Transactions of the ASME®

HEAT TRANSFER DIVISION
Chairman, J. M. CHENOWETH
Secretary, J. B. KITTO, JR.
Technical Editor, G. M. FAETH
Associate Technical Editors
J. V. BECK
R. O. BUCKIUS
I. CATTON
R. GREIF
F. P. INCROPERA
H. R. JACOBS
A. D. KRAUS
P. J. MARTO
D. M. McELIGOT
W. A. SIRIGNANO

BOARD ON COMMUNICATIONS
Chairman and Vice President
R. NICKELL

Members-at-Large
J. LLOYD
R. REDER
F. SCHMIDT
M. FRANKE
M. KUTZ
T. MIN
F. LANDIS
R. ROCKE
W. WINER
R. GENTILE
R. MATES

President, E. L. DAMAN
Executive Director,
D. L. BELDEN
Treasurer,
ROBERT A. BENNETT

PUBLISHING STAFF
Mng. Dir., Publ., JOS. SANSONE
Managing Editor,
CORNELIA MONAHAN
Sr. Production Editor,
VALERIE WINTERS
Editorial Prod. Asst.,
MARISOL ANDINO

Transactions of the ASME, Journal of Heat Transfer (ISSN 0022-1481) is published quarterly (Feb., May, Aug., Nov.) for $155 per year by The American Society of Mechanical Engineers, 345 East 47th Street, New York, NY 10017. Second class postage paid at New York, NY and additional mailing offices. POSTMASTER: Send address changes to The Journal of Heat Transfer, c/o THE AMERICAN SOCIETY OF MECHANICAL ENGINEERS, 22 Law Drive, Box 2300, Fairfield, NJ 07007-2300.
CHANGES OF ADDRESS must be received at Society headquarters seven weeks before they are to be effective. Please send old label and new address.
PRICES: To members, $29.00, annually; to nonmembers, $155.00.
Add $15.00 for postage to countries outside the United States and Canada.
STATEMENT from By-Laws. The Society shall not be responsible for statements or opinions advanced in papers or . . . printed in its publications (B7.1, para. 3).
COPYRIGHT © 1988 by the American Society of Mechanical Engineers. Reprints from this publication may be made on condition that full credit be given the TRANSACTIONS OF THE ASME, JOURNAL OF HEAT TRANSFER, and the author, and date of publication be stated.
INDEXED by Applied Mechanics Reviews and Engineering Information, Inc.

Journal of Heat Transfer

Published Quarterly by The American Society of Mechanical Engineers

VOLUME 110 • NUMBER 4(B) • NOVEMBER 1988

1035 Editorial

1037 Recent Developments in Computational Heat Transfer
S. V. Patankar

1046 Combined Parameter and Function Estimation in Heat Transfer With Application to Contact Conductance
J. V. Beck

1059 Recent Developments in Contact Conductance Heat Transfer
L. S. Fletcher

1071 Analysis of Extended Surface
A. D. Kraus

1082 Some Perspectives on Enhanced Heat Transfer—Second-Generation Heat Transfer Technology
A. E. Bergles

1097 Convection Heat Transfer in Electronic Equipment Cooling
F. P. Incropera

1112 On the Computation of Convective Heat Transfer in Complex Turbulent Flows
B. E. Launder

1129 Progress in Turbulent Forced Convection
R. H. Pletcher

1145 Heat Transfer in Fluid Flows Which Do Not Follow the Contour of Bounding Walls
E. M. Sparrow

1154 Wavenumber Selection in Bénard Convection
I. Catton

1166 Transient Response and Disturbance Growth in Vertical Buoyancy-Driven Flows
B. Gebhart

1175 Natural Convection in Enclosures
S. Ostrach

1191 Transitions and Bifurcations in Laminar Buoyant Flows in Confined Enclosures
K. T. Yang

1205 Heat Transfer During Melting and Solidification of Metals
R. Viskanta

1220 Thermal Radiation in Participating Media: The Past, the Present, and Some Possible Futures
J. R. Howell

1230 Thermal Radiation in Packed and Fluidized Beds
C. L. Tien

1243 Natural Circulation Loops
R. Greif

1259 Direct-Contact Heat Transfer for Process Technologies
H. R. Jacobs

1271 Burnout on Cylinders
J. H. Lienhard

1287 An Evaluation of Film Condensation on Horizontal Integral-Fin Tubes
P. J. Marto

Downloaded 04 Feb 2011 to 194.85.80.107. Redistribution subject to ASME license or copyright; see http://www.asme.org/terms/Terms_Use.cfm

Journal of Heat Transfer

Editorial

This special fifth issue of Volume 110 of the JOURNAL OF HEAT TRANSFER was prepared as part of the activities associated with the fiftieth anniversary of the Heat Transfer Division of the American Society of Mechanical Engineers. An anniversary is an appropriate occasion to reflect on the past, to take stock of the present, and to plan for the future. Thus, this special issue departs from the usual content of contributed articles and Technical Notes, and consists of twenty invited articles. The invited articles were prepared by leading specialists, chosen to be representative of the diverse interests of the heat transfer community. The articles are double length, to provide reasonable scope to develop each topic. The authors were given considerable latitude concerning the focus of their articles: Some emphasize historical background, some emphasize critical review, and some emphasize new information and methodologies. To an extent, however, all authors provide expert insight concerning future directions for research and development in heat transfer as the Heat Transfer Division ends its first fifty years.

The articles are organized in the normal format of the journal, beginning with general analytical and numerical methods and followed by conduction, convection, radiation, and multiphase heat transfer in order. The general areas of heat transfer that have been considered, and the authors that have contributed papers to each area, are as follows: computational methods for heat transfer, S. V. Patankar; conduction heat transfer, J. V. Beck and L. S. Fletcher; augmentation and high-intensity (electronic) cooling, A. E. Bergles, F. P. Incropera, and A. D. Kraus; forced convection, B. E. Launder, R. H. Pletcher, and E. M. Sparrow; natural convection, I. Catton, B. Gebhart, S. Ostrach, and K. T. Yang; melting and solidification, R. Viskanta; thermal radiation, J. R. Howell and C.-L. Tien; and multiphase flow and transport, R. Greif, H. R. Jacobs, J. H. Lienhard, and P. J. Marto.

The efforts of the authors to prepare articles in a timely manner, within stringent length limitations, are gratefully acknowledged. Finally, this special issue of the JOURNAL OF HEAT TRANSFER would not have been possible without the encouragement and support of the Executive Committee of the Heat Transfer Division.

Copyright © 1988 by ASME

Downloaded 16 Dec 2010 to 193.140.21.150. Redistribution subject to ASME license or copyright; see http://www.asme.org/terms/Terms_Use.cfm

Recent Developments in Computational Heat Transfer

S. V. Patankar
Department of Mechanical Engineering,
University of Minnesota,
Minneapolis, MN 55455

Recent developments in computational methods for heat transfer and fluid flow are reviewed. Emphasis is given to the treatment of convection and diffusion and solution of flow equations. Also, some interesting applications of the methods are mentioned. Whereas many attractive methods have been formulated in recent years, there exists no clear consensus about a preferred method. Careful and controlled evaluations of different methods are required. This and other tasks for future research are outlined.

Introduction

Background. Over the past twenty years, computational heat transfer has emerged as a new field, which promises to have significant impact on research, design, and education. With the rapid development of computer hardware, the computational techniques for heat transfer and fluid flow have been vigorously proposed, tested, and refined. Practicing engineers and researchers are beginning to recognize computational analysis as a cost-effective and convenient way of obtaining detailed solutions for complex physical situations. The purpose of this paper is to review some of the recent developments in this field and to comment on research requirements for the future.

Since the coverage of topics in this paper will be selective and limited, it is useful to mention here some other available sources of information. In the reviews of heat transfer literature published annually in the *International Journal of Heat and Mass Transfer* (such as Eckert et al., 1987), there is a section on numerical methods. Literature surveys on numerical heat transfer are periodically presented by Shih (1982, 1985, 1987). A recent article by Singhal (1985) takes a critical look at the progress in numerical heat transfer.

For a more in-depth treatment of the subject, the reader can turn to the textbooks published in recent years. These include the books by Patankar (1980), Baker (1983), Shih (1984), Anderson et al. (1984), and Jaluria and Torrance (1986). Also, the recently published handbook of numerical heat transfer (Minkowycz et al., 1988) contains many useful articles.

Scope and Limitations of the Paper. The literature on computational methods in heat transfer has grown very rapidly in recent years. An exhaustive review of all published papers in this field will not be attempted here. The purpose of this paper is to focus on the developments published after about 1980; earlier references will be mentioned only when required as a basis of discussion. Also, only papers published in major archival journals will be included in this review; papers included in conference proceedings and published in other places will not be reviewed.

Because of these restrictions and the choice of subjects (to be described shortly), it is quite possible that many important papers will be omitted from this review. However, omission from this review does not imply a judgment on the value of a particular paper.

The scope of the present paper is intentionally limited to certain subjects. This provides a focus for the paper and makes the review manageable. It is recognized that the topics included here do reflect the personal choices of the present author.

Among the different modes of heat transfer, radiation is not considered in this paper. Also, there is no explicit emphasis on conduction, although the methods for convection do include conduction problems as a limiting case. Thus, the paper is primarily concerned with convective heat transfer. No attention is given to freezing and melting problems, multiphase flows, and free-surface flows.

The computational analysis of convection can be considered to be the solution of the temperature field in the presence of a known velocity field. However, since the velocity field is seldom known, its calculation also becomes necessary. As a result, the computation of fluid flow becomes an essential part of computational heat transfer.

Among the techniques considered for fluid flow, supersonic flows and the associated methods of shock fitting and shock capturing are excluded. The primary focus is thus on incompressible flows. Although time-dependent phenomena are included, a greater emphasis is placed on the calculation of steady flows.

In this review, methods of general applicability, such as the finite-difference and finite-element method, are considered. Methods devised for very specific problems are excluded from consideration. Similarly, the boundary element method, the boundary integral method, and methods for *inverse* heat conduction problems are not considered.

For the treatment of irregular geometries, finite-difference methods often employ grids in curvilinear coordinates. The generation of appropriate grids is an important topic with its separate literature. Despite their importance, grid-generation techniques are not included in this paper.

The focus of this paper is on the methods rather than on their applications. However, at the end of the paper, a few recent applications to interesting and complex problems are briefly mentioned.

Ingredients of a Computational Technique. The aim of a computational method is to obtain the *values* of the dependent variables such as temperature, velocity, pressure, etc., at a number of discrete locations called nodes or grid points. These values are governed by algebraic equations known as discretization equations; they are derived from the governing differential equations and represent their discrete analogs.

Thus, the main ingredients of a computational technique are (*a*) the discretization equations and (*b*) an algorithm for their solution. The accuracy of the solution is dependent only on the first ingredient; the efficiency is, however, dictated by both ingredients since the nature of the discretization equations may control how efficiently they can be solved.

The main consideration in the derivation of the discretization equations is the formulation of the convection and diffusion terms. Since it is recognized that convection is an asymmetric phenomenon, i.e., the upstream conditions have a greater influence than the downstream ones, it is essential that the discretization scheme reflect this in some way. Otherwise, physically unrealistic solutions can occur. On the other hand,

Contributed by the Heat Transfer Division for publication in the JOURNAL OF HEAT TRANSFER. Manuscript received by the Heat Transfer Division May 2, 1988. Keywords: Numerical Methods, Reviews.

Copyright © 1988 by ASME
Downloaded 16 Dec 2010 to 193.140.21.150. Redistribution subject to ASME license or copyright; see http://www.asme.org/terms/Terms_Use.cfm

simple asymmetric schemes such as upwind differencing lead to significant errors in multidimensional situations.

The convection-diffusion formulation has relevance to the flow computation as well. The momentum equations and the equations for turbulence parameters also contain convection and diffusion terms. The extra feature required for the flow solution is an algorithm for handling the special coupling between the momentum and continuity equations.

Comparative Evaluation of Methods. The rapid growth of numerical methods for handling convection and diffusion and for solving flow equations has motivated a number of controlled comparisons of different methods. Such evaluations document the results of the methods on a few test problems. Sometimes, a standard test problem is given to a large number of groups who submit their solutions to that problem. Such Olympiads, although requiring considerable organization and raising expectations, have not produced useful conclusions. For example, in the study reported by Napolitano and Orlandi (1985), 15 different groups were asked to solve a standard flow problem. Their results were inconclusive. They commented, "Nothing definite can be said about the superior accuracy of finite elements or finite differences." They found that the comparisons of the computer time were also difficult to make. Different groups used different computers, different programming styles, and either general-purpose computer codes or specially "tuned" programs designed just for the test problem.

These experiences point to the difficulties in conducting large-scale evaluations. When the comparisons are made by a single group, its conclusions may not agree with the conclusions of another group. The situation seems very similar to that in the medical field where different controlled studies on the effect of tobacco, cholesterol, or exercise lead to contradictory conclusions.

After the rapid development of methods in recent years, the challenge for the future is going to be the careful evaluation and sifting of the methods so that useful recommendations can be given to the *users* of the methods.

Outline of the Remainder of the Paper. The presentation in this paper is divided into six major sections. In the first of these sections, methods for solving linear algebraic equations are reviewed. This is followed by a section on convection and diffusion. It contains a discussion of new formulations and a review of many studies involving a comparison of different schemes.

The next section focuses on the solution of the flow equations. The discussion there deals with a number of techniques for solving the coupled momentum and continuity equations. Both finite-difference and finite-element methods are reviewed. Additional topics such as spectral methods, irregular geometry, and adaptive grids are covered in a subsequent section.

The section on applications deals with the numerical solution of some interesting practical problems. Finally, some closing remarks are made about recent achievements and possible future developments.

Solution of Linear Equations

As already mentioned, the solution of simultaneous linear algebraic equations plays an important role in any overall calculation method. If the nodes are arranged along lines, the resulting algebraic equations have a pattern, which allows the use of particularly efficient techniques.

Whereas the Gauss–Seidel point-by-point or line-by-line methods have been commonly used for the solution of linear algebraic equations, a number of new techniques have recently been proposed. Some of these techniques are extensions of the strongly implicit method of Stone (1968). Lin (1985) has proposed the use of three free parameters to accelerate the convergence of Stone's method. In the methods formulated by Schneider and Zedan (1981) and Peric (1987), the five-diagonal matrix in Stone's method is replaced by a nine-diagonal matrix. As a result, these modified methods are applicable to the discretization formulations that lead to nine-diagonal matrices; they are also shown to be more efficient when applied to five-diagonal systems as well.

Phillips and Schmidt (1984) describe the use of multigrid techniques for solving the diffusion equation. The multigrid method is useful in resolving regions of large local gradients. A multilevel-multigrid method was found to be better than a simple multigrid method. The use of the multigrid method has also been demonstrated by Rieger et al. (1983).

Treatment of Convection and Diffusion

Background. In recent years, a significant amount of research effort has been directed toward discretization of the combined convection and diffusion fluxes. The formulation has direct consequences on the accuracy of the solution for the flow field, as well as the scalar variables such as temperature and concentration. Also, since many discretization schemes tend to become unstable at high flow rates, the ability to obtain a converged solution of the problem is also dependent on the underlying convection-diffusion formulation. If the solution contains an excessive amount of the numerical error known as false diffusion, the results may not reflect the true implications of physical models such as the turbulence model. In many cases, it is almost impossible to refine the grid sufficiently so that the numerical errors will be reduced to acceptable levels. Thus, there is a crucial need for a convection-diffusion formulation that leads to stable and accurate results with grids of modest fineness.

New Convection-Diffusion Formulations. Because of the shortcomings in terms of accuracy and stability of the established methods such as the central-difference scheme, upwind scheme, hybrid scheme (Spalding, 1973), and the power-law scheme (Patankar, 1980), a number of new formulations have been proposed. Some of them are based on the quadratic upstream (QUICK) scheme of Leonard (1979); a number of new schemes employ the concept of Raithby (1976), where the direction of the velocity vector is used in obtaining the convective influence from upstream.

Lillington (1981) has proposed a scheme that accounts for the magnitude of the source term in addition to the direction of the velocity vector. Another modification of Raithby's scheme is described by Hassan et al. (1983), where the negative influence coefficients in Raithby's (1976) scheme have been eliminated; the result is that spurious oscillations are suppressed but the false diffusion returns, albeit with a reduced magnitude.

A method based on a locally exact solution of the differential equation has been proposed by Stubley et al. (1980). A similar method, known as the finite analytic method, has been independently developed by Chen et al. (1981). These formulations do give stable and accurate results but are rather complex and expensive for regular use. A higher-order scheme, which employs Hermitian polynomials for convection, has been presented by Glass and Rodi (1982).

Convection-diffusion formulations in *finite-element* methods have followed a similar pattern. Baliga and Patankar (1980) introduced a control-volume formulation with triangular elements and employed a shape function based on the direction of the local velocity vector. The method has been extended to three dimensions by Muir and Baliga (1986). A similar procedure for quadrilateral elements has been developed by Ramadhyani and Patankar (1985).

In a Galerkin formulation of the finite-element method, Brooks and Hughes (1982) have employed a streamline up-

Downloaded 16 Dec 2010 to 193.140.21.150. Redistribution subject to ASME license or copyright; see http://www.asme.org/terms/Terms_Use.cfm

wind procedure. Rice and Schnipke (1985) have shown how the streamline upwind method can be constructed so that the spatial oscillations are completely eliminated.

Whereas many attempts have been made to improve accuracy without generating spurious overshoots and undershoots, Gresho and Lee (1981) argue that it is undesirable to suppress these "wiggles," which provide useful information about the inadequacy of the grid fineness or an incorrect boundary condition. In practice, however, it is difficult to follow this advice. In complex problems, one may not be able to distinguish between physical and nonphysical wiggles; moreover, the generation of wiggles during the iterative process may often lead to divergence of the iterations.

Comparisons of Convection-Diffusion Schemes. With a number of available schemes for the convection-diffusion formulation, it is natural to compare them on some standard problems and draw useful conclusions. A large number of such studies have been conducted and reported. Unfortunately, the matter is far from being resolved. Some studies are inconclusive, while the conclusions of the others conflict with one another. The need for a definitive study on the formulation of convection and diffusion still remains.

Smith and Hutton (1982) have reported the results of a compilation of 30 sets of solutions submitted by 19 groups. All solutions pertained to a standard problem, in which the specified flow made a 180 deg turn. On coarse grids, all methods showed oscillations or false diffusion.

Han et al. (1981) compared the results of the hybrid and QUICK schemes. Although QUICK was difficult to converge, it gave superior accuracy. Pollard and Siu (1982) worked out extended versions of QUICK that had better convergence behavior. Although they succeeded in getting convergence, it was slow and hence uneconomical. Beier et al. (1983) compared the performance of six methods for the calculation of a scalar field in the presence of a given recirculating flow field. They found that the higher-order methods gave superior accuracy.

Four different convection-diffusion schemes were employed by Huang et al. (1985) for the calculation of the flow equations. They found that QUICK gave very accurate results with only 65 percent more computational effort than the power-law scheme. A similar conclusion was reported by Aggarwal (1987) after applying many schemes to the convection-diffusion-reaction equations.

Shyy (1985) reported a study where many schemes, including QUICK, were employed. He found that the second-order upwind scheme was the most satisfactory. When different convection-diffusion schemes were used by Shyy et al. (1985) for a recirculating flow in nonorthogonal curvilinear coordinates, QUICK was found to be difficult to converge. The investigation of Demuren (1985) for three-dimensional flows found that QUICK produced overshoots and undershoots.

Patel et al. (1985) have tested seven discretization schemes on *one-dimensional* problems. Their conclusions are of little value in multidimensional situations where false diffusion occurs due to the obliquity of the flow. The two-dimensional problem has been addressed by Patel and Markatos (1986), who evaluated eight schemes. They found that QUICK and its variants gave accurate and cost-effective solutions when they converged. However, they failed to converge for high flow rates and coarse grids. Finally, Patel et al. (1987) reported the evaluation of 11 schemes for predicting flow in supersonic jets. Despite their best efforts, QUICK and the skew-differencing scheme (Raithby, 1976) failed to converge. The conclusion of their study was that the upwind scheme is the best choice.

Thus, we have gone around a full circle. Lower-order schemes such as upwind are stable and monotonic but lead to false diffusion. Higher-order schemes such as QUICK eliminate false diffusion but produce wiggles and often fail to converge. The search for the perfect method is still not over.

Among other studies of the convection-diffusion problem, Murphy and Prenter (1985) tested a number of higher-order methods, including the use of Hermite polynomials. Miller (1986) compared the flux-corrected transport and the TVD schemes with other candidates. Various finite-element formulations of the advection equations were examined by Neta and Williams (1986); they found that the best schemes were given by isosceles triangles with linear basis functions and rectangles with bilinear basis functions.

Solution of Flow Equations

Background. The prediction of convective heat transfer requires calculation of the underlying flow field. The convection-diffusion formulation developed for the transport of a scalar is applicable to the discretization of the equations for momentum and turbulence quantities. In addition, techniques are needed for handling coupling between the momentum and continuity equations.

The available methods for flow calculation can be roughly divided as finite difference or finite element, and as based on primitive variables or vorticity. Once the required convection-diffusion formulation is chosen, the essence of the method lies in its treatment of the coupling between the momentum and continuity equations.

A number of currently employed methods of flow calculation originate from the SIMPLE procedure of Patankar and Spalding (1972). In this section, a number of enhancements of SIMPLE will be reviewed. This will be followed by the description of multigrid methods for fluid flow. Also discussed will be coupled solution techniques and other flow calculation methods. Next, the general finite element methods and their subset of penalty methods will be reviewed. Finally, the development of nonstaggered grids and equal-order interpolation schemes will be discussed.

Enhancements of SIMPLE. The rather slow convergence of the original SIMPLE method and the need for heavy underrelaxation have motivated the development of more efficient variants of SIMPLE. Patankar (1980, 1981) introduced the SIMPLER method, in which an extra equation is solved for the evaluation of pressure. Another variant is the SIMPLEC procedure described by Van Doormaal and Raithby (1984); their method uses consistent underrelaxations for the momentum and pressure corrections. The SIMPLEST procedure was developed by Spalding (1980), who recommended an explicit treatment of convection and implicit treatment of diffusion in the momentum equations. Another enhancement of SIMPLE has been proposed by Issa (1985); the method is called PISO. Although at first sight it appears to be a separate method, a closer examination reveals that (except possibly for some very minor differences) PISO is the same as SIMPLER.

Connell and Stow (1986) have examined the pressure-correction method in general and proposed two extensions of SIMPLE. Latimer and Polard (1985) report a comparison of many enhancements of SIMPLE and describe a new algorithm called FIMOSE.

Multigrid Techniques. One way of handling the coupling between the velocity and pressure is to solve for them simultaneously at a grid point. However, this leads to a point-by-point scheme, which converges very slowly, especially for fine grids. Recently, in a series of papers, Vanka has shown that the use of a multigrid method with a coupled solution at a point can lead to a very efficient technique. His basic algorithm is described in Vanka (1986a); the application to two-dimensional recirculating flows is made in Vanka (1986b). He has also demonstrated a method for turbulent flows (Vanka, 1985), where the equations for the turbulence

Downloaded 16 Dec 2010 to 193.140.21.150. Redistribution subject to ASME license or copyright; see http://www.asme.org/terms/Terms_Use.cfm

parameters are handled by the Newton–Raphson technique. Applications have also been made to three-dimensional recirculating flows (Vanka, 1986c) and to three-dimensional sudden-expansion flows (Vanka, 1986d).

The concept of additive correction is used in a multigrid context by Hutchinson et al. (1988) for handling the coupling between velocity and temperature in natural convection problems.

One useful aspect of the multigrid technique is that it allows local grid refinement in the regions of large gradients. This aspect is described by Fuchs (1986). Also, Phillips and Schmidt (1985a) demonstrate that local grid refinement can be introduced in the solution of the convection-diffusion equation. They also describe a robust implementation of QUICK in the multigrid framework. A multilevel-multigrid technique for recirculating flows has been presented by Phillips and Schmidt (1985b). The performance of the technique has been compared with other methods by Miller and Schmidt (1988).

In the vorticity-stream function formulation, the coupled equations can be solved at a grid point. Then the overall convergence can be improved by the introduction of the multigrid method. Such a technique is reported by Lacroix et al. (1984).

Coupled Solution Methods. Multigrid is one framework in which a coupled solution of the interacting variables can be considered. A number of other techniques have also been developed.

Vanka and Leaf (1983) described a fully coupled solution of the momentum and continuity equations by the use of a sparse-matrix solver. Although the approach looks attractive for problems with a modest number of grid points, it requires excessive computer storage and time for fine grids and three-dimensional problems. Braaten and Shyy (1986) applied the direct solution technique to equations in body-fitted coordinates; they found that, because of the increased complexity, the method did not remain cost-effective.

The strongly implicit procedure of Stone (1968) can be extended to solve for velocity components and pressure in a coupled manner. Zedan and Schneider (1985) developed and tested such a procedure; they found that the new procedure, although better than the fully coupled direct solution, was marginally more costly than SIMPLE. Stone's method in a coupled form has also been developed for the stream function–vorticity system by Rubin and Khosla (1981). An alternative technique based on the conjugate gradient method has been described for the stream function–vorticity system by Khosla and Rubin (1981).

The continuity and momentum equations can be solved in a coupled manner along a grid line. Such a line solver has been developed by Galpin et al. (1985).

The nonlinearities in the momentum equations have been treated by the Newton–Raphson method in the framework of a direct solution by Galpin and Raithby (1986a). They also describe the use of a coupled line solver. The coupling between the momentum and energy equations has been treated in Galpin and Raithby (1986b).

Additional Fluid Flow Methods (Finite Difference). For two-dimensional problems, Farouk and Fusegi (1985) have proposed an alternative to the stream function–vorticity method. Their method solves the vorticity equation and two Poisson equations for the two velocity components. The equations are solved in a coupled manner along a line. Sone applications of the method are described in Fusegi and Farouk (1986).

Yang and Camarero (1986) have reported a method employing the vorticity vector and a *scalar* potential for three-dimensional duct flows. A discussion of various schemes for solving the Navier–Stokes equations is given by Connell and Stow (1986). They distinguish the methods as coupled and uncoupled depending on whether the nonlinearity is accounted for at a given stage of iteration. Methods for two-dimensional Navier–Stokes equations have been reviewed by Cebeci et al. (1981).

Finite-Element Methods for Fluid Flow. The ingredients of a finite element method for the calculation of the flow field include the type of the element used, the convection-diffusion formulation, and the solution technique. If the method is based on the primitive variables, there are two more considerations. To avoid a checkerboard pressure field, it may be necessary to employ unequal-order elements for the velocity components and pressure; this is the counterpart of the staggered grid that is commonly employed in finite-difference methods. Second, a suitable solution procedure is required for handling the special coupling between the momentum and continuity equations.

Not all finite-element methods now use unequal-order interpolation. The new equal-order methods will be described in a separate subsection along with the finite-difference methods for nonstaggered grids.

One method of handling the coupling between velocity and pressure is the penalty method, which is discussed in a separate subsection. If the penalty method is not used, then either the momentum and continuity equations are solved directly or a SIMPLE-like iterative procedure is devised.

Benim and Zinser (1986) have described a finite-element method with unequal-order interpolation and SIMPLE-like segregated solution technique. Similar strategy was used by Del Giudice et al. (1981) for a method for three-dimensional parabolic flows. Pepper (1987) has developed a time-stepping technique that uses quadrilateral elements, a line-by-line solution, and SIMPLE-like pressure corrections.

Whereas most finite-element methods are based on the variational principle or the Galerkin technique, Baliga and Patankar (1986) have developed a method based on the control-volume approach. It employs triangular grids with unequal-order interpolation, a shape function based on the local velocity vector, and a solution scheme that follows the spirit of SIMPLER.

For a natural convection problem, a mixed solution method has been proposed by McDonough and Catton (1982). They employ the Galerkin technique in the horizontal direction and finite differences in the vertical direction. A review of some finite-element methods for steady Navier–Stokes equations has been given by Segal (1985).

Penalty Methods. For incompressible flow, the continuity equation does not contain pressure. However, the zero right-hand side of the equation can be replaced by the product of pressure and a penalty parameter that is very small. Within the limits of the computer word length, one can reduce the value of this parameter and thereby nearly satisfy the continuity equation. The pressure is then given by the ratio of the (almost zero) divergence of the velocity vector and the vanishing penalty parameter. This expression for pressure is substituted into the momentum equations, thereby eliminating pressure. This is the essence of the penalty method.

A general discussion of the penalty method in finite elements has been given by Reddy (1982a). In another paper (Reddy, 1982b), he describes the application of the penalty method to a driven cavity and a natural convection problem.

Kheshgi and Scriven (1985) have proposed a method of varying the penalty parameter from element to element. Thus, even with large variations in element size, improved accuracy can be obtained. The method can then be used on computers with small word length.

In a review paper, Baker (1984) has described the use of the penalty method in three-dimensional parabolic flows. A number of elements with continuous velocity and discontinuous pressure approximation are described by Dhatt and Hubert (1986) in the context of the penalty method.

Downloaded 16 Dec 2010 to 193.140.21.150. Redistribution subject to ASME license or copyright; see http://www.asme.org/terms/Terms_Use.cfm

Nonstaggered Grids and Equal-Order Interpolation. In a finite-difference method, if the velocity components and pressure are located at the same grid points, a checkerboard pressure field can develop as an acceptable solution. This is described fully in Patankar (1980). Since such pressure fields are undesirable, one uses a staggered grid, which completely eliminates the checkerboard pressure field. In the staggered grid, the velocity components are stored at displaced or staggered locations such that the pressure drop between two pressure nodes can be used to "drive" the velocity component located between them. Methods such as SIMPLE and its variants all use the staggered grid. Although the staggered grid eliminates some major difficulties, it introduces some inconvenience, which becomes more serious when the method is extended to curvilinear nonorthogonal coordinates. Similarly, since there is no direct counterpart of the staggered grid in the finite element method, one has to resort to unequal-order interpolation, which reduces the accuracy of the overall solution. These reasons provide the motivation for a search for methods with nonstaggered grids or equal-order interpolation.

Rhie and Chow (1983) have presented a method that employs a nonstaggered grid in the framework of curvilinear nonorthogonal coordinates. The solution method uses a SIMPLE-like algorithm. Three different formulations with nonstaggered grids have been suggested by Shih and Ren (1984). Some of these employ the Poisson equation for pressure in place of the continuity equation.

In the method developed by Reggio and Camarero (1986) and Reggio et al. (1987), the staggering is introduced in the differencing formulas rather than in the grid. For the nonstaggered grid, forward differencing is used for the mass flow rate and backward differencing for the pressure gradients.

Although the nonstaggered-grid methods appear satisfactory on the surface, a number of them suffer from a subtle drawback. The solution produced by them depends on the values of the underrelaxation factors or the size of the time step. This feature is obviously very undesirable. That the nonstaggered-grid methods have this characteristic has been recognized by the present author and some others for quite some time. Recently, Majumdar (1988) has described this phenomenon and proposed a remedy for it. Incidentally, the same drawback is present in some of the finite-element methods with equal-order interpolation.

In finite-difference methods, the advantage of a nonstaggered grid is simply to avoid the inconvenience associated with the staggered grid. In finite-element methods, the matter becomes more important. The approximate counterpart of the staggered grid is the unequal-order interpolation, in which the pressure is interpolated by a lower-order shape function than the velocity components. In effect, pressure is calculated on a mesh coarser than the one used for velocity. As a result, the accuracy of the whole solution drops to the level appropriate to the coarse mesh. An equal-order method will increase accuracy in addition to providing convenience.

Prakash and Patankar (1985) have developed a control-volume finite-element method with equal-order velocity-pressure interpolation. Whereas the other details of the method are the same as those in Baliga and Patankar (1983), the velocities in the continuity equation are obtained from a formula that involves the pressure gradient. An extension of the method for three-dimensional parabolic flows has been described in Prakash and Patankar (1987). In an improved version of the method (Prakash, 1986), the pressure gradient is incorporated in the shape function for velocity; as a result, the pressure checkerboarding is avoided in a straightforward manner. Another control-volume finite-element method with equal-order interpolation has been described by Schneider and Raw (1987).

The finite-element method presented by Rice and Schnipke (1986) and Schnipke and Rice (1987) is based on a streamline upwind formulation, SIMPLE-like sequential solving of velocity and pressure, and the equal-order interpolation.

Additional Considerations

There are a number of other topics in which new developments have been made. These include the construction of spectral methods, treatment of irregular geometry, and adaptive grids. Some of these developments will be discussed in this section.

Spectral Methods. Although different versions of the spectral method have been around for some time, their applications have been mostly limited to simple problems. The possible reasons include the relative complexity of the method and the difficulty of handling general boundary conditions, internal discontinuities, and nonuniform transport properties and sources. The spectral method is capable of producing highly accurate solutions; however, the required computer time and storage seem to increase rapidly with the order of the method.

Nelsen and Douglass (1983) have described an application of the spectral method to natural convection. They report that the required computational effort increases as the cube of the number of terms retained in the series. Thus, the necessary computer storage and time become excessive at high Grashof numbers.

Basdevant et al. (1986) have compared the spectral and finite-difference methods for solving the Bergers equation. They conclude that the spectral method is not suitable for the calculation of thin inner layers unless a coordinate transformation or sufficient inner nodes are used. Ghaddar et al. (1986) have developed a spectral element method and applied it to the fully developed flow in periodic geometries.

The checkerboard pressure fields can also arise in the solutions via spectral methods. Montigny-Rannou and Morchoisne (1987) have proposed the use of the staggered grid with the spectral method for the Navier–Stokes equations; they show that the possibility of the checkerboard pressure field is then eliminated. A pseudospectral method for three-dimensional flows has been developed by Ku et al. (1987).

Treatment of Irregular Geometry. The significant difference between the finite-element method and the finite-difference method (on a regular coordinate grid) lies in their ability to handle irregular-shaped domains. Whereas any domain can easily be discretized into finite elements, the representation of curved or inclined boundaries on a Cartesian grid is not convenient. Thus, one way to handle irregular geometries is to use the finite-element methods, which have already been discussed. The other alternative is to formulate the finite-difference method on a curvilinear grid. Some of these developments will now be reviewed.

Vanka et al. (1980) have described a SIMPLE-like procedure that uses a staggered grid in body-fitted curvilinear coordinates. A different idea is proposed in Chung (1981), where the finite-difference method is based on a set of arbitrarily distributed nodes; each node is related to five neighbors through a shape function. Zedan and Schneider (1982) describe the use of the control-volume approach in a finite-difference solution of the conduction equation in generalized curvilinear coordinates.

The well-known MAC method has been extended by Patel and Briggs (1983) for use with boundary-fitted curvilinear coordinates. They use the contravariant velocity components in the discretization of the continuity equation. Raithby et al. (1986) have described a flow calculation method using general *orthogonal* coordinates. The method employs a staggered grid and SIMPLE-like solution procedure; the additional terms due to the grid curvature are obtained by treating the stresses and diffusion fluxes in a special manner. For domains where

Downloaded 16 Dec 2010 to 193.140.21.150. Redistribution subject to ASME license or copyright; see http://www.asme.org/terms/Terms_Use.cfm

one boundary does not lie along a coordinate line, Faghri et al. (1984) have developed a flow calculation method that employs an algebraic coordinate transformation.

Adaptive Grids. In both finite-element and finite-difference methods, the accuracy of the solution depends on the fineness of the mesh and on the mesh distribution. The regions of large gradients need to be represented by small elements or a fine grid. However, these regions are not known a priori. They must be guessed or determined from preliminary calculations. An adaptive grid method automatically calculates the locations of the nodes or the grid points in response to the evolving solution. Although the basic idea is attractive, general criteria for the distribution of grid points have not been worked out. Also, a dynamic adaptation in response to the evolving solution is prone to instability.

Acharya and Patankar (1985) have described an adaptive grid procedure for two-dimensional parabolic problems. The method employs a coarse fixed-grid solution from which guidance is obtained for the design of the adaptive fine grid. For a two-dimensional elliptic problem, Luchini (1987) has developed an adaptive-mesh solution method, which employs a technique of adding single points to a mesh independently of other mesh points.

Through the procedure of numerical grid generation, Kikuchi (1986) has formulated an adaptive finite-element method. Other adaptive techniques for finite-element methods for fluid flow have been reviewed and compared by Ewing (1986).

Applications

In recent years, a large number of computational methods have been developed, and have been applied to a variety of physical problems. Applications abound in natural and mixed convection, duct flows, convection in porous media, and freezing and melting. Review of these applications is outside the scope of this paper; however, a few recent interesting applications will now be mentioned. Some of the applications are conventional, while others demonstrate the use of computational methods in novel situations.

The forced convection heat transfer from a cylinder in cross flow has been predicted by Karniadakis (1988) by use of the spectral element method. The solutions include steady flow at low Reynolds numbers and unsteady vortex shedding at higher Reynolds numbers.

The three-dimensional natural convection in a spherical annulus has been calculated by Ozoe et al. (1985). They used the vorticity-vector potential formulation and solved the equations by ADI. Lee (1984) has presented laminar convection between concentric and eccentric heated rotating cylinders. The solutions were based on a special coordinate system devised for the annular geometry. As a practical application of natural convection, Ormiston et al. (1986) have reported numerical predictions for a Trombe wall system. They employed orthogonal curvilinear coordinates for the finite-difference calculation.

Calculations for three-dimensional natural convection of a liquid metal in a cavity (Viskanta et al., 1986) performed by using the SIMPLER algorithm indicate that, for low Prandtl numbers, the three-dimensional effects are present not only near the end walls but also in the center of the cavity. The effect of buoyancy on the laminar flow and heat transfer in a helically coiled tube have been predicted by Futagami and Aoyama (1988).

Lavine et al. (1987) have described a three-dimensional analysis of natural convection in a toroidal loop in a vertical plane. A finite-difference solution of the mixed convection heat transfer in a rectangular tank with rolling motion has been reported by Akagi and Kato (1987). The solution is relevant to oil tanks on ships experiencing a rollng motion.

In a very interesting application of the SIMPLE algorithm with body-fitted coordinates, Correa (1987) has predicted the natural convection in horizontal and vertical incandescent lamps. A finite-element simulation of an in-package pasteurization process has been described by Engelman and Sani (1983). They use the penalty method for the unsteady calculation. The results show interesting flow patterns in a milk bottle.

The increasing need for the cooling of electronic circuits has motivated a number of mathematical simulations of the process. Braaten and Patankar (1985) have presented the results for laminar mixed convection in a flow over electronic circuit boards with heat-generating components mounted on them. The buoyancy forces are shown to produce complex secondary flows and there are marked differences between the configurations of the heated blocks facing up and facing down.

Flows in electric arcs are produced by the action of the electric field on the fluid. The effect of this Lorentz force on the transport processes in the anode region of an electric arc have been demonstrated by Wilhelmi et al. (1985). They use a finite-difference technique employing the SIMPLE algorithm. In another arc-related application, Mostaghimi et al. (1985) have compared the use of the stream function-vorticity method with that of SIMPLER. They found that SIMPLER was more efficient and that it converged under conditions for which the other method diverged.

Whereas the results of computational analysis are usually reasonable and plausible, occasionally rather unexpected and surprising results are obtained. In a numerical prediction of the flow and heat transfer in tubes with internal circumferential fins, Rowley and Patankar (1984) found that the introduction of the fins actually *decreased* the heat transfer. The surprising outcome can be understood by examining the velocity field, which shows regions of almost stagnant flow in the vicinity of the fins.

Srinivasan and Basu (1986) have described an application of numerical techniques to the thermocapillary flow during laser melting. The flow is driven by surface tension gradients. By the use of a combination of polar and Cartesian grids, Fujii et al. (1984) have predicted the laminar flow and heat transfer in an in-line tube bank.

Finally, two rather complex applications will be mentioned. Jaluria (1984) has presented a prediction of the unsteady heat transfer in a furnace used for heat treatment. The calculation involves the interaction of conduction, convection, and radiation (including gas radiation). A numerical prediction of the three-dimensional transient flow and combustion through granulated propellants has been described by Markatos and Kirkcaldy (1983). The mathematical model includes chemical reaction and two-phase effects.

Concluding Remarks

Achievements. The computational analysis of heat transfer and fluid flow has made very substantial progress in recent years. About twenty years ago, the prediction of a two-dimensional boundary layer represented the upper limit of the computational capability. Now far more complex phenomena are being successfully computed. With the progress in available techniques, expectations have also grown. Practicing engineers and designers are increasingly turning to computational analysis to obtain insight into the physical phenomena and to quantify the effects of the main parameters.

Simultaneous advances in computer hardware have made it practical to obtain numerical solutions to practical problems. Very intensive computations such as the direct simulation of turbulence can now be undertaken on a supercomputer. Applications such as modeling of the flow over an entire airplane and simulation of the transport processes in a gas turbine engine are beginning to appear within reach. On the other hand, the availability of powerful personal computers and

Downloaded 16 Dec 2010 to 193.140.21.150. Redistribution subject to ASME license or copyright; see http://www.asme.org/terms/Terms_Use.cfm

workstations is facilitating the application of sophisticated computational techniques in a routine fashion.

That a number of improvements in the available numerical methods are still needed does not diminish what has already been achieved. The technology has come a long way from simple flat-plate boundary layer solutions to calculation of unsteady, recirculating, three-dimensional convection.

Further Developments in Computational Techniques. In this paper, recent developments in the various aspects of computational techniques have been reviewed. Although a number of new methods have been formulated and their comparative evaluations have been made, no clear consensus has emerged. In a rapidly developing field, this situation is understandable. However, in the coming years, attempts should be made to identify robust, efficient, and widely applicable techniques. For this purpose, comparative studies on a much larger scale are necessary, and they should be undertaken with very clear objectives and criteria for the selection of methods. Since the conclusions tend to be problem-dependent, a large number of different problems must be used as test cases.

It appears that both finite-difference and finite-element methods will continue to be used for many years, although a cross-fertilization of ideas between the two methods will increase. The finite-difference methods will increasingly use general curvilinear coordinates and the associated grid-generation techniques.

The formulation of a satisfactory convection-diffusion scheme still remains an unresolved question. The lower-order methods such as upwind or hybrid produce bounded and physically realistic solutions but involve significant false diffusion. The methods proposed for the elimination of false diffusion have negative influence coefficients, produce nonphysical overshoots and undershoots, and lead to oscillations and divergence. A more satisfactory scheme must be found.

A number of algorithms have been proposed for the solution of coupled momentum and continuity equations. These include the many variants of SIMPLE that have been formulated. A general *user* of these techniques now needs some guidance in choosing the proper algorithm. Again, there is an urgent need for a careful comparative study and a clear recommendation.

In most applications to complex situations the nonlinear coupling between different dependent variables is handled in a rather simple manner. That is why, whereas a laminar flow calculation converges quite quickly, the corresponding turbulent flow computation requires many iterations. In the future, greater emphasis must be placed on the proper treatment of the coupling between variables so that the solution of complex problems can be obtained reliably and efficiently.

Impact of Computer Hardware. Until a few years ago, all computers were based on nearly the same architecture, and a numerical analyst could use them simply as number-crunching devices. Now, the advent of supercomputers with their vector-processing and parallel-processing capabilities has made some impact on how computer programs and numerical algorithms are designed. In the coming years, there will be greater emphasis on the development of methods that properly exploit the vector- and parallel-processing capabilities.

At the other end of the scale are the microcomputers, which represent a convenient tool because of their easy availability. Because of their limitations of speed and memory, a separate class of methods and programming techniques is needed for the optimum use of these small computers.

Mathematical Models for Physical Phenomena. The ultimate success of computational analysis depends on the availability of reliable mathematical models for complex processes, such as turbulence, chemical reaction, multiphase flow, and so on. Over the last twenty years, the coordinated activities of numerical computation and research on mathematical models have produced many useful models for complex practical situations. It is this research that provides a framework for the results of experimental investigations and enables the observed generalizations to be used in other circumstances. With more powerful computers and numerical techniques, the research into mathematical models for complex processes is expected to grow in the coming years.

Educational Aspects. The significant progress in computational heat transfer over the past twenty years has also made an impact on the educational scene. A number of textbooks on the subject are now available. Many universities now teach separate graduate-level courses on computational heat transfer and fluid flow; introduction of this material into the undergraduate curriculum is also beginning.

As to the transfer of this information to practicing engineers and designers, the situation is not entirely satisfactory. As correctly pointed out by Singhal (1985), while the computational techniques are vigorously used in the aerospace industry, many other industries are not deriving the benefits of these new tools of analysis. Again, educational activities can play a major role here. Methods must be found for communicating the benefits of computational analysis to engineers dealing with many aspects of heat transfer and fluid flow.

In summary, there has been impressive progress in computational heat transfer during the past several years. Exciting and challenging tasks lie ahead in the development and evaluation of methods, the design of programs for proper computer hardware, research into mathematical models, and the dissemination of information to practicing engineers.

References

Acharya, S., and Patankar, S. V., 1985, "Use of an Adaptive Grid Procedure for Parabolic Flow Problems," *International Journal of Heat and Mass Transfer*, Vol. 28, pp. 1057–1066.

Aggarwal, S. K., 1987, "Numerical Study of Convection-Diffusion-Reaction Equations for Large Damkohler and Cell Reynolds Numbers," *Numerical Heat Transfer*, Vol. 11, pp. 143–164.

Akagi, S., and Kato, H., 1987, "Numerical Analysis of Mixed Convection Heat Transfer of a High Viscosity Fluid in a Rectangular Tank With Rolling Motion," *International Journal of Heat and Mass Transfer*, Vol. 30, pp. 2423–2432.

Anderson, D. A., Tannehill, J. C., and Pletcher, R. H., 1984, *Computational Fluid Mechanics and Heat Transfer*, Hemisphere, New York.

Baker, A. J., 1983, *Finite Element Computational Fluid Mechanics*, Hemisphere, New York.

Baker, A. J., 1984, "A Finite Element Penalty Algorithm for the Parabolic Navier–Stokes Equations for Turbulent Three-Dimensional Flow," *Computer Methods in Applied Mechanics and Engineering*, Vol. 46, pp. 277–293.

Baliga, B. R., and Patankar, S. V., 1980, "A New Finite-Element Formulation for Convection-Diffusion Problems," *Numerical Heat Transfer*, Vol. 3, pp. 393–409.

Baliga, B. R., and Patankar, S. V., 1983, "A Control Volume Finite Element Method for Two-Dimensional Fluid Flow and Heat Transfer," *Numerical Heat Transfer*, Vol. 6, pp. 245–261.

Basdevant, C., Deville, M., Haldenwang, P., Lacroix, J. M., Quazzani, J., Peyret, R., Orlandi, P., and Patera, A. T., 1986, "Spectral and Finite Difference Solutions of the Burgers Equation," *Computers and Fluids*, Vol. 14, pp. 23–41.

Beier, R. A., de Ris, J., and Baum, H. R., 1983, "Accuracy of Finite-Difference Methods in Recirculating Flows," *Numerical Heat Transfer*, Vol. 6, pp. 283–302.

Benim, A. C., and Zinser, W., 1986, "A Segregated Formulation of Navier–Stokes Equations With Finite Elements," *Computer Methods in Applied Mechanics and Engineering*, Vol. 57, pp. 223–237.

Braaten, M. E., and Patankar, S. V., 1985, "Analysis of Laminar Mixed Convection in Shrouded Arrays of Heated Rectangular Blocks," *International Journal of Heat and Mass Transfer*, Vol. 28, pp. 1699–1709.

Braaten, M. E., and Shyy, W., 1986, "Comparison of Iterative and Direct Solution Methods for Viscous Flow Calculations in Body-Fitted Coordinates," *International Journal for Numerical Methods in Fluids*, Vol. 6, pp. 325–349.

Brooks, A. N., and Hughes, T. J. R., 1982, "Streamline Upwind/Petrov-Galerkin Formulations for Convection Dominated Flows With Particular Emphasis on the Incompressible Navier–Stokes Equations," *Computer Methods in Applied Mechanics and Engineering*, Vol. 32, pp. 199–259.

Cebeci, T., Hirsh, R. S., Keller, H. B., and Williams, P. G., 1981, "Studies of Numerical Methods for the Plane Navier–Stokes Equations," *Computer Methods in Applied Mechanics and Engineering*, Vol. 27, pp. 13–44.

Downloaded 16 Dec 2010 to 193.140.21.150. Redistribution subject to ASME license or copyright; see http://www.asme.org/terms/Terms_Use.cfm

Chen, C.-J., Naseri-Neshat, H., and Ho, K.-S., 1981, "Finite-Analytic Numerical Solution of Heat Transfer in Two-Dimensional Cavity Flow," *Numerical Heat Transfer*, Vol. 4, pp. 179–197.

Chung, K. C., 1981, "A Generalized Finite-Difference Method for Heat Transfer Problems of Irregular Geometries," *Numerical Heat Transfer*, Vol. 4, pp. 345–357.

Connell, S. D., and Stow, P., 1986, "A Discussion and Comparison of Numerical Techniques Used to Solve the Navier–Stokes and Euler Equations," *International Journal for Numerical Methods in Fluids*, Vol. 6, pp. 155–163.

Connell, S. D., and Stow, P., 1986, "The Pressure Correction Method," *Computers and Fluids*, Vol. 14, pp. 1–10.

Correa, S. M., 1987, "Fluid Flow and Heat Transfer in Incandescent Lamps," *International Journal of Heat and Mass Transfer*, Vol. 30, pp. 663–672.

Del Giudice, S., Strada, M., and Comini, G., 1981, "Three-Dimensional Laminar Flow in Ducts," *Numerical Heat Transfer*, Vol. 4, pp. 215–228.

Demuren, A. O., 1985, "False Diffusion in Three-Dimensional Flow Calculations," *Computers and Fluids*, Vol. 13, pp. 411–419.

Dhatt, G., and Hubert, G., 1986, "A Study of Penalty Elements for Incompressible Fluid Flows," *International Journal for Numerical Methods in Fluids*, Vol. 6, pp. 1–19.

Eckert, E. R. G., Goldstein, R. J., Pfender, E., Ibele, W. E., Patankar, S. V., Ramsey, J. W., Simon, T. W., Decker, N. A., Kuehn, T. H., Lee, H. O., and Girshick, S. L., 1987, "Heat Transfer—a Review of 1986 Literature," *International Journal of Heat and Mass Transfer*, Vol. 30, pp. 2449–2523.

Engleman, M. S., and Sani, R. L., 1983, "Finite-Element Simulation of an In-Package Pasteurization Process," *Numerical Heat Transfer*, Vol. 6, pp. 41–54.

Ewing, R. E., 1986, "Efficient Adaptive Procedures for Fluid Flow Applications," *Computer Methods in Applied Mechanics and Engineering*, Vol. 55, pp. 89–103.

Faghri, M., Sparrow, E. M., and Prata, A. T., 1984, "Finite Difference Solutions of Convection-Diffusion Problems in Irregular Domains, Using a Nonorthogonal Coordinate Transformation," *Numerical Heat Transfer*, Vol. 7, pp. 183–209.

Farouk, B., and Fusegi, T., 1985, "A Coupled Solution of the Vorticity-Velocity Formulation of the Incompressible Navier–Stokes Equations," *International Journal for Numerical Methods in Fluids*, Vol. 5, pp. 1017–1034.

Fuchs, L., 1986, "A Local Mesh-Refinement Technique for Incompressible Flows," *Computers and Fluids*, Vol. 14, pp. 69–81.

Fujii, M., Fujii, T., and Nagata, T., 1984, "A Numerical Analysis of Laminar Flow and Heat Transfer of Air in an In-Line Tube Bank," *Numerical Heat Transfer*, Vol. 7, pp. 89–102.

Fusegi, T., and Farouk, B., 1986, "Predictions of Fluid Flow and Heat Transfer Problems by the Vorticity-Velocity Formulation of the Navier–Stokes Equations," *Journal of Computational Physics*, Vol. 65, pp. 227–243.

Futagami, K., and Aoyama, Y., 1988, "Laminar Heat Transfer in a Helically Coiled Tube," *International Journal of Heat and Mass Transfer*, Vol. 31, pp. 387–396.

Galpin, P. F., and Raithby, G. D., 1983a, "Treatment of Nonlinearities in the Numerical Solution of the Incompressible Navier–Stokes Equations," *International Journal for Numerical Methods in Fluids*, Vol. 6, pp. 409–426.

Galpin, P. F., and Raithby, G. D., 1986b, "Numerical Solution of Problems in Incompressible Fluid Flow: Treatment of Temperature-Velocity Coupling," *Numerical Heat Transfer*, Vol. 10, pp. 105–129.

Galpin, P. F., Van Doormaal, J. P., and Raithby, G. D., 1985, "Solution of the Incompressible Mass and Momentum Equations by Application of a Coupled Equation Line Solver," *International Journal for Numerical Methods in Fluids*, Vol. 5, pp. 615–625.

Ghaddar, N. K., Karniadakis, G. E., and Patera, A. T., 1986, "A Conservative Isoparametric Spectral Element Method for Forced Convection; Application to Fully Developed Flow in Periodic Geometries," *Numerical Heat Transfer*, Vol. 9, pp. 277–300.

Glass, J., and Rodi, W., 1982, "A Higher Order Numerical Scheme for Scalar Transport," *Computer Methods in Applied Mechanics and Engineering*, Vol. 341, pp. 337–358.

Gresko, P. M., and Lee, R. L., 1981, "Don't Suppress the Wiggles—They're Telling You Something!" *Computers and Fluids*, Vol. 9, pp. 223–253.

Han, T., Humphrey, J. A. C., and Launder, B. E., 1981, "A Comparison of Hybrid and Quadratic-Upstream Differencing in High Reynolds Number Elliptic Flows," *Computer Methods in Applied Mechanics and Engineering*, Vol. 29, pp. 81–95.

Hassan, Y. A., Rice, J. G., and Kim, J. H., 1983, "A Stable Mass-Flow-Weighted Two-Dimensional Skew Upwind Scheme," *Numerical Heat Transfer*, Vol. 6, pp. 395–408.

Huang, P. G., Launder, B. E., and Leschziner, M. A., 1985, "Discretization of Nonlinear Convection Processes: a Broad-Range Comparison of Four Schemes," *Computer Methods in Applied Mechanics and Engineering*, Vol. 48, pp. 1–24.

Hutchinson, B. R., Galpin, P. F., and Raithby, G. D., 1988, "Application of Additive Correction Multigrid to the Coupled Fluid Flow Equations," *Numerical Heat Transfer*, Vol. 13, pp. 133–147.

Issa, R. I., 1985, "Solution of the Implicity Discretized Fluid Flow Equations by Operator-Splitting," *Journal of Computational Physics*, Vol. 62, pp. 40–65.

Jaluria, Y., 1984, "Numerical Study of the Thermal Processes in a Furnace," *Numerical Heat Transfer*, Vol. 7, pp. 211–224.

Jaluria, Y., and Torrance, K. E., 1986, *Computational Heat Transfer*, Hemisphere, New York.

Karniadakis, G. E., 1988, "Numerical Simulation of Forced Convection Heat Transfer From a Cylinder in Crossflow," *International Journal of Heat and Mass Transfer*, Vol. 31, pp. 107–118.

Khesghi, H. S., and Scriven, L. E., 1985, "Variable Penalty Method for Finite Element Analysis of Incompressible Flow," *International Journal for Numerical Methods in Fluids*, Vol. 5, pp. 785–803.

Khosla, P. K., and Rubin, S. G., 1981, "A Conjugate Gradient Iterative Method," *Computers and Fluids*, Vol. 9, pp. 109–121.

Kikuchi, N., 1986, "Adaptive Grid-Design Methods for Finite-Element Analysis," *Computer Methods in Applied Mechanics and Engineering*, Vol. 55, pp. 129–160.

Ku, H. C., Hirsch, R. S., and Taylor, T. D., 1987, "A Pseudospectral Method for Solution of the Theee-Dimensional Incompressible Navier–Stokes Equations," *Journal of Computational Physics*, Vol. 70, pp. 439–462.

Lacroix, M., Camarero, R., and Tapucu, A., 1984, "Multigrid Scheme for Thermohydraulic Flow," *Numerical Heat Transfer*, Vol. 7, pp. 375–393.

Latimer, B. R., and Pollard, A., 1985, "Comparison of Pressure-Velocity Coupling Solution Algorithms," *Numerical Heat Transfer*, Vol. 8, pp. 635–652.

Lavine, A. S., Greif, R., and Humphrey, J. A. C., 1987, "A Three-Dimensional Analysis of Natural Convection in a Toroidal Loop—the Effect of Grashof Number," *International Journal of Heat and Mass Transfer*, Vol. 30, pp. 251–262.

Lee, T. S., 1984, "Numerical Experiments With Laminar Fluid Convection Between Concentric and Eccentric Heated Rotating Cylinders," *Numerical Heat Transfer*, Vol. 7, pp. 77–87.

Leonard, B. P., 1979, "A Stable and Accurate Convective Modelling Procedure Based on Quadratic Upstream Interpolation," *Computer Methods in Applied Mechanics and Engineering*, Vol. 19, pp. 59–98.

Lillington, J. N., 1981, "A Vector Upstream Differencing Scheme for Problems in Fluid Flow Involving Significant Source Terms in Steady-State Linear Systems," *International Journal for Numerical Methods in Fluids*, Vol. 1, pp. 3–6.

Lin, A., 1985, "The Parameterized Strongly Implicit Method for Solving Elliptic Difference Equations," *International Journal for Numerical Methods in Fluids*, Vol. 5, pp. 381–391.

Luchini, P., 1987, "An Adpative-Mesh Finite-Difference Solution Method for the Navier–Stokes Equations," *Journal of Computational Physics*, Vol. 8, pp. 283–306.

Majumdar, S., 1988, "Role of Underrelaxation in Momentum Interpolation for Calculation of Flow With Nonstaggered Grids," *Numerical Heat Transfer*, Vol. 13, pp. 125–132.

Markatos, N. C., and Kirkcaldy, D., 1983, "Analysis and Computation of Three-Dimensional Transient Flow and Combustion Through Granulated Propellants," *International Journal of Heat and Mass Transfer*, Vol. 26, pp. 1037–1053.

McDonough, J. M., and Catton, I., 1982, "A Mixed Finite Difference-Galerkin Procedure for Two-Dimensional Convection in a Square Box," *International Journal of Heat and Mass Transfer*, Vol. 25, pp. 1137–1146.

Miller, H. P., 1986, "A Comparison of High Resolution Schemes for the Two-Dimensional Linear Advection Equation," *Computers and Fluids*, Vol. 14, pp. 411–422.

Miller, T. F., and Schmidt, F. W., 1988, "Evaluation of a Multilevel Technique Applied to the Poisson and Navier–Stokes Equations," *Numerical Heat Transfer*, Vol. 13, pp. 1–26.

Minkowycz, W. J., Sparrow, E. M., Schneider, G. E., and Pletcher, R. H., 1988, *Handbook of Numerical Heat Transfer*, Wiley, New York.

Montigny-Rannous, F., and Morchoisne, Y., 1987, "A Spectral Method With Staggered Grid for Incompressible Navier–Stokes Equations," *International Journal for Numerical Methods in Fluids*, Vol. 7, pp. 175–189.

Mostaghimi, J., Proulx, P., and Boulos, M. I., 1985, "An Analysis of the Computer Modeling of the Flow and Temperature Fields in an Inductively Coupled Plasma," *Numerical Heat Transfer*, Vol. 8, pp. 187–201.

Muir, B. L., and Baliga, B. R., 1986, "Solution of Three-Dimensional Convection-Diffusion Problems Using Tetrahedral Elements and Flow-Oriented Upwind Interpolation Functions," *Numerical Heat Transfer*, Vol. 9, pp. 143–162.

Murphy, J. D., and Prenter, P. M., 1985, "Higher Order Methods for Convection-Diffusion Problems," *Computers and Fluids*, Vol. 13, pp. 157–176.

Napolitano, M., and Orlandi, P., 1985, "Laminar Flow in a Complex Geometry: a Comparison," *International Journal for Numerical Methods in Fluids*, Vol. 5, pp. 667–683.

Nelsen, J. M., and Douglass, R. W., 1983, "On Partial Spectral Expansions With Natural Convection in Spherical Enclosures as an Example," *Numerical Heat Transfer*, Vol. 6, pp. 67–84.

Neta, B., and Williams, R. T., 1986, "Stability and Phase Speed for Various Finite Element Formulations of the Advection Equation," *Computers and Fluids*, Vol. 14, pp. 393–410.

Ormiston, S. J., Raithby, G. D., and Hollands, K. G. T., 1986, "Numerical Predictions of Natural Convection in a Trombe Wall System," *International Journal of Heat and Mass Transfer*, Vol. 29, pp. 869–877.

Ozoe, H., Fujii, K., Shibata, T., Kuriyama, H., and Churchill, S. W., 1985, "Three-Dimensional Numerical Analysis of Natural Convection in a Spherical Annulus," *Numerical Heat Transfer*, Vol. 8, pp. 383–406.

Patankar, S. V., and Spalding, D. B., 1972, "A Calculation Procedure for Heat, Mass and Momentum Transfer in Three-Dimensional Parabolic Flows," *International Journal of Heat and Mass Transfer*, Vol. 15, pp. 1787–1806.

Downloaded 16 Dec 2010 to 193.140.21.150. Redistribution subject to ASME license or copyright; see http://www.asme.org/terms/Terms_Use.cfm

Patankar, S. V., 1980, *Numerical Heat Transfer and Fluid Flow*, Hemisphere, New York.

Patankar, S. V., 1981, "A Calculation Procedure for Two-Dimensional Elliptic Situations," *Numerical Heat Transfer*, Vol. 4, pp. 409–425.

Patel, M., Cross, M., Markatos, N. C., and Mace, A. C. H., 1987, "An Evaluation of Eleven Discretization Schemes for Predicting Elliptic Flow and Heat Transfer in Supersonic Jets," *International Journal of Heat and Mass Transfer*, Vol. 30, pp. 1907–1925.

Patel, M. K., and Markatos, N. C., 1986, "An Evaluation of Eight Discretization Schemes for Two-Dimensional Convection-Diffusion Equations," *International Journal for Numerical Methods in Fluids*, Vol. 6, pp. 129–154.

Patel, M. K., Markatos, N. C., and Cross, M., 1985, "A Critical Evaluation of Seven Discretization Schemes for Convection-Diffusion Equations," *International Journal for Numerical Methods in Fluids*, Vol. 5, pp. 225–244.

Patel, N. R., and Briggs, D. G., 1983, "A MAC Scheme in Boundary-Fitted Curvilinear Coordinates," *Numerical Heat Transfer*, Vol. 6, pp. 383–394.

Pepper, D. W., 1987, "Modeling of Three-Dimensional Natural Convection With a Time-Split Finite-Element Technique," *Numerical Heat Transfer*, Vol. 11, pp. 31–55.

Peric, M., 1987, "Efficient Semi-implicit Solving Algorithm for Nine-Diagonal Coefficient Matrix," *Numerical Heat Transfer*, Vol. 11, pp. 251–279.

Phillips, R. E., and Schmidt, F. W., 1984, "Multigrid Techniques for the Numerical Solution of the Diffusion Equation," *Numerical Heat Transfer*, Vol. 7, pp. 251–268.

Phillips, R. E., and Schmidt, F. W., 1985a, "Multigrid Techniques for the Solution of the Passive Scalar Advection-Diffusion Equation," *Numerical Heat Transfer*, Vol. 8, pp. 25–43.

Phillips, R. E., and Schmidt, F. W., 1985b, "A Multilevel-Multigrid Technique for Recirculating Flows," *Numerical Heat Transfer*, Vol. 8, pp. 573–594.

Pollard, A., and Siu, A. L.-W., 1982, "The Calculation of Some Laminar Flows Using Various Discretization Schemes," *Computer Methods in Applied Mechanics and Engineering*, Vol. 35, pp. 293–313.

Prakash, C., 1986, "An Improved Control Volume Finite-Element Method for Heat and Mass Transfer, and for Fluid Flow Using Equal-Order Velocity-Pressure Interpolation," *Numerical Heat Transfer*, Vol. 9, pp. 253–276.

Prakash, C., and Patankar, S. V., 1985, "A Control-Volume Based Finite-Element Method for Solving the Navier–Stokes Equations Using Equal-Order Velocity-Pressure Interpolation," *Numerical Heat Transfer*, Vol. 8, pp. 259–280.

Prakash, C., and Patankar, S. V., 1987, "A Control-Volume Finite-Element Method for Predicting Flow and Heat Transfer in Ducts of Aribtrary Cross Sections—Part I: Description of the Method," *Numerical Heat Transfer*, Vol. 12, pp. 389–412.

Raithby, G. D., 1976, "Skew Upstream Differencing Schemes for Problems Involving Fluid Flow," *Computer Methods in Applied Mechanics and Engineering*, Vol. 9, pp. 153–164.

Raithby, G. D., Galpin, P. F., and Van Doormaal, J. P., 1986, "Prediction of Heat and Fluid Flow in Complex Geometries Using General Orthogonal Coordinates," *Numerical Heat Transfer*, Vol. 9, pp. 125–142.

Ramadhyani, S., and Patankar, S. V., 1985, "Solution of the Convection-Diffusion Equation by a Finite-Element Method Using Quadrilateral Elements," *Numerical Heat Transfer*, Vol. 8, pp. 595–612.

Reddy, J. N., 1982a, "On Penalty Function Methods in the Finite Element Analysis of Flow Problems," *International Journal for Numerical Methods in Fluids*, Vol. 2, pp. 151–171.

Reddy, J. N., 1982b, "Penalty-Finite-Element Analysis of 3-D Navier–Stokes Equations," *Computer Methods in Applied Mechanics and Engineering*, Vol. 35, pp. 87–106.

Reggio, M., and Camarero, R., 1986, "Numerical Solution Procedure for Viscous Incompressible Flows," *Numerical Heat Transfer*, Vol. 10, pp. 131–146.

Rhie, C. M., and Chow, W. L., 1983, "A Numerical Study of the Turbulent Flow Past an Isolated Airfoil With Trailing Edge Separation," *AIAA Journal*, Vol. 21, pp. 1525–1532.

Rice, J. G., and Schnipke, R. J., 1985, "A Monotone Streamline Upwind Finite Element Method for Convection-Dominated Flows," *Computer Methods in Applied Mechanics and Engineering*, Vol. 48, pp. 313–327.

Rice, J. G., and Schnipke, R. J., 1986, "An Equal-Order Velocity-Pressure Formulation That Does Not Exhibit Spurious Pressure Modes," *Computer Methods in Applied Mechanics and Engineering*, Vol. 58, pp. 135–149.

Rieger, H., Projahn, U., and Beer, H., 1983, "Fast Iterative Solution of Poisson Equation With Neumann Boundary Conditions in Nonorthogonal Curvilinear Coordinate Systems by a Multiple Grid Method," *Numerical Heat Transfer*, Vol. 6, pp. 1–15.

Rowley, G. J., and Patankar, S. V., 1984, "Analysis of Laminar Flow and Heat Transfer in Tubes With Internal Circumferential Fins," *International Journal of Heat and Mass Transfer*, Vol. 27, pp. 553–560.

Rubin, S. G., and Khosla, P. K., 1981, "Navier–Stokes Calculations With a Coupled Strongly Implicit Method—I: Finite-Difference Solutions," *Computers and Fluids*, Vol. 9, pp. 163–180.

Schneider, G. E., and Raw, M. J., 1987, "Control Volume Finite-Element Method for Heat Transfer and Fluid Flow Using Colocated Variables—1. Computational Procedure," *Numerical Heat Transfer*, Vol. 11. pp. 363–390.

Schneider, G. E., and Zedan, M., 1981, "A Modified Strongly Implicit Procedure for the Numerical Solution of Field Problems," *Numerical Heat Transfer*, Vol. 4, pp. 1–19.

Schnipke, R. J., and Ricke, J. G., 1987, "A Finite Element Method for Free and Forced Convection Heat Transfer," *International Journal for Numerical Methods in Engineering*, Vol. 24, pp. 117–128.

Segal, A., 1985, "A Review of Some Finite Element Methods to Solve the Stationary Navier–Stokes Equations," *International Journal for Numerical Methods in Fluids*, Vol. 5, pp. 269–280.

Shih, T. M., and Ren, A. L., 1984, "Primitive-Variable Formulations Using Nonstaggered Grids," *Numerical Heat Transfer*, Vol. 7, pp. 413–428.

Shih, T. M., 1982, "A Literature Survey of Numerical Heat Transfer," *Numerical Heat Transfer*, Vol. 5, pp. 369–420.

Shih, T. M., 1984, *Numerical Heat Transfer*, Hemisphere, New York.

Shih, T. M., 1985, "A Literature Survey on Numerical Heat Transfer," *Numerical Heat Transfer*, Vol. 8, pp. 1–24.

Shih, T. M., 1987, "A Literature Survey on Numerical Heat Transfer," *Numerical Heat Transfer*, Vol. 11, pp. 1–29.

Shyy, W., 1985, "A Study of Finite Difference Approximations to Steady-State, Convection-Dominated Flow Problems," *Journal of Computational Physics*, Vol. 57, pp. 415–438.

Shyy, W., Tong, S. S., and Correa, S. M., 1985, "Numerical Recirculating Flow Calculation Using a Body-Fitted Coordinate System," *Numerical Heat Transfer*, Vol. 8, pp. 99–113.

Singhal, A. K., 1985, "A Critical Look at the Progress in Numerical Heat Transfer and Some Suggestions for Improvement," *Numerical Heat Transfer*, Vol. 8, pp. 505–517.

Smith, R. M., and Hutton, A. G., 1982, "The Numerical Treatment of Advection: a Performance Comparison of Current Methods," *Numerical Heat Transfer*, Vol. 5, pp. 439–641.

Spalding, D. B., 1972, "A Novel Finite-Difference Formulation for Differential Expressions Involving Both First and Second Derivatives," *International Journal for Numerical Methods in Engineering*, Vol. 4, pp. 557–559.

Spalding, D. B., 1980, "Mathematical Modelling of Fluid Mechanics, Heat Transfer and Mass Transfer Processes," Imperial College, London, Mechanical Engineering Department, Report No. HTS/80/1.

Srinivasan, J., and Basu, B., 1986, "A Numerical Study of Thermocapillary Flow in a Rectangular Cavity During Laser Melting," *International Journal of Heat and Mass Transfer*, Vol. 29, pp. 563–572.

Stone, H. L., 1968, "Iterative Solution of Implicit Approximation of Multidimensional Partial Differential Equations," *SIAM Journal of Numerical Analysis*, Vol. 5, pp. 530–558.

Stubley, G. D., Raithby, G. D., and Strong, A. B., 1980, "Proposal for a New Discrete Method Based on an Assessment of Discretization Errors," *Numerical Heat Transfer*, Vol. 3, pp. 411–428.

Van Doormaal, J. P., and Raithby, G. D., 1984, "Enhancements of the SIMPLE Method for Predicting Incompressible Fluid Flows," *Numerical Heat Transfer*, Vol. 67, pp. 147–163.

Vanka, S. P., and Leaf, G. K., 1983, "Fully Coupled Solution of Pressure-Linked Fluid Flow Equations," *Argonne National Laboratory Report*, ANL-83-73.

Vanka, S. P., 1985,"Block-Implicit Calculation of Steady Turbulent Recirculating Flows," *International Journal of Heat and Mass Transfer*, Vol. 28, pp. 2093–2103.

Vanka, S. P., 1986a, "Block-Implicit Multigrid Solution of Navier–Stokes Equations in Primitive Variables," *Journal of Computational Physics*, Vol. 65, pp. 138–158.

Vanka, S. P., 1986b, "Block-Implicit Multigrid Calculation of Two-Dimensional Recirculating Flows," *Computer Methods in Applied Mechanics and Engineering*, Vol. 59, pp. 29–48.

Vanka, S. P., 1986c, "A Calculation Procedure for Three-Dimensional Steady Recirculating Flows Using Multigrid Methods," *Computer Methods in Applied Mechanics and Engineering*, Vol. 55, pp. 321–338.

Vanka, S. P., 1986d, "Performance of a Multigrid Calculation Procedure in Three-Dimensional Sudden Expansion Flows," *International Journal for Numerical Methods in Fluids*, Vol. 6, pp. 459–477.

Vanka, S. P., Chen, B. C.-J., and Sha, W. T., 1980, "A Semi-implicit Calculation Procedure for Flows Described in Boundary-Fitted Coordinate Systems," *Numerical Heat Transfer*, Vol. 3, pp. 1–19.

Viskanta, R., Kim, D. M., and Gau, C., 1986, "Three-Dimensional Natural Convection Heat Transfer of a Liquid Metal in a Cavity," *International Journal of Heat and Mass Transfer*, Vol. 29, pp. 475–485.

Wilhelmi, H., Wimmer, W., and Pfender, E., 1985, "Modeling of the Transport Phenomena in the Anode Region of High Current Arcs," *Numerical Heat Transfer*, Vol. 8, pp. 731–749.

Yang, H., and Camarero, R., 1986, "An Improved Vorticity-Potential Method for Three-Dimensional Duct Flow Situations," *International Journal for Numerical Methods in Fluids*, Vol. 6, pp. 35–45.

Zedan, M., and Schneider, G. E., 1982, "A Physical Approach to the Finite-Difference Solution of the Conduction Equation in Generalized Coordinates," *Numerical Heat Transfer*, Vol. 5, pp. 1–19.

Zedan, M., and Schneider, G. E., 1985, "A Coupled Strongly Implicit Procedure for Velocity and Pressure Computation in Fluid Flow Problems," *Numerical Heat Transfer*, Vol. 8, pp. 537–557.

Downloaded 16 Dec 2010 to 193.140.21.150. Redistribution subject to ASME license or copyright; see http://www.asme.org/terms/Terms_Use.cfm

Combined Parameter and Function Estimation in Heat Transfer With Application to Contact Conductance

J. V. Beck
Heat Transfer Group,
Department of Mechanical Engineering,
Michigan State University,
East Lansing, MI 48824

This paper discusses parameter estimation, function estimation, and a combination of the two. An example of parameter estimation is the determination of thermal conductivity of solids from transient temperature measurements. An example of function estimation is the inverse heat conduction problem, which uses transient temperature measurements to determine the surface heat flux history. The examples used herein involve the determination of the thermal contact conductance. Two sets of very good data are analyzed. One set of steady-state data was obtained by Antonetti and Eid (1987). The other set was obtained by Moses and Johnson (1986) under transient conditions for periodic contact. Both sets of data are used to illustrate parameter, function, and combined estimation. It is demonstrated that the proposed methods are more powerful then commonly accepted methods. Many other heat transfer problems can be treated using the proposed techniques.

1 Introduction

Many inverse problems occur in engineering in general, and heat transfer in particular. Two general classes of inverse problem are parameter and function estimation. This paper discusses problems that have aspects of both types of estimation. The subject has many applications, but the main examples in this paper relate to the thermal contact conductance.

In this introduction, parameter and function estimation are briefly discussed and then several examples of combined estimation are given. This is followed by a literature review. The introduction ends with an outline of the scope of the remainder of the paper.

An example of parameter estimation (PE) in heat transfer is the determination of the contact conductance from steady-state temperature and heat flux measurements. Another is the estimation of the thermal diffusivity of a solid from transient temperature measurements in the solid. Engineers frequently use the expression "back out" in connection with such problems but the technical term is "parameter estimation." The word "estimation" is employed because there are measurements (which implies errors); consequently, the parameters are only found approximately.

An example of a function estimation problem is the inverse heat conduction problem (IHCP). In this problem the surface heat flux (or surface temperature) history is calculated for a solid from measured temperature histories at one or more internal locations. Other related problems are the determination of time-dependent heat transfer coefficients, contact conductances, and volume energy generations.

In many cases the distinction between parameter and function estimation is blurred. An example is the determination from transient measurements of a property such as thermal conductivity k, as a function of temperature T. The function for k can be approximated by a set of constants called parameters. One set of parameters is that associated with a straight line or parabola in T

$$k=\beta_1+\beta_2 T \tag{1a}$$

$$k=\beta_1+\beta_2 T+\beta_3 T^2 \tag{1b}$$

where β_1, β_2, β_3 are the parameters of interest. For either model shown in equation (1), the problem can be considered to be one of parameter estimation. A similar problem exists if k is approximated by linear segments of the form

$$k=k_i+\frac{k_{i+1}-k_i}{T_{i+1}-T_i}(T-T_i) \tag{2}$$

for the temperature interval $T_i<T<T_{i+1}$. For one or two linear segments, the estimation of the k_1, k_2, . . . values (here the parameters) is a parameter estimation problem. For ten or more linear segments, the problem becomes one of function estimation. The line of demarcation between parameter and function estimation is not clear in this and other applications. In general, the determination of a curve approximated by only a small number of constants is a parameter estimation problem but when a "large" number of constants is required to define the curve, the problem becomes one of function estimation. More differences are also cited in Section 2.

In addition to the blurring between parameter and function estimation, the distinction may be further confounded when both can exist in the same problem. The possibilities are very large. An example is the treatment of measured boundary conditions in PE as being errorless, such as the estimation of the thermal diffusivity of a solid from several internal temperature histories at locations $x_1, x_2, x_3, \ldots, x_m$, where

$$x_1<x_2<x_3<\ldots<x_m$$

and m is at least 3. The measured temperature histories at x_1 and x_m are used as boundary conditions. The thermal diffusivity is found by minimizing the sum of squares function

$$S=\sum_{j=2}^{m-1}\sum_{i=1}^{n}(Y_{ji}-T_{ji})^2 \tag{3}$$

with respect to the thermal diffusivity. The index i refers to time ($i=1, 2, \ldots, n$) and the index j to the location of the temperature sensor; Y_{ji} denotes the measured temperature at x_j and t_i, and T_{ji} is the corresponding calculated temperature. Notice that the boundary temperatures at x_1 and x_m are treated in a different way than those at $x_2, \ldots, x_{m-1}$. The calculated temperatures inside the body (at x_2 to x_{m-1}) are made to agree in the least-squares sense with the corre-

Contributed by the Heat Transfer Division for publication in the JOURNAL OF HEAT TRANSFER. Manuscript received by the Heat Transfer Division February 4, 1988. Keywords: Conduction, Numerical Methods, Transient and Unsteady Heat Transfer.

Copyright © 1988 by ASME
Downloaded 16 Dec 2010 to 193.140.21.150. Redistribution subject to ASME license or copyright; see http://www.asme.org/terms/Terms_Use.cfm

sponding measured temperatures. In contrast, the calculated boundary temperatures at x_1 and x_m are made equal to the measured temperatures

$$T_{1i} = Y_{1i}, \quad T_{mi} = Y_{mi} \tag{4}$$

Currently this is the standard method for solving this type of problem.

Except for computational simplicity, there is no justification for treating the boundary temperatures as errorless while the internal locations are assumed to be in error. Usually all measured temperatures in the same experiment have the same error characteristics. If all the measured temperature histories are treated in the same manner, then the temperature histories at x_1 and x_m must also be estimated. In other words, the quantities of interest become the thermal diffusivity and *two functions*, one at x_1 and the other at x_m. For equal treatment of all the measured temperatures, the function to be minimized is

$$S = \sum_{j=1}^{m} \sum_{i=1}^{n} (Y_{ji} - T_{ji})^2 \tag{5}$$

Notice that j goes from 1 to m, including the boundary locations. The S function is now minimized with respect to the thermal diffusivity α, and the temperature boundary functions

$$T_{1i}, \quad i = 1, 2, \ldots, n$$

$$T_{mi}, \quad i = 1, 2, \ldots, n \tag{6}$$

Thus this is a combined parameter estimation and function estimation problem.

Another type of combined estimation problem is for the simultaneous estimation of one or more parameters while estimating a function arising from inside the domain. An example is fluid flow in which there is viscous dissipation (Kays and Crawford, 1980). Suppose that the flow is laminar and that the describing equation is

$$\rho c_p \left(u \frac{\partial T}{\partial x} + v \frac{\partial T}{\partial y} \right) = \frac{\partial}{\partial y} \left(k \frac{\partial T}{\partial y} \right) + \Phi \tag{7}$$

where Φ is the dissipation function. If the velocity distributions $u(x, y)$ and $v(x, y)$ and the temperature distribution $T(x, y)$ are measured at many discrete positions (x_i, y_j), and ρc_p is known, then k and Φ can be estimated. If the thermal conductivity k is a constant, then it is a parameter to be estimated and the function of x and y to be found is ϕ. In most cases a relation between Φ and u may be known (such as $\Phi = \mu(\partial u/\partial y)^2$ where μ = viscosity). In other cases the fluid may not be Newtonian or there may be chemical reactions.

An example closely related to the one given by equation (7) is that of turbulent flow over a flat plate. The time-averaged thermal boundary-layer equation is

$$\bar{u} \frac{\partial \bar{T}}{\partial x} + \bar{v} \frac{\partial \bar{T}}{\partial y} = \frac{\partial}{\partial y} \left(\alpha \frac{\partial \bar{T}}{\partial y} - \overline{T'v'} \right) \tag{8}$$

The local time-averaged velocities $\bar{u}$ and $\bar{v}$ and the average temperature $\bar{T}$ are measured at many locations x_i, y_j. A combined parameter and function estimation problem is to estimate the parameter α and the function $\overline{T'v'}$.

A great many papers have been written on both parameter estimation and the inverse heat conduction problem. Both subjects use the method of least squares, which is thoroughly discussed by Lawson and Hansen (1974). The term "parameter estimation" used by Beck and Arnold (1977) was also called nonlinear least squares (Bevington, 1969), nonlinear estimation (Draper and Smith, 1968), nonlinear parameter estimation (Bard, 1974), response surface methodology (Myers, 1971), systems identification (Sage and Melsa, 1971; Goodwin and Payne, 1977), and nonlinear regression (Biles and Swain, 1980). Of the above books only one by Beck and Arnold specifically emphasizes heat transfer problems.

There are many papers on the inverse heat conduction problem and one book in English (Beck et al., 1985). The latter provides a comprehensive review through 1984. More recent papers are those of Scott and Beck (1985), Raynaud and Beck (1988), Osman and Beck (1987), and Hensel and Hills (1984). Inverse heat conduction is one of a class of ill-posed problems, on which there are some books (Tikhonov and Arsenin, 1977; Morozov, 1984). The determinations of functions of time or position are usually ill-posed, a result of extreme sensitivity to measurement errors. Another heat transfer example of an ill-posed problem is the estimation of the absorption coefficient distribution in flames (Chakravarty et al., 1988). The large and advanced literature on identification, systems, and controls contains methods that can be used both for parameter and function estimation. Two examples are Sage (1968) and Bryson and Ho (1969). The emphasis, notation, and required background in this identification literature make assimilation by the heat transfer community difficult.

Combined parameter estimation and function estimation problems should be based on as common a framework as possible. Techniques to be avoided are those (1) which are intrinsically linear, (2) which take advantage of certain numerical characteristics of finite differences, finite elements, or boundary elements, (3) which cannot have a statistical basis, (4) which are inherently parameter or function estimation procedures, and (5) which cannot readily be generalized from one to two or three dimensions. Methods with these restrictions are, for example, the inherently linear methods based upon the use of the Laplace transform or the convolution integral (Duhmel's integral or Green's functions), or the

Nomenclature

A_i = summation defined by equation (21) or (22)
B_i = summation defined by equation (23)
c_p = specific heat
e_i = residual $= Y_i - \hat{T}_i$
h = heat transfer coefficient
h_c = thermal contact conductance
H = reciprocal h_c
k = thermal conductivity
k_e = measured thermal conductivity
K = reciprocal k
L_1 = partial length of specimen 1
L_2 = partial length of specimen 2
n = number of temperature measurements
p = pressure
q = heat flux
q_e = measured heat flux
s_{h_c} = estimated standard deviation of $\hat{h}_c$
S = sum of squares function
t = time
T = temperature
x = coordinate
Y = measured quantity
z = coordinate
α = thermal diffusivity
α_0 = zeroth order regularization parameter
β_i = parameter
η = dependent variable
θ = temperature at $z = L_2$
ρ = density
σ = standard deviation
$\hat{}$ = denotes estimated parameter value

Downloaded 16 Dec 2010 to 193.140.21.150. Redistribution subject to ASME license or copyright; see http://www.asme.org/terms/Terms_Use.cfm

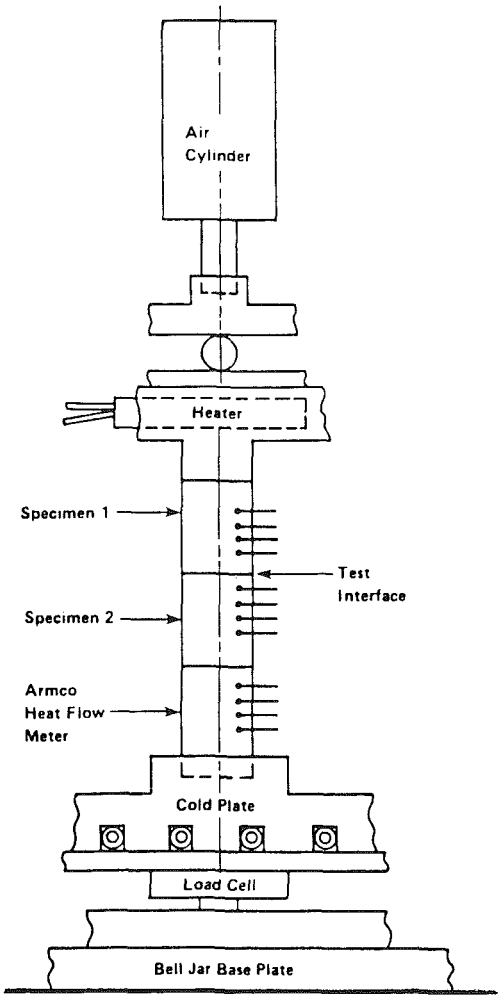

Fig. 1 Antonetti and Eid (1987) apparatus for measuring thermal contact conductance

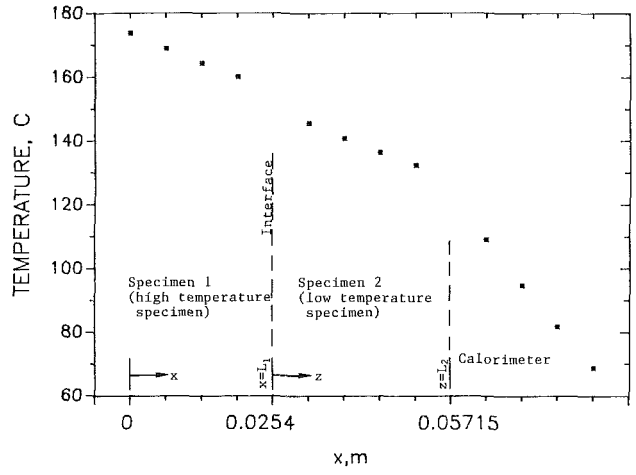

Fig. 2 Measured temperatures obtained by Antonetti and Eid (1987) for aluminum-aluminum contact with pressure of 2580 kN/m^2

one-dimensional space-marching methods for the IHCP, which do not readily extend to two and three dimensions and which are not relevant to parameter estimation problems.

The scope of this paper is restricted to the determination of thermal contact conductance for both steady-state and transient conditions. Also for conciseness, the parameter estimation and function estimation theories are not repeated. For a background in parameter estimation, see Beck and Arnold (1977), and in function estimation, see Beck et al., (1985). A more abridged treatment of each is given in Beck and Blackwell (1988). In Section 2 of this paper the steady-state case is considered and in Section 3 the transient case. The method of formulation is these cases can include both parameter and function estimation.

2 Steady-State Contact Conductance Estimation

A typical experiment for measuring the thermal contact conductance is described by Antonetti and Eid (1987) and is shown schematically in Fig. 1. The heat flow is approximately one-dimensional, orginates at the heater at the top, and exits through the calorimeter at the bottom. There are four thermocouples at equally spaced locations in each of the two specimens. The specimens can be made of the same or different materials. Held together at a prescribed pressure, the two specimens have a finite contact conductance at the interface between the two specimens. When a heat flow exists in the specimens, there is a temperature drop across the interface. Figure 2 shows the steady-state temperature profile obtained by Antonetti and Eid (1987).

The commonly accepted method of analysis is to pass a straight line using least squares through the temperature data of the specimen at higher temperatures and then extrapolate to find the interface temperature of that specimen. The same procedure is repeated for the specimen at lower temperatures, and then the temperature drop across the interface ΔT is calculated. Using a measured heat flux q, the contact conductance h_c is calculated from the simple equation

$$h_c = q/\Delta T \tag{9}$$

The advantages of using equation (9) in this manner include simplicity and acceptance of the method. There are several weaknesses, however. First, there is uncertainty in the q value. The heat flux can be estimated by using the measured power input, using the measured temperature in the calorimeter, and using the known thermal conductivity k and the temperature measurements in the specimens. Due to measurement errors and heat losses, each of these q values is (usually) different from the others. Second, another weakness of the method is that potential information regarding the thermal conductivity values of the specimens is disregarded. The apparatus shown schematically in Fig. 1 is also an apparatus for measuring k as well as h_c. As numerous measurements are made under different pressure, roughness, and other interface conditions (such as with fillers and oils), many measurements become available for estimation of the thermal conductivity of each specimen. A third weakness is that a straight line may not be appropriate due to T dependence of k or side heat losses. A fourth weakness is that continuity of heat flux is not required. Although there are heat losses off the sides of the specimens, the average heat flux leaving the high-temperature specimen must equal that entering the low-temperature specimen. Finally, the above method does not give meaningful residuals (temperature differences between the measured and calculated temperatures) that can be used to improve the mathematical model or to find confidence intervals. An improved model might include temperature dependence of the thermal conductivities of the specimens and the heat losses from the sides. The weighted least-squares method described in this section improves upon the direct use of equation (9) and eliminates each of these disadvantages.

For simplicity in presentation of the method, the thermal conductivity in each specimen is considered to be temperature independent and heat losses from the sides are not considered. Steady state is assumed to exist. For these assumptions the temperature distribution is given by

Downloaded 16 Dec 2010 to 193.140.21.150. Redistribution subject to ASME license or copyright; see http://www.asme.org/terms/Terms_Use.cfm

$$T=\theta+q\left[\frac{L_1-x}{k_1}+\frac{L_2}{k_2}+\frac{1}{h_c}\right], \quad 0<x<L_1 \tag{10a}$$

$$T=\theta+q\frac{L_2-z}{k_2}, \quad 0<z<L_2 \tag{10b}$$

where θ is the temperature at $z=L_2$. See Fig. 2. Since k_1, k_2, and h_c appear in the denominators in equations (10), it is convenient to define

$$K_1=\frac{1}{k_1}, \quad K_2=\frac{1}{k_2}, \quad H=\frac{1}{h_c} \tag{11}$$

Thus the temperature distributions given by equations (10) can also be written as

$$T=\theta+q[(L_1-x)K_1+L_2K_2+H], \quad 0<x<L_1 \tag{12a}$$

$$T=\theta+qK_2(L_2-z), \quad 0<z<L_2 \tag{12b}$$

In the estimation procedure using equations (10), the primary quantity of interest is h_c, but other parameters must be estimated also. These include k_1, k_2, θ, and q; k_1, k_2, and q are estimated because they are known only from measurements. When equations (12) are used as the model, the parameters are H, K_1, K_2, θ and q. The temperature at $z=L_2$, θ, is estimated because it is also measured and is a boundary condition; the interface temperatures are *not* boundary conditions and thus need not be parameters in the minimization procedure. In this formulation, the problem is basically treated as one of parameter estimation, although the inclusion of estimating a boundary condition (θ) is part of function estimation.

The procedure to estimate the parameters is to minimize the modified sum of squares function

$$S=+\sum_{i=1}^{2}(k_{ei}-k_i)^2\frac{1}{\sigma_{k_i}^2}+(q_e-q)^2\frac{1}{\sigma_q^2}+\sum_{i=1}^{n}(Y_i-T_i)^2\frac{1}{\sigma_i^2} \tag{13}$$

with respect to h_c, k_1, k_2, θ, and q. (When equations (12) are used for the model, lower case k is replaced by K in the first summation and S is minimized with respect to H, K_1, K_2, θ, and q). In minimizing with respect to these parameters it is assumed that each is independent of the others. In the summation over i in the last term of equation (13), there are n_1 T's in the first region ($0<x<L_1$), and $n-n_1$ T's in the second region ($0<z<L_2$). The e subscript on k and q denotes measured values; Y_i is the measured temperature and T_i is the corresponding calculated temperature obtained from equations (10) or (12). The determination of the standard deviations for the conductivity (σ_k), heat flux (σ_q), and temperature (σ) are discussed in connection with the solution using the algebraic method.

Two ways of minimizing S, which is given by equation (13), are discussed. One is to set the first partial derivatives of S with respect to the parameters equal to zero. This is called the direct algebraic method. This gives five algebraic equations for $\hat{h}_c$, $\hat{k}_1$, $\hat{k}_2$, $\hat{\theta}$, and $\hat{q}$ or equivalently $\hat{H}$, $\hat{K}_1$, $\hat{K}_2$, $\hat{\theta}$, and $\hat{q}$, where the $\hat{}$ symbol denotes an estimated value. The set of five algebraic equations, which are nonlinear, is solved simultaneously for the unknowns. With H, K_1, and K_2 as parameters, the complexity is reduced in the algebraic solution compared to using the original variables (h_c, k_1, k_2). Another method of solution uses the nonlinear sequential estimate procedure that is embedded in the computer program NLINA (Beck and Arnold, 1977). Both methods are discussed next.

Solution Using Direct Algebraic Method. The solution using the direct algebraic method involves first partial derivatives of S. The first of these is

$$\left.\frac{\partial S}{\partial H}\right|_{H=\hat{H},\ldots}=\sum_{i=1}^{n_1}\{Y_i-\hat{T}_i\}\frac{1}{\sigma_i^2}(-2\hat{q})=0 \tag{14}$$

The other derivatives are

$$\left.\frac{\partial S}{\partial K_1}\right|_{H=\hat{H},\ldots}=(K_{e1}-K_1)\frac{1}{\sigma_{K1}^2}(-2)+\sum_{i=1}^{n_1}\{Y_i-\hat{T}_i\}\frac{1}{\sigma_i^2}(-2\hat{q}(L-x_i))=0 \tag{15}$$

$$\left.\frac{\partial S}{\partial K_2}\right|_{H=\hat{H},\ldots}=(K_{e2}-K_2)\frac{1}{\sigma_{K2}^2}(-2)+\sum_{i=1}^{n}\{Y_i-\hat{T}_i\}\frac{1}{\sigma_i^2}\left(-2\frac{\partial\hat{T}_i}{\partial K_2}\right)=0 \tag{16}$$

$$\left.\frac{\partial S}{\partial\theta}\right|_{H=\hat{H},\ldots}=\sum_{i=1}^{n}\{Y_i-\hat{T}_i\}\frac{1}{\sigma_i^2}(-2)=0 \tag{17}$$

$$\left.\frac{\partial S}{\partial q}\right|_{H=\hat{H},\ldots}=(q_e-\hat{q})\frac{1}{\sigma_q^2}(-2)+\sum_{i=1}^{n}\{Y_i-\hat{T}_i\}\frac{-2}{\sigma_i^2}\frac{\partial\hat{T}_i}{\partial q}=0 \tag{18}$$

where

$$\hat{T}_i=\hat{\theta}+\hat{q}[\hat{K}_1(L-x_i)+\hat{K}_2L_2+\hat{H}], \quad 0<x_i<L_1 \tag{19a}$$

$$=\hat{\theta}+\hat{q}\hat{K}_2(L_2-z_i), \quad 0<z_i<L_2 \tag{19b}$$

$$\frac{\partial\hat{T}_i}{\partial K_2}=\begin{cases}\hat{q}L_2, & 0<x_i<L_1\\ \hat{q}(L_2-z_i), & 0<z_i<L_2\end{cases} \tag{20a}$$

$$\frac{\partial\hat{T}_i}{\partial q}=\begin{cases}\hat{K}_1(L-x_i)+L_2\hat{K}_2+\hat{H}\\ \hat{K}_2(L_2-z_i)\end{cases} \tag{20b}$$

The first derivative of the dependent variable with respect to a parameter is called a sensitivity coefficient; see for example equations (20). Equations (14)–(18) provide a set of five nonlinear algebraic equations for the five unknown: $\hat{H}$, $\hat{K}_1$, $\hat{K}_2$, $\hat{\theta}$, and $\hat{q}$. After rearrangement, the solution for the parameters is obtained by first selecting a reasonable value for q and then calculating

$$A_1=\sum_{i=1}^{n_1}\frac{1}{\sigma_i^2} \tag{21a}$$

$$A_2=\sum_{i=1}^{n_1}\frac{x_i}{\sigma_i^2} \tag{21b}$$

$$A_{22}=L_1A_2-\sum_{i=1}^{n_1}\frac{x_i^2}{\sigma_i^2}-\frac{1}{\hat{q}^2\sigma_{K_1}^2} \tag{21c}$$

$$A_3=\sum_{i=n_1+1}^{n}\frac{z_i}{\sigma_i^2} \tag{22a}$$

$$A_4=\sum_{i=n_1+1}^{n}\frac{1}{\sigma_i^2} \tag{22b}$$

Downloaded 16 Dec 2010 to 193.140.21.150. Redistribution subject to ASME license or copyright; see http://www.asme.org/terms/Terms_Use.cfm

$$A_{33} = L_2 A_3 - \sum_{i=n_1+1}^{n} \frac{z_i^2}{\sigma_i^2} - \frac{1}{\hat{q}^2 \sigma_{K_2}^2} \tag{22c}$$

$$B_1 = \sum_{i=1}^{n_1} \frac{Y_i}{\sigma_i^2} \tag{23a}$$

$$B_2 = \sum_{i=1}^{n_1} \frac{Y_i x_i}{\sigma_i^2} - \frac{K_{e1}}{\hat{q}\sigma_{K_1}^2} \tag{23b}$$

$$B_3 = \sum_{i=n_1+1}^{n} \frac{Y_i z_i}{\sigma_i^2} - \frac{K_{e2}}{\hat{q}\sigma_{K_2}^2} \tag{23c}$$

$$B_4 = \sum_{i=n_1+1}^{n} \frac{Y_i}{\sigma_i^2} \tag{23d}$$

Notice that only some of the terms in these equations depend on $\hat{q}$. The next step is to calculate $\hat{q}\hat{K}_2$ and $\hat{\theta}$ using

$$\hat{q}\hat{K}_2 = \frac{B_3 A_4 - B_4 A_3}{A_{33} A_4 - (L_2 A_4 - A_3) A_3} \tag{24a}$$

$$\hat{\theta} = \frac{A_{33} B_4 - (L_2 A_4 - A_3) B_3}{A_{33} A_4 - (L_2 A_4 - A_3) A_3} \tag{24b}$$

Using $\hat{q}\hat{K}_2$ and $\hat{\theta}$, $\hat{q}\hat{H}$ and $\hat{q}\hat{K}_1$ are found

$$\hat{q}\hat{H} = \frac{(B_1 - L_2 A_1 \hat{q}\hat{K}_2 - A_1\hat{\theta}) A_{22} - (B_2 - L_2 A_2 \hat{q}\hat{K}_2 - A_2\hat{\theta})(L_1 A_1 - A_2)}{A_1 A_{22} + A_2^2 - L_1 A_1 A_2} \tag{25a}$$

$$\hat{q}\hat{K}_1 = \frac{A_1 (B_2 - L_2 A_2 \hat{q}\hat{K}_2 - A_2\hat{\theta}) - A_2 (B_1 - L_2 A_1 \hat{q}\hat{K}_2 - A_1\hat{\theta})}{A_1 A_{22} + A_2^2 - L_1 A_1 A_2} \tag{25b}$$

The remaining equation used to obtain $\hat{q}$ is

$$\hat{q}\hat{K}_1 (K_{e1} - \hat{q}\hat{K}_1/\hat{q}) \frac{1}{\sigma_{K_1}^2} + \hat{q}\hat{K}_2 (K_{e2} - \hat{q}\hat{K}_2/\hat{q}) \frac{1}{\sigma_{K_2}^2} (q_e - \hat{q}) \frac{\hat{q}^2}{\sigma_q^2} = 0 \tag{26}$$

Equation (26) has been arranged to contain $\hat{q}\hat{K}_1$ and $\hat{q}\,\hat{K}_2$, which are obtained as indicated above. Equation (26) is a nonlinear function of $\hat{q}$; for that reason it is linearized using

$$\hat{q}^{(\nu+1)} = q^{(\nu)} + \delta q^{(\nu+1)} \tag{27}$$

The required correction, $\delta q^{(\nu+1)}$, is

$$\delta q^{(\nu+1)} = \frac{-\hat{q}\hat{K}_1 \left(K_{e_1} - \frac{\hat{q}\hat{K}_1}{\hat{q}^{(\nu)}}\right) \frac{1}{\sigma_{K_1}^2} - \hat{q}\hat{K}_2 \left(K_{e_2} - \frac{\hat{q}\hat{K}_2}{\hat{q}^{(\nu)}}\right) \frac{1}{\sigma_{K_2}^2} + (q_e - \hat{q}^{(\nu)}) \frac{(q^{(\nu)})^2}{\sigma_q^2}}{\left(\frac{(\hat{q}\hat{K}_1)^{(\nu)}}{\hat{q}^{(\nu)}}\right)^2 \frac{1}{\sigma_{K_1}^2} + \left(\frac{(\hat{q}\hat{K}_2)^{(\nu)}}{\hat{q}^{(\nu)}}\right)^2 \frac{1}{\sigma_{K_2}^2} + \frac{(q^{(\nu)})^2}{\sigma_q^2} - \frac{2(q_e - \hat{q}^{(\nu)})\hat{q}^{(\nu)}}{\sigma_q^2}} \tag{28}$$

After an estimate of $\hat{q}^{(\nu+1)}$ is obtained from equations (27) and (28), another iteration is started if

$$\left| \frac{\partial q^{(\nu+1)}}{\hat{q}^{(\nu)}} \right| < \epsilon \tag{29}$$

where ϵ is a small number such as 0.0001.

Before the iteration procedure is started, A_1, A_2, A_3, A_4, B_1, and B_4 are evaluated using equations (21*a*), (21*b*), (22*a*), (22*b*), (23*a*), and (23*d*). First, an estimate of $\hat{q}^{(\nu)}$ is found; usually it is q_e for $\nu = 0$. Second, the A_{22}, A_{33}, B_2, and B_3 coefficients given by equations (21*c*), (22*c*), (23*b*), and (23*c*) are evaluated. Third, $(\hat{q}\hat{K}_2)^{(\nu+1)}$ and $\hat{\theta}^{(\nu+1)}$ are estimated using equations (24*a*) and (24*b*). Fourth, equations (25*a*) and (25*b*) are used to estimate $(\hat{q}\hat{H})^{(\nu+1)}$ and $(\hat{q}\hat{K}_1)^{(\nu+1)}$. Fifth, equations (28) and (27) are used to get $\hat{q}^{(\nu+1)}$. Then, if equation (29) is not satisfied, ν is increased by 1 and the calculations continue from step 1.

Solution Using Sequential Program NLINA. In using the sequential estimation program NLINA, it is necessary to have a single summation term for the sum of squares function S, but there can be several models for the dependent variable and the weights can be different for each measurement. The sum of squares functions given by equation (13) can be written as

$$S = \sum_{j=1} (Y_j - \eta_j)^2 \frac{1}{\sigma_j^2} \tag{30}$$

where Y_j represents a measured or approximately known quantity such as thermal conductivity, heat flux, or temperature. The symbol η_j, represents a calculated quantity corresponding to Y_j and σ_j is the standard deviation of Y_j. Notice that σ_j has the same units as Y_j but all the Y_j's do not necessarily have the same units (since k, q, and T are included). In the use of program NLINA it is not necessary to use the groups of $K_1 = k_1^{-1}$, qK_1, . . . , which were used in the direct method. Also in this analysis, two measurements of heat flux q are considered to be available; at $x = 0$ the heat flux is known from the electric power input and at $x = L_1 + L_2$ the heat flux is found from temperature measurements in the calorimeter.

The measured and calculated quantities are related to the index j by

$j = 1$, $Y_1 = k_{e_1}$, $\eta_1 = k_1$ $\quad j = 2$, $Y_2 = k_{e_2}$, $\eta_2 = k_2$

$j = 3$, $Y_3 = q_{e_1}$, $\eta_3 = q$ $\quad j = 4$, $Y_4 = q_{e_2}$, $\eta_4 = q$

$J = 5$ to $n_1 + 5$, $Y_j = T_{ej}$, $\eta_j = T_j$ (temperatures in $0 < x < L_1$)

$j = n_1 + 6$ to $n_1 + n_2 + 6$, $Y_j = T_{ej}$, $\eta_j = T_j$ (temperatures in $0 < z < L_2$)

For simplicity in notation, the parameters are denoted β_i, $i = 1, 2, \ldots, 5$, and are

$$\beta_1 = h_c, \quad \beta_2 = k_1, \quad \beta_3 = k_2, \quad \beta_4 = \theta, \quad \beta_5 = q$$

In the model for the temperature given by equations (10), it is assumed that there is a steady state and there are no heat losses. Both assumptions can be relaxed. In this example, however, these assumptions are used and as a consequence q_{e_1} and q_{e_2} are considered to be measurements of the same true heat flux value q.

In program NLINA there is a provision for entering the model and the associated sensitivity coefficients. For conciseness, these are displayed in Tables 1, 2, and 3.

Example. Both the direct algebraic and the sequential

Downloaded 16 Dec 2010 to 193.140.21.150. Redistribution subject to ASME license or copyright; see http://www.asme.org/terms/Terms_Use.cfm

Table 1 Model and sensitivity coefficients for $j=1$, 2, 3, and 4 for Antonetti and Eid (1987) example

j	η_j	σ_j	Y_j	$\frac{\partial\eta_j}{\partial\beta_1}$	$\frac{\partial\eta_j}{\partial\beta_2}$	$\frac{\partial\eta_j}{\partial\beta_3}$	$\frac{\partial\eta_j}{\partial\beta_4}$	$\frac{\partial\eta_j}{\partial\beta_5}$
1	k_1	σ_{k_1}	k_{e_1}	0	1	0	0	0
2	k_2	σ_{k_2}	k_{e_2}	0	0	1	0	0
3	q	σ_{q_1}	q_{e_1}	0	0	0	0	1
4	q	σ_{q_2}	q_{e_2}	0	0	0	0	1

Table 2 Model and sensitivity coefficients for temperatures in $0<x<L$ for Antonetti and Eid (1987) example

$(j=5 \text{ to } n_1+4)$

$$\eta_j = \left[\frac{1}{h_c}+\frac{L-x_j}{k_1}+\frac{L_2}{k_2}\right]q+\theta$$

$$= \left[\frac{1}{\beta_1}+\frac{L-x_j}{\beta_2}+\frac{L_2}{\beta_3}\right]\beta_5+\beta_4$$

$$\frac{\partial\eta_j}{\partial\beta_1}=-\frac{\beta_5}{\beta_1^2},\quad \frac{\partial\eta_j}{\partial\beta_2}=-\frac{L-x_j}{\beta_2^2}\beta_5,\quad \frac{\partial\eta_j}{\partial\beta_3}=-\frac{L_2}{\beta_3^2}\beta_5$$

$$\frac{\partial\eta_j}{\partial\beta_4}=1,\quad \frac{\partial\eta_j}{\partial\beta_5}=\frac{1}{\beta_1}+\frac{L-x_j}{\beta_2}+\frac{L_2}{\beta_3}$$

Table 3 Model and sensitivity coefficients for temperatures in $0<z<L_2 (j=n_1+5$ to $n_1+n_2+4)$ for Antonetti and Eid (1987) example

$$\eta_j = \left[\frac{L_2-z_j}{k_2}\right]q+\theta$$

$$= \left[\frac{L_2-z_j}{\beta_3}\right]\beta_5+\beta_4$$

$$\frac{\partial\eta_j}{\partial\beta_1}=0,\quad \frac{\partial\eta_j}{\partial\beta_2}=0,\quad \frac{\partial\eta_j}{\partial\beta_3}=-\frac{L_2-z_j}{\beta_3^2}\beta_5$$

$$\frac{\partial\eta_j}{\partial\beta_4}=1,\quad \frac{\partial\eta_j}{\partial\beta_5}=\frac{L_2-z_j}{\beta_3}$$

Table 4 Steady-state data for aluminum–aluminum contact (Antonetti and Eid, 1987)

Temperature sensor No.	Bar number	x_i, m	z_i, m	T, °C
1	1	0	-	173.8
2	1	0.00635	-	169.0
3	1	0.0127	-	164.3
4	1	0.01905	-	160.1
5	2	-	0.00635	145.5
6	2	-	0.0127	140.7
7	2	-	0.01905	136.3
8	2	-	0.0254	132.3

Heat flux at x-0: 155,930 W/m^2
Heat flux at calorimeter: 145,000 W/m^2
Aluminum thermal conductivity: 220 W/m-K
Reciprocal thermal conductivity = 0.004545 m-K/W

methods are demonstrated in the following. The data displayed in Table 4 were obtained by Antonetti and Eid (1987); their curves were for a transient case with bare aluminum–aluminum contact, but near the end of the test steady state was approached. Also in Table 4 are the measured heat fluxes at $x=0$ and $x=L_1+L_2$; the former is obtained from the 100 W input to the 0.02858 m (1 1/8 in.) diameter cylinders and the latter value is obtained from the temperature gradient in the calorimeter. The thermal conductivity of the aluminum specimens is about 220 W/m-K, the value used by Antonnetti and Eid.

Two more ways to determine the heat flux are to pass a line in a least-squares sense through the data for each aluminum bar and to use $q=-kdT/dx$; the results are $q=158{,}700$ and 152,440 W/m^2 for bars 1 and 2, respectively. As expected from experimental measurements, all four values are different and there is a tendency for the heat flux to decrease with temperature (155,930, 158,700, 152,440 and 145,000 W/m^2). This decreasing tendency is usually attributed to heat losses. One of the problems encountered in contact conductance research is the selection of the proper heat flux. Some researchers report results for different heat fluxes (Antonetti and Eid, 1987), others use an average (Moses and Johnson 1986) and others use the electrical power input (namely, 155,930 W/m^2 in this case).

(*i*) *Example Solution Using Algebraic Method.* Consider now the algebraic solution procedure. Only one heat flux component, namely that at $x=0$, is used. In order to perform the analysis for the parameters (H, K_1, K_2, θ, and q) it is necessary to estimate values of the standard deviations of the measured quantities. The following values are used first:

$$\sigma=0.2\text{ K},\quad \sigma_{K_1}=\sigma_{K_2}=0.0000454\text{ m-K/W},\quad \sigma_q=5000\text{ W/m}^2$$

for which σ_{K_1} is 1 percent of K_1 ($=1/220$). The $\sigma=0.2$ K value is the estimated standard deviation of the measured temperatures; it is a value that is characteristic of many heat transfer experiments and can be verified by examining the temperature residuals. Since the heat flux values vary between 145,000 and 158,700, a standard deviation of 5000 W/m^2 is reasonable; this value is approximated by the use of the four values mentioned in the previous paragraph.

From these σ values and the measurements given in Table 4 (with just the $x=0$ q component) the following estimates are obtained: $\hat{q}\hat{H}=5.629$ K, $\hat{q}\hat{K}_1=710.6$ K/m, $\hat{q}\hat{K}_2=704.9$ K/m, $\theta=132.1$°C, and $q=155{,}716$ W/m^2; which in turn lead to $\hat{h}_c=27{,}660$ W/m^2-K, $k_1=219.1$ W/m-K, and $k_2=220.9$ W/m-K.

If the σ value of 0.2°C and $\sigma_q=5000$ W/m^2 are fixed and σ_K is given the values corresponding to 0.1, 1, and 10.0 percent of K_1 and K_2, the $\hat{h}_c$ values are respectively 27,860, 27,660, and 27,600 W/m^2-K. Evidently the $\hat{h}_c$ value is insensitive to the σ_K values in this analysis. These $\hat{h}_c$ values are grouped quite closely and also close to the value given by equation (9), which is 27,600 W/m^2-K.

(*ii*) *Sample Solution Using Sequential Method.* The sequential method is a powerful solution procedure. Compared to the algebraic method, it gives more information, is much easier to program, and is more adaptable to modifications for other models for the temperature distribution.

The example is solved using the sequential nonlinear estimation program NLINA (Beck and Arnold, 1977). Two components of q are used, one at $x=0$ and the other at $z=L_2$. The

Downloaded 16 Dec 2010 to 193.140.21.150. Redistribution subject to ASME license or copyright; see http://www.asme.org/terms/Terms_Use.cfm

Table 5 Sequential estimation for parameters of Antonetti and Eid (1987) data using $\sigma_i = 0.2°C$, $\sigma_{k_1} = \sigma_{k_2} = 2.2$ W/m-K, and $\sigma_q = 5000$ W/m^2

I	Eta	Residuals	$\hat{h}_c$	$\hat{k}_1$	$\hat{k}_2$	$\hat{\theta}$	$\hat{q}$
1	218.7	1.347	26390	220.0	220.4	132.0	154000
2	220.4	−0.4274	26390	220.0	220.0	132.0	154000
3	153956	1974	26390	220.0	220.0	132.0	155900
4	153956	−8696	26390	220.0	220.0	132.0	150600
5	173.5	0.2933	26380	220.0	220.0	133.3	150600
6	169.0	−0.0355	26390	219.5	220.0	132.6	152400
7	164.6	−0.2644	26390	218.8	220.0	131.7	155100
8	160.1	0.0067	26390	218.9	220.0	131.9	154700
9	145.4	0.1473	27530	218.9	220.0	132.1	154700
10	140.9	−0.2176	27250	219.1	219.6	131.9	155400
11	136.5	−0.1824	27310	219.1	219.5	131.8	155600
12	132.0	0.2527	26390	218.7	220.4	132.0	154000

Table 6 Summary of results of $\hat{h}_c$ values for Antonetti and Eid (1987) data

	Analysis	$\hat{h}_c$ values, W/m^2-K	$\hat{h}_c$, conf. interval
1	Antonetti and Eid (1987)	24,000 to 26,500	
2	Simple Least Squares		
	(*a*) heater q	27,600	
	(*b*) calorimeter q	25,660	
3	Direct analysis, heating q	27,660	23,160 to 32,160
4	Sequential anal., heater and cal. q	26,390	21,380 to 31,400

program has the ability to treat algebraic models readily; it is only necessary to enter the models in one subroutine and the sensitivity coefficients in another subroutine. The models and sensitivity coefficients are given in Tables 1, 2, and 3. In this estimation procedure, the parameters are h_c, k_1, k_2, θ, and q, respectively.

The parameters were estimated using the measured T and q values in Table 4 with

$$\sigma_i = 0.2\,K, \quad \sigma_{k_1} = \sigma_{k_2} = 2.2 \text{ W/m-K}, \quad \sigma_q = 5{,}000 \text{ W/m}^2$$

where σ_{k_1} and σ_{k_2} are 1 percent of the given k value of 220 W/m-K. The converged values of the parameters are $\hat{h}_c = 26{,}390$ W/m^2-K, $\hat{k}_1 = 218.7$ W/m-K, $\hat{k}_2 = 220.4$ W/m-K, $\theta = 132.0°C$, and $\hat{q} = 154{,}000$ W/m^2. The $\hat{h}_c$ estimate of 26,390 W/m^2-K is lower than the comparable "direct" value of 27,660 W/m^2-K because the measured heat flux in the calorimeter was used for the former value but not the latter.

Sequential results are displayed in Table 5. The first column, labeled I, is the measurement number, going from 1 to 12. Estimates of the parameters are given at each I value. The results are deemed sequential because at $I = 8$, for example, the estimates depend only upon the measurements $I = 1, 2, \ldots, 8$. Estimates are found for I values less than the number of parameters (5 in this case) by using prior information (see Beck and Arnold, 1977, p. 282). The best parameter estimates are obtained when all the data are used ($I = 12$). Notice that the sequential values of $\hat{h}_c$ vary from 26,380 to 27,530 W/m^2-K. The values of $\hat{h}_c$, particularly for $I = 5$ to 12, are revealing because they vary only slightly (about 4 percent) and there is not a systematic trend upward or downward. By not exhibiting a strong trend in $\hat{h}_c$, the heat conduction model, equations (10), is shown to be reasonable. However, the $\hat{h}_c$ values do tend to be larger for the cooler specimen ($I = 9 - 12$) than the hotter one ($I = 5 - 8$). The q measurements (Table 4) decrease about 7.5 percent from $x = 0$ to $x = L_1 + L_2$, suggesting heat losses that may account for the $\hat{h}_c$ differences.

Comparison of Results. It is instructive to compare the results of the different analyses. Antonetti and Eid (1987) did not provide a single $\hat{h}_c$ but gave curves of resistances as functions of time for four different ways of calculating the heat flow. Their transient values are consistent from 1000 to 4400 s and $\hat{h}_c$ varies between 24,000 and 26,500 W/m^2-K. The simple least-squares method using equation (9) and the heater input q of 155,930 W/m^2 gives $\hat{h}_c = 27{,}600$ W/m^2-K; for the calorimeter of q of 145,000 W/m^2, $\hat{h}_c$ is 25,660 W/m^2-K. These values along with others from the present analyses are given in Table 6. In general the $\hat{h}_c$ values of the direct and sequential analyses tend to be larger than those give by Antonetti and Eid (1987). If, however, a confidence interval is calculated, the results are consistent. Confidence intervals were obtained by using program NLINA to calculate the covariance matrix of the parameter estimates. This matrix contains an estimated variance of $\hat{h}_c$ and its square root is the estimated standard deviation s_{h_c}. An estimate of the 95 percent confidence interval of the true value of h_c is (Beck and Arnold, 1977)

$$\hat{h}_c - s_{h_c} t_{0.975}(7) < h_c < \hat{h}_c + s_{h_c} t_{0.975}(7) \tag{31}$$

where $t_{0.975}(7) = 2.375$ is the value of the t distribution for 7 degrees of freedom (12 measurements minus 5 parameters) and for the distribution function value of 0.975. The estimated 95 percent confidence intervals given in Table 6 include the range of values obtained by Antonetti and Eid (1987). The simple method given by equation (9) cannot generate a confidence interval in as consistent a manner as that just given.

Modification of the Model. The heat conduction model can be modified to include heat losses from the sides of the cylindrical specimens. The differential equation is the same as for a fin and includes a heat transfer coefficient h. If h is known, its value is used; if it is not, then h is estimated in the same manner as above but the algebraic model is more complex but still manageable using program NLINA. Another extension in the heat conduction model is to include temperature-variable thermal conductivity, which can also be treated but with increasing difficulty in an algebraic form. Algebraic forms are not necessary, however, as demonstrated in the transient contact conductance example.

The above analysis is basically a parameter estimation treatment. A modification closer to function estimation uses the results of several tests performed at the same temperature level for a range of pressures, p, at the interface. If the temperature level also is changed, a possible functional relation for h_c is

$$h_c = \beta_1 + \beta_2 T + \beta_3 p + \beta_4 T^2 + \beta_5 p^2 + \beta_6 pT \tag{32}$$

The parameters are $\beta_1, \ldots, \beta_6$ in this h_c relation. Other parameters, such as thermal conductivities, can be estimated simultaneously. There are many other possible models in addition to equation (32). The parameters in equation (32) (or in

Downloaded 16 Dec 2010 to 193.140.21.150. Redistribution subject to ASME license or copyright; see http://www.asme.org/terms/Terms_Use.cfm

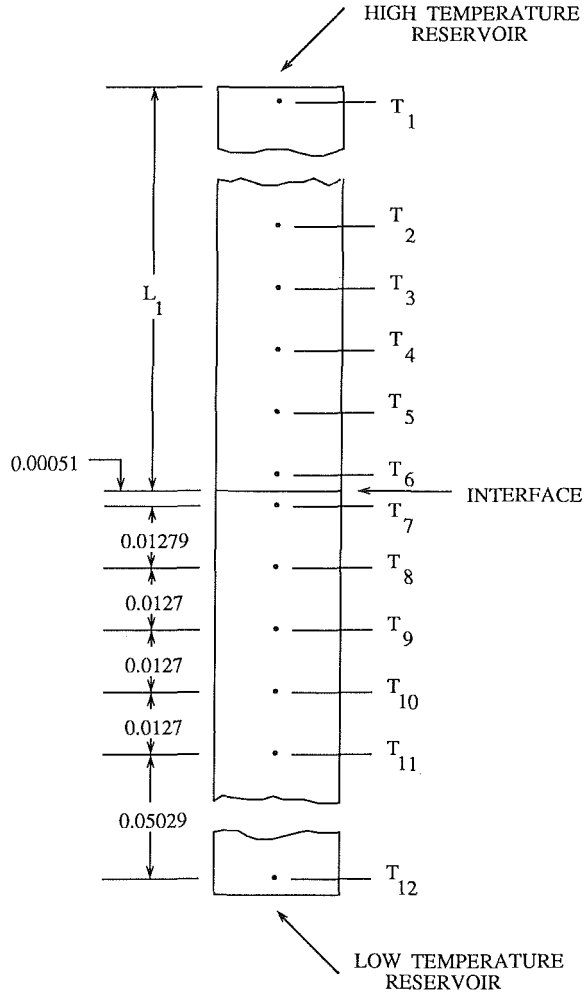

Fig. 3 Location of temperature sensors for Moses and Johnson (1986) experiment

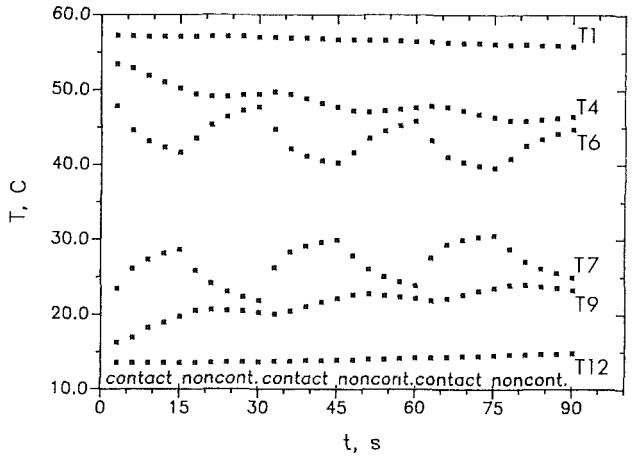

Fig. 4 Moses and Johnson (1986) temperature data for periodic contact case

related h_c models) are estimated by minimizing a sum of squares function similar to equations (13) or (30) with another summation over the experiments added. (In some cases involving function estimation, "smoothness" may be required; regularization is a method to accomplish this. See equation (39) given below and Beck et al., 1985). By using such a procedure, more accurate parameter estimates can be usually obtained than by treating each experiment separately. Furthermore, a compact model describing the conductance is found and investigation of the residuals can give insight into possible improvements in the model, such as dropping the $\beta_4 T^2$ or adding a T^3 term.

3 Transient Contact Conductance Estimation

The constant conductance varies with time, for cases such as periodic contact of valves with their seats, sliding contact of pistons with walls, and rolling contact of bearing elements. An experiment performed by Moses and Johnson (1986) employed periodic contact between two identical brass cylindrical specimens. The specimens were forced together at a constant pressure for 15 s and then moved apart for 15 s. The movement time is a small fraction of a second. Transient temperature measurements were taken at 3 s intervals for 25 cycles. There were twelve thermocouples, six in each specimen as shown in Fig. 3. The high and low temperature ends are caused by hot and cold circulating fluids, respectively. The transient temperatures are plotted in Fig. 4; the periods of contact and noncontact are shown. The objective of the experiment was to determine the contact conductance as a function of time for the case of periodic contact.

This experiment can be analyzed as either a parameter estimation or a function estimation problem. As a parameter estimation problem, the h_c value for each 15 s period of contact or noncontact is estimated. For example, the h_c value for time, $t=3$ to 15 s, is the first estimated and then h_c is estimated for $t=15$ to 30 s and so on. (Data were not given for $t=0$). During $t=3$ to 15 s, 30 to 45 s, . . . , the specimens were in contact; for $t=15$ to 30 s, . . . , the specimens were apart. In a sense, determination of h_c for these periods of contact or noncontact is function estimation but an analysis more properly termed function estimation gives a h_c value at each time step (3 s in this problem). Both methods of analysis are investigated in this section.

To illustrate these methods the contact conductance is estimated using the computer program called PROPOR, which is also described briefly in Beck and Arnold (1977). The solution of the transient heat conduction equation is incorporated into the computer program. The equation is

$$\frac{\partial}{\partial x}\left(k\frac{\partial T}{\partial x}\right)=\rho c_p\frac{\partial T}{\partial t} \tag{33}$$

which implies that side heat losses are not considered. The interface condition involving the contact conductance is

$$-k\frac{\partial T}{\partial x}\bigg|_{L_1^-}=-k\frac{\partial T}{\partial x}\bigg|_{L_1^+}=h_c[T(L_1^-,\,t)-T(L_1^+,\,t)] \tag{34}$$

where L_1 is the interface location. Program PROPOR can use prescribed time-dependent boundary conditions. In the analysis of the Moses and Johnson (1986) transient data, the temperature histories given by thermocouples 1 and 12 are used as the boundary conditions. These temperatures are nearly constant with time because they are near the high and low-temperature reservoirs, respectively. Since these T's are nearly constant, it is not necessary to include them in the estimation criteria. (See the discussion given in connection with equations (3) to (6).) At the start of the calculation, the initial temperature distribution is found by linear interpolation among the first values (which are at 3 s).

There are two basic parts in program PROPOR: a direct problem solver and an inverse algorithm. The direct problem solver uses the Crank–Nicolson (control volume) finite difference method. The heat flow leaving the high-temperature specimen is required to enter the low-temperature one. This important heat flux continuity condition is not imposed if the problem is solved as two separate inverse heat conduction problems, one for each specimen. Methods have been pro-

Downloaded 16 Dec 2010 to 193.140.21.150. Redistribution subject to ASME license or copyright; see http://www.asme.org/terms/Terms_Use.cfm

posed that do not include this condition. The requirement of continuity of q, the capability to treat T- variable properties and to use time-variable boundary conditions are important features of program PROPOR. Since the thermal properties of the brass specimens are not known as functions of temperature and also the temperature is not large, the k, ρ, and c values were considered to be constant. The brass k value used by Moses and Johnson (1986) was 106.1 W/m-K; ρc was taken from Holman (1976) and was 3280 kJ/m^3-K. (The use of PROPOR for estimating k is discussed in Section 3.4). The inverse algorithm is similar to those discussed in Section 2 and is discussed in more detail in Section 3.1.

Before describing the inverse algorithm in PROPOR, the Moses and Johnson (1986) method of analysis is outlined. This method is an extension of the accepted steady-state analysis associated with equation (9). Instead of temperature as a linear function of position, a quadratic curve was fitted to the data for each specimen, using the method of least squares. The temperature drop at the interface ΔT was found by evaluating both curves at the interface. Then the heat flux was found by differentiating each curve with respect to x and evaluating it at the interface. The two heat flux values were averaged to get the value used in equation (9). The resulting equation was

$$\hat{h}_c = \frac{k}{-2}\left[\left.\frac{\partial T}{\partial x}\right|_{L_1^-} + \left.\frac{\partial T}{\partial x}\right|_{L_1^+}\right]\left[T_{L_1^-} - T_{L_1^+}\right]^{-1} \tag{35}$$

where $x = L_1$ was the location of the interface. Equation (35) was used for each measurement time. This method has the advantages of simplicity and independence of the ρc_p value. Disadvantages are very similar to those for the steady-state analysis, which used equation (9). First, the same heat flux leaving the high-temperature specimen is not required to enter the low-temperature one. Second, the transient temperature measurements contain information regarding k, but the information is not used. Third, the use of a quadratic (or some other power) curve does not incorporate a physical model, such as equations (33) and (34). As a consequence, the residuals obtained in the quadratic fit cannot be used to improve the model. The use of a physical model, solved by an accurate method, overcomes each of these disadvantages.

An outline of the remainder of Section 3 is now given. Section 3.1 discusses parameter and function estimation algorithms. Section 3.2 provides a function estimation analysis of the Moses and Johnson (1986) data. Section 3.3 gives a parameter estimation analysis of that data for h_c; Section 3.4 discusses the parameter estimation of k using the Moses and Johnson (1986) data; and Section 3.5 gives some final comments regarding estimation of $h_c(t)$.

3.1 Inverse Algorithms. Algorithms for parameter and function estimation are usually different. For the Moses and Johnson (1986) data, however, the methods of analysis are nearly identical because the measurement time steps, $\Delta t = 3$ s, are "large." In this h_c problem, the condition of being large is determined by comparing $\alpha \Delta t/E^2$ to 1; α is the thermal diffusivity of the brass and E is the distance from the interface to the nearest thermocouple. The value is 373, which is very large compared to 1. Nevertheless, a few ideas regarding function estimation for h_c are given when $\alpha \Delta t/E^2$ is small compared to unity. In this section, algorithms for PE and FE are discussed briefly.

The parameter estimation algorithm in PROPOR is discussed first. The function to be minimized is S given by equation (3). PROPOR permits different weights for each temperature sensor; since only T is measured and each sensor has about the same accuracy, the weights are equal and thus can be omitted in equation (3).

When estimating h_c over the different time intervals (in contact, not in contact, in contact, etc.), the S function given by equation (3) can be written as

$$S_I = \sum_{j=2}^{m-1} \sum_{i=n_{I-1}}^{n_I} (Y_{ji} - T_{ji})^2 \tag{36}$$

where n_I is the beginning time index for the Ith time interval. The first few n_I values ($I = 0$, 1, 2, and 3) are 2, 5, 10, and 15 and correspond to times 6, 15, 30, and 45 s. The first time interval is anomalous because the initial temperatures (at $t = 0$) were not known. The procedure now requires the minimization of equation (36) with respect to h_c for the Ith time interval, assuming that the h_c values have been determined for the previous $I-1$ intervals. The problem is nonlinear. Program PROPOR uses a modified Gauss linearization procedure (Beck and Arnold, 1977); this is an iterative gradient technique. The minimization of equation (36) is accomplished by differentiating S with respect to h_c, setting the equation equal to zero, and evaluating at $\hat{h}_{c,I}$. The resulting equation is

$$\frac{\partial S_I}{\partial h_c} = 2\sum_{j=2}^{m-1} \sum_{i=n_{I-1}}^{n_I} (Y_{ji} - \hat{T}_{ji})\left(-\frac{\partial \hat{T}_{ji}}{\partial h_c}\right) = 0 \tag{37}$$

where the $\hat{}$ symbol on T_{ji} and the sensitivity coefficient, $\partial T_{ji}/\partial h_c$, indicates that they have been evaluated at $\hat{h}_{c,I}$. The calculated temperature $\hat{T}_{ji}$ is found from the finite control volume solution of the transient heat conduction model, equation (33). Sensitivity coefficient values are determined from the solution of equation (33) for given values of $h_c = \hat{h}_c$ and $\hat{h}_c + \delta h_c$

$$\frac{\partial \hat{T}_{ji}}{\partial h_c} \approx \frac{\hat{T}_{ji}(\hat{h}_c + \delta h_c) - \hat{T}_{ji}(\hat{h}_c)}{\delta h_c} \tag{38}$$

where δh_c is a small value compared to $\hat{h}_c$. The solution proceeds by using a Taylor series expression of T_{ji} in terms of h_c. The expansion is then introduced into equation (37) and solved for the correction of Δh_c. This iterative procedure is continued until $|\Delta h_c/\hat{h}_c|$ is less than 0.0001. Then I is increased by one and the $\hat{h}_c$ values is estimated for the next time interval, and so on. For more details, see Beck and Arnold (1977), Sections 7.4 and 7.8. The implementation of this algorithm has sequential aspects, which are discussed in Section 3.2.

The function estimation algorithm is now discussed. In generating numerical values for h_c at each time step of 3 s using the Moses and Johnson data, the same algorithm as described above is used. The only difference is that $n_{I+1} - n_I$ is always 1. This procedure can be used for the Moses and Johnson data because the time step is large, as discussed above. If the time step is small, then a procedure to stabilize the calculations is necessary. Two different stabilization procedures are described next; namely, function specification and regularization.

In the function specification method, the h_c component at time t_I is estimated using the measurements at r future times, during which h_c is specified to be a simple function, such as a constant. Then the component for time t_I is accepted, the t_I value is increased by Δt, and the process is repeated. The method is similar to the parameter estimation procedure described above, but only the *first* h_c component is accepted, so that future information is continually being used. Another reference is Osman and Beck (1987).

In the sequential regularization method, the augmented sum of squares function

$$S_I = \sum_{j=2}^{m-1} \sum_{i=n_I}^{n_{I+n}} (Y_{ji} - T_{ji})^2 + \alpha_0 \sum_{i=n_I}^{n_{I+r}} h_{ci}^2 \tag{39}$$

is minimized with respect to $h_{c,n_I}, \ldots h_{c,n_{I+r}}$. Only the h_{c,n_I} component is accepted and then n_I is increased by 1. The quantity α_0 in equation (39) is called a regularization parameter. Equation (39) is a zeroth order regularization

Downloaded 16 Dec 2010 to 193.140.21.150. Redistribution subject to ASME license or copyright; see http://www.asme.org/terms/Terms_Use.cfm

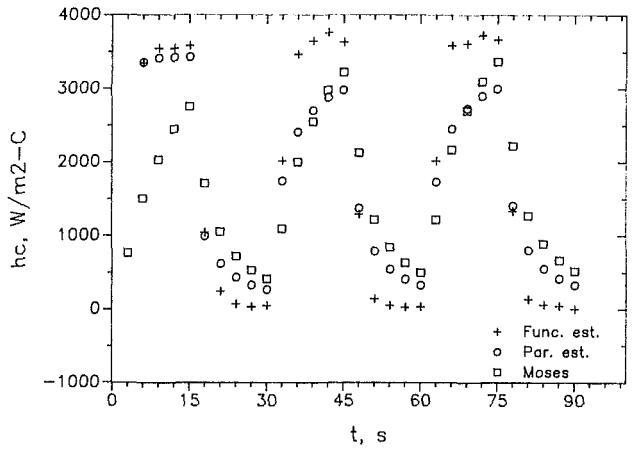

Fig. 5 Estimated h_c values for the Moses and Johnson (1986) data using the Moses and Johnson, sequential parameter estimation, and function estimation analyses

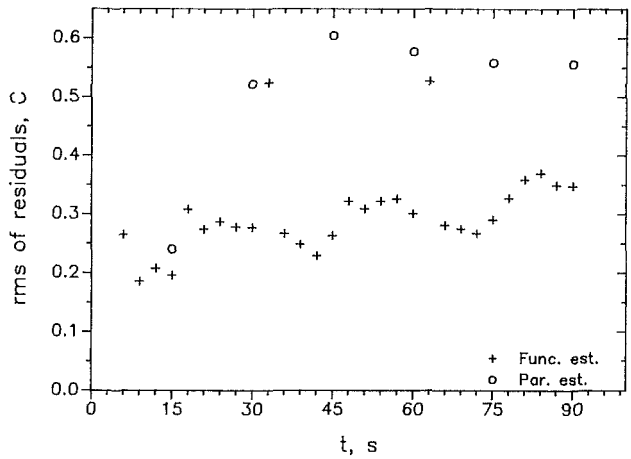

Fig. 6 The rms of temperature residuals for Moses and Johnson (1986) data for parameter and function estimation analyses

method because the last summation involves the zeroth difference of the h_{ci} values; equation (39) can be made a first-order regularization method by replacing h_{ci} inside the square by $h_{c,i+1}-h_{c,i}$ and reducing the upper limit in the summation by one. For more discussion, see Beck et al. (1985).

3.2 Function Estimation for Transient Contact Conductance Data. The transient temperatures for some of the thermocouples (Moses and Johnson, 1986) are shown in Fig. 4; from the highest to the lowest temperatures, the plotted values are for thermocouples 1, 4, 6, 7, 9, and 12. See Fig. 3 for the locations. The Moses and Johnson data are consistent and quite accurate. The highest and lowest temperature histories (thermocouples 1 and 12, respectively) are used as the boundary conditions. These two temperatures are maintained nearly constant by the high and low-temperature reservoirs shown in Fig. 3. A slight drift is noted in each; since the actual time-dependent temperature histories are used in PROPOR, the deviation from constant temperatures does not affect the validity of the analysis. The middle two temperature histories in Fig. 4 (numbers 6 and 7) are on either side of the interface and have the largest time variations. They are symmetric about a nearly horizontal line at 35°C. The high-temperature specimen is cooled during the contacting periods while the low-temperature specimen is heated. During the noncontacting periods, the high-temperature specimen increases in temperature and the low-temperature specimen decreases. For clarity, not all the measured temperature histories are shown in Fig. 4. In the calculations using PROPOR, temperatures given by thermocouples 4, 5, 6, 7, 8, and 9 were used in the sum of squares criterion, equation (36).

Estimated h_c values obtained by Moses and Johnson (1986) are shown as squares in Fig. 5. They obtained their values by passing a quadratic through the data, as discussed in the beginning of Section 3. The results from one period to another are quite consistent. During the contacting periods, the values start low and then increase rapidly with time. There is no contacting period in which the estimates are nearly constant with time. During the noncontacting periods, the results (squares in Fig. 5) continually decrease with time, and again do not reach constant values with time. One of the surprising aspects of the Moses and Johnson $\hat{h}_c$ values is that the noncontacting values remain large, with the minimum $\hat{h}_c$ values in the noncontacting periods between 409 and 516 W/m^2-K. These values are much larger than expected from natural convection, about 10 W/m^2-K.

In the function estimation analysis the transient heat conduction equation is solved numerically and $\hat{h}_c$ is found at each measured time. (The calculational time steps are 0.5 s, while the measurement steps are 3.0 s; the use of small calculational time steps improves the accuracy of the finite difference solution). Results for this analysis, displayed as crosses in Fig. 5, are more uniform over both the contacting and noncontacting periods than the Moses and Johnson values. Except for the first measurement after contact or noncontact, the function estimation values in Fig. 5 are roughly constant. Also note that the contacting values reach a maximum value of about 3600 W/m^2-K, while the Moses and Johnson values are about 10 percent lower. It is interesting to observe that the noncontacting $\hat{h}_c$ values are nearly constant and also have values about 20 W/m^2-K in several periods. The noncontacting values are reasonable, provided the first value after noncontact is neglected. There are probably larger measurement errors in the anomalous $\hat{h}_c$ values just after noncontact; this point is discussed further in connection with the residuals.

The residuals are defined by

$$e_{ji} = Y_{ji} - \hat{T}_{ji}$$

where Y_{ji} and $\hat{T}_{ji}$ are measured and calculated temperatures, respectively. The residuals can be sensitive indicators of the adequacy of the model and can yield insight into the measurement errors. Each residual can be examined; however, for conciseness the root mean square (rms) is found. One equation for the rms of the measured temperature is

$$\text{rms} = \left[\frac{1}{(n_I - n_{I-1})(m-2)-1}\sum_{j=2}^{m-1}\sum_{i=n_{I-1}}^{n_I}(Y_{ji}-\hat{T}_{ji})^2\right]^{1/2} \quad (40)$$

which can be compared with equation (36). The number of temperature sensors used in equation (40) is $m-2=6$. The number of measurement times for each $\hat{h}_c$ is $n_I - n_{I-1}$; namely, 1 in the function estimation analysis. Values of rms are denoted as crosses in Fig. 6 for the function estimation analysis. In most cases, the residual values just after contact or noncontact (6, 18, 33, 48, 63, and 78 s) are larger than those just before or later. Particularly noticeable are those at 33 and 63 s, which are just after contact. (The corresponding value at 3 s is not available because the temperature distribution was not measured at $t=0$ s.) These large rms values, about 0.5°C, compared with the other values, about 0.3°C, suggest that (1) the model is somewhat in error and/or (2) the temperature measurements have larger errors for sudden changes. The model can be in error because h_c might vary substantially over the 3 s period just after contact.

3.3 Parameter Estimation for Transient Contact Conductance Data. In the parameter estimation analysis, a single $\hat{h}_c$ value is estimated for each contacting or noncontacting

Downloaded 16 Dec 2010 to 193.140.21.150. Redistribution subject to ASME license or copyright; see http://www.asme.org/terms/Terms_Use.cfm

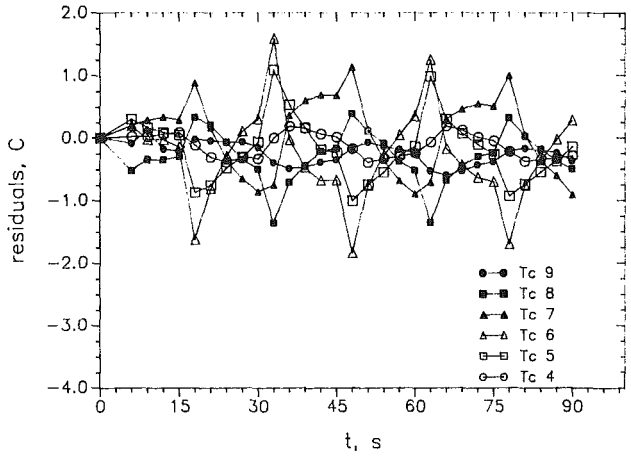

Fig. 7 *Temperature residuals for the Moses and Johnson (1986) data using the parameter estimation analyses*

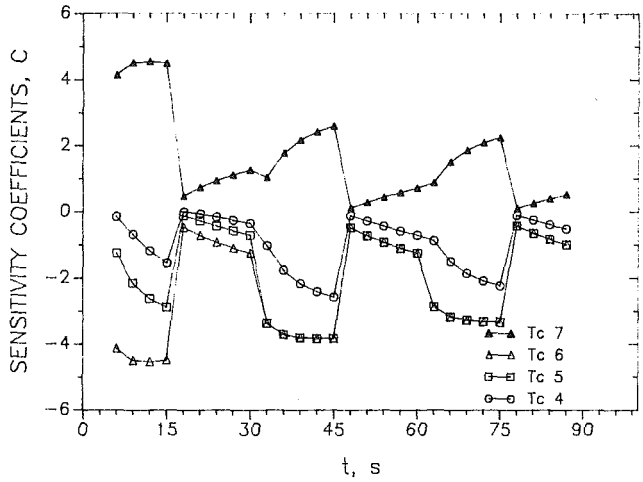

Fig. 8 **Sensitivity coefficients for the parameter estimation analysis (Moses and Johnson, 1986 data)**

period. For example, a contacting $\hat{h}_c$ estimate is found for the time period between 3 and 15 s. The estimate is found by minimizing the sum of squares function S with respect to h_c for this time period; the estimate is obtained in program PROPOR using the Gauss linearization procedure. After convergence is achieved, sequential estimates (which are *not* related to the iterative values) are calculated at times 6, 9, 12, and 15 s. The best $\hat{h}_c$ estimate for the complete contacting period (3 to 15 s) is the one given for 15 s. The other values are the $\hat{h}_c$ estimates if (*a*) fewer data are used and (*b*) the $\hat{T}_{ji}$ and sensitivity coefficients are evaluated at the converged $\hat{h}_c$ value for all the data in the time period of contact or noncontact. There are many benefits of presenting sequential results, some of which are discussed next.

Sequential parameter estimation $\hat{h}_c$ values for the Moses and Johnson (1986) data are shown in Fig. 5 as open circles. For the first time period (3 to 15 s), the $\hat{h}_c$ values are nearly constant. Note that the first values (at 6 s) for the parameter estimation (circles) and the function estimation (crosses) coincide, an expected result since the parameter estimation $\hat{h}_c$ values vary only slightly over this time period. This uniform behavior is not repeated again, possibly because this is the only case in which the first 3 s interval after contact is omitted. Even though the sequential parameter estimation values (circles) vary more than the function estimation values (crosses), they are less variable than the Moses and Johnson results (squares). The best PE $\hat{h}_c$ values given for the noncontacting periods (those at 30, 60, and 90 s) are between 264 and 326 W/m^2-K, which are slightly lower than the Moses and Johnson values but still considerably larger than the expected free convection value of about 10 W/m^2-K. It is possible that during contact $\hat{h}_c$ might change with time but it is not reasonable to expect that the noncontacting $\hat{h}_c$ should vary greatly with time. It is therefore concluded that the temperature measurements just after contact or noncontact possess larger errors than those at other times.

One way to investigate the possibility of larger measurement errors just after contact and noncontact is to calculate the rms of the residuals at each time. There is uncertainty regarding time variations of $\hat{h}_c$ during contacting periods but during noncontacting periods they are expected to be constant and very small. As noted in connection with Fig. 5, the parameter estimation algorithm produced values of $\hat{h}_c$ that are too large during the noncontacting period. If $\hat{h}_c$ is assumed to be constant in this period, the rms of the residuals (see the open circles in Fig. 6) are about twice as large as most of those for the function estimation analysis. More can be learned by looking at the actual residuals for the parameter estimation analysis; see Fig. 7. In every contacting and noncontacting period (except the 3 to 15 s period), the residuals are largest just after contact or noncontact. Since the noncontacting $\hat{h}_c$ values should be nearly constant (and nearer 10 than 300 W/m^2-K), the large residuals, almost 1.8°C, suggest that the temperature measurement errors significantly affect the accuracy of the estimation of h_c. The largest measurement errors are expected just after sudden surface temperature changes, which is consistent with the largest error amplitude in Fig. 7. It is very difficult to perform experiments that do not have such characteristics.

A quantity that can give much insight is the sensitivity coefficient; it is the partial derivative of T with respect to h_c. Figure 8 shows

$$h_c(\partial T/\partial h_c)$$

as a function of time. The sensitivity coefficient is multiplied by h_c to obtain the units of T and thus make comparisons with ΔT possible. The maximum magnitude in Fig. 8 is about 4.5°C, which can be compared with $\Delta T = 20$°C, an average of the temperature differences at the interface. (It could also be compared with the maximum ΔT of 45°C, Fig. 4.) Typically an accurate experiment has values of $|h_c\ \partial T/\partial h_c|$, which approach the maximum ΔT. Since 4 dividied by 20 (or 45) is 0.2 (or 0.09), this experiment does not have this desirable characteristic. However, it may not be possible to do better (Beck, 1969). The thermocouples nearest the interface have the largest magnitudes in the sensitivity coefficients, that is, thermocouples, 6 and 7. The sensitivity coefficients for the two specimens have the same magnitude; those in the high-temperature specimen are negative and those in the low-temperature one are positive. Notice that the sensitivity coefficients for thermocouples 6 and 7 are mirror images about the zero line. This means that the best locations for the thermocouples (for determining h_c) are near the interface and that sensors in both specimens ar equally effective. It is also significant that the $|h_c\ \partial T/\partial h_c|$ values decrease as time progresses from time period to time period. More uncertainty in the estimated $\hat{h}_c$ values is expected with decreasing values of $|h_c\ \partial T/\partial h_c|$. Since the sensitivity coefficients for the noncontacting time periods are quite small (about 1°C), the noncontacting h_c values are expected to have relatively large uncertainty; this is consistent with the parameter estimation results shown in Fig. 5 as the $\hat{h}_c$ values are much higher than expected.

3.4 Parameter Estimation for Thermal Conductivity. In the above analysis of the Moses and Johnson (1986) data, the thermal conductivity is assumed to be known. The data can also be used to estimate the thermal conductivity, provided the

Downloaded 16 Dec 2010 to 193.140.21.150. Redistribution subject to ASME license or copyright; see http://www.asme.org/terms/Terms_Use.cfm

ρc_p value is known. One way to do the estimation is to consider each specimen separately with thermocouples 1 and 6 providing the boundary temperatures in the high-temperature specimen, and 7 and 12 in the low-temperature one. The resulting estimates are 102 and 82 W/m-K for the high and low-temperature specimens, respectively. These should be compared with the Moses and Johnson value of 106.1 W/m-K. The difference between the estimated values is not unexpected because the use of temperature histories as boundary conditions without a knowledge of the heat flux is not characteristic of a well-designed experiment (Beck and Arnold, 1977, Chap. 8). The maximum value in this analysis of $|k\ \partial T/\partial k|$ is about 2.5, while in a better designed experiment (such as with a nonzero prescribed heat flux) the value would be almost ten times larger.

3.5 Final Comments About Transient Contact Conductance Analysis. There are several ways to analyze the transient contact conductance data of Moses and Johnson (1986). Some of these include the function and parameter estimation analyses given above. Some combined function and parameter estimation problems can also be suggested. One of these involves parameter estimation for the thermal conductivity, followed by function estimation for h_c. If the data solely from the experiment are used, accurate values of k are not obtained, as indicated above. However, if the standard deviation of prior k measurements is known, the k value obtained by using the transient temperature measurements would have a smaller standard deviation than if the data were not used. Another combined problem is (a) the parameter estimation of the same h_c value for all the contacting periods while either estimating the noncontacting h_c as the same value for all periods (or setting to a reasonable value such as 10 W/m^2-K) and (b) function estimation of the "best" boundary temperature histories at $x=0$ and $z=L_2$; this function estimation is discussed above in connection with equations (5) and (6). Yet other combined problems can be suggested when the pressure and temperature levels change; see equation (32).

4 Summary and Conclusions

Parameter, function, and combined parameter and function estimation problems are described. Each of these is an inverse problem. To date, the most commonly considered inverse problem in heat transfer is the inverse heat conduction problem, which is a function estimation problem. Other function estimation problems involve the determination of time-variable thermal contact conductances and heat transfer coefficients. A parameter estimation problem is the determination of the thermal diffusivity or thermal conductivity from transient temperature measurements.

There are cases in which there is not a clear difference between the parameter and function estimation problems and there are cases that involve a combination of the two. A problem that has a blurred distinction is the determination of thermal conductivity k as a function. If it is a constant, then it is parameter estimation problem but if k is approximated by 20 linear segments, it is a function estimation problem. Somewhere between these two extreme models for $k(T)$, the distinction between parameter and function estimation is blurred. In the beginning of the paper several problems of combined estimation are listed. Most of these problems have not been considered herein and thus are topics for research. One of these is the determination of parameters using interior temperature measurements and boundary condition functions.

Various types of estimation are illustrated for thermal contact conductance. Two experiments are analyzed. One was performed by Antonetti and Eid (1987) who used a transient experiment that approached steady state. Their steady-state data are analyzed using parameter estimation. The estimation includes finding a boundary condition that is typical of a function estimation problem. The other experiment was performed by Moses and Johnson (1986) and was transient. These data are analyzed using both parameter and function estimation techniques.

The temperature data of Antonetti and Eid (1987) and Moses and Johnson (1986) are found to be excellent. However, the methods of estimation given herein are believed to be superior to those commonly used, which involve independently curve-fitting the temperatures in the two specimens. Such commonly used methods (1) do not insure continuity of heat flux from the high to low-temperature specimens, (2) do not use the energy equation in a fundamental way, (3) do not utilize the potential to estimate the thermal conductivity of the specimens, and (4) cannot provide residuals (measured minus calculated temperatures) that can be employed for improving the mathematical model. Moreover, the commonly accepted methods cannot extend in a direct way to the treatment of side heat losses or temperature-dependent thermal properties. Each of these weaknesses can be overcome by using the parameter and function estimation techniques proposed in this paper.

The concepts are quite general and have wide application in the analysis of experimental data. The extension to combined parameter and function estimation is very important and can only be partly elucidated. For example, there are many convection problems that have yet to be explored. With the concurrent increasing availability of transient data acquisition equipment and computers (including supercomputers), there is a capacity to consider many new and challenging problems.

Acknowledgments

This research was partially funded by the State of Michigan through the Research Excellence Fund administered by the Composite Materials and Structure Center at Michigan State University. The suggestions of Professor C. R. St. Clair, Jr. are appreciated.

References

Antonetti, V. W., and Eid, J. C., 1987, "A Technique for Making Rapid Thermal Contact Resistance Measurements," *Proceedings of the International Symposium on Cooling Technology for Electronic Equipment*, W. Aung and P. Cheng, eds., Honolulu, HI, Mar. 17–21, pp. 449–460.

Bard, Y., 1974, *Nonlinear Parameter Estimation*, Academic Press, New York.

Beck, J. V., 1969, "Determination of Optimum, Transient Experiments for Thermal Contact Conductance," *Int. J. Heat Mass Transfer*, Vol. 12, pp. 621–633.

Beck, J. V., and Arnold, K. J., 1977, *Parameter Estimation in Engineering and Science*, Wiley, New York.

Beck, J. V., Blackwell, B., and St. Clair, C. R., 1985, *Inverse Heat Conduction, Ill-Posed Problems*, Wiley-Interscience, New York.

Beck, J. V., and Blackwell, B., 1988, "Inverse Problems," in: *Handbook of Numerical Heat Transfer*, W. J. Minkowycz, E. M. Sparrow, R. H. Pletcher, and G. E. Schneider, eds., Wiley, New York.

Bevington, P. R., 1969, *Data Reduction and Error Analysis for the Physical Sciences*, McGraw-Hill, New York.

Biles, W. E., and Swain, J. J., 1980, *Optimizaiton and Industrial Experimentation*, Wiley, New York.

Bryson, A. E., and Ho, Y., 1969, *Applied Optimal Control, Optimization, Estimation and Control*, Blaisdell Publishing Co., Waltham, MA.

Chakravarty, S., Menguc, M. P., Mackowski, D., and Altenkirch, 1988, "Application of Two Inversion Schemes to Determine the Absorption Coefficient Distribution in Flames," *Proceedings of the 1988 National Heat Transfer Conference*, Vol. 1, H. R. Jacobs, ed., pp. 171–178.

Draper, N. R., and Smith, H., 1968, *Applied Regression Analysis*, Wiley, New York.

Goodwin, G. C., and Payne, R. C., 1977, *Dynamic System Identification, Experiment Design and Data Analysis*, Academic Press, New York.

Hensel, E. C., and Hills, R. G., 1984, "A Space Marching Finite Difference Algorithm of the One-Dimensional Inverse Conduction Heat Transfer Problem," ASME Paper No. 84-HT-48.

Downloaded 16 Dec 2010 to 193.140.21.150. Redistribution subject to ASME license or copyright; see http://www.asme.org/terms/Terms_Use.cfm

Holman, J. R., 1976, *Heat Transfer*, 4th ed., McGraw-Hill, New York.

Kays, W. M., and Crawford, M. E., 1980, *Convective Heat and Mass Transfer*, 2nd ed., McGraw-Hill, New York.

Lawson, C. L., and Hansen, R. J., 1974, *Solving Least Squares Problems*, Prentice-Hall, NJ.

Morozov, V. A., 1984, *Methods for Solving Incorrectly Posed Problems*, Springer-Verlag, New York.

Moses, W. M., and Johnson, R. R., 1986, "An Experimental Study of the Transient Behavior of the Thermal Contact Conductance and Temperature Distribution in Periodically Contacting Surfaces," AIAA Paper No. AIAA-86-1244.

Osman, A., and Beck, J. V., 1987, "Nonlinear Inverse Problem for the Estimation of Time-and-Space Dependent Heat Transfer Coefficients," AIAA Paper No. AIAA-87-0150, to be published in *J. Thermophysics and Heat Transfer*.

Raynaud, M., and Beck, J. V., 1988, "Methodology for Comparison of Inverse Heat Conduction Methods," ASME JOURNAL OF HEAT TRANSFER, Vol. 110, pp. 30–37.

Sage, A. P., 1968, *Optimal Systems Control*, Prentice-Hall, Englewood Cliffs, NJ.

Sage, A. P., and Melsa, J. L., 1971, *System Identification*, Academic Press, New York.

Scott, E., and Beck, J. V., 1985, "Analysis of the Order of Sequential Regularization Solutions of Inverse Heat Conduction Problems," ASME Paper No. 85-WA/HT-43; to be published in the ASME JOURNAL OF HEAT TRANSFER.

Tikhonov, A. N., and Arsenin, V. Y., 1977, *Solutions of Ill-Posed Problems*, Wiley, New York.

Downloaded 16 Dec 2010 to 193.140.21.150. Redistribution subject to ASME license or copyright; see http://www.asme.org/terms/Terms_Use.cfm

Recent Developments in Contact Conductance Heat Transfer

L. S. Fletcher
Thomas A. Dietz Memorial Professor,
Department of Mechanical Engineering,
Texas A&M University,
College Station, TX 77843
Fellow ASME

The characteristics of thermal contact conductance are increasingly important in a wide range of technologies. As a consequence, the number of experimental and theoretical investigations of contact conductance has increased. This paper reviews and categorizes recent developments in contact conductance heat transfer. Among the topics included are the theoretical/analytical/numerical studies of contact conductance for conforming surfaces and other surface geometries; the thermal conductance in such technological areas as advanced or modern materials, microelectronics, and biomedicine; and selected topics including thermal rectification, gas conductance, cylindrical contacts, periodic and sliding contacts, and conductance measurements. The paper concludes with recommendations for emerging and continuing areas of investigation.

Introduction

The thermal contact conductance depends upon the thermal and physical characteristics of the material junction and the junction environment. The relative importance of the thermal conductance is directly related to the desirability of isolating or enhancing the energy transfer at a junction. As a consequence, the understanding of the thermal contact conductance phenomenon has taken on new dimensions as more and more researchers develop solutions to immediate problems.

When two surfaces are brought into contact, whether in the presence of an interstitial medium (epoxy, solder, grease, or other material) or a bare junction, an imperfect junction exists. While a uniform temperature gradient may exist in a homogeneous material, the junction between two surfaces creates a temperature difference between the surfaces. This difference is dependent upon the mechanical and thermophysical properties of the contacting materials, the characteristics of the contacting surfaces, the presence of gaseous and nongaseous interstitial media, and the overall environment of the junction.

Because two surfaces in contact are not perfectly flat, most of the heat or energy passes through a limited number of actual contact spots, as shown in Fig. 1. The contact resistance, then, is the resistance to heat flow because the actual area of contact is only a small fraction of the nominal or apparent area. This contact resistance is defined as the ratio of the temperature drop at the interface to the average heat flux across the junction, as shown in Fig. 2. The thermal contact resistance is related to the thermal contact conductance; however, the results of most analytical and experimental studies are reported in terms of thermal contact conductance.

The type of experimental facility generally used to obtain thermal contact conductance data consists of a vertical cylindrical column under axial load, with the contacting surfaces located at approximately the midpoint of the column. One end of the column serves as a heat source (heated by cylindrical heaters or other means), and the other end serves as the heat sink (cooled by water, liquid nitrogen, or other cooling media). The test materials, heat source, guard heaters, radiation shields, and heat sink usually are instrumented with thermocouples to provide information on the operation of the system and to measure axial temperatures in the column. Column loading is generally provided by dead weight, hydraulic, or pneumatic means. The test facility is generally located in a vacuum chamber to minimize convective heat transfer around the test materials and through gaseous interstitial media.

Since studies of thermal contact conductance or thermal contact resistance cover such a broad and diverse range and have been conducted over a substantial period of time, this paper is restricted to those investigations and studies that have been reported since 1980. This paper is further divided into recent reviews and summaries, theoretical and analytical studies, thermal conductance in such technological areas as advanced or modern materials, microelectronics, and biomedicine, and selected topics including thermal rectification, gas conductance, cylindrical contacts, periodic and sliding contacts, and conductance measurements.

Recent Reviews

A comprehensive review of thermal contact conductance literature for the period 1950 to 1980 was provided by Madhusudana and Fletcher (1981a, 1986). This review considered the advances in such areas as the resistance of single constrictions, including disk, conical, and others, as well as the effects of large-scale surface irregularities. Correlations were reviewed for thermal contact conductance in a vacuum through multiple contact spots for nominally flat, rough surfaces. The effects of both gaseous and nongaseous interstitial media and materials were summarized, including the effects of surface films and heat flow direction. Also considered were special topics of the time such as stacks of laminations, bolted joints, cylindrical joints, and nuclear reactor fuel elements.

Snaith et al. (1986) reviewed the literature in the area of the thermal resistance of pressed contacts in an effort to assist the designer in understanding the factors involved. The paper discussed mechanisms for heat transfer across solid metal/solid metal interfaces, influential parameters affecting thermal contact resistance, analytical predictions of the thermal resistance of pressed contacts with limitations, and empirical correlations. The comparison of the correlations suggested that a suitable general correlation for a bare metal junction has not yet been achieved, primarily because there is no standard method for measuring and reporting the topography of the contacting surfaces.

There have been other more recent reviews focused on selected areas. Antonetti and Yovanovich (1984) provided a selective review of the state of the art of thermal contact resistance as applied to microelectronic equipment. The review summarized analytical methods for determining the spreading resistance in microelectronic packages and presented techniques to predict, measure, and minimize the contact resistance across mechanical joints. The prediction and measurement of the contact resistance of bonded joints in integrated circuit packages was discussed, noting that there is considerable information on contact resistance available to the designer of microelectronic packages, but that the data

Contributed by the Heat Transfer Division for publication in the JOURNAL OF HEAT TRANSFER. Manuscript received by the Heat Transfer Division March 1, 1988. Keywords: Conduction, Reviews.

Copyright © 1988 by ASME
Downloaded 16 Dec 2010 to 193.140.21.150. Redistribution subject to ASME license or copyright; see http://www.asme.org/terms/Terms_Use.cfm

published are not comparable and are often difficult to interpret.

Because of the importance of heat dissipation in microelectronic components, the National Science Foundation sponsored a workshop on research needs in electronic cooling. As part of the workshop, Yovanovich et al. (1986b) summarized the issues related to internal resistance of microelectronic components, noting the dependence on internal design features, material selection, the integrity of assembly procedures, and mounting and cooling techniques. The conclusions and recommendations were divided into materials behavior and problems associated with thermal contact resistance. Standardized procedures for identification and assessment of materials used in multilayer composites and printed wiring boards were called for. It was suggested that the existing parameters and models pertaining to thermal contact conductance should be identified and disseminated to the microelectronics industry (noting the inaccuracy and limitations) and that a standardized test method for thermal resistance should be established.

The increasing focus on development of cooling technologies for electronic equipment resulted in an international symposium on the subject, at which Yovanovich (1987) presented a summary of the theory and applications of constriction and spreading resistance concepts for the thermal management of microelectronic components. The paper provided a timely review of the state of the art of thermal contact resistance problems and models, discussed the effect of thin metallic layers bonded to one surface of the contact, and presented recently developed dimensionless spreading resistance expressions suitable for solving many microelectronic thermal problems. A prediction expression for the thermal resistance of soldered joints was presented. The effects of thin metallic foils for minimization of joint resistances were also reported.

Yovanovich (1986) summarized recent developments in contact conductance models for point and line contacts and conforming rough surfaces. Theory was compared with experimental results, noting good to excellent agreement for point contact and conforming rough-surface models. The limited agreement observed at light loads was attributed to errors in form, or crowning, for line contact models. One of the major factors that caused differences in the conforming model at light loads was the high local strain due to very large local temperature gradients.

The influence of interstitial media on thermal contact conductance is of importance to the aerospace industry, as well as the electronics industry. Fletcher (1984) presented a review of the thermal contact conductance with interstitial materials useful in spacecraft thermal control. The paper was restricted to those investigations of appropriate spacecraft environments, and dealt with both gaseous and nongaseous interstitial media. The paper further divided nongaseous materials into four classifications, including synthetic or processed natural sheets, ceramic sheets and powders, metallic foils and screens, and greases and oils. An efficiency factor for thermal control materials was defined, which related the thermal conductance of the journal with an interstitial material to a bare metallic junction under the same conditions. Based on the range of materials reported, heat transfer was improved by as much as 40 percent or reduced by as much as 100 percent for the same junction conditions.

Fletcher and Peterson (1986) expanded on the review of interstitial materials for spacecraft systems to include a wide range of thermal systems with composite materials and similar and dissimilar metals. Both gaseous and nongaseous materials were considered, including polyethylene and elastomeric materials, sintered metallic fibers and powders, foils and grease-filled joints. It was noted that judicious use of interstitial materials could result in systems whose thermal behavior was not only optimized but predictable. A conductance efficiency was used to evaluate the relative merits of the various interstitial materials.

While there are numerous studies of sliding contacts with heat transfer, the review by Kennedy (1984) provides perspective on the thermal and thermomechanical effects in dry sliding. Among the topics reviewed are thermal deformation around sliding contacts, the changes in contact geometry caused by thermal deformation and thermoelastic instability, the thermomechanical stress distribution around frictionally heated and thermally deformed contact spots, the measurement and analysis of surface and near-surface temperatures resulting from frictional heating, and the mechanisms of frictional heating. The influence of thermal and thermomechanical contact phenomena on various modes of failure was also discussed.

General Theoretical/Analytical Studies

While there is thermal resistance associated with essentially all physical geometries in which heat flows across an interface, recent literature has focused on selected areas. Of specific interest has been the theoretical and analytical characterization of the thermal resistance problem.

Point Contacts. The reviews by Antonetti and Yovanovich (1984), Yovanovich et al. (1986), and Yovanovich (1987) provided an excellent overview of the state of the art in theoretical and analytical thermal contact resistance problems and models, particularly in the area of point contacts and conforming rough surfaces. In the last few years there have been some advances in the analyses of thermal contact resistance problems, and several of these are described here.

A numerical solution for the heat conduction through a joint composed of surfaces characterized as frustrums of cones was developed by Madhusudana (1980a) as a model for the asperities on contacting surfaces. The conical asperity was surrounded by a conducting medium or a vacuum. The model provided temperature profiles and demonstrated that the constriction resistance was reduced significantly because of the presence of a conducting fluid and that the resistance decreased with increasing cone semi-angle.

Yovanovich et al. (1982b) presented a series of thermal contact conductance models incorporating surface microhardness distributions. These models were based on the bulk hardness or isotropic hardness throughout the surface, an iterative approach based on a surface microhardness distribution, an in-

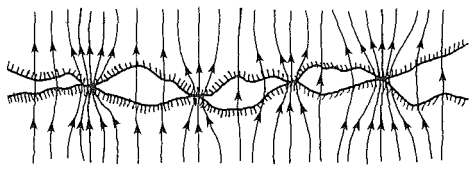

Fig. 1 Heat flow through a joint

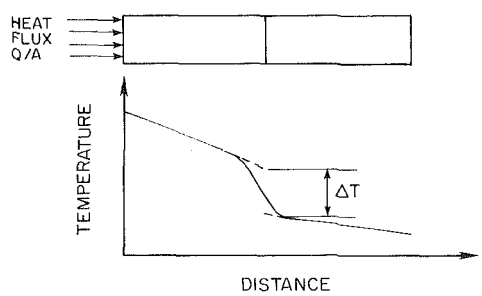

Fig. 2 Temperature variation along two bars joined together

Downloaded 16 Dec 2010 to 193.140.21.150. Redistribution subject to ASME license or copyright; see http://www.asme.org/terms/Terms_Use.cfm

tegral approach that assumed that each asperity has a hardness distribution corresponding to the hardness layer, and a direct approximation method, which involves the determination of an effective hardness for a particular surface at the mean contact pressure. The predictions of the contact conductance as determined with these models were compared with experimental data obtained by Yovanovich et al. (1983). In these comparisons, the use of the bulk hardness model significantly overpredicted the experimental data, whereas the iterated model resulted in reasonable agreement. The integral approach and direct approximation models resulted in excellent agreement with the data. Based on the comparisons, it was suggested that the direct approximation method would be the most suitable model to use for predicting the contact conductances for rough conforming surfaces.

Negus and Yovanovich (1984a) used an approximate technique for the solution of the thermal constriction resistance parameter for a wide range of relative contact sizes. The technique, which was used for an isothermal, circular disk supplying heat to a semi-infinite coaxial cylinder, consisted of superposing Neumann-specified solutions to Laplace's equation. A least-squares criterion was used so that the mixed boundary conditions could be approximated. Results of the analysis were compared by means of a correlation equation. Negus and Yovanovich (1984b) also obtained solutions to other combinations of other geometries for the case of uniform flux and various isothermal boundary conditions.

A thermal constriction resistance expression for an isotropic rough surface was developed by Negus et al. (1985) utilizing the method of infinite images. An elemental heat flux tube consisting of an elliptical contact on a semi-infinite adiabatic rod of rectangular cross section was used in the analysis. For small contact sizes, the constriction resistance was shown to be a perturbation of the half-space resistance. Through use of the surface element method and the method of infinite images, approximate expressions for the two low-order perturbations were developed. This approximation of the dimensionless thermal constriction resistance parameter provides a useful technique for analyzing the heat flow paths between real contacting surfaces.

The effect of a coating material (with different mechanical and thermal properties) on the short-time and steady-state constriction resistance was analyzed by Dryden et al. (1985) for an arbitrary axisymmetric contact spot flux. In the limit of very short times, the constriction resistance was equivalent to one-dimensional transient heat flow through a two-layer wall. For steady state, the effect of the coating was primarily dependent on the relative thermal properties of the coating and substrate.

Multiple Contacts. An approximate technique for determining the thermal contact resistance of a set of multiple circular contacts on half-spaces or circular flux tubes was developed by Saabas and Yovanovich (1985), using both surface element methods and superposition techniques. The results of this novel analytical-numerical method compared favorably with other models, and in the limiting case of a single elliptic contact on a half-space, compared favorably with published analytical solutions. Tabular results were presented for both half-spaces and flux tubes.

Ronzon et al. (1986) utilized the finite element method to analyze the thermal resistance across contiguous, rough interfaces. The interface shapes included saw-tooth, sine-wave, and square-wave profiles. Parametric studies were conducted to ascertain the influence of the interface profile on the thermal resistance. Results indicated that the resistance was decreased below the one-dimensional, smooth interface value. Solutions presented were estimated to be within 1 percent of the actual value of the incremental resistance. Observations indicated that the reduction in resistance increased as the interface material increased.

The contact pressure is extremely important in predicting the thermal contact conductance, and Song and Yovanovich (1987a) developed an explicit expression for the contact hardness and the relative contact pressure for nominally flat but microscopically rough surfaces. This expression was used for parametric studies and demonstrated the relative dependence of the contact pressure and hardness on the surface roughness, asperity slope, and Vickers microhardness correlations. Predictions utilizing the explicit expressions were in excellent agreement with experimental data obtained in their investigations and those of Eid and Antonetti (1986) and Peterson and Fletcher (1988b).

The theory of conforming rough surfaces was used by Negus et al. (1987) to predict the thermal contact resistance for dissimilar metal junctions, where mass diffusion processes produced a continuous alloy distribution. The diffusion process was found to raise or lower the constriction factor depending on whether it was a conductive or resistive alloy layer. The general expression for the thermal constriction factor for a circular flux tube with a layer of linearly varying thermal conductivity was determined for a circular contact with flux-specified boundary conditions. Results were presented in dimensionless thermal and geometric constriction parameters, using a copper–nickel diffusion interface as an example.

A new physically realistic thermomechanical model was developed by DeVaal et al. (1987) for predicting the contact conductance of both nominally flat, rough surfaces having variations in the surface slope with direction, and surfaces prepared by normal machining processes. The model was based on the assumption that the heat transfer across the interface was controlled by the constriction of heat passing through the individual contact regions, and that if the geometry of these individual contact regions were known, thermal models could be developed. The model represented a direct theoretical extension of previous correlations for isotropic, or slope invariant, surfaces, and was expected to be useful for finely ground, conforming surfaces. Based on a comparative study with the model, anisotropic surface pairs with aligned slope direction were found to be more resistive than similar surface pairs with perpendicular slope directions, and preliminary experimental data verified the suitability of the model for such surface geometries.

The thermal accommodation coefficient is used to represent the extent to which an interchange of energy takes place when a stream of gas molecules impacts a solid surface. A thermal accommodation coefficient correlation for engineering surfaces was developed by Song and Yovanovich (1987b) using experimental data for monatomic gases on several types of surfaces. It should be noted that the accommodation coefficient was significantly greater for engineering surfaces than that for clean surfaces. The correlation was used to predict the thermal accommodation coefficient for diatomic/polyatomic gases within 25 percent.

In recent years there have been significant advances in theoretical/analytical models used to predict the thermal contact resistance at an interface. Models and correlations suitable for selected conditions and geometries have been developed and refined with remarkable success and accuracy, and each new model has improved the overall understanding and knowledge of the phenomenon. Nevertheless, the diverse nature of the thermal contact conductance phenomenon is such that a generalized prediction technique has not been developed.

Thermal Conductance in Advanced Materials

There have been a number of investigations of heat conduction in engineering materials. Conduction occurs in such

Downloaded 16 Dec 2010 to 193.140.21.150. Redistribution subject to ASME license or copyright; see http://www.asme.org/terms/Terms_Use.cfm

diverse media as insulation materials, reinforced laminates, filament wound structures, geological strata, printed circuit boards, and aerospace components. As a consequence, there has been increasing interest in understanding the thermal contact conductance phenomenon and its relationship to porous, layered, and composite materials.

Porous Materials. Transient conduction and radiation heat transfer through planar porous thermal insulation was analyzed by Tong et al. (1984). The analysis was directed toward the use of transient methods for measuring the thermal conductivity of porous insulation, since steady-state methods require long times to establish thermal equilibriums. The analysis incorporated the thermal conductance of the material and the two flux equations for radiation heat transfer. The material was treated as an isotropic homogeneous porous medium that absorbed, scattered, and emitted thermal radiation. Results of the analysis suggested that when the porous material was a lightweight fiberglass insulation, neglecting radiation would result in significant errors in predicting the hot-wall temperature rise.

Zwart and Yovanovich (1985) modeled a simple packed system of identical spheres as an equivalent homogeneous substance having an effective thermal diffusivity, and they analyzed the transient, one-dimensional conduction within the system. The analysis incorporated the influence of the constriction resistance within the spheres and the gap resistance between the contacting spheres. The temperature profile in the material and the effective thermal conductivity of the heterogeneous material were evaluated. Results of the analysis showed that the effective thermal diffusivity is dependent upon the lumped parameter effective diffusivity, time, position within the system of spheres, and the total number of spheres. The sphere-packing arrangement and boundary conditions were also found to affect the effective diffusivity.

A theoretical model for the thermal conductivity of a consolidated mixture of two metal powders was developed by Hasley (1986), using the technique of volume averaging to produce working equations applicable to thermal conduction through mixtures. Modeling of mixtures is complex; therefore, the analysis was restricted to components that were well known and characterized. An experimental investigation was conducted for different mixture volume fractions of 70/30 Brass and 316 Stainless Steel to above 90 percent theoretical density, using both air and water as saturants. Experimental results were presented in both tabular and graphic form. Both the experimental data and the published data compared favorably with the values predicted by the model.

An inversion method for determining effective thermal conductivities of porous materials was developed by Kamiuto and Iwamoto (1987a). The method utilized numerical simulations and observed mean effective thermal conductivities. The effective thermal conductivity of glass beads was used successfully to predict temperature profiles within the glass bead layer. In an extension of the work, Kamiuto and Iwamoto (1987b) analyzed the combined conductive and radiative heat transfer through a layer of glass particles, using different layer thicknesses. The theory for predicting the effective conductivity of a glass particle layer by conduction was found to be accurate for ratios of the disperse phase to continuum phase of about 0.5 to 100. The present analytical method reported accurately predicts heat transfer and temperature profiles for a layer of glass particles having comparatively larger diameters.

As a result of increasing interest in moist porous media, Woodbury and Thomas (1985) conducted an experimental investigation to determine the variation of the effective thermal conductivity of a highly porous glass fiber insulation with moisture content ranging from zero to 100 percent on a dry mass basis. The experimental study utilized a spherical thermistor operating in a self-heating mode and providing local effective conductivity values. Results indicated that there was a strong nonlinear dependence of thermal conductivity on mositure content and that currently available models do not adequately reflect the observed thermal behavior of the moist fiberglass insulation.

Vafai and Alkire (1984) investigated the effects of an external boundary and variable porosity on heat transfer for flow through a variable-porosity medium. Packed beds for 5 and 8-mm-dia beads were used for different packings. Variable porosity close to an impermeable boundary led to flow maldistribution and channeling, or the occurrence of maximum velocity in a region close to an external boundary. It was noted that different packings do not significantly alter the heat transfer process for a given bead size. The average Nusselt number, which incorporates the effect of thermal work on the activity of the bed, was correlated with the Reynolds number based on bead diameter using a linear correlation. The experimental results were found to compare favorably with the resulting correlation for different packings.

Peterson and Fletcher (1987a) conducted an experimental investigation to determine the thermal contact conductance of packed beds of spherical particles in contact with flat surfaces. Beds comprised of Aluminum 2017-T4, Yellow Brass, Stainless Steel 304, and Chromium Alloy AISI 52100 were placed in contact with flat Stainless Steel 304 surfaces. Tests were conducted at a mean interface temperature of 66°C over an apparent contact pressure range of 0.2 to 8.0 MPa. An expression for the correlation of the data was developed utilizing the earlier work for single, large sphere–flat contacts and for large numbers of microscopic asperities. Data for both large single-point contacts and small, multiple contacts compared favorably with the correlation expression because the interface between beds of spherical particles and flat surfaces could be predicted with a high degree of accuracy.

Since heat pipe wicking is frequently comprised of sintered metal materials, Peterson and Fletcher (1986) conducted an experimental investigation of the effective thermal conductivity of sintered heat pipe wicks. The investigation included both sintered Nickel 200 and sintered copper powders over a temperature range of 25°C to 100°C, with several porosities in both dry and water-saturated conditions. The experimental results were found to compare favorably with Dul'nev (1965) and with other published experimental data. The effective thermal conductivity of the sintered materials was found to be a function of the thermal conductivity of the metal from which the sintered powder was made, the thermal conductivity of the fluid filling the pores, the porosity, and the mean sample temperature.

Layered Materials. The thermal contact resistance of layered materials has taken on increased importance in printed circuit boards, transformer systems, insulation, motor/generator armatures and fields, and surface oxides or material coatings. The determination of the thermal resistance of layered slabs is particularly important when energy dissipation is required.

In order to consider the influence of oxide films on the thermal resistance of contacts, Al-Astrabadi et al. (1980) developed an analysis for the thermal resistance of oxidized flat, randomly rough metallic surfaces using stochastic representations of surface microtopography with assumed uniform film thicknesses. Experimental data for oxidized contacts between EN3B mild steel surfaces were obtained and surface topographies and oxide film thicknesses were measured. The resulting data compared favorably with the theory developed for oxide films; however, the experimental data were obtained only for first loading of new surfaces.

Sheffield et al. (1980) investigated the steady-state thermal contact conductance of multilayered, electrically insulated sheets. Experimental tests were conducted for twelve combina-

Downloaded 16 Dec 2010 to 193.140.21.150. Redistribution subject to ASME license or copyright; see http://www.asme.org/terms/Terms_Use.cfm

tions of sheet materials and surface coatings in vacuum and low-pressure helium environments. The analysis considered a stack of laminations composed of a number of similar contact elements and evaluated the model utilizing the steady-state temperature distribution in a plate. The analysis compared favorably with Veziroglu et al. (1979) and comparison with experimental results indicates excellent agreement. Sheffield indicated that the predictive model could be improved, however, through the inclusion of an effective microhardness.

The heat transfer through a two-material, periodically layered, semi-infinite solid was investigated by Hagen (1987). The analysis utilized a Fourier series, and the specific heat and density of the layers were assumed equal. A perturbation expansion was used to provide a solution to the unsteady conduction problem. The analysis provided a reasonable prediction of the temperatures within the periodically layered, semi-infinite medium.

Luu et al. (1986) investigated the heat transfer in evacuated multilayer and mass insulations, considering relatively large amounts of residual gases. Models were used to study the contributions of gas conduction, solid conduction, and radiation. These models were based on the temperature jump theory and existing fibrous insulation formulations. Experimental data were obtained for two multilayer insulation specimens with residual gases of air and hydrogen. Results of the investigation indicated that the characteristic dimensions of an evacuated insulation significantly affected the performance in the presence of residual gases. The thermal accommodation coefficients between air and the materials were higher than those for hydrogen and the multilayer insulation materials.

Composite Materials. Although most composite material research has been directed toward the determination of mechanical properties, the use of composite materials in high-temperature applications and the thermal characteristics of such materials are equally important. The thermal contact conductance and thermal conductivity of composite materials are particularly important as new composite materials are developed. Han and Cosner (1981) summarized an analytical study of the steady-state effect of thermal conductivities of fiber-matrix type composites. Of particular importance was the proximity effect of embedded fibers dispersed uniformly in a matrix of region. The dispersion patterns included unidirectional fibers in a matrix and a configuration with fibers perpendicular to each other. The analysis was based on a two-region steady-state heat conduction solution. The results provided a technique for estimating the thermal conductivity of the fibrous composite.

Continuing the study of short-fiber reinforced composites, Takao and Taya (1986) developed a formulation for the effect of the thermal expansion coefficient and the thermal stresses induced around the fibers. Particular emphasis was placed on a carbon fiber/aluminum material. A parametric study was conducted, and the results were useful for the prediction of the thermal expansion coefficient for short fiber composites, as well as for the analysis of the stress in and around the fiber. Han et al. (1985) conducted an investigation of the effective thermal conductivity of graphite–epoxy composites with various fiber orientations and fiber content of 60 percent by volume. Analysis of the results suggested that there was a correspondence between the directional effect of conductivity of composites with unidirectional fibers. Further, the correspondence principle permitted an estimate of the conductivity of other balanced composite materials.

An investigation of the thermal resistance between cryogenic components was conducted by Yoo and Anderson (1983) in order to enhance the thermal resistance between mechanical contacts at temperatures below 4 K. A number of material junctions were considered, including copper, lithium fluoride, oxidized aluminum, sapphire, fiberglass, and thermal bonding cement. Results indicated that a thermally bonded metal/dielectric joint had the lowest resistance and that the use of sapphire plates separated by alumina powder increased the thermal impedance by a factor of more than 106.

Experimental thermal contact resistance values for selected metals and composites were obtained by Marchetti et al. (1987) for aerospace applications. Observed average values of thermal resistance indicate the relevance of the whole thermal resistance, particularly for small composite material thickness and metal/composite interfaces. Results were presented in graphic form for graphite-epoxy laminates and glass–epoxy laminates, as well as for traditional metals.

Madhusudana (1980b) conducted an experimental investigation of Zircaloy-2/uranium dioxide interfaces, and Madhusudana and Fletcher (1983) developed a power-law correlation to predict the dependence of nondimensional thermal contact conductance on nondimensional contact pressure for Zircaloy-2/uranium dioxide surfaces in contact. The correlation incorporated a wide range of data for joints formed by flat surfaces; however, cylindrical surfaces were not included since the contact pressure may only be inferred indirectly for these surfaces. The analysis took into account the effect of the mean interface temperature on the contact conductance, and utilized simple power laws to deduce the relationship between nondimensional conductance and nondimensional pressure. The correlation compared favorably with all of the data and results within a standard deviation of only 6.78 percent, as noted in Fig. 3.

The effect of the thermal conductivity of uranium dioxide fuel materials was investigated by Peterson et al. (1987a, 1987b) for the case in which fuel elements are comprised of packed beds of spherical or near-spherical particles. Analytical and experimental investigations were reviewed in order to develop a technique for determining the thermal conductivity of beds of packed spherical particles used in reactor fuel elements. Analytical techniques were presented and compared with existing experimental data. The results of the investigation indicated that additional analytical and experimental investigations are necessary in order to provide accurate predictions of the effective thermal conductivity of sphere-pac reactor fuels.

Thermal Conductance in Microelectronics

The optimization of microelectronic systems poses significant thermal design and analysis problems because of the in-

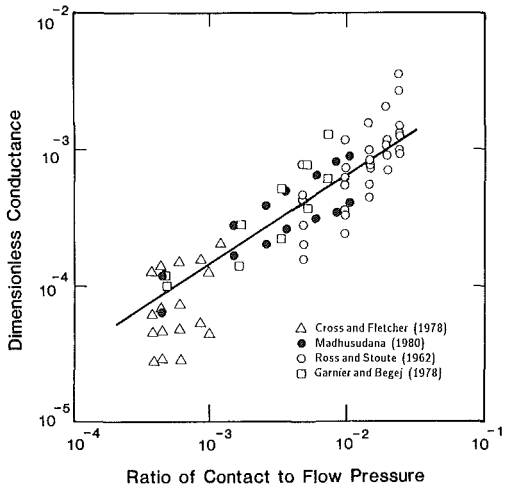

Fig. 3 Comparison of thermal contact conductance data for Zircaloy 2/uranium dioxide with a proposed correlation by Madhusudana and Fletcher (1983)

Downloaded 16 Dec 2010 to 193.140.21.150. Redistribution subject to ASME license or copyright; see http://www.asme.org/terms/Terms_Use.cfm

creased thermal loads that occur when components are miniaturized. The heat generation within microelectronic circuits, printed circuit boards, and multichip modules has become the primary factor that limits the physical size of both the individual components and multichip modules (Kraus and Bar-Cohen, 1983). The thermal environment and associated high temperatures could lead to overheating, significantly reducing component performance and increasing the possibility of total failure. As a consequence, there is an increasing interest in improving the thermal conductance at interfaces within microelectronic systems.

As a result of the increased interest in the cooling problems associated with microelectronic systems, an International Symposium on Cooling Technology for Electronic Equipment was held in 1987. This Symposium addressed such issues as air cooling techniques, liquid cooling techniques, thermal systems modeling, conduction cooling, and internal resistances. The conduction cooling and internal resistance area includes various aspects of thermal contact resistance. The recent literature concerned with thermal contact resistance in microelectronic systems may be divided into two general categories, those investigations dealing primarily with theoretical/analytical or numerical studies of heat transfer in microelectronic systems and components, and those investigations which are more experimental in nature.

Analytical Studies. In the area of theoretical analyses, Yovanovich et al. (1986a) developed analytical one and two-dimensional solutions for annular fins of constant thickness in a configuration that might be used as a heat sink for a microelectronic chip. The solutions were reduced to polynomial form for use in calculating the heat loss ratio as a function of dimensionless geometric and fin parameters. Numerical computations were performed for selected conditions, and graphic results were provided for the heat loss rate ratio as a function of the Biot number for selected fin-diameter ratios.

The contribution of contacting surfaces was statistically estimated by Haji-Sheikh and Lakshminarayana (1987) in an analytical/numerical Monte Carlo solution for temperature distribution within a silicon chip. The contact resistance values for the silicon chip analysis were developed by Chu et al. (1982). The resulting solution provided the temperature at critical points within the chip and surrounding bodies.

A three-dimensional finite difference numerical model with thermal resistance measurements was used by Chyu and Aghazadeh (1987) to study the thermal performance of an internally molded heat spreader for a 48-lead, plastic, dual, in-line package (PDIP) and a 68-lead, plastic, leaded chip carrier (PLCC). A parametric study of the heat spreader characteristics was conducted, and the results indicated that the package thermal resistance was strongly influenced by the area and location of the heat spreader but relatively insensitive to the heat spreader thermal conductivity and thickness. Favorable agreement was noted between the model and experimental measurements, and the use of such models was recommended for predictions of IC package thermal performances.

Negus and Yovanovich (1987) developed a thermal analysis procedure for semiconductor dies using fundamental solutions with surface element methods and arrays of images. The thermal analysis procedure was demonstrated with a complex contact distribution example, and the results indicated that for high power applications, silicon performed significantly better than gallium arsenide. As a consequence, the layout of gallium arsenide circuits appeared to be of importance due to the internal resistance. The thermal analysis procedure was developed as an efficient computational tool for designers involved in the circuit layout of semiconductor dies.

In view of the increased demands on microelectronic system design, Vanoverbeke et al. (1987) developed an approximate expression for the thermal resistance of bolted microelectronic chip carriers. The system investigated consisted of a semiconductor die mounted on a cylindrical carrier, which was bolted to a large heat sink. The thermal resistance of the carrier represented a significant portion of the overall thermal resistance. Parametric studies were conducted for a selection of geometric and loading criteria to provide the lowest possible thermal resistance. For carriers with a thickness less than optimum, there was a reduction in the thermal resistance. Conversely, for carriers with thicknesses above the optimum value, there will be an increase in the resistance.

Theoretical/analytical/numerical models of the heat transfer or thermal resistance of microelectronic systems and modules provide excellent opportunities for parametric studies. These studies permit the development of system designs that have reduced thermal resistance, greater heat dissipation, optimum spacing and sizing, and better materials selection. Such studies are extremely useful in analyzing new components and designs. While some of these theoretical/analytical/numerical investigations have included experimental data for comparison, other investigations have not. In most instances, real semiconductor systems and geometries are sufficiently complex that modeling techniques are difficult to use and experimental investigations have been conducted to provide data for analysis.

Experimental Studies. Because a majority of the thermal contact resistance data are not directly applicable to microelectronics applications, Eid and Antonetti (1986) conducted an experimental investigation of aluminum in contact with a silicon chip in air, argon, and vacuum environments. The test surfaces were appropriate for microelectronics applications, i.e., ground aluminum and polished silicon surfaces. The contact pressures were lower than those of previous studies, and the test samples were similar in size to semiconductor chips and modules, on the order of 4 mm^2. The experimental data compared favorably with correlations for the solid component of the thermal resistance in a vaccum, and the gap component compared well with the correlations of Yovanovich et al. (1983). Accommodation coefficients estimated from the data also compare well with published values.

The thermal contact resistance occurring at the bonded joints between silicon chips and substrate materials was investigated by Peterson and Fletcher (1987b), utilizing seven conductive epoxies (with a wide range of thermal conductivities) in contact with ground aluminum surfaces. Although the thermal contact resistances were relatively constant with respect to mean junction temperature, the contact resistance component of the overall joint resistance increased markedly with respect to the thermal conductivity of the diebond materials. Based on these data, an expression was developed for predicting the overall thermal resistance as a function of the void fraction, the thermal conductivity and thickness of the diebond material, and the void fraction.

Peterson and Fletcher (1988b) also evaluated the thermal resistance between substrate and mold compound materials. The investigation included four mold compounds and three heat spreader materials over a range of 20°C to 70°C at interface pressures of 0.5 to 5.0 MPa. Results of the investigation indicated that the mold compound and substrate/spreader interface in electronic equipment was relatively constant with respect to the mean interface temperature but varied significantly with changes in the interfacial pressure. The correlation proposed by Yovanovich et al. (1983) for metal-to-metal interfaces was shown to predict the thermal contact resistance at these interfaces accurately.

Downloaded 16 Dec 2010 to 193.140.21.150. Redistribution subject to ASME license or copyright; see http://www.asme.org/terms/Terms_Use.cfm

Techniques for enhancing the thermal conductance of a joint have been discussed by Fletcher (1984), Fletcher and Peterson (1986), and Yovanovich (1987). Thermal enhancement generally involves the use of interstitial fluids, greases, or metal foils at the interface. In view of the fact that greases migrate with time, metallic foils or metallic coating on surfaces may provide a more suitable technique for thermal enhancement of electronic chips and modules.

Peterson (1987) presented a summary of two methods by which the thermal contact resistance occurring at the metal-to-metal interfaces might be reduced. These methods included the use of thin metallic foils and metallic surface coatings. Comparative published data are presented for metallic foils and coatings for selected material combinations.

Peterson and Fletcher (1988a) presented a brief review of recent experimental and analytical investigations utilizing thin metallic foils with applications to microelectronic systems, along with the results of an experimental investigation of selected soft metallic foils. This investigation evaluated the effects of surface roughness along with foil hardness and thermal conductivity for optimum foil thicknesses. Results indicated that for optimum conditions of foil thickness and surface roughness, the thermal resistance could be reduced by a factor of as much as seven over the bare junction resistance. The study concluded that for metallic foils to be effective for thermal enhancement uses, the foils must be very thin, and that the parameter proposed by Yovanovich (1987), k/H, could be used to rank the thermal enhancement of various foils. Comparisons of metallic foil and coating characteristics are given in Figs. 4 and 5.

Chou and Jou (1987) conducted experiments to ascertain the effects of thermal greases with metal powder at the interface between two metallic surfaces in contact. The thermal grease was observed to serve as an interface filling medium, eliminating the air or gas trapped at the interface. Thermal grease with 10 to 20 weight percentage of copper powder decreases the thermal resistance; however, larger quantities of powder increase the thermal resistance and decrease the fluidity of the grease mixture.

Pinto and Mikic (1987) proposed a novel design concept for reduction of the equivalent thermal contact resistance for electronic equipment applications. The concept incorporated an increase in the apparent interface area without changing the projected area between the two components, utilizing two or three-dimensional matching features such as ribs and grooves, or pins and holes. The analysis indicated that the equivalent thermal contact resistance could be reduced substantially by modifying the contact area. The minimum contact resistance ratio possible was essentially the ratio between the flat interface and the extended surface areas.

Thermal Conductance in Biomedicine

Heat transfer mechanisms in and between biomaterials have received increasing attention with the development of synthetic organs, tissues, and other implantable devices. Knowledge of the thermal properties of biomaterials, as well as in situ tissue, is essential to modeling and to the development of new materials and organs. There are numerous circumstances in which the temperature gradient and the temperature difference between body tissues or fluids and implantable materials affect the overall performance or comfort of implantable devices. These circumstances include coronary angioplasty (removal of atherosclerotic plaque on arterial walls), the selection of appropriate bone cements for implantable replacement joints, measurement systems requiring

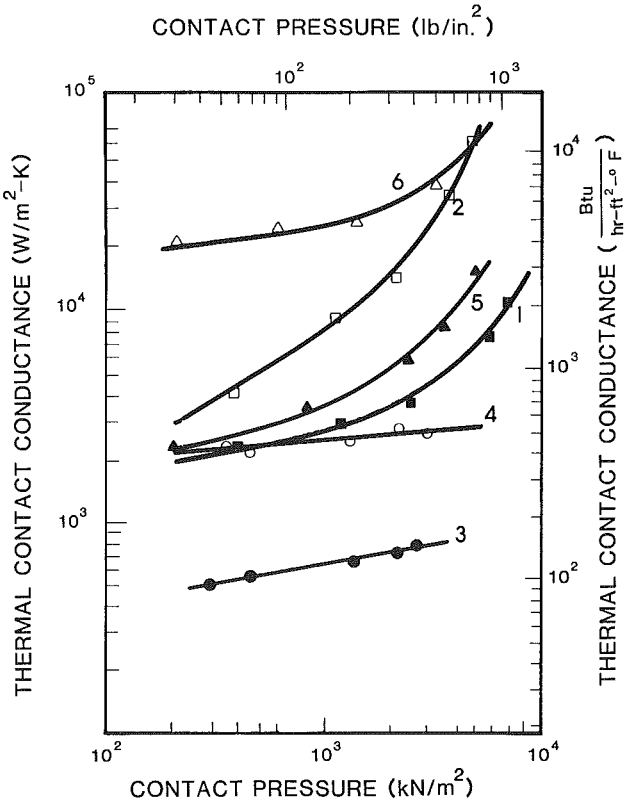

Fig. 4 Effect of metal foils on thermal contact conductance (Peterson, 1987): (1) SSKh18N9T bare interfaces; (2) SSKh18N9T interfaces with copper foil; (3) SSKhN789T bare interfaces; (4) SSKhN789T interfaces with copper foil; (5) molybdenum VM-1 bare interfaces; (6) molybdenum VM-1 interfaces with copper foils

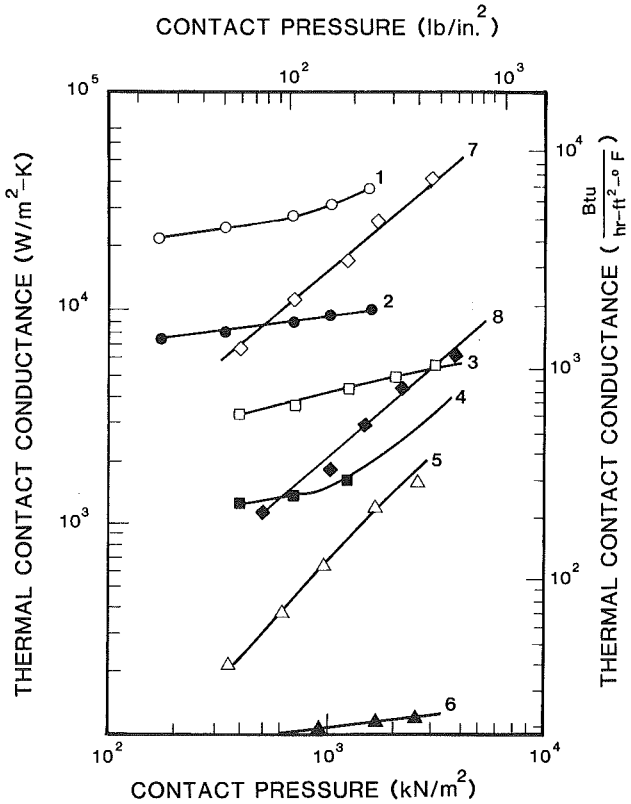

Fig. 5 Effect of metallic coatings on thermal contact conductance (Peterson, 1987): (1) bronze surface coated with tin/nickel alloy; (2) uncoated bronze alloy; (3) SS surface coated with silver; (4) uncoated SS surfaces; (5) SS surface coated with aluminum alloy; (6) uncoated SS surface; (7) nickel surface coated with nickel alloy; (8) uncoated nickel surfaces

Downloaded 16 Dec 2010 to 193.140.21.150. Redistribution subject to ASME license or copyright; see http://www.asme.org/terms/Terms_Use.cfm

intrusive catheters and probes, dental cements for installation of crowns or caps, and other biomedical applications.

A number of methods have been proposed for the dissolution or removal of atherosclerotic plaque utilizing surgical, chemical, and mechanical means. One recent technique deals with the use of a laser catheter for removal of plaque in both normal and diseased vessels by means of vaporization (Lee et al., 1981, 1983). Because excessive temperature at the artery wall may damage the artery as well as the surrounding tissue, the removal of plaque using laser techniques requires accurate temperature control as well as knowledge of the temperature gradients, tissue thermal conductivity, and thermal contact conductance of the plaque-arterial wall interface. Valvano et al. (1984) provided experimental measurements of the thermal conductivity and thermal diffusivity of atherosclerotic plaque and arterial walls from the human circulation system, using self-heated microthermistor probes over the temperature range of 25°C to 95°C. The atherosclerotic plaque investigated was categorized as fibrous, calcified, or fatty.

There are a number of factors that contribute to the failure of total joint prostheses, and one of the major factors is a loosening of the cement-bone interface, as noted by Liu et al. (1981). Failure at this interface is attributed to fatigue cracking of the bone-cement interface and resorption of bone. In addition, according to DiPisa et al. (1976), the high temperature attained by the cement during polymerization may cause tissue necrosis at the cement-bone interface. Further, the widely different material properties of bone and bone cement lead to a thermal discontinuity or a thermal resistance at the interface. This thermal contact resistance contributes to the loosening of the cement-bone interface. As in all thermal contact resistance problems, the surface characteristics of the bone and the replacement component are important, and Geiger and Greenwood (1981) proposed several surface preparation techniques. The characteristics of the thermal resistance at the cement-bone interface are not clearly understood and warrant further investigation.

Octerbeck et al. (1988) investigated the thermal contact conductance at the interface between bone, polymethylmethacrylate (PMMA)-based bone cements, and stainless steel. Measurements were made for both the thermal contact conductance of the bone-cement interfaces and the thermal conductivity of the bone for both saturated and dry conditions. The temperatures used, 286 K to 300 K, were similar to those presented previously for noncancellous bone. Both high-viscosity and low-viscosity bone cements were used for the investigation, with the high-viscosity cement resulting in the lower thermal contact resistance values.

Due to the surgical inaccessibility of some tumors, lesions, and cancerous regions of the human body, focused heat is used as a means for destroying diseased cells. Localized heat may be used as a therapeutic tool for precisely localized necrosis, particularly with reference to the central nervous system. Techniques for providing localized heating include thermal probes, radiofrequency probes, or ultrasound. Each of these techniques is appropriate for certain therapeutic uses. Thermal probes heated by temperature-controlled fluids or by electricity may be used for soft tissue as well as bones. Radiofrequency probes, such as those used in neurosurgery, may also have potential applications in bone surgery. Ultrasound has obvious advantages due to its nonintrusive nature, and offers selective heating in soft tissue. The use of ultrasound is not appropriate in bone due to the high absorption coefficient compared to soft tissue. Thermal probes or radiofrequency probes may be used for the treatment of certain cancers. The temperature of the treated area, however, must be carefully controlled and is generally measured with catheters composed of thermocouples and hypodermic needles. The primary problem with such measurements is perceived to be the thermal contact resistance between the thermocouple and hypodermic needle.

Selected Topics

Although the primary areas of recent contact heat transfer work have been reviewed in earlier sections of this paper, there are other equally interesting aspects of contact heat transfer that warrant consideration in this review. Special topics include the thermal conductance of dissimilar metals and the associated thermal rectification phenomenon, the contribution of interstitial gases to thermal contact resistance, the problems occurring in cylindrical contact surfaces, as well as periodic and sliding contacts, and the problems associated with the measurement of thermal contact conductance.

Thermal Rectification. There are many situations in which the thermal resistance of dissimilar metal interfaces may be important, including fin-tube heat exchangers, nuclear fuel rods, printed circuit boards, and cryogenic systems. The phenomenon of thermal rectification occurs when the thermal contact conductance of a junction composed of dissimilar metals varies with the direction of heat flow. Occasionally, thermal rectification is also observed for similar metal surfaces with different surface characteristics. Selected data for the thermal conductance of dissimilar metal interfaces are shown in Fig. 6. Padgett and Fletcher (1982) experimentally investigated the thermal contact conductance of aluminum/stainless steel interfaces for apparent contact pressure from 68.9 to 1.33×103 kPa, with mean junction temperatures up to 195°C, for a selected range of surface conditions. Data indicated thermal rectification effects at higher apparent contact pressures.

Williams and Fletcher (1983) reviewed the various, often conflicting, investigations of thermal rectification and found that directional effects existed but that experimental data were inconsistent. Contact behavior was found to be very sensitive to deviations in surface characteristics. Elastic deformations permitted directional effects to exist indefinitely as the heat flow direction was cycled, but plastic deformations resulted in diminishing effects after a few cycles. Published data conflict because of the wide variety of test materials and surface characteristics involved in thermal rectification tests.

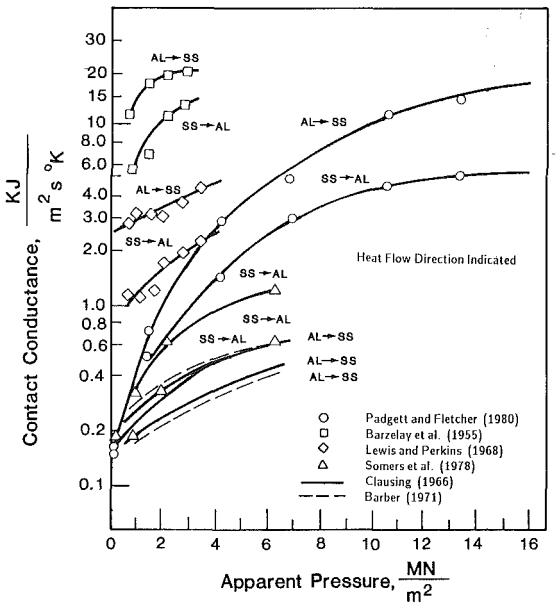

Fig. 6 Variation of contact conduct with apparent interface pressure for selected dissimilar metal surfaces (Padgett and Fletcher, 1982)

Downloaded 16 Dec 2010 to 193.140.21.150. Redistribution subject to ASME license or copyright; see http://www.asme.org/terms/Terms_Use.cfm

In an effort to understand the physical basis of thermal rectification, Somers (1983) and Somers et al. (1987) conducted a semi-quantitative study of an idealized contact between two smooth, frictionless spheres utilizing Hertzian methods. An expression defining the relationship between the contact length and the heat flux through the contact was derived. Thermal rectification was shown to exist between two elastic spheres through which heat was flowing, and this rectification was found to be a function of the thermal distortions on the contact interface which, in turn, were a function of the temperature fields within the contacting bodies. Observations of experimental trends indicated a thermal rectification increase due to increases in apparent contact load, a thermal rectification reversal due to contact surface changes, a thermal rectification reversal due to heat flux magnitude changes, and a reduction in thermal rectification due to the action of microscopic asperity contacts. The contact model developed may be used to explain the existence of these directional bias trends on a quantitative basis.

Gas Conductance. The gases filling the voids between a pair of contacting surfaces may significantly affect the overall heat transfer at a junction between contacting materials. Mentes et al. (1981) developed a model using mixed boundary conditions to determine the thermal contact conductance of coated, multilayered sheets. The fluid thermal conductivity and accommodation coefficient were introduced into the formulation as the equivalent fluid conductivity. Experimental contact conductance data were obtained with environments of vacuum, air, and helium, and the effective hardness values for coated surfaces were ascertained. Based on these values, the accommodation coefficients for the interfacial gas and surface coating combinations were estimated. Tabulated results for accommodation coefficients were included.

Madhusudana and Fletcher (1981c) compared the relationships between the peak-to-peak surface roughness, the effective gap width, and the temperature jump distances proposed by several authors. These comparisons required knowledge of the accommodation coefficient and the relationship between profilometer surface roughness readings and peak-to-peak roughness heights. The relationship between the effective gap width, peak-to-peak height, and temperature jump distance was compared for several different prediction techniques, as shown in Fig. 7. The gas conduction contributed to the overall heat transfer, started to decrease at a gas pressure called the threshold pressure, and became negligible below pressures of 0.13 kPa.

Cylindrical Contacts. The thermal contact conductance of concentric cylinders made of similar or dissimilar materials is somewhat different from planar thermal contact conductance. The apparent contact pressure in coaxial cylinders depends on the initial interference or clearance between cylinders, the differential expansion or contraction due to the temperature gradient, and the differential expansion or contraction due to the temperature difference at the interface between cylinders. For these reasons, it is generally more appropriate to express the contact conductance as a function of heat flux rather than interface contact pressure.

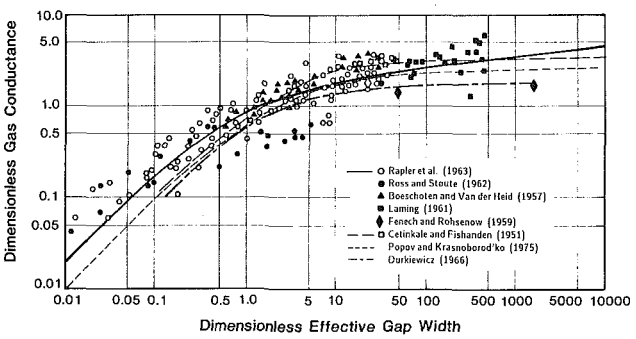

Fig. 7 Comparison of dimensionless gas conductance with dimensionless effective gap width (Madhusudana and Fletcher, 1981c)

Madhusudana and Fletcher (1981b) summarized an experimental investigation of heat transfer occurring across the interface of composite cylinders formed by stainless steel–stainless steel and armco iron–armco iron cylinders. Experimental tests were conducted in vacuum and in an air environment at atmospheric pressure. The data indicated that the conductance increased with increased contact pressure, which resulted from the differential expansion of the cylinders, caused by the radially outward heat flux.

The thermal constriction resistance for two cylindrical surfaces, one with longitudinal grooves, was evaluated by Wang nd Nowak (1981). In this geometric configuration, the lands were in contact, but the grooved area had no contact. This configuration was representative of a double tube heat exchanger for process fluids and lethal gases. The analysis of the cylindrical contacts was based upon steady heat flow, constant thermal conductivities, a two-dimensional temperature distribution, and a perfect contact at the contact land. In view of the mixed boundary conditions, no analytical solution was available. An equivalent heat flux distribution function was employed, however, and results were developed numerically. The results defined the limit of the thermal constriction resistance for cylindrical surfaces.

Chu et al. (1986) utilized the hyperbolic heat conduction equation to investigate the transient response of a finite, composite, hollow cylinder composed of two different materials. The cylinder was heated internally by a moving line source and cooled convectively on the exterior surface. Results of the investigation, which were calculated numerically, showed that the relaxation time and thermal conductivity ratio played an important role in the transient heat transfer. This work, however, assumed perfect contact at the interface.

A theory for prediction of the thermal contact conductance of concentric cylinders was developed by Madhusudana (1986). The contact pressure was calculated in terms of the temperature gradient in one of the cylinders, the initial allowance between cylinders, the surface characteristics, the cylinder radius ratios, the cylinder material properties, and the interstitial medium. The resulting formulation could be used to establish a relationship between the heat flux and thermal contact conductance. These results showed that conductance increased with increased heat flux, because of the resulting increased contact pressure. A surprising conclusion was that for cylindrical joints, a material combination with lower effective thermal conductivity may, in fact, exhibit higher thermal conductance than a combination with higher effective conductivity.

The design and construction of an apparatus to measure the heat transfer performance of cylindrical joints was reported by Madhusudana and Litvak (1987). The apparatus incorporated test specimens that were heated internally and cooled externally. Experimental data were presented for stainless steel interfaces and stainless steel–aluminum interfaces, and the results compared reasonably well with theoretical predictions.

Periodic and Sliding Contacts. Vick and Özişik, (1981) utilized the finite integral transform technique to obtain quasi-steady-state solutions for the problem of two periodically contacting finite regions with imperfect thermal contact at the interface. This investigation focused on the effects of contact duration, thermal contact conductance, thermal conductivity, and thermal diffusivity on the temperature distribution across two contacting surfaces. Moses and Johnson (1987) experimentally examined the problem of periodically contacting similar metal surfaces and obtained results that are comparable in both form and magnitude to those of Vick and Özişik (1981).

Downloaded 16 Dec 2010 to 193.140.21.150. Redistribution subject to ASME license or copyright; see http://www.asme.org/terms/Terms_Use.cfm

Moses and Johnson (1988) also experimentally examined the approach to the quasi-steady-state condition for similar metallic surfaces in periodic contact, focusing on the behavior of the thermal contact conductance during the contact portion of a cycle and on the number of cycles required to reach a quasi-steady-state condition. Results of these experiments indicated that, for cycles with short contact times, the thermal contact conductance varied throughout the contact period, while for longer contact times, a uniform value of thermal contact conductance was ultimately attained. The experimentally obtained temperature distributions from Moses and Johnson (1988) also were examined by Beck (1988) as an example of a parameter and function estimation technique for the inverse heat conduction problem. Utilizing this technique for computing values of the thermal contact conductance, Beck obtained values similar in both form and magnitude to those obtained by the experimental analysis. Utilizing the function estimation analysis, in which the transient conduction equation was solved numerically and the thermal contact conductance was computed at each measured time step, Beck obtained values for the thermal contact conductance that are considerably more uniform than either the experimental analysis or the parameter estimation analysis.

Dodd and Moses (1988) extended this set of experiments to consider periodic contacts between aluminum and stainless steel. Results for this single case of periodic contact between dissimilar metals indicated that the same transient behavior of the thermal contact conductance was observed for all metal pairs.

The flash temperatures of circular and elliptical contact spots for two materials in sliding contact were evaluated by Kuhlmann-Wilsdorf (1987). The parameters used in the analysis included experimental data, the coefficients of friction, known material properties, and the ellipticity and number of contact spots. The prediction equations were simplified for the limiting cases of very high and very low speeds. The effect of sliding rate on the flash temperature through the strain rate dependence of local hardness was considered, and demonstrated to be of considerable importance.

Yuen (1988) developed an analysis of the conduction between sliding solids with heat energy generated along the region of contact. An asymptotic solution for the heat flux position to each solid was used to develop closed-form expressions for the temperature fields in the solids. Based on the analysis, an appropriate parameter was recommended for use with correlations to estimate the thermal penetration into the solids.

Conductance Measurements. Intrinsic problems associated with accurately measuring the thermal contact conductance were discussed by Snaith et al. (1983). The specimen geometry and physical details, the apparatus design and temperature measurement procedures, the test schedules, and the experimental error all affect measurement accuracy. This suggests the need for a standard test procedure for measurement of thermal contact conductance. The authors recommended a number of special criteria for thermal contact conductance testing and analysis including a specimen form ratio, the reduction of transverse heat losses in the measurement system, specific arrangements for facility design and heat metering, temperature measurement and uncertainty procedures, and data presentation. While such a concept has merit, there has been little serious consideration or implementation of these recommendations.

The characteristic of thermal contact resistance was used in the development of a hardness tester by Goldsmid and Johnston (1981). When a probe of relatively low thermal conductivity was pressed against softer materials of higher conductivity, the thermal contact resistance depends upon the radius of contact. A ruby-tipped, heated, copper-constantan thermocouple was applied to several materials of high conductivity, and the resultant thermoelectric EMF generated was found to be directly related to the diagonal length of the indentation produced. Goldsmid (1982) extended the work utilizing a probe with a diamond tip. The load on the diamond-tipped probe was varied until the thermal contact resistance was the same as that of a heated copper-tipped probe. Experimental results for a range of materials indicated that the load required for balance was proportional to the Vickers hardness number.

Problems related to beaded and intrinsic thermocouples were studied both theoretically and experimentally by Cassagne et al. (1986). Analysis of the thermocouples indicated a temperature disturbance and the influence of thermal contact resistance. The perturbations produced in the temperature field were assumed to be the result of several phenomena including macroconstriction of the flux lines, contact resistance at the interface between the thermocouple bead and the material, and the wire environment heat transfer. Results of the analysis were experimentally verified and the errors introduced in the two methods of measurement were analyzed.

Antonetti and Eid (1987) proposed a new procedure for measuring steady-state thermal contact resistance that relied on monitoring the contact resistance rather than the specimen temperatures. The concept was based on the premise that the actual contact resistance should be invariant with time because the capacitance of the contact is extremely small compared to the thermal capacitance of the measurement systems involved. Based on experimental verification using transient techniques, apparent contact resistance reached actual contact resistance values considerably faster than with the traditional steady-state approach.

Conclusions and Recommendations

This review of recent developments in contact conductance heat transfer, although by no means exhaustive, has delineated areas in which recent experimental and theoretical studies have been conducted. The categorization of studies by area permits a more detailed comparison among similar analyses and experimental investigations. These comparisons have suggested several features to be considered in further analysis of contact conductance heat transfer.

Based on recent theoretical analyses, it is clear that the surface parameters are a major factor in thermal contact conductance. Conforming surfaces have been evaluated, and reliable models have been developed for predicting the apparent contact area. Further, effects of geometry have been studied, as have various surface preparation techniques. Nevertheless, further studies are needed to explore areas such as the combination of macroscopic elastic deformations and microscopic plastic distortions.

Inasmuch as each thermal contact conductance geometry is unique, knowledge of the surface characteristics and the material properties is essential to an analysis of the heat transfer. In addition, it can be expected that other characteristics such as load conditions, temperature regime, interstitial media, and geometry should be considered in any analysis of heat transfer at a junction.

There are a number of techniques available for the prediction of thermal contact conductance, although each prediction technique is appropriate for only selected conditions. Very few of these, however, appear to be successful, even over a limited range of conditions. At present, it does not appear possible to develop a generalized prediction technique for all test environments and conditions. While most prediction techniques are suitable for moderate-to-large loads, the studies of low apparent contact pressures have not led to comparable techniques for the prediction of heat transfer. Hence, it would ap-

Downloaded 16 Dec 2010 to 193.140.21.150. Redistribution subject to ASME license or copyright; see http://www.asme.org/terms/Terms_Use.cfm

pear that further investigations would be desirable at low apparent contact pressures.

In view of the increasing miniaturization of microelectronic components and the low apparent contact pressures involved, the dissipation of heat is directly related to the thermal contact resistance of chips, heat spreaders, and associated materials. Continuing investigations of new heat spreaders or chip carriers in conjunction with chip attachment techniques would be desirable.

The increasing focus on biomedical instrumentation and the limited knowledge of the thermal properties and characteristics of biological tissues suggest that further study of the thermal resistance of biological materials is warranted. Of particular interest would be bone/dental cements, catheters, body tissues, and prosthesis components.

With the advent of superconductivity and the continuing quest for higher temperature superconducting materials, it is essential that the thermal contact resistance of such materials be investigated. Initial studies should be conducted at cryogenic temperatures to assess the potential for superconducting material installation.

Plans for the development of a space station, and the continuing desire for more efficient space thermal power systems, suggest the need for a better understanding of thermal contact resistance as it relates to space applications. The desirability of providing optimum spacecraft systems necessitates the improvement of thermal control systems. Further study of contact conductance utilizing selected materials in space environments is important.

Modern composite materials, including metallic ceramics, are being considered for many high-temperature applications, especially in the gas turbine industry. The thermal characteristics of these materials, and the associated thermal contact resistance, will be important design parameters. Continuing experimental and theoretical studies of new materials would be instructive.

The characteristics of rolling and sliding contacts have been investigated from the perspective of frictional heating and the associated tribological behavior. There has been limited study of the thermal and thermomechanical effects in such contacts, and further studies are warranted. Significant thermal contact resistance leads to thermocracking and other forms of failure in rolling and sliding mechanical parts.

References

Al-Astrabadi, F. A., O'Callaghan, P. W., and Probert, S. D., 1980, "Thermal Resistance of Contact: Influence of Oxide Films," AIAA Paper No. 80-1467.

Antonetti, V. W., and Yovanovich, M. M., 1984, "Thermal Contact Resistance in Microelectronic Equipment," in: *Thermal Management Concepts in Microelectronic Packaging*, ISHM Technical Monograph Series 6984-003, International Society for Hybrid Microelectronics, Silver Spring, MD, pp. 135–151.

Antonetti, V. W., and Eid, J. C., 1987, "A Technique for Making Rapid Thermal Contact Resistance Measurements," *Proceedings of the International Symposium on Cooling Technology for Electronic Equipment*, Honolulu, HI, Mar., pp. 449–460.

Beck, J. V., 1988, "Combined Parameter and Function Estimation in Heat Transfer With Application to Contact Conductance," ASME JOURNAL OF HEAT TRANSFER, Vol. 110, this issue.

Cassagne, B., Bardon, J. P., and Beck, J. V., 1986, "Theoretical and Experimental Analysis of Two Surface Thermocouples," *Proceedings of the 8th International Heat Transfer Conference*, San Francisco, CA, pp. 483–488.

Chu, H. S., Chen, J. M., and Tzou, J. H., 1986, "Transient Response of a Composite Hollow Cylinder Heated by a Moving Line Source With Hyperbolic Heat Conduction Equation," *Proceedings of the 8th International Heat Transfer Conference*, San Francisco, CA, pp. 621–626.

Chu, R. C., Hwang, U. P., and Simons, R. E., 1982, "Conductance Cooling for an LSI Package: A One Dimensional Approach," *IBM Journal of Research and Development*, Vol. 26, No. 1, pp. 45–54.

Chyu, M. K., and Aghazadeh, M., 1987, "Modeling and Measurements of Heatspreader Thermal Performance in Molded Plastic Packages," *Proceedings of the International Symposium on Cooling Technology for Electronic Equipment*, Honolulu, HI, pp. 187–199.

DeVaal, J. W., Yovanovich, M. M., and Negus, K. J., 1987, "The Effects of Surface Slope Anisotropy on the Contact Conductance of Conforming Rough Surfaces," *Proceedings of the ASME Symposium on Developments in Contact Resistance*, ASME National Heat Transfer Conference, Pittsburgh, PA, pp. 123–134.

DiPisa, J. A., Sih, G. S., and Berman, A. T., 1976, "The Temperature Problem at the Bone–Acrylic Cement Interface of the Total Hip Replacement," *Clinical Orthopedics and Related Research*, No. 121, pp. 95–98.

Dodd, N. C., and Moses, W. M., 1988, "Heat Transfer Across Aluminum/Stainless Steel Surfaces in Periodic Contact," AIAA Paper No. 88-2646.

Dryden, J. R., Yovanovich, M. M., and Deakin, A. S., 1985, "The Effect of Coatings on the Steady-State and Short Time Constriction Resistance for an Arbitrary Axisymmetric Flux," ASME JOURNAL OF HEAT TRANSFER, Vol. 107, pp. 33–38.

Dul'nev, G. N., 1965, "Heat Transfer Through Solid Disperse Systems," *Inzhenero-Fizicheskii Zhurnal*, Vol. 9, No. 3, pp. 399–404.

Edmonds, M. J., Jones, A. M., and Probert, S. D., 1982, "Thermal Contact Resistance for Hard Machined Surfaces Pressed Against Relatively Soft Optical Flats," *Applied Energy*, Vol. 6, pp. 405–427.

Eid, J. C., and Antonetti, V. W., 1986, "Small Scale Thermal Contact Resistance of Aluminum Against Silicon," *Proceedings of the 8th International Heat Transfer Conference*, San Francisco, CA, pp. 659–664.

Feldman, K., Hong, Y., and Marjon, P., 1980, "Test of Thermal Joint Compounds to 200°C," AIAA Paper No. 80-1466.

Fletcher, L. S., 1984, "The Influence of Interstitial Media on Spacecraft Thermal Control," *Proceedings of the 14th International Symposium on Space Technology and Science*, Tokyo, Japan, pp. 527–532.

Fletcher, L. S., and Peterson, G. P., 1986, "The Effect of Interstitial Materials on the Thermal Contact Conductance of Metallic Junctions," *Proceedings of the Heat Transfer in Thermal Systems Seminar—Phase II*, National Cheng Kung University, Tainan, Taiwan, pp. 1–8.

Geiger, J. M., and Greenwood, A. S., 1981, "Surface Preparation Techniques at the Bone-Cement Interface," *Proceedings of the 34th ACEMB*, Houston, TX, p. 291.

Goldsmid, H. J., and Johnston, J. N., 1981, "A Hardness Tester Based on Thermal Contact Resistance," *J. Physics E: Sci. Instrum.*, Vol. 14, pp. 1329–1331.

Goldsmid, H. J., 1982, "A Thermal Balance for Hardness Testing," *J. Physics E: Sci. Instrum.*, Vol. 15, pp. 173–174.

Hagen, K. D., 1987, "A Solution to Unsteady Conduction in Periodically Layered, Composite Media Using a Perturbation Method," ASME JOURNAL OF HEAT TRANSFER, Vol. 109, pp. 1021–1023.

Haji-Sheikh, A., and Lakshminarayana, R., 1987, "A Multi-Method Study of Thermal Conduction in Bodies in Contact," *Proceedings of the International Symposium on Cooling Technology for Electronic Equipment*, Honolulu, HI, pp. 550–564.

Han, L. S., and Cosner, A. A., 1981, "Effective Thermal Conductivities of Fibrous Composites," ASME JOURNAL OF HEAT TRANSFER, Vol. 103, pp. 387–392.

Han, L. S., Boyee, W. M., and Glower, L., 1985, "Directional Thermal Conductivities of Graphite/Epoxy: 0/90 and 0/±45/90," AIAA Paper No. 85-0914.

Hasley, G. R., 1986, "Thermal Conductivity of Packed Metal Powders," *Int. J. Heat Mass Transfer*, Vol. 29, No. 6, pp. 909–920.

Kamiuto, K., and Iwamoto, M., 1987a, "Combined Conductive and Radiative Heat Transfer Through a Glass Particle Layer," *Proceedings of the 1987 ASME/JSME Thermal Engineering Joint Conference*, Honolulu, HI, pp. 77–84.

Kamiuto, K., and Iwamoto, M., 1987b, "Inversion Method for Determining Effective Thermal Conductivities of Porous Materials," ASME JOURNAL OF HEAT TRANSFER, Vol. 109, pp. 831–834.

Kennedy, F. E., Jr., 1984, "Thermal and Thermomechanical Effects in Dry Sliding," *Wear*, Vol. 100, pp. 453–476.

Kraus, A. D., and Bar-Cohen, A., 1983, *Thermal Analysis and Control of Electronic Equipment*, Hemisphere, New York.

Kuhlmann-Wilsdorf, D., 1987, "Temperatures at Interfacial Contact Spots: Dependence on Velocity and on Role Reversal of Two Materials in Sliding Contact," ASME *Journal of Tribology*, Vol. 109, April, pp. 321–329.

Lee, G., Ikeda, R. M., Kozina, J., and Mason, D. T., 1981, "Laser-Dissolution of Coronary Atherosclerotic Obstruction," *American Heart Journal*, Vol. 102, pp. 1074–1075.

Lee, G., Ikeda, R. M., Stobb, D., Ogata, C., Theis, J., Hussein, H., and Mason, D. T., 1983, "Laser Irradication of Human Atherosclerotic Obstructive Diseases: Simultaneous Visualization and Vaporization Achieved by a Dual Fiberoptic Catheter," *American Heart Journal*, Vol. 105, pp. 163–164.

Liu, Y. K., Stienstra, D., and Njus, G., 1981, "The Fatigue Life of Inorganic Bone—PMMA Composites," *Proceedings of the First Southern Biomedical Conference*, Shreveport, LA, pp. 12–15.

Luu, M., Allmon, B. A., Kneidel, K. E., and Stevens, J. G., 1986, "Study of Heat Transfer in Evacuated Insulations at Various Gas Loadings," *Proceedings of the 8th International Heat Transfer Conference*, San Francisco, CA, pp. 709–714.

Madhusudana, C. V., 1980a, "Heat Flow Through Conical Constrictions," *AIAA J.*, Vol. 18, No. 10, pp. 1261–1262.

Madhusudana, C. V., 1980b, "Experiments on Heat Flow Through Zicaloy-2/Uranium Dioxide Surfaces in Contact," *J. of Nucl. Mat.*, Vol. 2, pp. 345–348.

Madhusudana, C. V., 1983, "Contact Heat Transfer Between Coaxial

Downloaded 16 Dec 2010 to 193.140.21.150. Redistribution subject to ASME license or copyright; see http://www.asme.org/terms/Terms_Use.cfm

Cylinders of Similar or Dissimilar Materials," *Proceedings of the ASME-JSME Thermal Engineering Joint Conference*, Vol. III, Honolulu, HI, pp. 317–322.

Madhusudana, C. V., 1986, "On Heat Flow Across Cylindrical Joints," *Proceedings of the 8th International Heat Transfer Conference*, San Francisco, CA, pp. 651–658.

Madhusudana, C. V., and Fletcher, L. S., 1981a, "Thermal Contact Conductance: A Review of Recent Literature," NSF Grant MEA-8103230, Mechanical Engineering Department, Texas A&M University, Sept.

Madhusudana, C. V., and Fletcher, L. S., 1981b, "Thermal Conductance of Cylindrical Joints," *Proceedings of the Eight Canadian Congress of Applied Mechanics*, pp. 755–756.

Madhusudana, C. V., and Fletcher, L. S., 1981c, "Gas Conductance Contribution to Contact Heat Transfer," AIAA Paper No. 81-1163.

Madhusudana, C. V., and Fletcher, L. S., 1983, "Solid Spot Thermal Conductance of Zicaloy-2/Uranium Dioxide Interfaces," *Nucl. Sci. and Engrg.*, Vol. 83, pp. 327–332.

Madhusudana, C. V., and Fletcher, L. S., 1986, "Contact Heat Transfer—The Last Decade," *AIAA J.*, Vol. 24, No. 3, pp. 510–523.

Madhusudana, C. V., and Litvak, A., 1987, "Experimental Investigation of Heat Flow Across Cylindrical Joints," University of New South Wales, Report 1987/AM/1.

Mentes, A., Veziroglu, T. N., Samudrala, R., Sheffield, J. W., and Williams, A., 1981, "Effects of Interface Gases on Contact Conductance," AIAA Paper No. 81-0214.

Moses, W. M., and Johnson, R. R., 1987, "Experimental Results for the Quasi-Steady Heat Transfer Through Periodically Contacting Surfaces," AIAA Paper No. 87-1608.

Moses, W. M., and Johnson, R. R., 1988, "Experimental Study of the Transient Heat Transfer Across Periodically Contacting Surfaces," *AIAA Journal of Thermopyhysics and Heat Transfer*, Vol. 2, pp. 37–42.

Negus, K. J., and Yovanovich, M. M., 1984a, "Constriction Resistance of Circular Flux Tubes With Mixed Boundary Conditions by Linear Superposition of Neumann Solutions," ASME Paper No. 84-HT-84.

Negus, K. J., and Yovanovich, M. M., 1984b, "Application of the Method of Optimized Images to Steady Three Dimensional Conduction Problems," ASME Paper No. 84-WA/HT-110.

Negus, K. J., and Yovanovich, M. M., 1987, "Thermal Computations in a Semiconductor Die Using Surface Elements and Infinite Images," *Proceedings of the International Symposium on Cooling Technology for Electronic Equipment*, Honolulu, HI, pp. 474–485.

Negus, K. J., Yovanovich, M. M., and Devaal, J. W., 1985, "Development of Thermal Constriction Rough Surfaces by the Method of Infinite Images," ASME Paper No. 85-HT-17.

Negus, K. J., Vanoverbeke, C. A., and Yovanovich, M. M., 1987, "Thermal Constriction Resistance With Variable Conductivity Near the Contact Surface," *Proceedings of the ASME Symposium on Recent Developments in Contact Resistance*, ASME National Heat Transfer Conference, Pittsburgh, PA, Aug. 9–12, pp. 91–98.

Octerbeck, J. M., Fletcher, L. S., and Peterson, G. P., 1988, "Experimental Investigation of Thermal Contact Conductance at the Interface Between Bone and PMMA Cements," *Proceedings of the 6th Annual Conference on Biomedical Engineering Research in Houston*, University of Houston, Houston, TX, p. 26.

Padgett, D. L., and Fletcher, L. L., 1980, "An Apparatus to Determine the Thermal Contact Conductance Between Dissimilar Metals," University of Virginia, Charlottesville, VA, RLES Report UVA/526268/MAE80/101, Sept.

Padgett, D. L., and Fletcher, L. S., 1982, "The Thermal Contact Conductance of Dissimilar Metals," AIAA Paper No. 82-0885.

Peterson, G. P., 1987, "Thermal Contact Resistance in Waste Heat Recovery Systems," *Proceedings of the 8th ASME/ETCE Hyrdocarbon Processing Symposium*, Dallas, TX, pp. 45–51.

Peterson, G. P., and Fletcher, L. S., 1986, "Effective Thermal Conductivity of Sintered Heat Pipe Wicks," AIAA Paper No. 86-1362.

Peterson, G. P., and Fletcher, L. S., 1987a, "Thermal Contact Conductance of Packed Beds in Contact With a Flat Surface," ASME JOURNAL OF HEAT TRANSFER, Vol. 110, No. 1, pp. 38–41.

Peterson, G. P., and Fletcher, L. S., 1987b, "Thermal Contact Resistance of Silicon Chip Bonding Materials," *Proceedings of the International Symposium on Cooling Technology for Electronic Equipment*, Honolulu, HI, pp. 438–448.

Peterson, G. P., and Fletcher, L. S., 1988a, "Thermal Contact Conductance of Thin Metallic Foils," AIAA Paper No. 88-0544.

Peterson, G. P., and Fletcher, L. S., 1988b, "Evaluation of the Thermal Contact Conductance Between Mold Compound and Heat Spreader Materials," ASME JOURNAL OF HEAT TRANSFER, Vol. 110, No. 4(A), pp. 996–999.

Peterson, G. P., Fletcher, L. S., and Peddicord, K. L., 1987a, "Effective Thermal Conductivity in Multi-Fraction Reactor Fuels," *J. of Nucl. Sci. Tech.*, Vol. 24, No. 9, pp. 1–7.

Peterson, G. P., Fletcher, L. S., and Peddicord, K. L., 1987b, "Thermal Conductivity in Sphere-Pac Reactor Fuels," *Proceedings of the 2nd ASME/JSME Thermal Engineering Joint Conference*, Honolulu, HI, March 22–27, pp. 439–444.

Pinto, E. J., and Mikic, B. B., 1987, "A Novel Design Concept for Reduction of Thermal Contact Resistance," Keynote Address, *International Symposium on Cooling Technology for Electronic Equipment*, Honolulu, HI.

Rapier, A. C., Jones, T. M., and McIntosh, J. E., 1963, "The Thermal Conductance of Uranium Dioxide/Stainless Steel Interfaces," *Int. J. Heat Mass Trans.*, Vol. 6, pp. 397–416.

Ronzon, B. J., Galpin, P. F., Schneider, G. E., and Yovanovich, M. M., 1986, "The Effect of Geometry on Contact Conductance of Contiguous Interfaces," *AIAA J. Spacecraft*, Vol. 23, pp. 225–230.

Saabas, H. J., and Yovanovich, M. M., 1985, "Application of SEM and Superposition Techniques to Circular Microcontacts Distributed Over Elliptical Contour on Circular Flux Tubes and Half Spaces," AIAA Paper No. 85-1017.

Shai, I., and Santo, M., 1982, "Heat Transfer With Contact Resistance," *Int. J. Heat Mass Trans.*, Vol. 25, pp. 465–470.

Sheffield, J. W., Veziroglu, T. N., and Williams, A., 1980, "Thermal Contact Conductance of Multilayered Sheets," AIAA Paper No. 80-1468.

Snaith, B., O'Callaghan, P. W., and Probert, S. D., 1983, "Can Standards Be Set for Reliable Measurements of Thermal Contact Conductance," AIAA Paper No. 83-0533.

Snaith, B., Probert, S. D., and O'Callaghan, P. W., 1986, "Thermal Resistances of Pressed Contacts," *Applied Energy*, Vol. 22, pp. 31–84.

Sodha, M. S., Tiwari, G. N., and Kaushik, S. C., 1980, "Periodic Heat Flux Through a Three Layered Slab," *Energy Research*, Vol. 4, pp. 93–96.

Somers, R. R., II, 1983, "The Thermal Contact Conductance of Dissimilar Metals," Ph.D. Dissertation, University of Virginia, Charlottesville, VA.

Somers, R. R., II, Fletcher, L. S., and Flack, R. D., 1987, "Explanation of Thermal Rectification," *AIAA J.*, Vol. 25, No. 4, pp. 620–621.

Song, S., and Yovanovich, M. M., 1987a, "Explicit Relative Contact Pressure Expression: Dependence Upon Surface Roughness Parameters and Vickers Microhardness Coefficients," AIAA Paper No. 87-0152.

Song, S., and Yovanovich, M. M., 1987b, "Correlation of Thermal Accommodation Coefficient for 'Engineering' Surfaces," *Proceedings of the Symposium on Recent Developments in Contact Resistance*, ASME National Heat Transfer Conference, Pittsburgh, PA, Aug. 9–12, pp. 117–121.

Takao, Y., and Taya, M., 1986, "Thermal Expansion Coefficients and Thermal Stresses in an Aligned Short Fiber Composite With Application to a Short Carbon Fiber/Aluminum," ASME Paper No. 85-WA/ARM-11.

Tong, T. W., McElroy, D. L., and Yarbrough, D. W., 1984, "Transient Conduction and Radiation Heat Transfer in Porous Thermal Insulations," ASME Paper No. 84-WA/HT-102.

Vafai, K., and Alkire, R. L., 1984, "Heat Transfer in Variable Porosity Packed Beds: An Experimental Investigation," ASME Paper No. 84-WA/HT-100.

Valvano, J. W., Hayes, L. J., Welch, A. J., and Bajekal, S., 1984, "Thermal Conductivity and Diffusivity of Arterial Walls," ASME Paper No. 84-WA/HT-60.

Vanoverbeke, C. A., Negus, K. J., and Yovanovich, M. M., 1987, "Thermal Resistance of a Bolted Microelectric Chip Carrier: Effect of Contact Conductance," AIAA Paper No. 87-1613.

Veziroglu, T. N., Williams, A., Kakac, S., and Nayak, P., 1979, "Prediction and Measurement of the Thermal Conductance of Laminated Stacks," *Int. J. Heat Mass Trans.*, Vol. 22, No. 3, pp. 447–459.

Vick, B., and Ozişik, M. N., 1981, "Quasi-Steady-State Temperature Distribution in Periodically Contacting Finite Regions," ASME JOURNAL OF HEAT TRANSFER, Vol. 103, pp. 739–744.

Wang, J. C. Y., and Nowak, E. S., 1981, "Solution of Thermal Constriction Resistance Cylindrical Surfaces With an Isothermal Condition at the Contract Land," ASME Paper No. 81-WA/HT-5.

Williams, A., and Fletcher, L. S., 1983, "Thermal Rectification—Permanent or Transitory," *Proceedings of the Ninth Canadian Congress of Applied Mechanics*, University of Saskatchewan, Saskatoon, Canada, pp. 605–606.

Woodbury, K. A., and Thomas, C. T., 1985, "Effective Thermal Conductivity of a Moisture Laden Glass Fiber Insulation Matrix," ASME Paper No. 85-HT-70.

Yoo, K. H., and Anderson, A. C., 1983, "Thermal Impedance of Pressed Contacts at Temperatures Below 4 K," *Cryogenics*, Vol. 23, pp. 531–532.

Yovanovich, M. M., 1986, "Recent Developments in Thermal Contact, Gap and Joint Conductance Theories and Experiment," *Proceedings of the 8th International Heat Transfer Conference*, San Francisco, CA, pp. 35–45.

Yovanovich, M. M., 1987, "Theory and Applications of Constriction and Spreading Resistance Concepts for Microelectronic Thermal Management," Keynote Address, *Proceedings of the International Symposium on Cooling Technology for Electronic Equipment*, Honolulu, HI, Mar. 18–21.

Yovanovich, M. M., Culham, J. R., and Lemczyk, T. F., 1986a, "Simplified Solutions and Numerical Computation of One and Two-Dimensional Circular Fins With Contact Conductance and End Cooling," AIAA Paper No. 86-0149.

Yovanovich, M. M., Davidson, S., Mahalingham, M., and Sharma, A., 1986b, "Internal Resistance," in: *Research Needs in Electronic Cooling*, F. P. Incropera, ed., Purdue University, Dec., pp. 52–60.

Yovanovich, M. M., DeVaal, J., and Hegazy, A. H., 1982a, "A Statistical Model to Predict Thermal Gap Conductance Between Conforming Rough Surfaces," AIAA Paper No. 82-0888.

Yovanovich, M. M., Hegazy, A. H., and DeVaal, J., 1982b, "Surface Hardness Distributon Effects Upon Contact, Gap and Joint Conductance," AIAA Paper No. 82-0887.

Yovanovich, M. M., Hegazy, A., and Antonetti, V. W., 1983, "Experimental Verification of Contact Conductance Models Based Upon Distributed Surface Micro-Hardness," AIAA Paper No. 83-0532.

Yuen, W. Y. D., 1988, "Heat Conduction in Sliding Solids," *Int. J. Heat Mass Trans.*, Vol. 31, pp. 637–645.

Zwart, J., and Yavanovich, M. M., 1985, "Effective Thermal Diffusivity of a Simple Packed System of Spheres," ASME Paper No. 85-HT-52.

Downloaded 16 Dec 2010 to 193.140.21.150. Redistribution subject to ASME license or copyright; see http://www.asme.org/terms/Terms_Use.cfm

Analysis of Extended Surface

A. D. Kraus
Department of Electrical and Computer Engineering,
Naval Postgraduate School,
Monterey, CA

Previous work, by the author and others, pertaining to parameterizations for individual fins is reviewed. These parameterizations are the thermal transmission matrices and ratios that were devised to facilitate the analysis of an assembly of individual fins into an array of extended surface. An elaboration of the usefulness of these parameters, particularly with regard to their superiority over the notion of fin efficiency or fin effectiveness, is made. The concept of reciprocity is developed and the representation of an individual fin as a connection of just three simple resistances is developed. A procedure for the nodal analysis of finned arrays is developed via a matrix-oriented approach.

Introduction

Fins of various geometries and thermal conductivities respond differently to identical and uniform heat sources and sinks. Similarly, there are many ways in which the temperature and heat transfer coefficient relating the fin to the sources and sinks may vary. Important to the analysis of any fin geometry are the constraints or assumptions that are employed to define and limit the problem and, of course, to simplify its solution. Simplified constraint analysis of an extended surface employs the limiting assumptions that are attributed to Murray (1938) and Gardner (1945), which are:

1 The heat flow and temperature distribution throughout the fin are independent of time, i.e., the heat flow is steady.
2 The fin material is homogeneous and isotropic.
3 There are no heat sources in the fin itself.
4 The heat flow to or from the fin surface at any point is directly proportional to the temperature difference between the surface at that point and the surrounding fluid.
5 The thermal conductivity of the fin is constant with respect to temperature, time, and position.
6 The heat transfer coefficient is the same over all the fin surface.
7 The temperature of the surrounding fluid is uniform.
8 The temperature of the base of the fin is uniform and the joint between the fin and the prime surface is assumed to offer no bond resistance.
9 The thickness is so small compared to its height that temperature gradients normal to the surface may be neglected.
10 The heat transferred through the outermost edge of the fin is negligible compared to that passing through the faces.

To be sure, analyses based on the foregoing assumptions are not *real world* analyses. Indeed, there have been literally thousands of investigators who have revealed, in the historical advance of the technology, the inadequacies of the Murray–Gardner assumptions. Yet, while this attempt to adopt more realistic constraints has put the mathematical analysis models in closer agreement with the actual physical situation, the design of heat transfer equipment utilizing extended surfaces is still based on the simplified constraints that employ the limiting assumptions.

The next section presents a discussion of the design parameters of fin efficiency, fin effectiveness, and the recently proposed fin or array input admittance. This is followed by a section that deals with the mathematical representation of individual fins in terms of three matrices; the thermal transmission, the inverse thermal transmission, and the thermal admittance matrices. After a discussion of what are believed to be the deficiencies and limitations of the fin efficiency as a design parameter, it is shown that the use of the input admittance overcomes these deficiencies.

A detailed procedure for the determination of the thermal transmission matrix for any fin shape is then provided and it is shown how the input admittance can be obtained from the thermal transmission matrix. Algorithms for the assembly and combination of individual fins into an array are then presented and the paper concludes with a general method of finned array analysis.

Parameterizations

The convective fin efficiency, apparently first proposed by Harper and Brown (1922) and Parsons and Harper (1922) and then discussed in detail by Gardner (1945), is defined as the ratio of the heat dissipated by the fin to the amount of heat that would be dissipated if the fin were to operate throughout at the base temperature. An alternative definition is the ratio of the heat dissipated by the fin to the heat that would be dissipated by a fin of the same dimensions but with infinite thermal conductivity. Efficiencies were given by Gardner (1945), in a comprehensive and pioneering paper, for 11 common profiles of longitudinal fins, radial fins, and spines.

The fin efficiency is a design parameter that has been in use for half a century. It merely modifies (as a multiplier) the total fin surface to account for the fact that every point on the fin operates at a different temperature. Thus, the total surface to be employed in

$$q = hS\theta_b \tag{1}$$

is

$$S = S_b + \eta S_f \tag{2}$$

where the temperature excess $\theta = T - T_e$; η is the fin efficiency.

Another design parameter is the fin effectiveness defined by Gardner (1945) as the ratio of the heat transferred through the base of a fin to that which would be transferred, at the same temperature, through the same base area (prime surface area) if the fin were not present. Gardner showed that the fin effectiveness is related to the fin efficiency by

$$\phi = \left(\frac{S_f}{A_b}\right)\eta \tag{3}$$

Gardner (1945) was quick to point out that, in most practical cases, the addition of extended surface to a metal prime surface changes the base temperature. Two studies confirming this fact were conducted by Sparrow and Hennicke (1970) and Sparrow and Lee (1975). Thus, the use of the fin effectiveness as a design parameter is somewhat limited and the employment of the fin efficiency as the design parameter has prevailed. Trumpler (1945) pointed out that the simplistic approach utilizing the limiting assumptions should cause no concern because in most commercial installations, the fin efficiency is equal to or greater than 90 percent.

Contributed by the Heat Transfer Division for publication in the JOURNAL OF HEAT TRANSFER. Manuscript received by the Heat Transfer Division February 1, 1988. Keywords: Augmentation and Enhancement, Electronic Equipment, Finned Surfaces.

Copyright © 1988 by ASME

Downloaded 16 Dec 2010 to 193.140.21.150. Redistribution subject to ASME license or copyright; see http://www.asme.org/terms/Terms_Use.cfm

Manzoor et al. (1983), in a study that considered radiation as well as convection from the fin faces, contended that the heat flow through a finned assembly could be expressed conveniently in the form of an augmentation factor, defined as the ratio of the heat dissipated by the fin assembly to that of the unfinned surface operating under the same conditions. The augmentation factors proposed for both one-dimensional and two-dimensional heat transfer in the fins differ from the conventional fin effectivenss in that the latter fails to account for either the conductive heat flow within the supporting or prime surface or the convective heat dissipation from the unfinned side of the prime surface.

A completely new parameterization was proposed by Kraus et al. (1978). This parameterization, also based on the limiting assumptions, is a thermal transmission ratio or "input admittance" for an individual fin or a finned array. This input admittance is a thermal admittance and is defined as the ratio of the fin or array base heat flow to the fin or array base temperature excess

$$Y_i = q_b/\theta_b \tag{4}$$

and is related to the fin efficiency by

$$Y_i = \eta h S_f \tag{5}$$

Its use in conjunction with the base or prime surface is additive; the total input admittance Y_{iT} is merely the sum of Y_{iP} and Y_i and the heat dissipation is

$$q_T = Y_{iT}\theta_b = (Y_{iP} + Y_i)\theta_b \tag{6}$$

This new parameter is also particularly useful in the analysis and evaluation of finned arrays and the next section will be devoted to a short discussion of its origin.

The Fin or Array Input Admittance

Intuition dictates that conditions of temperature excess and heat flow at the tip of a fin (θ_a and q_a) are induced by similar conditions (θ_b and q_b) at the fin base. One may therefore assume that θ_b and q_b are independent analysis variables and θ_a and q_a are dependent variables related to the independent variables by the linear transformation

$$\begin{bmatrix} \theta_a \\ q_a \end{bmatrix} = \boldsymbol{\Gamma} \begin{bmatrix} \theta_b \\ q_b \end{bmatrix} = \begin{bmatrix} \gamma_{11} & \gamma_{12} \\ \gamma_{21} & \gamma_{22} \end{bmatrix} \begin{bmatrix} \theta_b \\ q_b \end{bmatrix} \tag{7}$$

where the matrix $\boldsymbol{\Gamma}$ is called the thermal transmission matrix. The elements of the thermal transmission matrix are called the thermal transmission parameters.

If one wants to represent conditions at the fin base in terms of conditions at the fin tip, it is easy to see that

$$\begin{bmatrix} \theta_b \\ q_b \end{bmatrix} = \boldsymbol{\Gamma}^{-1} \begin{bmatrix} \theta_a \\ q_a \end{bmatrix} = \mathbf{T} \begin{bmatrix} \theta_a \\ q_a \end{bmatrix} = \begin{bmatrix} \tau_{11} & \tau_{12} \\ \tau_{21} & \tau_{22} \end{bmatrix} \begin{bmatrix} \theta_a \\ q_a \end{bmatrix} \tag{8}$$

where the matrix $\mathbf{T}$ is the inverse of the matrix $\boldsymbol{\Gamma}$, and is called the inverse thermal transmission matrix having elements designated as the inverse thermal transmission parameters.

If the multiplication indicated by equation (8) is performed, one may represent the heat flow and temperature excess at the base of the fin as the superposition of two effects; one that is caused by the tip temperature excess and one that is a result of the heat leaving the tip

$$\theta_b = \tau_{11}\theta_a + \tau_{12}q_a \tag{9a}$$

$$q_b = \tau_{21}\theta_a + \tau_{22}q_a \tag{9b}$$

and from these, one may form the ratio called the input admittance

$$Y_i = \frac{q_b}{\theta_b} = \frac{\tau_{21}\theta_a + \tau_{22}q_a}{\tau_{11}\theta_a + \tau_{12}q_a} = \frac{\tau_{21} + \tau_{22}(q_a/\theta_a)}{\tau_{11} + \tau_{12}(q_a/\theta_a)} \tag{10}$$

Observe that the tip heat flow may be negligible, in which case, $q_a = 0$ and the input admittance simply becomes $Y_i = \tau_{21}/\tau_{11}$. It is also possible to consider fins or spines that taper to an edge or a point. In this case $q_a = 0$ because the metal cross-sectional area for the flow of heat is zero at the tip of the fin or spine even though the temperature gradient is not zero.

Fins or spines are categorized by the presence, or lack of, fin tip cross-sectional area and different parameterizations are required for each category; regular fins and spines possess a finite metal cross-sectional area at their tip and singular fins and spines do not.

The input admittance has been proposed by Kraus et al. (1978) as the new parameterization for the regular fins. As indicated by equation (10), it is easily obtained from the elements of the thermal transmission matrix, which have been provided by Kraus and Snider (1980) for the commonly used fin shapes. However, an attempt to follow the same procedure

Nomenclature

A = cross-sectional area
$\mathbf{A}$ = node-branch incidence matrix
b = fin height
C = arbitrary constant
$\mathbf{C}$ = a matrix
h = heat transfer coefficient
I = with subscript designates modified Bessel function
k = thermal conductivity
L = fin length
m = fin performance factor
n = fin performance factor for longitudinal fin of triangular profile
Q = heat flow
$\mathbf{Q}$ = heat flow vector
q = heat flow
S = surface area
T = temperature
$\Delta\mathbf{T}$ = branch temperature vector
x = height coordinate
Y = thermal admittance
$\mathbf{Y}$ = thermal transmission matrix, branch admittance matrix, or node admittance matrix
y = elements of the thermal transmission matrix
$\boldsymbol{\Gamma}$ = thermal transmission matrix
γ = elements of thermal transmission matrix
δ = fin width or thickness
η = fin efficiency
θ = temperature excess
$\boldsymbol{\Theta}$ = temperature excess vector
κ = taper angle
λ = a solution of a differential equation
μ = thermal transmission ratio
$\mathbf{T}$ = inverse thermal transmission matrix
τ = elements of inverse thermal transmission matrix
ϕ = fin effectiveness

Subscripts

a = designates tip of fin or augmented matrix
b = designated base of fin
c = designates a cluster
e = designates an equivalent or environment
f = designates fin
i = designates input condition
j = designates a matrix element
k = designates a matrix element
n = designates a total number of fins or a node or the node admittance matrix
o = designates characteristic value
P = designates prime surface
s = designates a source
T = designates a total

Downloaded 16 Dec 2010 to 193.140.21.150. Redistribution subject to ASME license or copyright; see http://www.asme.org/terms/Terms_Use.cfm

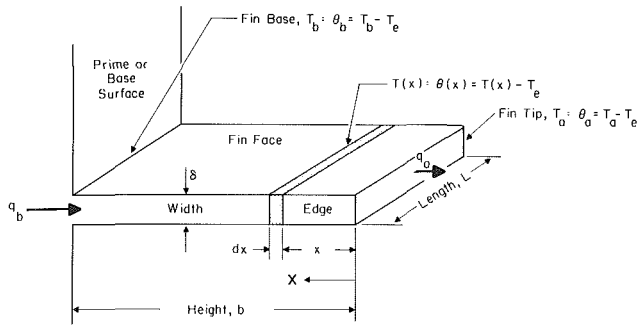

Fig. 1 Terminology for longitudinal fin of rectangular profile

for a singular fin is not valid because the determinant of the thermal transmission parameter matrix is equal to zero. This means that this matrix does not possess an inverse; the matrix is singular, hence the name singular fin. It is sufficient to parameterize the singular fin with a single parameter

$$\mu = q_b/\theta_b \tag{11}$$

called the thermal transmission ratio, which is seen to be, like the input admittance, the ratio of the fin base heat flow to the fin base temperature excess. For the longitudinal fin of triangular profile, the thermal transmission ratio is given by

$$\mu = \frac{k\delta_b}{b} nL \frac{I_1(2nb)}{I_0(2nb)} \tag{12}$$

where $n = h/k \sin \kappa$ and κ is the taper ratio ($\kappa = \arctan \delta_b/2b$).

For regular fins, it is convenient to relate both heat flow flows (at the base and tip of the fin) to both temperature excesses. This linear transformation is defined by the thermal admittance matrix

$$\begin{bmatrix} q_b \\ q_a \end{bmatrix} = Y \begin{bmatrix} \theta_b \\ \theta_a \end{bmatrix} = \begin{bmatrix} y_{11} & y_{12} \\ y_{21} & y_{22} \end{bmatrix} \begin{bmatrix} \theta_b \\ \theta_a \end{bmatrix} \tag{13}$$

whose elements are easily obtained, either from a conversion chart (Table 1) or from some simple manipulations involving matrix algebra.

It is contended that the fin or array input admittance should be considered as a viable alternative to the fin efficiency for design purposes. Most of this paper will be devoted to a review of the derivation and uses of this idea. However, the limitations and inadequacies of the fin efficiency should be further delineated and this is done in the next section.

The Limitations of the Fin Efficiency

The general idea of an efficiency as a performance parameter is sound; it is a dimensionless ratio comparing performance with a certain standard. However, the way that the efficiency has been defined for fins compares every fin with a different standard; how it performs compared with how it could perform if it were fabricated from a material with infinite thermal conductivity. Two fins in the same environment may have the same efficiency but they may transmit different quantities of heat. The following example, utilizing some realistic dimensions, shows that one fin can transmit more heat than another under identical environmental conditions and operate at a lower value of fin efficiency.

With the fin length, height, and width as indicated in Fig. 1, one may consider an aluminum longitudinal fin of rectangular profile (k = 202 W/m-K) with a base temperature of 200°C transferring heat to an environment at 100°C under natural convection conditions where h is taken as h = 10 W/m^2-K. The fin dimensions are: height b = 40 mm; width δ = 2.286 mm; and length L = 250 mm. Using the relationship for the heat entering the base

$$q_b = (2hk\delta)^{1/2} L\theta_b \tanh(mb) \tag{14}$$

where θ_b = 200 − 100 = 100°C is the base temperature excess and where $m = (2h/k\delta)^{1/2}$ m^{-1} is the fin performance factor, one may compute the heat dissipation as 43.85 W. Then, using the well-known expression

$$\eta = \tanh(mb)/mb \tag{15}$$

the efficiency may be computed as η = 0.877.

In a desire to save mass, it is proposed that a magnesium fin (k = 148 W/m-K) with the same dimensions operating at identical conditions be employed. Using the same heat dissipation of 43.85 W, one may solve equation (14) to obtain b = 106.4 mm, which shows that, because of its poorer conductivity, the height of the magnesium fin must be increased in order to accommodate an identical dissipating requirement. For the magnesium fin, the efficiency computed from equation (15) is η = 0.824. Observe that the magnesium fin, which has a huge advantage in a weight optimization, dissipates the same quantity of heat but at a lower fin efficiency. Yet, for both fins, the input admittance Y_i = 43.85/100 = 0.439 W/°C is identical.

If the heat transfer coefficient is reduced to, say, h = 8 W/m^2-K, equations (14) and (15) show that the magnesium fin (with the greater fin height) will dissipate 36.30 W at an efficiency of 0.853 while the aluminum fin will dissipate less heat, 35.94 W, at the higher efficiency of 0.899. In this case, the input admittances are 0.363 W/°C for the magnesium fin and 0.359 W/°C for the aluminum fin. The fins are no longer dissipating the same amount of heat and the magnesium fin is clearly outperforming its aluminum *design-point twin* at a lower efficiency.

At this point, it is noted that the fault is probably not in the efficiency concept but in the efficiency definition. If the efficiency had originally been called "the surface utilization factor" (which is exactly what it is) instead of the fin efficiency, it might never have entered either the preceding discussion or the calculations.

The usefulness of the fin efficiency is debatable when a finned array is considered. With the fin efficiency defined as the ratio of the heat dissipated, Q_1, to the heat dissipated if the fin possessed infinite thermal conductivity, $Q_0 = hS\theta_b$

$$\eta = Q_1/Q_0 \tag{16}$$

For a single fin without tip heat dissipation, $Q_1 = q_b$ and equation (16) prevails. A single fin with heat dissipation from the tip is governed by $q_a = h_a A_a \theta_a$. (Sparrow et al. (1978) and others have shown that h_a, the coefficient of heat transfer at the fin tip, does not necessarily equal the coefficient of heat transfer on the fin faces.) A_a is the fin cross-sectional area at the fin tip (equal to the fin surface area at the fin tip) and the entire convective dissipation passes through the base of the fin. Thus, with $Q_1 = q_b$, the efficiency is also given by equation (16).

In a finned array, if the fin tip heat flow q_a is injected into the base of another fin or a cluster of fins, then the heat dissipated is $Q_1 = q_b - q_a$ and the fin efficiency becomes

$$\eta = Q_1/Q_0 = (q_b - q_a)/Q_0 \tag{17}$$

Hence, the efficiency of a fin in a finned array depends on where the fin is mounted in the array, which is another inadequacy of the concept of the fin efficiency.

An example will help to illustrate the differences between η, Γ, and μ. Consider the finned array shown in Fig. 2 where the base temperature excess is 50°C. Fins 1, 2, 4, and 5 are identical longitudinal fins of rectangular profile and fins 3 and 6 are identical triangular profile fins. The specifications are as follows:

Fins 1, 2, 4, and 5: δ = 6.35 mm and b = 50.8 mm

Fins 3 and 6: δ_b = 6.35 mm and b = 40.0 mm

For all fins, the length L = 304.8 cm, k = 180 W/m-K, and h = 100 W/m^2-K. All of the heat flows and temperature ex-

Downloaded 16 Dec 2010 to 193.140.21.150. Redistribution subject to ASME license or copyright; see http://www.asme.org/terms/Terms_Use.cfm

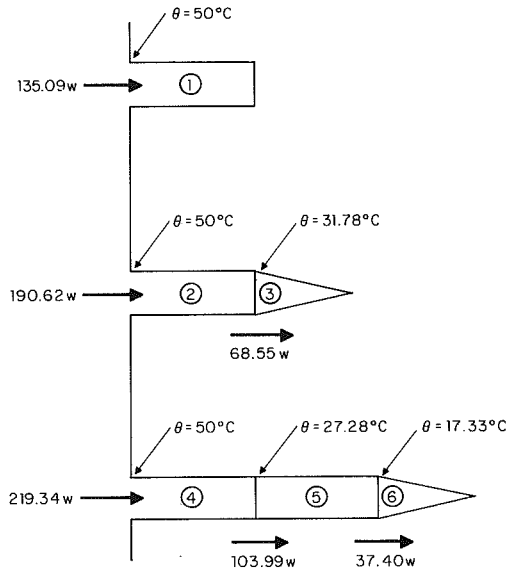

Fig. 2 A finned array containing six fins

cesses displayed in Fig. 2 were determined using the techniques developed by Kraus et al. (1978) and are discussed here in a later section.

One may compute the six fin efficiencies using equation (17) with hS = 3.0968 W/°C for fins 1, 2, 4, and 5, and hS = 2.4384 W/°C for fins 3 and 6.

$$\eta_1 = \frac{135.09}{50(3.0968)} = 0.872$$

$$\eta_2 = \frac{190.62 - 68.55}{50(3.0968)} = 0.788$$

$$\eta_3 = \frac{68.55}{31.78(2.4384)} = 0.885$$

$$\eta_4 = \frac{219.34 - 103.99}{50(3.0968)} = 0.745$$

$$\eta_5 = \frac{103.99 - 37.40}{27.28(3.0968)} = 0.788$$

$$\eta_6 = \frac{37.40}{17.33(2.4384)} = 0.885$$

Thus, the identical rectangular fins, all operating in the same environment, all have different efficiencies. Yet all have the same thermal transmission matrix, which can be evaluated from equations presented in the next section

$$\mathbf{\Gamma} = \begin{bmatrix} 1.2344 & -0.1570 \\ -3.3351 & 1.2344 \end{bmatrix}$$

On the other hand, the singular triangular fin, which can only be used as the most remote fin in any leg within the array, possesses a thermal transmission ratio computed from equation (12), μ = 2.1567 W/°C and it must have the same efficiency wherever it is employed.

Finding the Thermal Transmission Matrix

The temperature excess in any longitudinal or radial fin or spine is governed, in the steady state, by a differential equation of the form

$$\frac{d}{dx}\left[k(x)A(x)\frac{d\theta(x)}{dx}\right] - h(x)\frac{dS(x)}{dx}\theta(x) = 0 \qquad (18)$$

In most cases, x is a height coordinate measured from fin tip to base, but for radial fins, x is the radial coordinate measured from base to tip. Here $h(x)$ is the heat transfer coefficient and $k(x)$ is the thermal conductivity, which may vary with x. The cross-sectional area for the flow of heat by conduction is $A(x)$ and $dS(x)$ is the infinitesimal surface area of the fin faces over which a steady-state energy balance may be taken.

The theory of linear, homogeneous, second-order differential equations (with or without variable coefficients) shows that equation (18) is singular at all points where $k(x)A(x) = 0$ and is regular otherwise. Physically, because the thermal conductivity is not identically zero, singular points may only occur where the fin width is zero. In turn, this can take place at fin tips where $x = 0$ or $x = a$ depending on the origin of the height coordinate. The theory further dictates that equation (18) possesses two independent solutions $\lambda_1(x)$ and $\lambda_2(x)$, which satisfy the initial conditions at the base of the fin where $x = b$

$$\lambda_1(b) = 1: \ \lambda_1'(b) = 0 \qquad (19a)$$

where the prime indicates a first derivative and

$$\lambda_2(b) = 0: \ \lambda_2'(b) = \frac{1}{k(b)A(b)} \qquad (19b)$$

The heat flow $q(x)$ in the fin is always taken as positive from base to tip. Thus for nonradial fins, $q(x)$ is given by

$$q(x) = k(x)A(x)\frac{d\theta(x)}{dx} \qquad (20)$$

Therefore, one can use the solutions λ_1 and λ_2 to assemble the expressions for the temperature excess $\theta(x)$ and heat flow $q(x)$ at any point in the fin in terms of their values θ_b and q_b at the fin base

$$\theta(x) = \theta_b\lambda_1(x) + q_b\lambda_2(x) \qquad (21a)$$

$$q(x) = k(x)A(x)[\theta_b\lambda_1'(x) + q_b\lambda_2'(x)] \qquad (21b)$$

In matrix form, equations (21) become

$$\begin{bmatrix} \theta(x) \\ q(x) \end{bmatrix} = \begin{bmatrix} 1 & 0 \\ 0 & k(x)A(x) \end{bmatrix} \begin{bmatrix} \lambda_1(x) & \lambda_2(x) \\ \lambda_1'(x) & \lambda_2'(x) \end{bmatrix} \begin{bmatrix} \theta_b \\ q_b \end{bmatrix} \qquad (22)$$

The second matrix to the right of the equal sign can be seen to resemble the familiar Wronskian. The thermal transmission matrix is generated when x is set equal to a (a may equal zero) in equation (22)

$$\begin{bmatrix} \theta_a \\ q_a \end{bmatrix} = \mathbf{\Gamma}\begin{bmatrix} \theta_b \\ q_b \end{bmatrix} = \begin{bmatrix} \gamma_{11} & \gamma_{12} \\ \gamma_{21} & \gamma_{22} \end{bmatrix} \begin{bmatrix} \theta_b \\ q_b \end{bmatrix} \qquad (7)$$

where

$$\gamma_{11} = \lambda_1(a) \qquad (23a)$$

$$\gamma_{12} = \lambda_2(a) \qquad (23b)$$

$$\gamma_{21} = k(a)A(a)\lambda_1'(a) \qquad (23c)$$

and

$$\gamma_{22} = k(a)A(a)\lambda_2'(a) \qquad (23d)$$

Observe that if $A(a) = 0$, $\gamma_{21} = \gamma_{22} = 0$ and

$$\mathbf{\Gamma} = \begin{bmatrix} \lambda_1(0) & \lambda_2(0) \\ 0 & 0 \end{bmatrix}$$

This matrix has a determinant equal to zero and is termed singular because it has no inverse. This is why fins and spines that taper to a zero cross section are called singular and why the thermal transmission ratio μ was proposed to parameterize them. An example of the foregoing procedure used to determine $\mathbf{\Gamma}$ for the longitudinal fin of rectangular profile now follows.

Downloaded 16 Dec 2010 to 193.140.21.150. Redistribution subject to ASME license or copyright; see http://www.asme.org/terms/Terms_Use.cfm

Example: Finding the Parameters

In Fig. 1, consider that the origin of the coordinate is at the fin tip with positive orientation toward the fin base. Here, the fin width is constant, $\delta(x)=\delta$ so that $A(x)=\delta L$ and $dS(x)=Ldx$. With constant thermal conductivity, $k(x)=k$, equation (18) reduces to

$$\frac{d^2\theta}{dx^2}-m^2\theta=0$$

where $m=(2h/k\delta)^{1/2}$.

This differential equation has a general solution

$$\theta(x)=C_1e^{mx}+C_2e^{-mx}$$

where the arbitrary constants C_1 and C_2 are to be evaluated from the *initial value data*

$$\theta(x=b)=\theta_b$$

and

$$q(x=b)=q_b$$

This makes

$$\theta_b=C_1e^{mb}+C_2e^{-mb}$$

and

$$q_b=k\delta mL[C_1e^{mb}-C_2e^{-mb}]$$

or

$$q_b=Y_o[C_1e^{mb}-C_2e^{-mb}]$$

where $Y_o=k\delta mL=(2hk\delta)^{1/2}L$ having the units W/°C is designated as the characteristic admittance of the fin.

It is then a matter of algebra to evaluate C_1 and C_2 such that

$$\theta(x)=\cosh(b-x)\theta_b-\frac{1}{Y_o}\sinh m(b-x)q_b$$

and

$$q(x)=Y_o\sinh m(b-x)\theta_b+\cosh m(b-x)q_b$$

Here reference to equations (19) shows that

$$\lambda_1(x)=\cosh m(b-x);\qquad \lambda_1(b)=1$$

$$\lambda_2(x)=-\frac{1}{Y_o}\sinh m(b-x);\qquad \lambda_2(b)=0$$

$$\lambda_1'(x)=-m\sinh m(b-x);\qquad \lambda_1'(b)=0$$

$$\lambda_2'(x)=\frac{m}{Y_o}\cosh m(b-x);\qquad \lambda_2'(b)=\frac{m}{Y_o}=\frac{1}{k\delta L}$$

and at $x=a=0$ equations (23) yield the thermal transmission parameters that are the elements of the thermal transmission matrix.

$$\gamma_{11}=\lambda_1(0)=\cosh mb \tag{24a}$$

$$\gamma_{12}=\lambda_2(0)=-\frac{1}{Y_o}\sinh mb \tag{24b}$$

$$\gamma_{21}=k\delta L\lambda_1'(0)=-k\delta Lm\sinh mb=-Y_o\sinh mb \tag{24c}$$

and

$$\gamma_{22}=k\delta L\lambda_2'(0)=\frac{k\delta Lm}{Y_o}\cosh mb=\cosh mb \tag{24d}$$

Thus, for the longitudinal fin of rectangular profile

$$\boldsymbol{\Gamma}=\begin{bmatrix}\cosh mb & -(1/Y_o)\sinh mb\\ -Y_o\sinh mb & \cosh mb\end{bmatrix}$$

The inverse thermal transmission matrix is, as the name suggests, the inverse of the thermal transmission matrix. With the determinant of $\boldsymbol{\Gamma}$ equal to

$$\det\boldsymbol{\Gamma}=\cosh^2 mb-\sinh^2 mb=1$$

$\mathbf{T}$ becomes

$$\mathbf{T}=\boldsymbol{\Gamma}^{-1}=\begin{bmatrix}\cosh mb & (1/Y_o)\sinh mb\\ Y_o\sinh mb & \cosh mb\end{bmatrix}$$

where the inverse thermal transmission parameters, which are the elements of the inverse thermal transmission matrix, are

$$\tau_{11}=\cosh mb \tag{25a}$$

$$\tau_{12}=\frac{1}{Y_o}\sinh mb \tag{25b}$$

$$\tau_{21}=Y_o\sinh mb \tag{25c}$$

and

$$\tau_{22}=\cosh mb \tag{25d}$$

The thermal admittance matrix can then be obtained from an exercise in matrix algebra or from Table 1

$$\mathbf{Y}=\begin{bmatrix}Y_o\coth mb & -Y_o\operatorname{csch} mb\\ Y_o\operatorname{csch} mb & -Y_o\coth mb\end{bmatrix}$$

with thermal admittance parameters (elements)

$$y_{11}=Y_o\coth mb \tag{26a}$$

$$y_{12}=-Y_o\operatorname{csch} mb \tag{26b}$$

$$y_{21}=Y_o\operatorname{csch} mb \tag{26c}$$

and

$$y_{22}=-Y_o\coth mb \tag{26d}$$

For radial fins, a minus sign must be introduced into equation (20) because x, now the radial coordinate, is measured in the same direction as q (base to tip). The net result of this modification is to change the sign of γ_{12} and γ_{21} in equations (24*b*) and (24*c*).

The Array Input Admittance

The input admittance, which is the new parameterization

$$Y_i=\frac{q_b}{\theta_b} \tag{4}$$

is obtained from the elements of either the thermal transmission matrix

$$Y_i=\frac{\gamma_{21}-\gamma_{11}(q_a/\theta_a)}{-\gamma_{22}+\gamma_{12}(q_a/\theta_a)}$$

or the inverse thermal transmission matrix

$$Y_i=\frac{\tau_{21}+\tau_{22}(q_a/\theta_a)}{\tau_{11}+\tau_{12}(q_a/\theta_a)} \tag{27}$$

In either event, the ratio q_a/θ_a is known. For single fin analysis, $q_a=0$ or, if there is fin tip dissipation, $q_a/\theta_a=h_aA_a$. In this case, the input admittance Y_i is equal to the individual fin thermal transmission ratio μ. In array analysis, it must be recognized that the most remote connection in any array leg must either be an individual fin or a cluster of fins. If the connection is an individual fin, considerations of tip heat loss or no tip heat loss pertaining to individual fins prevail. If the connection is a cluster of fins, q_a/θ_a can be evaluated from the cluster algorithm, which is developed in a subsequent section. In this case, Y_i is called the array input admittance.

Algorithms for the Combination of Fins

A procedure for the determination of the performance of a finned array can be quite complicated and, as shown by Kays (1969) and Kern and Kraus (1972), can involve a solution of a system of many simultaneous linear differential equations. However, the reflection relationship or the thermal transmission matrix and the thermal admittance matrix can be

Downloaded 16 Dec 2010 to 193.140.21.150. Redistribution subject to ASME license or copyright; see http://www.asme.org/terms/Terms_Use.cfm

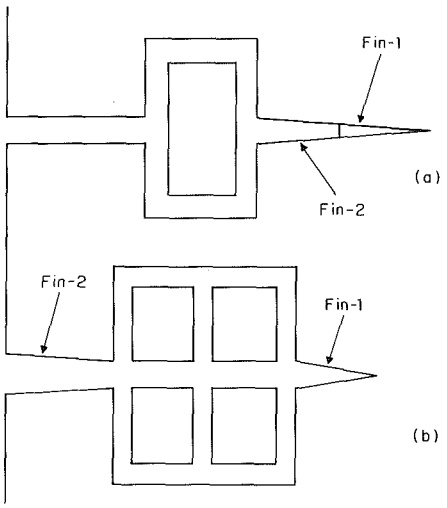

Fig. 3 Two arrays of extended surface, each with three longitudinal fin profiles. The array in (a) contains no loops in a graph theoretical sense; in both arrays, the fin of triangular profile is fin 1, the fin of trapezoidal profile is fin 2, and all other fins are fins of rectangular profile.

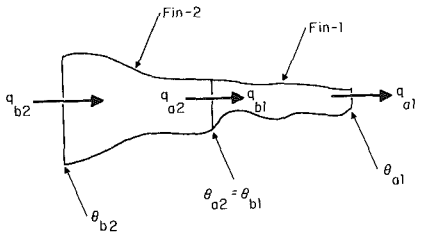

Fig. 4 Two fins in cascade

employed to evaluate the performance of a finned array rapidly through the use of three basic algorithms.

Figure 3 displays two finned arrays. Each of them contains three longitudinal fin profiles and in each, the fin of triangular profile is the most remote fin in the array. The array shown in Fig. 3(*b*) contains, as shown by Chan (1969), four loops in the graph theoretical sense; these four loops cannot be removed by a simple parallel combination. The array in Fig. 3(*a*) contains nine fins. Algorithms for the combination of fins in such an array that does not contain loops in the graph theoretical sense will be developed in this section.

The Cascade Algorithm. Consider the simplest case of two fins in cascade shown in Fig. 4. Here, continuity dictates that the heat leaving fin 2 must enter fin 1 and that at the point of intersection, the temperature excesses must match. Thus, one may set down a matrix equality embracing continuity and compatibility using *a* for tip conditions and *b* for base conditions

$$\begin{bmatrix} \theta_{a2} \\ q_{a2} \end{bmatrix} = \begin{bmatrix} \theta_{b1} \\ q_{b1} \end{bmatrix} \tag{28}$$

In addition, each fin has a **T** parameterization, which is a linear transformation from tip conditions to base conditions. For fin 1

$$\begin{bmatrix} \theta_{b1} \\ q_{b1} \end{bmatrix} = \mathbf{T}_1 \begin{bmatrix} \theta_{a1} \\ q_{a1} \end{bmatrix} \tag{29}$$

and for fin 2

$$\begin{bmatrix} \theta_{b2} \\ q_{b2} \end{bmatrix} = \mathbf{T}_2 \begin{bmatrix} \theta_{a2} \\ q_{a2} \end{bmatrix} \tag{30}$$

A simple exercise in matrix algebra shows that there is an equivalent **T** representation that maps conditions from the tip of fin 1 to the base of fin 2, which is at the base of the array. First take equation (29) and use equation (28)

$$\begin{bmatrix} \theta_{b1} \\ q_{b1} \end{bmatrix} = \begin{bmatrix} \theta_{a2} \\ q_{a2} \end{bmatrix} = \mathbf{T}_1 \begin{bmatrix} \theta_{a1} \\ q_{a1} \end{bmatrix}$$

and then use equation (30)

$$\begin{bmatrix} \theta_{b2} \\ q_{b2} \end{bmatrix} = \mathbf{T}_2 \begin{bmatrix} \theta_{a2} \\ q_{a2} \end{bmatrix} = \mathbf{T}_2\mathbf{T}_1 \begin{bmatrix} \theta_{a1} \\ q_{a1} \end{bmatrix} = \mathbf{T}_e \begin{bmatrix} \theta_{a1} \\ q_{a1} \end{bmatrix} \tag{31}$$

This shows the existence of an equivalent thermal transmission matrix that is a simple matrix product of the two individual inverse thermal transmission matrices (in the proper order because matrix multiplication, in general, is not commutative).

This may be extended to n fins in cascade

$$\mathbf{T}_e = \mathbf{T}_n\mathbf{T}_{n-1}\mathbf{T}_{n-2} \cdots \mathbf{T}_2\mathbf{T}_1 \tag{32}$$

and equation (32) is the cascade algorithm.

The array input admittance can be obtained using equation (27) with the elements of $\mathbf{T}_e$ with $q_a/\theta_a = 0$ or $q_a/\theta_a = h_{a1}A_{a1}$. Alternatively, the input admittance may be determined from two applications of equation (27), first using the elements of $\mathbf{T}_1$ for fin 1 with $q_a/\theta_a = 0$ or $h_{a1}A_{a1}$ to find the input admittance at the base of fin 1. This input admittance, by the continuity and compatibility conditions of equation (28), is the value of q_a/θ_a for fin 2. Another application of equation (27), this time using the elements of **T** for fin 2, will provide the sought-after result.

The foregoing seems to indicate an apparent equivalence between the use of equation (27), which is frequently called the "reflection relationship," and the use of the equivalent $\mathbf{T}_e$. Indeed, the usefulness of the cascade algorithm may be concealed by the simplicity of equations (27) and (32).

Consider, however, that the determination of an array input admittance for any convective heat transfer coefficient variation over the faces of any or all of the fins in the array is easily accomplished by an application of the cascade algorithm. One merely makes a piecewise continuous approximation (to the accuracy that is required) of the heat transfer coefficient. This dictates the number of subfins that must be employed to represent the original fin. The elements of **T** (via **Γ**) can then be obtained for each subfin using the average value of h in the individual segments of the h curve. A repeated matrix multiplication then gives the elements of $\mathbf{T}_e$ and then, equation (27) with $q_a = 0$ gives the required Y_i.

To be sure, efficiencies have been developed for various heat transfer coefficient variations on longitudinal fins of rectangular profile. Gardner (1951) proposed a power series variation, Han and Lefkowitz (1960) used a parabolic variation, and Chen and Zyskowski (1963) employed an exponential variation. However, the cascade algorithm will efficiently handle convective coefficients of any distribution on the faces of any fin or spine.

Fins in Cluster. Figure 5 shows n fins that are appended to fin m. These fins are said to be in a cluster arrangement and the tip of fin m is called a cluster point. Here, continuity dictates that the heat that leaves fin m must be divided among fins 1 through n. Moreover, compatibility dictates that the temperature excesses of all fins involved in the cluster must match. Thus, with the usage of subscripts *a* and *b* that has now become customary, it is observed that

$$q_{am} = q_{b1} + q_{b2} + q_{b3} + \cdots + q_{bn} \tag{33a}$$

and

$$\theta_{am} = \theta_{b1} = \theta_{b2} = \theta_{b3} = \cdots = \theta_{bn} \tag{33b}$$

Downloaded 16 Dec 2010 to 193.140.21.150. Redistribution subject to ASME license or copyright; see http://www.asme.org/terms/Terms_Use.cfm

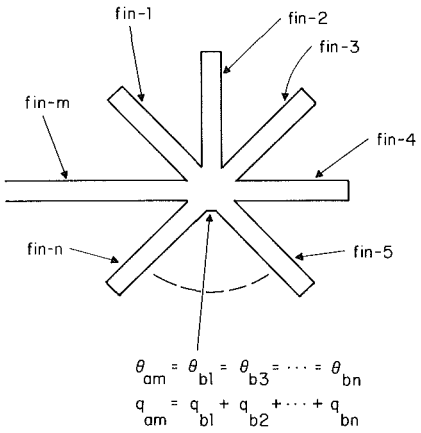

Fig. 5 Fins in cluster. There are *n* fins attached to the tip of fin *m* and the tip of fin *m* is designated as the cluster point.

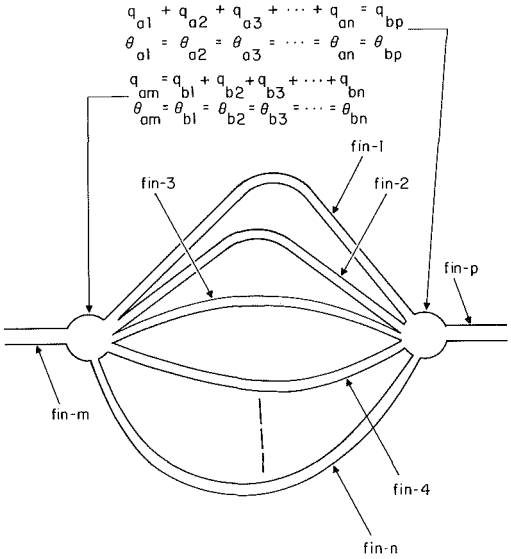

Fig. 6 Parallel combination of *n* fins

Consider the admittance at the tip of fin m, which is termed the cluster admittance Y_c

$$Y_{am} = Y_c = q_{am}/\theta_{am}$$

and employ equations (33). This yields

$$Y_{am} = Y_c = \frac{q_{b1} + q_{b2} + q_{b3} + \cdots + q_{bn}}{\theta_{am}}$$

or

$$Y_{am} = Y_c = \frac{q_{b1}}{\theta_{b1}} + \frac{q_{b2}}{\theta_{b2}} + \frac{q_{b3}}{\theta_{b3}} + \cdots + \frac{q_{bn}}{\theta_{bn}} \tag{34}$$

Each term on the right side of equation (34) represents an individual fin input admittance, or a thermal transmission ratio. Thus a cluster admittance may be defined as

$$Y_c = \sum_{i=1}^{n} Y_i = \sum_{i=1}^{n} \mu_i \tag{35}$$

This addition of input admittances to form the cluster input admittance is the cluster algorithm.

Fins in Parallel. A parallel arrangement of n fins is shown in Fig. 6. Notice that a single fin, designated as fin m, is delivering heat through its tip to the parallel combination and that a single fin, designated as fin p, is picking up, at its base, all of the heat leaving the parallel combination. In this case, continuity demands that

$$q_{am} = q_{b1} + q_{b2} + q_{b3} + \cdots + q_{bn} \tag{36a}$$

and

$$q_{bp} = q_{a1} + q_{a2} + q_{a3} + \cdots + q_{an} \tag{36b}$$

In addition, compatibility requires that at point m

$$\theta_{am} = \theta_{b1} = \theta_{b2} = \theta_{b3} = \cdots = \theta_{bn} \tag{37a}$$

and at point p

$$\theta_{bp} = \theta_{a1} = \theta_{a2} = \theta_{a3} = \cdots = \theta_{an} \tag{37b}$$

Use of the admittance parameter matrix defined by equation (13) permits a linear transformation of temperature excess to heat flow for any individual fin. Thus, from equations (36)

$$\begin{bmatrix} q_{am} \\ q_{bp} \end{bmatrix} = \begin{bmatrix} q_{b1} \\ q_{a1} \end{bmatrix} + \begin{bmatrix} q_{b2} \\ q_{a2} \end{bmatrix} + \begin{bmatrix} q_{b3} \\ q_{a3} \end{bmatrix} + \cdots + \begin{bmatrix} q_{bn} \\ q_{an} \end{bmatrix}$$

and the use of equation (13) provides

$$\begin{bmatrix} q_{am} \\ q_{bp} \end{bmatrix} = \mathbf{Y}_1 \begin{bmatrix} \theta_{b1} \\ \theta_{a1} \end{bmatrix} + \mathbf{Y}_2 \begin{bmatrix} \theta_{b2} \\ \theta_{a2} \end{bmatrix} + \mathbf{Y}_3 \begin{bmatrix} \theta_{b3} \\ \theta_{a3} \end{bmatrix} + \cdots + \mathbf{Y}_n \begin{bmatrix} \theta_{bn} \\ \theta_{an} \end{bmatrix} \tag{38}$$

But, by equations (37)

$$\begin{bmatrix} \theta_{am} \\ \theta_{bp} \end{bmatrix} = \begin{bmatrix} \theta_{b1} \\ \theta_{a1} \end{bmatrix} = \begin{bmatrix} \theta_{b2} \\ \theta_{a2} \end{bmatrix} = \begin{bmatrix} \theta_{b3} \\ \theta_{a3} \end{bmatrix} = \cdots = \begin{bmatrix} \theta_{bn} \\ \theta_{an} \end{bmatrix}$$

and when this is incorporated into equation (38)

$$\begin{bmatrix} q_{am} \\ q_{bp} \end{bmatrix} = [\mathbf{Y}_1 + \mathbf{Y}_2 + \mathbf{Y}_3 + \cdots + \mathbf{Y}_n] \begin{bmatrix} \theta_{am} \\ \theta_{bp} \end{bmatrix} \tag{39}$$

This shows that there is an equivalent thermal admittance matrix $\mathbf{Y}_e$ that relates the total heat flows to the temperature excesses at the base and tip of a parallel combination of fins

$$\begin{bmatrix} q_b \\ q_a \end{bmatrix} = \mathbf{Y}_e \begin{bmatrix} \theta_b \\ \theta_a \end{bmatrix}$$

where

$$\mathbf{Y}_e = \mathbf{Y}_1 + \mathbf{Y}_2 + \mathbf{Y}_3 + \cdots + \mathbf{Y}_n \tag{40}$$

Equation (40) is called the parallel algorithm

Example

The versatility of the algorithms developed in the preceding section can be demonstrated through an example. The array shown in Fig. 7 containing 15 individual longitudinal fins will be analyzed. Assume that the following groups of fins of rectangular profile possess identical dimensions:

fins 1, 2, and 3 (with no tip heat loss),
fins 6, 7, 10, and 11 (also with no tip heat loss),
fins 8, 12, and 13, and
fins 14 and 15

Observe that fin 4 is a fin of trapezoidal profile and that fins 5 and 9 are identical fins of triangular profile.

The key equation is equation (27), which will be referred to as the reflection relationship. A computationally efficient step-by-step procedure for the determination of the array input admittance now follows:

1 Determine the inverse thermal transmission parameters for fins 1 through 15 (except for fins 5 and 9) using the catalog

Downloaded 16 Dec 2010 to 193.140.21.150. Redistribution subject to ASME license or copyright; see http://www.asme.org/terms/Terms_Use.cfm

Table 1 Conversions between parameters

	Γ		T		Y	
Γ	γ_{11}	γ_{12}	τ_{22}	$-\tau_{12}$	$-y_{11}/y_{12}$	$1/y_{12}$
	γ_{21}	γ_{22}	$-\tau_{21}$	τ_{11}	$-\det\mathbf{Y}/y_{12}$	y_{11}/y_{12}
Γ	γ_{22}	$-\gamma_{12}$	τ_{11}	τ_{12}	$-y_{22}/y_{21}$	$1/y_{21}$
	$-\gamma_{21}$	γ_{11}	τ_{21}	τ_{22}	$-\det\mathbf{Y}/y_{21}$	y_{11}/y_{21}
Y	$-\gamma_{11}/\gamma_{12}$	$1/\gamma_{12}$	τ_{22}/τ_{12}	$-1/\tau_{12}$	y_{11}	y_{12}
	$-1/\gamma_{12}$	γ_{22}/γ_{12}	$1/\tau_{12}$	$-\tau_{11}/\tau_{12}$	y_{21}	y_{22}

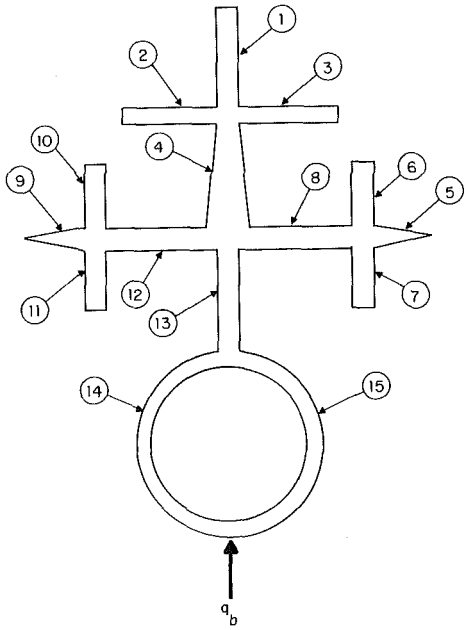

Fig. 7 Finned array composed of 15 individual fins

contained in Kraus et al. (1978) or Kraus and Snider (1980). For all of the rectangular profile fins, equations (25) pertain.

2 Determine the thermal transmission ratio for fins 5 and 9. For the triangular profile fin, equation (12) should be employed.

3 Fins 14 and 15 are in parallel and the thermal admittance parameters will be needed. These can be determined from the inverse thermal transmission parameters by using Table 1.

4 Use the reflection relationship of equation (27) with $q_a = 0$ to obtain the input admittance of fins 1, 2, and 3. Then use the cluster algorithm of equation (35) to find q_a/θ_a at the tip of fin 4. Another application of the reflection relationship will provide the input admittance at the base of fin 4.

5 Use the reflection relationship of equation (27) with $q_a = 0$ to determine the input admittance of fins 6 and 7. By the cluster algorithm, the value of q_a/θ_a at the tip of fin 8 will be equal to the sum of the input admittances of fins 6 and 7 plus the thermal transmission ratio of fin 5. Using this value of q_a/θ_a in the reflection relationship provides the input admittance at the base of fin 8.

6 An identical procedure to that given in step 5 will yield the input admittance at the base of fin 12. The input admittances at the bases of fin 8 and 12 will be equal because the applicable fin dimensions are all equal.

7 The cluster algorithm of equation (35) then yields the value of q_a/θ_a at the tip of fin 13. It says that the value of this *"tip admittance"* must be equal to the sum of the input admittances at the bases of fins 4, 8, and 12. The reflection relationship of equation (27) can then be used to determine the input admittance at the base of fin 13.

8 Fins 14 and 15 are identical and are in parallel. Table 1 was employed in step 3 to obtain the thermal admittance parameters for each of these fins. The equivalent thermal admittance matrix is then obtained in accordance with the parallel algorithm of equation (40) from the sum of the two individual thermal admittance matrices. An equivalent thermal transmission matrix can then be obtained from an application of Table 1. These are then used in the reflection relationship with the q_a/θ_a value determined at the end of step 7 to determine the sought-after total input admittance for the array.

There is no need to obtain the fin efficiency because the input admittance may be multiplied by the base temperature excess to obtain the heat dissipated by all 15 fins in the array.

Analysis of Finned Arrays Containing Loops

Finned arrays containing loops in the graph theoretical sense, such as the array shown in Fig. 3(*b*), may be analyzed by the general array algorithm proposed by Snider and Kraus (1981) or by a method of node analysis proposed by Kraus et al. (1982). The node analysis method is described here as a matrix-oriented method, which is believed to be more general than the more specific procedure given in the 1982 work.

Reciprocity, as Irwin (1984) shows, is an important concept in electrical network analysis and the equations describing the behavior of all regular fins and spines have the property of reciprocity. This can be exploited and regular fins can be represented by a thermal transmission matrix whose determinant is equal to unity (-1 in the case of the radial fins). Because of this, the off-diagonal elements of the thermal admittance matrix are related

$$y_{12} = -y_{21} \tag{41}$$

This permits any regular fin (called a reciprocal fin) to be represented as the equivalent pi network consisting of three thermal admittances shown in Fig. 8.

The Equivalent Pi Network. Application of continuity at points *a* and *b*, called node points or merely nodes, gives

$$q_b = q_1 + q_2$$
$$q_a = q_1 - q_3$$

However, each heat flow, q_1, q_2, and q_3 in Fig. 8, can be represented as a product of an admittance and a temperature excess

$$q_1 = Y_1(\theta_b - \theta_a)$$
$$q_2 = Y_2\theta_b$$
$$q_3 = Y_3\theta_a$$

so that

$$q_b = Y_1(\theta_b - \theta_a) + Y_2\theta_b$$
$$q_a = Y_1(\theta_b - \theta_a) - Y_3\theta_a$$

Downloaded 16 Dec 2010 to 193.140.21.150. Redistribution subject to ASME license or copyright; see http://www.asme.org/terms/Terms_Use.cfm

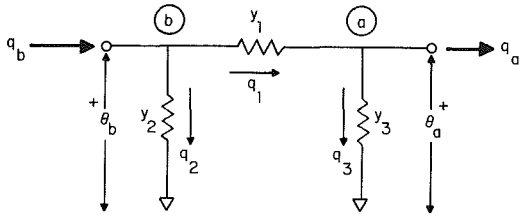

Fig. 8 Equivalent pi network

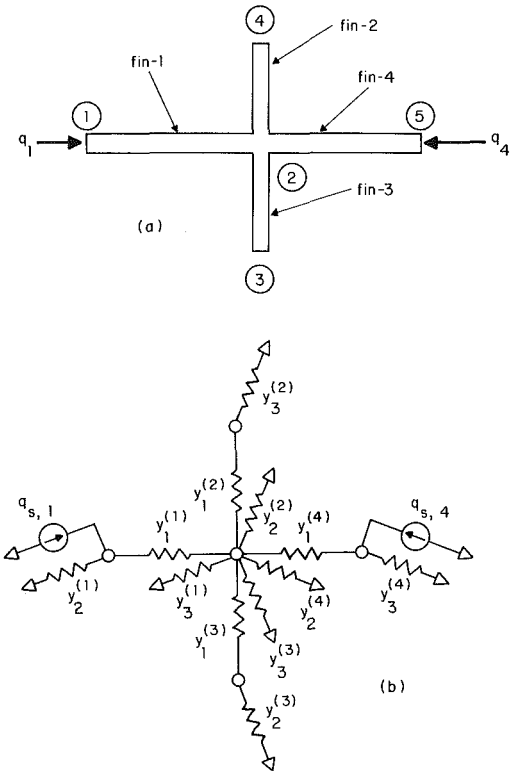

Fig. 9(*a*) An array of four fins with heat input at opposite ends; (*b*) an equivalent pi network to represent the array

or

$$q_b = (Y_1 + Y_2)\theta_b - Y_1\theta_a \tag{42a}$$

$$q_a = Y_1\theta_b - (Y_1 + Y_3)\theta_a \tag{42b}$$

Equations (42) may be put into matrix form

$$\begin{bmatrix} q_b \\ q_a \end{bmatrix} = \begin{bmatrix} (Y_1 + Y_2) & -Y_1 \\ Y_1 & -(Y_1 + Y_3) \end{bmatrix} \begin{bmatrix} \theta_b \\ \theta_a \end{bmatrix}$$

and then compared to equation (13), which defines the admittance parameter matrix

$$\begin{bmatrix} q_b \\ q_a \end{bmatrix} = \begin{bmatrix} y_{11} & y_{12} \\ y_{21} & y_{22} \end{bmatrix} \begin{bmatrix} \theta_b \\ \theta_a \end{bmatrix} \tag{13}$$

The comparison shows that

$$Y_1 + Y_2 = y_{11}$$

$$Y_1 = -y_{12} = y_{21}$$

and

$$Y_1 + Y_3 = -y_{22}$$

Then, it is only a matter of algebra to show that

$$Y_1 = -y_{12} = y_{21} \tag{43a}$$

$$Y_2 = y_{11} + y_{12} = y_{11} - y_{21} \tag{43b}$$

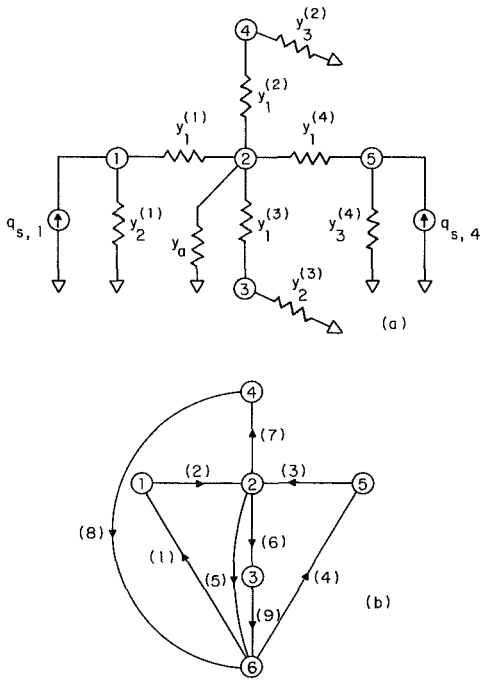

Fig. 10(*a*) A simplification of the network in Fig. 9(*b*), and (*b*) an oriented graph for the network of (*a*). The oriented graph contains six nodes and nine branches.

$$Y_3 = y_{12} - y_{22} = -(y_{21} + y_{22}) \tag{43c}$$

It is noted that as long as $y_{12} = -y_{21}$, any fin may be represented as an equivalent pi. All regular fins are reciprocal fins and may be represented as an equivalent pi network. Hence, arrays composed of regular fins may be treated as a combination of equivalent pi networks representing the individual fins in the array and connected as the array is connected. An example of a four-fin array with unequal heat inputs provided at the opposite ends is displayed, along with its network representation, in Fig. 9.

A simplification is shown in Fig. 10(*a*) where

$$Y_a = Y_3^{(1)} + Y_2^{(2)} + Y_3^{(3)} + Y_2^{(4)}$$

and Fig. 10(*b*) shows an oriented graph of the network in Fig. 10(*a*). The use of circles to designate nodes (points where two or more branches intersect) and numbers in parentheses to designate branches may be noted. The heat sources are included in branches 1 and 4 and the branch orientations are discretionary except for the branches containing the heat sources where the positive orientation must correspond to the direction of the heat input. The objective is to obtain all node temperature excesses in a computationally efficient manner and then, knowing the temperature excesses and heat flows at nodes 1 and 5, to determine the input admittances at nodes 1 and 5.

The General Branch. The most general case of the jth branch is the case, shown in Fig. 11, where a heat source q_{sj} and a temperature source ΔT_{sj} are present. The branch must also contain one of the thermal admittances.

Because the total temperature drop across each branch must be the sum of component temperature drops, it is easy to see that the temperature drop across the parallel combination of the heat source q_{sj}, and the admittance Y_j, must be $\Delta T_j - \Delta T_{sj}$ where ΔT_{sj} is the temperature source in branch j. Continuity then dictates that the branch heat flow q_j is represented, in matrix form, for all j branches, by

$$\mathbf{Q} = \mathbf{Q}_s + \mathbf{Y}(\Delta\mathbf{T} - \Delta\mathbf{T}_s) \tag{44}$$

Here, with b branches

Downloaded 16 Dec 2010 to 193.140.21.150. Redistribution subject to ASME license or copyright; see http://www.asme.org/terms/Terms_Use.cfm

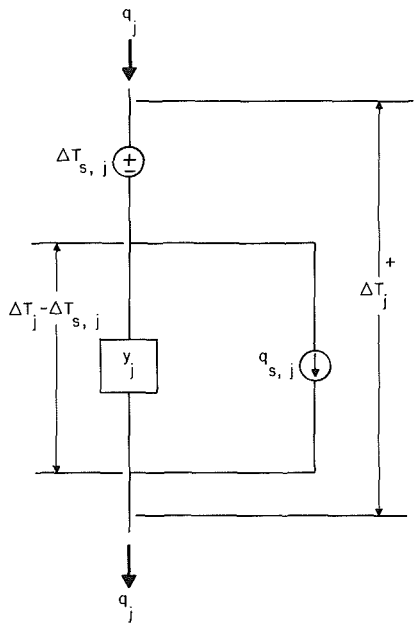

Fig. 11 General branch containing an admittance, a heat source, and a temperature source

$\mathbf{Q}$ is a $b \times 1$ heat flow vector

$\mathbf{Q}_s$ is a $b \times 1$ heat source vector (all nodes may possess heat sources)

$\mathbf{Y}$ is a $b \times b$ branch admittance matrix which is diagonal

$\Delta\mathbf{T}_s$ is a $b \times 1$ branch temperature source vector which may be (and most often is) null

$\Delta\mathbf{T}$ is a $b \times 1$ branch temperature vector.

The Node Branch Incidence Matrix. For a graph containing n_t nodes and b branches, a matrix that exactly represents the graph may be formulated. This matrix, which is called the node-branch incidence matrix, will have n_t rows and b columns and will contain elements $a_{jk} = +1, -1$, or 0 in accordance with the scheme.

$$a_{jk} = \begin{cases} +1 \text{ if branch } j \text{ leaves node } k \\ -1 \text{ if branch } j \text{ enters node } k \\ 0 \text{ if branch } j \text{ does not touch node } k \end{cases} \tag{45}$$

For example, the node-branch incidence matrix for the oriented graph in Fig. 10(b) will be $n = 6 \times b = 9$

$$\mathbf{A}_a = \begin{bmatrix} -1 & 1 & 0 & 0 & 0 & 0 & 0 & 0 & 0 \\ 0 & -1 & -1 & 0 & 1 & 1 & 1 & 0 & 0 \\ 0 & 0 & 0 & 0 & 0 & -1 & 0 & 0 & 1 \\ 0 & 0 & 0 & 0 & 0 & 0 & -1 & 1 & 0 \\ 0 & 0 & 1 & -1 & 0 & 0 & 0 & 0 & 0 \\ 1 & 0 & 0 & 1 & -1 & 0 & 0 & -1 & -1 \end{bmatrix} \tag{46}$$

It can be noted that every column contains a single $+1$ and a single -1 and that a summation of all elements in each column yields a zero.

The reduced incidence matrix contains $n-1$ rows and b branches. It is obtained from from $\mathbf{A}_a$ by merely deleting the row that represents the surrounding environment. In Fig. 10, node 6 represents the environment and when it is deleted

$$\mathbf{A} = \begin{bmatrix} -1 & 1 & 0 & 0 & 0 & 0 & 0 & 0 & 0 \\ 0 & -1 & -1 & 0 & 1 & 1 & 1 & 0 & 0 \\ 0 & 0 & 0 & 0 & 0 & -1 & 0 & 0 & 1 \\ 0 & 0 & 0 & 0 & 0 & 0 & -1 & 1 & 0 \\ 0 & 0 & 1 & -1 & 0 & 0 & 0 & 0 & 0 \end{bmatrix} \tag{47}$$

Because the row representing the environment has been deleted, the analysis becomes a node-to-datum analysis with the environment as the datum and all node temperatures to be considered as temperature excesses.

Continuity. The product $\mathbf{AQ}$, which postmultiplies an $n \times b$ matrix by a $b \times 1$ column vector, presents a statement of continuity at each node

$$\mathbf{AQ} = \begin{bmatrix} -1 & 1 & 0 & 0 & 0 & 0 & 0 & 0 & 0 \\ 0 & -1 & -1 & 0 & 1 & 1 & 1 & 0 & 0 \\ 0 & 0 & 0 & 0 & 0 & -1 & 0 & 0 & 1 \\ 0 & 0 & 0 & 0 & 0 & 0 & -1 & 1 & 0 \\ 0 & 0 & 1 & -1 & 0 & 0 & 0 & 0 & 0 \end{bmatrix} \begin{bmatrix} q_1 \\ q_2 \\ q_3 \\ q_4 \\ q_5 \\ q_6 \\ q_7 \\ q_8 \\ q_9 \end{bmatrix}$$

$$= \begin{bmatrix} q_2 - q_1 \\ q_5 + q_6 + q_7 - q_2 - q_3 \\ q_9 - q_6 \\ q_8 - q_7 \\ q_3 - q_4 \end{bmatrix} = \mathbf{O}$$

and this can be confirmed by an inspection of the oriented graph in Fig. 10(b). Thus the equation

$$\mathbf{AQ} = \mathbf{O} \tag{48}$$

is a matrix statement of the continuity at every node in the array.

A matrix that links the branch temperature drops can also be found. Define the elements c_{jk} of the matrix $\mathbf{C}$ in

$$\Delta\mathbf{T} = \mathbf{C}\Theta \tag{49}$$

by

$$c_{jk} = \begin{cases} +1 \text{ if branch } j \text{ leaves node } k \\ -1 \text{ if branch } j \text{ leaves node } k \\ 0 \text{ if branch } j \text{ does not touch node } k \end{cases} \tag{50}$$

The matrix $\mathbf{C}$ will contain b rows and n columns and the $b \times n$ matrix for the oriented graph of Fig. 10(b) (without node 6) will be

$$\mathbf{C} = \begin{bmatrix} -1 & 0 & 0 & 0 & 0 \\ 1 & -1 & 0 & 0 & 0 \\ 0 & -1 & 0 & 0 & 1 \\ 0 & 0 & 0 & 0 & -1 \\ 0 & 1 & 0 & 0 & 0 \\ 0 & 1 & -1 & 0 & 0 \\ 0 & 1 & 0 & -1 & 0 \\ 0 & 0 & 0 & 1 & 0 \\ 0 & 0 & 1 & 0 & 0 \end{bmatrix} \tag{51}$$

There are two kinds of branches. Those that touch two nodes, say nodes r and s, will possess a temperature drop, $\Delta T = \theta_r - \theta_s$. Those that touch a node and the datum node will have a temperature drop equal to the temperature excess for that node. In both cases, the branch temperature drops depend on the node temperature excesses. If equation (51) is put into equation (49), the result is

$$\mathbf{C}\Theta = \begin{bmatrix} -1 & 0 & 0 & 0 & 0 \\ 1 & -1 & 0 & 0 & 0 \\ 0 & -1 & 0 & 0 & 1 \\ 0 & 0 & 0 & 0 & -1 \\ 0 & 1 & 0 & 0 & 0 \\ 0 & 1 & -1 & 0 & 0 \\ 0 & 1 & 0 & -1 & 0 \\ 0 & 0 & 0 & 1 & 0 \\ 0 & 0 & 1 & 0 & 0 \end{bmatrix} \begin{bmatrix} \theta_1 \\ \theta_2 \\ \theta_3 \\ \theta_4 \\ \theta_5 \end{bmatrix} = \begin{bmatrix} -\theta_1 \\ \theta_1 - \theta_2 \\ \theta_5 - \theta_2 \\ -\theta_5 \\ \theta_2 \\ \theta_2 - \theta_3 \\ \theta_2 - \theta_4 \\ \theta_4 \\ \theta_3 \end{bmatrix} = \Delta\mathbf{T}$$

which is entirely correct. Moreover, a comparison of equations (47) and (51) shows that $a_{jk} = c_{kj}$, which indicates that

$$\mathbf{C} = \mathbf{A}^{\mathrm{T}}$$

and that

$$\Delta\mathbf{T} = \mathbf{A}^{\mathrm{T}}\Theta \tag{52}$$

Downloaded 16 Dec 2010 to 193.140.21.150. Redistribution subject to ASME license or copyright; see http://www.asme.org/terms/Terms_Use.cfm

Node-to-Datum Analysis of Finned Arrays. The method of node-to-datum analysis is based on the branch equation, which is a form of equation (44)

$$\mathbf{Q} = \mathbf{Q}_s - \mathbf{Y}\Delta\mathbf{T}_s + \mathbf{Y}\Delta\mathbf{T} \tag{53}$$

the expression of continuity

$$\mathbf{AQ} = \mathbf{O} \tag{48}$$

and the relationship between the branch temperature drops and the node temperature excesses

$$\Delta\mathbf{T} = \mathbf{A}^{\mathrm{T}}\boldsymbol{\theta} \tag{52}$$

If equation (51) is premultiplied by $\mathbf{A}$ and set equal to zero in accordance with equation (48)

$$\mathbf{AQ} = \mathbf{O} = \mathbf{AQ}_s - \mathbf{AY}\Delta\mathbf{T}_s + \mathbf{AY}\Delta\mathbf{T}$$

or

$$\mathbf{AY}\Delta\mathbf{T} = \mathbf{AY}\Delta\mathbf{T}_s - \mathbf{AQ}_s \tag{54}$$

Then define a heat source vector

$$\tilde{\mathbf{Q}} = \mathbf{AY}\Delta\mathbf{T}_s - \mathbf{AQ}_s \tag{55}$$

so that

$$\mathbf{AY}\Delta\mathbf{T} = \tilde{\mathbf{Q}}$$

If equation (52) is inserted here

$$\mathbf{AYA}^{T}\boldsymbol{\theta} = \tilde{\mathbf{Q}}$$

the node equations result

$$\mathbf{Y}_n\boldsymbol{\theta} = \tilde{\mathbf{Q}} \tag{56}$$

where the node admittance matrix $\mathbf{Y}_n$ is defined by

$$\mathbf{Y}_n = \mathbf{AYA}^{\mathrm{T}} \tag{57}$$

Solution of equation (56)

$$\boldsymbol{\theta} = \mathbf{Y}_{\mathrm{n}}^{-1}\tilde{\mathbf{Q}} \tag{58}$$

yields the temperature excess at each node and, if desired, input admittances can then be evaluated at each point where heat is injected into the array.

Conclusion

As heat rejection systems become more and more complicated, computationally efficient methods must be developed for their analysis and evaluation. This paper has attempted to summarize two methods for the analysis of complex finned arrays. One of them pertains to the array with no loops in the graph theoretical sense in which the analysis is carried out using three combinational algorithms based on a mathematical representation of a fin as either an inverse thermal transmission matrix or a thermal transmission ratio. The other is a general and matrix-oriented procedure that is used for arrays containing loops in the graph theoretical sense and is based on the principle of reciprocity and the representation of each individual fin as an equivalent pi network.

Acknowledgment

Some of the techniques presented in this article were developed under National Science Foundation Grant No. ENG-77-01297. The author also wishes to acknowledge the assistance of Mrs. Robert Limes, who generated the text, and Mr. Alvin W. Lau, who prepared the illustrations.

References

Chan, S. P., 1969, *Introductory Topological Analysis of Electrical Networks*, Holt, Rinehart and Winston, New York.

Chen, S. Y., and Zyskowski, G. L., 1963, "Steady State Heat Conduction in a Straight Fin With Variable Heat Transfer Coefficient," ASME Paper No. 63-HT-1.

Gardner, K. A., 1945, "Efficiency of Extended Surface," *Trans. ASME*, Vol. 67, p. 621.

Han, L. S., and Lefkowitz, S. G., 1960, "Constant Cross Section Fin Efficiencies for Non-uniform Surface Heat Transfer Coefficients," ASME Paper No. 60-WA-41.

Harper, D. R., and Brown, W. B., 1922, "Mathematical Equations for Heat Conduction in the Fins of Air Cooled Engines," NACA Report No. 158.

Irwin, J. D., 1984, *Basic Engineering Circuit Analysis*, McGraw-Hill, New York.

Kays, W. M., 1960, "Basic Heat Transfer and Flow Friction Characteristics of Six High Performance Heat Transfer Surfaces," ASME *Journal of Engineering for Power*, Vol. 80, p. 27.

Kern, D. Q., and Kraus, A. D., 1972, *Extended Surface Heat Transfer*, McGraw-Hill, New York.

Kraus, A. D., Snider, A. D., and Doty, L. F., 1978, "An Efficient Algorithm for Evaluating Arrays of Extended Surface," ASME JOURNAL OF HEAT TRANSFER, Vol. 100, p. 288.

Kraus, A. D., and Snider, A. D., 1980, "New Parameterizations for Heat Transfer in Fins and Spines," ASME JOURNAL OF HEAT TRANSFER, Vol. 102, p. 415.

Kraus, A. D., Snider, A. D., and Landis, F., 1982, "The Reciprocity of Extended Surface and the Node Analysis of Finned Arrays," *Proc. 7th Int. Heat Transfer Conf.*, Munich, Federal Repubic of Germany, Vol. 6, p. 223.

Manzoor, M., Ingham, D. B., and Heggs, P. J., 1983, "Improved Formulations for the Analysis of Convecting and Radiating Finned Surfaces," *AIAA J.*, Vol. 21, p. 120.

Murray, W. M. 1938, "Heat Transfer Through an Annular Disk or Fin of Uniform Thickness," ASME *J. Applied Mech.*, Vol. 60, p. A78.

Parsons, S. R., and Harper, D. R., 1922, "Radiators for Aircraft Engines," US Bureau of Standards, Technical Paper No. 211, p. 327.

Sparrow, E. M., Baliga, B. R., and Patankar, S. V., 1978, "Forced Convection Heat Transfer From a Shrouded Fin Array With and Without Tip Clearance," ASME JOURNAL OF HEAT TRANSFER, Vol. 100, p. 572.

Sparrow, E. M., and Hennecke, D. K., 1970, "Temperature Depression at the Base of a Fin," ASME JOURNAL OF HEAT TRANSFER, Vol. 92, p. 204.

Sparrow, E. M., and Lee, L., 1975, "Effects of Fin Base Depression in a Multifin Array," ASME JOURNAL OF HEAT TRANSFER, Vol. 97, p. 63.

Trumpler, P. R., 1945, "Discussion of Gardner, K. A., 1945, Efficiency of Extended Surface," *Trans. ASME*, Vol. 67, p. 630.

Downloaded 16 Dec 2010 to 193.140.21.150. Redistribution subject to ASME license or copyright; see http://www.asme.org/terms/Terms_Use.cfm

Some Perspectives on Enhanced Heat Transfer—Second-Generation Heat Transfer Technology

A. E. Bergles
Heat Transfer Laboratory,
Rensselaer Polytechnic Institute,
Troy, NY 12180-3590
Fellow ASME

During the past twenty-five years, heat transfer enhancement has grown at a rapid rate to the point where it can be regarded as a major field of endeavor, a second-generation heat transfer technology. After some historical background, mention of the driving trends, and a review of the various convective enhancement techniques, four areas of major contemporary interest are discussed: structured surfaces for shellside boiling, rough surfaces in tubes, offset strip fins, and microfin tubes for refrigerant evaporators and condensers. The review concludes with developments in the major areas of application.

Introduction

The enhancement of heat transfer has concerned researchers and practitioners since the earliest documented studies of heat transfer. In his pioneering paper directed toward development of a temperature scale, Newton (1701) suggested an effective way of increasing convective heat transfer ". . . not in a calm air, but in a wind that blew uniformly upon it. . . ."

Joule (1861) reported significant improvement in the "conductivity" or overall heat transfer coefficient for in-tube condensation of steam when a wire, spiralled around the condenser tube, was inserted in the cooling water jacket. Whitham (1896) reported increases up to 18 percent in fire-tube boiler efficiency when "retarders" or twisted-tape inserts were inserted in the tube; it was suggested that the inserts should by used only when "the boiler plant is pushed and the draught is strong." Enhanced surfaces for boiling were part of one of the first systematic studies of nucleate pool boiling by Jakob and Fritz (1931). The US Patent literature dealing with enhanced heat exchangers dates back to the 1920s (shell-side fins, Lea, 1921) as does the manufacturer's literature (corrugated tubes, Alberger Heater Company, 1921). The latter example of commercialization, albeit brief, is shown in Fig. 1; an increase of the hot water heating capacity of 50 percent was claimed as a result of enhancing both the tube-side single-phase flow and the shell-side condensing of steam.

In spite of these early efforts, this aspect of heat transfer received relatively little attention until about 30 years ago as evidenced by the small amount of technical and commercial literature. In the mid-1950s the field began to develop in response to the need for more efficient power and process heat exchangers, the advent of commercial nuclear power, and the demands of space flight systems. Another sharp increase in activity was associated with heat recovery and alternate energy systems stimulated by the 1973 oil embargo. The exponential increase in world technical literature is evident from Fig. 2 and a similar trend with US Patents is noted in Fig. 3. It is now estimated that each year over 500 papers, reports, and patents are published on this subject. ASME meeting sessions (often with bound volumes) are scheduled regularly, an ASME short course is given periodically, and over 10 percent of the papers at the quadrennial International Heat Transfer Conference concern this subject. In view of the level of activity and the continued growth, enhanced heat transfer has truly become a second-generation heat transfer technology.

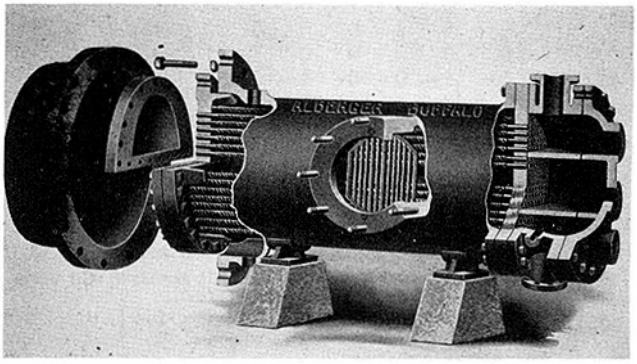

Fig. 1 Steam-heated water heater using corrugated tubes (Alberger, 1921)

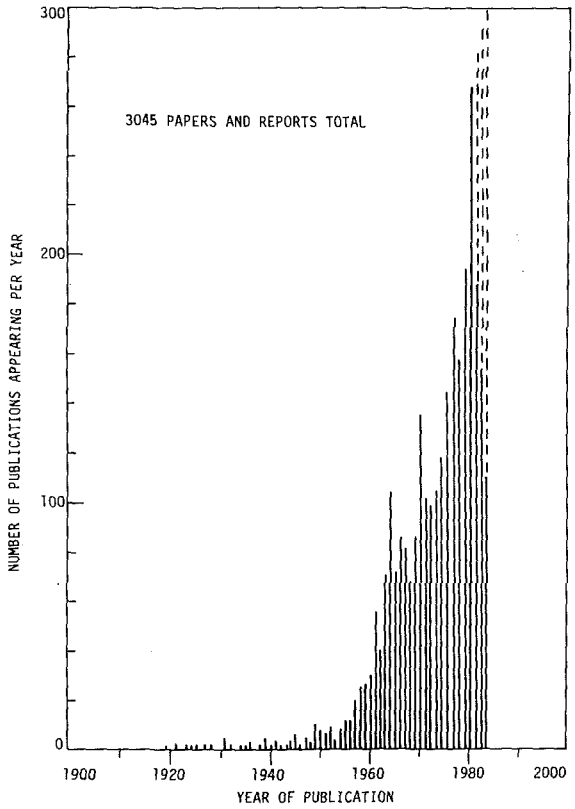

Fig. 2 Annual publications in heat transfer enhancement (Bergles et al., 1983)

Contributed by the Heat Transfer Division for publication in the JOURNAL OF HEAT TRANSFER. Manuscript received by the Heat Transfer Division March 1, 1988. Keywords: Augmentation and Enhancement, Boiling, Condensation, Reviews.

Copyright © 1988 by ASME

Downloaded 16 Dec 2010 to 193.140.21.150. Redistribution subject to ASME license or copyright; see http://www.asme.org/terms/Terms_Use.cfm

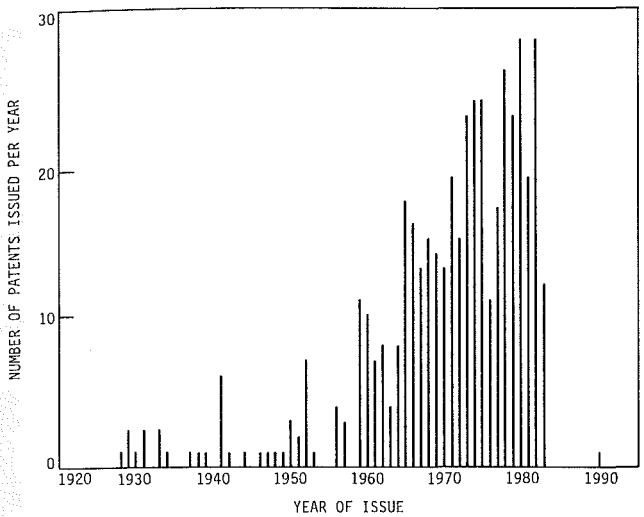

Fig. 3 US Patents issued annually in heat transfer enhancement (Webb et al., 1983)

There have been a number of recent survey articles and handbook sections prepared that deal with the field in general (e.g., Bergles, 1978, 1983, 1985; Nakayama, 1982) or with specific aspects (e.g., finned tubes: Webb, 1980; nucleate boiling: Webb, 1981; electrohydrodynamics: Kulacki, 1981; condensation: Marto, 1986). The purpose of the present review is not to repeat the extensive citations given in such reviews, but rather to single out recent examples of progress in understanding and predicting enhancement.

Some general observations can be made as to the evolution of enhancement technology during the past ten years. The widely scattered literature has been collected, classified, entered into a computerized data base, and published in several reports. Sophisticated experiments have been conducted to determine local heat transfer coefficients with complex geometries. Numerical simulations of increasingly complicated configurations are being attempted. Of greatest significance is the extent to which the more effective and feasible enhancement techniques have graduated from the laboratory to full-scale industrial equipment. This is documented by the over 200 manufacturers who offer products ranging from enhanced tubes to entire thermal systems incorporating enhancement technology (Bergles et al., 1984). Research and development at the present time is driven primarily by applications rather than by curiosity.

Before discussing some of the more recent progress in understanding and applications, the techniques will be briefly described.

The Techniques

Enhancement techniques can be classified as *passive* methods, which require no direct application of external power, or as *active* schemes, which require external power. The effectiveness of both types depends strongly on the mode of heat transfer, which might range from single-phase free convection to dispersed-flow film boiling. Brief descriptions of passive techniques, following the classification given by Bergles (1985), are given below.

Treated surfaces involve fine-scale alternation of the surface finish or coating (continuous or discontinuous). They are used for boiling and condensing; the roughness height is below that which affects single-phase heat transfer. The fine-scale structures used to enhance nucleate boiling are generally included in this category.

Nomenclature

A, A_p = projected or nominal surface area
C_q = constant in equation (5)
C_t = ratio of liquid film area to thickness
c_p = specific heat at constant pressure
d = tube diameter
d_b = bubble departure diameter
e = protuberance height
e^+ = roughness Reynolds number $= (e/d)\mathrm{Re}(f/2)^{0.5}$
F = function in equation (8)
f = Fanning friction factor
f_b = frequency of bubble emission
G = mass flux
$\bar{g}$ = function in equation (8)
h = heat transfer coefficient; height of offset strip fin
h_{fg} = enthalpy of vaporization
j = Colburn factor $= \mathrm{St}\,\mathrm{Pr}^{2/3}$
k = fluid thermal conductivity
k_1, k_L = liquid thermal conductivity
L = length of offset strip fin
m_1 = mass vaporized
N_A = number of nucleation sites
Nu = Nusselt number $= hd/k$
n = number of sharp corners facing flow
p = spacing between roughness elements
Pr = Prandtl number $= c_p\mu/k$
q = rate of heat transfer
q'' = heat flux
q_l'' = superficial latent heat flux
q_{ex}'' = superficial heat flux resulting from free convection
R_b = bubble radius
Re = Reynolds number $= Gd/\mu$
Re* = Reynolds number parameter defined by equation (17)
S = total surface area occupied by evaporating liquid film
St = Stanton number $= h/Gc_p$
s = spacing of offset strip fin
t = average liquid film thickness; thickness of offset strip fin plates
T_L = liquid film temperature at bubble interface
T_S = saturation temperature
T_V = vapor temperature
T_W = wall temperature
ΔT = temperature difference (wall superheat)
U_e^+ = Nikuradse similarity function $= (2/f)^{0.5} + 2.5\ \ln(2e/d) + 3.75$
v_{fg} = specific volume change during vaporization
x, y = exponents
α = angle from axis of helical rib roughness
β = geometry factor in equation (2); rib contact angle in equation (11)
θ = time
μ = dynamic viscosity
ρ = vapor density
σ = surface tension

Subscripts

1 = first period pertaining to Thermoexcel-E model
2 = second period pertaining to Thermoexcel-E model
a = pertains to enhanced tube
h = based on hydraulic diameter
L = based on fin element length
s = pertains to plain tube

Downloaded 16 Dec 2010 to 193.140.21.150. Redistribution subject to ASME license or copyright; see http://www.asme.org/terms/Terms_Use.cfm

Rough surfaces are produced in many configurations ranging from random sand-grain-type roughness to discrete protuberances. The configuration is generally chosen to promote turbulence rather than to increase the heat transfer surface area. The application of rough surfaces is directed primarily toward single-phase flow.

Extended surfaces are routinely employed in many heat exchangers. The development of new types of extended surfaces, such as integral inner-fin tubing, and the improvement of heat transfer coefficients on extended surfaces, by shaping or interrupting the surfaces, are of particular interest.

Displaced enhancement devices are inserted into the flow channel so as to improve energy transport indirectly at the heated surface. They are used with forced flow.

Swirl-flow devices include a number of geometric arrangements or tube inserts for forced flow that create rotating and/or secondary flow: coiled tubes, inlet vortex generators, twisted-tape inserts, and axial-core inserts with a screw-type winding.

Surface-tension devices consist of wicking or grooved surfaces to direct the flow of liquid in boiling and condensing.

Additives for liquids include solid particles and gas bubbles in single-phase flows and liquid trace additives for boiling systems.

Additives for gases are liquid droplets or solid particles, either dilute phase (gas–solid suspensions) or dense phase (fluidized beds).

The active techniques are described below.

Mechanical aids stir the fluid by mechanical means or by rotating the surface. Surface "scraping," widely used for viscous liquids in the chemical process industry, can also be applied to duct flow of gases. Equipment with rotating heat exchanger ducts is found in commercial practice.

Surface vibration at either low or high frequency has been used primarily to improve single-phase heat transfer.

Fluid vibration is the most practical type of vibration enhancement, given the mass of most heat exchangers. The vibrations range from pulsations of about 1 Hz to ultrasound. Single-phase fluids are of primary concern.

Electrostatic fields (d-c or a-c) are applied in many different ways to dielectric fluids. Generally speaking, electrostatic fields can be directed to cause greater bulk mixing of fluid in the vicinity of the heat transfer surface. An electrical field and a magnetic field may be combined to provide a forced convection via electromagnetic pumping.

Injection involves supplying gas to a flowing liquid through a porous heat transfer surface or injecting similar fluid upstream of the heat transfer section. Surface degassing of liquids can produce augmentation similar to gas injection. Only single-phase flow is of interest.

Suction involves either vapor removal through a porous heated surface in nucleate or film boiling, or fluid withdrawal through a porous heated surface in single-phase flow.

Two or more of the above techniques may be utilized simultaneously to produce an enhancement larger than that produced by only one technique. The simultaneous use is termed *compound enhancement*.

It should be emphasized that one reason for studying enhanced heat transfer is to assess the effect of an inherent condition on heat transfer. Some practical examples include roughness produced by standard manufacturing, degassing of liquids with high gas content, surface vibration resulting from rotating machinery or flow oscillations, fluid vibration resulting from pumping pulsation, and electric fields present in electrical equipment.

To give an idea of the greatest activity, Table 1 breaks down the citations represented in Fig. 2 according to technique and mode. It is clearly impossible in a brief space to give an overview of progress in all areas. Instead, just four commercially important passive techniques will be discussed. These techniques are typical of many in that they have been the object of sophisticated experiments and analysis.

Structured Surfaces for Shell-Side Boiling

As noted in the preceding section, this classification refers to fine-scale alteration of the surface finish, i.e., the tube surface appears rather smooth. A coating may be applied to the plain tube or the surface may be deformed to produce subsurface channels or pores.

Nucleate and transition pool boiling are usually quite strongly dependent on the surface condition as characterized by the material, the surface finish, and the surface chemistry. Certain types of roughness, fouling, and oxidation have been shown to reduce wall superheats, increase peak critical heat flux (CHF), and destabilize film boiling; however, these

Table 1 Classification of augmentation techniques and number or references in each category (Bergles et al., 1983)

	Single-phase natural convection	Single-phase forced convection	Pool boiling	Forced-convection boiling	Condensation	Mass transfer
Passive techniques (no external power required)						
Treated surfaces	NA	NA	149	17	53	NA
Rough surfaces	7	418	42	65	65	29
Extended surfaces	23	416	75	53	175	33
Displaced enhancement devices	NA	59	4	17	6	15
Swirl flow devices	NA	140	NA	83	17	10
Coiled tubes	NA	142	NA	50	6	9
Surface tension devices	NA	NA	12	1	NA	NA
Additives for liquids	3	22	61	37	NA	6
Additives for gases	NA	211	NA	NA	5	NA
Active techniques (external power required)						
Mechanical aids	16	60	30	7	23	18
Surface vibration	52	30	11	2	9	11
Fluid vibration	44	127	15	5	2	39
Electric or magnetic fields	50	53	37	10	22	22
Injection or suction	6	25	7	1	6	2
Jet impingement	NA	17	2	1	NA	2
Compound enhancement (two or more techniques)	2	50	4	4	4	2

NA = not applicable.

Downloaded 16 Dec 2010 to 193.140.21.150. Redistribution subject to ASME license or copyright; see http://www.asme.org/terms/Terms_Use.cfm

naturally occurring conditions are too unpredictable to permit their exploitation in commercial equipment. The action of nonwetting coatings, such as Teflon, for promoting boiling of water or aqueous solutions is well documented. Thin insulating coatings of Teflon may also be used to promote the rate of cooling of hot materials through reduction of the surface temperature to the level where transition or nucleate boiling occurs rather than film boiling. While the mechanisms of both situations are well understood, there have been no practical applications.

With highly wetting liquids (refrigerants, fluorochemicals, other organics, cryogens, alkali liquid metals), doubly reentrant cavities are required to ensure vapor trapping so that nucleation is stable. The probability of having such active nucleation sites is increased by selective machining, forming, or coating the surface with a porous material. Furthermore, the subsurface structures represent large surface areas that are conducive to high rates of vapor generation. The liquid flows via selected paths or channels to the interior where it is vaporized; the vapor is then ejected through other paths by a sort of "bubbling."

Boiling data for three of the most widely used structured surfaces are shown in Fig. 4. Note that the heat flux is based on the area of the equivalent smooth tube for a particular outside diameter. The shifts in the nucleate boiling curve to lower superheat are representative of the excellent performance of such surfaces. It must be emphasized, however, that the performance is very sensitive to surface configuration and the working fluid. The gap width, pore size, or particle size is tailored to the fluid and the pressure for optimum performance using empirical experience or guidelines inferred from models.

Porous Metallic Matrix Coating. Mechanistic models of the liquid–vapor exchange process have been proposed for the major commercial structured surfaces. Consider first the porous coatings consisting of sintered particles or fibers, particles bonded by electroplating, metal sprayed powder, or electroplated polyurethane foam. An example of sintered particles is shown in Fig. 5. Webb (1983) examined a wide variety of data for coatings of nearly spherical particles and concluded that particle diameter has very little effect on performance but that the preferred coating thickness is three to four layers of particles.

O'Neill et al. (1972) postulated a nucleate boiling model assuming an idealized matrix of uniform diameter spherical particles in a known packing arrangement with pores of uniform size each containing vapor bubbles. Thin liquid films exist on the surfaces of the particles. Heat flows from the prime surface through the particles and vaporizes the liquid film. The pores are assumed to be interconnected so that the vapor can exit to the surrounding liquid and liquid can be supplied to the interior of the matrix. Webb (1983) has clarified a number of the assumptions employed in this model.

The heat flux based on the projected area of the base surface A_p is simply

$$q'' = \frac{q}{A_p} = k_L \frac{S}{A_p} \frac{(T_W - T_L)}{t} \tag{1}$$

where k_L is the liquid thermal conductivity, S is the total surface area occupied by the liquid film, t is the average liquid film thickness, T_W is the particle surface temperature (assumed to be the base temperature), and T_L is the liquid film temperature at the surface of the bubble. Introducing the Gibbs equation, the wall superheat for a pore or bubble radius R_b is given by

$$T_W - T_S = \frac{\beta q'' R_b^2}{k_L} + \frac{2\sigma v_{fg} T_S}{h_{fg} R_b} \tag{2}$$

where the geometry factor β, a collection of terms involving geometry, can be calculated if the matrix thickness and the particle packing arrangement are known.

This model provides an optimum pore radius for which the wall superheat is a minimum. A relatively coarse matrix is required for water while a fine matrix is better for light hydrocarbons, fluorocarbons, and cryogens.

The packing arrangement may be deduced from measurement of the weight and volume of the coating or from measurement of the displacement of a wetting liquid. Using the latter method for the High Flux surface, O'Neill et al. (1972) found that the porosity ranged from 0.50 to 0.65; hence, an in-line packing was most appropriate.

Webb (1983) tested equation (2) against data for R-11 and R-113 and found that the predicted values of $T_W - T_S$ ranged from 0.62 to 2.05 times the observed values. While the model gave reasonably good results, considering the difficulty of accurately measuring temperature differences of the order of 1 K, the model has some shortcomings. As noted later by Czikk and O'Neill (1979), commercial coatings utilize powders that are not spherical and have a range of particle sizes. Also, since not all pores physically present are functionally active, it was necessary to determine the active sites from actual boiling data. With these modifications, the predictions were in rather good agreement with the data. Of course, by requiring the ac-

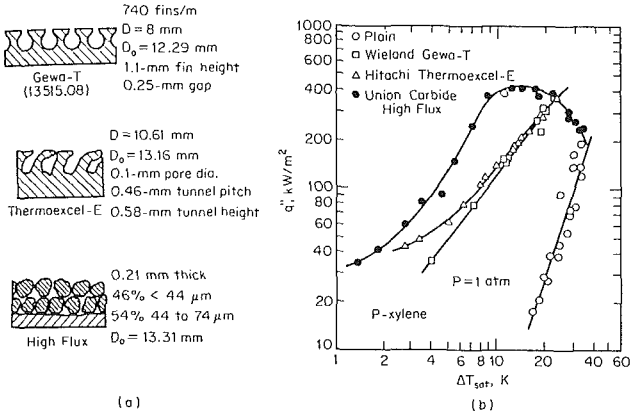

Fig. 4 Pool boiling from smooth and structured surfaces on the same apparatus: (a) cross-sectional sketches of surfaces; (b) boiling curves (Yilmaz et al., 1980)

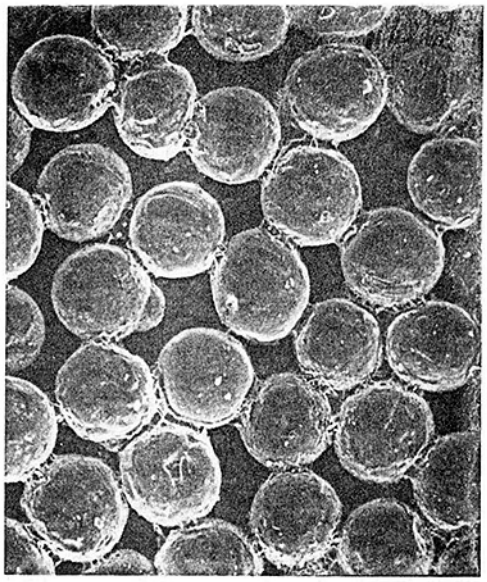

Fig. 5 Plan view of sintered surface, 50 × (Kim and Bergles, 1985)

Downloaded 16 Dec 2010 to 193.140.21.150. Redistribution subject to ASME license or copyright; see http://www.asme.org/terms/Terms_Use.cfm

tual boiling data, the model becomes an interpretive rather than a predictive tool. Its success suggests that the physics is correct.

On the other hand, Webb (1983) argues that even with this realism, the basic concept of a static model is incorrect and that proper modeling must take into account time-dependent two-phase flow within the matrix. No suggestions are offered as to how this might be accomplished.

While the established nucleate boiling performance of porous metallic matrix surfaces is excellent, there are concerns about the initiation of boiling. The typical fluids used with these surfaces are highly wetting; that is, they have contact angles approaching zero on all engineering surfaces. As a result, doubly re-entrant cavities are required if pure vapor nuclei are to be retained during subcooled liquid conditions. Such cavities are possible with spherical particles; however, Kim and Bergles (1985) have shown that even the fine particles normally employed are too large to allow re-entrant cavities small enough to permit significant subcooling without flooding the cavities. The burden of initiating boiling is thus placed on naturally occurring cavities on the base surface or on the particles. Since these are expected to be small, the wall superheat at incipient boiliing is expected to be high, as is observed (Bergles and Chyu, 1982; Kim and Bergles, 1985). As shown in Fig. 6, the incipient boiling superheats and subsequent temperature excursions are repeatable and large for a plain surface and several sintered surfaces. This results in the well-known boiling curve hysteresis. The significant reduction in superheat with the enhanced surfaces, from 30–40 K to 20–30 K, is attributed to the greater probability of finding re-entrant cavities in the large contorted surfaces within the matrix.

Given the impossibility of controlling incipient boiling superheat through geometry, other means must be found to insure the onset of boiling, particularly in systems that are ΔT controlled. Introduction of vapor or foreign gas is effective (Kim and Bergles, 1985), but the theory of its action is not well understood.

Tunnel-and-Pore Forming. The second type of structured surface is the Hitachi Thermoexcel-E surface characterized by well-defined pores that expose the subsurface channels. Nakayama et al. (1980) proposed a dynamic model based on the escape of vapor from some pores while liquid is being drawn into other pores. A substantial portion of the surface is subject to single-phase convection. The heat flux is based on the projected area corresponding to the outside diameter and is given by

$$q'' = q_l'' + q_{ex}'' \tag{3}$$

where q_l'' is the latent heat flux and q_{ex}'' is the enhanced free convection contribution. This is shown in Fig. 7.

The latent heat term was basically considered to involve three periods, a dormant period where the thin liquid film in the tunnel evaporates causing the pressure to build up, a bubbling period where some pores are active that leads to a reduction in pressure within the tunnel, and a short liquid intake period where the pressure is low enough to permit liquid to flow into the tunnel. The core of the analysis is to find for each period the amount of liquid evaporated or the total heat transfer and the duration, i.e.,

$$q_l'' = \frac{(m_{l1} + m_{l2})h_{fg}}{(\theta_1 + \theta_2)A} = \frac{k_l C_{t1}(T_W - T_{V1})}{A} + \frac{k_l C_{t2}(T_W - T_{V2})}{A} \tag{4}$$

where C_{t1} and C_{t2} are the ratios of liquid film area to liquid film thickness. Here, the two dynamic periods have been combined into the second period.

The single-phase contribution is related to the active site density

$$q_{ex}'' = \left(\frac{\Delta T}{C_q}\right)^{1/y} \left(\frac{N_A}{A}\right)^{-x/y} \tag{5}$$

The analysis is very complex and in places difficult to interpret (Ayub, 1986). Much empirical information is required to establish the basic characteristics of the heat transfer for a given surface. In particular, at an arbitrary reference state, say $\Delta T = 1$K, q'' is recorded and average values of the frequency of bubble emission, bubble departure diameter, and number of active sites are measured. This establishes the values of C_{t1} and C_{t2} along with two other key empirical parameters, the constant in the bubble departure equation and a constant characterizing the liquid curvature during the liquid intake.

Equation (5) was established from data for a variety of regular surfaces and several of the structured surfaces. It was necessary to estimate the natural convection component by subtracting the latent component from the total heat flux:

$$q_{ex}'' = q'' - \frac{\pi}{12} d_b^3 f_b h_{fg} \rho_v \frac{N_A}{A} \tag{6}$$

The exponents x and y were presumed to apply to all surfaces and fluids, but C_q was strongly dependent on the fluid.

For a given fluid and surface, once the five constants are determined, the boiling curve can be predicted with fair accuracy beyond the reference point. It is evident that this model is also interpretive and of no use in engineering calculations. Potentially important parameters such as the best pore size cannot be determined from the model. The general physics of

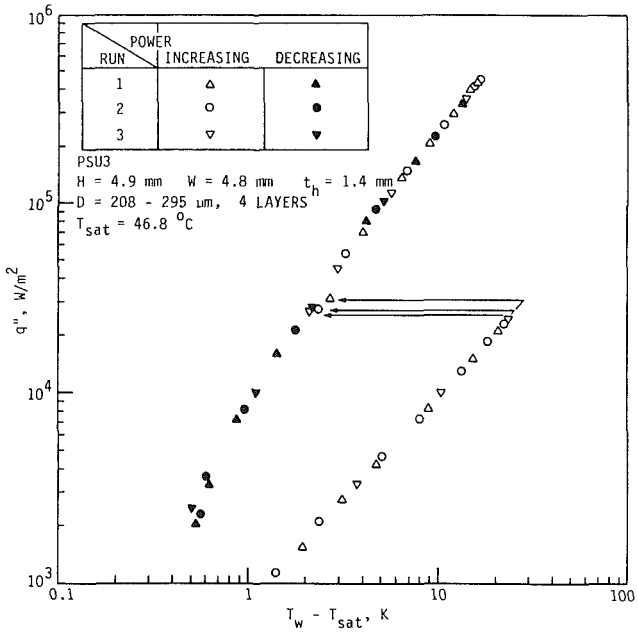

Fig. 6 Boiling data for a sintered surface illustrating the large wall superheat required to initiate boiling (Bergles and Kim, 1985)

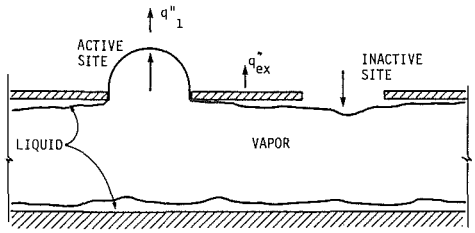

Fig. 7 Conceptual model of boiling from tunnel-and-pore surface (Ayub, 1986)

Downloaded 16 Dec 2010 to 193.140.21.150. Redistribution subject to ASME license or copyright; see http://www.asme.org/terms/Terms_Use.cfm

the process does seem to be correct, but the details cannot really be verified because of the large number of empirical constants. In spite of these shortcomings, the work of Nakayama et al. (1980) stands out as an example of original thinking and physical insight. They have shown that dynamic modeling is necessary for the structured surfaces and that it is possible to formulate the equations and obtain solutions.

The problem of incipient boiling with the Thermoexcel-E surface is similar to that described earlier. While such behavior is not well documented, Torii et al. (1978), among others, report considerable boiling curve hysteresis.

T-Shaped Fin Forming. Turning now to the final surface shown in Fig. 4, the Gewa-T surface has also been studied in detail in an attempt to obtain a first-order model of the even more complex liquid–vapor exchange mechanism. Here, the liquid and vapor are not constrained to flow through certain openings. Although it has been suggested that bubbles flow in the channels around the circumference and are ejected near the top (Stephan and Mitrovic, 1981), Marto and Hernandez (1983) observed that these bubbles ejected at other locations, even at the bottom of the tube. Ayub and Bergles (1987), on the basis of tests with simulators and actual tubes, confirmed that liquid flows in and vapor is ejected around the entire tube circumference when boiling at high flux. Their model shown in Fig. 8 is similar to that for the Thermoexcel-E surface except that the liquid and vapor are free to cross the tunnel opening at any point around the circumference.

Considering only time-averaged tube behavior, the total heat flux was formulated simply as

$$q'' = k_1 \frac{C_t \Delta T}{A} + \left(\frac{\Delta T}{C_q}\right)^{1/y} \left(\frac{N_A}{A}\right)^{-x/y} \tag{7}$$

where a single average vaporization term is considered. The values of C_q were essentially the same as those used by Nakayama et al. (1980). The value of N_A was measured and correlated as a function of ΔT. The film parameter C_t was then obtained from a $q'' - \Delta T$ reference point. The predicted values of other points along the boiling curve were found to be in good agreement with the data. In the case of water, the latent heat component dominated, whereas with R-113, the natural convection component was most important. This model ignores the dynamic behavior necessary for liquid–vapor exchange, but even with the simplifications, the resulting equation cannot be used for engineering predictions.

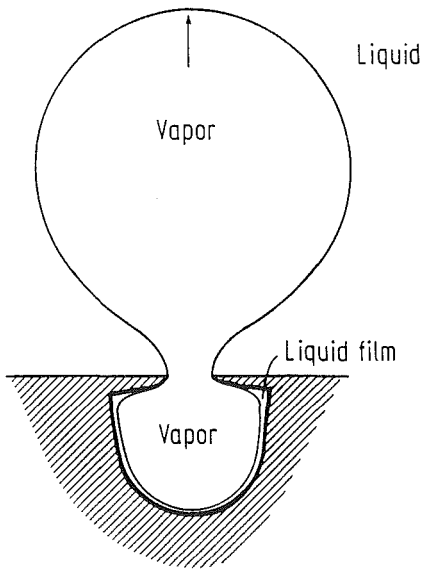

Fig. 8 Presumed configuration for boiling in a Gewa-T channel (Ayub and Bergles, 1987)

The Gewa-T tubes exhibit boiling curve hysteresis with wetting liquids but the effect is generally less than that observed with the Thermoexcel-E and High Flux surfaces (Ayub and Bergles, 1988). This is attributed to enhancement of the heat transfer prior to incipient boiling, through pumping of hot liquid from the channels or even by formation and trapping of vapor within the channels.

Tube Bundle Performance. The performance of enhanced tubes in horizontal bundles is receiving increased attention because this is the major application for these tubes. As in most other applications of enhancement technology, the understanding of enhanced tube behavior depends on the mechanism of the normal situation. Plain tube bundles often exhibit substantial increases in heat transfer coefficients above plain single tubes. This bundle factor is attributed to the convective effect in the upper portion of the bundle when the vapor quality is high. In the case of enhanced tubes, nucleate boiling overshadows the convective effect, with the result that the bundle performance tends to be reasonably close to that of the single tube. The result is a lesser increase in performance than would be expected from simply comparing the single tube data. This behavior is shown in Fig. 9. Although the opposite tendency is shown in Fig. 9 at low heat flux, there is some evidence that bundles of Gewa-T tubes perform better than

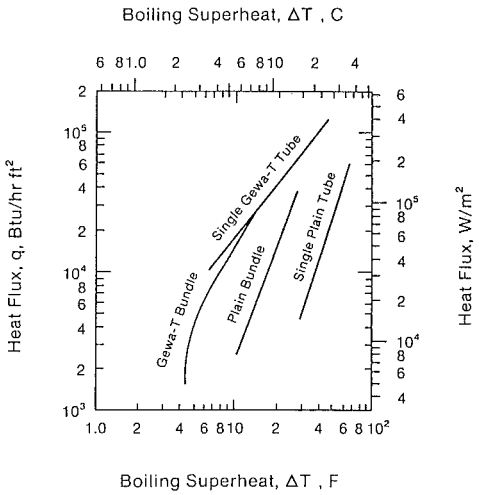

Fig. 9 Tube bundle boiling curves with plain tubes and Gewa-T tubes (Yilmaz et al., 1981)

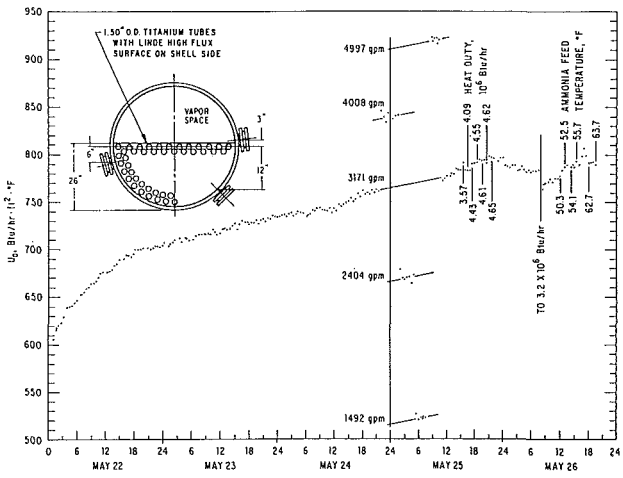

Fig. 10 Time variation of overall heat transfer coefficient in a High Flux flooded bundle ammonia evaporator, due to gradual spreading of boiling (Lewis and Sather, 1978)

Downloaded 16 Dec 2010 to 193.140.21.150. Redistribution subject to ASME license or copyright; see http://www.asme.org/terms/Terms_Use.cfm

single tubes (Menze, 1988). Arai et al. (1977) reported that the average performance of a bundle of Thermoexcel-E tubes was generally superior to the performance of a single tube, a conclusion that is disputed by Yilmaz et al. (1981). Several investigators (e.g., Czikk et al., 1970; Lewis and Sather, 1978) report that the performance of High Flux tubes in a bundle may be better than, essentially the same, or less than that of a single tube.

While in all cases, the enhanced bundle performs better than the plain bundle, there is clearly a lack of consensus on how to predict the bundle performance of enhanced tubes. Beyond this, there is a lack of knowledge as to how the enhanced tubes are affected by the two-phase crossflow. It is not even known what the two-phase flow characteristics are when there is intense promotion of nucleate boiling.

Bundles are not immune from the problem of boiling curve hysteresis with highly wetting fluids. As shown in Fig. 10, an ammonia flooded evaporator with enhanced tubes, intended for closed-cycle ocean thermal energy conversion, came up to full performance only after three days! While this problem does not occur in all systems because of normal vapor injection or favorable transients, the consequences of the inability to initiate boiling can be severe.

Fouling. The final issue that is very important with surfaces having small interior channels is fouling. It would be reasonable to expect solids to precipitate or less volatile components to hide out in the pores and render the normal boiling process ineffective. Only a few studies have considered fouling on either single tubes or tube bundles and the results are mixed.

Gottzmann et al. (1973) obtained overall performance data for industrial tube bundles under "lightly fouling conditions," those which might be encountered with cryogens, light hydrocarbons, and aqueous solutions. They found no detectable degradation in performance of High Flux surfaces over periods ranging from several hundred hours to several years. Their general recommendation is to use a pore size that keeps up the liquid circulation and to control the liquid chemistry. O'Neill et al. (1980) indicated that in certain circumstances typically associated with process upsets, significant fouling can occur. Lorenz et al. (1981) attributed the severe degradation of performance in an ammonia evaporator to prior fouling of the aluminum high flux coating. Chyu (1984) observed the gradual deterioration of performance of a high flux surface when boiling singly distilled water (Fig. 11); this was also attributed to some pre-existing contaminants on the surface.

Compressor lubricating oil is a possible contaminant in flooded refrigeration evaporators. The three surfaces under discussion have been tested with refrigerant-oil mixtures. Czikk et al. (1970) found that 2 percent oil in R-11 had no effect on the performance of the High Flux surface. More recently, however, Wanniarachchi et al. (1986) found that up to 3 percent oil in R-114 caused a 35 percent reduction in heat transfer coefficient at all heat fluxes. With 6 percent or more oil, the coefficient was sharply reduced at high heat flux. This behavior summarized in Fig. 12 was attributed to the creation of an oil-rich mixture within the porous structure.

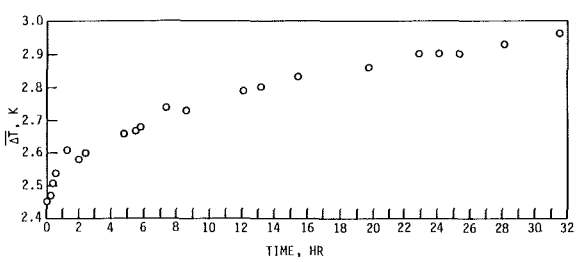

Fig. 11 Deterioration of boiling performance of a sintered surface due to boiling (Chyu, 1984)

Arai et al. (1977) studied the effect of up to 3.4 percent oil on the performance of a Thermoexcel-E bundle with R-12. At low heat fluxes, near the top of the bundle, the overall performance was increased, apparently due to foaming. The heat transfer at higher heat fluxes was degraded but not severely.

Stephan and Mitrovic (1981) found the degradation of heat transfer with R-12-oil mixtures to be nearly 40 percent at about 9 percent oil. Decreases in heat transfer coefficient with increasing concentration were observed at all concentrations except for intermediate concentrations at the highest heat flux where about 5 percent improvement was noted. In a subsequent paper, Stephan and Mitrovic (1982) discuss the thermodynamics of mixtures in an attempt to understand the phenomena.

Although the results for miscible oil–refrigerant mixtures are sometimes contradictory, it is important to note that the heat transfer coefficients for nucleate boiling with structured surfaces are above those for plain tubes under similar conditions. There is, however, a lack of understanding of why degradation relative to the pure refrigerant occurs in some cases but not in others and what the mechanism of degradation is.

Falling Film Evaporation. The use of structured surfaces in falling film (spray film) evaporation is another possibility. The same surfaces depicted in Fig. 4 were studied with single horizontal tubes subject to a feed of water (Chyu and Bergles, 1985). Both the High Flux and the Thermoexcel-E tubes exhibited low flux, nonboiling behavior similar to plain tubes. At high fluxes, nucleate boiling appeared to dominate and the data corresponded essentially to the extrapolation of pool boiling for the same surface with the same conditioning. Data for the Thermocexcel-E surface are shown in Fig. 13. The Gewa-T surface behaved similarly at high heat flux but the low flux heat transfer coefficient was enhanced due to effective use of the channels as extended surfaces.

In the other common configuration, the R-114 data of Fagerholm et al. (1985) indicate that vertical evaporator tubes with the same structured surfaces are enhanced by factor of 6 to 12. Although no reference data are given, these levels of enhancement are comparable to those observed with flooded pool boiling.

There appear to be fewer problems with inception of boiling with falling evaporating films than with flooded evaporation. Fagerholm et al. (1985) report only a slight thermal excursion with the High Flux tube. This is expected because the structure is full of vapor prior to system startup. Some erratic nucleation behavior has been observed by Hillis et al. (1979) with

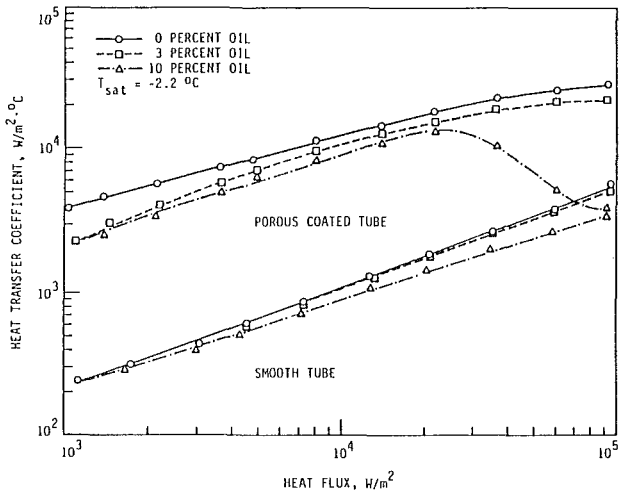

Fig. 12 Influence of oil on heat transfer performance of a smooth tube and a sintered surface tube (Wanniarachchi et al., 1986)

Downloaded 16 Dec 2010 to 193.140.21.150. Redistribution subject to ASME license or copyright; see http://www.asme.org/terms/Terms_Use.cfm

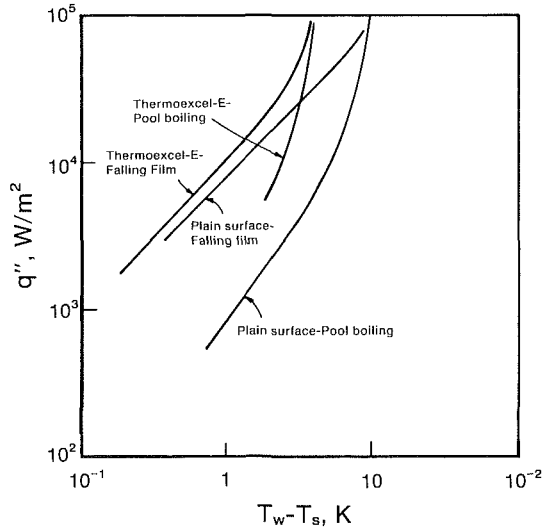

Fig. 13 Comparison of data for plain tube and Thermoexcel-E tube in both pool boiling and falling film evaporation (Chyu and Bergles, 1985)

horizontal bundles. When ammonia flowed over the unheated tubes, the vapor was removed from the High Flux surface and boiling was initiated only very slowly.

There do not appear to be any investigations of bundle effects with structured surface tubes. Although the film flows are likely to be quite disturbed, because of dripping and vapor shear, the convective effects will probably be overshadowed if there is nucleate boiling. This is likely to be the case because the structured surfaces exhibit boiling at very low superheat.

Fouling of enhanced tubes in falling film evaporation is expected to be similar to that for flooded boiling, with single or multiple tubes. There is, however, the additional complication of dryout with a long vertical tube evaporator.

Rough Surfaces in Tube-Side Single-Phase Flows

An enormous variety of surface roughnesses have been tested in both single- and two-phase flows under both natural and forced circulation. The roughness may be applied to any of the usual prime or extended heat exchange surfaces, e.g., tubes, plates, or fins. Both two- and three-dimensional integral roughness elements have been produced by the traditional processes of machining, forming, casting, or welding. Various inserts or wrap-around structures can also provide surface protuberances.

Attention is focused here on the helical repeated rib roughness that is readily manufactured and results in good heat transfer performance (up to 300 percent increases over the smooth tube) in single-phase turbulent flow without severe pressure drop penalty. Sketches of typical surface configurations are shown in Fig. 14. The main effect is that the ribs cause flow separation and reattachment, which results in higher average heat transfer coefficients. Analytical models, such as those of Lewis (1975) and Wessel and Mills (1979), have not been particularly successful because of the need for many empirical constants describing the heat transfer and flow friction or form drag. Furthermore, they have been applied only to transverse repeated ribs. Numerical simulations have thus far been applied only to single ribs (Hung et al., 1987). Accordingly, the fundamental work on this type of roughness has tended to focus on the development of semi-empirical correlations.

Analogy-Based Correlations. Following the lead of Dipprey and Sabersky (1963), Webb et al. (1971) used the heat transfer–momentum transfer analogy to correlated data for tubes with transverse repeated rib roughness. The procedure

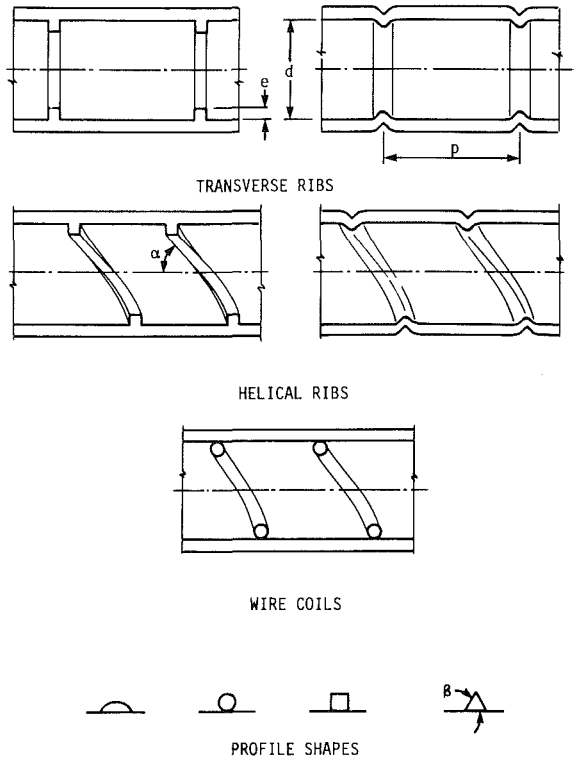

Fig. 14 Examples of repeated rib roughness (Ravigururajan and Bergles, 1985)

involves interpreting the friction factor data in terms of Nikuradse's similarity function U_e^+, and the roughness Reynolds number e^+. Applying the analogy, the general form of the heat transfer correlation is

$$\mathrm{St} = \frac{f/2}{1+(f/2)^{0.5}(\tilde{g}F - U_e^+)} \tag{8}$$

The functions $\tilde{g}$, F, and U_e^+ were obtained empirically for carefully constructed repeated rib roughnesses. As pointed out by Webb (1979), the correlation does not allow easy physical interpretation because of use of unconventional variables, e.g., roughness Reynolds number ($e^+ = (e/d)\mathrm{Re}\sqrt{f/2}$) instead of pipe Reynolds number. Originally, these variables were a barrier to understanding and accepting the correlations, but this has changed within the past ten years.

Strictly speaking, the analogy is valid for a single p/e, i.e., geometrically similar roughness. Since this would severely limit the application of the correlations, pitch is included in the friction correlation ($U_e^+ = f(e^+, p/e)$) and the heat transfer function ($\tilde{g} = f(e^+, p/e)$). Webb et al. (1971) found that for sufficiently high e^+, U_e^+ depends only on p/e and $\tilde{g}$ is dependent only on e^+.

Because most indenting or swaging processes lead to spiralled ribs, the helix angle is an additional variable that alters the geometric similarity. An angle correction factor is usually added to both the U_e^+ and $\tilde{g}$ expressions to complete the correlation. Correlations following this general strategy have been proposed by Withers (1980a, 1980b), Gee and Webb (1980), Li et al. (1982), Nakayama et al. (1983), and Sethumadhavan and Raja Rao (1986). Ganeshan and Raja Rao (1982) extended the method to non-Newtonian power law liquids, incorporating the flow behavior index into U_e^+.

The Withers correlations are not particularly useful because the friction correlation changes for each roughness configuration; however, a reasonably accurate friction correlation was obtained by Ravigururajan and Bergles (1986). They also proposed modifications to the Gee and Webb (1980) correlation

Downloaded 16 Dec 2010 to 193.140.21.150. Redistribution subject to ASME license or copyright; see http://www.asme.org/terms/Terms_Use.cfm

so that it agrees with the transverse rib limit of the Webb et al. (1971) correlation.

The analogy-based correlations are appealing because they represent a fundamental approach to the problem. Unfortunately, because of the need to correlate the effects of all the pertinent geometric parameters, similarity must be violated, with the result that the extended correlations are more empirical than fundamental. Furthermore, the correlations have had little testing against data outside of the particular study. For identical values of the basic parameters, the analogy correlations predict widely differing values of the heat transfer coefficient. In spite of these shortcomings, the analogy approach has emerged as a powerful tool for interpreting and correlating rough surface behavior.

Statistical Correlation. It is evident that the designer needs a wide-ranging correlation that can be used to predict the thermal-hydraulic performance of tubes with helical repeated ribs (or confirm manufacturer's specifications for such tubes) or to determine the optimum geometric parameters for a particular application. Given the large and growing data base that is now available for this type of roughness, it is now feasible to do this statistically using a large-scale computer.

Ravigururajan and Bergles (1985) developed such correlations from large data bases for friction factor and heat transfer. The 1807 heat transfer points covered the following ranges: Re from 6000 to 440,000, Pr from 0.66 to 37.6, e/d from 0.01 to 0.22, p/d from 0.1 to 17.8, and $\alpha/90$ from 0.3 to 1.0. Most ribs were of semicircular cross section, but many data points were included for circular, rectangular, and triangular cross sections.

The heat transfer correlation is given by

$$\mathrm{Nu}_a/\mathrm{Nu}_s = \{1 + [2.64\ \mathrm{Re}^{0.036}(e/d)^{0.212} \times (p/d)^{-0.21}(\alpha/90)^{0.29}(\mathrm{Pr})^{-0.024}]^7\}^{1/7} \quad (9)$$

where

$$\mathrm{Nu}_s = 0.5\, f\, \mathrm{RePr}/(1 + 12.7(0.5\, f)^{0.5}(\mathrm{Pr}^{0.667} - 1) \quad (10)$$

With this equation, 69 percent of the data were correlated to within ±20 percent.

The friction factor correlation is more complex because it was necessary to include a shape factor characterizing the profile by the number of sharp corners facing the flow and the contact angle

$$f_a/f_s = \left\{1 + \left[29.1\ \mathrm{Re}^{(0.67 - 0.06\, p/d - 0.49\, \alpha/90)} \times (e/d)^{(1.37 - 0.157\, p/d)} \times (p/d)^{(-1.66 \times 10^{-6}\,\mathrm{Re} - 0.33\, \alpha/90)} \times (\alpha/90)^{(4.59 + 4.11 \times 10^{-6}\mathrm{Re} - 0.15\, p/d)} \times \left(1 + \frac{2.94}{n}\right)\sin\beta\right]^{15/16}\right\}^{16/15} \quad (11)$$

where

$$f_s = (1.58\ \ln\ \mathrm{Re} - 3.28)^{-2} \quad (12)$$

In this case, 64 percent of the data were correlated to within ±20 percent. It should be noted that it is common to find data sets that have widely varying friction factors for nearly identical geometries.

The analogy correlations, extended if necessary, were applied to the same data base. It was concluded that equations (9) to (11) displayed all the right trends and were more accurate than any of the other correlations. The success of this approach suggests that statistical methods are an effective, if not elegant, way to correlate data for rough surfaces.

Offset Strip Fins

One of the most popular geometries for compact heat exchangers is the offset strip fin depicted in Fig. 15. Substantial enhancement over uninterrupted rectangular channels results from periodic development of laminar boundary layers and their at least partial dissipation in the fin wakes. As documented by Joshi and Webb (1987), a broad assault has been underway for over forty years to establish the flow friction and heat transfer characteristics as well as the basic transport mechanisms for this deceptively simple enhanced extended surface. The approaches include obtaining heat transfer and flow friction data for actual cores or scaled-up models, empirical correlations of such data, mass transfer data for scaled-up models, flow visualization, analytical models, and numerical solutions.

Empirical Data and Correlations. Although much data for prototype cores reside in company files, relatively few results are available in the open literature. Assuming many fins in the flow direction, the geometry should be described by fin height h, length L, transverse spacing s, and thickness t. The offset is usually uniform and equal to half the fin spacing;

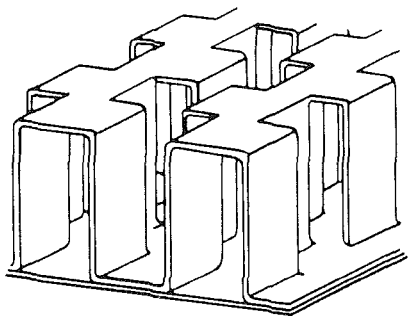

Fig. 15 Offset strip fins used in plate-fin heat exchangers

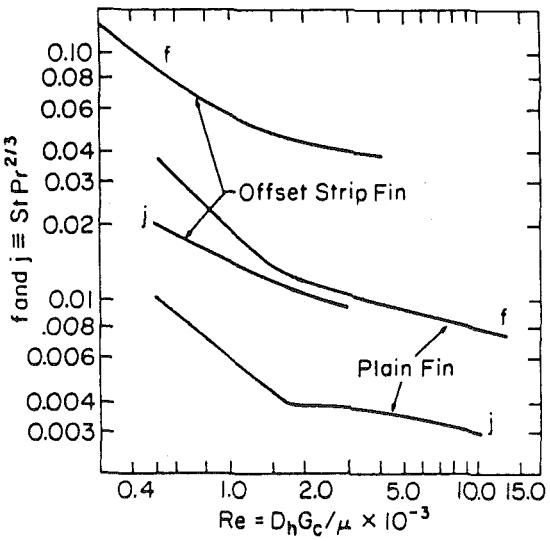

Surface Geometry

	Plain	Offset Strip
Surface designation	10-27	101
Fins/m	437	437
Plate spacing (mm)	12.2	11.9
Hydraulic diameter (mm)	3.51	3.51
Fin thickness (mm)	0.20	0.24
Offset strip length in flow direction (mm)	--	6.6

Fig. 16 Typical data for offset strip fins (Webb and Bergles, 1983)

Downloaded 16 Dec 2010 to 193.140.21.150. Redistribution subject to ASME license or copyright; see http://www.asme.org/terms/Terms_Use.cfm

if not, an additional geometric variable is introduced. The actual cores embody the usual manufacturing irregularities such as burred and scarfed fin edges, bonding imperfections, and separating plate roughness. The relatively old data presented in Kays and London (1984) are commonly referred to for design.

From such data, an example of the enhanced performance of the offset strip fin can be given. In Fig. 16, f and j data are presented for an offset strip fin and a plain fin scaled to provide the same hydraulic diameter. At $\mathrm{Re}_h = 1000$, the j factor of the offset strip fin is 150 percent higher than that for the plain fin; however the friction factor increase is 200 percent. The j/f ratio (at constant Reynolds number) is thus only 0.83; however, the benefits of the enhancement are better represented by one of the many thermal-hydraulic performance evaluation criteria. For example, if the flow rate and friction power are constrained to be constant, the offset strip fin will provide the same hA as the plain fin with 55 percent less surface area while requiring only 10 percent increase in flow frontal area (Webb and Bergles, 1983).

Until recently, the only broad-based correlations were those of Wieting (1975). He presented power-law curve fits of f and j data for 22 geometries. The correlations were broken down into low and high Reynolds number regions. For $\mathrm{Re}_h < 1000$, both f and j were functions of L/D_h, s/h, and Re_h. For $\mathrm{Re}_h > 2000$, f and j were found to be functions of L/D_h, t/D_h, and Re. Prandtl number does not appear because the tests were for the intended application of air.

Joshi and Webb (1987) re-examined some of the older data for 21 geometries and proposed a more accurate correlation that has a more refined limit on the laminar and turbulent regions:

For $Re_h \le Re_h^*$

$$f = 8.12(\mathrm{Re}_h)^{-0.74}(L/D_h)^{-0.41}(s/h)^{-0.02} \tag{13}$$

$$j = 0.53(\mathrm{Re}_h)^{-0.50}(L/D_h)^{-0.15}(s/h)^{-0.14} \tag{14}$$

For $Re_h \ge Re_h^* + 1000$

$$f = 1.12(\mathrm{Re}_h)^{-0.36}(L/D_h)^{-0.65}(t/D_h)^{0.17} \tag{15}$$

$$j = 0.21(\mathrm{Re}_h)^{-0.40}(L/D_h)^{-0.24}(t/D_h)^{0.02} \tag{16}$$

where

$$\mathrm{Re}_h^* = \frac{257(L/s)^{1.23}(t/L)^{0.58}D_h}{t + 1.328\ L/(\mathrm{Re}_L)^{0.5}} \tag{17}$$

Overall, 82 percent of the f data and 91 percent of the j data are correlated to within ±15 percent. The problem with these correlations as well as those of Wieting (1975) is the gap of 1000 in Reynolds numbers between laminar and turbulent. In any event, the Joshi and Webb (1987) work is a good example of the use of flow visualization to determine flow transition behavior.

Qualitative Observations. Many visual studies, usually of scaled-up arrays, have aided the interpretation of the experimental data. As the Reynolds number is increased, the wake exhibits time-dependent velocity behavior. Further increases in Reynolds number lead to vortex shedding. The oscillations thus created act as free-stream turbulence for the downstream fin. Even though the boundary layers are basically laminar, heat transfer and momentum transfer are increased. Loehrke and Lane (1982) and Joshi and Webb (1987), among others, found that the first disturbances corresponded approximately to the departure from the log-linear behavior of f and j. (See Fig. 16.) In their study of in-line arrays, Loehrke and Lane (1982) included acoustic measurements of the flow noise. At the departure from laminar friction behavior, there was a 10–20 db increase in sound pressure level clearly audible in the 1–2 kHz range. In a recent paper,

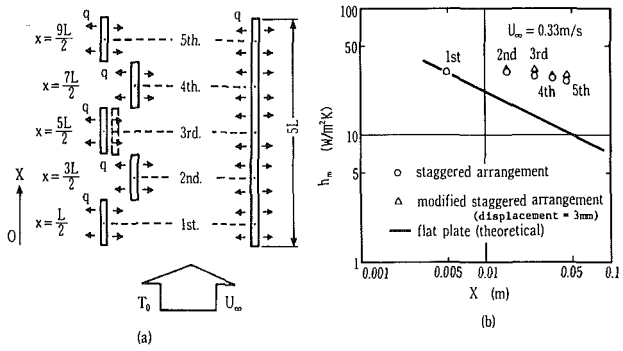

Fig. 17 Comparison of data for offset strip fins with various staggerings (Kurosaki, 1988)

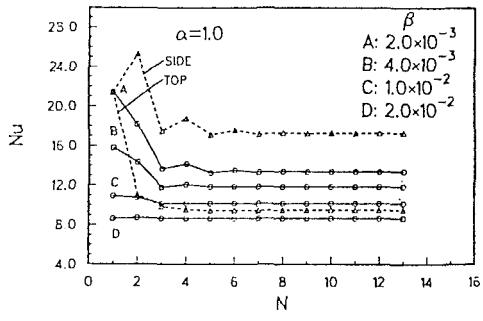

Fig. 18 Module-averaged heat transfer coefficient predictions for offset strip fins (Kelkar and Patankar, 1985)

Mullisen and Loehrke (1986) further confirm this behavior and show the periodic unsteady flow structure associated with the sequence of audible tones.

Other studies of flow patterns and flow structure provide qualitative support for the mechanisms of heat transfer enhancement. Mochizuki et al. (1988), using dye injection in a water channel, confirm the flow regimes with increasing Reynolds number: laminar, second laminar (also referred to as transitional, vortex shedding, or oscillating flow), and turbulent. The turbulence intensity was increased as compared to uninterrupted surfaces and this was considered to be responsible for the superior heat transfer performance.

A recent study by Kurosaki et al. (1988) involved holographic interferometry, which permitted both flow visualization and quantitative heat transfer measurements for scaled-up offset strip fins. The isotherms clearly showed that when the fins are offset uniformly, the wakes generated by upstream fins can have an adverse effect on heat transfer from downstream fins. This led to the proposal that the staggering be modified as shown in Fig. 17(*a*). The fin-average heat transfer coefficients for such an arrangement shown in Fig. 17(*b*) confirm an improvement of about 10 percent over the usual configuration. This seems to be a promising strategy for the development of higher performance surfaces.

Analytical Approach. The analytical approach of Kays (1972) modeled the fins as a series of short plates on which laminar boundary layers develop. Complete dissipation of the boundary layers is assumed in the wake region. Both f and j are calculated from the usual laminar boundary layer equations except that the former includes a term to account for profile drag. The rather poor agreement with data is attributed to neglect of any effect of the wake on the boundary layer. The analysis of Joshi and Webb (1987) is more refined in that they include heat transfer from fin ends and parting sheets (top and bottom walls) as well as the fin sides. The end heat transfer was assumed the same as the sides, and existing analytical solutions were used to model heat transfer from the other surfaces. The wall and side friction was handled the

Downloaded 16 Dec 2010 to 193.140.21.150. Redistribution subject to ASME license or copyright; see http://www.asme.org/terms/Terms_Use.cfm

same way and the effect of the ends was represented as a form drag. In the turbulent region, standard correlations were used to obtain f and j for the walls assuming that fully developed channel flow was applicable. The f and j for the fin sides were then backed out of the data for 21 surfaces and a correlation obtained. The agreement over the entire range of Reynolds numbers was about ± 20 percent, lending strong support to the methodology. Because the additive equations are somewhat cumbersome, the average f and j empirical correlations given by equations (13) to (17) were suggested as a more useful alternative.

Numerical Studies. The few numerical studies that have been attempted suffer from restrictions on the geometric parameters and the assumption of a stable laminar wake. The numerical predication of vortex shedding, through unsteady flow equations, has not yet been undertaken. The study of Kelkar and Patankar (1985) is more advanced in that the two-dimensional assumption (large h/s) is relaxed; however, zero fin thickness is assumed. The computations were carried out for the entrance region and continued until the flow exhibited periodically fully developed behavior, which occurred after 5–10 fins or modules. Figure 18 represents the module average heat transfer coefficients for various values of L/s. For $L/s = 0.002$, the fin and wall results are separated to show that the coefficient for the fin is substantially higher than that for the wall because the wall flow is not being interrupted.

The computed fully developed Nusselt numbers are generally higher than the data of Wieting (1975), while the computed friction factors are below the data. These discrepancies can be explained at least in part by neglect of the temperature gradient in the fin and by geometric irregularities such as burrs. While the numerical formulations are not yet accurate simulations, the calculations yield local flow and thermal fields rather than the gross averages deduced from experiments with actual or scaled-up cores. The only experimental confirmation could come from the interferometric measurements noted earlier or from local measurements of naphthalene sublimation. However, in the only cases where this has been done, Kurosaki et al. (1988) and Sparrow and Hajiloo (1980), respectively, only average coefficients for each fin were reported.

Micro-Fin Tubes for Refrigerant Evaporators and Condensers

The final detailed discussion concerns a new type of inner-fin tubing that is receiving much attention around the world. The original configurations for enhancement of in-tube evaporation of refrigerants were offset strip fin inserts soldered to the copper tubes or aluminum star-shaped inserts secured by drawing the tube over the insert. For reasons of cost and high pressure drop, these composite tubes are being replaced by tubes with integral inner fins of moderate number and height. The current trend is toward tubes with more numerous and very short fins that have good thermal-hydraulic performance and are cost effective.

Performance With Pure Refrigerants. Cross-sectional views of typical "micro-fin" tubes are shown in Fig. 19. These copper tubes are the popular 3/8 in. (9.5 mm) o.d. and have 60 to 70 spiral fins ranging from 0.10 to 0.19 mm in height. Representative data for evaporation of R-22 in these tubes are shown in Fig. 20. The heat transfer coefficients, based on area of an equivalent smooth tube, are increased 30 to 80 percent above the smooth tube values depending on the vapor quality and fin profile. The pressure drop penalties are in the same percentage range for this series of tests; however, some investigators report greater increases in average heat transfer coefficients than increases in pressure drop (Schlager et al., 1987). Similar favorable performance has been observed in condensation, but in this case the heat transfer coefficients (not the pressure drops) are more sensitive to the geometry (Khanpara et al., 1985). Regarding geometry, the higher fins performed better, flat valleys are preferred, but peak geometry is not critical. The outstanding thermal-hydraulic performance is related to increased surface area, increase in the turbulence level of the annular liquid film, extension of the dryout to higher quality, and alteration of the flow pattern. These tubes are at a stage that is often found in enhancement technology: They can be manufactured by several patented processes and are incorporated into commercial units, but relatively few experiments have been carried out to determine the performance, and no correlations are available. There is not even clear consensus on the combination of geometric parameters that yields optimum performance. Although the factors probably responsible for the enhancement can be identified, no mechanistic models have yet been proposed.

Influence of Oil. The usual contaminant in refrigeration systems is compressor lubricating oil, which may be present in concentrations up to 10 percent. Recent experiments have defined the effects of oil on the performance of a typical micro-fin tube. It is of interest to compare the average heat transfer coefficients with smooth tube and low-fin tube behavior. In Fig. 21 it is seen that oil generally degrades the performance of the low-fin tube while a small amount of oil slightly enhances the micro-fin tube performance at about 2 percent concentration. In contrast, the plain tube heat transfer coefficient is enhanced by oil throughout the test range, with a particularly sharp enhancement occurring at 3 percent concentration. With condensation, on the other hand, all three tubes exhibit a reduction in heat transfer coefficient with oil. While the inner-fin tubes always enhance heat transfer relative to the smooth tube, it is evident that the absolute performance and the enhancement are strongly dependent on the oil concentration.

Major Areas of Applications

To demonstrate the trends of applications of enhancement technology, seven industrial areas will be considered. Each of these areas has particular needs for enhancement and particular constraints, such as fouling or cost, that limit the techniques.

Heating, Ventilating, and Air Conditioning. This industry is well known for its ready adoption of enhancement for both air and refrigerant heat transfer. In the common evaporator or

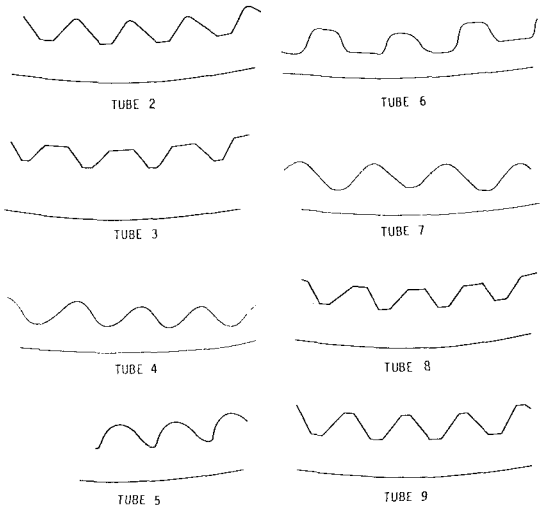

Fig. 19 Fin profiles for micro-fin tubes used in refrigerant evaporators and condensers (Khanpara et al., 1985)

Downloaded 16 Dec 2010 to 193.140.21.150. Redistribution subject to ASME license or copyright; see http://www.asme.org/terms/Terms_Use.cfm

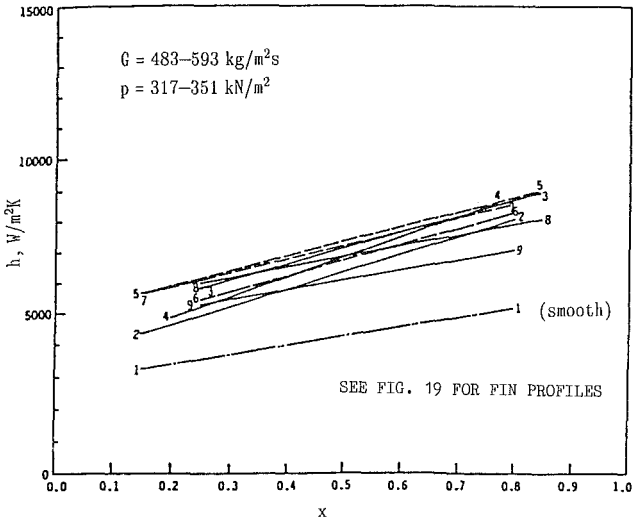

Fig. 20 Average heat transfer coefficients for vaporization of R-22 in micro-fin tubes (Khanpara et al., 1986)

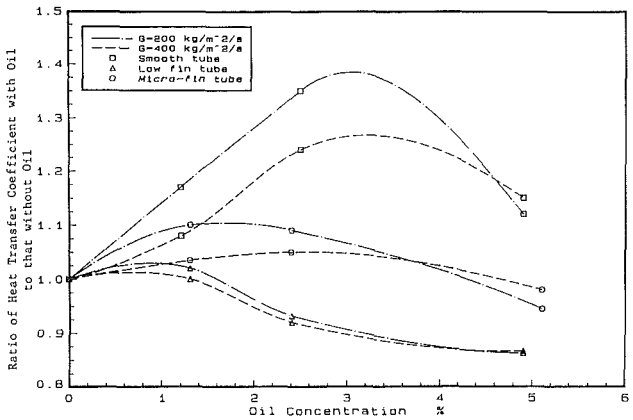

Fig. 21 Influence of oil on average evaporation heat transfer coefficients for plain and internally finned tubes (Schlager et al., 1988)

condenser coil, air-side heat transfer is routinely improved with fins that are louvered, corrugated, or serrated, as discussed in the section on offset strip fins. The intent is both to extend the area and to increase the heat transfer coefficient. With the reduction in the air-side thermal resistance, the refrigerant-side resistance becomes relatively more important. As discussed in the previous section, the micro-fin tube is one answer to double enhancement.

A satisfactory micro-fin configuration can usually be found that will work well in either evaporation or condensation. This is particularly important in heat pump air-conditioning systems where the roles of evaporator and condenser are periodically reversed. As another practical matter, the best flat tip profiles are preferable because mechanical expansion of the tube to secure the fins produces flat fins.

Noting the significant effect of oil on the heat transfer coefficient with enhanced tubes, methods have been developed to determine the oil concentration in refrigeration systems without sample removal (Baustian et al., 1988).

The structured boiling surfaces are being adopted more frequently for flooded refrigerant evaporators. Bundle simulator tests for this particular application, using High Flux tubes with R-11, are reported by Tatara and Payvar (1985). Their data confirm some previous observations that bundle convective enhancement is negligible with these tubes. This conclusion, although not validated in general, is justification for continuation of single-tube studies such as that of McManus et al. (1986). They included in the test program a new tube, the Turbo-B tube, which has a structured boiling surface on the outside and helical repeated ribs on the inside. The exterior boiling enhancement is made by rolling low integral fins, cutting diagonally across the fins, and rolling to compress the fins and give a uniform outside diameter. Re-entrant passageways are formed with a cross-hatched pattern. The wall superheat with pure R-114 was reduced by as much as a factor of 6.4. The maximum enhancement was reduced to a factor of 4.9 with 6 percent oil.

Low, integral fins have long been used for enhancement of shell-side condensation of refrigerants. The recent trend has been to configure the fins carefully (Webb et al., 1985; Rudy and Webb, 1985; Marto, 1986) and allow for drainage. Sauer et al. (1980) found that oil does not degrade the condensing performance of low fin tubes. As surveyed by Webb (1984) and Bergles (1985), three-dimensional extended surfaces yield higher performance than the low-fin tubes. For condensing as well as boiling, tubes are now provided with tube-side enhancements of the spiral repeated-rib type. These doubly enhanced tubes are indicative of the tendency to provide the highest possible overall heat transfer coefficients.

Automotive. Enhanced air-side surfaces have contributed to the dramatic reduction in size and weight of automotive radiators as well as the other heat exchangers found in modern vehicles. Mori and Nakayama (1980) report this reduction to be about 60 percent during the period 1957 to 1980. Additional gains have been made in the last eight years through the use of thin (down to 0.025 mm) copper fin stock that is louvered and tightly packed (up to 2000 fins/m).

There has been renewed interest in enhancement of the viscous flows that occur in oil coolers. Many types of convoluted channels and mixing inserts have been utilized; however, there is little in the way of analysis or correlations to guide the design. The one exception is twisted-tape inserts, which have received considerable attention.

Twisted-tape inserts have been tested with liquids of high viscosity under both heating and cooling conditions. The temperature difference has a strong influence on the heat transfer coefficient; however, the data are quite well correlated with a wall-to-bulk viscosity ratio correction similar to that used for smooth tubes. Manglik and Bergles (1987) developed the first correlation for uniform temperature tubes with twisted-tape inserts.

Power. High-performance air-side surfaces have been developed for dry cooling towers used for fossil power plant heat rejection. Current designs utilize structured boiling surfaces in the intermediate heat exchanger that evaporates the transfer fluid, ammonia.

Internally finned or rifled boiler tubes have been studied in more detail, particularly under dryout and post-dryout conditions. These tubes delay dryout to higher steam qualities and reduce wall temperatures in dispersed-flow film boiling (Kitto and Albrecht, 1988).

Although new nuclear plant construction in the US is nearing a standstill, there is a considerable business in reload fuel. The new bundles have specially designed rod spacers so that the dryout power is increased, thereby allowing an increase of plant power. Some rather sophisticated experiments have been run to define the spacer configurations; however, the data are generally proprietary (Groeneveld and Yousef, 1980).

Ocean thermal energy conversion is still in the planning stage, but enhanced boiling and condensing surfaces are vital to efficient designs. Many of the surfaces were developed for desalination, an area that has not fulfilled its promise relative to potential use of enhancement technology. The design of condensing surfaces is particularly well advanced because of recent analytical studies of surface-tension-driven condensate flow. The enhanced surfaces thus developed are being used for

Downloaded 16 Dec 2010 to 193.140.21.150. Redistribution subject to ASME license or copyright; see http://www.asme.org/terms/Terms_Use.cfm

evaporation and condensation of a variety of organic fluids being considered for organic Rankine cycles, both fired and driven by geothermal brine.

The potential degradation of heat transfer due to fouling has inhibited the use of tube-side enhancements in steam condensers. On the contrary, a rather optimistic report emerged from the retubing of a large power condenser for the Tennessee Valley Authority. Sartor (1982) found that the corrugated tubes (helical repeated rib roughness) did not have fouling rates greater than plain tubes. Standard cleaning methods were effective in restoring performance. In this application, the objective was to improve plant thermal efficiency through a lower turbine exhaust temperature. The payback period on initial investment was estimated to be less than one year.

Process. The chemical process industry has adopted enhancement technology sparingly because of concerns about fouling. Plant engineers do not wish to risk shutdown of an entire process facility because of degradation of a heat exchanger that is costwise a small part of the facility. The Cal Galvin Heatex wire loop inserts and Vapor Sphere Matrix fluted spheres (tube-side), or solid spheres (shell-side), not only improve heat transfer but reduce fouling with typical process fluids (Mascone, 1986). Once again, commercial installation has preceded research on these inserts.

Some attention has been given recently to the enhancement of heat transfer to laminar in-tube flow of non-Newtonian liquids. Percentage improvements in heat transfer coefficients with spirally corrugated tubes and twisted-tape inserts are comparable to those observed with Newtonian liquids.

The High Flux surface has been noted in connection with refrigeration applications, but its main application is in process plant reboilers. Numerous technical papers and economic analyses have been directed toward this application.

Since most process reboilers and evaporators involve mixtures, many of the structured boiling surfaces are being tested with mixtures of two or more components (Thome, 1988). Figure 22 compares the boiling curves for the new Gewa-TX tube with those of a plain tube for a five-component hydrocarbon mixture. This tube is similar to the Gewa-T tube shown in Fig. 4; however, the interior channels have small notches around the circumference. The performance gains are similar to those shown in Fig. 4 for a pure fluid.

Industrial Heat Recovery. Advanced surfaces for high-temperature heat recovery are being designed so that both convection and radiation are enhanced. Of particular interest recently are ceramic tubes that are enhanced externally and/or internally. These tubes show great promise for the recovery of heat from waste streams in excess of 850°C (Bergles, 1987).

Fouling and corrosion must be minimized if high-temperature heat recovery is to be practical. While most studies of fouling are with plain surfaces, serrated finned tubes and offset-strip-fin heat exchangers have been studied. These surfaces may remain effective in moderate fouling conditions; however, it is possible that nearly total plugging occurs with certain streams, e.g., diesel exhaust and glass furnace exhaust (Marner and Webb, 1983).

Electronics Cooling. Enhanced extended surfaces have long been used for air cooling of electronic devices ranging from radar tubes to transistors. The recent emphasis has been on the development of cooling schemes for microelectronic chips used in computers. Structures are provided to conduct the heat generated by an array of chips out to the air or water coolant. The final thermal coupling is through finned arrays that may be quite complex for air cooling or simple for liquid cooling. At present, much attention is being given to direct immersion of the chips in an inert, dielectric liquid. Saturated or subcooled boiling occurs due to the high chip powers. With

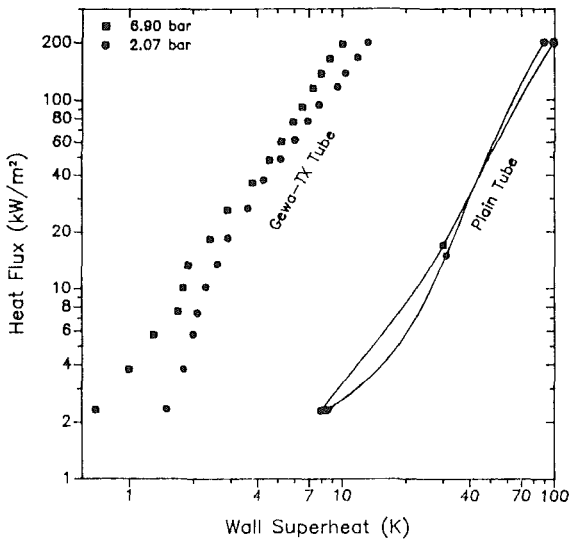

Fig. 22 Boiling of a five-component hydrocarbon mixture on a Gewa-TX tube (Thome, 1988)

the dual objective of reducing the wall superheat and increasing the burnout heat flux, enhanced boiling surfaces are attached to individual chips (Park and Bergles, 1986). There is much work yet to be done to establish configurations that achieve both objectives.

Jet impingement of dielectric liquid has recently been explored as a means of accommodating very high chip heat dissipations, over 2×10^6 W/m^2 (Ma and Bergles, 1983).

Aerospace. Gas turbine blade cooling has challenged the heat transfer community for the past decade. Several enhancement techniques are now being utilized to increase the heat transfer coefficient from blade wall to internal coolant, thereby reducing the wall temperature. Transverse repeated ribs and pin fins can be cast into the blade, or the air supply can be arranged to direct jets against the leading-edge wall (Simoneau, 1985).

Difficult heat transfer problems are being encountered in connection with the aerospace plane proposed for transatmospheric flight. In addition to protection of components in the propulsion system, active cooling of the vehicle will likely be required to reduce material temperatures during hypersonic flight. Enhancement of heat transfer will probably be required.

Concluding Remarks

Heat transfer enhancement today is characterized by vigorous activity in both research and industrial practice. Due to extensive research and much successful field experience during the past twenty-five years, enhancement techniques are routinely considered for improving convective heat transfer in a wide variety of equipment. Current research is driven primarily by applications rather than curiosity and typically involves multiple approaches. In many cases, however, analytical or numerical predictions of heat transfer and flow friction behavior are not yet possible and empirical correlations must be relied on for design. Modeling should be encouraged, however, because the resulting understanding of the phenomena can result in better predictions and improved surface or insert device configurations.

The growing maturity of this second generation heat transfer is evidenced by its incorporation into undergraduate textbooks (e.g., White, 1984) and it is likely that the subject will be featured in many of the new editions. At least two graduate courses (Penn State and RPI) are devoted entirely to enhanced heat transfer. The greatest challenge in the coming

Downloaded 16 Dec 2010 to 193.140.21.150. Redistribution subject to ASME license or copyright; see http://www.asme.org/terms/Terms_Use.cfm

years, perhaps, will be to collect the literature, evaluate it, and communicate it in concise form by way of formal courses, short courses, and review articles.

As the ASME Heat Transfer Division moves into its second fifty years, heat transfer enhancement will be a strong component of members' research, practice, and technical communications. Judging by the Division leadership in this field during the past quarter century, there is every reason to expect the development of much more advanced enhanced techniques that could become a third-generation heat transfer technology.

References

Alberger Heater Company, 1921, Catalog No. 3, Buffalo, NY.

Arai, N., Fukushima, T., Arai, A., Nakajima, T., Fujie, K., and Nakayama, Y., 1977, "Heat Transfer Tubes Enhancing Boiling and Condensation in Heat Exchanger of a Refrigerating Machine," *ASHRAE Transactions*, Vol. 83, Pt. 2, pp. 58–70.

Ayub, Z. H., 1986, "Pool Boiling From GEWA Surfaces in Water and R-113," Ph.D. Dissertation, Iowa State University, Ames, IA.

Ayub, Z. H., and Bergles, A. E., 1987, "Pool Boiling From GEWA Surfaces in Water and R-113," *Wärme- und Stoffübertragung*, Vol. 21, pp. 209–219.

Ayub, Z. H., and Bergles, A. E., 1988, "Nucleate Pool Boiling Curve Hysteresis for GEWA-T Surfaces in Saturated R-113," ASME *Proceedings of the Heat Transfer Conference*, HTD-Vol. 96, Vol. 2, pp. 515–521.

Baustian, J. T., Pate, M. B., and Bergles, A. E., 1988, "Measuring the Concentration of a Flowing Oil-Refrigerant Mixture: Instrument Test Facility and Initial Results," *ASHRAE Transactions*, Vol. 94, Pt. 1, pp. 167–177.

Bergles, A. E., 1978, "Enhancement of Heat Transfer," *Heat Transfer 1978*, Proceedings, 6th International Heat Transfer Conference, Hemisphere Publishing Corp., Washington, DC, Vol. 6, pp. 89–108.

Bergles, A. E., 1983, "Augmentation of Heat Transfer," *Heat Exchanger Design Handbook*, Vol. 2, Hemisphere Publishing Corp., Washington, DC, pp. 2.5.11-1–12.

Bergles, A. E., 1985, "Techniques to Augment Heat Transfer," *Handbook of Heat Transfer Applications*, McGraw-Hill, New York, NY, pp. 3-1–80.

Bergles, A. E., 1987, "Heat Transfer Enhancement—Application to High-Temperature Heat Exchangers," *Heat Transfer in High Technology and Power Engineering*, Hemisphere Publishing Corp., Washington, DC; Springer-Verlag, Berlin, Federal Republic of Germany, pp. 333–355.

Bergles, A. E., Nirmalan, V., Junkhan, G. H., and Webb, R. L., 1983, "Bibliography on Augmentation of Convective Heat and Mass Transfer—II," HTL-31, ISU-ERI-Ames-84222, DE-84018484, Iowa State University, Ames, IA.

Bergles, A. E., Nelson, R. M., Junkhan, G. H., and Webb, R. L., 1984, "Assessment, Development and Coordination of Technology Base Studies in Enhanced Heat Transfer," HTL-33, ISU-ERI-Ames-85024, DE-85004130, Iowa State University, Ames, IA.

Bergles, A. E., and Chyu, M. C., 1982, "Characteristics of Nucleate Boiling From Porous Metallic Coatings," ASME JOURNAL OF HEAT TRANSFER, Vol. 104, pp. 279–285.

Chyu, M. C., 1984, "Falling Film Evaporation on Horizontal Tubes With Smooth and Structured Surfaces," Ph.D. Dissertation, Iowa State University, Ames, IA.

Chyu, M. C., and Bergles, A. E., 1985, "Enhancement of Horizontal Tube Spray Film Evaporators by Structured Surfaces," *Advances in Enhanced Heat Transfer—1985*, HTD-Vol. 43, ASME, New York, pp. 39–48.

Czikk, A. M., Gottzmann, C. F., Ragi, E. G., Withers, J. G., and Habdas, E. P., 1970, "Performance of Enhanced Heat Transfer Tubes in Refrigerant-Flooded Liquid Coolers," *ASHRAE Transactions*, Vol. 1, Pt. 1, pp. 96–109.

Czikk, A. M., and O'Neill, P. S., 1979, "Correlations of Nucleate Boiling From Porous Metal Films," *Advances in Enhanced Heat Transfer*, ASME, New York, pp. 53–60.

Dipprey, D. G., and Sabersky, R. H., 1963, "Heat and Momentum Transfer in Smooth and Rough Tubes at Various Prandtl Numbers," *International Journal of Heat and Mass Transfer*, Vol. 6, pp. 329–353.

Fagerholm, N.-E., Kivioja, K., Ghazanfari, A.-R., and Jarvinen, E., 1985, "Using Structured Surfaces to Enhance Heat Transfer in Falling Film Flow," I.I.F.-I.I.R.—Commission E2 Trondheim (Norway), pp. 187–192.

Ganeshan, S., and Raja Rao, M., 1982, "Studies on Thermohydraulics of Single and Multistart Spirally Corrugated Tubes for Water and Time-Independent Power Law Fluids," *International Journal of Heat and Mass Transfer*, Vol. 25, pp. 1013–1022.

Gee, D. L., and Webb, R. L., 1980, "Forced Convection Heat Transfer in Helically Rib-Roughened Tubes," *International Journal of Heat and Mass Transfer*, Vol. 23, pp. 1127–1136.

Gottzmann, C. F., O'Neill, P. S., and Minton, P. E., 1973, "High Efficiency Heat Exchangers," *Chemical Engineering Progress*, Vol. 69, No. 7, pp. 69–75.

Groeneveld, D. C., and Yousef, W. W., 1980, "Spacing Devices for Nuclear Fuel Bundles: A Survey of Their Effect on CHF, Post-CHF Heat Transfer and Pressure Drop," *Proceedings of the ANS/ASME/NRC International Topical Meeting on Nuclear Reactor Thermal-Hydraulics*, NUREGI/CP 0014, Vol. 2, pp. 1111–1130.

Hillis, D. L., Lorenz, J. J., Yung, D. T., and Sather, N. F., 1979, "OTEC Performance Tests of the Union Carbide Sprayed-Bundle Evaporator," ANL/OTEC-PS-3, Argonne National Laboratory, Argonne, IL.

Hung, Y. H., Liou, T. M., and Syang, Y. C., "Heat Transfer Enhancement of Turbulent Flow in Pipes With an Internal Circular Rib," *Advances in Enhanced Heat Transfer—1987*, HTD-Vol. 68, pp. 55–63.

Jakob, M., and Fritz, W., 1931, "Versuche über den Verdampfungsvorgang," *Forschung auf dem Gebiete des Ingenieurwesens*, Vol. 2, pp. 435–447.

Joshi, H. M., and Webb, R. L., 1987, "Heat Transfer and Friction in the Offset Strip-Fin Heat Exchanger," *International Journal of Heat and Mass Transfer*, Vol. 30, pp. 69–84.

Joule, J. P., "On the Surface-Condensation of Steam," 1861, *Philosophical Transactions of the Royal Society of London*, Vol. 151, pp. 133–160.

Kays, W. M., 1972, "Compact Heat Exchangers," AGARD Lecture Series No. 57, Heat Exchangers, AGARD-LS-57-72.

Kays, W. M., and London, A. L., 1984, *Compact Heat Exchangers*, 3rd ed., McGraw-Hill, New York.

Kelkar, K. M., and Patankar, S. V., 1985, "Numerical Prediction of Heat Transfer and Fluid Flow in Rectangular Offset-Fin Arrays," *Augmentation of Heat Transfer in Energy Systems*, HTD-Vol. 52, ASME, New York, pp. 21–28.

Khanpara, J. C., Bergles, A. E., and Pate, M. B., 1985, "Augmentation of R-113 In-Tube Condensation With Micro-Fin Tubes," *Heat Transfer in Air Conditioning and Refrigeration Equipment*, HTD-Vol. 65, ASME, New York, pp. 21–32.

Khanpara, J. C., Bergles, A. E., and Pate, M. B., 1986, "Augmentation of R-113 In-Tube Evaporation With Micro-Fin Tubes," *ASHRAE Transactions*, Vol. 92, Part 2B, pp. 506–524.

Kim, C.-J., and Bergles, A. E., 1985, "Structured Surfaces for Enhanced Nucleate Boiling," HTL-36, ISU-ERI-Ames-86220, Iowa State University, Ames, IA.

Kitto, J. B., and Albrecht, M. J., 1988, "Elements of Two-Phase Flow in Fossil Boilers," *Two-Phase Flow Exchangers: Thermal Hydraulic Fundamentals and Design*, Kluwer Academic Publishers, The Netherlands, pp. 495–551.

Kulacki, F. A., 1981, "Electrohydrodynamic Enhancement of Convective Heat and Mass Transfer," *Advances in Transport Processes*, Vol. II, Halstead Press, New York, pp. 105–147.

Kurosaki, Y., Kashiwagi, T., Kobayashi, H., Uzuhashi, H., and Tang, S.-C., 1988, "Experimental Study on Heat Transfer From Parallel Louvered Fins by Laser Holographic Interferometry," *Experimental Thermal and Fluid Science*, Vol. 1, pp. 59–67.

Lea, R. B., 1921, "Oil Cooler," US Patent No. 1,367,881.

Lewis, M. J., 1975, "An Elementary Analysis for Predicting the Momentum- and Heat-Transfer Characteristics of a Hydraulically Rough Surface," ASME JOURNAL OF HEAT TRANSFER, Vol. 97, pp. 249–254.

Li, H. M., Ye, K. S., Tan, Y. K., and Deng, S. J., 1982, "Investigations on Tube-Side Flow Visualization, Friction Factors and Heat Transfer Characteristics of Helical-Ridging Tubes," *Heat Transfer 1982*, Proceedings, 7th International Heat Transfer Conference, Hemisphere Publishing Corp., Washington, DC, Vol. 3, pp. 75–80.

Loehrke, R. I., and Lane, J. C., 1982, "Heat Flow Through an Array of Interrupted, Parallel Plates," *Heat Transfer 1982*, Proceedings, 7th International Heat Transfer Conference, Hemisphere Publishing Corp., Washington, DC, Vol. 3, pp. 81–86.

Lorenz, J. J., Yung, D., Howard, P. A., Panchel, C. B., and Poucher, F. W., 1981, "OTEC-1 Power System Test Program: Performance of One-Megawatt Heat Exchangers," ANL/OTEC-PS-10, Argonne National Laboratory, Argonne, IL.

Lewis, L. G., and Sather, N. F., 1978, "OTEC Performance Tests of the Union Carbide Flooded-Bundle Evaporator," ANL-OTEC-PS-1, Argonne National Laboratory, Argonne, IL.

Mascone, C. F., 1986, "CPI Strive to Improve Heat Transfer in Tubes," *Chemical Engineering*, Feb., pp. 22–25.

Ma, C.-F., and Bergles, A. E., 1983, "Boiling Jet Impingement Cooling of Simulated Microelectronic Chips," *Heat Transfer in Electronic Equipment*, HTD-Vol. 28, ASME, New York, pp. 5–12.

Manglik, R. M., and Bergles, A. E., 1987, "A Correlation for Laminar Flow Enhanced Heat Transfer in Uniform Wall Temperature Circular Tubes With Twisted-Tape Inserts," *Advances in Enhanced Heat Transfer—1987*, HTD-Vol. 68, ASME, New York, pp. 35–45.

Marner, W. J., and Webb, R. L., 1983, "A Bibliography on Gas-Side Fouling," *Proceedings of the ASME-JSME Thermal Engineering Joint Conference*, Vol. 1, pp. 559–570.

Marto, P. J., 1986, "Recent Progress in Enhancing Film Condensation Heat Transfer on Horizontal Tubes," *Heat Transfer 1986*, Proceedings, 8th International Heat Transfer Conference, Vol. 1, Hemisphere Publishing Corp., Washington, DC, pp. 161–170.

Marto, P. J., and Hernandez, B., 1983, "Nucleate Pool Boiling Characteristics of a GEWA-T Surface in Freon-113," *AIChE Symposium Series*, No. 225, Vol. 79, pp. 1–10.

McManus, S. M., Marto, P. J., and Wanniarachchi, A. S., 1986, "An Evaluation of Enhanced Heat Transfer Tubing for Use in R-114 Water Chillers," *Heat Transfer in Air Conditioning and Refrigeration Equipment*, HTD-Vol. 65, ASME, New York, pp. 11–19.

Downloaded 16 Dec 2010 to 193.140.21.150. Redistribution subject to ASME license or copyright; see http://www.asme.org/terms/Terms_Use.cfm

Menze, K., 1988, Wieland-Werke, Ulm, Federal Republic of Germany, Personal Communication, Feb. 4.

Mochizuki, S., Yagi, Y., and Yang, W.-J., 1988, "Flow Pattern and Turbulence Intensity in Stacks of Interrupted Parallel-Plate Surfaces," *Experimental Thermal and Fluid Science*, Vol. 1, pp. 51–57.

Mori, Y., and Nakayama, W., 1980, "Recent Advances in Compact Heat Exchangers in Japan," *Compact Heat Exchangers—History, Technological Advancement and Mechanical Design Problems*, HTD-Vol. 10, ASME, New York, pp. 5–16.

Mullisen, R. S., and Loehrke, R. I., 1986, "A Study of the Flow Mechanisms Responsible for Heat Transfer Enhancement in Interrupted-Plate Heat Exchangers," ASME JOURNAL OF HEAT TRANSFER, Vol. 108, pp. 377–385.

Nakayama, W., Daikoku, T., Kuwhara, H., and Nakajima, T., 1980, "Dynamic Model of Enhanced Boiling Heat Transfer on Porous Surfaces, Part II: Analytical Modeling," ASME JOURNAL OF HEAT TRANSFER, Vol. 102, pp. 451–456.

Nakayama, W., 1982, "Enhancement of Heat Transfer," *Heat Transfer 1982*, Proceedings, 7th International Heat Transfer Conference, Hemisphere Publishing Corp., Washington, DC, Vol. 1, pp. 223–240.

Nakayama, W., Takahashi, K., and Daikoku, T., 1983, "Spiral Ribbing to Enhance Single-Phase Heat Transfer Inside Tubes," *ASME-JSME Thermal Engineering Joint Conference Proceedings*, Vol. 1, pp. 365–372.

Newton, I., (anon.), 1701, "Scala Graduum Caloris," *The Philosophical Transactions of the Royal Society of London*, Vol. 22, 1701, pp. 824–829; translated from the Latin in *The Philosophical Transactions of the Royal Society of London*, abridged, Vol. IV (1694–1702), London, 1809, pp. 572–575.

O'Neill, P. S., Gottzmann, C. F., and Turbot, J. W., 1972, "Novel Heat Exchanger Increases Cascade Cycle Efficiency for Natural Gas Liquefaction," *Advances in Cryogenic Engineering*, Vol. 17, pp. 420–437.

O'Neill, P. S., King, R. C., and Ragi, E. G., 1980, "Application of High Performance Evaporator Tubing in Refrigeration Systems of Large Olefins Plants," *AIChE Symposium Series*, No. 199, Vol. 76, pp. 289–300.

Park, K. A., and Bergles, A. E., 1986, "Boiling Heat Transfer Characteristics of Simulated Microelectronic Chips With Detachable Heat Sinks," *Heat Transfer 1986*, Proceedings, 8th International Heat Transfer Conference, Hemisphere Publishing Corp., Washington, DC, Vol. 4, pp. 2099–2104.

Ravigururajan, T. S., and Bergles, A. E., 1985, "General Correlations for Pressure Drop and Heat Transfer for Single-Phase Turbulent Flow in Internally Ribbed Tubes," *Augmentation of Heat Transfer in Energy Systems*, HTD-Vol. 52, ASME, New York, pp. 9–20.

Rudy, T. M., and Webb, R. L., 1985, "An Analytical Model to Predict Condensate Retention on Horizontal Integral-Fin Tubes," ASME JOURNAL OF HEAT TRANSFER, Vol. 107, pp. 361–368.

Sauer, H. S., Davidson, G. W., and Chungrungreong, S., 1980, "Nucleate Boiling of Refrigerant-Oil Mixtures From Finned Tubing," ASME Paper No. 80-HT-111.

Sartor, W. E., 1982, "Extended and Enhanced Tube Surfaces to Improve Heat Transfer," *Proceedings of the Second Symposium on Shell and Tube Heat Exchangers*, Houston, TX, pp. 411–418.

Sethumadhavan, R., and Raja Rao, M., 1986, "Turbulent Flow Friction and Heat Transfer Characteristics of Single- and Multistart Spirally Enhanced Tubes," ASME JOURNAL OF HEAT TRANSFER, Vol. 108, pp. 55–61.

Schlager, L. M., Pate, M. B., and Bergles, A. E., 1987, "A Survey of Refrigerant Heat Transfer and Pressure Drop Emphasizing Oil Effects and In-Tube Augmentation," *ASHRAE Transactions*, Vol. 93, Part 1, pp. 392–416.

Schlager, L. M., Pate, M. B., and Bergles, A. E., 1988, "Evaporation and Condensation of Refrigerant-Oil Mixtures in a Low-Fin Tube," *ASHRAE Transactions*, Vol. 94, Part 1.

Simoneau, R. J., 1987, "Heat Transfer in Aeropropulsion Systems," *Heat Transfer in High Technology and Power Engineering*, Hemisphere Publishing Corp., Washington, DC; Springer-Verlag, Berlin, Federal Republic of Germany, pp. 285–319.

Sparrow, E. M., and Haliloo, A., 1980, "Measurements of Heat Transfer and Pressure Drop for an Array of Staggered Plates Aligned Parallel to an Air Flow," ASME JOURNAL OF HEAT TRANSFER, Vol. 102, pp. 426–432.

Stephan, K., and Mitrovic, J., 1981, "Heat Transfer in Natural Convective Boiling of Refrigerants and Refrigerant-Oil-Mixtures in Bundles of T-Shaped Finned Tubes," *Advances in Enhanced Heat Transfer—1981*, HTD-Vol. 18, ASME, New York, pp. 131–146.

Stephan, K., and Mitrovic, J., 1982, "Heat Transfer in Natural Convective Boiling of Refrigerant-Oil Mixtures," *Heat Transfer 1982*, Proceedings, 7th International Heat Transfer Conference, Hemisphere Publishing Corp., Washington, DC, Vol. 4, pp. 73–87.

Tatara, R. A., and Payvar, P., 1986, "Pressure Drop and Heat Transfer Measurements of Boiling Refrigerant in Normal Flow Through a Porous Coated Tube Bundle," *Heat Transfer in Air Conditioning and Refrigerant Equipment*, HTD-Vol. 65, ASME, New York, pp. 1–9.

Thome, J. R., 1988, "Application of Enhanced Boiling Tubes to Reboilers," *Two-Phase Flow Heat Exchangers: Thermal-Hydraulic Fundamentals and Design*, Kluwer Academic Pub., The Netherlands, pp. 747–778.

Torii, T., Hirasawa, S., Kuwahara, H., Yanagida, T., and Fujie, K., 1978, "The Use of Heat Exchangers With Thermoexcel's Tubing in Ocean Thermal Energy Power Plants," ASME Paper No. 78-WA/HT-65.

Wanniarachchi, A. S., Marto, P. J., and Reilly, J. T., 1986, "The Effect of Oil Contamination on the Nucleate Pool-Boiling Performance of R-114 From a Porous Coated Surface," *ASHRAE Transactions*, Vol. 92, Pt. 2B, pp. 525–538.

Wassel, A. T., and Mills, A. F., 1979, "Calculation of Variable Property Turbulent Friction and Heat Transfer in Rough Pipes," ASME JOURNAL OF HEAT TRANSFER, Vol. 101, pp. 469–474.

Webb, R. L., Rudy, T. M., and Kedzierski, M. A., 1985, "Prediction of the Condensation Coefficient on Horizontal Integral-Fin Tubes," ASME JOURNAL OF HEAT TRANSFER, Vol. 107, pp. 369–376.

Webb, R. L., 1984, "Shell-Side Condensation in Refrigerant Condensers," *ASHRAE Transactions*, Vol. 90, Pt. 1, pp. 5–24.

Webb, R. L., 1979, "Toward a Common Understanding of the Performance and Selection of Roughness for Forced Convection," *Studies in Heat Transfer*, Hemisphere Publishing Corp., Washington, DC, pp. 257–272.

Webb, R. L., and Bergles, A. E., 1983, "Performance Evaluation Criteria for Selection of Heat Transfer Surface Geometries Used in Low Reynolds Number Heat Exchangers," *Low Reynolds Number Heat Exchangers*, Hemisphere Publishing Corp., Washington, DC; Springer-Verlag, Berlin, Federal Republic of Germany, pp. 735–752.

Webb, R. L., Bergles, A. E., and Junkhan, G. H., 1984, "Bibliography of U.S. Patents on Augmentation of Convective Heat and Mass Transfer-II," HTL-32, ISU-ERI-Ames-84257, Iowa State University, Ames, IA.

Webb, R. L., 1980, "Air-Side Heat Transfer in Finned Tube Heat Exchangers," *Heat Transfer Engineering*, Vol. 1, No. 3, pp. 33–49.

Webb, R. L., 1981, "The Evolution of Enhanced Surface Geometries for Nucleate Boiling," *Heat Transfer Engineering*, Vol. 2, Nos. 3–4, pp. 46–69.

Webb, R. L., 1983, "Nucleate Boiling in Porous Coated Surfaces," *Heat Transfer Engineering*, Vol. 4, Nos. 3–4, pp. 71–82.

Webb, R. L., Eckert, E. R. G., and Goldstein, R. J., 1971, "Heat Transfer and Friction in Tubes With Repeated-Rib Roughness," *International Journal of Heat and Mass Transfer*, Vol. 14, pp. 601–618.

White, F., 1984, *Heat Transfer*, Addison-Wesley Publishing Company, Reading, MA.

Whitham, J. M., 1896, "The Effect of Retarders in Fin Tubes of Steam Boilers," *Street Railway Journal*, Vol. 12, p. 374.

Wieting, A. R., 1975, "Empirical Correlations for Heat Transfer and Flow Friction Characteristics of Rectangular Offset-Fin Plate-Fin Heat Exchangers," ASME JOURNAL OF HEAT TRANSFER, Vol. 97, pp. 488–490.

Withers, J. A., 1980a, "Tube-Side Heat Transfer and Pressure Drop for Tubes Having Helical Ridging With Turbulent/Transitional Flow of Single-Phase Fluid, Part 1. Single-Helix Ridging," *Heat Transfer Engineering*, Vol. 2, No. 1, pp. 48–61.

Withers, J. A., 1980b, "Tube-Side Heat Transfer and Pressure Drop for Tubes Having Helical Internal Ridging With Turbulent/Transitional Flow of Single-Phase Fluid. Part 2. Multiple-Helix Ridging," *Heat Transfer Engineering*, Vol. 2, No. 2, pp. 43–50.

Yilmaz, S., Palen, J. W., and Taborek, J., 1981, "Enhanced Boiling Surfaces as Single Tubes and Bundles," *Advances in Enhanced Heat Transfer—1981*, HTD-Vol. 18, ASME, New York, pp. 123–129.

Yilmaz, S., Hwalck, J. J., and Westwater, J. N., 1980, "Pool Boiling Heat Transfer Performance for Commercial Enhanced Tube Surfaces," ASME Paper No. 80-HT-41.

Downloaded 16 Dec 2010 to 193.140.21.150. Redistribution subject to ASME license or copyright; see http://www.asme.org/terms/Terms_Use.cfm

Convection Heat Transfer in Electronic Equipment Cooling

F. P. Incropera
Professor,
Heat Transfer Laboratory,
School of Mechanical Engineering,
Purdue University,
West Lafayette, IN 47907
Fellow ASME

To maintain the best possible thermal environment in electronic packages, the engineer must establish the most efficient path for heat transfer from the electronic devices to an external cooling agent. The path is typically subdivided into internal and external components, representing, respectively, heat transfer by conduction through different materials and interfaces separating the devices from the package surface and heat transfer by convection from the surface to the coolant. Depending on the scale and speed of the electronic circuits, as well as on constraints imposed by nonthermal considerations, the coolant may be a gas or a liquid and heat transfer may be by natural, forced, or mixed convection or, in the case of a liquid, by pool or forced convection boiling. In this paper a comprehensive review of convection cooling options is provided.

1 Introduction

Since development of the first electronic digital computers, heat removal has played an important role in maintaining reliable operation. An important trend that initially alleviated, and subsequently exacerbated, the heat removal problem involved the integration of monolithic circuits on a silicon chip and the development of ever larger scales of circuit integration. From the large-scale integration (LSI) technologies of the 1970s, which involved up to 1000 gates per chip, to the very large-scale integration (VLSI) of the 1980s, which involved up to 100,000 gates per chip, there has been a steady increase in heat dissipation at the chip, module, and system levels. Such increases have made the role of heat transfer and thermal design more important than ever, and the development of future large-scale, high-speed circuits may well be limited by the inability to maintain effective cooling.

An appreciation for the diversity of heat transfer problems associated with today's electronic packages may be gained by examining representative multichip modules. Typically, moderate to large numbers of chips are mounted in close proximity on a ceramic substrate. Modules are enclosed in protective covers to which fins may be attached to enhance heat transfer to an external coolant and within which various materials and interfaces influence heat transfer from the chips to the cover. The materials may be interfaced mechanically (with bolts or springs) or with a bonding agent such as an epoxy or a low-temperature solder. An essential requirement of the interfaces is that they be characterized by low thermal resistances and stresses.

As examples, two air-cooled multichip modules for which considerable attention has been given to reducing both internal and external resistances are shown in Fig. 1. In the Hitachi Silicon-Carbide module (Okutani et al., 1984), heat is transferred from each chip through solder posts to a silicon circuit board and from the board to a SiC heat spreader. The spreader is joined to the board by a low-resistance gold eutectic bond and to an aluminum heat sink with longitudinal fins by a thin layer of silicone rubber. In addition to providing low internal thermal resistance, the use of silicon-based circuit board and heat spreader materials of nearly equal expansion coefficients substantially reduces thermal stresses at the soldered and gold eutectic interfaces. In the IBM 4381 module (Biskeborn et al., 1984), chips are attached to a multilayer ceramic by solder posts and to a ceramic cap through a layer of thermal grease. Most of the heat dissipated by the chips is transferred to the ceramic cap directly through the grease or indirectly through the solder bumps and the substrate. The aluminum heat sink consists of an array of hollow pin fins, which are cooled by air jet impingement. Although internal thermal resistances associated with the Hitachi and IBM modules are comparable, the IBM module is characterized by a much smaller external resistance.

The reduce the external thermal resistance further, increasing emphasis is being placed on the use of liquid cooling technologies. A distinction is made between *direct* liquid cooling, for which there is intimate contact between the coolant and the electronics, and *indirect* or *conduction* cooling, for which the electronics are physically separated from the liquid.

As originally conceived and implemented, indirect liquid cooling is synonymous with attachment of a water-cooled cold

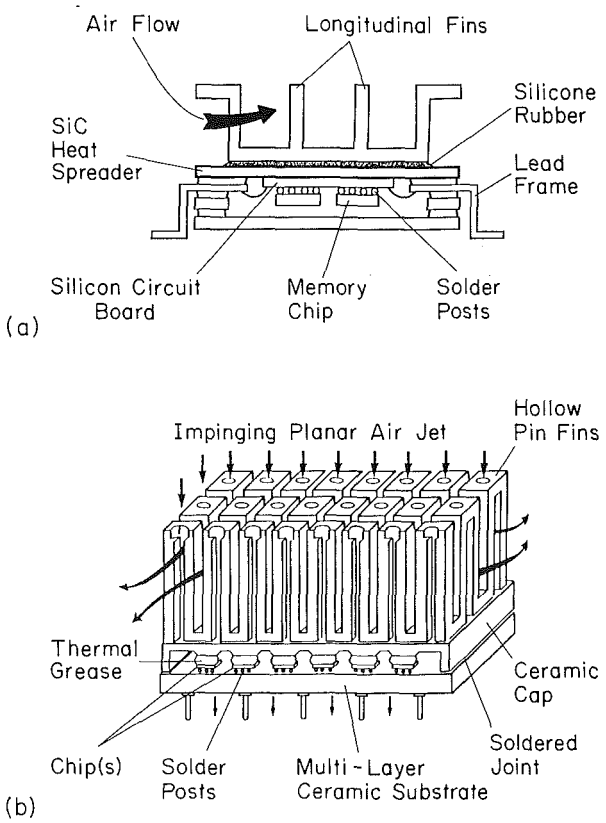

Fig. 1 Air-cooled, multichip modules: (*a*) Hitachi silicon carbide module, (*b*) IBM 4381 jet impingement module

Contributed by the Heat Transfer Division for publication in the JOURNAL OF HEAT TRANSFER. Manuscript received by the Heat Transfer Division February 8, 1988. Keywords: Boiling, Convection, Electronic Equipment, Reviews.

Copyright © 1988 by ASME

Downloaded 16 Dec 2010 to 193.140.21.150. Redistribution subject to ASME license or copyright; see http://www.asme.org/terms/Terms_Use.cfm

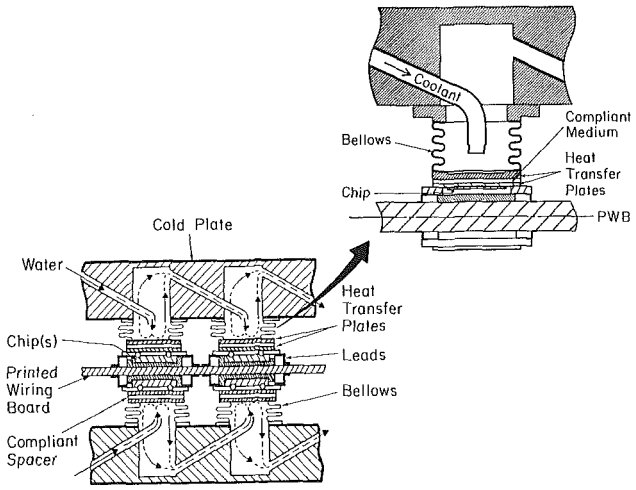

Fig. 2 Fujitsu FACOM M-780 water-cooled module with bellows interface

plate to the electronic package. A well-known example of this technology is the Thermal Conduction Module (TCM) used on the IBM 308X/3090 series of computers (Chu et al., 1982). In this system, however, there remains a substantial internal resistance to heat transfer between the chips and the cold plate. To reduce this resistance, the coolant flow must be brought in closer proximity to the electronics. One approach (Yamamoto et al., 1987) involves mounting chips to both sides of a printed wiring board and interfacing each side with a cold plate assembly (Fig. 2). The interface is provided by a bellows within which water flow maintains large convection heat transfer coefficients characteristic of a submerged jet. Alternatively, interface resistances between the cold plate and a multichip module may be eliminated by making the cold plate an integral part of the module. Such an approach has been adopted by Kishimoto and Osaki (1986).

Since direct liquid cooling maintains physical contact between the coolant and the electronic components, the coolant must have a very large dielectric strength and good chemical compatibility with the components. Typically, such coolants are characterized by low boiling points, and their use could involve pool or forced convection boiling, as well as single-phase convection (natural, forced, or mixed). Although the option of direct liquid cooling has been considered for well over a decade, actual application has been limited to a single computing system (Danielson et al., 1986). Vertical flow of the coolant (3MFC-77) between stacks of circuit modules precedes horizontal flow at approximately 25 mm/s through the modules. Memory and logic chips attached to the modules are immersed in the liquid, and heat transfer is likely to occur under single-phase, mixed convection conditions.

The foregoing brief review of electronic cooling technologies illustrates the great breadth of related heat transfer topics. The topics involve conduction and interfacial heat transfer phenomena occurring within electronic packages and convection heat transfer from the exterior surfaces of the packages. Free, forced, or mixed convection may be associated with coolants such as air, water, and dielectric liquids, while boiling may be associated with the use of liquid coolants.

The primary purpose of this paper is to assess the relationship of single-phase and multiphase convection heat transfer to electronic cooling. With respect to single-phase convection, it has become common practice to treat, separately, results obtained for air and liquid cooling. However, as applied to electronic packages, geometries and operating conditions are, in many cases, equivalent and results could possibly be collapsed in terms of the fluid Prandtl number. Hence, air and liquid results pertaining to a particular geometry or flow condition will be considered collectively. In sequence, the following sections deal with electronic cooling by single-phase natural, forced, and mixed convection; pool and forced-convection boiling; and two-phase thermosyphons.

2 Natural Convection

2.1 Parallel Plate Channels. One of the most common electronic equipment cooling configurations involves free convection in vertical (or inclined) parallel plate channels that are open to the ambient at opposite ends. As in an array of PCBs (Fig. 3*a*), heat dissipating components are mounted to the plates and heat transfer from the array is influenced by free convection to the coolant, as well as by conduction in the plates and (in the case of a gaseous coolant) by radiation exchange between the plates and their surroundings. Although the manner in which heat is dissipated along the wall varies with specific packaging and operating conditions, many ap-

Nomenclature

b = barrier height
C = fin tip-to-shroud clearance
g = gravitational acceleration
Gr = Grashof number
H = plate, enclosure, or channel height
$\bar{h}$ = average convection coefficient
h_{fg} = heat of vaporization
Ja = Jakob number
L = plate, fin, or heater length
$\overline{\mathrm{Nu}}$ = average Nusselt number
q = local heat flux
R_q = heating ratio for free convection between isoflux parallel plates $= q_2/q_1$
R_T = heating ratio for free convection between isothermal parallel plates $= (T_{s,2} - T_\infty)/(T_{s,1} - T_\infty)$
$\mathrm{Ra_S}$ = Rayleigh number for isothermal plates
$\mathrm{Ra_S^*}$ = modified Rayleigh number for isoflux plates
Re = Reynolds number based on duct hydraulic diameter
S = spacing between parallel plates; pitch
S_L, S_T = longitudinal and transverse pitches
t = fin, plate, or heater thickness
T = temperature
V = velocity
W = enclosure or channel width
We = Weber number
x = streamwise coordinate
θ = plate inclination or dimensionless temperature
ρ = density

Subscripts

c = chilled wall; chip microchannel; critical heat flux
f = fluid
g = vapor
h = heater
L = longitudinal
s = surface
sub = subcooled
T = total; transverse
∞ = free stream or inlet

Downloaded 16 Dec 2010 to 193.140.21.150. Redistribution subject to ASME license or copyright; see http://www.asme.org/terms/Terms_Use.cfm

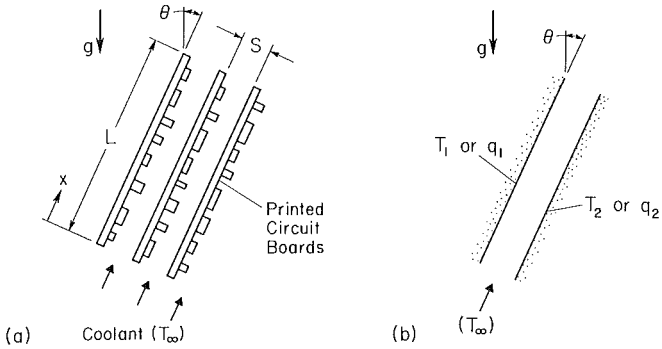

Fig. 3 Natural convection in parallel plate channels: (*a*) PCB array, (*b*) smooth plate approximation

plications are suitably approximated by smooth plates with isothermal or isoflux surfaces (Fig. 3*b*). Conditions may be symmetric ($T_{s,1}=T_{s,2}$; $q_1=q_2$) or asymmetric ($T_{s,1}\neq T_{s,2}$; $q_1\neq q_2$).

For vertical channels ($\theta=0$) buoyancy acts exclusively to induce motion in the streamwise (x) direction and, beginning at $x=0$, boundary layers develop on each surface. For short channels and/or large spacings, independent boundary layer development occurs at each surface and conditions correspond to those for an isolated plate in an infinite quiescent medium. For large L/S, however, boundary layers developing on opposing surfaces eventually merge to yield a fully developed condition. If the channel is inclined, there is a component of the buoyancy force acting normal, as well as parallel, to the streamwise direction, and conditions may be strongly influenced by development of a three-dimensional, secondary flow.

2.1.1 Vertical Channels. Beginning with the benchmark paper by Elenbaas (1942), the vertical channel orientation has been studied extensively for symmetrically and asymmetrically heated plates with isothermal or isoflux surface conditions. For *symmetrically heated, isothermal plates*, Elenbaas obtained the following semi-empirical correlation for the average Nusselt number $\overline{Nu}_S$ as a function of the parameter $Ra_S\,(S/L)$

$$\overline{Nu}_S=\frac{1}{24}Ra_S(S/L)\left\{1-\exp\left[-\frac{35}{Ra_S(S/L)}\right]\right\}^{3/4} \qquad (1)$$

In the fully developed limit ($S/L\to 0$), the correlation is in excellent agreement with the predictions of Bodoia and Osterle (1962), who numerically simulated developing flow with uniform inlet velocity and temperature profiles, and with the analytical fully developed flow solution of Aung (1972). Although there is reasonable agreement with the Bodoia and Osterle prediction in the isolated plate limit ($S/L\to\infty$), improved agreement was obtained by Aihara (1973), whose numerical simulation accounted for the pressure defect created by acceleration of the inviscid fluid at the channel inlet.

For *symmetrically heated, isoflux surfaces*, local heat transfer coefficients have been measured by Siegel and Norris (1957), and both fully developed and entry region solutions have been obtained (Aung, 1972; Aung et al., 1972). Experiments performed by Wirtz and Stutzman (1982) yielded a correlation for the maximum plate temperature, which is in good agreement with the predictions of Aung et al. (1972).

For *asymmetric heating* Aung (1972) obtained closed-form solutions for fully developed flow, while Aung et al. (1972) obtained numerical and experimental results for developing flow. Heating ratios were in the range $0\leq(R_T$ or $R_q)\leq 1$. For isothermal plates, results obtained for $\overline{Nu}_S$ were in good agreement with those for symmetric heating ($R_T=1$) when the average of the two surface temperatures, $\bar{T}_s\equiv(T_{s,1}+T_{s,2})/2$, was used to define $\bar{h}$. For a restricted range of $Ra_S(S/L)$, it was also concluded that expressions obtained for isoflux symmetric heating could be used to predict the maximum temperature on each of the asymmetrically heated surfaces. Miyatake and Fujii (1973, 1974) also simulated developing flow between asymmetrically heated isothermal and isoflux surfaces.

Conditions corresponding to heating at one plate, with the other plate insulated, have received special consideration. Numerical simulations (Miyatake and Fujii, 1972; Miyatake et al., 1973), as well as experiments (Sparrow et al., 1984b; Miyamoto et al., 1986) have been performed for both isothermal and isoflux conditions at the heated plate. For modified Rayleigh numbers up to 3×10^{14}, Miyamoto et al. (1986) observed transition to turbulence in upper portions of the channel, with an accompanying enhancement of the local Nusselt number at the heated (isoflux) surface.

Bar-Cohen and Rohsenow (1984) derived the limiting Nusselt number relations for fully developed laminar flow in symmetric isothermal and isoflux channels, as well as for channels with an insulated wall and an isothermal or isoflux wall. Using a well-established formalism for inferring general correlations from limiting results, the fully developed limits were combined with those for the isolated plate to obtain correlations for isothermal and isoflux conditions. Although data (in air) used to validate the correlations were in the range Ra_S (or $Ra_S^*)S/L\lesssim 10^4$, the correlations should remain applicable up to Rayleigh numbers associated with transition to turbulence. Bar-Cohen and Rohsenow used their Nusselt number correlations to infer optimum plate spacings for maximizing heat transfer from an array of isothermal plates, as well as the spacing needed to maximize heat transfer from each plate in the array. For water, Azevedo and Sparrow (1985) correlated heat transfer data for vertical isothermal surfaces in the isolated plate limit ($Ra_S S/L>200$).

Factors that may influence applicability of the foregoing results to PCBs include edge effects (Sparrow and Bahrami, 1980), board conduction (Zinnes, 1970; Burch et al., 1985; Jaluria, 1985), and the effect of protruding components. Studies concerning applicability of isothermal or isoflux correlations to PCBs with regular and irregular arrays of wall protrusions have yielded mixed results. Birnbrier (1981) found that uniform heat flux correlations did not provide reliable predictions of component temperatures on a printed circuit board. Ortega and Moffat (1985) measured heat transfer from a square in-line array of cubical elements mounted on one of opposing insulated boards, and average convection coefficients for air were as much as 50 percent larger than results for an equivalent parallel plate channel. Moreover, the data did not scale according to accepted fully developed and isolated plate limits. The data were reconsidered by Ortega and Moffat (1986) and Moffat and Ortega (1986) who, assuming good cross-stream mixing, presumed the channel flow over an element to consist of components due to global and local buoyancy effects. With respect to the elements, flow due to global buoyancy was viewed as forced convection and heat transfer could be calculated from an appropriate forced convection correlation.

In contrast to the foregoing results, Johnson (1986) found that existing parallel plate correlations for symmetric isoflux plates could be adapted to PCB conditions. Using available data for simulated PCB arrays, he concluded that, when expressed in terms of a board spacing reduced by the nominal height of the components, S', results for the range $10<Ra_{S'}^*(S'/L)<300$ were in good agreement with the correlations of both Wirtz and Stutzman (1982) and Bar-Cohen and Rohsenow (1984). Johnson also recommended use of these correlations for the fully developed limit, $Ra_{S'}^*(S'/L)<10$, and for the isolated plate limit corresponding to $300<Ra_{S'}(S'/L)<1000$.

Downloaded 16 Dec 2010 to 193.140.21.150. Redistribution subject to ASME license or copyright; see http://www.asme.org/terms/Terms_Use.cfm

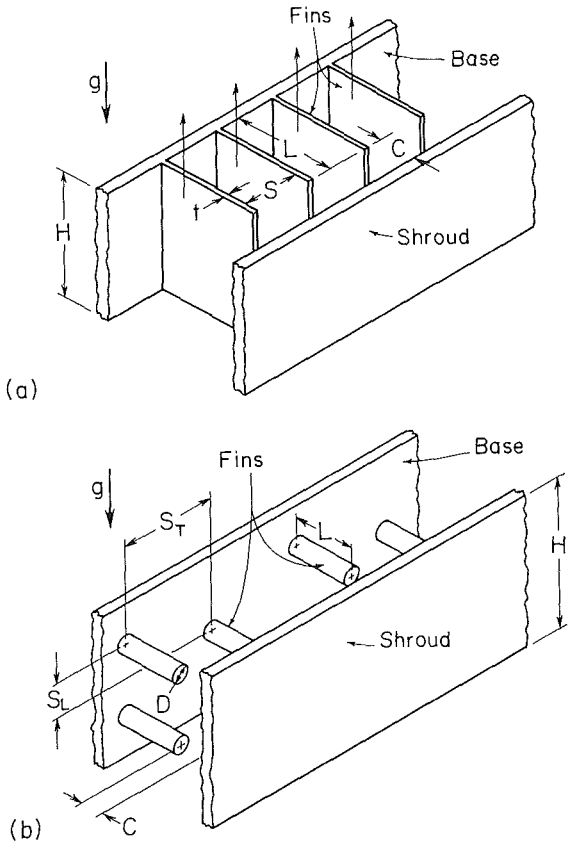

Fig. 4 Shrouded (*a*) plate and (*b*) pin fin arrays

2.1.2 Inclined Channels. Kennedy and Kanehl (1983) and Azevedo and Sparrow (1985) performed experiments for inclined channels in air and water, respectively. For isoflux plates and $30 \leq \theta \leq 90$ deg, Kennedy and Kanehl found that bottom plate temperatures ($T_{s,2}$) could be reduced by operating at a tilt angle of 75 deg. They also observed three-dimensional longitudinal vortices driven by the normal component of the buoyancy force that resulted from bottom heating. Longitudinal vortices due to bottom heating were also observed by Azevedo and Sparrow, who considered symmetric isothermal plates and isothermal/insulated plates for $0 \leq \theta \leq 45$ deg. For heated and insulated top and bottom plates, respectively, a two-dimensional recirculating flow was observed to exist near the unheated wall and the channel outlet. Data obtained for all experimental conditions, including vertical as well as inclined plates, were correlated to within ± 10 percent.

2.2 Fin Arrays. Fin arrays are widely used in heat sinks for cooling electronic components by natural convection. The most common configurations involve vertical surfaces to which plate or pin fins are attached (Figs. 4*a*, *b*). Average convection coefficients for unshrouded vertical arrays have been measured for various plate-fin geometries (Starner and McManus, 1963; Welling and Wooldridge, 1965). However, significant differences are associated with coefficients for the fin base, sides, and edges, and related correlations have been summarized by Aihara (1987). The optimum plate spacing, which maximizes the product of the plate convection coefficient and surface area, is known to decrease with increasing Rayleigh number. In a numerical study of free convection from a staggered array of discrete vertical plates, Sparrow and Prakash (1980) predicted substantial heat transfer enhancement relative to continuous vertical plates of the same heat transfer surface area. Enhancement is due to disruption of thermal boundary layer development. For horizontal, unshrouded plate fin arrays, average convection coefficients have been observed to be much less than those for the vertical array (Cengel and Zing, 1987).

The effect of attaching a shroud to a vertical fin array has been considered numerically (Karki and Patankar, 1984) and experimentally (Cengel and Zing, 1987). Assuming fins of infinite thermal conductivity and an insulated shroud, Karki and Patankar predicted increasing flowrate and heat transfer with increasing C, S, and H. Experimentally, Cengel and Zing found that use of the shroud increased the total heat rate and that enhancement was maximized for a clearance of $C \sim L$.

If a horizontal pin fin is attached to a heated vertical plate, the average convection coefficient for the pin is enhanced and degraded by the motion and temperature, respectively, of the upstream boundary layer flow. In air, these effects have been studied for a single cylinder (Sparrow and Chrysler, 1981) and for an in-line array of cylinders (Sparrow et al., 1982a). In addition to heat transfer enhancement and reduction by the motion and elevated temperature, respectively, of the boundary layer fluid, upstream (lower) cylinders generate buoyancy plumes whose motion and elevated temperature have competing effects on heat transfer from downstream (upper) cylinders.

Natural convection and radiation heat transfer from staggered, horizontal pin fin arrays on a vertical plate in air have been considered experimentally by Sparrow and Vemuri (1985). For an unshrouded array, up to order-of-magnitude enhancement in heat transfer was achieved. The relative contribution of radiation was significant and increased with increasing pin population. Shrouds attached close to the pin tips had the effect of reducing the total heat transfer rate.

2.3 Discrete Sources in a Quiescent Ambient. Energy dissipated by an electronic component in a quiescent ambient induces a buoyancy-driven flow that ascends from the component as a wake or plume. A common example concerns free convection heat transfer from a small rectangular component, flush-mounted to a vertical substrate. The problem was first considered by Baker (1972, 1973), who found that the heat transfer coefficient increased significantly with decreasing heater size and was underpredicted by accepted free convection correlations. Heat transfer coefficients in excess of standard predictions were also measured by Carey and Mollendorf (1977) and Park and Bergles (1987). In the latter study, the coefficient increased with decreasing width, and the effect was attributed to an induced flow of ambient fluid at the sides of the heater.

For a vertical, in-line array of heat sources, the plume ascending from a lower source can strongly influence heat transfer at an upper source. For laminar, two-dimensional flow associated with two isolated sources flush mounted on a vertical wall, Sparrow and Faghri (1980) and Jaluria (1982, 1985) numerically delineated the competing effects on heat transfer enhancement and degradation at the upper source due to fluid acceleration and preheating, respectively, by the lower source. The problem has been considered experimentally by Milanez and Bergles (1986) and Park and Bergles (1987), and a comprehensive theoretical and experimental study of heat transfer from a vertical plate with multiple, flush-mounted, heated elements in air has been performed by Kishinami et al. (1987).

Experiments for protruding heaters mounted on an unshrouded vertical plate have been performed in air (Ortega and Moffat, 1985) and in water and R-113 (Park and Bergles, 1987). Ortega and Moffat considered 10 rows of in-line cubical elements protruding 12.7 mm into the ambient and found that the average element convection coefficient decreased slightly from the first to the fourth rows and remained constant beyond the fourth row. Heat transfer data for the second to tenth rows were characterized by the functional

Downloaded 16 Dec 2010 to 193.140.21.150. Redistribution subject to ASME license or copyright; see http://www.asme.org/terms/Terms_Use.cfm

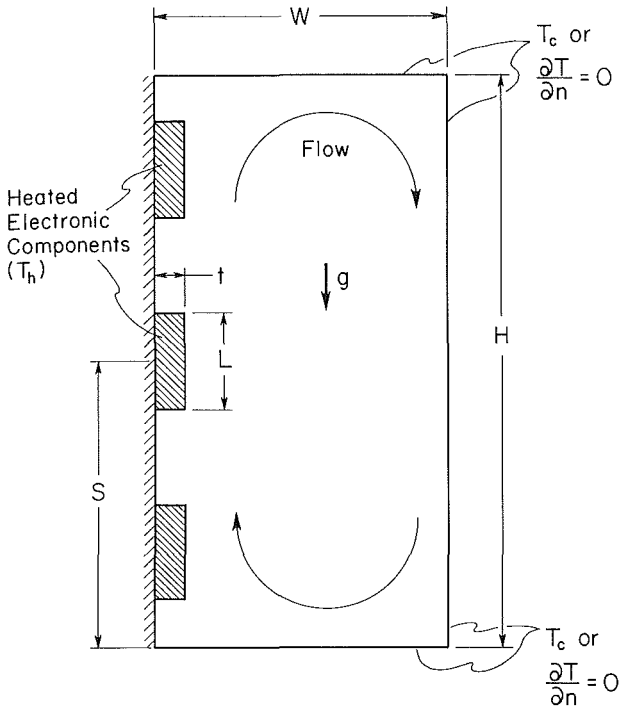

Fig. 5 Buoyancy-driven flow due to wall-mounted heaters in an enclosure

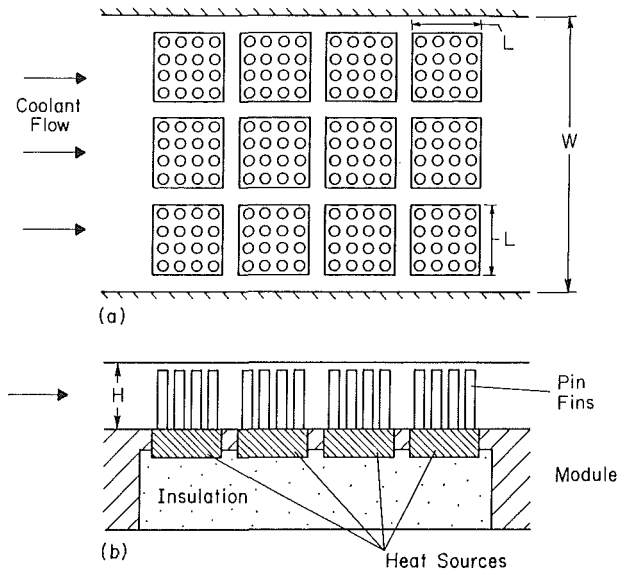

Fig. 6 Array of discrete sources mounted to one wall of a rectangular duct (experiments performed with and without pin fins)

dependence $Nu_x \sim Gr_x^{1/3}$, suggesting that disturbances induced by the protrusions were sufficient to induce turbulence in the buoyancy-driven flow. For an in-line array of two heaters protruding 1.1 mm from the substrate (Park and Bergles, 1987), convection coefficients exceeded those for flush heaters by approximately 14 percent and the coefficient for the top heater exceeded that for the bottom heater.

2.4 Enclosures. Numerous applications exist for which electronic components are packaged within rectangular enclosures (Fig. 5). The components may be mounted to one wall of the enclosure, while one or more of the other walls is cooled. Buoyancy forces induce a recirculating flow within the enclosure, and heat is transferred by natural convection from the component surfaces.

Although the literature on natural convection in enclosures is voluminous, comparatively little has been reported on the effects of discrete heat sources. The first such study was performed by Chu et al. (1976), who obtained a two-dimensional numerical solution for a single, isothermal (T_h) heater strip, flush-mounted ($t=0$) to a vertical wall of the cavity. The opposite wall was cooled (T_c), while all other surfaces were adiabatic. Calculations were performed for air, with Grashof numbers and aspect ratios in the ranges $0 \le Gr_H \le 10^5$ and $0.4 \le H/W \le 5$. The heater size L and position S were also varied. Over the range of conditions considered, the average Nusselt number was found to increase as Gr_H^n, where $n \approx 0.3$. It also increased with increasing L/H, exhibited a maximum for an optimal heater location of $S/H \approx 0.4$, and was approximately independent of aspect ratio. The $Gr_H^{0.3}$ dependence was also obtained in a subsequent numerical simulation for water (Yaghoubi and Incropera, 1980). Experiments performed in air for heating and cooling on opposite vertical walls (Turner and Flack, 1980; Flack and Turner, 1980) confirmed the L/H, S/H, and H/W trends predicted by Chu et al. (1976), but for larger Grashof numbers ($5 \times 10^6 \le Gr_H \le 9 \times 10^6$).

More recently, two-dimensional numerical simulations (Lee et al., 1987) and experiments (Kelleher et al., 1987) have been performed for an isothermal protruding heater (T_h) mounted to one vertical wall of a rectangular cavity. The remainder of the heater wall and the opposing wall were insulated, while the top and bottom surfaces were cooled (T_c). At large Rayleigh numbers, Nusselt number data were in good agreement with the predictions, but at small Rayleigh numbers the data, which were characterized by large uncertainty, were significantly overpredicted. Irrespective of heater location, both the numerical simulations and visualization revealed that the buoyancy-driven flow was concentrated in the region above the heater. A three-dimensional simulation has been performed for flow and heat transfer from a 3×3 array of blocklike electronic components mounted to one vertical wall of a rectangular cavity filled with a dielectric liquid (Liu et al., 1987). However, there is need for additional research to clarify the significance of three-dimensional effects of limitations associated with two-dimensional results.

3 Forced Convection

3.1 Rectangular Ducts. Electronic components may be cooled by single-phase forced convection, and available results may be differentiated according to whether the components are mounted flush with a substrate or protrude from the substrate. Results may also be distinguished according to whether they involve measures for heat transfer enhancement. Typically, components are mounted to the walls of a rectangular channel and conditions are complicated by the existence of multiple length scales.

3.1.1 Flush-Mounted Sources. Early experimental studies of forced convection heat transfer from flush-mounted sources were performed by Baker (1972, 1973), who considered silicone oil and R-113 in parallel flow over small, chiplike heaters. Single-phase forced convection coefficients increased significantly with decreasing surface area and substantially exceeded results associated with nucleate boiling, as well as predictions based on two-dimensional boundary layer theory. Enhanced convection was attributed to three dimensionality of the flow associated with small heating elements.

Studies related to heat transfer from an array of discrete isothermal sources flush-mounted to one wall of a rectangular channel have been performed by Incropera et al. (1986). The array (Fig. 6) consisted of four equally spaced rows, with three heaters in each row. Experiments were performed for water and FC-77 without the pin fins shown in the figure, and results

Downloaded 16 Dec 2010 to 193.140.21.150. Redistribution subject to ASME license or copyright; see http://www.asme.org/terms/Terms_Use.cfm

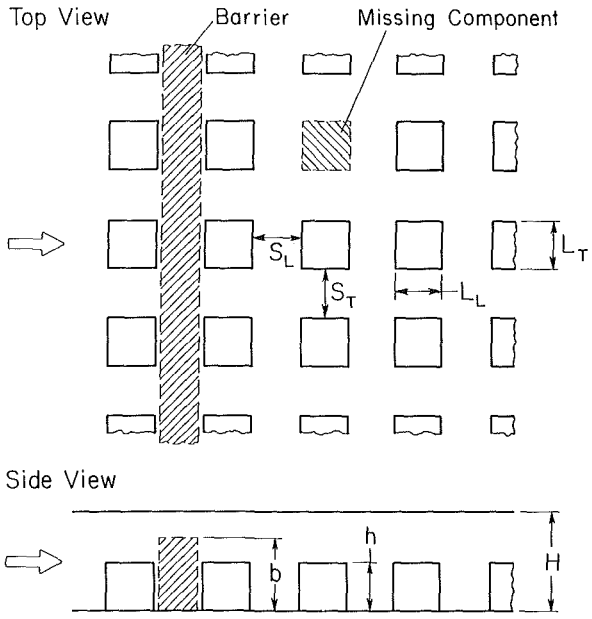

Fig. 7 Representative arrangement of electronic components in parallel plate channel with forced convection cooling

were compared with predictions based on two-dimensional, conjugate forced convection models for laminar and turbulent flow. The data were significantly underpredicted in laminar flow, and differences were attributed to the effects of buoyancy on the experimental results. In turbulent flow, however, agreement between the predicted and measured results was good, suggesting that three-dimensional boundary layer effects were negligible. Due to the effects of upstream thermal boundary layer development, average Nusselt numbers in the second row were approximately 25 percent less than those of the first row, while Nusselt numbers in the third row were approximately 10 percent less than those of the second row. The decrease between the third and fourth rows was only 3 percent, suggesting that a periodic fully developed condition was approached. An experimental study of heat transfer from a single source mounted flush with one wall of a rectangular duct has been performed by Samant and Simon (1986) for FC-72 and R-113. In R-113 a peak heat flux of 200 W/cm^2 was achieved without nucleation.

Although resistor network, finite-difference and finite-element methods have been used to predict heat transfer from a discrete source, it is common practice to ignore the coupling between heat transfer by conduction in substrate materials and convection to the coolant. However, the need to consider such coupling is dictated by the mutual dependence of conditions in the fluid, substrate, and heated component. The extent to which the component is more strongly coupled to the fluid or the substrate depends on the nature of the flow, as well as on the fluid and substrate thermophysical properties. For two in-line isothermal heat sources mounted flush to one wall of a parallel plate channel, this dependence has been considered by Ramadhyani et al. (1985) and Moffatt et al. (1986) for laminar and turbulent flows, respectively. Although the ratio of the substrate to total heat loss was found to be approximately the same for the two sources, thermal boundary layer development on the upstream source was found to attenuate local Nusselt numbers on, and therefore decrease convection heat transfer from, the downstream source.

3.1.2 Protruding Sources. A common electronic package is one that involves forced air cooling of protruding components on a printed circuit board. Typically, many such boards are stacked in a direction normal to the flow, forming parallel plate channels with the component covered board facing the smooth surface of an adjoining board (Fig. 7). However, unlike the regular array of cubical components illustrated in Fig. 7 ($L_T = L_L = h$), components of varying dimensions are often arranged in an irregular pattern. Even for a regular arrangement of uniformly sized components, there is considerable geometric variability and there is no definitive characteristic length. Three-dimensional flow within the channel is characterized by vortex shedding from component edges, separation downstream of the components, and bypass around the components. If the components occupy a large portion of the flow cross section, the flow is partitioned into two streams, one of which passes through the array, contributing to its cooling, while the other passes over the array with little effect on cooling. In addition to being influenced by such flow phenomena, heat transfer from a downstream component may be strongly affected by incomplete mixing in the channel cross section and hence location of the downstream component in the thermal wake of an upstream component. Further complications may result from the existence of missing components and the use of barriers or ribs to enhance heat transfer from downstream components.

Despite the enormous variability of geometric conditions, systematic attempts have been made to determine component coefficients and to develop methodologies for treating the effect of component location in an array. In an early study, Buller and Kilburn (1981) obtained heat transfer data for a single rectangular component and successfully correlated the data using a hybrid characteristic length based on features of both the flow and component geometries. In subsequent experiments, Sparrow and co-workers considered an array of components and systematically examined the effect of row number, missing and irregular components, and barriers on the average convection coefficient for a single component in the array (Sparrow et al., 1982b, 1984a; Sparrow and Otis, 1985). Conditions essentially corresponded to a single heated component in an array of unheated components. Lehmann and Wirtz (1985) also considered the effect of rib spacing and channel height by placing ten unheated, repeating ribs upstream of a heated, two-dimensional, rectangular component. Conjugate heat transfer calculations for two-dimensional developing flow over three repeating, heated, rectangular components (Davalath and Bayazitoglu, 1987) revealed the effect of recirculating zones and the existence of an optimum component spacing.

Several investigators have suggested methodologies for treating downstream effects of nonuniform heating in an array of components. Arvizu and Moffat (1982) proposed a superposition method to account for the effect of thermal wakes on the temperature rise of downstream components. In subsequent studies Moffat et al. (1985) obtained thermal wake functions for an in-line array of cubical elements, while Bieber and Sammakia (1986) applied a superposition method to an array of *flat packs*. Thermal wake effects in flat pack arrays have also been considered by Wirtz and Dykshoorn (1984) and Hollworth and Fuller (1987) for in-line and staggered arrangements, respectively. An alternative procedure for estimating the effects of imperfect mixing has been proposed by Ashiwake et al. (1983), who also found that the dispersion of thermal wakes and the reduction of downstream component temperatures improved when the components are staggered rather than in-line. Thermal wake dispersion is known to increase with increasing Reynolds number (Arvizu and Moffat, 1982; Wirtz and Dykshoorn, 1984).

3.1.3 Enhancement With Pin and Longitudinal Fins. The large convection coefficients associated with small surfaces render the use of single-phase forced convection an attractive method for cooling electronic devices. However, it is possible that additional enhancement may be realized by at-

Downloaded 16 Dec 2010 to 193.140.21.150. Redistribution subject to ASME license or copyright; see http://www.asme.org/terms/Terms_Use.cfm

taching fins directly to the devices, and a popular option involves mounting arrays of cylindrical pins to heat sources cooled in channel flows.

Experimental studies by Sparrow and Ramsey (1978) and Sparrow et al. (1980) for in-line and staggered arrays of pins with tip clearance revealed a row-by-row increase in the pin convection coefficient up to the fourth row, beyond which fully developed conditions were achieved. Convection coefficients and pressure drops were larger for the staggered array than for the in-line array. Van Fossen (1981) studied heat transfer from staggered arrays of short pin fins affixed between two heated copper plates and showed that the pins enhanced heat transfer by a factor of two over that for a plain channel with no fins. Metzger et al. (1982) performed experiments for staggered arrays of short pin fins and showed that convection coefficients increased over the first three to five rows, after which a gradual decline occurred over the remaining rows. Simoneau and Van Fossen (1984) reported results for in-line and staggered arrays of pins, and in both cases heat transfer from a row was enhanced by the presence of upstream rows. More recently, Steuber and Metzger (1986) performed a comprehensive experimental study of more than 20 in-line and staggered pin fin arrangements, with and without tip clearance. The effect of pin fin configuration on local convection coefficients at the wall of a rectangular channel to which the pins are attached has been experimentally determined by Lau et al. (1985).

All of the foregoing studies were performed in air, and no consideration was given to enhancement for discrete sources. However, in a recent study by Kelecy et al. (1987), experiments were performed for liquid flow over an in-line array of 12 flush-mounted heat sources, with a 4×4 array of copper pins attached to each source (Fig. 6). Use of the pins reduced the thermal resistance by factors up to 10 for water and 25 for FC-77. In a sequel study (Ramadhyani and Incropera, 1987), square fins integrally machined from each pin were found to further reduce the thermal resistance by only 20 percent.

Shrouded arrays of longitudinal fins may also be used to enhance heat transfer from electronic devices. Sparrow et al. (1978) and Sparrow and Hsu (1981) predicted local Nusselt number distributions on longitudinal fins for fully developed laminar flow. The results revealed highly nonuniform heat transfer distributions along the fin and base surfaces. With no tip clearance, the Nusselt number attained a maximum between the base and tip, and with tip clearance, the Nusselt number increased monotonically to the tip. Experiments have been performed to determine the effect of tip-to-shroud clearance on heat transfer from a shrouded longitudinal fin array in turbulent flow (Sparrow and Kadle, 1986), and numerical and experimental studies have been performed for turbulent flow in a shrouded array without tip clearance (Kadle and Sparrow, 1986).

Experiments have also been performed to assess the effect of longitudinal fins on heat transfer from discrete sources. Kishimoto et al. (1984) obtained heat transfer data for longitudinal fins mounted to an array of chips, while Yokono et al. (1987) obtained data for a single heater. In both cases, data were obtained for air flow over unshrouded fins of varying dimensions. Nakayama et al. (1987) obtained heat transfer data for a shrouded in-line array of heat sources with longitudinal fins in air.

3.1.4 Other Enhancement Schemes. Other surface arrangements may be used to enhance heat transfer from electronic components, and the success of such arrangements is determined as much by their ability to disrupt thermal boundary layer development and to deliver cold fluid directly to the heated region, as by the extent to which they increase the amount of surface area. Tailored surface arrangements that maximize the velocity and minimize the temperature of liquid flow over the heated surface are preferred.

As mentioned previously, heat transfer from electronic devices may be enhanced by inserting ribs in the flow. Implanted ribs disrupt or turbulate the developing flow, increasing convection heat transfer from downstream modules (Sparrow et al., 1982b, 1983; Hwang, 1984). A similar scheme has been considered for the enhancement of heat transfer from arrays of pins (Steuber and Metzger, 1986) and finned tubes (Rabas and Eckels, 1984). In addition to the use of implanted ribs, Rabas and Eckels considered the effect of deflectors placed upstream of the array and the effect of flow blockage in the array. In each case, heat transfer enhancement was accompanied by a significant increase in pressure drop. The effect of protruding ribs on flow and heat transfer in channels has been studied by Han et al. (1984), Lehmann and Wirtz (1984), Tanasawa et al. (1984), Webb and Ramadhyani (1985), Ichimiya (1987), and Kelkar and Patankar (1987).

Heat transfer enhancement may also be realized by modulating low Reynolds number laminar flows in a parallel plate channel. The process, known as resonant enhancement, may be effected in a grooved channel by actively modulating the flow rate at the natural frequency of the system or by achieving passive modulation through insertion of small vortex-shedding cylinders in crossflow (Greiner et al., 1986; Karniadakis et al., 1987). Significant heat transfer enhancement may be achieved with only a modest increase in pressure drop.

3.2 Indirect Liquid and Microchannel Cooling. Significant advances in the performance of indirect liquid cooling schemes must come from reductions in the internal resistances to heat transfer. A major step in this direction was made by Kishimoto and Osaki (1986), who considered an indirect scheme for which water was pumped through 800 μm wide by 400 μm high rectangular channels in a multilayer alumina substrate. However, the ultimate in indirect liquid cooling is achieved when the cold plate and chip are fabricated as an integral unit. This concept is illustrated in Fig. 8(*a*). With heat dissipating IC elements attached to one side of a silicon substrate, microchannels may be chemically etched or precision machined on the opposite side. The resulting structure resembles a miniature, longitudinally finned heat sink. Closure of the channels is achieved with a cover plate, and liquid is continuously pumped through the channels.

The microchannel concept was first considered by Tuckerman and Pease (1981, 1982), who chemically etched parallel channels of width $W_c = 50$ μm and height $H_c = 300$ μm on one side of a square ($L = 10$ mm) silicon substrate. The channel walls of width $W_w = 50$ μm act as microfins, enhancing heat transfer to the coolant. With water flow rates and attendant pressure drops up to 10 cm^3/s and 350 kPa, flow within the channels remained laminar and thermal resistances as low as 0.09°C/W were achieved (Fig. 8*b*). Accepting a coolant temperature rise of 71°C, a heat flux of 790 W/cm^2 could be dissipated. The superiority of microchannel cooling was confirmed by Mahalingham (1985), who reported thermal resistances in the range from 0.02 to 0.03°C/W for water flow rates up 63 cm^3/s.

Applications of microchannel cooling with air have also been considered. Mahalingham (1985) and Mahalingham and Andrews (1987) performed experiments for two different silicon substrates in which continuous parallel channels were machined. By operating at air velocities up to 37 m/s, thermal resistances as low as 0.75°C/W were achieved. Working with microchannel air velocities of approximately 10 m/s, Goldberg (1984) reported chip-to-air resistances ranging from approximately 4 to 10°C/W for an air velocity of approximately 10 m/s.

Theoretical models of microchannel thermal and

Downloaded 16 Dec 2010 to 193.140.21.150. Redistribution subject to ASME license or copyright; see http://www.asme.org/terms/Terms_Use.cfm

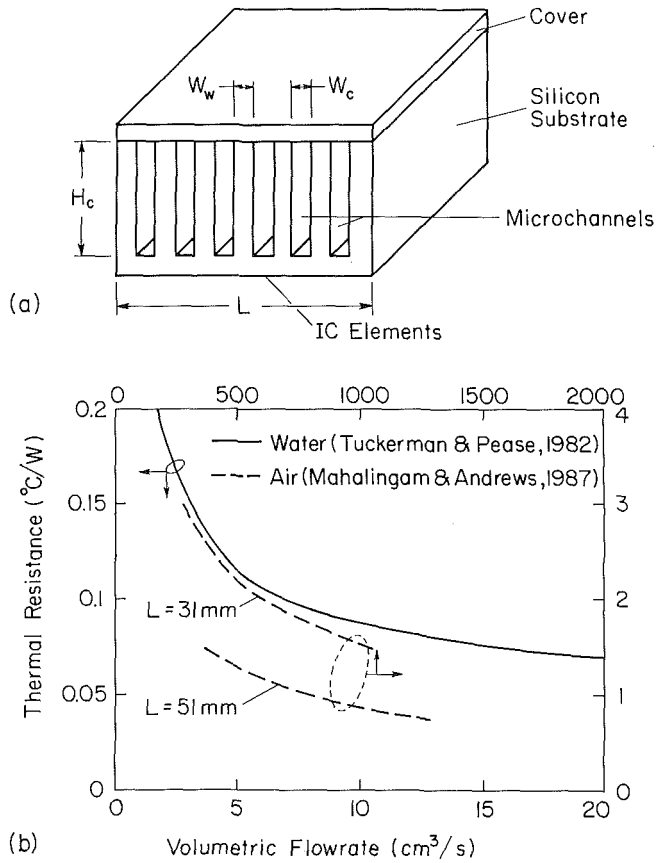

Fig. 8 Microchannel cooling of silicon substrate: (a) schematic, (b) thermal resistances

hydrodynamic conditions have been developed. Phillips et al. (1987) superimposed component thermal resistances in a model that predicted chip and coolant streamwise temperature variations, the total thermal resistance, and pump power requirements. Calculations suggested that enlarged channels for which turbulent flow is readily maintained provide equivalent or improved performance relative to smaller channels for which the flow is laminar. Calculations also suggested that, in lieu of fabricating microchannels in a chip, improved thermal performance could be achieved by machining channels in a separate heat sink of larger thermal conductivity (aluminum or copper) and using a low thermal resistance interface to mate the heat sink and chip. Performance characteristics of such a heat sink have been determined by Mahalingham and Andrews (1987). However, the issue of chip microchannels versus chip heat sinks is important and further investigation is warranted.

3.3 Jet Impingement Cooling. Air jet impingement cooling is used in the IBM 4381 multichip module (Biskeborn et al., 1984), where up to 36 chips are shrouded in a ceramic cap to which an array of 256 hollow aluminum pins is attached (Fig. 1*b*). With an impinging planar jet, an external thermal resistance of less than 8°C/W can be achieved. Impingement jet cooling has also been considered for a silicon heat sink that was 31 mm on a side and 1.5 mm thick (Mahalingham and Andrews, 1987). By machining two sets of narrow channels perpendicular to each other, an array of square microstuds (0.254 mm on a side and 1.143 mm deep) was formed on one side of the heat sink. A thermal resistance of less than 1°C/W could be maintained with air impinging normally on the pins at velocities in excess of approximately 45 m/s.

The specific consideration of impinging liquid jets to electronic cooling is relatively recent. Ma and Bergles (1983) made heat transfer measurements at the stagnation point of a 5 mm × 5 mm source cooled by a submerged 1 mm diameter jet of R-113. With the source mounted vertically and positioned 2 mm from the jet orifice, the data were correlated by an expression of the form $Nu \sim Re^{1/2}Pr^{0.4}$.

An extensive study of single-phase jet impingement cooling for microelectronic applications has been performed by Jiji and Dagan (1987). Heat transfer measurements were made for a single source, as well as for 2 × 2 and 3 × 3 heat source arrays. Using FC-77, each heat source was cooled by a single jet or a multijet array. Square arrays of four and nine jets were considered with jet diameters of 0.5 and 1.0 mm. For all of the cooling configurations, the average Nusselt number was correlated by a single expression, which included the effects of the number of jets and the heater length to nozzle diameter ratio. The results were independent of the nozzle to heat source spacing. The results also indicated that the thermal resistance associated with jet impingement cooling can be reduced by reducing the jet diameter and increasing the number of jets. Resistances as low as 0.15 cm²•°C/W and 1 cm²•°C/W were obtained with water and FC-77, respectively, and it was suggested that further improvements in thermal performance could be realized by seeking optimal arrays of small diameter jets.

Yamamoto et al. (1987) report local and average Nusselt numbers for the 3-mm-dia submerged water jet used to cool the heat transfer plate of the Fujitsu FACOM M-780 computer. The Nusselt number at the stagnation point exceeds the average value by approximately 75 percent, and both are correlated by an expression of the form $Nu_d \sim Re_d^{1/2}Pr^{0.4}$. In water, convection resistances as low as 0.7 cm²•°C/W were obtained.

4 Mixed Convection

Under mixed convection conditions, flow is driven by an externally imposed pressure gradient, as well as by buoyancy forces. If the channel is vertical, buoyancy acts to augment or retard the flow, according to whether the buoyancy force aids or opposes the imposed flow. If the channel is horizontal and heating occurs at the bottom surface, buoyancy may induce a secondary flow which, in combination with the main flow, produces a system of longitudinal vortices. If the channel is inclined, the buoyancy force has two components, one parallel to the surface, acting to accelerate or decelerate flow in the streamwise direction, and the other normal to the surface, acting to drive the secondary flow. The relative influence of these effects depends on the inclination angle.

Two-dimensional, elliptic models have been used to analyze laminar, mixed convection flow between vertical parallel plates with symmetric and asymmetric uniform wall temperatures. The models have addressed both developing (Aung and Worku, 1986a; Habchi and Acharya, 1986a) and fully developed (Aung and Worku, 1986b) flow conditions. Due to local fluid acceleration effects, buoyancy enhances heat transfer in the entrance region, particularly for the hotter of two walls, but buoyancy has no effect on heat transfer in the fully developed region. For asymmetric heating, flow reversal occurs when the parameter Gr/Re exceeds a threshold value, causing downflow along the cooler of the two walls.

Heat transfer enhancement is most pronounced when the channel is horizontal and heat is transferred from the bottom surface. In experiments performed for laminar flow between asymmetrically heated parallel plates (Osborne and Incropera, 1985a), convection coefficients at the bottom plate were found to exceed those corresponding to pure forced convection by up to a factor of 6. Enhancement was due to buoyancy-driven flow, which replaced warmer parcels of fluid ascending from the plate with cooler fluid descending from the main flow. In transitional and turbulent flows, the effects of buoyancy on

Downloaded 16 Dec 2010 to 193.140.21.150. Redistribution subject to ASME license or copyright; see http://www.asme.org/terms/Terms_Use.cfm

heat transfer enhancement at the bottom plate are much less pronounced (Osborne and Incropera, 1985b). Criteria for predicting the onset of a secondary flow have been established (Incropera et al., 1986), and a laminar, parabolic, three-dimensional model has been used to predict the flow morphology (Incropera and Schutt, 1985). In the absence of significant wall conduction, the developing secondary flow causes longitudinal variations in the Nusselt number, which have been confirmed experimentally (Incropera et al., 1987). The strength of the secondary flow and the attendant Nusselt number oscillations decrease with increasing inclination angle from a horizontal (Maughan and Incropera, 1987). The extent to which extended surfaces may be used to enhance mixed convection heat transfer has been considered by Acharya and Patankar (1981) and Zhang and Patankar (1984).

Braaten and Patankar (1985) considered laminar, fully developed flow of air and liquid freon between horizontal parallel plates, with heated rectangular blocks attached to the top or bottom plate. In both cases heat transfer is enhanced above that for pure forced convection, although enhancement is much more pronounced when the heated block is facing upward. Habchi and Acharya (1986b) considered laminar mixed convection in a vertical, parallel plate channel with one wall insulated and the opposing heated wall containing a rectangular blockage. Nusselt numbers on the block and the upstream surface were less than values corresponding to a bare surface.

Studies of mixed convection heat transfer from discrete sources are limited to the work of Kennedy and Zebib (1983) and Tomimura and Fujii (1987). For small heater strips flush-mounted to the walls of a horizontal channel, Kennedy and Zebib observed the formation of longitudinal and spanwise vortices in air due to heating at the bottom and top surfaces, respectively. Tomimura and Fujii applied a laminar, two-dimensional model to air flow between parallel plates, with the top surface insulated and an array of seven equally spaced discrete sources flush-mounted to the bottom surface. For vertical and near-vertical orientations, acceleration of the flow by the streamwise component of the buoyancy force enhances the local Nusselt number for each source significantly above that associated with forced convection.

5 Heat Transfer With Phase Change

Liquid immersion cooling in pool or forced convection boiling is by no means a new concept, with related studies and system designs traceable to the 1950s and 60s (Mark et al., 1958; Goltsos and Mark, 1962; Armstrong, 1967). However, the need for chemically inert coolants of high dielectric strength and low boiling point limits consideration to fluids for which boiling incipience is characterized by a *temperature overshoot*. That is, once boiling is initiated, the surface temperature drops sharply, following the typical boiling curve with increasing heat flux. If the heat flux is subsequently reduced, the surface temperature continues to follow the typical boiling curve, thereby exhibiting a *hysteresis* phenomenon. The phenomenon is attributed to the small surface tension of dielectric fluids and is exacerbated by the small cavities (bubble nucleation sites) associated with smooth chip surfaces. Boiling in dielectric fluids is also characterized by small values of the critical heat flux (CHF), and additional problems could include cyclic thermal stresses and electrical noise related to temperature fluctuations, device contamination due to impurities, and increased complexity associated with the need for sealed chambers (Baker, 1973).

5.1 Pool Boiling. Temperature overshoots up to 25°C have been observed for smooth silicon chips in Flutec PP liquids (Preston and Shillabeer, 1970) and perfluorinated liquids (Oktay, 1982; Moran et al., 1982), as well as for metallic surfaces in R-113 (Bergles and Chyu, 1982; Marto and Lepere, 1982; Park and Bergles, 1986a) and FC-72 (Marto and Lepere, 1982). The nature of the phenomenon is revealed by the representative results of Fig. 9, which also indicate the comparatively small CHF values (~20 W/cm^2) associated with dielectric fluids.

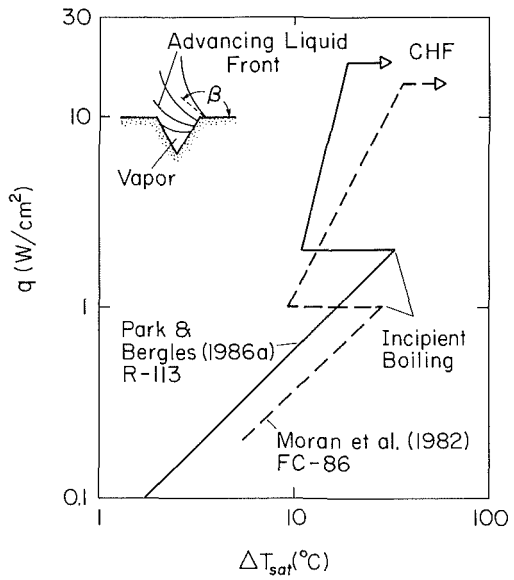

Fig. 9 Representative pool boiling curves with temperature overshoot

Bar-Cohen and Simon (1986) have reviewed existing literature on wall temperature overshoot and have suggested possible mechanisms for delayed nucleation. Boiling incipience at a heated surface is due to the nucleation of vapor bubbles from embryonic vapor/gas pockets in the surface cavities. If a vapor bubble is released from a cavity, surrounding liquid enters the cavity and the shape of the advancing liquid front is determined by its wetting angle β (insert, Fig. 9). Commonly, β exceeds the effective cone angle of the cavity, and the liquid cannot fill the cavity, thereby trapping residual vapor and restoring the nucleation site. However, dielectric liquids have uncommonly small surface tensions, and hence very small wetting angles. For all but the smallest cavities, an advancing liquid front may therefore flood a cavity, depleting it of the vapor embryo needed for the next bubble. Extensive deactivation of nucleation sites by flooding would then require elevated temperatures to initiate bubbles at the remaining smaller cavities or through homogeneous nucleation in the bulk liquid. Bar-Cohen and Simon obtained an upper bound for the incipience superheat excursion from a model based on homogeneous nucleation in the bulk liquid. The model and limited data indicate that the temperature excursion decreases with increasing subcooling and pressure, as well as with increasing velocity (forced convection boiling).

Options for reducing the temperature overshoot and enhancing pool boiling heat transfer have been considered. Considerable attention has been given to either altering the surface or attaching it to a heat sink. For example, Chu and Moran (1977) achieved enhancement by laser drilling holes in a chip surface, thereby forming re-entrant cavities, while Oktay (1982) also reported a reduction in the temperature overshoot for a sandblasted/KOH treated chip. Oktay and Schmeckenbecher (1974) found that, in FC-86, dendritic surfaces prepared by electrolytic deposition eliminated the temperature overshoot and enhanced heat transfer in the nucleate boiling regime. Oktay (1982) drilled 0.8-mm-dia vertical holes in a 1-mm-thick copper block and, relative to a

Downloaded 16 Dec 2010 to 193.140.21.150. Redistribution subject to ASME license or copyright; see http://www.asme.org/terms/Terms_Use.cfm

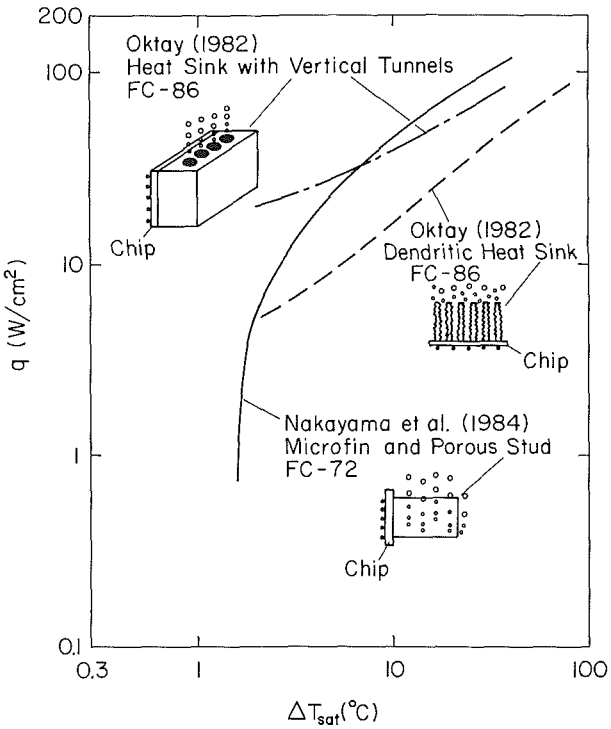

Fig. 10 Pool boiling curves for various heat sink configurations

plain silicon surface, obtained enhanced nucleate boiling and a reduced temperature overshoot in FC-86.

Extensive consideration has also been given to the use of commercially available surfaces (Bergles and Chyu, 1982; Marto and Lepere, 1982; Nakayama et al., 1984; Kim and Bergles, 1985; Park and Bergles, 1986b). The primary function of such surfaces is to provide re-entrant cavities, which enhance the availability of active nucleation sites. Bergles and Chyu (1982) studied nucleate pool boiling of R-113 from porous metallic coatings formed by brazing copper particles to a base surface (Linde High Flux surface). Although nucleate boiling heat transfer was significantly enhanced above that of an uncoated surface, the coating failed to eliminate the temperature overshoot. This result was confirmed by Marto and Lepere (1982) and Kim and Bergles (1985). Marto and Lepere (1982) also studied boiling of R-113 and FC-72 from commercially available grooved fin surfaces (Hitachi Thermoexcel E and Wieland Gewa-T), as well as from the High Flux porous coating. Pool boiling curves were characterized by overshoots of 5 to 10°C and CHF values were limited to approximately 20 W/cm^2.

In an effort to enhance the probability of bubble nucleation from small surfaces and hence boiling heat transfer, Nakayama et al. (1984) considered the effect of attaching a horizontal, cylindrical copper stud with fine structured surfaces to the heat dissipating component. The structures consisted of microfins, microfins covered by a porous plate, and a multilayered porous surface. Superior performance was achieved for a stud length-to-diameter ratio of $L/D \sim 1$, with microfins near the base and multilayered porous plates near the tip. With negligible hysteresis in FC-72, up to 100 W could be dissipated for a 1 cm base diameter, providing base heat fluxes of approximately 100 W/cm^2 at base temperatures up to 80°C.

Park and Bergles (1986b) evaluated the performance of several heat sinks attached to a 5 mm × 5 mm foil heater. The heat sinks included 1-mm-thick copper blocks with microholes or microfins machined parallel to the surface, as well as the High Flux and Thermoexcel-E surfaces. In R-113 the best overall performance was provided by the High Flux surface, which was, in turn, followed by the Thermoexcel-E surface and the copper block with 0.71 mm diameter vertical holes. Results associated with several heat sinks are contrasted in Fig. 10. Exclusion of the temperature overshoot is facilitated by plotting the data for decreasing heat flux. Superior performance is clearly associated with the microfin/porous surface stud of Nakayama et al. (1984). The good performance of the heat sink with vertical holes (Oktay, 1982) is attributed to liquid pumping, and hence enhanced velocities, due to bubble formation in the holes.

The effect of heater size on pool boiling in R-113 has been considered by Baker (1973) and Park and Bergles (1986a). Although Baker reported a pronounced shift in the fully established nucleate boiling curve to lower superheats with decreasing heater size, Park and Bergles observed no such effect. However, Park and Bergles do report increasing CHF with decreasing heater height and width. They also report that for two in-line vertical heaters, boiling incipience occurs at smaller superheats for the top surface, but that there is little difference in the established boiling curve for the two heaters.

5.2 Forced Convection Boiling. Forced convection boiling may occur when cooling is effected by an impinging jet, a channel flow, or a falling film. Impinging jets may be directed normal to the surface or at any angle off the normal. Katto and Ishii (1978) considered free, planar liquid jets impinging at various angles on rectangular surfaces that were 10 to 20 mm long and 15 mm wide. They observed a thickening of the wall jet due to bubble formation, and as CHF was approached, most of the liquid was driven from the surface by intense vapor effusion, leaving a very thin film at the surface. CHF was associated with evaporation of the film and the appearance of dry patches on the surface. Monde and Katto (1978) observed similar behavior for free jets impinging on circular heat sources with diameters ranging from 11 to 21 mm. They also proposed a critical heat flux correlation of the form

$$\frac{q_c}{\rho_g h_{fg} V} = C_1 \left(\frac{\rho_f}{\rho_g}\right)^{m_1} \mathrm{We}^{m_2} \left[1 + C_2 \left(\frac{\rho_f}{\rho_g}\right)^{n_1} \mathrm{Ja}^{n_2}\right] \qquad (2)$$

and for subcooled, normally impinging circular jets, they recommended the correlating coefficients $C_1 = 0.0745$, $m_1 = 0.725$, $m_2 = -0.333$, $C_2 = 2.7$, $n_1 = 0.5$, and $n_2 = 2.0$. For saturated planar jets, Katto and Ishii (1978) recommended the coefficients $C_1 = 0.0164$, $m_1 = 0.867$, and $m_2 = -0.333$.

Ma and Bergles (1983) performed experiments for submerged jets of R-113 impinging normally on a 5 mm × 5 mm heat source. Consistent with the results of Katto and Ishii (1978) and Monde and Katto (1978), CHF was found to increase with the cube root of velocity. It was also found to increase with the degree of subcooling, although the effect was not as pronounced as that observed by Monde and Katto (1978). CHF values up to 100 W/cm^2 were obtained, and temperature overshoots were observed to be negligible.

Katto (1985) considered forced convection boiling of water and R-113 at the heated lower and upper surfaces of a rectangular duct. For heater lengths as small as 10 mm, CHF was found to increase with decreasing length and with increasing velocity and subcooling. More recently, Samant and Simon (1986) investigated forced convection boiling of FC-72 at a 0.25 mm long by 2.0 mm wide heater attached to the lower surface of a rectangular duct. Fully developed, subcooled, turbulent flow was considered, with velocities and subcoolings extending to $V = 16.9$ m/s and $\Delta T_{sub} = 68.1$°C, respectively. Although a large temperature overshoot (27°C) was observed for small values of V and ΔT_{sub}, the overshoot decreased with increasing V and ΔT_{sub} and was essentially eliminated for $\Delta T_{sub} \gtrsim 50$°C. The critical heat flux increased with increasing V and ΔT_{sub}, reaching a value of 426 W/cm^2 for the maximum values of 16.9 m/s and 68.1°C.

Downloaded 16 Dec 2010 to 193.140.21.150. Redistribution subject to ASME license or copyright; see http://www.asme.org/terms/Terms_Use.cfm

Working with forced convection boiling data obtained for free and submerged jets (Monde and Katto, 1978; Ma and Bergles, 1983) and channel flow (Samant and Simon, 1986), Lee et al. (1987b) were able to correlate the data by using equation (2) with $C_1 = 0.0742$, $m_1 = 0.761$, $m_2 = -0.365$, $C_2 = 0.952$, $n_1 = 0.118$, and $n_2 = 1.414$. The data, and hence the correlation, are restricted to heater lengths in the range $0.25 \le L \le 5.0$ mm.

Forced convection boiling may also occur in free-falling, liquid films used to cool vertically mounted electronic chips. Related studies have been performed by Ueda et al. (1981) and Mudawwar et al. (1987). In the latter study liquid films of FC-72 were injected over vertical heaters ranging in length from 12.7 to 127 mm. Film thickness and velocity were varied from 0.25 to 1.50 mm and 0.50 to 2.0 m/s, respectively, while subcooling was maintained below 6°C. Boiling hysteresis was nonexistent, and conditions in the fully developed nucleate boiling regime were approximately independent of film thickness and velocity. The onset of CHF was characterized by separation of most of the film from the heater and subsequent dryout of a thin liquid subfilm, which maintained contact with the heater. The critical heat flux increased with increasing velocity and decreasing heater length and, for zero subcooling, could be correlated by equation (2) with $C_1 = 0.121$, $m_1 = 0.667$, and $m_2 = -0.42$. The largest critical heat flux ($q_c = 24$ W/cm^2) was obtained for the 12.7 mm heater and a velocity of 2 m/s.

Attempts to enhance CHF for falling films have been made by several investigators. Nakayama et al. (1982) considered a long (300 mm) heater in R-11 and studied the effects of structured surfaces, which included grooved (microfinned) surfaces with the grooves aligned (vertical) or perpendicular (horizontal) to the flow direction and a porous cover plate with horizontal subsurface tunnels. The largest heat transfer enhancement was provided by the porous plate, whose performance was independent of flow rate, although comparable performance was exhibited by the vertically grooved surface, when operated at an optimal flow rate.

For a falling film of FC-72 on a 63.5-mm-long heater, Grimley et al. (1988a) studied enhancement effects associated with the use of structured surfaces (vertical microfins or microstuds), subcooling, and a louvered plate mounted parallel to and 2.54 mm from the heated surface. Although both the microfin and microstud surfaces enhanced nucleate boiling heat transfer relative to a smooth surface, only the microfin surface provided significant enhancement of CHF. To establish upper limits for CHF enhancement, Grimley et al. (1988b) performed experiments for a subcooled film of FC-72 falling over a 12.7 mm microfinned surface with an attached flow deflector. It was found that, although CHF may be improved by the combination of reduced heater length, subcooling, and flow deflection, the effects are not independent and superposition does not apply. Since CHF could not be enhanced much above 30 W/cm^2, the large heat fluxes projected for VLSI devices are much more likely to be achieved with jet impingement or channel flows than with a falling film.

5.3 Two-Phase Thermosyphons. Of the many possibilities for two-phase, liquid immersion cooling of microelectronic assemblies, complete encapsulation is an attractive option. The option was first used for high power components and airborne electronic packages (Mark et al., 1958; Goltsos and Mark, 1962) and was subsequently advocated for densely populated PCBs and chip arrays (Megerlin and Vingerhoet, 1971; Aakalu et al., 1973). Typically, it provides for saturated or subcooled boiling at the surfaces of the electronic components and condensation within the liquid and/or at an encapsulated cold plate. As shown in the representative systems of Fig. 11, chips may be mounted to a substrate forming one wall of a module filled with a fluorocarbon. Heat is transferred from the chips to the coolant and from the coolant to the internal fins of a water-cooled cold plate or an air-cooled heat sink. Use of a submerged condenser facilitates maintenance of subcooled conditions in the coolant. Alternatively, the thermosyphon may use a vapor space condenser, in which case the liquid is saturated and condensate is returned from the upper portion of the chamber.

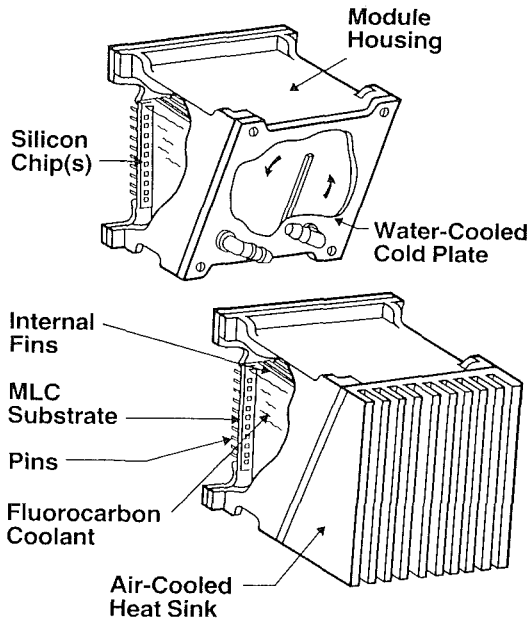

Fig. 11 Encapsulated two-phase thermosyphons

Megerlin and Vingerhoet (1971) considered boiling and condensation of FC-86 in a narrow cavity, with one vertical wall consisting of nine chips on an 8.5 cm^2 substrate and the opposite wall cooled. Heat fluxes up to 15.5 W/cm^2 were reported for a chip temperature of 69°C, and equivalent results were obtained for cavity widths of 3.4 mm and 6.8 mm. Mosinski et al. (1987) considered a similar system (a 3×3 array of simulated chips on one wall and a submerged condenser at the opposite wall), but for narrow cavity widths ranging from 0.43 to 0.81 mm. The wall superheat for a prescribed heat flux and the critical heat flux were found to decrease with decreasing cavity width. In FC-72, CHF values up to 20 W/cm^2 were achieved and were associated with formation of a vapor space and attendant dryout of the top row of heaters. In an alternative configuration intended to enhance condensation, Yokouchi et al. (1987) installed condenser tubes in both the liquid and vapor spaces and used porous nickel plates to trap bubbles in proximity to the submerged tubes. With 49 simulated chips mounted on each of two opposing circuit boards in FC-72, 10 W/cm^2 could be dissipated at the chip level and 1kW could be dissipated in the 900 cm^3 module volume. It was further determined that, by using an 80:20 mixture by volume of FC-72 and FC-75, respectively, temperature overshoot could be eliminated.

6 Summary

From the foregoing review it is evident that significant progress has been made in establishing a convection heat transfer knowledge base pertinent to the problems of electronic cooling. For a wide range of geometries, this knowledge base encompasses conditions corresponding to single-phase free, forced, and mixed convection, as well as pool and forced convection boiling. With such results, it is possible for the packaging engineer to assess, at least in an approximate sense, the relative merits of various options for a particular cooling problem. However, the knowledge base is by no means com-

Downloaded 16 Dec 2010 to 193.140.21.150. Redistribution subject to ASME license or copyright; see http://www.asme.org/terms/Terms_Use.cfm

plete, and research needs are extensive (Incropera, 1986; Nakayama, 1986). There is still room for improvement in air cooling systems through the development of advanced heat sink and/or flow distribution schemes. Significant improvements may also be made in current, state-of-the-art indirect cooling systems. Such improvements are likely to involve establishing intimate contact between the chips and miniature, high-performance, liquid-cooled heat sinks. With respect to direct liquid cooling, the literature is sparse and research needs encompass a broad spectrum. Single- and two-phase thermosyphons offer excellent opportunities for achieving moderate to large heat fluxes under passive operating conditions. Research is needed to understand related flow and heat transfer effects better and to identify optimal design and operating conditions. For two-phase thermosyphons an improved understanding of the behavior of submerged and vapor-space condensers is also needed. Similarly, moderate to large heat fluxes may be achieved under low flow, mixed convection conditions, while *very large fluxes* (~ 200 W/cm^2) require single-phase forced convection or forced convection boiling. In each case, an improved understanding of related flow phenomena is needed for the many possible geometries, and extended surface arrangements that offer significant heat transfer enhancement should be identified. Emphasis should, of course, be placed on schemes that minimize adverse effects associated with increased pressure losses and diminished reliability.

In all of the foregoing convection cooling options, upper limits of thermal performance should be determined. There is also a need for an improved understanding of effects related to the placement of discrete heat sources on a substrate. In many cases, flows are three-dimensional and conjugate effects are significant. There is clearly a need for numerical procedures that can accurately predict such effects in turbulent, as well as laminar, flows. In cooling options that involve boiling, the critical heat flux associated with dielectric liquids must be increased and a better understanding must be obtained of the hysteresis phenomenon and the means by which it may be suppressed. Finally, enhanced microelectronic circuit performance at cryogenic temperatures suggests that cryogenic cooling will be more widely used in future computing systems. Knowledge of heat transfer from small, discrete sources to a cryogenic fluid is sparse, and there is clearly a need for new research.

References

Aakalu, N. G., Chu, R. C., and Simons, R. E., 1973, "Liquid Encapsulated Air Cooling Module," U.S. Patent No. 3,741,292.

Acharya, S., and Patankar S. V., 1981, "Laminar Mixed Convection in a Shrouded Fin Array," ASME JOURNAL OF HEAT TRANSFER, Vol. 103, pp. 559–565.

Aihara, T., 1973, "Effects of Inlet Boundary Conditions on Numerical Solutions of Free Convection Between Vertical Plates," *Report of the Institute of High Speed Mechanics*, Tohoku Univ., Japan, Vol. 28, pp. 1–27.

Aihara, T., 1987, "Natural Convection Air Cooling," International Symposium on Cooling Technology for Electronic Equipment, Honolulu, HI, Mar. 17–21.

Armstrong, R. J., 1967, "Cooling Components With Boiling Halocarbons," *IEEE Transactions*, Vol. PMP-3, No. 4, pp. 135–142.

Arvizu, D. E., and Moffat, R. J., 1982, "The Use of Superposition in Calculating Cooling Requirements for Circuit Board Mounted Electronic Components," IEEE Paper No. CH1781-4/82-0133.

Ashiwake, N., Nakayama, W., Daikoku, T., and Kobayashi, F., 1983, "Forced Convective Heat Transfer From LSI Packages in an Air-Cooled Wiring Card Array," *Heat Transfer in Electronic Equipment—1983*, S. Oktay and A. Bar-Cohen, eds., ASME HTD-Vol. 28, pp. 35–42.

Aung, W., 1972, "Fully Developed Laminar Free Convection Between Vertical Plates Heated Asymmetrically," *International Journal of Heat and Mass Transfer*, Vol. 15, pp. 2293–2308.

Aung, W., Fletcher, L. S., and Sernas, V., 1972, "Developing Laminar Free Convection Between Vertical Flat Plates With Asymmetric Heating," *International Journal of Heat and Mass Transfer*, Vol. 15, pp. 2293–2308.

Aung, W., and Worku, G., 1986a, "Developing Flow and Flow Reversal in a Vertical Channel With Asymmetric Wall Temperatures," ASME JOURNAL OF HEAT TRANSFER, Vol. 108, pp. 299–304.

Aung, W., and Worku, G., 1986b, "Theory of Fully Developed, Combined Convection Including Flow Reversal," ASME JOURNAL OF HEAT TRANSFER, Vol. 108, pp. 485–488.

Azevedo, L. F. A., and Sparrow, E. M., 1985, "Natural Convection in Open-Ended Inclined Channels," ASME JOURNAL OF HEAT TRANSFER, Vol. 107, pp. 893–901.

Baker, E., 1972, "Liquid Cooling of Microelectronic Devices by Free and Forced Convection," *Microelectronics and Reliability*, Vol. 11, pp. 213–222.

Baker, E., 1973, "Liquid Immersion Cooling of Small Electronic Devices," *Microelectronics and Reliability*, Vol. 12, pp. 163–173.

Bar-Cohen, A., and Rohsenow, W. M., 1984, "Thermally Optimum Spacing of Vertical Natural Convection Cooled, Parallel Plates," ASME JOURNAL OF HEAT TRANSFER, Vol. 106, pp. 116–123.

Bar-Cohen, A., and Simon, T. W., 1986, "Wall Superheat Excursions in the Boiling Incipience of Dielectric Fluids," *Heat Transfer in Electronic Equipment—1986*, A. Bar-Cohen, ed., ASME HTD-Vol. 57, pp. 83–94.

Bergles, A. E., and Chyu, M. C., 1982, "Characteristics of Nucleate Pool Boiling From Porous Metallic Coatings," ASME JOURNAL OF HEAT TRANSFER, Vol. 104, pp. 279–285.

Bieber, C. R., and B. G. Sammakia, 1986, "Transport From Discrete Heated Components in a Turbulent Channel Flow," ASME Paper No. 86-WA/HT-68.

Birnbrier, H., 1981, "Experimental Investigations on the Temperature Rise of Printed Circuit Boards in Open Cabinets With Natural Ventilation," *Heat Transfer in Electronic Equipment*, M. D. Kelleher and M. M. Yovanovich, eds., ASME HTD-Vol. 20, pp. 19–23.

Biskeborn, R. G., Horvath, J. L., and Hultmark, E. B., 1984, "Integral Cap Heat Sink Assembly for the IBM 4381 Processor," *Proceedings Fourth Annual International Electronic Packaging Conference*, pp. 468–474.

Bodoia, J. R., and Osterle, J. F., 1962, "The Development of Free Convection Between Heated Vertical Plates," ASME JOURNAL OF HEAT TRANSFER, Vol. 84, pp. 40–44.

Braaten, M. E., and Patankar, S. V., 1985, "Analysis of Laminar Mixed Convection in Shrouded Arrays of Heated Rectangular Blocks," *International Journal of Heat and Mass Transfer*, Vol. 28, pp. 1699–1709.

Buller, M. L., and Kilburn, R. F., 1981, "Evaluation of Surface Heat Transfer Coefficients for Electronic Module Packages," *Heat Transfer in Electronic Equipment*, ASME HTD-Vol. 20, pp. 25–28.

Burch, R., Rhodes, T., and Acharya, S., 1985, "Laminar Natural Convection Between Finitely Conducting Vertical Plates," *International Journal of Heat and Mass Transfer*, Vol. 28, pp. 1173–1186.

Carey, V. P., and Mollendorf, J. C., 1977, "The Temperature Field Above a Concentrated Heat Source on a Vertical Adiabatic Surface," *International Journal of Heat and Mass Transfer*, Vol. 20, pp. 1059–1067.

Cengel, Y. A., and Zing, P. T. L., 1987, "Enhancement of Natural Convection Heat Transfer From Heat Sinks by Shrouding," *Proceedings of the Second ASME-JSME Thermal Engineering Joint Conference*, P. J. Marto and I. Tanasawa, eds., Vol. 3, pp. 451–457.

Chu, H. H.-S., Churchill, S. W., and Patterson, C. V. S., 1976, "The Effect of Heater Size, Location, Aspect Ratio, and Boundary Conditions on Two-Dimensional, Laminar Natural Convection in Rectangular Channels," ASME JOURNAL OF HEAT TRANSFER, Vol. 98, pp. 194–201.

Chu, R. C., and Moran, K. P., 1977, "Method for Customizing Nucleate Boiling Heat Transfer From Electronic Units Immersed in Dielectric Coolant," U.S. Patent No. 4,050,507.

Chu, R. C., Hwang, U. P., and Simons, R. E., 1982, "Conduction Cooling for an LSI Package: A One-Dimensional Approach," *IBM Journal of Research and Development*, Vol. 29, pp. 45–54.

Danielson, R. D., Krajewski, N., and Brost, J., 1986, "Cooling of a Superfast Computer," *Electronic Packaging and Production*, July, pp. 44–45.

Davalath, J., and Bayazitoglu, 1987, "Forced Convection Cooling Across Rectangular Blocks," ASME JOURNAL OF HEAT TRANSFER, Vol. 109, pp. 321–328.

Elenbaas, W., 1942, "Heat Dissipation of Parallel Plates by Free Convection," *Physica*, Vol. 9, pp. 1–28.

Flack, R. D., and Turner, B. L., 1980, "Heat Transfer Correlations for Use in Naturally Cooled Enclosures With High-Power Integrated Circuits," *IEEE Trans. on Components, Hybrids and Manufacturing Technology*, Vol. CHMT-3, pp. 449–452.

Goldberg, N., 1984, "Narrow Channel Forced Air Heat Sink," *IEEE Transactions on Components, Hybrids and Manufacturing Technology*, Vol. CHMT-7, pp. 154–159.

Goltsos, C. E., and Mark, M., 1962, "Packaging With a Flexible Container for Oil-Filled or Evaporative Cooled Electronic Equipment," *IRE Transactions*, Vol. PEP-6, pp. 44–48.

Greiner, M., Ghadder, N. K., Mikic, B. B., and Patera, A. T., 1986, "Resonant Convective Heat Transfer in Grooved Channels," in: *Heat Transfer 1986*, C. L. Tien, V. P. Carey, and J. K. Ferrell, eds., Hemisphere, New York, Vol. 6, pp. 2867–2872.

Grimley, T. A., Mudawwar, I., and Incropera, F. P., 1988a, "CHF Enhancement in Flowing Fluorocarbon Liquid Films Using Structured Surfaces and Flow Deflectors," *International Journal of Heat and Mass Transfer*, Vol. 31, pp. 55–65.

Grimley, T. A., Mudawwar, I., and Incropera, F. P., 1988b, "Limits to Critical Heat Flux Enhancement in a Liquid Film Falling Over a Structured Sur-

Downloaded 16 Dec 2010 to 193.140.21.150. Redistribution subject to ASME license or copyright; see http://www.asme.org/terms/Terms_Use.cfm

face That Simulates a Microelectronic Chip," ASME JOURNAL OF HEAT TRANSFER, Vol. 110, pp. 535-538.

Habchi, S., and Acharya, S., 1986a, "Laminar Mixed Convection in a Symmetrically or Asymmetrically Heated Vertical Channel," *Numerical Heat Transfer*, Vol. 9, pp. 605-618.

Habchi, S., and Acharya, S., 1986b, "Laminar Mixed Convection in a Partially Blocked Vertical Channel," *International Journal of Heat and Mass Transfer*, Vol. 29, pp. 1711-1722.

Han, J. C., Park, J. S., and Lei, C. K., 1984, "Heat Transfer Enhancement in Channels With Turbulence Promoters," ASME Paper No. 84-WA/HT-72.

Hollworth, B. R., and Fuller, H. A., 1987, "Heat Transfer and Pressure Drop in a Staggered Array of Aircooled Components," *Proceedings of the International Symposium on Cooling Technology for Electronic Equipment*, Honolulu, HI, Mar. 17-21, pp. 732-748.

Hwang, U. P., 1984, "Thermal Design Using Turbulators for Air-Cooled Electronic Modules on a Card Package," *Proceedings of the National Electronic Packaging and Production Conference (NEPCON)*, pp. 441-449.

Ichimiya, K., 1987, "Effects of Several Roughness Elements on an Insulated Wall for Heat Transfer From the Opposite Smooth Heated Surface in a Parallel Plate Duct," ASME JOURNAL OF HEAT TRANSFER, Vol. 109, pp. 68-73.

Incropera, F. P., and Schutt, J. A., 1985, "Numerical Simulation of Laminar Mixed Convection in the Entrance Region of Horizontal Rectangular Ducts," *Numerical Heat Transfer*, Vol. 8, pp. 707-729.

Incropera, F. P., Knox, A. L., and Schutt, J. A., 1986, "Onset of Thermally Driven Secondary Flow in Horizontal Rectangular Channels," in: *Heat Transfer—1986*, C. L. Tien, V. P. Carey, and J. K. Ferrel, eds., Hemisphere, New York, Vol. 3, pp. 1395-1400.

Incropera, F. P., Kerby, J., Moffatt, D. F., and Ramadhyani, S., 1986, "Convection Heat Transfer From Discrete Sources in a Rectangular Channel," *International Journal of Heat and Mass Transfer*, Vol. 29, pp. 1051-1058.

Incropera, F. P., ed., 1986, "Research Needs in Electronic Cooling," *Proceedings of National Science Foundation Workshop*, Andover, MA, June 4-6.

Incropera, F. P., 1987, "Research Needs in Electronic Cooling," *Proceedings of the International Symposium on Cooling Technology for Electronic Equipment*, Honolulu, HI, Mar. 17-21, pp. 749-761.

Incropera, F. P., Knox, A. L., and Maughan, J. R., 1987, "Mixed Convection Flow and Heat Transfer in the Entry Region of Horizontal Rectangular Duct," ASME JOURNAL OF HEAT TRANSFER, Vol. 109, pp. 434-439.

Jaluria, Y., 1982, "Buoyancy-Induced Flow Due to Isolated Thermal Sources on a Vertical Surface," ASME JOURNAL OF HEAT TRANSFER, Vol. 104, pp. 223-227.

Jaluria, Y., 1985, "Interaction of Natural Convection Wakes From Thermal Sources on a Vertical Surface," ASME JOURNAL OF HEAT TRANSFER, Vol. 107, pp. 883-892.

Jiji, L. M., and Dagan, Z., 1987, "Experimental Investigation of Single Phase Multi-Jet Impingement Cooling of an Array of Microelectronic Heat Sources," *Proceedings of the International Symposium on Cooling Technology for Electronic Equipment*, Honolulu, HI, Mar. 17-21, pp. 265-283.

Johnson, C. E., 1986, "Evaluation of Correlations for Natural Convection Cooling of Electronic Equipment," *Heat Transfer Engineering*, Vol. 7, Nos. 1-2, pp. 36-45.

Kadle, D. S., and Sparrow, E. M., 1986, "Numerical and Experimental Study of Turbulent Heat Transfer and Fluid Flow in Longitudinal Fin Arrays," ASME JOURNAL OF HEAT TRANSFER, Vol. 108, pp. 16-23.

Karki, K. C., and Patankar, S. V., 1984, "Cooling of a Vertical Shrouded Fin Array by Natural Convection: A Numerical Study," *Fundamentals of Natural Convection/Electronic Equipment Cooling*, L. C. Witte and L. S. Saxena, eds., ASME HTD-Vol. 32, pp. 33-40.

Karniadakis, G. E., Mikic, B. B., and Patera, A. T., 1987, "Heat Transfer Enhancement by Flow Destabilization: Application to the Cooling of Chips," *Proceedings of the International Symposium on Cooling Technology for Electronic Equipment*, Honolulu, HI, Mar. 17-21, pp. 498-521.

Katto, Y., and Ishii, K., 1978, "Burnout in a High Heat Flux Boiling System With a Forced Supply of Liquid Through a Plane Jet," *Proceedings Sixth International Heat Transfer Conference*, Toronto, Canada, Vol. 1, pp. 435-440.

Katto, Y., 1985, "Critical Heat Flux," in: *Advances in Heat Transfer*, Vol. 17, pp. 1-64.

Kelecy, F. J., Ramadhyani, S., and Incropera, F. P., 1987, "Effect of Shrouded Pin Fins on Forced Convection cooling of Discrete Heat Sources by Direct Liquid Immersion," *Proceedings of the Second ASME-JSME Thermal Engineering Joint Conference*, P. J. Marto and I. Tanasawa, eds., Vol. 3, pp. 387-394.

Kelkar, K. M., and Patankar, S. V., 1987, "Numerical Prediction of Flow and Heat Transfer in a Parallel Plate Channel With Staggered Fins," ASME JOURNAL OF HEAT TRANSFER, Vol. 109, pp. 25-30.

Kelleher, M. D., Knock, R. H., and Yang, K. T., 1987, "Laminar Natural Convection in a Rectangular Enclosure Due to a Heated Protrusion on One Vertical Wall—Part 1: Experimental Investigation," *Proceedings of the Second ASME-JSME Thermal Engineering Joint Conference*, P. J. Marto and I. Tanasawa, eds., Vol. 2, pp. 169-177.

Kennedy, K. J., and Zebib, A., 1983, "Combined Free and Forced Convection Between Horizontal, Parallel Planes: Some Case Studies," *International Journal of Heat and Mass Transfer*, Vol. 26, pp. 471-478.

Kennedy, K. J., and Kanehl, J., 1983, "Free Convection in Tilted Enclosures," *Heat Transfer in Electronic Equipment—1983*, S. Oktay and A. Bar-Cohen, eds., ASME HTD-Vol. 28, pp. 43-47.

Kim, C.-J., and Bergles, A. E., 1985, "Structured Surfaces for Enhanced Nucleate Boiling," Report HTL-36, ERI Project 1544, Iowa State University.

Kishimoto, T., Sasaki, E., and Moriya, K., 1984, "Gas Cooling Enhancement Technology for Integrated Circuit Chips," *IEEE Transactions on Components, Hybrids, and Manufacturing Technology*, Vol. CHMT-7, pp. 286-293.

Kishimoto, T., and Osaki, T., 1986, "VLSI Packaging Technique Using Liquid-Cooled Channels," *IEEE Transactions on Components, Hybrids, and Manufacturing Technology*, Vol. CHMT-9, pp. 328-335.

Kishinami, K., Saito, H., and Tokura, I., 1987, "Natural Convective Heat Transfer on a Vertical Plate With Discontinuous Surface Heating (Effect of Heat Conduction in Unheated Elements)," *Proceedings of the Second ASME-JSME Thermal Engineering Joint Conference*, P. J. Marto and I. Tanasawa, eds., Vol. 4, pp. 61-68.

Lau, S. C., Kim, Y. S., and Han, J. C., 1985, "Effects of Fin Configuration and Entrance Length on Local Endwall Heat/Mass Transfer in a Pin Fin Channel," ASME Paper No. 85-WA/HT-62.

Lee, J. J., Liu, K. V., Yang, K. T., and Kelleher, M. D., 1987a, "Laminar Natural Convection in a Rectangular Enclosure Due to a Heated Protrusion of One Vertical Wall—Part II: Numerical Simulations," *Proceedings of the Second ASME-JSME Thermal Engineering Joint Conference*, P. J. Marto and I. Tanasawa, eds., Vol. 2, pp. 179-185.

Lee, T. Y., Simon, T. W., and Bar-Cohen, A., 1987b, "An Investigation of Short-Heating-Length Effects on Flow Boiling Critical Heat Flux in a Subcooled Turbulent Flow," *Proceedings of the International Symposium on Cooling Technology for Electronic Equipment*, Honolulu, HI, Mar. 17-21, pp. 358-373.

Lehmann, G. L., and Wirtz, R. A., 1984, "Convection From Surface Mounted Repeating Ribs in a Channel Flow," ASME Paper No. 84-WA/HT-88.

Lehmann, G. L., and Wirtz, R. A., 1985, "The Effect of Variations in Streamwise Spacing and Length on Convection From Surface Mounting Rectangular Components," *Heat Transfer in Electronic Equipment—1985*, S. Oktay and R. J. Moffat, eds., ASME HTD-Vol. 48, pp. 39-47.

Liu, K. V., Yang, K. T., and Kelleher, M. D., 1987, "Three-Dimensional Natural Convection Cooling of an Array of Heated Protrusions in an Enclosure Filled With a Dielectric Fluid," *Proceedings of the International Symposium on Cooling Technology for Electronic Equipment*, Honolulu, HI, Mar. 17-21, pp. 486-497.

Ma, C. F., and Bergles, A. E., 1983, "Boiling Jet Impingement Cooling of Simulated Microelectronic Chips," *Heat Transfer in Electronic Equipment—1983*, S. Oktay and A. Bar-Cohen, eds., ASME HTD-Vol. 28, pp. 5-12.

Mahalingham, M., 1985, "Thermal Management in Semiconductor Device Packaging," *Proceedings of the IEEE*, Vol. 73, pp. 1396-1404.

Mahalingham, M., and Andrews, J., 1987, "High Performance Air Cooling for Microelectronics," *Proceedings of the International Symposium on Cooling Technology for Electronic Equipment*, Honolulu, HI, Mar. 17-21, pp. 608-625.

Mark, M. M., Stephenson, M., and Goltsos, C. E., 1958, "An Evaporative-Gravity Technique for Airborne Equipment Cooling," *IRE Transactions*, Vol. ANE-5, pp. 47-52.

Marto, P. J., and Lepere, V. J., 1982, "Pool Boiling Heat Transfer From Enhanced Surfaces to Dielectric Fluids," ASME JOURNAL OF HEAT TRANSFER, Vol. 104, pp. 292-299.

Maughan, J. R., and Incropera, F. P., 1987, "Experiments on Mixed Convection Heat Transfer for Airflow in a Horizontal Inclined Channel," *International Journal of Heat and Mass Transfer*, Vol. 30, pp. 1307-1318.

Megerlin, F. E., and Vingerhoet, P., 1971, "Thermal Control of Densely Packaged Microelectronics in Dielectric Fluids," *Proceedings National Aeronautical Electronics Conference*, pp. 254-259.

Milanez, L. F., and Bergles, A. E., 1986, "Studies in Natural Convection Heat Transfer From Thermal Sources on a Vertical Surface," *Heat Transfer—1986*, Proc. 8th Int. Heat Transfer Conf., Hemisphere Publishing Corp., Washington, Vol. 3, pp. 1347-1352.

Miyamoto, M., Katoh, Y., Kurima, J., and Sasaki, H., 1986, "Turbulent Free Convection Heat Transfer From Vertical Parallel Plates," *Heat Transfer—1986*, Proc. 8th Int. Heat Transfer Conf., Hemisphere Publishing Corp., Washington, Vol. 4, pp. 1593-1598.

Miyatake, O., and Fujii, T., 1972, "Free Convective Heat Transfer Between Vertical Plates—One Plate Isothermally Heated and the Other Thermally Insulated," *Heat Transfer—Japanese Research*, Vol. 1, pp. 30-38.

Miyatake, O., Fujii, T., Fujii, M., and Tanaka, H., 1973, "Natural Convective Heat Transfer Between Vertical Parallel Plates—One Plate With a Uniform Heat Flux and the Other Thermally Insulated," *Heat Transfer—Japanese Research*, Vol. 2, pp. 25-33.

Miyatake, O., and Fujii, T., 1973, "Natural Convection Heat Transfer Between Vertical Parallel Plates at Unequal Uniform Temperatures," *Heat Transfer—Japanese Research*, Vol. 2, pp. 79-88.

Miyatake, O., and Fujii, T., 1974, "Natural Convective Heat Transfer Between Vertical Parallel Plates With Unequal Heat Fluxes," *Heat Transfer—Japanese Research*, Vol. 3, pp. 29-33.

Moffat, R. J., Arvizu, D. E., and Ortega, A., 1985, "Cooling Electronic Components: Forced Convection Experiments With an Air-Cooled Array," *Heat Transfer in Electronic Equipment—1985*, S. Oktay and R. J. Moffat, eds., ASME HTD-Vol. 48, pp. 17-27.

Moffat, R. J., and Ortega, A., 1986, "Buoyancy Induced Forced Convection," *Heat Transfer in Electronic Equipment—1986*, A. Bar-Cohen, ed., ASME HTD-Vol. 57, pp. 135-144.

Moffatt, D. F., Ramadhyani, S., and Incropera, F. P., 1986, "Conjugate Heat Transfer From Wall Embedded Sources in Turbulent Channel Flow,"

Downloaded 16 Dec 2010 to 193.140.21.150. Redistribution subject to ASME license or copyright; see http://www.asme.org/terms/Terms_Use.cfm

Heat Transfer in Electronic Equipment—1986, A. Bar-Cohen, ed., ASME HTD-Vol. 57, pp. 177–182.

Monde, M., and Katto, Y., 1978, "Burnout in High Heat-Flux Boiling System With an Impinging Jet," *International Journal of Heat and Mass Transfer*, Vol. 21, pp. 295–305.

Moran, K. P., Oktay, S., Buller, L., and Kerjilian, G., 1982, "Cooling Concepts for IBM Electronic Packages," *Proceedings Second Annual Conference of International Electronic Packaging Society (IEPS)*, pp. 120–140.

Mosinski, T. A., Chen, S. J., and Chato, J. C., 1987, "Liquid Enhanced Cooling of Microchips," *Proceedings of the International Symposium on Cooling Technology for Electronic Equipment*, Honolulu, HI, Mar. 17–21, pp. 321–339.

Mudawwar, I. A., Incropera, T. A., and Incropera, F. P., 1987, "Boiling Heat Transfer and Critical Heat Flux in Liquid Films Falling on Vertically Mounted Surfaces," *International Journal of Heat and Mass Transfer*, Vol. 30, pp. 2083–2095.

Nakayama, W., Daikoku, T., and Nakajima, T., 1982, "Enhancement of Boiling and Evaporation on Structured Surfaces With Gravity Driven Film Flow of R-11," *Heat Transfer—1982*, Hemisphere Publishing Corporation, New York, pp. 409–414.

Nakayama, W., Nakayama, T., and Hirasaura, S., 1984, "Heat Sink Studs Having Enhanced Boiling for Cooling of Microelectronic Components," ASME Paper No. 84-WA/HT-89.

Nakayama, W., 1986, "Thermal Management of Electronic Equipment: A Review of Technology and Research Topics," *Applied Mechanics Reviews*, Vol. 39, pp. 1847–1868.

Nakayama, W., Matsushima, H., and Goel, P., 1987, "Forced Convective Heat Transfer From Arrays of Finned Packages," *Proceedings of the International Syposium on Cooling Technology for Electronic Equipment*, Honolulu, HI, Mar. 17–21, pp. 663–678.

Oktay, S., and Schmeckenbecher, A. F., 1974, "Preparation and Performance of Dendritic Heat Sinks," *Journal of the Electrochemical Society*, Vol. 21, pp. 912–918.

Oktay, S., 1982, "Departure From Natural Convection (DNC) in Low Temperature Boiling Heat Transfer Encountered in Cooling Micro-Electronic LSI Devices," *Heat Transfer—1982*, Proceedings 7th Int. Heat Transfer Conf., Hemisphere Publishing Corp., Washington, Vol. 4, pp. 113–118.

Okutani, K., Otsuka, K., Sahara, K., and Satoh, K., 1984, "Packaging Design of a SiC Ceramic Multi-Chip RAM Module," *Proceedings Fourth Annual International Electronics Packaging Conference*, pp. 299–304.

Ortega, A., and Moffat, R. J., 1985, "Heat Transfer From an Array of Simulated Electronic Components: Experimental Results for Free Convection With and Without a Shrouding Wall," *Heat Transfer in Electronic Equipment—1985*, S. Oktay and R. J. Moffat, eds., ASME HTD-Vol. 48, pp. 5–15.

Ortega, A., and Moffat, R. J., 1986, "Buoyancy Induced Convection in a Non-Uniformly Heated Array of Cubical Elements on a Vertical Channel Wall," *Heat Transfer in Electronic Equipment—1986*, A. Bar-Cohen, ed., ASME HTD-Vol. 57, pp. 123–134.

Osborne, D. G., and Incropera, F. P., 1985a, "Laminar Mixed Convection Heat Transfer for Flow Between Horizontal Parallel Plates With Asymmetric Heating," *International Journal of Heat and Mass Transfer*, Vol. 28, pp. 207–217.

Osborne, D. G., and Incropera, F. P., 1985b, "Experimental Study of Mixed Convection Heat Transfer for Transitional and Turbulent Flow Between Horizontal Parallel Plates," Vol. 28, pp. 1337–1344.

Park, K. A., and Bergles, A. E., 1986a, "Effects of Size of Simulated Microelectronic Chips on Boiling and Critical Heat Flux," *Heat Transfer in Electronic Equipment—1986*, ASME HTD-Vol. 57, A. Bar-Cohen, ed., pp. 95–102.

Park, K. A., and Bergles, A. E., 1986b, "Boiling Heat Transfer Characteristics of Simulated Microelectronic Chips With Detachable Heat Sinks," *Heat Transfer—1986*, C. L. Tien, V. P. Carey, and J. K. Ferrel, eds., Hemisphere, New York, Vol. 4, pp. 2099–2104.

Park, K. A., and Bergles, A. E., 1987, "Natural Convection Heat Transfer Characteristics of Simulated Microelectronic Chips," ASME JOURNAL OF HEAT TRANSFER, Vol. 109, pp. 90–96.

Phillips, R. J., Glicksman, L. R., and Larson, R., 1987, "Forced-Convection, Liquid Cooled Microchannel Heat Sinks for High-Power-Density Microelectronics," *Proceedings of the International Symposium on Cooling for Electronic Equipment*, Honolulu, HI, Mar. 17–21, pp. 227–248.

Preston, S. B., and Shillabeer, R. N., 1970, "Direct Liquid Cooling of Microelectronics," *Proceedings Int. Electronic Packaging and Production Conf. (INTER/NEPCON)*, pp. 10–31.

Rabas, T. J., and Eckels, P. W., 1984, "Effectiveness of Enhancement Devices for Three Row Inline Serrated Finned Tube Banks," ASME Paper No. 84-HT-96.

Ramadhyani, S., and Incropera, F. P., 1987, "Forced Convection Cooling of Discrete Heat Sources With and Without Surface Enhancement," *Proceedings of the International Symposium on Cooling Technology for Electronic Equipment*, Honolulu, HI, Mar. 17–21, pp. 249–264.

Ramadhyani, S., Moffatt, D. F., and Incropera, F. P., 1985, "Conjugate Heat Transfer From Small Isothermal Heat Sources Embedded in a Large Substrate," *International Journal of Heat and Mass Transfer*, Vol. 28, pp. 1945–1952.

Samant, K. R., and Simon, T. W., 1986, "Heat Transfer From a Small, High-Heat-Flux Patch to a Subcooled Turbulent Flow," ASME Paper No. 86-HT-22.

Siegel, R., and Norris, R. H., 1957, "Tests of Free Convection in a Partially Enclosed Space Between Two Heated Vertical Plates," ASME JOURNAL OF HEAT TRANSFER, Vol. 79, pp. 663–673.

Simoneau, R. J., and Van Fossen, G. J., Jr., 1984, "Effect of Location in an Array on Heat Transfer to a Short Cylinder in Crossflow," ASME JOURNAL OF HEAT TRANSFER, Vol. 106, pp. 42–48.

Sparrow, E. M., Baliga, B. R., and Patankar, S. V., 1978, "Forced Convection Heat Transfer From a Shrouded Fin Array With and Without Tip Clearance," ASME JOURNAL OF HEAT TRANSFER, Vol. 100, pp. 572–579.

Sparrow, E. M., and Ramsey, J. W., 1978, "Heat Transfer and Pressure Drop for a Staggered Wall-Attached Array of Cylinders With Tip Clearance," *International Journal of Heat and Mass Transfer*, Vol. 21, pp. 1369–1377.

Sparrow, E. M., and Faghri, M., 1980, "Natural Convection Heat from the Upper Plate of a Colinear, Separated Pair of Vertical Plates," ASME JOURNAL OF HEAT TRANSFER, Vol. 102, pp. 623–629.

Sparrow, E. M., and Prakash, C., 1980, "Enhancement of Natural Convection Heat Transfer by a Staggered Array of Discrete Vertical Plates," ASME JOURNAL OF HEAT TRANSFER, Vol. 102, pp. 215–220.

Sparrow, E. M., Ramsey, J. W., and Altemani, C. A. C., 1980, "Experiments on In-Line Pin Fin Arrays and Performance Comparisons With Staggered Arrays," ASME JOURNAL OF HEAT TRANSFER, Vol. 102, pp. 44–50.

Sparrow, E. M., and Bahrami, P. A., 1980, "Experiments on Natural Convection From Vertical Parallel Plates With Either Open or Closed Edges," ASME JOURNAL OF HEAT TRANSFER, Vol. 102, pp. 221–227.

Sparrow, E. M., and Chrysler, G. M., 1981, "Natural Convection Heat Transfer Coefficients for a Short Horizontal Cylinder Attached to a Vertical Plate," ASME JOURNAL OF HEAT TRANSFER, Vol. 103, pp. 630–637.

Sparrow, E.M., and Hsu, C.F., 1981, "Analytically Determined Fin-Tip Heat Transfer Coefficients," ASME JOURNAL OF HEAT TRANSFER, Vol. 103, pp. 18–25.

Sparrow, E. M., Cook, D. S., and Chrysler, G. M., 1982a, "Heat Transfer by Natural Convection From an Array of Short Wall Attached Horizontal Cylinders," ASME JOURNAL OF HEAT TRANSFER, Vol. 104, pp. 125–131.

Sparrow, E. M., Niethammer, J. E., and Chaboki, A., 1982b, "Heat Transfer and Pressure-Drop Characteristics of Arrays of Rectangular Modules Encountered in Electronic Equipment," *International Journal of Heat and Mass Transfer*, Vol. 25, pp. 961–973.

Sparrow, E. M., Vemuri, S. B., and Kadle, D. S., 1983, "Enhanced and Local Heat Transfer, Pressure Drop, and Flow Visualization for Arrays of Block-Like Components," *International Journal of Heat and Mass Transfer*, Vol. 26, pp. 689–699.

Sparrow, E. M., Yanezmoreno, A. A., and Otis, D. R., Jr., 1984a, "Convective Heat Transfer Response to Height Differences in an Array of Block-Like Electronic Components," *International Journal of Heat and Mass Transfer*, Vol. 27, pp. 469–473.

Sparrow, E. M., Chrysler, G. M., and Azevedo, L. F., 1984b, "Observed Flow Reversals and Measured-Predicted Nusselt Numbers for Natural Convection in a One-Sided Heated Vertical Channel," ASME JOURNAL OF HEAT TRANSFER, Vol. 106, pp. 325–332.

Sparrow, E. M., and Otis, D. R., 1985, "Duct Flow Heat Transfer at a Smooth Wall Which Faces a Wall Covered by Protuberances," *International Journal of Heat and Mass Transfer*, Vol. 28, pp. 1317–1326.

Sparrow, E. M., and Vemuri, S. G., 1985, "Natural Convection/Radiation Heat Transfer From Highly Populated Pin Fin Arrays," ASME JOURNAL OF HEAT TRANSFER, Vol. 107, pp. 190–197.

Sparrow, E. M., and Kadle, D. S., 1986, "Effects of Tip-to-Shroud Clearance on Turbulent Heat Transfer From a Shrouded Longitudinal Fin Array," ASME JOURNAL OF HEAT TRANSFER, Vol. 108, pp. 519–524.

Starner, K. E., and McManus, H. N., 1963, "An Experimental Investigation of Free Convection Heat Transfer From Rectangular Fin Arrays," ASME JOURNAL OF HEAT TRANSFER, Vol. 85, pp. 273–278.

Steuber, G. D., and Metzger, D. E., 1986, "Heat Transfer and Pressure Loss Performance for Families of Partial Length Pin Fin Arrays in High Aspect Ratio Rectangular Ducts," *Heat Transfer—1986*, Proceedings 8th Int. Heat Transfer Conf., Hemisphere Publishing Corp., Washington, Vol. 6, pp. 2915–2920.

Tanasawa, I., Nishio, S., Takano, K., and Miyazaki, H., 1984, "High Performance Surface for Forced Convection Heat Transfer Using Novel Turbulence Promoters," ASME Paper No. 84-HT-69.

Tomimura, T., and Fujii, M., 1987, "Laminar Mixed Convection Heat Transfer Between Parallel Plate With Localized Heat Sources," *Proceedings of the International Symposium on Cooling Technology for Electronic Equipment*, Honolulu, HI, Mar. 17–21, pp. 701–715.

Tuckerman, D. B., and Pease, R. F., 1981, "High-Performance Heat Sinking for VLSI," *IEEE Electronic Device Letters*, Vol. EDL-2, pp. 126–129.

Tuckerman, D. B., and Pease, R. F., 1982, "Ultrahigh Thermal Conductance Microstructures for Cooling Integrated Circuits," *Proceedings of 32nd IEEE Electronics Components Conference*, pp. 145–149.

Turner, B. L., and Flack, R. D., 1980, "Experimental Measurement of Natural Convective Heat Transfer in Rectangular Enclosures With Concentrated Energy Sources," ASME JOURNAL OF HEAT TRANSFER, Vol. 102, pp. 236–241.

Ueda, T., Inoue, M., and Nagatome, S., 1981, "Critical Heat Flux and Droplet Entrainment Rate in Boiling of Falling Liquid Films," *International Journal Heat and Mass Transfer*, Vol. 24, pp. 1257–1266.

Van Fossen, G. J., Jr., 1981, "Heat Transfer Coefficients for Staggered Arrays of Short Pin Fins," ASME Paper No. 81-GT-75.

Webb, B. W., and Ramadhyani, S., 1985, "Conjugate Heat Transfer in a

Downloaded 16 Dec 2010 to 193.140.21.150. Redistribution subject to ASME license or copyright; see http://www.asme.org/terms/Terms_Use.cfm

Channel With Staggered Ribs," *International Journal of Heat and Mass Transfer*, Vol. 28, pp. 1679–1687.

Welling, J. R., and Wooldridge, C. B., 1965, "Free Convection Heat Transfer From Rectangular Vertical Fins," ASME JOURNAL OF HEAT TRANSFER, Vol. 87, pp. 439–444.

Wirtz, R. A., and Stutzman, R. J., 1982, "Experiments on Free Convection Between Vertical Plates With Symmetric Heating," ASME JOURNAL OF HEAT TRANSFER, Vol. 104, pp. 501–507.

Wirtz, R. A., and Dykshoorn, P., 1984, "Heat Transfer From Arrays of Flat Packs in a Channel Flow," *Proceedings Fourth Annual International Electronics Packaging Conference*, pp. 318–326.

Yaghoubi, M. A., and Incropera, F. P., 1980, "Analysis of Natural Convection Due to Localized Heating in a Shallow Water Layer," *Numerical Heat Transfer*, Vol. 3, pp. 315–330.

Yamamoto, H., Udagawa, Y., and Suzuki, M., 1987, "Cooling System for FACOM M-780 Large Scale Computer," *Proceedings of the International Symposium on Cooling for Electronic Equipment*, Honolulu, HI, Mar. 17–24, pp. 96–109.

Yokono, Y., Sasaki, T., and Ishizuka, M., 1987, "Small Cooling Fin Performances for LSI Packages," *Proceedings of the International Symposium on Cooling Technology for Electronic Equipment*, Honolulu, HI, Mar. 17–21, pp. 679–688.

Yokouchi, K., Kamerhara, N., and Niwa, K., 1987, "Immersion Cooling for Higher Density Packages," *Proceedings IEEE Electronic Components Conference*, Boston, MA, May 11–13, pp. 545–549.

Zhang, Z., and Patankar, S. V., 1984, "Influence of Buoyancy on the Vertical Flow and Heat Transfer in a Shrouded Fin Array," *International Journal of Heat and Mass Transfer*, Vol. 27, pp. 137–140.

Zinnes, A. E., 1970, "The Coupling of Conduction With Laminar Natural Convection From a Vertical Plate With Arbitrary Surface Heating," ASME JOURNAL OF HEAT TRANSFER, Vol. 92, pp. 528–535.

Downloaded 16 Dec 2010 to 193.140.21.150. Redistribution subject to ASME license or copyright; see http://www.asme.org/terms/Terms_Use.cfm

On the Computation of Convective Heat Transfer in Complex Turbulent Flows

B. E. Launder
Mechanical Engineering Department,
UMIST,
Manchester, United Kingdom
Fellow ASME

The paper summarizes current strategies for computing heat transfer coefficients in complex turbulent flows based on numerical solution of the averaged equations for momentum and enthalpy and corresponding equations for averaged properties of the turbulent flow field. It argues that, for accuracy and width of applicability, a fine-grid low-Reynolds-number treatment should be employed near the wall in place of wall functions, despite the attractive simplicity of the latter approach. Several examples are provided that bring out the benefit from adopting second-moment closures, in which attention is focused on the turbulent stresses and heat fluxes themselves rather than on effective viscosities and thermal diffusivities. Directions for future research are briefly discussed, an important contribution to this effort being the direct numerical simulation of the near-wall dynamic and thermal turbulence field.

1 Introduction

One of my most clearly received truths of 1987 arrived, as is so often the case, by accident. A few days before, a colleague had shown me his numerical computations of convective heat transfer in a square-sectioned U-bend where the air flow at entry was fully developed: Agreement was only moderate, computed heat transfer coefficients being on average 20 percent below the measurements. A few days later, however, he discovered that, inadvertently, he had set the effective thermal diffusivity throughout the duct to zero except within a thin band adjacent to the duct walls with a width equal to 5 percent of that of the duct. He thereupon reinstated the intended turbulent thermal diffusivity model over the core region (which accounted for 81 percent of the duct's cross-sectional area) and repeated the computations. To our initial surprise, this modification raised the mean Nusselt number by a mere 15 percent! A detailed consideration of this flow is deferred until later. What the result emphatically brings out, however, is that, even for a gaseous flow, the local heat transfer coefficient is determined to a very large extent by the variation of the effective diffusivity *within the immediate vicinity of the wall*. This observation applies even more strongly where the fluid is water or one with an even higher Prandtl number.

These remarks do not necessarily mean that turbulent transport processes in the core of the flow are of small consequence. The turbulent stresses there may significantly affect the flow field development, which, in turn, can alter the wall heat transfer rate. Nevertheless, as far as heat transfer coefficients are concerned, it is generally the immediate near-wall region that is predominant and it is accordingly this region of the flow that is the main focus of the present article.

A popular and economical approach to computing convective heat transfer rates in turbulent flows is to assume that close to the wall (but far enough from it for the direct effects of molecular transport to be small) the velocity and temperature profiles are given by the so-called universal log laws

$$U^+ = \frac{1}{\tilde{\kappa}} \ln E\, y^+ \tag{1}$$

$$\Theta^+ = \frac{1}{\tilde{\kappa}} \ln \tilde{E}\, y^+ \tag{2a}$$

where κ, $\tilde{\kappa}$, and E are supposedly universal constants with values approximately equal to 0.42, 0.46, and 9.8, and $\tilde{E}$ is a function only of the molecular Prandtl number σ. U^+, Θ^+, and y^+ are the conventional velocity, temperature, and distance rendered dimensionless by the viscosity and density and the wall shear stress and heat transfer rate; thus

$$\Theta^+ \equiv \rho c_p (\Theta_w - \Theta)(\tau_w/\rho)^{1/2}/q_w$$

It is sometimes convenient to repackage equation (2*a*) with the help of equation (1) as

$$\Theta^+ = \sigma_\theta (U^+ + \mathcal{P}) \tag{2b}$$

where $\sigma_\theta \equiv \kappa/\tilde{\kappa}$ is effectively the turbulent Prandtl number for heat transport and $\mathcal{P} \equiv \ln\,(E/\tilde{E})/\tilde{\kappa}$ is the so-called "pee-function" correlated from pipe flow data by Jayatilleke (1969) as

$$\mathcal{P} = 9.24[(\sigma/\sigma_\theta)^{3/4} - 1][1 + 0.28 \exp(-0.007\sigma/\sigma_\theta)] \tag{3}$$

In a numerical computation, rather than apply boundary conditions at the wall, one would simply match one's velocity and temperature field to equations (1) and (2) along a line parallel to the wall and far enough from it for the nodes to lie in fully turbulent fluid. Since in a fairly coarse grid duct flow computation this line might well be situated about 5 percent of the duct width from the adjacent wall, it is evident from the discussion earlier that the accuracy of the overall prediction of Nusselt number hinges crucially on whether or not equations (1) and (2) do provide a good description of the velocity and temperature profiles in the near-wall region. While there are, indeed, many flows where these equations achieve a close fit to the actual profiles, it is equally certain that there are many where they do not. Indeed, for the purpose of this contribution, it is convenient to adopt the definition that a complex flow is one that near a wall does not adequately comply with equations (1) and (2). Equation (2) is in fact less widely valid than equation (1), for while, like the velocity field, it will cease to be applicable if the near-wall turbulence departs very far from a state of local equilibrium, it also fails to apply where the thermal boundary condition varies rapidly in the stream direction or where the thermal layer is very thin (e.g., Blom, 1970; Antonia et al., 1977).

The aim of the present paper is thus to provide an account of different approaches to computing heat transfer in turbulent flows not describable by the above equations. Attention is therefore limited to turbulent flows near walls and, within that subset, is especially given to the question of modeling the semiviscous sublayer. The different modeling strategies

Contributed by the Heat Transfer Division for publication in the JOURNAL OF HEAT TRANSFER. Manuscript received by the Heat Transfer Division March 4, 1988. Keywords: Forced Convection, Natural Convection, Reviews, Turbulence.

Copyright © 1988 by ASME
Downloaded 16 Dec 2010 to 193.140.21.150. Redistribution subject to ASME license or copyright; see http://www.asme.org/terms/Terms_Use.cfm

can conveniently be grouped into those that *refine* equations (1) and (2) while retaining the broad philosophy that underlies them, and those that *discard* them in favor of a detailed modeling of the turbulent diffusivities across the near-wall sublayer; these approaches are discussed in Sections 2 and 3, respectively. In Section 4 we consider higher-order approaches to modeling turbulent heat transport; most attention is given to the fully turbulent region but brief mention is also made of efforts to extend these approaches across the near-wall sublayer.

To help one get in the right frame of mind for the review ahead, Fig. 1 presents computed results for the Nusselt number downstream of an abrupt pipe expansion contributed by a dozen European research groups for an IAHR Workshop held at the Berkeley Nuclear Laboratories of the CEGB and consolidated by Hutton and Szczepura (1987). The computed results display at least an order of magnitude variation in the level of the predicted heat transfer coefficient; somewhere, buried beneath these predictions, lie the experimental data. This is a test case that will be repeatedly considered in the article as it serves to bring out the sharply different behavior generated by different turbulence models.

Of course, providing a physical model to represent turbulent transport rates is only one part of the problem of computing turbulent flow. The other lies in the procedures adopted for discretizing and solving the resulting nonlinear partial differential equations describing the convective transport processes of interest. In what follows, almost nothing is said about numerical practices, although Professor Patankar's article in the present volume covers at least some aspects of this problem. Likewise, explicit demonstrations will not be given that the various examples cited are grid-independent. Such grid-independence tests are, for the most part, reported in the original source articles and, in all cases presented, numerical and experimental uncertainties are believed to be small enough for differences between computed

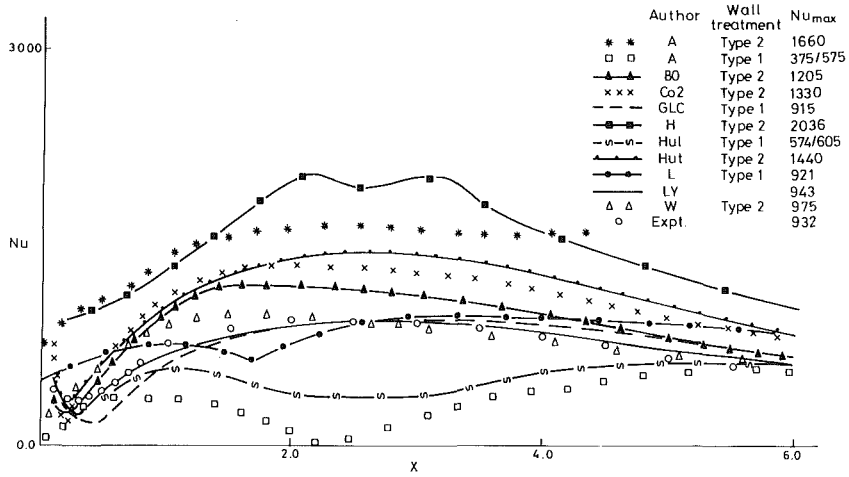

Fig. 1 Nusselt number distributions downstream of an abrupt pipe enlargement: computations submitted for IAHR Workshop, Hutton and Szczepura (1987)

Nomenclature

c_l = slope of length scale $k^{3/2}/\epsilon$ in near-wall equilibrium layer
c_p = specific heat at constant pressure
c_μ = coefficient in Prandtl-Kolmogorov viscosity formula equation (equation (5)) = 0.09
d_{ij}, $d_{i\theta}$ = net turbulent diffusion rate of u_iu_j and $u_i\theta$, respectively
E, E^* = additive constants in standard and * forms of universal velocity law, equations (1) and (9); $E = 9.8$, $E^* = 5.0$
$\tilde{E}$, $\tilde{E}^*$ = additive functions of Prandtl number in standard and * forms of universal temperature law equations (2) and (11)
F_{ij}, $F_{i\theta}$ = body force terms in u_iu_j and $u_i\theta$ equation
f_i = fluctuating body force per unit mass
g_i = gravitational acceleration vector
Gr = Grashof number
H = step height (for an abrupt pipe expansion from diameter D_1 to D_2, $H = (D_2 - D_1)/2$)
k = turbulent kinetic energy
K = dimensionless acceleration parameter $= (\nu/U_\infty^2)dU_\infty/dx$
l = length scale $= k^{3/2}/\epsilon$
l_m = mixing length
Nu = Nusselt number
$\mathrm{Nu_{DB}}$ = reference effective Nusselt number for fully developed pipe flow determined from Dittus-Boelter correlation
p = fluctuating part of pressure
P = production rate of turbulent kinetic energy by shear
$\mathcal{P}$ = function of σ characterizing relative resistance of sublayer to heat and momentum transfer (Jayatilleke, 1969), equation (3)
$\mathcal{P}^*$ = equivalent function to $\mathcal{P}$ for Θ^* profile
P_{ij} = production rate of u_iu_j by mean shear
$P_{i\theta 1}$, $P_{i\theta 2}$ = production rate of $u_i\theta$ by mean temperature and velocity gradients, respectively
q_w = heat flux from wall to fluid
Re = Reynolds number based on bulk velocity and pipe diameter (downstream value in the case of an abrupt expansion)
$\mathrm{Re_t}$ = local turbulent Reynolds number $= k^2/\nu\epsilon$
$\tilde{\mathrm{Re}}_t$ = local turbulent Reynolds number $= k^2/\nu\tilde{\epsilon}$
U, u = mean, fluctuating value of streamwise velocity
U^+ = streamwise velocity in standard wall-law form
U^* = streamwise velocity in modified wall-law form $= Uk^{1/2}/(\tau_w/\rho)$
U_i, u_i = mean and fluctuating velocity, tensor notation
$\overline{uv}$ = turbulent shear stress

Downloaded 16 Dec 2010 to 193.140.21.150. Redistribution subject to ASME license or copyright; see http://www.asme.org/terms/Terms_Use.cfm

and measured behavior mainly to arise from shortcomings in the modeling.

2 Wall Functions for Heat Transfer in Complex Flows

Equation (2) cannot be used to compute heat transfer in separated flows, for the definition of Θ^+ given above means that the Nusselt number falls to zero at separation and reattachment points. Experiments, in contrast, often show the maximum levels of heat transfer coefficient at reattachment! A first-order remedy for this problem was devised some twenty years ago by Professor D. B. Spalding's group at Imperial College, London (Wolfshtein, 1967; Spalding, 1967; Runchal, 1969). Its discovery was triggered by the recognition that transport of highly turbulent fluid with large-scale fluctuations to the surface was the primary mechanism for the augmentation of heat transfer in the vicinity of a stagnation point. In terms of modeling turbulent transport, this perception naturally led to the idea that Prandtl's (1925) mixing-length hypothesis, which in a generalized form can be written

$$\nu_t = l_m^2 \left(\left(\frac{\partial U_i}{\partial x_j} + \frac{\partial U_j}{\partial x_i} \right) \frac{\partial U_i}{\partial x_j} \right)^{1/2} \tag{4}$$

(and which, for a simply sheared constant-stress fluid near a wall, leads to equation (1)), should be replaced by the Prandtl-Kolmogorov formula

$$\nu_t = c_\mu \, k^{1/2} l \tag{5}$$

In the above, c_μ is a constant usually taken as 0.09, k is the turbulent kinetic energy, and l a turbulent length scale varying in much the same way through the flow as the mixing length l_m. Thus, essentially, the use of equation (5) replaces a velocity scale obtained via *mean* velocity gradients by one based directly on the energy of the turbulent motion itself. Wolfshtein's and Runchal's doctoral studies involved solving a transport equation for k over the flow domain. In the vicinity of the wall, however, they, like Spalding (1967), devised simplified one-dimensional models based on equation (5) to arrive at wall-law formulae appropriate to separated flows. The resultant formulations were rather cumbersome and, in practice, expressions directly analogous to equations (1) and (2) are nowadays usually adopted. They may be otained by applying equation (5) to a uniform-stress near-wall layer as follows. With the assumption that the length scale increases linearly with distance from the wall, $l = c_l y$:

$$\nu_t = \kappa^* k^{1/2} y \tag{6}$$

where $\kappa^* \equiv c_\mu c_l$ is approximately 0.22. Thus, for a uniform shear stress equal to that at the wall (and upon neglecting viscous transport)

$$\tau_w = \rho \kappa^* k^{1/2} y \frac{\partial U}{\partial y} \tag{7}$$

Now, in a fully turbulent region of constant stress, the turbulent kinetic energy is also essentially uniform so equation (7) may be integrated to give

$$U^* \equiv \frac{U k^{1/2}}{(\tau_w/\rho)} = \frac{1}{\kappa^*} \ln y + \text{function of integration} \tag{8}$$

As the wall is approached, turbulent mixing gradually gives way to direct viscous transport. If, as is often assumed, we imagine this transition from fully turbulent to viscous behavior to occur abruptly at a distance y_v from the wall, the velocity-distance relation there must simultaneously satisfy both the viscous relation

$$U = \frac{\tau_w}{\rho \nu} y$$

and equation (8), from which requirement the following may be written:

$$U^* = \frac{1}{\kappa^*} \ln E^* y^* \tag{9}$$

where $y^* \equiv y k_v^{1/2}/\nu$ and $E^* \equiv \exp(\kappa^* y_v^*)/y_v^*$.

The corresponding expression for the near-wall temperature emerges from considering a layer across which a uniform heat flux passes with the assumption that the turbulent thermal diffusivity is σ_θ^{-1} times the turbulent kinematic viscosity (a constant)

Nomenclature (cont.)

$\overline{u_i u_j}$ = Reynolds stress tensor
$\overline{u_i \theta}$ = turbulent heat flux vector
x = streamwise direction
x_i = Cartesian coordinate, tensor notation (x_1 streamwise, x_2 normal to wall)
y = Cartesian coordinate normal to (and with origin at) the wall
y^+ = distance normal to wall in standard wall coordinates
y^* = distance normal to wall in modified wall coordinates
y_v^* = thickness of viscous layer in modified wall coordinates
ϵ = dissipation rate of turbulent kinetic energy
$\tilde{\epsilon}$ = $\epsilon - 2\nu(\partial k^{1/2}/\partial x_k)^2$
ϵ_{ij} = viscous dissipation rate of $\overline{u_i u_j}$
ϵ_Θ = dissipation rate of $1/2\overline{\theta^2}$
Θ, θ = mean, fluctuating values of temperature
Θ^+, Θ^* = mean temperature in standard and modified wall coordinates
κ, κ^* = reciprocal of slope of log law velocity profile in standard and modified wall coordinates
$\tilde{\kappa}, \tilde{\kappa}^*$ = reciprocal of slope of log law temperature profile in standard and modified wall coordinates
ν, ν_t = molecular and turbulent kinematic viscosity
ρ = density
σ = molecular Prandtl number
σ_ϕ = turbulent Prandtl number for transport of ϕ (ϕ denoting Θ, k, or ϵ)
ϕ_{ij} = pressure-strain correlation
$\phi_{i\theta}$ = pressure-temperature gradient correlation
ω = turbulence "frequency," a quantity proportional to ϵ/k

Superscripts

$+$ = standard wall coordinates
$*$ = modified wall coordinates
$-$ = time or ensemble-averaged product of two or more fluctuating quantities *or* value of source/sink averaged over near-wall control volume

Subscripts

n = north face of near-wall control volume, Fig. 1
r = radial direction
t = turbulent
v = conditions at edge of viscous layer
∞ = free-stream value
2 = direction normal to wall

Downloaded 16 Dec 2010 to 193.140.21.150. Redistribution subject to ASME license or copyright; see http://www.asme.org/terms/Terms_Use.cfm

$$\frac{q_w}{\rho c_p} = \frac{\kappa^*}{\sigma_\theta} k^{1/2} y \frac{\partial}{\partial y}(\Theta_w - \Theta)$$

which, upon integration, gives

$$\Theta^* \equiv \frac{\rho c_p (\Theta_w - \Theta) k^{1/2}}{q_w} = \frac{\sigma_\theta}{\kappa^*} \ln y + \text{function of integration} \quad (10)$$

If the gradual shift from turbulent to molecular transport across the "buffer" layer is modeled as an abrupt changeover occurring at $y = y_c$, the temperature there must satisfy equation (10) and also the molecular condition relation

$$\Theta^* = \sigma y^*$$

It follows that the temperature profile for the fully turbulent region can be expressed

$$\Theta^* = \frac{\sigma_\theta}{\kappa} \ln \tilde{E}^* y^* \quad (11)$$

where $\tilde{E}^* \equiv \exp(\kappa^* y_c^* \sigma/\sigma_\theta)/y_c^*$.

Alternatively, eliminating y^* from (11) in favor of U^* (from equation (9))

$$\Theta^* = \sigma_\theta (U^* + \mathcal{P}^*) \quad (12)$$

where $\mathcal{P}^* \equiv \frac{1}{\kappa^*} \ln \tilde{E}^* E^*$.

Equations (9), (11), and (12) are directly analogous to equations (1), (2*a*), and (2*b*). In a constant stress flow they give identical results because then, with generation and dissipation rates of k in balance, $k = c_\mu^{-1/2}(\tau_w/\rho)$.

It thus follows that

$$U^* = c_\mu^{-1/4} U^+; \quad y^* = c_\mu^{-1/4} y^+; \quad \kappa^* = c_\mu^{-1/4} \kappa$$

From this we find that $y_v^* = 20.4$ and $E^* = 5.4$. Moreover, if the "*" form of the wall laws is to give the same behavior as the conventional "+" form in local equilibrium, $\tilde{E}^*/E^*$ must equal $\tilde{E}/E$ and thus

$$\mathcal{P}^* \kappa^* = \mathcal{P} \kappa \text{ or } \mathcal{P}^* = c_\mu^{-1/4} \mathcal{P}$$

where $\mathcal{P}$ is given by equation (3) above.

All the above results are obtained under the assumption of a constant-stress near-wall layer. But, as we have just seen, in this case the two formulations (i.e., U^+ or U^*, etc.) give identical behavior. The rationale behind the U^* approach is that it should give forms that extrapolate better to conditions far from equilibrium: where the shear stress varies rapidly with distance from the wall and where generation and dissipation rates of turbulence energy are not in balance. Certainly, the formulation based on turbulence energy does lead to more plausible relationships. For example, the use of U^* gives, for a fixed y^*, a wall shear stress that is directly proportional to the near-wall velocity and that simply changes sign if the velocity does, a behavior that is surely more plausible near separation than that implied by the traditional law of the wall (equation (1)). Equally, with Θ^* as the subject of the temperature equation, there is no requirement that the Nusselt number should vanish at a reattachment point, for while τ_w may be zero, $k_v^{1/2}$ will generally not be.

It remains to describe how the turbulence energy, which appears as an unknown in equations (9) and (11), is to be obtained. While it is the value of k at the edge of the viscous layer that emerges naturally from the analysis (Chieng and Launder, 1980), in practice it is more convenient and seems to be no less accurate to use the value of kinetic energy at the near-wall node in evaluating the above expressions for the nodal velocity and temperature. The nodal value of k is determined by reference to the closed transport equation governing this variable

$$\frac{Dk}{Dt} = d_k + P - \epsilon \quad (13)$$

where d_k, P, and ϵ denote, respectively, the net rate of gain of k by diffusion, the generation rate due to shear, and the viscous dissipation rate of turbulence energy.

As noted above, for a simple shear layer in local equilibrium ($P = \epsilon$) it is readily deduced that $k = c_\mu^{-1/2}(\tau_w/\rho)$. While this serves adequately as a boundary condition for k in many boundary layers, it is not appropriate for separated flows and other situations where transport effects on k are important close to the wall. In those cases, the near-wall value of turbulence energy is obtained from a numerical solution of equation (13). The required steps are particularly clear in terms of a finite-volume methodology as indicated in Fig. 2. As with the velocity field, the near-wall region is imagined to be comprised of a viscous sublayer where turbulent stresses are negligible and a fully turbulent layer where viscous transport can be ignored. But, while the turbulent shear stress is regarded as zero in the sublayer, the kinetic energy is not. Experiment suggests that, in the immediate vicinity of the surface, a linear increase in the fluctuating velocity parallel to the wall with distance occurs. This implies a parabolic variation of k; thus

$$k = k_v (y/y_v)^2 \quad (14)$$

Now, in a finite-volume approach to discretization, one seeks the mean contribution of the various terms on the right of equation (13) over the control volume in Fig. 2. In the immediate vicinity of the wall, diffusion of k occurs only by molecular gradient-driven transport so, from equation (14), there is no diffusion of k to the wall. The net diffusive flow to the control volume is simply that entering through the north face. Both the production and dissipation rates undergo spectacular variations across this region and a little care needs to be taken in evaluating appropriate mean values. We consider ϵ first. In the sublayer it may be shown (Jones and Launder, 1972) that

$$\epsilon = 2\nu \left(\frac{\partial k^{1/2}}{\partial y} \right)^2$$

So, on substituting for k from equation (14), we obtain

$$\epsilon = \frac{2\nu k_v}{y_v^2}$$

which is a constant. Over the fully turbulent region

$$\epsilon = k^{3/2}/l = \frac{k^{3/2}}{c_l y}$$

Thus, if k is taken as uniform there, we obtain the mean value of ϵ as

$$\bar{\epsilon} \equiv \frac{1}{y_n} \int_0^{y_n} \epsilon \, dy = \frac{2\nu k_v}{y_v y_n} + \frac{k^{3/2}}{c_l y_n} \ln \left(\frac{y_n}{y_v} \right) \quad (15)$$

Likewise, the assumption of a uniform turbulent shear stress equal to that at the wall for $y \geq y_v$ allows the mean turbulence energy generation to be expressed[1]

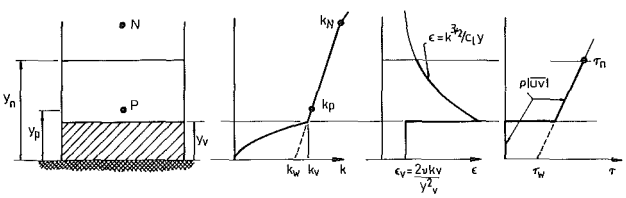

Fig. 2 Assumed distribution of variables across near-wall control volume

[1] It is still very common to find workers adopting $\tilde{P} = (\tau_w/\rho)(U_n/y_n)$ instead of the expression given in equation (16). This error, which typically gives a generation rate too large by a factor of four, arises from assuming that the turbulent shear stress equals the wall stress even in the viscous sublayer!

Downloaded 16 Dec 2010 to 193.140.21.150. Redistribution subject to ASME license or copyright; see http://www.asme.org/terms/Terms_Use.cfm

$$\bar{P} = \frac{1}{y_n}\int_{y_v}^{y_n} \frac{\tau_w}{\rho}\frac{\partial U}{\partial y}\cdot dy = \frac{\tau_w}{\rho}\frac{(U_n - U_v)}{y_n} \qquad (16)$$

We note, however, from equation (9) that

$$U = \frac{1}{\kappa^*}\frac{(\tau_w/\rho)}{k^{1/2}} l_n E^* y^*$$

and so with obvious substitution we obtain

$$\bar{P} = \frac{(\tau_w/\rho)^2}{\kappa^* y_n k^{1/2}} \ln(y_n/y_v) \qquad (17)$$

As already noted, in local equilibrium $(\tau_w/\rho) = c_\mu^{1/2} k$. Thus, since $c_\mu c_l \equiv \kappa^*$ we find that P equals $\bar{\epsilon}$ if the contribution of the viscous sublayer to the cell-averaged dissipation rate is neglected. The main uses of equations (15) and (17) are in conditions far removed from local equilibrium. Near separation or reattachment τ_w falls to zero faster than k and in such regions $\bar{P}$ will be considerably less than $\bar{\epsilon}$. Of course, the expressions for both quantities arise from assuming the energy and shear stress to be *uniform* over the fully turbulent region, so, as with the velocity profile (equation (9)), there is some inconsistency in applying equations (15) and (17) near separation. However, the sensitivity of the equations to moderate variations in k and $\overline{uv}$ is not great and, moreover, k and $\overline{uv}$ usually vary in the same sense; so these formulae are often used even in separated flows. One may alternatively assume a linear variation of energy and shear stress in evaluating the integrals of equations (15) and (16) (see Chieng and Launder, 1980), even though this leads to a very cumbersome formula for $\bar{\epsilon}$.

Nearly all applications employing wall functions of the type described here have determined the energy dissipation rate over the flow region by way of a semi-empirical transport equation for ϵ. This means that a boundary condition for this dependent variable needs to be supplied. The common approach is to presume that, at the near-wall node, the length scale will be the same as for a flow in local equilibrium, i.e., $l = c_l y$. This assumption is consistent with that used above in determining $\bar{\epsilon}$, the cell-averaged value of ϵ, and seems to be reasonably close to the truth for attached boundary layers, even close to separation (see East and Sawyer, 1980).

The strengths and weaknesses of the above approach to wall functions are well brought out by Yap's (1987) computations of heat transfer rates downstream of the 2.5:1 abrupt pipe expansion measured by Baughn et al. (1984b). Comparisons between the experimental and predicted Nusselt number profiles are provided in Figs. 3 and 4 at two Reynolds numbers. Two models of turbulence are used in the exterior flow, the standard k-ϵ eddy-viscosity model (EVM) (Jones and Launder, 1972; Launder and Spalding, 1974) and an algebraic second-moment closure (ASM) used earlier by Iacovides and Launder (1985) for computing heat transfer in bends. The mathematical details of these models are given in the appendix. Both schemes broadly capture the experimental observation of strongly augmented heat transfer coefficients over a wide region around the reattachment point (which occurs at $x/H \approx 10$). The ASM scheme clearly does better than the EVM, a topic to be considered in Section 4. Neither, however, shows the correct dependence of Reynolds number for the peak Nusselt number (here normalized by the value given by the Dittus-Boelter correlation for fully developed pipe flow, Nu_{DB}) nor the upturn in heat transfer coefficient for $x/H < 1$.

The above example serves to show that, while wall-function approaches offer a route to obtaining a better-than-qualitative indication of the distribution of Nu in complex flows, there is plenty of room for improvement. The incorrect trend with Reynolds number is of particular concern. In seeking a remedy, a number of the assumptions embedded in the derivation naturally suggest themselves for further scrutiny:

(*i*) the assumption that the dimensionless thickness of the sublayer y_v^* is a universal constant;

(*ii*) the assumption that the $\mathcal{P}$-function correlated from pipe-flow data extrapolates to recirculating-flow situations;

(*iii*) the assumption that the near-wall length scale is independent of the external flow, being fixed merely by the distance from the surface;

(*iv*) the assumption that an abrupt changeover from viscous to turbulent behavior at $y = y_v$ is adequate to cope with situations where the wall shear stress varies rapidly with distance from the wall.

Amano and his colleagues (Amano, 1985; Amano et al., 1983) have modified assumption (*iv*) by interposing a buffer layer between the viscous and fully turbulent regions where the turbulent shear stress varies as y^3.[2] The modification led to somewhat improved behavior for the cases examined. In the writer's view, a more important weakness than the two-layer viscous/turbulent interface is the assumption of a universal value of y_v^*. Even in boundary layers it is known that rapid variations in shear stress normal to the wall caused by pressure gradients, buoyancy, or mass transfer through the surface can appreciably modify the additive constant in the log law, which is directly related to y_v^*. If y_v^* is to vary, however, the question arises as to which parameter or parameters it should depend on. In two-dimensional boundary layers the dimensionless gradient of shear stress normal to the surface has often been used as a correlating parameter. That is not useful, however, for flows with no dominant direction because this magnitude and even the sign of this parameter depend on the orientation of axes. Johnson and Launder (1982) proposed that it was the

[2] Other refinements have been introduced by Rubesin and colleagues at NASA Ames (Viegas and Rubesin, 1983; Viegas et al., 1985) in applying wall-function treatments to complex shock-boundary-layer interactions.

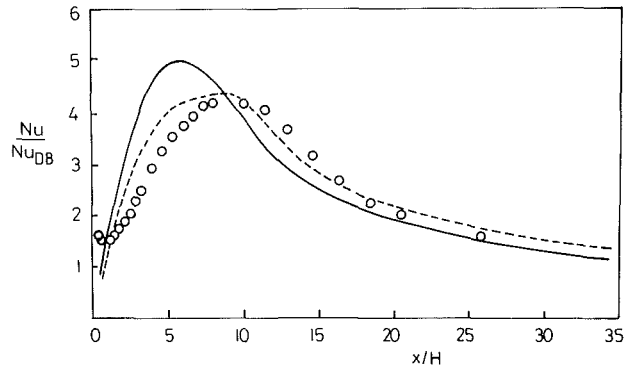

Fig. 3 Wall-function computation of Nusselt number in 2.5:1 abrupt pipe expansion: Re = 4 × 10⁴; ——— k-ϵ EVM; — — — k-ϵ ASM in main flow, Yap (1987); symbols: experiment, Baughn et al. (1984b)

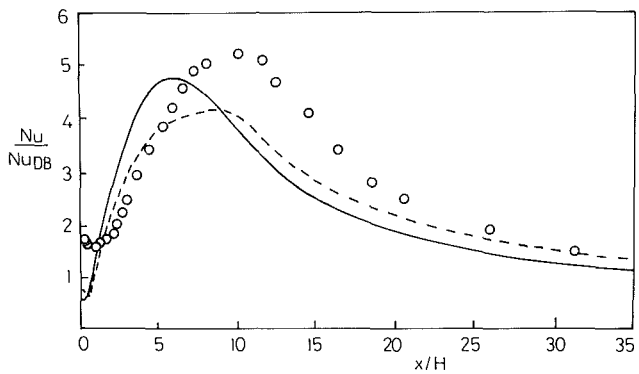

Fig. 4 Wall-function computation of Nusselt number in 2.5:1 abrupt pipe expansion: Re = 1.7 × 10⁴; key as in Fig. 3

Downloaded 16 Dec 2010 to 193.140.21.150. Redistribution subject to ASME license or copyright; see http://www.asme.org/terms/Terms_Use.cfm

inflow of turbulence energy to the sublayer region from the exterior by diffusion that principally caused a reduction in y_v^* in the vicinity of reattachment. They thus made y_v^* a linear function of the ratio of the rate of diffusive inflow of turbulent energy to the rate of turbulence energy dissipation in the sublayer, which after manipulation led to

$$y_v^* = 20/(1 + 3.1\beta^*) \tag{18}$$

where

$$\beta^* \equiv \frac{y_v}{k_v} \frac{\partial k}{\partial y}\bigg|_{y_{v_+}}$$

and the plus subscript on y_v indicates that the kinetic energy gradient is evaluated on the turbulent side of the viscous/turbulent interface in Fig. 2.

While the physical mechanism underlying this proposal seems plausible, it is now recognized that the wall does not exert as dominant an influence on the length scale in near-wall separated flows as equation (6) suggests. It has also become clear that the standard dissipation equation in such conditions gives erroneously high levels of length scale (e.g., Rodi and Scheuerer, 1983). With that being the case, any attempt at further refinement of wall functions before the question of an appropriate form of the ϵ equation in near-wall separated regions is established would be futile. For this reason, the writer's group has, since 1984, abandoned wall-function treatments (Launder, 1984) in favor of a detailed modeling of the near-wall sublayer. Perhaps, in due course, wall functions will have their day again; some awfully big questions need resolving first, however.

3 Low-Reynolds-Number Modeling

As the wall is approached, the local turbulent Reynolds number $\mathrm{Re}_t \equiv k^2/\nu\epsilon$ diminishes and, for values below about 150, direct viscous effects become important. Thus, a strategy that discards wall functions and, instead, prescribes a route for determining the various turbulence parameters all the way to the surface itself is often termed a *low-Reynolds-number model.*

The simplest and still widely used low-Reynolds-number model is Van Driest's (1956) extension of Prandtl's mixing-length hypothesis. This scheme and variants of it were extensively employed in the late 1960s and early 1970s to compute heat and mass transfer rates in two-dimensional boundary layers (e.g., Cebeci et al., 1972; Kays and Moffat, 1975; Jones and Launder, 1969; Launder and Priddin, 1973). This approach is still successfully applied in computing complex but unseparated flows in ducts, particularly where secondary flow is generated. When ducted fluid enters a bend, a secondary velocity field is created in the plane of the duct with the maximum secondary velocity occurring very close to the pipe wall, typically at the edge of the viscous sublayer. If a coarse-grid wall-function approach is employed to compute such flows, this peak is not properly resolved and the amount of secondary flow predicted will be significantly too low.[3] While some workers adopt the mixing-length model throughout the duct, others employ it only over a near-wall sublayer (i.e., over a comparable region to what would have been covered by way of wall functions), adopting a more elaborate transport-equation model over the rest of the duct. An example of the latter approach, shown in Figs. 5 and 6, is the computation of the three-dimensional thermal field and Nusselt number in a 180 deg circular-sectioned U-bend reported in Iacovides and Launder (1985). The velocity and temperature fields were

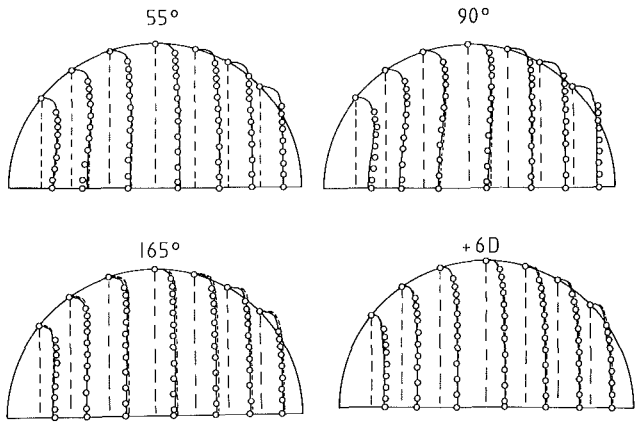

Fig. 5 Development of normalized temperature profiles around 180-deg bend from Iacovides and Launder (1985) (inside of bend on left of semi-circle): o o o experiments, Baughn et al. (1987); ——ASM; — — — EVM

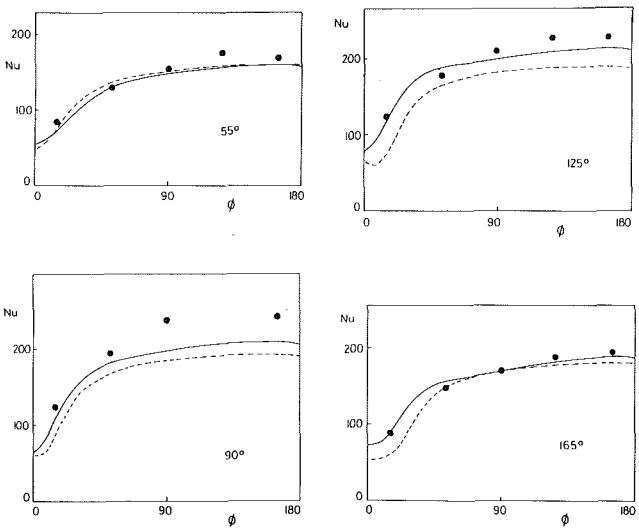

Fig. 6 Local Nusselt number in 180-deg U-bend: circumferential variation at four stations; key as in Fig. 5

computed on a 27 (radial) × 24 (circumferential) grid covering half the cross section[4] with 160 streamwise planes. The mixing-length hypothesis was employed for the first nine radial nodes nearest the pipe wall, covering 4 percent of the duct diameter. Over the core of the flow standard k–ϵ EVM or ASM models were employed (Appendix), as in the axisymmetric abrupt pipe expansion considered above. The computations correctly capture both the increase in the overall level of Nu as the flow develops around the bend and the strong circumferential variation between the inside and the outside of the bend, brought about partly by the induced secondary flow (that dumps slow-moving heated fluid at the inside of the bend) and partly by the different effects of streamline curvature on the mixing processes near the inside and outside of the bend. The difference between the ASM and EVM results will be discussed in Section 4.2

Recently computations have been made by the same workers of the flow around a square-sectioned bend using precisely the same physical model as in the foregoing example (Iacovides and Launder, 1988). In Fig. 7 the computed circumferential Nusselt number profile at a station 130 deg around the bend is compared with the experimental data and an earlier computation by Johnson (1984) who employed wall functions in conjunction with the standard k–ϵ EVM. This was

[3] Interesting, clear-cut differences can be seen, for example, among the computations submitted to the 1980-81 Stanford Conference (Kline et al., 1981) for the case of flow around a 90 deg bend.

[4] The flow is symmetric about the diametral line lying in the plane of the bend.

Downloaded 16 Dec 2010 to 193.140.21.150. Redistribution subject to ASME license or copyright; see http://www.asme.org/terms/Terms_Use.cfm

the case referred to in the Introduction where computations had also been made with the thermal diffusivity inadvertently set to zero everywhere except within the near-wall sublayer, where the mixing length had been employed. The relatively small difference between the latter results and those that included the appropriate thermal diffusivity arising from the EVM or ASM treatments in the core confirms the predominant effect of the sublayer region in determining the level of heat transfer coefficient. The present mixing-length model certainly gives a closer agreement with the experimental data than do the wall functions. The agreement is, however, not complete, the heat transfer coefficients being markedly too low in the corners of the duct. Our suspicion is that this is due to the neglect of turbulent transport that is implicit with the mixing-length hypothesis: In the corners, mean velocity gradients are relatively low because the fluid is constrained by two adjacent walls at right angles. Turbulence energy generation rates there are thus lower. However, the strong secondary flow is likely to transport substantial turbulence energy into the corner region, thus raising the level of heat transfer coefficient above that currently predicted.

The U-bend computations discussed above have adopted a uniform turbulent Prandtl number of 0.9 across the sublayer region. Kays and Moffat (1975) have reported that for air, at least, the temperature profiles across this low-Reynolds-number sublayer are better correlated by a turbulent Prandtl number varying with y^+. The following is the simpler of two correlations they recommend:

$$\sigma_\theta = 1.43 - 0.17y^{+1/4} \tag{19}$$

Recently Malhotra and Kang (1984) extensively reviewed the data for heat transfer in a circular pipe for liquids ($1 \lesssim \sigma \lesssim 10^4$). Using Van Driest's mixing-length profile (modified to reduce levels of l_m in the core of the pipe) to determine the velocity field, for each value of σ they adjusted the (uniform) value of σ_θ until agreement with the experimental Nu was obtained. In this way a dependence of σ_θ on σ was obtained. Their results indicated that the mean value of σ_θ diminished monotonically as the molecular Prandtl number was raised, from 0.9 for $\sigma = 1$ to about 0.15 for $\sigma \simeq 10^4$. From a physical point of view it is difficult to imagine that in the fully turbulent regime the transport of heat is affected by molecular transport properties (at least for values of σ of order unity or greater). This dependence on σ runs counter to that suggested by equation (19), though it is supported consistently across the various data sets they considered. What it seems to suggest is that, while equation (19) may describe the increase in σ_θ as one moves toward the wall in the buffer region ($10 \lesssim y+ \lesssim 30$), at points closer to the surface there must be a rapid reduction in σ_θ.

When fluids other than air have been considered, Cebeci's (1973) proposal for a damped thermal mixing length also has some attraction. The resultant expression for the turbulent thermal diffusivity is

$$\lambda_t = \tilde{\kappa}\, \kappa\, y^2(1 - \exp - y^+/A^+)(1 - \exp - y^+/B^+) \tag{20}$$

where, following Na and Habib (1973)

$$B^+ = \sum_{i=1}^{5} c_i(\log_{10}\, \sigma)^{i-1}$$

with $(c_1, c_2, c_3, c_4, c_5) = (34.96, 28.79, 33.95, 6.33, -1.186)$. Barba (1984) (see also Barba et al., 1984) has adopted this formulation together with Van Driest's model for momentum transport as the sublayer model for the computation of heat transfer rates in spirally fluted tubes.

As discussed in Section 2, mixing-length models cannot be used for computing heat transfer in separated flows and, as has been suggested above, even in unseparated duct flows their failure to capture turbulence energy transport may be the main cause of underprediction of Nu in corner regions. A one-equation sublayer model is, naturally enough, the first step in raising the level of the turbulence model. It is also a particularly interesting level at which to draw comparisons with wall-function computations, for the approach described in Section

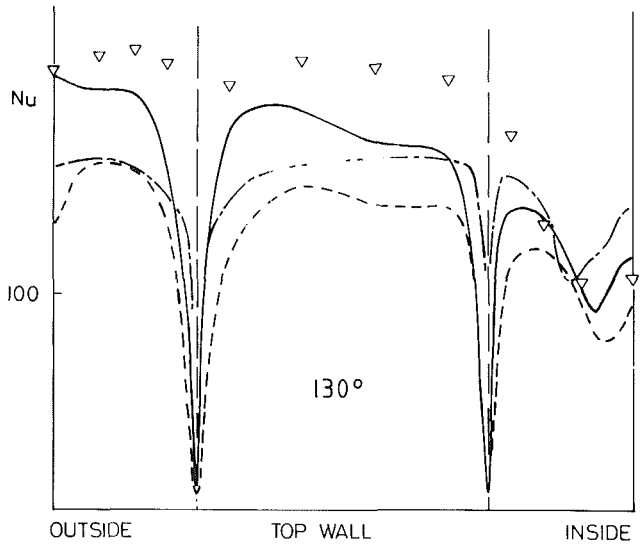

Fig. 7 Local Nusselt number for flow around 180-deg square-sectioned bend: circumferential variation at 130-deg station: ▽ experiments (Johnson, 1984); ——— ASM/mlh computations; — — — ASM/mlh computations with thermal diffusivity set to zero in ASM region (Iacovides and Launder, 1988); ——— EVM/wall-function computations (Johnson, 1984)

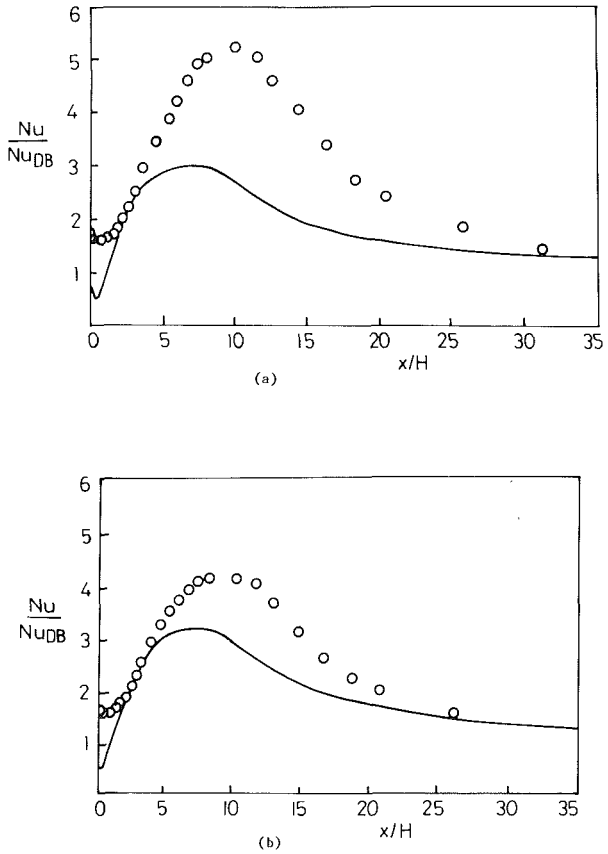

Fig. 8 Nusselt number in 2.5:1 abrupt expansion: ——— EVM low-Re one-equation model; symbols: experiment (Baughn et al., 1984b); (a) Re = 1.7 x 10⁴; (b) Re = 4 x 10⁴

Downloaded 16 Dec 2010 to 193.140.21.150. Redistribution subject to ASME license or copyright; see http://www.asme.org/terms/Terms_Use.cfm

2 amounts to a very simplified mathematical treatment of a one-equation model. Yap (1987) converted Wolfshtein's (1969) one-equation model to a form that facilitated its interfacing with the high-Reynolds-number form of the k–ϵ EVM or ASM:

$$\begin{aligned} \nu_t &= c_\mu k^{1/2} l_\mu; \quad \epsilon = k^{3/2}/l_\epsilon \\ l_\mu &= c_l y(1-\exp - A_\mu \tilde{\mathrm{Re}}_t) \\ l_\epsilon &= c_l y(1-\exp - A_\epsilon \tilde{\mathrm{Re}}_t) \\ \sigma_\theta &= 0.90 \end{aligned} \tag{21}$$

where $c_\mu = 0.09$; $c_l = 2.4$; $A_\mu = 0.0055$; $A_\epsilon = 0.0855$; and $\tilde{\mathrm{Re}}_t = k^2/\nu\tilde{\epsilon}$ where $\tilde{\epsilon} \equiv \epsilon - 2\nu(\partial k^{1/2}/\partial y)^2$. The turbulence energy k is obtained from the transport equation

$$\frac{Dk}{Dt} = \frac{\partial}{\partial x_j}\left((\nu+\nu_t)\frac{\partial k}{\partial x_j}\right) + \nu_t \frac{\partial U_i}{\partial x_j}\left(\frac{\partial U_i}{\partial x_j} + \frac{\partial U_j}{\partial x_i}\right) - \epsilon \tag{22}$$

Now, for air flow through pipes (where the near-wall layer is essentially one of constant stress) this model gives virtually the same behavior as do wall functions. For the flow downstream of the 2.5:1 abrupt pipe expansion, however, results illustrated in Fig. 8 show that the inclusion of the low-Reynolds-number one-equation model leads to a marked deterioration in the predicted Nusselt number compared with that obtained with wall functions, cf. Figs. 3 and 4.

The shortcomings of the one-equation approach suggested that the sublayer damping coefficients (especially A_μ) could not be treated as constants and that, quite probably, the presumed length-scale distribution was far from the truth, i.e., even close to the wall the length-scale profile in a separated flow was affected by events far from the wall. The implication was that the near-wall length scale was not the same as in local-equilibrium flows and that therefore one needed to solve both the k and ϵ equations through the sublayer.

In the early 1970s Jones and Launder (1972, 1973) developed a low-Reynolds-number k–ϵ EVM specifically with a view to predicting laminarization by acceleration and other phenomena related to a thickening of the viscous sublayer due to a rapid decrease in shear stress with distance from the wall. Various applications of the model have been reported in predicting condensation (Jones and Renz, 1974), the effects of polymer additives (Durst and Rastogi, 1977), and transonic and supersonic flows (Viegas and Horstmann, 1978). In terms of heat transfer, however, perhaps the most convincing computations are those recently reported by Cotton and Jackson (1987a, 1987b) of turbulent mixed convection in vertical tubes. Figure 9 provides a comparison of their computed fully developed flow behavior with data from various sources spanning a wide range of buoyant conditions; the model adopted was a minor variant of the original Jones–Launder formulation with re-optimized coefficients (Launder and Sharma, 1974). The abscissa is a buoyancy parameter that effectively provides a dimensionless measure of the decrease in shear stress due to buoyancy that occurs across the viscous sublayer in the case of upflow. For this situation the impairment of heat transfer coefficient results from the progressive thickening of the sublayer region, which the decrease in shear stress across the sublayer provokes. Eventually, when the heat input is raised sufficiently, the near-wall peak in velocity produces appreciable velocity gradients across the fully turbulent region, increasing the turbulence energy level and thus raising the Nusselt number again. This acrobatic behavior of Nu is faithfully reproduced by the computations. The behavior in downflow, while less spectacular, is equally well captured. Other impressive buoyant flow predictions with a model of the same type have been reported by To and Humphrey (1986) for natural convection on a vertical plate.

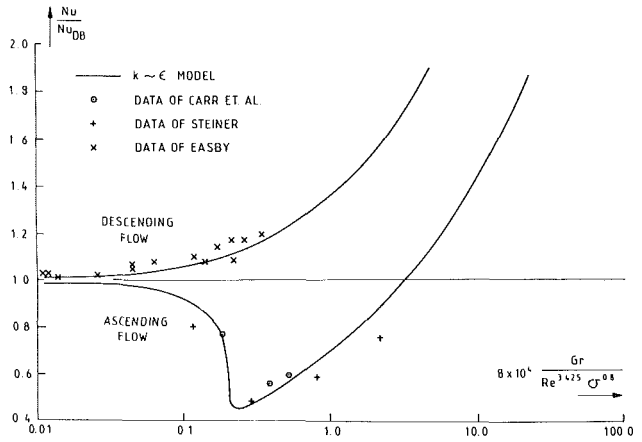

Fig. 9 Effects of buoyancy on levels of Nusselt number in vertical pipe flow (Cotton and Jackson, 1987b): symbols: experiments; line: k–ϵ computations

These applications were all for situations where the shear stress either decreased rapidly or increased only slowly across the low-Reynolds-number sublayer. An early attempt by Chieng and Launder (1980) to apply a low-Re k–ϵ model to the abrupt pipe expansion led to the tentative conclusion that heat-transfer coefficients in the vicinity of the reattachment point were predicted some *seven times* too high! There were several numerical uncertainties in these computations, but Yap (1987) re-examined the position for a somewhat different expansion ratio using a finer grid, a higher-order discretization scheme, and a much tighter convergence criterion, and obtained effectively the same results. The cause of the problem is the excessive level of near-wall length scales that are generated in separated flows—or, to be more precise, in situations where large diffusive transport rates of energy occur toward the wall. Such diffusive transport always arises near reattachment points but it may also occur in a horizontal free surface jet (where the free surface acts in many respects like a wall) and, as we shall shortly see, in buoyantly driven flow in a tall enclosure. In an attempt to cure this problem, Yap (1987) added a further source term S_ϵ to the right-hand side of the $\tilde{\epsilon}$ equation

$$S_\epsilon \equiv 0.83\left(\frac{\tilde{\epsilon}^2}{k}\right)\left(\frac{k^{3/2}}{c_l y\tilde{\epsilon}} - 1\right)\left(\frac{k^{3/2}}{c_l y\tilde{\epsilon}}\right)^2 \tag{23}$$

where y is the distance from the wall. The term has no effect in a flow in local equilibrium because then, near the wall, $k^{3/2}/\tilde{\epsilon} = c_l y$ and the term vanishes. In nonequilibrium flow the term acts to reduce the departure of the turbulent length scale from its local equilibrium value. Yap (1987) found that inclusion of this source term not only reduced $\mathrm{Nu}_{\max}$ to levels comparable with the measurements but also improved the Reynolds-number dependence. An example of his results will be presented in Section 4. Before that we consider the effect of this effective source on the fully developed buoyant flow between vertical walls, one heated and the other cooled. Betts and Dafa'Alla (1986) have reported that, for this case, the Launder–Sharma version of the k–ϵ model (while performing better than the other k–ϵ variants tested) gives appreciably too low peak velocities but too high heat transfer rates; see Table 1. Subsequent computations by Ince and Launder (1988) have confirmed this result but have also shown that inclusion of the above source term, equation (23), greatly improves the level of agreement (see Table 1 and Fig. 10). Their computations of the local Nusselt number in a 30:1 narrow cavity are compared with measured values in Fig. 11. Agreement between the two is excellent except near the start (top) of the cold wall. The reason for the discrepancy seems to be that, in practice, a small heat loss through the insulated top wall reduces the

Downloaded 16 Dec 2010 to 193.140.21.150. Redistribution subject to ASME license or copyright; see http://www.asme.org/terms/Terms_Use.cfm

Table 1

Basis	Nu	Maximum vertical velocity, cm/s
Experiment (midheight value in 30:1 cavity)	4.9	11.40
Betts and Dafa'Alla (1986)	6.53	8.96
Ince and Launder (1988) (with equation (23))	4.74	12.10

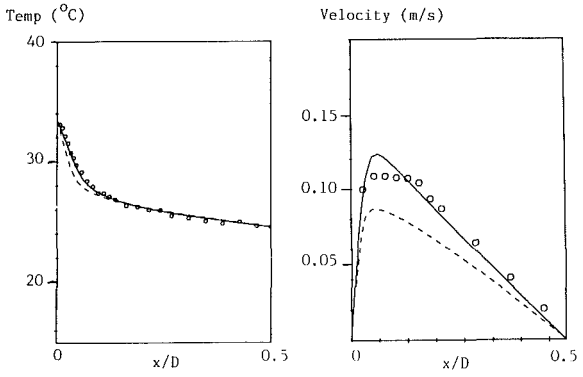

Fig. 10 Comparison of velocity and temperature profiles in infinite buoyant cavity (Ince and Launder, 1988): ——— k-ϵ EVM including equation (23); — — — standard Launder-Sharma model; o o o experiment (Ince, 1984)

strength of the stable stratification of fluid moving horizontally at the top of the cavity and, in consequence, turbulent mixing is not damped as completely as in the computation (which assumed adiabatic endwalls).

An interesting if unorthodox near-wall treatment for separated flows downstream of abrupt expansions and backward-facing steps has been developed by Gooray et al. (1982, 1983, 1985). They applied a wall-function approach to the separated flow region immediately downstream of the expansion and a k-ϵ low-Reynolds-number model downstream of the reattachment point. Generally satisfactory predictions of Nusselt number were reported.[5] Their low-Reynolds-number ϵ equation differed in only minor respects from that given in the appendix and it contained no term similar to that of equation (23) to limit the growth of ϵ near the wall. The inference would seem to be that in some way the fixed near-wall length scales in the separated-flow region were preventing the appearance of excessive length scales in the region immediately downstream of the reattachment point.

Although most workers adopting low-Reynolds-number two-equation models have worked within the k-ϵ framework, there is no necessity so to do. Wilcox and Rubesin (1980) developed a model in which, in place of ϵ, the second dependent variable was taken as ω^2, where formally $\omega = \epsilon/kc_\mu$. While the generation and principal dissipation terms in their ω^2 equation are just direct transforms of those in the standard ϵ equation, it also contains a further term proportional to $(\epsilon/k)^3(\partial l/\partial x_j)^2$.[6] Another low-Reynolds-number EVM has been developed by Kawamura and his co-workers (Kawamura, 1979; Tanaka et al., 1982) based on the solution of transport equations for k and kl. The model has been successfully applied to two problems of laminarization, the earlier paper considering gaseous flow in tubes subject to severe heating, which in turn both reduces the Reynolds number and causes a rapid acceleration, and the later one the effects of (gradual) reduc-

[5]Their computations for the abrupt pipe expansion gave an exponent n (in the relation $\mathrm{Nu} = c\,\mathrm{Re}^n$) of 0.75, however, compared with a value of about 0.67 indicated by the most recent experimental data.

[6]A similar proposal has been made by Ilegbusi and Spalding (1985), though working within the framework of wall functions.

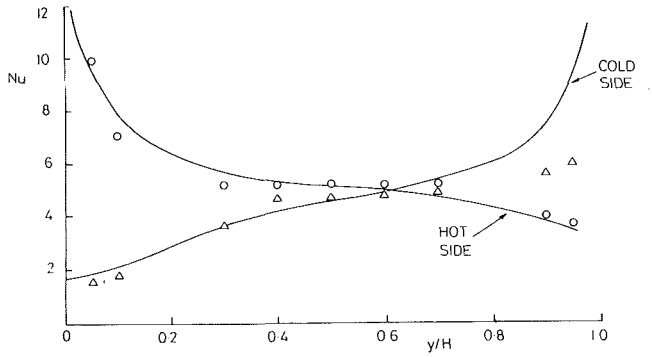

Fig. 11 Nusselt number in 30:1 cavity (Ince and Launder, 1988): ——— computations k-ϵ EVM; ▽ o experiments (Ince, 1984)

tions in cross-sectional area on the Nusselt number in ducted flows.

Besides the source and sink terms that are directly comparable with those in the dissipation equation, the kl equation devised by Kawamura (1979) contains sink terms whose magnitude (like that of equation (23)) depend on the ratio of the length scale $k^{3/2}/\epsilon$ to the distance from the wall. Convenient though this ratio may be for trimming turbulence levels near the wall to bring accord with experimental observation, the explicit inclusion of wall distance greatly limits the possibility of extending such models to more complex flows; for example, in flow over finned walls or spirally fluted tubes with deeply crenellated surfaces it is difficult to see that any of the possible choices for "distance to the wall" will bear a simple relationship to turbulence structure. It would obviously be preferable if the desired effect could be brought about by terms involving length scale *gradients* rather than wall distances (such as in the terms proposed by Wilcox and Rubesin (1980) and Ilegbusi and Spalding (1985) above). At present Ince (personal communication) is exploring the replacement of equation (23) by a term proportional to $(\epsilon/k^{1/2})(\partial k/\partial x_j)(\partial l/\partial x_j)$. Near a reattachment point the energy and length scale gradients normal to the wall are both positive and the term acts to raise ϵ and reduce k and l. The term brings satisfactory agreement to the flow field of the free surface jet but it still awaits application to the more searching test cases of heat transfer in separated flows.

4 Higher-Order Approaches to Modeling Heat Transfer

4.1 General Considerations. Although the concept of a locally determined, isotropic, effective turbulent diffusivity is too useful to be relegated to the closet for the foreseeable future, as one seeks greater reliability and width of applicability, it is nevertheless this fundamental basis of the models discussed so far that most research workers agree should be replaced. There are plenty of signposts in the experimental data to show that heat transfer in turbulent flow is not driven by an isotropic diffusivity. Inferred values of diffusivities in asymmetric heat or mass transfer in pipes indicate circumferential values several times larger than radial (e.g., Quarmby and Quirk, 1972); measurements of turbulent heat transfer in pipes and boundary layers (e.g., Bremhorst and Bullock, 1973) have shown that turbulent heat fluxes in the flow direction are two or three times larger than normal to the rigid wall even though the streamwise temperature gradient is negligible compared with that normal to the surface. Finally (though this is by no means an exhaustive list), in buoyancy-dominated natural convection between horizontal parallel planes (the lower one being the hotter), there is a uniform vertical heat flux between the plates; yet, away from the immediate vicinity of the planes there is often an imperceptible

Downloaded 16 Dec 2010 to 193.140.21.150. Redistribution subject to ASME license or copyright; see http://www.asme.org/terms/Terms_Use.cfm

variation of temperature with height (e.g., Deardorff and Willis, 1970).

None of the above features can be accommodated with an isotropic thermal diffusivity. However, two of them can be, at least in part, by adopting what is known as the *generalized* gradient diffusion hypothesis (GGDH)

$$\overline{u_i\theta} = -c_\theta \frac{\overline{u_k u_i}\, k}{\epsilon} \frac{\partial \Theta}{\partial x_k} \tag{24}$$

apparently first introduced by Daly and Harlow (1970). Equation (24) implies, for example, that the ratio of the circumferential to radial diffusivities in asymmetrically heated pipe flow is

$$\frac{\lambda_\theta}{\lambda_r} = \frac{\overline{u_\theta^2}}{\overline{u_r^2}} \tag{25}$$

a formulation successfully applied by Chieng and Launder (1979) and Baughn et al. (1984a, 1988) to account for several hitherto paradoxical results. It has also been shown by Bergeles et al. (1978) to lead to markedly superior predictions of the rate of dilution of coolant downstream of an obliquely inclined cooling hole (on a gas turbine blade, for example) to those obtained assuming an isotropic diffusivity.

Equation (24) also indicates that a streamwise heat flux in pipe flow can be produced by radial temperature gradients; thus, if $\partial\Theta/\partial x$ is small compared with $\partial\Theta/\partial r$

$$\overline{u_x\theta} = \overline{u_r\theta}\ \overline{u_x u_r}/\overline{u_r^2} \tag{26}$$

Near a wall $-\overline{u_x u_r} \approx \overline{u_r^2}$, so equation (26) implies that the magnitudes of the radial and streamwise heat-flux components are about the same. While this relative magnitude of $\overline{u_x\theta}$ is less than half the measured value, it is at least a considerable improvement on that given by anisotropic diffusivity: essentially zero.

Yet, while equation (24), with c_θ set to a value of about 0.3, *is* a significant advance, its utility depends on how accurately the component values of the Reynolds stress tensor are known. For example, an isotropic eddy-viscosity model for $\overline{u_i u_j}$ gives equal turbulence intensities in all directions, which would imply from equation (25) that λ_θ and λ_r were also equal. Now, the routes adopted for obtaining more realistic values of the Reynolds stresses usually start from the exact transport equation for $\overline{u_i u_j}$, which may be obtained by taking a velocity-weighted moment of the Navier–Stokes equation and averaging. For a fluid with negligible density fluctuations except in the body force term F_{ij}, the result may be written

$$\frac{D\overline{u_i u_j}}{Dt} = \underbrace{-\left\{\overline{u_i u_k}\frac{\partial U_j}{\partial x_k} + \overline{u_j u_k}\frac{\partial U_i}{\partial x_k}\right\}}_{P_{ij}} + \underbrace{\{\overline{f_i u_j} + \overline{f_j u_i}\}}_{F_{ij}}$$

$$+ \underbrace{\overline{\frac{p}{\rho}\left(\frac{\partial u_i}{\partial x_j} + \frac{\partial u_j}{\partial x_i}\right)}}_{\phi_{ij}} - \underbrace{2\nu\,\overline{\frac{\partial u_i}{\partial x_k}\frac{\partial u_j}{\partial x_k}}}_{\epsilon_{ij}} \tag{27}$$

$$\underbrace{-\frac{\partial}{\partial x_k}\left[\overline{u_i u_j u_k} + \frac{\overline{p u_i}}{\rho}\delta_{jk} + \frac{\overline{p u_j}}{\rho}\delta_{ik} - \nu\frac{\partial \overline{u_i u_j}}{\partial x_k}\right]}_{d_{ij}}$$

The analogous equation for the turbulent heat flux vector $\overline{u_i\theta}$ may be obtained by multiplying the Navier–Stokes equation by the fluctuating temperature and adding it to the (thermal) energy equation multiplied by u_i. Upon averaging and rearranging we obtain

$$\frac{D\overline{u_i\theta}}{Dt} = \underbrace{-\left\{\overline{u_i u_k}\frac{\partial \Theta}{\partial x_k} + \overline{\theta u_k}\frac{\partial U_i}{\partial x_k}\right\}}_{P_{i\theta}} + \underbrace{\overline{f_i\theta}}_{F_i\theta}$$

$$+ \underbrace{\overline{\frac{p}{\rho}\frac{\partial \theta}{\partial x_i}}}_{\phi_{i\theta}} - \underbrace{\nu\left[\overline{\frac{\partial \theta}{\partial x_k}\left(\frac{\partial u_i}{\partial x_k} + \frac{\partial u_k}{\partial x_i}\right)} + \sigma^{-1}\,\overline{\frac{\partial u_i}{\partial x_k}\frac{\partial \theta}{\partial x_k}}\right]}_{\epsilon_{i\theta}} \tag{28}$$

$$\underbrace{-\frac{\partial}{\partial x_k}\left[\overline{u_i\theta u_k} + \frac{\overline{p\theta}}{\rho}\delta_{ik} - \nu\left(\overline{\theta\frac{\partial u_i}{\partial x_k}} + \overline{\theta\frac{\partial u_k}{\partial x_i}} + \sigma^{-1}\,\overline{u_i\frac{\partial \theta}{\partial x_k}}\right)\right]}_{d_{i\theta}}$$

Many of the terms on the right of equations (27) and (28) are not directly determinable and must be modeled. It is beyond the scope of the present article to give a comprehensive review of alternative approaches to closing equations (27) and (28).[7] Nevertheless, a few comments are in order. Firstly, the generation terms P_{ij}, F_{ij}, $P_{i\theta}$, and $F_{i\theta}$ contain only mean-field quantities and second-moment products; they thus do not require further approximation. This is probably the greatest strength of second-moment closure, for it directly indicates the way that force fields or subtleties in the strain or thermal fields may modify the generation of the various second-moment products. Indeed, without bothering about the details of how to approximate the unknown terms in equations (24) and (25), one might directly invoke the following proposition:

$$\underline{\text{W}}\text{ealth} \propto \underline{\text{E}}\text{arnings} \times \underline{\text{T}}\text{ime}$$

sometimes called the WET hypothesis (Launder, 1987). As an economic statement it is a gross oversimplification, yet there is more than a grain of truth in it. Applied to turbulent fluxes the WET idea leads to

Value of second moment	$\propto$	Generation rate of second moment	$\times$	Turbulent time scale

So, for the heat flux, with the turbulent time scale taken as k/ϵ:

$$\overline{u_i\theta} = -c_\theta \frac{k}{\epsilon}\left(\overline{u_i u_k}\frac{\partial \Theta}{\partial x_k} + \overline{u_k\theta}\frac{\partial U_i}{\partial x_k} + \overline{f_i\theta}\right) \tag{29}$$

We notice that the first term on the right of this equation is just the GGDH approximation for $\overline{u_i\theta}$, equation (24). Indeed, for asymmetrically heated pipe flow in the absence of buoyancy effects, equation (29) gives the same connection between λ_r and λ_θ as equation (24), i.e., equation (25). In other cases it is clearly superior to the GGDH formulation; for example, the inclusion of the second term on the right leads to essentially the correct ratio of $\overline{u_x\theta}/\overline{u_r\theta}$, both in pipe flow and in a free jet, while in buoyancy-driven flow (for which, in a perfect gas, $f_i = -g_i\,\theta/\Theta$) ones sees that a vertical heat flux can be driven by the temperature variance $\overline{\theta^2}$ in the absence of mean temperature or velocity gradients.

One must take a little care in applying the WET hypothesis

[7] Surveys are provided in the books by Bradshaw (1978) and Launder et al. (1984); Lumley's (1978) extensive article develops several important ideas, while current research efforts are discussed in the more recent of the papers cited in the present section.

Downloaded 16 Dec 2010 to 193.140.21.150. Redistribution subject to ASME license or copyright; see http://www.asme.org/terms/Terms_Use.cfm

to the Reynolds stresses, for while in isotropic turbulence $\overline{u_i\theta}$ is zero, the turbulent stresses are equal to 2/3 $\delta_{ij}k$. This suggests that our formalism should be applied to describe *departures* from the isotropic state. Thus, we would conclude

$$(\overline{u_iu_j} - 2/3\ \delta_{ij}k) = -c_s \frac{k}{\epsilon}(P_{ij} + F_{ij} - 1/3\ \delta_{ij}\ (P_{kk} + F_{kk})) \tag{30}$$

In a simple shear flow, $U_1(x_2)$, unaffected by external force fields, the turbulent shear stress $\overline{u_1u_2}$ is thus given by

$$\overline{u_1u_2} = -c_s \frac{k\overline{u_2^2}}{\epsilon} \partial U_1/\partial x_2 \tag{31}$$

From proposals of Gibson and Launder (1978) one may infer the value 0.26 for c_s. Equation (30) has been quite extensively used in the computation of free shear flows, though it is usually justified in terms of specific closure approximations in equation (27) (e.g., Launder et al., 1975) coupled with the representation of the transport of $\overline{u_iu_j}$ in terms of turbulence energy transport (Rodi, 1976). On its own, however, it is not useful as a basis for predicting wall heat transfer rates because it leads to much too large values of $\overline{u_2^2}$, the mean fluctuation levels normal to the wall. To tackle this problem requires going back to equation (27). In a simple shear there is negligible generation of $\overline{u_2^2}$ (because the mean velocity U_2 is so small), yet this component nevertheless contains a significant fraction of the fluctuating kinetic energy: In a free shear flow $\overline{u_2^2}$ is typically about 0.5 k. Such a level is due to the action of the pressure-strain term ϕ_{ij} in deflecting kinetic energy from the x_1 (streamwise) direction, where it is produced, to x_2. However, the presence of a rigid plane surface impedes this transfer process: Effectively pressure fluctuations are reflected from the surface interfering with the energy flow to the component normal to the wall. A "wall reflection" agency thus needs to be introduced in modeling ϕ_{ij}, primarily to reduce the level of $\overline{u_2^2}$ as the wall is approached. Specific proposals have been detailed in Launder et al. (1975) and Gibson and Launder (1978). This damping of $\overline{u_2^2}$ in the vicinity of the wall is in fact the main reason that, in the k-ϵ EVM approach, a Reynolds-number damping term f_μ must be introduced. This may be seen from Fig. 12, in which the variation of $\overline{u_2^2}/k$ across the near-wall region is shown. Now, with the k-ϵ EVM

$$\overline{u_1u_2} = -c_\mu f_\mu \frac{k^2}{\epsilon} \frac{\partial U_1}{\partial x_2} \tag{32}$$

Comparing equations (31) and (32) indicates that over the region of their mutual validity

$$\frac{\overline{u_2^2}}{k} = \frac{c_\mu f_\mu}{c_s} = 0.34 f_\mu$$

The distribution of $0.34f_\mu$ determined by Patel et al. (1985) (from measurements of all the other terms in equation (32)) and direct measurements and computer simulations of $\overline{u_2^2}/k$ (Launder, 1986) are shown in Fig. 12. There is a good deal of uncertainty attaching to both estimates, but what seems to be suggested by the results appearing in Fig. 12 is that the two quantities vary in essentially the same way across the region considered. If one thus accepts that the damping of the turbulent shear stress is predominantly due to the reduction in $\overline{u_2^2}$, some doubt is thrown on the universal practice of correlating near-wall damping coefficients in terms of x_2^+ or Re_t since, even in pipe flow, the variation of $\overline{u_2^2}$ near the wall does not, for different bulk Reynolds numbers, appear to scale particularly well on either parameter.

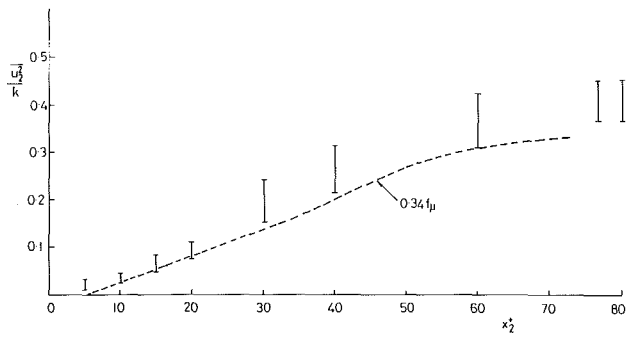

Fig. 12 Variation of $\overline{u_2^2}/k$ and f_μ across the near-wall region: — — — 0.34 f_μ (Patel et al., 1985); II estimate of range of $\overline{u_2^2}/k$ from data (Launder, 1986)

4.2 Applications of Second-Moment Closures. The first efforts in computing turbulent heat transport processes by solving closed forms of equations (27) and (28) were made by meteorological fluid dynamicists, their subject being the earth's atmospheric boundary layer. Here we note contributions by Monin (1965), Donaldson (1971), Mellor and Yamada (1974), Wyngaard (1975), André et al. (1976), and Zeman and Lumley (1979) among many others. In these studies the main focus has been on regions of the boundary layer above the immediate vicinity of the ground, for example the diurnal growth pattern of the turbulent mixed layer due to solar radiation (Zeman and Lumley, 1979).

Among the first applications of full second-moment closure to engineering heat transfer problems are those reported by Launder and Samaraweera (1979) to two-dimensional flows and, with the same model, Baughn et al. (1979) to the three-dimensional thermal field in pipe flow. The latter included a solution of the equation for heat conduction in the pipe wall simultaneously with those for the mean and turbulent field within the flow in order to take proper account of circumferential conduction in the pipe wall. However, both studies retained the very simple near-wall logarithmic laws, equations (1) and (2).

Although, adopting tensor notation, the transport equations for the components of Reynolds stress and heat flux are expressible as single equations (the exact forms of which are equations (27) and (28)), it must be remembered that in three-dimensional flows there are six independent components of the former and three for the latter. If one adds to this an equation for ϵ to give a turbulent time or length scale (and possibly one for ϵ_θ, the dissipation rate of $1/2\overline{\theta^2}$, to provide an independent thermal turbulence time scale), one sees that a very considerable computing task is involved. For this reason, heat transport studies in complex flows have usually adopted very simple approximations of the transport processes in equations (27) and (28) that have allowed the second-moment *differential* equations to be simplified to a system of *algebraic* equations (Rodi, 1976; Gibson and Launder, 1976). In these approaches transport effects on the stresses and heat fluxes are expressed via the transport of turbulent kinetic energy k and the mean-square temperature variance $\overline{\theta^2}$. Thus, as many as nine transport equations are replaced by two, a truncation that may typically reduce overall computing time by a factor of two. Unfortunately, recent studies (Fu et al., 1988) have shown that this simplification greatly reduces the width of applicability of the basic model in free flows; it is, however, less of a problem in flows near walls because then transport effects are generally small compared with local source and sink terms in the $\overline{u_iu_j}$ and $\overline{u_i\theta}$ equations. A commonly adopted form for such *algebraic* second-moment (ASM) closures is given in the appendix.

In elliptic or three-dimensional flows the algebraic stress and heat flux equations are usually solved on a grid staggered relative to the mean velocity, a stability-enhancing feature that has been rediscovered several times since its first introduction in the context of atmospheric flows in the early 1970s. In two-dimensional parabolic flows it is possible to simplify the

Downloaded 16 Dec 2010 to 193.140.21.150. Redistribution subject to ASME license or copyright; see http://www.asme.org/terms/Terms_Use.cfm

algebraic stress and heat-flux equations to expressions for the effective viscosity and turbulent Prandtl number, both of which are dependent upon the relative generation and dissipation rates of turbulence energy and, in buoyancy-affected flows, on a local Richardson number (Rodi, 1976; Gibson and Launder, 1976; Ljuboja and Rodi, 1981). This is the approach adopted by De Lemos and Sesonske (1985) to compute mixed convection in a mercury pipe flow. Although in this study the usual turbulent wall function, equation (1), was used for the near-wall boundary condition on velocity, the *molecular* thermal diffusivity at this near-wall location was still much larger than the turbulent value; consequently, a purely laminar temperature–distance relation was assumed.

Quite frequently, for the heat fluxes, workers have adopted the simpler GGDH formula, equation (24), in place of the full ASM truncation, equation (A15). This practice was followed in the 180-deg-bend computations shown earlier in Fig. 6. One notices from that figure that the ASM treatment achieves somewhat closer agreement with the experimental data than the eddy-viscosity model. Due to the sensitivity of the ASM closure to the different effects of streamline curvature near the inside and outside of the bend (augmentation of turbulence energy on the outside and damping on the inside), a greater circumferential variation in Nu is produced, a behavior that better accords with the experiment. On the outside of the bend, however, even the ASM scheme does not show quite the augmentation of Nu found in the experiment (Baughn et al., 1987).

A much greater difference between EVM and ASM computations is found in the case of the abrupt pipe expansion for which Yap's (1987) computations are presented in Fig. 13. Here a low-Reynolds-number k–ϵ EVM is adopted across the sublayer, while either an EVM or ASM is employed beyond (in the latter case again using equation (24) for $\overline{u_i\theta}$). In both cases the extra source term, equation (23), is included in the ϵ equation to diminish the otherwise excessive near-wall length scales that would result. From the comparison of Fig. 13 it is clear that the ASM computations not only capture the general shape of the Nusselt-number profile a good deal more successfully[8]; they also exhibit a Reynolds-number dependence much closer to that of the experiments. There are a number of factors contributing to the large difference between ASM and EVM results in this example. For example, the peak Nusselt number occurs farther downstream, partly because the ASM scheme gives a longer reattachment length and partly because the use of equation (24) gives relatively larger radial diffusivities near the wall in the vicinity of the reattachment point, i.e., at a fixed (small) distance from the pipe wall $\overline{u_2^2}/k$ is larger near the stagnation point than elsewhere. As a result, $\mathrm{Nu}_{\max}$ for the ASM closure essentially occurs at the stagnation point, whereas for the k–ϵ EVM it is located nearly two step heights upstream. Experiments do in fact indicate the virtual coincidence of the position of maximum Nu and the stagnation point in these abrupt-expansion geometries (e.g., Vogel and Eaton, 1985), giving further support to the ASM results.

Of course, if in a recirculating flow there are such clear-cut improvements in predicting heat transfer from using an ASM rather than an EVM formulation in the fully turbulent part of the flow, it would seem highly desirable to introduce this refinement also in the semiturbulent near-wall sublayer where, as noted earlier, the distribution of the effective transport coefficient exerts such a dominant influence on Nu. In fact To and Humphrey (1986) have done this (see also Humphrey and To, 1986) in their studies of natural convection on vertical plates and in cavities. With but minor adjustments they simply applied the ASM stress and heat flux formulae, in conjunction

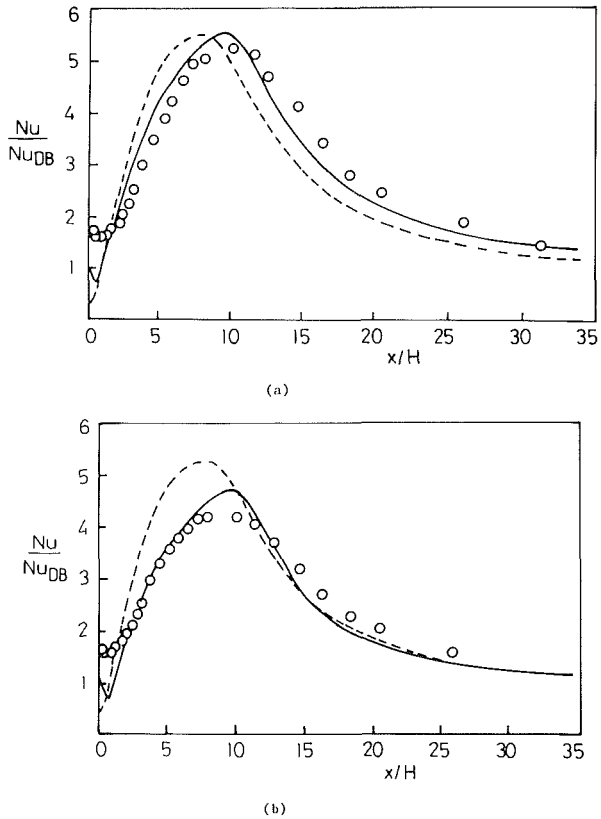

Fig. 13 Computations of Nusselt number in 2.5:1 near-wall abrupt pipe expansion; near-wall ϵ source and low-Re k–ϵ EVM across near-wall sublayer (Yap, 1987): ——— ASM; — — — — EVM in core; (*a*) $\mathrm{Re} = 1.7 \times 10^4$; (*b*) $\mathrm{Re} = 4 \times 4^4$

with the low-Reynolds-number kinetic energy and ϵ equations, all the way to the wall. This brought definite improvements to their predictions of the natural convection boundary layer though, to be fair, their k–ϵ EVM results were also quite impressive.

In the Humphrey–To applications considered above the flow streamlines were essentially parallel to the surface. It is likely that in more general circumstances—to include, for example, separating and reattaching flows and a wide range of Prandtl numbers—a more extensive reappraisal of the model will be needed to make it entirely suitable for handling the low-Reynolds-number sublayer. This view is based on the crucial role that the variation of $\overline{u_2^2}$ in the immediate vicinity of the wall plays in determining heat transfer and wall-friction coefficients (cf. the discussion above concerning Fig. 12). In fact, continuity requires that, as the wall is approached, u_2 should fall to zero faster than the velocity fluctuations parallel to the surface; that is, as $x_2 \to 0$, wall turbulence approaches a two-component limit which requires *inter alia* that ϕ_{22} should vanish. Now, the models for ϕ_{ij} commonly used for computing wall shear flows do not comply with this limiting behavior (see, for example, equation (A7)). This weakness is arguably of little consequence if the second-moment closure is sewn on to a simpler model at the edge of the low-Reynolds-number sublayer, but it assumes considerable importance if the computations are to extend to the wall itself. Lumley (1978) has shown how, in principle, it is possible to build the desired limiting behavior of $\overline{u_2^2}$ into the formulation of invariant models for ϕ_{ij}. Recently, versions rigorously satisfying these limits and other kinematic constraints have been devised by Shih and Lumley (1985) and Fu et al. (1987).

Work is now in progress to incorporate these proposals into a second-moment model for the near-wall sublayer. Although definitive results are not yet available for near-wall flows, it is

[8] This feature is also present when wall functions are employed, see Figs. 3 and 4.

Downloaded 16 Dec 2010 to 193.140.21.150. Redistribution subject to ASME license or copyright; see http://www.asme.org/terms/Terms_Use.cfm

at least encouraging that the version of Fu et al. (1987) has brought marked improvement to the prediction of several free shear flows. A rather simpler formulation (Launder and Shima, 1988) has aimed at retaining broadly the Gibson–Launder (1978) dynamic model given in the appendix but extending its applicability to the near-wall sublayer through the introduction of two invariant measures of anisotropy of the stress field. In this way the vanishing of ϕ_{ij} at the wall can be ensured. Figure 14 presents streamwise mean and turbulent velocity and shear stress profiles for two cases of strongly accelerated flows measured by Simpson and Wallace (1975). At the lower acceleration level $K = 2.2 \times 10^{-6}$ the velocity distribution departs strongly from the (all-too-non-) universal log laws but remains turbulent, while for $K = 3.2 \times 10^{-6}$ complete collapse to laminar flow ensues. The computations entailed solution of transport equations for the four nonzero Reynolds-stress components and ϵ in addition to the mean velocity. The computed behavior is in virtually complete agreement with the measurements and also with the recent direct numerical simulations of Spalart (1986), whose results suggested that the critical sustained value of K beyond which laminarization would ensue was about 2.8×10^{-6}. No heat transfer computations have yet been made with the model nor have any impinging flow cases been examined; so the width of applicability of the proposals is, as yet, by no means established. Nevertheless, the clear indications that second-moment closure offers a more broadly valid approach for handling complex turbulent transport phenomena near boundaries than eddy-diffusivity models should ensure an intensive research effort in this area over the next several years.

An important development destined to give great impetus to and doubtless to reshape many current ideas in turbulence modeling is that computers are now sufficiently powerful that it is just possible to make full computer simulations of inhomogeneous wall turbulence. Landmark computations of channel and boundary-layer flows have been reported by workers at the NASA Ames Research Center (Moser and Moin, 1984; Spalart and Leonard, 1985). While some lament that these simulations are at rather low Reynolds number, in the writer's view a comprehensive study of channel turbulence at a number of discrete values of Re below 10^4 would provide invaluable information partly *because* the low-Reynolds-number region is *not* one of constant stress. These direct simulations provide not only the best available indicators of the variation of $u_i u_j$ and ϵ in the vicinity of the wall but of higher-order correlations like $u_i u_j u_k$ and the "unmeasurable" pressure-strain correlation. Although generating the initial data tapes of these results was an enormous undertaking, they should provide the basis for further research for the next decade. Moreover, while computing the three-dimensional time-dependent velocity field was a formidable undertaking, it is a relatively modest task to obtain solutions for a passive scalar field (such as temperature) imposed on the velocity field for different thermal boundary conditions and Prandtl numbers. Major steps in this direction have already been taken by Kim and Moin (1988) and Rogers et al. (1986).

5 Concluding Remarks

From the point of view of making conclusive statements about the computation of heat transfer in complex flows, it's a pity that the JOURNAL OF HEAT TRANSFER has already reached

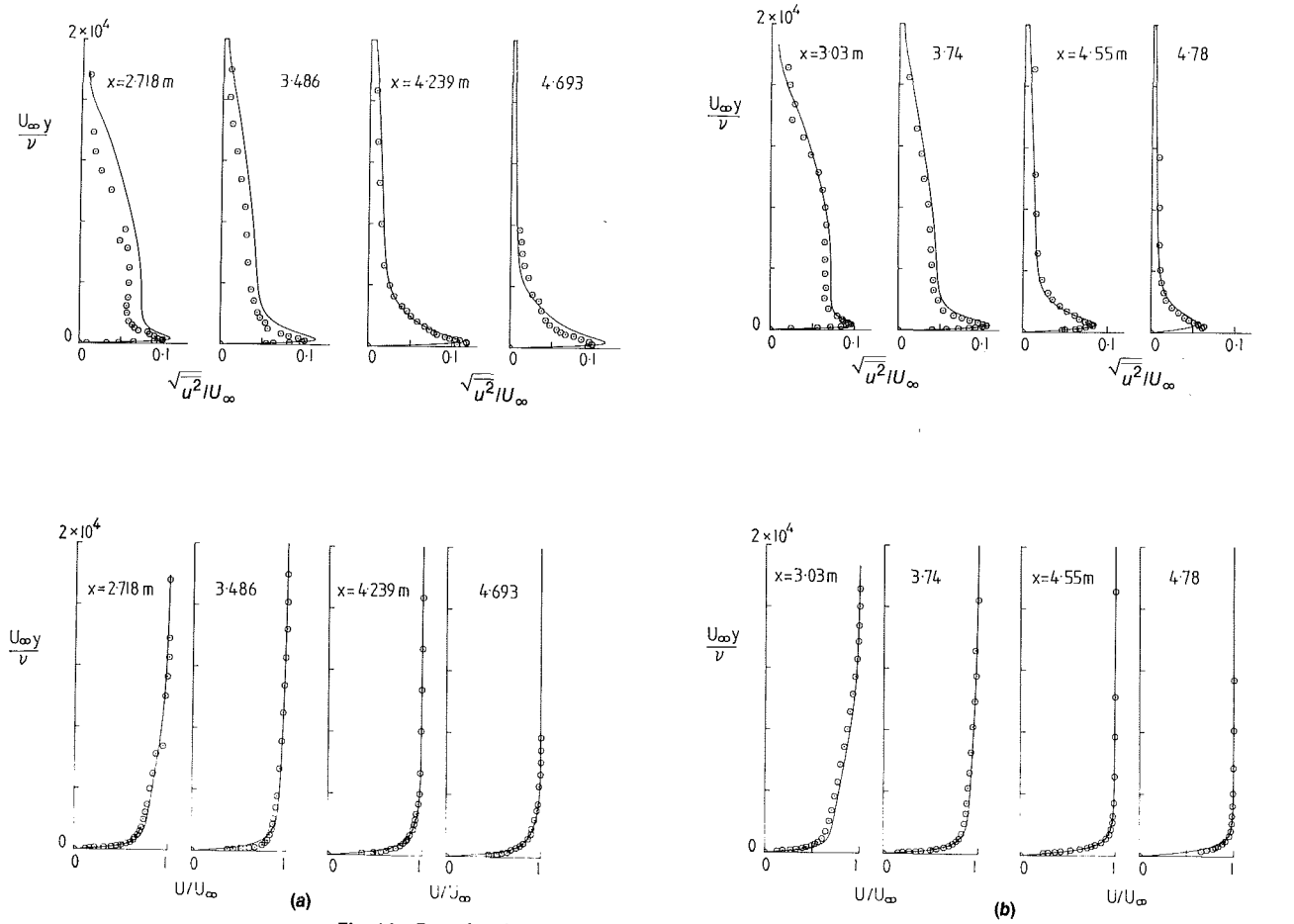

Fig. 14 Boundary layer development in strongly accelerated boundary layers: symbols: Simpson and Wallace (1975); lines: Launder and Shima (1988); (a) $K = 2.2 \times 10^{-6}$; (b) $K = 3.2 \times 10^{-6}$

Downloaded 16 Dec 2010 to 193.140.21.150. Redistribution subject to ASME license or copyright; see http://www.asme.org/terms/Terms_Use.cfm

its half-centenary. Were it now a mere 45-year-old stripling, there seems, to this writer at any rate, the likelihood that the present flurry of turbulence modeling activity would have been translated to a substantial body of concrete results in time for the fiftieth anniversary celebrations. The current resurgence of research in modeling seems to be driven by three factors linked to the rapid growth in computing power:

(*i*) Software and hardware are now available that allow large-scale computations of industrially important heat-convection problems without numerical errors muffling the impact of the turbulence model;

(*ii*) increased computing power has made it feasible to adopt low-Reynolds-number turbulence models in complex flows and these provide greater scope for representing the turbulent transport processes in the sublayer than do wall functions;

(*iii*) direct computer simulations of the dynamic and thermal structure of wall turbulence are now being generated, notably by the Stanford-NASA Ames turbulence-simulation group, which provide details of the statistics of the fluctuating field far beyond what any laboratory experiment could ever hope to achieve.

Thus, for the next few years we can foresee much activity as workers try to accommodate the implications of these direct computer simulations into turbulence models, of the type discussed in this article, for use with the *averaged* equations.

However, even if, by 1993 or thereabouts, the computation of convective heat transfer in single-phase turbulent flows has reached a more settled state, there will remain no shortage of problems to contend with; for example, in the handling of multiphase flow processes, non-Newtonian fluids or chemically reacting flows. Therein lie problems that will surely occupy the JOURNAL OF HEAT TRANSFER for the *next* half century.

Acknowledgments

The work reported in this article owes much to present and former PhD students in the CFD group at UMIST, particularly Dr. Hector Iacovides, Dr. Christopher Yap, Dr. Nadir Ince, Mr. Song Fu, and Mr. Dimitri Tselepidakis. It is a pleasure to acknowledge their contributions and those of their sponsors: the Science and Engineering Research Council, Rolls-Royce plc, and the Central Electricity Generating Board. Thanks are also due to Dr. M. A. Cotton, Mr. A. G. Hutton, Dr. R. T. Szczepura, and Professor N. Shima for making figures available to me for inclusion in the article. Mrs. L. J. Ball prepared the typescript for publication against a very tight deadline working from a continually changing and incomplete manuscript.

Finally, my thanks go to the editors of the JOURNAL OF HEAT TRANSFER for inviting me to contribute to this anniversary volume. Preparing the article has been something of a nostalgic experience for me for the JOURNAL also published my first technical contribution (originally a term paper written for Warren Rohsenow). I still have the letter of acceptance from one Thomas F. Irvine, Jr., dated April 18, 1963—half-way back to the birth of this great journal.

References

Amano, R., 1985, "A Numerical Study of Laminar and Turbulent Heat Transfer in a Periodically Corrugated Wall Channel," ASME JOURNAL OF HEAT TRANSFER, Vol. 107, pp. 564–569.

Amano, R., Jensen, M. K., and Goel, P., 1983, "A Numerical and Experimental Investigation of Turbulent Heat Transport Downstream From an Abrupt Pipe Expansion," ASME JOURNAL OF HEAT TRANSFER, Vol. 105, pp. 862–869.

André, J.-C., de Moor, G., Lacarrere, P., and Du Vachat, R., 1976, "Turbulence Approximation for Inhomogeneous Flows: Part I. The Clipping Approximation," *J. Atmos. Sci.*, Vol. 33, pp. 476–481.

Antonia, R. A., Danh, H. Q., and Prabhu, A., 1977, "Response of a Turbulent Boundary Layer to a Step Change in Surface Heat Flux," *J. Fluid Mech.*, Vol. 80, pp. 153–177.

Barba, A., 1984, "The Prediction of Convective Heat Transfer in Spirally Fluted Tubes," Ph.D. Thesis, Faculty of Technology, University of Manchester, United Kingdom.

Barba, A., Gosman, A. D., and Launder, B. E., 1984, "The Prediction of Heat-Transfer Performance in Spirally Fluted Tubes: The Turbulent Flow Regime," Inst. Chem. Engrs. Symp. Series 86, First UK National Heat Transfer Conference, University of Leeds, Paper 11.1, pp. 695–706.

Baughn, J. W., Dingus, C. W., Hoffman, M. A., and Launder, B. E., 1988, "Turbulent Heat Transport in a Circular Duct With a Narrow Strip Heat Flux Boundary Condition," submitted to ASME JOURNAL OF HEAT TRANSFER.

Baughn, J. W., Hoffman, M. A., Launder, B. E., and Samaraweera, D. S. A., 1978, "Three-Dimensional Turbulent Heat Transport in Pipe Flow: Experiment and Model Validation," ASME Paper No. 78-WA-HT-15.

Baughn, J. W., Hoffman, M. A., Launder, B. E., and Takahashi, R. K., 1984a, "Turbulent Heat Transport in Circular Ducts With Circumferentially Varying Heat Flux," ASME JOURNAL OF HEAT TRANSFER, Vol. 106, pp. 64–70.

Baughn, J. W., Hoffman, M. A., Takahashi, R., and Launder, B. E., 1984b, "Local Heat Transfer Downstream of an Abrupt Pipe Expansion in a Circular Channel With Constant Wall Heat Flux," ASME JOURNAL OF HEAT TRANSFER, Vol. 106, pp. 789–796.

Baughn, J. W., Iacovides, H., Jackson, D. C., and Launder, B. E., 1987, "Local Heat Transfer Measurements in Turbulent Flow Around a 180-deg Pipe Bend," ASME JOURNAL OF HEAT TRANSFER, Vol. 109, pp. 43–48.

Bergeles, G., Gosman, A. D., and Launder, B. E., 1978, "The Turbulent Jet in a Cross Stream at Low Injection Rates: A 3-Dimensional Numerical Treatment," *Numerical Heat Transfer*, Vol. 1, pp. 217–242.

Betts, P. L., and Dafa'Alla, A. A., 1986, "Turbulent Buoyant Air Flow in a Tall Rectangular Cavity," in: *Significant Questions in Buoyancy Affected Enclosure or Cavity Flows*, ASME HTD-Vol. 60, pp. 83–92.

Blom, J., 1970, "An Experimental Study of the Turbulent Prandtl Number in a Developing Temperature Boundary Layer," Ph.D. Thesis, The Technological University, Eindhoven, The Netherlands.

Bradshaw, P., ed., 1978, *Turbulence*, 2nd ed., Springer, Heidelberg.

Bremhorst, K., and Bullock, K. J., 1973, "Spectral Measurements of Turbulent Heat and Momentum Transfer in Fully Developed Pipe Flows," *Int. J. Heat Mass Transfer*, Vol. 16, pp. 2141–2154.

Byrne, J., and Ejiogu, E., 1971, "Combined Free and Forced Convection Heat Transfer in a Vertical Pipe," IMechE Symp. on Heat and Mass Transfer by Combined Forced and Natural Convection, London, Paper No. C118/71.

Cebeci, T., 1973, "A Model for Eddy Conductivity and Turbulent Prandtl Number," ASME JOURNAL OF HEAT TRANSFER, Vol. 95, pp. 227–234.

Cebeci, T., Smith, A. M. O., and Mosinskis, G., 1970, "Solution of the Incompressible Turbulent Boundary Layer Equations With Heat Transfer," ASME JOURNAL OF HEAT TRANSFER, Vol. 92, p. 499.

Chieng, C. C., and Launder, B. E., 1979, "On the Calculation of Turbulent Transport in Flow Through an Asymmetrically Heated Pipe," *Numerical Heat Transfer*, Vol. 2, pp. 359–371.

Chieng, C. C., and Launder, B. E., 1980, "On the Calculation of Turbulent Heat Transport Downstream From an Abrupt Pipe Expansion," *Numerical Heat Transfer*, Vol. 3, pp. 189–207.

Cotton, M. C., and Jackson, J. D., 1987a, "Calculation of Turbulent Mixed Convection Using a Low-Reynolds-Number k-ϵ Model," Sixth Turbulent Shear Flows Symp., Toulouse, Sept., Paper No. 9-6.

Cotton, M. C., and Jackson, J. D., 1987b, "Comparison Between Theory and Experiment for Turbulent Flow of Air in a Vertical Tube With Interaction Between Free and Forced Convection," in: *Mixed Convection Heat Transfer 1987*, V. Prasad, I. Catton, and P. Cheng, eds., ASME HTD-Vol. 84, pp. 43–50.

Daly, B. J., and Harlow, F. H., 1970, "Transport Equations in Turbulence," *Physics of Fluids*, Vol. 13, pp. 2634–2649.

Deardorff, J. W., and Willis, G. E., 1967, "Investigation of Turbulent Thermal Convection Between Horizontal Plates," *J. Fluid Mech.*, Vol. 28, pp. 675–704.

De Lemos, M. J. S., and Sesonske, A., 1985, "Turbulence Modeling in Combined Convection in Mercury Pipe Flow," *Int. J. Heat Mass Transfer*, Vol. 28, pp. 1067–1088.

Donaldson, C. du P., 1971, "Calculation of Turbulent Shear Flows for Atmospheric and Vortex Motions," *AIAA J.*, Vol. 10, pp. 4–12.

Durst, F., and Rastogi, A. K., 1977, "Calculations of Turbulent Boundary Layer Flows With Drag Reducing Polymer Additives," *Physics of Fluids*, Vol. 20, pp. 1975–1985.

East, L. F., and Sawyer, W. G., 1980, "An Investigation of the Structure of Equilibrium Boundary Layers," *Turbulent Boundary Layers—Experiments, Theory and Modelling*, AGARD CP 271, Paper No. 6.

Fu, S., Huang, P. G., Launder, B. E., and Leschziner, M. A., 1988, "A Comparison of Algebraic and Differential Second-Moment Closures for Axisymmetric Turbulent Shear Flows With and Without Swirl," ASME *Journal Fluids Engineering*, Vol. 110, pp. 216–221.

Fu, S., Launder, B. E., and Tselepidakis, D. P., 1987, "Accommodating the Effects of High Strain Rates in Modelling the Pressure-Strain Correlation," Mech. Eng. Dept. Report TFD/87/5, UMIST, Manchester, United Kingdom.

Gibson, M. M., and Launder, B. E., 1976, "On the Calculation of Horizontal, Turbulent Free Shear Flows Under Gravitational Influence," ASME JOURNAL OF HEAT TRANSFER, Vol. 98, pp. 379–386.

Gibson, M. M., and Launder, B. E., 1978, "Ground Effects on Pressure

Downloaded 16 Dec 2010 to 193.140.21.150. Redistribution subject to ASME license or copyright; see http://www.asme.org/terms/Terms_Use.cfm

Fluctuations in the Atmospheric Boundary Layer," *J. Fluid Mech.*, Vol. 86, pp. 491–511.

Gooray, A. M., Watkins, C. B., and Aung, W., 1981, "Numerical Calculations of Turbulent Heat Transfer Downstream of a Rearward Facing Step," *Proc. 2nd Int. Conf. Numerical Methods in Laminar and Turbulent Flows*, C. Taylor and B. A. Schefler, eds., Pineridge Press, Swansea, United Kingdom.

Gooray, A. M., Watkins, C. B., and Aung, W., 1983, "Improvements to the k–ϵ Model for Calculation of Turbulent Separated Forced Convection," *Proc. 4th Turbulent Shear Flows Symp.*, Univ. of Karlsruhe, Federal Republic of Germany.

Gooray, A. M., Watkins, C. B., and Aung, W., 1985, "Turbulent Heat Transfer Computations for Rearward-Facing Steps and Sudden Pipe Expansions," ASME JOURNAL OF HEAT TRANSFER, Vol. 107, pp. 70–76.

Hossain, M. S., and Rodi, W., 1982, "A Turbulence Model for Buoyant Flows and Its Application to Vertical Buoyant Jets," in: *Turbulent Buoyant Jets and Plumes*, W. Rodi, ed., Pergamon, New York.

Humphrey, J. A. C., and To, W. M., 1986, "Numerical Simulation of Buoyant, Turbulent Flow—II. Free and Mixed Convection in a Heated Cavity," *Int. J. Heat Mass Transfer*, Vol. 29, pp. 593–610.

Hutton, A. G., and Szczepura, R. T., 1987, "Turbulent Flow and Heat Transfer in a Sudden Pipe Expansion: A Comparison of Current Models of Turbulence," CEGB Report TPRD/B/0926/R87.

Iacovides, H., and Launder, B. E., 1985, "ASM Predictions of Turbulent Momentum and Heat Transfer in Coils and U-Bends," *Proc. 4th Int. Conf. on Numerical Methods in Laminar and Turbulent Flow*, C. Taylor et al., eds., Pineridge Press, Swansea, Vol. 2, pp. 1023–1045.

Iacovides, H., and Launder, B. E., 1988, "Prediction of Turbulent Flow and Heat Transfer in a 180° Bend of Square Cross-Section," *Proc. Second United Kingdom National Heat Transfer Conf.*, IMechE, London, pp. 735–743.

Ilegbusi, J. O., and Spalding, D. B., 1985, "An Improved Version of the k–W Model of Turbulence," ASME JOURNAL OF HEAT TRANSFER, Vol. 107, pp. 65–69.

Ince, N. Z., and Launder, B. E., 1988, "Computation of Turbulent Natural Convection in Closed Cavities," *Proc. Second United Kingdom National Heat Transfer Conf.*, IMechE, London, pp. 1389–1400.

Jayatilleke, C. L. V., 1969, "The Influence of Prandtl Number and Surface Roughness on the Resistance of the Laminar Sublayer to Momentum and Heat Transfer," *Prog. Heat Mass Transfer*, Vol. 1, p. 193.

Johnson, R. W., 1984, "Turbulent Convecting Flow in a Square Duct With a 180° Bend; An Experimental and Numerical Study," Ph.D. Thesis, Faculty of Technology, University of Manchester, United Kingdom.

Johnson, R. W., and Launder, B. E., 1982, "Discussion of 'On the Calculation of Turbulent Heat Transport Downstream from an Abrupt Pipe Expansion'," *Num. Heat Transfer*, Vol. 5, pp. 493–496.

Jones, W. P., and Launder, B. E., 1972, "The Prediction of Laminarization With a Two-Equation Model of Turbulence," *Int. J. Heat Mass Transfer*, Vol. 15, pp. 301–314.

Jones, W. P., and Launder, B. E., 1973, "The Calculation of Low-Reynolds-Number Phenomena With a Two-Equation Model of Turbulence," *Int. J. Heat Mass Transfer*, Vol. 16, pp. 1119–1130.

Jones, W. P., and Renz, U., 1974, "Condensation From a Turbulent Stream Onto a Vertical Surface," *Int. J. Heat Mass Transfer*, Vol. 17, pp. 1019–1028.

Kawamura, H., 1979, "Analysis on Laminarization of Heated Turbulent Gas Using a Two-Equation Model of Turbulence," *Proc. 2nd Turbulent Shear Flows Symp.*, London, pp. 18.16–18.21.

Kays, W. M., and Moffat, R. J., 1975, "Behavior of Transpired Turbulent Boundary Layers," *Studies in Convection*, B. E. Launder, ed., Academic, London, Vol. 1, pp. 223–319.

Kim, J., and Moin, P., 1988, "Transport of Passive Scalars in a Turbulent Channel Flow," in: *Turbulent Shear Flows—6*, Springer-Verlag, Heidelberg (to appear).

Kline, S. J., Cantwell, B., and Lilley, G., eds., 1981, *Proc. 1980-81 AFOSR/HTTM Stanford Conf. on Complex Turbulent Flows*, Vol. 1, Mech. Eng. Dept., Stanford University, CA.

Launder, B. E., 1984, "Numerical Computation of Convective Heat Transfer in Complex Turbulent Flows: Time to Abandon Wall Functions?" *Int. J. Heat Mass Transfer*, Vol. 27, pp. 1485–1491.

Launder, B. E., 1986, "Low-Reynolds-Number Turbulence Near Walls," Mech. Eng. Dept. Report TFD/86/4, UMIST, Manchester, United Kingdom.

Launder, B. E., 1987, "An Introduction to Single-Point Closure Methodology," *An Introduction to the Modelling of Turbulence*, Lecture Series 1987-06, Von Karman Inst. for Fluid Dynamics, Rhode-Saint-Genese, Belgium (also available as UMIST Mech. Eng. Dept. Report TFD/87/7).

Launder, B. E., and Priddin, C. H., 1973, "A Comparison of Some Proposals for the Mixing Length Near a Wall," *Int. J. Heat Mass Transfer*, Vol. 16, pp. 700–702.

Launder, B. E., Reece, G. J., and Rodi, W., 1975, "Progress in the Development of a Reynolds-Stress Turbulence Closure," *J. Fluid Mech.*, Vol. 68, pp. 537–566.

Launder, B. E., Reynolds, W. C., and Rodi, W., 1984, *Turbulence Models and Their Application*, Vol. 2, Eyrolles, Paris.

Launder, B. E., and Samaraweera, D. S. A., 1979, "Application of a Second-Moment Turbulence Closure to Heat and Mass Transport in Thin Shear Flows. I: 2-Dimensional Transport," *Int. J. Heat Mass Transfer*, Vol. 22, pp. 1631–1643.

Launder, B. E., and Sharma, B. I., 1974, "Application of the Energy-Dissipation Model of Turbulence to the Calculation of Flow Near a Spinning Disc," *Letters in Heat Mass Transfer*, Vol. 1, pp. 131–138.

Launder, B. E., and Shima, N., 1988, "A Second-Moment Closure for the Near-Wall Sublayer: Development and Application," submitted to *AIAA J.*

Launder, B. E., and Spalding, D. B., 1974, "The Numerical Computation of Turbulent Flows," *Comp. Meth. Appl. Mech. Eng.*, Vol. 3, pp. 269–289.

Ljuboja, M., and Rodi, W., 1981, "Prediction of Horizontal and Vertical Turbulent Buoyant Wall Jets," ASME JOURNAL OF HEAT TRANSFER, Vol. 103, pp. 343–349.

Lumley, J. L., 1978, "Computational Modeling of Turbulent Flows," *Adv. Applied Mech.*, Vol. 18, pp. 123–176.

Malhotra, A., and Kang, S. S., 1984, "Turbulent Prandtl Number in Circular Pipes," *Int. J. Heat Mass Transfer*, Vol. 27, pp. 2158–2161.

Mellor, G. L., and Yamada, T., 1974, "A Hierarchy of Turbulence Closure Models for Planetary Boundary Layers," *J. Atmos. Sci.*, Vol. 31, pp. 1791–1806.

Monin, A. S., 1965, "On the Symmetry of Turbulence in the Surface Layer of Air," *IZV Atm. and Oceanic Phys.*, Vol. 1, pp. 45–54.

Moser, R. D., and Moin, P., 1984, "Direct Numerical Simulation of Curved Channel Flow," NASA TM85974; see also *Proc. 5th Turbulent Shear Flows Symp.*

Na, T. Y., and Habib, I. S., 1973, "Heat Transfer in Turbulent Pipe Flow Based on a New Mixing Length Model," *Appl. Sci. Res.*, Vol. 28, p. 302.

Prandtl, L., 1925, "Bericht uber Untersuchungen ausgebildeten Turbulenz," *ZAMM*, Vol. 5, p. 136.

Quarmby, A., and Quirk, R., 1972, "Measurements of the Radial and Tangential Eddy Diffusivities of Heat and Mass in Turbulent Flow in a Plain Tube," *Int. J. Heat Mass Transfer*, Vol. 15, pp. 2309–2327.

Rodi, W., 1976, "A New Algebraic Relation for Calculating the Reynolds Stresses," *ZAMM*, Vol, 56, p. 219.

Rodi, W., and Scheuerer, G., 1983, "Scrutinizing the k–ϵ Model Under Adverse Pressure Gradient Conditions," *Proc. 4th Turbulent Shear Flows Symp.*, Karlsruhe, pp. 2.8–2.14.

Rogers, M. M., Moin, P., and Reynolds, W. C., 1986, "The Structure and Modelling of the Hydrodynamic and Passive Scalar Fields in Homogeneous Turbulent Shear Flow," Thermosciences Division Report TF-25, Mech. Eng. Dept., Stanford University, CA.

Runchal, A. K., 1969, "Transfer Processes in Steady Two-Dimensional Separated Flows," Ph.D. Thesis, Faculty of Engineering, University of London, United Kingdom.

Shih, T.-H., and Lumley, J. L., 1985, "Modelling of Pressure Correlation Terms in Reynolds Stress and Scalar Flux Equations," Report FDA-85-3, Sibley School of Mech. and Aerospace Eng., Cornell University, NY.

Simpson, R., and Wallace, D. B., 1975, "Laminarescent Turbulent Boundary Layers," Project SQUID, Tech. Report SMU-1-PU.

Spalart, P. R., 1986, "Numerical Study of Sink-Flow Boundary Layers," *J. Fluid Mech.*, Vol. 172, pp. 307–328.

Spalart, P., and Leonard, A., 1985, "Direct Numerical Simulation of Equilibrium Turbulent Boundary Layers," *Proc. 5th Turbulent Shear Flows Symp.*, Cornell University, NY, pp. 9.35–9.40.

Spalding, D. B., 1967, "Heat Transfer From Turbulent Separated Flows," *J. Fluid Mech.*, Vol. 27, pp. 97–109.

Tanaka, H., Kawamura, H., Tateno, A., and Hatamiya, A., 1982, "Effect of Laminarization and Retransition on Heat Transfer for Low Reynolds Number Flow Through a Converging to Constant Area Duct," ASME JOURNAL OF HEAT TRANSFER, Vol. 104, pp. 363–371.

To, W. M., and Humphrey, J. A. C., 1986, "Numerical Simulation of Buoyant Turbulent Flow; Part 1: Free Convection Along a Heated Vertical Flat Plate," *Int. J. Heat Mass Transfer*, Vol. 29, pp. 573–592.

Van Driest, E. R., 1956, "On Turbulent Flow Near a Wall," *J. Aero. Sci.*, Vol. 23, p. 1007.

Viegas, J. R., and Horstmann, C. C., 1978, "Comparison of Multi-Equation Turbulence Models for Several Shock-Separated Boundary-Layer Interaction Flows," AIAA Paper No. 78-1165.

Viegas, J., and Rubesin, M., 1983, "Wall Function Boundary Conditions in the Solution of the Navier-Stokes Equations for Complex Compressible Flows," AIAA Paper No. 83-1694.

Viegas, J., Rubesin, M., and Horstmann, C. C., 1985, "On the Use of Wall Functions as Boundary Conditions for Two-Dimensional Separated Compressible Flows," AIAA Paper No. 85-0180.

Vogel, J. C., and Eaton, J. K., 1985, "Combined Heat Transfer and Fluid Dynamic Measurements Downstream of a Backward-Facing Step," ASME JOURNAL OF HEAT TRANSFER, Vol. 107, pp. 922–929.

Wilcox, D., and Rubesin, M. W., 1980, "Progress in Turbulence Modelling for Complex Flow Fields Including Effects of Compressibility," NASA Tech. Paper 1517, NASA Ames Research Center, CA.

Wolfshtein, M. W., 1967, "Convection Processes in Turbulent Impinging Jets," Ph.D. Thesis, Faculty of Engineering, University of London, United Kingdom.

Wolfshtein, M. W., 1969, "The Velocity and Temperature Distribution in One-Dimensional Flow With Turbulence Augmentation and Pressure Gradient," *Int. J. Heat Mass Transfer*, Vol. 12, pp. 301–318.

Wyngaard, J. C., 1975, "Modeling the Planetary Boundary Layer—Extension to the Stable Case," *Boundary Layer Meteorology*, Vol. 9, pp. 441–460.

Yap, C., 1987, "Turbulent Heat and Momentum Transfer in Recirculating and Impinging Flows," Ph.D. Thesis, Faculty of Technology, University of Manchester, United Kingdom.

Downloaded 16 Dec 2010 to 193.140.21.150. Redistribution subject to ASME license or copyright; see http://www.asme.org/terms/Terms_Use.cfm

Zeman, O., and Lumley, J. L., 1979, "Buoyancy Effects in Entraining Turbulent Boundary Layers," *Turbulent Shear Flows-1*, Springer, Heidelberg, pp. 295–306.

APPENDIX

For illustration, the details of three levels of turbulence model for computing heat transfer in near-wall flows are presented.

Level 1: Eddy Viscosity Model (EVM)

General review by Patel et al. (1985); particular form cited Launder and Sharma (1974):

$$-(\overline{u_iu_j}-1/3\ \delta_{ij}\overline{u_ku_k})=\nu_t\left(\frac{\partial U_i}{\partial x_j}+\frac{\partial U_j}{\partial x_i}\right)$$

$$-\overline{u_i\theta}=\frac{\nu_t}{\sigma_\theta}\frac{\partial\Theta}{\partial x_i}$$

where

$$\nu_t = c_\mu f_\mu k^2/\tilde{\epsilon};\quad \sigma_\theta=0.9$$

$$\frac{Dk}{Dt} = \frac{\partial}{\partial x_k}\left(\left(\frac{\nu_t}{\sigma_k}+\nu\right)\frac{\partial k}{\partial x_k}\right)+P-\tilde{\epsilon}\ -2\nu\left(\frac{\partial k^{1/2}}{\partial x_k}\right)^2 \quad \text{(A1)}$$

$$\frac{D\tilde{\epsilon}}{Dt} = \frac{\partial}{\partial\epsilon}\left(\left(\frac{\nu_t}{\sigma_\epsilon}+\nu\right)\frac{\partial\epsilon}{\partial x_k}\right)+c_{\epsilon1}\frac{P\tilde{\epsilon}}{k}$$
$$-c_{\epsilon2}\,f_\epsilon\,\frac{\tilde{\epsilon}\,2}{k}+2\nu\nu_t\left(\frac{\partial^2U_i}{\partial x_k\partial x_j}\right)^2 \quad \text{(A2)}$$

c_μ	$c_{\epsilon1}$	$c_{\epsilon2}$	σ_k	σ_ϵ	σ_θ
0.09	1.44	1.92	1.0	1.3	0.9

$f_\mu=\exp(-3.4/(1+\mathrm{Re}_t/50)^2)$; $f_\epsilon=1.0-0.3\ \exp(-\mathrm{Re}_t^2)$; $\mathrm{Re}_t\equiv k^2/\nu\tilde{\epsilon}$ with wall boundary conditions $\tilde{\epsilon}=k=0$.

In the high-Reynolds-number form of the model, the last term in equations (A1) and (A2) is dropped, f_μ and f_ϵ are set equal to unity, and $\tilde{\epsilon}$ becomes identical to ϵ.

Level 3: Differential Second-Moment Closure (DSM)

General review by Bradshaw (1978); Lumley (1978); Launder et al. (1984); particular form cited Gibson and Launder (1978) (applicable in high-Reynolds-number regions only).

$$\frac{D\overline{u_iu_j}}{Dt}=P_{ij}+F_{ij}+\phi_{ij}-\epsilon_{ij}+d_{ij} \quad \text{(A3)}$$

$$\frac{D\overline{u_i\theta}}{Dt}=P_{i\theta1}+P_{i\theta2}+F_{i\theta}+\phi_{i\theta}-\epsilon_{i\theta}+d_{i\theta} \quad \text{(A4)}$$

$$\frac{D\epsilon}{Dt}=c_{\epsilon1}\frac{P\epsilon}{k}-c_{\epsilon2}\frac{\epsilon^2}{k}+d_\epsilon \quad \text{(A5)}$$

where

$$P_{ij}\equiv-\left\{\overline{u_iu_k}\frac{\partial U_j}{\partial x_k}+\overline{u_ju_k}\frac{\partial U_i}{\partial x_k}\right\};\ F_{ij}\equiv(\overline{f_iu_j}+\overline{f_ju_i})$$
$$\epsilon_{ij}=2/3\ \delta_{ij}\epsilon;\quad \epsilon_{i\theta}=0 \quad \text{(A6)}$$
$$P_{i\theta1}\equiv-\overline{u_iu_k}\frac{\partial\Theta}{\partial x_k};\ P_{i\theta2}\equiv-\overline{\theta u_k}\frac{\partial U_i}{\partial x_k};\ F_{i\theta}\equiv\overline{f_i\theta}$$

$$\phi_{ij}=-c_1\frac{\epsilon}{k}(\overline{u_iu_j}-1/3\ \delta_{ij}\overline{u_ku_k})-\underbrace{c_2(P_{ij}-1/3\ \delta_{ij}P_{kk})}_{\phi_{ij2}}$$

$$\underbrace{-c_3(F_{ij}-1/3\ \delta_{ij}F_{kk}+\phi_{ij}^w)}_{\phi_{ij3}} \quad \text{(A7)}$$

$$\phi_{i\theta}=-c_{1\theta}\frac{\epsilon}{k}\overline{u_i\theta}-\underbrace{c_{2\theta}P_{i\theta2}}_{\phi_{i\theta2}}-\underbrace{c_{3\theta}P_{i\theta3}}_{\phi_{i\theta3}}+\phi_{i\theta}^w \quad \text{(A8)}$$

and the "wall-reflection" parts of the pressure interaction are approximated by

$$\phi_{ij}^w = \left\{c_1^w\frac{\epsilon}{k}(\overline{u_ku_m}n_kn_m\delta_{ij}-3/2\ \overline{u_ku_i}n_kn_j-3/2\ \overline{u_ku_j}n_kn_i)\right.$$
$$+\ c_2^w(\phi_{km2}n_kn_m\ \delta_{ij}-3/2\ \phi_{ki2}\ n_kn_j-3/2\ \phi_{kj2}n_kn_i) \quad \text{(A9)}$$
$$\left.+\ c_3^w(\phi_{km3}n_kn_m\ \delta_{ij}-3/2\ \phi_{ki3}\ n_kn_j-3/2\phi_{kj3}n_kn_i)\right\}k^{3/2}/(\epsilon c_l x_n)$$

$$\phi_{i\theta}^w = \left\{-c_{1\theta}^w\frac{\epsilon}{k}\overline{u_k\theta}n_in_k-c_{2\theta}^w\phi_{k\theta2}n_in_k\right.$$
$$\left.-c_{3\theta}^w\phi_{k\theta3}n_in_k\right\}k^{3/2}/(\epsilon c_l\ x_n) \quad \text{(A10)}$$

$$d_\phi = c_\phi\frac{\partial}{\partial x_k}\left(\overline{u_iu_k}\frac{k}{\epsilon}\frac{\partial\phi}{\partial x_i}\right);\ \phi=\overline{u_iu_j},\ \overline{u_i\theta},\ \epsilon,\ \overline{\theta^2},\ k \quad \text{(A11)}$$

When f_i denotes a buoyant force, $F_{i\theta}$ contains the mean square temperature variance as an unknown, which may be determined from its own transport equation

$$\frac{D\bar{\theta}^2}{Dt}=-2\overline{u_k\theta}\frac{\partial\Theta}{\partial x_k}-2\epsilon_\theta+d_{\theta^2} \quad \text{(A12)}$$

where d_{θ^2} is approximated by equation (A11) and

$$\epsilon_\theta=R^{-1}\frac{\epsilon}{k}\frac{\bar{\theta}^2}{2} \quad \text{(A13)}$$

R denotes the thermal to dynamic time-scale ratio, a quantity habitually taken as constant in computing flows near walls.

The following values are suggested for the coefficients:

c_1	c_2	c_3	c_{θ_1}	c_{θ_2}	c_{θ_3}	c_1^w	c_2^w	c_3^w	$c_{1\theta}^w$	$c_{2\theta}^w$	$c_{3\theta}^w$	c_{ϵ_1}	c_{ϵ_2}	R
1.8	0.6	0.5	3.0	0.40	0.33	0.5	0.3	*	0.75	*	*	1.44	1.90	0.8

*Set to zero as no cases were examined in which these terms appeared to be significant.

Diffusion coefficients for:

$\overline{u_iu_j}$	$\overline{u_i\theta}$	ϵ	k	$\overline{\theta^2}$
0.20	0.20	0.15	0.20	0.11

Downloaded 16 Dec 2010 to 193.140.21.150. Redistribution subject to ASME license or copyright; see http://www.asme.org/terms/Terms_Use.cfm

Level 2: Algebraic Second Moment Closure (ASM)

A truncation of the Level 3 model to express transport of $\overline{u_i u_j}$ and $\overline{u_i \theta}$ in terms of that of k and $\overline{\theta^2}$ thereby reducing the number of variables to be obtained via transport equations (see, for example, Hossain and Rodi, 1982).

$$\left(\frac{\overline{Du_i u_j}}{Dt} - d_{ij}\right) = \frac{\overline{u_i u_j}}{k}\left(\frac{Dk}{Dt} - d_k\right) = \frac{\overline{u_i u_j}}{k}(P-\epsilon) \quad \text{(A14)}$$

$$\left(\frac{D\overline{u_i\theta}}{Dt} - d_{i\theta}\right) = \frac{1/2\overline{u_i\theta}}{\sqrt{k^{1/2}\overline{\theta^2}}}\left((P-\epsilon) + (P_\theta - \epsilon_\theta)\right) \quad \text{(A15)}$$

Sometimes one or both of the following further simplifications are made:

$\overline{\theta^2}$ in local equilibrium: $P_\theta = \epsilon_\theta$; $\overline{\theta^2} = -2R\,\frac{k}{\epsilon}\,\overline{\theta u_k}\,\frac{\partial \Theta}{\partial x_k}$ (A16)

GGDH approximation (equation (A11)) for $\overline{u_i\theta}$: $\overline{u_i\theta} = -c_\theta\,\frac{k}{\epsilon}\,\overline{u_i u_k}\,\frac{\partial \Theta}{\partial x_k}$ (A17)
with a coefficient of proportionality of about 0.3.

Downloaded 16 Dec 2010 to 193.140.21.150. Redistribution subject to ASME license or copyright; see http://www.asme.org/terms/Terms_Use.cfm

R. H. Pletcher
Department of Mechanical Engineering
and Computational Fluid Dynamics Center,
Iowa State University,
Ames, IA 50010
Fellow ASME

Progress in Turbulent Forced Convection

This paper presents a brief account of some recent progress toward the understanding and prediction of turbulent forced convection. The impact of technological advances in electronics and optical methods is pointed out. Coverage includes observations on structure, measurement techniques, experimental results, numerical strategies, turbulence modeling, and large eddy and full simulation.

Introduction

Turbulent forced convection occurs in many important technological applications. It is observed in applications of interest to mechanical, aerospace, chemical, and civil engineers, and in flows of interest to meterologists and earth scientists. Turbulence itself is one of the important unresolved problems in engineering and science. At the present time, no workable general theory is known by which the phenomena can be accurately predicted in configurations of practical interest. The time-dependent, three-dimensional Navier-Stokes equations, along with appropriate forms of the energy and continuity equation, are believed to govern turbulent flow. However, despite advances in computer technology and simulation methods, it is still not feasible to solve the exact governing equations numerically for turbulent flows occurring in most practical applications. Such direct simulations are very expensive and at the present time are carried out for relatively simple geometries in order to gather information on very fundamental questions. Research on direct simulation of turbulence will be discussed further in a section to follow. In spite of the difficulties in computing turbulent flows from first principles, considerable progress has been made toward understanding turbulent convective flows and in developing data correlations, formula, and predictive procedures suitable for design purposes. Some of this progress will be reviewed in the present paper.

In order to discern whether events represent progress, the objectives or goals of research in turbulent convection need to be clarified. Ultimately, it is desirable to predict the performance of devices in which or over which turbulent convection occurs. This means it should be possible to determine in advance the local and average Nusselt number and the temperature distribution throughout the convective flow. It is also desirable to understand the important features and mechanisms of turbulent flow. Such understanding can contribute toward the development of sound predictive procedures and set the stage for the development of methods for controlling turbulence to reduce or enhance heat transfer. Ideally, the understanding should precede the development of predictive methods, but this is not always feasible. Quite often the urgency of the application forces development on the basis of empirical information and only limited understanding is possible. Broadly then, the goal of research in turbulent convection has been and is the accumulation of understanding and the development of theories or procedures by which turbulent convective phenomena can be predicted in configurations of interest.

Space does not permit an exhaustive review of all aspects of turbulent forced convection in this article. The subject encompasses many facets including experimental methods, experimental results, transition, computational methods, and turbulence modeling. Most of these subtopics are extensive enough to be the focus of a full-length review article. The present paper will simply express the author's limited perspective on the highlights of recent progress. Omission of some important references seems inevitable, although such omissions were not intended. Coverage will likely be more complete in the areas of computational methods and turbulence modeling due to the author's greater experience with those subjects.

A number of technological advances have had an impact on research in turbulent convection. Among these are advances in electronics, including the electronic digital computer, and in optical methods of measurement. The impact of the advances in electronics and computer technology has been especially far reaching, affecting significantly the way both experiments and analysis are carried out. The computer has, in fact, stimulated the rapid growth of the "numerical" or "computational" approach to solving problems in convection (Pletcher and Patankar, 1983). A number of finite-difference solutions to laminar flow problems appeared in the literature in the 1950s, although some discussion of other numerical methods for the boundary-layer equations can be found from the literature of the 1930s and 1940s. Finite-difference solutions for laminar convective problems began to appear in the early 1960s, one of the first being the solution for entrance region heat transfer between parallel plates (Hwang and Fan, 1964). Application of similar numerical procedures to turbulent flow soon followed (Patankar and Spalding, 1967; Herring and Mellor, 1968; Bankston and McEligot, 1970; Cebeci, 1970; Pletcher, 1970).

At the time of these early numerical studies, certain "universal" characteristics of turbulent wall boundary layers had been known for many years, such as the "law of the wall." Such characteristics could be explained or interpreted through Prandtl's mixing length hypothesis, which provided a basis for computing an "effective" turbulent viscosity. A noteworthy result of the early computational research in turbulent flows was the revelation that the numerical solutions of the Reynolds-averaged form of the governing conservation equations using a Boussinesq (1877) representation for the turbulent shear stress and heat flux terms along with a model based largely on the mixing length concept for the effective viscosity and conductivity could provide amazingly accurate detailed solutions for velocities and temperatures in a class of internal and external flows. From the mid-1960s on the idea grew that it might be possible to simulate turbulent flows through the Reynolds equations numerically in a manner that would parallel simulations for laminar flows. For the most part, the early numerical calculations utilized the boundary-layer form of the conservation equations. The idea of modeling the effective turbulent viscosity and conductivity was not new, but the availability of the computer as a tool by which the models could be evaluated through numerical solution of the Reynolds-averaged governing equations provided even greater motivation for research on turbulence models. Other lines of turbulent research such as large eddy and direct simulation have also flourished because of the steady improve-

Contributed by the Heat Transfer Division for publication in the JOURNAL OF HEAT TRANSFER. Manuscript received by the Heat Transfer Division April 15, 1988. Keywords: Forced Convection, Reviews, Turbulence.

Copyright © 1988 by ASME

Downloaded 16 Dec 2010 to 193.140.21.150. Redistribution subject to ASME license or copyright; see http://www.asme.org/terms/Terms_Use.cfm

ment in computer hardware and algorithms.

The paper begins with a review of a number of experimental observations that have had great influence on our perception of turbulence structure. This is followed by a discussion of experimental methods and the results from a broad class of experiments designed to increase understanding of effects important in applications. The paper concludes with a discussion of computational methods, turbulence modeling, and large eddy and full simulation.

Observations on Structure

Progress in turbulent convection has been very dependent upon experimental observations. Many experiments have been carried out with the main objective being to establish values of engineering parameters for flows of interest in applications. These will be discussed in a section to follow. In the present section, some of the recent observations on structure that have had the greatest impact on our understanding of turbulent motion will be discussed.

The ability of engineers to predict turbulent flow phenomena accurately and reliably is severely limited. There has been the hope that with greater understanding of the basic physics of turbulent motion, some analytical approach will emerge that will greatly simplify the prediction of turbulent flows. This simplification has been slow in coming but may someday be achieved.

Many features of turbulent shear flows were well established by the 1940s and 1950s. These include the existence of the viscous sublayer, the buffer layer, and the logarithmic and outer layer for wall boundary layers. The remarkable universality of the inner region had been recognized. It is common to measure the "inner" region in terms of y^+ defined as

$$y^+ = yu^*/\nu_w \tag{1}$$

where $u^* = (\tau_w/\rho_w)^{1/2}$. In terms of y^+, the viscous sublayer extends from $0 < y^+ \lesssim 5$ and in this region, the mean velocity is given to a good approximation for constant property flows by

$$u^+ = y^+ \tag{2}$$

where $u^+ = u/u^*$. The region from y^+ of 5 to about 30 is known as the buffer layer and the velocity distribution for constant property flows can be obtained from the formula due to Spalding (1961)

$$y^+ = u^+ + e^{-\kappa B}\left[e^{\kappa u^+} - 1 - \kappa u^+ - \frac{(\kappa u^+)^2}{2} - \frac{(\kappa u^+)^3}{6}\right] \tag{3}$$

where κ is the von Kármán constant (0.40) and B is a constant (5.5). Other authors (Kleinstein, 1967) have suggested 0.41 and 5.0 for the two constants.

Outside of the buffer layer, a region invariably exists where the famous logarithmic law holds

$$u^+ = \frac{1}{\kappa} \ln y^+ + C_1 \tag{4}$$

where κ is the von Kármán constant ($\simeq 0.41$) and $C_1 \simeq 5.15$. Values of κ between 0.39 and 0.44 and C_1 between 4.9 and 5.2 can be found in the literature. The y^+ range over which equation (4) is valid generally varies with Reynolds number, but for external wall boundary layers in zero or very mild pressure gradients, the logarithmic law will only hold for the inner 20–25 percent of the boundary layer. This is one commonly accepted definition of the extent of the inner region. Although a degree of universality has been observed in the outer layer (that is, outside of the logarithmic region), the pressure gradient becomes a parameter. A number of expressions have been proposed to correlate the velocity distribution in the outer wakelike layer (Clauser, 1954, 1956; Coles, 1956). The expression proposed by Coles,

$$u^+ = \frac{1}{\kappa} \ln y^+ + C_1 + \frac{\Pi}{\kappa} 2 \sin^2\left(\frac{\pi}{2}\frac{y}{\delta}\right) \tag{5}$$

is valid for both the logarithmic and the outer region. In equation (5), Π is a pressure gradient parameter equal to 0.55 for a zero pressure gradient. For internal flow, such as in a circular duct, similar universal behavior is observed for the mean velocity, except that the wake component in equation (5) is nearly negligible due largely to the favorable pressure gradients that generally prevail in internal flows. It has long been recognized that similar relationships can be developed for the temperature distribution in a nearly constant property turbulent boundary layer except that the Prandtl number will now be a parameter. Dimensional analysis suggests that in the near wall region

$$T^+ = \frac{T_w - T}{q_w/\rho c_p u^*} = f\left(y^+, \text{Pr}, \frac{\rho u^{*3}}{q_w}\right) \tag{6}$$

The quantity $q_w/\rho c_p u^*$ is known as the friction temperature T^*, and $T^+ = (T_w - T)/T^*$. The last parameter on the right-hand side of equation (6), $\rho u^{*3}/q_w$, measures the relation importance of viscous dissipation, and can be neglected for low-speed flows. Many expressions for the "universal" temperature distribution have been reported in the literature (see, for example, Kader and Yaglom, 1972; Kader, 1981). For low-speed flow, these usually show a logarithmic portion of the form

$$T^+ = \frac{1}{\kappa_h} \ln y^+ + C_h \tag{7}$$

where $\kappa_h \simeq (0.4 - 0.44)$ and C_h is a function of Prandtl number. For $\text{Pr} \simeq 1$, $C_h \simeq 5.0$.

During the 1950s, more measurements of fluctuating quantities and turbulence energy became available. The sharp peak in the fluctuating quantities very near the wall indicating a high rate of production of turbulence energy was noted (Klebanoff, 1954; Laufer, 1954) and served to arouse interest in the near-wall region. It seemed to be a region of contradiction. Why should production be so large very close to a no-slip boundary that ought to serve to damp the turbulent (and all) motion?

The near-wall region became the focus of more intense study. Flow visualization by Kline and Rundstadler (1959) indicated that the flow in the viscous sublayer was not steady and laminar at all. With further studies (Kline et al., 1967), a description of events in the near-wall region evolved. Kline and co-workers found that hydrogen bubbles released in the viscous sublayer, $y^+ = 2.7$, accumulated in an alternating array of high and low-speed regions called "streaks." They observed that the streaks interacted with the outer flow through a process of gradual outflow, liftup, sudden oscillating growth, and breakup. This sequence of events has been termed "bursting." The oscillations were observed in the region $y^+ = 8$–12. The abrupt breakup was observed in the region $10 < y^+ < 30$. After the breakup, the streak of bubbles was ejected outward along an identifiable trajectory. This is illustrated in Fig. 1 taken from the work of Kim et al. (1971).

Corino and Brodkey (1969) also observed "ejections" near the wall in fully developed pipe flow although they reported that ejections originated outside the viscous sublayer, $y^+ \sim 5$ to 15. They also noticed that the ejection phase ended with an axial movement, called a "sweep," of upstream higher momentum fluid sweeping out fluid from the previous ejection event. Among the many other experimental studies confirming the earlier observations on bursting and contributing new details are those due to Grass (1971), Kim et al. (1971), Wallace et al. (1972), Nychas et al. (1973), Willmarth and Lu (1972), Sirkar and Hanratty (1970), Blackwelder and Kaplan (1976), Bakewell and Lumley (1967), and Blackwelder and Eckelmann (1979). By the early 1970s it seemed fairly clear

Downloaded 16 Dec 2010 to 193.140.21.150. Redistribution subject to ASME license or copyright; see http://www.asme.org/terms/Terms_Use.cfm

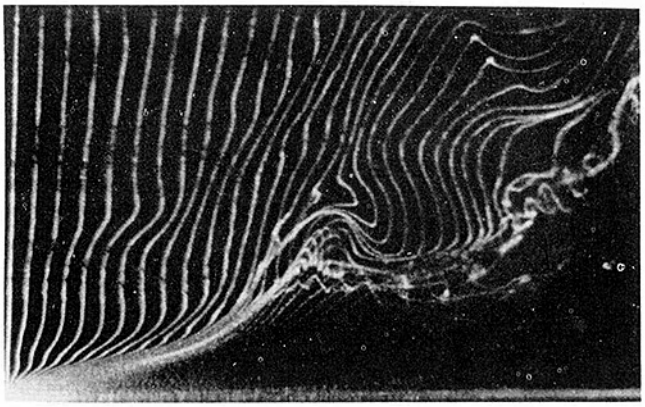

Fig. 1 Visualization of bursting process near wall by hydrogen bubble time lines released from wire perpendicular to wall at left; formation of transverse vortex, from Kim et al. (1971)

that nearly all of the net production of turbulent energy in the wall region occurs during bursts. Similarly, studies showed that bursts, including the sweep phase, accounted for the generation of nearly all of the Reynolds stresses in the region $0 < y^+ < 100$.

Prior to the discovery of the bursting phenomena, turbulence was thought to be totally a statistically random process. That belief was shaken by discoveries of the 1960s, which suggested that the transport properties of most shear flows were not random but the result of "organized" or "coherent," repeatable, unsteady motions. At first the organized bursting process was thought to be essentially a wall-related phenomenon that interacted with the outer flow, but was governed by wall parameters. This perception was shattered when Rao et al. (1971) showed that the mean burst period scales with outer variables as

$$\frac{u_\infty t}{\delta} \simeq 6 \tag{8}$$

where t is the time between bursts, and δ is the boundary layer thickness.

Organized motions have also been discovered in the outer part of wall boundary layers (including pipe flow) and in free shear flows (Brown and Roshko, 1974). Generally, the organized activity is characterized by relatively large-scale vortex motions. The form and scale of these motions vary from flow to flow. The observations have been numerous and important, but will not be described in detail here because of space limitations. Further details on this important progress can be found in the excellent review articles by Mollo-Christensen (1971), Laufer (1975), Willmarth (1975), Roshko (1976), Cantwell (1981), and Hirata et al. (1982).

The discovery of organized structures in turbulent flow has had a great impact on current perceptions of turbulence and has influenced the direction of much experimental research over the past 25–30 years. It is important to recognize that new experimental techniques were required to identify and study the organized structures. Measurements of mean and fluctuating quantities alone do not easily reveal coherent structures that often become very obvious (Brown and Roshko, 1974) when flow visualization is employed. Flow visualization, generally, has contributed much to present knowledge of turbulent motion.

Although the bursting phenomena and other organized structures have been recognized for more than 25 years, their impact on prediction methods for practical applications has been very slight. In the early years of work on the organized structures, there was a sense of optimism that the mysteries of turbulent motion were being solved and soon a predictive scheme that cleverly accounts for the organized motion would be in place. This hasn't happened. Perhaps early on, workers were overly optimistic that a universal aspect to the organized motion would be uncovered, i.e., a common thread would be found relating the organized motion in all types of turbulent flows. Instead, with additional study, the coherent structures were often found to be more complex than originally thought. The majority of the prediction schemes (vortex methods, large eddy, and direct simulation are exceptions) utilize numerical solutions to the Reynolds-averaged form of the conservation equations. It is doubtful that this form of the equations can capture the unsteady organized motions responsible for the apparent stresses and heat flux quantities associated with the time mean flow. Another mathematical model will likely be required. In time, an approach may well be developed that is both consistent with the observed organized motion and economical enough to be used for practical calculations.

Experiments

General. The previous section highlighted the experimental observations that had the greatest impact on our perception of turbulence structure. In this section a broader category of experiments will be considered, including those designed to provide heat transfer results for configurations of interest in applications.

Measurement Techniques. Innovative measurement techniques have contributed much to the understanding of turbulent transport. Over the past 20–25 years, continued refinement in hot-wire and hot-film technology has been observed (Comte-Bellot et al., 1981; Perry, 1982). The wires and films have been used extensively for mean velocity and temperature measurements. Transducer signals must be analyzed carefully when films or wires are used in nonisothermal applications because the signal is influenced by both temperature and velocity variations. The use of a wire probe as a resistance thermometer (operating at constant current) for mean and fluctuating temperature measurements has been attempted, among others, by Corrsin (1949), Chevray and Tutu (1972), Hashida and Nagano (1978), Pimenta et al. (1975), LaRue et al. (1975), Fabris (1978), and Andreopoulos (1983).

Chevray and Tutu (1972) and Hashida and Nagano (1978) described techniques employing two wires that are capable of providing separate and simultaneous signals directly proportional to velocity and temperatures. Fabris (1978) used a four-wire probe to measure instantaneous temperature and the three velocity components in turbulent flow. Even when used in nominally isothermal fluids, slow drift of the ambient temperature can introduce error if compensation of some sort is not used. These problems are more severe when operating in water. A recent discussion of corrections to the output response of a hot-film anemometer due to temperature drift can be found in Sherif and Pletcher (1986).

Hot-wire signals in flows at high levels of turbulence and in flows in which mean flow reversal occurs have been difficult to interpret through conventional anemometry. Two techniques have been proposed for such conditions. In the "flying hot-wire" technique (Coles and Wadcock, 1979), a standard probe is moved through the flow field so that relative to the probe, no flow reversal occurs. A number of applications and refinements to this technique have been reported (Cantwell and Coles, 1983; Watmuft et al., 1983; Thompson and Whitelaw, 1984; Walker and Maxey, 1985). These studies demonstrated that the flying hot-wire technique can be used in complex flows not accessible by standard techniques. The experimental arrangement and data acquisition procedures are necessarily quite complex for the flying hot wire. The thermal

Downloaded 16 Dec 2010 to 193.140.21.150. Redistribution subject to ASME license or copyright; see http://www.asme.org/terms/Terms_Use.cfm

tuft concept (Kovasznay, 1948) has also been used to determine flow direction. In this approach, the thermal wake created by a heated wire is detected by additional wires on both sides of the wake generating wire (Eaton et al., 1979). A pulsed wire version of this concept was developed by Bradbury and Castro (1971) and Bradbury (1976) in which the velocity was determined from the time required for the fluid heated by the pulse in wire current to reach a second senser positioned a known distance away. The technique has been further developed and utilized for measurements, including Reynolds stresses in some cases, by Castro and Cheun (1982), Dengel et al. (1981), Jaroch (1985), and Ruderich and Fernholz (1986).

Laser-Doppler anemometry has become an important technique for obtaining mean velocity and fluctuating quantities in flows not easily accessible to hot wires. The laser-Doppler anemometer (LDA) is a relatively new instrument, coming into widespread use only in the 1970s. The method is based on the measurement of the Doppler shift of laser light scattered from small particles carried along with the fluid. It is increasingly becoming the instrument of choice for use in liquids and high-speed and recirculating flows. The technique is nonintrusive, which alone is a distinct advantage in many applications. The theory of the LDA is discussed by Durst et al. (1981) and Durrani and Greated (1977). Some of the limitations and problems encountered in use of the LDA are discussed by Buchhave et al. (1979). Temperature variations or fluctuations within the medium will cause fluctuations in the refractive index which in turn causes the path of the laser beam to bend. Errors introduced by this effect are discussed by Buchhave et al. (1979). Technology supporting the LDA is advancing rapidly. Use of fiber optics for laser light transmission is allowing the LDA to be used in large-scale wind tunnels. The LDA is now being used for flow field scanning (Durst et al., 1981; Chehroudi and Simpson, 1985) which permits measurements of space–time correlations. Laser light has also been used in several ingenious ways to aid in flow visualization. It is likely that we are still at an early point in the evolution of laser-related technology for obtaining measurements in turbulent flow. Other optical techniques such as interferometry (Hauf and Grigull, 1970; Goldstein, 1978; Lauterborn and Vogel, 1984) have played an important role in experimental studies in turbulent forced convection.

Digital image processing is another evolving technology that should soon be playing a major role in turbulent flow research (Gonzalez and Wintz, 1977; Castleman, 1979; Hall, 1979; Hesselink, 1988). In a sense, it represents a marriage of two approaches or technologies, flow visualization and digital computation, each of which has been responsible for some of the most significant advances in understanding of turbulent flows over the past two decades. The input to the digital imaging process can be from flow visualization experiments or numerical flow simulations, which can create an immense amount of data, especially for a three-dimensional time-evolving flow. Objectives of the imaging process include global structure identification and classification, enhancement of images, feature extraction, and three-dimensional representations of fluid structures to aid understanding and interpretation (Hesselink, 1988).

Temperature-sensitive liquid crystals are being used increasingly to obtain a quantitative measure of surface temperature in heat transfer experiments and to infer near-wall turbulence structure. Liquid crystals have been used for indicating temperature changes for many years (Fergason, 1964; Cooper et al., 1975). However, relatively recently such crystals have become available in a convenient composite of liquid crystal and heating element. In the composite, the lower sheet is typically coated with a conducting material (gold or carbon), which serves as an electrical heater. The upper sheet contains a thin layer of the liquid crystal. The composite can be bonded to the heat transfer test surface to allow determination of local heat transfer coefficient. Hippensteele et al. (1981) reported that the liquid crystal composite was found to indicate a temperature to within 0.2°C. This allowed the local heat transfer coefficient to be determined to within 8 percent when conduction and radiation losses were properly accounted for. Other investigators utilizing liquid crystals in convective studies include Simonich and Moffat (1982). The thin gold film heater on a plastic substrate, which forms the lower part of the composite, has also been widely used in experiments that employed thermocouples, rather than liquid crystal, to determine surface temperature (Baughn et al., 1984).

The mass transfer analogy has been widely developed in recent years as a means by which heat transfer coefficients can be computed from mass transfer experiments. One widely used technique utilizes the sublimation of naphthalene. The procedure has been used to determine both local and average mass transfer coefficients. It is possible to determine the amount of mass that sublimes at a particular location with great accuracy without the need for corrections to account for conduction or radiation. The feasibility of using the sublimation mass transfer analogy has been recognized since the 1940s. The most commonly used vapor pressure–temperature equation for naphthalene was provided by Sogin (1958). A large number of experiments have been based on this transfer analogy, especially by E. M. Sparrow and co-workers at the University of Minnesota (see, for example, Garcia and Sparrow, 1987). Mass transfer in electrochemical solutions has also been used to obtain heat transfer data and to study turbulent structure by analogy (Newman, 1973; Mizushina, 1971). Such techniques have been employed in turbulent flows by Mitchell and Hanratty (1966), Shaw and Hanratty (1977a, 1977b), and Sirkar and Hanratty (1970), among others.

Experimental Results—General. The main characteristics of turbulent forced convective flow in straight smooth ducts and over simple shapes have been known for some time. Heat transfer correlations of experimental results for a wide range of such flows can be found in handbooks and textbooks covering forced convection. For duct flows, the fully developed condition has been investigated the most exhaustively and generally under conditions where the effects of property variations were small. Less extensive and conclusive information is available on turbulent developing flows and flows with significant property variations, although such conditions are considered by Bhatti and Shah (1987) and Kakac (1987).

Much of the recent experimental research in turbulent forced convection has dealt with what might be called "special effects." These include the effects of secondary flows in noncircular ducts, the effects of curvature, swirl, surface transpiration, and roughness, strong pressure gradients, free stream turbulence, and separation. These effects occur very frequently in applications and are only "special" in the sense that they are absent in the simplest baseline flows of the straight, smooth circular duct and the flat plate. They are also special in that the simplest turbulence models require adjustments in order to predict the flows accurately. Experiments containing such complicating features are very important, not only because the flows are characteristic of those occurring in applications, but also because they provide guidance and motivation for the development of much needed prediction schemes.

Transpiration. A good example of this is flows with transpiration. One way to provide cooling for a surface exposed to a hot external stream is to inject a coolant through a porous section of the surface into the hot boundary layer. A considerable amount of experimental data has been accumulated for the transpiration of air into a turbulent low-speed airstream (Kays and Moffat, 1975). The experiments included flows with both blowing and suction over a range of

Downloaded 16 Dec 2010 to 193.140.21.150. Redistribution subject to ASME license or copyright; see http://www.asme.org/terms/Terms_Use.cfm

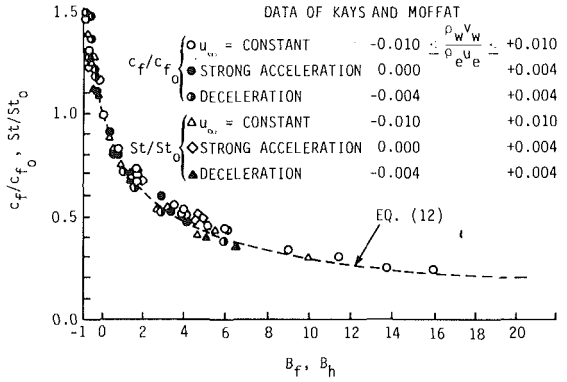

Fig. 2 Effect of transpiration on Stanton number and skin-friction coefficient for an incompressible turbulent boundary layer, from Kays and Crawford (1980)

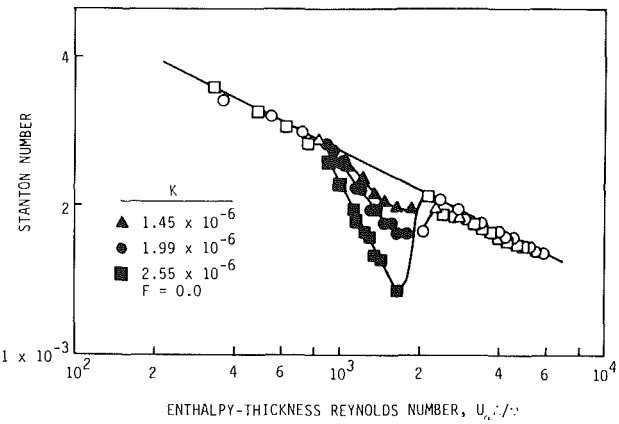

Fig. 3 The effects of acceleration on Stanton number, from Moffat and Kays (1984)

pressure gradients. Property variations were small. The results have been well correlated making use of the parameters

$$B_f = \frac{2\rho_w v_w}{c_f \rho_e u_e} \tag{9}$$

$$B_h = \frac{\rho_w v_w}{\mathrm{St}\ \rho_e u_e} \tag{10}$$

and the enthalpy thickness

$$\Delta = \int_0^\infty \frac{\rho u (H - H_e)}{\rho_e u_e (H_w - H_e)}\, dy \tag{11}$$

The same correlation can be used for the skin-friction coefficient and Stanton number in the form

$$\frac{c_f}{c_{f_0}}\bigg|_\theta = \frac{\mathrm{St}}{\mathrm{St}_0}\bigg|_\Delta = \left[\frac{\ln(1+B)}{B}\right]^{1.25} (1+B)^{1/4} \tag{12}$$

where $B = B_f$ when c_f is to be determined; $B = B_h$ when St is to be determined; θ is the momentum thickness. The c_{f_0} in equation (12) is to be taken as the skin-friction coefficient for a flow without transpiration but at the same value of Re_θ as the transpired flow. Similarly, St_0 is taken as the Stanton number for a flow without transpiration but at the same Re_θ as the transpired flow. The range of applicability of equation (12) appears to be quite broad. Experimental results for St and c_f are shown in Fig. 2 along with equation (12). As can be deduced from the figure, blowing reduces both the local skin friction coefficient and the local Stanton number. The effect of suction is just the opposite. The experimental results available for compressible turbulent flows are limited to a relatively narrow range of flow conditions (Jeromin, 1970; Coles, 1972; Voisinet, 1979; Squire, 1970) and no simple correlation is available.

Pressure Gradients. Low-speed studies indicating the effects of pressure gradients (acceleration, deceleration) on heat transfer to the turbulent boundary layer include the work of Moretti and Kays (1965), Moffat and Kays (1968), Blackwell (1972), Orlando et al. (1974); Kearney (1970), Thielbahr (1969), and Whitten (1967). The results of these studies have been summarized by Moffat and Kays (1984). The effect of flow acceleration is to reduce the Stanton number toward a laminarlike value. An example of this is shown in Fig. 3. The pressure gradient parameter K is defined as

$$K = \frac{\nu}{u_e^2}\frac{du_e}{dx} \tag{13}$$

On the other hand, deceleration was observed (Moffat and Kays, 1984) to have little effect on Stanton number when examined as a function of enthalpy thickness Reynolds number. That is, even the effects of blowing and suction on Stanton number in decelerating flows were found to be the same as for zero pressure gradient flows.

Roughness. A number of studies have considered the effects of roughness on heat transfer, some of them in combination with transpiration (Moffat et al., 1978; Ligrani, 1979; Pimenta et al., 1979; Coleman, 1976; Healzer et al., 1974; Hill et al., 1980; Holden 1982). The low-speed rough-wall (packed copper balls) data (Moffat et al., 1978) with no blowing were found to fit the equation

$$\mathrm{St} = 0.00317\,(\Delta/r) \tag{14}$$

where r is the radius of the balls forming the roughness elements.

Curvature. Streamwise curvature has been observed to have a significant effect on heat transfer in a turbulent boundary layer (Thomann, 1968). Convex curvature in the streamwise direction reduces heat transfer while concave curvature augments it. The effect of convex curvature is quite dramatic as illustrated in Fig. 4, taken from the work of Simon et al. (1980) for a case in which the ratio of the boundary layer thickness to the radius of curvature, δ_{99}/R, was 0.10. The experiment was run at constant pressure in order to isolate the effect of the curvature. The effect of the convex curvature seems to be to restrict the effects of turbulence to a thin layer near the wall. This effect is illustrated in Fig. 5 (Moffat and Kays, 1984) where the mixing length calculated from measured stress profiles and mean velocities is plotted for stations near the end of curvature. The mixing length is seen to level off at a value which is only about 30 percent of that expected for a flat plate boundary layer. The outer region of the boundary layer is apparently turbulent, but the turbulence is uncorrelated with nearly zero Reynolds stresses.

The increase in heat transfer observed for concave curvature has often been attributed to streamwise vortices similar to Taylor-Görtler vortices. However, a visualization study by Simonich and Moffat (1982) and a study of the turbulence structure by Jeans and Johnston (1982) showed no evidence of streamwise vortices or roll cells developing inside the curved region. This suggests that two-dimensional computational models might be adequate for predicting heat transfer on concave walls.

Free-Stream Turbulence. Although investigators have been in general agreement that increasing the free-stream turbulence level increases the skin friction, the reported effects on heat transfer have been contradictory. However, the recent comprehensive studies by Blair (1983a, 1983b) provided convincing evidence that the effect of free-stream turbulence is to

Downloaded 16 Dec 2010 to 193.140.21.150. Redistribution subject to ASME license or copyright; see http://www.asme.org/terms/Terms_Use.cfm

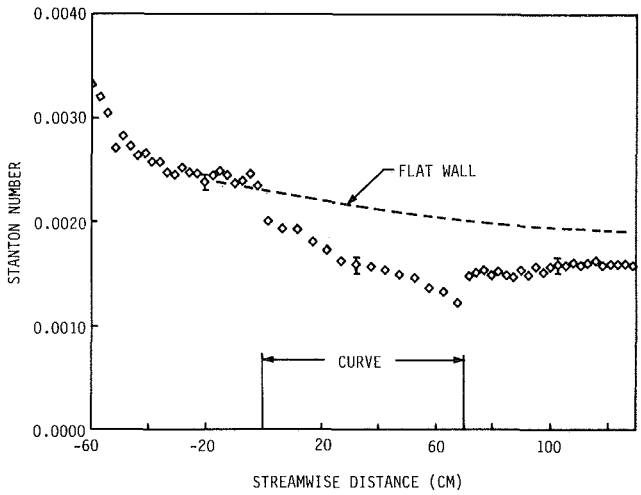

Fig. 4 Effect of convex curvature on Stanton number, from Simon et al. (1980)

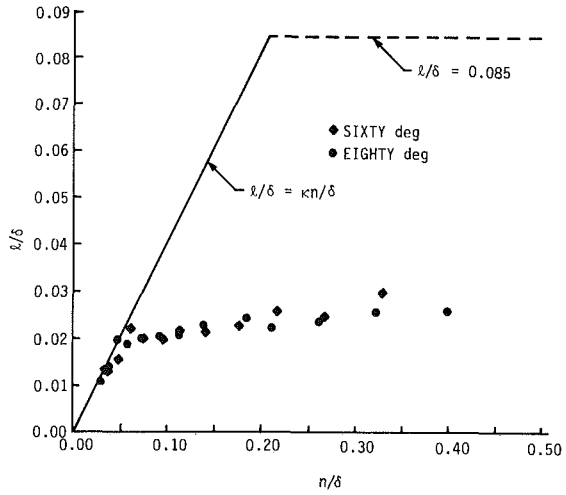

Fig. 5 Effect on convex curvature on mixing length, from Moffat and Kays (1984)

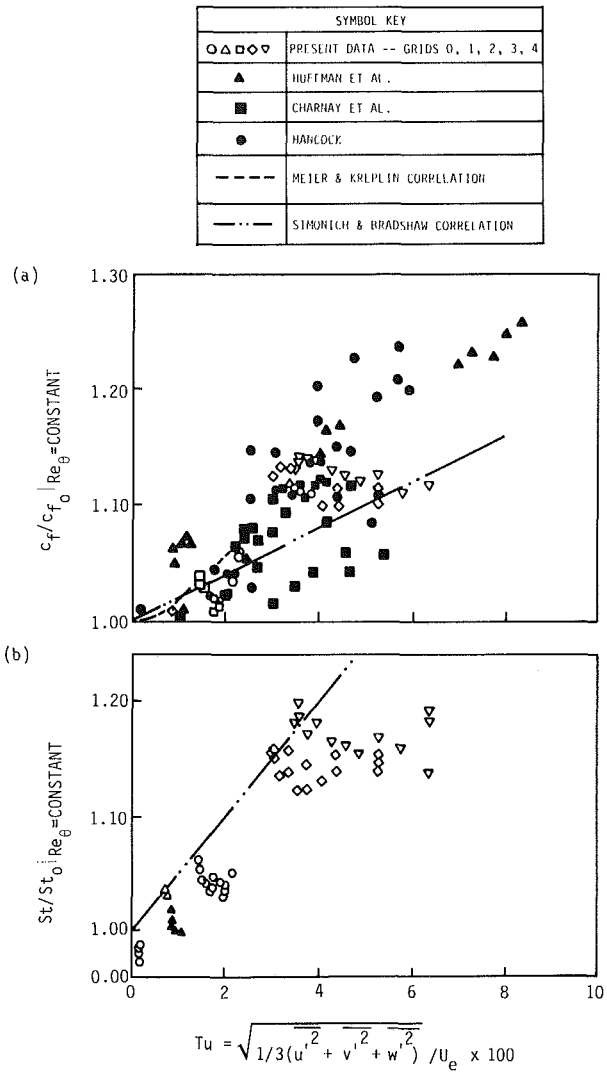

Fig. 6 Influence of free-stream turbulence intensity on skin friction and heat transfer coefficients, from Blair (1983b)

enhance the heat transfer through a turbulent boundary layer by as much as 20 percent for free-stream turbulence levels in the range 4–7 percent. His studies also indicated that the Reynolds analogy factor, $2St/c_f$, increased linearly with increasing turbulence level according to the correlation

$$2St/c_f = 1.18 + 1.3Tu \tag{15}$$

where Tu is the free-stream turbulence intensity defined by

$$Tu = [1/3(\overline{u'^2} + \overline{v'^2} + \overline{w'^2})]^{1/2}/u_e \tag{16}$$

The skin friction and Stanton number data of Blair and several previous investigators (Huffman et al., 1972; Charnay et al., 1971; Hancock, 1980) are shown in Fig. 6, taken from Blair (1983b). The correlations proposed by Meier and Kreplin (1980) and Simonich and Bradshaw (1978) are also shown in the figure. The values of c_{f_0} and St_0 are for negligible free-stream turbulence at the same value of Re_θ. The main effect of the free-stream turbulence on velocity and temperature profiles is to reduce the wake component, as can be seen in Fig. 7. In fact, Bradshaw (1974) has proposed a correlation for c_f/c_{f_0} based on the change in wake strength. In Blair's (1983b) study, the wake component disappeared entirely when the free-stream turbulence reached 5.3 percent. Not only is the effect of free-stream turbulence important in applications, but understanding and simulating the mechanism by which the free-stream turbulence influences skin friction and heat transfer is important to those developing accurate and general numerical prediction schemes.

Secondary Flows. It has been known for a long time that secondary flows are established in turbulent flow through noncircular ducts. The secondary flows (known as Prandtl's secondary flow of the second kind) are driven by gradients in the Reynolds stresses and have been studied most extensively in ducts of square or rectangular cross section. These secondary flows influence the distribution of wall shear stress and heat flux in the duct and present a major challenge to turbulence models. A great many investigators have addressed the hydrodynamic problem, experimentally and through computational studies (see, for example, the review articles by Bradshaw, 1987, and Nallasamy 1987). Similar secondary flow patterns are observed in external corner flows and open channels. Only a few investigators have reported measurements and/or predictions for such flows with heat transfer. Among these are the studies of Emery et al. (1979, 1980), and Launder and Ying (1973).

Separated Flows. Forced convection flows with zones of recirculation have received attention recently probably

Downloaded 16 Dec 2010 to 193.140.21.150. Redistribution subject to ASME license or copyright; see http://www.asme.org/terms/Terms_Use.cfm

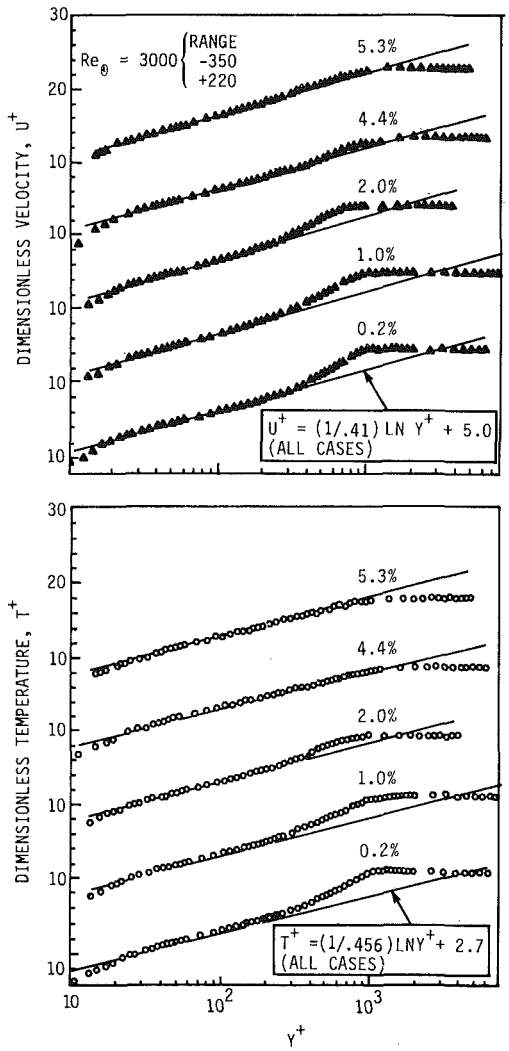

Fig. 7 Effect of free-stream turbulence on mean velocity and temperature profiles, from Blair (1983b)

because of their importance in applications and because they represent a class of flows in which the controlling mechanisms are largely unknown. Such flows can be viewed as comprised of two types. The first are flows that separate due to adverse pressure gradients in or on smoothly varying geometries, and the second are flows that separate due to abrupt changes in geometry. Flow through a diffuser or over a turbine blade are examples of the first type and flows through a sudden pipe expansion (rearward-facing step) are an example of the second type. The most detailed experimental studies highlighting the separated and reattachment zones have been for the second type. The experiments of Vogel and Eaton (1985) were obtained for a planar expansion over a rearward-facing step in a channel of aspect ratio 12 and for an area expansion ratio of 1.25. Stanton number profiles were obtained at four different step height Reynolds numbers ranging from 13,000 to 42,000 on a constant heat flux surface. The reattachment caused a local augmentation of heat transfer by a factor of about two with the maximum heat transfer coefficient occurring slightly upstream of reattachment. Mean velocities and temperatures and the mean skin friction were also reported. The Reynolds analogy fails completely in this type of flow because the Stanton number is near its maximum value at the point where the mean skin friction passes through zero. This presents a major challenge for prediction schemes.

Baughn et al. (1984) recently measured the local heat transfer coefficients downstream of an abrupt expansion in a circular channel with constant wall heat flux. The flow upstream of the expansion was fully developed. Measurements were made at five diameter ratios from 0.267 to 0.800 and over a range of Reynolds (based on downstream diameter) from 5300 to 87,000. Peak Nusselt numbers exceeded ten times the fully developed values at the largest expansion ratio. No supporting hydrodynamic measurements were reported. Other heat transfer measurements in pipe expansion flows were reported by Zemanick and Dougall (1970). Earlier heat transfer experiments are described in the review by Fletcher et al. (1974). There have been many more experimental studies on separated flows carried out under isothermal conditions. A description of many of these can be found in the review by Simpson (1985).

Predictions. The experimental studies mentioned in this section have all dealt with effects not easily accounted for by conventional prediction methods. Only in a few exceptional cases has it beeen possible to develop correlations for engineering parameters from the results of these studies. In most cases, the flows have been too complex with too many important parameters to permit the development of a working correlation. On the other hand, the experiments have provided the guidance needed for modifying turbulence models so that most of these effects can now be predicted using finite-difference solutions to the governing partial differential equations. In a sense, the empirical turbulence models then contain the correlating information. In some instances, it has been possible to correlate (using experimental data) model parameters to exhibit the influence of an effect such as blowing or pressure gradient. Although simple correlations for engineering parameters will always be in demand, the numerical solution does provide more detailed information including velocities, pressures, and temperatures throughout the convective flow.

Computational Methods

Numerical Strategies. A wide range of numerical techniques has been used to solve turbulent flow problems in forced convection. For the most part, these methods can be categorized as (1) integral methods, (2) finite-difference methods, (3) finite-element methods. The objective of all three of these methods is to transfer the problem posed through partial differential equations to one having an algebraic representation. The methods differ in the procedures used to implement this discretization. Currently, the finite-difference method appears to be the most widely used numerical approach for convective flows.

Boundary-Layer Approximation. A large number of solutions to important problems in convection have been based on the boundary-layer approximation. Certain external flows as well as the developing flow in a two-dimensional or axisymmetric channel are good examples of this. Some of the earliest work of this type was cited in the Introduction. Quite a wide range of flows has been fairly well predicted using a simple algebraic turbulence model to evaluate the Reynolds stress $-\rho\overline{v'u'}$ through the Boussinesq (1877) assumption, $-\rho\overline{v'u'} = \mu_T\,(\partial u/\partial y)$ where

$$\mu_T = \rho l^2 (\partial u/\partial y) \tag{17}$$

In the inner region of wall flows,

$$l = \kappa y(1 - e^{-y^+/A^+}) \tag{18}$$

with $\kappa = 0.41$ and $A^+ = 26.0$. The quantity $(1 - e^{-y^+/A^+})$ is the Van Driest (1956) damping function used to bridge the gap between the fully turbulent region where $l = \kappa y$ and the viscous sublayer where $l \to 0$. Numerous variations on the exponential function have been utilized in order to account for effects of

Downloaded 16 Dec 2010 to 193.140.21.150. Redistribution subject to ASME license or copyright; see http://www.asme.org/terms/Terms_Use.cfm

property variations, pressure gradients, transpiration, and surface roughness. A discussion of modifications to account for several of these effects can be found in Cebeci and Smith (1974) and Moffat and Kays (1984). In the outer region,

$$l_0 = C_0 \delta_{99} \tag{19}$$

where a value of $C_0 = 0.089$ has been found to work well, but values as low as 0.085 are found in the literature. An alternative formulation for the outer region employs the form (Cebeci and Smith, 1974)

$$\mu_{T(\text{outer})} = \alpha \rho u_e \delta_k^* \tag{20}$$

where α is a function reflecting intermittency effects or Reynolds number dependence and δ_k^* is the kinematic displacement thickness defined as

$$\delta_k^* = \int_0^\infty (1 - u/u_e)\, dy \tag{21}$$

Closure for the apparent heat flux $\rho c_p \overline{v'T'}$ in the boundary-layer energy equation can be obtained by extending the Boussinesq assumption to the heat flux, $\rho c_p \overline{v'T'} = k_T(\partial T/\partial y)$, and using a turbulent Prandtl number, $\text{Pr}_T = \mu_T c_p / k_t$ to obtain the form

$$-\rho c_p \overline{v'T'} = (\rho c_p \mu_T / \text{Pr}_T)\partial T/\partial y \tag{22}$$

Experiments for wall boundary layers indicate that Pr_T varies from between $0.6 \sim 0.7$ at the outer edge of the boundary layer to about 1.5 near the wall (Moffat and Kays, 1984). Despite this, good predictions are obtained with algebraic turbulence models by letting Pr_T be a constant value of $0.9 \sim 1.0$.

Finite-difference methods easily accommodate step changes in thermal boundary conditions, permitting solutions to be obtained for conditions under which simple correlations may not be applicable. An example of this can be observed in Fig. 8 where finite-difference predictions (Pletcher, 1970) based on an algebraic turbulence model are compared with the measurements of Moretti and Kays (1965) for flow over a cooled flat plate in a favorable pressure gradient. Numerous computational studies have demonstrated that the effects of property variations are accurately accounted for through the numerical solution of the governing conservation equations, even with algebraic turbulence models. For example, the same numerical scheme and turbulence model used for the low-speed flow of Fig. 8 has been used to predict the local Stanton number and skin friction on a cooled flat plate at a free-stream Mach number of 6.8. The results are compared with the measurements of Neal (1966) and theory of Van Driest (1956) and the Spalding-Chi (1964) correlation in Fig. 9. Many more comparisons demonstrating the applicability of finite-difference solutions to the boundary-layer form of the conservation equations for internal and external convective flows can be found in the works of Cebeci and Smith (1974), Cebeci and Bradshaw (1984), Bankston and McEligot (1970), McEligot et al. (1970), Pletcher and Nelson (1974), and Malik and Pletcher (1981).

Over the last decade it has become apparent that the boundary-layer equations can be employed to compute flows containing regions of recirculation. Previously, it was generally thought that the validity of the boundary-layer approximation ended as the separation point was approached. This was because of the Goldstein (1948) singularity of the standard boundary-layer formulation at separation and because the entire boundary-layer approximation is subject to question as the boundary layer thickens and the normal component of velocity becomes somewhat larger (relative to u) than in the usual high Reynolds number flow. It is now known that the singularity can be removed by employing on "inverse" calculation procedure (Klineberg and Steger, 1974). The inverse methods differ from direct or conventional calculation methods only in the specification of boundary conditions. In

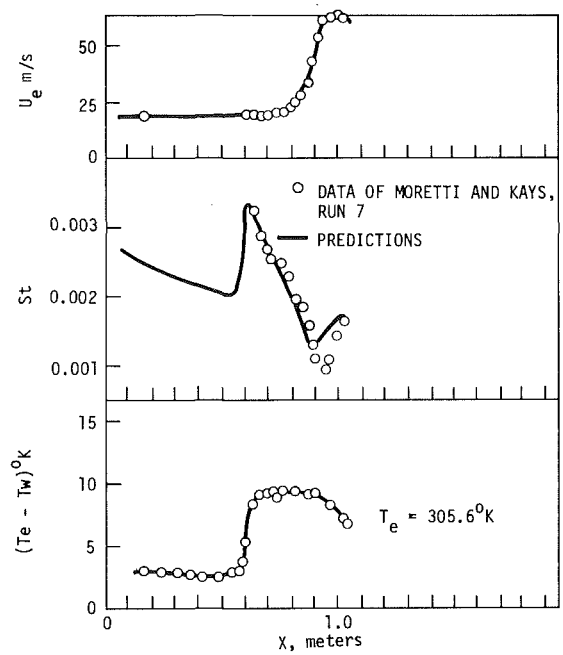

Fig. 8 Comparison of prediction of algebraic turbulence model with measurements for turbulent flow over a cooled flat plate with acceleration, from Pletcher (1970)

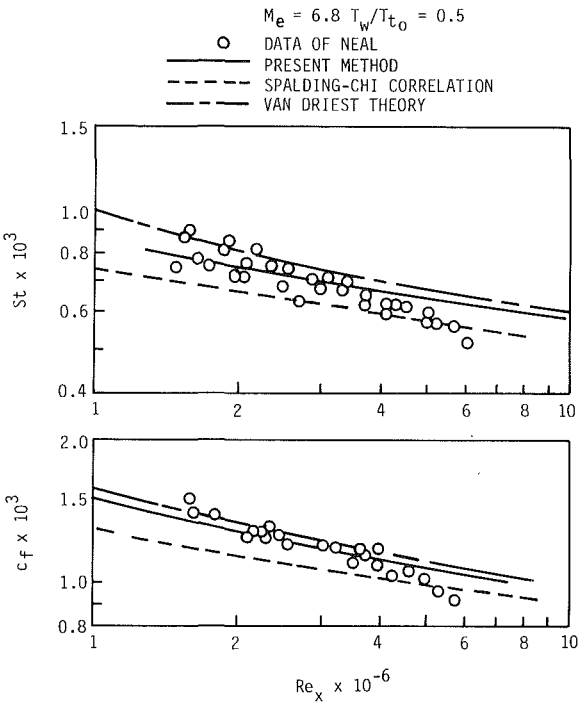

Fig. 9 Comparison of predictions of algebraic turbulence model with measurements for a cooled flat plate at Mach 6.8, from Pletcher (1971)

an inverse method, the specification of the pressure gradient is replaced by the specification of a displacement thickness or wall shear stress (Carter and Wornom, 1975; Pletcher, 1978; Cebeci, 1976). When flow reversal occurs, the treatment of the convective terms must be altered through the FLARE approximation (Reyhner and Flugge-Lotz, 1968) or the use of type-dependent differencing (Anderson et al. 1984).

Inverse boundary-layer methods have been combined with numerical procedures for inviscid flows to form viscous-inviscid interaction (or interacting boundary-layer) calculation

Downloaded 16 Dec 2010 to 193.140.21.150. Redistribution subject to ASME license or copyright; see http://www.asme.org/terms/Terms_Use.cfm

methods. Such schemes have been used to compute separated turbulent flows on airfoils and axisymmetric bodies (Cebeci and Stewartson, 1983; Carter, 1979; Carter, 1981; Veldman, 1981; Van Dalsem and Steger, 1983; Kwon and Pletcher, 1979, 1984; Lee and Pletcher, 1987) and separated flows resulting from abrupt expansions in channels formed by rearward-facing steps (Kwon and Pletcher, 1986). None of the above studies featured heat transfer, although viscous-inviscid interaction has been applied to laminar flows with heat transfer (Hall and Pletcher, 1985). The strategy is applicable to turbulent flows with heat transfer, but the problem of turbulence modeling for heat transfer becomes very difficult for separated regions (Johnson and Launder, 1982; Gooray et al., 1985; Amano et al., 1983). An inverse boundary-layer procedure without interaction has been used (Lewis and Pletcher, 1986a) to predict heat transfer for fully developed turbulent pipe flow undergoing a sudden expansion. For fully developed flows, the conventional interaction approach is not applicable because no inviscid core can be identified. Although the applicability of this noninteractive inverse boundary-layer analysis for turbulent separated has not been fully established, such an approach was observed to provide very good results for developed laminar flows undergoing a sudden expansion (Lewis and Pletcher, 1986b).

Finite-difference solutions to the boundary-layer equations only require a modest amount of computer time by present standards. The calculation can be carried out easily on a microcomputer, if necessary. When viscous-inviscid interaction is included, the computational effort increases but, depending on the algorithm and specific problem, still requires only 1/5 to 1/100 of the computational time required for solving the Reynolds-averaged Navier–Stokes equations for the same problem. No specific algorithm has emerged as superior to all others. Most of the algorithms used for inverse methods solve the boundary-layer momentum and continuity equations in a coupled manner using implicit finite-difference procedures.

Although the range of applicability of the boundary-layer mathematical model has been extended considerably in recent years, the approach does have limitations and it is often necessary to solve a more complete set of conservation equations in order to predict certain turbulent flows adequately. Examples of such flows include flows in three-dimensional corner configurations such as wing–body junctions. The main shortcomings of the interacting boundary layer model are that it cannot account for pressure variations across viscous regions and cannot correctly account for viscous forces in corner regions. The full Reynolds-averaged Navier–Stokes equations can be used for such flows, although somewhat reduced forms are sometimes adequate.

Reynolds-Averaged Navier–Stokes Equations. There has been steady improvement in numerical algorithms and computer hardware in recent years. The computer time required to perform a given calculation on the fastest available machines continues to decrease by a factor of 10 about every 8 years. It is hard to generalize about the computational effort required to solve various problems because problems vary a great deal in complexity. However, the solution of many two-dimensional steady problems using the full Navier–Stokes or Reynolds-averaged Navier–Stokes equations can be obtained in a matter of a few seconds or, at most, a few minutes on machines available to most practicing engineers. High Reynolds number flows about complex configurations, three-dimensional flows, and unsteady two- and three-dimensional flows all require considerably more computational effort. In fact, calculations are in progress today that are estimated to require hundreds of hours on the fastest supercomputers. It is perhaps good that our imaginations and ambitions continue to outpace the available computational resources.

The limiting factor in obtaining accurate numerical solutions to complex turbulent flow problems using the full Reynolds-averaged conservation equations is the turbulence modeling. This does not mean that algorithms are now perfect, but rather that advances in algorithms have been outpacing advances in turbulence modeling. The result of this is that a fair amount of uncertainty must be attached to many turbulent flow calculations, especially those involving unsteady, recirculating, or three-dimensional flows. It seems that the flows that have sufficient complexity as to require solution to the full Reynolds-averaged equations, rather than the reduced boundary layer set, are the same flows for which the turbulence modeling is the most uncertain. This is due in part to a lack of experimental data to guide development and verification of models.

A very large number of algorithms have been proposed for solving the Reynolds-averaged Navier–Stokes equations. The variations proposed must number more than one hundred. For the most part, algorithms have first been proposed and demonstrated for laminar flows and then extended to turbulent flows, usually with an algebraic turbulence model. Shock capturing methods for compressible flows usually employ a time-dependent formulation, with steady solutions being obtained as the time-asymptotic limit of the time-dependent calculation. One of the earliest widely used methods was the explicit procedure proposed by MacCormick (1969). Other early methods are discussed in the review by Peyret and Vivand (1975). The implicit central difference schemes proposed by Lindemuth and Killeen (1973), McDonald and Briley (1975), and Beam and Warming (1978) can all be classed as alternating direction implicit schemes (ADI). Implicit schemes of the ADI type have been widely used and many improvements and variations have been proposed. Additional references to explicit and implicit procedures can be found in Anderson et al. (1984). More recently, several upwind schemes have been developed for the compressible Navier–Stokes and Reynolds-averaged Navier–Stokes equations (see, for example, Thomas and Walters, 1987; Ying et al., 1986). Two classes of upwind schemes, total variation diminishing (TVD) and essentially nonoscillatory (ENO), provide especially accurate and nonoscillatory solutions near shock and contact discontinuities. The TVD and ENO formulations are relatively new and been evaluated most extensively for inviscid flows (Yee, 1987a; Harten and Osher, 1987; Van Leer, 1979; Roe, 1986) although the approach can be extended to the Navier–Stokes equations (Chakravarthy, 1985) and presumably to the Reynolds-averaged Navier–Stokes equations. Additional references on these new formulations can be found in the review by Yee (1987b).

Many of the time-dependent algorithms developed primarily for the compressible Navier–Stokes or Reynolds-averaged Navier–Stokes equations become very inefficient and/or inaccurate at low subsonic Mach numbers of approximately 0.1 or less. This has been especially well recognized for approximate factorization algorithms where it can be shown that the truncation errors associated with the factorization increase without bound for decreasing Mach number. Vanishingly small time steps are often required to maintain stability for explicit methods as the Mach number approaches zero. Some of these problems have been discussed in the papers by Choi and Merkle (1985) and Briley et al. (1983). Partly because of these difficulties, a different set of algorithms has become popular for low-speed and incompressible applications. Some of these have been shown also to be workable for compressible flows containing shock discontinuities, but it is not clear that they are as efficient in the high-speed applications as the algorithms cited above.

A number of algorithms have been developed for fully constant density (incompressible) flows. With density removed

Downloaded 16 Dec 2010 to 193.140.21.150. Redistribution subject to ASME license or copyright; see http://www.asme.org/terms/Terms_Use.cfm

from the continuity equation, a way must be found to link changes in the velocity field to changes in pressure while maintaining conservation of mass. This problem has been overcome in two dimensions by utilizing stream function–vorticity variables whereby the pressure is eliminated from the governing equations (Mallinson and DeVahl Davis, 1973). In three dimensions the stream function does not exist. Extensions to three dimensions can be made through the definition of a vector potential (see, for example, Wong and Reizes, 1986) but this introduces additional variables to be determined as part of the solution. Another approach that shows promise utilizes variables of vorticity and velocity (Gatski et al., 1982). The formulations utilizing vorticity as a variable instead of pressure have been used more frequently for laminar natural convection in enclosures than for turbulent forced convection.

The most widely used algorithms for solving Reynolds-averaged Navier-Stokes equations for incompressible turbulent forced convection problems utilize the primitive variables of velocity, pressure, and temperature. The velocity-pressure linkage has been handled in three basic ways although there have been many variations of each approach. The first of these follows a pattern set by the early work of Harlow and Welch (1965), Welch et al. (1966) and Amsden and Harlow (1970) in which the conservation equations are solved in an uncoupled or segregated fashion. The pressure is determined from the solution of a Poisson equation formed with the use of the velocities from the solutions of the momentum equations, which themselves were solved using an approximate pressure distribution. The process is iterative. The pressure and velocity fields must evolve so that mass is conserved. Details on several ways in which this procedure can be carried out have been provided by Raithby and Schneider (1979). The widely used SIMPLE (Patankar and Spalding, 1972) and SIMPLER (Patankar, 1981) algorithms are of this type as are the variations proposed by Rhie and Chow (1983), Issa (1986), and Van Doormaal and Raithby (1984).

The second strategy frequently used for the pressure–velocity coupling for steady flows follows the early work of Chorin (1967) and is known as the artificial compressibility method. In this method, a fictitious time derivative of pressure is added to the continuity equation. With an equation of state, this transforms the incompressible equations to a system that can be solved in a coupled manner by standard implicit time marching methods of the type used successfully for the compressible Navier-Stokes equations. Recent applications of such an approach have been reported by Kwak et al. (1986) and Soh (1987). Extensions of this approach to unsteady flows are discussed by Merkle and Athavale (1987).

It recently became clear that the full conservation equations for steady incompressible and low-speed compressible flows can be solved accurately in a coupled manner without using a separate Poisson equation for pressure. The use of artificial compressibility is not essential for the coupling. Examples of this can be found in the work of Galpin et al. (1985), Vanka (1985), Patankar et al. (1987), and TenPas and Pletcher (1987). The latter scheme is a compressible formulation that seems to remain efficient in the incompressible limit. Such coupled algorithms, comprising the third approach for the pressure velocity coupling, were reported (Galpin et al., 1985) to be more robust than those based on the segregated (uncoupled) strategy and comparable in execution time to the best of the segregated methods.

Parabolized Equations. To this point, numerical strategies for solving the boundary-layer equations (including viscous-inviscid interaction) and the full Reynolds-averaged Navier-Stokes equations have been discussed. In addition to these two classical sets of governing equations, several other approximate formulations, intermediate in complexity, have been found useful. Many of these are described in Anderson et al. (1984). Two such mathematical models that have been especially widely used for numerical solutions in applications are the parabolized Navier-Stokes equations (Rudman and Rubin, 1968; Lubard and Helliwell, 1974), used effectively for three-dimensional, steady, predominantly supersonic flows, and the three-dimensional parabolic procedures (Gosman and Spalding, 1971; Patankar and Spalding, 1972; Briley and McDonald, 1979) used for subsonic confined flows. Both of these formulations permit solutions to be obtained by an efficient once-through space marching procedure for steady flows having a predominant flow direction and no flow reversals.

Turbulence Modeling—General. As was pointed out previously, turbulence modeling is the most uncertain feature of numerical prediction schemes for turbulent forced convection. Because turbulent flows are very important in applications and because the closure problem is difficult, considerable effort has been devoted to the development and evaluation of turbulence models. Some progress has been made, but to date no model has been found to be both accurate and general. It seems that with enough effort, models can be developed or adjusted to account for most complicating effects, roughness, transpiration, curvature, etc., but to date, generalization of a single approach to account for all effects in all classes of shear flows has been difficult.

The models most widely used in applications have been based on the Boussinesq (1877) assumption

$$\overline{\rho u_i' u_j'} = \mu_T \left(\frac{\partial u_i}{\partial x_j} + \frac{\partial u_j}{\partial x_j} \right) - \frac{2}{3} \delta_{ij} \left(\mu_T \frac{\partial u_k}{\partial x_k} + \rho \bar{k} \right) \quad (23)$$

where $\bar{k}$ is the kinetic energy of turbulence. A boundary layer form of the Boussinesq assumption was given in a previous section in connection with an example of an algebraic turbulence model. For a suitable characteristic length scale l and velocity scale v_T, analogy with kinetic theory as well as dimensional reasoning suggests that the turbulent viscosity can be evaluated as

$$\mu_T = \rho v_T l \quad (24)$$

Closure through the Boussinesq assumption can be thought of as specifying suitable values of v_T and l. This has been attempted in numerous ways in efforts to achieve the major goals of accuracy and generality. Models based on the Boussinesq assumption are frequently called simply turbulent viscosity models. However, such models can range considerably in complexity depending on how v_T and l are evaluated.

Although experimental evidence indicates that the turbulent viscosity hypothesis (Boussinesq assumption) is reasonably valid in many flow circumstances, there are exceptions. A class of models has been developed that effect closure without this assumption. These generally require the solution of transport partial differential equations for the Reynolds stresses and are known as stress equation models or Reynolds stress models.

Turbulence models are often classified according to the number of supplementary partial differential equations that must be solved in order to supply the modeling parameters. This number ranges from zero for the simplest "algebraic" models to about 12 for the more complex Reynolds stress models (Donaldson and Rosenbaum, 1968).

Algebraic Models. An example of an algebraic model was given in a previous section. In this, following Prandtl, the characteristic velocity of turbulence was obained from $l|\partial u/\partial y|$ and l was evaluated from the local geometry of the flow, i.e., distance from the wall and the boundary-layer thickness. Algebraic models have proven to be accurate and reliable for relatively simple flows but need to be modified in order to predict flows with complicating features. Modifications to account for low Reynolds number effects have been

Downloaded 16 Dec 2010 to 193.140.21.150. Redistribution subject to ASME license or copyright; see http://www.asme.org/terms/Terms_Use.cfm

proposed by Herring and Mellor (1968), McDonald (1970), Cebeci and Smith (1974), Bushnell et al. (1976), and Pletcher (1976). Recommended adjustments to account for surface roughness can be found in the work of Cebeci and Smith (1974), Bushnell et al. (1976), McDonald and Fish (1973), Healzer et al. (1974), Adams and Hodge (1977), Christoph and Pletcher (1983), and Finson (1982). Modifications to account for wall blowing and suction have been proposed by Cebeci and Smith (1974), Pletcher (1974), Baker and Launder (1974), and Kays and Moffat (1975). Modifications to account for strong pressure gradients are discussed in Cebeci and Smith (1974), Bushnell et al. (1976), Adams and Hodge (1977), Pletcher (1974), Baker and Launder (1974), and Kays and Moffat (1975). Adjustments to algebraic models to account for effects of streamwise curvature have been discussed by several authors including Bradshaw (1973) and Johnston and Eide (1976).

The main criticism of algebraic models has been their lack of generality. The corrections and adjustments needed to accommodate special effects are mostly ad hoc and the constants in the models must be changed to handle different classes of shear flows. Closures of all levels suffer from these shortcomings to a certain degree, but some advantage in generality can be obtained through the use of certain of the more complex models. Algebraic models are still widely used, especially for the calculation of flows that already demand large computer resources due to unsteadiness, three dimensionality, or geometric complexity.

One-Half Equation Model. To make improvements over the algebraic models, it is natural to permit v_T or l to be more general functions of the flow. Models in which the model parameters vary in a manner determined by an ordinary differential equation have become known as one-half equation models. The ordinary differential equation usually results from neglecting or assuming the variation of the model parameter with one coordinate direction. These models have been quite successful in dealing with certain specific effects, often performing better than one and two-equation models for a specific class of flow. Some examples include the models that employ an ordinary differential equation for the length scale in the outer portion of the flow (McDonald and Camerata, 1968; Kreskovskey et al., 1974; McDonald and Kreskovsky, 1974; Chan, 1972; Adams and Hodge, 1977; Malik and Pletcher, 1978; Pletcher, 1978). Models have also been suggested that obtain the turbulent viscosity in the outer region by means of solving an ordinary differential equation (Reyhner, 1968; Shang and Hankey, 1975). One of the more recent one-half equation models (Johnson and King, 1985) designed especially for separating boundary layers obtains the maximum shear stress from the solution to an ordinary differential equation. These one-half equation models have been successful in accounting for effects not easily handled through algebraic models and which are not well predicted by standard forms of one and two-equation models, such as transition, relaminarization, merging shear layers, and flows with separation.

One-Equation Models. The most common one-equation model follows the suggestions of Prandtl and Kolomogorov made in the 1940s to let v_T be proportional to the square root of the turbulent kinetic energy $\bar{k}$. This has proven to be a very fruitful suggestion. The kinetic energy of turbulence is a measurable quantity and can be readily interpreted physically. A transport partial differential equation for the turbulent kinetic energy can be derived from the Navier–Stokes equations, but the terms representing diffusion, generation, and dissipation of $\bar{k}$ introduce yet additional unknowns involving higher moments of fluctuating quantities. These must also be modeled through additional assumptions. In general, the predictions of the one-equation model have only been marginally better than can be obtained from algebraic models. An exception is in certain flows with heat transfer where algebraic models indicate $k_T=0$ where $\partial u/\partial y=0$. The one-equation model correctly gives $K_T\neq 0$ where $\partial u/\partial y=0$ and results in better predictions of temperature profiles (Malik and Pletcher, 1978) in certain flows.

Two-Equation Models. Two-equation models permit the determination of both a characteristic velocity v_T and a length scale l from the solution of transport partial differential equations. One of these transport equations is invariably for the determination of k. Although a second transport equation can be developed for a length scale, the terms in this are apparently not easily modeled and better success has been achieved by solving a transport equation for a length-scale-related parameter rather than the length scale itself. One of the most widely used two-equation models is the $\bar{k}$–ϵ model first proposed by Harlow and Nakayama (1968) and further developed by Jones and Launder (1972). The parameter ϵ is the turbulence dissipation rate and is assumed to be related to the length scale through

$$\epsilon = C_D \bar{k}^{3/2}/l \tag{25}$$

The turbulent viscosity is evaluated in terms of $\bar{k}$ and ϵ by

$$\mu_T = C_\mu \rho \bar{k}^2/\epsilon \tag{26}$$

A considerable amount of work has been done with models within the two-equation framework and the literature on this topic is extensive. Some of these have been compared and discussed by Launder and Spalding (1974). The reviews by Nallasamy (1987), Patel et al. (1985), and Lakshminarayana (1986) describe many other variations and critically compare some of the model proposals. The two-equation models, particularly the $\bar{k}$–ϵ form, are widely used for engineering calculations. As with all models, weaknesses have been observed and predictions are often poor for flows with recirculation, streamline curvature, and buoyancy effects unless the constants in the model are adjusted.

Reynolds Stress Models. Although two-equation models have a reasonable degree of flexibility, they are restricted by the assumption of a scalar turbulent viscosity and the assumption that the stresses are proportional to the rate of mean strain. Reynolds stress models are free of these restrictions. Transport partial differential equations are solved for the Reynolds stresses and heat fluxes.

Keller and Friedmann (1924) appear to the first to suggest that the Reynolds stresses could be determined from a transport equation and Rotta (1951) made early contributions to the modeling of the resulting equations. The transport equations can be derived in an exact form but contain terms that must be approximated to close the system. Several closure schemes have been proposed. One that is widely used follows from the work of Launder et al. (1975). Another is based on the closure proposals of Lumley and co-workers (Lumley and Khajeh-Nouri, 1974; Lumley, 1975) and a third due to Donaldson and associates (Donaldson and Rosenbaum, 1968; Lewellen et al., 1976). The Reynolds stress models contain the greatest number of model partial differential equations and constants and can, in principle, account for effects such as buoyancy, curvature, and rotation without ad hoc adjustments. On the other hand, the determination of the optimum modeling formulation and values of constants is not easy. The computational effort required by the Reynolds stress models is significantly greater than for the less complex models and to date they have only received limited use in engineering predictions. Although the Reynolds stress models can overcome some of the deficiencies of simpler models, on balance the improvements have not been impressive, especially considering the additional computational effort required to use them. In recent years many modifications have been pro-

Downloaded 16 Dec 2010 to 193.140.21.150. Redistribution subject to ASME license or copyright; see http://www.asme.org/terms/Terms_Use.cfm

posed for these models and a number of interesting computations have been carried out. A description of many of these can be found in the reviews by Rodi (1980), Nallasamy (1987), Patel et al. (1985), and Lakshminarayana (1986),

Algebraic Reynolds Stress Models. Rodi (1976) has proposed an interesting and useful algebraic simplification to the Reynolds stress model. Rodi assumed that the transport of $\overline{u_i'u_j'}$ was proportional to the transport of $\bar{k}$ and that the proportionality factor was $\overline{u_i'u_j'}/\bar{k}$. The result is an algebraic relationship between the stresses and $\bar{k}$, ϵ, and derivatives of mean flow quantities. Transport equations are solved for $\bar{k}$ and ϵ so that the algebraic Reynolds stress model can be considered as an extended $\bar{k}$-ϵ model. For nonbuoyant thin shear layers Rodi shows that the expression for Reynolds stress becomes equivalent in form to that used in the $\bar{k}$-ϵ model, but with the C_μ being a function of the ratio of production of turbulent kinetic energy to its dissipation. For this case, the algebraic Reynolds stress model become equivalent to the $\bar{k}$-ϵ turbulent viscosity model but with a variable C_μ. The model appears attractive for accounting for effects of buoyancy, rotation, and streamline curvature in an economical fashion. It is not, however, equivalent to a full Reynolds stress model because of the additional assumptions made to convert the expressions for Reynolds stresses to algebraic form. Some applications of algebraic stress models can be found in the work of Meroney (1976), Rodi (1976), Leschziner and Rodi (1981), Pourahmadi and Humphrey (1983), and Gibson (1978).

Large Eddy and Full Simulations. Turbulent flows can be computed by numerically solving the full three-dimensional time-dependent Navier–Stokes equations without the use of turbulence models. This is known as "direct" or "full" simulation. The full simulations attempt to resolve the smallest details of the turbulent flow. Continuing advances in computer technology have made such calculations possible, but to date they have been limited to simple geometries at low Reynolds numbers. The calculations are useful more for providing information about the turbulence than for providing predictions of engineering parameters.

In large eddy simulation, only the large-scale motion that is expected to be influenced by the boundary conditions of the particular problem under study is computed. The smaller-scale motions that are assumed to be more universal are modeled. Thus, large eddy simulation represents a compromise between the direct simulation in which no model is required and solutions to the Reynolds-averaged equations that depend completely upon modeling.

The early work in simulation was carried out by meteorologists at the National Center for Atmospheric Research (Fox and Lilly, 1972). Advances have been paced largely by available computing power. For full simulations the grid spacing must be fine enough to resolve the dissipation length scale while the computational domain must be large enough to contain the largest turbulence scales and/or the physical device influencing the nature of the flow. For wall-bounded flows in particular this requires enormous computer memory. Rogallo and Moin (1984) provide an example of the requirements for simulating developed turbulent channel flow at a Reynolds number of 10^4 (based on half-width). Resolving the smallest eddies with four grid points in each direction would require 5×10^{10} grid points and 2×10^3 time steps would be needed for the flow to reach a statistical steady state, a matter of a few seconds of real flow time. Such a full simulation is beyond the capabilities of present computers. A calculation more typical of what can be achieved today would employ a $64 \times 64 \times 64$ grid and require several hours of supercomputer time. Important information results from such calculations including flow properties that cannot be measured.

Many applications of large eddy and full simulation are described in the reviews by Rogallo and Moin (1984) and Ferziger (1983). Particularly impressive are the large eddy simulation results of Moin and Kim (1982) for channel flow at a Reynolds number of 13,800. The computed velocity and pressure field was used to study the time-dependent structure of the flow. In particular, a motion picture was made simulating hydrogen bubble visualization. Frames from this film look remarkably like the hydrogen bubble experimental results illustrating aspects of the wall bursting phenomena obtained by Kim et al. (1971) and shown in Fig. 1. Very recently Kim (1987) reported direct simulations including both momentum and heat transport (passive scalar) in a channel at a Reynolds number of 3300 using a $128 \times 129 \times 128$ grid. The near-wall temperature profiles showed remarkable agreement with the formula recommended by Kader (1981) based on a consensus of experimental data.

Large eddy and direct simulation will likely play an increasingly important role in the study of turbulence in the future as computing power continues to increase. For quite some time to come, however, these methods may be more valuable as tools for scientific exploration and study than for engineering design. It is likely, however, that information obtained through direct simulations will aid in the development of better prediction methods for engineering purposes in the near term. The day may eventually come, perhaps in the twenty-first century, when it will be feasible to directly simulate most turbulent flows arising in engineering applications. At that time, turbulence modeling will become a thing of the past.

Concluding Remarks

A number of important advances have been made in recent years toward the understanding of turbulent flow phenomena. A clearer picture of the structure of turbulent flow has been made possible primarily through the development of numerous innovative experimental techniques. Steady progress has also been made in computational methods for prediction and computer hardware. Still, it is not possible to predict turbulent convective flows accurately in many configurations of practical interest. With computational resources available now and anticipated for the near future, some level of turbulence modeling will be required for mathematical closure to the convective problem. Since turbulence modeling is the weakest link in the predictive procedure, improvements in predictive capability will come mainly through the development and verification of improved turbulence models. It is not clear at present whether the best hope for reliable predictions is through the "zonal" approach in which a number of models each finely tuned for specific conditions are employed, or the development of a single general model for the Reynolds equations capable of predicting a wide range of flows. There is hope, of course, that a successful new approach, not necessarily relying on the Reynolds-averaged equations, will emerge. Efforts to incorporate more of the new information becoming available on structure into models should be encouraged.

The future outlook for the role of large eddy and direct simulation is bright. At a minimum, knowledge gained from application of this approach will contribute significantly to the understanding of structure and may be instrumental in the development of improved turbulence models and modeling approaches. It seems certain that computer technology will continue to advance rapidly and that more and more ambitious large eddy and direct simulations will be possible. Slowly this approach will likely become feasible for obtaining predictions of engineering parameters in more and more applied configurations. Increases in computer power will also permit greater attention to be given to the development of predictive schemes for unsteady and three-dimensional flows.

Downloaded 16 Dec 2010 to 193.140.21.150. Redistribution subject to ASME license or copyright; see http://www.asme.org/terms/Terms_Use.cfm

References

Adams, J. C., Jr., and Hodge, B. K., 1977, "The Calculation of Compressible, Transitional, Turbulent, and Relaminarizational Boundary Layers Over Smooth and Rough Surfaces Using an Extended Mixing Length Hypothesis," AIAA Paper No. 77-682.

Amano, R. S., Jensen, M. K., and Goel, P., 1983, "A Numerical and Experimental Investigation of Turbulent Heat Transport Downstream From an Abrupt Pipe Expansion," ASME JOURNAL OF HEAT TRANSFER, Vol. 105, pp. 862-869.

Amsden, A. A., and Harlow, F. H., 1970, "The SMAC Method: A Numerical Technique for Calculating Incompressible Fluid Flows," Los Alamos Scientific Laboratory Report LA-4370, Los Alamos, NM.

Anderson, D. A., Tannehill, J. C., and Pletcher, R. H., 1984, *Computational Fluid Mechanics and Heat Transfer*, Hemisphere, New York.

Andreapoulos, J., 1983, "Heat Transfer Measurements in a Heated Jet-Pipe Flow Issuing Into a Cross Stream," *Phys. Fluids*, Vol. 26, pp. 493-499.

Baker, R. J., and Launder, B. E., 1974, "The Turbulent Boundary Layer With Foreign Gas Injection: II—Predictions and Measurements in Severe Streamwise Pressure Gradients," *Int. J. Heat Mass Trans.*, Vol. 17, pp. 293-306.

Bakewell, H. P., and Lumley, J. L., 1967, "Viscous Sublayer and Adjacent Wall Region in Turbulent Pipe Flow," *Phys. Fluids*, Vol. 10, pp. 1880-1889.

Bankston, C. A., and McEligot, D. M., 1970, "Turbulent and Laminar Heat Transfer to Gases With Variable Properties in the Entry Region of Circular Ducts," *Int. J. Heat Mass Trans.*, Vol. 13, pp. 319-344.

Baughn, J. W., Hoffman, M. A., Takahashi, R. K., and Launder, B. E., 1984, "Local Heat Transfer Downstream of an Abrupt Expansion in a Circular Channel With Constant Wall Heat Flux," ASME JOURNAL OF HEAT TRANSFER, Vol. 106, pp. 789-796.

Beam, R. M., and Warming, R. F., 1978, "An Implicit Factored Scheme for the Compressible Navier-Stokes Equations," *AIAA J.*, Vol. 16, pp. 393-401.

Bhatti, M. S., and Shah, R. K., 1987, "Turbulent and Transition Flow Convective Heat Transfer in Ducts," *Handbook of Single-Phase Convective Heat Transfer*, Chap. 3, Wiley, New York.

Blackwelder, R. F., and Kaplan, R. E., 1976, "On the Wall Structure of the Turbulent Boundary Layer," *J. Fluid Mech.*, Vol. 76, pp. 89-112.

Blackwelder, R. F., and Eckelmann, H., 1979, "Streamwise Vortices Associated With the Bursting Phenomenon," *J. Fluid Mech.*, Vol. 94, pp. 577-594.

Blackwell, B. F., 1972, "The Turbulent Boundary Layer on a Porous Plate: An Experimental Study of the Heat Transfer Behavior With Adverse Pressure Gradients," Ph.D. Dissertation, Stanford University, CA.

Blair, M. F., 1983a, "Influence of Free-Stream Turbulence in Turbulent Boundary Layer Heat Transfer and Mean Profile Development, Part I—Experimental Data," ASME JOURNAL OF HEAT TRANSFER, Vol. 105, pp. 33-40.

Blair, M. F., 1983b, "Influence of Free-Stream Turbulence on Turbulent Boundary Layer Heat Transfer and Mean Profile Development, Part II—Analysis of Results," ASME JOURNAL OF HEAT TRANSFER, Vol. 105, pp. 41-47.

Boussinesq, J., 1877, "Essai Sur La Theorie Des Eaux Courantes," *Mem. Presentes Acad. Sci.*, Vol. 23, Paris, p. 46.

Bradbury, L. J. S., and Castro, I. P., 1971, "A Pulsed-Wire Technique for Velocity Measurement in Highly Turbulent Flow," *J. Fluid Mech.*, Vol. 49, pp. 657-691.

Bradbury, L. J. S., 1976, "Measurements With a Pulsed-Wire and a Hot-Wire Anemometer in the Highly Turbulent Wake of a Normal Flat Plate," *J. Fluid Mech.*, Vol. 77, pp. 473-497.

Bradshaw, P., 1973, "Effects of Streamline Curvature on Turbulent Flow," AGARD-AG 169.

Bradshaw, P., 1974, "Effect of Free Stream Turbulence on Turbulent Shear Layers," Aeron. Res. Council (Great Britain) Paper No. 35648.

Bradshaw, P., 1987, "Turbulent Secondary Flows," *Ann. Rev. Fluid Mech.*, Vol. 19, pp. 53-74.

Briley, W. R., and McDonald, H., 1979, "Analysis and Computation of Viscous Subsonic Primary and Secondary Flows," AIAA Paper No. 79-1453.

Briley, W. R., McDonald, H., and Shamroth, S. J., 1983, "A Low Mach Number Euler Formulation and Application to Time-Iterative LBI Schemes," *AIAA J.*, Vol. 21, pp. 1467-1469.

Brown, G. L., and Roshko, A., 1974, "On Density Effects and Large Structure in Turbulent Mixing Layers," *J. Fluid Mech.*, Vol. 64, pp. 775-816.

Buchhave, P., George, W. K., Jr., and Lumley, J. L., 1979, "The Measurement of Turbulence With the Laser-Doppler Anemometer," *Ann. Rev. Fluid Mech.*, Vol. 11, pp. 443-503.

Bushnell, D. M., Cary, A. M., Jr., and Harris, J. E., 1976, "Calculation Methods for Compressible Turbulent Boundary Layers," von Karman Institute for Fluid Dynamics Lecture Series 86, Vol. 2, Rhode-Saint-Genese, Belgium.

Cantwell, B. J., 1981, "Organized Motion in Turbulent Flow," *Ann. Rev. Fluid Mech.*, Vol. 13, pp. 457-515.

Cantwell, B. J., and Coles, D., 1983, "An Experimental Study of Entrainment and Transport in the Turbulent Near Wake of a Circular Cylinder," *J. Fluid Mech.*, Vol. 136, pp. 321-374.

Carter, J. E., and Wornom, S. F., 1975, "Forward Marching Procedure for Separated Boundary Layer Flows," *AIAA J.*, Vol. 13, pp. 1101-1103.

Carter, J. E., 1979, "A New Boundary-Layer Inviscid Iteration Technique for Separated Flow," AIAA Paper No. 79-1450.

Carter, J. E., 1981, "Viscous-Inviscid Interaction Analysis of Transonic Turbulent Separated Flow," AIAA Paper No. 81-1241.

Castleman, K. R., 1979, *Digital Image Processing*, Prentice-Hall, Englewood Cliffs, NJ.

Castro, I. P., and Cheun, B. S., 1982, "The Measurement of Reynolds Stresses With a Pulsed Hot-Wire Anemometer," *J. Fluid Mech.*, Vol. 118, pp. 41-58.

Cebeci, T., 1970, "Application of 'Exact' Turbulent-Boundary-Layer Equations as a Means of Calculating Heat and Mass Transfer in Incompressible and Compressible Flows," *Heat Transfer 1970*, Proceedings of the Fourth International Heat Transfer Conference, Vol. 2, FC 2.4.

Cebeci, T., and Smith, A. M. O., 1974, *Analysis of Turbulent Boundary Layer*, Academic Press, New York.

Cebeci, T., 1976, "Separated Flows and Their Representation by Boundary Layer Equations," Rept. ONR-CR215-234-2, Office of Naval Research, Arlington, VA.

Cebeci, T., and Stewartson, K., 1983, "On the Calculation of Separation Bubbles," *J. Fluid Mech.*, Vol. 133, pp. 287-296.

Cebeci, T., and Bradshaw, P., 1984, *Physical and Computational Aspects of Convective Heat Transfer*, Springer-Verlag, New York.

Chakravarthy, S. A., 1985, "Application of a New Class of High Accuracy TVD Schemes to the Navier-Stokes Equations," AIAA Paper No. 85-0165.

Chan, Y. Y., 1972, "Compressible Turbulent Boundary Layer Computations Based on an Extended Mixing Length Approach," *Canadian Aeron. and Space Inst. Trans.*, Vol. 5, pp. 21-27.

Charnay, G., Comte-Bellot, G., and Mathiew, J., 1971, "Development of a Turbulent Boundary Layer on a Flat Plate in an External Turbulent Flow," AGARD CP 93 Paper No. 27.

Chehroudi, B., and Simpson, R. L., 1985, "Space-Time Results for a Separating Turbulent Boundary Layer Using a Rapidly Scanning Laser Anemometer," *J. Fluid Mech.*, Vol. 160, pp. 77-92.

Chevray, R., and Tutu, N. K., 1972, "Simultaneous Measurements of Temperature and Velocity in Heated Flows," *Rev. of Scientific Instruments*, Vol. 43, pp. 1417-1421.

Choi, D., and Merkle, C. L., 1985, "Application of Time-Iterative Schemes to Incompressible Flow," *AIAA J.*, Vol. 23, pp. 1518-1524.

Chorin, A. J., 1967, "A Numerical Method for Solving Incompressible Viscous Flow Problems," *J. Computational Physics*, Vol. 2, pp. 12-26.

Christoph, G. H., and Pletcher, R. H., 1983, "Prediction of Rough-Wall Skin Friction and Heat Transfer," *AIAA J.*, Vol. 21, pp. 509-515.

Clauser, F. H., 1956, "The Turbulent Boundary Layer," *Advances in Appl. Mech.*, Vol. 4, pp. 1-51.

Coleman, H. W., 1976, "Momentum and Energy Transport in the Accelerated Fully Rough Turbulent Boundary Layer," Ph.D. Dissertation, Stanford University, CA.

Coles, D. E., 1956, "The Law of the Wake in the Turbulent Boundary Layer," *J. Fluid Mech.*, Vol. 1, pp. 191-226.

Coles, D., 1972, "A Survey of Data for Turbulent Boundary Layers With Mass Transfer," Turbulent Shear Flows, AGARD-CP-93.

Coles, D., and Wadcock, A. J., 1979, "Flying Hot-Wire Study of Two-Dimensional Turbulent Separation on a NACA 4412 Airfoil at Maximum Lift," *AIAA J.*, Vol. 17, pp. 321-329.

Comte-Bellot, G., Charnay, G., and Sabot, J., 1981, "Hot-Wire and Hot-Film Anemometry and Conditional Measurements: A Report on Euromech 132," *J. Fluid Mech.*, Vol. 110, pp. 115-128.

Cooper, T. E., Field, R. J., and Meyer, J. F., 1975, "Liquid Crystal Thermography and Its Application to the Study of Convective Heat Transfer," ASME JOURNAL OF HEAT TRANSFER, Vol. 97, pp. 442-450.

Corrino, E. R., and Brodkey, R. S., 1969, "A Visual Investigation of the Wall Region in Turbulent Flow," *J. Fluid Mech.*, Vol. 37, pp. 1-30.

Corrsin, S., 1949, "Extended Applications of the Hot-Wire Anemometer," NACA Technical Note No. 1864.

Dengel, P., Fernholz, H. H., and Vagt, J.-D., 1981, "Turbulence and Mean Flow Measurement in an Incompressible Axisymmetric Boundary Layer With Incipient Separation," *Proc. of Third Symposium on Turbulent Shear Flow*, Davis, CA.

Donaldson, C. duP., and Rosenbaum, H., 1968, "Calculation of Turbulent Shear Flows Through Closure of the Reynolds Equations by Invariant Modeling," Aero. Res. Assoc. of Princeton Report No. 127.

Durrani, T. S., and Greated, C. A., 1977, *Laser Systems in Flow Measurement*, Plenum, New York.

Durst, F., Melling, A., and Whitelaw, J. H., 1981, *Principles and Practice of Laser-Doppler Anemometry*, 2nd ed., Academic Press, London.

Eaton, J. K., Jeans, A. H., Ashjaee, J., and Johnston, J. P., 1979, "A Wall-Flow Direction Probe for Use in Separating and Reattaching Flows," ASME *J. Fluids Engr.*, Vol. 101, pp. 364-366.

Emery, A. F., Neighbors, P. K., and Gessner, F. B., 1979, "A Computational Procedure for Developing Turbulent Flow and Heat Transfer in Square Ducts," *Num. Heat Trans.*, Vol. 2, pp. 379-416.

Emery, A. F., Neighbors, P. K., and Gessner, F. B., 1980, "The Numerical Prediction of Developing Turbulent Flow and Heat Transfer in a Square Duct," ASME JOURNAL OF HEAT TRANSFER, Vol. 102, pp. 51-57.

Fabris, G., 1978, "Probe and Method for Simultaneous Measurements of True Instantaneous Temperature and Three Velocity Components in Turbulent Flow," *Rev. of Scientific Instruments*, Vol. 49, pp. 654-664.

Fergason, J. L., 1964, "Liquid Crystals," *Scientific American*, Vol. 211, No. 2, pp. 76-85.

Downloaded 16 Dec 2010 to 193.140.21.150. Redistribution subject to ASME license or copyright; see http://www.asme.org/terms/Terms_Use.cfm

Ferziger, J. H., 1983, "Higher-Level Simulations of Turbulent Flows," *Computational Methods for Turbulent, Transonic, and Viscous Flows*, J. A. Essers, ed., Hemisphere, Washington, pp. 93-182.

Finson, M. L., 1982, "A Model for Rough Wall Turbulent Heating and Skin Friction," AIAA Paper No. 82-0199.

Fletcher, L. S., Briggs, D. G., and Page, R. H., 1974, "Heat Transfer in Separated and Reattached Flows: An Annotated Review," *Israel J. Technology*, Vol. 12, pp. 236-261.

Fox, D. G., and Lilly, D. K., 1972, "Numerical Simulation of Turbulent Flows," *Rev. Geophys. Space Phys.*, Vol. 10, pp. 51-72.

Galpin, P. F., Van Doormaal, J. P., and Raithby, G. D., 1985, "Solution of the Incompressible Mass and Momentum Equations by Application of a Coupled Line Solver," *Int. J. Numer. Meth. Fluids*, Vol. 5, pp. 615-625.

Garcia, A., and Sparrow, E. M., 1987, "Turbulent Heat Transfer Downstream of a Contraction-Related, Forward-Facing Step in a Duct," ASME JOURNAL OF HEAT TRANSFER, Vol. 109, pp. 621-626.

Gatski, T. B., Grosch, C. E., and Rose, M. E., 1982, "A Numerical Study of the Two-Dimensional Navier-Stokes Equations in Vorticity-Velocity Variables," *J. Comp. Phys.*, Vol. 48, pp. 1-22.

Gibson, M. M., 1978, "An Algebraic Stress and Heat Flux Model for Turbulent Shear Flow With Streamline Curvature," *Int. J. Heat Mass Trans.*, Vol. 21, pp. 1609-1617.

Goldstein, R. J., 1978, "Some Measurement Techniques in Heat Transfer," *Heat Transfer 1978*, Proceedings of the 6th International Heat Transfer Conference, Vol. 6, pp. 495-508.

Goldstein, S., 1948, "On Laminar Boundary Layer Flow Near a Position of Separation," *Q. J. Mech. Appl. Math.*, Vol. 1, pp. 43-69.

Gonzales, R. C., and Wintz, P., 1977, *Digital Image Processing*, Addison-Wesley, Reading, MA.

Gooray, A. M., Watkins, C. B., and Aung, W., 1985, "Calculations of Heat Transfer in Redeveloping Turbulent Boundary Layers Downstream of Reattachment," ASME JOURNAL OF HEAT TRANSFER, Vol. 107, pp. 70-76.

Gosman, A. D., and Spalding, D. B., 1971, "The Prediction of Confined Three-Dimensional Boundary Layers," Salford Symposium on Internal Flows, Paper No. 19, IMechE, London.

Grass, A. J., 1971, "Structural Features of Turbulent Flow over Smooth and Rough Boundaries," *J. Fluid Mech.*, Vol. 50, pp. 233-255.

Hall, E. J., and Pletcher, R. H., 1985, "Application of a Viscous-Inviscid Interaction Procedure to Predict Separated Flows With Heat Transfer," ASME JOURNAL OF HEAT TRANSFER, Vol. 107, pp. 557-563.

Hall, E. L., 1979, *Computer Image Processing and Recognition*, Academic Press, Toronto.

Hancock, P. E., 1980, "Effect of Free-Stream Turbulence on Turbulent Boundary Layers," Ph.D. Dissertation, Imperial College, London University.

Harlow, F. H., and Welch, J. E., 1965, "Numerical Calculation of Time-Dependent Viscous Incompressible Flow of Fluid With a Free Surface," *Phys. Fluids*, Vol. 8, pp. 2182-2189.

Harlow, F. H., and Nakayama, P. I., 1968, "Transport of Turbulence Energy Decay Rate," Loss Alamos Scientific Laboratory Report LA-3854, Los Alamos, NM.

Harten, A., and Osher, S., 1987, "Uniformly High-Order Accurate Nonoscillatory Schemes I," *SIAM J. Num. Analysis*, Vol. 24, pp. 279-309.

Hashida, M., and Nagano, Y., 1978, "Simultaneous Measurements of Velocity and Temperature in Nonisothermal Flows," ASME JOURNAL OF HEAT TRANSFER, Vol. 100, pp. 340-345.

Hauf, W., and Grigull, U., 1970, "Optical Methods in Heat Transfer," *Advances in Heat Transfer*, Vol. 6, pp. 134-366.

Healzer, J. M., Moffat, R. J., and Kays, W. M., 1974, "The Turbulent Boundary Layer on a Rough Porous Plate: Experimental Heat Transfer With Uniform Blowing," Report No. HMT-18, Dept. of Mech. Engr., Stanford University, CA.

Herring, H. J., and Mellor, G. L., 1968, "A Method of Calculating Compressible Turbulent Boundary Layers," NASA CR-1144.

Hesselink, L., 1988, "Digital Image Processing in Flow Visualization," *Ann. Rev. Fluid Mech.*, Vol. 20, pp. 421-85.

Hill, J. A. F., Voisinet, R. L. P., and Wagner, D. A., 1980, "Measurements of Surface Roughness Effects on Heat Transfer to Slender Cones at Mach 10," AIAA Paper No. 80-0345.

Hippensteele, S. A., Russell, L. M., and Stepka, F. S., 1981, "Evaluation of a Method for Heat Transfer Measurements and Thermal Visualization Using a Composite of a Heater Element and Liquid Crystals," NASA TM 81639.

Hirata, M., Tanaka, H., Kawamura, H., and Kasagi, N., 1982, "Heat Transfer in Turbulent Flows," *Heat Transfer 1982*, Proceedings of the 7th International Heat Transfer Conference, Vol. 1, pp. 31-57.

Holden, M. S., 1982, "Experimental Studies of Surface Roughness, Entropy Swallowing and Boundary Layer Transition Effects on Skin Friction and Heat Transfer Distribution in High Speed Flows," AIAA Paper No. 82-0034.

Huffman, G. D., Zimmerman, D. R., and Bennet, W. A., 1972, "The Effect of Free-Stream Turbulence Level in Turbulent Boundary Layer Behavior," AGARD AG 164, pp. 91-115.

Hwang, C.-L., and Fan, L.-T., 1964, "Finite Difference Analysis of Forced Convection Heat Transfer in the Entrance Region of a Flat Rectangular Duct," *Appl. Sci. Res.*, Sec. A, Vol. 13, pp. 401-422.

Issa, R. I., 1986, "Solution of the Implicitly Discretised Fluid Flow Equations by Operator Splitting," *J. Comp. Phys.*, Vol. 62, pp. 40-65.

Jeromin, L. O. F., 1970, "The Status of Research in Turbulent Boundary Layers with Fluid Injection," *Prog. Aero. Sci.*, Vol. 10, pp. 55-189.

Jaroch, M., 1985, "Development and Testing of Pulsed-Wire Probes for Measuring Fluctuating Quantities in Highly Turbulent Flows," *Exp. Fluids*, Vol. 3, pp. 315-322.

Jeans, A. H., and Johnston, J. P., 1982, "The Effects of Streamwise Concave Curvature on Turbulent Boundary Layer Structure," Rept. No. MD-40, Dept. of Mechanical Engr., Stanford University, CA.

Johnson, D. A., and King, L. S., 1985, "A Mathematically Simple Turbulence Closure Model for Attached and Separated Turbulent Boundary Layers," *AIAA J.*, Vol. 23, pp. 1684-1692.

Johnson, R. W., and Launder, B. E., 1982, Discussion of "On the Calculation of Turbulent Heat Transport Downstream From an Abrupt Expansion," *Num. Heat Trans.*, Vol. 5, pp. 493-496.

Johnston, J. P., and Eide, S. A., 1976, "Turbulent Boundary Layers on Centrifugal Compressor Blades: Prediction of the Effects of Surface Curvature and Rotation," ASME *J. Fluids Eng.*, Vol. 98, pp. 374-381.

Jones, W. P., and Launder, B. E., 1972, "The Prediction of Laminarization With a Two-Equation Model of Turbulence," *Int. J. Heat Mass Trans.*, Vol. 15, pp. 301-314.

Kader, B. A., and Yaglom, A. K., 1972, "Heat and Mass Transfer Laws for Fully Turbulent Wall Flows," *Int. J. Heat Mass Trans.*, Vol. 15, pp. 2329-2351.

Kader, B. A., 1981, "Temperature and Concentration Profiles in Fully Turbulent Boundary Layers," *Int. J. Heat Mass Trans.*, Vol. 24, pp. 1541-1544.

Kakac, S., 1987, "The Effects of Temperature-Dependent Fluid Properties on Convective Heat Transfer," *Handbook of Single-Phase Convective Heat Transfer*, Chap. 18, Wiley, New York.

Kays, W. M., and Crawford, M. E., 1980, *Convective Heat and Mass Transfer*, 2nd ed., McGraw-Hill, New York.

Kays, W. M., and Moffat, R. J., 1975, "The Behavior of Transpired Turbulent Boundary Layers," *Studies in Convection: Theory, Measurements, and Applications*, Vol. 1, Academic Press, New York, pp. 223-319.

Kearney, D. W., 1970, "The Turbulent Boundary Layer: Experimental Heat Transfer With Strong Favorable Pressure Gradients and Blowing," Ph.D. Dissertation, Stanford University, CA.

Keller, L., and Friedmann, A., 1924, "Differential gleichungen fur die turbulente bewegung einer kompressibleen flussigkeit," *Proc. First Intern. Congress Appl. Mech.*, Delft, pp. 395-405.

Kim, H. T., Kline, S. J., and Reynolds, W. C., 1971, "The Production of Turbulence Near a Smooth Wall in a Turbulent Boundary Layer," *J. Fluid Mech.*, Vol. 50, pp. 133-160.

Kim, J., 1987, "Investigation of Heat and Momentum Transport in Turbulent Flows Via Numerical Simulations," *Proc. 2nd Symp. on Transport Phenomena in Turbulent Flows*, Tokyo, pp. 707-721.

Klebanoff, P. S., 1954, "Characteristics of Turbulence in a Boundary Layer With Zero Pressure Gradient," NACA TN 3178.

Kleinstein, G., 1967, "Generalized Law of the Wall and Eddy-Viscosity Model for Wall Boundary Layers," *AIAA J.*, Vol. 5, pp. 1402-1407.

Kline, S. J., and Runstadler, P. W., 1959, "Some Preliminary Results of Visual Studies of the Flow Model of the Wall Layers of the Turbulent Boundary Layer," ASME *J. Appl. Mech.*, Vol. 26, pp. 166-170.

Kline, S. J., and Reynolds, W. C., Schraub, F. A., and Runstadler, P. W., 1967, "The Structure of Turbulent Boundary Layers," *J. Fluid Mech.*, Vol. 30, pp. 741-773.

Klineberg, J. M., and Steger, J. L., 1974, "On Laminar Boundary Layer Separation," AIAA Paper No. 74-94.

Kovasznay, L. S. G., 1942, "Some Improvements in Hot-Wire Anemometry," *Hung. Acta Phys.*, Vol. 1, No. 13, pp. 25-51.

Kreskovskey, J. P., Shamroth, S. J., and McDonald, H., 1974, "Parametric Study of Relaminarization of Turbulent Boundary Layers in Nozzle Walls," NASA CR-2370.

Kwak, D., Chang, J. L. C., Shanks, S. P., and Chakravarthy, S. R., 1986, "An Incompressible Navier-Stokes Flow Solver in Three-Dimensional Curvilinear Coordinate System Using Primitive Variables," *AIAA J.*, Vol. 24, pp. 390-396.

Kwon, O. K., and Pletcher, R. H., 1979, "Prediction of Incompressible Separated Boundary Layers Including Viscous-Inviscid Interaction," ASME *J. Fluids Eng.*, Vol. 101, pp. 466-472.

Kwon, O. K., and Pletcher, R. H., 1984, "Prediction of Subsonic Separation Bubbles on Airfoils by Viscous-Inviscid Interaction," *Numerical and Physical Aspects of Aerodynamic Flows*, Vol. II, T. Cebeci, ed., Springer-Verlag, New York, pp. 163-172.

Kwon, O. K., and Pletcher, R. H., 1986, "A Viscous-Inviscid Interaction Procedure Part 2: Application to Turbulent Flow Over a Rearward-Facing Step," ASME *J. Fluids Eng.*, Vol. 108, pp. 71-75.

Lakshminarayana, B., 1986, "Turbulence Modeling for Complex Shear Flows," *AIAA J.*, Vol. 24, pp. 1900-1917.

LaRue, J. C., Deaton, T., and Gibson, C. H., 1975, "Measurement of High Frequency Turbulent Temperature," *Rev. Sci. Instr.*, Vol. 46, pp. 757-764.

Laufer, J., 1954, "The Structure of Turbulence in Fully Developed Pipe Flow," NACA TN 2954.

Laufer, J., 1975, "New Trends in Experimental Turbulence Research," *Ann. Rev. Fluid Mech.*, Vol. 7, pp. 307-326.

Launder, B. E., Reece, G. J., and Rodi, W., 1975, "Progress in the Development of a Reynolds Stress Closure," *J. Fluid Mech.*, Vol. 68, pp. 537-566.

Launder, B. E., and Ying, W. M., 1973, "Prediction of Flow and Heat Transfer in Ducts of Square Cross Section," *Heat and Fluid Flow*, Vol. 3, pp. 115-121.

Downloaded 16 Dec 2010 to 193.140.21.150. Redistribution subject to ASME license or copyright; see http://www.asme.org/terms/Terms_Use.cfm

Lauterborn, W., and Vogel, A., 1984, "Modern Optical Techniques in Fluid Mechanics," *Ann. Rev. Fluid Mech.*, Vol. 16, pp. 223-244.

Lee, D., and Pletcher, R. H., 1987, "A Simultaneous Viscous-Inviscid Interaction Calculation Procedure for Transonic Turbulent Flows," AIAA Paper No. 87-1155.

Leschziner, M. A., and Rodi, W., 1981, "Calculation of Annular and Twin Parallel Jets Using Various Discretization Schemes and Turbulence Model Variations," ASME *J. Fluids Eng.*, Vol. 103, pp. 352-360.

Lewellen, W. S., Teske, M., and Donaldson, C. duP., 1976, "Variable Density Flows Computed by a Second-Order Closure Description of Turbulence," *AIAA J.*, Vol. 14, pp. 382-387.

Lewis, J. P., and Pletcher, R. H., 1986a, "A Boundary-Layer Computational Model for Predicting the Flow and Heat Transfer in Sudden Expansions," Technical Report HTL-41, CFD-14, ISU-ERI-Ames-87018.

Lewis, J. P., and Pletcher, R. H., 1986b, "Limitations of the Boundary-Layer Equations for Predicting Laminar Symmetric Sudden Expansion Flows," ASME *J. Fluids Eng.*, Vol. 108, pp. 208-213.

Ligrani, P. M., 1979, "The Thermal and Hydrodynamic Behavior of Thick, Rough-Wall, Turbulent Boundary Layers," Ph.D. Dissertation, Stanford University, CA.

Lindemuth, I., and Killeen, J., 1973, "Alternating Direction Implicit Techniques for Two-Dimensional Magnetohydrodynamics Calculations," *J. Comp. Phys.*, Vol. 13, pp. 181-208.

Lubard, S. C., and Helliwell, W. S., 1974, "Calculation of the Flow on a Cone at High Angle of Attack," *AIAA J.*, Vol. 12, pp. 965-974.

Lumley, J. L., and Khajeh-Nouri, B., 1974, "Computation of Turbulent Transport," *Adv. in Geophys.*, A18, pp. 169-192.

Lumley, J. L., 1975, "Prediction Methods for Turbulent Flows," Lecture Series 76, Von Karman Institute, Belgium.

MacCormack, R. W., 1969, "The Effect of Viscosity in Hypervelocity Impact Cratering," AIAA Paper No. 69-354.

Malik, M. R., and Pletcher, R. H., 1978, "Computation of Annular Turbulent Flows With Heat Transfer and Property Variations," *Heat Transfer 1978*, Proceedings of the Sixth International Heat Transfer Conference, Vol. 2, Hemisphere, pp. 537-542.

Malik, M. R., and Pletcher, R. H., 1981, "A Study of Some Turbulence Models for Flow and Heat Transfer in Ducts of Annular Cross Section," ASME JOURNAL OF HEAT TRANSFER, Vol. 103, pp. 146-152.

Mallinson, G. D., and deVahl Davis, 1973, "The Method of False Transient for the Solution of Coupled Elliptic Equations," *J. Comp. Phys.*, Vol. 12, pp. 435-461.

McDonald, H., and Camerata, F. J., 1968, "An Extended Mixing Length Approach for Computing the Turbulent Boundary Layer Development," *Proc. Computation of Turbulent Boundary Layers 1968 AFOSR-IFT*, Stanford Conference Vol. 1, Stanford University, CA, pp. 83-98.

McDonald, H., 1970, "Mixing Length and Kinematic Eddy Viscosity in a Low Reynolds Number Boundary Layer," United Aircraft Research Laboratory Report J2 14453-1, East Hartford, CT.

McDonald, H., and Fish, R. W., 1973, "Practical Calculations of Transitional Boundary Layers," *Int. J. Heat Mass Trans.*, Vol. 16, pp. 1729-1744.

McDonald, H., and Kreskovsky, J. P., 1974, "Effect of Free Stream Turbulence on the Turbulent Boundary Layer," *Int. J. Heat Mass Trans.*, Vol. 17, pp. 705-716.

McDonald, H., and Briley, W. R., 1975, "Three-Dimensional Supersonic Flow of a Viscous or Inviscid Gas," *J. Comp. Phys.*, Vol. 19, pp. 150-178.

McEligot, D. M., Smith, S. B., and Bankston, C. A., 1970, "Quasi-Developed Turbulent Pipe Flow With Heat Transfer," ASME JOURNAL OF HEAT TRANSFER, Vol. 92, pp. 641-650.

Meier, H. V., and Kreplin, H. P., 1980, "Influence of Freestream Turbulence on Boundary Layer Development," *AIAA J.*, Vol. 18, pp. 11-15.

Meroney, R. N., 1976, "An Algebraic Stress Model for Stratified Turbulent Shear Flows," *Computers and Fluids*, Vol. 4, pp. 93-107.

Merkle, C. L., and Athavale, M., 1987, "Time-Accurate Unsteady Incompressible Flow Algorithms Based on Artificial Compressibility," AIAA Paper No. 87-1137.

Mitchell, J. E., and Hanratty, T. J., 1966, "A Study of Turbulence at a Wall Using an Electrochemical Wall Shear-Stress Meter," *J. Fluid Mech.*, Vol. 26, pp. 199-221.

Mizushina, T., 1971, "The Electrochemical Method in Transport Phenomena," *Advances in Heat Transfer*, Vol. 7, pp. 87-161.

Moffat, R. J., and Kays, W. M., 1968, "The Turbulent Boundary Layer on a Porous Plate: Experimental Heat Transfer With Uniform Blowing and Suction," *Int. J. Heat Mass Transfer*, Vol. 11, pp. 1547-1560.

Moffat, R. J., Healzer, J. M., and Kays, W. M., 1978, "Experimental Heat Transfer Behavior of a Turbulent Boundary Layer on a Rough Surface With Blowing," ASME JOURNAL OF HEAT TRANSFER, Vol. 100, pp. 134-142.

Moffat, R. J., and Kays, W. M., 1984, "A Review of Turbulent-Boundary-Layer Heat Transfer Research at Stanford, 1958-1983," *Adv. in Heat Transfer*, Vol. 16, pp. 241-365.

Moin, P., and Kim, J., 1982, "Numerical Investigation of Turbulent Channel Flow," *J. Fluid Mech.*, Vol. 188, pp. 341-377.

Mollo-Christensen, E., 1971, "Physics of Turbulent Flow," *AIAA J.*, Vol. 9, pp. 1217-1228.

Moretti, P. M., and Kays, W. M., 1965, "Heat Transfer to a Turbulent Boundary Layer With Varying Free-Stream Velocity and Varying Surface Temperature—An Experimental Study," *Int. J. Heat Mass Trans.*, Vol. 8, pp. 1187-1202.

Nallasamy, M., 1987, "Turbulence Models and Their Applications to the Prediction of Internal Flows: A Review," *Computers and Fluids*, Vol. 15, pp. 151-194.

Neal, L., Jr., 1966, "A Study of the Pressure, Heat Transfer, and Skin Friction on Sharp and Blunt Flat Plates at Mach 6.8," NASA TN-D-3312.

Newman, J. S., 1973, *Electrochemical Systems*, Prentice-Hall, Englewood Cliffs, NJ.

Nychas, S. G., Hershey, H. C., and Brodkey, R. S., 1973, "A Visual Study of Turbulent Shear Flow," *J. Fluid Mech.*, Vol. 61, pp. 513-540.

Orlando, A. F., Moffat, R. J., and Kays, W. M., 1974, "Heat Transfer in Turbulent Flows Under Mild and Strong Adverse Pressure Gradient Conditions for an Arbitrary Variation of Wall Temperature," *Proc. of the 24th Heat Transfer and Fluid Mechanics Institute*, pp. 91-104.

Patel, V. C., Rodi, W., and Scheuerer, 1985, "Turbulence Models for Near-Wall and Low Reynolds Number Flows: A Review," *AIAA J.*, Vol. 23, pp. 1308-1319.

Patankar, S. V., and Spalding, D. B., 1967, "A Finite-Difference Procedure for Solving the Equations of the Two-Dimensional Boundary Layer," *Int. J. Heat Mass Trans.*, Vol. 10, pp. 1389-1411.

Patankar, S. V., and Spalding, D. B., 1972, "A Calculation Procedure for Heat, Mass and Moment Transfer in Three-Dimensional Parabolic Flows," *Int. J. Heat Trans.*, Vol. 15, pp. 1787-1806.

Patankar, S. V., 1981, "A Calculation Procedure for Two-Dimensional Elliptic Situations," *Num. Heat Trans.*, Vol. 4, pp. 409-425.

Patankar, S. V., Karki, K. C., and Mongia, H. C., 1987, "Development and Evaluation of Improved Numerical Schemes for Recirculating Flows," AIAA Paper No. 87-0061.

Perry, A. E., 1982, *Hot-Wire Anemometry*, Clarendon Press, Oxford.

Peyret, R., and Viviand, H., 1975, "Computation of Viscous Compressible Flows Based on the Navier-Stokes Equations," AGARD-AG-212.

Pimenta, M. M., Moffat, R. J., and Kays, W. M., 1975, "The Turbulent Boundary Layer: An Experimental Study of the Transport of Momentum and Heat With the Effect of Roughness," Report No. HMT-21, Dept. of Mech. Engr., Stanford University, CA.

Pimenta, M. M., Moffat, R. J., and Kays, W. M., 1979, "The Structure of a Boundary Layer on a Rough Wall With Blowing and Heat Transfer," ASME JOURNAL OF HEAT TRANSFER, Vol. 101, pp. 193-198.

Pletcher, R. H., 1971, "On a Calculation Method for Compressible Turbulent Boundary Layer Flows With Heat Transfer," AIAA Paper No. 71-165.

Pletcher, R. H., 1974, "Prediction of Transpired Turbulent Boundary Layers," ASME JOURNAL OF HEAT TRANSFER, Vol. 96, pp. 89-94.

Pletcher, R. H., and Nelson, R. M., 1974, "Heat Transfer to Laminar and Turbulent Flow in Tubes With Variable Fluid Properties," *Heat Transfer 1974*, Proceedings of the Fifth International Heat Transfer Conference, Vol. 2, pp. 146-150.

Pletcher, R. H., 1976, "Prediction of Turbulent Boundary Layers at Low Reynolds Numbers," *AIAA J.*, Vol. 14, pp. 696-698.

Pletcher, R. H., 1978, "Prediction of Incompressible Turbulent Separating Flow," ASME *J. Fluids Eng.*, Vol. 100, pp. 427-433.

Pletcher, R. H., and Patankar, S. V., 1983, "Computers in Analysis and Design," *Mechanical Engineering*, Vol. 105, No. 6, pp. 73-79.

Pletcher, R. H., 1970, "On a Solution for Turbulent Layer Flows With Heat Transfer, Pressure Gradients, and Wall Blowing and Suction," *Heat Transfer 1970*, Proceedings of the Fourth International Heat Transfer Conference, Vol. 2, FC 2.9.

Pourahmadi, F., and Humphrey, J. A. C., 1983, "Prediction of Curved Channel Flow With an Extended k-ϵ Model of Turbulence," *AIAA J.*, Vol. 21, pp. 1365-1373.

Ragallo, R. S., and Moin, P., 1984, "Numerical Simulation of Turbulent Flows," *Ann. Rev. Fluid Mech.*, Vol. 16, pp. 99-137.

Raithby, G. D., and Schneider, G. E., 1979, "Numerical Solution of Problems in Incompressible Fluid Flow: Treatment of the Velocity-Pressure Coupling," *Num. Heat Trans.*, Vol. 2, pp. 417-440.

Rao, K. K., Narashimha, R., and Badri Narayanan, M. A., 1971, "The 'Bursting' Phenomenon in a Turbulent Boundary Layer," *J. Fluid Mech.*, Vol. 48, pp. 339-352.

Reyhner, T. A., and Flugge-Lotz, I., 1968, "The Interaction of a Shock Wave With a Laminar Boundary Layer," *Int. J. Non-Linear Mech.*, Vol. 3, pp. 173-199.

Rhie, C. M., and Chow, W. L., 1983, "A Numerical Study of the Turbulent Flow Past an Isolated Airfoil With Trailing Edge Separation," *AIAA J.*, Vol. 21, pp. 1525-1532.

Rodi, W., 1976, "A New Algebraic Relation for Calculating the Reynolds Stresses," *ZAMM*, Vol. 56, T219-T221.

Rodi, W., 1980, *Turbulence Models and Their Application in Hydraulics—A State of the Art Review*, International Association for Hydraulic Research, Delft.

Roe, P. L., 1986, "Characteristic-Based Schemes for the Euler Equations," *Ann. Rev. Fluid Mech.*, Vol. 18, pp. 337-365.

Roshko, A., 1976, "Structure of Turbulent Shear Flows: A New Look," *AIAA J.*, Vol. 14, pp. 1349-1357.

Rotta, J., 1951, "Statische Theorie nichthomogener Turbulenz," *Z. Phys.*, Vol. 129, pp. 547-572.

Ruderich, R., and Fernholz, H. H., 1986, "An Experimental Investigation of a Turbulent Shear Flow With Separation, Reverse Flow, and Reattachment," *J. Fluid Mech.*, Vol. 163, pp. 283-322.

Downloaded 16 Dec 2010 to 193.140.21.150. Redistribution subject to ASME license or copyright; see http://www.asme.org/terms/Terms_Use.cfm

Rudman, S., and Rubin, S. G., 1968, "Hypersonic Flow Over Slender Bodies With Sharp Leading Edges," *AIAA J.*, Vol. 6, pp. 1883–1889.

Shang, J. S., and Hankey, W. L., Jr., "Supersonic Turbulent Separated Flows Utilizing the Navier-Stokes Equations," *Flow Separation*, AGARD-CCP-168.

Shaw, D. A., and Hanratty, T. J., 1977a, "Turbulent Mass Transfer to a Wall for Large Schmidt Numbers," *AIChE J.*, Vol. 23, pp. 28–37.

Shaw, D. A., and Hanratty, T. J., 1977b, "Influence of Schmidt Number on the Fluctuations of Turbulent Mass Transfer to a Wall," *AIChE J.*, Vol. 23, pp. 160–169.

Sherif, S. A., and Pletcher, R. H., 1986, "Temperature Correction for the Output Response of a Constant-Temperature Hot-Film Anemometer in Nonisothermal Flows With a Strong Property-Temperature Dependence," *Heat Transfer 1986*, Proceedings of the Eighth International Heat Transfer Conference, Vol. 2, pp. 549–554.

Simon, T., Johnston, J. P., Kays, W. M., and Moffat, R. J., 1980, "Turbulent Boundary Layer Heat Transfer Experiments: Convex Curvature Effects Including Introduction and Recovery," Rept. No. HMT-32, Dept. of Mech. Engr., Stanford University, CA.

Simonich, J. C., and Bradshaw, P., 1978, "Effect of Free-Stream Turbulence on Heat Transfer Through a Turbulent Boundary Layer," ASME JOURNAL OF HEAT TRANSFER, Vol. 100, pp. 671–677.

Simonich, J. C., and Moffat, R. J., 1982, "A New Technique for Mapping Heat Transfer Coefficient Contours," *Rev. Sci. Instr.*, Vol. 53, pp. 678–683.

Simpson, R. L., 1985, "Two-Dimensional Turbulent Separated Flow," AGARD-AG-287, Vol. 1.

Sirkar, K. K., and Hanratty, T. J., 1970, "Relation of Turbulent Mass Transfer to a Wall at High Schmidt Numbers to the Velocity Field," *J. Fluid Mech.*, Vol. 44, pp. 589–603.

Sogin, H. H., 1958, "Sublimination From Disks to Air Streams Flowing Normal to Their Surfaces," *Trans. ASME*, Vol. 80, pp. 61–71.

Soh, W. Y., 1987, "Time-Marching Solution of Incompressible Navier-Stokes Equations for Internal Flow," *J. Comp. Phys.*, Vol. 70, pp. 232–252.

Spalding, D. B., 1961, "A Single Formula for the Law of the Wall," ASME *J. Appl. Mech.*, Vol. 28, pp. 455–57.

Spalding, D. B., and Chi, S. W., 1964, "The Drag on a Compressible Turbulent Boundary Layer on a Smooth Flat Plate With and Without Heat Transfer," *J. Fluid Mech.*, Vol. 18, pp. 117–143.

Squire, L. C., 1970, "Further Experimental Investigations of Compressible Turbulent Boundary Layers With Air Injection," Aeronaut. Res. Council (Great Britain) Rep. and Memo. No. 3627.

TenPas, P. W., and Pletcher, R. H., 1987, "Solution of the Navier-Stokes Equations for Subsonic Flow Using a Coupled Space-Marching Method," AIAA Paper No. 87-1173.

Thielbahr, W. H., 1969, "The Turbulent Boundary Layer: Experimental Heat Transfer With Blowing, Suction, and Favorable Pressure Gradient," Ph.D. Dissertation, Stanford University, CA.

Thomann, H., 1968, "Effect of Streamwise Wall Curvature on Heat Transfer in a Turbulent Boundary Layer," *J. Fluid Mech.*, Vol. 33, pp. 283–292.

Thomas, J. L., and Walters, R. W., 1987, "Upwind Relaxation Algorithms for the Navier-Stokes Equations," *AIAA J.*, Vol. 25, pp. 527–534.

Thompson, B. E., and Whitelaw, J. H., 1984, "Flying Hot-Wire Anemometry," *Exp. Fluids*, Vol. 2, pp. 47–56.

Van Dalsem, W. R., and Steger, J. L., 1983, "Finite-Difference Simulation of Transonic Separated Flow Using Full Potential-Boundary Layer Interaction Approach," AIAA Paper No. 83-1689.

Van Doormaal, J. P., and Raithby, G. D., 1984, "Enchancements of the SIMPLE Method for Predicting Incompressible Fluid Flows," *Num. Heat Trans.*, Vol. 7, pp. 147–163.

Van Driest, E. R., 1956, "On Turbulent Flow Near a Wall," *J. Aero. Sci.*, Vol. 23, pp. 1007–1011.

Vanka, S. P., 1985, "Block Implicit Calculation of Steady Turbulent Recirculating Flows," *Int. J. Heat Mass Trans.*, Vol. 28, pp. 2093–2103.

van Leer, B., 1979, "Towards the Ultimate Conservation Difference Scheme V, A Second-Order Sequel to Godunov's Method," *J. Comp. Phys.*, Vol. 32, pp. 101–136.

Veldman, A. E. P., 1981, "New, Quasi-Simultaneous Method to Calculate Interacting Boundary Layers," *AIAA J.*, Vol. 19, pp. 79–85.

Vogel, J. C., and Eaton, J. K., 1985, "Combined Heat Transfer and Fluid Dynamics Measurements Downstream of a Backward-Facing Step," ASME JOURNAL OF HEAT TRANSFER, Vol. 107, pp. 922–929.

Voisinet, R. L. P., 1979, "Influence of Roughness and Blowing on Compressible Turbulent Boundary Layer Flow," Naval Surface Weapons Center TR 79-153, Silver Spring, MD.

Walker, M. D., and Maxey, M. R., 1985, "A Whirling Hot-Wire Anemometer With Optical Data Transmission," *J. Phys. E.: Sci. Instru.*, Vol. 18, pp. 516–521.

Wallace, J. M., Eckelmann, H., and Brodkey, R. S., 1974, "The Wall Region in Turbulent Shear Flow," *J. Fluid Mech.*, Vol. 54, pp. 39–48.

Watmuff, J. H., Perry, A. E., and Chong, M. S., 1983, "A Flying Hot-Wire System," *Exp. Fluids*, Vol. 1, pp. 63–71.

Welch, J. E., Harlow, F. H., Shannon, J. P., and Daly, B. J., 1966, "The MAC Method," Los Alamos Scientific Laboratory Report LA-3425, Los Alamos, NM.

Whitten, D. G., 1967, "The Turbulent Boundary Layer on a Porous Plate: Experimental Heat Transfer With Variable Suction, Blowing and Surface Temperature," Ph.D. Dissertation, Stanford University, CA.

Willmarth, W. W., and Lu, S. S., 1972, "Structure of the Reynolds Stress Near the Wall," *J. Fluid Mech.*, Vol. 55, pp. 65–92.

Willmarth, W. W., 1975, "Structure of Turbulence in Boundary Layers," *Advances in Appl. Mech.*, Vol. 15, pp. 159–254.

Wong, A. K., and Reizes, J. A., 1986, "The Vector Potential in the Numerical Solution of Three-Dimensional Fluid Dynamics Problems in Multiply Connected Regions," *J. Comp. Phys.*, Vol. 62, pp. 124–142.

Yee, H. C., 1987a, "Construction of Explicit and Implicit Symmetric TVD Schemes and Their Applications," *J. Comp. Phys.*, Vol. 68, pp. 151–179.

Yee, H. C., 1987b, "Upwind and Symmetric Shock Capturing Schemes," NASA TM 89464.

Ying, S. X., Steger, J. L., and Schiff, L. B., 1986, "Numerical Simulation of Unsteady Viscous, High-Angle-of-Attack Flows Using a Partially Flux-Split Algorithm," AIAA Paper No. 86-2179.

Zemanick, P. P., and Dougall, R. S., 1970, "Local Heat Transfer Downstream of Abrupt Circular Channel Expansion," ASME JOURNAL OF HEAT TRANSFER, Vol. 92, pp. 53–60.

Downloaded 16 Dec 2010 to 193.140.21.150. Redistribution subject to ASME license or copyright; see http://www.asme.org/terms/Terms_Use.cfm

Heat Transfer in Fluid Flows Which Do Not Follow the Contour of Bounding Walls

E. M. Sparrow
Division Director,
Chemical, Biochemical, and Thermal Engineering,
National Science Foundation,
Washington, DC 20550

This paper is dedicated to the generations of students who honored me by their willingness to join their hearts and minds with mine, and to my wife who taught all of us that it is heart, rather than mind, that makes the world go 'round. The paper showcases a highly personalized style of research characterized by intense human involvement and a minimum of material resources, and exemplifies the notion that "less is more." The technical content of the paper is a collection of themewise-related pieces of research, all of which have to do with fluid flows which do not follow the contour of the bounding wall(s) and with the related heat transfer ramifications. Two classes of such flows are considered. In one, the fluid is acted on by forces directed normal to the wall, causing lift-off. The other non-wall-adhering class of flows to be considered is separated flows.

Introduction

The aim of this paper is to convey a research philosophy, a style, and a way of thinking, with specific results and details of particular problems being of lesser concern. This aim has also been the basis of all the seminars and public lectures that I have given over the years. Because of this commonality of purpose, I felt that it would be quite proper that this paper be a written version of a seminar that I have presented to various audiences in recent times.

In accord with the aforementioned goal, it is natural that the research underlying the presentation be work with which I have been personally and intimately involved. As a result, what I will present here and what I have presented in seminars is a highly personalized view of a subject. Furthermore, consistent both with the objective of minimizing specifics in favor of general style and approach with the seminar nature of the paper, there is no need for a detailed review of the literature. Indeed, it should be underscored that the paper makes no claim to conveying an assessment of the status of the subjects to be discussed.

Another feature of the paper is its focus on experimental work. This reflects a personal belief in the primacy of experiment as the ultimate source of truth. The experimental focus is also consistent with the seminar nature of the paper, since experiments are easier to visualize and are usually more physical than is analysis or computation.

In view of the fact that papers appearing in this special issue of the journal are, in some way, concerned with the history or the present status of heat transfer, certain history-related comments about the research to be described in this paper are appropriate. The techniques and instrumentation used in the research may well be those of an era that is rapidly passing from the scene. In general, the research was performed with a maximum of human involvement and a minimum of automation. This high degree of involvement led to unusual attention to detail and concern about accuracy. The experimental techniques were unsophisticated, thereby enabling the experimenter to be a more integral part of the research than might be possible when more sophisticated techniques are used. Control of the experiments was entirely manual. Data were collected by means of simple but highly accurate instrumentation and recorded by hand. Even in the data reduction, there was considerable human involvement. Analogy methods were used whenever possible as an alternative to direct heat transfer experiments, and flow visualization was often an integral part of the research. All of the research was low budget, in keeping with the underlying philosophy, "less is more."[1]. The research was performed at The University of Minnesota.

Attention will now be turned to the technical theme of the paper. Most fluid flows that participate in convective heat transfer are more or less parallel to the walls with which they exchange heat. There are, however, a great many technologically important situations where the fluid flow does not follow the contour of the wall. Such non-wall-adhering flows will be the subject of this paper. Two classes of such flows will be discussed. In one, the fluid is acted on by forces directed normal to the surface. These forces tend to push the fluid away from the surface, causing lift-off and giving rise to complex flow patterns. Examples of this type of force include buoyancy (for a nonvertical surface) and the centripetal force.

The other non-wall-adhering class of flows to be considered here is separated flows. Such flows most commonly occur when the contour of the bounding wall changes too rapidly for the flowing fluid to follow the change. As a consequence, the mainstream is no longer bounded by the wall. Between the mainstream and the wall, there is a pocket of recirculating fluid. Depending on the downstream extent of the wall and the trajectory of the mainstream, there may ultimately be a reattachment of the mainstream to the wall.

The two classes of non-wall-adhering flows will be illustrated here with the aid of several visualization techniques. The heat transfer characteristics of these flows will also be discussed.

Flows Which Lift Off From Surfaces

Occasionally, a piece of research produces a work of art as well as information of technical value. Such an event is illustrated in Fig. 1. The figure contains a pair of photographs showing graceful, flowing, abstract shapes, which are artistically pleasing. These shapes also provide information about a flow created by forces that tend to push a fluid away from a surface. To facilitate the discussion, attention may first be focused on the lower photograph.

Contributed by the Heat Transfer Division for publication in the JOURNAL OF HEAT TRANSFER. Manuscript received by the Heat Transfer Division February 1, 1988. Keywords: Flow Separation, Forced Convection, Natural Convection, Reviews.

[1] This was the motto of the great modern architect, Ludwig Mies van der Rohe (1886-1969), representative samples of whose work may be seen on Lake Shore Drive in Chicago.

Copyright © 1988 by ASME
Downloaded 16 Dec 2010 to 193.140.21.150. Redistribution subject to ASME license or copyright; see http://www.asme.org/terms/Terms_Use.cfm

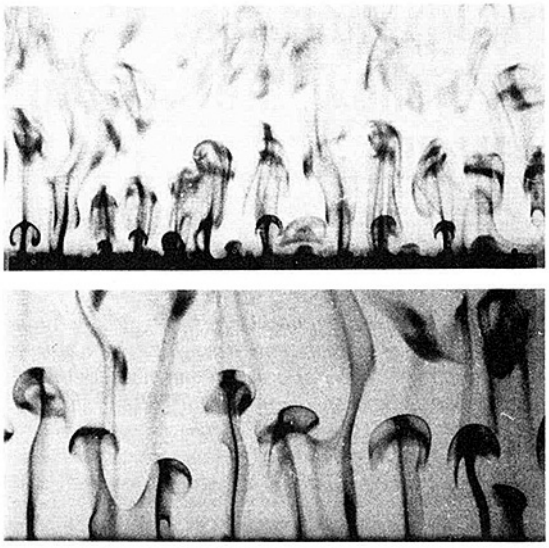

Fig. 1 Flow pattern adjacent to a heated horizontal plate

The black band at the bottom of the lower photograph represents a heated, horizontal isothermal plate. The space above the plate is filled with water whose temperature, far from the plate, is room temperature. Since in this temperature range the density of water decreases with increasing temperature, the fluid adjacent to the heated plate is lighter than the fluid far above the plate. An arrangement where a heavy object is atop a light object is not comfortable, and some corrective action is in order. A wholesale interchange of the light and heavy fluids is not easily accomplished, and nature opts for a selective exchange as illustrated in the photograph.

The photograph shows a succession of black, vertical, rounded-top structures deployed more or less periodically across the span of the plate. These structures are the tracks of upward-moving buoyant packets of fluid, i.e., the tracks of fluid that has lifted off from the surface. Between the periodically deployed upflows are mass-conserving downflows from the far field toward the plate.

Not only are the buoyant upflows spatially periodic, but they are also timewise periodic, as can be seen in the upper photograph of Fig. 1. In that photograph, three generations of buoyant packets are in evidence. The newest generation of packets is in the process of developing adjacent to the plate surface. The earlier generation has moved away from the plate and, at the instant of the photograph, is deployed at a distance above the plate. A still earlier generation, smeared out but still distinct, is situated near the top of the photograph.

The flow visualization patterns displayed in Fig. 1 were obtained by means of the thymol blue method. This is an electrochemical technique in which a change in the color of the fluid is produced by changes in pH brought about by an imposed d-c voltage. The tracer fluid generated is neutrally buoyant and precisely follows the fluid motions.

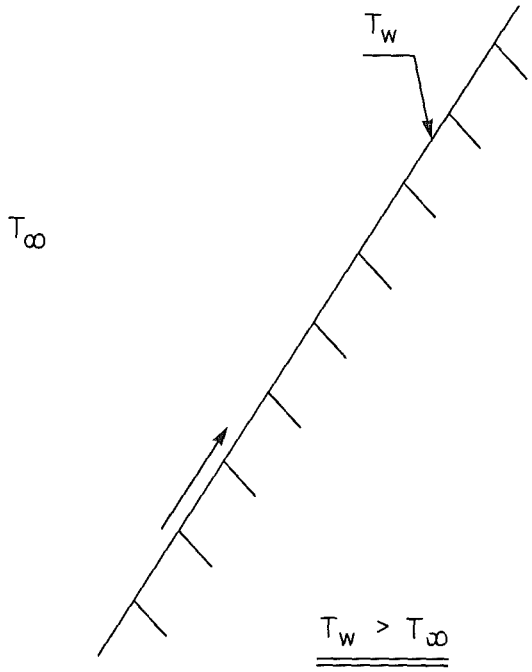

Fig. 2 Inclined, upward-facing, heated plate

Minute amounts of three substances were added to the water in order to enable the desired changes in color to take place. They are: an acid (hydrochloric acid), a base (sodium hydroxide), and a pH indicator (thymol blue). The thymol blue was the first substance to be added to the water, and it was dissolved by vigorous stirring. This solution was then titrated to the end point with the addition of sodium hydroxide. The color of the solution at this stage is deep blue. The solution is next made slightly acidic by the addition of hydrochloric acid. A red-yellow color results from this operation.

If a small d-c voltage (less than 6 V) from an adjustable supply is applied across two electrodes situated in the solution, an electrochemical reaction will take place and the pH of the solution in the neighborhood of the negative electrode will change from the acidic to the basic side. This change in pH is accompanied by a change in the color of the fluid, from red-yellow to blue. In the present instance, the heated horizontal plate served as the negative electrode, and the black buoyant structures in evidence in Fig. 1 are blue tracer fluid rising from the plate.

An interesting variant of the instability phenomena set forth in Fig. 1 is encountered on an inclined, upward-facing, heated plate. The physical situation is depicted schematically in Fig. 2, which shows a side view of an inclined plate whose uniform

Nomenclature

D = cylinder diameter
$\mathfrak{D}$ = mass diffusion coefficient
H = duct height
h = heat transfer coefficient
K = mass transfer coefficient
k = thermal conductivity
L = length of cylinder or duct
$\dot{m}$ = rate of mass transfer per unit area
Nu = Nusselt number
R = cylinder radius
Ra = Rayleigh number
Re = Reynolds number
r = radial coordinate
Sh = Sherwood number
T_w = wall temperature
T_∞ = ambient temperature
U_∞ = free stream velocity
u = streamwise velocity
x = axial coordinate
z = distance across the width of a surface
ν = kinematic viscosity

Downloaded 16 Dec 2010 to 193.140.21.150. Redistribution subject to ASME license or copyright; see http://www.asme.org/terms/Terms_Use.cfm

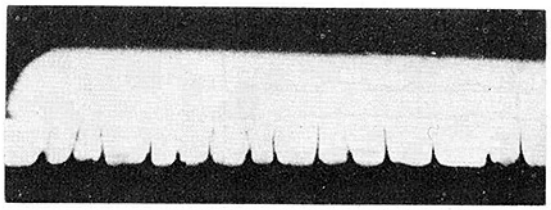

Fig. 3 Flow pattern adjacent to an inclined, upward-facing, heated plate

surface temperature exceeds the temperature of the surrounding fluid in which the plate is situated. At the plate surface, the buoyancy force can be resolved into two components, respectively along the surface and normal to the surface. The former creates an upflow which is essentially parallel to the surface, as indicated schematically in the figure. The latter tends to push the fluid away from the surface, thereby setting the stage for flow instability and lift-off.

To examine the results of the instability, the electrochemical flow visualization technique described in the foregoing may be used. To this end, visualization experiments were performed with an inclined, heated plate situated in water. Although a diagram such as Fig. 2 implies a two-dimensional situation, the instability causes the flow to be three-dimensional. Indeed, the main action occurs across the width of the plate, i.e., in the direction normal to the plane of Fig. 2. To view fluid flow phenomena across the width, the camera was set up to look upward along the plate from the leading edge. A photograph is presented in Fig. 3 to convey the observed flow visualization pattern for plate inclinations from the vertical of 15 deg or greater.

The horizontal, solid black band at the bottom of the photograph (excluding the attached vertical structures) represents the inclined heated plate, while the adjacent near-white zone is the fluid. The vertical structures, which are more or less periodically distributed across the width of the plate, are the traces of fluid moving away from the surface (i.e., lifting off) under the action of the normal component of the buoyancy force. Between these structures, fluid from the surroundings moves toward the plate surface. This incoming fluid undergoes a change of direction in the neighborhood of the surface, whereafter it feeds the outflow driven by the buoyancy force. The succession of inflow and outflow zones distributed across the width of the plate is superimposed on the mainflow, which moves upward along the inclined plate.

The heat transfer ramifications of the three-dimensional fluid flow pattern were investigated by making use of the analogy between heat and mass transfer. Measurements were made of the mass transfer coefficient and of its dimensionless counterpart, the Sherwood number. According to the analogy, at a given Reynolds number, the Sherwood number corresponding to a Schmidt number Sc is equal to the Nusselt number corresponding to a Prandtl number whose numerical value is equal to Sc.

The particular mass transfer technique used for the inclined plate experiments was electrochemical mass transfer, with an electrolyte consisting of aqueous solutions of cupric sulfate and sulfuric acid serving as the fluid environment. The electrochemical mass transfer system was isothermal, and the buoyancy forces were created by density differences associated with variations in species concentrations. The inclined plate was operated as a constant voltage surface, which modeled the uniform temperature boundary condition at the plate surface for the analogous heat transfer problem. With this electrochemical technique, the rate of mass transfer is determined by measuring the ion current associated with the transfer of copper ions at the surface. By using very small electrodes

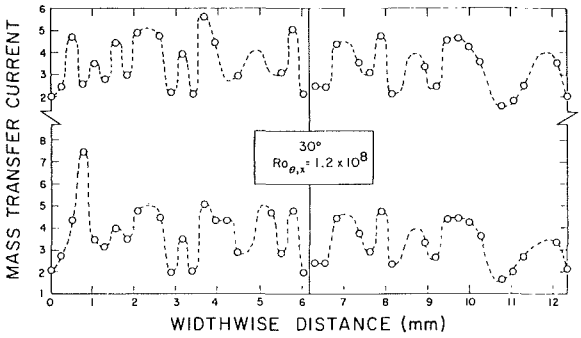

Fig. 4 Variations of the local mass transfer rate across the width of an inclined plate

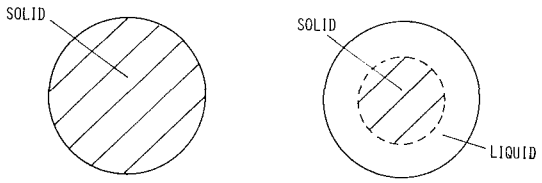

Fig. 5 Schematic diagrams for melting of a solid in a horizontal tube

embedded in the surface, highly localized current flows can be measured, giving correspondingly localized mass transfer coefficients. Indeed, the capability to provide highly localized results was a decisive factor in the decision to use the mass transfer technique instead of making direct heat transfer measurements.

Representative results for the distribution of the local mass transfer rate across the width of the inclined plate are presented in Fig. 4. The ordinate is the mass transfer current, and the abscissa is the horizontal distance across the width. Since the results tended to shift with time, two distributions are shown, each referred to its own ordinate scale. For these results, the plate was inclined at 30 deg with respect to the vertical, and the local Rayleigh number was 1.2×10^8. Inspection of the figure shows that there is a major variation in the magnitude of the mass transfer rate across the width of the plate. Therefore, the three-dimensional fluid flow pattern induced by forces acting normal to the surface has a significant effect on the mass (heat) transfer.

The presence of normal forces which tend to push fluid away from surfaces and cause lift-off occurs in a wide variety of physical situations, sometimes unexpectedly. Consider, for example, the melting of a solid contained in a horizontal tube. Before the onset of melting, suppose that the solid and tube wall are at a common uniform temperature equal to the melting temperature. This initial condition is illustrated in the left-hand diagram of Fig. 5. Heating is initiated at $t = 0$ and maintained such that the tube is at a steady, circumferentially uniform temperature that exceeds the melting temperature.

At some instant during the melting process, the situation may be *tentatively* represented as in the right-hand diagram of Fig. 5, which shows an unmelted core of solid surrounded by an annulus of liquid melt. If it is noted that the tube wall corresponds to the highest temperature of the system and the surface of the solid to the lowest temperature, it is evident that there is a different thermal structure in the upper and lower halves of the cross section.

In the lower half, the solid is above the tube, so that heavy fluid is atop light fluid. This is an instability situation of the type discussed earlier, and it is not unreasonable to expect a

Downloaded 16 Dec 2010 to 193.140.21.150. Redistribution subject to ASME license or copyright; see http://www.asme.org/terms/Terms_Use.cfm

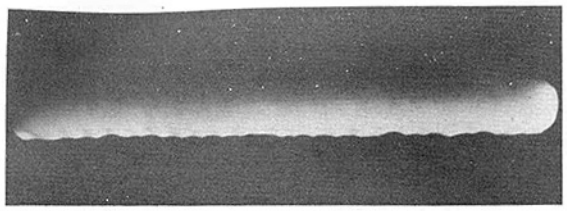

Fig. 6 Longitudinal view of a solid which was partially melted in a horizontal tube

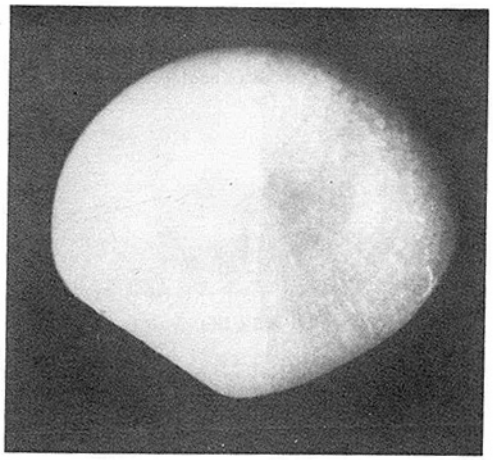

Fig. 7 End view of a solid which was partially melted in a horizontal tube

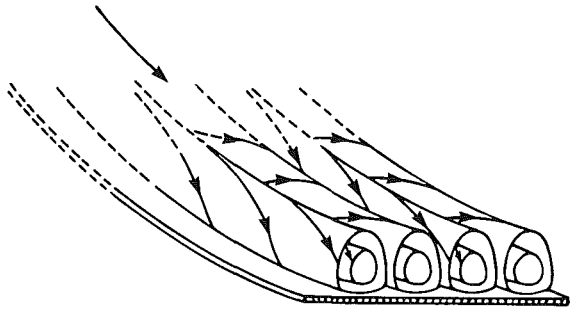

Fig. 8 Pattern of longitudinal vortices for forced convection flow along a plate which has concave curvature in the flow direction

periodic pattern of buoyancy-induced flow welling up from the tube and impinging on the solid. On the other hand, in the upper half, the tube is above the solid. This corresponds to light fluid atop heavy fluid, a situation where instability is not expected. In view of these considerations, the symmetric melting implied by the right-hand diagram of Fig. 5 is, in all likelihood, not realistic. Rather, different patterns of melting should occur in the upper and lower halves of the cross section.

This issue is explored photographically in Figs. 6 and 7, which display melting patterns for 99-percent pure, *n*-eicosane paraffin which has a melting temperature of 36.3°C. In the experiments from which Figs. 6 and 7 were taken, the solid, which is more dense than the liquid, was constrained not to fall to the bottom of the tube.

Figure 6 is a longitudinal view of the melting solid with the camera looking at the side of the solid. Careful examination of the lower edge of the solid reveals an undulating contour indicative of the expected periodic pattern of buoyant flow. The valleys in the surface correspond to the impingement of hot fluid rising from the tube wall, while the peaks are at locations where hot-fluid impingement is absent. Although the photograph is somewhat vague about the upper surface of the solid, it was, in fact, perfectly smooth.

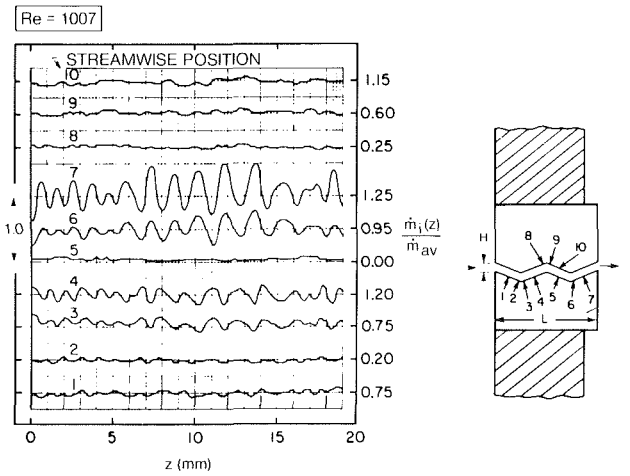

Fig. 9 Variations of the local mass transfer rate across the width of the walls of a corrugated duct

Figure 7 is an end view of the solid. The distinctly different shapes of the upper and lower surfaces provide clear evidence of the differences in the transfer mechanisms acting in the upper and lower portions of the liquid annulus. It is noteworthy that more melting actually occurred at the upper surface of the solid. This is because there is a general, buoyancy-driven circulation pattern in the annulus whereby liquid rises along the tube wall and descends along the solid. The circulation delivers warmer fluid to the upper portion of the annulus and cooler fluid to the lower portion. The aforementioned instability in the lower portion is superposed on the general circulation.

Although it might appear from the preceding discussion that the lift-off of a flow from a surface is a buoyancy-related process, this is by no means always the case. To make this point, reference may be made to Fig. 8, which is reproduced from Schlichting's Boundary Layer Theory. The figure illustrates fluid flow along a plate which has concave curvature in the mainflow direction. The complex flow pattern illustrated in the figure results from the presence of forces which tend to push the fluid away from the surface.

These forces are a direct consequence of the curved path taken by the fluid particles in response to the curvature of the plate. It is well known that particles moving on curved trajectories are acted on by a force (the centripetal force) directed toward the center of curvature. For the case of fluid gliding smoothly along a concave plate, the centripetal force would act normal to the plate surface and would promote a tendency for the fluid to lift off the surface.

A wholesale lift-off is, of course, unrealistic. Instead, as seen in Fig. 8, there is selective lift-off, which occurs at spatially periodic locations across the width of the plate. Between the successive lift-off locations, there is a mass-conserving flow directed toward the plate. This pattern of alternating inflows and outflows is reminiscent of that discussed earlier in connection with buoyancy-related lift-off.

The superposition of the inflow-outflow cells on the forced convection mainflow gives rise to the longitudinal vortices depicted in Fig. 8. These fluid structures are often called Gortler vortices.

With this as background, attention may be turned to the case of the corrugated duct, which is illustrated in schematic side view at the right in Fig. 9. A forced convection flow passes through the duct as indicated by the inflow and outflow vectors in the diagram. The flow rates to be considered here are those appropriate to compact heat exchangers, i.e., primarily in the laminar and transitional range.

Downloaded 16 Dec 2010 to 193.140.21.150. Redistribution subject to ASME license or copyright; see http://www.asme.org/terms/Terms_Use.cfm

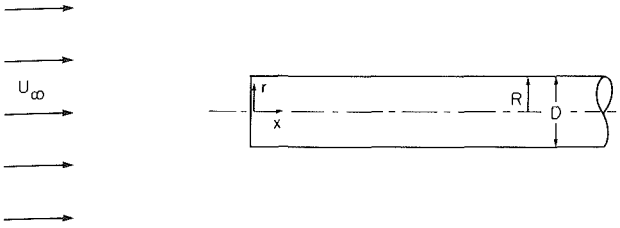

Fig. 10 Blunt-faced circular cylinder situated in a longitudinal flow

From a consideration of the expected streamline shapes for relatively slow flow through the corrugated duct, it is not unreasonable to conjecture that the fluid particles would move along curved paths. If this were so, then the centripetal forces could give rise to three-dimensional flows of the type discussed in connection with Fig. 8. In the presence of such flows, the heat transfer coefficients would vary in the direction of the width of the duct, i.e., in the direction normal to the plane of the right-hand diagram of Fig. 9.

The exploration of the possible variation of the heat transfer coefficient in the direction of the width of the duct requires the capability to make highly localized measurements. Once again, a mass transfer technique appears to be advantageous. The specific technique used for the corrugated duct is naphthalene sublimation. The walls of the duct were made of naphthalene, which had been cast in a special mold to produce the desired surface shape. In the presence of forced convection air flow through the duct, the sublimation of the naphthalene is analogous to the transfer of heat for the corresponding thermal problem. The boundary condition for the sublimation process is uniform concentration of naphthalene vapor along the surface, which corresponds to the isothermal wall condition for the thermal analogue.

In general, the naphthalene sublimation technique offers several advantages compared with direct heat transfer measurements. It affords smaller extraneous losses, higher measurement accuracy, and simpler fabrication and assembly. It also enables ready attainment of standard boundary conditions that are the analogues of uniform wall temperature and zero heat flux. Highly localized measurements of high accuracy are readily performed, a task which is particularly difficult in the case of the isothermal wall boundary condition in the thermal analogue.

Surface contour measurements having an instrument resolution of 0.00001 in. were made both before and after each data run, and the difference yielded the local rate of mass transfer. Such contour measurements were carried out across the width of the duct at each of the ten streamwise stations indicated in the diagram at the right of Fig. 9. Readings of the contour were recorded every 0.2 mm along a 19 mm section of the width.

Widthwise distributions of the local sublimation mass flux are presented graphically in Fig. 9 at each of the ten investigated streamwise positions. Each distribution has its own ordinate origin, which is indicated along the right-hand edge of the graph. The average mass flux which normalizes the local distributions corresponds to either one of the corrugated walls as a whole—the lower wall for positions $i=1$ through 7 and the upper wall for positions $i=8$, 9, and 10. The widthwise coordinate is z.

Inspection of Fig. 9 indicates the presence of regular widthwise variations at positions 3, 4, 6, and 7. These variations provide strong evidence of the existence of three-dimensional flows of the type illustrated in Fig. 8 (i.e., longitudinal vortices superimposed on the mainflow).

It is, however, somewhat perplexing as to why widthwise variations are not seen at other locations. On leeward facets of

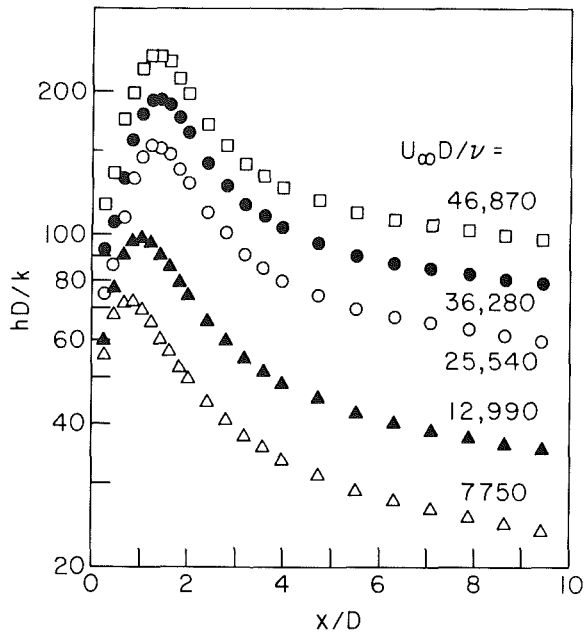

Fig. 11 Axial distributions of the local Nusselt number along the cylindrical surface of a blunt-faced cylinder in a longitudinal flow

the corrugated wall, flow separation may interfere with the development of the longitudinal vortices. This explanation, however, does not apply to location 10, which is situated on a windward facet. A tentative rationalization may be based on the change of direction of the centripetal force as the flow moves from the valleys to the peaks of the corrugated wall. Such a change of direction might cancel out the vortex pattern which exists in the first valley as the flow moves to the first peak. Subsequent to the cancellation, a new vortex pattern can develop as the flow moves to the second valley.

This concludes the discussion of flows which lift off from surfaces in response to forces which act normal to the surface. The lift-off occurs periodically in a direction transverse to the mainflow direction and may give rise to periodic variations of the heat transfer coefficient in that direction.

Flows Which Separate From Surfaces

Fluid flows that are unable to follow a rapid change in the contour of the surface which bounds the flow are said to separate from the surface. A representative physical situation where separation occurs is pictured schematically in Fig. 10. The figure shows a circular cylinder situated longitudinal to a uniform free stream, with the blunt end of the cylinder facing upstream toward the oncoming flow.

The fluid impinging on the blunt face is deflected and becomes a radial outflow along the face. The radial flow cannot negotiate the sharp corner at the intersection of the end face and the cylindrical surface, and so it separates. After separation, the radial flow is bent downstream. It arches over the upstream portion of the cylindrical surface and eventually reattaches to it. The space between the arching separated flow and the cylindrical surface is occupied by recirculating fluid. This space is often referred to as a separation bubble. Once the flow reattaches to the surface, boundary layer development ensues.

Experiments, performed to explore the heat transfer ramifications of the flow separation, were carried out in a low-speed, low-turbulence wind tunnel (turbulence intensity ~ 0.4 percent). The cylindrical surface of the cylinder was heated uniformly, and local measurements of the surface temperature

Downloaded 16 Dec 2010 to 193.140.21.150. Redistribution subject to ASME license or copyright; see http://www.asme.org/terms/Terms_Use.cfm

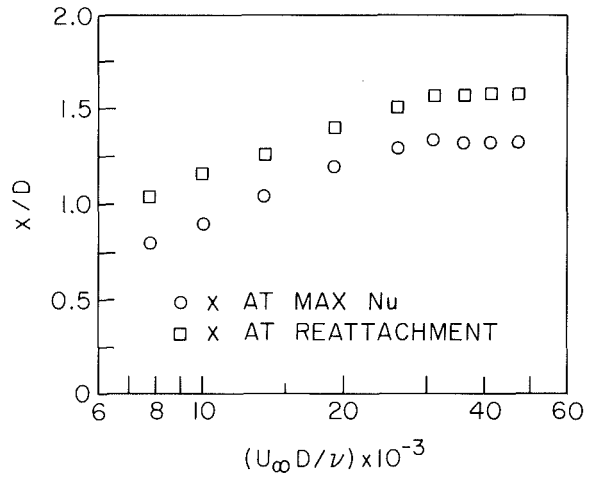

Fig. 12 Locations of the maximum Nusselt number and the flow reattachment at the cylindrical surface of a blunt-faced cylinder in a longitudinal flow

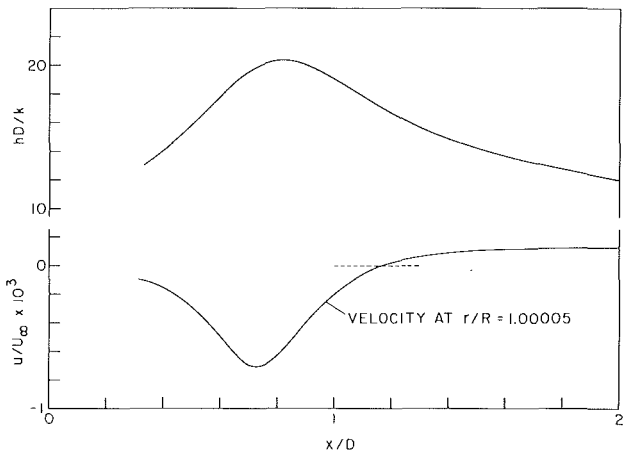

Fig. 13 Numerically determined axial distributions of the local Nusselt number and the near-wall streamwise velocity along the cylindrical surface of a blunt-faced cylinder in a longitudinal flow

were made from which local heat transfer coefficients were readily determined. The blunt face of the cylinder was unheated.

Axial distributions of the local Nusselt number along the cylindrical surface are presented in Fig. 11 for parametric values of the Reynolds number ranging from 7750 to approximately 47,000. For all of the Reynolds numbers, the axial distributions have a common shape characterized by an initial increase, the attainment of a maximum, and a subsequent decrease.

The aforementioned pattern in the Nusselt number distribution is characteristic of numerous separated flows. For instance, it is encountered just downstream of a sharp-edged inlet in a tube. It is also encountered downstream of both forward-facing and backward-facing steps. In general, the Nusselt numbers associated with this type of distribution are higher than those for a corresponding unseparated flow, especially in the region of the maximum and, to a lesser extent, in the flanks of the distribution both upstream and downstream of the maximum (e.g., Sparrow and Ohadi, 1987; Garcia and Sparrow, 1987). Therefore, the flow separation and reattachment function as a mechanism for enhancing heat transfer.

It is natural to question whether the streamwise location of the maximum in the Nusselt number distribution coincides with the location at which the separated flow reattaches to the surface. To explore this issue, it is necessary to determine the reattachment location, and this was accomplished by flow visualization by means of the oil-lampblack technique.

To prepare for a visualization run, the cylindrical surface was first covered with white, plasticized, self-adhering contact paper, and a thin film of engine oil was then applied to the contact paper. Next, a circular toothpick with a conical tip was dipped into a container filled with a mixture of oil and lampblack powder, and an array of small dots of the oil-lampblack solution was deployed axially along the topmost horizontal line of the cylinder. The dots were about 0.5 mm in diameter, and the distance between the centers of consecutive dots was 1.5 mm. The presence of the aforementioned thin film of oil enabled the dots to move readily even when subjected to very small airflow-induced shear stresses.

When the dots were in place, the airflow was initiated. It was soon observed that all dots upstream of a certain station moved in the direction opposite to the free stream, while all dots downstream of that station moved in the direction of the free stream. The reattachment location is situated between the adjacent pair of dots which move in opposite directions, and it was assumed to occur midway between these dots. This assumption gave rise to an uncertainty of $0.02D$ in the reattachment location (D = cylinder diameter). Additional visualization runs were made to verify that the reattachment was circumferentially uniform.

The dimensionless axial coordinate x/D at reattachment is plotted as a function of the Reynolds number in Fig. 12. The reattachment data are represented by the square symbols. Also plotted in the figure are circular data symbols. Each such data point corresponds to the x/D coordinate of the maximum of the Nusselt number distribution.

The figure clearly shows that for the case of the blunt-faced longitudinal cylinder, the points of reattachment and maximum Nusselt number do not coincide. Indeed, the Nusselt number maximum consistently occurs upstream of the reattachment point.

Further exploration of the relationship between the points of reattachment and maximum Nusselt number was undertaken by means of numerical solutions of the conservation laws for mass, momentum, and energy. The flow was assumed to be laminar and, correspondingly, the parametrically assigned values of the Reynolds number had to be suitably low (lower than those of the experiments).

The numerically determined axial distributions of the local Nusselt number and of the streamwise velocity immediately adjacent to the cylindrical surface are presented in Fig. 13 for a Reynolds number of 2000 and a Prandtl number of 0.713. The Nusselt number distribution of Fig. 13 exhibits the same qualitative trends as the experimentally determined distributions of Fig. 11 (note that the enlarged abscissa scale of Fig. 13 flattens the maximum). The velocity adjacent to the cylindrical surface is negative for $x/D < 1.17$ and becomes positive thereafter. The negative velocities correspond to the backflow leg of a recirculation loop. Since the wall shear stress is proportional to the surface-adjacent velocity, it follows that the shear changes sign at $x/D = 1.17$, signaling the reattachment of the flow. Consequently, the separation bubble extends from $x/D = 0$ to 1.17.

From Fig. 13, the value of x/D at the maximum of the Nusselt number distribution can be read as 0.82, while, as noted in the foregoing, the reattachment occurs at $x/D = 1.17$. Thus, as in the experiments, the Nusselt number attains its maximum in the separated region upstream of the point of reattachment of the flow.

Within the separated region, the magnitude of the wall-adjacent velocity increases at first, attains a maximum, and

Downloaded 16 Dec 2010 to 193.140.21.150. Redistribution subject to ASME license or copyright; see http://www.asme.org/terms/Terms_Use.cfm

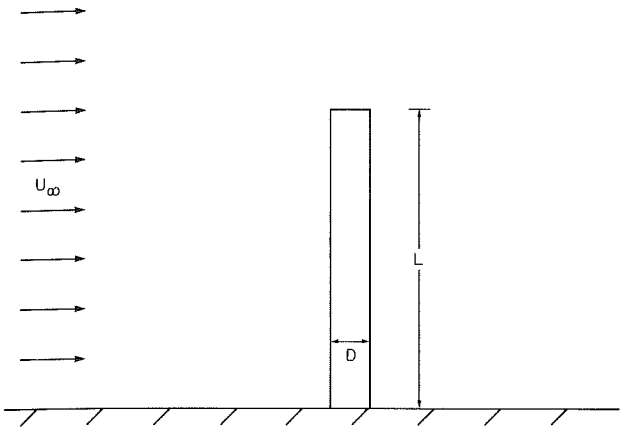

Fig. 14 Cylinder in crossflow with one end free and the other end attached to a wall

then decreases toward zero. The maximum occurs where the ellipselike streamlines which characterize the recirculating flow in the separation bubble approach most closely to the cylinder surface. Note that the Nusselt number maximum is attained quite close to the location where the velocity magnitude attains its maximum.

Although there is no separated flow that is truly simple, the separated flow discussed in connection with Figs. 10-13 is relatively simple because the entire flow field is axisymmetric. When the flow field is three-dimensional, a correspondingly complex separated flow occurs. Attention is now turned to an example of a three-dimensional separated flow.

The physical situation to be considered is the flow adjacent to the free end of a cylinder in crossflow, a schematic diagram of which is presented in Fig. 14. As seen there, the cylinder is of length L and diameter D. The lower end of the cylinder is attached to a wall, and the upper end is free.

The length of the cylinder was chosen sufficiently great so that wall effects were confined to only a small fraction of the length. Indeed, the flow adjacent to the free end was altogether unaffected by the presence of the wall. In fact, in the central region of the cylinder, away from both the wall and the free end, the flow was that corresponding to an infinitely long cylinder in crossflow.

The first focus of the discussion is the pattern of fluid flow adjacent to the flat face situated at the free end of the cylinder. By imagining the path of the fluid which approaches the upper portion of the cylinder, it is not unreasonable to expect that the flow will rise upward toward the free space above the end face in order to escape the blockage imposed by the cylinder. This upwelling fluid is unable to turn the sharp corner where the end face and the cylindrical surface intersect, so that separation occurs. The separated flow can be envisioned as arching over the end face and then bending toward it, but without definitive measurements it is not known whether the flow will reattach on the end face or miss it altogether. The occurrence or nonoccurrence of reattachment on the end face is expected to have a major effect on the heat transfer coefficient for that surface.

The oil-lampblack technique was used to help visualize the pattern of fluid flow adjacent to the end face. This technique was alluded to briefly in connection with the identification of the reattachment point for separation on a blunt-faced cylinder in longitudinal flow. In view of the simplicity of the technique, its ease of implementation, its extremely low cost, and the considerable amount of information that it provides, a more detailed description is appropriate.

Lampblack is a very fine black power now primarily available as an ingredient of paint. It mixes readily with oil,

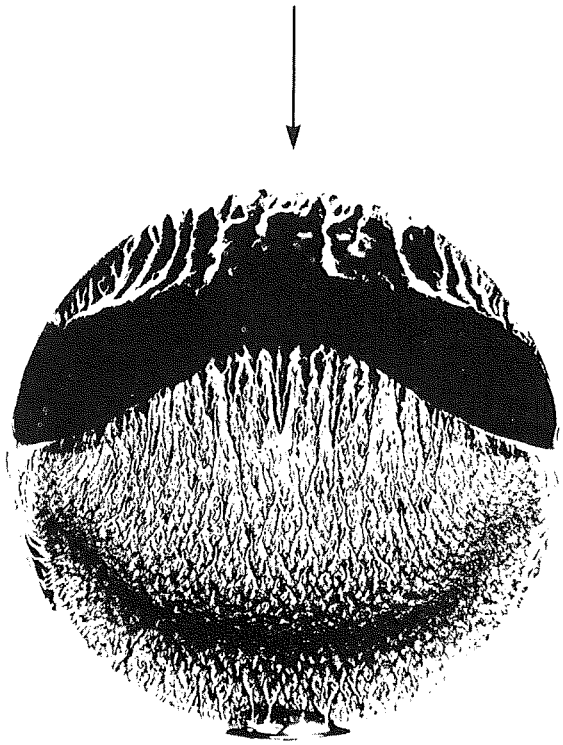

Fig. 15 Flow pattern adjacent to the free end of a cylinder in crossflow

and the mixture, when brushed on a surface, produces a smooth, glossy-black coating. The fluidity of the mixture can be regulated by the selection of the viscosity of the oil and by the proportions of the oil and the lampblack powder. The general procedure for using the technique is to brush the oil-lampblack mixture on a surface and then to expose the surface to the airflow whose characteristics are to be studied. Under the action of the forces exerted by the flow, the mixture will move along the surface, following the paths of the fluid particles that pass adjacent to the surface. In regions of low velocity (e.g., stagnation regions), the forces are small and the mixture will remain stationary, so that such regions show themselves as black streak-free zones on the surface.

The ideal fluidity is such that the mixture will move slowly over the surface under the action of the applied forces. For such an ideal mixture, any excess will be blown off, leaving an array of streaks which indicate the direction of the fluid flow adjacent to the surface. A mixture that is too fluid will be completely blown off the surface, so that no indication of the flow pattern remains. In addition, a too-fluid mixture tends to sag under the action of gravity, particularly when the surface is inclined or vertical. On the other hand, a too-stiff mixture will not move at all, again providing no information about the flow. The attainment of the proper mixture fluidity is a trial and error process. Furthermore, a fluidity that is appropriate at a particular Reynolds number may not be effective at another Reynolds number, owing to differences in the shear stresses that are exerted.

The oil-lampblack technique can provide flow pattern information via three types of observations. First, observation of the movement of the freshly applied mixture immediately after initiation of the airflow reveals the direction of fluid motion. Next, after the excess mixture is blown off the surface, a fixed pattern of streaks is established, which gives further confirmation of the flow direction. Finally, in separate experiments, the mixture can be applied locally at selected positions on the surface to identify the details of the motion at those positions.

For the visualization runs performed for the end face of the

Downloaded 16 Dec 2010 to 193.140.21.150. Redistribution subject to ASME license or copyright; see http://www.asme.org/terms/Terms_Use.cfm

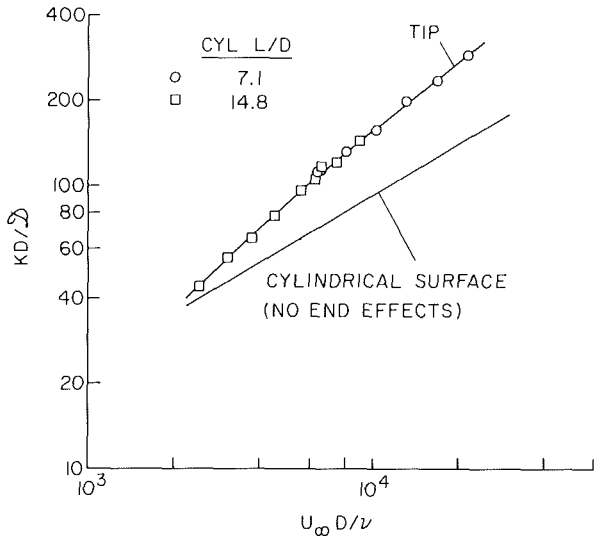

Fig. 16 Comparison of Sherwood numbers at the free end face of a cylinder in crossflow with those for the cylindrical surface

cylinder in crossflow, the surface of the face was covered with white, plasticized, self-adhering contact paper, which provided a contrasting background for the oil-lampblack mixtures which were brushed on it. During a visualization run, once the oil-lampblack mixture had arranged itself into a final pattern, a photograph of the pattern was taken with the camera looking down through the plexiglass wall of the wind tunnel at the end face of the cylinder. During the photography, the airflow in the tunnel was maintained at the same value as that for the visualization run proper.

The photographs that resulted from the flow visualization are another instance where art and science overlap. A representative visualization photograph is presented in Fig. 15, where many interesting textures and structures are in evidence. Overall, the photograph has the appearance of a smiling face.

For purposes of orientation with respect to Fig. 15, it should be noted that the flow approaching the cylinder lies in planes parallel to the plane of the figure. The flow approaches the cylinder in the direction shown by the arrow. Inspection of Fig. 15 reveals six distinct zones. In discussing these zones, the term forward flow will be used to denote fluid motion that is in the same direction as the oncoming flow, while the term backflow will denote fluid motion whose direction is opposite to that of the oncoming flow.

As discussed earlier, the free-stream flow approaching the upper portion of the cylinder can be envisioned as rising to avoid the blockage created by the cylinder. The rising fluid tends to brush lightly against the forward portion of the end face, thereby creating the broad, sideward-curving streaks that are seen in the topmost zone of Fig. 15. This is a zone of weak forward flow.

The rising flow separates from the tip of the cylinder, and it is the recirculation of the separated flow and the reattachment downstream of the separated region that shapes most of the other zones seen in the figure.

The dark crescent-shaped region situated in the lower part of the photograph marks the reattachment of the separated flow, so that the separated region and its recirculating flow are located fore of the crescent. The curvature of the reattachment line is indicative of the three-dimensional nature of the flow. The sharply etched lines that populate the separated region are lines of backflow (i.e., opposite to the freestream direction). These backflow lines terminate in a broad black band. The black band is a zone of very low velocity. It is, in a sense, a neutral zone that stands between the forward and backflows that exist at its upstream and downstream edges. Careful local probing within the black band, utilizing local application of the oil-lampblack mixture, revealed regions of weak forward flow, especially near the flanks of the band.

Aft of the crescent, the flow is reattached and is forward in direction (i.e., in the same direction as the freestream). At the downstream extremity of the end face, at the rim, there is a small black region. Extensive visual observation indicated this to be a stagnation zone, from which flow could not pass over the rim because of a blocking current which moved upward along the cylindrical surface.

Considering the complexity of the just-discussed pattern of fluid flow and comparing it with the well-documented flow around a cylinder in a crossflow (also complex, but very different), there is ample reason to expect different heat transfer coefficients at the end face and the cylindrical surface. This issue was explored quantitatively by making use of the naphthalene sublimation technique, whereby sublimation mass transfer measurements are made instead of direct heat transfer measurements. The naphthalene technique was discussed earlier in the paper. As noted there, the Sherwood numbers obtained from the mass transfer experiments are equal to Nusselt numbers for heat transfer, provided that the Prandtl number is equal to the Schmidt number.

The experimentally determined Sherwood number results are presented in Fig. 16, both for the end face (labeled *tip* in the figure) and for the cylindrical surface. As indicated on the ordinate, the Sherwood number includes the mass transfer coefficient K, the cylinder diameter D, and the coefficient of mass diffusion $\mathcal{D}$. The Reynolds number on the abscissa spans the range from about 2500 to 25,000.

The figure shows that in the investigated Reynolds number range, the end-face (i.e., tip) Sherwood numbers exceed those for the end-effect-free cylindrical surface, with deviations that increase with Reynolds number. At the upper end of the range, the end-face Sherwood numbers are twice as large as those for the cylindrical surface. To rationalize this finding, reference may be made to the flow patterns portrayed in Fig. 15. There, it can be seen that most of the end face is washed by flows that are highly responsive to the Reynolds number—namely, in the separated region and the reattachment zone. On the other hand, for the cylindrical surface, away from the ends, about half of the circumference—the forward half—is washed by a flow (i.e., a laminar boundary layer) whose Sherwood number is less responsive to the Reynolds number. It is, therefore, quite reasonable that the variation of Sh with Re at the end face has a steeper slope than that for the end-effect-free cylindrical surface.

From the results of Fig. 16, it is evident that the end-face heat transfer would be underestimated if it were to be calculated using the conventional cylinder-in-crossflow Nusselt number correlation.

The just-discussed separation at the end face was overtly three-dimensional because of the geometry of the system. However, even in nominally symmetric situations, nonsymmetric flow separation has been observed, giving rise to a higher degree of complexity than would have been expected on the basis of geometrical considerations alone. This occurred, for example, just downstream of an abrupt, geometrically symmetric enlargement of a parallel-plate channel (Sparrow and Kalejs, 1977). By making use of the naphthalene sublimation technique, the axial distribution of the local Sherwood number was measured on each of the principal walls of the enlarged channel. In the separated region, the Sherwood numbers at the respective walls were distinctly different. Indeed, there were clear differences in the lengths of the respective separated regions. Far downstream, after reattachment

Downloaded 16 Dec 2010 to 193.140.21.150. Redistribution subject to ASME license or copyright; see http://www.asme.org/terms/Terms_Use.cfm

and redevelopment, the Sherwood numbers were the same at the two walls.

Concluding Remarks

This paper was intended to convey a particular personal style of research characterized by intense human involvement and a minimum of material resources. The philosophical basis of this style is the notion that "less is more." The description of the style was conveyed by a sequence of research problems which have to do with fluid flows which do not follow the contour of the bounding wall(s) and with the related heat transfer ramifications. These research problems span a period of almost 20 years and represent work with which I was personally intimately involved.

The paper is neither a review nor a status report of the technical areas which are dealt with therein. As noted in the foregoing, it was written to describe a personalized approach.

References

Garcia, A., and Sparrow, E. M., 1987, "Turbulent Heat Transfer Downstream of a Contraction-Related, Forward-Facing Step in a Duct," ASME JOURNAL OF HEAT TRANSFER, Vol. 109, pp. 621–626.

Sparrow, E. M., and Kalejs, J. P., 1977, "Local Convective Transfer Coefficients in a Channel Downstream of a Partially Constricted Inlet," *International Journal of Heat and Mass Transfer*, Vol. 20, pp. 1241–1249.

Sparrow, E. M., and Ohadi, M. M., 1987, "Comparison of Turbulent Thermal Entrance Regions for Pipe Flows With Developed Velocity and Velocity Developing From a Sharp-Edged Inlet," ASME JOURNAL OF HEAT TRANSFER, Vol. 109, pp. 1028–1030.

Downloaded 16 Dec 2010 to 193.140.21.150. Redistribution subject to ASME license or copyright; see http://www.asme.org/terms/Terms_Use.cfm

Wavenumber Selection in Bénard Convection

I. Catton
Mechanical, Aerospace and Nuclear Engineering Department, University of California, Los Angeles, Los Angeles, CA 90024-1597

The results of three related studies dealing with wavenumber selection in Rayleigh-Bénard convection are reported. The first, an extension of the power integral method, is used to argue for the existence of multi-wavenumbers at all supercritical wavenumbers. Most existing closure schemes are shown to be inadequate. A thermodynamic stability criterion is shown to give reasonable results but requires empirical measurement of one parameter for closure. The third study uses an asymptotic approach based in part on geometric considerations and requires no empiricism to obtain good predictions of the wavenumber. These predictions, however, can only be used for certain planforms of convection.

Introduction

Natural convection in horizontal fluid layers is a commonly occurring phenomena in nature, but has eluded theoretical as well as physical description due to the highly complicated nature of turbulent flow. Sound theoretical and physical understanding is required if realistic modeling and predictive capability are ever to be achieved for many of the complex systems we must deal with. For example in astrophysics, the validity of star models depends to a large degree on the validity of energy transport in the outer regions of stellar atmospheres. In geophysics current theories of continental drift depend on possible convective motion in the earth's mantle caused by internal heat generation due to radioactive decay. In meteorology, theories and prediction of current weather phenomena as well as long-term effects like ice ages depend on the validity of theories of convective energy transport in the Earth's atmosphere. In engineering, numerous examples can be found in the field of energy production and transport. For example, in solar energy collectors heat losses due to natural convection can be significantly reduced by appropriately placed cell boundaries. The cell spacing in turn has a significant effect on the economics of solar energy production.

The modeling of such systems is normally done by one of two methods. The first method is to devise an experiment that is similar to the system under investigation and use principles of dynamic similarity to correlate and extrapolate the experimentally measured data. The second involves integrating the governing partial differential equations. Both have drawbacks. Experiments are usually limited by materials, by technology, and by certain effects not being present in the experiment. Exact integration of the governing equations can only be accomplished for a few special cases with approximate methods being required for the others. Even so, approximate methods must overcome the limitations of computer storage and speed as well as numerically induced phenomena such as diffusive truncation (Hirt, 1968) and round-off errors. With modern numerical algorithms and computer hardware, these are only truly limiting for problems whose solutions contain a large range of length or time scales. Relevant examples include turbulence and convection in large-aspect-ratio containers.

The physical problem to be addressed here is a fluid layer contained between two infinite parallel horizontal surfaces, which is heated from below and cooled from above (see Fig. 1). If the heating is high enough, the Rayleigh number Ra_c will exceed 1707.762 and convection will begin with a wavenumber a_c of 3.117. This particular problem has received a great deal of attention because of its importance to a wide class of physical phenomena. It is commonly called Bénard convection. An extensive body of theoretical as well as experimental work has been devoted to this problem. One reason is that it provides a simple form of turbulence for study.

A large number of experimental studies of Bénard convection have been carried out since the classical experiments of Bénard (1900). They cover stability, heat transfer, planform, transitions, and temperature distributions. An extensive survey of the literature was prepared by Catton (1978).

Most experiments and engineering applications are carried out in large-aspect-ratio (horizontal length to height) convection cells. Thus, there are two very different length scales: the horizontal length of the cell, and the size of an individual convection roll. This makes both analytical and numerical work difficult. However, the dependence on the horizontal length scale can be eliminated by assuming periodic solutions with a given wavenumber. Analysis of the Bénard problem very quickly reduces to attempting to eliminate the nonuniqueness of the wavenumber of the motion resulting at supercritical Rayleigh numbers (greater than the Rayleigh number at which convection first occurs). If one knew how the wavenumber changed with increasing Rayleigh number, one could easily calculate the heat transport and other physical parameters of interest. McDonough and Catton (1982) used the mean field equations to demonstrate that even Prandtl number effects, at least below the second transition, could be accounted for if one knew the wavenumber. The focus thus becomes prediction of the wavenumber.

Visual observations of the flow patterns, which have been made by numerous investigators, indicate that a "textured" (as opposed to an ordered) pattern of rolls will usually appear at Rayleigh numbers slightly above critical. The characteristic wavenumber is a decreasing function (larger wavelength) of the Rayleigh number in contrast with many theoretical efforts, which have predicted that the wavenumber is an increasing function of Rayleigh number. Further, in contrast to ones' intuition, supercritical Rayleigh numbers yield a temperature gradient reversal in the central regions of the layer. Farhadieh

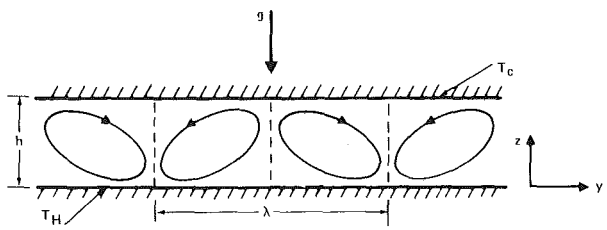

Fig. 1 Two-dimensional Rayleigh-Bénard convection

Contributed by the Heat Transfer Division for publication in the JOURNAL OF HEAT TRANSFER. Manuscript received by the Heat Transfer Division February 4, 1988. Keywords: Flow Instability, Flow Transition, Natural Convection, Turbulence.

Copyright © 1988 by ASME
Downloaded 16 Dec 2010 to 193.140.21.150. Redistribution subject to ASME license or copyright; see http://www.asme.org/terms/Terms_Use.cfm

and Tankin (1974) observed this reversal in a water layer at Rayleigh numbers as low as 6000, and Gille (1967) in an air layer at 27,000. Chu and Goldstein (1973) observed the reversal at Rayleigh numbers as high as 500,000, beyond which they seem to disappear. Numerical predictions of gradient reversals have been made by Kuo (1961) and by Veronis (1966).

As the Rayleigh number is increased to a value of about 22,000 (the actual value is a function of the Prandtl number; see Krishnamurti, 1970) a transition to bimodal convection (two wavenumbers) occurs. The bimodal state of convection is characterized by a set of cross rolls perpendicular to and superimposed on the original set of rolls. The cross rolls have larger wavenumbers than the initial set of wavenumbers. The wavenumber behavior of the fundamental and the cross rolls with increasing Rayleigh number have not been reported in the literature nor has the effect of random initial conditions. One must first understand the fundamental then attempt to understand the cross rolls or higher transitions. Bimodal convection has been reported at Rayleigh numbers less than 22,000 by Krishnamurti (1970) making it important to heat transport even at relatively low Rayleigh numbers.

The transition to bimodal convection is accompanied by a discrete change in the heat flux curve. The transition has been measured by Krishnamurti (1970), Malkus (1954), Willis and Deardorff (1967), Carrol (1971), and Somerscales and Parsapour (1982) among others. There is some disagreement as to the exact value of the transition Rayleigh number, but there is little disagreement about its occurrence. The first and higher transitions in the heat transfer curve were first reported by Malkus (1954) yet their existence remains controversal because changes in the slope of the heat transfer data used to find the transitions are small relative to the precision of the experiments. The transition to three-dimensional motion takes place near the upper boundary of the stability envelope shown in Fig. 2. Further increases in the Rayleigh number result in periodic behavior in time, aperiodic behavior, and finally chaotic behavior or turbulence. Here we will emphasize the region within the stability balloon shown in Fig. 2. The focus will be on means by which one can select a wavenumber. Three approaches will be described that have each had a limited amount of success in predicting wavenumbers of convection in commonly encountered geometries.

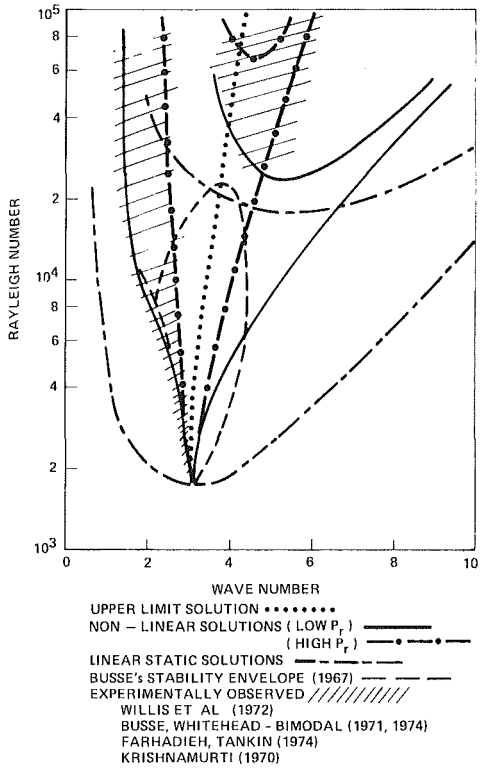

Fig. 2 Relationship between wavenumbers and the Rayleigh number

Extended Power Integral Solutions

Forty years ago Landau (1944) postulated that turbulent flow develops as a series of instabilities sequentially occurring as the driving potential (in this case the Reynolds number) is increased until the flow is fully turbulent. The rate at which these instabilities appear as the driving potential is increased depends on the nature of the flow. The best example of such a route to turbulence is provided by Rayleigh-Bénard convection where the driving potential is characterized by the Rayleigh number. As the Rayleigh number increases the flow passes from a steady quiescent state to singly periodic and then to doubly periodic and higher periodicity cells. These transitions have been the subject of much discussion and research since the early work of Malkus (1954). An overview of this work is given by Somerscales and Parsapour (1982).

Landau (1944) points out that with each new frequency an arbitrary phase is introduced giving the flow added degrees of freedom. The successive instabilities are, therefore, in some sense associated with the appearance of additional degrees of freedom, which support higher frequency modes in the mo-

Nomenclature

a = wavenumber
e = internal energy
f = horizontal solution of Helmholtz equation
g = gravitational constant
k = thermal conductivity
$\mathbf{k}$ = unit vertical vector
L = layer depth
N = number of eigenvalues
Nu = Nusselt number
P = pressure
Pr = Prandtl number
q = heat flux
Q = volumetric heat source
$\mathbf{r}$ = radial horizontal vector
Ra = Rayleigh number $(=g\,\beta(T_H - T_c)L^3/\nu\kappa)$
s = entropy
t = time
T = temperature
$\bar{T}$ = horizontal average temperature
T' = temperature deviation from horizontal average
$\mathbf{u}$ = velocity vector
u, v, w = components of velocity
W = z component of vertical dimension
z = normalized vertical dimension
β = isobaric coefficient of thermal expansion
γ = Liapunov function
δ = finite difference
δ = thermohydrodynamic functional
θ = z component of temperature deviation
∇ = gradient operator
κ = thermal diffusivity
λ = wave length $(\lambda = 2\pi/a)$
ν = kinematic viscosity
ρ = density

Subscripts

i, j, k, m = summation integers
$L, 0$ = lower surfaces
$u, 1$ = upper surface
c = "critical value"
O = reference quantity
H = hot boundary
C = cold boundary

Downloaded 16 Dec 2010 to 193.140.21.150. Redistribution subject to ASME license or copyright; see http://www.asme.org/terms/Terms_Use.cfm

tion. Unfortunately the hydrodynamic equations of motion are nonlinear, precluding simple superposition of these modes. The global nonlinear effects, however, have been found to be small for a certain class of problems where the driving potential is not changed by the appearance of the instabilities. Malkus and Veronis (1958) and Stuart (1958) formulated an averaging procedure (called the power integral), in a pair of papers appearing almost simultaneously in the *Journal of Fluid Mechanics*, following Landau's suggested methodology that addresses the Bénard and Taylor problems. Embodied in the procedure are two critical assumptions about the nonlinear structure of the convective process:

1 Nonlinear self-distortion of a given mode is small so that only the amplitude, and not the shape, of the convective motion changes as the driving potential is increased (the "Stuart Shape Assumption").

2 The global effect of nonlinear interactions between successive modes arising from the instabilities is small so that global transport contributions from succcessive modes may be summed (Malkus and Veronis).

With these two assumptions, Landau's successive instabilities are distinctly associated with the eigenvalues of the linear problem and the convective mode shapes are given by the corresponding eigenfunctions of the lienar problem. Catton (1966) has used this approach very effectively for a number of problems. It was found that the overall transport (Nusselt number) was predicted well; however, velocities and temperatures were not well predicted much beyond the onset of motion. In particular, when the motion changed the driving potential, for example in convection driven by volumetric heating, even the transport characteristics were not well predicted. An extended or nonlinear power integral is described here that to a great degree overcomes these problems.

Many methods have been used in the past to solve the partial differential equations for a heated layer. The method to be used here is a separation of variables technique that results in a set of equations called the mean field equations. The method is chosen because it retains some of the characteristics of three-dimensional flows and allows both the number and values of the wavenumber to be determined implicitly. In using this approach, the flow is assumed to be periodic in the horizontal plane, which, in turn, leads to a coupled set of differential equations for the vertical structure. These equations are solved in terms of wavenumbers to yield useful details of the flow and temperature structure. Their derivation is found in Appendix A.

It has long been known that the Navier–Stokes and energy equations do not have unique solutions. The Navier–Stokes equation has a unique solution only if it is considered as an initial value problem (see Serrin, 1959). Thermal convection experiments have been performed by many and all have found essentially the same result. Thus, it appears that some governing principle(s) must exist, which forces uniqueness or closure. Earlier investigators have left the number and values of the wavenumbers as parameters. A close inspection of the equations (see Appendix A) reveals that a characteristic problem exists for the wavenumbers. Thus, both the numbers and values of the wavenumbers are determined by the equations as eigenvalues, which depend on the mean temperature profile under study. This eigenvalue problem does not remove the degeneracy since there are essentially an infinite number of possible mean temperature profiles within the solution envelope. One set of limits is the familiar curves of marginal stability. Several sets of results are given in Fig. 2, two of which are the curves of marginal stability for the static case of Bénard convection. Each curve for the static case represents a mode of convection. These modes occur alternately in even and odd type solutions with the number of sign changes in the vertical velocity determining its character. Each mode has two branches, which will be denoted the left and right-hand branch with subscripts l and r.

The nonlinear solutions have wavenumbers that lie within the curves of the lower-limit solution. Two typical wavenumber relationships are shown in Fig. 2 as solid and dot-dash curves. Note that the onset of the second mode is raised above the linear static case.

The upper-limit solution, the dotted line, completely suppresses the onset of the higher modes. The left and right branches have collapsed to a single line leaving only a single wavenumber. This solution bisects the wavenumber space for the first mode so that all other solutions have wavenumbers that lie on either side.

From Fig. 2, it is apparent that all solutions have a multiwavenumber character except the upper limit solution. Since there are essentially an infinite number of possible solutions, closure must be sought. The simplest method might be to obtain the extremal of some property of the flow. The extremal, if it is found, must allow one to calculate temperature and velocities that are in agreement with experimental data. We will return to this topic below.

At slightly supercritical Rayleigh numbers a single mode exists that has two eigenvalues corresponding to the right and left wavenumbers. There are two degrees of freedom rather than one as has previously been assumed. Properties of these solutions represent surfaces in the space of eigenfunction amplitudes and not simple graphs. As the Rayleigh number is increased a second mode will appear, with its right and left wavenumber adding two more degrees of freedom, yielding four degrees of freedom in the bimodal convection regime. Further increases in Rayleigh number will lead to further increases in the degrees of freedom as more modes are excited. Here we will only focus on the first mode.

At this point it is perhaps best to discuss the degrees of freedom associated with the mean field equations. It was found that each set of eigenfunctions (ω_i and θ_i) constitutes a degree of freedom. Thus at slightly supercritical Rayleigh numbers a single mode exists, which has two sets of eigenfunctions corresponding to the left and right-hand branches of the Rayleigh number wavenumber curve. Properties of these solutions represent surfaces in the space of eigenfunction amplitudes and not simple graphs. As the Rayleigh number is increased, a second mode will appear, adding two more degrees of freedom. Graphic representation in this range is practically impossible since the dependent variables lie in four-dimensional space. As the Rayleigh number is further increased more and more degrees of freedom are added. For example at Ra = 60,000 in Bénard convection Suo-Antilla (1977) calculated twelve degrees of freedom.

The independent variables are the amplitudes of the eigenfunctions. They can be treated in terms of two variables that are more familiar: the Nusselt number, and a separation parameter ϵ. They are related by evaluating the horizontally averaged energy equation (see equation A.12) at the upper boundary. The result is

$$(\mathrm{Nu}-1)\mathrm{Ra} = <\overline{w\theta}>_r + <\overline{w\theta}>_l \tag{1}$$

$$<\overline{w\theta}>_l = (1-\epsilon)(\mathrm{Nu}-1)\mathrm{Ra} \tag{2}$$

$$<\overline{w\theta}>_r = \epsilon(\mathrm{Nu}-1)\mathrm{Ra} \tag{3}$$

where the overbar denotes a horizontal average over a cell and the carets a vertical average from plate to plate. By varying Nu and ϵ, all possible combinations of eigenfunction amplitudes can be found. The Nusselt number can vary from unity (pure conduction) to the maximum value found by Roberts (1966). Nusselt numbers outside this range result in no solution to the equations being found.

The steps followed to obtain solutions to the set of equations derived in Appendix A were

Downloaded 16 Dec 2010 to 193.140.21.150. Redistribution subject to ASME license or copyright; see http://www.asme.org/terms/Terms_Use.cfm

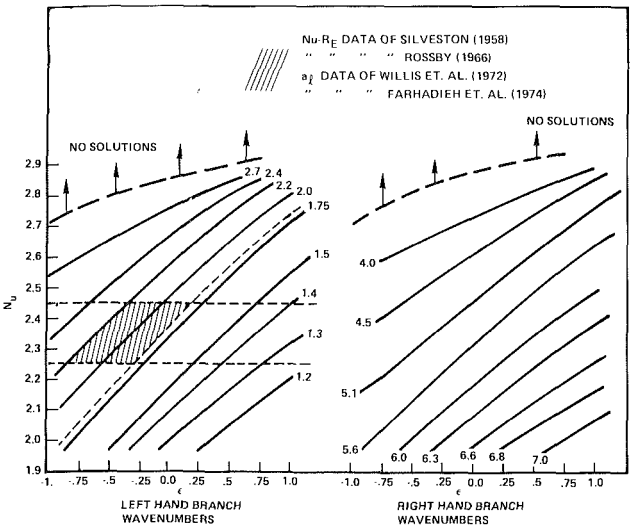

Fig. 3 Lines of constant wavenumber at Ra = 10,000

1 Select an initial temperature gradient (either the conduction solution or the simple power integral result) and the two independent parameters Nu and ϵ.

2 Obtain the amplitude of the eigenfunctions from equations (2) and (3) with the chosen values of ϵ and Nu for a given Ra. When bimodal convection results are being sought, three values of ϵ and Nu are needed to treat the four wavenumbers that result.

3 Set $\sigma_k = 0$ in equation (A.19) and solve the characteristic equation for a_k.

4 Calculate the eigenvectors $C_{m,k}$ and the normalized shapes of w_k and θ_k.

5 Integrate equation (A.21) forward a small amount of time and use the result of equation (A.20) to obtain a new $T(Z)$.

6 Calculate a new temperature gradient $\partial T/\partial Z$ using the results of step 5.

7 Repeat steps 3–6 until the residual $F < 10^{-6}$, where

$$F = \int_0^1 \left[\int_0^z \frac{\partial T}{\partial t}\, dz' - \int_0^z \frac{\partial T}{\partial t}\, d_{z'} \right]^2 dz$$

$$= \int_0^1 \left[\frac{\partial T}{\partial z} + R + \sum_k - < w\theta >_k \left(1 - \frac{\overline{w\theta}_k}{< \overline{w\theta} >_k} \right) \right]^2 dz \quad (4)$$

It can be seen that F is the mean square time derivative. At one time it was used as functional for a variational approach that was abandoned due to numerical difficulties. It does, however, have some interesting properties. For a converged solution, it will be identically zero, and its derivative with respect to $< w\theta >_i$ will be zero, yielding

$$\left[\int_0^1 \left(1 - \frac{\overline{w\theta}_k}{< w\theta >_k} \right) \left(1 - \frac{\overline{w\theta}_i}{< \overline{w\theta} >_i} \right) dz \right] | < \overline{w\theta} >_k | =$$

$$- \left| \int_0^1 \left(\frac{\partial T}{\partial z} + \mathrm{Ra} \right) \left(1 - \frac{\overline{w\theta}_i}{< \overline{w\theta} >_i} \right) dz \right| \quad (5)$$

and for internal stability the determinant of the second variation

$$D = \left| \left| \int_0^1 \left(1 - \frac{\overline{w\theta}_k}{< \overline{w\theta} >_k} \right) \left(1 - \frac{\overline{w\theta}_i}{< \overline{w\theta} >_i} \right) dz \right| \right| > 0 \quad (6)$$

must be positive. The expression above will be used below in a discussion of closure.

Determination of the appropriate values of Nu and ϵ at a given Ra is done by selecting values in the vicinity of measured values. Figure 3 shows lines of constant wavenumber for the left and right-hand branch solutions at an Ra of 10,000. Experiments indicate that the number is between 2.25 and 2.45 (Silveston, 1958; Rossby, 1969) and the wavenumbers are between 1.8 and 2.2 (Willis et al., 1972; Faradieh and Tankin, 1974) for water and air. The cross-hatched area in Fig. 3(*a*) delineates where the experimental observations are located.

Since the cross-hatched region in Fig. 3(*a*) is centered at $\epsilon \simeq -0.25$, certain inferences can be drawn. First, the flow is inherently multi-wavenumber in nature. Single wavenumber flows are represented by $\epsilon = 0$ or $\epsilon = 1$. The experimental data suggest only a small region where $\epsilon = 0$. Thus it could be concluded that Bénard-type convection may always be multi-wavenumber except at the onset of motion. Further, the negative eigenfunction amplitudes ($\epsilon < 0$) mean that the velocity and temperature fields of the right-hand branch are out of phase. The amplitudes of the eigenfunctions $< w\theta >$ for $\epsilon = -0.25$ and Nu = 2.35 are 1.69 for the left-hand branch and -0.34 for the right-hand branch. The left-hand branch, the most frequently observed, has five times the amplitude of the right-hand branch. It is not clear what this means.

It is not surprising that the right-hand branch has gone unnoticed. A close examination of the photographic plates made by Willis et al. (1972) reveals that the convective "rolls" are actually multi-wavenumber in nature. The convective rolls show up as alternating bands of light and dark regions at all Rayleigh numbers. Superimposed on these bands are perpendicular bands, which might correspond to the right-hand branch wavenumbers. By measuring the wavelengths of the rolls and cross rolls for water it was found that the wavenumber ratio (i.e., a_r/a_l) at Ra = 11,000 is approximately 2.7 and at Ra = 17,500 it is 3.2. These measurements can be compared to the values resulting from the mapping given in Fig. 3 (2.6) and from Fig. 2 at Ra = 17,500 (3.4). The experimental results seem to confirm the existence of multi-wavenumbers even at relatively low Ra.

Figure 2, referred to earlier, presents results obtained by insuring that agreement with experimental data was obtained. In this figure the nonlinear solutions for water are shown as solid lines and for very high-Pr material (oil) as dash-dot lines. Two important effects of the nonlinearity and Prandtl number can be ascertained from these efforts. First, nonlinear solutions fall well within the linear theory solutions and increasing Prandtl number suppresses the onset of higher modes. For water (Pr = 6.7) the onset of the second mode is at Ra $\simeq$ 25,000, whereas for high-Pr fluids, Ra $\simeq$ 60,000. This is in agreement with the experimental results of Krishnamurti (1970).

An unexpected result is the shape of the velocity and temperature profiles when four wavenumbers exist. Figure 4 shows the relative shapes of the vertical velocity w and temperature deviation θ. The first mode of even eigenfunctions describes the first set of cross rolls. Shown are left and right-hand branch solutions and they are seen to be symmetric about the centerline of the layer. The lower half of the figure gives the shape of the velocity and temperature fields for the left and right-hand branches for the second or odd mode. Only half of the curves are shown because the shapes are antisymmetric about the centerline. The antisymmetry implies that the second mode is a double vertical roll. The eddy diffusivity $\overline{w\theta}$ at Ra = 40,000 is shown in Fig. 5 normalized to unity on the vertical scale by the Nusselt number. Note that even though symmetric and antisymmetric functions are involved, the result is an even function.

The mean field method presented here was used to map out the eigenfunction product amplitude dependence on Rayleigh number for water using available data, which are sparse. The result is shown in Fig. 6. The arrows indicate the uncertainty in the data. Above a Rayleigh number of 25,000 the uncertainty is very large and the results shown are based on reasonably shaped temperature profiles. The right-hand eigenfunction product amplitude is seen to be of relatively small amplitude.

Downloaded 16 Dec 2010 to 193.140.21.150. Redistribution subject to ASME license or copyright; see http://www.asme.org/terms/Terms_Use.cfm

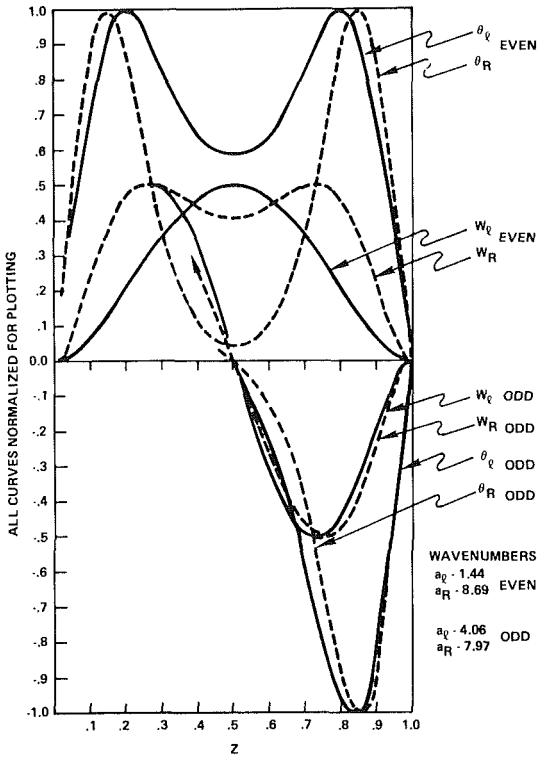

Fig. 4 Eigenfunctions at Ra = 40,000 with Nu = 3.3 in Bénard convection

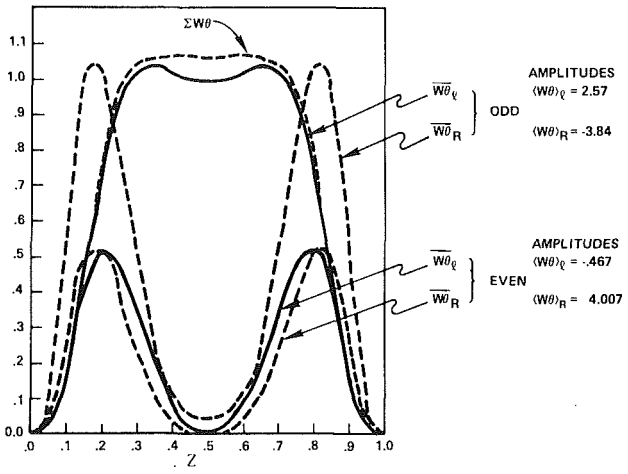

Fig. 5 Product of eigenfunctions in Bénard convection at Ra = 40,000 with Nu = 3.3

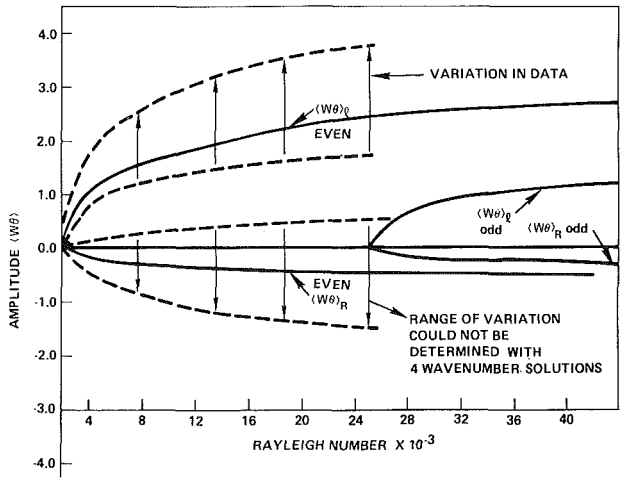

Fig. 6 Range of eigenfunction amplitudes as a function of the Rayleigh number in Bénard convection at Ra = 40,000 with Nu = 3.3

This may explain why it has not been seen in earlier experiments. The transition from two-dimensional motion to three-dimensional motion may not be sudden but rather a gradual process as the right-hand branch grows in amplitude.

The results presented above required experimental data for closure. Convection experiments initiated from almost random initial conditions result in the final state where the mean temperature distribution $\bar{T}(Z)$ is remarkably reproducible and stationary in time. A similar preferred state is found for turbulent pipe flow mean velocity profiles when far enough downstream. All of the experimental evidence seems to suggest that a preferred state exists that is independent of the flow history and initial conditions. Determining what this preferred state is has captured the attention of many researchers, none of them completely successful.

Maximizing heat transfer has been the most widely used closure principle. It was originally suggested by Malkus (1954) and received minor revision by Howard (1963) and Busse (1969). The heat transfer overprediction still exists and unless there are heretofore undiscovered additional constraints, maximizing heat transfer does not achieve the proper closure. Maximizing heat transfer can be shown to be maximum or minimum in entropy production depending on the boundary conditions, and to a maximum in viscosity dissipation mean square vorticity. Malkus and Veronis (1958) suggested maximization of the mean square temperature gradient. Figure 7 shows the results of a number of attempts at closure for Ra = 10,000, and there is no sign of an extremal in the vicinity of measured values.

Another approach to find closure is to use a relative stability criterion. Busse (1967) carried out such an analysis, by computing where the growth rate of a new disturbance would decay and outside which it would grow. Roberts' (1966) analysis is similar and his upper limit solution passes through the stability envelope of Busse (see Fig. 2). In examining experimental data it is found that a large amount of data falls outside the stability envelope and virtually no data fall in the

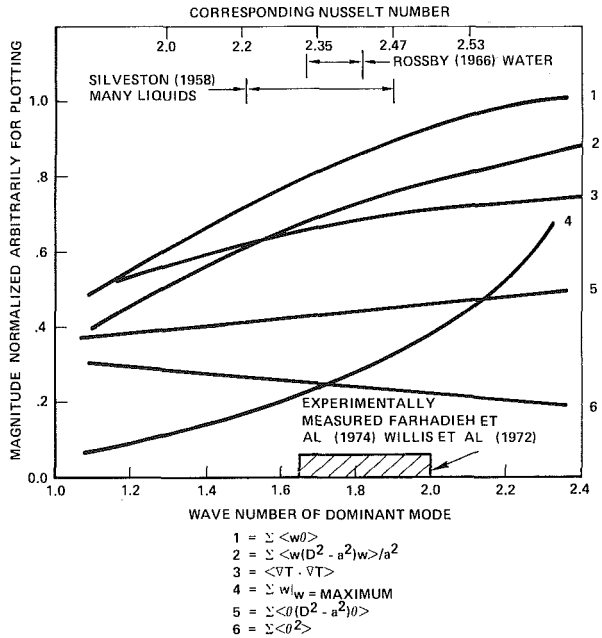

Fig. 7 Various closure attempts at Ra = 10,000

Downloaded 16 Dec 2010 to 193.140.21.150. Redistribution subject to ASME license or copyright; see http://www.asme.org/terms/Terms_Use.cfm

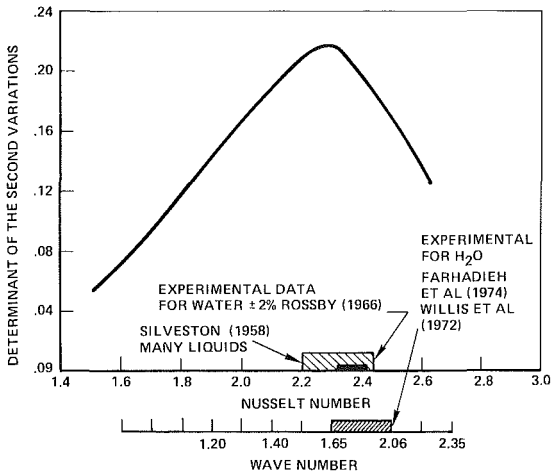

Fig. 8 Magnitude of the determinant of the second variation at Ra = 10,000

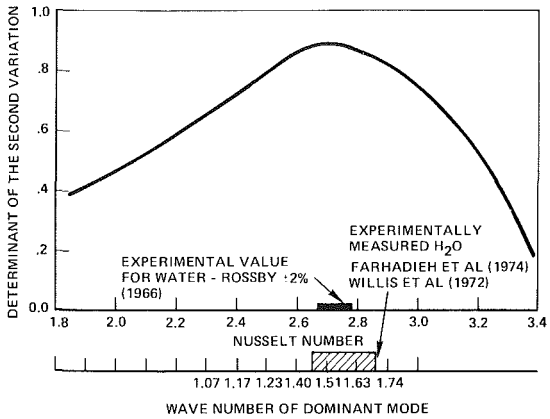

Fig. 9 Magnitude of the determinant of the second variation at Ra = 20,000

right half. Thus, it appears that the stability analysis of Busse may be incomplete, although it certainly does reduce the range of uncertainty.

Some encouraging results were obtained when the determinant of the second variation of the mean square time derivative of the mean temperature (see equation (6)) was plotted as a function of the dominant wavenumber. It was found that the determinant was positive, as it should be, and that it exhibited a maximum in the vicinity of the experimental data for both Ra = 10,000 and Ra = 20,000. This very encouraging result deserves more attention. The physical meaning of the parameter plotted is not yet understood nor has the range of applicability been fully explored. It clearly shows more promise than all past attempts at closure.

In summary, the mean field equations will yield excellent agreement with all aspects of experimental data given some closure. Multi-wavenumbers appear to exist from the onset of convection by experiment. Closure of the problem by past methods does not result in the experimentally observed behavior.

A Thermodynamic Principle for Wavenumber Selection

As remarked above, the conservation equations possess stable solutions for a whole continuum of values of the wavenumber between the bounding linear stability values at a given Ra. Hence, unless, the wavenumber is prescribed, solutions to the conservation equations are not unique and an additional relationship is necessary before a unique solution to the complete problem can be obtained. To derive this extra relationship we begin with the nonequilibrium thermodynamic theory presented by Glansdorff and Prigogine (1971). Although the initial steps have been given by McDonough and Catton (1979), they are repeated here for completeness.

It is worth noting at the outset that Rayleigh–Bénard convection constitutes a physical situation that is far from thermodynamic equilibrium, and as a consequence the often misused principle of minimum entropy production is not applicable. The valid generalization introduced by Glansdorff and Prigogine (1971) takes the form of a Liapunov stability functional, which includes both thermodynamic and hydrodynamic contributions; namely

$$\gamma = s - \frac{1}{2} T_0^{-1} |\mathbf{U}|^2 \tag{7}$$

where $\mathbf{U} \equiv (v, w) \in \mathrm{Ra}^2$, and $|\cdot|$ is notation for the inner product $\mathbf{U}\cdot\mathbf{U}$. T_0 is a suitable reference temperature (here taken to be the horizontally average mean temperature of the fluid layer), and s is specific entropy. The only major assumption needed to obtain the desired stability functional from equation (7) is that, although the convecting system, as a whole, may be far from the equilibrium state, locally within the system thermodynamic equilibrium prevails. This is known as the local thermodynamic equilibrium assumption, abbreviated LTE. For this to be valid, it is only necessary that the same equation of state hold throughout the system, and that this equation be independent of gradients of the state variables. This is, of course, true for Bénard convection in a Boussinesq fluid.

In the equilibrium case, thermodynamic stability is guaranteed when the time rate of change of the second differential of entropy is nonnegative. Application of this to equation (7) yields

$$\frac{\partial}{\partial t}(d^2\gamma) = \frac{\partial}{\partial t}(d^2 s) - T_0^{-1}\frac{\partial}{\partial T}|dU|^2 \geq 0 \tag{8}$$

Then, by invoking the local thermodynamic equilibrium (LTE) assumption, and in particular the Gibbs relation, we obtain

$$d^2 s = dT^{-1} de + d(pT^{-1}) dv$$

and substitution into equation (8) leads to the local thermohydrodynamic stability condition[1]

$$dT^{-1}\frac{\partial}{\partial T}(de) + d(pT^{-1})\frac{\partial}{\partial t}(dv) - T_0^{-1}\frac{\partial}{\partial T}|d\mathbf{U}|^2 \geq 0$$

From the Boussinesq approximation we have $dv = 0$; and by taking

$$dT^{-1} = -\frac{1}{T_0^2} dT$$

as in Glansdorff and Prigogine (1971), and noting that $de = c_v dT$, we obtain

$$-c_v dT \frac{\partial}{\partial t}(dT) - 2T_0 d\mathbf{U}\cdot\frac{\partial}{\partial t}(\partial\mathbf{U}) \geq 0$$

Finally, we replace differentials with "*"-notation, observe that dimensionally $c_v \sim \beta g L$, and introduce the same scalings employed for equations (A.1)–(A.3). The result is the local thermohydrodynamic stability condition for Rayleigh–Bénard convection

$$-T^*\frac{\partial T^*}{\partial t} - \frac{2}{\mathrm{Pr}} T_0 \mathbf{U}^*\cdot\frac{\partial \mathbf{U}^*}{\partial t} \geq 0$$

To obtain the global condition we merely integrate over a

[1] Note that this expression differs from the corresponding result in McDonough and Catton (1979) by a factor of 2 in the last term. This, and replacing c_v by $\beta g h$, does not affect the linearity properties, and accomplishes a convenient rescaling of the kinetic and thermal energy contributions.

Downloaded 16 Dec 2010 to 193.140.21.150. Redistribution subject to ASME license or copyright; see http://www.asme.org/terms/Terms_Use.cfm

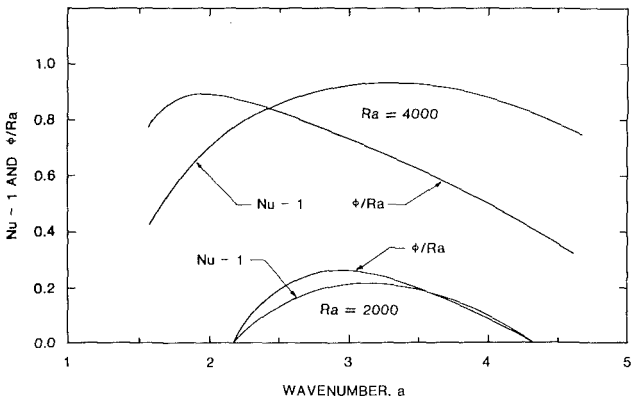

Fig. 10 Comparison of Nusselt number and stability functional as a function of wavenumber and Rayleigh number

Bénard cell. In the two-dimensional case this yields the global stability functional ϕ, and the associated stability condition

$$\phi = \int_0^1 \int_0^{\pi/a} \left(-T^* \frac{\partial T^*}{\partial t} - \frac{2}{\mathrm{Pr}} T_0 \mathbf{U}^* \cdot \frac{\partial \mathbf{U}^*}{\partial t} \right) dydz \geq 0 \quad (9)$$

The time derivatives are evaluated from

$$\frac{1}{\mathrm{Pr}} \frac{\partial \mathbf{U}^*}{\partial t} = -\frac{1}{\mathrm{Pr}} \mathbf{U}^* \cdot \nabla \mathbf{U}^* - \nabla p^* + T^* \mathbf{e}_3 + \Delta \mathbf{U}^* \quad (10a)$$

and

$$\frac{\partial T^*}{\partial t} = -\mathbf{U}^* \cdot \nabla T^* + \Delta T^* \quad (10b)$$

where U^*, T^*, and p^* are obtained from solutions to equations (A.1)-(A.3).[2]

It must first be remarked that the stability condition equation (9) is satisfied for all wavenumbers within the bounds of the neutral stabiltiy curve for any given Ra. It is also important to observe that ϕ attains a unique maximum interior to the interval of stable wavenumbers. This is indicated in Fig. 10, which compares ϕ and Nu for $Ra = 2000$ and 4000. As can be seen, the maximum of ϕ moves toward smaller values of wavenumber as Ra increases, while Nu exhibits just the opposite trend. It is tempting to associate the preferred wavenumber with the maximum of ϕ for each Ra; but comparisons with experimental results show that this value of wavenumber would quickly become much smaller than observed values as Ra increases.

When equations (10) are substituted into equation (9) there results an expression that can be rearranged as the difference between dissipative and convective effects. Chandrasekhar (1961) has shown that at the onset of convective motion, dissipation of kinetic energy (by viscous effects) must just balance the internal energy release due to buoyancy (i.e., the thermal potential). Moreover, the critical wavenumber a_c ($=3.117$) can be predicted on the basis of this. Koschmieder (1969) has conjectured that maintenance of such a balance is the physical basis for wavenumber selection when Ra is only slightly greater than Ra_c. The stability functional (9) provides a generalization of these ideas, which includes thermal (conductive) dissipation and convection. Thus, it should be applicable even when Ra is much greater than Ra_c. Because ϕ is more general, we do not expect the simple balance between viscous dissipation and thermal potential, but conjecture that instead the stability functional ϕ should be a general linear function of the thermal potential. Since Ra is the dimensionless thermal potential, it follows that wavenumbers should be selected in such a way that

$$\frac{d^2\phi}{dRa^2} = 0 \quad (11)$$

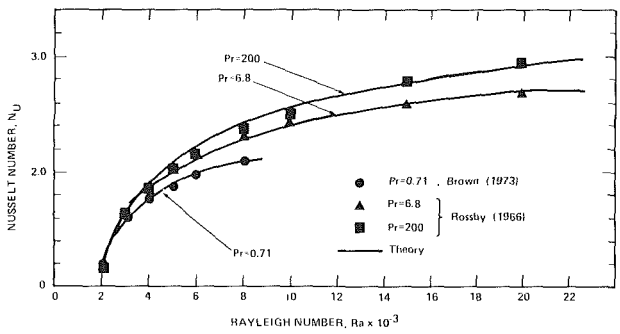

Fig. 11 Comparison of theoretical and experimental heat transfer

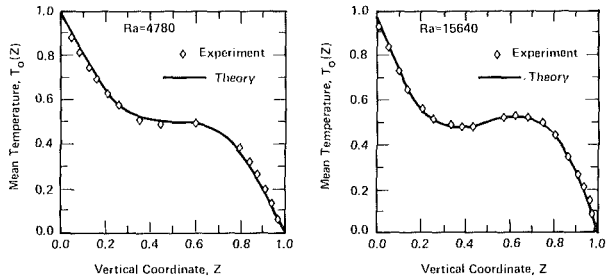

Fig. 12 Comparison of theoretical and experimental mean temperatures (note: experimental data from Farhadieh and Tankin, 1974, for Ra = 15,640 are midcell temperatures, rather than mean temperatures)

for ϕ evaluated at the preferred wavenumber. The validity of equation (11) has been demonstrated for $0.71 < \mathrm{Pr} < 450$ between the first two critical values by calculating ϕ at the experimentally measured wavenumbers of Willis et al. (1972). The results of the calculation are shown in Fig. 10.

Based on the experimental verification of equation (11), a wavenumber equation is obtained by noting that with Pr fixed, ϕ is a function only of Ra and a. Thus,

$$\frac{d\phi}{d\mathrm{Ra}} = \frac{\partial \phi}{\partial \mathrm{Ra}} + \frac{\partial \phi}{\partial \mathrm{Ra}} \frac{da}{d\mathrm{Ra}}$$

and

$$\frac{d^2\phi}{d\mathrm{Ra}^2} = \frac{d}{d\mathrm{Ra}} \left(\frac{\partial \phi}{\partial \mathrm{Ra}} \right) + \frac{\partial \phi}{\partial a} \frac{d^2 a}{d\mathrm{Ra}^2} + \frac{d}{d\mathrm{Ra}} \left(\frac{\partial \phi}{\partial a} \right) \frac{da}{d\mathrm{Ra}}$$

which can be rewritten

$$\frac{\partial \phi}{\partial a} a'' + 2 \frac{\partial^2 \phi}{\partial a \partial \mathrm{Ra}} a' + \frac{\partial^2 \phi}{\partial a^2} (a')^2 + \frac{\partial^2 \phi}{\partial \mathrm{Ra}^2} = 0 \quad (12)$$

where the prime denotes ordinary differentiation with respect to Ra.

Equation (12) will be treated as an evolution operator by supplying it with two initial conditions. If we begin at the onset of convection, it is clear that one condition is

$$a(\mathrm{Ra}_c) = a_c = 3.117$$

The second required condition is $a'(\mathrm{Ra}_c)$. No completely satisfactory prescription of this value has yet been given. Thus, in this work $a'(\mathrm{Ra}_c)$ is derived from experiment.

$$a'(\mathrm{Ra}_c, \mathrm{Pr}) = -\frac{4.2148 \times 10\ \mathrm{Pr} + 7.2761 \times 10^{-3}}{3.55257 \times 10^{-2} \mathrm{Pr} + 1} \quad (13)$$

The theoretical calculations shown in Fig. 11 were done using equation (12) with (13) as closure. The Pr number dependence is seen to be correct for $\mathrm{Ra} \leq 5000$. Figure 12 shows predictions of the corresponding mean temperature profiles. Agreement between theory and experiment is seen to be quite good.

Downloaded 16 Dec 2010 to 193.140.21.150. Redistribution subject to ASME license or copyright; see http://www.asme.org/terms/Terms_Use.cfm

There are two main implications of the wavenumber initial value problem. The first is that experimental wavenumbers can be predicted, despite the fact that they may vary among experiments. The initial wavenumber derivatives (calculated using one data point) appear to provide a quantification of variations in experimental procedures and geometry, which is adequate for accurate theoretical wavenumber predictions via the wavenumber equation. The only qualification is that the experiments themselves be performed in an evolutionary manner.

The second implication concerns the hysteresis phenomena often observed in Bénard convection experiments. The principal feature of hysteresis is that the wavenumber path in decreasing Ra experiments does not retrace the path followed for increasing Ra. With respect to this, there are two predictions that can be made on the basis of the initial value problem. First, if the wavenumber path has not proceeded through a bifurcation point prior to reversing the direction of δRa, the original path should be retraced to within experimental error. On the other hand, if a bifurcation point has been crossed, there is no reason to expect retracing of the original path beyond the bifurcation point when the Ra direction is reversed.

In the first case, because there is no significant structural change in the Bénard cells, we should expect that reversing the direction of δRa at any particular Ra should have no effect on a'. But in the second case, where significant changes in cell structure occur when the bifurcation point is crossed, it does not seem likely that, for instance, $a'(\mathrm{Ra}_{c2})$ would be the same for Ra increasing and cellular structure changing from two- to three-dimensional, as $a'(\mathrm{Ra}_{c2})$ with Ra decreassing and structure changing from three- to two-dimensional.

We note that there have been few experiments in which any systematic investigations of hysteresis have been conducted. There are limited data for very high Pr fluids in Willis et al. (1972) that support the above contentions, while results in Krishnamurti (1970) are inconclusive in this respect.

An Asymptotic Approach to the Preferred Wavenumber

The lack of success with thermodynamic principles has led to a more physical approach to wavenumber selection. One argues that a large uniform thickness region bounded by gently tapering regions will allow the wavenumber in the uniform region to take on the preferred value expected in an infinite domain. These "soft" boundaries allow the wavenumber to change easily and continuously, thereby allowing the convection pattern to achieve an "ordered" steady state in a relatively short time. Although the concept is a simple one the mathematics are complex. Several recent papers have shown that various types of soft boundaries select unique wavenumbers. Kramer et al. (1982) and Kramer and Riecke (1985) varied one or more external parameters so that the system became subcritical near one boundary. For Bénard convection ramping of both temperature and plate spacing were considered. It was found that although the behavior near the critical wavenumber was unique it depended on the variable being ramped. Their results were limited to very near the critical Rayleigh number. Cannel et al. (1983) conducted an experiment to determine whether or not unique wavenumbers would result for the Taylor problem (fluid between concentric cylinders with the inner one spinning). They varied the gap between the cylinders and found unique wavenumbers, in contrast to the constant spacing case where a wide range of wavenumbers are found. There are no theoretical calculations for the Taylor problem using Kramer and Riecke formalism, but the qualitative similarities between the Taylor problem and the Bénard problem are close enough to be encouraging.

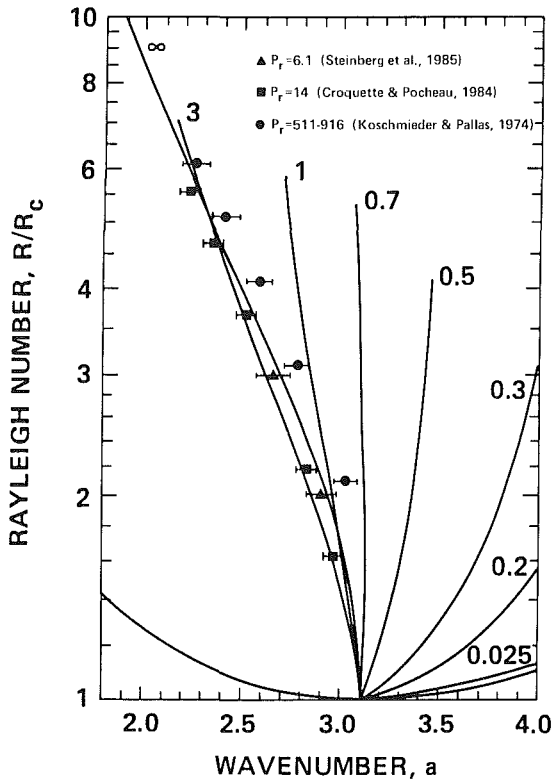

Fig. 13 Predicted preferred wavenumber

Buell and Catton (1985) extended these ideas by calculating wavenumbers for Rayleigh numbers between the first two critical values. The analysis is for slightly bent rolls (very large radius of curvature) and assumes that there is a horizontal pressure gradient strong enough to force the net flow induced by curvature to zero. These assumptions are certainly satisfied for axisymmetric convection in a large-aspect-ratio cylinder. The governing partial differential equations are given in Appendix C. They were solved using a mixed finite-difference Galerkin procedure and an iterative scheme to find the preferred wavenumber.

Results for preferred wavenumber are shown as a function of Rayleigh number for several Prandtl numbers in Fig. 13. Some experimental data of Pocheau and Croquette (1984), Steinberg et al. (1985), and Koschmeider and Pallas (1974) are also shown. The analysis, represented by solid curves, extends up to where straight parallel rolls are thought to become unstable. The experiments shown were done with either water (Prandtl number of about 6) or oil (70, 500), and agree very well with the theory. For Prandtl numbers less than 0.7 the wavenumber is seen always to be larger than its value at critical. This is a surprising result. Unfortunately, no axisymmetric experimental results could be found for comparison. The slope of the wavenumber-Rayleigh number curve at the critical point agrees with the analytical work of Manneville and Piquemal (1983). In particular, their results show that the initial slope is positive for Prandtl numbers smaller than 0.784, although they did not mention the significance of this. The slope at the critical point is seen to be quite different from its value at higher Rayleigh numbers. As a result one cannot extrapolate wavenumber behavior from regions of small amplitude behavior to high Rayleigh numbers with any confidence. The nonlinear problem must be solved to obtain reliable wavenumber predictions.

At high Prandtl numbers, the preferred wavenumber depends very weakly on the Prandtl number. This appears to take place for Prandtl numbers greater than 3. The results at

Downloaded 16 Dec 2010 to 193.140.21.150. Redistribution subject to ASME license or copyright; see http://www.asme.org/terms/Terms_Use.cfm

the higher Prandtl numbers compare well with experimental data, but more calculations and comparisons of other parameters such as temperature, temperature gradient reversal and its location, and heat transfer are needed before the asymptotic method used by Buell and Catton (1985) is fully verified. It is, however, the first set of calculations for roll cell convection extending over the domain of Rayleigh numbers where they are stable that does not require empirical data for closure.

Conclusion

Large amplitude Rayleigh–Bénard convection was studied using an extended power integral approach. This yielded some rather interesting results. First it was possible to obtain all the important aspects of large-amplitude convection, providing one matched the measured heat transfer. The solutions showed that there is a possibility of multi-wavenumber solutions at all supercritical Rayleigh numbers. The onset of time dependence was found to consist of two wavenumbers, with the temperature and velocity of the right-hand branch being out of phase. Experimental measurements seem to give credence to the multiple wavenumber solutions.

Some closure schemes were looked at and none were found to be fully satisfactory. The one closure scheme that showed some potential needs more testing against data. It was concluded that extremals based on simple properties of the flow may not exist for horizontal fluid layers of infinite extent.

A thermodynamic stability criterion was used to obtain an equation for the wavenumber. The criterion still required experimental data. The amount of data required was, however, much less in that all that was needed was the initial rate of change of the wavenumber with Rayleigh number. Given these data, the first predictions of the proper wavenumber–Rayleigh number behavior were obtained. Temperature and heat transfer results compared well with experiment up to the onset of bimodal convection. Here the wavenumber found is the left-hand wavenumber, which is the dominant one, of the results discussed above. This seems to be a contradiction and maybe it is. The thermohydrodynamic stability criterion needs to be extended to multi-wavenumber. Another possibility is to use it with the mean field equations, as was done in extending the power integral. The wavenumber expansion used in Appendix B may not be appropriate. In a similar problem, convection in a porous medium, the flow has been observed to take on a different wavenumber but not simultaneously. Further, as noted above, one can interpret some of the available experimental data as showing the existence of multi-wavenumbers at relatively low Rayleigh numbers.

Calculations of the preferred wavenumber using an asymptotic approach were found to agree well with experimental studies using large Prandtl number fluids ($Pr > 3$). The prediction that the wavenumber increases with increasing Rayleigh number when the Prandtl number is below 0.7 or so is new but lacks experimental verification. These calculations required no experimental data to eliminate the nonuniqueness in wavenumber. This result is encouraging. Its extension to multi-wavenumbers is conceptually possible. What mathematical difficulties one might encounter are, at this point, unknown.

It still seems to us that a principle of some sort must exist. The experimentally observed wavenumbers are usually consistent with one another without the "soft" wall needed in the analysis. Heat transfer results are consistent and independent of aspect ratio as long as the aspect ratio is large enough. Here large enough is on the order of ten or so. At this point we are left with the possibility of multi-wavenumbers, a thermodynamic principle that needs help and a geometric asymptotic approach that appears to have a great deal of promise.

Acknowledgments

The work presented here is the result of a number of students: in particular, A. J. Suo-Anttila, J. M. McDonough, and J. C. Buell. It has been supported by both the National Science Foundation and the Department of Energy, most recently by NSF Grant No. MEA 81-10552.

References

Bénard, H., 1900, "Les Tourbillons Cellulaires Dans une Nappe Liquide," *Revue General des Sciences Pures et Appliquees*, Vol. 11, pp. 1261–1271; 1309–1328.

Brown, W., 1973, "Heat Flux Transitions at Low Rayleigh Number," *J. Fluid Mech.*, Vol. 60, pp. 539–559.

Buell, J. C., 1986, "Wavenumber Selection in Steady Rayleigh–Bénard Convection," Ph.D. Dissertation, University of California, Los Angeles.

Buell, J. C., and Catton, I., 1985, "Wavenumber Selection in Large-Amplitude Axisymmetric Convection," *Phys. of Fluids*, Vol. 29, pp. 23–30.

Busse, F. H., 1967, "On the Stability of Two Dimensional Convection Heated From Below," *J. Mathematics and Physics*, Vol. 46, pp. 140–149.

Busse, F. H., 1969, "On Howard's Upper Bound for Heat Transport by Turbulent Convection," *J. Fluid Mech.*, Vol. 4, pp. 225–260.

Busse, F. H., 1969, "On Howard's Upper Bound for Heat Transport by Turbulent Convection," *J. Fluid Mech.*, Vol. 37, pp. 457–477.

Busse, F. H., and Whitehead, J. A., 1971, "Instabilities of Convection Rolls in High Prandtl Number Fluid," *J. Fluid Mech.*, Vol. 47, pp. 305–320.

Busse, F. H., and Whitehead, J. A., 1974, "Oscillatory and Collective Instabilities in Large Prandtl Number Convection," *J. Fluid Mech.*, Vol. 66, pp. 67–69.

Cannel, D. S., Dominquez-Lerma, M. A., and Ahlers, G., 1983, "Experiments on Wave-number Selection in Rotating Convette-Taylor Flow," *Phys. Rev. Lett*, Vol. 50.

Carrol, J., 1971, "The Structure of Turbulent Convection," Ph.D. Thesis, University of California, Los Angeles.

Catton, I., 1966, "Natural Convection in Horizontal Layers," *Phys. Fluids*, Vol. 9, pp. 2521–2522.

Catton, I., 1978, "Natural Convection in Enclosures," *Proc. Sixth Int'l. Heat Transfer Conf.*, Vol. 6, Hemisphere Press, Washington, DC, pp. 13–31.

Chandrasekhar, S., 1961, *Hydrodynamic and Hydromagnetic Stability*, Oxford Clarendon Press.

Chu, T. Y., and Goldstein, R. J., 1973, "Turbulent Convection in a Horizontal Layer of Water," *J. Fluid Mech.*, Vol. 60, pp. 141–159.

Farhadieh, R., and Tankin, R. S., 1974, "Interferometric Study of Two Dimensional Bénard Convection Cells," *J. Fluid Mech.*, Vol. 66, pp. 739–752.

Gille, J., 1967, "Interferometric Temperature Measurement of Temperature Gradient Reversal in a Layer of Convecting Air," *J. Fluid Mech.*, Vol. 30, pp. 371–384.

Glandsdorff, P., and Prigogine, I., 1971, *Thermodynamic Theory of Structure, Stability and Fluctuations*, Wiley Interscience, New York.

Hirt, C. W., 1968, "Heuristic Stability Theory for Finite Different Equations," *J. Computational Physics*, Vol. 21, pp. 339–343.

Howard, L. N., 1963, "Heat Transport by Turbulent Convection," *J. Fluid Mech.*, Vol. 17, pp. 405–412.

Koschmieder, E. L., 1966, "On Convection Over a Uniformly Heat Plate," *Beitr. Phys. Atmos.*, Vol. 39, pp. 1–11.

Koschmieder, E. L., 1969, "On the Wavelength of Convective Motions," *J. Fluid Mech.*, Vol. 35, pp. 527–530.

Koschmieder, E. L., and Pallas, S. G., 1974, "Heat Transfer Through a Shallow Horizontal Convecting Fluid Layer," *Int'l. J. Heat and Mass Trans.*, Vol. 17, pp. 991–1002.

Kramer, L., Ben-Jacob, E., Brand, H., and Cross, M. C., 1982, "Wavelength Selection in Systems Far From Equilibrium," *Phys. Rev. Lett.*, Vol. 49, pp. 1891–1894.

Kramer, L., and Riecke, H., 1985, "Wavelength Selection in Rayleigh–Bénard Convection," *Zeitschrift für Physik*, Vol. 59B, pp. 245–251.

Krishnamurti, R., 1970, "On the Transition to Turbulent Convection," *J. Fluid Mech.*, Vol. 42, pp. 295–320.

Kuo, H. L., 1961, "Solution of the Non-linear Equations of Cellular Convection and Heat Transport," *J. Fluid Mech.*, Vol. 10, pp. 611–634.

Landau, L. D., 1944, "On the Problem of Turbulence," *Papers of the Academy of Science of the USSR, Doklady*, Vol. 44, pp. 44–??.

Malkus, W. V. R., 1954, "The Heat Transfer and Spectrum of Thermal Turbulence," *Proceedings of the Royal Society*, Series A, Vol. 225, pp. 185–196.

Malkus, W. V. R., and Veronis, G., 1968, "Finite Amplitude Cellular Convection," *J. Fluid Mech.*, Vol. 4, pp. 225–260.

Manneville, P., and Piquemal, J. M., 1983, "Zigzag Instability and Axisymmetric Rolls in Rayleigh–Bénard Convection: The Effects of Curvature," *Phys. Rev. A*, Vol. 28, pp. 1774–1790.

McDonough, J. M., 1980, "The Rayleigh–Bénard Problem on a Horizontally Unbounded Domain: Determination of the Wavenumber of Convection," Ph.D. Dissertation, University of California, Los Angeles.

McDonough, J. M., and Catton, I., 1980, "Wavenumber Selection via Thermodynamic Stability for Two-Dimensional Bénard Convection," ASME Paper No. 79-WA/HT-14.

Downloaded 16 Dec 2010 to 193.140.21.150. Redistribution subject to ASME license or copyright; see http://www.asme.org/terms/Terms_Use.cfm

McDonough, J. M., and Catton, I., 1982, "A Mixed Finite Difference Galerkin Method for Two-Dimensional Convection in a Square Box," *Int'l. J. Heat Mass Trans.*, Vol. 25, pp. 1137-1146.

McDonough, J. M., and Catton, I., 1982, "Accuracy of the Mean Field Approximation and the Physical Effect of Prandtl Number in Bénard Convection," *Phys. Fluids*, Vol. 25, pp. 1502-1505.

Pocheau, A., and Croquette, V., 1984, "Dislocation Motion: A Wavenumber Selection Mechanism in Rayleigh-Bénard Convection," *J. Phys. (Paris)*, Vol. 45, pp. 35-48.

Pomeau, Y., and Manneville, P., 1981, "Wavelength Selection in Axisymmetric Cellular Structures," *J. Physique*, Vol. 42, pp. 1067-1074.

Roberts, P. H., 1966, "On Non-linear Bénard Convection," *Non-Equilibrium Thermodynamics, Variation Techniques and Stability*, R. J. Donnely, R. Herman, and I. Prigogine, eds., University of Chicago Press, pp. 125-162.

Rossby, H. T., 1966, "An Experimental Study of Bénard Convection With and Without Rotation," Ph.D. Dissertation, Massachusetts Institute of Technology.

Serrin, J., 1959, "On the Stability of Viscous Fluid Motions," *Arch. Ration. Mech. Anal.*, Vol. 1, pp. 1-13.

Silveston, P. L., 1958, "Warmedurchgang in Waagerechtern Flussigkeitsschicten," *Forsch. Ing. Wes.*, Vol. 24, pp. 59-69.

Somerscales, E. F. C., and Pasapour, H. G., 1982, "An Application of the Optical Correlation Computer to the Detection of the Malkus Transitions in Free Convection," ASME JOURNAL OF HEAT TRANSFER, Vol. 104, pp. 255-263.

Somerton, C. W., McDonough, J. M., and Catton, I., 1984, "Natural Convection in a Volumetrically Heated Porous Layer," ASME JOURNAL OF HEAT TRANSFER, Vol. 106, pp. 241-244.

Steinberg, V., Ahlers, G., and Cannel, D. S., 1985, "Pattern Formation and Wavenumber Selection by Rayleigh-Bénard Convection in a Cylindrical Container," *Physica Scripta*, Vol. 32, pp. 334-347.

Stuart, J. T., 1958, "On the Non-linear Mechanics of Hydrodynamic Stability," *J. Fluid Mech.*, Vol. 4, pp. 1-10.

Suo-antilla, A. J., 1977, "Natural Convection in Horizontal Fluid Layers," Ph.D. Dissertation, University of California, Los Angeles.

Veronis, G., 1966, "Large Amplitude Bénard Convection," *J. Fluid Mech.*, Vol. 26, pp. 49-68.

Willis, G. E., Deardorff, J. W., and Somerville, R. C. J., 1972, "Roll Diameter Dependence in Rayleigh Convection and Its Effect on Heat Flux," *J. Fluid Mech.*, Vol. 54, pp. 351-367.

Willis, G. E., and Deardorff, J. W., 1967, "Confirmation and Renumbering of the Discrete Heat Flux Transitions of Malkus," *Phys. of Fluids*, Vol. 10, pp. 1861-1866.

APPENDIX A

Mean Field Equations

The conservation equations are:

Mass

$$\nabla \cdot \mathbf{v} = 0 \tag{A.1}$$

Momentum

$$\frac{1}{\mathrm{Pr}}\left[\frac{\partial \mathbf{v}}{\partial t} + \mathbf{v}\cdot\nabla\mathbf{v}\right] = -\nabla P + \nabla^2\mathbf{v} + T'\mathbf{k} \tag{A.2}$$

Energy

$$\frac{\partial T}{\partial t} + \mathbf{v}\cdot\nabla T = \nabla^2 T \tag{A.3}$$

where it has been assumed that

$$T = T + T', \qquad T' = 0 \tag{A.4}$$

and $-T\mathbf{k}$ has been combined with the pressure in the momentum equation. Velocity $\mathbf{v}$, temperature T, and pressure are measured in units of κ/L, $\beta L^3 g/\nu\kappa$, and $\rho\nu\kappa/L^2$, respectively, and Pr is the Prandtl number ν/κ. Assuming periodicity in the horizontal plane, the velocity and temperature deviations are represented by

$$U = \sum_i \frac{1}{a_i^2}\frac{\partial f_i}{\partial x}\frac{\partial w_i}{\partial z} \tag{A.5}$$

$$V = \sum_i \frac{1}{a_i^2}\frac{\partial f_i}{\partial y}\frac{\partial w_i}{\partial z} \tag{A.6}$$

$$w = \sum_i f_i w_i \tag{A.7}$$

$$T' = \sum_i f_i \theta_i \tag{A.8}$$

where

$$\nabla_\perp^2 f_i + a_i^2 f_i = 0, \qquad a_i = \frac{2\pi}{\lambda_i} \tag{A.9}$$

Substitution of the assumed forms into the momentum equation, operating with $f_k\mathbf{k}\cdot\,\mathrm{curl}^2$, and horizontally averaging yields

$$(D^2 - a_k^2)^2 W_k = a^2\theta_k - \frac{1}{\mathrm{Pr}}\sum_{l,m}\overline{f_m f_l f_k}/2\left\{\frac{a_{m,k,l}}{a_l^2 a_m^2} W_m (D^2 - a_l^2)\frac{\partial W_e}{\partial z} + \frac{a_{m,k,l} + a_{k,l,m}}{a_l^2 a_m^2}\frac{\rho W_m}{\partial z}(D^2 - a_l^2)W_l\right\} - \frac{1}{\mathrm{Pr}}\frac{\partial}{\partial t}[(D^2 - a_k^2)W_k] \tag{A.10}$$

where the overbar denotes horizontal averaging, $k = 1, 2$, $a_{k,l,m} = a_k^2(a_l^2 + a_m^2 - a_k^2)$, $D = \partial/\partial z$. Similarly, substitution of the assumed forms of v and T into the energy equation, weighting with f_k, and averaging yields

$$\frac{\partial \theta_k}{\partial t} + W_k\frac{\partial T}{\partial z} = (D^2 - a_k^2)\theta_k - \sum_{l,m}\overline{f_k f_l f_m}\left\{\frac{(a_m^2 + a_l^2 - a_k^2}{2a_l^2}\theta_m\frac{\partial W_l}{\partial z} + W_l\frac{\partial \theta_m}{\partial z}\right\}, \quad k = 1,2 \tag{A.11}$$

Horizontally averaging the energy equation gives

$$\frac{\partial T}{\partial t} + \frac{\partial}{\partial z}\sum_k W_k\theta_k = \frac{\partial^2 T}{\partial z^2} \tag{A.12}$$

The boundary conditions are

$$\begin{aligned} &\theta_k = W_k = DW_k = T = 0 && \text{at } z = 0 \\ &\theta_k = W_k = DW_k = 0, \quad T = -R && \text{at } z = 1 \end{aligned} \tag{A.13}$$

and the initial condition is

$$T(z, 0) = T_0(z) \tag{A.14}$$

Note, for rolls and rectangular plan forms $\overline{f_k f_l f_m} = 0$. The momentum equation (A.10) with $\overline{f_k f_l f_m} = 0$ is solved for W_k using

$$a_k^2\theta_k = \sum_m C_{m,k}\sin(m\pi z)e^{\sigma_k t} \tag{A.15}$$

yielding

$$W_k = \sum_m C_{m,k}W_{m,k} = \sum_m \frac{C_{m,k}}{(m^2\pi^2 + a_k^2)^2}\{B_1^{(m,k)}\sinh(a_k z) + A_2^{(m,k)} z\cosh(a_k z) B_2^{(m,k)} z\sinh(a_k z) + \sin m\pi z\}e^{\sigma_k t} \tag{A.16}$$

with

$$\begin{aligned} B_1^{(m,k)} &= m\pi(a_k + (-1)^m)/\Delta \\ A_2^{(m,k)} &= -m\pi\{\sinh^2(a_k) + (-1)^m a_k \sinh(a_k)\}/\Delta \\ B_2^{(m,k)} &= m\pi\{\sinh(a_k)\cosh(a_k) - a_k \\ &\quad + (-1)^m(a_k\cosh(a_k) - \sinh(a_k))\}/\Delta \\ \Delta &= \sinh^2(a_k) - a_k^2 \end{aligned} \tag{A.17}$$

Downloaded 16 Dec 2010 to 193.140.21.150. Redistribution subject to ASME license or copyright; see http://www.asme.org/terms/Terms_Use.cfm

Substituting for the expression for W_k into equation (A.11), multipling by $\sin(n\pi z)$, and integrating yields, for $\overline{f_k f_l f_m} = 0$,

$$\sum_m C_{m,k}\left\{\frac{m^2\pi^2 + a_k^2}{2a^2}\,\delta_{nm} - \int_0^1 W_{m,k}\,\frac{\partial T}{\partial z}\,\sin(k\pi z)\,dz - \frac{\sigma_k}{2}\,\delta_{nm}\right\} = 0, \qquad k = 1, 2, \ldots \tag{A.18}$$

For $C_{m,k}$ to be nontrivial, the determinant of the coefficient matrix must vanish

$$\left|\left|\frac{(m^2\pi^2 + a_k^2)}{2a_k^2}\,\delta_{nm} - \int_0^1 - W_{m,k}\,\frac{\partial T}{\partial z}\,\sin(k\pi z)\,dz - \sigma_k\,\frac{\delta_{nm}}{2}\right|\right| = 0 \tag{A.19}$$

Equation (A.19) will yield a_k as eigenvalues and $C_{m,k}$ as eigenvectors. The Nusselt number is found by integrating the steady form of equation (A.12). It is easily found to be

$$\mathrm{Nu} = 1 + \sum_{k=1}^{2} <\overline{w_k\theta_k}> \tag{A.20}$$

where the symbol $< >$ denotes averaging along a line between the heated and cooled surface

$$<A> = \int_0^1 A\,dz \tag{A.21}$$

APPENDIX B

Solutions to equation (A.1)-(A.3) are obtained using the mixed finite-difference-Galerkin procedure of McDonough and Catton (1982). Periodic solutions of the form

$$\begin{aligned} V(y, z) &= \sum_{K=0}^{\infty} V_K(z)\,\sin\,(a_K y) \\ W(y, z) &= \sum_{K=0}^{\infty} W_K(z)\,\cos\,a_K y \\ T(y, z) &= \sum_{K=0}^{\infty} T_K(z)\,\cos\,(a_K y) \\ P(y, z) &= \sum_{K=0}^{\infty} P_K(z)\,\cos\,(a_K y) \end{aligned} \tag{B.1}$$

with $a_K \equiv K \cdot a$ and $a = 2\pi/\lambda$ are chosen. It is assumed that solutions of this form (rolls) exist between the first two critical values of Ra.

Substitution of the assumed forms into equations (A.1)-(A.3) yields

$$a_K V_K + DW_K = 0 \qquad \text{(continuity)} \tag{B.2a}$$

$$(D^2 - a_K^2)V_K + a_K P_K = \frac{1}{\mathrm{Pr}}\,\hat{f}_{1,K} \qquad (y\text{-momentum}) \tag{B.2b}$$

$$(D^2 - a_K^2)W_K - DP_K + T_K = \frac{1}{\mathrm{Pr}}\,\hat{f}_{2,K} \qquad (z\text{-momentum}) \tag{B.2c}$$

for $K = 1, 2, \ldots, K$ and

$$(D^2 - a_K^2)T_K = f_{3,K} \qquad \text{(energy)} \tag{B.2d}$$

for $K = 0, 1, \ldots, K$ where D denotes differentiation with respect to z and $\hat{f}_{1,u}$ are the Galerkin inner products given by

$$\hat{f}_{1,K} \equiv <(VV_y + WV_z),\ \sin a_K y> \tag{B.3a}$$

$$\hat{f}_{2,K} \equiv <(VW_y + WV_z),\ \cos a_K y> \tag{B.3b}$$

$$\hat{f}_{3,K} \equiv <(VT_y + WT_z),\ \cos a_K y> \tag{B.3c}$$

with $<,>$ denoting integration over $[0, \pi/a]$. The boundary conditions are

$$V_K(0) = V_K(1) = W_K(0) = W_K(1) = T_K(0) = T_K(1) = 0 \tag{B.4a}$$

for $K = 1, \ldots, K$ and

$$T_0(0) = 0, \quad T_0(1) = -\mathrm{Ra} \tag{B.4b}$$

Eliminating P_K and V_K from equations (B.2b) and (B.2c) yields, with equation (B.2a), the equations to be solved

$$(D^2 - a_K^2)^2 W_K = a_K^2 T_K - \frac{1}{\mathrm{Pr}}\,(a_K^2 \hat{f}_{2,K} + a_K D\hat{f}_{1,K}) \tag{B.5a}$$

$$(D^2 - a_K^2)^2 T_K - \hat{f}_{3,K} \tag{B.5b}$$

$$V_K = -\frac{1}{a_K}\,DW_K \tag{B.5c}$$

for $K = 1, \ldots, K$ and

$$D^2 T_0 = \hat{f}_{3,0} (\hat{f}_{3,0} = <(VT_y + WT_z),\ 1>) \tag{B.5d}$$

for $K = 0$.

Given a value of the wavenumber a, equation (B.5) can be solved for V, W, and T. With

$$T^* = T - T_0 = \sum_{K=1}^{\infty} T_K(z)\,\cos\,a_K y$$

$$\mathbf{U}^* = \mathbf{j}V + \mathbf{K}W$$

and

$$P^* = \frac{1}{\mathrm{Pr}}\,\hat{f}_{1,K} - (D^2 - a_K^2)V_K$$

the time derivatives for equation (9) can be evaluated.

APPENDIX C

Governing Equation and Solvability Condition for Large Radius of Curvature Convection Cells

Dimensionless axisymmetric equations for the radial and vertical velocity and temperature are obtained using

$$\mathbf{V} = \mathrm{curl}(\mathrm{curl}\phi\,\mathbf{k}) \tag{C.1}$$

for the velocities and operating on the vector momentum equation with $\mathbf{k} \cdot \mathrm{curl}(\mathrm{curl})$. In operator notation the result is

$$M[U] = \frac{\partial}{\partial t}\,S[U] \tag{C.2}$$

where $U = (\phi, \theta)^T$, and

$$M = M_0 + \frac{1}{\eta}\,M_1 + \frac{1}{\eta^2}\,M_2\,\frac{1}{\eta^3}\,M_3 + \frac{1}{\eta^4}\,M_4 \tag{C.3}$$

$$S = S_0 + \frac{1}{\eta}\,S_1 + \frac{1}{\eta^2}\,S_2 + \frac{1}{\eta^3}\,S_3 + \frac{1}{\eta_4}\,S_4 \tag{C.4}$$

with r being the distance from the axis to the center of a convection cell. The effect of curvature is determined by r while the details of the convection cell are a function of x. Following Pomeau and Manneville (1981)

$$U(\eta, z, t) + U^{(0)}(x, z) + \frac{1}{r}\,U^{(1)}(x, z, t) + \ldots \tag{C.5}$$

where $U^{(i)}$, $i = 0, 1, \ldots$ are periodic in x with wavenumber a and satisfy the no-slip and perfectly conducting boundary conditions

$$\frac{\partial \phi^{(i)}}{\partial z} = \phi^{(i)} = \theta^{(i)} = 0; \qquad z = 0, 1 \tag{C.6}$$

At the zeroth order of $1/r$ the equations for study convection result in

$$M_0[U^{(0)}] = 0 \tag{C.7}$$

Downloaded 16 Dec 2010 to 193.140.21.150. Redistribution subject to ASME license or copyright; see http://www.asme.org/terms/Terms_Use.cfm

and at order $1/r$ there results

$$M_1[U^{(0)}] + L[U^{(1)}] = \frac{\partial}{\partial t} S[U^{(1)}] \tag{C.8}$$

where L is M_0 linearized around $U^{(0)}$. The operators are

$$M_i = \begin{bmatrix} M_{i,1} \\ M_{i,2} \end{bmatrix} \qquad L = \begin{bmatrix} L_{1,1} & L_{1,2} \\ L_{2,1} & L_{2,1} \end{bmatrix} \qquad S_0 = \begin{bmatrix} S_{0,1} \\ S_{0,2} \end{bmatrix}$$

where

$$M_{0,1}[U] = \nabla^4 \phi_{xx} - R\theta_{xx} - \frac{1}{\mathrm{Pr}} (\phi_{xz} \nabla^2 \phi_{xx} - \phi_{xx} \nabla^2 \phi_{xz})_z$$

$$M_{0,2}[U] = \nabla^2 \theta - \phi_{xx} - \phi_{xz} \theta_x + \phi_{xx} \theta_z$$

$$M_{1,1}[U] = \nabla^4 \phi_x + 2\nabla^2 \phi_{xxx} + \frac{1}{\mathrm{Pr}} [\phi_{xx}(3\phi_{xxxz} + 2\phi_{xzzz}) + \phi_x \nabla^2 \phi_{xxz} + \phi_{xxz} \nabla^2 \phi_x - \phi_{xz} \phi_{xxxx} - u^m \nabla^2 \phi_{xxx} + u^m_{zz} \phi_{xxx}] - \mathrm{Ra}\theta x$$

$$M_{1,2}[U] = \theta_x - \phi_x + \phi_x \theta_z - u^m \theta_x$$

$$S_{0,1}[U] = \frac{1}{\mathrm{Pr}} \nabla^2 \phi_{xx}$$

$$S_{0,2}[U] = \theta$$

$$L_{1,1}[U] = \nabla^4 \phi_{xx} - \frac{1}{\mathrm{Pr}} [\phi^{(0)}_{xz} \nabla^2 \phi_{xxx} + \nabla^2 \phi^{(0)}_{xxx} \phi_{xz} - \phi^{(0)}_{xx} \nabla^2 \phi_{xxz} - \nabla^2 \phi^{(0)}_{xxz} \phi_{xx} + \phi^{(0)}_{xxz} \nabla^2 \phi_{xx} + \nabla^2 \phi^{(0)}_{xx} \phi_{xxz} - \phi^{(0)}_{xxx} \nabla^2 \phi_{xz} - \nabla^2 \phi^{(0)}_{xz} \phi_{xxx}]$$

$$L_{1,2}[U] = -\mathrm{Ra}\theta_{xx}$$

$$L_{2,1}[U] = -\phi_{xx} - \theta^{(0)}_x \phi_{xz} + \theta^{(0)}_z + \phi_{xx}$$

$$L_{2,2}[U] = \nabla^2 \theta - \phi^{(0)}_{xz} \theta_x + \phi^{(0)}_{xxz} \theta_z \tag{C.9}$$

The subscripts denoted partial differentiation and U^m is the mean flow obtained from the horizontal average, denoted by $< >$, of the x momentum equation

$$\frac{d^2 U^m}{dz^2} = P + \frac{1}{\mathrm{Pr}} < -\phi^{(0)}_x \phi^{(0)}_{xxz} + \phi^{(0)}_x \phi^{(1)}_{xxzz} \phi^{(0)}_{xzz} \phi^{(1)}_{xx} > \tag{C.10}$$

and

$$P^m = r < P_x >$$

with

$$P^m = 0 \text{ (boundary of the zigzag instability)}$$

$$\int_0^1 u^m dz = 0 \text{ (axisymmetric convection)}$$

steady solutions for $U^{(1)}$ result only if

$$L[U^{(1)}] = -M_1[U^{(0)}] \tag{C.11}$$

is satisfied and since L is singular, the solvability condition

$$(U^*, M_1[U^{(0)}]) = 0 \tag{C.12}$$

must be fulfilled, where U^* is the solution of the adjoint of the linearized equations

$$[U^*] = 0 \tag{C.13}$$

For a given wavenmber a, equation (C.7) is solved for $U^{(0)}$, equation (C.11) for $U^{(1)}$, equation (C.10) for U^m, equation (C.13) for U^*, then equation (C.12) is evaluated. An iterative procedure is used to force the solvability condition to be met. Details of the solution procedure and results are given by Buell and Catton (1985).

Downloaded 16 Dec 2010 to 193.140.21.150. Redistribution subject to ASME license or copyright; see http://www.asme.org/terms/Terms_Use.cfm

Transient Response and Disturbance Growth in Vertical Buoyancy-Driven Flows

B. Gebhart
Samuel Landis Gabel Professor of Mechanical Engineering, Mechanical Engineering and Applied Mechanics, University of Pennsylvania, Philadelphia, PA 19104-6315
Fellow ASME

The basic physical characteristics of flow response to a changed bounding-surface energy input is reviewed. Response regimes are delineated in terms of locally laminar, unstable, transition, and turbulent flows and dimensionality and regimes intermediate to the others. Very large transient heat transfer effects arise. A key general question is how such regimes become unstable and progress to turbulence. Transient disturbance growth analysis is very difficult and few results are available. This paper develops a general and purely numerical formulation for two-dimensional transient response and disturbance growth. It relies on imposed random flow and associated temperature and disturbance motion pressure disturbances. It applies to any boundary region regime and is specialized here to disturbance growth in a developing buoyancy-driven flow, as an example.

Introduction

Each important kind of steady fluid flow and heat transfer configuration also has, in practice, a number of transient regimes. These arise, for example, as the transport circumstance is begun, changes during the period, and is terminated. Some of these transients may be of equal or greater importance in design than the steady-state process. Transients also frequently involve behavior regimes not encountered in the comparable steady circumstance. Perhaps these are often the principal reasons such processes have not received comparable attention. However, the accelerating shift to reliance on numerical computations is likely to increase investigation of transient effects and of the resulting instantaneous transport mechanisms.

The purpose here is to discuss in detail the transient response generated in a fluid adjacent to a vertical surface, due to the changing thermal conditions that generate buoyancy forces. The mechanisms include laminar response, transient motion pressure fields, flow instability, disturbance growth, transition to turbulence, and relaminarization. Interpretations are given of most recent experimental observations, their interpretations in terms of transport regimes, and the nature and analysis of the several disturbance growth mechanisms that arise. Based on this background, a new formulation of instability and disturbance growth is given. It is based on the introduction of purely random and very small disturbances. It applies to either steady or transient flows. Its use is discussed in detail.

The anlaysis of transient flow response is in terms of the temperature t, velocity field u, v, the motion pressure field p, and the buoyancy force $\rho\beta$ $(t - t_\infty)$. Motion pressure is the static minus the local hydrostatic pressure. For a planar flow, adjacent to a vertical surface, the conservation equations, neglecting pressure work and viscous dissipation, are

$$\frac{\partial u}{\partial x}+\frac{\partial v}{\partial y}=0 \tag{1}$$

$$\frac{\partial u}{\partial \tau}+u\frac{\partial u}{\partial x}+v\frac{\partial u}{\partial y}=\nu\left(\frac{\partial^2 u}{\partial x^2}+\frac{\partial^2 u}{\partial y^2}\right)+g\beta(t-t_\infty)-\frac{1}{\rho}\frac{\partial p}{\partial x} \tag{2}$$

$$\frac{\partial v}{\partial \tau}+u\frac{\partial v}{\partial x}+v\frac{\partial v}{\partial y}=\nu\left(\frac{\partial^2 v}{\partial x^2}+\frac{\partial^2 v}{\partial y^2}\right)-\frac{1}{\rho}\frac{\partial p}{\partial y} \tag{3}$$

$$\frac{\partial t}{\partial \tau}+u\frac{\partial t}{\partial x}+v\frac{\partial t}{\partial y}=\alpha\left(\frac{\partial^2 t}{\partial x^2}+\frac{\partial^2 t}{\partial y^2}\right) \tag{4}$$

The boundary conditions here will be an unstratified quiescent ambient medium at t_∞, zero fluid velocity at the surface, at $y = 0$, and in the distant ambient. The other condition is the changing thermal effect in the surface, which drives the transient. There are several common kinds of input. One is an abrupt surface temperature change, to t_0, or a changing value in time $t_0 = F(\tau)$. Another is an imposed or changing heat flux q'' or $q'' = G(\tau)$. An often more realistic condition is a flux input q'' to a surface element having a thermal capacity of c'' per unit surface area. If the element is thin or has, relatively, a very high thermal conductivity, the flux effect is divided between heating the surface element and the heat conduction outward into the adjacent fluid. This is expressed as

$$q''(\tau)=c''\frac{\partial t}{\partial \tau}-k\frac{\partial t}{\partial y}\quad \text{at } y=0 \tag{5}$$

The surface element material is assumed to have negligible temperature gradient, locally, normal to the surface.

The above general equations and specific boundary conditions are sufficient for all the physical effects considered here. They may be specialized to cover, for example, one-dimensional transients and transient instability.

Formulations of such transients, for study, are in terms of the kinds of processes that occur. As an example, consider a vertical surface in a quiescent ambient fluid, all at t_∞. If the surface temperature is suddenly "changed" to $t_0 > t_\infty$, an upward transient flow will begin. This kind of idealized temperature condition received most of the earliest study. Illingworth (1950) modeled the initial response, a laminar one-dimensional conduction transient, out into the fluid. This temperature field, through buoyancy, is followed by a one-dimensional velocity field. Additional kinds of surface condition were also analyzed by Schetz and Eichhorn (1962) and Menold and Yang (1962). Yang (1960) also considered nonuniform temperature conditions and also found some conditions for similar boundary layer solutions.

Sugawara and Michiyoshi (1951), Hellums and Churchill (1961), Ingham (1978a, 1978b), and Callahan and Marner (1976) used the step in the surface temperature condition in numerical analyses of flow response. The boundary region

Contributed by the Heat Transfer Division for publication in the JOURNAL OF HEAT TRANSFER. Manuscript received by the Heat Transfer Division February 4, 1988. Keywords: Flow Transition, Natural Convection, Reviews.

Copyright © 1988 by ASME

Downloaded 16 Dec 2010 to 193.140.21.150. Redistribution subject to ASME license or copyright; see http://www.asme.org/terms/Terms_Use.cfm

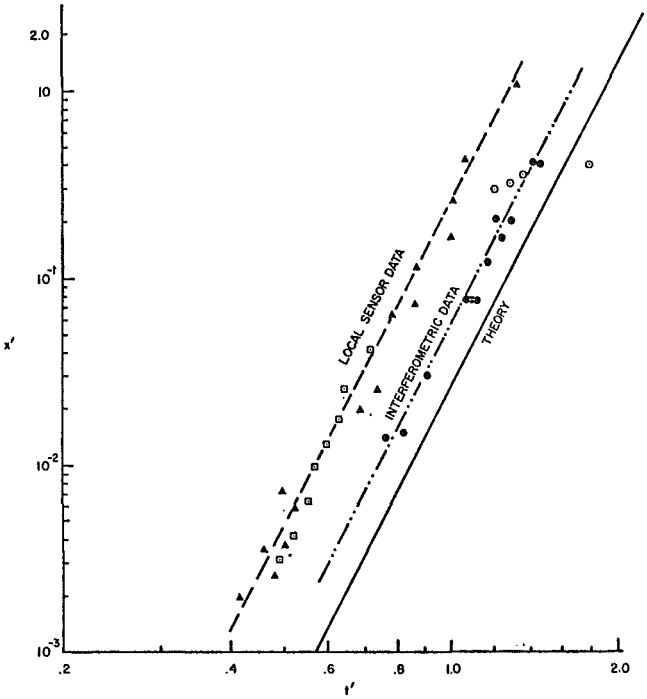

Fig. 1 Comparison of first observed waves to the leading edge propagation rate and other data: interferometer data, Gebhart and Dring (1967) and Mollendorf and Gebhart (1970); local sensor data, Mahajan and Gebhart (1978); and theory, Goldstein and Briggs (1964)

formulation thus modeled the progression through the one-dimensional regime, to the eventual steady state. The questions of transient temperature overshoot and heat transfer undershoot arose from these results.

Leading Edge Effects—LEE. These numerical results did not relate directly to several mechanisms in such a transient. One is the time duration of the one-dimensional flow transient regime. This must initially arise and persist at early times, for a step or for any rapid change in surface condition. At each downstream location x, the flow becomes two dimensional as the leading edge effect (LEE) reaches that location. This effect arises due to the finite distance from the leading edge and from the ambient entrainment which begins there and propagates downstream.

Goldstein and Briggs (1964) developed a method of predicting the propagation of the LEE. This is expressed as the time τ that elapses in the transient until the local flow field, at x_{LEE}, is affected by the presence of the leading edge. It was calculated as follows:

$$x_{\mathrm{LEE}}(\tau) = \max\left\{\int_0^{\tau} u(y, \tau')d\tau'\right\} \tag{6}$$

where $u(y, \tau')$ is the instantaneous downstream velocity in the growing one-dimensional flow field. The maximization is over y at given τ. A similar analysis by Brown and Riley (1973) assumes that the fastest downstream signal travels at the maximum velocity in the velocity layer. It yields essentially the same result.

Calculated LEE propagation is compared with measured propagation in Fig. 1. The measurements were for a practical physical circumstance, the sudden imposition of an electrical current input into a very thin, wide and stretched vertical metal foil structure. Local sensor data in the flow are a much more accurate determination of the maximum LEE propagation rate, since an interferometer averages over the horizontal span of the flow field. The trend of the measured propagation rate data matches the calculation, equation (6), very closely.

However, the actual rate is about 50 percent greater, in spite

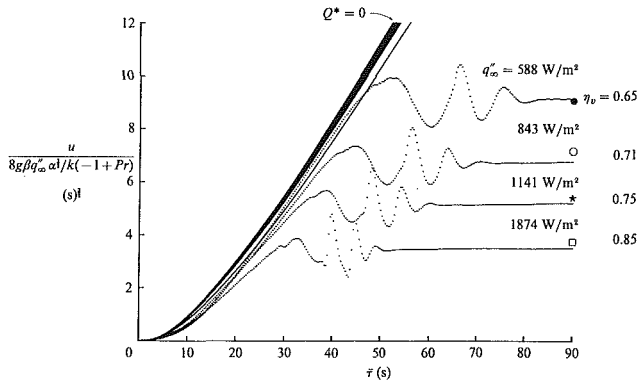

Fig. 2 Transient velocity response $u(x, \tau)$ for various q''_∞ at $x = 0.29$ m. The short-time solutions with and without the effects of surfce thermal capacity are contained within two separate bands. The nondimensional normal distance variable $\eta_\nu = yG^*/5x$ is shown for each curve. Symbols at the right show the laminar-boundary-layer predictions at Pr = 6.2.

of the damping thermal capacity, c'' per unit surface area, of the experimental surface structure. One likely prinicpal cause of this large difference is that the one-dimensional flow field analysis does not completely represent the physical mechanisms. The LEE region is the interaction of a transient and entraining upstream two-dimensional flow, with the one-dimensional downstream flow. Large fluctuations in u have been measured there as seen, for example, in Fig. 2. These data are for a surface in water, at four different input heat flux levels q''_∞. The clear and darkened bands at the left are the calculated one-dimensional velocity response, accounting for the variation of the thermal capacity parameter Q^* due to fluid property variation in the experiments. The two bands are for $Q^* = 0$ and the Q^* of the actual experiment, respectively, where

$$Q^* = c''\left[\frac{g\beta\nu^2 q''_\infty}{k^5}\right]^{1/4} \tag{7}$$

Very large velocity fluctuations, about 30 to 50 percent in magnitude, arise in the LEE propagation mechanism. These are strongly damped in time, in the apparently stable two-dimensional flow, arising at the x, q''_∞ conditions in Fig. 2. This clearly implies that very large motion pressure fluctuations are central to the LEE propagation mechanism, as they have long been known to be in disturbance behavior in flows generally. Therefore, $p(x, y, \tau)$ must be retained in the analysis, for a more representative assessment of the LEE on detailed local transport during transients. This becomes a much more complicated formulation.

Other Measurements of Transient Response. There have been many experiments concerning response characteristics, adjacent to vertical surfaces, as summarized in Table 1. These, collectively, amount to the measurement of several aspects and regimes of transient response.

Those by Klei (1957), Martin (1961), Lurie and Johnson (1962), Gebhart and Adams (1963), and Gebhart et al. (1967) considered average transport during the transient. Goldstein (1959) studied the local transport and the transient development of the thermal boundary layer, in air and water. Rajan and Picot (1971) report local heat transfer coefficients in four different fluids.

Using the interferometric data of Gebhart et al. (1967), Gebhart and Dring (1967) determined the termination of one-dimensional processes, as occurring earlier than the predictions. Even faster propagation rates in pressurized nitrogen were found by Mahajan and Gebhart (1978), using very fine local sensors.

Sammakia et al. (1980) measured transient local surface-temperature response in air, with appreciable radiation ef-

Downloaded 16 Dec 2010 to 193.140.21.150. Redistribution subject to ASME license or copyright; see http://www.asme.org/terms/Terms_Use.cfm

Table 1 Summary of experimental studies of natural-convection transients adjacent to a vertical surface

Investigator(s)	Fluid	Gr*	Gr	Q^*	ΔT (°C)	Height of surface (cm)	Experimental technique
Klei† (1957)	Air	—	7.9 to 12×10^4	12.6 to 15.4	50.6 to 110.6	2.5	Thermocouple measurements
Goldstein (1959)	Water	1.8 to 4.8×10^8	3.4 to 7.8×10^6	0.06 to 0.08	0.3 to 0.6	16.5	Interferometry
	Air	4.3 to 7.7×10^8	1.3 to 1.9×10^7	20.1 to 23.2	5.9 to 21.2	20.3	
Martin (1961)	Water	1.3 to 23×10^7	4.3 to 34×10^5	0.4 to 0.8	6.7 to 52.8	2.5	Resistance thermometry
	Water	2.8 to 21×10^9	5.3 to 23×10^6	0.3 to 0.5	5.3 to 23.1	6.4	
	Water	1.4 to 6.5×10^9	1.9 to 5.9×10^7	0.3 to 0.5	6.9 to 21.4	8.9	
Lurie and Johnson (1962)	Water	1.8 to 10^{11}	9.2 to 10^8	1.2	63.3	7.6	Resistance thermometry
Gebhart and Adams (1963)	Air	7.7×10^6	5.0×10^5	282.3	129.4	3.8	Infrared detector
	Air	4.5×10^7	2.2×10^6	24.8	125.0	6.4	
	Air	8.7×10^7	4.6×10^6	7.3	110.0	7.6	
Gebhart et al. (1967)	Pressurized nitrogen	2.4 to 510×10^9	5.4 to 400×10^7	2.3 to 12.8	2.7 to 41.9	18.4	Interferometry
Mollendorf and Gebhart (1970)	Pressurized nitrogen	1.8 to 61×10^{12}	9.1 to 120×10^9	2.7 to 5.1	5.6 to 27.3	50.2	Interferometry
Rajan and Picot (1971)	$Pr\sim6-10^6$	4.1×10^1 to 2.4×10^{10}	—	—	~3	25.4	Thermocouple measurements
Mahajan and Gebhart (1978)	Pressurized nitrogen	2.5 to 150×10^9	—	2.9 to 32.3	2 to 80	38.5	Hot-wire and thermocouple
Sammakia et al. (1980)	Air	3.7 to 69×10^{11}	—	284	~4.1 to 95.9	130.5	Thermocouple measurements
Sammakia et al. (1982)	Water	6.7×10^5 to 12×10^8	—	1.2 to 2.0	—	130.5	Thermocouple measurements
Joshi and Gebhart (1978)	Water	2.7×10^8 to 10^{13}	—	0.86 to 1.14	~2 to 8.7	124.0	Hot-film and thermocouple measurements and flow visualization

†Based on data reported by Siegel (1958).

fects. The same configuration was considered by Sammakia et al. (1982), to obtain local surface and fluid temperature data in laminar transients in water. These latter measurements also included transients following the cessation of surface heating, as the surface returned to the ambient water temperature level. Numerical calculations by Sammakia and Gebhart (1978, 1981) were in general agreement with their measurements. Recent measurements were made by Joshi and Gebhart (1988) of flow response following a change in surface heat flux from q_1'' to q_2''. Very large heat transfer effects were seen to follow such changes, caused by both transient transition and turbulence.

Mollendorf and Gebhart (1970) studied more vigorous transients. These began as laminar flow but were primarily turbulent in steady state. Using a Mach-Zehnder interferometer, convection layers were observed in nitrogen gas adjacent to a vertical foil, in the downstream region. The initially one-dimensional laminar flow response became turbulent soon after the arrival of leading-edge disturbances. Two heat input levels were studied. At the lower value, the flow relaminarized. At the higher input, the flow remained turbulent. The interferometric data did not give information about flow features during the transient, such as entrainment and development. The more extensive recent measurements and observations of Joshi and Gebhart (1987, 1988) in water will be discussed in detail in the next section.

The initial one-dimensional transient response was calculated by Joshi and Gebhart (1984) for a vertical surface in cold water. The calculations concerned imposed temperature conditions that resulted in a density extremum and buoyancy force reversal across the flow region. Upward, downward, and bidirectional flows were found. Measurements and visualizations were also made by Joshi and Gebhart (1986) under similar temperature conditions in water. Similar mechanisms were found. Such transient flows were also often extremely unstable. Complete transition occurred under some conditions. The anomalous behavior had many additional quite different characteristics.

The following section concerns the collection of constituent regimes that have been observed in transients. For small changes in conditions, a purely laminar response is found and may be quite simply treated. More vigorous transients go into instability and short lived turbulence. Very vigorous transients have additional one and two-dimensional regimes.

Transient Response Regimes

Purely laminar transients, following a changed bounding condition, consist of only the initial one-dimensional response, the propagation of the LEE downstream, and the simultaneous and continuing development into a steady flow. At the other extreme are the more vigorous conditions. These also begin in a one-dimensional laminar response and LEE propagation. However, each of the three flow regimes may be sufficiently vigorous to be very unstable.

Thereby, many different kinds of downstream regimes arise. This is seen, for example, in terms of the measurements and observations made by Joshi and Gebhart (1987), in water, at input levels of $q_\infty'' = 92$ to 1879 W/m^2. Figure 3 is the resulting response diagram. It is in terms of time τ into the transient, at a given downstream location x, as $\mathrm{Fo} = \alpha\tau/x^2$, versus the local flux Grashof number at x, $\mathrm{Gr}_x^* = gx^4\beta q_\infty'' / kv^2$. On these coordinates, at any condition q_∞'', at any surface location x, that is, Gr_x^*, the transient follows a vertical path, in Fo, through time. It eventually reaches steady state, correlated as $\mathrm{Fo}_{ss} = 0.596\ \mathrm{Gr}_x^{*-0.35}$.

Regime I is the laminar one-dimensional response. It ends with the LEE appearance in regime II, for Gr_x^* less than about 2×10^{11}. For larger Gr_x^*, it terminates in one-dimensional transient transition, Regime IIA. This regime, and the five additional later ones seen, will be discussed in detail in a later subsection.

Laminar Transient Response Regimes. There have been a number of integral analyses of response, based on the boundary layer approximations of the full equations (1)–(4), neglecting, of course, also, the motion pressure terms.

The analysis of Siegel (1958), and the variable fluid property treatment of Miyamoto (1977), determined flow response following an abrupt change in bounding surface temperature, from t_∞ to t_0. The results implied the sequence of events to steady state discussed in the preceding section. They also provided estimates for the progression of the LEE and the times to the eventual local steady state.

Downloaded 16 Dec 2010 to 193.140.21.150. Redistribution subject to ASME license or copyright; see http://www.asme.org/terms/Terms_Use.cfm

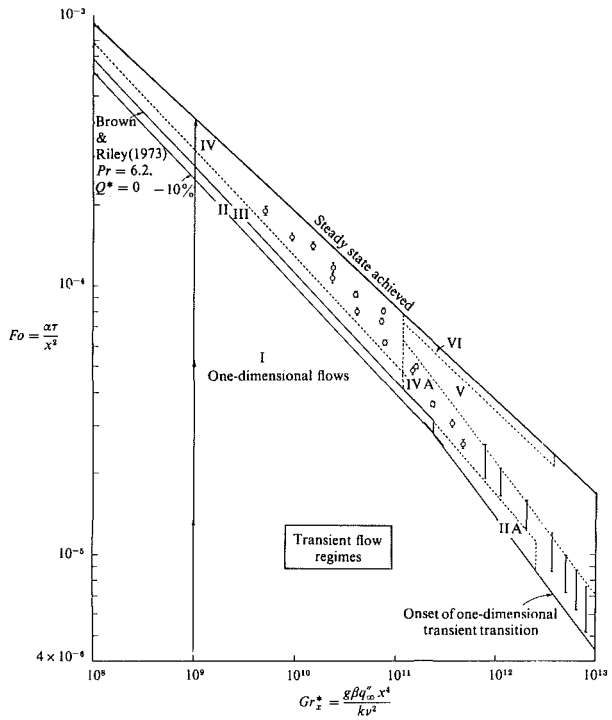

Fig. 3 Regime diagrams for the transient and steady flows. The transient regimes identified are (I) laminar one-dimensional, (II) entrainment development in laminar flow, (IIA) entrainment development following onset of one-dimensional transient transition, (III) laminar two-dimensional flow, (IV) damping disturbances, (IVA) transient disturbance growth, (V) turbulent flow, and (VI) partial relaminarization. The data shown are: I, sensor measurements; Φ, times when vortices were observed from steady sensor data.

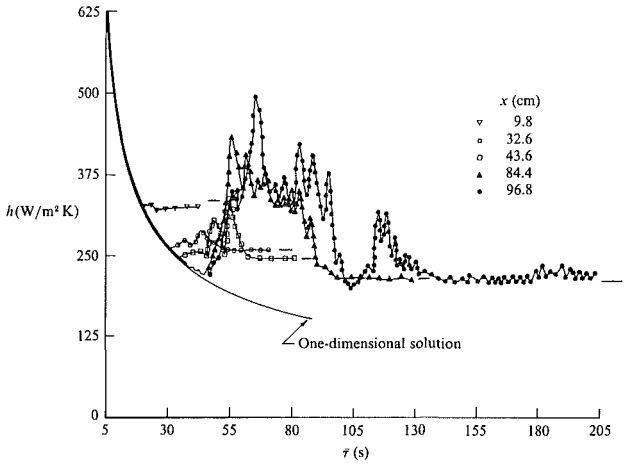

Fig. 4 Instantaneous local heat transfer coefficient at various downstream locations x for q''_∞ = 1874 W/m^2. One-dimensional predictions with and without surface thermal capacity are indistinguishable on the plot. The short horizontal lines for each x are laminar-boundary-layer predictions for Pr = 6.0.

Actual transients, in both practice and experiments, arise instead from a change in energy input to a bounding surface, having some thermal capacity. Rapid increases in heat flux input often arise, for example, with radiation or direct electrical heating. This is the condition in equation (5), when $q''(\tau)$ is perhaps, in general, a changing heat flux input.

An integral formulation (Gebhart, 1961) was expressed in terms of the average surface element temperature response, the changing average buoyancy-induced velocity level, and the changing thickness of the transport region adjacent to the surface element. Suitable constants in the formulation covered the range Pr = 0.01 to 1000. Transient response was calculated, for a sudden uniform step of input q'', from zero to a constant value, over a wide range of a thermal capacity parameter, as $Q \propto c''$, similar to Q^* in equation (7).

In terms of overall flow response, the results indicated three regimes, in terms of Q. For $Q < 0.1$, the response was essentially one dimensional all the way to steady state. For $0.1 \leq Q < 1$, the transient convection terms, and the LEE, were very important contributions during the transient. For $Q \geq 1$ the flow response was essentially a quasi-static process. Extensive measurements in air, for Q large, and in water, for Q small, were in very close agreement with the calculated responses; see Gebhart and Adams (1963).

More Vigorous Transients. The above regimes are related to the recent and more detailed experimental determinations summarized in Fig. 3. Since Q^* is around 1 (see Table 1), these latter transients lie in the region Q around 1 in the earlier formulation. Therefore, the nominal laminar response, in region I (Fig. 3), corresponds to both the laminar one-dimensional and the convection transient regimes.

However, in these much more vigorous flows, instability and even transition arise later in the response, as characterized in regions II through VI. The several distinct mechanisms found will be discussed, in preparation for the later application of a new model for instability analysis in steady and in transient flows.

Figure 3 is in terms of a local flow and condition, at x, as Gr_x^*, the abscissa, as the flow changes with increasing time, Fo $= \alpha\tau/x^2$. For Gr_x^* less than about 2×10^{11}, regime I ends in laminar entrainment and in the LEE, regime II. A subsequent period of vigorous unstable two-dimensional flow, regime III, amplifies disturbances. These are damped, in regime IV, to an eventual largely laminar steady flow. The regimes of appreciable naturally occurring disturbances, regimes III and IV, are transient and laminar two-dimensional flows. This is hereafter called disturbance regime D2.

However, for $\mathrm{Gr}_x^* > 2 \times 10^{11}$, the one-dimensional laminar transient ends in a very different way, in regime IIA. The more vigorous flows, up to $\mathrm{Gr}_x^* = 2.5 \times 10^{12}$, become unstable while the flow is still in one-dimensional form. This is called disturbance regime D1. At the beginning of regime IIA the flow has undergone transient transition and the LEE subsequently arrives. In regime IVA there is continuing transient disturbance growth, to regime V, a completely turbulent transient. This ends in regime VI, with partial relaminarization. For the yet higher range of Gr_x^*, disturbance regime D1, transition and further disturbance growth follow. This sequence ends in a steady turbulent flow, over most of the range.

Disturbance Growth Characteristics. Thus, two different disturbance regimes, D1 and D2, arise in these vigorous transients. Both regimes also initiated transistion, in one and two-dimensional transient flows, respectively. Past calculations and measurements of growth and transition in buoyancy-driven flows have largely concerned steady base flows. Therefore, these results do not necessarily provide any direct guidance in these transient events.

These events were found to have very large effects on instantaneous heat transfer, for example, for q''_∞ = 1874 W/m^2 (see Fig. 4). The local instantaneous convection coefficient $h(x, \tau)$ is plotted from the response of thermocouples laminated into the thin surface structure, at five heights x. Very large fluctuations are seen, before all transients disappear at τ = 140 s at x = 96.8 cm. At this x location, the range of transient variation has been up to 200 percent above the eventual average value.

The recent disturbance measurements of Joshi and Gebhart (1987), in water, showed a very surprising characteristic for the D1 and D2 transient disturbance regimes. Figure 5 is a

Downloaded 16 Dec 2010 to 193.140.21.150. Redistribution subject to ASME license or copyright; see http://www.asme.org/terms/Terms_Use.cfm

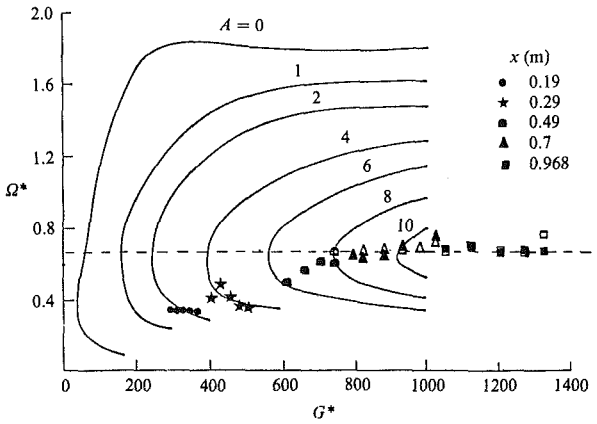

Fig. 5 Observed frequencies of sinusoidal disturbances during the transient, by Joshi and Gebhart (1987). Solid curves are constant-amplification contours for Pr = 6.7, for a steady base flow, vertical natural-convection boundary layer, from Gebhart and Mahajan (1982). Unfilled symbols correspond to disturbances observed in the eventual steady-state flow.

steady boundary region flow disturbance amplification plane for water. It is in terms of $\Omega^* = 2\pi f[k/g\beta q''_\infty]^{1/2}$, which is proportional to physical disturbance frequency f, and $G^* = 5\sqrt[5]{\mathrm{Gr}_x^4}/5$. A given naturally occurring disturbance component f travels downstream along a horizontal line, like the dashed one shown at $\Omega^* = 0.675$. This is seen to be the most amplified component to $A \approx 8$, at $G^* \approx 620$. On this plane e^A is the amplitude at any downstream location G^*, divided by that of the same frequency component when it crossed the neutral curve at $A = 0$.

The very strong tendency of selective amplification seen has long been known and has been abundantly confirmed in experiments with different fluids. The unfilled symbols in Fig. 5 are merely additional confirmation, based on the measurements of the dominant frequency by Joshi and Gebhart (1987), at the end of the transient flow development.

The filled symbols are the disturbance frequencies, which were measured in the obviously unstable one and two-dimensional transient flow regimes, D1 and D2. These new data indicate the very surprising conclusion that the growth mechanisms of transient wavelike disturbance components followed the same mechanisms as those in a steady downstream-developing two-dimensional flow.

The above formulations, calculations, and experimental measurements are the collective basis for the following development of a general numerical method of determining instability in buoyancy-driven transients. The following section develops the governing relations and formulations for numerical analysis. Preliminary results of an application of this formulation to a steady flow are then mentioned.

Disturbance Growth in Transients

In contrast to steady flows, there has been relatively little calculation or measurement of either disturbance growth or of transition in transient buoyancy driven flows. Gunness and Gebhart (1969) found that accelerating flows in a vertical passage were more stable than decelerating ones. The general criterion for instability in a transient given by Shen (1961) is

$$\mathrm{Gro}(\tau) = \frac{1}{E}\frac{dE}{d\tau} > 0 \tag{8}$$

where E is the ratio of the instantaneous disturbance and base flow kinetic energy levels. This kind of criterion has been applied for disturbance growth in the less demanding circumstance of quasi-static flows, where the base flow is known. These results do not apply to the vigorous transients in which base-flow response time becomes comparable to the rate of disturbance growth.

Another approach is in considering the whole process, as arising form an initial state. There have been many studies of transient instability applying disturbances in regular modes. There have also been some in which disturbances were imposed in some kind of random manner, as summarized below.

In a transient Couette flow, instability was investigated by Chen and Kirchner (1971). One technique considered an initial value problem, imposing random disturbances of given wavelength and following their evolution. The resulting critical wavelengths agreed with the experiments of Kirchner and Chen (1970). A quasi-static analysis yielded similar results, for marginal stability. Liu and Chen (1973) also analyzed Couette instability, imposing initial and random wave disturbances over characteristic axial lengths comparable to those found in experiments. Taylor vortices resulted. Chen and Sanford (1977) used random disturbances, in vorticity, to calculate instability in doubly diffusive convection, in an inclined slot.

The Bénard instability was analyzed by Jhaveri and Homsy (1980) as a random initial value problem, in terms of the Fourier modes. The onset of convection was a mean of the individual components, some showing appreciable convective motion. A similar initial-value analysis by Jhaveri and Homsy (1982) used random forcing to determine transient responses in Bénard instability. Related numerical studies of instability of steady laminar forced flows are those of Fasel (1970), flow over a flat surface (Blasius); and Orszag and Kells (1980), plane Couette and Poiseuille flows, respectively. The first introduced small periodic disturbances. Their subsequent evolution was followed numerically and the results were in reasonable agreement with both linear theory and data. The second study used a spectral method representing the velocity field by a Fourier series and a Chebyshev expansion across the flow.

Disturbance Growth Formulation. The technique given here, for buoyancy-driven flows, uses the full planar flow formulation, equations (1)–(4). The general instantaneous flow region is shown in Fig. 6, in terms of the three characteristic downstream regions. The dependent variables, u, v, t, and p, are all considered to be functions of x, y, and τ. They are expressed below as

$$u = U + u', \quad v = V + v', \quad t = T + t', \text{ and } p = P + p'$$

where U, V, T, and P are the base flow, that is a steady or transient flow which would result from the imposed conditions, in the absence of disturbances or instability. If this flow is taken to be of boundary layer form, $P = 0$, and all terms in equations (1)–(4) that depend only on U, V and T disappear. However, accurately modeling the LEE in transients will require retaining $P(x, y, \tau)$. Recall Fig. 2. Also, there are no spanwise effects or secondary means flows, since u', v', t', and p' are formulated to depend only on x, y, and τ. Only linear disturbance quantities are retained. Therefore, all disturbance quantities should average, in time, to zero, if they do at the input location. This formulation is similar to that which results, for example, in the Orr–Sommerfeld equations, as applied to many kinds of steady flow. The resulting equations for u', v', t', and p' are

$$\frac{\partial u'}{\partial x} + \frac{\partial v'}{\partial y} = 0 \tag{9}$$

$$\frac{\partial u'}{\partial \tau} + \frac{1}{\rho}\frac{\partial p'}{\partial x} = \nu\nabla^2 u' + g\beta t' - \left[U\frac{\partial u'}{\partial x} + u'\frac{\partial U}{\partial x} + V\frac{\partial u'}{\partial y} + v'\frac{\partial U}{\partial y}\right] = A \tag{10}$$

Downloaded 16 Dec 2010 to 193.140.21.150. Redistribution subject to ASME license or copyright; see http://www.asme.org/terms/Terms_Use.cfm

$$\frac{\partial v'}{\partial \tau}+\frac{1}{\rho}\frac{\partial p'}{\partial y}=\nu\nabla^2 v'-\left[U\frac{\partial v'}{\partial x}+u'\frac{\partial V}{\partial x}+V\frac{\partial v'}{\partial y}+v'\frac{\partial V}{\partial y}\right]=B \tag{11}$$

$$\frac{\partial t'}{\partial \tau}=\alpha\nabla^2 t'-\left[U\frac{\partial t'}{\partial x}+u'\frac{\partial T}{\partial x}+V\frac{\partial t'}{\partial y}+v'\frac{\partial T}{\partial y}\right]=C \tag{12}$$

in terms of forward differences of u', v', and t'. Note that base flow derivative terms are retained here that are neglected in the simplest ordinary linear stability formulation. All terms in U, V, and T are for the instantaneous transient flow or for a converged steady-state flow.

The boundary conditions are as below, where Y is taken well outside both the instantaneous boundary region and the region where disturbances arise, or into which they grow.

$$u'(x,0)=v'(x,0)=u'(x,Y)=v'(x,Y)$$
$$=t'(x,Y)=p'(x,Y)=0 \tag{13a}$$

$$t'(x,0)=0(\text{air},\ Q^*\ \text{large});\quad \partial t'/\partial y=0(\text{water},\ Q^*\ \text{small}) \tag{13b}$$

All of the above variables, such as u, v, p, etc., will be retained in dimensional form, since the generalizations to be used depend on the particular flow circumstance to be considered.

The right-hand sides of equations (10)–(12) are known at all locations x_i, y_j from the current flow condition, at any time level n. That is $A = A^n_{i,j}$, $B = B^n_{i,j}$, $C = C^n_{i,j}$. Therefore, the formulation is explicit and the following time step changes in u', v', and t' are expressed as

$$\left(\frac{\partial u'}{\partial \tau}\right)^n_{i,j}+\frac{1}{\rho}\left(\frac{\partial p'}{\partial x}\right)^n_{i,j}=A^n_{i,j} \tag{14}$$

$$\left(\frac{\partial v'}{\partial \tau}\right)^n_{i,j}+\frac{1}{\rho}\left(\frac{\partial p'}{\partial y}\right)^n_{i,j}=B^n_{i,j} \tag{15}$$

$$\left(\frac{\partial t'}{\partial \tau}\right)^n_{i,j}=C^n_{i,j} \tag{16}$$

Thus, the pressure field $p'^n_{i,j}$, or actually its gradients, must be determined to calculate $(u', v', t')^{n+1}_{i,j}$. To this end, continuity equation (9) may be used, in conjunction with equations (14) and (15) to yield a Poisson equation in $p'^n_{i,j}$

$$\frac{\partial}{\partial x}\left(\frac{\partial u'}{\partial \tau}\right)=\frac{\partial}{\partial x}\left(A-\frac{1}{\rho}\frac{\partial p'}{\partial x}\right)=-\frac{\partial}{\partial y}\left(\frac{\partial v'}{\partial \tau}\right)$$
$$=-\frac{\partial}{\partial y}\left(B-\frac{\partial p'}{\partial y}\right) \tag{17}$$

Therefore

$$\frac{1}{\rho}\nabla^2 p'^n_{i,j}=\frac{\partial A^n_{i,j}}{\partial x}+\frac{\partial B^n_{i,j}}{\partial y}=D^n_{i,j} \tag{18}$$

The current values of A and B yield the $D^n_{i,j}$. Therefore, $p'^n_{i,j}$ could be calculated from equation (18), at each time step, if conditions are sufficiently specified at all boundaries of the region. However, in general, they are not, as discussed below.

An Alternative Formulation. Consider the flow in Fig. 7. This may be either a steady or transient flow. However, it is assumed that there is a stable laminar upstream region, extending to at least $x = x_2$, and perhaps beyond. This is a region of downstream flow development. Very small random disturbances are to be added at x_3, y_j through time. The calculation procedure is thereafter to follow the time evolution of the downstream flow and of any disturbances in the flow.

For this region, the calculation of $p'^n_{i,j}$ from equation (18) would require conditions at the four boundaries: (*a*) x_i, y_1; (*b*) x_1, y_j; (*c*) L, y_j; and (*d*) x_i, Y. However, for this flow configuration, the only information available on boundary (*d*) is that Y must be chosen sufficiently large to include all distur-

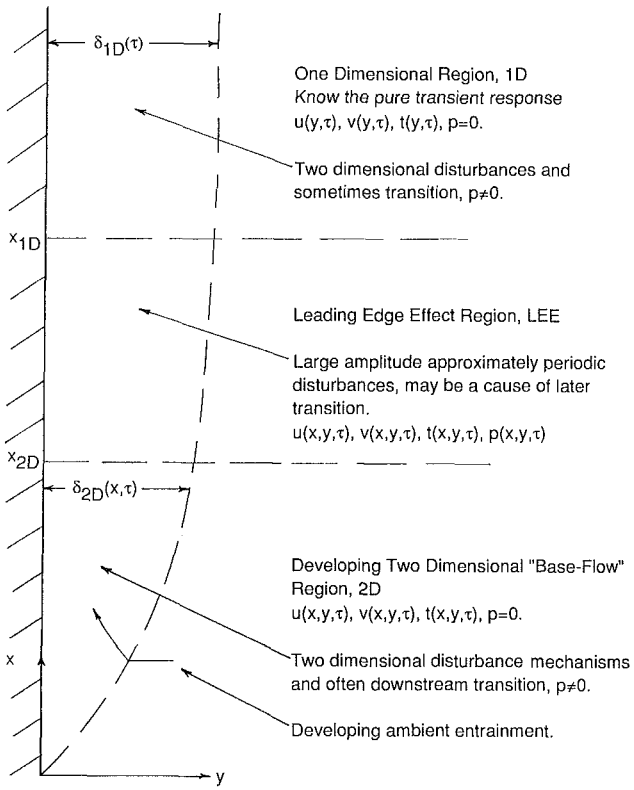

Fig. 6 Transient regimes, enlarged, during the transient

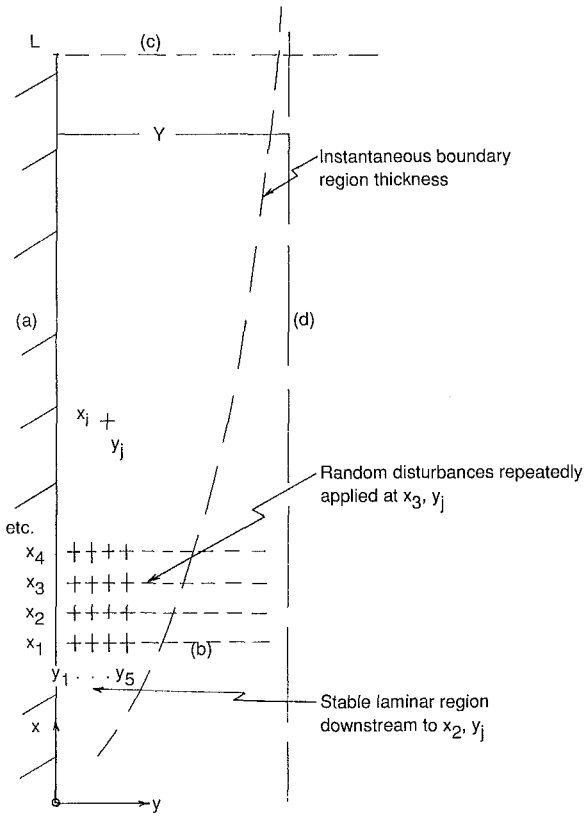

Fig. 7 A two-dimensional flow region

Downloaded 16 Dec 2010 to 193.140.21.150. Redistribution subject to ASME license or copyright; see http://www.asme.org/terms/Terms_Use.cfm

bance effects. Also, there is no a priori information for boundary (c) in this geometry. Therefore, the formation in equation (18) is not used and equation (17) is rewritten as

$$\frac{\partial A^n_{i,j}}{\partial x}-\frac{1}{\rho}\left(\frac{\partial}{\partial x}\frac{\partial p'}{\partial x}\right)^n_{i,j}=-\frac{\partial B^n_{i,j}}{\partial x}+\frac{1}{\rho}\left(\frac{\partial}{\partial y}\frac{\partial p'}{\partial y}\right)^n_{i,j}\equiv$$

$$\equiv K^n_{i,j}=\left(\frac{\partial^2 u'}{\partial x\partial\tau}\right)^n_{i,j}=-\left(\frac{\partial^2 v'}{\partial y\partial\tau}\right)^n_{i,j} \tag{19}$$

Therefore, the two equations, in terms of p', A, B, and K, are

$$\frac{1}{\rho}\left(\frac{\partial}{\partial x}\frac{\partial p'}{\partial x}\right)^n_{i,j}=\frac{\partial A^n_{i,j}}{\partial x}-K^n_{i,j} \text{ or } \frac{1}{\rho}\Delta\left(\frac{\Delta p'}{\Delta x}\right)^n_{i,j}$$

$$=\Delta A^n_{i,j}-K^n_{i,j}\Delta x \tag{20}$$

$$\frac{1}{\rho}\left(\frac{\partial}{\partial y}\frac{\partial p'}{\partial y}\right)^n_{i,j}=\frac{\partial B^n_{i,j}}{\partial y}+K^n_{i,j} \text{ or } \frac{1}{\rho}\Delta\left(\frac{\Delta p'}{\Delta y}\right)^n_{i,j}$$

$$=\Delta B^n_{i,j}+K^n_{i,j}\Delta y \tag{21}$$

The only values of $K^n_{i,j}$ that are known at each time level n are $K^n_{i,1}=K^n_{1,j}=0$, from equations (19)–(21). That is $K^n_{i,1}=0$ since $u'=v'=0$ at the surface. Also, x_1 and x_2 are to be chosen sufficiently far upstream that small disturbances, introduced at x_3, are not felt. Then

$$p'_{1,j}=p'_{2,j}=0=A^n_{1,j}=A^n_{2,j},\quad K^n_{1,j}=0 \text{ and } t'^n_{1,j}=0 \tag{22}$$

These considerations supply the conditions at the bottom boundary of the disturbance region.

The remaining necessary boundary conditions arise at the surface, at $x_{i,1}$. They will permit the calculation of the $K^n_{i,j}$ over $K^n_{2,j}$ to $K^n_{L,j}$. From equations (10)–(12)

$$\frac{1}{\rho}\frac{\partial p'}{\partial x}\Big)^n_{i,1}=\nu\nabla^2 u')^n_{i,1}+g\beta t'^n_{i,1}$$

$$=\nu\frac{\partial^2 u'}{\partial y^2}\Big)^n_{i,1}+g\beta t'^n_{i,1}=A^n_{i,1} \tag{23}$$

$$\frac{1}{\rho}\frac{\partial p'}{\partial y}\Big)^n_{i,1}=\nu\nabla^2 v')^n_{i,1}=\nu\left(\frac{\partial^2 v'}{\partial y^2}\right)^n_{i,1}=B^n_{i,1} \tag{24}$$

$$\frac{\partial t'}{\partial\tau}\Big)^n_{i,1}=\alpha\nabla^2 t')^n_{i,1}=\alpha\frac{\partial^2 t'}{\partial x^2}\Big)^n_{i,1}$$

$$+\alpha\left(\frac{\partial^2 t'}{\partial y^2}\right)^n_{i,1}=C^n_{i,1} \tag{25}$$

Clearly, the second derivatives in y above may each be estimated at x_i, y_1, at time n, in terms of u'^n, v'^n, and t'^n at x_i, y_2; x_i, y_3, etc., for example, in terms of polynomials. Although $u'^n_{i,1}=v'^n_{i,1}=0$, $t'^n_{i,1}$ in equation (22) is influenced by the relative thermal capacity of the surface, as an additional boundary condition. For a surface element flux input

$$q''=c''\frac{\partial t}{\partial\tau}-k\frac{\partial t}{\partial y}=c''\frac{\partial T}{\partial\tau}-k\frac{\partial T}{\partial y}+c''\frac{\partial t'}{\partial\tau}-k\frac{\partial t'}{\partial y}$$

Since the base flow is to be calculated consistent with the relation in equation (5), the two disturbance effects balance as follows:

$$c''\left(\frac{\partial t'}{\partial\tau}\right)^n_{i,1}=k\left(\frac{\partial t'}{\partial y}\right)^n_{i,1} \tag{26}$$

This amounts to the condition that determines $\partial t'/\partial\tau)^n_{i,1}$ for locations along the surface. If $c''=0$ then $(\partial t/\partial y)^n_{i,1}=0$ and $t')^n_{i,1}\neq 0$ in general. Therefore $C^n_{i,1}\neq 0$ and $\partial t'/\partial\tau)^n_{i,1}$ is calculated from equation (12). The highly idealized condition of an imposed temperature level at the surface results in $t'^n_{i,1}=0$.

The above considerations determine the pressure conditions that apply along the horizontal boundary (b), x_1, y_j, and the surface (a), x_i, y_1. On (b) $p'^n_{1,j}=p'^n_{2,j}=0$ and

$$\left(\frac{\partial p'}{\partial x}\right)^n_{1,j}=\left(\frac{\partial^2 p'}{\partial x^2}\right)^n_{1,j}=0 \tag{27}$$

Along (a), from equation (23), given equation (27), $(\partial p'/\partial x)^n_{i,1}$ and $p'^n_{i,1}$ may be calculated. Also, equation (24) determines $(\partial p'/\partial y)^n_{i,1}$, or $p'^n_{i,2}$, knowing $p^n_{i,1}$. These conditions are applied, in conjunction with equations (20) and (21), to determine the field of pressure gradient throughout the region. The following subsection indicates the procedure for making these calculations, in terms of the initially unknown $K^n_{i,j}$ over the region.

Calculation Procedure. The determination of the pressure field, throughout the region at each time step, uses equations (20) and (21), with boundary conditions, equations (22), (23), (24), and (27). The essential feature of this system is that the values of $K^n_{i,j}$ inside the region are unknown. However, for any grid point interior to the region, there are two completely independent paths whereby the pressure at that point, $p'^n_{i,j}$ may be calculated, in terms of the unknown $K^n_{i,j}$. This allows the determination of the $K^n_{i,j}$. For example, consider the location x_3, y_2 in Fig. 7. At any time level n

$$(p'_{2,1}-p'_{1,1})^*+(p'_{3,1}-p'_{2,1})+(p'_{3,2}-p'_{3,1})=(p'_{1,2}-p'_{1,1})^*$$

$$+(p'_{2,2}-p'_{1,2})^*+(p'_{3,2}-p'_{2,2})$$

The starred quantities are zero. The terms $(p'_{3,1}-p'_{2,1})$ and $(p'_{3,2}-p'_{3,1})$ may be determined from equations (23) and (24), respectively. Then $(p'_{3,2}-p'_{2,2})$ is calculated. From this $K^n_{2,2}$ may be calculated from equation (20). The next step, to x_4, y_2, involves the unknown $K^n_{3,2}$. However, $(p'_{4,1}-p'_{3,1})$ and $(p'_{4,2}-p'_{4,1})$ are again known, as is $(p'_{3,2}-p'_{3,1})$, from above. Thus $(p'_{4,1}-p'_{3,1})$ is used in equation (21) to determine $K^n_{3,2}$. Thereby, the $K^n_{i,2}$ are determined. The whole procedure is then repeated, starting with the two paths from x_1, y_1 to x_3, y_3. Thereby $K^n_{2,3}$ is determined, etc.

The field of calculation extends upward as far as the boundary condition equation (23), which results in the determination of $K^n_{i,j}$ up to $x_i=L-\Delta x$. Over that range, calculations may be extended outward as far as the disturbances propagate, as indicated by the remaining presence of appreciable values of $p'^n_{i,j}$. Thus, this formulation determines the whole disturbance field, requiring boundary conditions only at x_i, y_1 and x_1, y_j.

The above calculation technique determines the pressure gradient field at time n. Then $(u', v', \text{ and } t')^{n+1}_{i,j}$ are determined from equations (14)–(16), etc. Growth and spectral characteristics are calculated from these results. The next matter is the nature of the disturbance inputs to the flow.

Random Disturbance Inputs and Downstream Growth. The calculation step through time $\Delta\tau$, over times τ^n, and the grid sizes $\Delta x\geq\Delta y$, are to be determined by numerical stability and by disturbance spatial resolution considerations. Random disturbances, in u', v', t', and p', are applied along x_3, y_j, at time intervals $\Delta\tau^d=m\Delta\tau$, where $m\geq 1$. Values of m and therefore of $\Delta\tau^d$ may also be randomly chosen, in terms of some maximum value M during the calculation.

At each time step $m\Delta\tau$, at time level τ^d, and across x_3, y_j for $j>1$, values of $u'^d_{3,j}$ are generated, of random sign and magnitude, up to a specified maximum value $|u'^d_{\max}|$. This value must be very small compared to $U_{\max}$, the maximum value of the base flow at x_1. Using continuity, equation (9), $v'^d_{3,j}$ is calculated at τ^d, from $u'^d_{3,j}$ and $u'^d_{2,j}$.

The values $u'^d_{3,j}$ and $v'^d_{3,j}$ are then added to the $u'^n_{3,j}$ and $v'^n_{3,j}$ at the time $\tau^n=\tau^d$. Thereby, A, B, and C are changed in equations (10)–(12) in the next time step. Thereby, the effects of the random disturbances have entered the subsequent

Downloaded 16 Dec 2010 to 193.140.21.150. Redistribution subject to ASME license or copyright; see http://www.asme.org/terms/Terms_Use.cfm

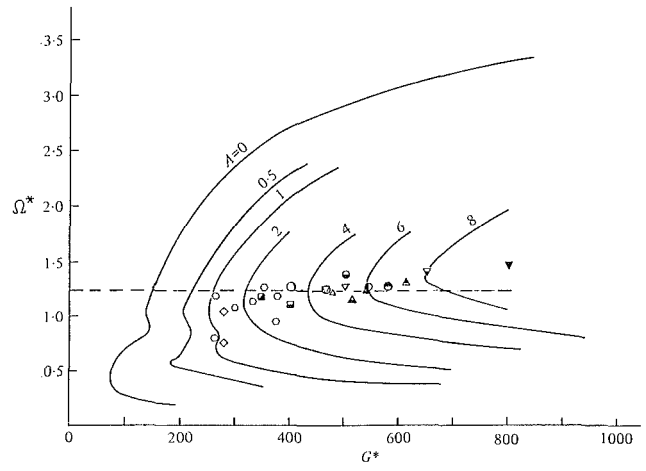

Fig. 8 Stability plane for Pr = 0.733 showing principal measured frequencies, arising in the flow, as open symbols, and in the laminar portion of transitional flows as partially or fully shaded symbols. The dashed line is a downstream path at constant physical frequency. From Mahajan and Gebhart (1982).

calculations, through equations (14)–(16). Alternatively, the calculations at $\tau^n = \tau^d$ could be redone, in terms of the added disturbances u'^d and v'^d, to calculate the left sides of equations (14)–(16). This would change all of the $K^n_{i,j}$ associated with points x_3, y_j.

Calculation of Instability and Disturbance Growth

The specific condition considered to date is the instability of a steady flow, U, V, and T, for Pr = 0.72 and 6.7. The driving boundary condition at x_i, y_1 was a steady uniform flux q'' from a surface having a very large thermal capacity c''. Therefore $t'^n_{i,1} = 0$.

Since the inputs at x_3, y_j are random in equations that have been linearized in disturbance quantities, all such quantities should have a zero time-average value, throughout the region above x_1, y_j. The aim of the method, formulation, and calculation is to determine any downstream amplification and/or order that results from the random inputs upstream. This approach is the numerical analogue of the Orr-Sommerfeld analysis, which resulted in the strongly selective amplification seen in Fig. 5, for water.

Conclusions

The foregoing formulation, in terms of random disturbances, does not require any preliminary specification or initiation of input disturbance form, such as periodic modes, which have been used in numerical computations of transient instability. The new numerical method also avoids restrictive special requirements and approximations, such as a quasi-static base flow.

The particular numerical formulation used above also avoids the property of requiring either arbitrary initial or boundary conditions. This is seen in the particular example, which follows the general formulation. Nominally, it appears there, in equation (18), that a Poisson equation must be solved, for the motion pressure field, over the domain, at each time step. For each solution, this would require specified conditions at all four boundaries. However, the conditions out in the undisturbed ambient region and at the downstream edge of the flow field of interest are unknown. This difficulty is avoided by calculating the instantaneous pressure field, in steps, away from the known undisturbed conditions far upstream and from disturbance conditions along the vertical boundary.

Preliminary calculations, for a steady vertical flow, show that the required computer time is quite large in the conventional sequential calculation format. This calculation is being done first to compare results with this formulation with those determined from the Orr-Sommerfeld equations (Figs. 5 and 8). The results, in terms of both downstream disturbances and spectral analysis, indicate that the initial random disturbances are again selectively amplified for favored frequency components. These calculations are preliminary to calculation of transient disturbance behavior in regimes like IIA, IV, and IVA in Fig. 3.

References

Brown, S. N., and Riley, N., 1973, "Flow Past a Suddenly Heated Vertical Plate," *J. Fluid Mech.*, Vol. 59, pp. 225–237.

Callahan, G. D., and Marner, W. J., 1976, "Transient Free Convection With Mass Transfer on an Isothermal Vertical Flat Plate," *Int. J. Heat Mass Trans.*, Vol. 19, pp. 165–174.

Chen, C. F., and Kirchner, R. P., 1971, "Stability of Time-Dependent Rotational Couette Flow, Part II, Stability Analysis," *J. Fluid Mech.*, Vol. 48, pp. 365–384.

Chen, C. F., and Sanford, R. D., 1977, "Stability of Time Dependent Double-Diffusive Convection in an Inclined Slot," *J. Fluid Mech.*, Vol. 83, pp. 83–96.

Fasel, H., 1976, "Investigation of the Stability of Boundary Layers by a Finite Difference Model of the Navier-Stokes Equations," *J. Fluid Mech.*, Vol. 78, pp. 355–384.

Gebhart, B., 1961, "Transient Natural Convection From Vertical Elements," ASME JOURNAL OF HEAT TRANSFER, Vol. 83, pp. 61–70.

Gebhart, B., and Adams, D. E., 1963, "Measurements of Transient Natural Convection on Flat Vertical Surfaces," ASME JOURNAL OF HEAT TRANSFER, Vol. 85, pp. 25–28.

Gebhart, B., and Dring, R. P., 1967, "The Leading Edge Effect in Transient Natural Convection Flow From a Vertical Plate," ASME JOURNAL OF HEAT TRANSFER, Vol. 89, pp. 274–275.

Gebhart, B., Dring, R. P., and Polymeropoulos, C. E., 1967, "Natural Convection From Vertical Surfaces, the Convection Transient Regime," ASME JOURNAL OF HEAT TRANSFER, Vol. 89, pp. 53–59.

Gebhart, B., and Mahajan, R. L., 1982, "Instability and Transition in Buoyancy-Induced Flows," *Adv. Appl. Mech.*, Vol. 22, pp. 231–315.

Goldstein, R. J., 1959, "Interferometric Study of the Steady State and Transient Free Convection Thermal Boundary Layers in Air and in Water About a Uniformly Heated Vertical Flat Plate," Ph.D. Dissertation, University of Minnesota, Minneapolis, MN.

Goldstein, R. J., and Briggs, D. G., 1964, "Transient Free Convection About Vertical Plates and Cylinders," ASME JOURNAL OF HEAT TRANSFER, Vol. 86, pp. 490–500.

Hellums, J. D., and Churchill, S. W., 1961, "Transient and Steady State, Free and Natural Convection, Numerical Solutions," presented at the International Heat Transfer Conference, Boulder, CO, Paper No. 18.

Illingworth, C. R., 1950, "Unsteady Laminar Flow of Gas Near an Infinite Flat Plate," *Proc. Camb. Phil. Soc.*, Vol. 46, pp. 603–611.

Ingham, D. B., 1978a, "Transient Free Convection on an Isothermal Vertical Flat Plate," *Int. J. Heat Mass Trans.*, Vol. 21, pp. 67–69.

Ingham, D. B., 1978b, "Numerical Results for Flow Past a Suddenly Heated Vertical Plate," *Phys. Fluids*, Vol. 21, pp. 1891–1895.

Jhaveri, B., and Homsy, G. M., 1980, "Randomly Forced Rayleigh–Bénard Convection," *J. Fluid Mech.*, Vol. 98, pp. 329–348.

Jhaveri, B., and Homsy, G. M., 1982, "The Onset of Convection in Fluid Layers Heated Rapidly in a Time-Dependent Manner," *J. Fluid Mech.*, Vol. 114, pp. 251–260.

Joshi, Y., and Gebhart, B., 1984, "Vertical Transient Natural Convection Flows in Cold Water," *Int. J. Heat Mass Trans.*, Vol. 27, pp. 1573–1582.

Joshi, Y., and Gebhart, B., 1986, "Measurements and Visualizations of Transient and Steady-State Vertical Natural Convection Flow in Cold Water," *Int. J. Heat Mass Trans.*, Vol. 29, pp. 1723–1740.

Joshi, Y., and Gebhart, B., 1987, "Transition of Transient Natural Convection Flows in Water," *J. Fluid Mech.*, Vol. 179, pp. 407–438.

Joshi, Y., and Gebhart, B., 1988, "Transient Response of a Steady Vertical Flow, Subject to a Change in Surface Heating Rate," *Int. J. Heat Mass Trans.*, Vol. 31, pp. 743–757.

Kirchner, R. P., and Chen, C. F., 1970, "Stability of Time-Dependent Rotational Couette Flow, Part I, Experimental Investigation," *J. Fluid Mech.*, Vol. 40, pp. 39–48.

Klei, H. E., 1957, "A Study of Unsteady State Natural Convection for a Vertical Plate," B.S. Thesis, MIT, Cambridge, MA.

Liu, D. C. S., and Chen, C. F., 1973, "Numerical Experiments on Time-Dependent Rotational Couette Flow," *J. Fluid Mech.*, Vol. 59, pp. 77–96.

Lurie, H., and Johnson, H. A., 1962, "Transient Pool Boiling of Water on a Vertical Surface With a Step in Heat Generation," ASME JOURNAL OF HEAT TRANSFER, Vol. 84, pp. 217–224.

Mahajan, R. L., and Gebhart, B., 1978, "Leading Edge Effects in Transient Natural Convection Flow Adjacent to a Vertical Surface," ASME JOURNAL OF HEAT TRANSFER, Vol. 100, pp. 731–733.

Downloaded 16 Dec 2010 to 193.140.21.150. Redistribution subject to ASME license or copyright; see http://www.asme.org/terms/Terms_Use.cfm

Martin, J. H., 1961, "An Experimental Study of Unsteady State Natural Convection From Vertical Plates," M.S. Thesis, Cornell University, Ithaca, NY.

Menold, E. R., and Yang, K.-T., 1962, "Asymptotic Solutions for Unsteady Laminar Free Convection on a Vertical Plate," ASME *Journal of Applied Mechanics*, Vol. 84, pp. 124–126.

Miyamoto, M., 1977, "Influence of Variable Properties Upon Transient and Steady State Free Convection," *Int. J. Heat Mass Trans.*, Vol. 20, pp. 1258–1261.

Mollendorf, J. C., and Gebhart, B., 1970, "An Experimental Study of Vigorous Transient Natural Convection," ASME JOURNAL OF HEAT TRANSFER, Vol. 20, pp. 628–634.

Orszag, S. A., and Kells, L. C., 1980, "Transition to Turbulence in Plane Poiseuille and Plate Couette Flow," *J. Fluid Mech.*, Vol. 96, pp. 159–205.

Rajan, V. S. V., and Picot, J. J. C., 1971, "Experimental Study of the Laminar Free Convection From a Vertical Plate," *Ind. Engng. Chem. Fundam.*, Vol. 10, pp. 132–134.

Sammakia, B., and Gebhart, B., 1978, "Transient and Steady-State Numerical Solutions in Natural Convection," *Numer. Heat Trans.*, Vol. 1, pp. 529–542.

Sammakia, B., and Gebhart, B., 1981, "Transient Natural Convection Adjacent to a Vertical Flat Surface: The Thermal Capacity Effect," *Numer. Heat Trans.*, Vol. 4, pp. 331–334.

Sammakia, B., Gebhart, B., and Qureshi, Z. H., 1980, "Measurements and Calculations of Transient Natural Convection in Air," *Int. J. Heat Mass Trans.*, Vol. 23, pp. 571–576.

Sammakia, B., Gebhart, B., and Qureshi, Z. H., 1982, "Measurements and Calculations of Transient Natural Convection in Water," ASME JOURNAL OF HEAT TRANSFER, Vol. 104, pp. 644–648.

Schetz, J. A., and Eichhorn, R., 1962, "Unsteady Natural Convection in the Vicinity of a Doubly Infinite Vertical Plate," ASME JOURNAL OF HEAT TRANSFER, Vol. 84, pp. 334–338.

Shen, S. F., 1961, "Some Considerations on the Laminar Stability of Time-Dependent Basic Flows," *J. Aero. Sci.*, Vol. 28, p. 397.

Siegel, R., 1958, "Transient Free Convection From a Vertical Flat Plate," ASME JOURNAL OF HEAT TRANSFER, Vol. 80, pp. 347–359.

Sugawara, S., and Michiyoshi, I., 1951, "The Heat Transfer by Natural Convection in the Unsteady State on a Vertical Flat Wall," *Proc. First Japan Natl. Cong. for Appl. Mech.*

Yang, K.-T., 1960, "Possible Similarity Solutions for Laminar Free Convection on Vertical Plates and Cylinders," ASME *Journal of Applied Mechanics*, Vol. 82, pp. 230–236.

Downloaded 16 Dec 2010 to 193.140.21.150. Redistribution subject to ASME license or copyright; see http://www.asme.org/terms/Terms_Use.cfm

Natural Convection in Enclosures

S. Ostrach
Wilbert J. Austin
Distinguished Professor of Engineering,
Department of Mechanical
and Aerospace Engineering,
Case Western Reserve University,
Cleveland, OH 44106
Fellow ASME

There exists a great diversity of buoyancy flows in enclosures that are of interest in science and technology. These buoyancy flows pose new and challenging physical and mathematical problems. Emphasis is given to the complexities of the phenomena, viz., the coupling of the flow and transport and of the boundary-layer and core flows, the interaction between the flow and the driving force, which alters the regions in which the buoyancy acts, and the occurrence of flow sub-regions (cells and layers). The importance of scaling analysis and experiments to determine flow details are discussed and the essentials of scaling techniques are outlined. The implications of these for numerical methods are presented, and the inadequacies of purely numerical solutions are pointed out. Representative works covering a broad range of problems are discussed.

Introduction

For the past 30 years, there has been an ever-increasing awareness that fluid motions and transport processes generated or altered by buoyancy are of interest and significance in many fields of science and technology. As a result, this subject is currently discussed in conferences and journals covering such diverse areas of meteorology, geophysics, astrophysics, nuclear reactor systems, materials processing, solar energy systems, energy storage and conservation, fire control, and chemical, food, and metallurgical industries, as well as in the more conventional fields of the fluid and thermal sciences.

Modern developments in buoyancy-driven flows had rather ignominious beginnings in the late 1940s. After World War II, German and Japanese scientists worked on this subject because it was not considered to be of any practical importance. Also, the present author, in desperation for a doctoral thesis topic, chose a completely confined buoyancy-flow problem, the subject of the present article and a configuration not previously studied in detail. It is ironic that such a choice was made by a young and naïve student, for it took nearly two decades of work by numerous researchers before the problem was properly described and somewhat longer for most of the complexities of confined buoyancy flows to be understood. However, this introduction to this fascinating subject led him to persist in exploring it further, with little interest by others for a number of years.

Buoyancy-induced flows are complex because of the essential coupling between the flow and transport. The problems can be classified as either external ones (free convection) or internal ones (natural convection). The first unified and comprehensive review of this subject was made by Ostrach (1964). Later summaries of free convection were presented by Ede (1967) and Gebhart (1979) and other reviews of natural convection were compiled by Ostrach (1972), Catton (1978), Ostrach (1982a), and Hoogendoorn (1986). Each of the last three emphasize essentially different aspects of the subject.

It was first pointed out by Ostrach (1968) that internal problems are considerably more complex than external ones. This is because at large Rayleigh numbers (the product of Prandtl and Grashof numbers) classical boundary-layer theory yields the same simplifications for external problems that are so helpful in other fluid-flow problems, viz., the region exterior to the boundary layer is unaffected by the boundary layer. For confined natural convection, on the other hand, boundary layers form near the walls but the region exterior to them is enclosed by the boundary layers and forms a core region. Because the core is partially or fully encircled by the boundary layers, the core flow is not readily determined from the boundary conditions but depends on the boundary layer, which, in turn, is influenced by the core. The interactions between the boundary layer and core constitute a central problem that has remained unsolved and is inherent to all confined convection configurations, namely, that the flow pattern cannot be predicted a priori from the given boundary conditions and geometry. In fact, the situation is even more intricate because it often appears that more than one global core flow is possible and flow subregions, such as cells and layers, may be imbedded in the core. This matter, which has been discussed more fully by Ostrach (1972, 1982a), and Ostrach and Hantman (1981), is not merely a subtlety for analysis, but has equal significance for numerical and experimental studies, as will be indicated later.

It is distressing to note that this crucial aspect of natural convection seems to be essentially ignored in most existing literature or is treated in a cavalier manner. The core flow is often merely assumed, estimated in an ad hoc manner, or specified from seemingly similar problems. However, experience has shown that natural convection is extremely sensitive to changes in the container configuration and the imposed boundary conditions so that use of results from "similar" problems is dangerous. In numerical studies, the entire matter generally is ignored and, as a consequence, there have been no truly reliable *predictive* results of velocity and temperature distributions. Until the problem is resolved, numerical studies must be guided and closely coupled with experiments.

Lack of progress on this crucial aspect of natural convection can be attributed to two reasons, one old and one relatively new. The first is related to proper normalization of the equations, sometimes referred to as dimensional or scaling analysis. As was pointed out by Ostrach (1982), it is disturbing to note that despite the existence of clear and explicit delineations of how to normalize natural-convection problems (Ostrach, 1964, 1982b), they are scaled in many different inappropriate ways (even for identical problems) in the literature. This can lead to errors in analysis and to considerable numerical problems (see de Vahl Davis, 1986), some of which even lead to misrepresentation of the physics. Scaling analysis is also essential for indicating the resolution required in both numerical and experimental studies. The disregard or lack of appreciation of such vital aspects, which are well documented, is hard to understand. The second aspect alluded to above

Contributed by the Heat Transfer Division for publication in the JOURNAL OF HEAT TRANSFER. Manuscript received by the Heat Transfer Division April 15, 1988. Keywords: Enclosure Flows, Modeling and Scaling, Natural Convection.

Copyright © 1988 by ASME

Downloaded 16 Dec 2010 to 193.140.21.150. Redistribution subject to ASME license or copyright; see http://www.asme.org/terms/Terms_Use.cfm

concerns an inherent coupling between the flow and the buoyancy-driving force. This was first indicated by Hantman and Ostrach (1969) and later noted more specifically by Cormack et al. (1974a, 1974b), but was not fully appreciated until relatively recently. In essence, this coupling causes the principal driving force to act in different regions of the enclosure, depending on conditions. This unusual physical characteristic of natural convection must be properly accounted for if meaningful results are to be obtained.

To add to all the complexity it should be recalled (Ostrach, 1964) that there are essentially two basic modes of flow generated by buoyancy. The first, usually referred to as conventional convection, occurs whenever a density gradient (due to thermal and/or concentration effects) is normal to the gravity vector. In such a case a flow ensues immediately. The second mode, called unstable convection, occurs when the density gradient is parallel but opposed to the gravity vector. In this situation the fluid remains in a state of unstable equilibrium (due to heavier fluid being above lighter) until a critical density gradient is exceeded. A spontaneous flow then results that eventually becomes steady and cellular-like. If the density gradient is parallel but in the same direction as gravity the fluid is stably stratified. As if all this were not sufficiently difficult to deal with, both conventional and unstable (or stratified) modes can interact in a given configuration.

For many years research on natural convection in enclosures centered around two basic configurations, viz., horizontal cylinders and rectangular cavities. The height-to-width (aspect) ratio of the rectangular cavities ranged from values equal to or greater than unity. Most attention has been given to each mode of convection separately, i.e., where the density gradients in a gravitational field were either horizontal or vertical with the gradient increasing upward. Most density variations were considered to be the result of temperature gradients. Less attention has been given to situations in which the buoyancy is due to concentration differences. Catton (1978) reviewed work done when both modes occurred simultaneously, as, e.g., in tilted rectangular enclosures.

More recently, due to motivations from diverse applications, the research scope has expanded in many ways. The configurations now being considered are low-aspect-ratio rectangles, parallelograms, annuli, and three-dimensional enclosures. The fluids now may be radiation participating media, or be changing phase, or be in porous media. Some problems are now being considered with heat flow in more than a single direction, either by direct imposition or by inclination of the cavity. Problems are being considered in which the imposed thermal conditions are not specified but must be determined from the interaction between the enclosure heat transfer and the environment or cover only part of the surface. Increasing attention is being given to situations in which the buoyancy is due to the combined effects of temperature and concentration gradients, which have various orientations relative to themselves and to gravity.

Clearly, with the limited space allotted to this paper, it is impossible to present a comprehensive review of all ongoing research. Because many physical and mathematical questions remain unresolved and others are introduced by some new work, emphasis will be given to refocusing on the crucial aspects of the conventional convection problem and on presenting insights on how to deal with them. In this way, some other older work will be revisited and some of the more recent work will be discussed. Fewer details will be given on material that is well documented and more on newer topics, but the presentation will be essentially descriptive and narrative due to space restrictions.

Overview of Early Work

The early work done on fully developed flows in channels and tubes, closed-end tubes, and in a shallow right circular cylinder that rotates about its axis and is heated at its lower surface was reviewed by Ostrach (1964, 1972).

The earliest investigation of natural convection in a completely confined configuration seems to have been made by Lewis (1950), who considered the heat transfer of "foam" type commercial insulating materials, which consist of gas-filled cells dispersed throughout a solid material. The natural convection in the cells was of particular interest. To simplify the analysis a spherical cell was treated as a horizontal cylinder of circular cross section and infinite length. A cosine wall temperature was specified, with the maximum and minimum wall temperatures on opposite ends of the horizontal diameter. This temperature corresponds to that which would occur in the solid without gas bubbles. Since the cells were very small, Lewis considered only the case of Rayleigh number less than unity for which no boundary-layer phenomena are encountered. A similar problem was treated by Zhukovitskii (1952). An excellent survey of low Rayleigh number problems is presented by Ostroumov (1952). Low Rayleigh number convection in a spherical cavity was investigated to Drakhlin (1952).

The heat transfer through gas layers confined in rectangular cavities composed of isothermal vertical walls and either perfectly conducting or perfectly insulating horizontal surfaces was investigated by Batchelor (1954) for the cases of height-to-width ratios of layers between 5 and 200. It was reasoned that several different flow regimes could occur

Nomenclature

A = aspect (height-to-width) ratio
ΔC = concentration difference
D = species diffusion coefficient
d = width
Gr = Grashof number $= \beta g \Delta T L^3/\nu^2$
g = acceleration of gravity
H = height
L = length
l = height
Le = Lewis number $= \alpha/D$
N = buoyancy ratio $= \beta\Delta C/\beta\Delta T$
$\overline{\text{Nu}}$ = average Nusselt number
P = dimensional pressure
p = dimensionless pressure
Pe = Peclet number = PrRe
Pr = Prandtl number $= \nu/\alpha$
Re = Reynolds number $= UL/\nu$
Ra = Rayleigh number = PrGr
Ra_H = Rayleigh number based on height
Sc = Schmidt number $= \nu/D$
T = temperature
ΔT = temperature difference
U = dimensional velocity
u, v = dimensionless velocities
$\bar{v}$ = velocity defined by equation (4)
X = dimensional coordinates
x, y = dimensionless coordinates
$\bar{y}$ = stretched coordinate
α = thermal diffusivity
β = volumetric expansion coefficient
$\bar{\beta}$ = concentration densification coefficient
δ_x = horizontal length scale
θ = azimuthal coordinate
ν = kinematic viscosity
ρ = density
ϕ = phase angle (Fig. 1)
ψ_R = characteristic stream function

Subscripts

H = horizontal
i = inner
V = vertical
w = wall
0 = entering
∞ = ambient

Downloaded 16 Dec 2010 to 193.140.21.150. Redistribution subject to ASME license or copyright; see http://www.asme.org/terms/Terms_Use.cfm

within the cavity depending on the values of the height-to-width ratio l/d and the Rayleigh number Ra. For small Ra Batchelor (1954) used a perturbation scheme similar to that of Lewis (1959) and, as expected, concluded that convection was unimportant compared to conduction. Conduction was also found to be the sole means of heat transfer in the asymptotic case of $l/d \to \infty$ and general Ra. In such cases, the temperature distribution in the air was found to vary linearly between the walls and the fluid flow was entirely vertical. Convection was restricted to the upper and lower ends of the cavity and as Ra approached values appropriate for boundary layers, these effects propagated into the rest of the cavity. This asymptotic case of infinite aspect ratio had been investigated earlier by Ostrach (1952) who treated it as a special case in a general analysis of natural convection between parallel, vertical, isothermal plates.

None of the aforementioned difficulties were encountered in those problems because the flows were not of the boundary-layer type.

Horizontal Cylinders

The first work dealing with the much more difficult large Rayleigh number internal natural convection problem was by Ostrach (1950), who studied the same configuration as Lewis (1950). Without any particular regard for applications, this problem was chosen because for large Rayleigh number it had a boundary-layer character, a subject of considerable interest at that time. The problem thus posed some interesting physical and mathematical questions; how difficult these were would not be appreciated fully for many years. It was formally shown that the equations for a compressible, viscous, heat-conducting fluid subject to a body force reduced to quasi-incompressible equations if $\beta\Delta T$ is less than unity. This is now usually referred to as the Boussinesq approximation. Also, the characteristic 1/4 power variation of the boundary-layer thickness was determined by a formal stretching transformation.

Specifically, Ostrach (1950) considered the steady laminar flow generated in a horizontal circular cylinder of infinite extent by an imposed cosine temperature distribution on the cylinder wall. The temperature extrema were on opposite ends of the horizontal diameter, a situation which will be referred to as heating-from-the side (conventional convection). For large Rayleigh number (specifically large Grashof number and unit-order Prandtl number) it was concluded that both a thermal and a flow boundary layer would exist adjacent to the cylinder wall and that they encircle a core. Using physical reasoning it was assumed that the core should be isothermal and have solid-body rotation. This assumption appeared to be reasonable and satisfied seemingly appropriate equations and accordingly was used by many investigators for years. However, later experiments on a somewhat similar configuration by Martini and Churchill (1960) raised doubts about it. The experiments were made for the same conditions and configuration as Ostrach's analysis except for the thermal boundary condition. The cylinder wall was divided along a vertical plane and the two halves were maintained at different uniform temperatures. Although this boundary condition differs from the cosine wall distribution, the similarity to the heating-from-the-side case is apparent. The experiment did indicate that flow and thermal boundary layers existed as a narrow circulating band of fluid along the cylinder wall. The core was, however, found to be thermally stratified with essentially horizontal isotherms and it was relatively stagnant. Because a positive vertical temperature gradient was observed in the core, Martini and Churchill (1960) argued that the core resisted rotation because of its increasing density from top to bottom, analogous to a "weighted disk."

Ostrach's thesis problem was reconsidered by Weinbaum (1964), Ostrach (1968), and Ostrach and Menold (1968). Each of these introduced new ideas to obtain meaningful solutions. Weinbaum (1964) generalized the original configuration by including a phase angle ϕ (see Fig. 1), which corresponds to heating-from-the-side (conventional convection) when $\phi = 0$ and heating-from-below (unstable mode) when $\phi = \pi/2$. In the latter two works, the Rayleigh number was considered large by taking the Prandtl number to be large and the Grashof number to be of unit order, rather than the reverse. The advantages of this model are that there is no flow boundary layer and the nonlinear terms in the vorticity transport equation are negligible. The modified Oseen linearization (Lewis and Carrier, 1949) was used in all the above-cited work; however, it was only required in the energy equation in the latter two. Considerable analysis of the core flow failed to yield a stagnant stratified solution for the heating-from-the-side case, although Ostrach and Menold (1968) did show that two core configurations were possible. The theory, however, did not discriminate between them.

At this point, it was deemed necessary to investigate this problem experimentally. Results from experimental analogues of the analyses are reported by Ostrach (1968, 1972), Ostrach and Menold (1968), Sabzevari and Ostrach (1974), and Brooks and Ostrach (1970). It should be noted that all the work of Ostrach and his students started in the early 1960s although, for many reasons, it was reported later as cited. It, together with Weinbaum's (1964) work, is reviewed in a unified manner by Ostrach and Hantman (1981).

In summary, the character of the core velocity and temperature distributions for natural convection at large Rayleigh number in a closed cavity appears to depend on the imposed thermal boundary conditions. A review of work for both rectangular and cylindrical enclosures indicates that experiments similar to the heating-from-below configuration (e.g., Schmidt and Saunders, 1938 in an infinite layer bounded by parallel horizontal planes) seem to yield core streamlines that are closed (i.e., a rotating core) and an isothermal core although the flows are three dimensional. In contrast, experiments applicable to the heating-from-the-side configuration (Martini and Churchill, 1969; Eckert and Carlson, 1961; Brooks and Ostrach, 1970, Elder, 1965a) indicated horizontal core streamlines, which begin and end in the boundary layer, and a thermally stratified core such that the isotherms and streamlines coincide.

All theoretical work, with the exception of Gill (1966), assumed an isothermal rotating core regardless of the thermal boundary conditions. The failure of this assumption in the heating-from-the-side case was brought out especially by Weinbaum (1964) and Ostrach (1968). Gill's (1966) analysis was strongly guided by Elder's (1965a) experiments and yields an adequate description for a high-aspect-ratio rectangular cavity with vertical side walls at different uniform temperatures.

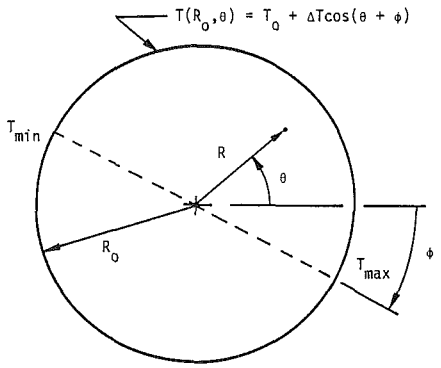

Fig. 1 Geometry

Downloaded 16 Dec 2010 to 193.140.21.150. Redistribution subject to ASME license or copyright; see http://www.asme.org/terms/Terms_Use.cfm

Since these analyses failed to predict the proper core behavior and the effect of the thermal boundary conditions (phase angle effects) the problem was reconsidered by Hantman and Ostrach (1969) with particular emphasis on two specific points. Firstly, the core streamlines had always been assumed to be closed. Therefore, it seemed advisable to formulate the problem without any assumptions about the nature of the core flow and temperature distribution. Secondly, the modified-Oseen linearization that was employed for tractability decoupled the core variables from those in the boundary layer. Since the core is driven by the boundary layer, a stronger coupling should be anticipated.

The limiting case of large Prandtl number and unit-order Grashof number was retained so that the nonlinear inertia terms can be neglected. This simplification facilitates the mathematical solution without losing the significant physical behavior. The methods of analysis described by Ostrach and Hantman (1981) are equally applicable to the alternative case of large Grashof number and unit-order Prandtl number. To deal with the first of the two points made above, consideration was given to the complete nonlinear and coupled equations. The equations are a well-defined set with no apparent singularities, the circular geometry presents no difficulties (e.g., no corners), and the boundary conditions are easily treated. Thus, if an approximate analytical technique would yield solutions to this one-point boundary-value problem that properly describe the physics, then no boundary-layer orderings or decisions about the nature of the core at the outset would be needed. Various generalizations of the modified Oseen linearization were tried (see Hantman and Ostrach, 1969, for details) but they all led to temperature distributions that yield an isothermal core. These solutions, which were obtained with no assumptions about the core, were shown to be equivalent to those of Ostrach (1968) and Ostrach and Menold (1968) and, hence, are valid for heating angles away from $\pi/2$ but not near $\phi = 0$.

Since solutions for heating from the side could not be obtained in the manner described above, a return was made to the boundary-layer approach. However, now the method of matched asymptotic expanisons (Van Dyke, 1964) was formally applied. Without prior assumptions about the nature of the core a number of physical characteristics of the core were obtained. However, these could be satisfied by either of the two possible core configurations. Proper matching conditions could, however, be obtained to yield solutions appropriate to heating from the side that were in consonance with experimental observations. The details of the boundary-layer analysis are presented by Ostrach and Hantman (1981) and will not be repeated herein because of space limitations.

The flow field described by the solutions obtained is one with a circumferentially oriented boundary layer, which joins a horizontal crossflow in the core. The core flow is in opposite directions in the upper and lower halves of the cylinder; in the lower half the flow is from left to right and in the upper half from right to left. Thus, the boundary layer in the first and third quadrants ejects fluid into the core and entrains fluid from the core in the second and fourth quadrants.

In order to match velocity fields properly for the boundary layer and stratified core a matching condition was derived from the requirement that the mass flux through the boundary layer must balance the mass flux across the core. The model, therefore, requires continuous circumferential flow in the boundary layer for all values of the azimuthal angle θ. This precludes any stagnation regions or any reversals of flow direction. From the matching condition it was also found that the core flow is weaker (i.e., of order $\mathrm{Pr}^{-3/4}$) than the azimuthal boundary-layer flow (of order $\mathrm{Pr}^{-1/2}$).

The boundary-layer energy equation was linearized in a new way (consistent with a stratified core) by replacing both convection terms with θ derivatives by functions of ϕ that are related to the core distributions. This linearization also reduced the coupled boundary-layer energy and vorticity equations to ordinary differential equations.

Despite the many advantages that resulted from the use of linearization, it also has some characteristics that limit the range of applicability of the results. The solutions obtained were not valid near the top and bottom of the cylinder; the validity covers -90 deg $< \theta <$ 70 deg. Also, the azimuthal coordinate plays the role of a parameter and, therefore, the solution along a ray $\theta = \text{const}$ is independent of that on any other ray. This decoupling prevents any circumferential diffusion of heat.

The heating phase angle, ϕ, appears in the solutions as a factor $\cos\phi$. For ϕ near zero the solutions for the horizontal diameter are representative for the presented model and, in fact, agree in form with Gill's (1966) evaluated at midheight of a rectangular high-aspect-ratio cavity.

Considerably more analytical study has been made for the horizontal cylinder configuration than for any other. This is possibly because only two parameters are associated with this configuration because the aspect ratio does not enter, there are no corner effects (and, therefore, no mixed boundary conditions), and the inclusion of a heating phase angle permits a complete variation of the thermal boundary conditions from heating from the side to heating from below. Since the core configuration is strongly affected, if not determined, by the thermal boundary condition, some insight was obtained into that aspect of the problem. Despite all these seeming advantages it is surprising that, to the best of the present author's knowledge, there has been no further work done on this configuration since the work of Hantman and Ostrach (1969). This configuration was recently reconsidered by Kassemi et al. (1987) for thermosolutal convection, i.e., when the buoyancy is due to the combined effects of thermal and concentration gradients.

Before embarking on the more complex problem of thermosolutal convection in a horizontal cylinder it was deemed necessary by Kassemi et al. (1987) to reconsider the purely thermal convection problem to resolve the uncertainty in the determination of the core configuration and to minimize or eliminate the arbitrariness due to linearizations made to obtain solutions. Focus was again given to the case of large Pr and unit-order Gr with heating from the side, because it was the most troublesome and there existed experimental results with which to compare solutions. The analysis of the core equations by Ostrach and Hantman (1981) was generalized so that explicit first-order core solutions could be obtained. The isothermal rotating core possibility was rejected on the basis of a more careful examination of the nature of the boundary-layer flow. Then an analytic iteration procedure was developed that started with the first-order solutions being introduced into integral forms of the full (nonsimplified) core equations. A somewhat similar integral procedure with strict conditions imposed on the velocity and temperature distributions was developed to obtain the boundary-layer solutions. Careful matching of the core and boundary-layer solutions yielded analytical results that agreed very well with experimental data. The use of integral forms of the equations eliminated the arbitrariness of the various linearizations that were previously used. The accuracy did not suffer because sufficiently realistic conditions, as determined by careful analysis, were imposed on the profiles. Although the accuracy of solutions obtained by integral methods is generally not known and ultimately must be checked by data, the method of analysis developed by Kassemi et al. (1987) seems promising because it gave additional physical insight into the problem and also good results in analytic form. The method has been generalized for thermosolutal convection.

The only numerical solution of the horizontal cylinder configuration known to this author is that of Hellums and Chur-

Downloaded 16 Dec 2010 to 193.140.21.150. Redistribution subject to ASME license or copyright; see http://www.asme.org/terms/Terms_Use.cfm

chill (1962), which is the analogue of the Martini and Churchill (1960) experiments. Because of the guidance from the experiments, reasonably good agreement was obtained between numerical and experimental results. Numerical methods would seem to have one advantage over the analytical boundary-layer approach. The numerical work can be carried out as a one-point boundary value problem for forward integrations and, therefore, requires no a priori knowledge of the core configuration. However, numerical work in the 1960s was seriously limited for confined natural convection problems because the solution of coupled higher-order equations requires machines of large capacity. Also, because numerical solution techniques were still relatively primitive, considerable ingenuity and trial and error were needed, which resulted in very high costs for solutions. Furthermore, numerical solutions of boundary-layer problems in which there are steep gradients are difficult to obtain and severe problems of numerical stability arise. More recently, there has been a proliferation of numerical solutions, almost to the exclusion of analytical work, but those are not without difficulties, as will be discussed in a subsequent section.

High-Aspect-Ratio Rectangular Enclosures

Square cavities will also be included in this section. Batchelor (1952) formulated the boundary-layer case corresponding to large Rayleigh numbers with general aspect ratios for rectangular enclosures. Based on the work of Pillow (1952) the interior was taken to be isothermal and have constant vorticity. However, Pillow's work dealt with the thermally unstable mode of convection between two infinite horizontal planes, the lower of which was at a higher temperature than the upper one. This is distinctly different from the conventional convection mode of interest to Batchelor. Clearly, the distinction between the two basic modes and the influence of thermal boundary conditions on the core was not appreciated in those days.

In a formal manner Batchelor (1956) investigated the nature of the interior region of a closed streamline flow in which viscous effects are restricted to a region near a solid boundary. As a theorem he was able to show that as long as the interior is not stagnant, the vorticity there is constant. The proof applied only to isothermal regions, and the boundary of the interior region has to be a closed streamline outside the viscous boundary layer. With this work it appeared that the nature of the core was well understood and described. Unfortunately, it took a number of years (Ostrach and Menold, 1968) before the other possibility, dismissed by Batchelor (1956), viz., that the core could be stagnant, was theoretically considered. Interestingly, Poots (1958) obtained numerical solutions that agreed with Batchelor's formulation, which illustrates that such solutions can be biased by inappropriate expectations.

Eckert and Carlson (1961) experimentally investigated air layers enclosed between vertical isothermal walls, the situation studied analytically by Batchelor (1954). The temperature field was determined in great detail by interferometry and no velocity measurements were made. As predicted by Batchelor (1954) the experimental results showed that below a certain Rayleigh number (prior to the formation of boundary layers) and above a certain height-to-width ratio, heat was transferred from the hot to the cold wall by conduction in the central part of the layer, with convection effects restricted to the corner regions. However, in the boundary layer regime (above a certain Ra and below a certain aspect ratio) the core of the layer was not found to be isothermal as predicted by Batchelor (1956), but instead, the temperature was uniform along horizontal lines only and increased in the vertical direction. The various flow regimes are delimited by Eckert and Carlson (1961) and are also shown by Ostrach (1972) in terms of the range of Grashof numbers and aspect ratio values. Based on their experiments, Eckert and Carlson (1961) concluded that it was extremely doubtful that a core of uniform temperature would ever exist at large Ra unless the height-to-width ratio was very small.

Experiments that further support the stratified core configuration are reported by Elder (1965a). Velocity measurements, made by direct observation of aluminum powder suspended in the fluid, were obtained in addition to temperature measurements. The fluids were medicinal paraffin and silicone oil, which have Prandtl numbers near 1000. The upper end of the cavity was open to the environment (air) so that thermocouples could be inserted. This resulted in different boundary conditions at the two ends, as a consequence, this configuration is not identical to the configuration studied by Batchelor (1954) and Eckert and Carlson (1961). The Elder experiments essentially confirmed the picture portrayed by Eckert and Carlson, but found that for $\mathrm{Ra} = 3 \times 10^5 \pm 30$ percent secondary cells appeared in the fluid. Further increases in Ra caused the cell wavelength to decrease and more cells to appear. As the Rayleigh number is increased still further after the occurrence of the secondary cells, a pronounced and rapid change occurs in the weak shear layers between successive secondary cells near $\mathrm{Ra} = 10^6$. A tertiary flow then ensues in the form of a circulation with closed streamlines and it has motion opposite to the clockwise motions of the primary and secondary flows.

The transition in a vertical slot from laminar to unsteady and then to turbulent flow is studied by Elder (1965b). For Rayleigh numbers above approximately 8×10^8 $(\mathrm{Pr}^{1/2}/A^3)$ travelling wavelike motions grow up the hot wall of the slot and down the cold wall. These waves grow most readily midway between the two ends. At higher Rayleigh numbers when the wave amplitude is finite the phase of successive wave fronts becomes increasingly random until near $\mathrm{Ra} = (1.0 \times 10^{10})/A^3$ an intense entrainment and mixing process starts between the wall region and the interior. The middle portion of the interior is then turbulent and the extent of this region grows further toward the ends as Ra increases.

Guided by the experiments of Elder (1965a) a theoretical model was developed by Gill (1966) for the limit of large Prandtl number. Approximate solutions were obtained that agree with the main aspects of the laminar flow experiments. This work is particularly significant because it was the first analytical treatment that did not assume an isothermal rotating core.

A number of numerical solutions for the vertical slot problem were obtained by Wilkes (1963), Geshuni et al. (1968), de Vahl Davis (1968), and Newell and Schmidt (1970). A comparison of these is presented by de Vahl Davis (1968) and somewhat more fully by Ostrach (1972). A correlation equation and table are given in the last two papers, which permit reasonable predictions of heat transfer to be made over a range of conditions. A more recent and comprehensive review of numerical methods for natural convection in rectangular cavities is presented by de Vahl Davis (1986).

On the basis of all the work described to date a few points need to be emphasized. Firstly, it is ill-advised to make ad hoc physical assumptions for complex problems. The original assumption of an inappropriate core configuration, which was universally accepted for too many years, certainly delayed proper description of the problem and misled users of the information. Scaling analysis coupled with formal mathematical procedures gave deeper insight into the physics and ultimately led to meaningful results. Also, careful assessments should be made of any approximation used to obtain solutions. The modified Oseen linearization, which proved so helpful in other problems, led only to incorrect results in the present one. Secondly, experimental guidance and verification are required for new and complex problems. The experiments should be carefully defined by scaling analysis, which can also indicate

Downloaded 16 Dec 2010 to 193.140.21.150. Redistribution subject to ASME license or copyright; see http://www.asme.org/terms/Terms_Use.cfm

the required resolution, and they should be conducted over appropriate ranges of parametric values. The present author's skepticism of purely numerical solutions is based on the reasons outlined above and will be further documented later.

Discrete Boundary Conditions. In all the work discussed thus far the bounding walls were isothermal or insulated. In numerous applications, however, such as home heating or the cooling of electric equipment, the heating is imposed over only a portion of the vertical walls. Some representative studies of this type will now be discussed.

Chu et al. (1976) determined the influence of the size and location of the heating element on the flow field and the rate of heat transfer for laminar two-dimensional situations. Although most practical cases involve three-dimensional turbulent motions, it was felt that the investigation could be a first step to the more general one and it did have some practical significance. The enclosure is a long horizontal channel with a rectangular cross section. The heating element is a long, horizontal, isothermal strip on an otherwise insulated vertical wall. The width and location of the heating element are variables. The opposing vertical wall is maintained at a lower uniform temperature. The upper and lower surfaces are insulated or maintained at the lower temperature. Numerical calculations and experiments were carried out for aspect ratios h/w from 0.4 to 5, a range of Rayleigh numbers from 0 to 10^5, and $\mathrm{Pr} = 0.7$.

After due consideration of convergence and stability problems, numerical solutions were obtained by a nonconservative finite difference technique using the ADI (alternating-direction-implicit) method. In the experiments temperatures were measured by thermocouples mounted in various locations on the heater strips and bounding surfaces and cigarette smoke was used to visualize the flow pattern.

The agreement between the theoretical and experimental streamlines was very good, as were comparisons of heat transfer rates computed for the limiting case of a completely heated wall with similar calculations made by others. These comparisons, together with tests for convergence, stability, independence from the initial condition, and step size, gave confidence in the numerical results.

The effects of the enclosure aspect ratio and thermal boundary conditions on the horizontal walls were numerically investigated, as well as the effects of heater size and location. The results were presented in terms of the Rayleigh number based on the height of the enclosure, the ratio of distance of the heating element from the top of the enclosure, and the ratio of the width of the heating to the enclosure height. The relationship between the circulation pattern and the heat transfer rate was found to be quite complex and indicates the possibility of maximizing or minimizing the rate of circulation

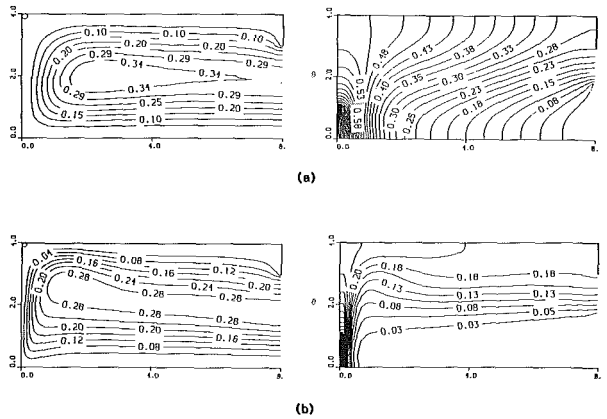

Fig. 2 Streamlines and isotherms for buoyancy-driven flow with $H = 4$, $L = 8$, $H_d = 3$: (*a*) $\mathrm{Ra} = 10^2$, and (*b*) $\mathrm{Ra} = 10^4$ (from Abib and Jaluria, 1988)

for a given heat transfer rate or vice versa. Conduction was found to be the predominant mechanism for heat transfer for $\mathrm{Ra} < 1000$ even though some circulation occurs for all $\mathrm{Ra} > 0$. Vertical plate boundary layer theory does not appear to be useful for prediction or correlation of the computed results.

Another problem of this type, related to solar collection systems, room fires, and electronic circuitry, was studied by Abib and Jaluria (1988). Particular interest was given to the buoyancy-induced flow in partially open enclosures. The spread and growth of combustion products in a room are largely determined by the location and size of doors and windows and the cooling of electronic components is substantially enhanced by openings in the enclosure. Since little detailed information on such problems exists, attention is focused on the interaction between the buoyancy flow and the flow through the opening. The configuration is a rectangular cavity with an isothermal heater of finite size extending upward from the bottom on the left vertical wall and an opening extending upward with different heights from the bottom on the right vertical wall. Except for the isothermal heater all bounding walls are adiabatic. At the opening the temperature from the ambient region is set and the temperature leaving the enclosure satisfies an "upwind" condition, i.e., no change in the normal direction. The horizontal velocity entering the cavity is obtained from a mass balance and the vertical velocity is taken to be zero. A finite-difference ADI scheme is used to obtain the solutions. Results are presented for Ra ranging from 10^2 to 10^7, $\mathrm{Pr} = 0.72$, and a range of openings from 1/4 to fully open, and a height to width ratio of 1/2. It is found that at Rayleigh numbers about 100 the effect of the opening does not penetrate very far into the cavity (Fig. 2*a*). However, for high Ra (10^4 to 10^7) the effect is significant since cold fluid penetrates much farther into the cavity and a boundary layer forms adjacent to the left vertical wall (Fig. 2*b*). A thermally stratified region forms outside the boundary layer. This thermal stratification becomes stronger as Ra increases and convection becomes the dominant mode of heat transfer. A recirculation region is established in the cavity, which reduces in size and moves to the left as $\mathrm{Ra} > 10^5$. The recirculation region increases as the size of the opening is reduced but the wall boundary layer is not significantly affected by the opening size. The thermal field is somewhat affected by the large recirculation region.

A more comprehensive treatment of the interaction between a fluid stream that passes through an enclosure and natural convection is presented by Sparrow and Samie (1982). A generic problem is treated to represent some geometric specific situations like oven cavities of electric stoves and air circulation in rooms with vents. The specific problem analzyed is a hollow vertical circular cylinder with small circular apertures centered in the upper and lower ends. A fluid stream enters the cylindrical enclosure through the lower aperture and exits through the upper one. The entering fluid has a temperature T_0, and the inner walls are at a different uniform temperature T_w. Two of the associated dimensionless parameters are the Reynolds number Re of the throughflow and the Rayleigh number Ra of the natural convection in the enclosure. There are two geometric parameters, the ratio of the aperture to cylinder diameters and the ratio of the cylinder height to its diameter. The fifth parameter is the Prandtl number. The two flows can augment or oppose each other depending on the sign of $(T_w - T_0)$. Even when natural convection is negligible (i.e., small Ra) the anticipated flow pattern in the enclosure is quite complex. The throughflow itself takes on a recirculatory pattern that washes the walls of the cylinder. At higher Ra the natural convection within the enclosure interacts with the recirculation and at still higher Ra it may interact with the throughflow stream itself. Thus, for a given Re it is of interest to identify the Ra at which these interactions occur. The effect of fluid flow interactions on the wall heat transfer, of course,

Downloaded 16 Dec 2010 to 193.140.21.150. Redistribution subject to ASME license or copyright; see http://www.asme.org/terms/Terms_Use.cfm

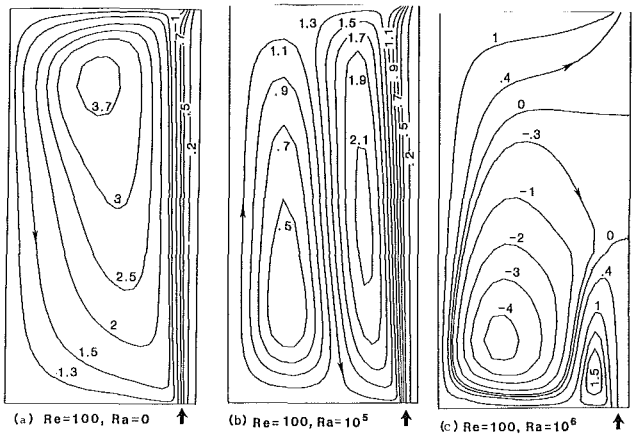

Fig. 3 Streamline maps, the curve parameter is $\psi/\nu d$ (from Sparrow and Samie, 1982)

must almost be determined. It would appear that when the two flows augment each other the heat transfer would be enhanced and, contrariwise, the counterflow would diminish the heat transfer. However, this overlooks the fact that the large-scale recirculation driven by the upward throughflow actually moves downward along the vertical wall. Thus, it is not clear which situation will enhance the heat transfer.

The problem was formulated in cylindrical coordinates and assumed to be axisymmetric. The usual no-slip and impermeability conditions are specified at the solid boundaries and inflow through the lower aperture is described as a constant purely vertical flow. Since the outflow condition is uncertain, simple conditions are specified at the upper aperture and the grid is structured so that those conditions do not penetrate very far into the solution domain. The thermal boundary conditions have already been described. Because of the recirculating nature of the flow, boundary-layer equations are not used, so the problem is elliptic. A specific elliptic finite-difference method was used in terms of primitive variables.' Calculations were made for a cylinder height-to-diameter ratio of unity and an aperture-to-cylinder diameter ratio of 0.1. Reynolds numbers were 100 and 250 and for each of these Ra was varied systematically from -10^6 to 10^6. For all cases $\mathrm{Pr}=0.7$. Detailed streamline and isotherm patterns are presented, as are lists of surface-integrated heat transfer rates for the individual surfaces of the enclosure and distributions of local heat transfer. A succession of complex interactions are indicated between the throughflow stream and the natural convection, which have a major influence on the heat transfer at the walls of the enclosure. In the absence of buoyancy the throughflow induces a large recirculating eddy in which the flow moves radially outward adjacent to the upper wall, downward along the side wall, and radially inward adjacent to the lower wall (Fig. 3*a*). Positive Rayleigh number natural convection ($T_w > T_0$) tends to induce a reverse direction for the circulation. At small and intermediate Ra the throughflow-driven recirculation is dominant and the natural convection weakly opposes it. As Ra increases a buoyancy-driven eddy is formed in the outer portion of the enclosure and it grows and utimately dominates the recirculating motion (Fig. 3*b*). At still higher Ra the buoyancy draws the throughflow stream outward along the lower wall and propels it upward along the side wall (Fig. 3*c*). In contrast, negative Ra ($T_w < T_0$) reinforces the throughflow-driven recirculation and the flow field in the enclosure is essentially unchanged from that without natural convection.

The temperature distributions in the enclosures show that regions of large temperature gradients shift from the upper wall to the lower wall as the direction of the recirculation reverses. These effects are reflected in both local and surface-integrated heat transfer results. For positive Ra the upper wall heat transfer decreases as Ra increases, with an opposite trend at the lower wall. At the side wall the heat transfer decreases initially, then increases and at sufficient high Ra may again decrease. The surface-integrated heat transfer rate for the enclosure as a whole decreases as Ra increases from zero, attains a minimum, and then increases. When the buoyancy is completely dominant (for positive Ra) the heat transfer is significantly larger than for buoyancy-free flow. The heat transfer is very little different for negative Ra from that at zero Rayleigh number.

Annuli. The studies of natural convection between vertical cylinders of different height and diameter by Charmchi and Sparrow (1982), Sparrow and Charmchi (1983), and Sparrow et al. (1984) are, in a sense, of the same general type as those with discrete boundary conditions. The inner cylinder was taken to be concentric, eccentric, and off center in that work. The inner cylinder was smaller in both height and diameter than the outer cylinder. Each cylinder is isothermal at different temperatures and the aspect ratio for each was unity. In the first reference cited above numerical solutions were obtained for concentric cylinders by an elliptic finite-difference method, assuming axisymmetry, and for a range of diameter ratios of 0.1 to 0.3, $0 \le \mathrm{Ra}_i \le 10^5$, $\mathrm{Pr}=0.7$, and three different axial locations of the inner cylinder. Streamline and isotherm maps, velocity profiles, per-surface and overall heat transfer rates and Nusselt numbers, and local Nusselt numbers are presented. Natural convection increased with Ra, with the most vigorous motion tending to be concentrated in the upper portion of the enclosure and with an accompanying stable stratification. For fixed Ra the flow is stronger for smaller diameter ratios. In the presence of vigorous natural convection the overall inner-cylinder Nusselt number for a given Ra is nearly independent of the geometric parameters (diameter ratio, inner cylinder evaluation). The local Nusselt number distributions are more responsive to the geometry changes.

The experimental analogue of the numerical study is described by Sparrow and Charmchi (1983) and in addition eccentric cases were considered. Temperature data enabled only evaluation of the average heat transfer coefficent and Nusselt number for each cylinder for a fixed cylinder-to-cylinder diameter ratio. The last agreed very closely with values determined numerically. Furthermore, it was found that the average Nusselt number was nearly independent of both elevation and eccentricity of the inner cylinder so that the average Nusselt number could be correlated only with Ra and the cylinder-to-cylinder diameter ratio. The close agreement between numerical and experimental results is regarded as validation of the numerical method. This is not too convincing because the average Nusselt number is obviously not very sensitive to flow details as is evidenced by the fact that geometric factors did not influence it. One wonders whether integral methods, which are much simpler, would not yield equally good heat transfer results. Examination of streamline and isotherm maps in Charmchi and Sparrow (1982) for the simpler case of concentric cylinders indicates that although the former are qualitatively similar (especially for smaller inner cylinders), the flow at a given Ra is considerably stronger when the inner cylinder is at its lowest elevation compared to its highest in accord with the results of Chu et al. (1976). For the larger inner cylinder cases the patterns are not quite as similar and a secondary cell appears above the inner cylinder when it is at its highest elevation. The maximum stream function ratio for the lowest and highest elevations is nearly two. The isotherm maps for the higher elevations are much more compressed toward the upper part of the enclosure and the isotherms indicate steeper stabilized zones beneath the inner cylinder at the lowest elevation.

In Sparrow et al. (1984) experiments were made with the inner cylinder position varied parametrically within the

Downloaded 16 Dec 2010 to 193.140.21.150. Redistribution subject to ASME license or copyright; see http://www.asme.org/terms/Terms_Use.cfm

enclosure and the orientation of the enclosure (outer cylinder) was varied relative to the gravity field. Again, the average Nusselt number for the inner body was insensitive to both the innerbody position and enclosure orientation.

Natural convection within both concentric and eccentric horizontal cylindrical enclosures was studied experimentally with an interferometer by Sun and Zhang (1986) and numerically in the three-dimensional annulus between concentric and horizontal cylinders by Fusegi and Farouk (1986). Optimum spacing of two low-conductivity, radial baffles in the air-filled annuli between horizontal concentric and eccentric cylinders at different temperatures was investigated by Babus'Hag et al. (1986).

More General Boundary Conditions. The problems discussed to this point were well defined by specifying thermal conditions on the interior surfaces of the enclosures. These boundary conditions are somewhat restrictive in the sense that they do not account for possible interactions between the enclosure and its surroundings. In fact, it is quite difficult to simulate experimentally such theoretically defined problems. Furthermore, there is also practical interest in problems in which the enclosure interacts with the environment. Examples are provided by heat transfer through windows or in cellular structures where the enclosure is embedded in a solid. Some representative problems dealing with such situations will now be described.

Sparrow and Parkash (1981) consider the interaction between internal natural convection in a square enclosure and an external free-convection boundary-layer flow. One vertical wall is cooled by an external free-convection flow and the opposite one is maintained at an uniform temperature with the horizontal walls adiabatic. Thus, the left wall temperature is specified to be T_w and the ambient fluid temperature is T_∞. The temperature at the right wall is unknown and its magnitude and distribution must be determined by the dynamics of the heat transfer process. Thus, complete thermal boundary conditions to solve either the internal or external are not known in advance. Consequently, interactions between the two flows must be considered such that the wall-temperature distribution emerges as one of the results. Problems involving coupling like the present ones are often referred to as being of the conjugate type.

It should be noted that the two buoyancy flows are fundamentally different in nature. The external flow is a boundary layer, which is mathematically characterized as parabolic, whereas the internal circulating flow is elliptic. Since numerical solutions are sought, the need to deal with interacting parabolic and elliptic problems is another special feature of this paper. The conjugate internal-external problem was solved numerically for $Pr = 0.7$ and Grashof numbers Gr between 10^3 and 10^7. Approximate solutions were also obtained with a model that avoids conjugate-type computations. For comparison purposes calculations were made for the internal problem with fixed different isothermal walls. Unfortunately, no detailed velocity and thermal distributions were presented. For overall conjugate heat transfer characteristics the average Nusselt number could be well represented by $\overline{Nu} = 0.0907\ Gr^{0.285}$ for $Gr > 10^4$. These $\overline{Nu}$ are about 60 percent of those for the standard enclosure for the same Gr. This should not be surprising since the conjugate wall imposes a stabilizing thermal gradient on the flow. These gradients increased with Gr. Two representative streamline maps are presented. For low Gr the pattern was symmetric and it is claimed that at high Gr there is a "modest" asymmetry due to the different boundary conditions at the two active walls. For the external free convection the local heat transfer coefficients were generally larger than those predicted by local application of classical isothermal plate results.

Another type of conjugate problem is experimentally and numerically treated by Kim and Viskanta (1984a) who considered the interaction between the natural convection in a square cavity and the conduction of heat in the walls that form the enclosure. Buoyancy flow are considered to be driven in each of three different ways: heating from the side, above, and below. An interferometer was used to determine the temperature distributions in the air. Numerical solutions of the transient elliptic equations were obtained by the ADI method. The accuracy was checked for the nonconjugate problem with the benchmark results of de Vahl Davis and Jones (1983). On the outer walls, two were specified to have different isothermal values and two were insulated. The thermal conditions at the interior walls (solid-fluid interface) were continuity of temperature and heat flux. As a result, the ratios of the solid and fluid thermal diffusivities and thermal conductivities and the void fraction are dimensionless parameters that appear in addition to the usual Pr, Ra, and aspect ratio. Only representative results for each heating configuration are presented. The effect of wall conduction was found to be greatest for heating from above and less significant but still important for heating from the side and the bottom. Wall conduction induces convection in the first configuration and convection induces conduction in the other two. Heat conduction along the conducting adiabatic (on the outside) walls simultaneously stabilizes and destabilizes the fluid in the cavity.

The concept of heat transfer coefficient may not be meaningful in conjugate problems because the Nusselt number depends not only on flow but also on thermal and geometric parameters of the solid that surrounds the cavity. Agreement between numerical and experimental temperature distributions is good but there are discrepancies.

Extension of the work described above is reported by Kim and Viskanta (1984b) to include effects of radiation heat exchange between the cavity surfaces. Yang (1986) presents additional information on interactions between natural convection and radiation in multidimensional enclosure, with emphasis on numerical modeling.

Simultaneous Imposition of Horizontal and Vertical Temperature Differences. In almost all existing work the buoyancy was induced by imposing a heat flux either horizontally (for conventional convection) or vertically from below (for thermal instabilities). Exceptions are the works dealing with enclosures that are tilted relative to the gravity vector. In many applications, however, heat fluxes are directly imposed simultaneously in more than one direction. Also, recently, there has been interest in reducing or eliminating natural convection in some processes, such as crystal growth, wherein natural convection is considered detrimental to good crystal morphology. Imposition of a stabilizing (vertical) heat flux on the driving (horizontal) heat flux would seem to offer a design option to accomplish this. One then wonders as to the magnitude of such a retarding flux. Research directed to obtain such information on natural convection is a rectangular enclosure with temperature differences imposed simultaneously in both the horizontal and vertical directions was done by Ostrach and Raghavan (1979) and Fu and Ostrach (1981) and will be described here.

Actually, the first work that indicated the effect of heat fluxes in more than one direction was that of Ostrach (1954, 1955a, 1955b). Stabilizing and destabilizing temperature gradients were imposed on the fully developed natural convection between two parallel vertical plates. Because the destabilizing gradients gave the first indication of thermal instabilities in vertical fluid layers, emphasis was focused on that case. However, results for the stabilizing configurations were included and the velocities were shown to decrease with increasing vertical stabilizing temperature gradients, but the implications were not appreciated at the time.

Experimental investigation of stabilizing thermal gradients

Downloaded 16 Dec 2010 to 193.140.21.150. Redistribution subject to ASME license or copyright; see http://www.asme.org/terms/Terms_Use.cfm

in a rectangular enclosure was made by Ostrach and Raghavan (1954). The flows correspond to Pr of order of 10^4 and unit order Gr. It was found that the reduction in the velocities depended on the aspect ratio, Gr (based on the horizontal temperature difference), and on the ratio of vertical to horizontal temperature differences. It was not possible to stop completely the flow generated by the horizontal temperature difference within the range of stabilizing gradients imposed.

A more detailed continuation of that work was made by Fu and Ostrach (1981) in which more quantitative data were obtained for the same range of conditions in a square cavity and some numerical results were obtained. The four walls of the enclosure were either heated or cooled to provide the desired boundary conditions. For a given pair of horizontal and vertical temperature differences, ΔT_H and ΔT_V, there are many ways to impose the wall temperatures. Most of the work dealt with those cases in which the averages of the vertical and the horizontal temperatures were identical, i.e., symmetric cases. Some asymmetric cases were also studied. Streamlines and velocities were determined by dye-injection visualization and isotherms were measured by a copper-constantan thermocouple that traversed the center plane of the enclosure. The stabilizing gradients cause the symmetric streamline pattern for the basic flow ($\Delta T_V = 0$) to become skewed into a parallelogram-like pattern with secondary counterrotating cells sometimes appearing in two diametric corners. The isotherms are very much more stably stratified in the core. The greatest decrease in total mass flux was found to be 62 percent when $\Delta T_V/\Delta T_H = 6$ is imposed symmetrically. Other aspects such as proper scaling, core secondary flows, and imposed asymmetries we studied. For the same $\Delta T_V/\Delta T_H$ symmetric imposition of the stabilizing gradient yields the greater reduction of natural convection.

Shiralkar and Tien (1982) numerically investigated the problem treated by Fu and Ostrach (1981). However, they considered $\mathrm{Pr} = 0.71$ rather than large values and Rayleigh numbers up to 10^6, more than an order of magnitude greater than Fu and Ostrach (1981). Despite the differences in parametric values the streamline and isotherm maps displayed similar qualitative features and large velocity reductions were also predicted. Shiralkar and Tien (1982) also considered the effects of imposing destabilizing gradients too. They determine heat transfer rates on the horizontal and vertical walls by integrating the normal temperature gradients over the length of the walls and claim that, surprisingly, the stabilizing temperature gradients increased both horizontal and vertical heat transfer. This, however, is misleading because the temperature gradients are singular at the corners of the enclosure and how they are evaluated can significantly affect the results. The large heat transfer in the corner regions is due to the large temperature differences between adjacent walls and not to the stratification. Fu and Ostrach (1981) were primarily interested in flow decreases because of its relevance to improved crystal quality and they only inferred concomitant reduced heat transfer by showing that the pure conduction isotherms were not distorted much by the slow flows. More quantitative heat transfer results are required to verify this.

Kirkpatrick and Bohn (1986) experimentally studied the natural convection in a cubical enclosure for different configurations of differentially heated and cooled surfaces, all of which were variations on the heating-from-below case. Thus, that work is the inverse of that just discussed in the sense that unstable gradients were imposed on the flows. The heated floor, as would be expected, promoted heating in the enclosure and reduced thermal stratification. For the conditions investigated the heat transfer from the horizontal surfaces was not strongly affected by the presence of a horizontal temperature gradient.

A related problem of natural convection in a rectangular cavity with constant heat flux on the bottom wall with an isothermal adjacent vertical wall with the other two insulated is studied experimentally and numerically by Anderson and Lauriat (1986).

Low-Aspect-Ratio Enclosures. A great deal of attention has been given to natural convection in shallow enclosures heated from the side during the past decade or so, motivated by applications such as auxiliary cooling equipment for high-temperature gas-cooled reactors and solar collectors (Boyack and Kearney, 1972) and crystal growth by closed-tube vapor deposition (Klosse and Ullersma, 1973; Solan and Ostrach, 1979). The extensive analytical, numerical, and experimental work on this configuration was reviewed by Ostrach (1982) and only the essential results will be presented herein. It was found by Cormack et al. (1974a) that for fixed Gr and diminishing A, the flow is parallel to the horizontal boundaries except near the ends of the cavity, that it is driven across the entire enclosure by an essentially linear horizontal temperature gradient, and the heat transfer is by conduction. For fixed $A < 1$ and Gr increasing the driving buoyancy force becomes concentrated at the ends and the flow is of a boundary-layer type. The core flow structure is no longer parallel and assumed various forms depending on values of the basic parameters and the thermal boundary conditions on the horizontal boundaries. Under certain conditions secondary cells or stagnation regions can occur in the core (Ostrach et al., 1980). The secondary cells were shown by Kamotami et al. (1983) to influence the heat transfer significantly. The existence of such flow subregions within the core even further complicates the determination of the core flow patterns. However, if meaningful analytical, numerical, or experimental results are to be obtained, at very least, the resolution required to predict or observe such subregions must be known. The present writer, therefore, returned to the central unresolved problem in natural convection and undertook to develop a method for obtaining a qualitative description of the overall flow pattern from the given geometric configuration, the fluid, and the boundary conditions. Because of the interest in low-aspect-ratio enclosures and because that configuration contains all the characteristics of the general problem, emphasis was given to it. The first phase of that work was completed by Lee and Ostrach (1982) and the essence of the method and the results will now be described.

In shallow rectangular enclosures the flow pattern can, on a geometric basis alone, be divided into two regions, viz., one, the region near the endwalls (the end region) and the other, the core, is the region outside the end regions and bounded by the horizontal boundaries.

In order to be able to predict the core flow pattern and, thus, the entire flow correctly, the physical mechanisms that pertain to each region must be clear. Recall, for example, that in the limit of pure conduction the buoyancy force acts over the entire enclosure, whereas in the boundary-layer limit it acts only in the end regions; clearly, intermediate cases also exist. Since the flow characteristic can be different and coupled in each region it is not possible to consider all the important physical mechanisms in the enclosure from equations that apply in a single region. In addition, the equations are nonlinear and bidirectionally coupled. Any simplifications must, therefore, be carefully made and ad hoc assumptions are dangerous. In order to ensure that an assumption (or physical statement) made in one equation is consistently transmitted to the other equations, a somewhat formal procedure is employed based on the method of multiple scales (Nayfeh, 1973). Multiple scales are introduced to give mathematical degrees of freedom that enable statements to be made of the proper physical mechanisms in the enclosure. Analytically the method of multiple scales yields single uniformly valid expansions, in contrast to the method of matched asymptotic expan-

Downloaded 16 Dec 2010 to 193.140.21.150. Redistribution subject to ASME license or copyright; see http://www.asme.org/terms/Terms_Use.cfm

sions, which leads to two expansions that must be matched. The method of multiple scales formally gives equations valid in each region as well as in the interaction region. This, implications of physical statements (force or energy balances) made in one region are formally and consistently transmitted to the other region as well as to the interactive one. It is easy to identify the equations that describe the core flow from the general equations. An outline of the procedure follows.

To identify the dominant physical mechanisms and the regions of the enclosure in which they apply a global scaling analysis is made first. The basic equations are normalized using geometric length scales. The order of magnitude of each term can then be estimated from the dimensionless parameters that appear as coefficients of the various terms to give the desired results. With this information as a guide a subregion scaling is made with the method of multiple scales where the geometric lengths are replaced by arbitrary ones that are determined from the proper physical statements. The occurrence of subregions is considered to be possible when the arbitrary length scales are found (on the basis of physical arguments) to be less than the geometric ones. This is a necessary, but not sufficient condition for flow subregions. The results obtained on this premise are compared with existing experimental data.

The analysis of Lee and Ostrach (1982) pertains essentially to enclosures with adiabatic horizontal surfaces and the vertical endwalls at different constant temperatures. Other horizontal thermal conditions were examined for some situations. The effects of horizontal wall boundary conditions are discussed by Ostrach (1982) and Cormack et al. (1974c).

The results of Lee and Ostrach (1982) are summarized in Table 1. The basic force and energy balances in each region are indicated therein as are also the proper scaling for the characteristic stream function, ψ_R, and the horizontal end region length scale, δ_x, and the physical conditions for which the various core configurations will be obtained. Note that the proper scalings for the variables obtained in this way indicate the resolution required to determine flow subregions both numerically and experimentally.

Three specific situations are analyzed depending on where the buoyancy (driving) force is operative. As determined from the global scaling when $\mathrm{Ra}_H A^2 \leq 1$ and $\mathrm{PrRa}_H A^2 << 1$ the temperature distribution is linear across the entire enclosure and the flow is driven by the buoyancy in the core. Depending on the magnitude of the Grashof number Gr, the core flow will be parallel when there is no flow boundary layer ($\mathrm{Gr}A^2 < 1$) and nonparallel when there is a flow boundary layer ($\mathrm{Gr}A^2 > 1$). No flow subregions are expected under these conditions.

When there are thermal boundary layers near the endwalls ($\mathrm{Ra}_H A^2 >> 1$) the flow will be driven by the buoyancy acting there. Then, depending on the magnitude of Pr the flow will be stagnant in the midcore, distinct horizontal thermal boundary layers will exist, or the core temperature distribution will be stratified. Secondary cells can be expected for some conditions.

In the intermediate flow regime the core temperature distribution varies with both space variables so that the buoyancy force acts throughout the enclosure and there are interactions between the core and end flows. In this case both parallel and nonparallel core flows can occur under the conditions specified and multicell patterns are possible.

Comparison of the predictions of the core flow patterns show good agreement with existing experimental results for $\mathrm{Pr} \geq 1$. For $\mathrm{Pr} < 1$ there are insufficient data for a comparable configuration. Predictions of the overall core flow patterns are generally satisfactory, but further work is required to define the flow subregions better. The method of analysis has clarified much of the physics of such problems and can be generalized to other configurations. It thus represents a good first step in resolving the key problem that has confronted workers on this subject since its inception.

Hart (1983) finds the conditions for which a parallel core flow will exist at low Pr for the same configuration studied by Lee and Ostrach (1982). Beyond those secondary vortices appear. The results are in agreement with the predictions of Lee and Ostrach. The stability of natural convection in a shallow cavity is analzyed by Kuo et al. (1986). The various types of cells and rolls that occur for various Pr as a result of instabilities are described.

Drummond and Korpela (1987) present numerical solutions for natural convection in shallow enclosures emphasizing low Pr, with some calculations made up to values of unity. For sufficiently small Pr they find a series of transverse cells distributed over the enclosure, which they attribute to a hydrodynanic instability as indicated by Kuo et al. (1986). Under those circumstances conduction prevails so that the buoyancy force is operative over the entire enclosure. As Pr is increased, ultimately convective unicellular flows occur. The authors, themselves, wonder whether the cell flows that they calculated could occur in reality or are artifacts of their two-dimensional simulation.

It should be said that the secondary cells determined experimentally by Ostrach et al. (1980) and Kamatoni et al. (1983) and analyzed by Lee and Ostrach (1982) are considered to result from the interaction between the velocity and temperature fields that cause the buoyancy driving force to change its location. This mechanism is a result of the inherent dynamics of the problem and not due to an instability. Clearly, the ranges of parametric values are different in the two problems. It is unfortunate, however, that Drummond and Korpela (1987) did not simulate the experimental results (some of which they cited) since their numerical program seemed to have the capabilities to do that. Greater confidence in their numerical procedure would have been obtained in this way.

Three-dimensional natural convection of a liquid metal in a differentially heated rectangular cavity was investigated numerically and experimentally by Viskanta et al. (1986). They found that for low-Prandtl-number fluids three-dimensional effects develop not only near the walls but also in the center of the cavity. Despite this, average Nusselt numbers calculated two dimensionally were in good agreement with three-dimensional ones. Agreement between measured and computed temperatures was only fair and the reasons for the discrepancies are discussed.

Thermosolutal Convection. In studies of natural convection the buoyancy driving force has, mostly, been considered to be due to temperature differences or gradients. Less attention has been given to situations in which concentration gradients alone are the cause of buoyancy. Although much has been learned there are still many aspects that are not fully understood or predictable. Despite this, even more complex situations are now being investigated.

Fluids flows generated by buoyancy due to the simultaneous action of both temperature and concentration gradients are generally referred to as thermosolutal convection. If there is a disparity in their associated diffusivities (Lewis number $\mathrm{Le} = \alpha/D \neq 1$) the flows are also said to be double diffusive. In reviews of this subject Ostrach (1980, 1982) indicated that various modes of convection are possible depending on the orientation of the temperature and concentration gradients relative to themselves and relative to the gravity vector. Most attention has been given to unbounded regions in which the gradients are alined with gravity in such a way as to lead to the Rayleigh–Bénard instability with double-diffusive effects (Turner, 1974) and some similarity solutions have been found for other orientations of the gradients by Gebhart and Pera (1971). For confined flows emphasis was given to the influence

Downloaded 16 Dec 2010 to 193.140.21.150. Redistribution subject to ASME license or copyright; see http://www.asme.org/terms/Terms_Use.cfm

of horizontal temperature gradients on stably stratified salt layers by Chen et al. (1971).

The simultaneous action of temperature and concentration gradients can be found in numerous technologies, such as cleaning and drying proceses, liquid-gas storage, and condensation through a noncondensing gas. Recently, it has been recognized that thermosolutal convection occurs in many aspects of materials processing, such as solidification, oxidation, and crystal growth. In some crystal-growth methods, e.g., closed-tube vapor transport and horizontal Bridgman growth, the completely confined fluid phase is subject to both horizontal temperature and concentration gradients. To gain insight on such flows an experimental program was initiated by Kamotani et al. (1985) to study thermosolutal flow in shallow rectangular enclosures with lateral temperature and concentration gradients between the vertical end walls, configurations that had not been investigated previously.

An electrochemical system based on a diffusion-controlled electrode reaction is employed to create the horizontal concentration gradients. The vertical endwalls can be heated or cooled so that the imposed horizontal temperature gradient can either augment or oppose the concentration gradient. Details of the apparatus and test procedure are given by Kamotani et al. (1985) and Ostrach et al. (1987). The flow structures and mass transfer are studied in detail under various conditions.

Ostrach (1980) derived the dimensionless parameters that describe thermosolutal convection, viz:

thermal Grashof number,	$\mathrm{Gr} = \beta g \Delta T H^3/\nu^2$
Prandtl number,	$\mathrm{Pr} = \nu/\alpha$
Schmidt number,	$\mathrm{Sc} = \nu/D$
buoyancy ratio,	$N = \tilde{\beta}\Delta C/\beta\Delta T$
aspect ratio,	$A = H/L$

Note that mostly $\tilde{\beta}$ and β have different signs so that positive values of N correspond to situations in which the thermal and solutal buoyancy forces augment each other and for negative N they are in opposition. The ranges of parametric values in the experiments are essentially limited by the electromechanical system and are: Gr up to 1.7×10^6, $\mathrm{Pr}=7$, $\mathrm{Sc}=2583$ to 2701, N to 45, and $A=0.13$ to 0.55 for both augmenting and opposing forces. The Lewis number $\mathrm{Le}=\mathrm{Sc}/\mathrm{Pr}=\alpha/D$ ranges from 369 to 386, which indicates that the diffusion of heat is much larger than the diffusion of species, so that double diffusion is to be expected. It should be noted that the flows generated with this system are thermally dominated in the sense that the thermal boundary layer is about six times larger than the solutal one and solutal boundary-layer velocities are 1/3 to 1/10 as slow as the thermal velocities. Although some tests were made by starting the solutal flow first and then imposing the thermal effects, the majority were made by establishing a steady thermal flow first and then the solutal effects were introduced. The results presented herein are all for the latter situation.

The flow patterns were found to depend strongly on the buoyancy ratio N (see Fig. 4). Multilayer flows occur when N is greater than about 6 when the two buoyancy forces are augmenting and for $N>10$ for opposing forces. The fluid is layered in three cells with the sense of circulation in each layer being toward the cold wall. The cell boundaries are clearly visible because the fluid color changes markedly across them and is quite uniform within each layer. The fluid concentration is lowest in the top layer and highest in the bottom one.

The layered flow structures develop because of double diffusion. Although the patterns look alike for augmenting and opposing buoyancy forces the mechanisms for their development are quite different, with counterflow entrainment an important aspect in the latter case. The development of the layered patterns is described in detail by Ostrach et al. (1987). The aspect ratio does not influence the multilayer flow significantly for augmenting situations, but for opposing cases, zonal mutilayers occur for $A=0.55$ and the top and bottom layers are tilted for $A=0.13$.

For N less than about 6 in the augmenting cases and less than but 10 in the opposing cases the flow forms unicellular patterns with secondary cells near the endwalls, very similar to the patterns for pure thermal convection. This is not unexpected since the lower values of N indicate stronger thermal effects. Representative changes in the flow patterns with N are presented in Fig. 4 for opposing forces and the smallest aspect ratio.

Temperature distributions and mass transfer are profoundly influenced by different flow patterns. Details are presented by Ostrach et al. (1987).

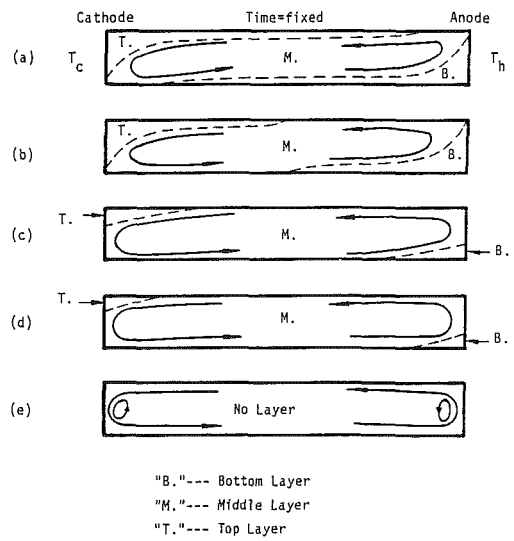

Fig. 4 Effects of thermal convection on multilayer for opposing case with $A=0.13$ and $G_{r,s}=8.2\times10^4$: (a) $G_{r,T}=-2.9\times10^3$, (b) $G_{r,T}=-5.9\times10^3$, (c) $G_{r,T}=-7.2\times10^3$, (d) $G_{r,T}=-1.0\times10^4$, (e) $G_{r,T}=-1.3\times10^4$

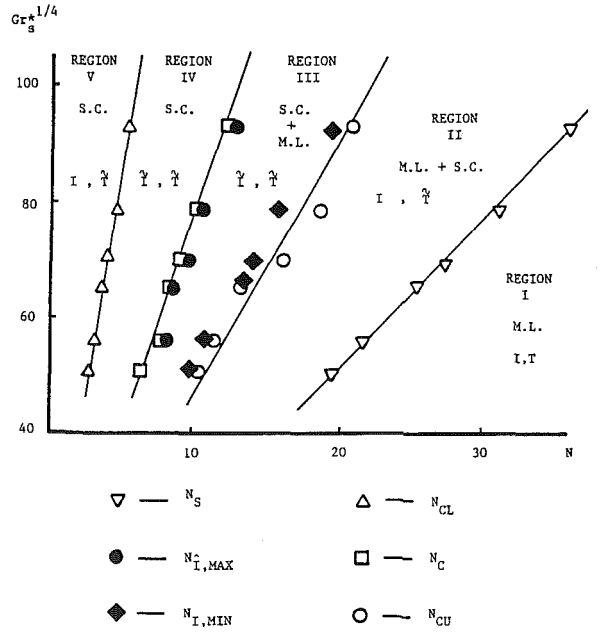

Fig. 5 Relation between the flow regimes and the fluctuations of temperature and current (including the minimum mass transfer rate I_{min} and the maximum current fluctuation intensity $\hat{I}_{max}$) in the ($Gr_s^{*1/4}$, N) plane

Downloaded 16 Dec 2010 to 193.140.21.150. Redistribution subject to ASME license or copyright; see http://www.asme.org/terms/Terms_Use.cfm

Under certain conditions with opposing forces, fluctuations in the cell potential occurred that are directly related to an unsteady mass transfer process that is ultimately due to changes in the solutal boundary-layer flow. To gain a deeper understanding of these unsteady characteristics of thermosolutal convection and to delineate the conditions for their occurrence a comprehensive experimental investigation of such flows due to opposing forces in shallow enclosures was undertaken. This research is described by Jiang et al. (1988).

Recall that for opposing buoyancy forces, the thermosolutal convection induces counterflows in the disparate thermal and solutal boundary layers that lead to very complex phenomena. In order to provide an overall view of the process a summary of the flow patterns and associated thermal and solutal fields will be presented. More details are given by Jiang et al. (1988).

The thermosolutal flow field is classified by its visible structures into three regimes: (*i*) a multilayer flow regime with $N \geq N_S$, where N_S is the value of the buoyancy ratio at which secondary cells appear, (*ii*) a secondary-cell flow regime with $N \leq N_C$, where N_C is the value at which the multilayer pattern disappears, and (*iii*) a mixed-flow regime consisting of both multilayers and secondary cells with $N_C < N < N_S$. These are delimited on Fig. 5.

The flow fields can also be characterized by the mass transfer. For $N \geq N_{CU}$ and $N \leq N_{CL}$ the mass transfer (current) is steady and it fluctuates when $N_{CU} > N > N_{CL}$, where N_{CL} and N_{CU} denote lower and upper bounds of N values for current fluctuations. These are also indicated on Fig. 5. Since N_{CU} and N_{CL} do not coincide with N_S and N_C, five regions are identified in Fig. 5. In the multilayer-flow regime ($N \geq N_S$), Region I, both the temperature and current, I, are steady and the convective flow near the cold cathode is laminar and bidirectional. Similar conditions occur near the hot anode. In part of the mixed-flow regime, Region II, defined by $N_S > N \geq N_{CU}$ the current is steady but the temperature fluctuates. The flow near the cold cathode is steady and bidirectional and there is a weak secondary cell there. Region III includes the remainder of the mixed-flow regime defined by $N_{CU} > N > N_C$. The flow near the cold cathode is quite complex and consists of an upper steady region and a lower unsteady one in both of which the flow is bidirectional, together with a fairly strong secondary cell. For some values of N the upper part of the steady-flow region also becomes unsteady. Both the temperature and current fluctuate in Region III. A part of the secondary cell flow regime with $N_C \geq N > N_{CL}$ is defined as Region IV. Both temperature and current fluctuate and the flow near the upper part of the cold cathode is steady and unidirectional and it is unsteady and bidirectional near the lower part. A secondary cell also occurs. The remainder of the secondary-cell regime with $N \leq N_{CL}$ is defined as Region V. A steady unidirectional flow covers the major part of the cathode and a steady bidirectional flow is found near the lower part of the cathode. A secondary cell also exists. The temperature fluctuations are weak in this region and the current is steady. The secondary cell flows are locally unsteady due to a thermosolutal instability associated with the interaction of the viscous shear and thermal and solutal buoyancy forces. The instability depends not only on the solutal Rayleigh number but also on the buoyancy ratio and the Lewis number.

To summarize, the temperature and current (mass-flow rate) are always steady in the multilayer flow regime, whereas in the mixed and secondary-cell regimes the temperature always fluctuates and the current fluctuates except when the secondary cells are either very weak or very strong. The detailed mechanisms for the observed behavior are described by Jiang et al. (1988). The maximum current fluctuations occur when the flow changes from the mixed flow to the secondary-cell flow regime.

The complexity of thermosolutal convection has been observed experimentally in a different configuration near a vertical ice surface melting in saline water by Carey and Gebhart (1982), Johnson (1978), and Josberger and Martin (1981). From those studies, and the one just described, the important aspects of thermosolutal convection are evident. In thermosolutal convection with large Le the opposing thermal and solutal buoyancy forces generate countercurrent flows in certain ranges of N. The flow near the solutal boundary-layer interface is destabilized by the counterflow and becomes sensitive to the buoyancy ratio N. Very different and complex flow patterns can then result.

Since there was no theoretical study of thermosolutal convection in enclosures Kassemi et al. (1987) undertook such an investigation. Because of the advantages of the horizontal cylinder configuration and the experience gained from analysis of the purely thermal case, as discussed previously, they considered that case with imposed cosine wall temperature and concentration distributions, which correspond to augmenting or opposing thermal and buoyancy forces imposed "from the side" (i.e., conventional convection mode). The analytic iteration method used in conjunction with integral equations that was developed for the case of pure thermal convection was generalized to include the simultaneous mass transfer. The thermal and solutal Grashof numbers were of unit order of magnitude and the Lewis number was arbitrary to take advantage of the simplifications that were previously described.

Approximate analytic solutions were obtained in closed form, which displayed many of the thermosolutal flow phenomena: double-cell and multilayer streamline patterns. For augmenting bouyancy forces, velocities were enhanced relative to purely thermal ones and were retarded for opposing forces. The core temperature and concentration were both stratified. Although the range of parameters and configuration are different from any existing experiments there were qualitative similarities with the data for shallow enclosures.

Concluding Remarks

In the foregoing the rich diversity of natural convection problems in science and technology has been demonstrated. These pose new and challenging physical and mathematical problems. The complexities of the phenomena have also been discussed, i.e., the coupling of the flow and transport and of the boundary layer and core flows, the interaction between the flow and the driving force, which alters the regions in which the buoyancy acts, and the occurrence of flow subregions (cells and layers).

The early research on natural convection in enclosures was almost entirely analytical or experimental, and although the former gave important insights, the latter were usually critical in revealing the true nature of the flows and new aspects. The experiments also indicated the folly of ad hoc physical assumptions for such complex problems. Examples are afforded by the experiments of Martini and Churchill (1960), Ostrach and Menold (1968), and Sabzevari and Ostrach (1974), who showed that the core in a horizontal cylinder heated from the side was stagnant and stratified and not rotating and isothermal and Eckert and Carlson (1961) did the same for high-aspect-ratio rectangular enclosures. Secondary cells for side heating were found by Brooks and Ostrach (1970) for the horizontal cylinder, Elder (1965a) for vertical rectangular enclosures, and Ostrach et al. (1980) and Kamotani et al. (1983) for shallow enclosures. None of these crucial aspects of the problems were predicted by the early numerical work and, in fact, some of that, Poots (1958) for example, actually gave incorrect results.

Despite this, there is an ever-increasing proliferation of purely numerical solutions to problems of this type with even more complications than the relatively straightforward early

Downloaded 16 Dec 2010 to 193.140.21.150. Redistribution subject to ASME license or copyright; see http://www.asme.org/terms/Terms_Use.cfm

problems. To give credence to the numerical results, usually numerical stability and convergence tests are made and then the calculations are compared to others made for simpler problems or are compared to such experimental data as the average Nusselt number. However, this last is a gross parameter, which is generally insensitive to details such as velocity and temperature distributions so that agreement with numerical calculations does not ensure that the details are correct. Incredibly, in some papers in which such comparisons are used as validation of the numerical work, the insensitivity of the average Nusselt number to many details is actually indicated, but this does not seem to concern the authors. The insensitivity of gross parameters to details is precisely the reason that integral methods are so useful for their determination. Comparison with simpler numerical solutions can also not be convincing either because the simpler solutions may not have been validated or, even if they have, different apsects may appear in the new problem due to the sensitivity of natural convection to changes in configuration and boundary conditions.

Another problem with numerical solutions has been alluded to earlier, viz., that the equations have rarely been normalized, i.e., not only been made dimensionless but also of unit order of magnitude. The result is that the dimensionless parameters appear as coefficients of various terms and the relative magnitude of each term in thus not properly indicated by its coefficient (parameter). Incidentally, this has not deterred some authors from simplifying such equations by ordering procedures. Even without ordering, numerical difficulties and errors arise, as indicated by Ostrach (1982) and deVahl Davis (1986), because the large parametric values associated with such problems cause the terms to have disparate magnitudes that require more computer storage and also lead to calculations of large differences of small numbers, or vice versa. An even more serious consequence of improper normalization of scaling is that the proper physics may be misrepresented. Recall that it was previously indicated that due to the coupling of the flow and temperature gradient, the regions in which the buoyancy driving force acts changes. In almost every numerical paper reviewed herein and in the literature the velocity is made nondimensional (not normalized) by using either the viscous or thermal diffusion velocity. Ostrach (1982) has indicated the implications and consequences of various reference velocities. As a consequence the Grashof or Rayleigh number appears as the coefficient of the buoyancy term. Since for laminar flows these parameters can easily have values on the order of 10^4 to 10^8, the buoyancy force is made the dominant term in the equations. There are, however, regions in which there is no buoyancy, such as the core for boundary layer flows, but a very small numerical error in the buoyancy term can cause it improperly to contribute to the solution there and, thus, misrepresent the true physics.

Finally, there is the difficulty of finding the proper mesh for the numerical solutions, i.e., finding the resolution required to give meaningful results. If no a priori information exists on the flow patterns it is difficult to know if and where to expect unusual aspects, such as flow subregions. The work of Lee and Ostrach (1982) represents a first step in providing such information but it must be further extended and generalized. Until such time that it or other developments will be able to give at least qualitative information on the flow patterns to be expected for a given configuration and boundary conditions, experimental guidance and validation for theoretical and numerical analyses of natural convection is essential. The problems outlined above make it difficult to avoid skepticism of purely numerical solutions. This may seem like an unusual position for an applied mathematician to take, but many years of experience on problems of this type have led to the views expressed herein.

As much care must, of course, be taken in defining experimental models as numerical ones. Many of the more recent experimental studies yield only gross parameters, which are useful for applications. However, for determining the nature and extent of new phenomena one must be certain that all the relevant physics are included and that the resolution of the instrumentation is sufficient to obtain the desired information. Again, scaling analysis is essential for these purposes.

Since so much emphasis has been given to proper normalization of equations and scaling analysis herein and these have been generally ignored and, more recently, are being obfuscated, this paper would be incomplete if more were not said on this matter. Unfortunately, there is not enough space available to present a comprehensive account of this powerful method herein. Therefore, a brief historical account will be given to set some matters straight and then the essentials of the techniques will be outlined and relevant references for more details will be presented.

One of the few articulations of the value of scaling analysis and descriptions of its applications to several problems was presented by Ostrach (1966). It is indicated therein that the dimensionless parameters that are derived in that way are of value for many reasons, not the least of which is to indicate the dominant physical aspects of the problem of interest. This is because those parameters can be interpreted as ratios of such physical quantities as forces. Clearly, these parameters can take on different values in various regions of a given problem, which was the basis of the multiscale analysis of Lee and Ostrach (1982). Bejan (1984) apparently unaware of the distinction between global and local scalings uses a force balance in the boundary layer and states unequivocally that the parameters have no such meaning. He confuses global and local scalings. This is a most unfortunate misconception to be presented in a textbook, because the dimensionsless parameters provide the only way to ensure that the proper physics is included in both numerical and experimental simulations of complex phenomena. Many real problems of current significance are ones in which there can be several driving forces, multiple transport modes, and chemical reactions and phase separations. Evaluation of the dimensionless parameters for protoype conditions will indicate which of all those are signficiant in a global sense and, thereby, lead to more tractable and still meaningful problems. If this procedure is disregarded, only intuition can be used for simplifications and the literature is replete with extensive numerical solutions and experiments where the essence of the problem has been omitted.

The scalings developed by Ostrach (1952) for free convection about a vertical plate were essentially limited to unit-order Prandtl numbers. Nevertheless, Ostrach's numerical results, even for extreme values of Pr, were found by asymptotic methods for vanishing and infinite values of Pr (Le Fevre, 1956) and other numerical solutions for low Pr (Sparrow and Gregg, 1958 and 1959) to be accurate to within one percent. Bejan (1984), based on arguments relative to extreme values of Pr, refers to Ostrach's (1952) scaling as fictitious, improper, and incorrect. He does not mention that they are, however, valid for unit-order Pr, a rather important range. Proper scalings for small and large Pr were derived by Braun et al. (1961) and reported by Ostrach (1964, 1982b). These are identical to those found later by Bejan (1984). This seeming lack of awareness of the existing literature has led Bejan (1987) to claim a need for correcting the traditional and established (and presumably incorrect) scalings. Such spurious arguments confuse those uninitiated in scaling analysis and, thereby, lead to their disenchantment with it. This is not to say that all matters concerning scaling analysis are settled, because they are not. Efforts should be expended to resolve the new issues and there are many opportunities to make contributions thereby.

To obtain the scales the variables must be normalized (made dimensionless and of unit order). Thus,

Downloaded 16 Dec 2010 to 193.140.21.150. Redistribution subject to ASME license or copyright; see http://www.asme.org/terms/Terms_Use.cfm

$u = U/U_R, \quad x = X/L, \quad \phi = (T - T_\infty)/T_w - T_\infty), \quad p = p/\rho U_R^2$

where U_R denotes a (unknown) reference velocity, because no velocity scale is imposed in buoyancy-driven flows. Schematically, the dimensionless equations with parameters are:

$$\text{(Inertia)} \approx (\nu/U_R L)\,\text{(Viscous)} + \\ + (\beta g \Delta T L/U_R^2)\,\text{(Buoyancy)} - \text{(Pressure)} \quad (1)$$

$$\text{(Convection)} \approx (\alpha/U_R L)\,\text{(Conduction)} \quad (2)$$

The mathematical expressions for the various quantities in parentheses are omitted both for simplicity and also since they should be of unit order if the variables are properly normalized. Thus, the magnitude of each term is indicated by its coefficient. To determine the reference velocity U_R, it is necessary to know the dominant forces involved and those, in turn, depend on the parameters, $\text{Re} = U_R L/\nu$, $\text{Pr} = \nu/\alpha$, $\text{Pe} = \text{PrRe} = U_R L/\alpha$.

All possible combinations of these parameters are presented in the table below, where S denotes small (less than unity), U denotes unit order, and L denotes large (greater than unity). The last column indicates dominant forces or other qualitative features of the problem.

Case	Re	Pr	Pe	Comments
1	S	S	S	Buoyancy and viscous forces balance
2	S	U	S	Buoyancy and viscous forces balance
3	S	L	U	Buoyancy and viscous forces balance
4	S	L	L	Thermal boundary layer
5	U	S	S	All forces of same order
6	U	U	U	All forces of same order
7	U	L	L	Thermal boundary layer
8	L	S	S	Velocity boundary layer
9	L	S	L	Velocity and thermal boundary layers
10	L	U	L	Velocity and thermal boundary layers
11	L	L	L	Velocity and thermal boundary layers

Note that since the buoyancy force is generating the flow it must always, on a global scale, be one of the dominant forces.

For cases 1 to 3 a balance of coefficients of buoyancy and viscous forces in equation (1) yields

$$U_R = \beta g \Delta T L^2/\nu = \text{Gr}(\nu/L) \quad (3)$$

Whenever a thermal boundary layer exists (cases 4, 7, and 9 to 11) its thickness is the fundamental length because it is over that length that the buoyancy force acts. Therefore, a coordinate stretching is required to make both terms in equation (2) of the same order, so we let

$$\bar{y} = [\text{Pr}(U_R L/\nu)]^{1/2} y \text{ and } \bar{v} = [\text{Pr}(U_R L/\nu]^{1/2} v \quad (4)$$

Then, equations (1) and (2) become

$$\text{(Inertia)} = \text{Pr(Viscous)} \\ + (\beta g \Delta T L/U_R^2)\,\text{(Buoyancy)} \quad (5)$$

$$\text{(Convection)} = \text{(Conduction)}$$

where the axial viscous and conduction tems are neglected, the transverse velocity in the inertia and convection terms is now v as given by equation (4), and the pressure term is omitted for brevity. For small Pr the appropriate balance between the buoyancy and inertia forces gives

$$U_R = (\beta g \Delta T L)^{1/2} = (\text{Gr})^{1/2}(\nu/L) \quad (6)$$

and for large Pr the balance between buoyancy and viscous forces yields

$$U_R = (\beta g \Delta T L/\text{Pr})^{1/2} = (\text{Gr/Pr})^{1/2}(\nu/L) \quad (7)$$

When there is only a velocity boundary layer (case 8) buoyancy and inertia forces must balance and the reference velocity is given by equation (6). When all forces are of the same order (cases 5 and 6) either equation (6) or (7) is applicable.

If the appropriate reference velocity, as given by equations (3), (6), and (7), is substituted into the Reynolds and Peclet numbers, criteria, in terms of buoyancy flow parameters, for use of those velocities are obtained. Thus, for

$\text{Gr} \le 1$ and $\text{Ra} \le 1$	use equation (3)
$(\text{Gr})^{1/2} > 1$ and $\text{Pr} < 1$	use equation (6)
$(\text{Gr})^{1/2} > 1$ and $\text{Pr} > 1$	use equation (7)

With this presentation of the elements of scaling analysis it is hoped that the heat transfer community will begin to appreciate its power and utility and use it to obtain meaningful models of complex phenomena.

References

Abib, A. H., and Jaluria, Y., 1988, "Numerical Simulation of the Buoyancy-Induced Flow in a Partially Open Enclosure," *Num. Heat Trans.*, in press.

Anderson, R., and Lauriat, G., 1986, "The Horizontal Natural Convection Boundary Layer Regime in a Closed Cavity," *Proceedings of the Eighth International Heat Transfer Conference*, Vol. 4, Hemisphere Publishing Corp., Washington, DC, pp. 1453–1458.

Babus'Haq, R. F., Probert, S. D., and Shilston, M. J., 1986, "Influence of Baffles Upon Natural-Convective Steady-State Heat Transfer Across Horizontal Air-Filled Annuli," *Proceedings of the Eighth International Heat Transfer Conference*, Vol. 4, Hemisphere Publishing Corp., Washington, DC, pp. 1557–1561.

Batchelor, G. K., 1954, "Heat Transfer by Free Convection Across a Closed Cavity Between Vertical Boundaries at Differenrt Temperatures," *Quart. Appl. Math.*, Vol. 12, pp. 209–233.

Batchelor, G. K., 1956, "On Steady Laminar Flow With Closed Streamlines at Large Reynolds Number," *J. Fluid Mech.*, Vol. 1, pp. 177–190.

Bejan, A., 1984, Convection Heat Transfer, Wiley, New York.

Bejan, A., 1987, "Stressing the 'Free' in Free Convection Research: The Basic Scales of Heat and Mass Transfer in Fluids and Fluid-Saturated Porous Media," *Proc. 1987 ASME/JSME Thermal Engineering Joint Conference*, Vol. 2, pp. 195–202.

Boyack, B. E., and Kearney, D. W., 1972, "Heat Transfer by Laminar Natural Convection for Low Aspect Ratio Cavities," ASME Paper No. 72-HT-52.

Braun, W. H., Ostrach, S., and Heighway, J. E., 1961, "Free-Convection Similarity Flows About Two-Dimensional and Axisymmetric Bodies With Closed Lower Ends," *Int. J. Heat Mass Trans.*, Vol. 2, pp. 121–135.

Brooks, I., and Ostrach, S., 1970, "An Experimental Investigation of Natural Convection in a Horizontal Cylinder," *J. Fluid Mech.*, Vol. 44, pp. 545–561.

Carey, V. P., and Gebhart, B., 1982, "Transport Near a Vertical Ice Surface Melting in Saline Water: Experiments at Low Salinities," *J. Fluid Mech.*, Vol. 117, pp. 403–423.

Catton, I., 1978, "Natural Convection in Enclosures," *Proceedings of the Sixth International Heat Transfer Conference*, Toronto, Vol. 6, Hemisphere Publishing Corp., Washington, DC, pp. 13–30.

Charmchi, M., and Sparrow, E. M., 1982, "Analysis of Natural Convection in the Space Between Concentric Vertical Cylinders of Different Height and Diameter," *Num. Heat Trans.*, Vol. 5, pp. 119–144.

Chen, C. F., Briggs, D. G., and Wirtz, R. A., 1971, "Stability of Thermal Convection in a Salinity Gradient Due to Laterial Heating," *Int. J. Heat Mass Trans.*, Vol. 14, pp. 57–65.

Chu, H. H.-S., Churchill, S. W., and Patterson, C. V. S., 1976, "The Effect of Heater Size, Location, Aspect Ratio, and Boundary Conditions on Two-Dimensional, Laminar Natural Convection in Rectangular Channels," ASME JOURNAL OF HEAT TRANSFER, Vol. 98, pp. 194–199.

Cormack, D. E., Leal, L. G., and Imberger, J., 1974a, "Natural Convection in a Shallow Cavity With Differentially Heated End Walls, Pt. 1, Asymptotic Theory," *J. Fluid Mech.*, Vol. 65, Pt. 2, pp. 209–229.

Cormack, D. E., Leal, L. G., and Seinfield, J. H., 1974b, "Natural Convection in a Shallow Cavity With Differentially Heated End Walls, Pt. 2, Numerical Solutions," *J. Fluid Mech.*, Vol. 65, Pt. 2, pp. 231–246.

Cormack, D. E., Stone, G. P., and Leal, L. G., 1974c, "The Effect of Upper Surface Conditions on Convection in a Shallow Enclosure With Differentially Heated End Walls," *Int. J. Heat Mass Trans.*, Vol. 18, pp. 635–648.

deVahl Davis, G., 1968, "Laminar Natural Convection in a Rectangular Cavity," *Int. J. Heat Mass Trans.*, Vol. 11, pp. 167–1693.

deVahl Davis, G., 1986, "Finite Difference Methods for Natural and Mixed Convection in Enclosures," *Proceedings of the Eighth International Heat Transfer Conference*, San Francisco, Vol. 1, Hemisphere Publishing Corp. Washington, DC, pp. 190–109.

deVahl Davis, G., and Jones, I. P., 1983, "Natural Convection in a Square Cavity, a Comparison Exercise," *Int. J. Num. Meth. Fluids*, Vol. 13, pp. 227–248.

Drakhlin, E., 1952, "On Spherical Convection in an Enclosure," *Soviet Journal of Technical Physics*, Vol. 22, pp. 829–832.

Downloaded 16 Dec 2010 to 193.140.21.150. Redistribution subject to ASME license or copyright; see http://www.asme.org/terms/Terms_Use.cfm

Drummond, J. E., and Korpela, S. A., 1987, "Natural Convection in a Shallow Cavity," *J. Fluid Mech.*, Vol. 182, pp. 543–564.

Eckert, E. R. G., and Carlson, W. O., 1961, "Natural Convection in an Air Layer Enclosed Between Two Vertical Plates at Different Temperatures," *Int. J. Heat Mass Trans.*, Vol. 2, pp. 106–129.

Ede, A. J., 1967, "Advances in Free Convection," *Advances in Heat Transfer*, Vol. 4, Academic Press, pp. 1–62.

Elder, J. W., 1965a, "Laminar Free Convection in a Vertical Slot," *J. Fluid Mech.*, Vol. 23, Part 1, pp. 77–98.

Elder, J. W., 1965b, "Turbulent Free Convection in a Vertical Slot," *J. Fluid Mech.*, Vol. 23, pp. 99–111.

Fu, B.-I., and Ostrach, S., 1981, "The Effects of Stabilizing Thermal Gradients on Natural Convection Flows in a Square Enclosure," *Natural Convection*, I. Catton and R. N. Smith, eds., ASME HTD-Vol. 16, pp. 91–104.

Fusegi, T., and Farouk, B., 1968, "A Three-Dimensional Study of Natural Convection in the Annulus Between Horizontal Concentric Cylinders," Vol. 4, Hemipshere Publishing Corp., Washington, DC, pp. 1575–1579.

Gebhart, B., 1979, "Buoyancy Induced Fluid Motions Characteristic of Applications in Technology," The 1978 Freeman Scholar Lecture, *J. Fluids Engr.*, Vol. 101, pp. 5–28.

Gebhart, B., and Pera, L., 1971, "The Nature of Vertical Natural Convection Flows Resulting From the Combined Buoyancy Effects of Thermal and Mass Diffusion," *Int. J. Heat Mass Trans.*, Vol. 14, pp. 2025–2050.

Gershuni, G. Z., Zhukovitskii, E. M., and Tarunin, E. L., 1968, "Secondary Convective Motions in a Plane Vertical Fluid Layer," *Mechanics of Liquids and Gases*, Academy of Sciences, USSR, No. 5, pp. 56–62.

Gill, A. E., 1966, "The Boundary-Layer Regime for Convection in a Rectangular Cavity," *J. Fluid Mech.*, Vol. 26, Part 3, pp. 515–536.

Hantman, R. G., and Ostrach, S., 1969, "Natural Convection Inside a Horizontal Circular Cylinder," Case Western Reserve University, Cleveland, OH, FTAS/TR-69-36.

Hart, J. E., 1983, "Low Prandtl Number Convection Between Differentially Heated End Walls," *Int. J. Heat Mass Trans.*, Vol. 26, No. 7, pp. 1069–1074.

Hellums, J. D., and Churchill, S. W., 1962, "Transient and Steady-State, Free and Natural Convection, Numerical Solutions: Part II—The Region Inside a Horizontal Cylinder," *AIChE J.*, Vol. 8, pp. 692–695.

Hoogendoorn, C. J., 1986, "Natural Convection in Enclosures," *Proc. Eighth International Heat Transfer Conference*, San Francisco, Vol. 1, Hemisphere Publishing Corp., Washington, DC, pp. 111–120.

Jiang, H. D., Ostrach, S., and Kamotani, Y., 1988, "Thermosolutal Convection With Opposed Buoyancy Forces in Shallow Enclosures," Case Western Reserve University, Cleveland, OH, FTAS/TR-87-192.

Johnson, R. S., 1978, "Transport From a Melting Vertical Ice Surface in Saline Water," M. S. Thesis, State University of New York at Buffalo.

Josberger, E. G., and Martin, S., 1981, "A Laboratory and Theoretical Study of the Boundary Layer Adjacent to a Vertical Melting Ice Wall in Salt Water," *J. Fluid Mech.*, Vol. 111, pp. 439–473.

Kamotani, Y., Wang, L. W., and Ostrach, S., 1983, "Experiments on Natural Convection Heat Transfer in Low Aspect Ratio Enclosures," *AIAA J.*, Vol. 21, pp. 290–294.

Kamotani, Y., Wang, L. W., Ostrach, S., and Jiang, H. D., 1985, "Experimental Study of Natural Convection in Shallow Enclosures With Horizontal Temperature and Concentration Gradients," *Int. J. Heat Mass Transfer*, Vol. 28, No. 1, pp. 165–173.

Kassemi, S. A., Ostrach, S., and Kamotani, Y., 1987, "Thermal and Double-Diffusive Convection Inside a Horizontal Cylinder," Case Western Reserve University, Cleveland, OH, FTAS/TR-87-191.

Kim, D. M., and Viskanta, R., 1984a, "Study of the Effects of Wall Conductance on Natural Convection in Differently Oriented Square Cavities," *J. Fluid Mech.*, Vol. 144, pp. 153–176.

Kim, D. M., and Viskanta, R., 1984b, "Effect of Wall Conduction and Radiation on Natural Convection in a Rectangular Cavity," *Num. Heat Trans.*, Vol. 7, pp. 449–470.

Kirkpatrick, A. T., and Bohn, M., 1986, "An Experimental Investigation of Mixed Cavity Natural Convection in the High Rayleigh Number Regime," *Int. J. Heat Mass Transfer*, Vol. 29, No. 1, pp. 69–82.

Klosse, K., and Ullersma, P., 1973, "Convection in Vapor Transport Process," *J. Crystal Growth*, Vol. 18, pp. 167–174.

Kuo, H. P., Korpela, S. A., Chait, A., and Marcus, P. S., 1986, "Stability of Natural Convection in a Shallow Cavity," *Proceedings of the Eighth International Heat Transfer Conference*, Hemisphere Publishing Corp., Washington, DC, pp. 1539–1544.

Lee, J., and Ostrach, S., 1982, "Prediction of Natural Convection Flow Patterns in Low Aspect Ratio Enclosures," Case Western Reserve University, Cleveland, OH, FTAS/TR 82-158.

LeFevre, E. J., 1956, "Laminar Free Convection From a Vertical Plane Surface," Ninth International Congress of Appl. Mech., Brussels, Belgium, Paper No. I-168.

Lewis, J. A., and Carrier, G. F., 1949, "Some Remarks on the Flat Plate Boundary Layer," *Quart. Appl. Math.*, Vol. 7, pp. 228–234.

Lewis, J. A., 1950, "Free Convection in Commercial Insulating Materials," Ph.D. Thesis, Graduate Division of Applied Mathematics, Brown University, Providence, RI.

Martini, W. R., and Churchill, S. W., 1960, "Natural Convection Inside a Horizontal Cylinder," *AIChE J.*, Vol. 6, pp. 251–257.

Nayfeh, A., 1973, *Perturbation Methods*, Wiley, New York, Chap. 6.

Newell, M. E., and Schmidt, F. W., 1970, "Heat Transfer by Laminar Natural Convection Within Rectangular Enclosures," ASME JOURNAL OF HEAT TRANSFER, Vol. 92, No. 1, pp. 159–168.

Ostrach, S., 1950, "A Boundary Layer Problem in the Theory of Free Convection," Ph.D. Thesis, Graduate Division of Applied Mathematics, Brown University, Providence, RI.

Ostrach, S., 1952, "An Analysis of Laminar Free-Convection Flow and Heat Transfer About a Flat Plate Parallel to the Direction of the Generating Body Force," NACA TN 2635.

Ostrach, S., 1952, "Laminar Natural-Convection Flow and Heat Transfer of Fluids With and Without Heat Sources in Channels With Constant Wall Temperatures," NACA TN 2863.

Ostrach, S., 1954, "Combined Natural- and Forced-Convection Laminar Flow and Heat Transfer of Fluids With and Without Heat Sources in Channels With Linearly Varying Wall Temperatures," NACA TN 3141.

Ostrach, S., 1955a, "Unstable Convection in Vertical Channels With Heating From Below, Including the Effects of Heat Sources and Frictional Heating," NACA TN 3458.

Ostrach, S., 1955b, "On the Flow, Heat Transfer, and Stability of Viscous Fluids Subject to Body Forces and Heated From Below in Vertical Channels," 50 Jahre Grenzschichtforschung, H. Goertler, ed., Vieweg, Braunschweig.

Ostrach, S., 1964, "Laminar Flows With Body Forces," *High Speed Aerodynamics and Jet Propulsion*, Vol. 4, Theory of Laminar Flows, F. K. Moore, ed., Princeton University Press, pp. 528–718.

Ostrach, S., 1966, "Role of Analysis in the Solution of Complex Physical Problems," *Proceedings of the Third International Heat Transfer Conference*, Chicago, IL, Vol. VI, pp. 31–43.

Ostrach, S., 1968, "Completely Confined Natural Convection," *Development in Mechanics*, Vol. 4, Proc. Tenth Midwestern Mechanics Conf., Johnson Publ. Co., Fort Collins, CO, pp. 53–81.

Ostrach, S., 1972, "Natural Convection in Enclosures," *Advances in Heat Transfer*, Vol. 8, Academic Press, New York, pp. 161–227.

Ostrach, S., 1980, "Natural Convection With Combined Driving Forces," *PCH PhysicoChemical Hydrodynamics*, Vol. 1, pp. 233–247.

Ostrach, S., 1982a, "Natural Convection Heat Transfer in Cavities and Cells," *Proceedings of Seventh International Heat Transfer Conference*, Munich, Vol. 1, Hemisphere Publishing Corp., Washington, DC, pp. 365–379.

Ostrach, S., 1982b, "Low-Gravity Fluid Flows," *Ann. Rev. Fluid Mech.*, Vol. 14, pp. 313–345.

Ostrach, S., and Hantman, R. G., 1981, "Natural Convection Inside a Horizontal Cylinder," *Chem. Engr. Comm.*, Vol. 9, pp. 213–243.

Ostrach, S., Jiang, H. D., and Kamotani, Y., 1987, "Thermosolutal Convection in Shallow Enclosures," *Proceedings of the 1987 ASME/JSME Thermal Engineering Joint Conference*, P. J. Marto and I. Tanasawa, eds., Vol. 2, pp. 159–168.

Ostrach, S., Loka, R. R., and Kumar, A., 1980, "Natural Convection in Low Aspect Ratio Rectangular Enclosures," *Natural Convection in Enclosures*, K. Torrance and I. Catton, eds., ASME HTD-Vol. 8.

Ostrach, S., and Menold, E. R., 1968, "Natural Convection in a Horizontal Cylinder," *Teplo- y Massoperenos*, A. V., Luikov and B. M. Smol'kovu, eds., Proc. Third All Union Conference on Heat and Mass Transfer, Minsk, BSSR, pp. 640–660.

Ostrach, S., and Raghavan, C., 1979, "Effects of Stabilizing Thermal Gradients on Natural Convection in Rectangular Enclosures," ASME JOURNAL OF HEAT TRANSFER, Vol. 101, pp. 238–243.

Ostroumov, G. A., 1952, "Free Convection Under Conditions of the Internal Problem," State Publishing House, Technio-Theoretical Literature, Moscow, Leningrad, (also available as NACA TM 1407, 1958).

Pillow, A. F., 1952, "The Free Convection Cell in Two Dimensions," Aeronautical Research Laboratory, Rept. A79.

Poots, G., 1958, "Heat Transfer by Laminar Free Convection in Enclosed Plane Layers," *Quart. J. Mech. Appl. Mech.*, Vol. II, pp. 257–273.

Sabzevari, A., and Ostrach, S., 1974, "Experimental Studies of Natural Convection in a Horizontal Cylinder," *Proceedings Fifth International Heat Transfer Conference*, Tokyo, Vol. III, pp. 100–104.

Schmidt, R. J., and Saunders, O. A., 1938, "On the Motion of a Fluid Heated From Below," *Proc. Royal Soc. Lodon*, Series A, Vol. 165, pp. 215–228.

Shiralkar, G. S., and Tien, C. L., 1982, "A Numerical Study of the Effect of a Vertical Temperature Difference Imposed on a Horizontal Enclosure, " *Num. Heat Trans.*, Vol. 5, pp. 185–197.

Solan, A., and Ostrach, S., 1979, "Convection Effects in Crystal Growth by Closed-Tube Vapor Transport," *Preparation and Properties of Soild State Materials*, Vol. 4, W. Wilcox, ed., Marcell Dekker, Inc., New York.

Sparrow, E. M., and Gregg, J., 1958, "'Low Prandtl Number Free Convection," *Z. Angew. Math. Phys.*, Vol. 9, pp. 383–387.

Sparrow, E. M., and Gregg, J. L., 1959, "'Details of Exact Low Prandtl Number Boundary-Layer Solutions for Forced and Free Convection," NASA Mem. 2-27-59E.

Sparrow, E. M., and Charmchi, M., 1983, "Natural Convection Experiments in an Enclosure Between Eccentric or Concentric Vertical Cylinders of Different Height and Diameter," *Int. J. Heat Mass Transfer*, Vol. 26, No. 1, pp. 133–143.

Sparrow, E. M., and Prakash, C., 1981, "Interaction Between Internal Natural Convection in an Enclosure and an External Natural Convection Boundary-Layer Flow," *Int. J. Heat Mass Transfer*, Vol. 24, No. 5, pp. 895–907.

Sparrow, E. M., and Samie, F., 1982, "Interaction Between a Stream Which

Downloaded 16 Dec 2010 to 193.140.21.150. Redistribution subject to ASME license or copyright; see http://www.asme.org/terms/Terms_Use.cfm

Passes Through an Enclosure and Natural Convection Within the Enclosure," *Int. J. Heat Mass Transfer*, Vol. 25, No. 10, pp. 1489–1502.

Sparrow, E. M., Stryker, P. C., and Ansari, M. A., 1984, "Natural Convection in Enclosures With Off-Center Innerbodies," *Int. J. Heat Mass Transfer*, Vol. 27, No. 1, pp. 49–56.

Sun, J.-H., and Zhang, X., 1986, "An Experimental Study of the Natural Convection Within the Horizontal Cylindrical Annular Enclosures," *Proceedings of the Eighth International Heat Transfer Conference*, Vol. 4, Hemisphere Publishing Corp., Washington, DC, pp. 1569–1574.

Turner, J. S., 1974, "Double-Diffusive Phenomena," *Ann. Rev. Fluid Mech.*, Vol. 6, pp. 37–56.

Van Dyke, M., 1964, *Perturbation Methods in Fluid Mechanics*, Academic Press, New York.

Viskanta, R., Kim, D. M., and Gau, C., 1986, "Three-Dimensional Natural Convection Heat Transfer of a Liquid Metal in a Cavity," *Int. J. Heat Mass Transfer*, Vol. 29, No. 3, pp. 475–485.

Weinbaum, S., 1964, "Natural Convection in a Horizontal Cylinder," *J. Fluid Mech.*, Vol. 18, p. 409.

Wilkes, J. O., 1963, "The Finite Difference Computation of Natural Convection in an Enclosed Rectangular Cavity," Ph.D. Thesis, University of Michigan, Ann Arbor, MI.

Yang, K. T., 1986, "Numerical Modeling of Natural Convection-Radiation Interactions in Enclosures," *Proceedings of the Eighth International Heat Transfer Conference*, Vol. 1, Hemisphere Publishing Corp., Washington, DC, pp. 131–140.

Zhukovitskii, E. M., "On Thermal Convection in an Infinite Cylinder," *Soviet Journal of Technical Physics*, Vol. 22, p. 832.

Downloaded 16 Dec 2010 to 193.140.21.150. Redistribution subject to ASME license or copyright; see http://www.asme.org/terms/Terms_Use.cfm

Transitions and Bifurcations in Laminar Buoyant Flows in Confined Enclosures

K.T. Yang
Department of Aerospace and Mechanical Engineering, University of Notre Dame, Notre Dame, IN 46556
Fellow ASME

Recent advances in experimental and numerical studies of flow instability, bifurcation, and transition to turbulence for buoyant flow in three-dimensional rectangular enclosures heated from below and from the sides are reviewed, with emphasis on the physical causes of various instabilities and bifurcations as well as the observed and calculated routes to chaotic motions. Also discussed are the current successes and shortcomings of numerical simulations of experimental data and observations. Finally, unresolved critical issues and needs for future research are also addressed.

Introduction

Buoyancy-driven natural convection in confined enclosures has received much attention in recent years; this is motivated by several seemingly unrelated considerations. First there are many traditional and more recent application areas where basic data for buoyant enclosure flows are needed; these include building systems containing multilayered walls, double windows, and other air gaps in unventilated spaces; energy systems such as solar collectors, energy storage devices, furnaces, heat exchangers, and nuclear reactors; materials processing such as solidification phenomena and growing crystals; and large-scale geophysical and astrophysical phenomena and other natural convection processes in the natural environment such as spread of fire. Secondly, natural convection in enclosures represents one of the simplest multiple-scale coupled nonlinear fluid-flow problems, and provides a convenient vehicle for the development of new methods of analysis, either analytical or numerical. Finally, certain buoyant enclosure-flow problems for simple geometries and thermal boundary conditions have well-established base solutions for the velocity and temperature fields so that they can be utilized as a basis for studying experimentally and theoretically their instabilities and the subsequent flow bifurcations, leading eventually to the study of the onset of turbulence. While this turbulence may be atypical among all real turbulent-flow phenomena, such studies nevertheless provide us with a firm foundation and physical insight to our understanding of the complex laminar-to-turbulent flow transitions and also of turbulent flows in general.

The purpose of this paper is to present a review of some of the very exciting research findings of the recent past on flow instabilities, bifurcations, and routes to chaotic motion and turbulence within the framework of laminar buoyant flow in three-dimensional confined enclosures. Primarily because of space limitations, this review is centered on the simple geometry of rigid rectangular enclosures with differentially heated opposite walls and side walls adiabatic or perfectly conducting. Relative to the normal gravity vector, the enclosure may be heated from below or from the side, and the enclosure aspect ratios, Prandtl number of the fluid medium, and the temperatures of the heated and cooled walls are all arbitrarily prescribed. While the choice of the rectangular-enclosure geometry may seem to be too restrictive, it is, however, not really so in view of the fact that the physical mechanisms responsible for flow instabilities, bifurcations, and other transitions in this geometry are very similar, at least qualitatively, to those of other more complex enclosures. In the present review, emphasis will be placed on the physical conditions for the occurrence of various flow instabilities and bifurcations and how the physical parameter in the problem affects them, and also on the experimentally observed and calculated scenarios of successive bifurcations, which eventually lead to the onset of chaotic motions and turbulence. In particular, the overall heat transfer across the enclosure will not be emphasized, but will only be discussed if it is relevant to indications of flow transitions.

Since flow bifurcations and transitions are central to what is discussed in this paper, it is pertinent here to briefly define their meanings in the context of the problem under consideration. The buoyant enclosure problem represents a dissipative dynamic system that contains a control or forcing parameter, the Rayleigh number Ra. At a specific value of Ra, the system is well defined and known, and the corresponding motions settle down eventually to a temporal asymptotic state, which may be stationery or periodic. When the parameter Ra is changed to another prescribed value, the asymptotic state may also change to a different flow structure. Such a change of flow structure is known as flow bifurcation and a bifurcation point is one at which such a change of flow structure takes place. Usually, a series of bifurcations corresponding to a sequence of increasing Ra can be considered as flow transition. An example here is the transition to turbulence as represented by a series of flow bifurcations occurring in a heated-from-below rectangular enclosure containing a fluid with a given Prandtl number Pr, when Ra is increased quasi-statically. According to these definitions, therefore, there is no transition point, since transition always takes place over a range of the control parameter, with the exception that the transition consists of only one bifurcation. Other more detailed flow characteristics, which are also important in describing the physical dynamic system in the enclosure, will be introduced and defined in the next section.

In the following sections, the basic buoyant enclosure-flow problem is first formulated and the various physical parameters identified and discussed. This is then followed by a general discussion of the possible bifurcated states and transitions to chaotic motion and turbulence. The specific enclosure problems with heated-from-below and heated-from-the-side conditions, as well as those for tilted enclosure, are then described separately in terms of our current understanding for each. Finally, unresolved critical issues and needs for future research are delineated. At the outset, as will become clear from the present review, our current knowledge of the transition processes of the buoyant enclosure-flow phenomena is still incomplete, despite our ability to predict and essentially

Contributed by the Heat Transfer Division for publication in the JOURNAL OF HEAT TRANSFER. Manuscript received by the Heat Transfer Division February 3, 1988. Keywords: Enclosure Flows, Flow Instability, Flow Transition, Reviews.

Copyright © 1988 by ASME
Downloaded 16 Dec 2010 to 193.140.21.150. Redistribution subject to ASME license or copyright; see http://www.asme.org/terms/Terms_Use.cfm

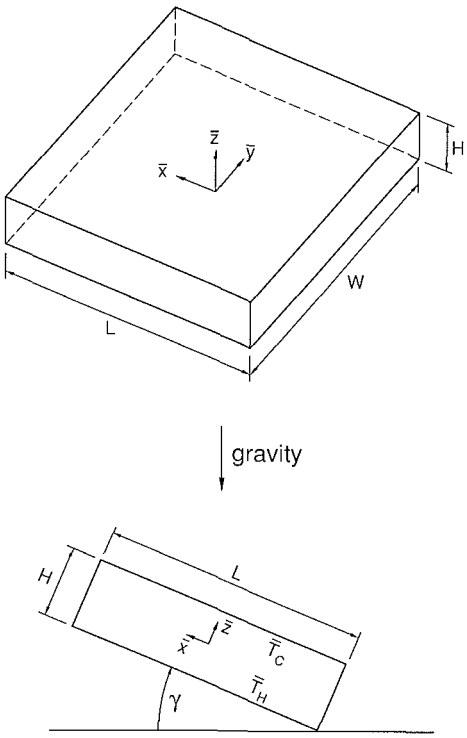

Fig. 1 Confined rectangular enclosure geometry

understand several of the bifurcations that have been observed in the experiments. Furthermore, our inability to determine the specific route or transition to turbulence under a given set of conditions is deeply rooted in the unpredictability characteristics of deterministic chaos of dynamic systems.

Problem Statement, Parameters, and Bifurcation States

A generic three-dimensional rectangular enclosure is shown in Fig. 1. The coordinates are fixed at the center of the enclosure and the geometry is described by two aspect ratios: $A_x = L/H$ and $A_y = W/H$. Surfaces $z = -H/2$ and $z = +H/2$ are differentially heated and maintained at constant temperatures T_H and T_C, respectively, with $T_H > T_C$. The other four walls are either adiabatic or perfectly conducting. The single tilt angle γ is the angle that the hot wall makes with the horizontal. When $\gamma = 0$ deg, the enclosure is in the heated-from-below condition, and the density gradient is parallel, but opposite to gravity. The linear conduction and zero motion situations prevail and are stable until a critical Ra, a bifurcation point, is exceeded for the onset of convection. For $\gamma = 180$ deg, the enclosure is heated from the top, and is thus stable thermally. When the density gradient is normal to the gravity from side-wall heating, i.e., $\gamma = 90$ deg, convective motion commences immediately, and the enclosure is generally referred to as a vertical enclosure. This motion may become unstable beyond another critical Ra, thus also undergoing a bifurcation. All these phenomena and other bifurcations including the onset of turbulence can be described by the following set of dimensionless equations under the usual assumptions of a Boussinesq fluid and negligible viscous dissipation and pressure work:

$$\nabla \cdot \mathbf{V} = 0 \tag{1}$$

$$\frac{1}{\mathrm{Pr}} \frac{\partial \mathbf{V}}{\partial t} + \mathbf{V} \cdot \nabla \mathbf{V} = -\nabla p + \nabla^2 \mathbf{V} - \mathrm{Ra}\theta \frac{\mathbf{g}}{g} \tag{2}$$

Nomenclature

A_x = L/H
A_y = W/H
a = wave number
a_c = critical wave number
a_{lm}, b_{lm} = coefficients in base flow expansions
$\hat{a}_{lm}$, $\check{a}_{lm}$, $\hat{b}_{lm}$, $\check{b}_{lm}$, $\hat{c}_{lm}$, $\check{c}_{lm}$ = coefficients in expansions for the perturbations
B = characteristic spatial dimension of roll
b_n = subharmonic bifurcation points
CR = cross-roll instability
c_x, c_y = disturbance wave numbers
E = Eckhaus instability
f = frequencies
f_{lm}, g_{lm} = functions of z in base flow expansions
f_m, g_m = functions of z in expansions for the perturbations
Gr_c = critical Grashof number
g = gravitational acceleration
$\mathbf{g}$ = gravity vector with components in negative coordinate directions (Fig. 1)
H = height or distance between heated and cooled surfaces
KN = knot instability
k = thermal conductivity
$\mathbf{k}$ = unit vector in the z direction
L = length of enclosure (x direction)
L = phase-locking state
N = nonperiodic state
OS = oscillatory instability
$P(f)$ = power spectrum
p = pressure
Pr = Prandtl number
P_n = subharmonic bifurcations
QP_n = quasi-periodic state
Ra = Rayleigh number
Ra_c = critical Rayleigh number
S = stationary state
S = stratification parameter
SV = skewed varicose instability
T = temperature
t = time
u, v, w = velocity components
$\mathbf{V}$ = velocity vector
W = width of enclosure (y direction)
X, Y, Z = dependent variables in the Lorenz equations
x, y, z = coordinates
X_n^* = perturbations
ZZ = zig-zag instability
α = thermal diffusivity
β = coefficient of volumetric expansion
γ = single tilt angle
γ_c = critical tilt angle
δ, ϵ = vector operators defined in equation (8)
Θ = $\mathrm{Ra}\theta$
θ = dimensionless temperature excess over the conduction profile
λ_n = Lyapunov exponents
ν = kinematic viscosity
ϕ, ψ = base flow scalar functions
ϕ, ψ = perturbation functions of ϕ and ψ, respectively

Subscripts

H = heated surface
C = cooled surface

Superscript

$\bar{\ }$ = dimensional quantities

Downloaded 16 Dec 2010 to 193.140.21.150. Redistribution subject to ASME license or copyright; see http://www.asme.org/terms/Terms_Use.cfm

$$\frac{\partial \theta}{\partial t} + \mathbf{V} \cdot \nabla \theta = \mathbf{V} \cdot \mathbf{k} + \nabla^2 \theta \tag{3}$$

where $\mathbf{V}$ is the velocity vector having dimensionless velocity components (u, v, w) normalized with H and the diffusion time H^2/α as the length and time scales, respectively; θ is the dimensionless temperature excess over the linear temperature profile in the z direction for the pure conduction state normalized with the temperature difference ($\bar{T}_H - \bar{T}_C$); p and t are, respectively, the dimensionless pressure and time variable; $\mathbf{g}$ is the gravity vector; and $\mathbf{k}$ is the unit vector in the z direction. The quantity $\mathbf{g}/g$ also represents a unit vector with components of $(-\sin\gamma, 0, -\cos\gamma)$. The Rayleigh number Ra and the Prandtl number are defined by

$$\mathrm{Ra} = \frac{\beta g (\bar{T}_H - \bar{T}_C) H^3}{\alpha \nu} \tag{4}$$

$$\mathrm{Pr} = \frac{\nu}{\alpha} \tag{5}$$

respectively, where β is the coefficient of volumetric expansion, and ν is the kinematic viscosity. For the boundary conditions, the three velocity components vanish at all six walls, and so does θ for the perfectly conducting side-wall cases. For the adiabatic side-wall cases, θ is still zero at the hot and cold walls, but its normal gradients vanish at the other walls. The aspect ratios A_x and A_y are inherently present in these boundary conditions. Consequently, in addition to the control or forcing parameter Ra, flow transitions are also expected to be affected by the Prandtl number Pr, the aspect ratios A_x and A_y, the tilt angle γ, and the side-wall thermal boundary conditions. In fact the determination of these effects is one of the central issues in flow instability and bifurcation studies for buoyant enclosure flows.

In general, these same parameters and the initial conditions determine whether a given Ra is a critical Rayleigh number for bifurcation and also the nature of the bifurcated state. To facilitate the discussion of such bufurcations and also the transition or route to chaotic motion and turbulence, several concepts used in the theory of nonlinear dynamics are very helpful and important. One is the notion of an attractor, which is used to describe the temporal asymptotic behavior of a trajectory in the phase space, which corresponds to a flow bifurcation. The phase space is essentially a plot of the time derivative of a dynamic quantity versus the quantity itself with time as a parameter. For small changes in the initial conditions or when the starting trajectories are close to each other, the corresponding temporal asymptotic motions will remain essentially the same on an attractor, and the region of starting trajectories which all lead to the same attractor is known as the basin of the attractor. Such attractors can be classified as a stationary attraction (S), using the notation of Gollub and Benson (1980), which represents a stationary flow and is a fixed point in the phase space; a periodic time-dependent attractor (P) represented by a limit cycle; a quasi-periodic attractor (QP_n) represented by a torus; and a subharmonic bifurcation (P_n), sometimes known as period doubling bifurcations. All these attractors have specific signatures in their power spectra (e.g., for the velocity). Briefly, the power spectrum of the P attractor contains a single sharp peak and its harmonics; that of the QP_n attractor has two ($n = 2$) or three ($n = 3$) distinct or incommensurate frequencies, along with linear combinations of the basic frequencies; and the spectrum for P_n contains frequencies for which the period is twice ($n = 2$) or four times ($n = 4$) the original frequency. Sometimes the two frequencies in QP_2 can lock (phase locking) into a constant rational ratio and this may persist for a range of Ra, and can be denoted by L. Furthermore, there is another attractor known as intermittance (I), which results from the collision of a stable S and an unstable S (Pomeau and Manneville, 1980a).

In addition, when the power spectrum contains any broadband noise even with the presence of sharp peaks, the flow then is definitely nonperiodic (N), and this is known as a chaotic attractor or strange attractor. While there is some controversy as to whether this motion can be considered as turbulence, it certainly is at best weak turbulence in view of the relatively small magnitude of the Reynolds number involved (~ 100). One characteristic of the chaotic attractor is the extreme sensitivity of its dependence on the initial conditions, even though the resulting motion satisfies deterministic descriptions such as those in equations (1) to (3). Consequently, the motion in a chaotic attractor is also known as deterministic chaos and in general the predictability of such motions is all but impossible (Lighthill, 1986). In addition to the power spectra, the various attractors can also be quantitatively distinguished by the Lyapunov exponents λ_n, which can be numerically determined by (Haken, 1984)

$$\lambda_n = \lim_{t \to \infty} \sup \frac{\ln |x_n^*(t)|}{t} \tag{6}$$

The limit superior is referred to the largest value of λ_n and $x_n^*(t)$ is simply the perturbation of a dynamic quantity such as a velocity component or temperature around the attractor. The exponent λ_n in a dynamic system is the growth rate of the perturbation given by $\exp(\lambda_n t)$. For a three-dimensional system, $n = 1$, 2, and 3 and the Lyapunov exponents λ_1, λ_2, and λ_3 for the various attractors, for example, have the following characteristics: $S(-, -, -)$, $P(-, -, 0)$, $QP_2(-, 0, 0)$, and $N(+, 0, -)$, where $+$, $-$, and 0 in the parentheses refer to positive, negative, and zero exponents, respectively. Because of the importance of the Lyapunov exponents, especially in characterizing a strange and chaotic attractor, methods have been proposed for their determinations from a temporal sequence of experimental and numerical data (Wolf et al., 1985; Eckmann and Ruelle, 1985; Sano Sawada, 1985). One shortcoming of the use of the Lyapunov exponents is that they do not give any information about the geometric structure (topology) of the attractor. One way to characterize this structure is to determine the geometric fractal dimension of the dynamic system based on the phase-space plots from either the experimental or numerical data (Thompson and Stewart, 1986). For an example, Urata (1986), in a numerical study of a rectangular enclosure heated from below with $A_x = A_y = 2$ and $\mathrm{Pr} = 1$ at a $\mathrm{Ra} = 2 \times 10^4$, together with free boundaries and adiabatic side walls, has determined a fractal dimension of the chaotic attractor of 3.3 with two positive and one zero Lyapunov exponents. The integer part of the dimension denotes the least degree of freedom of the chaotic attractor (or turbulence), while the fractional part gives an indication of the disorder of the system. It is particularly interesting to note that the degree of freedom of the turbulence here is so low (low-dimensional chaos), despite the fact it is admittedly very weak turbulence. A similar indication has recently been given by Sreenivasan (1985) for the turbulent wake behind a circular cylinder with a number of degrees of freedom of the order of only 20 even at a Reynolds number of 7000.

While the attractors mentioned above have all been observed experimentally and obtained numerically, it is still not clear as to what conditions must prevail before a bifurcation to a specific attractor is achieved. In view of the fact that it is now known that the expected turbulence in confined buoyant flows has only a few degrees of freedom, it would then be reasonable to expect that the transition (or route) to turbulence would only involve a few bifurcations. Several scenarios for such transitions are known (Behringer, 1985; Oertel, 1985) and are briefly described in the following. It must, however, be said again that the turbulence referred to here is defined as motions involving only temporal nonperiodicity with some broadband noise and a case can be

Downloaded 16 Dec 2010 to 193.140.21.150. Redistribution subject to ASME license or copyright; see http://www.asme.org/terms/Terms_Use.cfm

made that such is not full turbulence in view of the lack of the corresponding spatial behaviors.

The simplest transition model is the classical one due to Landau with the stipulation that turbulence is the result of an infinite cascade of Hopf bifurcations, in each of which a new discrete frequency is added (in Landau and Lifshitz, 1982). According to this model, only quasi-periodic flows can result and all Lyapunov exponents are negative, and consequently there is no mechanism for generation of broadband noise. There is also the scenario involving a snap-through bifurcation represented by $S \rightarrow N$ (Joseph, 1976) within a very small range of Ra, even though within this small range there is possibility of several successive secondary stationary bifurcations (Ahlers and Behringer, 1978; Chang and Shirer, 1984). Then there is the Ruelle–Takens–Newhouse scenario (Ruelle et al., 1978), which may be represented by $S \rightarrow P \rightarrow QP_2 \rightarrow N$. Three Hopf bifurcations are needed and a chaotic attractor is present and sensitive to the initial conditions. The Feigenbaum sequence (Feigenbaum, 1979) is a scenario in which an infinite cascade of period doublings (subharmonic bifurcations) leads to turbulence. It may be represented by $S \rightarrow P \rightarrow P_2 \rightarrow P_4, \ldots$, but no broadband spectrum is possible. It is of interest to note that in the latter part of the cascade

$$\lim_{n \to \infty} \frac{b_n - b_{n-1}}{b_{n+1} - b_n} = 4.6642016\ldots \tag{7}$$

which is known as the Feigenbaum number and is universal. In the above equation b_n is the control parameter, or the Rayleigh number for the confined buoyant-flow problem. Also, the spectral peaks of the subsequent consecutive bifurcations are also in a universal ratio of about 6.574. Finally, there is the Pomeau–Manneville scenario (Pomeau and Manneville, 1980a), which involves flow intermittency (I), resulting from combinations of stable and unstable stationary attractors. Discussions on other possible scenarios for chaos are given by Oertel (1985) and Shirer and Wells (1986).

While some elements of the above scenarios, as will be described later, have indeed been observed experimentally and calculated numerically, the real phenomena of confined buoyant flows are considerably more complex, and there is no reason to suspect that no other scenarios exist. That this is the case becomes clear when we note that the nonlinearities in equations (1) to (3), which have theoretically infinite degrees of freedom, would suggest many different stationary or periodic states, which would then lead to many transitions to turbulence.

In the following sections, the individual physical situations of confined rectangular enclosures heated from below and heated from the side wall, which is tilted with the gravity vector, are discussed separately. Emphasis will be placed on the results from both experimental data and detailed numerical calculations in terms of instability, bifurcation, and transition (or route) to turbulence as affected by changes in the physical parameters. Also, we will note the close interplay between experiments and numerical simulations in advancing our understanding of the complex phenomena. Furthermore, there is a rich literature on the experimental techniques of LDV interferometry for instantaneous velocity measurements and differential interferometry and other optical systems for full-field density measurements as well as such numerical tools as the Galerkin methods, the spectral methods, and the finite-difference methods, which have all been used to address the confined buoyant-flow problem. It is beyond the scope of this review to describe them in any detail, and the readers are referred to individual papers for their descriptions.

Rectangular Enclosure Heated From Below

Rayleigh–Bénard convection deals with an infinite horizontal fluid layer contained between two isothermal surfaces heated from below; its linear stability analysis based on the set of governing equations (1)–(3) is now well documented (Chandrasekhar, 1961). The important result is that when the Rayleigh number Ra is below a minimum critical value Ra_c, there is no motion and the temperature field is that of pure conduction. The minimum critical Rayleigh number Ra_c is only a function of the boundary conditions, and specifically not a function of the Prandtl number Pr, except for the limiting Pr $\rightarrow$ 0 cases (Chao et al., 1982). For rigid upper and lower surfaces, the linear stability theory shows that $\mathrm{Ra}_c = 1707.76$ and the corresponding dimensionless wave number based on the layer thickness is $a_c = 3.117$. The stable convective mode is given by long rolls of almost square cross section. While the problem treated in this paper deals with confined rectangular enclosures, the infinite-layer Rayleigh–Bénard case is still of particular relevance for several important reasons. One is that fluid layers used in laboratory experiments must necessarily be of finite extent and enclosed, and consequently vertical side walls must be provided to form confined enclosures. A second reason is that the infinite-layer situation can be approached by utilizing large values of the two aspect ratios A_x and A_y. Finally, the infinite-layer results can conveniently be used as a reference to examine the all important effects of the aspect ratios on the flow instability, bifurcation, and transition to turbulence.

Several significant results of the infinite-layer Rayleigh–Bénard convection problem can be mentioned here. Both Ra_c and a_c from the linear stability theory have been essentially verified for a large range of Pr (Koschmieder, 1974; Catton, 1978), even though the planforms of the convection rolls appear to be in general somewhat irregular, contrary to the predictions. Several causes can be cited for such differences. The eigenvalue problem for the prediction of the onset of convection is a degenerate one and there are many possible solutions at Ra_c. It is also known that the roll planforms are very sensitive to defects such as nonuniformities in the boundary temperatures and geometric irregularities. Then there is the problem of the effect of the vertical side walls as mentioned previously. As it will become clear later, such irregular roll forms, if they persist into the supercritical Ra range, will have a profound effect on subsequent bifurcations and transition to turbulence. When the Rayleigh number crosses into the supercritical region, the admissibility of multiple convective roll planforms with different wave numbers in the nonlinear theories is contrary to the unique planforms found in the experiments, and the determination of an additional criterion for the wave number selection is one of the central issues of the nonlinear Rayleigh–Bénard convection problems. Various criteria have been recently proposed and reviewed by Catton (1985) and Catton and Buell (1986). Two- and three-dimensional finite-difference calculations based on the governing equations, which do not require an additional criterion for wave-number selection, have been carried out by Lipps and Somerville (1971) and Lipps (1976). Despite the reasonable agreement of the calculated wave number (Lipps, 1976) with that from the experiments of Willis et al. (1972), the accuracy of the calculations is still somewhat uncertain because of the use of aspect ratios that may not be sufficiently large to approximate infinite layers and the boundary conditions used at the side walls. Consequently, it seems that the wave-number selection issue is still not closed, despite some partial successes achieved so far (Catton and Buell, 1986). Another closely related issue is the variation of the preferred wave numbers with Ra in the near supercritical region. Experimental data have consistently shown that the wave number decreases as $\mathrm{Ra} > \mathrm{Ra}_c$ increases (Koschmieder, 1974; Faradieh and Tankin, 1974; Berge, 1980), and on the other hand several early theoretical studies all predict the opposite behavior (Koschmieder, 1982). However, according to more recent theories, the reduction in the wave number for increasing Ra,

Downloaded 16 Dec 2010 to 193.140.21.150. Redistribution subject to ASME license or copyright; see http://www.asme.org/terms/Terms_Use.cfm

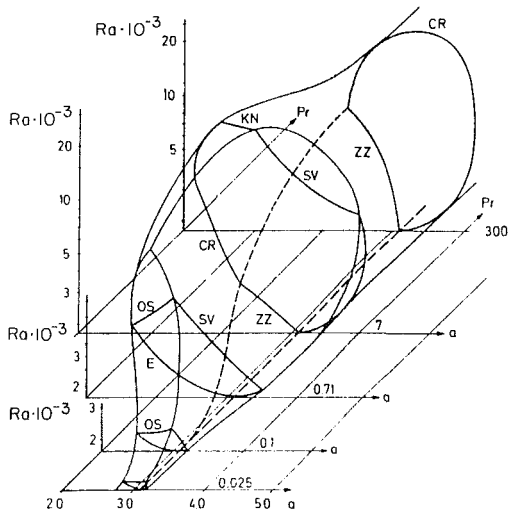

Fig. 2 Stability diagram of stable two-dimensional convection rolls in infinite layer (Busse, 1978)

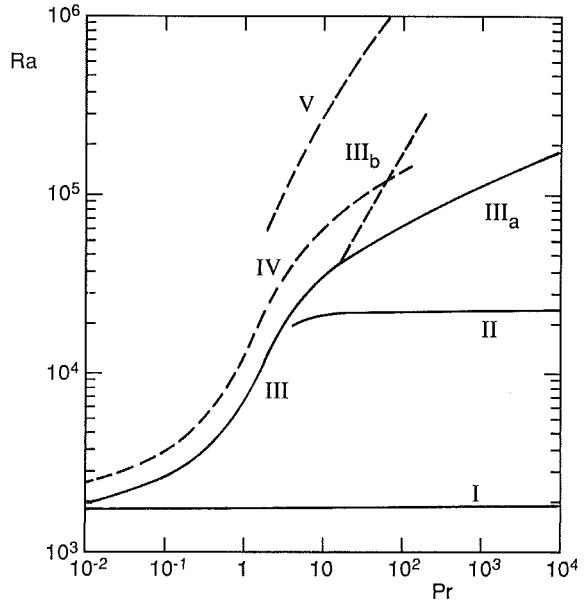

Fig. 3 Experimental observations for flow bifurcations in Rayleigh-Bénard convection: (I) onset of two-dimensional steady rolls, (II) three-dimensional convection, (III) time-dependent convection (a) in isolated spots, (b) uniformly throughout layer, (IV, V) turbulent convection (Busse, 1978)

sometimes referred to as the loss of convection rolls, is either caused by three-dimensional instabilities (skewed varicose instability) (Busse, 1978; Busse and Clever, 1979; Busse, 1982), or by the presence of the vertical side walls (Pomeau and Manneville, 1980b; Oertel, 1980; Cross et al., 1980).

Nonlinear analysis in the supercritical region is always difficult, if not impossible. Most early analytical studies deal with an Ra range only slightly higher than Ra_c so that perturbation analyses in terms of $(\mathrm{Ra}/\mathrm{Ra}_c^{-1})^{1/2}$ can be performed. However, linear stability analysis can still be utilized to reveal regions of various instabilities for $\mathrm{Ra} > \mathrm{Ra}_c$ if the base flow is taken to be that of the two-dimensional convection rolls (Busse, 1978; Busse and Clever, 1979; Busse, 1982). Here arbitrary three-dimensional disturbances are superimposed on the two-dimensional base flow, and the growth rates of such disturbances are examined to determine the limits of the various stable regions. It is, however, understood that such linear stability analyses cannot resolve the wave-number selection problem, and the wave numbers remain as parameters in the result. Briefly, for a Boussinesq fluid, the velocity vector $\mathbf{V}$ can be represented by a solenoidal vector field as

$$\mathbf{V} = \nabla \times (\nabla \times \mathbf{k}\phi) + \nabla \times \kappa\psi = \delta\phi + \epsilon\psi \tag{8}$$

where δ and ϵ are vector operators and ϕ and ψ are scalars. For the two-dimensional base flow, $\psi = 0$ and the unknowns in equations (2) and (3) may then be written in terms of the following orthogonal functions:

$$\phi = \sum_l \sum_m a_{lm} \cos(lax) f_{lm}(z) \tag{9}$$

$$\Theta = \mathrm{Ra}\theta = \sum_l \sum_m b_{lm} \cos(lax) g_{lm}(z) \tag{10}$$

where functions f_{lm} and g_{lm} satisfying the boundary conditions at $z = \pm 1/2$, i.e., $\phi = \partial\phi/\partial z = \Theta = 0$, have been given by Busse (1978) and Busse and Clever (1979). By using arbitrary three-dimensional infinitesimal disturbances $\tilde{\phi}$, $\tilde{\psi}$, and $\tilde{\Theta}$ of the following forms:

$$\phi = \sum_l \sum_m [\hat{a}_{lm} \cos(lax) + \check{a}_{lm} \sin(lax)] f_m(z) \exp[i(c_x x + c_y y) + \lambda t] \tag{11}$$

$$\tilde{\psi} = \sum_l \sum_m [\hat{c}_{lm} \cos(lax) + \check{c}_{lm} \sin(lax)] g_m(z) \exp[i(c_x x + c_y y) + \lambda t] \tag{12}$$

$$\tilde{\Theta} = \sum_l \sum_m [\hat{b}_{lm} \cos(lax) + \check{b}_{lm} \sin(lax)] g_m(z) \exp[i(c_x x + c_y y) + \lambda t] \tag{13}$$

where c_x and c_y are disturbance wave numbers and λ is the eigenvalue of the growth rate, the linear perturbation equations

$$\Delta_2(\nabla^4\tilde{\phi} - \tilde{\Theta}) = \mathrm{Pr}^{-1}\delta\cdot[\delta\phi\cdot\nabla(\delta\tilde{\phi} + \epsilon\tilde{\psi}) + (\delta\tilde{\phi} + \epsilon\tilde{\psi}) \cdot \nabla\delta\phi + \lambda\delta\tilde{\phi}] \tag{14}$$

$$\nabla^2\Delta_2\psi = \mathrm{Pr}^{-1}\epsilon\cdot[\delta\phi\cdot\nabla(\delta\tilde{\phi} + \epsilon\tilde{\psi}) + (\delta\tilde{\phi} + \epsilon\tilde{\psi})\cdot\nabla\delta\phi + \lambda\epsilon\tilde{\psi}] \tag{15}$$

$$\nabla^2\tilde{\Theta} - \Delta_2\tilde{\phi} = (\delta\tilde{\phi} + \epsilon\tilde{\psi})\cdot\nabla\Theta + \delta\phi\cdot\nabla\tilde{\Theta} + \lambda\tilde{\Theta} \tag{16}$$

can be solved as an eigenvalue problem, yielding $\lambda = \lambda$ (Ra, Pr, a, c_x, c_y). For given parameters of Ra, Pr, and a, the steady solution is unstable or stable depending on whether the maximum real part of λ is positive or not. The resulting stability diagram is shown in Fig. 2 in accordance with Busse (1978), which also shows a diversity of various instabilities given by the lettering symbols. The zig-zag instability (ZZ) refers to the steady bending of the rolls in a periodic manner and normally occurs at low wave numbers and moderate to high Prandtl numbers. The cross-roll instability (CR) refers to additional new rolls generated at right angles to the base rows, which eventually lead to bimodal convection (Yang et al., 1988). Eckhaus instability (E) usually occurs at small Pr and is a two-dimensional side-band phenomenon with $c_y = 0$. The oscillatory instability (OS) is the only temporally periodic instability found in the linear analysis and the oscillations represent translational waves traveling along the roll axis. The critical Ra for this instability increases strongly with Pr. The knot instability (KN) is also the result of cross roll instability as Ra increases and is characterized by a small value of c_y, resulting in a knotlike structure. Finally, the skewed varicose instability (SV) also occurs only at moderately high Prandtl numbers and is characterized by finite nonzero values of c_x and c_y. It is responsible for the increase in the wavelengths of the convection rolls with increasing Ra at the Prandtl number for air. The strong dependence of the instabilities on Pr based on the result of the linearized analysis shown in Fig. 2 agrees

Downloaded 16 Dec 2010 to 193.140.21.150. Redistribution subject to ASME license or copyright; see http://www.asme.org/terms/Terms_Use.cfm

well with earlier experimental observations as given in Fig. 3 (Krishnamurti, 1973; Busse, 1978), and this dependence is primarily due to the interplay of the advection terms in equations (2) and (3). It is of particular interest to note that despite the linearized nature of the stability analysis in the supercritical regions, many of the instabilities found in the analysis have also been found in experiments as well as in full numerical simulations based on equations (1) to (3), even at Ra levels well beyond the range where the analysis is expected to be valid. The more recent relevant simulation studies for the infinite-layer problem deal with three-dimensional bimodal convection (Frick et al., 1983), three-dimensional time-dependent oscillatory convection (Clever and Busse, 1987), and transition from periodic convection to chaotic motions (McLaughlin and Orszag, 1982).

Discussions of the supercritical Rayleigh–Bénard infinite-layer problem cannot be considered complete without mentioning the Lorenz model (Lorenz, 1963). Although it is not considered as a good model for the real problem, it is nevertheless rooted in Rayleigh–Bénard convection and also demonstrates that chaotic motion is possible with low dimensions. Consider the two-dimensional problem with a Boussinesq fluid and free–free boundaries. The stream function and departure of temperature from that for conduction can both be expanded in double Fourier series in x and z, which can then be substituted into the governing equations (2) and (3), resulting in, after rearranging, an infinite system of ordinary differential equations in time. If the series is truncated to include only three terms, the following Lorenz equations for the amplitudes of the Fourier components are obtained:

$$\frac{dX}{dt} = \mathrm{Pr}(Y - X) \tag{17}$$

$$\frac{dY}{dt} = -XZ + \left(\frac{\mathrm{Ra}}{\mathrm{Ra}_c}\right)X - Y \tag{18}$$

$$\frac{dZ}{dt} = XY - BZ \tag{19}$$

where X represents the intensity of the convective motion, Y the horizontal temperature gradient, and Z the vertical temperature gradient, Ra_c the minimum critical Rayleigh number according to the classical stability theory, and B the characteristic spatial dimension of the convection roll (B = 8/3 for the free–free boundary problem). These equations can be numerically integrated, and with B = 8/3 and Pr = 10, the results are shown in Fig. 4 for increasing values of $\mathrm{Ra}/\mathrm{Ra}_c$ (Oertel, 1985). At $\mathrm{Ra}/\mathrm{Ra}_c$ = 20, the solution represents a damped oscillation and is therefore a stationary point in the phase space (S). At $\mathrm{Ra}/\mathrm{Ra}_c$ = 23.5, there is a limit cycle representing temporal periodic oscillation (P). Intermittent periodic and nonperiodic oscillations set in at $\mathrm{Ra}/\mathrm{Ra}_c$ = 24.5, and finally at $\mathrm{Ra}/\mathrm{Ra}_c$ = 28, a chaotic attractor is present after a characteristic time. As pointed out by Oertel (1985), the chaotic solutions of the Lorenz equations are very sensitive to the initial conditions and no prediction can be made regarding which side the trajectory is likely to settle in (Lighthill, 1986). Despite the shortcomings of the Lorenz model for describing Rayleigh–Bénard convection, it is interesting to note that the simple model does produce bifurcations and transition to chaos that are common to the routes to turbulence found in the real phenomena, as will be seen later.

As already pointed out previously, the infinite-layer results are expected to be good approximations to those of confined enclosures of large aspect ratios, and vice versa. As the aspect ratios are reduced, the confined geometry starts to have its effect on the heated-from-below phenomena in a significant way. The thermal boundary conditions at the confining vertical walls are also expected to change the local conditions sufficiently to alter the instability and bifurcation characteristics. The Prandtl-number effects for the infinite-layer problem may also be affected by the presence of vertical side walls. All in all, the physical phenomena for the confined enclosure cases are certainly much more complex. Fortunately, the systematic advances made in recent studies on confined enclosures, especially in the heated-from-below situation, begin to shed some light on the detailed processes involved so that it is now possible to sort out the different physical effects.

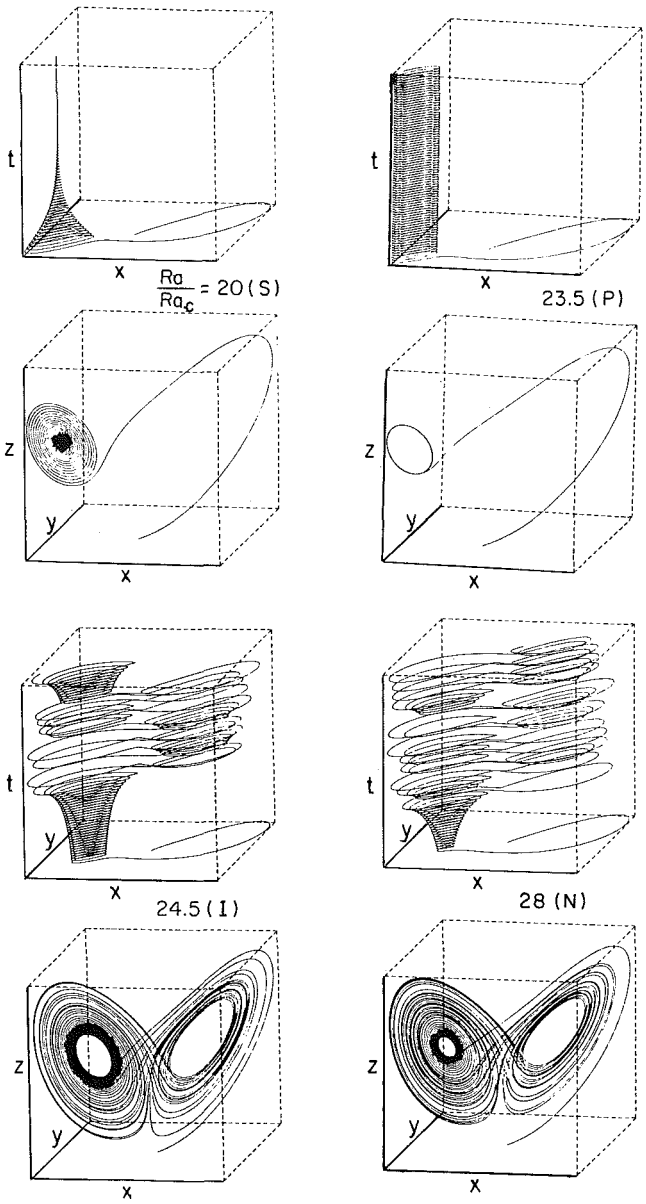

Fig. 4 Route to chaos for the Lorenz model (Oertel, 1985)

The first effect of the vertical side walls is on the minimum critical Rayleigh number Ra_c. In view of the increased drag by these side walls, Ra_c is expected to increase as compared to the infinite-layer case. The determination of Ra_c as a function of the aspect ratio is, however, no longer simple because the variables are no longer separable in the linear stability analysis for the onset of convection. Calculations have been made by the approximate Galerkin method for both adiabatic and perfectly conducting side walls (Davis, 1967; Catton, 1970). The results for the former case are shown in Fig. 5, and the corresponding experimental data, as shown by Müller (1982) lie somewhat below by only a few percentage points. More re-

Downloaded 16 Dec 2010 to 193.140.21.150. Redistribution subject to ASME license or copyright; see http://www.asme.org/terms/Terms_Use.cfm

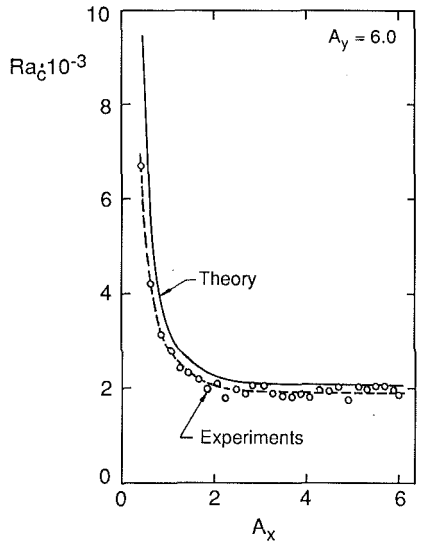

Fig. 5 Critical Rayleigh numbers for confined enclosures with adiabatic vertical walls and A_y = 6.0 (Muller, 1982)

cent calculations based on different base functions in the Galerkin method have produced even better agreement with the experimental data (Oertel, 1982). For narrow vertical gaps with $A_x < 1$, measurements of Ra_c have also been carried out for both thermal boundary conditions by Catton and Edwards (1967). The latest compilation of these values of Ra_c is given by Holland and Raithby (1985). As shown in Fig. 5, the increase in Ra_c with decreasing A_x is self-evident.

In the supercritical region, it is generally recognized that convection is always three dimensional, contrary to the infinite-layer case. Its influence on the basic two-dimensional rolls, however, depends on the aspect ratio, Pr, and also the thermal boundary conditions on the vertical walls. In general, for large and moderate-size enclosures equal to and greater than about $10(A_x) \times 4(A_y) \times 1$, the influence of the vertical wall only extends into the enclosure over one unit of gap size with a very slight modulation along the axis of other rolls in the enclosure middle (Oertel, 1982; Yang et al., 1986). For smaller enclosures, this influence becomes much more complex, especially for low-Pr fluids with different thermal boundary conditions (Kessler, 1987), as will be discussed later.

Mention has been previously made for infinite horizontal layers that the increase in the wavelengths of the two-dimensional rolls as Ra increases is continuous and it is related to the mechanism of skewed varicose instability (SV) analyzed by Busse (1978). In the case of confined enclosures, the change of wavelengths with Ra is discrete or in steps. The transition over a range of Ra involving such step changes in the number of rolls can be thought of as a series of bifurcations to stable stationary states. Sometimes this is known as the loss of rolls when Ra is increased. Most of the loss of rolls studies have been carried out with either air or N_2 with Pr = 0.71. In a small enclosure with a size of $4 \times 2 \times 1$, Kessler et al. (1984) have observed bifurcations from four rolls to three rolls at Ra = 24,000 and then to two rolls at Ra = 100,000, and the bifurcations are sharp (snap-through). In a more moderate enclosure of $10 \times 4 \times 1$ with N_2, Oertel (1980) has found nine rolls at Ra = 2,300, eight rolls at 5650, and seven rolls at 8900 before oscillations set in at Ra = 11,300. Leith (1987) has made measurements and observations in air in larger enclosures with $A_x \times 4 \times 1$ and A_x ranging from 8 to 12. For the largest enclosure $12 \times 4 \times 1$, the initial bifurcations from 12 to 11 and then to ten rolls are relatively simple and three-dimensional and all occur at the same end. However, the situation becomes very complex at the bifurcation (Ra = 11,000) from ten to nine rolls, which occurs at opposite ends of the enclosure, in a back and forward limit-cycle behavior. It is now clear that when the enclosure is small to moderate size, there exist only a few bifurcations up to relatively high Ra before oscillations occur. On the other hand, many bifurcations may occur for large aspect ratio enclosures, but only up to moderate Ra before oscillations set in. Hysteresis effects have also been observed in the enclosures of Leith (1987), but not in the large-width square enclosure of Willis et al. (1972). The loss roll phenomena are still not well understood, and may well have multiple causes. Among them are the skewed varicose instability, pinched wall ends, mismatch between natural roll and enclosure geometries, and other side-wall effects as postulated by Pomeau and Manneville (1980b) and Cross et al. (1980).

As already shown in Fig. 3, flow oscillations lie beyond the region of stable three-dimensional stationary flows, regardless of Prandtl number, and this has also been found the case in confined enclosures. In accordance with Busse (1982), these oscillations represent translational waves traveling along the axes of the rolls. However, when vertical side walls are present in the case of small aspect ratios, the outer rolls oscillate both spatially and temporally, while the middle rolls remain stationary, but oscillate. The situation with a large-aspect-ratio enclosure is much more complex. There is a complex three-dimensional reorientation of the rolls, resulting in a variety of oscillation modes (Oertel, 1982).

It is also of interest to mention that the aspect ratios also have an effect on the transition to chaotic motions. For moderate and large aspect ratios ($A_x > 4$ or 5), there is a bifurcation from the stationary state (S) to an oscillation state (P) with an almost immediate appearance of chaos. Ahlers and Behringer (1978) have provided such an example in which the bifurcation occurs at $Ra = 1.1\ Ra_c$. For small enclosures, many transitions to turbulence, as will be later seen, are possible and in general occur within a broad range of Ra.

In many theoretical studies of confined enclosures heated from below, both adiabatic and perfectly conducting vertical side walls are utilized. In the corresponding experimental studies, these conditions are very difficult to achieve, and consequently, it is always difficult to compare the theoretical results with those of the experiments because of possible mismatches in the boundary conditions. Efforts have been made to study the sensitivity of these boundary conditions on the instability and bifurcations in the supercritical region. In this regard, the three-dimensional numerical study of Kessler (1987) is particularly relevant, and treats a small enclosure $4 \times 2 \times 1$ with Pr = 0.71 and 7.0 by means of the Galerkin method, utilizing both thermal boundary conditions. Up to Ra beyond 30,000, convection is given by steady three-dimensional rolls. Results for Pr = 0.71 in the plane of symmetry ($y = 0$) are shown in Fig. 6(*a*) for the conducting walls and Fig. 6(*c*) for the adiabatic walls. Both of these figures show that the streamlines are not closed, but spiral out of the roll centers, and there is communication and mass exchange between the rolls. The streamlines that originate in the roll centers for the conducting wall case end up in the corner vortices, which are caused by additional buoyancy there. For the adiabatic wall case, the mass transfer is from the outer rolls to the central roll. The experimental light-sheet photograph in Fig. 6(*b*) (Jäger, 1982) corresponds directly to that of Fig. 6(*a*) and can be directly compared, and it is seen that the agreement is good, including the presence of corner vortices. The numerical results also show that the bifurcation point for oscillatory motion is at Ra = 33,200 ± 50 for conducting walls and 33,400 ± 50 for adiabatic walls, and these may be compared with the value of Jäger (1982) of 34,000, the value of Gollub et al. (1980) of 29,000 ± 1700 for an enclosure of $3.5 \times 2.1 \times 1$ and Pr = 2.5, and the value of Maurer and Libchaber (1980) of 23,500 for an enclosure of $3.5 \times 1.9 \times 1$ and

Downloaded 16 Dec 2010 to 193.140.21.150. Redistribution subject to ASME license or copyright; see http://www.asme.org/terms/Terms_Use.cfm

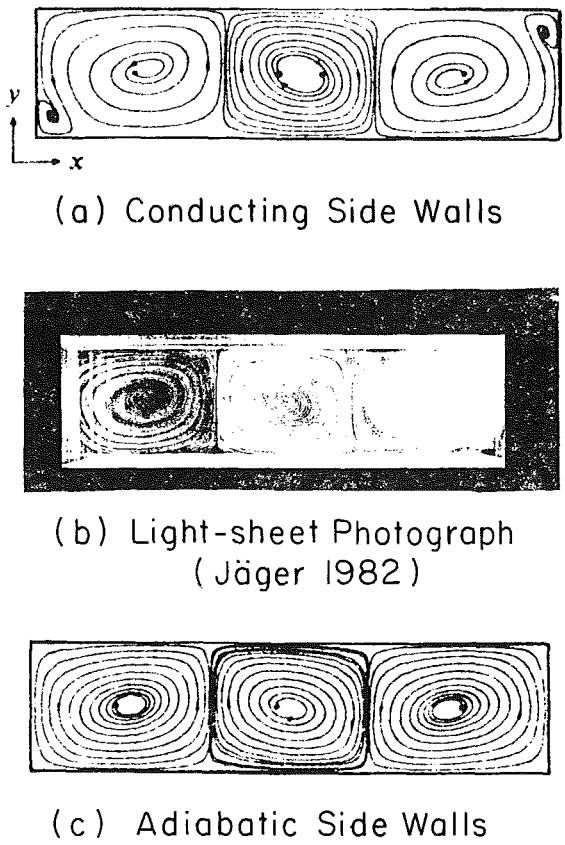

Fig. 6 Streamlines for steady convection at Ra = 30,000 and Pr = 0.71 in plane y = 0 (Kessler, 1987)

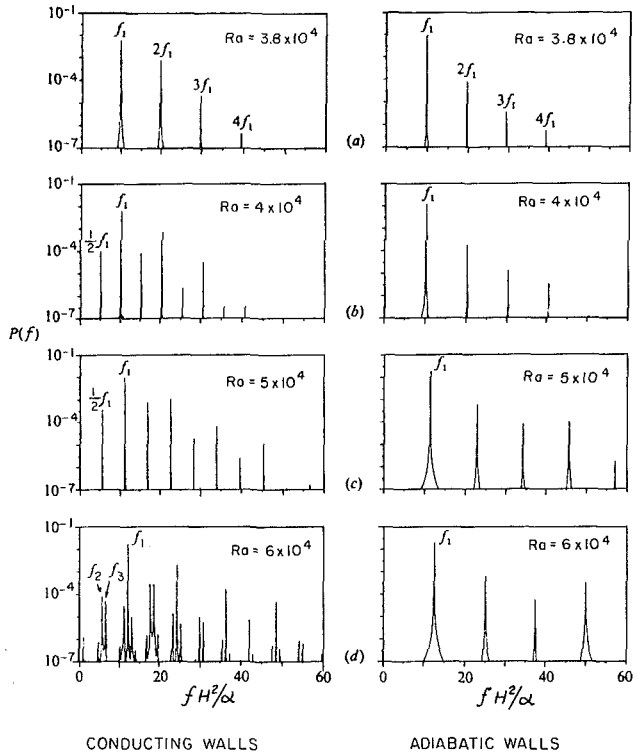

Fig. 7 Power spectra of θ (0.0, −0.4) for Pr = 0.71 (Kessler, 1987)

Pr = 0.71 for liquid helium. The last data were based on the more unstable configuration of two convection rolls initially. Even though the thermal boundary conditions do not seem to affect the bifurcation point for oscillatory motions, they do have profound effects on the subsequent bifurcations at higher Ra, again as demonstrated by Kessler (1987) in Fig. 7 for Pr = 0.71, which shows the power spectra for the temperature excess θ oscillations at a fixed location $(-0.4H, 0, 0)$. It is clearly seen that for adiabatic side walls the periodic oscillatory flow remains stable up to Ra = 60,000. However, the behaviors for conducting walls are very different. A subharmonic bifurcation (P_2) occurs just beyond Ra = 38,000 and it is stable until Ra = 56,000, at which the subharmonic peak splits into two new incommensurate frequencies, resulting in a quasi-periodic flow. Detailed analysis of the results show that the subharmonic bifurcation is very sensitive to the spatial structure of the time-dependent flow and is caused by the corner vortices. Similar conclusions on the importance of the spatial structure have been drawn by Gollub et al. (1980) and McLaughlin and Orzag (1982). For steady-steady bifurcations in the loss-of-rolls experiments of Leith (1987), there appear to be no significantly different effects of the two thermal boundary conditions. This perhaps can be expected in view of the A_x aspect ratios.

As noted previously, the Prandtl number exerts its influence through the advection terms in the momentum and energy equations. Physically, at low Pr inertia effects are more important, while at increased Pr, the thermal effects become more important. In the numerical study of Kessler (1987) for small aspect ratios, the three dimensionality of the flow for Pr = 7.0 is limited essentially to the wall regions, while the flow in the central region of the enclosure remains two dimensional. This is in contrast to the Pr = 0.71 case where the entire enclosure is affected by the three dimensionality. The Prandtl number also has an effect on the onset of oscillatory flows. At Pr = 7.0, the thermal instability becomes more important, and is the main cause of oscillations. This results in a higher bifurcation point for oscillations at 39,000 ± 100 for both boundary conditions, as compared to that for Pr = 0.71 of 33,200 ± 50 for the perfectly conducting wall case. Other Prandtl number effects are very similar to those for infinite layers, even though it is expected that the corresponding bifurcation points will be at higher Ra because of the presence of side walls, and those pertaining to the transition to turbulence will be discussed in the following section.

Even for fixed Pr, aspect ratios, and thermal boundary conditions at the side walls, the transition or route to turbulence as Ra is raised beyond the onset of convection is certainly not unique. Since the transition is known to be very sensitive to detailed spatial structure in the flow in the supercritical region, which in turn depends on the uncontrolled initial conditions and also affects the subsequent instabilities and bifurcations, it is impossible even to speculate as to how many such transitions are possible. Nevertheless, experiments and full numerical simulations have been carried out to follow and document specific transitions to turbulence. The documented experimental cases obviously represent possible routes and numerical simulations allow the examination of detailed numerical data for obtaining physical insight and exploring physical mechanisms. This combined effort has so far been reasonably successful in advancing our current knowledge. Unfortunately, the numerical simulations do not always correspond to possible real routes because of the shortcomings of the numerical techniques and computer resources (McLaughlin and Orszag, 1982). In the following, three documented series of possible transitions to turbulence at three levels of Pr, all obtained experimentally, will be described as illustrations, and these cases all deal with relatively small, confined (low-aspect-ratio) enclosures. It is known that for such small enclosures the transition to turbulence consists of just a few well-defined bifurcations.

Downloaded 16 Dec 2010 to 193.140.21.150. Redistribution subject to ASME license or copyright; see http://www.asme.org/terms/Terms_Use.cfm

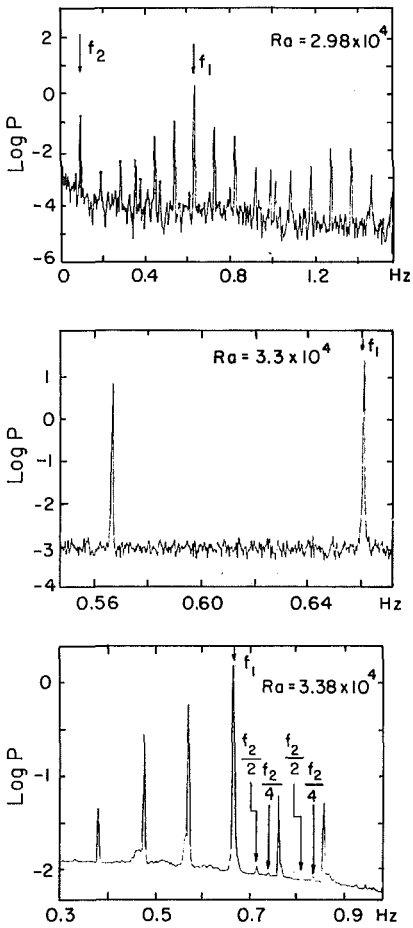

Fig. 8 Power spectra for 3.129 × 1.88 × 1 enclosure with liquid helium (Pr = 0.5) (Maurer and Libchaber, 1979)

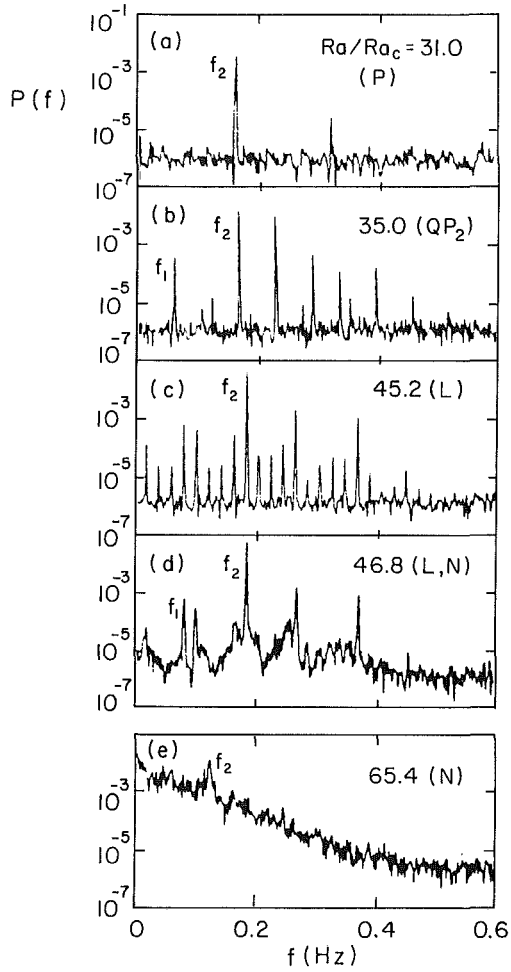

Fig. 9 Route to turbulence for a 3.51 × 2.08 × 1 enclosure with water (Pr = 5.0) and two convection rolls initially (Gollub and Benson, 1980)

The superfluid liquid helium ^{4}He is one of the preferred fluids for Rayleigh-Bénard convection studies (Behringer, 1985) in view of the fact that it is a liquid, but has a Prandtl number range of 0.1 to 0.8, overlapping that for gases, and also it has a high thermal conductivity so that flows can be monitored by thermal measurements. A relatively simple transition to turbulence is found in a 2.8 mm × 1.6 mm × 0.85 mm (3.29 × 1.88 × 1) enclosure with insulated side walls at Pr = 0.5 by Maurer and Libchaber (1979):

$$S_{\mathrm{Ra_{II}}} \rightarrow P_{\mathrm{Ra_{III}}} \rightarrow QP_{2_{\mathrm{Ra_{IV}}}} \rightarrow L_{\mathrm{Ra_V}} \rightarrow L_{\mathrm{Re_{VI}}} \rightarrow P_2,\ P_{4_{\mathrm{Ra_{VII}}}} \rightarrow N$$

The steady convection state S is represented by two rolls parallel to the short side of the enclosure and it is in a metastable state, since the wave number $a = 2\pi/A_x = 1.90$ is considerably less than that corresponding to the stable case. When the Rayleigh number is raised to $\mathrm{Ra_{II}} = 2 \times 10^4$, temperature oscillations at a frequency f_1 of about 0.55 Hz together with its harmonics are observed (P). These oscillations are consistent with the oscillatory instability (OS) described by Busse (1982) and represent translational waves along the roll axis. Another bifurcation at $\mathrm{Ra_{III}} = 2.7 \times 10^4$ produces a lower second frequency f_2 of about 0.09 together with linear combinations of the two frequencies (QP_2). This is followed by two phase-locking states (L), one starting at $\mathrm{Ra_{IV}} = 4.2 \times 10^4$ with $f_1/f_2 = 6.5$ and the other, at $\mathrm{Ra_V}$ with $f_1/f_2 = 7.0$. The second phase-locked state persists until $\mathrm{Ra_{VI}} = 3.38 \times 10^4$ where subharmonic bifurcations of f_2 occur (P_2, P_4). At slightly higher $\mathrm{Ra_{VII}} \geq 3.38 \times 10^4$, phase locking disappears and a nonperiodic or chaotic region is reached (N). It is also of interest to note that considerable hysteresis exists at the phase-locking states, particularly the second one with $f_1/f_2 = 7.0$. This transition to turbulence is depicted in Fig. 8 in terms of the power spectrum $P(f)$ of the temperature oscillations at a fixed point. A subsequent study (Maurer and Libchaber, 1980) utilizes three different enclosures with a = 1.8, 2.3, and 2.8 and variations of Pr between 0.4 and 0.8. The same transitions to turbulence are observed for the two lower wave-number cases for all Pr. However, for the case of a = 2.8 and Pr ≥ 0.59, another oscillation, which is believed to be caused by the three-dimensional skewed varicose instability of Busse (1982), precedes OS, and the subsequent bifurcations produce a third incommensurate frequency, locking among the three frequencies, and then turbulence, in a way similar to the Ruelle-Takens-Newhouse scenario described previously. In another similar enclosure with a = 2.7 and Pr = 0.62, also initially with two convection rolls, intermittency (I) has been observed before full turbulence sets in.

Based on LDV measurements in enclosures of 3.51 × 2.08 × 1 and 2.42 × 1.23 × 1 and two Prandtl numbers of 2.5 and 5.0 (water), Gollub and Benson (1980) have identified four different transitions to the onset of turbulence: $QP_2 \rightarrow L \rightarrow N$, $P_2 \rightarrow P_4 \rightarrow N$, $QP_3 \rightarrow N$, and $I \rightarrow N$. All these transitions start with a stationary state S, which bifurcates to a periodic attractor P. Gollub and Benson (1980) have found different mean flow states ranging from two stable symmetric rolls parallel to the short side of the enclosure to three rolls of somewhat irregular shapes, which are likely responsible for the variety of transitions observed. The first transition $QP_2 \rightarrow L \rightarrow N$ is for the enclosure 3.51 × 2.08 × 1 and Pr = 5.0 with initially two stable rolls, and the scenario, as demonstrated in

Downloaded 16 Dec 2010 to 193.140.21.150. Redistribution subject to ASME license or copyright; see http://www.asme.org/terms/Terms_Use.cfm

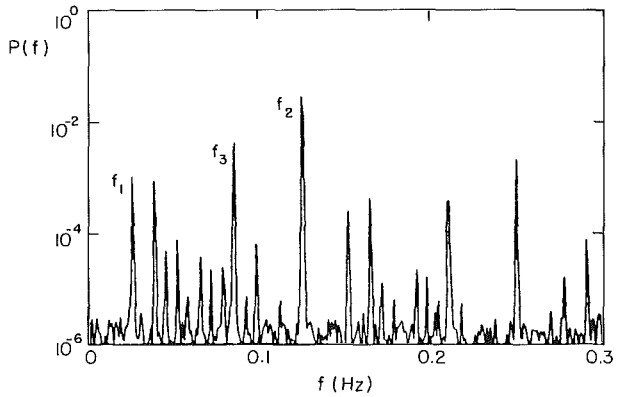

Fig. 10 Three incommensurate frequencies at Ra/Ra_c = 42.3 for a 3.51 × 2.08 × 1 enclosure with water (Pr = 5.0) and three convection rolls initially (Gollub and Benson, 1980)

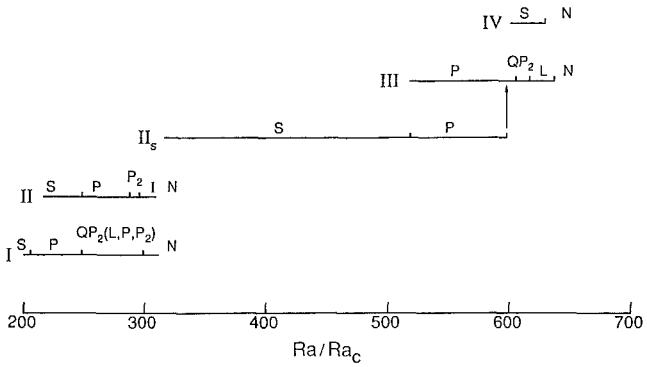

Fig. 11 Routes to turbulence for a 2 × 1.2 × 1 enclosure with silicone oil (Pr = 130) (Berge et al., 1982)

Fig. 9 at various bifurcation points of Ra/Ra_c in terms of the power spectra of the velocity, is similar to that previously described for liquid helium by Maurer and Libchaber (1979). Figure 9(*a*) shows a P state with a single peak and its harmonics at Ra/Ra_c = 31.0; Fig. 9(*b*) clearly gives a QP_2 state and several linear combinations of the base frequencies at Ra/Ra_c = 35.0; Fig. 9(*c*) is for Ra/Ra_c = 45.2, sharing a phase locking (L) at the integer ratio of f_2/f_1 = 9/4; Fig. 9(*d*) shows already a nonperiodic state (N) at Ra/Ra_c = 46.8, even though f_1 and f_2 are still noticeable; and finally Fig. 9(*e*) clearly shows featureless broadband noise. The second route of $P_2 \rightarrow P_4 \rightarrow N$ features period doubling in accordance with the Feigenbaum scenario (Feigenbaum, 1979), for the same enclosure but with Pr = 2.5 and two initial stable rolls. The onset for P for this case is at Ra/Ra_c = 17.0, as compared to 27.2 for the previous case because of the Prandtl number effect. The first period doubling (P_2) occurs at Ra/Ra_c = 21.5, and the second (P_4) at Ra/Ra_c = 26.5. The onset of N occurs at Ra/Ra_c = 28.0. The third route $QP_3 \rightarrow N$ is for the same enclosure with Pr = 5.0 and three rolls. Three incommensurate frequencies occur at Ra/Ra_c values of 30 for f_2, 39.5 for f_1, and 41.5 for f_3 and the power spectrum at Ra/Ra_c = 42.3 is shown in Fig. 10 with all three frequencies present and their linear combinations. The onset of broadband noise is at Ra/Ra_c = 43.0. This scenario very much reminds one of the Ruelle–Takens–Newhouse scenario for the route to turbulence described earlier. The final transition route to turbulence is by $I \rightarrow N$ found in the 2.42 × 1.23 × 1 enclosure with Pr = 5.0 and three rolls. The intermittencies are at irregular intervals between quasi-periodic and nonperiodic states, also similar to that found for liquid helium by Maurer and Libchaber (1980), even though in the latter case the Prandtl number is lower at 0.62 and the enclosure is 2.33 × 1.16 × 1 with two initial rolls.

The third and last example of routes to turbulence is that of Berge et al. (1982), who have observed transition in a small enclosure 2 × 1.2 × 1 with H = 2 cm filled with silicone oil at Pr = 130. The side walls are insulated. Here again, several spatial steady states have been obtained, namely, structures I (2 x rolls, 1 y roll), II (2 x rolls, 2 y rolls), III (3 x rolls, 2 y rolls), and IV (4 x rolls, 2 y rolls). These structures in slightly different enclosures have also been numerically simulated recently (Yang et al., 1988). Figure 11 gives a complete schematic diagram of the various routes to turbulence experimentally observed. It is noted that the structure II_s is the same as II except that the rolls are very symmetric with respect to the axis of the enclosure. Consequently, the roll convection is very stable and stationary for a broad range of Ra. After another range of Ra in which the flow is periodic, it bifurcates to a III or IV structure as indicated by the vertical arrows. For structure I, QP_2 (L, P, P_2) indicates that in this interval of Ra, L, P, and P_2 can also be observed in between the QP_2 states. One characteristic of the high-Prandtl-number fluid is that bifurcations occur at much higher Ra because of low inertia effects; this is consistent with the stability diagrams in Figs. 2 and 3.

One conclusion that can be drawn from the above examples is that at least for small enclosures the transitions or routes to turbulence involve relatively small numbers of bifurcations, regardless of the Prandtl number, and are very sensitive to the detailed spatial structure of the initial convection rolls, which in turn may depend on disturbances such as nonuniformities in geometry and boundary conditions, thermal history, and other experimental conditions, as well as on Rayleigh and Prandtl numbers. One difficulty with experimental measurements, regardless of the quality of the measurements, is that they are necessarily limited in terms of detailed information that may be needed to determine the various mechanisms for bifurcations and transitions to turbulence. On the other hand, numerical simulations based, for instance, on equations (1), (2), and (3) are capable of yielding such detailed information (e.g., McLaughlin and Orszag, 1982; Kessler, 1987). Unfortunately, numerical simulations still have shortcomings in terms of approximations due to limitations on computing resources and simulation of convection rolls as observed in experiments. However, there is a great deal of interplay going on between these two approaches, and the recent advances in the field would not have been successful without such cooperation of the researchers.

Before we turn our attention to confined vertical and tilted rectangular enclosures heated from the side, there is also another class of rectangular enclosures heated from below that deals with the Hele-Shaw cells (Müller, 1982; Yang et al., 1987; Buhler et al., 1987), and that also offers a rich variety of possible bifurcations as the corresponding Ra increases. The flow and temperature fields, however, are essentially two dimensional with $W \rightarrow 0$, and hence are not discussed here.

Vertical and Tilted Enclosures Heated From the Side

If the heated-from-below phenomenon is called a horizontal-layer problem with side walls, then the case for the single tilt angle γ = 90 deg is that of a vertical enclosure with heating from the side (Fig. 1). Here motion starts immediately for $Ra > 0$ in view of the fact that the gravity vector is perpendicular to the direction of density gradient. Recent reviews on vertical enclosures have been given by Catton (1978), Ostrach (1982), and Yang (1987). Instabilities also occur when Ra becomes sufficiently high. For other values of γ, a rich variety of flow patterns is possible due principally to the partitioning of inertia and gravity forces by the tilt angle, in addition to the usual parameters of Pr, A_x, A_y, Ra, and boundary conditions.

Downloaded 16 Dec 2010 to 193.140.21.150. Redistribution subject to ASME license or copyright; see http://www.asme.org/terms/Terms_Use.cfm

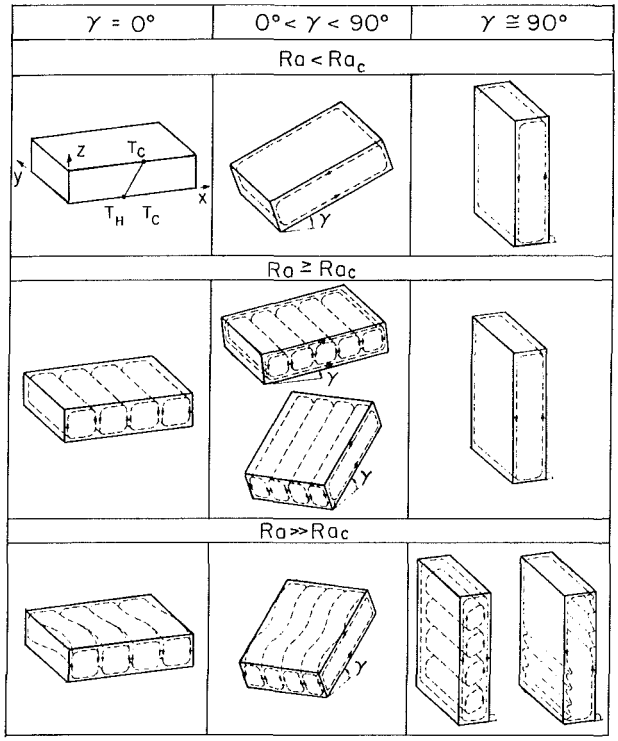

Fig. 12 Flow structure examples for tilted enclosures (Kirchartz et al., 1982)

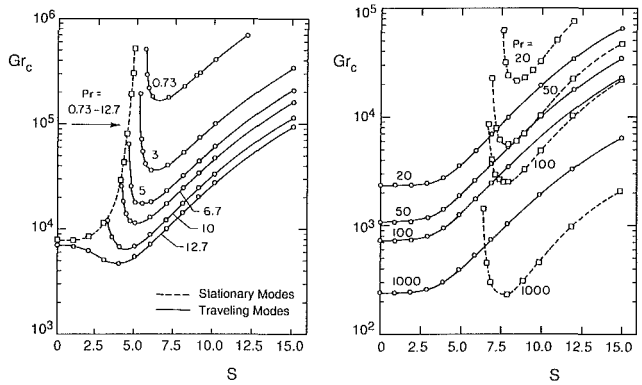

Fig. 13 Stability diagram for vertical enclosures with large aspect ratios (Bergholz, 1978)

Typical flow structures can be seen in Fig. 12 for $0 \leq \gamma \leq 90$ deg. Here for $\gamma \neq 0$, the critical Rayleigh number Ra_c is the first bifurcation point from a steady flow field. For $Ra \gg Ra_c$, the flow fields in general also become time-dependent and oscillatory, even though the mechanisms involved are different from those for $\gamma = 0$ deg. The flow behaviors for 90 deg $< \gamma <$ 180 deg are very similar to those at $\gamma = 90$ deg, while at $\gamma = 180$ deg the temperature field is stably stratified and there is no motion. These flow structures and the corresponding heat transfer across the enclosures have been reviewed by Catton (1978) and more recently by Yang (1987). Because the tilt angle γ partitions the driving forces relative to the gravity vector, it can also be viewed as a forcing parameter, in addition to Ra. Thus, bifurcations can also be expected to occur when γ is changed. Because of this complexity, it is not surprising that the corresponding bifurcation phenomena and transition to turbulence have not been studied as extensively as those for the heated-from-below cases, i.e., $\gamma = 0$ deg. In the following the cases for the vertical enclosures ($\gamma = 90$ deg) and other tilted enclosures are discussed separately.

Extensive observations of the flow structures for essentially two-dimensional vertical enclosures filled with water for a wide range of aspect ratios ($1 \leq A_x \leq 60$, A_y large) and insulated horizontal surfaces have been made by Elder (1965a, 1965b) and later analyzed by Ayyaswamy (see Catton, 1978). For Ra based on H less than 10^3, the flow is weak and of a unicellular structure as shown in Fig. 12; there is no vertical stratification. In the range $10^3 < Ra < 10^5$, the unicellular structure persists, but the flow and temperature fields are of the boundary layer type along the heated and cooled walls, and the core has weak circulation and is vertically stably stratified. Onset of secondary flow occurs at $Ra = 10^5$ and that of tertiary flow, at $Ra = 10^6$. At $Ra \sim 10^7$, boundary layers become unstable with growing traveling waves. In the central portion of the enclosure, the flow becomes turbulent at $Ra \sim 10^9$. Consequently, it is seen that hydrodynamic instability plays a much more important role in vertical enclosures.

Linear stability analyses are now known for both the conduction regime, where there is no vertical stratification, and the boundary-layer regime, for which stable stratification exists in the enclosure core. As pointed out in the recent review by Yener et al. (1985), the analyses can be greatly facilitated in the limit as $A_x \to \infty$ so that the base flow and temperature profiles are only functions of z, which can be obtained analytically, and also with the additional condition that the stable stratification in the core is taken to be linear and can be incorporated into the boundary conditions. A dimensionless stratification parameter S, defined by

$$S = \left[\frac{Ra}{4} \frac{|\partial \bar{T}/\partial x|}{(\bar{T}_H - \bar{T}_c)} \right]^{1/4} \tag{20}$$

must, however, be prescribed in the standard eigenvalue problem. The results show that there are two distinct instabilities in both regimes. One is in the form of stationary multicell secondary flow and has a hydrodynamic origin, while the other is in the form of traveling waves originating from the temperature perturbations. As shown in Fig. 13 for the critical Grashof number Gr_c, the boundaries of these two instabilities are complex functions of the stratification parameter S and the Prandtl number (Bergholz, 1978). For the conduction regime, $S = 0$, it is seen that for $Pr \leq 12.7$, the preferred instability is that of multicells and Gr_c is essentially independent of Pr. However, as Pr increases beyond 12.7, the instability is that of the traveling waves and Gr_c decreases due to increased thermal effects. In the boundary-layer regime ($S > 0$), the traveling-wave instabilities reappear as the preferred mode at higher values of S. Detailed two-dimensional finite-difference calculations based on equations (1), (2), and (3) have been made (see Yener et al., 1985), and most notably by Korpela et al. (1982) and Lee and Korpela (1983) for air in the range $10 < A_x < 40$. These numerical results, though not without uncertainties, can be utilized to assess the validity of the linear stability analysis as well as to provide basic information on the effect of large, but still finite aspect ratios. For an aspect ratio of $A_x = 20$, the calculations of Lee and Korpela (1983) show that the bifurcation to a multicell flow for air occurs in the range $10^4 < Gr_c < 1.1 \times 10^4$, which compares well with the experimental data of Hollands and Konicek (1973). In accordance with Fig. 13, the corresponding Gr_c for negligible S is 0.804×10^4, also confirming the validity of the linear stability theory. The slight discrepancy is due to the fact that S is not identically zero and A_x is large but still finite in the numerical case. Also, the lowest value of A_x under which multicell bifurcation does not take place is around 10 or 12.5, depending on the Prandtl number. This critical value becomes

Downloaded 16 Dec 2010 to 193.140.21.150. Redistribution subject to ASME license or copyright; see http://www.asme.org/terms/Terms_Use.cfm

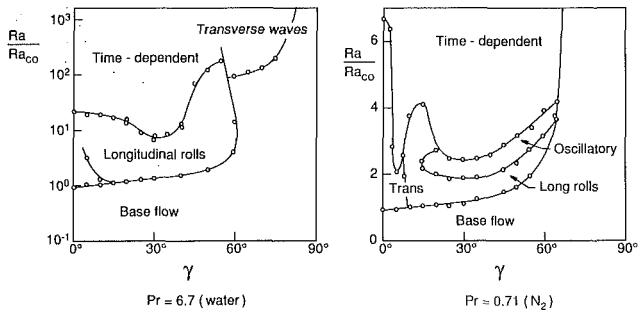

Fig. 14 Stability diagrams for a tilted enclosure (Kirchartz et al., 1982)

lower for decreasing Pr. The numerical solutions also show traveling waves at $A_x = 25$ with Gr increased from 2×10^4 to 4×10^4. For high Prandtl numbers Pr $\geq$ 20, the validity of the instability boundaries for traveling waves from the linear analysis is somewhat uncertain when compared to the numerical solutions even when the same S is used in the theory. At least for two-dimensional high-aspect-ratio vertical enclosures, the instabilities and their mechanisms have been identified and there is a basic agreement between the linear stability theory, full numerical solution, and experimental data. As observed in the experiments by Elder (1965a, 1965b), tertiary flows occur at Ra beyond the onset of multicell flows. This second bifurcation has not been heretofore studied. There is a high possibility that such bifurcations based on the three-dimensional disturbances can be analyzed by a stability analysis similar to that of Busse (1982) for the Rayleigh-Bénard problem. However, the condition of $A_x \to \infty$ must still be invoked. Linear stability analysis is difficult for vertical enclosures with finite aspect ratios primarily due to the difficulty of determining the base flows that account for the presence of horizontal surfaces. However, it is now known that for aspect ratios between unity and the critical aspect ratio mentioned previously, the base flow is essentially of unicellular structure and the critical Ra for the traveling-wave instability increases with the Prandtl number, but varies inversely with the aspect ratio. An experimental study has recently been carried out by LeQuere and Penot (1987) for an air-filled enclosure with aspect ratios given by $4 \times 4.67 \times 1$ that is differentially heated, together with a two-dimensional numerical simulation based on the governing equations for a Boussinesq fluid. The experimentally determined Ra_c for the traveling-wave instability is about 1.16×10^5, which lies between numerically obtained results for adiabatic and perfectly conducting boundary conditions at the horizontal surfaces, and is also consistent with the data of Hart (1971) for air. The results also show that at least two solutions can be found in the supercritical vicinity of the critical Rayleigh number, indicating different bifurcations. Transition routes to turbulence for vertical enclosures have not been studied so far. However, in view of the prominence of traveling-wave instabilities, some routes to turbulence are expected to be similar to those of external buoyant flow over vertical surfaces (Jaluria, 1986).

As pointed out previously, the single tilt angle γ can be interpreted as a second forcing parameter in addition to Ra, in view of the fact that it partitions the gravity into the usual thermal effect and a shear effect. This becomes clear when it is noted that a rich variety of steady flows is possible at a given Ra but with changing γ. Primarily depending on aspect ratios and the Prandtl number, such base flows may include unicellular flow, transverse and longitudinal rows (Fig. 12), and superimposed rolls in two perpendicular directions (Yang et al., 1988). Bifurcations may occur as a function of γ for fixed Ra, or as a function of Ra for a fixed tilt angle. Different bifurcations may also occur when both γ and Ra change. Good examples include the bifurcation at γ_c from traverse rolls to unicellular flow at a fixed Ra with increases of γ from zero with the corresponding presence of minimum heat transfer (Catton, 1978; Yang et al., 1986), and the bifurcation from transverse to longitudinal rolls when both Ra and γ increase from the critical point of the heated-from-below case (Kirchartz, 1980).

Very little is known regarding the instability characteristics of tiled three-dimensional enclosures. Sets of experimental data for water (Pr = 6.7) and N_2 (Pr = 0.71) in a $10 \times 4 \times 1$ enclosure have been provided by Kirchartz (1980) as shown in Fig. 14 (Kirchartz et al., 1982), where Ra_{co} is the critical Rayleigh number corresponding to the heated-from-below case. Base flow refers to the initial steady motion, which may either be transverse rolls for small γ, longitudinal rolls for larger γ, or unicellular flow for γ close to 90 deg. It is seen that for Pr = 6.7 in the region of small γ, thermal and buoyancy effects still dominate and the shear in the base flow has a destabilizing effect on the onset of three-dimensional time-dependent flow. The effect is reversed at larger tilt angles. At high Ra and γ close to 90 deg, the hydrodynamic traveling waves appear and represent the preferred instability mode in the region. The corresponding diagram for N_2 shows the Prandtl number effect, and the bifurcations appear at much lower Ra. These results agree well with those observed by Hart (1971). As also given by Hart (1971), the traveling-wave instability boundaries persist beyond $\gamma = 90$ deg and intersect with another longitudinal-roll instability curve in the region 90 deg $< \gamma <$ 180 deg at even higher Rayleigh numbers. This indicates that in this high γ region, where both thermal and hydrodynamic effects are small but comparable, the unicellular flow is very stable. As also indicated by Hart (1971), the instability boundaries for both traveling waves and longitudinal rolls in the region $\gamma < 60$ deg are shifted to high Ra for higher Pr due to reduced inertia effects. Routes-to-turbulence studies for tilted enclosures do not seem to have been undertaken in the recent literature.

Research Needs and Concluding Remarks

From the above discussions, it is now clear that our knowledge is much more advanced in the confined Rayleigh-Bénard problem than those for vertical and tilted enclosures. For the confined Rayleigh-Bénard problem, linear stability analysis for the infinite-layer problem provides several types of instability, which have also been observed in confined enclosures, even at Rayleigh numbers considerably higher than those that are considered valid in the linear analysis. Several sets of successive bifurcations, starting from a stationary state, and transitions to turbulence have been experimentally documented for small-aspect-ratio enclosures. Many of the bifurcations have been numerically simulated based on the governing equations to provide the corresponding physical mechanisms. Unfortunately, it is still not clear as to what exact conditions must prevail before specific bifurcations take place. What specific route to turbulence a given flow is likely to follow is very uncertain at this time. Different initial conditions and our inability to determine minor details of the spatial structure of the flow may be responsible. Therefore, there is a critical need for identifying and categorizing the initial conditions as well as the spatial structures of the flow. More new and refined experimental and numerical techniques are needed to get better and more accurate resolutions of the spatial and temporal flow details. It is absolutely essential to be able to avoid spurious results in the calculations and in this regard other numerical techniques than those prevailing, such as higher-order finite-difference methods, may prove to be viable alternatives. Routes to turbulence observed in experiments are physically possible routes, while those from the numerical solutions may not be.

Downloaded 16 Dec 2010 to 193.140.21.150. Redistribution subject to ASME license or copyright; see http://www.asme.org/terms/Terms_Use.cfm

Therefore, it is important to be able to simulate numerically the experimentally observed route, in hopes of discovering what is responsible for the successive bifurcations and the onset of chaotic motions. Thus, more well-documented cases from experiments are needed. The corresponding studies for vertical and tilted enclosures are very sketchy at best, and systematic studies, both experimental and numerical, are very much needed to identify the many routes to turbulence. The mere fact that for large aspect ratios the existence of multicell and traveling-wave instabilities may lead to very different subsequent bifurcations and routes is an indication of the complexities involved. In addition to the limited geometries and conditions considered in this paper, there are many more that are now at different stages of development and study. Good examples are cylindrical enclosures, enclosures subject to time-dependent heating, enclosures containing a porous medium, thermal boundary conditions other than adiabatic and perfectly conducting, more complex geometries and body-force fields, non-Boussinesq fluids, enclosures with internal heat sources, enclosures involving other interacting effects such as thermal radiation, melting, and solidification, electric and magnetic effects, thermocapillary effects, and many others. Since each of those areas is closely related to important applications, significant research is needed and should be pursued. Even more importantly, all this research is likely to provide us with further insight into turbulence.

Acknowledgments

The author wishes to acknowledge the support and help from his former students Drs. K. V. Liu, L. C. Chang, H. S. Kou, V. F. Nicolette, Z. Y. Zhong, and H. Q. Yang, who have been involved in confined buoyant flow studies under NSF grants at Notre Dame. He also would like to thank his colleagues, Professor M. Sen of the University of Notre Dame and Professor J. R. Lloyd of the Michigan State University, and his current student, Mr. Devadatta Mukutmoni for their discussions on flow bifurcation and routes to turbulence.

References

Ahlers, G., and Behringer, R. P., 1978, "The Rayleigh-Bénard Instability and the Evolution of Turbulence," *Supplement of the Progress of Theoretical Physics*, No. 64, pp. 186-201.

Behringer, R. P., 1985, "Rayleigh-Bénard Convection and Turbulence in Liquid Helium," *Review of Modern Physics*, Vol. 57, pp. 657-687.

Berge, P., 1980, "Systems Far From Equilibrium," *Lecture Notes in Physics 132*, Springer-Verlag, Berlin, pp. 381-394.

Berge, P., Dubois, M., and Croquette, V., 1982, "Approach to Rayleigh-Bénard Turbulent Convection in Different Geometries," in: *Convective Transport and Instability Phenomenon*, J. Zierep and H. Oertel, Jr., eds., G. Braun, Karlsruhe, pp. 123-148.

Bergholz, R. F., 1978, "Instability of Steady Natural Convection in a Vertical Fluid Layer," *Journal of Fluid Mechanics*, Vol. 84, pp. 743-768.

Buhler, L., Ehrhard, P., Gunther, C., Müller, U., and Zimmerman, G., 1987, "Natural Convection in Vertical Gaps Heated at the Lower Side—An Experimental and Numerical Study," in: *Bifurcation Phenomena in Thermal Processes and Convection*, H. Bau, L. A. Bertram, and S. A. Korpela, eds., ASME HTD-Vol. 94, pp. 67-74.

Busse, F. H., 1978, "Nonlinear Properties of Thermal Convection," *Reports on Progress in Physics*, Vol. 41, pp. 1929-1967.

Busse, F. H., 1982, "Transition to Turbulence in Thermal Convection," in: *Convective Transport and Instability Phenomena*, J. Zierep and H. Oertel, Jr., eds., G. Braun, Karlsruhe, pp. 149-170.

Busse, F. H., and Clever, R. M., 1979, "Instability of Convection Rolls in a Fluid of Moderate Prandtl Number," *Journal of Fluid Mechanics*, Vol. 91, pp. 319-335.

Catton, I., 1970, "Convection in a Closed Rectangular Region: The Onset of Motion," ASME JOURNAL OF HEAT TRANSFER, Vol. 92, pp. 186-187.

Catton, I., 1978, "Natural Convection in Enclosures," *Proceedings of 6th International Heat Transfer Conference*, Toronto, Vol. 2, pp. 13-31.

Catton, I., 1985, "Natural Convection in Horizontally Unbounded Plane Layers," in: *Natural Convection: Fundamentals and Applications*, S. Kakac, W. Aung, and R. Viskanta, eds., Hemisphere, Washington, DC, pp. 97-134.

Catton, I., and Buell, J. C., 1986, "The Wave Number at Supercritical Rayleigh Numbers," in: *Stability in Convection Flows*, W. S. Saric and A. A. Szewczyk, eds., ASME HTD-Vol. 54, pp. 17-29.

Catton, I., and Edwards, D. K., 1967, "Effects of Side Walls on Natural Convection Between Horizontal Plates Heated From Below," ASME JOURNAL OF HEAT TRANSFER, Vol.89, pp. 295-299.

Chandrasekhar, S., 1961, *Hydrodynamic and Hydromagnetic Stability*, Oxford University Press, Oxford.

Chang, H. R., and Shirer, X. X., 1984, "Transitions in Shallow Convections: An Explanation for Lateral Cell Expansion," *Journal of Atmospheric Sciences*, Vol. 41, pp. 2334-2346.

Chao, P., Churchill, S. W., and Ozoe, H., 1982, "The Dependence of the Critical Rayleigh Number on the Prandtl Number," in: *Convective Transport and Instability Phenomena*, J. Zierep and H. Oertel, Jr., eds., G. Braun, Karlsruhe, pp. 55-70.

Clever, R. M., and Busse, F. H., 1987, "Nonlinear Oscillatory Convection," *Journal of Fluid Mechanics*, Vol. 176, pp. 403-417.

Cross, M. C., and Danhiels, P. G., Hohenberg, P. C., and Siggia, E. D., 1980, "Effect of Sidewalls on Wavenumber Selection in Rayleigh-Bénard Convection," *Physical Review Letters*, Vol. 45, pp. 898-901.

Davis, S. H., 1967, "Convection in a Box: Linear Theory," *Journal of Fluid Mechanics*, Vol. 30, pp. 465-478.

Eckmann, J. P., and Ruelle, D., 1985, "Ergodic Theory of Chaos and Strange Attractors," *Review of Modern Physics*, Vol. 57, pp. 617-656.

Elder, J. W., 1965a, "Laminar Free Convection in a Vertical Slot," *Journal of Fluid Mechanics*, Vol. 23, pp. 77-98.

Elder, J. W., 1965b, "Turbulent Free Convection in a Vertical Slot," *Journal of Fluid Mechanics*, Vol. 23, pp. 99-111.

Faradieh, R., and Tankin, R. S., 1974, "Interferometric Study of Two-Dimensional Bénard Convection Cells," *Journal of Fluid Mechanics*, Vol. 66, pp. 739-751.

Feigenbaum, M. J., 1979, "The Onset Spectrum of Turbulence," *Physics Letters*, Vol. A74, pp. 375-378.

Frick, H., Busse, F. H., and Clever, R. M., 1983, "Steady Three-Dimensional Convection at High Prandtl Numbers," *Journal of Fluid Mechanics*, Vol. 127, pp. 141-153.

Gollub, J. P., and Benson, S. V., 1980, "Many Routes to Turbulent Convection," *Journal of Fluid Mechanics*, Vol. 100, pp. 449-470.

Gollub, J. P., Benson, S. V., and Steinman, 1980, "A Subharmonic Route to Turbulent Convection," *Annals New York Academy of Sciences*, Vol. 357, pp. 22-27.

Hakin, H., 1984, "Instability Hierarchies of Self Organizing Systems and Devices," in: *Advanced Synergetics*, Springer-Verlag, Berlin.

Hart, J., 1971, "Stability of the Flow in a Differentially Heated Inclined Box," *Journal of Fluid Mechanics*, Vol. 47, Pt. 3, pp. 547-476.

Hollands, K. G. T., and Konicek, L., 1973, "Experimental Study of the Stability of Differentially Heated Inclined Layers," *International Journal of Heat and Mass Transfer*, Vol. 16, pp. 1467-1476.

Jäger, W., 1982, "Oszillatorische und Turbulente Konvection," Dissertation, Universität Karlsruhe, West Germany.

Jaluria, Y., 1986, "Nonlinear Disturbance Growth and Transition in Natural Convection Flows," in: *Stability in Convective Flows*, W. S. Saric and A. A. Szewczyk, eds., ASME HTD-Vol. 54, pp. 1-9.

Joseph, D. D., 1976, *Stability of Fluid Motions I/II*, Springer-Verlag, Berlin.

Kessler, R., 1987, "Nonlinear Transition in Three-Dimensional Convection," *Journal of Fluid Mechanics*, Vol. 174, pp. 357-379.

Kessler, R., Dallman, U., and Oertel, H., 1984, "Nonlinear Transitions in Rayleigh-Bénard Convection," in: *Turbulence and Chaotic Phenomena in Fluids*, T. Tatsumi, ed., Elsevier, Amsterdam, pp. 173-178.

Kirchartz, K. R., 1980, "Zeitabhängige Zellularkonvektion in Horizontalen und Geneigten Behältern," Ph.D. Thesis, Universität Karlsruhe.

Kirchartz, K. R., Oertel, H., Jr., and Zierep, J., 1982, "Time-Dependent Convection," in: *Convective Transport and Instability Phenomena*, J. Zierep and H. Oertel, Jr., eds., G. Braun, Karlsruhe, pp. 101-122.

Korpela, S. A., Lee, Y., and Drummond, J. E., 1982, "Heat Transfer Through a Double Pane Window," ASME JOURNAL OF HEAT TRANSFER, Vol. 104, pp. 539-544.

Koschmieder, E. L., 1974, "Bénard Convection," *Advances in Chemical Physics*, Vol. 26, pp. 177-211.

Koschmieder, E. L., 1982, "Rayleigh-Bénard Convection and Taylor Vortex Flow," in: *Convective Transport and Instability Phenomena*, J. Zierep and H. Oertel, Jr., eds., G. Braun, Karlsruhe, pp. 39-54.

Krishnamurti, R., 1973, "Some Further Studies on the Transition to Turbulent Convection," *Journal of Fluid Mechanics*, Vol. 60, pp. 285-303.

Landau, L., and Lifshitz, E. M., 1982, *Fluid Mechanics*, Vol. 6, Course of Theoretical Physics, Pergamon Press, New York.

Lee, Y., and Korpela, S. A., 1983, "Multicellular Natural Convection in a Vertical Slot," *Journal of Fluid Mechanics*, Vol. 126, pp. 91-121.

LeQuere, D., and Penot, F., 1987, "Numerical and Experimental Investigation of the Transition to Unsteady Natural Convection of Air in a Vertical Differentially Heated Cavity," in: *Bifurcation Phenomena in Thermal Processes and Convection*, H. H. Bau, L. A. Bertram, and S. A. Korpela, eds., ASME HTD-Vol. 94, pp. 75-82.

Lighthill, J., 1986, "The Recently Recognized Failure of Predictability in Newtonian Dynamics," *Royal Society of London*, Vol. A407, pp. 35-50.

Lipps, F. B., 1976, "Numerical Simulation of Three-Dimensional Bénard Convection in Air," *Journal of Fluid Mechanics*, Vol. 75, Pt. 1, pp. 113-148.

Lipps, F. B., and Somerville, R. D. J., 1971, "Dynamics of Variable Wavelength in Finite Amplitude Bénard Convection," *Physics of Fluids*, Vol. 14, pp. 759-765.

Lorenz, E. N., 1963, "Deterministic Nonperiodic Flow," *Journal of Atmospheric Sciences*, Vol. 20, pp. 130-141.

Downloaded 16 Dec 2010 to 193.140.21.150. Redistribution subject to ASME license or copyright; see http://www.asme.org/terms/Terms_Use.cfm

Maurer, J., and Libchaber, A., 1980, "Effect of the Prandtl Number on the Onset of Turbulence in Liquid ^{4}He," *Journal of Physics Letters*, Vol. 41, pp. L515–L518.

Maurer, J., and Libchaber, A., 1979, "Rayleigh-Bénard Experiment in Liquid Helium: Frequency Locking and the Onset of Turbulence," *Journal of Physics Letters*, Vol. 40, pp. L419–L423.

McLaughlin, J. B., and Orszag, S. A., 1982, "Transition From Periodic to Chaotic Thermal Convection," *Journal of Fluid Mechanics*, Vol. 122, pp. 123–142.

Müller, U., 1982, "Bénard Convection Gaps and Cavities," in: *Convective Transport and Instability Phenomena*, J. Zierep and H. Oertel, Jr., eds., G. Braun, Karlsruhe, pp. 71–100.

Oertel, H., Jr., 1980, "Three-Dimensional Convection Within Rectangular Boxes," in: *Natural Convection in Enclosures*, K. E. Torrence and I. Catton, eds., ASME HTD-Vol. 8, pp. 11–16.

Oertel, H., Jr., 1982, "Thermal Instabilities," in: *Convective Transport and Instability Phenomena*, J. Zierep and H. Oertel, Jr., eds., G. Braun, Karlsruhe, pp. 3–24.

Oertel, H., Jr., "Nonlinear Dynamics, Temporal and Spatial Structures in Fluid Mechanics," in: *Nonlinear Dynamics of Transcritical Flows*, H. L. Jordan, H. Oertel, and K. Robert, eds., Springer-Verlag, Berlin, pp. 1–36.

Ostrach, S., 1982, "Natural Convection Heat Transfer in Cavities and Cells," *Proceedings of the 7th International Heat Transfer Conference*, Munich, Vol. XX, pp. 365–379.

Pomeau, Y., and Manneville, P., 1980a, "Intermittent Transition to Turbulence in Dissipative Dynamic Systems," *Communications of Mathematic Physics*, Vol. 74, pp. 189–197.

Pomeau, Y., and Manneville, P., 1980b, "Wavelength Selection in Cellular Flows," *Physical Letters*, Vol. 75A, pp. 296–298.

Raithby, G. D., and Hollands, K. G. T., "Natural Convection," in: *Handbook of Heat Transfer Fundamentals*, 2nd ed., W. M. Rohsenow, J. P. Hartnett, and E. N., Ganie, eds., McGraw-Hill, New York, Chap. 6, pp. 6-1 to 6-94.

Ruelle, D., Takens, F., and Newhouse, S. E., 1978, "Occurrence of Strange Axiom A Attractors Near Quasi Periodic Flows on T^m, $m \geq 3$," *Communications Mathematics Physics*, Vol. 64, pp. 35–40.

Sano, M., and Sawada, Y., 1985, "Measurement of the Lyapunov Spectrum From a Chaotic Time Series," *Physical Review Letters*, Vol. 55, p. 1082.

Shirer, H. N., and Wills, R., 1986, "Steady States: Keys to Classifying the Routes to Chaos," in: *Stability in Convective Flows*, W. S. Saric and A. A. Szewczyk, eds., ASME HTD-Vol. 54, pp. 11–16.

Sreenivasen, K. R., 1985, "Transition and Turbulence in Fluid Flows and Low-Dimensional Chaos," in: *Frontiers in Fluids Mechanics*, S. H. Davis and J. L. Lumley, eds., Springer-Verlag, Berlin, pp. 41–67.

Thompson, J. M. T., and Stewart, H. B., 1986, *Nonlinear Dynamics and Chaos*, Wiley, Chichester, United Kingdom.

Willis, G. E., Deardorff, J. W., and Somerville, R. C. J., 1972, "Roll-Diameter Dependence in Rayleigh Convection and Its Effect Upon the Heat Flux," *Journal of Fluid Mechanics*, Vol. 54, pp. 351–376.

Wolf, A., Swift, J. B., Swinney, H. L., and Vastano, J. A., 1985, "Determining Lyapunov Exponents From a Time Series," *Physica*, Vol. 16D, p. 285.

Urata, K., 1986, "Low Dimensional Chaos in Boussinesq Convection," *Fluid Dynamics Research*, Vol. 1, pp. 257–282.

Yang, H. Q., Yang, K. T., and Lloyd, J. R., 1986, "Flow Transition in Laminar Buoyant Flow in a Three-Dimensional Tilted Rectangular Enclosure," *Proceedings of 8th International Heat Transfer Conference*, San Francisco, Vol. 4, pp. 1495–1500.

Yang, K. T., 1987, "Natural Convection in Enclosures," in: *Handbook of Single-Phase Convective Heat Transfer*, S. Kakac, R. K. Shah, and W. Aung, eds., Wiley-Interscience, New York, Chap. 13, pp. 13-1 to 13-51.

Yang, H. Q., Yang, K. T., and Lloyd, J. R., 1987, "Laminar Natural-Convection Flow Transitions in Tilted Three-Dimensional Longitudinal Rectangular Enclosures," *International Journal of Heat and Mass Tranfer*, Vol. 3, pp. 1637–1644.

Yang, H. Q., Yang, K. T., and Lloyd, J. R., 1988, "Three-Dimensional Bimodal Flow Transitions in Tilted Enclosures," *International Journal of Heat and Fluid Flow*, Vol. 9, pp. 90–97.

Yener, Y., Kakac, S., and Maia, F. F., 1985, "Stability of Natural Convection in a Vertical Layer," in: *Natural Convection: Fundamentals and Applications*, S. Kakac, W. Aung, and R. Viskanta, eds., Hemisphere, Washington, DC, pp. 135–155.

Downloaded 16 Dec 2010 to 193.140.21.150. Redistribution subject to ASME license or copyright; see http://www.asme.org/terms/Terms_Use.cfm

Heat Transfer During Melting and Solidification of Metals

R. Viskanta
Heat Transfer Laboratory,
School of Mechanical Engineering,
Purdue University,
West Lafayette, IN 47907

Recent advances in the understanding of melting and solidification heat transfer in metals and alloys are discussed. Since heat transfer is generally the rate-determining process, the emphasis in the paper is on fundamental heat transfer processes during solid–liquid phase transformation and comparison between mathematical-numerical model predictions with experimental data. After a brief discussion of theoretical considerations, unidirectional and multidirectional melting and solidification processes are reviewed. The important role played by buoyancy-driven fluid flow is discussed and problem areas needing research attention are identified.

1 Introduction

Melting and solidification of metals is of particular interest in materials processing, metallurgy, purification of metals, growth of pure crystals from melts and solutions, solidification of castings and ingots, welding, electroslag melting, zone melting, and various other solidification technologies. Melting of ice and freezing of water are phase transformation processes that are familiar to everyone. However, there is little appreciation for the fact that the manufacture of almost every man-made object involves melting and solidification at some stage. Metals have been principal materials of man for about five millenia (5000 years since the bronze age and 3000 years since the iron age). It is, therefore, not surprising that a perusal of *Metals Abstracts* reveals an extremely large body of literature on metals processing, particularly on solidification of pure metals and alloys. Some important processes that involve solidification include casting (continuous, die, form, ingot, precision), rapid solidification processing, welding, soldering/brazing, and directional solidification (Bridgman, Czochralski, electroslag remelting, liquid metal cooling). Special conferences and symposia on casting and materials processing attest to the continuing and ever increasing interest in the field (Kou and Mehrabian, 1986; Fredericksson, 1986; Smith, 1987; Samanta et al., 1987).

Melting and solidification are phase transformation processes that are accompanied by either absorpotion or release of thermal energy. The essential and common features of systems undergoing solid–liquid (*s/l*) phase change (melting or solidification) are that a moving boundary exists that separates the two phases of differing thermophysical properties and at which thermal energy is absorbed or liberated. Melting and solidification are just two processes in an entire class of problems that are referred to as moving or free boundary problems. There is a very large body of literature concerned with a variety of such problems in applied sciences, geophysics, and engineering (Cryer, 1977; Tarzia, 1981/82).

The major problem in melting is to add, and in solidification to extract, the latent heat of the phase transformation in a controlled manner. In general, the latent and sensible heat of the system are added or removed by convection or radiation from the boundary. For example, during solidification of a casting or an ingot the superheat in the melt and the latent heat of fusion liberated at the *s/l* interface are transferred across the solidified metal, the metal–mold interface, and the mold (Fig. 1), encountering at each one of these steps a certain thermal resistance. As the metal solidifies it shrinks, an air gap may form, and the metal may oxidize. In addition, a lubricant may sometimes be used to facilitate removal of the solidified metal from the mold. The heat transfer processes occurring across such a complex mold–metal contact are complex and not well understood (Ho and Pehlke, 1985; Gozlan and Bamberger, 1987). The process of controlled heat addition and removal from a system undergoing phase transformation is an important issue and is beginning to receive fundamental research attention.

There is a close relationship between the mechanical behavior of polycrystalline metallic materials (i.e., castings, ingots, etc.) and their microstructural soundness, which, in turn, is affected by species distribution on the macroscopic and microscopic scales (Kurz and Fisher, 1984). For example, the mechanical strength of metallic alloys is directly connected to the grain size or dendrite arm spacing, the lamellar or fibrous spacing, the number and size of inclusions, and the crystallographic texture of microstructural matrices, in other words, the directionality or anisotropy of the solid material. Both the structural perfection and the microstructure of castings and ingots greatly depend on solidification parameters, such as the growth rate, temperature gradients at the *s/l* interface, and thermal undercooling. As expected, there is a close interaction between these parameters and heat transfer in the solid and the melt during solidification of metals and alloys. Heat transfer is very important as the cooling rates employed range from 10^{-5} to 10^{10} K/s and correspond to solidification systems extending from several meters to a few micrometers. These various cooling rates produce differing microstructures as well as metallurgical and mechanical properties.

The purpose of this paper is to review the significant role that heat transfer plays during melting and solidification of metals and alloys and to draw attention to the new developments in modeling the processes. The emphasis in the discussion is on the fundamental macroscopic transport processes in the solid and the melt that affect the *s/l* interface shape and motion and not on external heat exchange (see Fig.

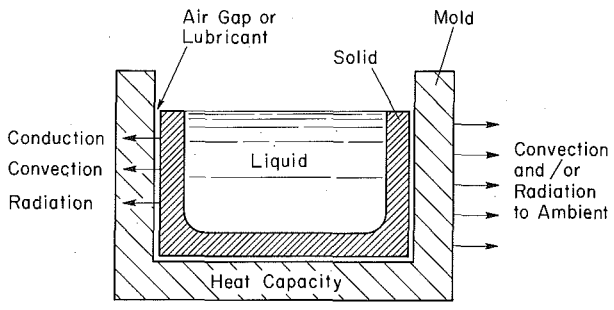

Fig. 1 Schematic representation of external heat exchange from a solidifying ingot

Contributed by the Heat Transfer Division for publication in the JOURNAL OF HEAT TRANSFER. Manuscript received by the Heat Transfer Division February 22, 1988. Keywords: Liquid Metals, Materials Processing and Manufacturing Processes, Moving Boundaries, Natural Convection, Phase-Change Phenomena.

Copyright © 1988 by ASME

Downloaded 16 Dec 2010 to 193.140.21.150. Redistribution subject to ASME license or copyright; see http://www.asme.org/terms/Terms_Use.cfm

1). Since the subject matter is very broad and encompasses thermodynamics, phase transformation kinetics, transport phenomena, and other related fields, a thorough review is not possible. The paper is not intended to be a definitive or even a critical review of this topic but is a guide to recent work in the area. The focus of the discussion is on macroscopic heat transfer phenomena during phase transformation, and there is no attempt to repeat several recent reviews (Viskanta, 1983; Cheung and Epstein, 1984; Viskanta, 1985; Fukusako and Seki, 1987). In these accounts the emphasis has been on ordinary materials (i.e., nonmetallic liquids and solids) undergoing *s/l* phase change. Experimental and theoretical details cannot be included, and no attempt is made to be complete as ample references to the original literature are included where further information may be obtained. In spite of the fact that forced convection effects (i.e., due to shear forces, rotational forces, magnetic and electric fields, etc.) are very important in materials processing and metallurgy (Minkoff, 1986; Gleave and Hawkins, 1987), they are intentionally omitted from this discussion, because they depend on the particular system considered. In this brief review, it is also not possible to discuss many other interesting topics such as rapid solidification and welding.

2 Theoretical Considerations: Pure Substances

The main mathematical difficulty in analyzing solid–liquid phase change heat transfer problems is caused by the motion of the solid–liquid interface, which makes the posed problem nonlinear. Since the position of the interface is not known *a priori* and its location must be determined by the solution of the problem, few exact solutions are available (Carslaw and Jaeger, 1959; Rubinsthein, 1971; Ozisik, 1980; Crank, 1984). One-dimensional problems are often solved approximately or numerically, while multidimensional problems usually require numerical solution techniques. Literally hundreds of papers have been written on melting and solidification, including applications. Reviews are available (Bankoff, 1964; Muehlbauer and Sunderland, 1965; Mori and Aoki, 1976; Ozisik, 1980; Viskanta, 1983; Cheung and Epstein, 1984; Fukusako and Seki, 1987) and will not be repeated here.

2.1 Mathematical Formulation of a Phase Change Problem. Two mathematical methods have been proposed and developed for convection/diffusion solid–liquid phase change problems, based on the choice of the dependent variable used in the energy conservation equation. In the more general classical method, the temperature is the sole dependent variable, and energy conservation equations are written separately for the solid and liquid regions (Carslaw and Jaeger, 1959). This is referred to as the temperature-based method. In the second formulation, the enthalpy is used as a dependent variable along with the temperature (Ozisik, 1980; Lewis and Roberts, 1987). This method is called the enthalpy method or sometimes the weak formulation. Details of the enthalpy method are given by a number of authors (see Voller et al., 1987; Lewis and Roberts, 1987 for an extensive list of references). Unfortunately, the method suffers from a number of deficiencies, which are detailed in the literature (Viskanta, 1983; Voller et al., 1987; Smith and Hoadley, 1987).

The set of differential equations for a temperature-based solid–liquid phase change heat transfer model has been formulated and will be presented here without derivation. The energy conservation equation for the solid phase is given by

$$\rho_s c_s \partial T_s/\partial t = \nabla \cdot (k_s \nabla T_s) + \dot{q}_s \tag{1}$$

and in the liquid phase by

$$\rho_l c_l (\partial T_l/\partial t + \mathbf{v} \cdot \nabla T_l) = \nabla \cdot (k_l \nabla T_l) + \dot{q}_l \tag{2}$$

Equation (2) clearly shows that heat flow in the melt is coupled to the flow field $\mathbf{v}$. This represents a potential source of difficulty, since the determination of the flow field will require simultaneous solution of the mass, momentum, energy, and possibly species conservation equations. Fortunately, in two special cases, which pertain to many practical problems, the velocity field need not be computed. In the first case, the influence of density change due to phase change is assumed to be negligible, and heat transfer in the liquid is assumed to be by conduction only, so that $\mathbf{v} = 0$. In the second case, the different densities of the liquid and the solid are accounted for, but the liquid is assumed to be at the fusion (melting) temperature. Hence, if freezing is induced by heat removal at the external boundary, the liquid remains at the fusion temperature T_m until it solidifies.

2.2 Interface Conditions. We consider the situation in which melting (or solidification) takes place at a definite melting (fusion) temperature T_m and, as a result, the solid and liquid phases are segregated by a sharp interface defined by the equation

$$F(x, y, z, t) = 0 \tag{3}$$

Nomenclature

A = aspect ratio $= H/L$
C = molar fraction
c = specific heat, J/kg K
Fo = Fourier number
G = temperature gradient, K/m
H = height, m
h = enthalpy, J/kg, or heat transfer coefficient, W/m^{2}K
h_i = heat transfer coefficient at metal/mold interface, W/m^{2}K
Δh_m = latent heat of fusion, J/kg
k = thermal conductivity, W/mK
L = width, m
l_c = characteristic length of melt region, m
$\overline{Nu_c}$ = Nusselt number $\bar{h} l_c/k$
$\mathbf{n}$ = unit vector normal to the interface
q = heat flux, W/m^2
Ra = Rayleigh number $= g\beta\Delta T l_c^3/\nu\alpha$
Ste = Stefan number $= c_l(T_w - T_m)/\Delta h_m$, for melting, and Stefan number for solidification $= c_s(T_m - T_w)/\Delta h_m$
T = temperature, K
T_o = surface temperature, K
t = time, s
x = horizontal coordinate, m
y = vertical coordinate, m
α = thermal diffusivity, m$^2/s$
δ = normalized interface position $= s(t)/H$
ρ = density, kg/m^3
τ = dimensionless time $=$ Fo $\times$ Ste

Subscripts

c = cold
E = equilibrium
h = hot
i = initial or interface
L = liquidus
l = liquid
M = melting point
o = boundary
S = solidus
s = solid
w = wall
Σ = interface

Downloaded 16 Dec 2010 to 193.140.21.150. Redistribution subject to ASME license or copyright; see http://www.asme.org/terms/Terms_Use.cfm

There are two fundamental relations that must be satisfied at such an interface. First, the temperature at the solid–liquid interface must be continuous

$$T_s(x, y, z, t) = T_l(x, y, z, t) = T_m \text{ at } F(x, y, z, t) = 0 \quad (4)$$

where T_s and T_l are the temperatures of the solid and liquid phases, respectively, and T_m is the melting temperature, which is constant for a pure substance. Second, an energy balance must be satisfied at the interface. In general the densities of the solid and liquid phases are not the same; therefore, some bulk motion of liquid resulting from the density difference is expected. Usually the solid density ρ_s is greater than the liquid density ρ_l (antimony, bismuth, and gallium are exceptions) at the melting point and, as a result, some liquid motion occurs. If $\rho_s > \rho_l$, then the material shrinks; if $\rho_s < \rho_l$, then the material expands upon solidification. If a material shrinks upon solidification, there is a net flow in the melt toward interface.

With the foregoing considerations, an energy balance across such a surface, Σ, can be expressed as (Ozisik, 1980)

$$(\rho_s h_s - \rho_l h_l)\ v_\Sigma + \rho_l h_l v_l = (k\partial T/\partial n)_s - (k\partial T/\partial n)_l \quad (5)$$

where v_Σ and v_l are the local velocities of the interface (normal to itself) and the liquid, respectively, and the subscripts s and l represent values on the solid and the liquid side of Σ, respectively.

The interfacial mass balance equation can be expressed as

$$(\rho_s - \rho_l)v_\Sigma + \rho_l v_l = 0 \quad (6)$$

This equation can be used to eliminate v_l from equation (3) to obtain the relation

$$\rho_s \Delta h_m v_\Sigma = (k\partial T/\partial n)_s - (k\partial T/\partial n)_l \quad (7)$$

where $\Delta h_m = h_l - h_s$ represents the latent heat of fusion of the material. Equation (7) is the interfacial energy balance equation employed in the conventional temperature-based models.

If the change in density due to phase transformation is to be included in the analysis, then the momentum equation for the liquid phase should include the velocity components normal to the interface as boundary conditions. A unique feature of solid–liquid phase change heat transfer problems is associated with the requirements of conservation of mass and energy at the moving solid–liquid interface. More general boundary conditions than those given above have been derived from the control volume forms of the conservation of mass and energy equations for the special case of phase change along a vertical wall (Lapadula and Miller, 1970).

2.3 System-Environment Heat Transfer. The heat addition (melting) or extraction (solidification) rates from the system control the process, and several models are available for simulating melt/environment and solid/environment heat exchange. Of these, the specification of constant boundary temperature and heat flux are the simplest, but may not be appropriate in real applications. The most realistic approach involves relating the heat flux on the side of the material to the heat transfer addition or removal rate. This can be expressed as

$$-(k\partial T/\partial n)_{s \text{ or } l} = q_o \quad (8)$$

For cases where the heat transfer rate to the environment q_o is by convection and radiation these rates can be related to the surface temperature at the boundary of the system T_o and the environment temperature T_e through appropriate phenomenological or empirical relations. Both T_o and T_e could possibly vary with time. In the case of solidification of castings and ingots, where the interface heat transfer between the solid and the mold is complex, probably the best compromise between mathematical simplicity and physical similitude is to define an effective thermal conductance of the solid–mold interface, which accounts for conductive, convective, and radiative heat exchange across the gap (Ho and Pehlke, 1985). This should be a fair representation of conductive and convective heat transfer, but radiative exchange is sensitive to absolute values of the temperatures involved. This exchange can, of course, be handled separately, although the complication arises that the experimental values of the interface thermal conductance actually include a radiative contribution.

2.4 Methods of Solution. Exact solutions of the problem are available for a few limiting cases (Carslaw and Jaeger, 1959; Rubinshtein, 1971; Ozisik, 1980), mostly in the absence of fluid motion in the melt. During the past decade, multidimensional phase change (melting and solidification) problems in which convection in the melt has been accounted for have been receiving increased research attention not only in the heat transfer (Viskanta, 1983, 1985; Fukusako and Seki, 1987) but also in the materials processing literature (Ridder et al., 1980; Bertram and Zanner, 1985; Ohnaka and Kobayashi, 1986). Reference is made to the above publications for more complete literature sources. Suffice it to mention that finite difference, finite element, and direct finite difference methods are being used to solve the model equations. In the absence of convection in the melt, heat transfer in the liquid is by conduction, and the problem reduces to one of diffusion in the solid and the melt. There is a very large body of literature dealing with exact, approximate, and numerical approaches. It is not possible to review them here, and reference is made to published accounts (Ozisik, 1980; Viskanta, 1983; Poirier and Salcudean, 1986; Fukusako and Seki, 1987).

2.5 An Example: Phase Change in the Absence of Convection in the Liquid. As a result of the nonlinearity of the equations introduced by the motion of the phase change boundary there are but a few exact solutions of problems concerned with melting and solidification (Carslaw and Jaeger, 1959; Ozisik, 1980). One such problem is the melting of a subcooled solid (Fig. 2*a*) or solidification of a superheating liquid (Fig. 2*b*) confined to a semi-infinite region. The solution was obtained some time ago and is known as Neumann's solution. For the case of temperature-independent thermophysical properties, the two problems are mathematically identical and for the sake of concreteness we consider solidification.

A liquid at a uniform temperature T_i that is higher than the melting temperature T_m of the solid is confined to the half-space $x > 0$. At time $t = 0$ the boundary surface at $x = 0$ is lowered to a temperature T_o below T_m and maintained at that temperature for time $t > 0$. As a result, solidification starts at the surface $x = 0$ and the solid–liquid interface moves in the positive x direction. This is referred to as a two-region problem because the temperatures are unknown in both the solid and liquid phases. This is a classical problem and the solution is well known in the literature (Carslaw and Jaeger, 1959; Ozisik, 1980).

Omitting the mathematical details, one can show that the temperature distributions in the solid and liquid phases are given by

$$\frac{T_s(x, t) - T_o}{T_m - T_o} = \frac{\text{erf}[x/2(\alpha_s t)^{1/2}]}{erf(\lambda)} \quad (9)$$

and

$$\frac{T_l(x, t) - T_o}{T_m - T_o} = \frac{\text{erfc}[x/2(\alpha_l t)^{1/2}]}{\text{erfc}(\lambda)} \quad (10)$$

The solid–liquid interface position is given by the equation

$$s(t) = 2\lambda(\alpha_s t)^{1/2} \quad (11)$$

The interface energy balance equation, i.e., equation (7), is used to find a relation for the evaluation of the parameter λ.

Downloaded 16 Dec 2010 to 193.140.21.150. Redistribution subject to ASME license or copyright; see http://www.asme.org/terms/Terms_Use.cfm

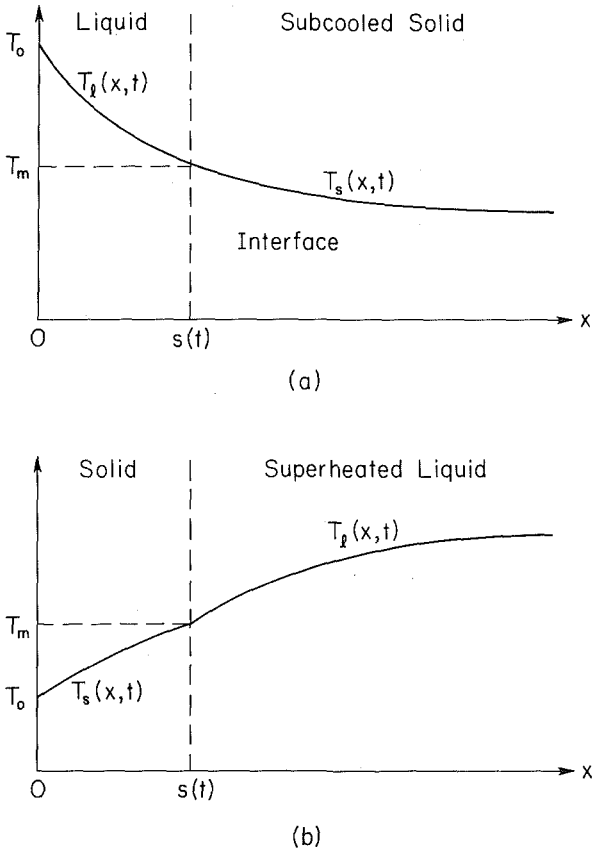

Fig. 2 Solid-liquid phase change in a semi-infinite region: (a) melting of a subcooled solid and (b) solidification of a superheated liquid

This yields a transcendental equation for λ,

$$\frac{\exp(-\lambda^2)}{\text{erf}(\lambda)} + (k_l/k_s)(\alpha_s/\alpha_l)^{1/2}\, S\, \frac{\exp(-\lambda\alpha_s/\alpha_l)}{\text{erfc}[\lambda(\alpha_s/\alpha_l)^{1/2}]} = \lambda\pi/\text{Ste}_s \tag{12}$$

where

$\text{Ste}_s = c_s(T_m - T_o)/\Delta h_m$ = Stefan number for solidification
$S = (T_i - T_m)/(T_o - T_m)$ = Superheating parameter

Once λ is known from the solution of equation (12), $s(t)$ is determined from equation (11), and the temperature in the solid and liquid phases from equations (9) and (10), respectively. Note that in general λ is a function of four parameters, $\lambda = f(\text{Ste}_s, S, \alpha_s/\alpha_l, k_s/k_l)$. Available experimental results have confirmed the validity of the Neumann solution for both ordinary substances (Hale and Viskanta, 1980) and metals (Gau and Viskanta, 1985a). It has been further verified that in the absence of superheating, the dimensionless time ($\tau = \text{Ste} \times \text{Fo}$) is the only parameter that controls the rate of formation of the new phase.

3 Melting

Melting is relevant to processing and purification of metals, nuclear reactor safety, and many other technologies. Heat transfer during melting is a rate determining process that needs to be understood for process assessment, design, and optimization (Minkoff, 1986). While the effects of natural convection during melting of ordinary (nonmetallic) materials has received considerable research attention (Viskanta, 1985), melting of metals has been studied relatively little. For example, buoyancy (temperature and composition) driven convection during melting of metal systems has not been studied and is not understood. In this section of the paper we discuss

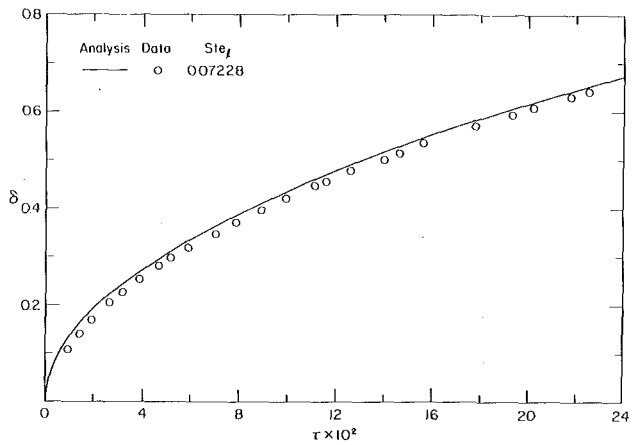

Fig. 3 Comparison of measured and predicted s/l interface position during melting of pure gallium from above (from Gau and Viskanta, 1985a)

transport processes that occur during melting of metals as well as mathematical modeling of heat transfer.

A number of important physical phenomena have been identified to take place during melting of pure metals and eutectics as well as metallic alloys. Pure metals and eutectics melt at a discrete temperature, and the local heat transfer rate normal to the *s/l* interface determines its motion and shape. It is well recognized that density differences between the solid and liquid phases and motion of the *s/l* interface can produce convective motion in the melt. The effect of thermal convection on the rate of melting, *s/l* interface shape, and morphology has been well recognized in the metallurgy and heat transfer literature (Cole, 1969; Kattamis, 1981; Clyne, 1984; Viskanta, 1985). Convective motion generated by surface temperature gradients and turbulence generated by buoyancy forces in the liquid have not been studied, but they are recognized as being important (Gleave and Hawkins, 1987). Experiments with pure gallium have shown that crystallographic effects caused by anisotropic heat conduction in the solid can produce a macroscopically nonplanar interface during melting from above and below (Gau and Viskanta, 1985a, 1986).

3.1 Unidirectional Melting. Melting of a pure metal from above is gravitationally stable, and the *s/l* interface is planar, except for the crystallographic effects (Gau and Viskanta, 1985a). The average interface position predicted by a conduction model using an average thermal conductivity of gallium (arithmetically averaged over the A, B, and C crystalline axes) has yielded good agreement between the experimental data and predictions (Fig. 3). Melting of a Lipowitz eutectic (Bi, 50 percent, Pb, 26.7 percent, Sn, 13.3 percent, and Cd, 10 percent) from above also yielded good agreement between predictions based on the Neumann model and experimental data (Gau and Viskanta, 1984). Thus, results obtained have confirmed the validity of the model for predicting the temperature distribution and heat transfer during melting of metals and alloys under stable conditions.

Melting of a pure metal from below, however, produces a gravitationally unstable situation with a development of natural convection shortly after a thin layer (1 to 2 mm) of melt has formed on the heated surface (Gau and Viskanta, 1984, 1985b). Natural convection develops as the melt layer thickness increases, and the flow undergoes transition from small Bénard-type hexagonal capped cells to semi-cylindrical capped rolls with their axes perpendicular to the short edge of the relatively small test cell. The *s/l* interface departs gradually from a macroscopically planar one to a hexagonal capped and finally to an irregular three-dimensional one as the melting

Downloaded 16 Dec 2010 to 193.140.21.150. Redistribution subject to ASME license or copyright; see http://www.asme.org/terms/Terms_Use.cfm

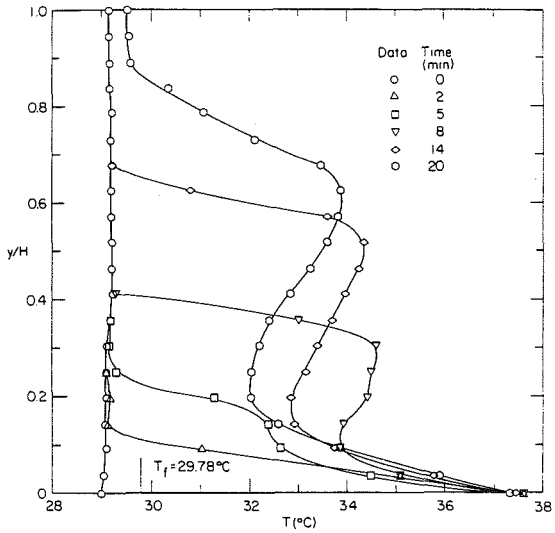

Fig. 4 Vertical temperature distribution at the center of the test cell during melting of pure gallium from below (from Gau and Viskanta, 1985b)

progresses. Superimposed on the *s/l* interface is a microstructure that is controlled by the crystallographic effects of gallium (Gau and Viskanta, 1985b). The measured interface position averaged over the cross-sectional area of the test cell (i.e., the instantaneous melt volume) is considerably higher than predicted on the basis of the Neumann model (Carslaw and Jaeger, 1959), particularly at late times. Improved agreement between measured and predicted melted volume can be obtained by accounting for convective heat transfer at the phase change boundary using steady-state heat transfer coefficient for natural convection in the absence of phase change (Gau and Viskanta, 1985b).

The local temperatures in the melt fluctuate as the interface advances and the flow structure changes from one pattern to another with time. Typical vertical temperature (time-averaged) distributions at the center of the test cell during melting of pure gallium from below are shown in Fig. 4. In the early stages of the process ($t=2$ min), the temperature increases almost linearly with the distance from the heated bottom of the test cell. The temperature distributions shown in the figure exhibit a very interesting feature. After natural convection has been established in the melt layer ($t \geq 8$ min), the temperature gradients in the melt near the heated bottom and below the interface remain high, but the gradients in the melt core are reversed. This difference in the temperature distribution suggests a change in the flow structure in the melt layer with time. Highly chaotic ("turbulent") natural convection was believed to have been initiated. This has caused significant increase of heat transport from the bottom of the test cell to the central core region and to the *s/l* interface. The temperature profiles and *s/l* interface position data (Gau and Viskanta, 1985b) suggest that the buoyancy-induced transport is so intense that thermal energy from near the bottom of the plate is advected to the upper region of the melt core where the temperatures are higher. This is in the opposite direction of the temperature gradient imposed by the heat source and the heat sink. These findings are consistent with published results for steady-state, turbulent natural convection in fluid layers heated from below. The temperature gradient reversal is attributed to the dissipation of the thermals before reaching the *s/l* interface. A more detailed discussion of the temperature gradient reversal in horizontal layers of ordinary fluids is given by Chu and Goldstein (1973). With increasing melt layer thickness (i.e., Rayleigh number) the temperature gradient reversal becomes more gradual but does not vanish.

Melting and resolidification of a Lipowitz eutectic produced

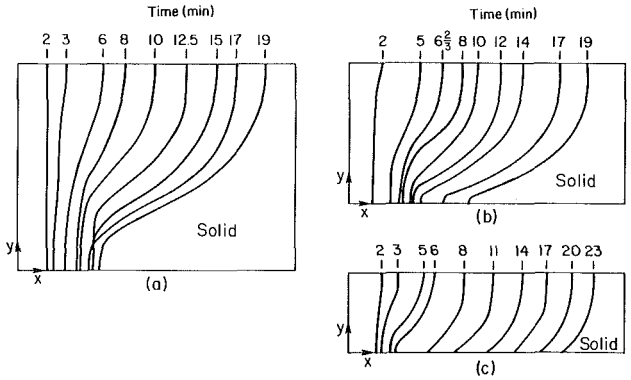

Fig. 5 Interface shapes during melting of pure gallium determined by the pour-out method: (a) $T_h = 38.0°C$, $A = 0.714$, (b) $T_h = 33.3°C$, $A = 0.5$, (c) $T_h = 38.7°C$, $A = 0.286$ (from Gau and Viskanta, 1986)

segregation of its constituents, and after several cycles the metal system was constitutionally stratified. Upon melting from below, natural convection was completely suppressed by the stable melt (Gau and Viskanta, 1984).

3.2 Multidirectional Melting. The importance of natural convection on heat transfer in metal melts has been recognized in the metallurgical literature (Cole, 1969; Kattamis, 1981; Clyne, 1984), but few studies have been reported. The effect of natural convection is often modeled by simply increasing the effective thermal conductivity of the melt by an arbitrary factor. For example, heat transfer measurements through liquid tin contained in a rectangular (thin) test cell heated by imposing a horizontal temperature gradient demonstrated that heat transfer increased by a factor of up to 9.6 in comparison to the heat flow by pure conduction (Harrison and Weinberg, 1985). It is, therefore, expected that natural convection in the melt could affect the melting rate of the metal and the *s/l* interface motion, in spite of the fact that the thermal conductivity of metals is two to three orders of magnitude higher than that of ordinary materials.

The effect of natural convection on the shape and motion of the *s/l* interface during melting of gallium (Gau and Viskanta, 1986) and tin (Wolff and Viskanta, 1987) from a vertical wall has been investigated. The results have clearly established that for larger aspect ratio cavities, melting of the solid near the top can be significantly enhanced, and melting near the bottom of the test cell can be completely terminated, by natural convection in the melt.

The *s/l* interface shapes during melting of pure gallium from a vertical wall are shown in Fig. 5. At very early times, before the buoyancy-driven flow is initiated, the interface is parallel to the heated vertical wall of the test cell. During this period of time, heat transfer in the melt layer is dominated by conduction. As the heating progressed, natural convection in the melt started to develop and continued to intensify. This is evidenced by the appearance of a nonuniform melt layer, receding from the top to the bottom of the test cell. As Fig. 5 clearly shows, the interface departed from one parallel to the heated wall earlier in time ($t<2$ min) for the smaller aspect ratio cavities. The liquid heated at the vertical wall rises along the hot left wall. The flow is deflected 90 deg by the top wall, flows along it, and impinges at the *s/l* interface at the top of the cavity, producing more melting in this region. The liquid is turned 90 deg, flows along the interface, and is cooled to the fusion temperature as it moves downward. At the bottom of the test cell the liquid is turned another 90 deg by the wall and flows toward the heated wall, thus forming a clockwise rotating cell. Fluid motion associated with the phase change at the interface was negligible since there is very little difference in the density between the solid and liquid phases. Note that melting at the bottom of the test cell is nearly terminated in the

Downloaded 16 Dec 2010 to 193.140.21.150. Redistribution subject to ASME license or copyright; see http://www.asme.org/terms/Terms_Use.cfm

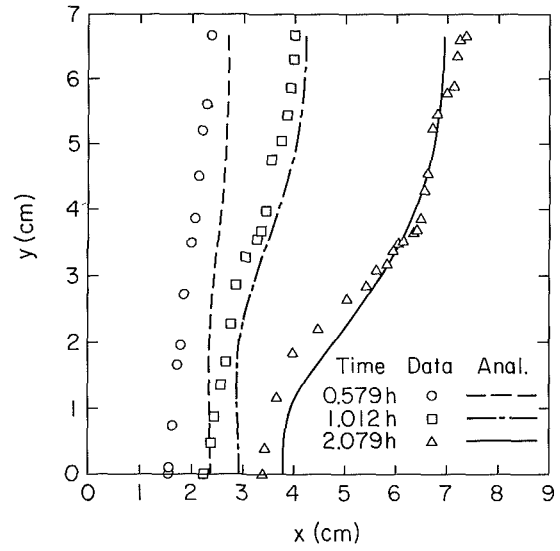

Fig. 6 Comparison between measured and predicted s/l interface locations during melting of pure tin from a vertical wall, $T_h = 233.9$, $A = 0.75$, Ste = 0.0848 (from Wolff and Viskanta, 1987)

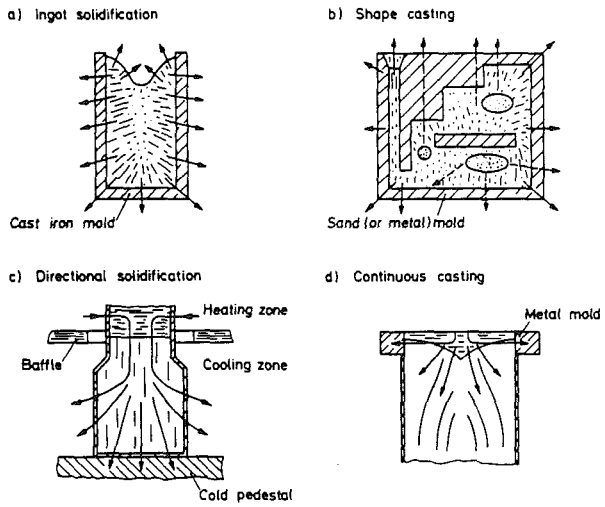

Fig. 7 Schematic diagrams of commonly used solidification technologies and heat flow diagrams (from Sahm, 1982)

larger aspect ratio cavity (Fig. 5*a*) at later times (for $t \geq 12.5$ to 17 min). This is due to the fact that in this region the flow of the liquid is in the opposite direction of the imposed temperature gradient and the liquid has been cooled to near its melting temperature. In fact, results show that near the bottom of the test cell the local melting rate is always smaller than that predicted by the Neumann model (Gau and Viskanta, 1986). In the middle and the top of the test cell the Neumann model greatly underpredicts the melting rate.

A numerical model has been developed to predict melting of pure metal from a vertical wall, initially at its fusion temperature (Webb and Viskanta, 1986a). Because of the subcooling of the solid and the finite heat capacity of heated vertical wall in the experiments (Gau and Viskanta, 1986a), the numerical model overpredicted the advancement of the interface and the melting rate. The finding suggests that initial subcooling of the solid can result in a large reduction of the melting of higher thermal conductivity solids such as metals. A comparison between experimentally measured and theoretically predicted solid-liquid interface positions for melting of tin from a vertical wall is given in Fig. 6. Since the initial subcooling of the solid is negligibly small in the experiments, the discrepancy between data and predictions may be explained by the thermal inertia of the experimental system. In the numerical analysis, the constant-temperature boundary condition on the vertical wall is assumed to be imposed impulsively, and the Stefan number is held constant throughout the simulation. In the experiments, approximately seven minutes (5.6 percent of the total time) elapsed before the desired constant wall temperature boundary condition is reached. At later times the difference between the experimental and numerical results becomes smaller. This rather critical comparison between data and predictions is encouraging and appears to validate the mathematical model. Unfortunately, the computer resources needed to perform the calculations for a rather simple physical situation are very large, and more efficient numerical algorithms are needed to solve the model equations.

Heated-area-averaged heat transfer coefficients for melting of gallium from a vertical wall have been measured (Gau and Viskanta, 1986). Even though the entire melting process was transient and quasi-steady melting conditions (Viskanta, 1985) were not reached, the experimental data were correlated by a least-square equation of the form

$$\overline{\mathrm{Nu}}_{l_c} = \frac{\bar{h} l_c}{k_l} = 0.0631(\mathrm{Ra}_{l_c}/\mathrm{Ste})^{0.274} \tag{13}$$

where l_c is a characteristic length of the melt region (i.e., average melt layer thickness). This length scale was determined from the knowledge of the instantaneous volume of the gallium melted and the area of the heated wall. The correlating equation (13) is valid in the conduction, transition, and convection regimes (Viskanta, 1985), but it is not useful for design calculations because the characteristic length l_c would not be known *a priori*. This length is a function of time, Stefan and Rayleigh numbers, aspect ratio, and subcooling parameter, and would have to be measured or predicted from a detailed analysis. To contrast, for quasi-steady convection-dominated melting from an isothermal, vertical surface the numerically predicted average Nusselt number at the wall was correlated by the equation (Webb and Viskanta, 1986a)

$$\overline{\mathrm{Nu}}_H = \bar{h}H/k = 0.157\ \mathrm{Ra}_H^{0.263} \tag{14}$$

In this equation the height H of the wall is used as a characteristic length in the dimensionless parameters.

Attempts to correlate melt volume fraction data, which are closely related to the heat transfer rate, have been only partially successful (Webb and Viskanta, 1986b). This is attributed to the lack of an appropriate length scale (which depends on the melt pool shape and volume and changes as the melting progresses) for use in the dimensionless parameters. The length scale for phase-change heat transfer problems is an important parameter and needs theoretical research attention.

4 Solidification

Solidification is of great importance simply because one of its major practical applications is casting – an economical method of forming a component if the melting point of the metal is not too high (Kurz and Fisher, 1984). Some of the most common solidification technologies are illustrated schematically in Fig. 7. If the physical and mechanical properties of castings were easier to control, then solidification would be an even more imporant process. Solidification of pure, binary, and multicomponent metal systems is an important and broad field encompassing basic understanding of thermodynamics, phase-transformation kinetics, transport processes, and solid mechanics, in addition to application of these principles to the improvement and fabrication of materials. Solidification theory is beginning to play a vital role, since it forms the basis for controlling the microstructure and hence improving the quality of metal products (Flemings, 1974; Kurz and Fisher, 1984; Minkoff, 1986). Three levels of

Downloaded 16 Dec 2010 to 193.140.21.150. Redistribution subject to ASME license or copyright; see http://www.asme.org/terms/Terms_Use.cfm

approach are distinguished in studying solidification: (1) microscopic-crystal growth: atomic level simulation, (2) intermediate-solidification front morphology: stability calculations, and (3) macroscopic-casting geometry: foundary process modeling. In the discussion to follow the focus is on the macroscopic approach.

The main characteristics of solidification fronts in metals hve been well established and described in textbooks (Flemings, 1974; Kurz and Fisher, 1984; Minkoff, 1986). It is known that at low rates of advance the solidification front tends to a planar, minimum energy configuration, but with increasing rates of solidification (e.g., increasing departure from equilibrium conditions) the front breaks down, first into a cellular and then a dendritic structure. In pure or nearly pure metals, departure from equilibrium conditions and the breakdown of the solidification front are associated with the supercooling of the liquid. The front becomes unstable in the presence of supercooled liquid and is thus liable to breakdown if perturbed in any way. The breakdown of the solidification front occurs more readily when solute elements are present, either as impurities or as deliberate alloying components. Again, the explanation for this effect is in terms of instability of the interface due to undercooling. The undercooling arises from the zone of solute-enriched liquid that is generated ahead of the solidification front, which is below its liquidus temperature and is therefore constitutionally undercooled (Mullins and Sekerka, 1964).

Dendritic solidification is the usual form of growth in either solutions or pure melts, whenever supersaturation or supercooling exists ahead of the growing *s/l* interface. Accompanying dendritic growth in a pure melt, the latent heat of fusion is transferred from the moving interface into the supercooled melt. This internal heat transfer gives rise to a thermal field around a growing dendrite, whereby transformtion kinetics are driven by thermal gradients. The presence of temperature gradients is responsible for conductive heat flow. These gradients lead to buoyancy forces, which induce thermal convective flows that affect growth.

Fluid flow in the melt plays an important role in nucleation, growth, and coarsening phenomena and affects microsegregation and macrosegregation in metallic alloys. Five major types of fluid flow in the melt, which are encountered during solidification of ingots, castings, etc. are: (1) thermal convection driven by temperature gradients, (2) constitutional convection driven by solutal (concentration) gradients, (3) solidification shrinkage induced convection, (4) fluid flow induced by the nucleation and growth of phases that are heavier or lighter than the melt, and (5) forced convection (i.e., due to shear forces, rotational forces, magnetic forces, etc.). The effects of fluid flow during solidification on microscopic and macroscopic *s/l* morphologies have been discussed (Kattamis, 1981; Fisher, 1981; Fisher and Kurz, 1984).

The effect of convective flow on the structure of the solid formed was shown experimentally by Cole and Bolling (1965). However, the first attempt at a quantitative treatment of convective motion and its effect on unidirectional solidification was made by Szekely and Stanek (1970). It is now recognized that the natural convective flow developed in the melt due to thermal gradients. Natural convection is very important as it not only affects the rate of solidification, the shape of the *s/l* interface, and the distribution of impurities, but can also have a large influence on the structure of the solid formed (Winegard and Cole, 1964; Morizane et al., 1967; Szekely and Stanek, 1970; Szekely and Chhabra, 1970; Chiesa and Guthrie, 1974).

As an illustration of the effect of natural convection on solidification, consider the experimental conditions shown in Fig. 8(*a*). A pure metal melt is brought into intimate contact with a metallic mold. The mold cools the melt and causes the metal to solidify. The temperature profile at a certain time

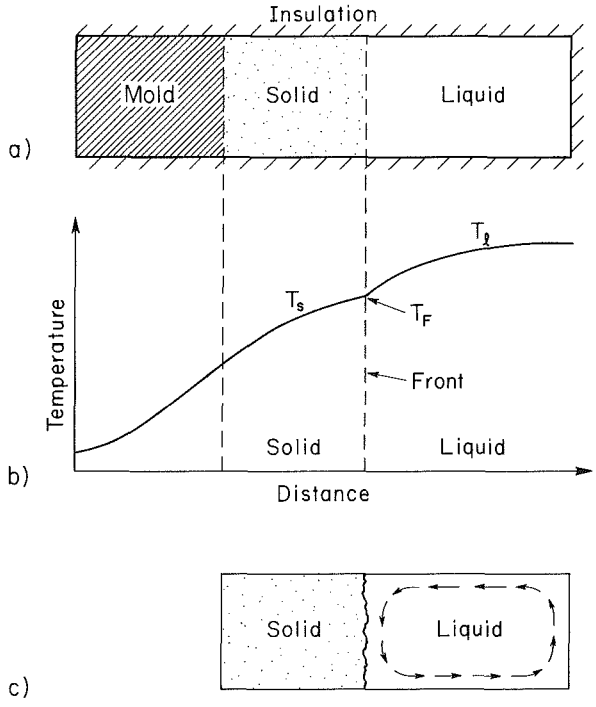

Fig. 8 Unidirectional solidification and conditions: (*a*) schematic of conditions, (*b*) temperature distribution, and (*c*) natural convection circulation ahead of a growing front

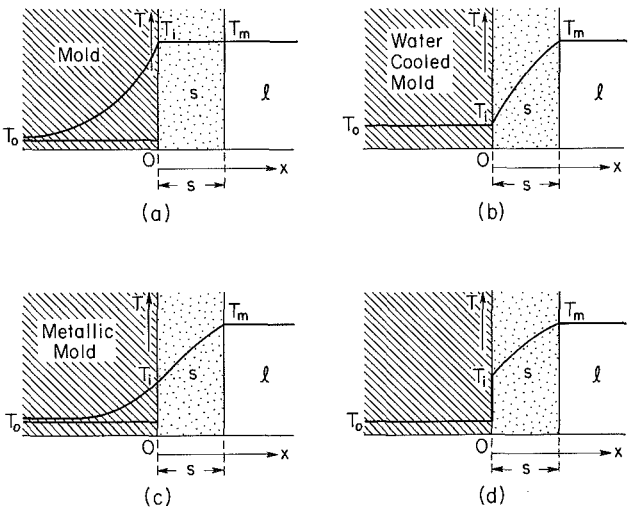

Fig. 9 Temperature distribution across the melt, solid, and the mold: (*a*) insulating mold, (*b*) water-cooled (constant temperature) mold, (*c*) metallic mold, and (*d*) casting solidifying in the presence of significant thermal resistance to heat flow metal-mold interface (after Kattamis, 1981)

after the solidification process has started is given in Fig. 8(*b*). Due to the lower temperature at the solidification front T_F, the melt will sink at the front and rise in some other part of the melt region, producing a counterclockwise natural circulation motion (panel *c* in Fig. 8). Estimates show that even though the superheat may be dissipated very rapidly (in the order of seconds), natural convection in the melt may be maintained across the region.

During solidification the melt superheat and the latent heat of fusion must be removed through the solid metal formed, the metal-mold interface, and the mold, encountering at each one of the these steps a certain thermal resistance. The heat transfer processes are complex, and simplifying assumptions need to be made to analyze the problem. Four idealized cases are identified in Fig. 9. The thermal characteristics of the mold

Downloaded 16 Dec 2010 to 193.140.21.150. Redistribution subject to ASME license or copyright; see http://www.asme.org/terms/Terms_Use.cfm

determine the rate of solidification, and a more detailed discussion is available elsewhere (Kattamis, 1981). Suffice it to say that the cooling rate is a very important factor, which determines the microstructure of the casting, but the details cannot be discussed here because of space limitations.

The properties of cast metals can be linked directly to their chemical homogeneity and grain structure. The major cause of structural defects and nonhomogeneities (macrosegregation) is now understood to be the state of convection in the melt close to the *s/l* interface during the solidification. Hence, detailed knowledge of the convective phenomena is crucial for the proper control of the casting processes. To make matters more complicated in large solidifying ingots, for example, the thermosolutally induced convective flow may be turbulent. Neither the macroscopic type of convection (crucible or mold dimensions) nor microscopic type of convection (dimensions of microstructural elements such as cells, dendrites, eutectic lamellae, or fibers) have so far been treated and understood in a rigorously quantitative manner on a broad scale (Kurz and Fisher, 1984; Minkoff, 1986).

In the next two sections, we review the recent progress in understanding heat transfer during solidification of pure metals and alloys. An engineering-phenomenological and not a more basic-microscopic point of view is followed in the discussion.

4.1 Solidification of Pure Metals

4.1.1 Relevant Physical Processes. Pure substances and eutectic mixtures solidify at a discrete temperature and the solidification rates are, in general, determined by the heat transfer rates normal to the solid–liquid interface. In the absence of superheat in the liquid and density differences between the solid and liquid phases, heat transfer during solidification is by pure conduction. The effects of highly anisotropic crystalline structures on the heat conduction in the solid have been demonstrated, but have not been studied in detail. For example, experiments with pure gallium have shown that anisotropic heat conduction in the solid can produce a highly irregular solidification front morphology (Gau and Viskanta, 1985a).

It is well recognized that density differences between the phases, solidification front motion, temperature gradients in the melt, and surface temperature gradients can produce convective motion in the melt. In the Earth environment, the effect of thermal convection on the rate of solidification, *s/l* interface shape, and interface morphology has been well recognized in the metallurgy and heat transfer literature (Cole, 1969; Kattamis, 1981; Viskanta, 1985). There are a number of studies reported in the literature that have modeled the effects of thermal convection in the melt during solidification (Wolff and Viskanta, 1988). It has been shown that the natural convection flow structures in liquid metals can be quite different from those in nonmetallic substances (Viskanta, 1983, 1985). The effects of these flow structures on the front shape and movement during solidification of metals are not well understood. Furthermore, the influences of the orientation of the system with respect to the gravitational field, cellular or turbulent convection, and three-dimensional flow structures (Viskanta et al., 1986) have not been studied in solidifying metals and are not understood. The density difference between the phases poses an additional complexity, because more than one moving boundary (solid–liquid, liquid–gas, and solid–gas) can result simultaneously, and no mathematical models appear to have been developed to handle multiple moving boundaries resulting from shrinking or mold filling during solidification. The fact that the motion of the solidification front can produce bulk convection in the melt has been recognized, but does not appear to have been modeled. The effect is usually not significant, except under conditions of very rapid solidification.

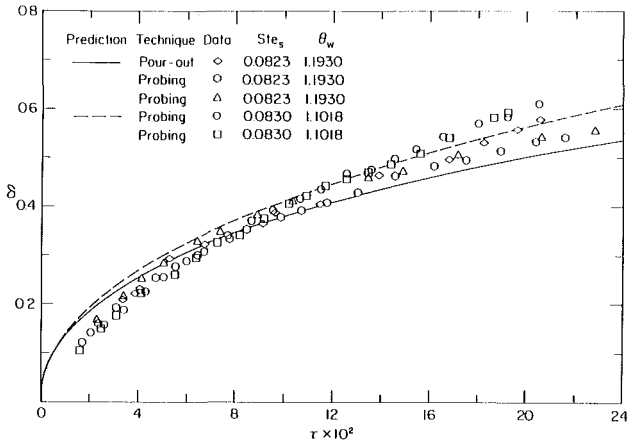

Fig. 10 Comparison of the measured and predicted interface positions during solidification of pure gallium from above (from Gau and Viskanta, 1985)

4.1.2 Unidirectional Solidification. Mathematical models that can be used to predict the solidification rate and temperature distribution during the solidification of pure metals in molds cooled by fluids (Garcia and Prates, 1978) and through uncooled molds of effectively semi-infinite thickness (Garcia et al., 1979) have been developed and verified experimentally. The heat transfer model is essentially an extension of the classical Neumann solution (Carslaw and Jaeger, 1959) while retaining the advantage of convenience over numerical solutions. The exact analytical solution can also serve as a benchmark to determine the accuracy of numerical models. In order to verify the applicability of the model to air-cooled molds, the model predictions are compared with experimental results in the literature for lead, tin, and a lead–tin eutectic (Garcia and Prates, 1978). For water-cooled molds, the experimental results for lead and aluminum of commercial purity (not less than 99.8 percent) are compared with the model predictions (Garcia and Prates, 1978). For massive molds the model (Garcia et al., 1979) permits the measurement of the heat transfer coefficient at the metal–mold interface. This enables a complete description of the kinetics and thermal characteristics of solidification.

An exact analysis has recently been presented (Garcia and Prates, 1978; Garcia et al., 1979) to treat the generalized, unidirectional solidification problem, subject only to the constraint that the interfacial thermal resistance (heat transfer coefficient) between the mold and solid be invariant. The technique involves the mathematical expedient of representing components of the interfacial thermal resistance by virtual layers of solid metal and/or mold. It is demonstrated (Clyne and Garcia, 1980) that the kinetic and thermal description of the model reduces to the expected in the three simple limiting cases previously subjected to exact analysis.

Even though gallium crystals are highly anisotropic and the *s/l* interface is nonplanar, the average interface position predicted using an extended Neumann model agreed well with experimental data for solidification from below (Gau and Viskanta, 1985a). In the model, the crystal was assumed to be isotropic and a thermal conductivity averaged over the three crystalline axes is used in the calculations. Solidification of 99.9 percent pure gallium from above produced natural convection in the melt, which together with the anisotropy in the thermal conductivity of the crystals resulted in a macroscopically and microscopically nonplanar solidification front. Comparison of experimental average solidification front data with predictions based on a one-dimensional model, which accounted for natural convection in the melt (Fig. 10), show relatively poor correspondence at early and at late times (Gau and Viskanta, 1985b). This is due to

Downloaded 16 Dec 2010 to 193.140.21.150. Redistribution subject to ASME license or copyright; see http://www.asme.org/terms/Terms_Use.cfm

anisotropic heat conduction in the crystalline solid at early times and the effects of interface morphology and natural convection in the melt at late times, which were not modeled mathematically.

4.1.3 Multidirectional Solidification. Since metals have a high thermal conductivity, a usual simplification in analyzing solidification of metals is that conduction is the sole mode of heat transfer (Hills et al., 1975). However, numerous solidification experiments (Winegard and Cole, 1964; Szekely and Chhabra, 1970; Chiesa and Guthrie, 1974) had previously established that natural convection in the melt affects the shape of the solidification front on a vertical wall resulting in multidirectional motion of the front. Szekely and Chhabra (1970) appear to be the first to demonstrate conclusively both experimentally and analytically the importance of natural convection on the *s/l* interface shape in a rectangular tank with the heat source and sink on two opposite vertical sidewalls. Experiments with pure lead and lead-tin alloys (Chiesa and Guthrie, 1974) have shown that under unstable conditions natural convection in the melt also affects the *s/l* interface shape and motion during solidification.

Carefully controlled experiments with pure tin have been performed and have yielded solidification front position and temperature distribution data (Wolff and Viskanta, 1988). A comparison of the measured positions with predictions, based on a mathematical-numerical model developed by Ramachandran et al. (1981), during solidification of tin on a vertical wall is given in Fig. 11. At early times ($t = 0.077$ h) the numerical model overpredicts the solidified volume. This discrepancy may be partly attributed to supercooling and thermal inertia of the experimental apparatus. Due to the inertia of the apparatus it is impossible to lower the temperature impulsively at the vertical wall to initiate the solidification process. At later times ($t = 1.462$ h) the agreement between data and predictions is disappointing, and the discrepancies are attributed to differences between the predicted flow structures and those present during solidification. This is due to several factors: (1) shrinkage of the solid due to phase transformation and change of the boundary condition at the top from a no-slip to a slip, (2) neglect of the finite velocity at the solidification front, (3) unavoidable heat losses from the bottom of the test cell, (4) crystallographic effects at the solidification front, and (5) numerical errors due to an insufficiently fine grid. All of these factors could affect the flow structure in the melt and alter the solidification front shape and motion.

The flow structure in the melt could not be measured, but the analysis predicted secondary roll cells in the four corners of the melt region. Such secondary recirculation cells have also been predicted during laminar natural convection of gallium and tin in rectangular cavities heated on one vertical wall and cooled at the opposite wall in the absence of phase change (Wolff et al., 1988). Since liquid metals are not transparent, visualization of the flow structure is not possible. Although attempts were made in some laboratories to infer the flow field in metals with radiotracer methods or x-ray techniques, very little is known about flow patterns in liquid metals. A novel magnetic probe (Ricou and Vives, 1982; Oreper and Szekely, 1983) has been developed for measuring instantaneous local velocities in forced flow, and there appears to be a possibility of extending its range to low velocities corresponding to those expected in buoyancy-driven flows in the presence of temperature gradients.

Solidification experiments with 99.9 percent pure gallium on an isothermal vertical wall have shown that not only natural convection in the liquid but also the anisotropy of the thermal conductivity and the crystallographic effects play an important role in establishing the solidification front shape and the morphology (Gau and Viskanta, 1986). The front was irregular and nonreproducible. The crystallographic effects

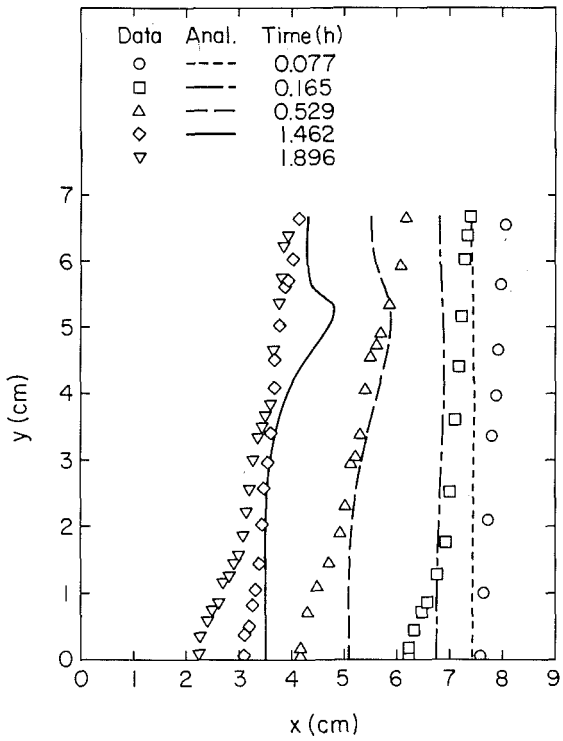

Fig. 11 Comparison between the predicted and measured interface locations during solidification of pure tin from a vertical wall: $T_i = 233.0°C$, $T_h 233.0°C$, $T_c = 229.0°C$, $A = 0.75$, $Ste = 0.0132$, $Ra_w = 1.59 \times 10^5$ (from Wolff and Viskanta, 1988)

were important not only during the early times when conduction in the solid predominated over convection in the liquid, but also at times when natural convection in the melt played an important role in controlling the solidification front advance. The local flow and heat transfer near the front are expected to be influenced by the irregular front morphology and vice versa.

4.2 Solidification of Metal Alloys

4.2.1 Physical Phenomena. During solidification of binary and multicomponent alloys the physical phenomena become much more complicated. In this section, we consider solidification of multicomponent alloys, with the emphasis on binary alloys. Solidification of binary or multicomponent mixtures differs in many respects from solidification of pure substances. Usually, the phase transformation takes place over a range of temperatures, rather than at a discrete temperature as occurs in pure substances or eutectics. In other words, the solid and liquid phases can coexist in equilibrium at various temperatures, depending on the composition of the mixture. Furthermore, in most systems the chemical components have different solubilities in the solid and liquid phases. Hence, during phase change a chemical species may be preferentially incorporated or rejected at the solidification front. A number of new and important physical phenomena have been identified to take place during solidification (Viskanta and Beckermann, 1987), and reference for a more detailed discussion is made to this recent account.

During solidification of binary and multicomponent alloys, the solidification front is not always smooth and, under most practical conditions, a variety of microscopically complicated growth structures develops, as shown in Fig. 12. The solidification fronts can be divided into a planar, cellular, and dendritic morphology (Sahm, 1982). The interfacial structure is a function of the temperature gradient (G) to the front velocity (v) ratio and of the freezing temperature range ($T_l - T_s$). The transition from the planar to the dendritic

Downloaded 16 Dec 2010 to 193.140.21.150. Redistribution subject to ASME license or copyright; see http://www.asme.org/terms/Terms_Use.cfm

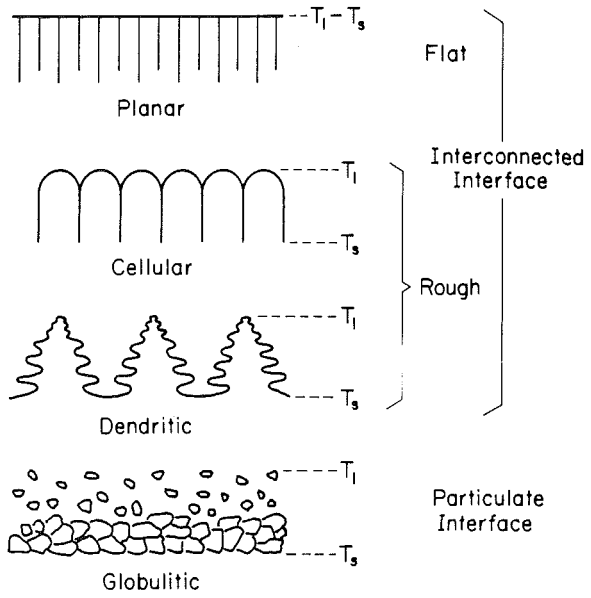

Fig. 12 Basic types of solidification fronts distinguished (from Sahm, 1982)

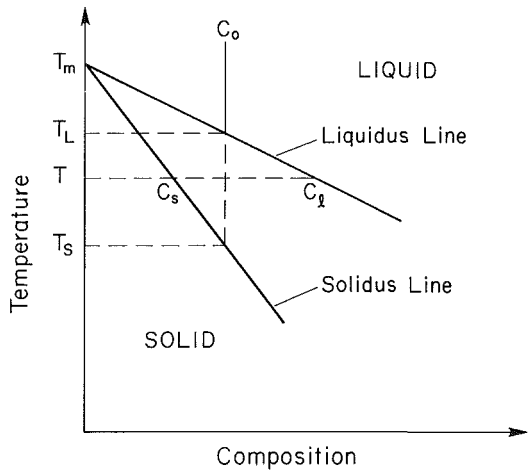

Fig. 13 A corner of a binary equilibrium diagram

solidification front is linked with a reduction in the G/v ratio. The region characterized by the presence of such irregular interfaces is often called a mushy zone. In industrial castings and ingots as well as in many phase-change processes occurring in nature, the normal growth mode is dendritic (Fisher, 1981). The dendrite exists in alloy castings because it is the most efficient morphology for the diffusion of solute and the dissipation of heat in order to reduce the supercooling in the melt. Dendritic growth in castings can be further subdivided into two categories, columnar and equiaxed. In columnar dendritic growth, long aligned dendrite stalks are produced due to unidirectional heat flow. Equiaxed dendritic crystals growth to roughly the same extent in several directions indicating a multidirectional heat flow.

The temperature range over which a binary alloy solidifies can be obtained from an equilibrium phase diagram (Flemings, 1974). An outline of a typical corner of such a diagram is shown in Fig. 13. In thermal and phase equilibrium, the phase diagram reflects the difference of the component solubilities in the liquid and solid phases at a particular temperature. For a certain temperature T one notes first that the solid of composition C_s is in equilibrium with liquid of composition C_l. Expressed differently, one can say that a melt of composition C_l indicated on the liquidus line at a certain temperature T will always solidify with composition C_s indicated on the solidus line at the same temperature T. If a melt of composition C_o solidifies, according to this diagram, it will start to solidify at temperature T_L and solidification will be complete at temperature T_S with the solid at an average composition C_o.

The *s/l* interface constitutes the location for a thermodynamic transformation, which to a large extent is determined by kinetic factors. In general, driving forces for solidification of binary mixtures are the chemical (concentration or activity) and thermal (temperature) gradients at the *s/l* interface. These forces act through thermal and constitutional undercooling (Flemings, 1974; Kurz and Fisher, 1984). At very high heat and mass transfer rates, solidification is controlled by kinetic factors (i.e., incorporation of molecules in the crystal lattice), which is beyond the scope of this brief account. Fluid motion has a profound influence on the melting and solidification process in that it will affect the melt composition and temperature at the *s/l* interface. Directly at the growth front ("near field"), the so-called microconvection determines the microstructure of the solidification front (i.e., the interface morphology).

Fisher (1981) has discussed the relationship between macroscopic fluid convection in the melt and the process of macrosegregation, which referes to the large-scale separation of alloy components and is a major source of nonhomogeneities in castings. During solidification of a binary mixture, solute enrichment or depletion of the remaining liquid phase results from differences in the component solubilities in the solid and liquid phases. For example, the study of steel ingot solidification revealed the formation of V-type segregates near the bottom of the casting, which was attributed to natural convection of the melt and settling of free crystals (Gomer and Andrews, 1969; Engler and Ellerbrok, 1977). The structure of the grains (microstructure) and, therefore, the mechanical properties of an alloy are also strongly influenced by melt convection (i.e., interdendritic fluid flow) and heat and species transfer on microscopic and macroscopic levels during solidification. A remarkable effect of convection on macroscopic orientation of dendritic microstructure is the orientation of the dendrites toward the direction of the flow, and "bending" of dendrites also appears possible (Sahm, 1982).

The complicated interfacial geometries (Fig. 12) make it virtually impossible to utilize a "microscopic" formulation of the fundamental conservation equations and interface conditions. Therefore, present methods of analysis are largely based on simplified ("macroscopic") models of the phase-change process during solidification. Macroscopic conservation equations that are capable of accounting for fluid flow in the mushy and pure melt regions have been derived, and the interested reader is referred to recent accounts (Smith and Hoadley, 1987; Viskanta and Beckermann, 1987) for a more detailed discussion.

The importance of convection during solidification of metal alloys has been well recognized, but little systematic experimental and theoretical work has been done to provide a general understanding of the various transport phenomena involved. The effects of a nonstationary solid, i.e., the floating and settling of equiaxed crystals, convection due to surface tension gradients, and penetration of bulk liquid into the mushy zone are not well understood. Other important physical phenomena associated with solidification include remelting of the solid in different parts of the system, effects of anisotropic crystal structures, volume deficit, and interaction of particulate matter with the solidification front.

4.2.2 Unidirectional Solidification. As a concrete example consider unidirectional solidification of a binary alloy (Clyne, 1982b). The physical model of the system, together with the temperature distribution, is shown in Fig. 14. The solid frac-

Downloaded 16 Dec 2010 to 193.140.21.150. Redistribution subject to ASME license or copyright; see http://www.asme.org/terms/Terms_Use.cfm

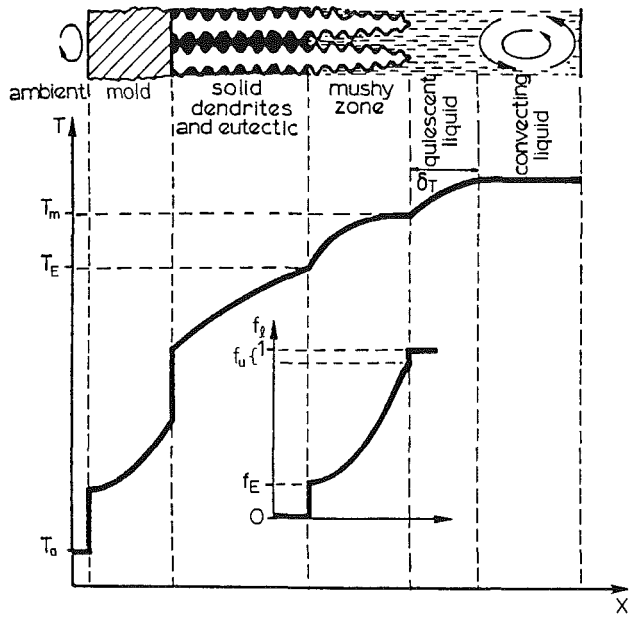

Fig. 14 Schematic diagram of a unidirectional solidification model and temperature profile (from Clyne, 1982b)

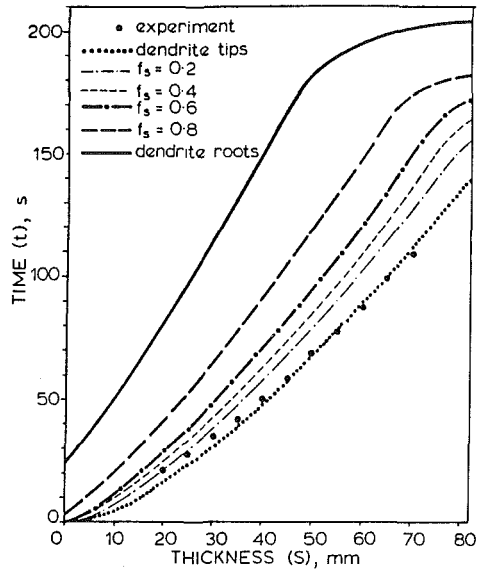

Fig. 15 Comparison between isotherm advance predictions and dipstick penetration measurements for solidification of Al–4.5 percent Cu; $\Delta T_i = 3$ K and $h_i = 1.9$ kW/m^{2}K (from Clyne, 1982b)

tion profile (f_s) is given as an inset in the figure. In the presence of a known flow field u, the energy equation may be written as

$$\rho c\left[\frac{\partial T}{\partial t}+\frac{\partial}{\partial x}(uT)\right]=\frac{\partial}{\partial x}\left(k\frac{\partial T}{\partial x}\right)+\dot{q} \tag{15}$$

where $\dot{q}$ represents the local volumetric rate of latent heat evolved and may be treated as a source term. For solidification of metal alloys that freeze over a finite temperature range, the local rate of latent heat evolved $\dot{q}$ can be expressed as

$$\dot{q}=\rho\Delta h_m\frac{\partial f_s}{\partial t}\approx\rho\Delta h_m\frac{\partial f_s}{\partial T}\frac{\partial T}{\partial t} \tag{16}$$

where $f_s(T)$ is the solid (volume) fraction (Kurz and Fischer, 1984). The form of the function $f_s(T)$ depends on the nature of the solute redistribution occurring in the mushy zone.

It should be emphasized at this point that the solidification characteristics, both in terms of the progression of the freezing and of the resultant microsegregation, are highly sensitive to the temperature dependence of the latent heat evolution. The actual f_s versus T relationship is controlled by the growth kinetics and the solute redistribution (microsegregation). The solid volume fraction $f_s(T)$ can be obtained from the lever rule of Scheil, Brody and Flemings, and other models (Flemings, 1974). Under normal conditions the solidification front velocity is low enough for thermodynamic equilibrium to prevail so that f_s (T) depends primarily on the solute redistribution in the mushy zone. Substitution of equation (14) into equation (15) yields

$$\rho c\left[\left(1-\frac{\Delta h_m}{c}\frac{\partial f_s}{\partial T}\right)\frac{\partial T}{\partial t}+\frac{\partial T}{\partial x}(uT)\right]=\frac{\partial}{\partial x}\left(k\frac{\partial T}{\partial x}\right) \tag{17}$$

An analytical model has been presented that describes the temperature distribution and the positions of the solidus and liquidus isotherms in the unidirectional solidification of binary alloys (Lipton et al., 1982). The model is an extension of the one developed earlier by Garcia and Prates (1978) described in Section 4.1.2 of this paper and involves accounting of the latent heat of fusion by adjusting the specific heat over the solidification temperature range. The model employs the mathematically expedient technique of replacing the interfacial thermal resistance by equivalent layers of material. Temperature distributions are predicted in the solid, mushy, and liquid regions, and positions of the mushy–solid interface (solidus isotherm) and the mushy–liquid interface (liquidus isotherm) are also determined. The application of the model is demonstrated by comparison with experimental data for an Al–4.5 percent Cu alloy and with the numerical results of a finite difference method. The model was checked for simplicity in a variety of casting situations; it gives a rapid, reliable prediction of any isotherm position and temperature distribution.

Some of the basic characteristics of alloys that freeze over a finite temperature range have been examined both experimentally (Clyne, 1982a) and numerically (Clyne, 1982b) with the help of an explicit finite difference model. In the model (Fig. 14) for numerical treatment of directional freezing of alloys, the emphasis is on modeling the detailed internal response of the metal. Particular attention is devoted to the handling of latent heat of evolution (as it is influenced by segregation phenomena) and representation of the mushy zone. For a phase diagram with linear liquidus and solidus lines, the f_s–T relationship for use in equation (16) is specified. Convection heat flow in the melt is modeled by means of a thermal boundary layer ahead of the advancing dendrite tip. Heat transfer within the quiescent liquid layer is then assumed to be only by conduction, while assumed convection currents maintain a uniform temperature in the rest of the melt (Fig. 14). A boundary condition relates the heat flux at the edge of the quiescent layer to the cooling rate of the convection liquid. Modeling results are presented for both laboratory experiments and industrial processes, and examples are given of how this type of analysis can assist in process optimization and control (Clyne, 1982b).

Comparison has been made between observed and predicted changes in local cooling conditions during directional solidification and deductions made about thermal features and the growth behavior (Clyne, 1982a; Clyne, 1982b). For example, a comparison between thermal histories recorded via thermocouples located in an Al–4.5 percent Cu melt and their corresponding predictions show good agreement (Clyne, 1982b). A comparison of the isotherms corresponding to different f_s values for an experiment with Al–4.5 percent Cu is illustrated in Fig. 15, together with experimental probe (dipstick) readings. The speedup of isotherms corresponding to higher solid fractions toward the end of the ingot results from the progressive elimination of the "superheat" ahead of them (Clyne, 1982b). Some conclusions regarding the speedup of the dendrite tip and root isotherms, other end effects,

Downloaded 16 Dec 2010 to 193.140.21.150. Redistribution subject to ASME license or copyright; see http://www.asme.org/terms/Terms_Use.cfm

fects, elimination of melt superhead by convection current, and the effect of isothermal latent heat evolution are discussed. Some general conclusions about the relevance of the model to real solidification processes and the importance of numerical modeling in future developments are presented (Clyne, 1982a; Clyne, 1982b). The relative effects on the growth behavior of interfacial conductance, pouring superheat, liquid convection, and mold characteristics may be examined for different types of alloys. Finally, only by numerical modeling is it possible to explore the effect of the overall cooling characteristics on dendrite penetration into the melt, solute-dependent thermal conductivity changes, microsegregation phenomena, dendrite tip undercooling, eutectic reactions, etc.

A more detailed mathematical model in which macroscopic and microscopic aspects of equiaxed solidification are combined has been developed by Rappaz et al. (1985, 1986). The macroscopic model deals with a standard conduction-type energy equation; however, the heat release by the phase transformation phenomena, as well as dendritic and eutectic growth, are being calculated from the temperature distributions. The macroscopic/microscopic models have been integrated into an explicit finite-difference calculation of one-dimensional heat flow and cooling curves for Al–4.7 percent Si alloy and gray iron casting have been calculated and compared with experimental data. The advantage of the approach is that it is able to furnish, on the scale of the whole casting, microstructural features such as number of grains, microstructure spacings, and fraction of eutectic.

4.2.3 Multidirectional Solidification. The displacement of segregated solid and liquid phases, which accompanies solidification, leads to a redistribution of constituents known as macrosegregation. While the floating or settling of unattached solid grains can contribute to several types of observed segregation, fluid motion in the mushy region and in the bulk of the melt are considered to be the most important causes of macrosegregation. Detailed discussions of the transport mechanisms responsible are available (Flemings, 1974). More up to date accounts of segregation (both macro and micro), including some specific applications, can be found in more recent publications (Ridder et al., 1981; Kattamis, 1981; Bennon and Incropera, 1987c).

A detailed discussion of proposed solidification models that can handle fluid flow is available (Viskanta and Beckermann, 1987). Suffice it to mention that the models can be grouped with those based on the continuum mixture theory and on the local volume averaging method. The model based on the mixture theory originally developed by Flemings and co-workers (see Ridder et al., 1980) has been generalized and put on firmer theoretical grounds by a number of researchers (Stiller, 1982; Hills et al., 1983; Prantil and Dawson, 1983; Bennon and Incropera, 1987a, 1987b). The local volume-averaging method differs from the continuum theory of mixtures in that each phase is treated separately and the irregular interfaces are regarded as moving boundaries. The classical conservation equations are applied only within each phase but not over the entire mixture. The transport equations for each phase are supplemented by appropriate interfacial and boundary conditions (Beckermann, 1987). The interested reader is referred to the original references for details. Here, we briefly mention some of the applications of the two approaches.

Ridder et al. (1981) have simulated two-dimensional fluid flow and heat flow in axisymmetric ingots. Incorporation of variable mesh spacing in the finite-difference equations allowed a smooth transition near the solidus and liquidus boundaries, resulting in a more stable solution of the macrosegregation equations. The model couples the flow in the liquid metal pool above the liquids isotherm to the interdendritic flow in the mushy zone during solidification. The

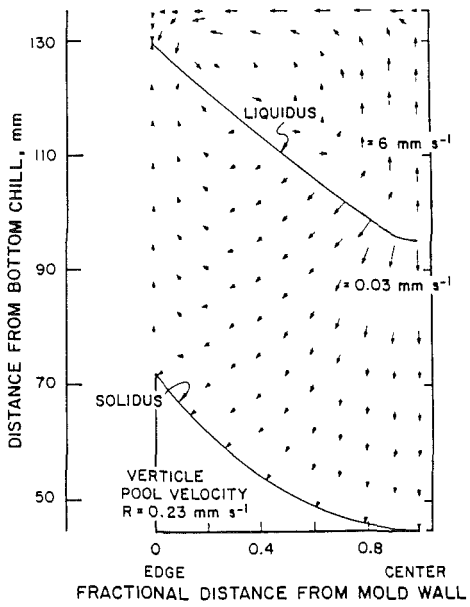

Fig. 16 Calculated steady-state flow velocities for axisymmetric solidification of Pb-26.5 percent Sn ingot (from Ridder et al., 1981)

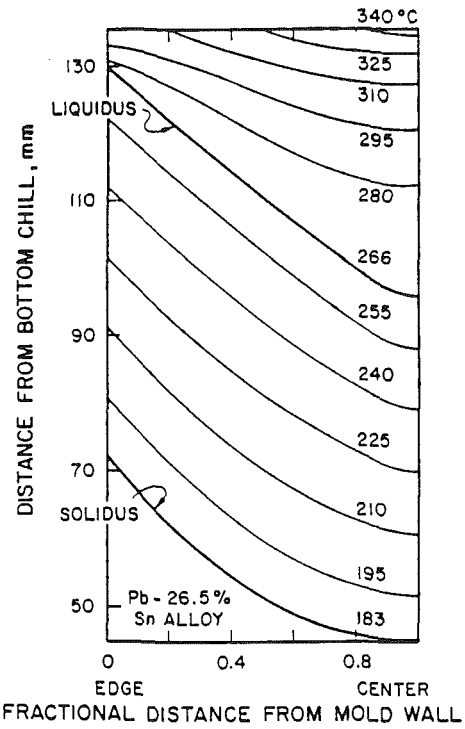

Fig. 17 Calculated steady-state isotherms for axisymmetric solidification of Pb-26.5 percent Sn ingot (from Ridder et al., 1981)

predicted steady-state isotherms in the Pb–25.4 percent Sn ingot and the resulting velocity vectors are shown in Figs. 16 and 17, respectively. Experimental data were used for the initial values and boundary conditions where applicable, and a value of $2.3 \times 10^{-5} \text{mm}^2$ was used for the permeability at the centerline of the ingot. Since the flow in the liquid metal pool of the Pb-rich ingot is in the same direction as in the Sn-rich ingot and opposing the flow in the mushy region, a decrease in the segregation profile is predicted if this flow is included in the calculations. The results of calculations revealed (Ridder et al., 1981) that convection in the bulk melt is only very weakly coupled to the interdendritic fluid flow and that, while the former has a marked influence on the thermal field, the latter makes very little contribution to heat transfer in the mushy

Downloaded 16 Dec 2010 to 193.140.21.150. Redistribution subject to ASME license or copyright; see http://www.asme.org/terms/Terms_Use.cfm

zone. The work also has illustrated the relative importance of thermal and solutal buoyancy forces, and good correlations were obtained with experimentally measured macrosegregation profiles. Comparisons of predicted and experimental segregation profiles show that natural convection in the liquid metal pool has little effect on the interdendritic fluid flow and hence macrosegregation.

Recently Bennon and Incropera (1987b, 1987c) have investigated macrosegregation in a statically cast NH_4Cl–H_2O system. They used ammonium chloride–water as an analog system for dendritically solidifying metals. Mushy region dendrite erosion and formation of segregates have been predicted. Unstable and double-diffusive conditions that accompany the discharge of interdendritic fluids into the liquid core have shown to result in localized growth variations, remelting, and fluctuating bulk fluid transport behavior. The authors compare their results with qualitative experimental observations, but no quantitative validation of the model is presented.

The transport and solidification model based on the volume-averaging method developed by Beckermann (1987) has been applied by Beckermann and Viskanta (1988) to solidification of a NH_4Cl–H_2O solution inside a vertical cavity. Experiments were performed to visualize the phase-change and convection processes in the cavity. It was found that the solidification induces a variety of double-diffusive phenomena, but the predicted behavior showed considerable disagreement with the measured data. While the model accounts for thermal and solutal convection in both the melt and mushy regions, it has not yet been used to study solidification of binary metal systems.

Since the Peclet number within the mushy zone is much smaller than unity ($Pe < 1$), convective heat transfer in the mushy zone has often been neglected (MacAuley and Weinberg, 1973; Szekely and Jassal, 1978; Ridder et al., 1978). To improve understanding of the importance of flow and heat transfer in a mushy zone, a mathematical model based on volume-averaged transport equations (with phase change assumed to occur over a temperature range) has recently been developed and the predictions have been compared with experimental data for solidification of gallium and glass beads as the fluid and porous matrix, respectively (Beckermann and Viskanta, 1988a). Numerical results show reasonably good agreement with interface position and temperature measurements. Natural convection in the melt and heat conduction in the solid are found to influence the interface shape and motion considerably during both solidification and melting. A recent experimental and numerical investigation has revealed that the degree of penetration of the fluid into the porous region depends strongly on the porous-layer geometry (Beckermann et al., 1988). The intensity of natural convection is always much stronger in the fluid region than in the porous medium. The degree of penetration of fluid into the porous layer increases with increasing permeability (i.e., the Darcy number) and the Rayleigh number.

Prediction of only the temperature distribution during continuous casting of a metal does not appear to require detailed modeling of the flow and species transport processes in the melt. For example, a steady, two-dimensional energy equation-based model has been developed to compute the temperature distribution and estimate optimal casting conditions for the continuous casting of metals (Bamberger and Prinz, 1986). The model takes into account natural convection (empirically) at the solidification front, the influence of temperature on the thermophysical properties, release of latent heat at a rate proportional to the solidification rate for both pure metals and alloys, and convective heat exchange between the mold and the secondary cooling zone. The model has been tested, and the calculated temperatures agree with the measurements. Equally good agreement has been obtained between predicted and measured results for aluminum alloy ingots. It appears that the good agreement between model predictions and data is obtained through a reliable prescription of the heat flow between the metal and the mold. This heat flux was specified by the following empirical correlation:

$$q = C_1 - C_2\sqrt{z/V} \tag{18}$$

where the parameters C_1 and C_2 are empirical constants, which depend on the metal cast and the construction of the mold; z is a coordinate in the direction of casting; and V is the casting speed. These results suggest that for certain purposes, energy equation based models can be useful to understand and optimize the process; however, such models cannot be used to predict nonhomogeneities in the chemical composition of a solidified material (i.e., macrosegregation) caused by uncontrolled species transport by melt convection.

There is currently very intense interest in mathematical-numerical modeling of solidification. Methods are being designed to model one or more of the many physical processes. The interested reader is directed to the more specialized accounts detailing numerical simulation of metal solidification under different conditions and a wide range of practical applications (Erickson, 1980; Brody and Apelian, 1981; Sahm and Hansen, 1984; Dantzig and Berry, 1984; Kou and Mehrabian, 1986; Fredricksson, 1986; Smith, 1987; Samanta et al., 1987).

5 Concluding Remarks

A wide range of transport (heat, mass, species, and momentum) processes arise during melting and solidification of pure metals and alloys. Significant progress has been made in understanding the phenomena, often with the main emphasis treating the heat flow, but many of the processes have not been studied and are poorly understood. The research in the past has been motivated by the need to solve practical technological problems, and there has been inadequate communication between the scientists who understand the process and the engineers who apply it.

Despite the accomplishments represented by the research just discussed, further challenges remain in quantifying the influence of a range of transport phenomena that occur simultaneously with conductive heat transfer and include: nature and transport processes in an anisotropic mushy zone, the effect of micro- and macroconvection on the growth of dendrites, cellular structures, globules, etc., the effect of thermosolutal convection originating in the mushy zone and its vicinity on the microstructure, behavior of double-diffusive plumes and breakup and merging process of the double-diffusive layers on the flow in the melt, effect of convection on the microstructure and solidification front kinetics, turbulent transport induced by temperature and composition gradients (including dispersion in the mushy zone), and floating and settling of equiaxed crystals in the melt as well as their detachment process from the mushy zone. In addition to the above, chemical species transport can have other effects that may be of intrinsic interest, particularly with reference to solidification macrostructure.

Mathematical modeling is a powerful tool to aid in the task of understanding and control of complex processes during solidification, especially when supplemented by experimental modeling. In this connection, problems that warrant research attention include: establishment of fundamental time, length, and velocity scales during phase transformation, development of efficient numerical algorithms for solving multidimensional transport equations with multiple phase-change boundaries (Rickert and Engler, 1984) to reduce costs associated with numerical simulations, design and conduct of fundamental model experiments to provide a rational basis for making adjustments to improve qualitative and quantitative agreement

Downloaded 16 Dec 2010 to 193.140.21.150. Redistribution subject to ASME license or copyright; see http://www.asme.org/terms/Terms_Use.cfm

between data and model predictions, and measurement of thermophysical, transport, and mechanical properties for multicomponent metal systems to reduce the uncertainty on predicted transport behavior.

Many important physical processes that occur during solidification of metals have not been adequately studied and are not understood. Superb computations with wrong models of some of the transport processes will yield meaningless results, just as an inefficient numerical algorithm will prevent any results from being obtained. For this reason interaction between those engaged in the physical phenomena and the analysis is much needed, because today many fundamental physical theories evolve through numerical studies.

Acknowledgments

Preparation of this review paper was initiated by the author as part of the 1986 Max Jakob Memorial Award lecture presented at the 24th National Heat Transfer Conference, Pittsburgh, PA, in August 1987. The author is grateful to Professor C. Beckermann for many helfpul discussions. He also wishes to acknowledge the support of his research on solid-liquid phase change heat transfer by the Thermal Systems and Engineering Program of the National Science Foundation under Grant No. CBT-8313573.

References

Bankoff, S. G., 1964, "Heat Conduction or Diffusion With Change of Phase," in: *Advances in Chemical Engineering*, T. B. Drew, J. W. Hoppes, Jr., and T. Vermeulen, eds., Academic Press, New York, Vol. 5, pp. 75–150.

Beckermann, C., 1987, "Melting and Solidification of Binary Mixtures With Double-Diffusive Convection in the Melt," Ph.D. Thesis, Purdue University, West Lafayette, IN.

Beckermann, C., Viskanta, R., and Ramadhyani, S., 1988, "Natural Convection in Vertical Enclosures Containing Simultaneously Fluid and Porous Layers," *Journal of Fluid Mechanics*, Vol. 186, pp. 257–284.

Beckermann, C., and Viskanta, R., 1988a, "Natural Convection Solid/Liquid Phase-Change in Porous Media," *International Journal of Heat and Mass Transfer*, Vol. 31, pp. 34–46.

Beckermann, C., and Viskanta, R., 1988b, "Double-Diffusive Convection During Dendritic Solidification of a Binary Mixture," *Physico Chemical Hydrodynamics*, Vol. 10, pp. 195–213.

Bennon, W. D., and Incropera, F. P., 1987a, "A Continuum Model for Momentum, Heat and Species Transport in Binary Solid-Liquid Phase Change Systems – I. Model Formulation," *International Journal of Heat and Mass Transfer*, Vol. 30, pp. 2161–2170.

Bennon, W. D., and Incropera, F. P., 1987b, "A Continuum Model for Momentum, Heat and Species Transport in Binary Solid-Liquid Phase Change Systems – II. Application to Solidification in a Rectangular Cavity," *International Journal of Heat and Mass Transfer*, Vol. 30, pp. 2171–2187.

Bennon, W. D., and Incropera, F. P., 1987c, "The Evolution of Macro-Segregation in Statically Cast Binary Ingots," *Metallurgical Transactions B*, Vol. 18, pp. 611–616.

Bertram, L. A., and Zanner, F. J., 1986, "Convective Simulation in Metal Solidification," in: *Stability in Convective Flows*, W. S. Saric and A. A. Szewczyk, eds., ASME, New York, pp. 99–107.

Brody, H. D., and Apelian, D., eds., 1981, *Modelling of Casting and Welding Processes*, AIME, New York.

Brown, R. A., Chang, C. J., and Adornato, P. M., 1983, "Finite Element Analysis of Directional Solidification of Dilute and Concentrated Binary Alloys," in: *Modeling of Casting and Welding Processes II*, J. A. Dantzig and J. T. Berry, eds., Society of TMS-AIME Publishing, Warrendale, PA.

Brown, R. A., Sackinger, P. A., Thomas, P. D., Derby, J. J., and Atherton, L. J., 1987, "Application of Large-Scale Simulation to Intelligent Materials Processing: Modeling of Czochralski Growth of Single Crystals," in: *Interdisciplinary Issues in Materials Processing and Manufacturing*, S. K. Samanta, R. Komanduri, R. McMeeking, M. M. Chen and A. Tseng, eds., ASME, New York, Vol. 1, pp. 331–348.

Caldwell, T. W., Campagna, A. J., Flemings, M. C., and Mehrabian, R., 1977, "Refinement of Dendrite Arm Spacings in Aluminum Ingots Through Heat Flow Control," *Metallurgical Transactions B*, Vol. 8, pp. 261–270.

Carslaw, H. S., and Jaeger, J. C., 1959, *Conduction of Heat in Solids*, 2nd ed., Clarendon Press, Oxford.

Cheung, F. B., and Epstein, M., 1984, "Solidification and Melting in Fluid Flow," in: *Advances in Transport Processes*, Vol. III, A. S. Majumdar and R. A. Mashelkar, eds., Wiley Eastern Ltd., New Delhi, pp. 35–117.

Chiesa, F. M., and Guthrie, R. I. L., 1974, "Natural Convection Heat Transfer Rates During Solidification and Melting of Metals and Alloys Systems," ASME JOURNAL OF HEAT TRANSFER, Vol. 96, pp. 377–384.

Chu, T. Y., and Goldstein, R. J., 1973, "Turbulent Convection in a Horizontal Layer of Water," *Journal of Fluid Mechanics*, Vol. 60, pp. 141–159.

Clyne, T. W., and Garcia, A., 1980, "Assessment of a New Model for Heat Flow During Unidirectional Solidification of Metals," *International Journal of Heat and Mass Transfer*, Vol. 23, pp. 773–782.

Clyne, T. W., 1982a, "The Use of Heat Flow Modeling to Explore Solidification Phenomena," *Metallurgical Transactions B*, Vol. 13, pp. 471–478.

Clyne, T. W., 1982b, "Numerical Modelling of Directional Solidification of Metallic Alloys," *Metal Science*, Vol. 16, pp. 441–450.

Clyne, T. W., 1984, "Modelling of Heat Flow in Solidification," *Materials Science and Engineering*, Vol. 65, pp. 111–124.

Cole, G. S. and Bolling, G. F., 1965, "The Importance of Natural Convection in Casting," *Transactions of Metallurgical Society AIME*, Vol. 233, pp. 1568–1572.

Cole, G. S., 1969, "Transport Processes and Fluid Flow in Solidification," in: *Solidification*, T. J. Hugel and G. F. Bolling, eds., AIME, Metal Park, OH, pp. 201–274.

Cornellissen, M. C. M., 1986, "Mathematical Model for Solidification of Multicomponent Alloys," *Ironmaking and Steelmaking*, Vol. 13, pp. 204–211.

Crank, J., 1984, *Free and Moving Boundary Problems*, Clarendon Press, Oxford.

Cryer, C. W., 1977, "Bibliography of Free Boundary Problems," Report 1793, Mathematics Research Center, University of Wisconsin, Madison, WI.

Dantzig, J. A., and Berry, J. T., eds., 1984, *Modeling of Casting and Welding Processes – II*, TMS-AIME Publishing, Warrendale, PA.

Engler, S., and Ellerbrok, R., 1977, "On the Formation of the Equiaxed Zone in Castings," in: *Symposium on Quality Control of Engineering Alloys and the Role of Metals Science*, Delft, The Netherlands.

Erickson, W. C., 1980, "Computer Simulation of Solidification," *AFS International Cast Metals Journal*, Vol. 5, pp. 30–41.

Fisher, K. M., 1981, "The Effects of Fluid Flow on the Solidification of Industrial Castings and Ingots," *Physico Chemical Hydrodynamics*, Vol. 2, pp. 311–326.

Flemings, M. C., 1974, *Solidification Processing*, McGraw-Hill, New York.

Fredricksson, H., ed., 1986, *State of the Art Computer Simulation of Casting and Solidification Process – 1986*, Les Editions de Physique, Zone Industrielle de Courtabeoff, France.

Fukusako, S., and Seki, N., 1987, "Fundamental Aspects of Analytical and Numerical Methods on Freezing and Melting Heat Transfer Problems," in: *Annual Review of Numerical Fluid Mechanics and Heat Transfer*, Vol. 1, T. C. Chawla, ed., Hemisphere Publishing Corporation, Washington, Vol. 1, pp. 351–402.

Garcia, A., and Prates, M., 1978, "Mathematical Model for the Unidirectional Solidification of Metals: 1. Cooled Molds," *Metallurgical Transactions B*, Vol. 9, pp. 449–457.

Garcia, A., Clyne, T. W., and Prates, M., 1979, "Mathematical Model for the Unidirectional Solidification of Metals: II. Massive Molds," *Metallurgical Transacttions B*, Vol. 10, pp. 85–92.

Gau, C., and Viskanta, R., 1984, "Melting and Solidification of a Metal System in a Rectangular Cavity," *International Journal of Heat and Mass Transfer*, Vol. 27, pp. 113–123.

Gau, C., and Viskanta, R., 1985a, "Effect of Crystal Anisotropy on Heat Transfer During Melting and Solidification of a Pure Metal," ASME JOURNAL OF HEAT TRANSFER, Vol. 107, pp. 706–709.

Gau, C., and Viskanta, R., 1985b, "Effect of Natural Convection on Solidification from Above and Melting from Below of a Pure Metal," *International Journal of Heat and Mass Transfer*, Vol. 28, pp. 573–587.

Gau, C., and Viskanta, R., 1986, "Melting and Solidification of a Pure Metal on a Vertical Wall," ASME JOURNAL OF HEAT TRANSFER, Vol. 108, pp. 174–181.

Gleave, M. C., and Hawkins, R. J., 1987, "Application of PCH in the Steel Industry," *Physico Chemical Hydrodynamics*, Vol. 9, pp. 115–125.

Gomer, C. R., and Andrews, K. W., 1969, "Study of Steel Solidification by the Use of Radioactive Isotopes," *Journal of Iron and Steel Institute*, Vol. 207, No. 1, pp. 26–35.

Gozlan, E., and Bamberger, M., 1987, "Heat Flow and Solidification in a Metal Mold," *Zeitschrift fur Metallkunde*, Vol. 78, pp. 677–682.

Hale, N. W., Jr., and Viskanta, R., 1980, "Solid-Liquid Phase-Change Heat Transfer and Interface Motion in Materials Cooled or Heated From Above or Below," *International Journal of Heat and Mass Transfer*, Vol. 23, pp. 283–292.

Harrison, C., and Weinberg, F., 1985, "The Influence of Convection on Heat Transfer in Liquid Tin," *Metallurgical Transactions B*, Vol. 16, pp. 355–357.

Hills, A.W.D., Malhotra, S. L., and Moore, M. R., 1975, "The Solidification of Pure Metals (and Eutectics) Under Unidirectional Heat Flow Condition: II. Solidification in the Presence of Superheat," *Metallurgical Transactions B*, Vol. 6, pp. 131–142.

Ho, K., Pehlke, R. D., 1985, "Metal-Mould Interfacial Heat Transfer," *Metallurgical Transactions B*, Vol. 16, pp. 585–594.

Kattamis, T. Z., 1981, "Heat Transfer and Mass Transfer During Solidification," in: *Heat and Mass Transfer in Metallurgical Systems*, D. B. Spalding and N. H. Afgan, eds., Hemisphere, Washington, pp. 375–401.

Kou, S., and Mehrabian, R., eds., 1986, *Modeling of Casting and Welding Processes – III*, TMS-AIME Publishing, Warrendale, PA.

Kuo, S., and Sun, D. K., 1985, "Flow Field and Weld Penetration in Stationary Arc Welds," *Metallurgical Transactions A*, Vol. 166, pp. 203–203.

Downloaded 16 Dec 2010 to 193.140.21.150. Redistribution subject to ASME license or copyright; see http://www.asme.org/terms/Terms_Use.cfm

Kurz, W., and Fisher, D. J., 1984, *Fundamentals of Solidification*, Trans Tech Publications, Switzerland.

Lapadula, C. A., and Miller, W. K., 1970, "The Effect of Buoyancy on the Formation of a Solid Surface Freezing Onto a Vertical Surface," *International Journal of Heat and Mass Transfer*, Vol. 13, pp. 13–26.

Lewis, R. W., and Roberts, P. M., 1987, "Finite Element Simulation of Solidification Problems," *Applied Scientific Research*, Vol. 44, pp. 61–92.

Lipton, J., Garcia, A., and Heinemann, W., 1982, "Analytical Solution of Directional Solidification With Mushy Zone," *Archiv fur Eisenhuttenwesen*, Vol. 53, pp. 469–473.

Minkoff, I., 1986, *Solidification and Cast Structure*, Wiley, New York.

MacAuley, L. C., and Weinberg, F., 1972, "Liquid Metal Flow in Horizontal Rods," *Metallurgical Transactions B*, Vol. 4, pp. 2097–2107.

Mori, A., and Araki, K., 1976, "Methods for Analysis of the Moving Boundary Surface Problem," *International Chemical Engineering*, Vol. 16, pp. 734–743.

Morizane, K., Witt, A. F., and Gatos, H. C., 1967, "Impurity Distribution in Single Crystals," *Journal of the Electrochemical Society*, Vol. 114, pp. 738–742.

Muehlbauer, J., and Sunderland, J., 1965, "Heat Conduction With Freezing and Melting," *Applied Mechanics Reviews*, Vol. 18, pp. 951–959.

Mullins, W. W., and Sekerka, W. W., 1964, "Stability of Planar Interface During Solidification of a Dilute Binary Alloy," *Journal of Applied Physics*, Vol. 35, pp. 444–451.

Ohnaka, I., and Kobayashi, K., 1986, "Flow Analysis During Solidification by the Direct Finite Difference Method," *Transactions of the Iron and Steel Institute of Japan*, Vol. 26, pp. 781–789.

Oreper, G., and Szekely, J., 1983, "The Effect of an Externally Imposed Magnetic Field on Buoyancy Driven Flow in a Rectangular Cavity," *Journal of Crystal Growth*, Vol. 64, pp. 505–515.

Ozisik, N. M., 1980, *Heat Conduction*, Wiley-Interscience, New York, Chap. 10.

Perkins, A., and Irving, W. R., 1975, *Mathematical Process Models in Iron- and Steelmaking*, The Metals Society, London, pp. 187–199.

Poirier, D., and Salcudean, M., 1986, "On Numerical Methods in Mathematical Modeling of Phase Change in Liquid Metals," ASME Paper No. 86-WA/HT-22.

Prantil, V. C., and Dawson, P. R., 1983, "Application of a Mixture Theory to Continuous Casting," in: *Transport Phenomena in Materials Processing*, M. M. Chen, J. Mazumder, and C. L. Tucker III, eds., ASME, New York, pp. 47–54.

Ramachandran, N., Gupta, J. P., and Jaluria, Y., 1981, "Two-Dimensional Solidification With Natural Convection in the Melt and Convective and Radiative Boundary Conditions," *Numerical Heat Transfer*, Vol. 4, pp. 469–484.

Rappaz, M., Thevoz, Ph., and Kurz, W., 1985, "Micro-/Macroscopic Modelling of Equiaxed Solidification," in: *Numerical Methods in Thermal Problems 1*, R. W. Lewis and K. Morgan, eds., Pinbridge Press, Swansea, United Kingdom, pp. 251–261.

Rappaz, M., The'voz, Ph., Zon Jie, Gabatzhuler, J.-P., and Lindscheid, H., 1986, "Micro-Macroscopic Modelling of Equiaxed Solidification," in: *State of the Art of Computer Simulation of Casting and Solidification Processes – 1986*, H. Fredericksson, ed., les Editions de Physique, Zone Industrielle de Courtaboeuff, France, pp. 277–284.

Rickert, A., and Engler, S., 1984, "Solidification Behaviour of Gravity Die Cast Iron," *Giesserei Forschung*, Vol. 36, pp. 99–108.

Ricou, R., and Vives, C., 1982, "Local Velocity and Mass Transfer Measurements in Molten Metals Using an Incorporated Probe," *International Journal of Heat and Mass Transfer*, Vol. 25, pp. 1579–1588.

Ridder, S. D., Reyes, F. C., Charkravorty, S., Mehrabian, R., Nanman, J. D., Chen, J. H., and Klein, H. J., 1978, "Steady State Segregation and Heat Flow in ESR," *Metallurgical Transactions B*, Vol. 9, pp. 415–425.

Ridder, S. D., Mehrabian, R., and Kou, S., 1980, "A Review of our Present Understanding of Macrosegregation in Axi-Symmetric Ingots," in: *Modeling of Casting and Welding Process I*, H. D. Brody and D. Apelian, eds., Metallurgical Society of AIME, Ridge, NH, pp. 261–284.

Ridder, S. D., Kou, S., and Mehrabian, R., 1981, "Effect of Fluid Flow on Macro-Segregation in Axi-Symmetric Ingots," *Metallurgical Transactions B*, Vol. 12, pp. 435–447.

Rubinshtein, L., 1971, *The Stefan Problem*, American Mathematical Society, Providence, RI.

Sahm, P. R., 1982, "The Role of Convection in Solidification," in: *Convective Transport and Instability Phenomena*, J. Zierep and H. G. Oertel, eds., Braun, Karlsruhe, pp. 515–556.

Sahm, P. R., and Hansen, P. N., 1984, *Numerical Simulation and Modeling of Casting and Solidification Processes for Foundary and Cast-House*, International Committee of Foundary Technical Association (CIATF).

Samanta, S. K., Komanduri, R., McMeeking, R., Chen, M. M., and Tseng, A., eds., 1987, *Interdisciplinary Issues in Materials Processing and Manufacturing*, ASME, New York, Vols. 1 and 2.

Smith, T. J., ed., 1987, *Modelling the Flow and Solidification of Metals*, Martinus Nijhoff Publishers, Dodrecht–Boston–Lancaster.

Smith, T. J., and Hoadley, A.F.A., 1987, "Recent Developments in Modelling Metal Flow and Solidification," in: *Modelling of Flow and Solidification of Metals*, T. J. Smith, ed., Martinus Nijhoff Publishers, Dodrecht–Boston–Lancaster, pp. 277–302.

Stiller, W., 1982, "Warme- und Stofftransport bei der Erstarrung von Kokillenguss," Doktor-Ingenieur Dissertation, Universitat Hannover, Hannover, Federal Republic of Germany.

Szekely, J., and Stanek, V., 1970, "Natural Convection Transients and Their Effects on Unidirectional Solidification," *Metallurgical Transactions*, Vol. 1, pp. 2243–2251.

Szekely, J., and Chhabra, 1970, "The Effect of Natural Convection on the Shape and Movement of the Melt-Solid Interface in the Controlled Solidification," *Metallurgical Transactions B*, Vol. 1, pp. 1195–1203.

Szekely, J., and Jassel, A., 1978, "An Experimental and Analytical Study of the Solidification of a Binary Dendritic System," *Metallurgical Transactions B*, Vol. 9, pp. 389–401.

Tarzia, D. A., 1981/82, "Una revision sobre problems de frontera movil y libre para la ecuacion del calor. El problema de Stefana," *Mathematical Notae*, Vol. XXIX, pp. 147–241.

Viskanta, R., 1983, "Phase-Change Heat Transfer," in: *Solar Heat Storage: Latent Heat Materials*, G. A. Lane, ed., CRC Press, Inc., Boca Raton, FL, pp. 153–222.

Viskanta, R., 1985, "Natural Convection in Melting and Solidification," in: *Natural Convection: Fundamentals and Applications*, S. Kakac, W. Aung, and R. Viskanta, eds., Hemisphere, Washington, pp. 845–877.

Viskanta, R., and Beckermann, C., 1987, "Mathematical Modeling of Solidification," in: *Multidisciplinary Issues in Materials Processing and Manufacturing*, S. K. Samanta, R. Komanduri, R. McMeeking, M. M. Chen, and A. Tseng, eds., ASME, New York, Vol. 2, pp. 501–526.

Voller, V. R., Cross, M., and Markatos, N. C., 1987, "An Enthalpy Method for Convection/Diffusion Phase Change," *International Journal for Numerical Methods in Engineering*, Vol. 24, pp. 271–284.

Webb, B. W., and Viskanta, R., 1986a, "Analysis of Heat Transfer During Melting of Pure Metal From an Isothermal Vertical Wall," *Numerical Heat Transfer*, Vol. 5, pp. 539–558.

Webb, B. W., and Viskanta, R., 1986b, "On the Characteristic Length Scale for Correlation Melting Heat Transfer Data," *International Communications of Heat and Mass Transfer*, Vol. 12, pp. 245–253.

Winegard, W. C., and Cole, G. S., 1964, "Thermal Convection During Horizontal Solidification of Pure Metals and Alloys," *Journal Institute of Metals*, Vol. 93, pp. 153–164.

Wolff, F., and Viskanta, R., 1987, "Melting of a Pure Metal From a Vertical Wall," *Experimental Heat Transfer*, Vol. 1, pp. 17–30.

Wolff, F., and Viskanta, R., 1988, "Solidification of a Pure Metal at a Vertical Wall in the Presence of Liquid Superheat," *International Journal of Heat and Mass Transfer* (in press).

Wolff, F., Beckermann, C., and Viskanta, R., 1988, "Natural Convection of Liquid Metals in Vertical Cavities," *Experimental Thermal and Fluid Science*, Vol. 1, pp. 83–91.

Downloaded 16 Dec 2010 to 193.140.21.150. Redistribution subject to ASME license or copyright; see http://www.asme.org/terms/Terms_Use.cfm

Thermal Radiation in Participating Media: The Past, the Present, and Some Possible Futures

J. R. Howell
Department of Mechanical Engineering,
The University of Texas at Austin,
Austin, TX 78712
Fellow ASME

A review of major events in the development of the engineering treatment of radiative transfer in participating media is presented. This review is followed by a discussion of the major analytical methods presently used for this class of problems, along with their strengths and limitations. Some comments are added concerning important areas of research that remain to be completely treated, and some areas of potential future application.

Introduction and a Short History

The history of early measurements of spectral and total radiation as contained in the seminal references makes fascinating reading. Herschel's evident amazement at the discovery of energy outside the visible part of the spectrum (referring to it as "invisible light") (Herschel, 1800) and the delight expressed by Nobili and Meloni (1831) at the sensitivity of their thermopile radiometer still reverberate from the antique chronicles to bring excitement even to the modern reader. Nobili and Meloni note, following their measurements of the temperatures of over 400 different insects, that they observed the following law concerning caterpillars: "The caterpillars always possess a more elevated temperature than the butterflies or chrysalides." They also noted that the reflectivity of metals follows the same progression as does their electrical conductivity, an observation that antedates the formulation of the Hagen-Rubens relation by nearly seventy years.

The ingenuity and accuracy of experimental measurements by these early workers, plus the later benchmark measurements of the blackbody total and spectral emissive power by Lummer and Pringsheim (1897, 1899, 1901) over the range 300 to 1300°C, provided a precise touchstone for the later theoretical work of Planck and others. Barr (1960) has provided an interesting review of the early measurements in radiation.

Because of its impact on the development of modern physics, thermal radiation is arguably the most fruitful of all the elements in the study of heat transfer. It is well known that Planck, after a series of attempts to match classical theory with experimental measurements of the blackbody spectrum, was forced to hypothesize the existence of quantized energy states. This led him to the development of quantum theory (Planck, 1959). Albert Einstein, in building on Planck's ideas, showed that an alternative derivation of the blackbody spectral distribution required consideration of the presence of induced emission and the coupling of the equilbrium radiation field with the emission of radiation by matter (Einstein, 1916, 1917). The explanation of the observed line absorption and emission spectra of gases led Neils Bohr to develop his theory of the structure of the hydrogen atom (Bohr, 1913), further opening the door to the modern quantum interpretation of the structure of matter and its interaction with energy.

We are now so confident of the theoretical basis of radiative transfer that most engineering radiative transfer calculations are accepted without experimental confirmation.

Engineering Radiative Heat Transfer in Absorbing-Scattering-Emitting Media

By the 1920s, the need for design tools that could adequately predict radiative transfer in industrial furnaces was becoming obvious. Exchange between simply arranged surfaces was previously worked out by ray-tracing techniques, i.e., following the history of emitted radiation from one surface through its history of reflections among the surfaces, and attempting to find a closed-form solution for the resulting infinite series (Christiansen, 1883). This method had serious flaws when many surfaces were present, or an attenuating medium was present between the bounding surfaces.

The pioneering work by Hottel (1931, 1933) systematically developed a methodology for such applications. The absence of high-speed computational capability at that time caused Hottel to develop methods that were amenable to hand calculation or that made reference to auxiliary tools such as graphs of gas emittance. These graphs were constructed from data that were painstakingly measured and extrapolated to useful parameter ranges.

Hottel's early work on configuration or view factors showed insight into these useful quantities. His derivation of the "crossed-string" method for factors between parallel, infinitely long bodies, as well as his original derivation of many commonly used factors, are perhaps no longer accorded their due regard (Hottel, 1931, 1933, 1954).

A very significant paper by Poljak (1935) introduced the net-radiation method, which simplifies the formulation of radiative exchange in enclosures by casting the formulation in terms of the net radiative energy at a given surface; i.e., the difference between the incident radiative energy flux (irradiance) and the outgoing radiant energy flux (radiosity). This approach allows radiative exchange to be set up in terms of a closed set of linear equations, rather than through use of an infinite series obtained by ray-tracing.

Hottel continued development of analytical treatments of radiative transfer in enclosures, including the effects of medium absorption. His treatment of an absorbing isothermal gas by using the mean beam length is an extremely clever engineering approximation. The exposition of this method in the various editions of the text edited by McAdams (Hottel, 1954) was the major reference for radiative transfer analysis throughout the 1940s and well into the middle 1950s. Further extensions culminated in the zoning method (Hottel and Cohen, 1958; Hottel and Sarofim, 1967), which allows consideration of nonuniform gas temperatures. This method continues to influence practitioners of furnace design.

Innovative applications of thermal radiation principles outside the conventional engineering of power plants and furnaces during the 1950s and 1960s put increasing demands on the accuracy of radiative transfer calculations. The greatest

Contributed by the Heat Transfer Division for publication in the JOURNAL OF HEAT TRANSFER. Manuscript received by the Heat Transfer Division February 4, 1988. Keywords: Radiation, Radiation Interactions, Reviews.

Copyright © 1988 by ASME
Downloaded 16 Dec 2010 to 193.140.21.150. Redistribution subject to ASME license or copyright; see http://www.asme.org/terms/Terms_Use.cfm

impetus was probably the emergence of NASA and the need for heat transfer calculations applicable to new propulsion systems and space vehicles, and the parallel need to determine radiative transfer in very high and very low temperature systems. This forced consideration of spectral, directional, and temperature-dependent property variations and their effects on radiative transfer, and required analytical methods that could include these effects. In addition, more accurate data for surface properties and the properties of attenuating media were required. The data gathered by Hottel and others for the total emittance of common gases and gas mixtures found in combustion processes became inadequate, although still useful for some applications.

Also during the 1960s, the greater availability, speed, and capacity of the electronic computer turned researchers toward alternative methods of calculation that were previously impractical. Certain drawbacks to the zoning method had long been obvious, notably the inability to treat variations in the properties of the absorbing medium within the enclosure easily, the incompatibility of practical zone structures with the grid size needed for fluid mechanical/convection/conductive analysis, and the difficulty of treating geometries that stray from purely rectangular or cylindrical. Although it is possible using the zoning method to account for spectral effects through the "sum of gray gases" method (Hottel and Sarofim, 1967), results are not completely satisfactory. Also, zoning allows no accounting for anisotropic scattering.

The intensified interest and the need for greater sophistication in the treatment of engineering radiative transfer encouraged the publication of a number of texts devoted to the subject during this time, including those by Wiebelt (1966), Sparrow and Cess (1978, first edition 1966), Hottel and Sarofim (1967), Love (1968), and Siegel and Howell (1972, based on their NASA reports of 1968, 1969, and 1971).

Attempts to treat the spectral properties of absorbing gases during the late 1960s and early 1970s were based on the total emittance charts developed by Hottel, or were borrowed from atmospheric physics, where the so-called narrow-band models (Goody, 1968; Ludwig et al., 1973) had been developed and used. Edwards and his co-workers (Edwards and Menard, 1964; Edwards, 1968; Edwards and Balakrishnan, 1973) provided the basis for much more useful engineering approaches to modeling the spectral properties of the gases most often encountered in engineering problems by the development of "wide-band" models. These provide relatively simple expressions for the band emittance of these gases as a function of total and partial pressure, path length, and temperature. They also make the band properties of gas mixtures relatively easy to calculate.

The problem of incorporating other modes of heat transfer into radiation-dominated problems also began in the 1960s, bringing to light the difficulties in grid-size matching and convergence. The solutions presented by Viskanta and Grosh (1962a, 1962b) long remained benchmark solutions for the planar geometry when conduction and radiation are present.

Throughout the 1970s and up to the present, the search has continued for methods that could be applied broadly to multidimensional radiative transfer in enclosures, with the additional capability of handling spectral and anisotropic characteristics in absorbing-emitting-scattering media. Interest was strong in the older methods and their extensions, and some newer approaches showed promise, such as the finite-element methods described later. New solutions for standard problems have provided benchmarks for comparing existing and emerging methods for accuracy and ease of solution. Notable among these are the solutions for two-dimensional gray enclosures given by Crosbie and Schrenker (1985) and Crosbie and Farrell (1985) and the three-dimensional solutions in rectangular enclosures given by Larsen (1983) using the zonal method and by Menguc (1985) using the P-3 method.

Methods developed for other applications have long been appropriated for use in engineering radiative transfer. These include the Schuster–Schwarzschild [now more commonly called the two-flux model; see Schuster (1905), Schwarzschild (1906), Chandrasekhar (1944)], Milne–Eddington, discrete ordinate, (S_n), and diffusion methods from astrophysics; and Monte Carlo, differential, P–N, invariant embedding, and others from nuclear physics and engineering.

Many of the methods developed in atmospheric science, astrophysics, and nuclear engineering are not directly applicable to the enclosure problems found in engineering. This is for two reasons. First, intensity at the boundary is often given as a boundary condition in the nonengineering fields, while temperature and boundary absorptance are the usual engineering boundary conditions. Second, the radiative flux divergence term in the energy equation is required for solution of many engineering problems, and evaluation of this term requires that the local radiative intensity be integrated over the sphere of solid angles, as is outlined in a later section. The additional complexity required by the engineering boundary conditions and the need to have much more detailed knowledge of the radiative intensity field at each point in the medium makes some methods impractical for engineering application.

Each of the developing methods was successfully applied to simple one-dimensional gray gas problems. When they were extended to multidimensional geometries with nongray media with various boundary conditions, drawbacks emerged in

Nomenclature

a = linear absorption coefficient
$\overline{gg}$ = gas volume-to-gas volume exchange area in zoning method
$\overline{gs}$ = gas volume-to-surface exchange area in zoning method
h = enthalpy of medium
i' = radiative intensity
I' = radiative source function
k = thermal conductivity of medium
P = pressure
s = distance from origin of intensity
$\overline{sg}$ = surface-to-gas volume exchange area in zoning method
$\overline{ss}$ = surface-to-surface exchange area in zoning method
q = energy flux; energy transiting normal to a given area per unit time per unit area
q''' = volumetric internal energy generation rate
T = absolute temperature
V = volume
κ = optical depth
λ = wavelength
ρ = density of medium
σ = linear scattering coefficient
τ = time
Φ = dissipation function
ϕ = scattering phase function
ω = solid angle
Ω = albedo $= \sigma/(\sigma+a)$

Subscripts

b = blackbody
g = property of participating medium
i = incident
i, j = surface indices
r = radiative
s = scattering
γ, μ = volume indices
λ = spectrally dependent

Downloaded 16 Dec 2010 to 193.140.21.150. Redistribution subject to ASME license or copyright; see http://www.asme.org/terms/Terms_Use.cfm

every case. No single method is now accepted as being the best for all problems. The greatest stumbling blocks remain those found in applying the zoning method: inability to treat nonuniform gas absorption and scattering coefficients easily; difficulty in matching the required grid size for radiation with that needed for concomitant computation of convection, conduction, or fluid mechanics (although many methods do much worse than the zoning method in grid matching); incorporation of spectral effects in an accurate yet tractable way; and complete treatment of anisotropic scattering.

Exact solution techniques for the integral equation of transfer were found for some simples cases. Crosbie and Dougherty (1981) have reviewed exact solution methods for some one-dimensional problems, and Viskanta and Menguc (1987) discuss recent multidimensional exact solutions. All of the exact solutions assume that the properties of the attenuating medium are spatially uniform. Lin (1987) has presented detailed formulations of the exact integral radiative transfer equation for various simple configurations in one- and multidimensional geometries.

Additional problems arise as more complicated problems are addressed. An example is the difficulty in obtaining converged numerical solutions to problems in which radiation interacts with chemical energy release in flame fronts (Chen et al., 1987). In these problems, the temperature gradients are very steep within the combustion zone, and the reaction rate depends strongly on the temperature. If multi-step chemistry is considered, the resulting very stiff equations are quite difficult to bring to convergence. In a sense, this is another manifestation of the problem of matching the numerical grid for radiation with that necessary for the other parts of the energy equation, in this case for combustion relations.

The Radiative Transfer Equation and the Energy Conservation Equation

To explore further the present state of investigation into solving radiative transfer problems, it is necessary to look in some detail at the governing relations involved in a general formulation.

The radiative transfer equation (RTE), which describes the spectral radiation intensity i'_λ in a particular solid angle ω and at a local optical depth κ_λ, can be cast in terms of the gradient in radiative intensity in an absorbing-emitting-scattering medium. This *differential form* of the RTE is

$$\frac{\partial i'_\lambda}{\partial \kappa_\lambda} + i'_\lambda(\kappa_\lambda) = I'_\lambda(\kappa_\lambda,\omega) \tag{1}$$

The optical depth κ_λ depends on the local linear spectral absorption coefficient $a_\lambda(s)$ and the local spectral linear scattering coefficient, $\sigma_\lambda(s)$, and is defined by

$$\kappa_\lambda(s) = \int_{s^*=0}^{s} (a_\lambda + \sigma_\lambda)\, ds^* \tag{2}$$

where s is the distance from a boundary to the local position of interest. The linear spectral coefficients describe the magnitude of the logarithmic reduction in spectral intensity due to absorption and scattering, respectively.

The I'_λ is the *source function*, which defines the intensity in direction ω at a local position s arising from the emission of radiation by the medium, plus the intensity scattered into the directon ω at the local position due to incoming intensity from all directions. The source function is defined by

$$I'_\lambda(\kappa_\lambda,\omega) = (1-\Omega_\lambda) i'_{\lambda b}(\kappa_\lambda) + \frac{\Omega_\lambda}{4\pi} \int_{\omega_i=4\pi} i'_\lambda(\kappa_\lambda,\omega)\phi(\lambda,\omega,\omega_i)\, d\omega_i \tag{3}$$

Here, $\Omega_\lambda = \sigma_\lambda/(\sigma_\lambda + a_\lambda)$ is the albedo, and ϕ is the scattering phase function, which defines the intensity incident from direction ω_i that is scattered into direction ω. Note that the term $i'_{\lambda b}$, the local blackbody intensity, depends explicitly upon local temperature of the medium, which is normally not given in engineering radiation problems; rather, it is the unknown of interest.

The intensity in equation (1) is both spectrally and directionally dependent, and the albedo is also spectrally dependent. The differential RTE can be formally integrated by using an integrating factor to give the *integrated form* of the RTE, which describes the intensity of radiation at some optical depth κ_λ in the medium in terms of the intensity reaching that position from other locations κ^*_λ in the medium and from the medium boundary at $\kappa_\lambda = 0$. Its form is

$$i'_\lambda(\kappa_\lambda) = i'_\lambda(0)\exp(-\kappa_\lambda) + \int_0^{\kappa_\lambda} I'_\lambda(\kappa_\lambda,\omega)\exp[-(\kappa_\lambda - \kappa^*_\lambda)]\, d\kappa^*_\lambda \tag{4}$$

The local divergence of the radiative flux can be determined from the local intensity (if it is assumed, as is usually the case, that the scattering phase function ϕ is independent of the direction of incidence ω_i) by the relation

$$\nabla \cdot q_r = \int_{\lambda=0}^{\infty} a_\lambda(\lambda)\left[4\pi i'_{\lambda b}(\lambda) - \int_{\omega=0}^{4\pi} i'_\lambda(\lambda,\omega,\kappa_\lambda)\, d\omega\right] d\lambda \tag{5}$$

For most engineering problems that include radiation, it is necessary to solve an energy conservation relation that explicitly provides the local temperature. The form of this relation depends on the particular forms of energy that must be treated in a given problem, but it can be written for a one-component fluid in the general form

$$\rho\frac{Dh}{D\tau} = \frac{DP}{D\tau} + \nabla\cdot(k\nabla T - q_r) + q''' + \Phi \tag{6}$$

Here, the term $\nabla \cdot q_r$ represents the divergence of the radiative flux, which must be found by use of equation (5). The form $(D/D\tau)$ represents the substantial derivative. The term $\rho(Dh/D\tau)$ represents contributions due to convection, $DP/D\tau$ expansion work, $\nabla \cdot k\nabla T$ conduction, q''' internal generation, and Φ is the dissipation function. Some, none, or all of these terms may be present in a given radiation problem.

The fact that the radiative flux divergence depends upon the temperature at each point throughout the medium and at the boundaries through equations (4) and (5), and that this temperature distribution is the objective of solving equation (6), is what makes these problems challenging. The problems are always implicit in temperature, and therefore require iterative solution unless the temperature distribution is specified.

Present Methods of Choice

A survey of the literature over the past few years plus discussions with other workers in the field show that some methods are receiving much attention, while others that appeared promising at one time have fallen out of favor. In some cases, extension of methods that were quite easy to apply in one-dimensional geometries has proven difficult or intractable in two and three dimensions. For other methods, the addition of important effects, such as anisotropy, nonuniform properties, or spectral effects, has proven to be the difficulty.

The following methods are attracting interest at present:

P-N Methods. The use of expansions of the local intensity in terms of spherical harmonics, with truncation to N terms in the series and substitution into the moments of the differential form of the equation of transfer, leads to the so-called *P-N* approximation. In general, the higher the value of N, the better

Downloaded 16 Dec 2010 to 193.140.21.150. Redistribution subject to ASME license or copyright; see http://www.asme.org/terms/Terms_Use.cfm

will be the agreement with exact solutions. When $N=1$, this method is also called the differential approximation.

Usually, odd expansions (P-1, P-3, etc.) are used in the P-N method, for two reasons. First, the even terms are difficult to incorporate into useful engineering boundary condition formulations (Ratzel, 1981). The odd-order expansions work well in the so-called Marshak boundary conditions (Marshak, 1946), which have a physical interpretation in terms of the net boundary radiative flux for first order terms. Second, for one- and two-dimensional problems in many geometries, it is found that second-order terms are negligible or drop out of the formulation of the radiative transfer equation or its moments, indicating that second-order expansions often will provide only marginal increases in accuracy over first-order solutions.

Even-order expansions can be carried out if the boundary condition formulations proposed by Mark (1945) or their modified version used by Shokair and Pomraning (1981) are used. As expected, however, Shokair and Pomraning found that second order expansions provide little increase in accuracy over first-order.

According to Davison (1958), for higher order expansions ($N>7$), the Mark conditions provide better accuracy than the Marshak conditions. However, unless only the intensity of radiation is of interest in a particular problem, the use of expansions of order $N>3$ becomes very difficult. Since the intensity itself is seldom of interest in engineering radiative transfer problems (because the flux or its divergence is needed in the energy equation), the Marshak conditions are used most generally in engineering formulations.

The P-N method is now used widely because the differential form of the resulting transfer equations makes them compatible with the gridding requirements of the energy and fluid-mechanics equations often present in the numerical formulation of a given problem. It has usually been found that $N=3$ provides good accuracy in one-, two-, and three-dimensional problems (Higenyi, 1979; Bayazitoglu and Higenyi, 1979; Ratzel, 1981; Menguc, 1985; Menguc and Viskanta, 1985), while going to $N=5$ provides little additional increase in accuracy (Menguc and Viskanta, 1982).

Extension of the P-N method to include anisotropic scattering has made it useful in modeling combustion systems using coal, where anisotropic scattering is an important factor. Menguc (1985) used the delta-Eddington phase function in a P-3 solution in three dimensions.

Two-Flux and Discrete Ordinate Methods. The two-flux method is based on a simple physical model in which the positive-direction and negative-direction radiative intensity are each assumed isotropic over their respective hemisphere of solid angles. Anisotropic scattering can be considered, but is used as an integrated average fraction for forward and backscattering. The method works well in one-dimensional systems, where it is simple to apply. It has been used in analysis of packed beds (Brewster and Tien, 1982; Brewster, 1986); radiative transfer through fibers and powders (Wang and Tien, 1983; Tong and Tien, 1983); combustion in composite solids (Brewster and Patel, 1987); and porous layers with penetrating flow and an external radiation source (Lee and Howell, 1986). Viskanta (1982) has reviewed the pertinent literature on the two-flux model through 1982.

When the solid angles about a location are divided into more than the two directions with uniform intensities used in the two-flux method, the method is known as the multi-flux, discrete ordinate, or S_n method (Chandrasekhar, 1960; Lathrop, 1966). Fiveland (1984, 1987) has developed and implemented the discrete ordinate method as part of a general code for the analysis of heat transfer in coal-fired furnaces. Menguc and Viskanta (1987) present a comprehensive review of recent work using the method.

Finite Element Methods. Finite element solutions (Sokmen and Razzaque, 1987; Razzaque et al., 1983, 1984; Chung and Kim, 1984; Wu and Ferguson, 1981; Fernandes et al., 1981; Nice, 1983) have been applied to the nonlinear combined-mode problems of conduction and/or convection with radiation, including scattering and both known temperature and known heat flux boundary conditions. Most of these solutions have used the Galerkin finite element method. The finite element method in principle gives exact solutions within the errors introduced by the numerical solution itself; i.e., no approximations need be made in the formulation of a problem. Each finite element of the medium volume can have its temperature (or the fourth power of its temperature) described in terms of various degrees of accuracy. If each element is taken to be isothermal, then the method is equivalent to a zoning technique. Usually, the elements in two-dimensional problems have their temperature described by biquadratic functions, which allow a continuous temperature profile to be prescribed in the medium by matching the element boundary temperatures to the temperatures at the boundaries of adjacent elements. Higher order functions for the temperatures allow matching of temperature slopes at the element boundaries as well.

Sokmen and Razzaque (1987) and Chung and Kim (1984) have included isotropic scattering in their analysis of two-dimensional systems, and Sokmen and Razzaque also were able to include known-heat-flux boundary conditions in their analysis of enclosures with absorbing-emitting-scattering conducting media.

Much remains to be done to exploit the finite element approach. The method offers the possibility of high accuracy and a built-in match of the numerical grids for the radiation field and the energy equation. However, most solutions to date have used large grid size, because computer running time for this method tends to be long, especially for problems in which the conduction is relatively small in comparison with radiation. If a creative way can be found to use the generated temperature profiles within the individual elements to carry out analytically all or part of the radiative field integrals, the method could be greatly speeded up and perhaps used to develop radiative transfer subroutines to existing thermal analysis programs. Perhaps this can be done by the use of a partial integration of the general form of the integrals followed by numerical evaluation of the remaining simplified form.

Tan (1988) has proposed and applied the product-integration method (Baker, 1977) to radiative transfer problems. This approach is closely related to the finite element method but reduces the dimension of the required integrations, thus significantly reducing required computation time. This reduction occurs because for a given degree of approximation of the temperature (i.e., constant, linear, binomial, etc.) within each of n finite volume or surface elements, the number of calculations in zonal or finite element approaches increases as n^2, while in the product-integration method it increases as n. For example, Tan was able to carry out analysis of a square enclosure divided into 8×8 volume elements on an IBM XT computer, while the finite element analysis used by Razzaque et al. (1983, 1984) was limited to 4×4 elements by computer time requirements on a CDC Cyber system. Tan included linear-anisotropic scattering effects in analysis of a two-dimensional emitting-absorbing-scattering medium. This approach appears to hold great promise.

Zoning Method. Considerable literature continues to appear that is based on the zoning method, or that extends its capabilities. Naraghi and Chung (1985) developed an explicit matrix formulation for the zoning method that significantly reduces the programming necessary for computer solution. Larsen and Howell (1986) derived a method based on the same assumptions used by Hottel. Their method uses "exchange

Downloaded 16 Dec 2010 to 193.140.21.150. Redistribution subject to ASME license or copyright; see http://www.asme.org/terms/Terms_Use.cfm

factors," which are physically measurable quantities related to radiative exchanges among surface and volume elements. These appear in the analysis in place of the "exchange areas" used in the zoning method, which can only be computed. They show the mathematical relation between exchange factors and exchange areas. Liu and Howell (1987) then measured exchange factors using a scale model of an enclosure filled with a near-isotropically scattering medium, and compared radiative transfer results with those calculated by the zoning method. Their approach allows treatment of enclosures that are not limited to rectangular or cylindrical shapes. The required experimental measurements, however, are quite tedious.

Naraghi et al. (1987) developed a continuous exchange factor method that improves the accuracy of the zoning method, but was difficult to program and execute. Naraghi (1988) has proposed a unified matrix formulation that reduces the computational time of the earlier work. The exchange factors defined in the work by Naraghi et al. (1987, 1988) differ from those used by either Hottel and Sarofim (1967) or Larsen and Howell (1985). In Larsen's work, the factors are defined for the absorbing medium in radiative equilbrium, and a separate gas–gas exchange factor is invoked to account for deviations from radiative equilibrium when energy sources or sinks are present in the absorbing/emitting medium. Gas-to-gas exchange for radiative equilibrium in the Larsen paper is thus included in the gas–surface, surface–gas, and surface–surface factors, and the gas–gas factor is not needed or calculated for such problems. In the Naraghi and Chung work, the gas–gas factor is used for all gas-to-gas exchange, whether the system is in radiative equilibrium or not. The original Hottel formulation, Larsen's work, and the work by Naraghi et al. (1987, 1988) each present different mathematical and, to some extent, physical interpretations of the transfer mechanism. There are probably other formulations that could be used as well. Each of the methods described has computational advantages in certain situations.

Sowell and O'Brien (1972), Vercammen and Froment (1980), and Larsen and Howell (1986) have all presented methods for normalizing and smoothing exchange areas so that round-off, truncation, or other errors in individually computed or measured values obey the required conservation relations. Sowell and O'Brien give a methodology for using the conservation relations on exchange areas, defined as

$$(4aV)_\gamma = \sum_{i=1}^{N} \overline{g_\gamma s_i} + \sum_{\mu=1}^{\Gamma} \overline{g_\gamma g_\mu} \tag{7}$$

$$A_i = \sum_{j=1}^{N} \overline{s_i s_j} + \sum_{\gamma=1}^{\Gamma} \overline{s_i g_\gamma} \tag{8}$$

to evaluate the $M=N+\Gamma$ exchange areas from the unique $M(M+1)/2$ exchange areas that must be specified after reciprocity is invoked. Here, $\overline{s_i s_j}$, $\overline{s_i g_\gamma}$, $\overline{g_\gamma s_j}$, and $\overline{g_\gamma g_\mu}$ are the surface-to-surface, surface-to-gas, gas-to-surface, and gas-to-gas exchange areas, respectively. This method assures that the set of exchange factors thus found will satisfy equations (7) and (8); however, if the unique factors used in the method have any computation or round-off errors, then there is no guarantee that the individual factors in the calculation are correct. Vercammen and Froment (1980) use a regression technique to smooth the factors. Larsen and Howell (1986) invoke error minimization through the method of Lagrangian multipliers using equations (7) and (8) as constraints.

Siddall (1986) presents a method for accurate calculation of direct exchange areas in rectangular geometries by a transformation that reduces the order of the integrations normally involved to a single numerical integration. He states that five-figure accuracy is readily obtained. Edwards and Balakrishnan (1972) present simplified expressions for exchange areas, while Rasmussen (1986) presents a fast approximate method of determining exchange areas between zones of finite size by formulating a distance correction between zone centers that is used in the element-to-element expressions.

Smith et al. (1981) and Farag and Allam (1981) have presented recent work on the "sum of gray gases" approach to incorporating spectral effects into the zone method. Steward and Kocaefe (1986) have used band emission data to generate total gas emittance and absorptance values for carbon dioxide, water vapor, and their mixtures, and provide algebraic expressions for these properties as functions of the temperature, pressure, and path length. Skocypec and Buckius (1984) have presented a method for determining the total emittance of a mixture of emitting gases and scattering particles, using wide-band models for the gas emittance. Goodwin and Ebert (1987) questioned the results presented by Skocypec and Buckius, and presented an alternative method based on individual spectral bands. The latter paper led to a lively debate (Skocypec and Buckius, 1987; Self, 1987), with final agreement that the total emittance of an emitting gas containing scattering particles could be expressed as

$$\epsilon_\lambda = \epsilon_{\lambda,g} + C\epsilon_{\lambda,s} \tag{9}$$

where ϵ_λ is the emittance of the mixture, $\epsilon_{\lambda,g}$ is the emittance of the gas, $\epsilon_{\lambda,s}$ is the emittance of the scattering medium, and C is a multiplier.

Monte Carlo Methods. Sufficiently low computer costs will allow solution of almost any problem if even an inefficient method is available to model a given problem exactly. We have had such a method for a long time: The Monte Carlo method can in principle be programmed to include an exact simulation of all important physical processes. The sole remaining difficulty with Monte Carlo, given sufficiently fast and cheap computation capability, is the grid-size incompatibility problem, in that the computational element size required for statistical accuracy in the Monte Carlo solution may not be compatible with the grid size necessary for numerical solution of the energy equation. Given enough computer power, that problem too can be overcome by taking a sufficiently small Monte Carlo computation element size (with a resulting increase in the number of statistical simulations required for accuracy) to match other gridding needs. Of course, some elegant grid-matching procedures may also emerge that will make Monte Carlo the method of choice in the near term.

Reviews of the method are available (Howell, 1968; Halton, 1970; Haji-Sheikh, 1988). Recent work on reducing computation time includes that by Mishkin and Kowalski (1983), who used the transient form of the energy equation to predict a temperature field, and then used the predicted temperature field in a Monte Carlo evaluation of the radiation field. The radiative flux divergence from the Monte Carlo solution was then introduced into the energy equation at each succeeding time step, and the procedure was repeated until convergence at a steady-state solution.

Recent applications of the Monte Carlo method have appeared that exploit its flexibility and power to examine difficult problems. A few of these can be cited to give the overall flavor of these applications. Slater et al. (1982), Bernes (1979), Meier and Lee (1978), Katkovskii et al. (1983), and Vlasov (1979) all have used Monte Carlo approaches to solve problems in which the medium was not assumed to be in local thermodynamic equilibrium (LTE). Carter et al. (1978) used the method to include the effects of polarization on radiative transfer. Egan and Hilgeman (1978) examined the spectral reflectance of particulates. Dunn (1983) has applied the method to inhomogeneous media. Gupta et al. (1983) include anisotropic scattering in their Monte Carlo analysis of coal furnaces with fly-ash. Lewis and Miller (1984) and Meier et al.

Downloaded 16 Dec 2010 to 193.140.21.150. Redistribution subject to ASME license or copyright; see http://www.asme.org/terms/Terms_Use.cfm

(1978) present valuable information on Monte Carlo applications in scattering problems.

Some discussion of the possibilities for significant improvement in the calculation times for Monte Carlo solutions is presented later.

The Present: Emerging Directions

Radiation continues to emerge as an important and indeed necessary consideration in applications where it often was previously ignored. For example, turbine and diesel engines are approaching operating temperatures at which radiation must be explicitly treated (Menguc et al., 1985; Chang and Wang, 1987).

General combustion problems have attracted a major research effort, recently reviewed in detail by Viskanta and Menguc (1987) and, for the case of flames, by Faeth (1986). More specialized combustion systems are also being investigated in which radiation plays a primary role, such as in fluidized bed combustion (Brewster, 1986; Brewster and Tien, 1982) and combustion within highly porous foamed ceramics (Echigo et al., 1986; Chen et al., 1987; Tong et al., 1987; Yoshizawa et al., 1987).

Renewed interest in space power systems and the space station has also triggered interest in novel radiation problems, such as the use of radiative transfer from free flowing droplets of working fluid in a space power system to replace large space radiator assemblies (Siegel, 1987a, 1987b).

Echigo has exploited the idea of placing a highly emitting solid matrix (metallic screen or ceramic foam) into a flowing hot gas stream, thus converting a portion of the gas enthalpy into emitted radiation from the matrix. He has analyzed the application of this idea for recovering stack gas enthalpy in industrial furnaces (Echigo, 1982), combustion of materials with low energy content (Echigo et al., 1983; Yoshizawa et al., 1987), and for enhancing radiative transfer to water tubes in steam boilers (Echigo, 1985).

Much attention is being paid to treating anisotropic scattering because of the importance of this effect in atmospheric radiation transfer, furnaces with particulate matter (ash, soot) present, and other technologies. Almost without exception, a basic assumption in this work is that the individual particles scatter as if they were independent point scatterers; i.e., particle interactions do not affect the distribution of scattered intensity. The important papers by Tien and co-workers (Brewster and Tien, 1982; Cartigny et al., 1986; Yamada et al., 1986) definitively show the effect of wavelenth, particle number density and size, and particle scattering and absorption cross section, on the regions of dependent and independent scattering, and give confidence that the assumption of independent scattering is indeed justified in most (but not all) engineering situations. Buckius (1986) reviews much of the work that deals with the properties of scattering media, and outlines the scattering properties of various particles of regular and irregular shape for independent scattering.

Methods of solution that can incorporate anisotropic effects are being investigated and, at the same time, realistic scattering phase functions are being tried that will allow treatment of scattering without the complexity necessary if the complete Mie scattering phase functions are used. The delta-Eddington function (Joseph et al., 1976) and the Henyey–Greenstein approximation (Kamiuto, 1987; McKellar and Box, 1981) offer a reasonable degree of simplification while allowing good accuracy. The varous Dirac-delta phase function approximations have been reviewed by Crosbie and Davidson (1985). Lee and Buckius (1986) have shown that radiation scaling laws allow some anisotropic scattering problems to be reduced to, and solved as, nonscattering problems. Menguc and Viskanta (1986) have investigated radiative transfer in a cylindrical furnace by the P-3 method, including the effects of spectral absorption and anisotropic scattering (delta-Eddington) in the gas.

The interaction of turbulence with radiation in combustion is drawing attention. Gore et al., (1986, 1987) have examined the effect both experimentally and analytically for the case of a turbulent diffusion flame, with emphasis on finding how turbulence affects the emission of radiation from a flame. Significant enhancement (as much as 20 percent) over the emission predicted using mean properties was found for hydrogen/air flames when a stochastic turbulence model was invoked, and the predicted enhancement agreed with measurements. The inverse question of how much effect radiation has on the scale and intensity of turbulence in a flame has not been carefully investigated.

Fundamental studies of the nature of the radiative exchange process, and the implications of the Second Law of Thermodynamics when applied to radiative exchange, are drawing the attention of some researchers (Bejan, 1987; and Arpaci, in a series of papers including Arpaci (1987a, 1987b) and Arpaci and Selamet (1986)). Just where these studies will lead in terms of engineering applications is not yet clear, but they do give insight and unification to some puzzling results from earlier work that was carried out separately. For example, Arpaci (1987b) shows the relationship among the Rosseland, Eddington, and thin gas (Planck) mean absorption coefficients that arise in the various approximate forms of the equation of transfer, proceeding from a single general formulation based on the radiative stress tensor. Bejan uses a classical thermodynamic analysis of radiative exergy to show the possible work extraction from enclosed radiation under various constraints, and shows the interrelation of work by some earlier approaches to this problem by Petela (1964), Spanner (1964), and Jeter (1981).

Future Work

A few problems are not yet being widely addressed. For example, anisotropic scattering is universally treated as if the scattering were independent of incident angle. This is the case for many practical systems, such as those with particle suspensions, because the particles are randomly oriented even if individually they have a nonspherical form. However, in some important cases, such as in radiative transfer within fixed solid matrices such as foamed ceramics, the scattering material may have a fixed orientation. The scattering phase function then depends on the angle of incidence as well as the angle of reflection, lending a new degree of difficulty to the analysis of scattering. Methods for treating this situation have not been developed.

Numerical difficulties still exist in treating radiative transfer problems. Combustion problems present an energy equation that is extremely stiff, and in some cases the addition of radiation terms can exacerbate the problem, leading to slow or lack of convergence for these problems. Numerical techniques for rapid solution of this class of problem need development.

The burgeoning speed and capability of supercomputers, with their ability to use vector and parallel processing, may soon make many of the concerns about methods moot (Shih et al., 1986; Howell, 1985). Adaptation of radiative transfer methods to these new capabilities has just begun, and can be expected to have one of the major impacts on this field in the next few years. The analyst will need to choose the best methodology for multimode heat transfer calculations that takes advantage of parallel processing. One method of exploiting parallel processing is perhaps to solve the radiative transfer equation using an initial assumed temperature field on one processor while simultaneously solving the energy equation to compute the temperature field from an initial assumed radiation field on another. Then, the calculated

Downloaded 16 Dec 2010 to 193.140.21.150. Redistribution subject to ASME license or copyright; see http://www.asme.org/terms/Terms_Use.cfm

radiation field and temperature from each parallel path are traded and used as new initial guesses, and iteration proceeds until convergence. This could significantly reduce computation time.

Denning (1985) has reviewed the state of the art in parallel processing, and says that we are presently in *stage I* of its use. Present computers make parallel processing available by having their operating systems access more than one processor, so that successive tasks need now await completion of prior tasks, or by having multiple memory banks, or by the use of "vector pipelines." Newer machines, called *reduced instruction set computers*, or RISC's, are structured so that their compilers carefully analyze programs in a way that keeps the pipeline of instructions busy much of the time. Such methods are effectively invisible to the user, but result in much faster execution time.

To use the parallel processing capability efficiently, software must be structured in such a way as to make use of the inherent features of the parallel processing system. If the software is structured with linear commands, then much of the benefit of parallel processing may be lost. Even if the program is structured carefully, the software must have the capability of *microtasking*, i.e., telling the computer to access a parallel processor for a given task.

Stage II of the parallel processing evolution will make use of such advanced languages as parallel PASCAL (Reeves et al., 1980) or OCCAM, a derivative of PASCAL. These languages allow the structuring of programs so that the information required for continuation of a given calculation is supplied from a parallel processor when available, and the calculation proceeds. Such a language allows parallel processing even on separate machines, as long as a communication link is established.

Denning (1985) notes that, although these systems are well along in their development, their application to practical engineering computations has not been exploited. Also, the newer languages such as LISP and APL have not been structured internally to take full advantage of parallel processing, nor to allow discrete program parts, which Denning calls "chunks," to be processed independently and then rejoined. Such restructuring will be *stage III*, which Denning believes will lead in turn to *stage IV*, when program-user interaction will allow the program to structure itself into chunks automatically.

Arvind (1980) discusses the use of high-level dataflow programs to control the flow of individual calculations dynamically to parallel processors as a program is executed. He believes that existing programs of this type probably are not useful for the classes of calculation typically found in fluid mechanics (and radiative transfer). Rather, careful structuring by the programmer with static mapping of results into memory that can be accessed by parallel processors when information is needed may be most efficient.

Monte Carlo methods in particular stand to improve significantly in reduced computer time. The use of multiprocessor systems to handle the multiple path trees describing the distribution of radiation in complex systems should reduce the computing time by the number of parallel processors used. Lord et al. (1983) discuss some attempts to use vectorized Monte Carlo approaches in quantum field theory by Moriarity (1981) and by Barkai (1981), and describe these as not very successful in terms of reduced computation time in comparison with standard computation. Barkai and Moriarity (1982) are more positive about their work in a later report. Pawley and Dove (1983) report on the use of parallel processors for molecular dynamics calculations using Monte Carlo, and Genz (1982) applies parallel processing in the evaluation of multiple integrals, both with some success. The latter two are closely related to the needs of radiative transfer calculations.

As multiprocessor computers become widely available, other approaches will undoubtedly emerge.

Another relatively untouched tool in radiative transfer is the use of computer graphics. Emery et al. (1988) have used some elements of computer graphics in engineering configuration factor analysis. Some work on configuration factor analysis as applied to architectural lighting problems shows the potential for even more sophisticated approaches (Cohen and Greenberg, 1985; Goral et al., 1984; Nishita and Nakamae, 1985; Cohen et al., 1986). This work uses increasingly complex models of surface radiosity (in some recent work using nondiffuse reflectance models) to depict surface appearance graphically under varying conditions of illumination; it is a simple step to compute numerical values concurrently for configuration factors. All of the shading and blocking problems common to radiant exchange within a multisurfaced enclosure must be treated in these programs, and the visual representation of shading and blocking can be shown directly in color. Thus, confidence in the results is much greater than when a canned numerical program giving only tabular results is used. Also, this work has led to extensive re-examination of ray-tracing methods by the computer graphics community (Arvo and Kirk, 1987; Bentley, 1975; Cook et al., 1984; Fujimoto et al., 1986; Fussell and Subramanian, 1988; Glassner, 1984; Kaplan, 1985; Kay and Kajiya, 1986; Maxwell et al., 1986), which may lead to efficient new tools for configuration factor analysis or other uses in radiative transfer. Although the work to date has concentrated on surface-to-surface exchange, some initial work is being directed to systems with participating media (Rushmeier and Torrance, 1987; Nishita et al. 1987).

Some Observations

Based on the above exposition of the growth of capability in the computation of radiative transfer, some observations may be in order. First, the community of workers in radiative transfer labors in two fairly distinct areas. These are the *development of more efficient methods* for treating radiative transfer within the context of engineering heat transfer problems, and the *application* of existing methods to technical problems of immediate interest.

Those working on method development often start with applications to problems with little technical interest, such as the ubiquitous solution of the heat transfer and temperature profile in a uniform gray gas in radiative equilibrium between infinite parallel plates at fixed temperatures. This may have had merit in the past, because few accurate methods existed to treat even such a simple geometry. Presently, however, the problem has little intrinsic interest, since the real questions about a new method are these: Can it be applied in multidimensional problems? Will it work well if the properties of the attenuating medium are nonuniform in space? Does the method lend itself to a match with the gridding requirements of related conduction/convection equations? Can spectral properties be easily incorporated? Can anisotropic scattering be treated?

If a new method cannot be shown to have advantages over existing techniques in at least one of these areas, then publication of another one-dimensional gray-gas solution is pointless, even if the mathematical technique is novel or elegant. No one will bother to use elegant solutions that cannot be applied to problems of technical interest.

Looking at the progress in engineering radiative heat transfer over the past half-century, as we have progressed from the treatment of simple enclosures with an isothermal absorbing-emitting medium of uniform composition, to the present day, when we can treat multidimensional enclosures with an absorbing-emitting-anisotropically scattering medium with spectrally dependent properties that vary within the

Downloaded 16 Dec 2010 to 193.140.21.150. Redistribution subject to ASME license or copyright; see http://www.asme.org/terms/Terms_Use.cfm

enclosure (with, it must be admitted, some considerable difficulty), we can see the steady, continuing progress. New methods, computational tools, and applications continue to appear, and the study of radiation heat transfer remains a robust area for both applications and research.

References

Arpaci, V. S., 1987a, "Radiative Entropy Production—Lost Heat Into Entropy," *Int. J. Heat Mass Transfer*, Vol. 30, No. 10, pp. 2115–2124.

Arpaci, V. S., 1987b, "Hooksean and Stokesean Implications of the Radiative Stress," in: *Radiation, Phase Change Heat Transfer, and Thermal Systems*, Y. Jaluria, V. P. Carey, W. A., Fiveland, and W. Yuen, eds., ASME, HTD-Vol. 81, pp. 1–5.

Arpaci, V. S., and Selamet, A., 1986, "Radiative Entropy Production," *Proc. 8th Int. Heat Tansfer Conf.*, Vol. 2, C. L. Tien, V. P. Carey, and J. K. Farrell, eds., pp. 729–734.

Arvind, 1980, "Decomposing a Program for Multiple Processor Systems," *Proc. 1980 Conf. on Parallel Processing*, IEEE Computer Soc., New York, pp. 5–6.

Arvo, J., and Kirk, D., 1987, "Fast Ray Tracing by Ray Classification," *Computer Graphics*, Vol. 21, No. 4, pp. 269–278.

Baker, C. T. H., 1977, *The Numerical Treatment of Integral Equations*, Clarendon Press, Oxford.

Barkai, D., 1981, *Vectorizing the Monte Carlo*, Control Data, Ltd., London.

Barkai, D., and Moriarity, K. J. M., 1982, "Vectorizing the Monte Carlo Algorithm for Lattice Gauge Theory Calculations on the CDC Cyber 205," *Computer Phys. Comms.*, Vol. 26, pp. 349–352.

Barr, E. S., 1960, "Historical Survey of the Early Development of the Infrared Spectral Region," *Am. J. Phys.*, Vol. 28, No. 1, pp. 42–54.

Bayazitoglu, Y., and Higenyi, J., 1979, "Higher Order Differential Equations of Radiative Transfer: P_3 Approximation," *AIAA J.*, Vol. 17, No. 4, pp. 424–431.

Bejan, A., 1987, "Unification of Three Different Theories Concerning the Ideal Conversion of Enclosed Radiation," ASME JOURNAL OF HEAT TRANSFER, Vol. 109, No. 1, pp. 46–51.

Bentley, J. L., 1975, Multidimensional Binary Search Trees Used for Associative Searching," *Communications of the ACM*, Vol. 18, No. 9.

Bernes, C., 1979, "A Monte-Carlo Approach to Non-LTE Radiative Transfer Problems," *Astron. Astrophys.*, Vol. 73, pp. 67–73.

Bohr, N., 1913, *Phil. Mag.*, Vol. 26, p. 1.

Brewster, M. Q., 1986, "Effective Absorptivity and Emissivity of Particulate Media With Application to a Fluidized Bed," ASME JOURNAL OF HEAT TRANSFER, Vol. 108, No. 3, pp. 710–712.

Brewster, M. Q., and Patel, R., 1987, "Selective Radiative Preheating of Aluminum in Composite Solid Propellant Combustion," ASME JOURNAL OF HEAT TRANSFER, Vol. 109, No. 1, pp. 179–184.

Brewster, M. Q., and Tien, C. L., 1982, "Radiative Transfer in Packed Fluidized Beds: Dependent Versus Independent Scattering," ASME JOURNAL OF HEAT TRANSFER, Vol. 104, No. 4, pp. 573–579.

Buckius, R. O., 1986, "Radiative Heat Transfer in Scattering Media: Real Property Contributions," *Proc. 7th Int. Heat Transfer. Conf.*, Vol. 1, Munich, pp. 141–150.

Carter, L. L., Horak, H. G., and Sandford, M. T., III, 1978, "An Adjoint Monte Carlo Treatment of the Equations of Transfer for Polarized Light," *J. Comp. Phys.*, Vol. 26, pp. 119–128.

Cartigny, J. D., Yamada, Y., and Tien, C. L., 1986, "Radiative Transfer With Dependent Scattering by Particles: Part 1—Theoretical Investigation," ASME JOURNAL OF HEAT TRANSFER, Vol. 108, No. 3, pp. 608–613.

Chang, S. L., and Wang, C. S., 1987, "Thermal Radiation and Fuel Spray Group Combustion in Diesel Engines," in: *Radiation, Phase Change Heat Transfer, and Thermal Systems*, Y. Jaluria, V. P. Carey, W. A. Fiveland, and W. Yuen, eds., ASME HTD-Vol. 81, p. 34.

Chandrasekhar, S., 1960, *Radiative Transfer*, Dover, New York.

Chandrasekhar, S., 1944, *Astrophys. J.*, Vol. 100, p. 76.

Chen, Y.-K., Matthews, R. D., and Howell, J. R., 1987, "The Effect of Radiation on the Structure of Premixed Flame Within a Highly Porous Inert Medium," in: *Radiation, Phase Change Heat Transfer, and Thermal Systems*, Y. Jaluria, V. P. Carey, W. A. Fiveland, and W. Yuen, eds., ASME HTD-Vol. 81, pp. 35–41.

Christiansen, C., 1883, "II. Absolute Bestimmung des Emissions- and Absorptionsvermogens fur Warmes," *Ann. Phys. Wied.*, Vol. 19, pp. 267–283.

Chung, T. J., and Kim, J. Y., 1984, "Two-Dimensional Combined-Mode Heat Transfer by Conduction, Convection and Radiation in Emitting, Absorbing and Scattering Media—Solution by Finite Elements," ASME JOURNAL OF HEAT TRANSFER, Vol. 106, No. 2, pp. 448–452.

Cohen, M. F., Greenberg, D. P., Immel, D. S., and Brock, P. J., 1986, "An Efficient Radiosity Approach for Realistic Image Synthesis," *IEEE Computer Graphics and Applications*, Vol. 6, No. 3, pp. 26–35.

Cohen, M. F., and Greenberg, D. P., 1985, "The Hemi-Cube: A Radiosity Solution for Complex Environments," *ACM Computer Graphics Proc. (1985)*, Vol. 19, No. 3, pp. 31–40.

Cook, R. L., Porter, T., and Carpenter, L., 1984, "Distributed Ray Tracing," *Computer Graphics*, Vol. 18, No. 3, pp. 137–145.

Crosbie, A. L., and Shrenker, R. G., 1985, "Multiple Scattering in a Two-Dimensional Rectangular Medium," *J. Quantitative Spectroscopy and Radiative Transfer*, Vol. 33, No. 2, pp. 101–125.

Crosbie, A. L., and Davidson, G. W., 1985, "Dirac-Delta Function Approximation for Radiative Transfer," *J. Quantitative Spectroscopy and Radiative Transfer*, Vol. 33, No. 4, pp. 391–409.

Crosbie, A. L., and Farrell, J. R., 1984, "Two-Dimensional Isotropic Scattering in a Finite Cylindrical Medium Exposed to Uniform Diffuse Radiation," *J. Quantitative Spectroscopy and Radiative Transfer*, Vol. 31, No. 5, pp. 397–416.

Crosbie, A. L., and Dougherty, R. L., "Two-Dimensional Radiative Transfer in a Cylindrical Geometry With Anisotropic Scattering," *J. Quantitative Spectroscopy and Radiative Transfer*, Vol. 25, No. 6, pp. 551–569.

Davison, B., 1958, *Neutron Transport Theory*, Clarendon Press, Oxford.

Denning, P. J., 1985, "The Science of Computing: The Evolution of Parallel Processing," *Am. Scientist*, Vol. 73, No. 5, pp. 414–416.

Dunn, W. L., 1983, "Inverse Monte Carlo Solutions for Radiative Transfer in Inhomogeneous Media," *J. Quantitative Spectroscopy and Radiative Transfer*, Vol. 29, No. 1, pp. 19–26.

Echigo, R., Yoshizawa, Y., Hanamura, K., and Tomimura, T., 1986, "Analytical and Experimental Studies on Radiative Propagation in Porous Media With Heat Generation," *Proc. 8th Int. Heat Transfer Conf.*, Vol. II, San Francisco, pp. 827–832.

Echigo, R., *1985*, "Radiative Heat Transfer Enhancement to a Water Tube by Combustion Gases in Porous Media," *Proc. Int. Conf. on Heat Transfer*, Vol. 3, Beijing, pp. 186–193.

Echingo, R., Kurusu, M., Ichimiya, K., and Yoshizawa, Y., 1983, "Combustion Augmentation of Extremely Low Calorific Gases (Application of the Effective Energy Conversion Method From Gas Enthalpy to Thermal Radiation)," *Proc. 1983 ASME/JSME Thermal Engineering Joint Conference*, Vol. IV, Honolulu, pp. 99–103.

Echigo, R., 1982, "Effective Energy Conversion Method Between Gas Enthalpy and Thermal Radiation and Application to Industrial Furnances," *Proc. 7th Int. Heat Transfer Conf.*, Vol. VI, Munich, pp. 361–366.

Edwards, D. K., and Balakrishnan, A., 1973, "Thermal Radiation by Combustion Gases," *Int. J. Heat Mass Transfer*, Vol. 16, No. 1, pp. 25–40.

Edwards, D. K., and Balakrishnan, A., 1972, "Volume Interchange Factors for Nonhomogeneous Gases," ASME JOURNAL OF HEAT TRANSFER, Vol. 94, No. 2, pp. 181–187.

Edwards, D. K., 1968, "Molecular Gas Band Radiation," in: *Advances in Heat Transfer*, T. F. Irvine, Jr., and J. P. Hartnett, eds., Academic Press, New York, Vol. 12, pp. 115–193.

Edwards, D. K., and Menard, W. A., 1963, "Comparison of Models for Correlation of Total Band Absorption," *Applied Optics*, Vol. 3, p. 621.

Egan, W. G., and Hilgeman, T., 1978, "Spectral Reflectance of Particulate Materials: A Monte Carlo Model Including Asperity Scatterng," *Applied Optics*, Vol. 17, No. 2, pp. 245–252.

Einstein, A., 1916, "Emission and Absorption of Radiation According to the Quantum Theory," *Verh. Dtsch. Phys. Ges.*, Vol. 18, pp. 318–323.

Einstein, A., 1917, "On the Quanta Theory of Radiation," *Phys. Z.*, Vol. 18, pp. 121–128.

Emery, A. F., Johansson, O., Lobo, M., and Abrous, A., 1988, "A Comparative Study of Methods for Computing the Diffuse Radiation Viewfactors for Complex Structures," *AIAA/ASME/ASCE/ASH 29th SDM Conference*, AIAA Paper No. 88-2223.

Faeth, G. M., 1986, "Heat and Mass Transfer in Flames," *Proc. 7th Int. Heat Transfer Conf.*, Vol. 1, Munich, pp. 151–160.

Farag, I. H., and Allam, T. A., 1981, "A Mixed Gray-Gas Model to Calculate Water Vapor Standard Emissivities," ASME Paper No. 81-HT-63.

Fernandes, R., Francis, J., and Reddy, J. N., 1981, "A Finite Element Approach to Combined Conductive and Radiative Heat Transfer in a Planar Medium," in: *Heat Transfer and Thermal Control*, A. L. Crosbie, ed., AIAA, New York, pp. 93–109.

Fiveland, W. A., 1987, "Discrete Ordinate Methods for Radiative Heat Transfer in Isotropically and Anisotropically Scattering Media," ASME JOURNAL OF HEAT TRANSFER, Vol. 109, No. 3, pp. 809–812.

Fiveland, W. A., 1984, "Discrete-Ordinates Solutions of the Radiative Transport Equation for Rectangular Enclosures," ASME JOURNAL OF HEAT TRANSFER, Vol. 106, No. 4, pp. 699–706.

Fujimoto, A., Takayuki, T., and Iwata, K., 1986, "ARTS: Accelerated Ray-Tracing System," *IEEE Computer Graphics and Applications*, Vol. 6, No. 4, pp. 16–26.

Fussell, D., and Subramanian, K. R., 1988, "Fast Ray-Tracing Using *k-d* Trees," paper submitted to SIGGRAPH '88.

Genz, A. C., 1982, "Numerical Multiple Integration of Parallel Computers," *Computer Phys. Comms.*, Vol. 26, pp. 349–352.

Glassner, A. S., 1984, "Space Subdivision for Fast Ray Tracing," *IEEE Computer Graphics and Applications*, Vol. 4, No. 10, pp, 15–22.

Goodwin, D. G., and Ebert, J. L., 1987, "Rigorous Bounds on the Radiative Interaction Between Real Gases and Scattering Particles," *J. Quantitative Spectroscopy and Radiative Transfer*, Vol. 37, No. 5, pp. 501–508.

Goody, R. M., 1964, *Atmospheric Radiation: Part 1—Theoretical Basis*, The Clarendon Press, Oxford.

Goral, C. M., Torrance, K. E., Greenberg, D. P., and Battaile, B., 1984, "Modeling the Interaction of Light Between Diffuse Surfaces," *ACM Computer Graphics (Proc. 1984)*, Vol. 18, No. 3, pp. 213–222.

Gore, J. P., Jeng, S.-M., and Faeth, G. M., 1986, "Spectral and Total Radia-

Downloaded 16 Dec 2010 to 193.140.21.150. Redistribution subject to ASME license or copyright; see http://www.asme.org/terms/Terms_Use.cfm

tion Properties of Turbulent Carbon Monoxide/Air Diffusion Flames," AIAA Paper No. 86-0294.

Gore, J. P., and Jeng, S.-M., and Faeth, G. M., 1987, "Spectral and Total Radiation Properties of Turbulent Hydrogen Air Flames," ASME *Journal of Heat Transfer*, Vol. 109, No. 1, pp. 165–171.

Gupta, R. P., Wall, T. F., and Truelove, J. S., 1983, "Radiative Scatter by Fly Ash in Pulverized-Coal-Fired Furnaces: Application of the Monte Carlo Method to Anisotropic Scatter," *Int. J. Heat Mass Transfer*, Vol. 26, No. 11, pp. 1649–1660.

Haji-Sheikh, A., 1988, "Monte Carlo Methods," in: *Handbook of Numerical Heat Transfer*, W. J. Minkowycz, E. M. Sparrow, R. H. Pletcher, and G. E. Schneider, eds., Wiley, New York, Chap. 16.

Halton, J. H., "A Retrospective and Prospective Review of the Monte Carlo Method," *SIAM Review*, Vol. 12, No. 1, pp. 1–63.

Herschel, W. 1800, "Investigation of the Powers of the Prismatic Colours to Heat and Illuminate Objects: with Remarks, That Prove the Different Refrangibility of radiant Heat. To which is added, an Inquiry into the Method of viewing the Sun advantageously, with Telescopes of large Apertures and high magnifying Powers," *Philos. Trans.*, Vol. MDCCC, pp. 255–326.

Higenyi, J., 1979, "Higher Order Differential Approximation of Radiative Energy Transfer in a Cylindrical Gray Medium," PhD Dissertation, Rice University.

Hottel, H. C., and Sarofim, A. 1967, *Radiative Transfer*, McGraw-Hill, New York.

Hottel, H. C., and Cohen, E. S., 1958, "Radiant Heat Exchange in a Gas Filled Enclosure: Allowance for Non-uniformity in Temperature," *AIChE J.*, Vol. 4, No. 1, pp. 3–14.

Hottel, H. C., 1954, "Radiant Heat Transmission, " in: *Heat Transmission*, W. H., McAdams, ed., 3rd ed., McGraw-Hill, New York, Chap. 4.

Hottel, H. C., and Keller, J. D., 1933, "Effect of Reradiation on Heat Transmission in Furnaces and Through Openings," *Trans. ASME*, Vol. 55, pp. 39–49.

Hottel, H. C., 1931, "Radiant Heat Transmission Between Surfaces Separated by Non-absorbing Media," *Trans. ASME*, Vol. 53, pp. 265–273.

Howell, J. R., 1986, "Improving the Monte Carlo Method for Radiative Transfer by the Use of Parallel Processors," *Proc. Heat Transfer in Thermal Systems Seminar, Phase ii*, National Cheng Kung University, Taiwan, pp. 53–58.

Howell, J. R., 1968, "Application of Monte Carlo to Heat Transfer Problems," in: *Advances in Heat Transfer*, J. P. Hartnett and Tom Irvine, eds., Vol. 5, Academic Press, New York.

Jeter, S. M., 1981, "Maximum Conversion Efficiency for the Utilization of Direct Solar Energy," *Solar Energy*, Vol. 26, No. 3, pp. 231–236.

Joseph, J. H., Wiscombe, W. J., and Weinman, J. A., 1976, "The Delta-Eddington Approximation for Radiative Heat Transfer," *J. Atm. Sci.*, Vol. 33, pp. 2452–2459.

Kaplan, M. R., 1985, "The Uses of Spatial Coherence in Ray Tracing," *ACM SIGGRAPH Course Notes 11.*

Kamiuto, K., 1987, "Study of the Henyey—Greenstein Approximation to Scattering Phase Functions," *J. Quantitative Spectroscopy and Radiative Transfer*, Vol. 37, No. 4, pp. 411–414.

Katkovskii, L. V., Khodyko, Yu. V., and Leparskaya, L. V., 1983, "Monte Carlo Calculation of Outgoing Radiation in Vibrational-Rotational Band of CO from a Cylindrical Supersonic Molecular Gas Jet in the Absence of Local Thermodynamic Equilibrium," trans. from *Zh. Prikladnoi Spectroskopii*, Vol. 38, No. 2, pp. 256–262.

Kay, T. L., and Kajiya, J. T., 1986, "Ray Tracing Complex Scenes," *Computer Graphics*, Vol. 20, No. 4, pp. 269–278.

Larsen, M. E., and Howell, J. R., 1986, "Least-Squares Smoothing of Direct-Exchange Areas in Zonal Analysis," ASME JOURNAL OF HEAT TRANSFER, Vol. 108, No. 1, pp. 239–242.

Larsen, M. E., and Howell, J. R., 1985, "The Exchange Factor Method: An Alternative Zonal Formulation of Radiating Enclosure Analysis," ASME JOURNAL OF HEAT TRANSFER, Vol. 107, No. 4, pp. 936–942.

Lathrop, K. D., 1966, "Use of Discrete Ordinate Methods for Solution of Photon Transport Problems," *Nucl. Sci. and Engineering*, Vol. 24.

Lee, H., and Buckius, R., 1986, "Combined Mode Heat Transfer Utilizing Radiating Scaling," ASME JOURNAL OF HEAT TRANSFER, Vol. 108, No. 3, pp. 626–631.

Lee, K.-B., and Howell, J. R., 1986, "Effect of Radiation on the Laminar Convective Heat Transfer Through a Layer of Highly Porous Medium," in: *Radiation in Energy Systems*, T. Tong and M. Modest, eds., ASME HTD-Vol. 55, pp. 51–59.

Lewis, E. E., and Miller, W. F., Jr., 1984, *Computational Methods of Neutron Transport*, Wiley, New York.

Lin, J.-D., 1987, "Exact Formulation for Radiative Transfer in an Arbitrary Geometry Exposed to Radiation," *J. Quantitative Spectroscopy and Radiative Transfer*, Vol. 37, No. 6, pp. 591–601.

Liu, H.-P., and Howell, J. R., 1987, "Measurement of Radiation Exchange Factors," ASME JOURNAL OF HEAT TRANSFER, Vol. 109, No. 2, pp. 470–477.

Lord, N. W., Girogosian, P. A., Ouellette, R. P., Clerman, R. J., and Cheremisinoff, P. N., 1983, *Advanced Computers and Parallel Processors*, Ann Arbor Science Publishers, Ann Arbor, MI.

Love, T. J., 1968, *Radiative Heat Transfer*, Charles E. Merrill, Columbus, OH.

Ludwig, C. B., Malkmus, W., Reardon, J. E., and Thomson, J. A. L., 1973, *Handbook of Infrared Radiation From Combustion Gases*, R. Goulard and J. A. L. Thomson, eds., NASA SP-3080, Washington, D. C.

Lummer, O., and Pringsheim, E., 1897, *Ann. der Physik LXIII*, p. 395.

Lummer, O., and Pringsheim, E., 1899, *Verh. der Deutsch Phys. Ges.*

Lummer, O., and Pringsheim, E., 1901, *Ann. der Physik VI*, p. 192.

Marshak, R. E., 1946, "Note of the Spherical Harmonic Method as Applied to the Milne Problem for a Sphere," *Phys. Rev.*, Vol. 71, pp. 443–446.

Mark, J. C., 1945, *The Spherical Harmonic Method—Part I and II*, National Research Council of Canada, Atomic Energy Reports MT 92-1944 and MT 97-1945.

Maxwell, G. M., Bailey, M. J., and Goldschmidt, V. W., 1986, "Calculations of the Radiation Configuration Factors Using Ray Casting," *Computer Aided Design*, Vol. 18, pp. 371–379.

McKellar, B. H. J., and Box, M. A., 1981, "The Scaling Group of the Radiative Transfer Equation," *J. Atm. Sci.*, Vol. 38, pp. 1063–1068.

Meier, R. R., Lee, J.-S., and Anderson, D. E., 1978, "Atmospheric Radiation of Middle UV Radiation From an Internal Souce," *Applied Optics*, Vol. 17, No. 20, pp. 3216–3225.

Meier, R. R., and Lee, J.-S., 1978, "A Monte Carlo Study of Frequency Redistribution in an Externally Excited Medium," *Astrophys. J.*, Vol. 219, pp. 262–273.

Menguc, M. P., and Viskanta, R., 1986, "An Assessment of Spectral Radiative Heat Transfer Predictions for a Pulverized Coal-Fired Furnace," *Proc. 8th Int. Heat Transfer Conf.*, C. L. Tien, V. P. Carey, and J. K. Farrell, eds., Vol. 2, pp. 815–820.

Menguc, M. P., Viskanta, R., and Ferguson, C. R., 1985, "Multidimensional Modeling of Radiative Heat Transfer in Diesel Engines," SAE Paper No. 850503.

Menguc, M. P., 1985, "Modeling of Radiative Heat Transfer in Multidimensional Enclosures Using Spherical Harmonics Approximation," PhD Thesis, Purdue University.

Menguc, M. P., and Viskanta, R., 1985, "Radiative Transfer in Three-Dimensional Enclosures Containing Inhomogeneous, Anisotropically Scattering Media," *J. Quantitative Spectrosc. and Radiat. Transfer*, Vol. 33, No. 6, pp. 533–549.

Menguc, M. P., and Viskanta, R., 1982, "Comparison of Radiative Transfer Approximations for Highly Forward Scattering Medium," ASME Paper No. 82-HT-17.

Miskin, M., and Kowalski, G., 1983, "Application of Monte Carlo Techniques to the Steady State Radiative and Conductive Heat Transfer Problem Through a Participating Medium," ASME Paper No. 83-WA/HT-27.

Moriarity, K. M., *Vectorizing the Monte Carlo*, Dept. of Mathematics, Royal Holloway College, Egham, Surrey, UK.

Naraghi, M. H. N., 1988, "On the Explicit Matrix Formulations for the Exchange Factor Methods," ASME JOURNAL OF HEAT TRANSFER, submitted.

Naraghi, M. H. N., and Chung, B. T. F., 1985, "A Unified Matrix Formulation for the Zone Method: A Stochastic Approach," *Int. J. Heat Mass Transfer*, Vol. 28, No. 2, pp. 245–251.

Naraghi, M. H. N., Chung, B. T. F. and Litkouhi, B., 1987, "A Continuous Exchange Factor Method for Radiative Exchange in Enclosures With Participating Media," presented at ASME/AIChE National Heat Transfer Conf., Pittsburgh.

Nishita, T., and Nakamae, E., 1985, "Continuous Tone Representation of Three-Dimensional Objects Taking Account of Shadows and Interreflections," *Computer Graphics*, Vol. 19, No. 3, pp. 23–30.

Nishita, T., Miyawaki, Y., and Nakamae, E., 1987, "A Shading Model for Atmospheric Scattering Considering Luminous Intensity Distribution of Light Sources," *Computer Graphics*, Vol. 21, No. 4, pp. 303–310.

Nobili, L., and Melloni, M., 1831, "New Experiments in Caloric Performed by Means of the Thermo-multiplier," *Am. J. Sci. and Arts*, Vol. 23, No. 1, pp. 185–190, (trans. from *Annales de Chim, et de Phys.*).

Nice, M. L., 1983, "Application of Finite Element Method to Heat Transfer in a Participating Medium," in: *Numerical Properties and Methodologies in Heat Transfer*, T. M. Shih, ed., Hemisphere, Washington, DC, pp. 497–514.

Pawley, G. S., and Dove, M. T., 1983, "Molecular Dynamics on a Parallel Computer," *Helvetica Physica Acta*, Vol. 56, pp. 583–592.

Petela, R., 1964, "Exergy of Heat Radiation," ASME JOURNAL OF HEAT TRANSFER, Vol. 86, No. 1, pp. 187–192.

Planck, M., 1959, *The Theory of Heat Radiation*, 2nd ed., M. Masius, translator, Dover Publications, New York.

Poljak, G., 1935, "Analysis of the Heat Exchange by Radiation Between Gray Surfaces by the Saldo-Method," *Tech. Phys. USSR*, Vol. 1, No. 5/6, pp. 555–590.

Ratzel, A. G., 1981, "P-N Differential Approximation for Solution of One- and Two-Dimensional Radiation and Conduction Energy Transfer in Gray Participating Media," PhD Dissertation, Department of Mechanical Engineering, The University of Texas, Austin, TX.

Rasmussen, N. B. K., 1986, "Radiant Heat Exchange Between Zone Elements: A Simplified Method," *Int. Comm. Heat Mass Transfer*, Vol. 13, pp. 335–347.

Razzaque, M. M., Klein, D. E., and Howell, John, R., 1983, "Finite Element Solution of Radiative Heat Transfer in a Two-Dimensional Rectangular Enclosure With Gray Participating Media," ASME JOURNAL OF HEAT TRANSFER, Vol. 105, No. 4, pp. 933–934.

Razzaque, M. M., Klein, D. E., and Howell, J. R., 1984, "Coupled Radiative and Conductive Heat Transfer in a Two-Dimensional Rectangular Enclosure With Gray Participating Media Using Finite Elements," ASME JOURNAL OF HEAT TRANSFER, Vol. 106, No. 3, pp. 613–619.

Reeves, A. P., Bruner, J. D., and Poret, M. S., 1980, "The Programming

Downloaded 16 Dec 2010 to 193.140.21.150. Redistribution subject to ASME license or copyright; see http://www.asme.org/terms/Terms_Use.cfm

Language Parallel PASCAL," *Proc. 1980 Conf. on Parallel Processing*, IEEE Computer Society, New York, pp. 5, 6.

Rushmeier, H. E., and Torrance, K. E., 1987, "The Zonal Method for Calculating Light Intensities in the Presence of a Participating Medium," *Computer Graphics*, Vol. 21, No. 4, pp. 293-302.

Schuster, A., 1905, *Astrophys, J.*, Vol. 21, p. 1

Schwarzschild, K., 1906, *Gottinger Nachrichten*, p. 41.

Self, S., 1987, "Comments on 'Rigorous Bounds on the Radiative Interaction Between Real Gases and Scattering Particles," *J. Quantitative Spectroscopy and Radiative Transfer*, Vol. 37, No. 5, pp. 513-515.

Shih, T.-M., et al., 1986, "Parallel Computations in Heat Transfer," *Num. Heat Transfer*, Vol. 9, pp. 639-662.

Shokair, I. R., and Pomraning, G. C., 1981, "Boundary Conditions for Differential Approximations," *J. Quantitative Spectroscopy and Radiative Transfer*, Vol. 25, No. 4, pp. 325-337.

Siddall, R. G., 1986, "Accurate Evaluation of Radiative Direct-Exchange Areas for Rectangular Geometries," *Proc. 8th. Int. Heat Transfer Conf.*, C. L. Tien, V. P. Carey, and J. K. Farrell, eds., Vol. 2, pp. 751-756.

Siegel, R., 1987, "Transient Radiative Cooling of a Droplet Filled Layer," ASME JOURNAL OF HEAT TRANSFER, Vol. 109, No. 1, pp. 159-164.

Siegel, R., 1987, "Radiative Cooling of a Solidifying Droplet Layer Including Absorption and Scattering," *Int. J. Heat Mass Transfer*, Vol. 30, No. 8, pp. 1762-1765.

Siegel, R., and Howell, J. R., 1972, *Thermal Radiation Heat Transfer* (1st ed.; 2nd ed., 1981). McGraw-Hill, New York.

Siegel, R., and Howell, J. R., 1971, *Thermal Radiation Heat Transfer: Vol. III: Radiation Transfer With Absorbing, Emitting, and Scattering Media*, NASA SP-164.

Siegel, R., and Howell, J. R., 1969, *Thermal Radiation Heat Transfer; Vol. II: Radiation Exchange Between Surfaces and in Enclosures*, NASA SP-164.

Siegel, R., and Howell, J. R., 1968, *Thermal Radiation Heat Transfer; Vol I: The Blackbody, Electromagnetic Theory, and Material Properties*, NASA SP-164.

Skocypec, R. D., and Buckius, R. O., 1987, "Comments on 'Rigorous Bounds on the Radiative Interaction Between Real Gases and Scattering Particles'," *J. Quantitative Spectroscopy and Radiative Transfer*, Vol. 37, No. 5, pp. 509-512.

Skocypec, R. D., and Buckius, R. O., 1984, "Total Hemispherical Emittances for CO_2 and H_2O Including Particle Scattering," *Int. J. Heat Mass Transfer*, Vol. 27, No. 1, pp. 1-13.

Slater, G., Salpeter, G. G., and Wasserman, I., 1982, "Monte Carlo Calculations of Resonance Radiative Transfer Through a Semi-Infinite Medium," *Astrophys. J.*, Vol. 255, pp. 293-302.

Smith, T. F., Shen, Z. F., and Friedman, J. N., 1982, "Evaluation of Coefficients for Weighted Sum of Gray Gases Model," ASME JOURNAL OF HEAT TRANSFER, Vol. 104, No. 4, pp. 602-608.

Sobolev, A. M., 1982, "The Monte Carlo Method for Multi-level Problems of Radiative Transfer With Allowance for Processes in the Continuum," *Sov. Astron.*, Vol. 6, No. 3, pp. 366-367.

Sokman, C. N., and Razzaque, M. M., 1987, "Finite Element Analysis of Conduction Radiation Heat Transfer in an Absorbing-Emitting and Scattering Medium Contained in an Enclosure With Heat Flux Boundary Conditions," in: *Radiation, Phase Change Heat Transfer, and Thermal Systems*, Y. Jaluria, V. P. Carey, W. A. Fiveland, and W. Yuen, eds., ASME HTD-Vol. 81, pp. 17-23.

Sowell, E. F., and O'Brien, R. F., 1972, "Efficient Computation of Radiant-Interchange Configuration Factors Within an Enclosure," ASME JOURNAL OF HEAT TRANSFER, Vol. 94, No. 3, pp. 326-328.

Spanner, D. C., 1964, *Introduction to Thermodynamics*, Academic Press, London.

Sparrow, E. M., and Cess, R. D., 1978, *Radiation Heat Transfer*, Hemisphere, Washington (augmented ed.).

Steward, F. R., and Kocaefe, Y. S., 1986, "Total Emissivity and Absorptivity Models for Carbon Dioxide, Water Vapor, and Their Mixtures," *Proc. 8th Int. Heat Transfer Conf.*, C. L. Tien, V. P. Carey, and J. K. Farrell, eds., Vol. 2, pp. 735-740.

Tan, Z.-Q., 1988, "Radiative Heat Transfer in Multidimensional Emitting, Absorbing and Anisotropic Scattering Media—Mathematical Formulation and Numerical Method," ASME JOURNAL OF HEAT TRANSFER, in press.

Tong, T. W., Lin, W.-Q., and Peck, R. E., 1987, "Radiative Heat Transfer in Porous Media With Spatially Dependent Heat Generation," in: *Radiation, Phase Change Heat Transfer, and Thermal Systems*, Y. Jaluria, V. P. Carey, W. A. Fiveland, and W. Yuen, eds. ASME HTD-Vol. 81, pp. 43-50.

Tong, T., and Tien, C. L., 1983, "Radiative Heat Transfer in Fibrous Insulations—Part I: Analytical Study," ASME JOURNAL OF HEAT TRANSFER, Vol. 105, No. 1, pp. 70-75.

Vercammen, H. A. J., and Froment, G. F., 1980, "An Improved Zone Method Using Monte Carlo Techniques for the Simulation of Radiation in Industrial Furnaces," *Int. J. Heat and Mass Transfer*, Vol. 23, No. 3, pp. 329-336.

Viskanta, R., 1982, "Radiation Heat Transfer: Interaction With Conduction and Convection and Approximate Methods in Radiation," *Proc. 7th Int. Heat Transfer Conf.*, U. Grigull, E. Hahne, K. Stephan, and J. Straub, eds., Vol. 1, pp. 103-122.

Viskanta, R., and Menguc, M. P., 1987, "Radiation Heat Transfer in Combustion Systems," *Prog. Energy Combus. Sci.*, Vol. 13, pp. 97-160.

Viskanta, R. and Grosh, R. J., 1962a, "Heat Transfer by Simultaneous Conduction and Radiation in an Absorbing Medium," ASME JOURNAL OF HEAT TRANSFER, Vol. 84, No. 1, pp. 63-72.

Viskanta, R., and Grosh, R. J., 1962b, "Effect of Surface Emissivity on Heat Transfer by Simultaneous Conduction and Radiation," *Int. J. Heat Mass Transfer*, Vol. 5, pp. 729-734.

Vlasov, Yu, P., and Titarchuk, L. G., 1982, "Monte Carlo Calculations of Resonance-Line Formation in a Plane Layer," *Sov. Astron.*, Vol. 8, No. 5, pp. 304-307.

Wang, K. Y., and Tien, C. L., 1983, "Radiative Transfer Through Opacified Fibers and Powders," *J. Quantitative Spectroscopy and Radiative Transfer*, Vol. 30, No. 3, pp. 213-223.

Wiebelt, J., 1966, *Engineering Radiation Heat Transfer*, Holt, Rinehart and Winston, New York.

Wu, S. T., and Ferguson, R. E., 1981, "Application of Finite Element Techniques to the Interaction of Conduction and Radiation in Participating Media," in: *Heat Transfer and Thermal Control*, A.L. Crosbie, ed., AIAA, New York, pp. 61-92.

Yamada, Y., and Cartigny, J. D., and Tien, C. L., 1986, "Radiative Transfer With Dependent Scattering by Particles: Part 2—Experimental Investigation," ASME JOURNAL OF HEAT TRANSFER, Vol. 108, No. 3, pp. 614-618.

Yoshizawa, Y., Sasaki, K., and Echigo, R., 1987, "Analytical Study of the Structure of Radiation Controlled Flame," ASME Paper No. 87-HT-57.

Yoshizawa, Y., Echigo, R., Suzuki, H., and Jugjai, S., 1987, "Combustion Augmentation of Solid Poor Cumbustibles With an Extremely High Water Content," *Proc. Western States and Japanese Sections Joint Meeting*, The Combustion Institute, Honolulu, HI.

Downloaded 16 Dec 2010 to 193.140.21.150. Redistribution subject to ASME license or copyright; see http://www.asme.org/terms/Terms_Use.cfm

Thermal Radiation in Packed and Fluidized Beds

C. L. Tien
A. Martin Berlin Chair Professor,
Department of Mechanical Engineering,
University of California at Berkeley,
Berkeley, CA 94709
Fellow ASME

The present work gives an overview of the existing knowledge on radiative transfer in packed and fluidized beds. Special emphasis is given to the proper usage and determination of radiation characteristics of the particles in these systems. Models that treat the particulate bed as a continuum are discussed along with those that consider the system as discontinuous, i.e., accounting for the phase boundaries between the gas and the particles. Existing experimental techniques for determining the radiative properties are presented, and the published bed transmittance and reflectance data are discussed and compared with the theoretical predictions. Interaction of radiation with other modes of heat transfer is also examined.

1 Introduction

Many modern technologies and industrial processes utilize packed and fluidized beds of solid particles operating at temperatures high enough for thermal radiation to be a significant mechanism of heat transfer (Flamant and Arnaud, 1984; Saxena et al., 1978). Some examples are coal combustors, chemical reactors, and nuclear fuel rods. Other types of packed beds in which thermal radiation is important, even though the temperatures may not be high, are those where other modes of heat transfer have been suppressed, such as packed cryogenic microsphere insulations (Tien and Cunnington, 1973). Since most packed and fluidized beds are characterized by either high volume fractions of particles or large particles, or both, many features are unique for analyzing such systems. These features are discussed in this paper. Only gas systems are considered here since most applications of interest, such as those mentioned above, fall in the category of gas fluidized and packed beds.

Packed beds are usually characterized by densely packed particles that do not move during normal operation. The high volume fraction is generally coupled with either an absence of fluid motion or low fluid velocities. This restricts the convection contribution and renders radiation a dominant mode of energy transport. Fluidized beds, on the other hand, have lower volume fractions but higher fluid velocities. In many applications, however, the contribution of radiation to the total energy transport remains significant due to the high operating temperatures. Table 1 shows various representative values that characterize packed and fluidized beds (Ulrich, 1984; Flamant and Arnaud, 1984). A schematic depiction of the various types of packed and fluidized beds is presented in Fig. 1. A review by Haughey and Beveridge (1969) describes the structural properties of packed bed systems.

Previous studies of radiative heat transfer through packed and fluidized beds have employed a variety of analytical and experimental techniques. Vortmeyer (1978) summarized some earlier radiation models using unit cell representations for analyzing packed beds. Such cell and layer models, in conjunction with Monte-Carlo methods, are also used by Chan and Tien (1974a) to evaluate radiative characteristics of packed beds of fixed porosity and regular structure, by Yang et al. (1983) for randomly packed beds of uniform spheres, and by Kudo et al. (1985) who examined different types of packing and variation in volume fraction. Brodulya and Kovensky (1983) used the cell approach by evaluating exact view factors in the unit cell by assuming the surfaces to be isothermal and diffuse. Heat transfer in fluidized beds was reviewed by Saxena et al. (1978). Glicksman and Decker (1982) examined the role of radiation and particle packing on the heat transfer from immersed surfaces to particles in fluidized beds. Combined wall-to-fluidized bed heat transfer was studied by Flamant and Menigault (1987). Brewster and Tien (1982a) examined the issue of dependent versus independent scattering in packed and fluidized beds.

Table 1 Characteristics of gas fluidized and fixed beds

	Type of Bed	
	Fluidized	Fixed
Bed diameter (m)	1-10	0.3-4.0
Bed height (m)	0.3-15.0	0.3-30.0
Porosity	0.6-0.8	0.35-0.70
Particle diameter (m)	10^{-5}–10^{-2}	<0.1×(bed dia.)
Fluid velocity (m/s)	0.1-5.0	0.005-1.0
Pressure drop (kPa/m)	5-15	0.001-1.0
Temperature (°C)		
Carbon steel	450	450
Stainless steel	750	750
Nickel alloys	1200	1200
Brick-lined	1500	1500
Overall heat transfer coefficient (J/sm^2K)	400-800	20-80
Percent of radiation in total heat transfer (750°C)	10-40	-

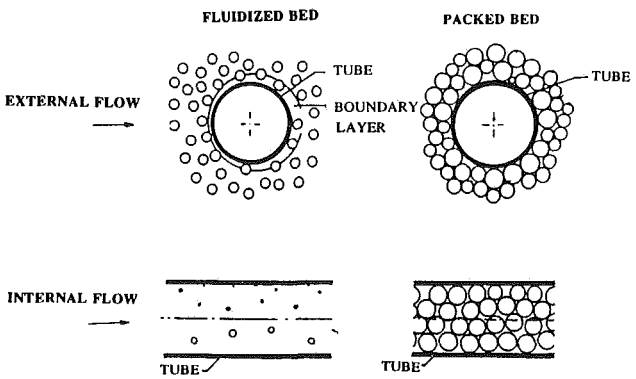

Fig. 1 Types of packed and fluidized beds

Contributed by the Heat Transfer Division for publication in the JOURNAL OF HEAT TRANSFER. Manuscript received by the Heat Transfer Division February 22, 1988. Keywords: Packed and Fluidized Beds, Radiation, Radiation Interactions.

Copyright © 1988 by ASME
Downloaded 16 Dec 2010 to 193.140.21.150. Redistribution subject to ASME license or copyright; see http://www.asme.org/terms/Terms_Use.cfm

Combined radiative and conductive heat transfer in packed beds has been the subject of many studies (Chan and Tien, 1974b; Bergquam and Seban, 1971). Simultaneous radiative-convective transfer in packed and fluidized beds has also been studied (Echigo et al., 1974; Tabanfar and Modest, 1987). Experimental measurements of radiant transmission through packed and fluidized media have been reported by various researchers. The effective scattering and absorption cross sections of isothermal beds of glass, aluminum oxide, steel, and silicon carbide spheres, cylinders, and irregular grains were obtained by Chen and Churchill (1963). Similar measurements through packed and fluidized beds of glass beads were reported by Cimini and Chen (1987). Local heat transfer coefficients in large-particle fluidized beds were measured by Goshayeshi et al. (1986) and wall-to-bed heat transfer by Flamant and Menigault (1987).

2 Theoretical Basis of Thermal Radiation in Packed/Fluidized Beds

Packed and fluidized beds are multiphase systems consisting of solid particulates and gases (liquid systems are not considered here). Thermal radiation within these beds usually is the result of emission by the hot walls and the gas–particle mixture. This radiation undergoes complex interactions with the bed primarily due to absorption and scattering processes. The three primary radiative properties that characterize the interactions of radiation with the particulate bed are the scattering coefficient, the extinction coefficient (i.e., sum of scattering and absorption coefficients), and the scattering phase function. These properties are adopted primarily due to the following considerations: (*i*) the theory of electromagnetic interaction with particles yields these values first, (*ii*) they can be directly obtained from experimental measurements, and (*iii*) other values can be inferred from these primary properties. For example, the absorption coefficient cannot be directly measured from light scattering experiments. It is obtained indirectly by measuring the scattering and extinction losses from the incident beam and evaluating the difference between the corresponding extinction and the scattering coefficients.

Computation of the transport of thermal radiation in the particulate system requires an accurate knowledge of these primary radiative characteristics. This is evident by considering the propagation of radiation within an absorbing, emitting, and scattering medium, which is governed by the equation of transfer (Kerker, 1961; Siegel and Howell, 1981; Ozisik, 1973):

$$\mathbf{e}_\Omega \cdot \nabla I_\lambda(\mathbf{r}, \mathbf{e}_\Omega) = -(\sigma_{a\lambda} + \sigma_{s\lambda}) I_\lambda(\mathbf{r}, \mathbf{e}_\Omega) + \sigma_{a\lambda} I_{b\lambda}(T(\mathbf{r})) + \frac{\sigma_{s\lambda}}{4\pi} \int_{4\pi} I_\lambda(\mathbf{r}, \mathbf{e}_{\Omega'}) \Phi(\mathbf{e}_{\Omega'} \rightarrow \mathbf{e}_\Omega) d\Omega' \quad (1)$$

where I_λ is the monochromatic radiation intensity, T the medium local temperature, $\mathbf{r}$ the position vector, $\mathbf{e}_\Omega$ the unit vector in the direction of consideration, and Ω the solid angle centered around $\mathbf{e}_\Omega$. The coefficients are denoted by σ and the subscripts a, e, s refer to absorption, extinction, and scattering, respectively. The first term on the right-hand side of the equation of transfer represents the attenuation of intensity due to absorption and scattering, the second term represents the gain due to emission, and the last term is the gain due to the in-scattering into the direction $\mathbf{e}_\Omega$ from all other directions. The intensity I_λ is defined as the energy per unit area per unit solid angle per unit wavelength and the scattering phase function $\Phi(\mathbf{e}_{\Omega'} \rightarrow \mathbf{e}_\Omega)$ is a specification of the radiation intensity scattered from the direction $\mathbf{e}_{\Omega'}$ into the direction under consideration, normalized by the isotropic scattered radiation intenstiy, i.e., $\Phi(\mathbf{e}_{\Omega'} \rightarrow \mathbf{e}_\Omega) = 1$ for isotropic scattering. The dif-

Nomenclature

b = single-particle back-scatter fraction
B = bed back-scatter fraction
c = interparticle clearance
C = cross section
C_p = specific heat at constant pressure
D = diameter of the particles
$\mathbf{e}$ = unit vector
E = exchange factor
f_v = solid volume fraction $= 4N\pi(D/2)^3/3V$
$F(\theta)$ = form factor to account for coherent addition of intensities
$g(R)$ = radial distribution of number density, normalized by N/V
G = geometric cross-sectional area
$H(\beta)$ = $3(\sin\beta - \beta\cos\beta)/\beta^3$
i = $\sqrt{-1}$
I = intensity, energy/steradian/projected area
k = propagation constant $= 2\pi/\lambda$; thermal conductivity
L = length of the one-dimensional medium
m = complex refractive index $= n + i\kappa$
n = index of refraction
N = number of particles in volume V
P = radiation transmission number
q = heat flux
Q = efficiency
$\mathbf{r}$ = position vector
R = ratio of radial distance to particle diameter $= r/D$; reflectance
t = time
T = transmittance; temperature
$\mathbf{v}$ = velocity vector
V = volume
x, y, z = Cartesian coordinates
α = size parameter $= \pi D/\lambda$
β = $4\alpha \sin(\theta/2)$
γ = function defined by equation (22)
ϵ = m^2; emissivity
ζ = near-field complex correction factor
η = function defined by equation (26)
θ = polar angle
κ = index of absorption
λ = wavelength of incident radiation
Λ = function defined in Table 4
μ = $\cos\theta$
ν = frequency of incident radiation
Ξ = function defined in Table 4
ρ = reflectivity
σ = radiative coefficients
τ = optical path length
ϕ = azimuthal angle
Φ = scattering phase function
χ = parameter in the liquid model
ω = angular frequency $= 2\pi\nu$; scattering albedo $= \sigma_s/\sigma_e$
Ω = solid angle

Subscripts

a = absorption
b = blackbody
d = diffraction
e = extinction
i = incident radiation
j, l = particle identification
L = length of medium
M = Mie theory for one particle
N = N particles
r = radiative
ref = reflection
s = scattering; specular
t = transmission
0 = background dielectric matrix; coordinate origin
λ = wavelength

Downloaded 16 Dec 2010 to 193.140.21.150. Redistribution subject to ASME license or copyright; see http://www.asme.org/terms/Terms_Use.cfm

ferent methodologies for solving equation (1) are discussed in Section 4.

The radiative coefficients are defined as the fraction of the corresponding energy loss from the propagating wave, per length of travel. The units for the coefficients σ are inverse of length, whereas the phase function is dimensionless. The radiative coefficients are functions of the optical constants of the bed materials and of the particle size, shape, and packing, where the optical constants are functions of the wavelength. The phase function is a strong function of shape and varies from the predominantly forward scattering for large particles to the semi-diffuse for small.

Thermal radiation in packed and fluidized beds is unpolarized by nature and I_λ represents the unpolarized intensity. Another important quantity, which is of greater interest than the intensity, is the heat flux. The radiative heat flux vector $\mathbf{q}_r$ is given as (Ozisik, 1973)

$$\mathbf{q}_r(\mathbf{r}) = q_r \mathbf{e}_q = \int_\lambda \int_{4\pi} I_\lambda(\mathbf{r}, \mathbf{e}_\Omega)\mathbf{e}_\Omega \cdot \mathbf{e}_q d\Omega \tag{2}$$

where $\mathbf{e}_q$ is the unit normal vector to the unit area across which the flux is being measured. Integrating equation (1) over all angles and wavelengths yields the following equation for the divergence of the radiative flux (Ozisik, 1973):

$$\nabla \cdot \mathbf{q}_r(\mathbf{r}) = 4\pi \int_\lambda \sigma_{a\lambda} I_{\lambda b}(T(\mathbf{r}))d\lambda - \int_\lambda \sigma_{a\lambda} \int_{4\pi} I_\lambda(\mathbf{r}, \mathbf{e}_\Omega)d\Omega d\lambda \tag{3}$$

The energy equation accounts for radiation, convection, and conduction modes of energy transfer and can be written in the form (Siegel and Howell, 1981)

$$\rho C_p \left[\frac{\partial T}{\partial t} + (\mathbf{v} \cdot \nabla)T\right] = \nabla \cdot k \nabla T + \nabla \cdot \mathbf{q}_r \tag{4}$$

where T is the temperature, $\mathbf{v}$ the velocity vector, ρ the density, C_p the specific heat, k the thermal conductivity, and t time. The effect of viscous dissipation has been neglected in the above equation. The energy equation obtained by combining equations (1), (3), and (4) is integro-differential and nonlinear, and cannot be simplified to a differential equation in most situations without neglecting readiative processes in the energy transfer. The full equation does not lend itself to simple closed-form solutions and direct numerical solutions require immense computational effort. Combinations of radiation with the other modes of heat transfer were first studied for cases where only radiation and conduction were present, which is characteristic of packed beds. In fluidized-bed systems, convection and radiation are the important mechanisms of energy transfer as indicated by experimental studies (Goshayeshi et al., 1986). Solutions have been obtained by incorporating simplifying approximations such as an isotropically scattering gray medium (Yener and Ozisik, 1986), and a linearly anisotropic scattering medium (Azad and Modest, 1981).

The focus of this section so far has been on the transport of radiative energy as described by the equation of transfer. The equation of transfer treats the medium as a continuum where each volume element absorbs, emits, and scatters radiation. The exact positions of the different particles in the volume are not considered; only volume-averaged values of the radiative properties are used. Other methods, which do not treat the medium as a continuum and, instead, take into account the position of particles and the boundaries between the solid and the gas phase, are termed the discrete models of radiative transfer. Such models usually utilize ray-tracing or view-factor techniques and are most useful for analyzing beds with large particles and high volume fractions. These models are discussed in Section 4.

3 Thermal Radiation Characteristics of Packed/Fluidized Beds

In homogeneous media such as gases, absorption and emission are the major radiative mechanisms. If the medium contains inhomogeneities, such as the particles in packed or fluidized beds, the additional mechanism of scattering is introduced. These absorption and scattering processes are governed by electromagnetic field equations and their associated boundary conditions at all interfaces. The resulting analytical problem is formidable and is usually solved by using simplifying assumptions: idealized geometry of the scatterers, independent scattering and absorption, homogeneous distribution of particles, and others discussed in the following sections.

Absorption and Scattering by a Single Particle. The absorption and scattering characteristics of a single particle are described by the solution of the electromagnetic field equations. Physically, they can be explained by the processes of reflection, refraction, and diffraction. When an electromagnetic wave strikes the particle surface, a portion of it is reflected while the remainder penetrates the particle. The beam within the particle may experience some absorption and multiple internal reflections before it escapes out of the particle in different directions, giving rise to scattering. This scattering is the contribution by refraction. The diffraction scattering process originates from the bending of the incident beams near the edge of the particle. Consequently, even a completely absorbing particle scatters radiation.

Scattering and absorption characteristics of a particle are governed by three factors: the particle shape, the particle size relative to the wavelength of the incident radiation, and the optical properties of the particle and the background medium (Tien, 1985). For the particle shape, general solutions are available for only a few common shapes such as spheres, cylinders, and spheroids (Kerker, 1961; Bohren and Huffman, 1983). The solutions are complicated even for these simple cases. The second factor is commonly expressed by a size parameter α, which is defined as $(\pi D/\lambda)$ for spheres, where D is the diameter and λ is the wavelength. The last factor is represented by the complex refractive index m defined as $(n + i\kappa)$ where n is the index of refraction and κ is the index of absorption. It should be noted that $m = (n - i\kappa)$ if the incident wave is assumed proportional to $\exp(i\omega t)$, where ω is the angular velocity and t is time. In this paper it is assumed that the proportionality is $\exp(-i\omega t)$ and hence $m = (n + i\kappa)$. The background medium is assumed to be nonparticipating, i.e., $m = 1.0$, and thus requires no further consideration.

The solution of the electromagnetic field equations yields the internal and scattered electromagnetic fields from which the corresponding extinction and scattering cross sections C_e and C_s are obtained. The cross sections are defined as the ratio of the energy loss to the incident energy flux and have the units of area. Efficiencies are defined as the dimensionless ratios of cross sections to the geometric cross-sectional area G, i.e.,

$$Q_p = C_p/G \qquad (p = a, e, s) \tag{5}$$

where $G = \pi D^2/4$ for spheres of diameter D. The phase function for spheres is defined as

$$\Phi(\mathbf{e}_\Omega \rightarrow \mathbf{e}_{\Omega'}) = \frac{\pi^2 D^2}{C_s} \frac{I_s(\mathbf{e}_\Omega \rightarrow \mathbf{e}_{\Omega'})}{I_i} \tag{6}$$

where I_i is the intensity of the incident wavelength. The scattering phase functions for spherical particles of three different sizes have been plotted in Fig. 2. Figure 3 shows the absorption, extinction, and scattering efficiencies for a range of size parameters $0 < \alpha < 15$, $m = 1.29 + i0.472$.

The solutions of the electromagnetic fields are usually in the form of an infinite series (Bohren and Huffman, 1983; Wiscombe, 1980) or complicated functions of α and m.

Downloaded 16 Dec 2010 to 193.140.21.150. Redistribution subject to ASME license or copyright; see http://www.asme.org/terms/Terms_Use.cfm

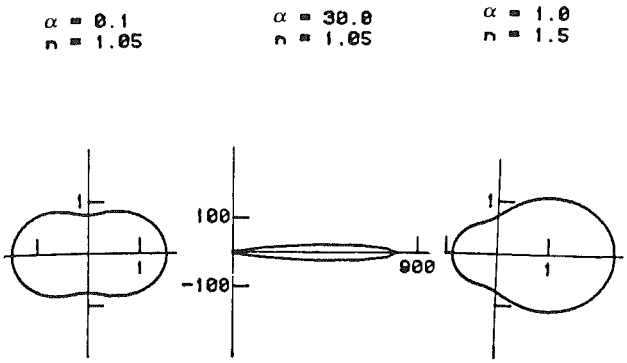

Fig. 2 Scattering phase functions for small, intermediate, and large values of α and m

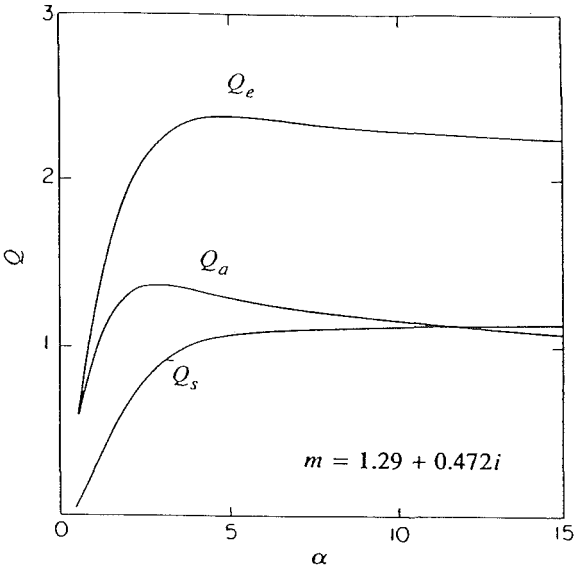

Fig. 3 Absorption, scattering, and extinction efficiencies of a spherical particle

However, simple expressions exist for some limiting cases that are of greatest importance for fluidized and packed bed applications. The first of these is the small particle limit, i.e., $\alpha \ll 1$, which is important for packed-bed systems such as microsphere insulations. This is called the Rayleigh limit. The second is the large particle, or geometric limit, characteristic of packed and fluidized bed combustors. The Rayleigh limit offers simple algebraic equations for radiative properties of small particles though no significant saving of computational time. In contrast to this limited numerical expediency, large computational savings are possible by using geometric scattering assumptions over the Mie theory.

For a small (Rayleigh) isolated particle of size parameter α, the extinction and scattering efficiencies corresponding to unpolarized incident radiation, obtained from the Mie theory (to terms of order α^4, $\alpha \ll 1$) are (Kerker, 1961; Bohren and Huffman, 1983)

$$Q_e(\alpha, \epsilon) = 4\alpha \mathrm{Im}\left\{\left(\frac{\epsilon-1}{\epsilon+2}\right)\left[1 + \frac{1}{15}\alpha^2\left(\frac{\epsilon-1}{\epsilon+2}\right)\frac{\epsilon^2+27\epsilon+38}{2\epsilon+3}\right]\right\} + \frac{8}{3}\alpha^4 \mathrm{Re}\left\{\left(\frac{\epsilon-1}{\epsilon+2}\right)^2\right\} \quad (7)$$

$$C_s(\alpha, \epsilon) = \frac{8}{3}\alpha^4\left|\frac{\epsilon-1}{\epsilon+2}\right|^2 \quad (8)$$

where $\epsilon = m^2$. The corresponding phase function is

$$\Phi(\theta) = \frac{3}{4}(1+\cos^2\theta) \quad (9)$$

where θ is the polar angle between scattering and incident directions.

The simplicity of the Rayleigh-scattering approximations makes them appealing for computing radiative characteristics of small particles. Even though the limit $\alpha \ll 1$ is used to indicate the Rayleigh limit, Ku and Felske (1984) have discussed in some detail the range of parameters α and m for which the above equations can be used without causing significant error. Packed beds of microspheres and ultrafine powder, used for insulation purposes, and certain fluidized beds fall in these categories.

The geometric or large-particle limit is difficult to handle through exact solutions involving series expansions because large numbers of terms (approximately $2\alpha+2$) are required to obtain convergence (Wiscombe, 1980). Additionally the large value of the arguments of the mathematical functions involved makes the terms in the series very difficult to evaluate. To overcome these hurdles concepts from geometric optics are introduced to analyze particles with large size parameters. Geometric optics uses the method of tracing rays as they undergo refractions and multiple reflections at the interfaces and absorption within the particle.

The total energy scattered by a large sphere may be written as the sum of diffracted, reflected, and transmitted components. Consequently the scattering efficiency is expressed as

$$Q_s = Q_d + Q_{ref} + Q_t, \qquad Q_d = 1 \quad (10)$$

where the subscripts d, ref, and t denote diffraction, external reflection, and transmission, respectively. For large absorbing spheres all the energy entering the sphere is eventually absorbed, yielding $Q_t = 0$. The extinction efficiency for large spheres is shown to be (Boheren and Huffman, 1983; Kerker, 1961)

$$\lim_{\alpha\to\infty} Q_e = 2 \quad (11)$$

implying $Q_a = 1 - Q_{ref} - Q_t$. The phase function for large particles is strongly forward scattering and must be determined by ray-tracing methods.

For large opaque spheres the efficiencies can be approximated as (Siegel and Howell, 1981)

$$Q_a = \epsilon_\lambda, \qquad Q_s = 1 - \epsilon_\lambda \quad (12)$$

where ϵ is the emissivity of the surface of the particles. The phase function is approximately isotropic, i.e., $\Phi(\theta) = 1$, if the sphere is specularly reflecting, and is

$$\Phi(\theta) = \frac{8}{3\pi}(\sin\theta - \theta\cos\theta) \quad (13)$$

if the spheres reflect diffusely. Since large particles in most packed and fluidized beds such as chemical reactors and coal combustors are diffuse, the expressions presented above represent a significant saving of computational resources compared to the complete Mie series solution.

If the diffraction component is treated as part of the propagating beam, restrictions are placed on the lower size limit for the geometric scattering to ensure that the scattered portion due to diffraction is indeed in the forward direction. The extinction efficiency is taken to be equal to unity instead of two since the diffraction portion is omitted. Similarly $Q_s = Q_{ref} + Q_t = 1 - Q_a$. If the scattered light in a cone of half angle of 5 deg is considered as part of the propagating wave, the lower limit for geometric optics (without diffraction) is $\alpha \approx 115$.

Absorption and Scattering of a Particulate System. Scattering and absorption characteristics of many particles in close packing or fluidization can be obtained from the single-

Downloaded 16 Dec 2010 to 193.140.21.150. Redistribution subject to ASME license or copyright; see http://www.asme.org/terms/Terms_Use.cfm

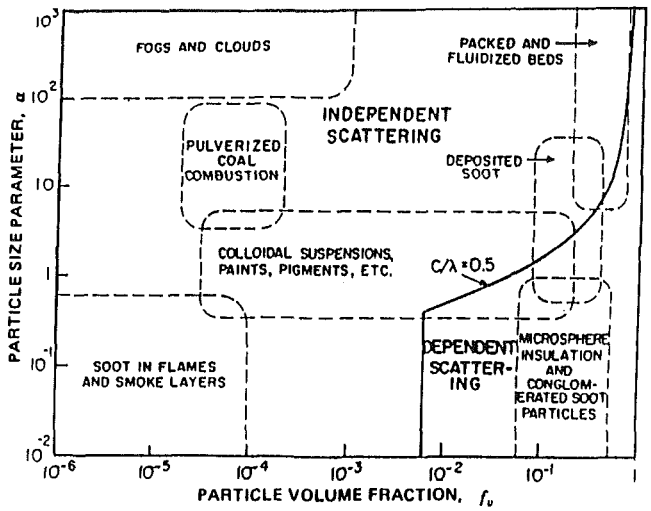

Fig. 4 Independent and dependent scattering regime map

particle characteristics. The procedure depends on the scattering regime to which the system of particles belongs. Based on the size parameter α and the particle volume fraction f_v, the regime map shown in Fig. 4 is divided into regimes: one where independent theory is an adequate representation, and the other where interparticle interactions must be accounted for.

The independent theory is based on the assumption that each particle in the assembly scatters and absorbs radiation unaffected by the presence of other particles. Thus the extinction and scattering of energy by the system is expressed by a simple algebraic addition of the energy extinguished and scattered by each primary particle. The cross section for the system of N particles is the sum of the cross sections of each particle, and the individual particles are assumed to scatter and absorb radiation independently of the others. For identical particles this leads to the following expressions (Bohren and Huffman, 1983; Ozisik, 1973):

$$I_{sN} = \sum_{j=1}^{N} I_{sj} = NI_{sM}, \quad C_{eN} = \sum_{j=1}^{N} C_{ej} = NC_{eM},$$

$$C_{sN} = \sum_{j=1}^{N} C_{sj} = NC_{sM}, \quad \Phi_N = \Phi_M, \quad Q_{eN} = Q_{eM}, \quad Q_{sN} = Q_{sM} \tag{14}$$

Here the subscript M indicates the value obtained for a single particle (Mie theory). The corresponding coefficients for the medium are obtained by

$$\sigma_p = \frac{C_{pN}}{V} = \frac{NC_{pM}}{V} \qquad (p = a, e, s) \tag{15}$$

where V is the volume containing N particles. For beds of monodisperse spherical particles of diameter D

$$\sigma_p = \frac{3}{2}\frac{f_v Q_{pN}}{D} \qquad (p = a, e, s) \tag{16}$$

In essence, the independent theory assumes no electromagnetic interaction between the various particles in the system and that each particle has the same incidence. Interference of the waves scattered from the different particles is also neglected. Thus the resultant properties of the system are simply an algebraic sum of the corresponding properties of the individual particles that constitute the system, where each particle is assumed to be alone in the imposed incident field.

Intuitively the assumptions associated with the independent theory seem valid when the clearance between particles is significantly larger than the diameter and the wavelength, as well as when the particles are randomly distributed in space and time. As discussed in the following sections the ratio of interparticle clearance to the diameter of the particles is not of consequence for randomly distributed homogeneous particles whereas the ratio of clearance to the wavelength is.

Results using the independent theory are far simpler, and wherever justified it is advantageous to use them over the exact expressions that account for interparticle effects.

Departure from independent theory occurs in a densely packed system, where the close spacing of the particles renders invalid the assumption that each particle acts independently of the others. Dependent effects are introduced into the radiative characteristics by two mechanisms. The first is the near-field interparticle effect by which the net incidence on the particles is modified as well as the internal fields, and consequently both the extinction and scattering characteristics of the system are changed. The second is due to coherent addition of scattered radiation in the far field, which is manifested by a change in the scattering characteristics only (Tien and Drolen, 1987; Kumar and Tien, 1987). In reality, dependent effects are always present but may be neglected under certain conditions. It is thus important to quantify demarcation criteria that separate the regions where the independent assumption is a good approximation from those where dependent effects cannot be ignored.

It is seen that the dependent effects are a function of size α and the volume fraction f_v. These can also be replaced by c/λ and f_v, since c is directly related to α and f_v by the following relation:

$$\frac{c}{\lambda} = \frac{\alpha}{\pi}\left(\frac{0.905}{f_v^{1/3}} - 1\right) \tag{17}$$

by assuming a rhombohedral lattice structure. Here c is the clearance between particles defined as the difference between the center-to-center distance between two particles and the sum of their radii. The realization that dependent effects are a function of c/λ and f_v was first introduced by Hottel et al. (1971). Prior to this, dependent effects were believed to be a function of center-to-center particle separation only. Hottel et al. (1971) suggested that the dependent scattering was important when $c/\lambda_0 < 0.3$ and presented the following correlation:

$$\log_{10}\log_{10}\left(\frac{Q_{sM}}{Q_{sN}}\right) = 0.25 - 4.1\frac{c}{\lambda_0}, \qquad \frac{c}{\lambda_0} < 0.3 \tag{18}$$

where λ_0 is the wavelength in a vacuum. The correlation is based on experimental data for a limited range of size parameter, $\alpha = 0.78$ to $\alpha = 2.39$.

Figure 4 shows a regime map (Tien and Drolen, 1987) for dependent and independent scattering efficiencies considering only coherent addition effects. The transition from dependent to the independent asymptote is gradual and thus a sharp transition demarcation is not apparent. The line separating dependent and independent regimes in Fig. 4 corresponds to a 5 percent deviation from the independent (Mie) theory. It is given by $c/\lambda = 0.5$, which is slightly higher than $c/\lambda = 0.3$ (Brewster and Tien, 1982a) but is in good agreement with that of Hottel et al. (1971), who stated that the measured scattering efficiency is within 5 percent of the independent theory if $c/\lambda_0 = 0.37$, which for their case yields $c/\lambda = 0.49$. Experimental verification of these limits has been discussed in the literature (Brewster and Tien, 1982a; Yamada et al., 1986; Drolen et al., 1987) and has been reviewed in depth by Tien and Drolen (1987). Some experimental data have been plotted in Fig. 5 indicating the origin of the demarcation line.

Even though the demarcation criterion for coherent addition has been established in the literature as indicated above, i.e., $c/\lambda = 0.5$, the demarcation for the near-field interactions has not been studied. Coherent addition is not dependent on the refractive index m of the material, whereas the near-field correction is a strong function of m. This introduces another parameter that must be considered and thus precludes a cor-

Downloaded 16 Dec 2010 to 193.140.21.150. Redistribution subject to ASME license or copyright; see http://www.asme.org/terms/Terms_Use.cfm

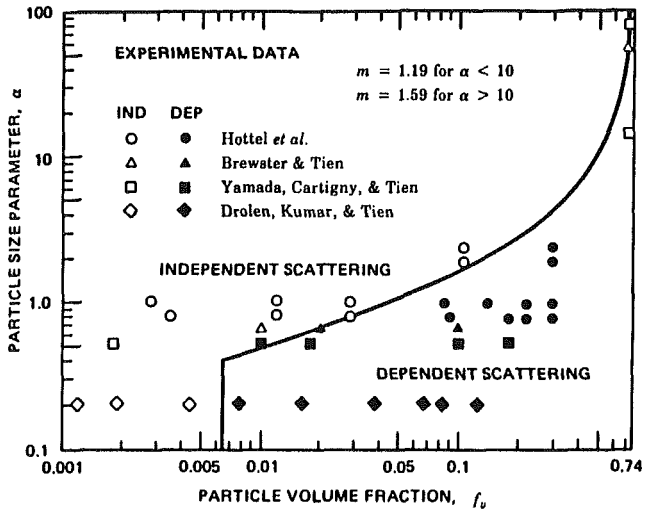

Fig. 5 Experimental data for independent and dependent scattering regime

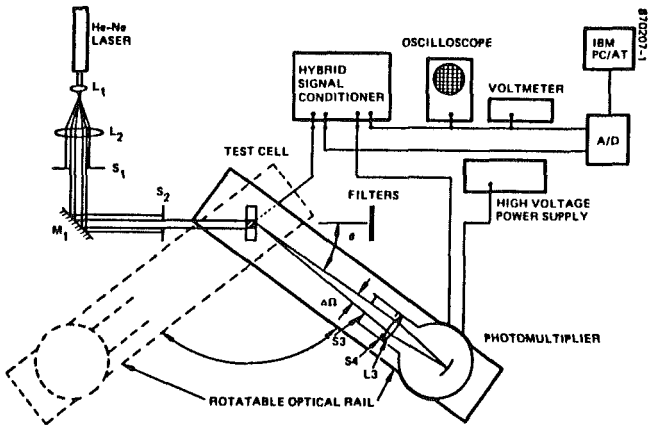

Fig. 6 Experimental apparatus for particulate radiation characteristics

responding regime map from being two-dimensonal until other appropriate variables are identified that can adequately indicate the demarcation limits.

The expressions for the radiative characteristics that include dependent effects have been developed in the literature. The absorption efficiency is obtained as (Kumar and Tien, 1987)

$$Q_{aN} = 4\alpha \mathrm{Im}\left[\zeta\left(\frac{\epsilon-1}{\epsilon+2}\right)\right] \tag{19}$$

for Rayleigh particles, where ζ is the near-field correction factor. The scattered intensity and scattering cross section are evaluated by defining a form-factor $F(\theta)$ as (Tien and Drolen, 1987; Kumar and Tien, 1987)

$$F(\theta) = |\zeta|^2\left\{1 + 24 f_v \int_0^\infty R^2[g(R)-1]\frac{\sin\beta R}{\beta R}\,dR\right\} \tag{20}$$

yielding

$$I_{sN}(\theta) = N I_{sM}(\theta) F(\theta), \quad \Phi_N(\theta) = \Phi_M(\theta)\frac{F(\theta)}{\gamma} \tag{21}$$

where θ is the angle between the direction of incidence and scattering and

$$\gamma = \frac{1}{4\pi}\int_{4\pi} \Phi_M(\theta) F(\theta)\, d\Omega \tag{22}$$

From this definition

$$Q_{sN} = Q_{sM}\gamma \tag{23}$$

The expressions for the near-field factor ζ and far-field

Table 2 Expressions for ζ for Rayleigh particles

$g(R)$	ζ
Gas model	$\left[1-\frac{\epsilon-1}{\epsilon+2}f_v(1+1.6\alpha^2)\right]^{-1}$
Packed-sphere model	$\left[1-\frac{\epsilon-1}{\epsilon+2}f_v(1+0.7134\alpha^2)\right]^{-1}$
Liquid model	$\left[1-\frac{\epsilon-1}{\epsilon+2}f_v(1+1.6\alpha^2(\chi^2-0.5541))\right]^{-1}$

Table 3 Expressions for $F(\theta)$

$g(R)$	$F(\theta)/\lvert\zeta\rvert^2$
Gas model	$1 - 8f_v H(\beta)$
Packed-sphere model	$1 - 8f_v[H(\beta) - 0.831(\sin\beta)/\beta]$
Liquid model	$1 - 8f_v[\chi^3 H(\chi\beta) - 0.831(\sin\beta)/\beta]$
Percus-Yevick model	$(1-f_v)^4/(1+2f_v)^2$, $\alpha\to 0$
$\beta = 4\alpha\sin(\theta/2)$	
$H(\beta) = 3(\sin\beta - \beta\cos\beta)/\beta^3$	
$\approx 1 - \beta^2/10$, $\theta\to 0$, $\alpha\to 0$	

Table 4 Expressions for γ using Rayleigh phase functions

$g(R)$	$\gamma/\lvert\zeta\rvert^2$
Gas model	$1 - 8f_v\Lambda(4\alpha)$
Packed-sphere model	$1 - 8f_v[\Lambda(4\alpha) - 0.831\Xi(4\alpha)]$
Liquid model	$1.0 - 8f_v[\chi^3\Lambda(\chi 4\alpha) - 0.831\Xi(4\alpha)]$
Percus-Yevick model	$(1-f_v)^4/(1+2f_v)^2$, $\alpha\to 0$
$\Lambda(\xi) = \frac{9}{\xi^2}\left[\frac{\sin\xi}{\xi}\left(-1+\frac{16}{\xi^2}\right)+\frac{\cos\xi}{\xi^2}\left(-4+\frac{16}{\xi^2}\right)+\left(1-\frac{4}{\xi^2}-\frac{16}{\xi^4}\right)\right]$	
$\Xi(\xi) = \frac{3}{\xi^2}\left[\frac{\sin\xi}{\xi}\left(4-\frac{48}{\xi^2}\right)+\cos\xi\left(-1+\frac{20}{\xi^2}-\frac{48}{\xi^4}\right)+\left(1+\frac{4}{\xi^2}+\frac{48}{\xi^4}\right)\right]$	

coherent addition corrections are presented in Tables 2–4. These expressions are developed by using statistical particle-distribution functions $g(R)$. The distribution g is the ratio of the number of particles at a radial distance $R = r/D$ from the central particle to the average number density N/V of the particulate bed. Different distribution functions have been used in Tables 2–4, namely the gas model, packed-sphere model, liquid model, and Percus–Yevick model, which have been discussed in the review by Tien and Drolen (1987) and by Kumar and Tien (1987). It has been shown that the theoretical results obtained by using the Percus–Yevick distribution (Percus and Yevick, 1958) show the best agreement with experimental measurements (Drolen et al., 1987). This model is however very computationally intensive and is therefore

Downloaded 16 Dec 2010 to 193.140.21.150. Redistribution subject to ASME license or copyright; see http://www.asme.org/terms/Terms_Use.cfm

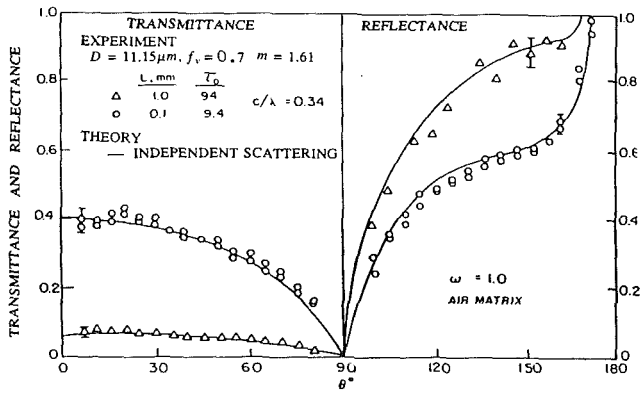

Fig. 7 Transmittance and reflectance for packed beds

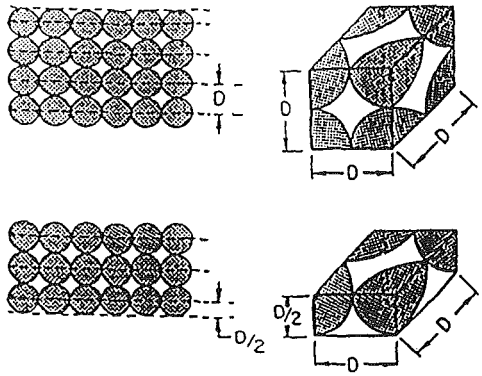

Fig. 8 Example of unit cell geometry used in discontinuous models

cumbersome to use. The simple expressions obtained by using the gas and packed-sphere models are also close to the experimental data and are thus good approximations. The review by Tien and Drolen (1987) discusses the various distribution functions and their applicability.

Experimental Determination. The radiative characteristics of packed beds are determined experimentally by the following sequence. First the extinction characteristics are obtained from direct transmission measurements. Next, the scattering cross section and phase function are obtained by measuring the angular distribution of scattered thermal radiation. Finally, the absorption characteristics are inferred from the difference between the extinction and scattering of the incident radiation. The radiation source in the experiment is either a laser or glow-bar. An experimental apparatus employing laser scattering is schematically depicted in Fig. 6 (Drolen et al., 1987). Similar setups have been used by Hottel et al. (1971), Brewster and Tien (1982a), and Yamada et al. (1986).

The experimental results consist of transmittance and reflectance data for a planar slab containing the scatterers from the particulate bed. Data reduction to yield the desired radiative properties is achieved by adopting a suitable radiative transfer model. Brewster and Tien (1982a) used the two-flux model (Brewster and Tien, 1982b) for the data inversion, yielding the following expressions for the transmittance T and reflectance R:

$$T = \frac{I(L)}{I_i} = \left[\cosh(\eta L) + \frac{\bar{\sigma}_s + \bar{\sigma}_a}{\eta}\sinh(\eta L)\right]^{-1} \tag{24}$$

$$R = (1-\delta^2)\sinh(\eta L) \tag{25}$$

where

$$\eta = [\bar{\sigma}_a(\bar{\sigma}_a + 2\bar{\sigma}_s)]^{1/2}, \quad \bar{\sigma}_a = 2\sigma_a, \quad \bar{\sigma}_s = 2B\sigma_s \tag{26}$$

and

$$B = \frac{1}{4\pi}\int_{\phi-\phi'=0}^{2\pi}\int_0^1\int_{-1}^0 \Phi(\mu, \phi \to \mu', \phi')d\mu d\mu' d(\phi-\phi') \tag{27}$$

is the back-scatter fraction.

Chen and Churchill (1963) used an open-ended tubular electric furnace as a blackbody source. The test section, comprised of packed spheres supported on a screen and the source, was placed underneath. Using thermocouples as detectors the characteristics of glass, aluminum oxide, steel, and silicon carbide spheres, cylinders, and irregular grains were found for various source temperatures. Two-flux models, with the inclusion of an emission term, were used for the data inversion.

Whereas characteristics of packed beds can be measured in ex-situ situations, the thermal radiation characteristics of fluidized beds have to be measured in-situ, usually to preserve the operating conditions. This is achieved by laser scattering techniques. Alavizadeh et al. (1984) have designed an instrument for the measurement of the radiative component of heat transfer in a high-temperature gas fluidized bed. The design uses a silicon window to transmit the radiative flux to a thermopile detector located at the base of a cavity.

4 Analytical Modeling of Radiative Transfer in Packed/Fluidized Beds

Several methods have been used for modeling radiative transfer in packed and fluidized beds. These approaches can be classified, according to the modeling of the medium itself, into two major groups: discontinuous or discrete models, and continuous or pseudocontinuous models.

In discontinuous or discrete models the medium is considered as a regular assembly of units or cells of idealized geometry, resulting in a simple algebraic formulation of the problem. In this case, volume-average radiative properties of the medium, determined from the radiative characteristics of particles, are used in the equation of transfer. The second approach visualizes the medium as a random collection of particles with some number density N/V, a reasonable approximation when the characteristic dimension of the system is much larger than the characteristic size of the particles in the system. In this case the radiative transfer modeling involves either the integro-differential equation of radiative transfer or a simplified version of this equation, or Monte-Carlo and/or ray-tracing methods.

A few general comments are in order regarding the models that had been proposed to predict the radiative transfer in particulate systems. Models have been developed to predict primarily the transmission of radiation and/or the effective radiant conductivity of the particulate medium. Corresponding experiments have been performed to test these two different approaches. Of these two major experimental methods the measurement of radiation transmittance through an evacuated and isothermal bed of spheres is the fundamental and by far more reliable method for evaluating theoretical models, since these experiments completely isolate the radiation from other modes of heat transfer. An excellent review of many models developed to predict radiant conductivity can be found in the literature (Vortmeyer, 1978). Here emphasis is placed on some of the models for prediction of radiative transmission through a particulate medium. Some of the models developed to predict radiant conductivity are discussed later.

Discontinuous or Discrete Models. Discontinuous models characteristically treat a particulate system as a regular assembly of cells or units of idealized geometry such as parallel flat plates, close-packed spheres, and cubic-packed spheres. In these models the scattering diagram of a unit or cell is first determined. Standard resistance network or layer theory approaches are then applied to calculate radiation

Downloaded 16 Dec 2010 to 193.140.21.150. Redistribution subject to ASME license or copyright; see http://www.asme.org/terms/Terms_Use.cfm

transfer through the system. Vortmeyer (1978) reviews many models that fall into this category for predicting radiant conductivity. Figure 8 shows some representative unit-cell geometries.

Chan and Tien (1974a) examined a single cubic cell, which is representative of a cubic packed geometry. Using ray-tracing techniques and assuming specular surfaces, they calculated the optical properties of a single layer based on the fraction of rays transmitted, reflected, and absorbed by a single cell. The transmittance and reflectance of an N-layer thick bed were then calculated based on single-layer properties with multiple reflections and transmissions accounted for by the layer theory (similar to the treatment of multiple-pane windows).

Borodulya and Kovensky (1983) presented a somewhat different unit cell consisting of four quarters of a sphere located at each corner of the midplane. Note that in this model the spherical sections need not be in contact and thus the volume fraction is variable. Rather than using ray tracing they assumed diffuse, isothermal surfaces and calculated view factors exactly. A radiative flux was imposed on the bottom of the cell and a set of six equations were solved for the transmitted, absorbed, and reflected fluxes for the single layer. The net properties of an N-layer bed were calculated in a similar manner to the approach used by Chan and Tien (1974a), which accounted for multiple reflections.

Kudo et al. (1985) also assumed diffuse spheres. They examine two different packings, a pyramidal arrangement of four spherical octants contained in a cubic cell with one octant per diagonal and a cubic cell with sides of length L_c containing a sphere of diameter D at its center ($L_c \geq D$). They suggested that the first of these cases is the most dependent scattering case and that the second is the most independent scattering. Actually they were not examining independent versus dependent scattering. What they did show was the effect of single versus multiple scattering on a unit cell basis. The volume fraction in their model is variable at the unit cell level as in the case of Borodulya and Kovensky (1983). They also allowed for global variations in the volume fraction, i.e., cell-to-cell variations. In contrast to Borodulya and Kovensky (1983), Kudo et al. (1985) used a Monte-Carlo technique to calculate the reflected, transmitted, and absorbed energy. Results of these models will be discussed and compared later.

Predictions of radiative transfer in packed/fluidized beds based on discontinuous or discrete models are expected to be very sensitive to the packing geometry assumed. Nevertheless, the discontinuous approach is the natural one to apply in order to predict radiative transfer in many discrete systems, such as nuclear fuel rods, solid-matrix beds, screens, and packed beds of low tube-particle diameter ratio, such as the packed-bed tubular reactors widely used in the chemical industry. Careful consideration of the solid particle arrangement and recourse to ray-tracing/Monte-Carlo method or to other more complicated methods is then required to predict radiative transfer accurately in these systems. Furthermore, the modification of the ray-tracing technique to account for energy diffracted, especially for intermediate particle size parameters, is then required. The application of the theory of geometric diffraction, originally developed by Keller (1962), to radiative transfer problems deserves special attention.

Continuous or Pseudocontinuous Models. In this approach the particulate medium is modeled as a random assembly of particle with some number density N/V. The medium extinction characteristics can be calculated by a Monte-Carlo and/or ray-tracing approach, or by the solution of an integro-differential transport equation such as equation (1), or a simplified version of this equation, such as the two-flux model and the diffusion approximation.

The Monte-Carlo and/or ray-tracing models are best represented by the work of Yang et al. (1983) who recently presented a novel approach for modeling packed-bed radiative transfer. In their model, a randomly packed bed of spheres is created, mathematically, using a model that describes the slow sequential settling of individual rigid spheres of equal diameter, where each sphere must be supported by at least three others, and no sphere can overlap. This generates a random loose packing with $f_v = 0.58$. With the sphere centers located, a ray tracing is performed in conjunction with Monte-Carlo techniques, to determine the cumulative distribution function. This function represents the probability that a ray has interacted with at least one surface and is a function of dimensionless distance from a base sphere. For this packing, rays are most likely to have their first interaction at about one quarter of a sphere diameter. They also found that the mean penetration depth is about 0.66 sphere diameter, and that virtually all rays have hit a sphere surface after traveling a distance of six diameters. The abovementioned probability information was then used to perform a ray-tracing analysis on thick beds. A ray was projected in a random direction across a randomly chosen distance based upon the cumulative distribution function. The process was then continued by randomly choosing the position of a sphere around the endpoint of this ray and assuming specular reflections at the sphere surface. Results of this model are presented later in comparison with those of other models.

Abbasi and Evans (1982) used the analogy between Kundsen diffusion of a gas in a porous solid and radiant transport in a packed bed composed of adiabatic, diffusely reflecting spheres. They emphasized that the assumption of adiabatic pore walls does not necessarily imply that the surfaces are totally reflecting. Clearly they were alluding to a balance between absorbed and emitted energy at the pore walls.

Each of the models that were previously discussed neglects the diffraction contribution by the particles. As discussed earlier, this is a reasonable assumption for large α ($\alpha > 100$) since the diffracted energy is concentrated in the direction of propagation. However, for intermediate and small α the diffracted energy can no longer be considered as part of the propagating beam. Thus reflection at the particle surface is not the only contributor to the scattered energy; diffraction must be considered as well.

The integro-differential approach involves the solution of an equation of transfer as if the medium were a continuum. The extinction characteristics of this continuum are based on the properties of the discrete particles. Chen and Churchill (1963) used a two-flux approximation of the equation of transfer to correlate their experimental data for transmission of radiation through a packed bed of spheres. These results provide a standard for comparison of several of the analytical models discussed herein. The equation of transfer under the two-flux approximation, assuming a quasi-isotropic phase function with diffuse incident flux and no emission, takes the following form:

$$\frac{dI^+}{dx} = -(\bar{\sigma}_s + \bar{\sigma}_a)I^+ + \bar{\sigma}_s I^- \tag{28}$$

$$-\frac{dI^-}{dx} = -(\bar{\sigma}_s + \bar{\sigma}_a)I^- + \bar{\sigma}_s I^+ \tag{29}$$

where the boundary conditions are

$$I^+(x=0) = I_i; \quad I^-(x=L) = 0 \tag{30}$$

This set of equations can be solved for I^+ and I^- yielding the expression for transmittance presented previously, equations (24)–(27).

In contrast to the ray-tracing and Monte-Carlo models, the effect of diffraction and transmission can be incorporated in equations (26) and (27) through the scattering and absorption efficiencies, and the scattering phase function. The two-flux model as given by equations (28)–(30) is not always an ac-

Downloaded 16 Dec 2010 to 193.140.21.150. Redistribution subject to ASME license or copyright; see http://www.asme.org/terms/Terms_Use.cfm

curate approximation, since the model assumes semi-isotropic scattering. As shown in Fig. 2, the scattering for large particles is highly anisotropic. The results of Brewster and Tien (1982b) indicate that for $n=1.21$, the simple two-flux model only performs well for $\alpha<1$, where the phase function is quasi-isotropic. Other authors have presented comparisons between two-flux and "exact" results as a function of α and optical thickness for the same refractive index (Truelove, 1984; Fiveland, 1985). Truelove (1984) described a modified two-flux model for strongly anisotropic forward scattering that approximates the phase function as the superposition of a forward-directed delta function and a linearly anisotropic phase function. He showed excellent agreement to the exact results over the range of $0.1<\alpha<100$ and $0.1<\tau<100$.

Chandrasekhar (1960) extended the two-flux model by approximating the radiation field in terms of a number (N) of discrete streams. This reduced the problem to the solution of N coupled differential equations. The directions of these streams, $\mu_i=\cos\omega_i$, are typically chosen so as to correspond to the zeros of the Legendre polynomials, $P_N(\mu)$. The integral in equation (1) can then be approximated by Gaussian quadrature. The model just discussed is called the method of discrete ordinates and can be thought of as the exact solution to the problem given a large enough N, say $N\geq 20$. It is best applied to problems involving anisotropic scattering and/or requiring directional results. A simple algorithm for solving the general equation of transfer using discrete ordinates is presented by Kumar et al. (1988). Other methods for analyzing the radiative transfer equation have been reviewed by Viskanta (1982, 1984) and Menguc and Viskanta (1983).

The diffusion approximation method greatly simplifies the equation of transfer in the case of optically thick media, by assuming the radiative transfer to be a diffusion process. In this optically thick case, the radiant heat flux is approximated as

$$q_r=-k_r\frac{dT}{dx} \tag{31}$$

where k_r is the radiant conductivity. Many different definitions exist for the k_r under an equal number of assumptions. Wang and Tien (1983) gave the following solution for radiative flux assuming a two-flux model for the radiative transfer in a one-dimensional planar geometry, including emission,

$$q_r=\int_0^\infty \frac{I_{b\lambda,1}-I_{b\lambda,2}}{(1/\epsilon_{\lambda,1})+(1/\epsilon_{\lambda,2})-1+(1-\omega_\lambda+2B_\lambda\omega_\lambda)\sigma_{e\lambda}L}\,d\lambda \tag{32}$$

where ω is the scattering albedo, equal to σ_s/σ_e. In the above equation the slab back-scattering fraction B, defined in equation (27), was used. Originally, Wang and Tien (1983) used the particle back-scatter fraction b

$$b=\frac{2}{\alpha^2 Q_s}\int_{-1}^{0} I\,d\mu \tag{33}$$

However in a multiple-scattering, one-dimensional planar geometry, B is the correct choice (Brewster and Tien, 1982b).

Although equation (32) is far from a general solution to the problem, this equation can be used to derive an expression for k_r. First, assume gray radiative properties and black boundaries. This gives the following result:

$$q_r=\frac{\sigma(T_1^4-T_2^4)}{1+(1-\omega+2B\omega)\sigma_e L} \tag{34}$$

If the system is optically thick, equation (34) can be approximated as follows:

$$q_r=\frac{\sigma}{(1-\omega+2B\omega)\sigma_e}\frac{T_1^4-T_2^4}{T_1-T_2}\frac{T_1-T_2}{L} \tag{35}$$

For $(T_1-T_2)<200$ K the above equation can be linearized yielding

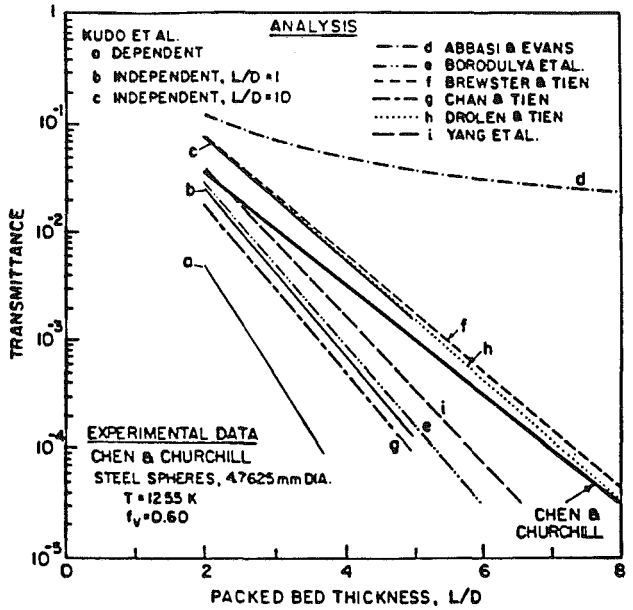

Fig. 9 Experimental data and analytical predictions for the transmittance of a packed bed of steel spheres

$$q_r=\frac{4\sigma T_m^3}{(1-\omega+2B\omega)\sigma_e}\frac{\Delta T}{L} \tag{36}$$

Thus the radiant conductivity can be defined as

$$k_r=\frac{4\sigma T_m^3}{(1-\omega+2B\omega)\sigma_e} \tag{37}$$

Equation (37) is equivalent to that used by Chen and Churchill (1963).

The validity of the various models discussed in the previous sections is assessed by comparing their results with reliable experimental data. The experimental results consist of transmittance and radiant conductivity data through packed spheres as well as bidirectional transmittance and reflectance data for a planar slab containing Mie scatterers.

By far the most quoted experimental data relating to radiant transport in packed beds are those of Chen and Churchill (1963). Many of the authors previously referenced have compared results of their respective models to these experimental data. This experiment was the first to isolate the radiant mode of heat transfer from the convective and conductive modes. This was achieved by illuminating a bed of spheres (2–16 diameters deep) with a modulated, high-temperature (700–1366 K), blackbody source and measuring the transmitted energy via a spectrally independent detector. Four different materials in various shapes and sizes were tested (carbon steel, boro-silicate glass, Al_2O_3, and SiC). For the purpose of comparison only two of these materials are discussed here, polished carbon steel spheres with $D=4.76$ mm and $f_v=0.60$, and boro-silicate glass spheres with $D=5$ mm and $f_v=0.61$.

First examine the results of eight different analytical models for the steel spheres, as shown in Fig. 9. Note that the results of Kudo et al. (1985) ("dependent") and those of Abbasi and Evans (1982) ("totally reflecting") are in poor agreement with the data. The two Monte Carlo models that seem to work the best in this case are those of Yang et al. (1983) and Kudo et al. (1985) ("independent," $L_c/D=10$). Of these two models, that of Yang et al. (1983) is far more physical since they use $f_v=0.58$, whereas at $L_c/D=10$ the Kudo et al. model gives a volume fraction of 0.004. This is clearly inconsistent with the conditions of Chen and Churchill (1963) experiments.

Brewster and Tien (1982b) used equations (12) and (13), suggested by Siegel and Howell (1981), for Q_a, Q_s and the

Downloaded 16 Dec 2010 to 193.140.21.150. Redistribution subject to ASME license or copyright; see http://www.asme.org/terms/Terms_Use.cfm

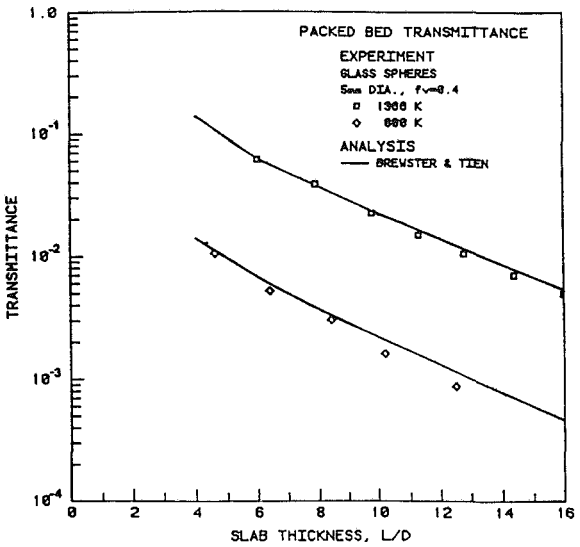

Fig. 10 Experimental data and analytical predictions for the transmittance of a packed bed of glass spheres

phase function. The phase function used is for a diffusely reflecting sphere and the emittance used was $\epsilon = 0.4$ as given by Chen and Churchill (1963). It is quite interesting that such a simple model matches the data so closely.

Drolen and Tien (1987) did not use $\epsilon = 0.4$ to approximate Q_a and Q_s, since it was not actually measured by Chen and Churchill (1963). Instead, Mie scattering calculations were performed using $\lambda = \lambda_{max}$ and the n and k values of iron provided by Siegel and Howell (1981), $n = 1.51$, $\kappa = 1.63$ at $\lambda = 0.589$ μm. These were scaled to $\lambda_{max} = 2.3$ μm using the Hagen-Rubens formula

$$n = \kappa = \sqrt{0.003\lambda_o / r_o} \tag{38}$$

This resulted in $n = \kappa = 3.0$. For the size parameter $\alpha = 6505$, Mie scattering theory yields $Q_a = 0.50$, $Q_s = 1.52$, and $B = 0.17$. The two-flux parameters were then calculated using equations (26) and (27). The results of this model fit the experimental data slightly better than those of Brewster and Tien (1982b). The greatest difficulty in calculating scattering and absorption coefficients directly is the paucity of accurate n and κ data for the appropriate temperature and wavelength.

The values of $\bar{\sigma}_e$ and $\bar{\sigma}_s$ calculated using Mie scattering theory, $\bar{\sigma}_s = 97.7\ \mathrm{m}^{-1}$ and $\bar{\sigma}_a = 190.0\ \mathrm{m}^{-1}$, can be compared to those correlated by Chen and Churchill (1963), $\bar{\sigma}_s = 1056\ \mathrm{m}^{-1}$ and $\bar{\sigma}_a = 28.5\ \mathrm{m}^{-1}$. Although these values of $\bar{\sigma}_s$ and $\bar{\sigma}_a$ are radically different, they give very similar results. Because of this ambiguity, the practice of correlating transmittance data using equation (24) can lead to nonphysical results.

Packed-bed transmittance data for the 5 mm glass spheres are shown in Fig. 10. Brewster and Tien (1982a) achieved an excellent prediction of these results based on $\epsilon = 0.8$ and $B = 0.265$ (from geometric optics) for $\lambda < 2.7$ μm, and $\epsilon = 0.9$ and $B = 0.5$ for $\lambda > 2.7$ μm. This appears to be the only available prediction of the glass-sphere case. Perhaps Monte-Carlo models have not been used due to the complexity of treating semitransparent particles.

As discussed previously, radiation transport through optically thick media, such as packed beds, can be treated as a diffusion process for which a radiant conductivity can be defined. Many definitions for k_r have been suggested, e.g., equations (37), and can be put in the form

$$k_r = 4ED\sigma T_m^3 \tag{39}$$

where E, the exchange factor, varies from model to model. Vortmeyer (1978) discussed eight of these models, four of which are given in Table 5. The first of these is the Argo and Smith (1953) model, which treats a packed bed of spheres as an alternating series of solid and gas layers, perpendicular to the direction of transfer. If the separation between layers is equal to the particle diameter the following exchange factor results:

$$E = \frac{2}{2 - \epsilon} \tag{40}$$

A different model proposed by Schotte (1960) approximates the exchange factor by the particle emissivity. He justified this by assuming that the irregular surface, presented by the surrounding particles, appears essentially black.

Vortmeyer (1978) modified the plane-layer model of Argo and Smith (1953) to incorporate transmission of energy through void spaces in the layer. The voids were introduced through the radiation transmission number P, which is a function of the volume fraction and the particle emissivity. His expression for the radiation exchange factor is as follows:

$$E = \frac{2P + \epsilon(1-P)}{2(1-P) - \epsilon(1-P)} \tag{41}$$

He also stated that for $f_v = 0.6$ the parameter is approximately 0.1.

Table 5 Radiant conductivity exchange factor E

Author	E (model)	E (result) ϵ=0.35	E (result) ϵ=0.85
Kasparek	experimental	0.54	1.02
Argo and Smith (1953)	$\frac{\epsilon}{(2-\epsilon)}$	0.21	0.74
Schotte (1960)	ϵ	0.35	0.85
Chen and Churchill (1963) Wang and Tien (1983)	$\frac{2}{D(\sigma_a+2\sigma_s)}$	1.11	1.06
Vortmeyer (1978)	$\frac{2P + \epsilon(1-P)}{2(1-P)-\epsilon(1-P)}$	0.35	0.93

Each of these expressions was used to predict two experimentally correlated values of k_r given by Kasparek, as described by Vortmeyer (1978). The Kasparek experiment used numerous planar layers of welded steel spheres. The layers were oriented perpendicular to the direction of heat transfer. To eliminate conduction no direct contact was allowed between the adjacent layers. Convection was eliminated by performing the experiment in a vacuum. Kasparek's experimental results are shown at the top of Table 5 followed by the predictions of each of the abovementioned models. The two cases examined were polished steel spheres ($\epsilon = 0.35$) and chromium-oxide coated spheres ($\epsilon = 0.85$). In each case, the diameter of the spheres was 1 cm and the volume fraction was 0.6. Equations (26) and (27) were used to calculate $\bar{\sigma}_a$ and $\bar{\sigma}_s$ in the two-flux model. The values of Q_a and Q_s and B for the steel spheres were calculated from the Mie theory, whereas for the chromium-oxide spheres equations (12) and (13) were used. The two-heat model predicts consistently high values of E. Furthermore, as the emittance is increased the experimental data indicate an increase in E, whereas the two-flux model predicts a decrease. In the two-flux model, the individual spheres are assumed to be isothermal and scattering independently. These may be poor assumptions for welded-steel spheres. Vortmeyer's (1978) model ap-

Downloaded 16 Dec 2010 to 193.140.21.150. Redistribution subject to ASME license or copyright; see http://www.asme.org/terms/Terms_Use.cfm

pears to give the best predictions while Schotte's (1960) extremely simple model gives surprisingly good results.

5 Radiation Interaction With Other Heat Transfer Modes

The role of thermal radiation in gas–particulate systems is of major importance in the design of fluidized beds, packed beds, catalytic reactors, and many other advanced energy conversion systems, especially at high temperatures. The formulation of the combined conduction/radiation and convection/radiation heat transfer problem and its solution are quite complex due to the different nature of thermal radiation when compared with the local and differential characteristics of diffusion and convection phenomena. Rigorous calculation of the general heat transfer problem requires the solution of the energy equation (4) in conjunction with the equation of radiative transfer given by equation (1), and their boundary conditions.

Equations (1)–(4) are all formulated in terms of volumetric-averaged variables and are coupled through temperature. This set of equations is a highly nonlinear system of differential and integro-differential equations and it is a formidable task even to attempt a numerical solution. The general equation of radiative transfer alone has been the subject of many investigations, with several approximate methods being proposed for its solution (Chandrasekhar, 1960; Siegel and Howell, 1981; Viskanta, 1984; Menguc and Viskanta, 1983). An iterative method or a variant of this method has been traditionally used to solve the coupled energy and radiative transfer equation. Here a temperature profile is assumed and used in equation (3) to calculate the divergence of the radiative heat flux, this being then substituted in equation (4) for recalculating temperature distributions. The solution of these complex problems has been substantially facilitated with the recent development of the Differential-Disctete-Ordinate (DDO) method (Kumar et al., 1988) for solving the general equation of radiative transfer. This powerful but simple method allows the simultaneous solution of equations (1)–(4) in a direct and computationally efficient way. The method uses a discrete-ordinate technique to reduce the integro-differential equation (1) to a system of ordinary differential equations. The resulting set of coupled differential equations is then solved utilizing existing software routines.

Many engineering applications require a simple yet approximate method for modeling the radiative transfer part of the problem. This has motivated the development of many simplified versions of the equation of transfer (Deissler, 1964; Rosseland, 1936). The utility of these approximate methods, however, is still highly limited.

Radiation in packed and fluidized beds brings up additional challenging aspects in the analysis. Difficulties in analyzing packed and fluidized beds arise in two major areas: the development of a radiation transfer model and the corresponding radiative properties for the model, and the development of a heat conduction and/or convection model with properly determined thermophysical properties.

Combined Conduction and Radiation. Heat transfer by simultaneous conduction and radiation between two reflecting surfaces with an intervening medium that absorbs, emits, and scatters thermal radiation is a problem of considerable practical importance in stagnant packed beds such as microsphere insulation and nuclear fuel rods.

The interaction of radiation with conduction for an absorbing but nonscattering medium has been well reported in the literature (Viskanta, 1982) where the effects of boundary emissivities, radiation to conduction parameter, optical thickness, and wall temperature ratio were investigated. The combined conduction and radiation problem in a gray absorbing and isotropic scattering medium bounded by two infinite parallel planes at constant temperature was parametrically studied by Viskanta (1982). He studied the effect of various governing parameters and reported exact numerical solutions that became benchmark cases. Similar numerical solutions to the same problem, but in an absorbing, emitting, and anisotropic scattering medium, were reported by Yuen and Wong (1980).

Earlier Bergquam and Seban (1971) took another approach using the two-flux model for the radiation contribution to the total heat transfer flux. Their results show that the total heat transfer flux can be adequately predicted using the two-flux model instead of the equation of transfer in one-dimensional conduction/radiation problems.

Chan and Tien (1974b) analyzed combined conduction and radiation through a bed of packed spheres bounded by two infinite plane surfaces at different temperatures. They modeled the medium as a continuum with effective thermophysical properties. Their analysis involves the determination of the effective thermophysical properties of the medium such as the effective thermal conductivity, and the effective absorption and scattering coefficients in terms of the material properties and geometric characteristics of the medium. The solution of the two-flux equations together with the energy equation is then used to predict the thermal effectiveness of a slab of microspheres and the prediction compares favorably with experimental data of Cunnington and Tien (1973). The effective conductance and the radiation properties of the medium were determined from a simple-cubic packing model. For the range of system parameters evaluated, the effective thermal conductivity of the medium was found to be independent of the insulation thickness, indicating that optically thick conditions existed inside the medium. The effect of particle size and particle emissivities was also investigated. It was shown that thermal radiation increases with increasing particle diameter and increasing particle emissivities, in agreement with experiments of Cunnington and Tien (1973).

Similar results were obtained by Vortmeyer (1974) using the diffusion approximation for an optical thick medium. The radiation exchange factor of equation (38), required for the determination of the radiant conductivity through equation (40), was derived by modifying the plane-layer model of Argo and Smith (1953) to incorporate transmission of energy through voids in the layer. They stated that the parameter P in equation (41) is a function of bed porosity and emissivity of the particle and that in a packed bed an average value for this parameter is 0.1.

Combined Convection and Radiation. The solution of combined convection and radiation in a particulate medium is even more complicated than the previous cases because of the difficulties in the modeling of fluid and particle motion in these systems, particularly in fluidized beds. Fluidized beds have remarkable heat transfer characteristics and have been employed in many applications such as coal combustors and catalytic reactors. Gas and particle conduction, gas convection, and gas and particle radiation render the heat transfer from the fluidized bed to an immersed surface a very complex phenomenon. The heat transfer coefficients measured are much higher than those for a single-phase (gas) case. To a first approximation, the heat transfer can be assumed to be equal to the resultant contribution from conduction, convection, and radiation, each acting separately.

The modeling of heat transfer from a fluidized bed to an immersed surface has traditionally followed a mechanistic approach. The packed model originally used by Mickley et al. (1955) has been generally accepted as an explanation for the much higher heat transfer rates. Many variants of the packed model have been proposed in order to match with experimen-

Downloaded 16 Dec 2010 to 193.140.21.150. Redistribution subject to ASME license or copyright; see http://www.asme.org/terms/Terms_Use.cfm

tal data (Saxena et al., 1978). Glicksman and Decker (1982) have pointed out some of the limitations of this model.

Several studies for high-temperature fluidized beds, where thermal radiation becomes significant, have recently been presented in the literature (Flamant and Menigault, 1987; Glicksman and Decker, 1982; Renzhang et al., 1987; Goshayeshi et al., 1986). Difficulties in analyzing experimental data to determine the conditions at which thermal radiation becomes important arise due to variations in the conductive and convective heat flux with temperature as well as from the large number of variables involved. However, all these studies agree that thermal radiation becomes an important mode of heat transfer in fluidized beds at temperatures above 750°C.

The understanding of convection heat transfer in packed beds has developed substantially in recent years. Theoretical models that include wall porosity-variation effects and inertia effects (non-Darcy effects) have yielded results in excellent agreement with experiment (Hunt and Tien, 1987). The problems of combined convection and radiation in these systems have not been fully investigated. However, this should not present major difficulties. In a recent experimental study reported by Harris and Lenz (1985), conduction, convection, and radiation are all important.

Heat transfer in internal flows of gases and solid or liquid particles is of increasing importance in engineering systems such as furnaces, combustion chambers, and advanced solar collector systems. Much of the work in this area has been oriented to numerical investigations on the interaction of these heat transfer modes. Chawla and Chan (1980) studied the case of laminar flow between parallel plates with isotropic scattering. Azad and Modest (1981) investigated the interaction of thermal radiation with conduction and convection in thermally developing gas–particulate turbulent flow in a circular tube with black walls. The numerical investigation was carried out for a gray gas and absorbing, emitting, and anisotropically scattering particulate medium. The nongray gas case was recently investigated by Tabanfar et al. (1987). Very little experimental information, however, is available at this time.

References

Abbasi, M. H., and Evans, J. W., 1982, "Monte Carlo Simulation of Radiant Transport Through an Adiabatic Packed Bed or Porous Solid," *AIChE Journal*, Vol. 28, pp. 853–854.

Alavizadeh, N., Adams, R. L., Welty, J. R., and Goshayeshi, A., 1984, "An Instrument for Local Radiative Heat Transfer Measurment in a Gas-Fluidized Bed at Elevated Temperatures," ASME HTD-Vol. 31, pp. 1–8.

Argo, W. B., and Smith, J. M., 1953, "Heat Transfer in Packed Beds," *Chemical Engineering Progress*, Vol. 49, pp. 443–451.

Azad, F. H., and Modest, M. F., 1981, "Combined Radiation and Convection in Absorbing, Emitting and Anisotropically Scattering Gas-Particulate Tube Flow," *International Journal of Heat and Mass Transfer*, Vol. 24, pp. 1681–1698.

Bergquam, J. B., and Seban, R. A., 1971, "Heat Transfer by Conduction and Radiation in Absorbing and Scattering Materials," ASME JOURNAL OF HEAT TRANSFER, Vol. 93, pp. 236–239.

Bohren, C. F., and Huffman, D. R., 1983, *Absorption and Scattering of Light by Small Particles*, Wiley, New York.

Borodulya, V. A., and Kovensky, V. I., 1983, "Radiative Heat Transfer Between a Fluidized Bed and a Surface," *International Journal of Heat and Mass Transfer*, Vol. 26, pp. 277–287.

Brewster, M. Q., 1986, "Effective Absorptivity and Emissivity of Particulate Media With Application to a Fluidized Bed," ASME JOURNAL OF HEAT TRANSFER, Vol. 108, pp. 710–713.

Brewster, M. Q., and Tien, C. L., 1982a, "Radiative Transfer in Packed Fluidized-Beds: Dependent Versus Independent Scattering," ASME JOURNAL OF HEAT TRANSFER, Vol. 104, pp. 573–579.

Brewster, M. Q., and Tien, C. L., 1982b, "Examination of the Two-Flux Model for Radiative Transfer in Particulate Systems," *International Journal of Heat and Mass Transfer*, Vol. 25, pp. 1905–1907.

Buckius, R. O., 1986, "Radiative Heat Transfer in Scattering Media: Real Property Contributions," *Proceedings, 8th International Heat Transfer Conference (San Francisco)*, Vol. 1, pp. 141–150.

Cartigny, J. D., Yamada, Y., and Tien, C. L., 1986, "Radiative Transfer With Dependent Scattering by Particles: Part 1—Theoretical Investigation," ASME JOURNAL OF HEAT TRANSFER, Vol. 108, pp. 608–613.

Chan, C. K., and Tien, C. L., 1974a, "Radiative Transfer in Packed Spheres," ASME JOURNAL OF HEAT TRANSFER, Vol. 96, pp. 52–58.

Chan, C. K., and Tien, C. L., 1974b, "Combined Radiation and Conduction in Packed Spheres," *Proceedings, 5th International Heat Transfer Conference (Tokyo)*, Vol. 1, pp. 72–74.

Chandrasekhar, S., 1960, *Radiative Transfer*, Dover, New York.

Chawla, T. C., and Chan, S. H., 1980, "Combined Radiation and Convection in Thermally Developing Poiseuille Flow With Scattering," ASME JOURNAL OF HEAT TRANSFER, Vol. 102, pp. 297–302.

Chen, J. C., and Churchill, S. W., 1963, "Radiant Heat Transfer in Packed Beds," *AIChE Journal*, Vol. 9, pp. 35–41.

Cimini, R. J., and Chen, J. C., 1987, "Experimental Measurements of Radiant Transmission Through Packed and Fluidized Media," *Experimental Heat Transfer*, Vol. 1, pp. 45–56.

Cunnington, G. R., and Tien, C. L., 1973, "Heat Transfer in Microsphere Cryogenic Insulation," *Advances in Cryogenic Engineering*, Vol. 18, pp. 103–111.

Deissler, R. G., 1964, "Diffusion Approximation for Thermal Radiation in Gases With Jump Boundary Condition," ASME JOURNAL OF HEAT TRANSFER, Vol. 86, pp. 240–246.

Drolen, B. L., Kumar, S., and Tien, C. L., 1987, "Experiments on Dependent Scattering of Radiation," *AIAA 22nd Thermophysics Conference (Honolulu)*, Paper 87-1485, June 8–10.

Drolen, B. L., and Tien, C. L., 1987, "Independent and Dependent Scattering in Packed-Sphere Systems," *Journal Thermophysics and Heat Transfer*, Vol. 1, pp. 63–68.

Echigo, R., Hasegawa, S., and Nakano, S., 1974, "Simultaneous Radiative and Convective Heat Transfer in a Packed Bed With High Porosity," *Transactions of JSME*, Vol. 40, p. 479.

England, W. A., 1986, "An In Situ X-Ray Small Angle Scattering Study of Soot Morphology in Flames," *Combustion Science and Technology*, Vol. 46, pp. 83–93.

Fiveland, W. A., 1985, "Discrete Ordinate Methods for Radiative Heat Transfer in Isotropically and Anisotropically Scattering Media," *Proceedings, 23rd National Heat Transfer Conference ASME*, HTD-Vol. 49, pp. 1–8.

Flamant, G., and Arnaud, G., 1984, "Analyse et Modèlisation du Transfert de Chaleur Entre une Paroi et Lit Fluidisé à Haute Température (Analysis and Theoretical Study of High-Temperature Heat Transfer Between a Wall and a Fluidized Bed)," *International Journal of Heat and Mass Transfer*, Vol. 27, pp. 1725–1735.

Flamant, G., and Menigault, T., 1987, "Combined Wall-to-Fluidized Bed Heat Transfer. Bubbles and Emulsion Contributions at High Temperature," *International Journal of Heat and Mass Transfer*, Vol. 30, pp. 1803–1812.

Glicksman, L. R., and Decker, N., 1982, "Heat Transfer From an Immersed Surface to Adjacent Particles in a Fluidized Bed: The Role of Radiation and Particle Packing," *Proceedings, 7th International Heat Transfer Conference (Munchen)*, Vol. 6, pp. 45–50.

Goshayeshi, A., Welty, J. R., Adams, R. L., and Alavizadeh, N., 1986, "Local Heat Transfer Coefficients for Horizontal Tube Arrays in High-Temperature Large-Particle Fluidized Beds: An Experimental Study," ASME JOURNAL OF HEAT TRANSFER, Vol. 108, pp. 907–912.

Harris, J. A., and Lenz, T. G., 1985, "Experimental Heat Transfer in a Packed Bed in Which Radiation, Conduction, and Convection are all Significant," ASME HTD-Vol. 46, pp. 49–59.

Haughey, D. P., and Beveridge, G. S. G., 1969, "Structural Properties of Packed Beds—A Review," *Canadian Journal Chemical Engineering*, Vol. 47, pp. 130–140.

Hottel, H. C., Sarofim, A. F., Dalzell, W. H., and Vasalos, I. A., 1971, "Optical Properties of Coatings. Effect of Pigment Concentration," *AIAA Journal*, Vol. 9, pp. 1895–1898.

Keller, J. B., 1962, "Geometrical Theory of Diffraction," *Journal of Optical Society of America*, Vol. 52, pp. 116–130.

Kerker, M., 1961, *The Scattering of Light and Other Electromagnetic Radiation*, Academic Press, New York.

Kolar, A. K., Grewal, N. S., and Saxena, S. C., 1979, "Investigation of Radiative Contribution in a High Temperature Fluidized-Bed Using the Alternate Slab Model," *International Journal of Heat and Mass Transfer*, Vol. 22, pp. 1695–1704.

Ku, J. C., and Felske, J. D., 1984, "The Range of Validity of the Rayleigh Limit for Computing Mie Scattering and Extinction Efficiencies," *Journal of Quantitative Spectroscopy and Radiative Transfer*, Vol. 31, pp. 569–574.

Kudo, K., Yang, W. J., Taniguchi, H., and Hayasaka, H., 1985, "Radiative Heat Transfer in Packed Spheres by Monte Carlo Method," *Proceedings, U.S.-Japan Heat Transfer Joint Seminar*, J-4, p. 1–12.

Kumar, S., and Tien, C. L., 1987, "Dependent Scattering and Absorption of Radiation by Small Particles," *24th National Heat Transfer Conference (Pittsburgh)*, Aug. 9–12, HTD-Vol. 72, A.M. Smith and T. F. Smith, eds., pp. 1–7.

Kumar, S., Majumdar, A., and Tien, C. L., 1988, "The Differential-Discrete-Ordinate Method for Solving the General Equation of Radiative Transfer," *25th National Heat Transfer Conference (Houston)*, July 24–27.

Mengüç, M. P., and Viskanta, R., 1986, "An Assessment of Spectral Radiative Transfer Predictions for a Pulverized Coal-Fired Furnace," *Proceedings, 8th International Heat Transfer Conference (San Francisco)*, Vol. 2, pp. 815–820.

Mengüç, M. P., and Viskanta, R., 1983, "Comparison of Radiative Transfer Approximations for Highly Forward Scattering Planar Medium" *Journal of Quantitative Spectroscopy and Radiative Transfer*, Vol. 29, pp. 381–394.

Downloaded 16 Dec 2010 to 193.140.21.150. Redistribution subject to ASME license or copyright; see http://www.asme.org/terms/Terms_Use.cfm

Mickley, H. S., and Fairbanks, D. F., 1955, "Mechanism of Heat Transfer to Fluidized Beds," *AIChE Journal*, Vol. 1, pp. 374–384.

Ozisik, M. N., 1973, *Radiative Transfer and Interactions With Conduction and Convection*, Wiley, New York.

Percus, J. K., and Yevick, G. J., 1958, "Analysis of Classical Statistical Mechanics by Means of Collective Coordinates," *Physics Review*, Vol. 110, pp. 1–13.

Purcell, E. M., and Pennypacker, C. R., 1973, "Scattering and Absorption of Light by Nonspherical Dielectric Grains," *Astrophysics Journal*, Vol. 186, pp. 705–714.

Renzhang, Q., Wendi, H., Yunsheng, X., and Dechang, L., 1987, "Experimental Research of Radiative Heat Transfer in Fluidized Beds," *International Journal of Heat and Mass Transfer*, Vol. 30, pp. 827–831.

Rosseland, S., 1939, *Theoretical Astrophysics*, Oxford University Press, Clarendon, United Kingdom, pp. 113–115.

Sarofim, A. F., and Hottel, H. C., 1978, "Radiative Transfer in Combustion Chambers: Influence of Alternative Fuels," *Proceedings, 6th International Heat Transfer Conference* (*Toronto*), Vol. 6, pp. 199–217.

Sarofim, A. F., Hottel, H. C., and Fahimian, E. J., 1968, "Scattering of Radiation by Particle Layers," *AIAA Journal*, Vol. 6, pp. 2262–2266.

Saxena, S. C., Grewal, N. S., Gabor, J. D., Zabrodsky, S. S., and Galershtein, D. M., 1978, "Heat Transfer Between a Gas Fluidized Bed and Immersed Tubes," *Advances in Heat Transfer*, Academic Press, Vol. 14, pp. 150–248.

Schotte, W., 1960, "Thermal Conductivity of Packed Beds," *AIChE Journal*, Vol. 6, pp. 63–67.

Schuster, A., 1905, "Radiation Through a Foggy Atmosphere," *Astrophysics Journal*, Vol. 21, pp. 1–22.

Siegel, R., and Howell, J. R., 1981, *Thermal Radiation Heat Transfer*, 2nd ed., Hemisphere, New York.

Schwarzchild, K., 1906, "Equilibrium of the Sun's Atmosphere," *Ges. Wiss*, Gottingen, Vol. 1, pp. 41–53.

Tabanfar, S., and Modest, M. F., 1987, "Combined Radiation and Convection in Absorbing, Emitting, Nongray Gas-Particulate Tube Flow," ASME JOURNAL OF HEAT TRANSFER, Vol. 109, pp. 478–484.

Tien, C. L., 1985, "Radiation Properties of Particulates," *Handbook of Heat Transfer Fundamentals*, 2nd ed., Hemisphere, New York, pp. 14.83–14.91.

Tien, C. L., and Drolen, B. L., 1987, "Thermal Radiation in Particulate Media With Dependent and Independent Scattering," *Annual Review of Numerical Fluid Mechanics and Heat Transfer*, Vol. 1, pp. 1–32.

Tien, C. L., and Cunnington, G. R., 1973, "Cryogenic Insulation Heat Transfer," *Advances in Heat Transfer*, Vol. 9, pp. 349–417.

Tien, C. L., and Hunt, M., 1987, "Boundary-Layer Flow and Heat Transfer in Porous Beds," *Chemical Engineering Processes* (*Grenzchichtsrömung und Wärmeüdergang in Schüttungen*), Vol. 21, pp. 53–63.

Truelove, J. S., 1984, "The Two-Flux Model for Radiative Transfer With Strongly Anisotropic Scattering," *International Journal of Heat and Mass Transfer*, Vol. 27, pp. 464–466.

Ulrich, G. B., 1984, *A Guide to Chemical Engineering Process Design and Economics*, Wiley, New York.

van de Hulst, H. C., 1981, *Light Scattering by Small Particles*, Dover Publications, New York.

van de Hulst, H. C., 1980, *Multiple Light Scattering*, Vols. 1 and 2, Academic Press, New York.

Viskanta, R., 1982, "Radiation Heat Transfer: Interaction With Conduction and Convection and Approximate Methods in Radiation," *Proceedings, Seventh International Heat Transfer Conference* (*Munchen*), Vol. 1, pp. 103–121.

Viskanta, R., 1984, "Radiative Heat Transfer," *Progress Chemical Engineering* (*Fortschritte der Verfahrenstechniks*), Section A, Vol. 22, pp. 51–81.

Viskanta, R., 1966, "Radiation Transfer and Interaction of Convection With Radiation Heat Transfer," *Advances in Heat Transfer*, Vol. 3, T. F. Irvine and J. P. Hartnett, eds., Academic Press, New York, pp. 176–252.

Viskanta, R., and Mengüç, M. P., 1987, "Radiation Heat Transfer in Combustion Systems," *Progress Energy Combustion Science*, Vol. 13, pp. 97–160.

Vortmeyer, D., 1974, "Radiation Interaction With Conduction and Convection," *Proceedings, 5th International Heat Transfer Conference* (*Tokyo*), Vol. 6, pp. 129–135.

Vortmeyer, D., 1978, "Radiation in Packed Solids," *Proceedings, 6th International Heat Transfer Conference* (*Toronto*), Vol. 6, pp. 525–539.

Wang, K. Y., and Tien, C. L., 1983, "Radiative Heat Transfer Through Opacified Fibers and Powders," *Journal of Quantitative Spectroscopy and Radiative Transfer*, Vol. 30, pp. 213–223.

Wiscombe, W. J., 1980, "Improved Mie Scattering Algorithms," *Applied Optics*, Vol. 19, pp. 1505–1509.

Yamada, Y., Cartigny, J. D., and Tien, C. L., 1986, "Radiative Transfer With Dependent Scattering by Particles: Part 2—Experimental Investigation," ASME JOURNAL OF HEAT TRANSFER, Vol. 108, pp. 614–618.

Yang, Y. S., Howell, J. R., and Klein, D. E., 1983, "Radiative Heat Transfer Through a Randomly Packed Bed of Spheres by the Monte Carlo Method," ASME JOURNAL OF HEAT TRANSFER, Vol. 105, pp. 325–332.

Yener, Y., and Özişik, M. N., 1986, "Simultaneous Radiation and Forced Convection in Thermally Developing Turbulent Flow Through a Parallel-Plate Channel," ASME JOURNAL OF HEAT TRANSFER, Vol. 108, pp. 985–988.

Young, A. T., 1982, "Rayleigh Scattering," *Physics Today*, Vol. 35, pp. 42–48.

Yuen, W. W., and Wong, L. W., 1980, "Heat Transfer by Conduction and Radiation in a One-Dimensional Absorbing, Emitting, and Anisotropically Scattering Medium," ASME JOURNAL OF HEAT TRANSFER, Vol. 102, pp. 303–307.

Downloaded 16 Dec 2010 to 193.140.21.150. Redistribution subject to ASME license or copyright; see http://www.asme.org/terms/Terms_Use.cfm

Natural Circulation Loops

R. Greif
Department of Mechanical Engineering,
University of California,
Berkeley, CA 94720
Fellow ASME

Natural circulation loops encompass a broad range of applications and phenomena. Basic experimental and theoretical studies as well as overall performance and systems testing and analyses have been carried out on natural circulation loops. Research in this important area is being vigorously conducted throughout the world and a number of representative works and programs are discussed.

Introduction

Natural circulation loops are systems in which the flow is driven by thermally generated density gradients so that pumping is not required. The loops are often heated from below and cooled from above, which then establishes an unstable density gradient in the fluid. (Side heating and cooling are also common configurations.) Under the influence of gravity the lighter fluid rises and the heavier fluid falls and the fluid is said to flow due to natural convection.

Natural circulation loops provide for the transfer of energy without a pump and have many practical applications. For example, their extensive use in solar water heaters has resulted in many operating systems. In one configuration, solar radiation is absorbed by a collector surface, which transfers energy to an elevated tank by natural circulation of the heated fluid. The heated fluid then transfers energy by direct mixing or through a heat exchanger and finally returns to the collector. In the direct configuration, water is the circulating fluid; for the indirect system, a "nonfreezing" liquid is used. The operation is analogous to that of a gravity hot water system in a building with a boiler as the heat source. Natural circulation loops have also been used as cooling systems for internal combustion engines. In this application, engine heating causes the water in the engine jacket to rise and flow to the radiator. There it is cooled and returned to the engine jacket. Applications abound and also appear in nuclear reactor cooling, turbine blade cooling, computer cooling, permafrost protection, geothermal energy, highway de-icing, energy storage, etc. General reviews have been given by McKee (1970), Ostrach (1972), Japikse (1973), Zvirin (1981a), Mertol et al. (1981b), Norton and Probert (1982, 1986), and Mertol and Greif (1985, 1987). Japikse (1973) makes a distinction between natural circulation loops (sometimes called loop thermosyphons), where the flow is generally in one direction around the loop, and "thermosyphons," where, for example, the flow might be upward along the heated wall of a tube with an associated downward return flow in the core.[1] Japikse's comprehensive review emphasizes the latter systems and in view of this coverage, and the many recent contributions on natural circulation loops, this work will emphasize loop systems.

Theoretical Modeling of Natural Circulation Loops – Basic Assumptions and One-Dimensional Modeling

Some of the early experiments with natural circulation loops were carried out with fluids under conditions that were close to the thermodynamic critical point. Instabilities were observed in these experiments that were assumed to be caused by the large variations of the fluid properties in this region. However, Keller (1966) and Welander (1967) showed analytically that instabilities in natural circulation loops could result from the dynamics of the system independent of fluid property variations. In particular, they developed a one-dimensional model that was applicable to a simplified loop consisting of a point heat source and a point heat sink, which were connected by two vertical insulated branches. A comprehensive study was carried out by Creveling et al. (1975) for a torus located in a vertical plane. This work provided basic experimental data and made also direct comparisons with one-dimensional calculations for the stability characteristics of the flow in a natural circulation loop (also cf. Damerell and Schoenhals, 1979). Subsequently, many studies have been carried out for a large number of configurations and applications utilizing one-dimensional formulations.

To exemplify the basic approach, a closed toroidal loop of circular geometry is considered as shown in Fig. 1. The loop is heated continuously with a constant heat flux q over the bottom half of the area and is cooled continuously with a heat exchanger over the top half. For the cooled region, a constant wall temperature T_w and a constant heat transfer coefficient h are taken. Variations in the radial and circumferential directions are not considered so that the temperature and velocity are values that are averaged over the cross section and the only space coordinate θ runs along the loop. Axial conduction, viscous dissipation, and pressure work are neglected along with the effects of curvature. The flow is taken to be laminar and the fluid properties are considered to be constant except for the evaluation of the density in producing buoyancy. For this term only, the density is assumed to vary linearly with respect to the temperature.

From the equation of continuity for one-dimensional incompressible flow, the velocity is a function of time only; that is, $v = v(t)$. Integrating the momentum equation in the θ direction around the loop eliminates the pressure term and using the relation $\rho = \rho_w [1-\beta(T-T_w)]$ in the body force term yields

$$\rho_w \frac{dv}{dt} = \frac{g\rho_w\beta}{2\pi}\int_0^{2\pi} (T-T_w)\cos\theta\, d\theta - \frac{2\tau_w}{a} \qquad (1)$$

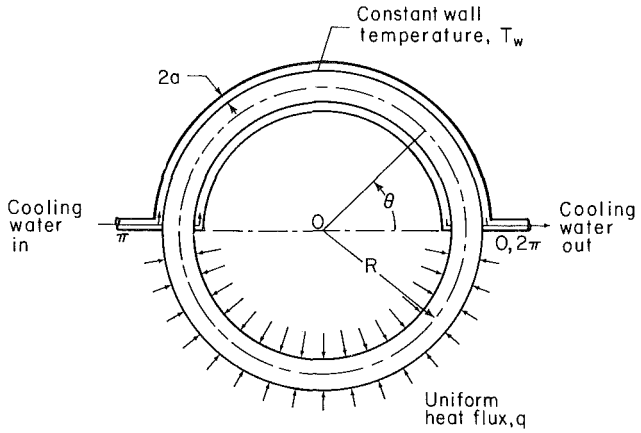

Fig. 1 Schematic diagram of the circular toroidal loop (Greif et al., 1979)

[1] Unfortunately, these designations are not unique; i.e., thermosyphon is also sometimes used to describe a natural circulation loop. For completeness, it is noted that both systems possess closed and open configurations.

Contributed by the Heat Transfer Division for publication in the JOURNAL OF HEAT TRANSFER. Manuscript received by the Heat Transfer Division February 4, 1988. Keywords: Heat Pipes and Thermosyphons, Natural Convection, Reviews.

Copyright © 1988 by ASME

Downloaded 16 Dec 2010 to 193.140.21.150. Redistribution subject to ASME license or copyright; see http://www.asme.org/terms/Terms_Use.cfm

To solve for the velocity from equation (1), it is necessary to obtain the temperature variation $T(\theta, t)$. The energy equations for the heated lower and cooled upper regions are given by

$$\rho_w c\left(\frac{\partial T}{\partial t}+\frac{v}{R}\frac{\partial T}{\partial \theta}\right)=\begin{cases}\dfrac{2h}{a}(T-T_w), & 0<\theta<\pi \quad (2a)\\ \dfrac{2}{a}q, & \pi<\theta<2\pi \quad (2b)\end{cases}$$

The solutions for the velocity and the temperature must be obtained by solving equations (1) and (2) simultaneously.

The governing equations are made dimensionless according to the following definitions:

$$\phi=\frac{T-T_w}{q/h}, \quad w=\frac{v}{V}, \quad \tau=\frac{t}{2\pi R/V}, \quad V=\left(\frac{g\beta \mathrm{Ra} q}{2\pi c\mu}\right)^{1/2} \quad (3)$$

where V is a characteristic velocity. The wall shear stress in equation (1) is expressed as $\tau_w = f\rho_w v^2/2$ and the friction coefficient for fully developed laminar flow (omitting buoyant effects) is used; that is, $f = 16/\mathrm{Re}$ with $\mathrm{Re} = \rho_w v 2a/\mu$. It is noted that in studying turbulent flows a friction coefficient that is independent of velocity, i.e., $\tau_w \sim v^2$, is sometimes used. This results in a characteristic velocity that is proportional to the one-third power of the heat input, i.e., $V \sim q^{1/3}$. Discussion of the friction and the heat transfer coefficients is presented later.

The dimensionless forms of equations (1) and (2) then become

$$\frac{dw}{d\tau}+\Gamma w=\frac{\pi\Gamma}{4D}\int_0^{2\pi}\phi\cos\theta\, d\theta \quad (4)$$

$$\frac{\partial\phi}{\partial\tau}+2\pi w\frac{\partial\phi}{\partial\theta}=\begin{cases}-2D\phi, & 0<\theta<\pi \quad (5a)\\ 2D, & \pi<\theta<2\pi \quad (5b)\end{cases}$$

The parameters D and Γ are defined by

$$D=\frac{2\pi Rh}{\rho_w caV}, \quad \Gamma=\frac{16\pi\mu R}{\rho_w a^2 V}=\frac{32\pi}{E} \quad (6)$$

E being the parameter used by Creveling et al. (1975).

The steady-state temperature profile $\phi_{ss}(\theta)$, may be obtained by solving equations (5*a*) and (5*b*) with $\partial\phi/\partial\tau = 0$, subject to the condition that the temperature is continuous at $\theta = 0, 2\pi$ and at $\theta = \pi^-, \pi^+$. The resulting expressions for $\phi_{ss}(\theta)$ are given by Creveling et al. (1975) and Greif et al. (1979). Then, substituting the results for $\phi_{ss}(\theta)$ into the integral of the momentum equation (4) with $dw/d\tau = 0$ yields the steady-state values of the velocity w_{ss}. At the steady-state condition, the buoyancy driving force is balanced by the frictional force and w_{ss} depends only on D. For small values of D, $w_{ss} \equiv v_{ss}/V \approx 1$. Note that ϕ_{ss} depends on both D and θ. Discussion of the transient and stability behavior is presented in the following sections.

Stability, Time-Dependent, and Steady-State Results

Introduction. As noted earlier, Keller (1966) and Welander (1967) developed a one-dimensional model to study the stability of the natural circulation in a tube that is bent into a rectangular shape that is standing in a vertical plane. The fluid is heated at the "center" of the lower horizontal segment (point heat source) and cooled at the "center" of the upper horizontal segment (point heat sink) with two vertical insulated tubes comprising the rest of the loop. Welander (1967) noted that at first glance it seems likely that the system would always be stable. The intuitive argument (also refer to Creveling et al., 1975) is that if the flow rate should increase above the steady-state value, there would be a corresponding increase in the friction and a decrease in the total buoyancy. This results in a decreased flow rate, which then acts to return the system to the original steady-state condition. A decrease in the flow rate produces the opposite effects, so the system is presumed to be self-correcting and stable. In general, the same reasoning is valid for more complex loop configurations.

Since it is known that natural circulation loops can be unstable, the simplified argument given above must be incomplete; Welander (1967) and Creveling et al. (1975) provided a plausible argument to clarify the possibility of instabilities. The loop is presumed to be operating in the steady-state condition. Then a small thermal disturbance causes a "pocket" of fluid to leave the heating section (at the bottom) at a temperature that is higher than normal for the steady-state condition. The hotter-than-normal pocket then moves upward more rapidly than is usual (due to the increased buoyancy) and

Nomenclature

a = radius of the toroid, Fig. 1; coefficient in the friction relation
A = surface area
b = exponent in the friction relation
c = specific heat
d = diameter
D = dimensionless parameter, equation (6)
E = dimensionless parameter, equation (6)
f = friction coefficient = $2\tau_w/\rho_v v^2$, frequency
g = acceleration of gravity
$\mathrm{Gr_m}$ = modified Grashof number
Gz = Graetz number
h = heat transfer coefficient per unit length
h_{fg} = heat of vaporization
k = thermal conductivity
L = length
p = pressure
Pr = Prandtl number
q = heat flux
Q = heat transfer rate
R = radius of the circular loop, Fig. 1
Ra = Rayleigh number
Re = Reynolds number
T = temperature
t = time
U = heat transfer conductance
V = characteristic velocity, equation (3)
v = velocity of the fluid
w = dimensionless velocity, equation (3)
W = flow rate
x = distance
α = angle of inclination
β = thermal expansion coefficient
Γ = dimensionless parameter, equation (6)
θ = space coordinate, Fig. 1
μ = absolute viscosity
ρ = density
τ = dimensionless time, equation (3)
τ_w = shear stress
ϕ = dimensionless temperature, equation (3)

Subscripts

c = condenser
ch = characteristic
e = evaporator
g = vapor
i = initial value
l = liquid
ss = steady state
w = wall
0 = location at $\theta = 0$

Downloaded 16 Dec 2010 to 193.140.21.150. Redistribution subject to ASME license or copyright; see http://www.asme.org/terms/Terms_Use.cfm

therefore, when it emerges from the cooling section (at the top), it is at a temperature that is higher than normal. As the pocket now moves downward, it is lighter and decelerates. Thus, the pocket enters the heated section once more, but at a higher inlet temperature and at a lower velocity. When it emerges from the heater, it is even hotter than before, and moves still more rapidly (upward) than before; the process is repeated and ultimately results in an unstable flow. A similar description holds for a cold pocket that originates at the exit from the cooling section. This argument provides a simple physical description for the possible build-up of oscillations.

Closed Toroidal Loop Studies. Welander (1967), Creveling et al. (1975), and Zvirin (1979) analyzed the stability of natural circulation systems by superimposing small disturbances, $w'(\tau)$ and $\phi'(\theta, \tau)$, on the steady-state results, w_{ss} and $\phi_{ss}(\theta)$. These variations for the velocity and the temperature were substituted into the momentum and energy equations and the resulting equations were then solved. The flow was considered to be stable if the disturbances were damped out and to be unstable if the disturbances were amplified. In carrying out their calculations for the toroidal loop, Creveling et al. (1975) used a friction factor relation of the form $f = a/\mathrm{Re}^b$ with $a = 151$, $b = 1.17$ for laminar flow and $a = 0.88$, $b = 0.45$ for turbulent flow; Zvirin (1979) used the relation $f = 16/\mathrm{Re}$. Marginal or neutral stability curves were obtained and the results are presented in Fig. 2. The stable and unstable regions are denoted by S and U, respectively; points to the right of the neutral stability curve are stable, points to the left are unstable.

Experimental confirmation of the instabilities in a loop containing water at a pressure of one atmosphere and at moderate temperatures was reported by Creveling et al. (1975). The experimental apparatus consisted of a glass tube of circular geometry, which was heated from below by ribbon type heating elements and cooled from above by a concentric cooling jacket. The heating approached a constant wall heat flux condition over the bottom and the coolant flow rate was large enough so that the upper wall was essentially at a uniform temperature. Two thermocouples were inserted inside the loop at the ends of the heater section to measure the temperature of the circulating fluid. The measured temperatures revealed that in some cases, steady-state conditions were achieved, and in other cases the flow did not reach a steady state and instead oscillated continually. For unstable operation, the fluid temperatures fluctuated with large amplitudes, corresponding to variations in the flow rate as well as to reversals of the flow direction. A flow reversal was indicated by sign changes in the temperature difference across the heating section and this was verified by visual observation of the motions of small particles in the circulating water. A neutrally stable condition corresponded to sustained fluctuations of the temperature of approximately constant amplitude.

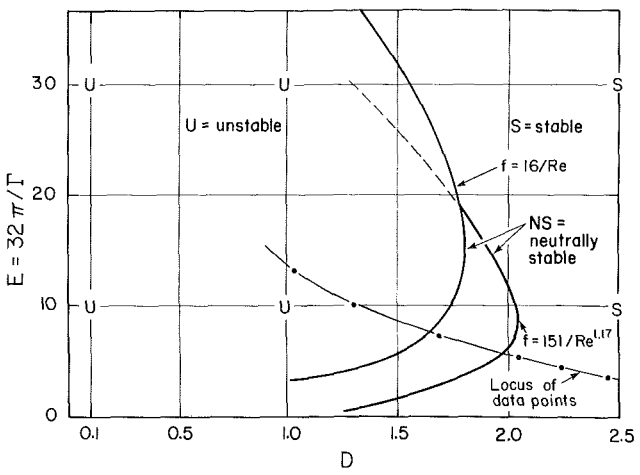

Fig. 2 Stability map for the toroidal loop (Greif et al., 1979)

The locus of unstable experimental data points in laminar flow is shown on the stability map of Fig. 2. For laminar flow, stable experimental conditions exist for values of D larger than 2.5 (not shown on the figure), which correspond to values of q less than 0.11 W/cm^2. It is noted, however, that the system is predicted to be stable for q less than 0.21 W/cm^2 (D larger than 2.0). This disagreement between the data and both neutral stability curves (which are based on the two friction factors) is significant but not surprising in view of the complexity of the problem.

Damerell and Schoenhals (1979) used the same apparatus to investigate the effect of an angular displacement (tilt) of the heated and cooled sections on the flow and the stability in the toroidal loop. For values of the angular displacement between -6 and $+6$ deg, there was a range of input heat fluxes for which instabilities were observed; namely, from ~ 500 to 9500 W/m^2 for no tilt angle to the limiting case of one value of the heat flux, ~ 4000 W/m^2, at a tilt angle of ± 6 deg. For operating points outside the unstable region, steady flow was reported when sufficient time was allowed for transient effects to die out.

Britt and Wood (1983) also carried out experiments in a toroidal loop and the results for the heat transfer and the temporal variation of the temperatures were in agreement with those reported by Creveling et al. (1975). Their results confirmed the observations of three distinctive regions of operation; namely, stable flow at low power, oscillatory flow at intermediate power, and stable flow again at high power. Flow reversals (recirculating cells) were also observed. The flow reversals occur because the fluid that flows along the loop wall changes temperature more rapidly than the bulk of the fluid. One of the cells consisted of warm fluid from the heated section of the loop mixing with the bulk fluid and the other cell consisted of cool fluid from the cooled section mixing with the bulk fluid. These changes in temperature are accompanied by changes in density, which cause the fluid along the wall to travel against the mainstream flow. Tests were also carried out with the loop rotated 90 deg so that the heating now begins at the bottom and terminates at the top; similarly, the cooling commences at the top and is completed at the bottom. In this heating and cooling configuration, the fluid near the wall always moves in the direction of the bulk flow and no reversals were observed.

The transient and stability behavior of the toroidal loop was also studied by Greif et al. (1979). They solved numerically the governing equations using a finite difference method to calculate the spatial and temporal variation of the temperature and the temporal variation of the velocity. Typical results are shown in Figs. 3 and 4 for a specified initial velocity w_i in the counterclockwise direction and an initial temperature $\phi_i = 0$. As the fluid emerges at $\theta = 2\pi$ (or $\theta = 0$) from the heated region, which extends over the range $\pi \leq \theta \leq 2\pi$, it cools by convection to the cold wall, which is maintained at a constant temperature $\phi_w = 0$ over the range $0 \leq \theta \leq \pi$. The results for the temperature profile $\phi(\theta, \tau)$ are for values of $\Gamma = 1$, $D = 2.5$, and $w_i = 1.5$ (see Fig. 3). The corresponding variation of the velocity $w(\tau)$ is shown in Fig. 4 along with results for other values of the initial velocity w_i. The results shown are characteristic of flows that attain steady-state values and are designated as stable flows. The steady-state results are shown dotted.

The stability of the toroidal loop was also studied. Calculations were carried out using as the initial conditions the steady-state distributions for the temperature and small perturbations from the steady-state values for the velocity. Results from these calculations were in agreement with the linearized stabili-

Downloaded 16 Dec 2010 to 193.140.21.150. Redistribution subject to ASME license or copyright; see http://www.asme.org/terms/Terms_Use.cfm

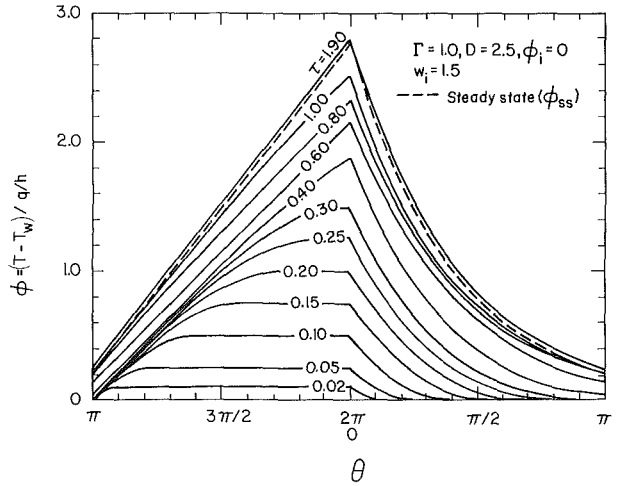

Fig. 3 Temperature distribution at different times for stable condition (Greif et al., 1979)

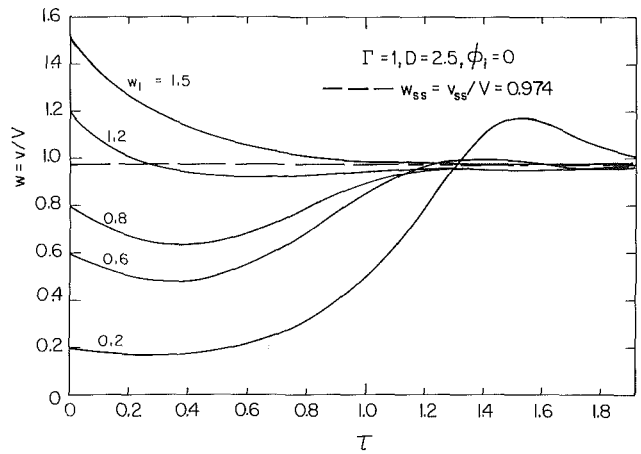

Fig. 4 Velocity variation for different initial velocities for stable condition (Greif et al., 1979)

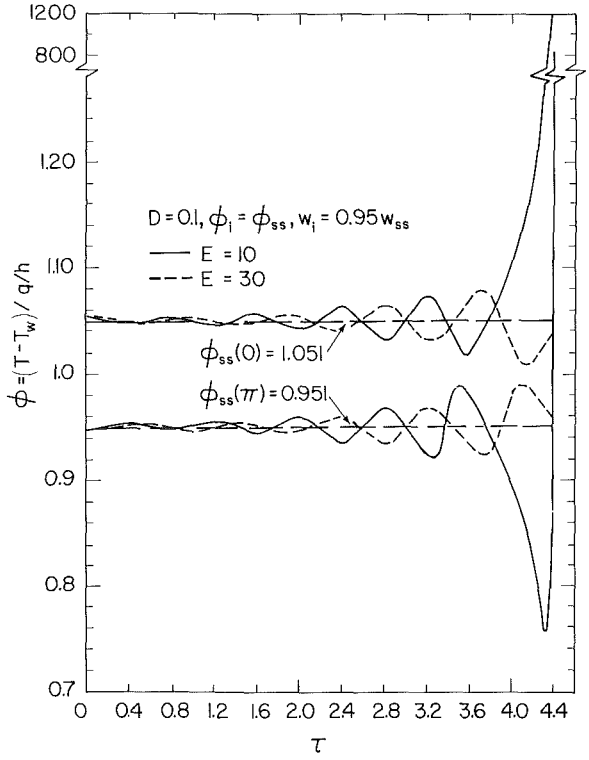

Fig. 5 Temperature variation for unstable condition (Greif et al., 1979)

ty analysis as exemplified in Fig. 2. Points located to the left of the stability curve exhibited a build-up of oscillations as shown, for example, in Fig. 5. The results show that the period of the oscillations is approximately equal to the time required for an element of fluid to circulate once around the loop; that is, $\Delta\tau \sim 1$ for $w_{ss} \sim 1$, which is in accord with the observations of Creveling et al. (1975). Calculations were also carried out for conditions close to the neutral stability curve (for f = 16/Re) shown in Fig. 2. For these cases, the magnitudes of the oscillations about the steady-state value remain almost constant, which is consistent with the linearized analysis.

The transient and stability behavior of the closed toroidal loop has been studied in regard to a number of considerations. Mertol (1980) included axial conduction in the energy equation and showed that the system then became more stable. The result was that the neutral stability curve shown in Fig. 2 was shifted to the left, thereby increasing the range of conditions for stable operation. Note that axial conduction reduces the temperature gradients, which results in less buoyancy and hence, smaller driving forces and velocities.

The effect of throughflow, that is, the addition and withdrawal of fluid from the loop, was studied by Zvirin (1980) for the loop consisting of a point heat source and sink and two vertical branches and by Mertol et al. (1981a) for the toroidal loop. It was shown that the effect of throughflow increased the stability of the system since some perturbations that might have led to instabilities (in the absence of throughflow) were now carried out of the loop.

Wacholder et al. (1982) analyzed the stability and transient behavior of a toroidal thermosyphon that is connected to a pressurized (or a surge tank) module. In most of the previous analyses the integral of the momentum equation around the loop is used, cf. equation (1). Wacholder et al. (1982) did not follow this approach. They solved numerically the differential momentum equation along with the equations of continuity and energy. Their equations also included the exchange of mass, momentum, and energy between the loop and the pressurizer. They concluded that over a wide range of cases studied, both with and without a pressurizer, there was no significant effect of the pressure distribution on the temperature distribution, mass flux, etc. The main effect of the pressurizer was to damp out the pressure oscillations and keep the pressure effectively constant. They also concluded that the prediction of instability depends largely on the assumed relations for the heat transfer coefficient and friction factor and their transient dependences on local and instantaneous thermodynamic and transport properties.

The effects of viscous dissipation and pressure work were examined by Bau and Torrance (1983) for several loops under different heating conditions. It was shown that the effects of viscous dissipation and pressure work have opposing influences on the flow and that both effects are of comparable magnitude.

Sen et al. (1985b) studied the steady-state velocity occurring in the inclined toroidal loop. It was demonstrated that the flow can have zero, one, two, or three steady-state velocities. It was also found that the maximum velocity is not always obtained at zero angle of inclination. The usefulness, as well as the limitations, of approximate solutions were also discussed.

The transient, steady-state, and stability behavior of a toroidal loop with a counterflow heat exchanger was studied by Mertol and Greif (1982a) and with a parallel flow exchanger by Mertol et al. (1983). Temperature profiles and stability maps were presented along with detailed physical descriptions of the mechanisms for the instabilities in these systems.

Downloaded 16 Dec 2010 to 193.140.21.150. Redistribution subject to ASME license or copyright; see http://www.asme.org/terms/Terms_Use.cfm

Another approach to the study of time-dependent flows has been carried out by Malkus (1972), Yorke and Yorke (1982), Hart (1984), Sen et al. (1985c), and Gorman et al. (1986). In general, it was assumed in these studies that the angular variation of the temperature could be expanded in the form of a Fourier series with unknown time-dependent coefficients. These expressions were then substituted into the governing partial differential equations and a set of ordinary differential equations was obtained. Steady solutions were obtained and the stability of these solutions was determined by perturbing the ordinary differential equations about the steady roots. The results have shown that steady, periodic, and chaotic motions are possible depending on the values of the parameters. Hart (1985) studied the motion in a loop containing a two-component fluid mixture. The boundaries of the loop were impermeable and gradients in the solute resulted from Soret diffusion, i.e., where a molecular flux of the solute was generated by an internal temperature gradient. Hart (1985) examined the existence and stability of steady-state solutions over a range of Rayleigh numbers and dimensionless Soret coefficients, $Q = \Gamma^* S_0(1-S_0)\beta/\alpha$, where Γ^* is the Soret coefficient, S_0 is the ambient salinity, β is the volumetric expansion coefficient, and α is the coefficient of thermal expansion. For positive Soret coefficients and Rayleigh numbers greater than one, the flows were found to be primarily thermally controlled and solute diffusion was of little importance. However, if the Rayleigh number was somewhat less than one, a wide variety of flow patterns was obtained including steady flow, period-doubling cascades, and chaos. For negative Soret coefficients, periodic and chaotic oscilllations analogous to those of thermohaline convection are predicted.

Gorman et al. (1984, 1986) carried out experiments in a toroidal thermosyphon to study the nonlinear dynamics of this system. The characteristics of five flow regimes were discussed encompassing no flow, steady circulation, and three different chaotic flow regimes. A systematic and detailed comparison between the observed flows and the nonlinear dynamics of the Lorenz model showed consistent results.

Closed Loops in Varied Configurations and Applications. The preceding coverage has emphasized the closed circular loop because of the number of theoretical and experimental studies that have been made for this configuration. Other geometries will now be discussed.

Holman and Boggs (1960) conducted experiments to investigate the heat transfer to Freon 12 near the critical state in a natural circulation loop. No results were presented for conditions where boiling could have occurred. The system consisted of two vertical branches, a horizontal bottom section with large curvatures at the corners, and a curved top section. A lower portion of one vertical branch was heated by passing an electric current through the tube while the upper portion of the other vertical branch was cooled in a heat exchanger. Measurements were made of the power input, the outside wall temperature, and the temperature, pressure, and pressure drop in the fluid. To correlate the results for the heat transfer, steady-state momentum and energy balances were made using relationships for the friction for laminar and for turbulent flows. Holman and Boggs observed fluctuations in the pressure on the order of 20 to 30 psi in the regions close to the critical state. These fluctuations were accompanied by intense vibrations of the test apparatus. When the cooling water flow rate was increased, the pressure was reduced and the fluctuations subsided. However, when the cooling water flow rate decreased or the power was increased, the fluctuations became more severe and did not subside until the pressure had risen well above the critical value.

Zvirin et al. (1977) modeled a natural circulation solar water heater to obtain the steady-state temperature distribution and the flow rate. A simpler model of the system assuming a linear distribution for the temperature was also presented and the usefulness and limitations of the simpler analysis were demonstrated. Zvirin et al. (1978) studied the stability of a solar water heater by superimposing small disturbances on the steady-state results. Linear temperature distributions were utilized and it was found that perturbation modes decayed very slowly and oscillatory modes had periods on the order of the time required to circulate around the loop. It was concluded that system instabilities could occur at high rates of energy utilization. Shitzer, et al. (1979) carried out measurements in a solar water heater. It was concluded that the temperature profiles inside the collector tubes could be assumed to be almost linear for most of the day. Fluctuations in the water flow rate were measured in the absence of significant fluctuations in the solar insolation.

Mertol et al. (1981b) analyzed the performance of the natural circulation solar water heater by solving the unsteady equations of continuity, momentum, and energy over the entire loop. The temperatures, flow rates, and system efficiencies were calculated using a detailed loop model in a system that included a heat exchanger in a storage tank. The circulating fluid was taken to be a propylene–glycol solution and withdrawal of water from the storage tank was permitted. Detailed spatial and temporal variations were obtained. The calculations showed that the daytime system performance is generally insensitive to the tank stratification, to the tank elevation relative to the collector, and to the flow resistances for the commonly available configurations.

Chato (1963) analyzed the natural circulation in vertical multiple channel systems with different heat inputs. In particular, a detailed analytical and experimental investigation was made for a system with three vertical tubes contained between two constant temperature headers. The results showed that such systems can be unstable due to multiple metastable flow patterns. The velocity was estimated using ink injection and it was noted that transition to turbulence was observed at low Reynolds numbers.

Zvirin et al. (1981b) also carried out a theoretical and experimental study of natural circulation in an apparatus with parallel loops. Their system, which was relevant to a pressurized water reactor, consisted of an electrically heated core and two parallel loops with once-through heat exchangers. Tests were performed for steady-state and transient conditions with heat removal from either or both heat exchangers. It was shown that the core flow resistance, input heat distribution, and upper plenum geometry yielded three-dimensional flow effects, which contributed to the overall difference (of 30 percent) between the analytical and experimental results. Under certain conditions, oscillations in the flow were observed, which were accompanied by instabilities and flow reversals. The analysis utilized the assumption of a single equivalent loop. Under steady-state conditions, the flow rate was obtained from the solution to the energy equation and the integral of the momentum equation. For the transient behavior, overall energy balances were used to estimate the characteristic time constant of the system.

Gruszczynski and Viskanta (1983) and Hallinan and Viskanta (1985, 1986) studied the flow and heat transfer for water in a rectangular loop in which tube bundles served as the source of heat in one vertical leg and as the heat sink in the other vertical leg. The purpose of the work was to gain improved understanding of the behavior of a natural circulation loop containing tube bundles. Fluid temperatures were measured along the loop and a fluorescent dye was injected for flow visualization. Transient and steady-state tests were conducted and an unsteady one-dimensional formulation was used to model the flow. Detailed comparisons were made between the predicted and measured temperatures and good agreement was obtained under both transient and steady-state conditions.

Downloaded 16 Dec 2010 to 193.140.21.150. Redistribution subject to ASME license or copyright; see http://www.asme.org/terms/Terms_Use.cfm

Sen and Fernandez (1985a) modeled multiple-loop systems for the case when branches start from one point and finish at another point. All branches consisted of tubes that were of the same cross-sectional area but could be of different lengths. The governing equations were obtained for both conducting and nonconducting fluids. The authors presented a methodology for solving the resulting equations and emphasized that the effect of small differences, between seemingly identical branches, on the steady-state operation of the loop has yet to be fully determined.

Chen (1985) studied the stability of the flow in a rectangular loop that is heated over the lower horizontal segment and cooled over the upper horizontal segment. A range of loop diameters and aspect ratios was considered for both laminar and turbulent flows. In an earlier study under steady-state conditions, Chen (1982) introduced a modified Grashof number G_m, which incorporated the influences of loop diameter and geometry. Under steady-state conditions, the loop configuration for maximum heat transfer rate was determined to be

$$G_m(\max Q) = 2^{\frac{b-n-1}{1-n}} \tag{7}$$

where b and n are the exponents in the expressions for the friction and heat transfer coefficients, respectively. In the stability analysis, it is shown that the flow is stable provided that G_m is less than a critical value. Since the calculated critical value is found to be much larger than G_m (max Q), it is concluded that it is possible to design a loop so that it can operate efficiently and without oscillations. Calculations that were carried out for values of G_m above the critical value showed that oscillatory instabilities occurred over a narrow range of values of the friction parameter. The calculated neutral stability conditions showed that the flow is least stable for a square loop, that is, when the aspect ratio of the loop approaches unity. It is also found that the frequency of the convection-induced oscillation is slightly higher than the angular frequency of a fluid particle traveling around the loop.

The thermal performance of a rectangular loop was studied by Huang and Zelaya (1988). The loop is shown in Fig. 6 and contained an electrical heating ribbon attached to the lower portion of the hot leg and a cooling jacket with coolant flowing upward over the upper portion of the cold leg. The loop had an inside diameter of 2.8 cm, a total length of 450 cm, with L_c = 0.48 m, L_h = 0.60 m, H = 1.5 m, and Δz = 0.96 m. Thermocouples were installed along the centerline of the tube and the measured temperature distribution is presented in Fig. 7 at different times including steady-state conditions. The calculated curves were obtained using a one-dimensional analysis of the form presented in equations (4) and (5) for the toroidal loop. The overall heat transfer coefficient between the water in the loop and the coolant water was obtained from the measurements in conjunction with an energy balance. The friction was calculated by using a conventional correlation with an effective length L_{ec}, obtained from piping equations. The steady-state calculations yielded results for the heat transfer that were in good agreement with the measurements. It was noted that the relation for the heat transfer was almost identical to the correlation obtained by Holman and Boggs (1960) for their data with Freon 12 as the loop fluid. It was also pointed out that oscillations occurred during the starting period but these were damped out and steady-state operation was obtained.

A stability analysis of the rectangular loop was carried out by Huang and Zelaya (1987). Their results indicated that reducing the loop friction and increasing the distance between the heated and cooled sections would improve the system efficiency but might, in turn, result in instabilities, which would then reduce the system efficiency.

A more complex configuration is related to the Savannah River power plant, which has nuclear reactors filled with tubular assemblies containing uranium. Under certain conditions after the reactor is shut down, the residual decay heat is removed by natural convection only. The study of this phenomenon prompted the work of Steimke (1985) who carried out an experimental and theoretical investigation of the natural circulation of water in a loop where the flow channels are the annuli between three concentric cylindrical surfaces. The system consisted of a central rod, a concentric cylindrical heater, and a concentric cylindrical casing (see Fig. 8). The surfaces have longitudinal ribs that separate them and form annular passages. During operation, water in the inner annulus, i.e., between the central rod and the inner surface of the heater, is heated and rises. Water in the outer annulus, i.e., between the outer surface of the heater and the casing, descends as it loses heat to the cooler casing and the water surrounding it. The casing, heater, and inner rod were made from aluminum, stainless steel, and glass-filled polyester, respectively. Stainless steel was chosen for the heater because it has a relatively high electrical resistivity and has a thermal conductivity similar to that of uranium. The entire assembly was placed in a tank of water and the upper portion of the casing was above the surface of the water. The apparatus contained

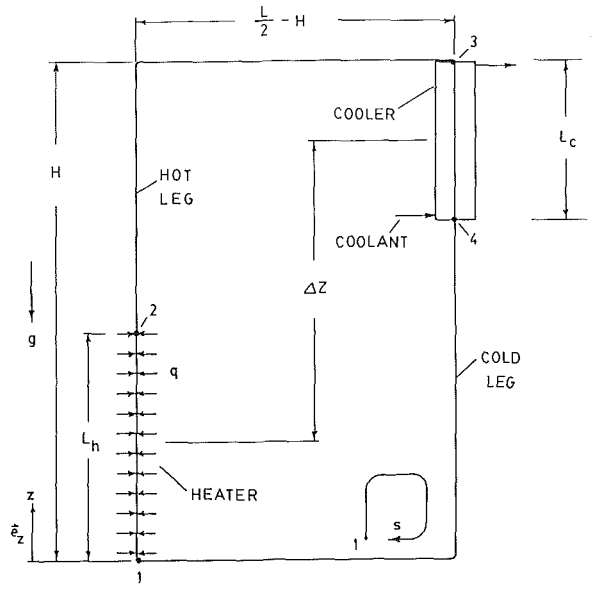

Fig. 6 Schematic diagram of the rectangular loop (Huang and Zelaya, 1988)

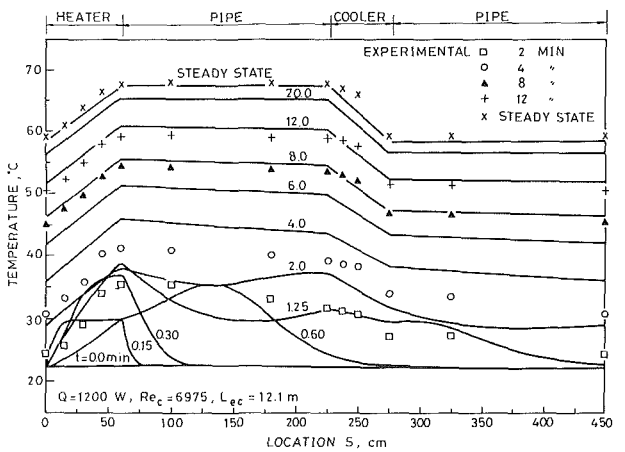

Fig. 7 Temperature distribution in the rectangular loop (Huang and Zelaya, 1988)

Downloaded 16 Dec 2010 to 193.140.21.150. Redistribution subject to ASME license or copyright; see http://www.asme.org/terms/Terms_Use.cfm

four electrical conductivity probes, one at each end of the two annuli. The probes were used to measure the time required for a pulse of salt tracer, made neutrally buoyant with the addition of ethanol, to travel the length of the loop. The system also contained five thermocouples, one at each end of both annuli and one embedded in the heater near the top.

An analysis was made based on a one-dimensional model. Results were obtained from the numerical solution to the conservation equations of mass, momentum, and energy for steady laminar flow. Friction factors and heat transfer coefficients were specified for the annuli and the heat transfer from the casing to the surrounding tank water was also included. Agreement between the calculated and measured temperatures, velocities, and Nusselt numbers was reasonably good. The discrepancies were presumed to result from the approximate specifications for the friction and the heat transfer coefficients and the complicated heater support was also noted. A comparison of the results for the velocity of the water in the inner annulus is shown in Fig. 9.

Seki et al. (1980) carried out an experimental study with a concentric two-tube configuration with water and fluorocarbon R-11 as the circulating fluids. Heat was supplied to the outer tube whose inner surface was maintained at a constant temperature. The inner tube was open at both the bottom and the top and the heating caused an upflow in the annulus between the tubes. At the top, the fluid entered a tank (reservoir), was cooled by a heat exchanger, and then descended via the inner tube to the bottom. At the bottom, the fluid continued outward to the annulus between the tubes and then upward. Steimke (1985) analyzed the flow and heat transfer in the experiments of Seki et al. (1980) utilizing the one-dimensional approach discussed above. The calculated results, which were expressed in terms of overall Nusselt and Rayleigh numbers, were in good agreement with the experimental data.

Acosta et al. (1987) made an experimental and theoretical study of a tilted square loop. Heating was carried out with an electrical resistance heater and cooling utilized a coaxial cylindrical heat exchanger. The heating and cooling were on opposite sides of the square loop. The loop was mounted on a vertical frame that permitted rotation about its horizontal axis. Different types of flow patterns were observed. These included time-independent flows as well as oscillatory flows, which persisted for at least 40 min with no apparent change in amplitude or frequency. In addition, flow instability due to a small change in the tilt angle was also observed. However, chaotic behavior, which had been previously reported for the toroidal loop, was not seen in the tilted square loop. Acosta et al. (1987) also demonstrated experimentally the existence of two stable solutions for certain values of the heat input and the tilt angle. The existence of multiple steady-state flows in natural circulation loops had been predicted by Damerell and Schoenhals (1979), Ramos et al. (1985), and Sen et al. (1985b) and this work represented an experimental verification. However, it was stated that the complete behavior is much more complex than that envisioned by a simple theory.

Takeda and Fischer (1987) studied the use of the natural circulation of a liquid lead–bismuth eutectic to transport the energy deposited by a high-intensity proton beam from a spallation neutron source. An earlier concept used natural convection in a simple tall cylindrical pot, without a guide tube, to transfer the energy to a heat exchanger. However, analytical and experimental investigations showed flow instabilities such as swaying or bifurcation and for this reason a new configuration with a guide tube was modeled. The loop consisted of an interior channel with an internal heat source at the bottom. The heated liquid metal rose to the top of the enclosure where it then divided outward into an annular channel surrounding the interior. A heat exchanger was placed at the upper portion of the annular region. A simplified model of the loop was used to analyze the thermal and fluid behavior.

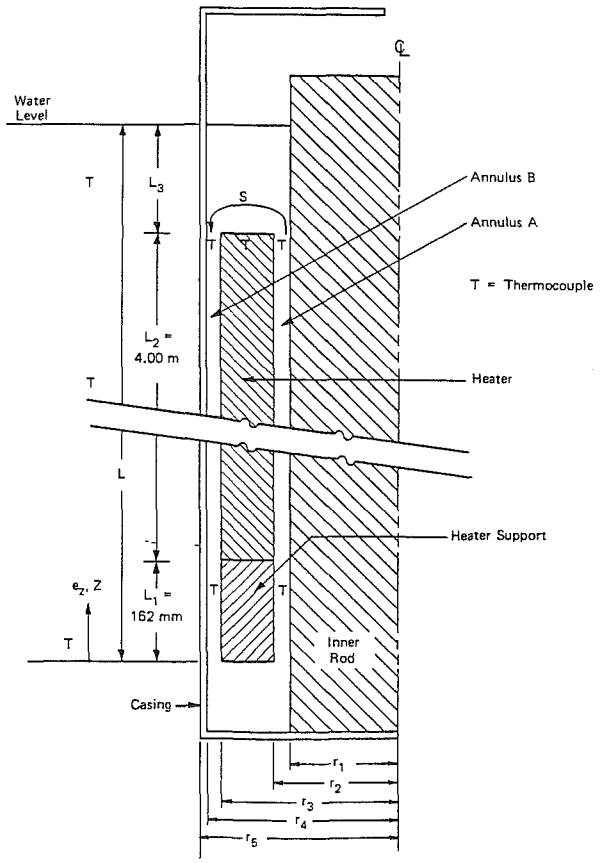

Fig. 8 Schematic diagram of concentric cylinder loop (Steimke, 1985)

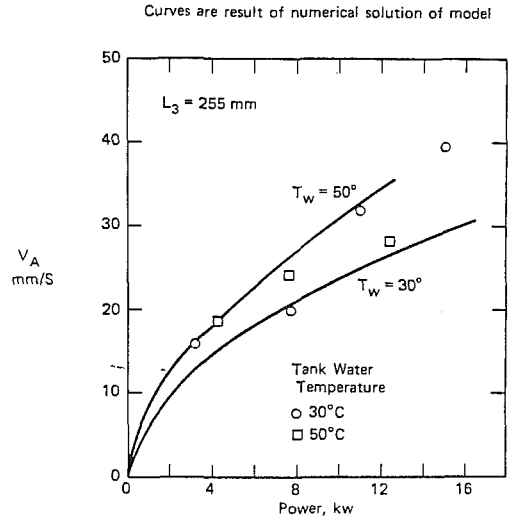

Fig. 9 Results for the velocity in the concentric cylinder loop (Steimke, 1985)

The model consisted of two vertical legs, one leg simulating the interior channel and the other corresponding to the outside annular region. An internally heated section located along the lower portion of one leg represented the target of the proton beam. A heat exchanger was located along the upper portion of the other leg and was simulated by a volumetric heat source.

The flow and energy transfer were studied by utilizing a one-dimensional model. The momentum equation corresponded to equation (4) while the energy equation differed from equation (5) by including the axial conduction contribu-

Downloaded 16 Dec 2010 to 193.140.21.150. Redistribution subject to ASME license or copyright; see http://www.asme.org/terms/Terms_Use.cfm

tion. The equations were solved numerically using a finite difference formulation for the derivatives with a Simpson formula for the integral. The results showed oscillations in the velocity and temperature profiles which damped out, resulting in steady-state behavior. The pressure loss from the turning of the flow at the bottom of the target was modeled (by modifying the friction coefficient to include a contribution for a 180 deg turn). It was noted that the general oscillatory behavior was the same as for the calculations, excluding this contribution, but the steady-state value of the velocity was lower, which resulted in a higher maximum temperature. The effect of energy deposition outside the guide tube was also studied.

Zvirin (1985) studied the onset of motion in a symmetric natural circulation loop. The loop consisted of two vertical insulated branches, which connect two reservoirs at the bottom and the top. The fluid completely filled the system and the temperature at the bottom reservoir was maintained at the constant value T_D and at the upper reservoir the value was T_U. Heating from below was investigated, i.e., $T_D > T_U$. The one-dimensional conservation equations were used and the steady-state solution for the velocity yielded the critical Rayleigh number, $\mathrm{Ra}_c = 6$, below which there is no steady flow possible. Note that $\mathrm{Ra} = V_{ch}h/\alpha$, where $V_{ch} = \beta g(T_D - T_U)a^2/16\,\nu$ is the steady-state velocity omitting axial conduction, h is the height of the loop, and a is the radius of the connecting tubes. A linearized stability analysis showed that for $\mathrm{Ra} > \mathrm{Ra}_c$, the rest state is always unstable, i.e., there exists a monotonically growing perturbation that increases with Ra and decreases with the modified Prandtl number, $8(h/a)^2\nu/\alpha$.

Open Loop Studies. Reid et al. (1975) modeled the behavior of a concentric tube open loop that is used for protection of permafrost. The device is called an air convection (or air) pile and makes use of a 0.457 m diameter pipe that is used for pilings. A smaller diameter (and shorter) tube is inserted concentric with the larger pipe. In winter, the ground is warmer than the ambient air. Thus, the air in the annulus is heated by the surrounding ground and rises up the annulus while the colder air within the smaller tube moves to the bottom. A heat exchange is thereby established and heat is continually removed from the ground surrounding the pile. In the summer the ground is colder than the air and the air in the device is cold and stable. In the analysis, a boundary layer flow was assumed and both laminar and turbulent flows were considered. The authors compared the predicted vertical mean temperature profiles, total heat removal rates, and average velocities with the available experimental data and concluded that the model correctly predicted the gross performance of the loop. However, it was noted that the unavailability of detailed experimental data precluded comparisons of the local temperature and velocity profiles.

Kreitlow et al. (1978) studied the heat transfer in downhole heat exchangers that are used to extract energy from relatively low-temperature geothermal walls. They considered the convection through and around a wellbore casing that was perforated at different depths. Analytical models were developed for the flow in the cased well both with and without a heat exchanger. Temperature measurements showed that the uncased wells have a substantial temperature gradient with the hottest temperature at the bottom and considerably lower temperatures at the static water level. For the cased well, with the downhole heat exchanger not operating, an essentially constant temperature resulted from the water level to the bottom. For the condition with the downhole heat exchanger operating, the temperatures of the well fluid were highest at the water level and decreased with depth. The model that was used to study the convection considered a vertical impermeable cylindrical tube located concentrically within a vertical cylindrical "hole" that is surrounded by an infinite impermeable medium. The inner cylinder represented the casing while the cylindrical hole in the medium represented the wellbore, which was surrounded by the earth. A flow can take place in the vertical annulus that is formed between the inner cylinder and the earth. In the analysis, it was assumed that there was an open, constant temperature aquifer at the bottom. Water fills both the inner cylinder and the annulus to a level just below the top of the cylinders. Just below the water level, the casing has perforations that allow fluid to flow from inside the (impermeable) casing to the annulus or vice versa. The temperature of the medium was assumed to increase linearly with depth. A motion results from the temperature difference between the hot reservoir fluid and the relatively cooler well walls. The casing of the well isolates the upward and downward flows, which results in a greatly increased bulk fluid flow relative to the uncased situation, and a nearly uniform temperature profile inside the casing. Because both the well walls and the casing were assumed to be impermeable, the mass flow rate through the casing is the same as that through the annulus but in the opposite direction. The well walls provide the cooling so that the flow is expected to be down the annulus and up the inside of the casing. A one-dimensional analysis was used with the variations in the vertical direction; heat transfer was assumed to occur only in the radial direction. Without a heat exchanger, it was found that the model predicted flows that were of the same order of magnitude, but were somewhat less, than the experimental values. The difference was attributed to the influence of the wall boundary conditions. Also, mixing at the bottom of the two cylinders was neglected in the analysis. An analysis was also made with a downhole heat exchanger with downward flow inside the casing. This model was used to predict the influence of design variables on the behavior of the system and results showed that minor design changes could increase the energy output by over 50 percent.

Torrance (1979) investigated the natural convection flow in an open loop that connected two reservoirs. The loop is embedded in an impermeable medium of high thermal conductivity, which is heated uniformly. The temperature of both the medium and the loop walls is assumed to increase linearly with depth. These loops or aquifers may occur in the earth's crust and result from the flow of groundwater through a connected sequence of fractures or through permeable layers in folded sedimentary formations. Torrance (1979) developed a one-dimensional analytical model with the water flowing through the aquifers being heated by the geothermal gradient. The water in the ascending leg was warmer than that in the descending leg, which resulted in a net buoyant head and natural circulation. Results were obtained for steady-state operation over a wide range of loop geometries and system parameters. The limits of a very narrow (vertical) loop and wide (elliptical) loop were examined and generally higher exit temperatures were achieved for the latter configuration. The results showed that higher exit temperatures require long residence times at or near the maximum depth of the loop. For a semicircular loop (half-torous), the result for the critical Rayleigh number for the onset of convection was obtained; namely, $\mathrm{Ra}_{\mathrm{crit}} = 4fL\mathrm{ReNu}/b\pi$, where L is the length of the loop and b is the principal radius (or the maximum depth). The addition of a horizontal, underground section between the ascending and descending portion of the loop was introduced to study the behavior of thermal springs. For this configuration, reasonable agreement was obtained with the exit temperatures and flow rates observed in the Virginia thermal springs region.

Torrance and Chan (1980) extended the work of Torrance (1979) by assuming finite conductivity for the impermeable solid surrounding the semicircular loop. Steady-state flow and heat transfer were studied with conduction in the surrounding medium. Results for the mean velocity, exit temperature, convective heat transfer rate and critical Rayleigh number for the onset of motion were obtained.

Downloaded 16 Dec 2010 to 193.140.21.150. Redistribution subject to ASME license or copyright; see http://www.asme.org/terms/Terms_Use.cfm

Bau and Torrance (1981a, 1981b) performed experiments and developed analytical models to study the transient and steady behavior and stability of a U-shaped open loop. The top of the loop was open to an isothermal reservoir. For symmetric heating, the lower (horizontal) segment of the loop was heated and the vertical legs were adiabatic. For asymmetric heating, the horizontal segment and one vertical leg were heated at rates Q_1 and Q_2, respectively. The loop was filled with water or with a water-saturated porous medium. Experimental results for symmetric heating included the starting transients and the friction factors and heat transfer rates at steady state for flow Reynolds numbers varying from 4 to 1000; the input heat flux ranged from 0 to 2300 W. Temperatures were measured at the inlets and outlets of the heated and cooled sections, at the center of the heated section, and at the inlet and exit to the reservoir. For the analysis, a one-dimensional model was formulated for a loop consisting of three straight tubes of diameter d, height b, horizontal length a, and overall length L.

For symmetric heating, experiments were initiated after allowing the entire system to come into equilibrium with the room. Flows developed in either direction through the loop and a small amount of heating was then applied to create a temperature difference between inlet and outlet to support a unidirectional flow. The experiments suggested that the quiescent initial state (the rest state) is unstable when heated from below. Stability analyses showed that the rest state is always unstable; the critical Rayleigh number for the onset of motion is zero and the steady-state motion for such symmetric heating is stable. Also, the starting transients in the loop were observed experimentally and were simulated numerically and a strong qualitative similarity between the observed and the calculated results was obtained. After the start of heating, experimental observations revealed that heat was transferred to the fluid, for the porous loop, in the horizontal section by conduction and by local convective circulation. Following the transients, stable, nonoscillating, steady-states were achieved.

For asymmetric heating, Bau and Torrance (1981b) examined the influence of adding Q_2 to a vertical leg while simultaneously adding heat Q_1 to the horizontal leg. Stable motion was obtained when heat is added to an ascending flow in the vertical leg and oscillatory flow may result when heat is added to a descending flow in the vertical leg. The heat supply Q_2 to the descending leg was increased in small steps. During this transient step heating, the flow first decelerated due to the reduced buoyancy effect and then accelerated to a new steady state. For large Q_2, a steady state was not achieved and the flow oscillated with a period about twice the flow time through the loop. The oscillations amplified until the flow reversed its direction. This corresponded to an ascending motion in the heated vertical leg, which was stable after the disturbances damped out. In the porous loop, time intervals as long as 36 h were observed between the start of oscillations and an ensuing flow reversal. The stability behavior was also studied by using both linearized stability analysis and numerical solutions of the governing equations. It was found that the cases of symmetric heating, asymmetric heating favoring the ascending flow, and weak asymmetric heating favoring the descending flow were all stable. When the descending leg was heated to a critical value, the flow was observed to start to oscillate and eventually reverse.

Multidimensional Studies: Theoretical and Experimental Results

Many investigators have emphasized the importance of multidimensional effects. With respect to analytical work, one-dimensional formulations are limited by the a priori specifications of the friction and heat transfer coefficients, f and h, respectively; in multidimensional approaches, these quantities are determined from the solution to the governing equations. Mertol et al. (1982b) analyzed the steady-state flow and heat transfer in a toroidal loop and included variations in both the radial, r, and axial, θ, directions. The parameters are the Prandtl, Graetz, and characteristic Reynolds numbers:

$$\mathrm{Pr}=\frac{\mu c}{k}\,,\quad \mathrm{Gz}=\mathrm{Re}_{ch}\mathrm{Pr}\left(\frac{2a}{2\pi R}\right)=\frac{2\rho_w c a^2 V}{\pi k R}\,,\quad \mathrm{Re}_{ch}=\frac{\rho_w V a}{\mu} \tag{8}$$

where V is defined in equation (3). It was shown that the friction parameter $f\mathrm{Re}$ increased significantly as a function of the Graetz number. The heat transfer coefficients, or the local Nusselt numbers, in the heated and cooled sections decreased with respect to distance along the loop with the Graetz number as a parameter. The heat transfer increased for increasing values of the Graetz number and this was accompanied by smaller temperature differences. The numerical predictions were also compared with the experimental data of Creveling et al. (1975) for the steady-state heat flux and good agreement was obtained. Mertol et al. (1984) subsequently utilized a two-dimensional formulation to investigate the transient flow and heat transfer in the toroidal loop. Results were obtained for the velocity and temperature profiles and the transient variations of the friction and heat transfer coefficients were presented.

Stern and Greif (1987) carried out detailed fluid temperature measurements in a toroidal loop using a small, movable thermocouple probe. The loop was oriented in the vertical plane and was heated over the lower half and cooled over the upper half. Averaged and fluctuating temperature measurements were made along the tube diameter extending from the inside to the outside surface at the entrance and exit of the heating sections. The inside surface refers to the tube location that is closest to the center of the torus, radial location $R-a$; the outside surface corresponds to $R+a$. Averaged results are shown in Figs. 10 and 11. A prominent feature of the temperature profiles leaving the heated section (flowing upward) was that the maximum value of the temperature occurred at the inside surface for all heat inputs. The magnitude of this peak and the steepness of the profile near the inside surface increased with increasing values of the heat input. For the fluid entering the heating section (flowing downward), the maximum temperature also occurred at the inner surface. At this location, the magnitude of the temperature difference between the wall and the middle of the profile was greatest for an intermediate heat input. Results from one-dimensional calculations yielded temperatures that were substantially greater than the measured values. Temperature histograms and strip chart recordings were also obtained that showed that the greatest amplitudes of the fluctuations occurred at the locations near the inner surfaces. Flow visualization indicated that this may result from recirculating flow regions at the entrances to the heating and cooling sections.

The experiments of Creveling et al. (1975), Damerell and Schoenhals (1979), Acosta and Manero (1984), and Stern and Greif (1987) reported the presence of three-dimensional effects, such as flow reversals, nonzero cross-stream velocities, and nonaxisymmetric temperature profiles. The one- and two-dimensional analyses all assumed that the flow was solely in the axial direction and that the effect of pipe curvature was negligible. Therefore, three-dimensional effects could not be predicted in these studies.

Lavine et al. (1986, 1987) carried out three-dimensional analyses of the flow and heat transfer in a toroidal loop. The flow was assumed to be steady, laminar, and symmetric about the vertical plane containing the circle of radius R formed by the pipe centerline. The conservation equations were solved using a modified version of the TEACH code (cf. Gosman and Ideriah, 1983; Patankar, 1980; Humphrey, 1978; Lavine,

Downloaded 16 Dec 2010 to 193.140.21.150. Redistribution subject to ASME license or copyright; see http://www.asme.org/terms/Terms_Use.cfm

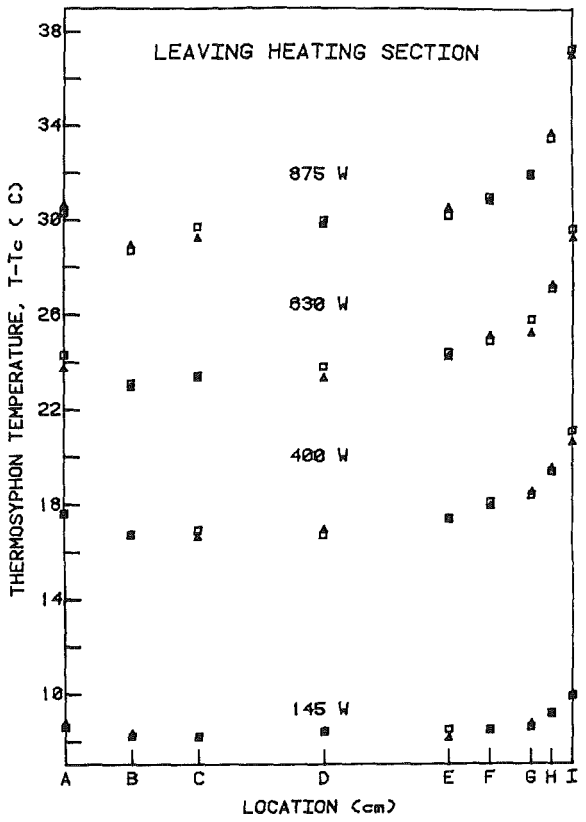

Fig. 10 Temperature profiles leaving heating section of toroidal loop; A is outside, I is inside (reprinted with permission from C. Stern and R. Greif, *Warme- und Stoffubertragung*, Vol. 21, p. 279. © 1987, Springer-Verlag)

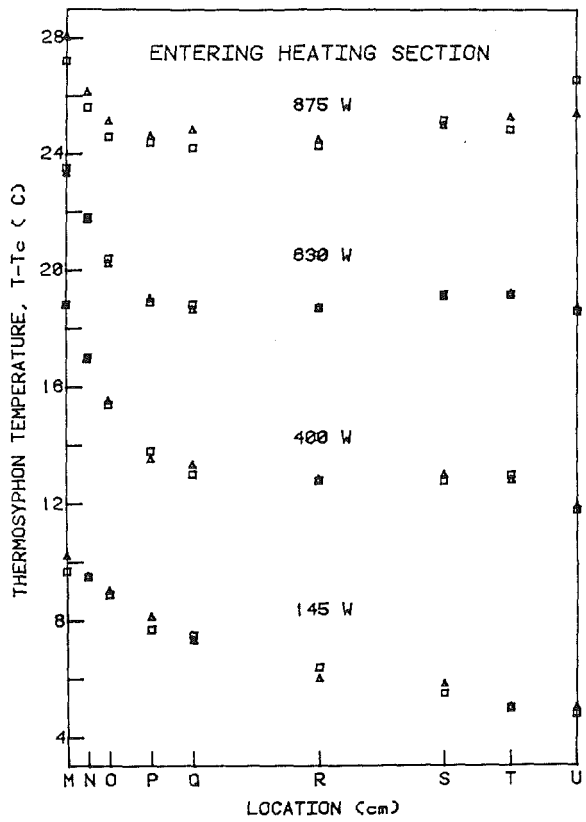

Fig. 11 Temperature profiles entering heating section of toroidal loop; M is inside, U is outside (reprinted with permission from C. Stern and R. Greif, *Warme- und Stoffubertragung*, Vol. 21, p. 279. © 1987, Springer-Verlag)

1984). Results for the dimensionless temperature and velocity profiles in the symmetry plane, near the entrance to the cooling section that extends from $\theta \approx 10$–20 deg, are shown in Figs. 12 and 13. At $\theta = 9.8$ deg, i.e., before the flow enters the cooling section (flowing upward), the temperature peak is at the inner wall. This is because in the bottom half of the loop the hotter, lighter fluid rises toward the inner wall. At $\theta = 10.3$ deg, the fluid has entered the cooling section and the temperature at the wall drops to the specified wall temperature. The temperature then decreases as the flow continues through the cooling section. In Fig. 13, it is seen that at $\theta = 9.4$ deg, i.e., before the flow enters the cooling section, the velocity peak is toward the inner wall. Once inside the cooling section ($\theta > 10$ deg), the flow begins to decelerate near the walls due to the rapid cooling there. The cross-stream, secondary motion brings the cold, slowly moving fluid that is in the neighborhood of the (entire) tube wall toward the inner wall (see Fig. 14). A flow reversal results at the inner wall, and the axial velocity peak shifts toward the outer wall. The temperature is considerably lower in the region of flow reversal than over the remainder of the cross section (see Fig. 12). Detailed results and discussion are provided for the flow and heat transfer over the entire loop for Grashof numbers of 1.9×10^3 and 3.6×10^3. It was shown that the one- and two-dimensional analyses overpredicted the total buoyancy, and consequently, overpredicted the average axial velocity by 31 and 47 percent, respectively, at the higher Grashof number. Also, the peripherally averaged Nusselt number does not continue to decrease monotonically in the two sections.

Lavine et al. (1986) also analyzed the effect of tilting the toroidal loop. Calculations were carried out at tilt angles of 10, 45, and 90 deg and a detailed analysis was made of the effects of the flow reversals. Although results were not obtained for the larger values of the Grashof number corresponding to the experimental data, i.e., from 10^4 to 10^6, the phenomena predicted have been experimentally observed at the higher Grashof numbers.

Stern et al. (1988) recently presented velocity and temperature profiles that were measured at the entrance and exit to the heating section of a toroidal loop. The velocity measurements were made with a laser-Doppler velocimeter and the temperature measurements utilized a thermocouple probe. Flow visualization techniques were also used to observe the complex flow field. In particular, flow recirculation in the longitudinal (axial) direction and circumferential secondary flows were noted, as well as transient motions. Detailed measurements of the velocity and temperature profiles were carried out and typical results are shown in Fig. 15 for four heating levels, which correspond to the Grashof number range from 1×10^5 to 9×10^5. The longitudinal velocity and temperature profiles are in the region leaving the heating section and are along the diameter that extends from the inner surface at the radial distance $R-a$, to the outer surface at $R+a$. The velocity profiles shown in Fig. 16 are along the diameter perpendicular to this direction. For all the heat inputs, the circumferential velocities exhibit the secondary flow pattern shown in Fig. 16. The magnitude of this component of velocity increased with increasing heat input and was approximately proportional to the longitudinal velocity. Results were also presented at the entrance to the heating section where the presence of a prominent recirculating flow region at the lowest heat input was noted. It was emphasized that accurate calculations for the heat transfer require that three-dimensional analyses be carried out.

Two-Phase Loops

It is convenient to begin this section with the work of Cundy and Ha (1982), who investigated the performance of a two-

Downloaded 16 Dec 2010 to 193.140.21.150. Redistribution subject to ASME license or copyright; see http://www.asme.org/terms/Terms_Use.cfm

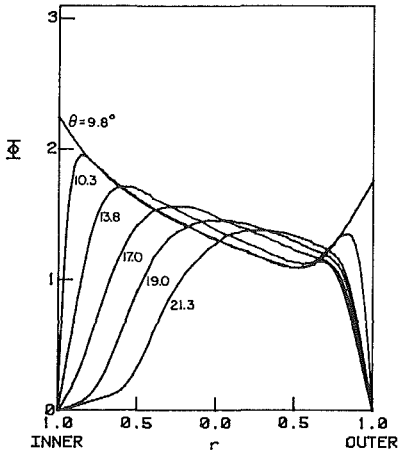

Fig. 12 Temperature profiles in symmetry plane near cooling section entrance (reprinted with permission from A. S. Lavine, R. Greif, and J. A. C. Humphrey, *Int. J. Heat Mass Transfer*, Vol. 30, p. 254. © 1987, Pergamon Journals Ltd.)

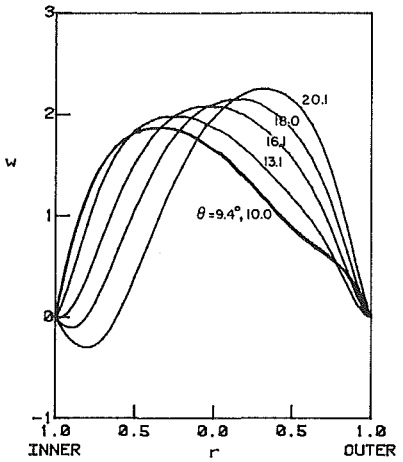

Fig. 13 Axial velocity profiles in symmetry plane near cooling section entrance (reprinted with permission from A. S. Lavine, R. Greif, and J. A. C. Humphrey, *Int. J. Heat Mass Transfer*, Vol. 30, p. 255. © 1987, Pergamon Journals Ltd.)

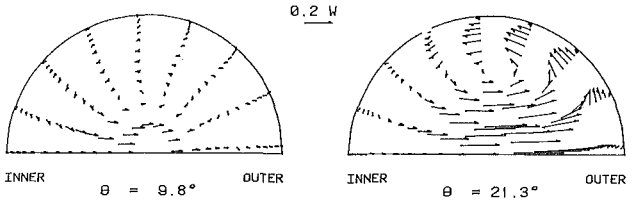

Fig. 14 Secondary velocity vectors near cooling section entrance (reprinted with permission from A. S. Lavine, R. Greif, and J. A. C. Humphrey, *Int. J. Heat Mass Transfer*, Vol. 30, p. 255. © 1987, Pergamon Journals Ltd.)

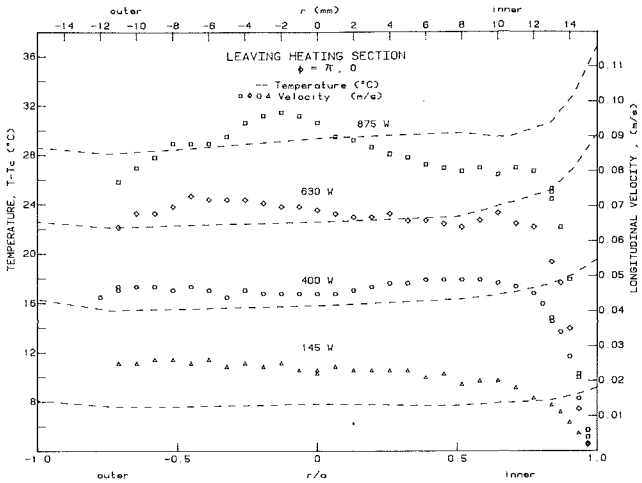

Fig. 15 Longitudinal velocity and temperature profiles leaving the heating section (Stern et al., 1988)

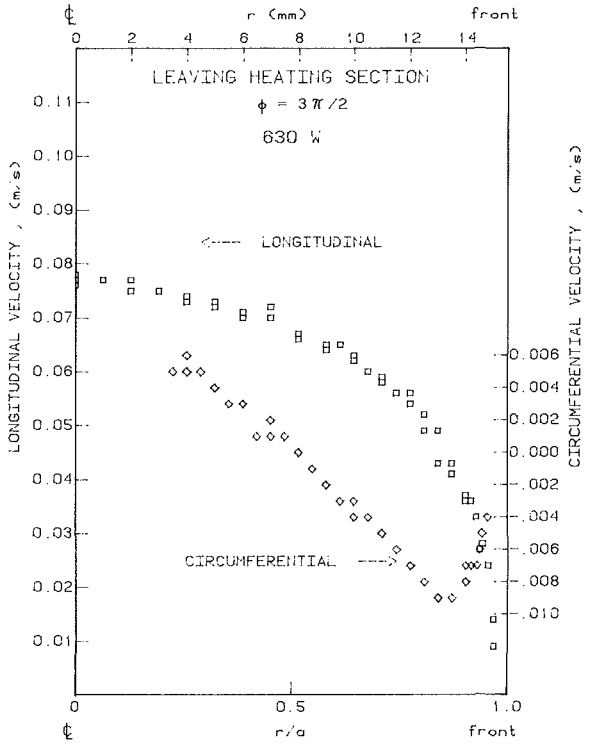

Fig. 16 Longitudinal and circumferential velocity profiles leaving the heating section (Stern et al., 1988)

phase loop. They carried out experiments in a closed loop with an evaporator section located at the bottom of the loop and a condenser section on the side of the loop, these sections being connected by an adiabatic section (cf. Fig. 17). A U-shaped tube served as a vapor barrier blocking the flow of vapor generated in the evaporator, thereby forcing the vapor to travel to the adiabatic section. Tests were conducted in two systems; one was made of stainless steel and employed ethanol as the working fluid; the other was made of copper and was filled with water. It was noted that compatibility problems with ethanol and stainless steel that were previously reported did not occur, primarily because the fluids were changed after one week of operation. Thermocouples were installed along the tube walls and the axial variation of the temperature was presented. The unidirectional flow pattern was verified indirectly from the temperature measurements and directly by measuring the condensate flow. The importance of the parallel, downward flow of both the vapor and the condensate, which enhances the heat transfer by thinning the condensate film and removing it, was cited. It was also noted that, during the initial heating period, the temperatures increased in an unpredictable and fluctuating manner.

McDonald et al. (1977a, 1977b) and Ali and McDonald (1977) studied a waste heat recovery system that evolved from the concept of combining the physical flexibility of a liquid coupled heat exchanger with the natural circulation characteristics of a two-phase loop thermosyphon. The studies were carried out to recover ventilation waste heat and the authors emphasized that vast amounts of energy are lost with ventilation air if it is not reclaimed to preheat incoming air. Experiments were carried out in two separate test loops; one was used only for data acquisition and the second was used for

Downloaded 16 Dec 2010 to 193.140.21.150. Redistribution subject to ASME license or copyright; see http://www.asme.org/terms/Terms_Use.cfm

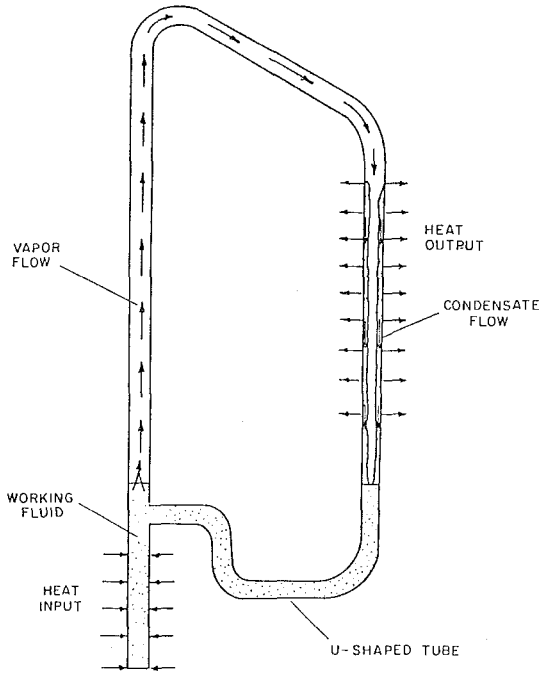

Fig. 17 Two-phase natural circulation loop (reprinted with permission from V. A. Cundy and L. N. Ha, *Thermal Sciences 16*, Proceedings of the 16th Southeastern Seminar, Vol. 2, p. 602. © 1983, Hemisphere Publishing Corporation)

data acquisition and for flow visualization (cf. McDonald et al., 1977a). The performance of the loops was evaluated in terms of a loop conductance U defined by the relation

$$U = (Q/A_e)/(T_e - T_c) \tag{9}$$

where Q is the rate of energy transfer, A_e is the inside surface area of the evaporator tube, and T_e and T_c are the temperatures of the evaporator and condenser tube surfaces, respectively. Tests were carried out using two different working fluids, R-113 and R-11, for various fills (or charges), orientations, and source and sink temperatures. In general, the conductance increased with increasing angles of rotation of the loop as a result of the decreased flooding in the condenser and dryout in the evaporator (especially for small fillings). For the small fillings at high inclination angles, the conductance drops off as a result of the increased transport resistance due to the necessity of pumping liquid along with the vapor up the vapor header through a change in elevation. It was also shown that an optimum filling exists that will yield the maximum conductance for a given loop rotation angle and temperature difference.

Ali and McDonald (1977) presented a computer program that simulated the experimentally observed behavior reported by McDonald et al. (1977a). In developing the program, some of the correlations available in the literature had to be used at conditions beyond the range of variables over which they were established. The authors also noted a difficulty in determining the best method to treat the transition regions between the various flow regions in the evaporator. In spite of these difficulties the computer program predicted values of the surface temperature, heat flux, and overall loop conductance that were in good agreement with the experimental results. Using this program, McDonald and Ali (1977b) presented the results for a number of calculations to illustrate the typical behavior of thermosyphon loops. The calculations were performed for unidirectional and bidirectional studies. The results for the unidirectional systems showed that the angle of inclination of the condenser had a very significant effect on the loop conductance whereas the inclination of the evaporator did not. The calculations yielded a peak loop performance with the condenser inclined 10 deg that was nearly twice the value with the condenser vertical. For the bidirectional loop, the condenser was steadily flooding as the filling increased. This caused the performance to be slightly lower and yielded a more gradual variation with the amount of filling than occurred for the unidirectional case. For large fillings, the performance of the unidirectional loop rapidly decreased due to the fact that the liquid carried over must be pumped thermally to a higher elevation, thereby causing a greater pressure drop and hence saturation temperature drop within the loop.

Experiments and calculations for multiple-loop two-phase thermosyphons were carried out by McDonald et al. (1978) for unidirectional operation and by McDonald and Sampath (1980) for bidirectional operation. It was shown for both systems that a careful selection of the coil tube diameter and length, as well as the loop filling, could provide very good loop conductance values over a wide range of temperature differences in multiple-tube, two-phase thermosyphon loops. The operational range of the systems was found to be limited by evaporator tube dryout for large temperature differences and by boiling suppression for small differences. The bidirectional system was found to yield a smaller loop conductance than the corresponding unidirectional system. This was primarily due to flooding in the condenser which thus decreased its performance. In addition, the bidirectional system was found to be much more sensitive to the loop filling.

The steady-state operating and heat transfer characteristics of a closed-loop, two-phase thermosyphon system for low grade heat recovery from liquid heat sources were studied by Cheng and Rovang (1987). Their system consisted of an evaporator, a condenser located above the evaporator, a liquid–vapor separator, and connecting tubes. Tests were carried out over a range of liquid heat source temperatures (45–85°C), cooling water flow rates (25–75 mL/s), and initial liquid charge levels (20–100 percent) defined as the fraction of the vertical distance between the evaporator inlet tube and the horizontal axis of the condenser. The mass flux of the natural circulation flow of Freon R-113 was measured with a turbine flow meter and the values covered a range from 100 to 240 kg/m^{2}s. The natural circulation flow was immediately self-starting with the application of external heating and cooling. The flow regime in the riser line ranged from a two-phase flow to superheated vapor. The heat transfer was found to be primarily in the form of latent heat and the mass flow rate remained small even with increasing input heat flux. The optimum performance of the system resulted with operation in the saturation region with vapor quality near unity without superheating. Both an increase in the cooling water flow rate and a lower charge level were found to assist vapor generation by lowering the system pressure and thus the saturation temperature of the working fluid.

Fluctuations of the flow rate and the system pressure were observed to be of the same order of magnitude as the mean flow rate and the pressure. The fundamental frequency was found to be essentially constant with a value between 0.35 and 0.375 cycles/s and the mechanism of the two-phase instability was due to density wave oscillations.

Bau and Torrance (1981a) performed experiments in the symmetrically heated, open, U-shaped loop previously discussed. Boiling was observed in both the porous and the water loops during the starting transients and at steady state. Boiling in the porous loop occurred when the heater temperature reached the saturation temperature during the transient. The heater temperature remained at saturation until the induced convective flow quenched the boiling process with an influx of cold water. The heater temperature then dropped below saturation and the resulting transient was similar to the nonboiling condition. With the appearance of boiling during steady-state operation, the temperature data indicated the presence of oscillations. For boiling in the water loop, small-

Downloaded 16 Dec 2010 to 193.140.21.150. Redistribution subject to ASME license or copyright; see http://www.asme.org/terms/Terms_Use.cfm

amplitude oscillations with a period of 15–20 s, corresponding to the flow time in the loop, appeared in the outlet temperature. Also, approximately once per hour, a large-amplitude oscillation occurred that was associated with the formation and escape of a large vapor bubble from the heater. For the porous loop, relatively small oscillations were observed because the porous medium restricts the bubble motion. Reversals of the flow direction in the loop were not observed after the start of boiling.

Britt and Wood (1983) carried out experiments with several systems to determine the operational characteristics of a multiple-loop container used to cool nuclear reactor assemblies at the Savannah River Plant (cf. previous discussion of Steimke, 1985). The container, commonly called a "HARP" because of the resemblance to the musical instrument, was designed to isolate and cool failed nuclear reactor assemblies. One set of experiments was carried out in a rectangular flow loop that had one vertical section wrapped with heating tape. The other vertical section was cooled and contained a window for flow visualization. Oscillatory flow was present at the higher heating rates and the oscillations in the cooling section were at a frequency that was equal to the formation and release of vapor (nucleate boiling) in the heated section. It was also noted that the buoyant force increases when vapor bubbles are released in the heating section. This results in an increase in the fluid velocity, which sweeps the vapor from the heated section and increases the heat transfer in the cooling section. Thus, "cooler" vapor-free fluid fills the heating section; the buoyancy then decreases and a flow reversal occurs. The effect is temporary because the fluid is heated in the heating section; the buoyant driving force is increased, which re-establishes the original direction of the flow. Experiments were also carried out in a replica assembly of the HARP. Momentum and energy balances were used to obtain a correlation for the heat transfer. It was noted that the simplicity of the analysis and the complexity of the flow pattern precluded the use of standard frictional correlations.

Simplified analyses of the flow and heat transfer in two-phase natural circulation loops have proven to be very useful in illustrating some of the many effects that take place in these systems. Sen et al. (1983) considered a closed loop in which the flowing liquid was confined to a region $0 < x < d$ and the vapor to the remaining region $d < x < L$, the location $x=0$ being identical to $x=L$. This "sharp interface model" assumed a point heat source (evaporator) of strength Q at $x=d$ and a point heat sink of strength $-Q$ at $x = 0, L$. The system was assumed to be under saturation conditions. Ramos et al. (1985) extended the analysis to permit two-phase zones over which there was heat addition and extraction; the single-phase regions were adiabatic. In the two-phase zones the properties were assumed to vary linearly from one phase to the other. Several cases were studied and a particular example showed that friction forces were unimportant; this resulted in simplified expressions for the mass flow rate and the maximum velocity. It was also shown that heat could be transferred from one point to another regardless of their relative position when certain geometric conditions were satisfied. Multiple solutions were also found and it was noted that one or both solutions could be unstable.

Natural circulation represents a means of cooling for light water reactors (LWRs) during transients and accidents. Three distinct modes of natural circulation relevant to small breaks and transients for pressurized water reactors (PWRs) are identified as a function of quality (Burchill and Abramson, 1985; Duffey and Sursock, 1987): (*i*) single-phase water flow, in which the water is subcooled and there are no voids, (*ii*) two-phase flow, in which voids formed by core heat addition are circulated and condensed, and (*iii*) reflux condensation, or boiler-condenser, where single-phase steam flow is condensed in a *U*-tube (UTSG) or once-through (OTSG) steam generator. Duffey and Sursock (1987) developed a theoretical model to analyze the natural circulation phenomena relevant to small breaks and transients for PWRs and boiling water reactors (BWRs) and also reviewed the relevant experimental data. A small-break, loss of coolant accident (LOCA) is characterized by relatively slow reactor cooling system (RCS) depressurization rates and by relatively slow mass loss from the RCS so that flashing and acceleration effects are negligible. Accordingly, the entire circulation process can be considered to be quasi-steady. This assumption has been confirmed experimentally on the semiscale PWR loop in natural circulation, which shows that the loop flow response duplicates that obtained in steady-state tests for a range of loop inventories. It is also pointed out that the experimentally obtained maximum flow rate W is very much less than the value that is calculated for a flow that is produced solely by void production. For this limiting case, the maximum theoretical flow rate is given by $W_m = (\rho_l/\rho_g)\ (Q_c/h_{lg})$. The experimental data show that for PWRs the core flow is a maximum for intermediate liquid inventories or loop voidage, while for BWRs the core flow is a maximum for high downcomer levels. To obtain expressions for the flow rate as a function of the inventory, the equations of continuity, momentum, and energy are solved under steady-state conditions. For PWR single-phase flow, the authors refer to the study of Zvirin et al. (1981b) and note the applicability of the result for the flow rate to model studies and to LWR plant data (Zvirin, 1981a). For PWR two-phase flow, unequal densities, ρ_1 and ρ_2, are assumed on the hot and cold sides, respectively, with flow qualities X_1 and X_2. The flow rate is obtained from momentum balance considerations and the integral of the momentum equation around the loop is utilized. The core void fraction is calculated by using the drift-flux model with uniform power in the core. For the reflux condensation rate, the net loop flow W drops virtually to zero, being pure steam from the core. It is noted that the static heads nearly balance on the hot and cold sides so that the equations obtained for the two-phase natural circulation can be simplified by assuming the void fractions in the cold and hot legs to be equal. Results are then obtained for the maximum flow rate and the inventory for PWRs. For BWRs, the authors obtained a relation for the "collapsed" liquid level, i.e., the effective inventory on the hot side, from mass conservation. By assuming that the outlet losses dominate, the momentum equation is written in terms of the downcomer level and the "collapsed" liquid level. The result for the maximum flow rate in the BWR system is found to be independent of power and dependent on the square root of the downcomer level for the case when the two-phase level is in the separators above the core. This can be interpreted as the balancing of the downcomer head by the steam venting losses, and is a direct result from the momentum balance. When the level drops below the separator and recirculation ceases, the two-phase level penetrates the bundle and the steam production is dependent on the two-phase level height. For this condition, the mass conservation equation derived by Sun et al. (1981) was used to obtain the flow rate. To first order, it was found that the flow rate depends on the downcomer head and bundle power for low powers.

Predictions of the PWR models with experimental data were made using the power Q, flow rate W, and the relationship for single-phase flow; namely, $W = CQ^{1/3}$, where the constant C was empirically determined. It was found that this power law dependence agrees well with the experimental data. For the flow rate in a BWR test facility, a simplified correlation was written in the form:

$$W \sim z_D \left(\frac{Q_0}{1+Q_0} \right) \tag{10}$$

where z_D is the downcomer level and Q_0 is the bundle power. The study demonstrated that natural circulation flow rates in

Downloaded 16 Dec 2010 to 193.140.21.150. Redistribution subject to ASME license or copyright; see http://www.asme.org/terms/Terms_Use.cfm

PWRs are strongly dependent on the liquid inventory but weakly dependent on power level; in BWRs, the flow rates are strongly dependent on both vessel level, or inventory, and on power level.

Manero et al. (1987) carried out an experimental study of the two-phase flow and heat transfer in a toroidal loop. The torus had a diameter of 500 mm with a cross-sectional diameter of 10 mm. The heat input was supplied from an electrically heated nicromel wire that was wound around the evaporator section and the heat was removed through a condenser consisting of a double tube, counterflow heat exchanger. The evaporator and condenser sections were located at opposite ends of a diameter of the torus. The apparatus permitted visualization of the boiling process and the liquid motion. Tests were performed with methyl alcohol at different heat inputs Q, for different angles of inclination α of the evaporator-condenser diameter with respect to the horizontal. At $\alpha = 0$ deg, the evaporator and condenser are at the same elevation; at $\alpha = 90$ deg, the evaporator is at the bottom and the condenser is at the top of the loop. Measurements of the temperature and the pressure were made for different values of Q and α.

From an overall system point of view, it was demonstrated that the toroidal loop with two-phase natural circulation could be effectively used to transfer heat from a lower source to a higher sink. However, the operation of the system proved to be highly complex. Except for low heat inputs and small angles of inclination, the system was never in a time-independent condition. The results for the variation in pressure for $Q = 60$ W at $\alpha = 15$ deg and 45 deg are shown in Fig. 18. The frequency f of the pressure oscillations was correlated by the relation $f/\cos\alpha = 4.9$ (s^{-1}) excluding $\alpha = 90$ deg. This result was in good agreement with a model presented by the authors for bubble formation.[2] However, a predicted inversely proportional relationship between the bubble frequency and the heat input was not in agreement with the measurements. This was attributed to such effects as surface tension and condensation, which were not included in the model. The authors noted that bubbling at higher heat inputs may be desirable because of the higher heat transfer that was obtained. Combining this effect with a submerged evaporator, the liquid carryover effect of the vapor bubbles contributed significantly to the efficiency of the system.

Bar-Cohen and Schweitzer (1985) noted that the high heat fluxes and moderate temperature differences associated with boiling heat transfer make immersion cooling one of the primary candidates for the thermal control of microelectronic components. For this application, they cited the need for information on the thermal transport from vertical arrays of parallel, densely packaged, printed circuit boards or ceramic modules. They therefore studied the boiling heat transfer from a pair of flat, closely spaced vertical plates that are immersed in a large container of saturated water. Saturated boiling from these surfaces is expected to produce a vapor fraction gradient in the vertical channel formed by each pair of surfaces. The resulting density difference between the two-phase mixture in the channel and the ambient saturated liquid should increase the flow past the circuit board and improve the thermal performance relative to pool boiling. Bar-Cohen and Schweitzer (1985) expressed the heat flux in the form

$$q = \phi q_c + \gamma q_b \tag{11}$$

where q_b is taken to be the pool boiling contribution and q_c is the convective heat flux, which is obtained by using a convection heat transfer coefficient that is averaged over the height of the channel. The parameter γ was set equal to unity and a correlation for ϕ was obtained. For the test conditions, the usual nucleate pool boiling behavior was obtained for channel spacings greater than 15 mm. For a constant imposed heat flux, the wall temperature decreased as the spacing narrowed below approximately 10 mm.

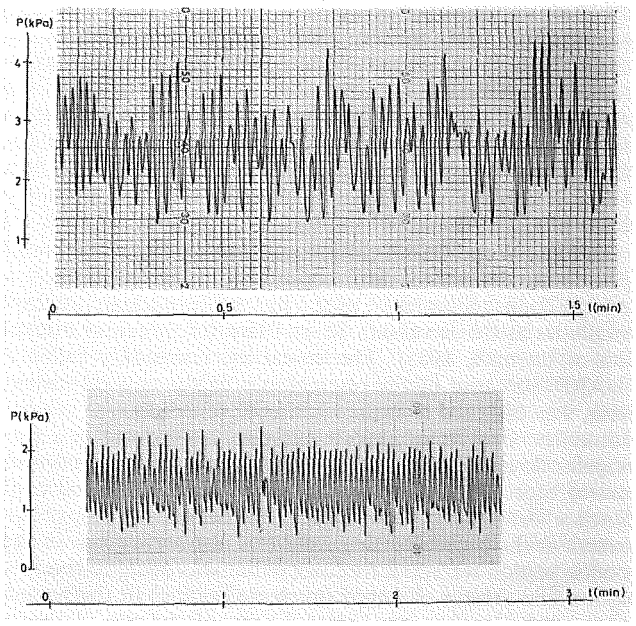

Fig. 18 Pressure oscillations in two-phase toroidal loop; $\alpha = 15$ deg, $\alpha = 45$ deg (reprinted with permission from E. Manero, M. Sen, and E. Ramos, *Warme- und Stoffubertragung*, Vol. 21, p. 47. © 1987, Springer-Verlag)

Summary

Natural circulation loops encompass a broad range of applications and phenomena as has been exemplified, in part, by the preceding coverage. In virtually every aspect, including, for example, one-dimensional modeling, detailed numerical calculations, system performance, experimental studies, turbulent transport, etc., there is an urgent need for additional work on both fundamentals and applications. In the last decade, there has been a greatly expanded effort in this field. Reference to the recent International Symposium on Natural Circulation that was held during the 1987 Winter Annual Meeting of the American Society of Mechanical Engineers (Kim and Hassan, 1987) testifies directly to the continued importance, vitality, and interest in the field of natural circulation loops.

Acknowledgments

The interest and participation of Dr. A. Mertol, Science Applications International Corporation, in the preparation of this manuscript is gratefully acknowledged. The support from the National Science Foundation and the University of California at Berkeley is greatly appreciated.

References

Acosta, R., Sen, M., and Ramos, E., 1987, "Single-Phase Natural Circulation in a Tilted Square Loop," *Warme- und Stoffübertragung*, Vol. 21, pp. 269-275.

Acosta, R., and Manero, E., 1984, "Theoretical and Experimental Study of Thermosyphons in One and Two Phases," Professional Thesis, UNAM, Mexico City.

Ali, A. F. M., and McDonald, T. W., 1977, "Thermosiphon Loop Performance and Characteristics: Part 2. Stimulation Program" *ASHRAE Transactions*, Vol. 83, Part 2, pp. 260-278.

Bar-Cohen, A., and Schweitzer, H., 1985, "Thermosyphon Boiling in Vertical Channels," ASME JOURNAL OF HEAT TRANSFER, Vol. 107, pp. 772-778.

Bau, H. H., and Torrance, K. E., 1981a, "Transient and Steady Behavior of

[2] It is also pointed out that steady oscillations due to periodic boiling were observed by Chato (1963). This occurred in a parallel channel apparatus, which was previously discussed.

Downloaded 16 Dec 2010 to 193.140.21.150. Redistribution subject to ASME license or copyright; see http://www.asme.org/terms/Terms_Use.cfm

an Open Symmetrically-Heated Free Convection Loop," *Int. J. Heat Mass Transfer*, Vol. 24, pp. 597–609.

Bau, H. H., and Torrance, K. E., 1981b, "On the Stability and Flow Reversal of an Asymmetrically Heated Open Convection Loop," *J. Fluid Mech.*, Vol. 106, pp. 417–433.

Bau, H. H., and Torrance, K. E., 1983, "On the Effects of Viscous Dissipation and Pressure Work in Free Convection Loops," *Int. J. Heat Mass Transfer*, Vol. 26, pp. 727–734.

Britt, T. E., and Wood, D. C., 1983, "Free Convection in a Partially Submerged Fluid Loop," ASME Paper No. 83-HT-67.

Burchill, W. E., and Abramson, P. B., 1985, "PWR Small Break LOCA," in: *Guidebook to Light Water Reactor Safety Analysis*, Chap. 3, P. B. Abramson, ed., Hemisphere, New York.

Chato, J. C., 1963, "Natural Convection Flows in Parallel-Channel Systems," ASME JOURNAL OF HEAT TRANSFER, Vol. 85, pp. 339–345.

Chen, K., 1982, "The Influence of Loop Configuration on Closed-Loop Thermosyphons," ASME Paper No. 82-WA/HT-63.

Chen, K., 1985, "On the Oscillatory Instability of Closed-Loop Thermosyphons," ASME JOURNAL OF HEAT TRANSFER, Vol. 107, pp. 826–832.

Cheng, K. C., and Rovang, G. W., 1987, "Operating and Heat Transfer Characteristics of a Closed-Loop Two-Phase Thermosyphon System for Low Grade Waste Heat Recovery," in: *Proc. ASME-JSME Thermal Engineering Joint Conf.*, Vol. 3, P. J. Marto and I. Tanasawa, eds., ASME, pp. 179–186.

Creveling, H. F., DePaz, J. F., Baladi, J. Y., and Schoenhals, R. J., 1975, "Stability Characteristics of a Single-Phase Free Convection Loop," *J. Fluid Mech.*, Vol. 67, pp. 65–84.

Cundy, V. A., and Ha, L. N., 1983, "The Characterization of a Gravity Assisted Heat Pipe With Internal Two-Phase Parallel Flow Throughout," in: *Thermal Sciences 16*, Vol. 2, T. N. Veziroglu, ed., Hemisphere, Washington, pp. 599–612.

Damerell, P. S., and Schoenhals, R. J., 1979, "Flow in a Toroidal Thermosyphon With Angular Displacement of Heat and Cooled Sections," ASME JOURNAL OF HEAT TRANSFER, Vol. 101, pp. 672–676.

Duffey, R. B., and Sursock, J. P., 1987, "Natural Circulation Phenomena Relevant to Small Breaks," *Nucl. Engng. and Design*, Vol. 102, pp. 115–128.

Gorman, M., Widman, P. J., and Robbins, K. A., 1984, "Chaotic Flow Regimes in a Convection Loop," *Phys. Rev. Lett.*, Vol. 52, pp. 2241–2244.

Gorman, M., Widman, P. J., and Robbins, K. A., 1986, "Nonlinear Dynamics of a Convection Loop: A Quantitative Comparison of Experiment With Theory," *Physica*, Vol. 19D, pp. 255–267.

Gosman, A. D., and Ideriah, F. J. K., 1983, "TEACH-2E: A General Computer Program for Two-Dimensional, Turbulent, Recirculating Flows," Imperial College, London; revised, University of California, Berkeley, FM-83-2.

Greif, R., Zvirin, Y., and Mertol, A., 1979, "The Transient and Stability Behavior of a Natural Convection Loop," ASME JOURNAL OF HEAT TRANSFER, Vol. 101, pp. 684–688.

Gruszczynski, M. J., and Viskanta, R., 1983, "Heat Transfer From a Vertical Tube Bundle Under Natural Circulation Conditions," *ASME-JSME Thermal Engineering Joint Conf. Proc.*, Y. Mori and W. J. Yang, eds., Vol. 3, pp. 403–410.

Hallinan, K. P., and Viskanta, R., 1985, "Heat Transfer From a Vertical Tube Bundle Under Natural Circulation Conditions," *Int. J. Heat and Fluid Flow*, Vol. 6, pp. 256–264.

Hallinan, K. P., and Viskanta, R., 1986, "Dynamics of a Natural Circulation Loop: Analysis and Experiments," *Heat Transfer Engineering*, Vol. 7, pp. 45–51.

Hart, J. E., 1984, "A New Analysis of a Closed Loop Thermosyphon," *Int. J. Heat Mass Transfer*, Vol. 27, pp. 125–136.

Hart, J. E., 1985, "A Model of Flow in a Closed-Loop Thermosyphon Including the Soret Effect," ASME JOURNAL OF HEAT TRANSFER, Vol. 107, pp. 840–849.

Holman, J. P., and Boggs, J. H., 1960, "Heat Transfer to Freon 12 Near the Critical State in a Natural Circulation Loop," ASME JOURNAL OF HEAT TRANSFER, Vol. 82, pp. 221–226.

Huang, B. J., and Zelaya, R., 1987, "Stability Analysis of a Thermosyphon Loop," ISES Solar World Congress, Hamburg, Federal Republic of Germany.

Huang, B. J., and Zelaya, R., 1988, "Heat Transfer Behavior of a Rectangular Thermosyphon Loop," ASME JOURNAL OF HEAT TRANSFER, in press.

Humphrey, J. A. C., 1978, "Numerical Calculation of Developing Laminar Flow in Pipes of Arbitrary Curvature Radius," *Canadian J. Chem. Engng.*, Vol. 56, pp. 151–164.

Japikse, D., 1973, "Advances in Thermosyphon Technology," *Advances in Heat Transfer*, by T. F. Irvine, Jr. and J. P. Hartnett, eds., Academic Press, New York, Vol. 9, pp. 1–111.

Keller, J. B., 1966, "Periodic Oscillations in a Model of Thermal Convection," *J. Fluid Mech.*, Vol. 26, pp. 599–606.

Kim, J. H., and Hassan, Y. A., eds., 1987, *Natural Circulation*, ASME, FED – Vol. 61, HTD – Vol. 92, New York.

Kreitlow, D. B., Reistad, G. M., Miles, C. R., and Culver, G. G., 1978, "Thermosyphon Models for Downhole Heat Exchanger Applications in Shallow Geothermal Systems," ASME JOURNAL OF HEAT TRANSFER, Vol. 100, pp. 713–719.

Lavine, A. G., 1984, "A Three-Dimensional Analysis of Natural Convection in a Toroidal Loop," Ph.D. Dissertation, University of California, Berkeley.

Lavine, A. S., Greif, R., and Humphrey, J. A. C., 1986, "Three-Dimensional Analysis of Natural Convection in a Toroidal Loop: Effect of Tilt Angle," ASME JOURNAL OF HEAT TRANSFER, Vol. 108, pp. 796–805.

Lavine, A. S., Greif, R., and Humphrey, J. A. C., 1987, "A Three-Dimensional Analysis of Natural Convection in a Toroidal Loop – The Effect of Grashof Number," *Int. J. Heat Mass Transfer*, pp. 251–261.

Malkus, W. R. V., 1972, "Non-periodic Convection at High and Low Prandtl Number," *Mem. Soc. R. Sci. Liege*, Vol. 4, pp. 125–128.

Manero, E., Sen, M., and Ramos, E., 1987, "Two-Phase Natural Circulation in a Toroidal Loop," *Wärme- und Stoffübertragung*, Vol. 21, pp. 41–49.

McDonald, T. W., Hwang, K. S., and DiCiccio, X. X., 1977, "Thermosiphon Loop Performance Characteristics: Part 1. Experimental Study," *ASHRAE Trans.*, Vol. 82, Part 2, pp. 250–259.

McDonald, T. W., and Ali, A. F. M., 1977b, "Thermosiphon Loop Performance Characteristics: Part 3. Simulated Performance," *ASHRAE Trans.*, Vol. 83, Part 2, pp. 279–287.

McDonald, T. W., Ali, A. F. M., and Sampath, S., 1978, "The Unidirectional Coil Loop Thermosiphon Heat Exchanger," *ASHRAE Trans.*, Vol. 84, Part 2, pp. 27–37.

McDonald, T. W., and Sampath, S., 1980, "The Bidirectional Coil Loop Thermosiphon Heat Exchanger," *ASHRAE Trans.*, Vol. 86, Part 2, pp. 37–47.

McKee, H. R., 1970, "Thermosiphon Reboilers – A Review," *Industrial and Engineering Chemistry*, Vol. 62, pp. 76–82.

Mertol, A., 1980, "Heat Transfer and Fluid Flow in Thermosyphons," Ph.D. Dissertation, University of California, Berkeley.

Mertol, A., Greif, R., and Zvirin, Y., 1981a, "The Transient Steady-State and Stability Behavior of a Natural Convection Loop With a Throughflow," *Int. J. Heat Mass Transfer*, Vol. 24, pp. 621–633.

Mertol, A., Place, W., Webster, T., and Greif, R., 1981b, "Detailed Loop Model (DLM) Analysis of Liquid Solar Thermosyphons With Heat Exchangers," *Solar Energy*, Vol. 27, pp. 367–386.

Mertol, A., and Greif, R., 1982a, "Study of a Thermosyphon With a Counter-Flow Heat Exchanger," in: *Proc. 7th Int. Heat Transfer Conf.*, Munich, Federal Republic of Germany, Vol. 2, pp. 239–244.

Mertol, A., Greif, R., and Zvirin, Y., 1982b, "Two-Dimensional Study of Heat Transfer and Fluid Flow in a Natural Convection Loop," ASME JOURNAL OF HEAT TRANSFER, Vol. 104, pp. 508–514.

Mertol, A., Greif, R., and Giz, A. T., 1983, "The Transient, Steady-State and Stability Behavior of a Toroidal Thermosyphon With a Parallel-Flow Heat Exchanger," ASME *Journal of Solar Energy Engineering*, Vol. 105, pp. 58–65.

Mertol, A., Greif, R., and Zvirin, Y., 1984, "Two-Dimensional Analysis of Transient Flow and Heat Transfer in a Natural Circulation Loop," *Wärme- und Stoffübertragung*, Vol. 18, pp. 89–98.

Mertol, A., and Greif, R., 1985, "A Review of Natural Circulation Loops," in: *Natural Convection*, S. Kakac, W. Aung, and R. Viskanta, eds., Hemisphere, New York, pp. 1033–1071.

Mertol, A., and Greif, R., 1987, "Review of Thermosyphon Solar Water Heaters," in: *Solar Energy Utilization*, H. Yuncu, E. Paykoc, and Y. Yener, eds., Martinus Nijhoff, Amsterdam, pp. 537–569.

Norton, B., and Probert, S. D., 1982, "Natural-Circulation Solar-Energy Stimulated Systems for Heating Water," *Applied Energy*, Vol. 11, pp. 167–196.

Norton, B., and Probert, S. D., 1986, "Thermosyphon Solar Energy Water Heaters," in: *Advances in Solar Energy*, K. W. Boer, ed., American Solar Energy Society, Boulder, CO, Vol. 3, pp. 125–170.

Ostrach, S., 1972, "Natural Convection in Enclosures," in: *Advances in Heat Transfer*, T. F. Irvine, Jr. and J. P. Hartnett, eds., Academic Press, New York, Vol. 8, pp. 161–227.

Patankar, S. V., 1980, *Numerical Heat Transfer and Fluid Flow*, McGraw-Hill, New York.

Ramos, E., Sen, M., and Trevino, C., 1985, "A Steady-State Analysis for Variable Area One and Two-Phase Thermosyphon Loops," *Int. J. Heat Mass Transfer*, Vol. 28, pp. 1711–1719.

Reid, R. L., Tennant, J. S., and Childs, K. W., 1975, "The Modeling of a Thermosyphon Type Permafrost Protection Device," ASME JOURNAL OF HEAT TRANSFER, Vol. 97, pp. 382–386.

Seki, N., Fukusako, S., and Koguchi, K., 1980, "Single-Phase Heat Transfer Characteristics of Concentric-Tube Thermosyphon," *Wärme- und Stoffübertragung*, Vol. 14, pp. 189–199.

Sen. M., Trevino, C., Ramos, E., and Raychaudhuri, B. C., 1983, "Natural Circulation Driven Two Phase Flow Loops," in: *Alternative Energy Sources V. Part A: Solar Radiation/Collection/Storage*, T. N. Veziroglu, ed., Elsevier, Amsterdam, pp. 435–441.

Sen, M., and Fernandez, J. L., 1985a, "One-Dimensional Modeling of Multiple Loop Thermosyphons," *Int. J. Heat Mass Transfer*, Vol. 28, pp. 1788–1790.

Sen, M., Ramos, E., and Trevino, C., 1985b, "On the Steady-State Velocity of the Inclined Toroidal Thermosyphon," ASME JOURNAL OF HEAT TRANSFER, Vol. 107, pp. 974–977.

Sen, M., Ramos, E., and Trevino, C., 1985c, "The Toroidal Thermosyphon With Known Heat Flux," *Int. J. Heat Mass Transfer*, Vol. 28, pp. 219–233.

Shitzer, A., Kalmanoviz, D., Zvirin, Y., and Grossman, G., 1979, "Experiments With a Flat Plate Solar Water Heating System in Thermosyphonic Flow," *Solar Energy*, Vol. 22, pp. 27–35.

Steimke, J. L., 1985, "Natural Convection Heat Transfer for a Concentric Tube Thermosiphon," ASME JOURNAL OF HEAT TRANSFER, Vol. 107, pp. 583–588.

Stern, C., and Greif, R., 1987, "Measurements in a Natural Convection Loop," *Wärme- und Stoffübertragung*, Vol. 21, pp. 277–282.

Stern, C., Greif, R., and Humphrey, J. A. C., 1988, "An Experimental Study

Downloaded 16 Dec 2010 to 193.140.21.150. Redistribution subject to ASME license or copyright; see http://www.asme.org/terms/Terms_Use.cfm

of Natural Convection in a Toroidal Loop," ASME JOURNAL OF HEAT TRANSFER, accepted for publication.

Sun, K. H., Duffey, R. B., and Peng, C. M., 1981, "The Prediction of Two-Phase Mixture Level and Hydrodynamically Controlled Dryout Under Low Flow Conditions," *Int. J. Multiphase Flow*, Vol. 7, pp. 521–543.

Takeda, Y., and Fischer, W. E., 1987, "Thermofluid Behavior of the SINQ Target, a Natural Circulation Loop as a Target," *Natural Circulation*, J. H. Kim and Y. A. Hassan, eds., ASME, New York, pp. 141–148.

Torrance, K. E., 1979, "Open-Loop Thermosyphons With Geological Applications," ASME JOURNAL OF HEAT TRANSFER, Vol. 101, pp. 677–683.

Torrance, K. E., and Chan, V. W. L., 1980, "Heat Transfer by a Free-Convection Loop Embedded in a Heat Conducting Solid," *Int. J. Heat Mass Transfer*, Vol. 23, pp. 1091–1097.

Wacholder, E., Kaizerman, S., and Elias, E., 1982, "Numerical Analysis of the Stability and Transient Behavior of Natural Convection Loop," *Int. J. Engineering Science*, Vol. 20, pp. 1235–1254.

Welander, P., 1967, "On the Oscillatory Instability of a Differentially Heated Fluid Loop," *J. Fluid Mech.*, Vol. 29, pp. 17–30.

Yorke, J. A., and Yorke, E. D., 1981, "Chaotic Behavior and Fluid Dynamics," in: *Topics in Applied Physics, Hydrodynamic Instabilities and the Transition to Turbulence*, H. L. Swinney and J. P. Gollub, eds., Springer-Verlag, Berlin, Chap. 4, pp. 77–96.

Zvirin, Y., Shitzer, A., and Grossman, G., 1977, "The Natural Circulation Solar Heater-Models With Linear and Nonlinear Temperature Distributions," *Int. J. Heat Mass Transfer*, Vol. 20, pp. 997–999.

Zvirin, Y., Shitzer, A., and Bartal-Bornstein, A., 1978, "On the Stability of the Natural Circulation Solar Heat," in: *Proceedings of the 6th International Heat Transfer Conference*, Toronto, Canada, Vol. 2, pp. 141–145.

Zvirin, Y., 1979, "The Effect of Dissipation on Free Convection Loops," *Int. J. Heat Mass Transfer*, Vol. 22, pp. 1539–1546.

Zvirin, Y., 1980, "The Effects of Throughflow on the Steady State and Stability of a Natural Circulation Loop," *19th National Heat Transfer Conference*, AIChE Symposium Series, Orlando, FL, pp. 238–249.

Zvirin, Y., 1981a, "A Review of Natural Circulation Loops in Pressurized Water Reactors and Other Systems," *Nuclear Engineering and Design*, Vol. 67, pp. 203–225.

Zvirin, Y., Jeuck, P. R., III, Sullivan, C. W., and Duffey, R. B., 1981b, "Experimental and Analytical Investigation of a Natural Circulation System With Parallel Loops," ASME JOURNAL OF HEAT TRANSFER, Vol. 103, pp. 645–652.

Zvirin, Y., 1985, "The Instability Associated With the Onset of Motion in a Thermosyphon," *Int. J. Heat Mass Transfer*, Vol. 28, pp. 2105–2111.

Downloaded 16 Dec 2010 to 193.140.21.150. Redistribution subject to ASME license or copyright; see http://www.asme.org/terms/Terms_Use.cfm

Direct-Contact Heat Transfer for Process Technologies

H. R. Jacobs

Department of Mechanical Engineering,
The Pennsylvania State University,
University Park, PA 16802

Direct-contact heat transfer processes between fluid streams are reviewed for situations that may be found in process technologies. While not all of the past work could be referenced in the space available, many current and review articles are cited that provide sources of detailed information. Included in this review are topics that relate to direct contact evaporation, condensation, and boiling as well as simple sensible heat transfer between the fluid streams.

Introduction

Direct-contact heat transfer in process equipment occurs between two process streams, which can either be identical media or different ones. For example, in an open feedwater heater in a steam power plant, the feedwater may be heated by a submerged steam jet or a series of jets. Alternatively, two immiscible fluids can be used in a spray column with the purpose of extracting heat from the warmer stream. Direct-contact heat transfer can take place between solids and fluid streams as in drying processes, or between two fluid streams as in pyrolysis-gas quenchers. It is even possible to design direct-contact heat exchange systems to exchange heat between two particle streams, as in the case of cooling large chunks of material from used tires by smaller fragmented pieces that have been cryogenically cooled in order to achieve their fracture. This latter example is just one of many that has application to the recovery of energy and raw materials from waste.

Direct-contact heat transfer processes have myriads of applications. Why then are they not more widely used and discussed in textbooks on heat transfer? It is this writer's viewpoint that they are more widely used than imagined, and that they are not discussed more by textbook writers due to their lack of experience with them. In order for me to support my first premise, let me point out that a wet cooling tower is a direct-contact heat exchanger, as is a grain dryer. Quenching processes are also direct-contact heat exchange processes. Distillation columns and fractionation columns in a petroleum refinery include sections where direct-contact heat exchange is the primary goal. I support my second premise by citing the lack of examples present in textbooks as well as the lack of discussion of the appropriate theory.

Direct-contact heat exchange is in no way a new field of endeavor for the heat transfer practitioner. Hausbrand's book, *Evaporation, Condensing and Cooling Apparatus*, appearing in its first German edition in 1900 and later appearing in five English editions through 1933, deals with several types of direct contactors including barometric condensers. The earliest edition dealt with the, then, theoretical aspects of the equipment as well as with their commercial design. Despite this early start, the development of a true understanding of their nature lagged, and still lags behind the understanding of surface-type heat exchangers.

Due to the myriads of applications of direct-contact heat exchange, it is not possible to cover all aspects of this fascinating subject in the space provided, nor has this author the knowledge to do so. Therefore, primary attention will be paid to the direct-contact heat exchange between two fluid streams. This, then, is the field where conventional surface-type heat exchangers might offer an attractive alternative. Prior reviews of direct-contact heat transfer dealing with this subject have been published in *Advances in Chemical Engineering*, Vol. 6, 1966 (Sideman, 1966), and *Advances in Heat Transfer*, Vol. 15, 1982 (Sideman, 1982). The later review dealt primarily with direct-contact condensation, while the former was broad in scope.

Contributed by the Heat Transfer Division for publication in the JOURNAL OF HEAT TRANSFER. Manuscript received by the Heat Transfer Division February 16, 1988. Keywords: Multiphase Flows, Phase-Change Phenomena, Reviews.

Advantages and Disadvantages in Utilizing Direct Contactors

Direct-contact heat exchangers have several advantages over surface-type heat exchangers. They also have several drawbacks. The drawbacks are quite obvious. If two fluid streams are placed in direct contact they will mix, unless the streams are immiscible. Thus, stream contamination may occur. This could be extremely expensive if later purification of the contaminated stream or streams is necessary. The two streams must also be at the same pressure in a direct contactor, which could lead to additional costs. The advantages in utilizing direct contact include the lack of surfaces to corrode and/or foul, or otherwise deteriorate the heat transfer performance. Other advantages include the potentially superior heat transfer for a given volume of heat exchanger due to the larger heat transfer surface area and the ability to transfer heat at much lower temperature differences. Still another advantage is the much lower pressure drop associated with direct contactors as compared with their tubular counterparts. A final advantage is the much lower capital cost as direct-contact heat exchangers can be constructed of little more than a pressure vessel, inlet nozzles for the fluid streams, and exit ports. Of course it is sometimes advantageous to provide internals, as will be discussed later.

It is clear that direct-contact heat exchangers offer in many cases a clear alternative to tubular heat exchangers; however, it is also clear that they offer no panacea to all heat exchange problems, and that their selection must be done with care. Further, it is necessary that an equally well-established data base for their design be established if they are to reach their full potential use in process technology.

Typical Equipment Used for Facilitating Direct-Contact Heat Transfer Between Fluid Streams

The types of heat exchange between fluid streams that are normally encountered in processes include the simple heating or cooling of one fluid by the other, cooling with the vaporization of the coolant, cooling of a gas–vapor mixture with partial condensation, cooling of a vapor or vapor mixture with total condensation, and cooling of a liquid with partial or complete solidification. All of these applications can be carried out using a variety of direct contactor configurations. Most of the direct-contact applications can be accomplished with the following devices:

(*a*) Spray columns
(*b*) Baffle tray columns

Copyright © 1988 by ASME

Downloaded 16 Dec 2010 to 193.140.21.150. Redistribution subject to ASME license or copyright; see http://www.asme.org/terms/Terms_Use.cfm

(*c*) Sieve tray or bubble columns
(*d*) Packed columns
(*e*) Pipeline contactors
(*f*) Mechanically agitated contactors

Examples of each of the above are shown in Figs. 1 through 6. With the exception of the last two, the heat transfer takes place between a continuous phase and a clearly defined disperse phase in the form of droplets, bubbles, jets, sheets, or thin supported films in the case of packed beds. For the pipeline contactor, the two fluid streams are brought together in a turbulent flow so as to obtain near perfect mixing and a mean temperature that is dependent on the thermal capacity of the two fluids, their inlet temperatures, and their flow rates. Separation, if desired and possible, requires an additional device.

Most mechanically agitated devices are strongly dependent on the configuration of the agitator as well as the vessel and are not readily susceptible to analysis. They are typically proprietary in their design and the process engineer is at the tender mercy of the manufacturer in establishing the adequacy of the device to perform the necessary role.

Spray columns, sieve tray columns, baffle tray columns, and even packed columns are more amenable to analyses. They have many things in common, including the need for further research. In discussing them, this review will concentrate on their similarities through the nature of the dispersed phase, i.e., droplets or bubbles, jets, sheets, or thin films.

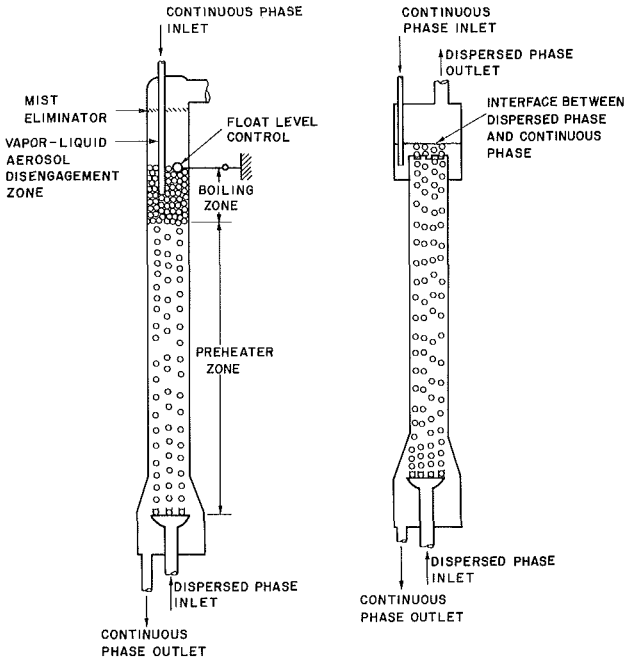

Fig. 1 Spray columns for boiling and for liquid-liquid heat transfer (Jacobs, 1988)

Direct-Contact Heat Transfer With Drops or Bubbles

Direct contactors such as spray or sieve tray columns, shown in Figs. 1 and 3, are designed to produce, as the dispersed phase, either droplets or bubbles depending on whether the dispersed phase is a liquid or gas. Ideally, the drops or bubbles move vertically through the continuous phase before coalescing at the top or bottom of the column and being withdrawn. In process equipment, the formation of the drops or bubbles is typically achieved through the breakdown of jets. By providing the appropriate flow rate through a given nozzle, it is possible to form nearly uniform size drops of a predictable diameter. This uniformity is achievable only if the velocity of the dispersed phase is carefully controlled. Thus, off-design operation of these contactors is limited as noted in the discussion of the hole or nozzle design provided next.

The perforations in a sieve tray or the nozzles in the injection plate for a spray columnn should typically be punched holes and the material of the tray or distributor should not be wettable by the dispersed fluid (Jacobs, 1988b). Actual design of the holes is not critical as long as the velocity through them is equal to the jetting velocity but less than the critical jetting

Nomenclature

α_d = thermal diffusivity of disperse phase
α_{eff} = effective thermal diffusivity
C_{pd} = drop specific heat
d_D = drop diameter
d_{DC} = critical drop diameter
d_{jc} = critical jet diameter
d_n = nozzle diameter
D_{CR} = critical diameter for transition to a circulating drop, defined in equation (17)
$\Delta\rho$ = difference in density of dispersed and continuous phases
Eö = Eötvos number, defined in equation (11)
Eö_n = Eötvos number using the nozzle diameter
ϵ = void fraction or holdup
g = gravitational acceleration
G_c = continuous phase volumetric flow rate
G_d = dispersed phase volumetric flow rate
γ = density ratio, defined in equation (14)
h_{fg} = enthalpy of vaporization
Ja = Jakob number, defined in equation (23)
K = defined by equation (4)
K_1 = defined in equation (13)
K_v = defined in equation (16)
M = M-group, defined in equation (10)
μ_c = continuous phase dynamic viscosity
μ_d = disperse phase dynamic viscosity
Nu_{ci} = Nusselt number for internal to drop heat transfer for rapidly circulating drop
Nu_{co} = external to drop Nusselt number for circulating and oscillating drops, defined in equation (18)
ρ_c = density of continuous phase gravity
ρ_d = density of dispersed phase
ρ_l = density of condensate
Pe = Peclet number based on continuous phase properties and drop to continuous phase relative velocity
r = radial coordinate
Re_c = Reynolds number, defined in equation (10)
R_f = final radius
R_i = initial radius
$R(t)$ = radius at time t
σ = interfacial tension
T_{Ri} = temperature at initial drop surface
$T(r, t)$ = temperature at r at time t
T_{SAT} = saturation temperature
$T(t=0)$ = temperature of drop at time zero
U_v = volumetric heat transfer coefficient
V_d = drop velocity in a quiescent medium
V_j = jetting velocity
V_{jc} = critical jetting velocity
V_n = mean nozzle velocity

Downloaded 16 Dec 2010 to 193.140.21.150. Redistribution subject to ASME license or copyright; see http://www.asme.org/terms/Terms_Use.cfm

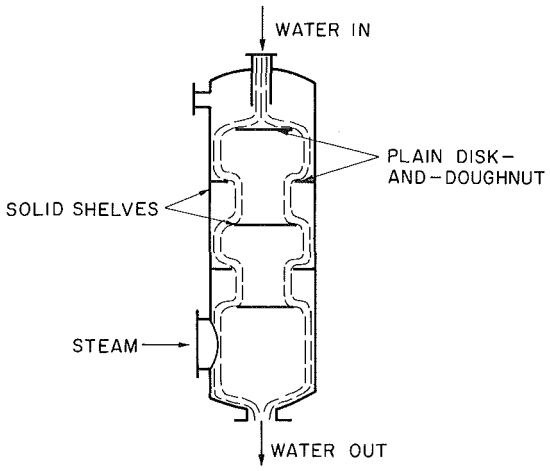

Fig. 2 A baffle tray column used as a direct contact condenser (Jacobs and Nadig, 1987)

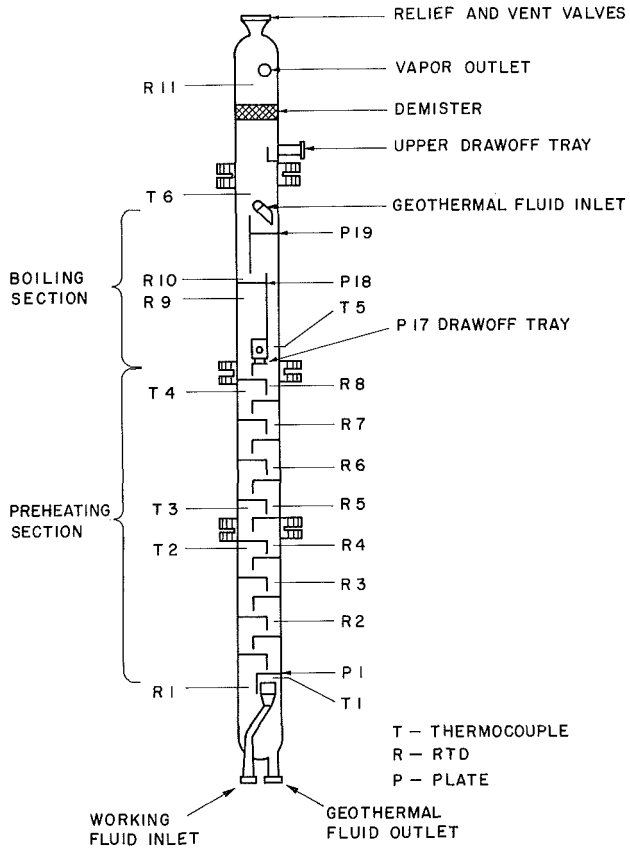

Fig. 3 A sieve tray column used for extracting heat from geothermal brine using isobutane as a dispersed phase (Jacobs and Eden, 1986)

velocity. Exceeding or equaling the jetting velocity is important due to the fact that lower velocities can lead to situations where not all of the nozzles are flowing, and due to the fact that drops formed when it is exceeded are very regular in size. As noted previously, regular size drops are important in order to prevent premature coalescence and to predict column performance. Steiner and Hartland (1983) recommend that the jetting velocity be calculated from

$$V_j = \frac{2\sigma}{\rho_d d_n}\left(1.07\text{–}0.75\,\frac{\Delta\rho d_n^2 g}{4\sigma}\right) \tag{1}$$

where σ is the interfacial tension and d_n is the nozzle diameter.

It is also necessary not to exceed the critical jetting velocity. Above this velocity, the length of the jet decreases dramatically followed quickly by atomization of the dispersed phase. This requires a large pressure drop across the nozzle. It is generally undesirable for spray columns and requires too large of a coalesced zone below or above each tray in a sieve tray column, depending upon whether the dispersed fluid is heavier or lighter than the continuous one. The critical jet diameter and the corresponding critical velocity can be calculated according to Skelland and Johnson (1974) as follows:

$$d_{jc} = \frac{d_n}{0.485K^2 + 1} \quad \text{for } K < 0.785 \tag{2}$$

or

$$d_{jc} = \frac{d_n}{1.51K + 0.12} \quad \text{for } K > 0.785 \tag{3}$$

where

$$K = \frac{d_n}{\sqrt{\sigma/(\Delta\rho g)}} \tag{4}$$

$$V_{jc} = 2.69\left(\frac{d_{jc}}{d_n}\right)^2 \left(\frac{\sigma}{d_{jc}(0.514\rho_d + 0.472\rho_c)}\right)^{1/2} \tag{5}$$

At this critical velocity, Treybal (1963) recommends the following equations for the critical drop size:

$$d_{DC} = \frac{2.07 d_n}{0.485\text{Eö}_n + 1} \quad \text{for } \text{Eö}_n < 0.615 \tag{6}$$

and

$$d_{DC} = \frac{2.07 d_n}{1.51\text{Eö}_n^{1/2} + 0.12} \quad \text{for } \text{Eö}_n \geq 0.615 \tag{7}$$

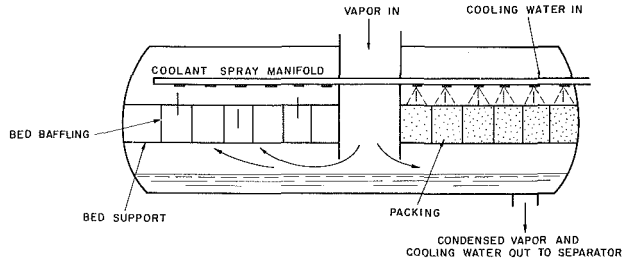

Fig. 4 A possible configuration of a packed bed condenser (Jacobs, Section 2.6.8, *Design Handbook*, 1986)

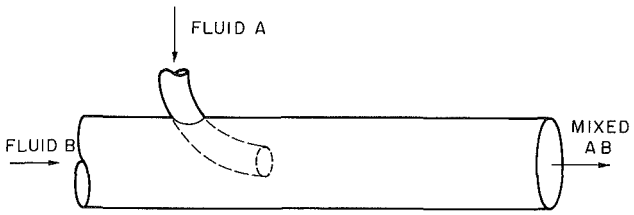

Fig. 5 Turbulent pipe contactor

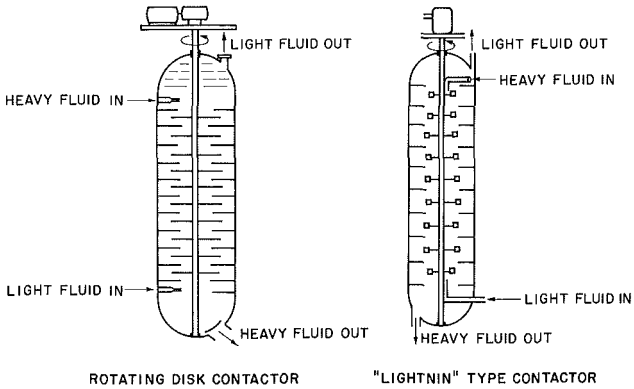

Fig. 6 Typical mechanically agitated towers (Treybal, 1966)

Downloaded 16 Dec 2010 to 193.140.21.150. Redistribution subject to ASME license or copyright; see http://www.asme.org/terms/Terms_Use.cfm

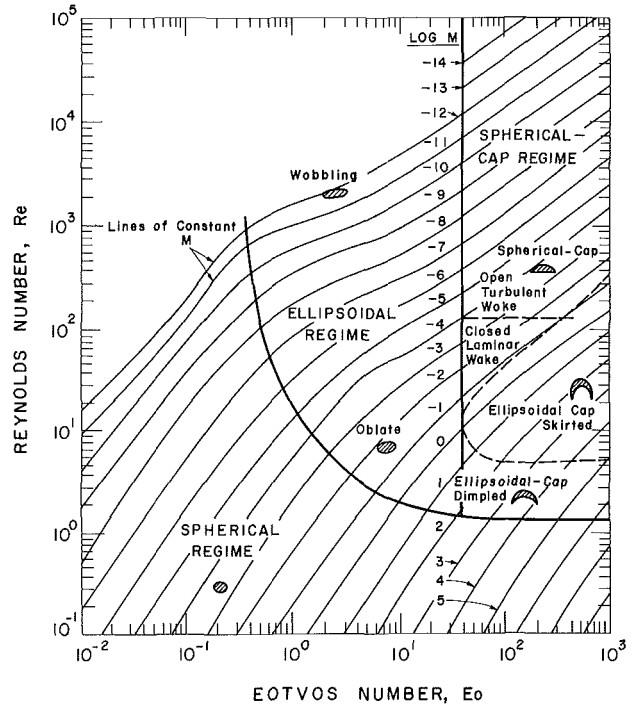

Fig. 7 Drop characterization map (Grace, 1983)

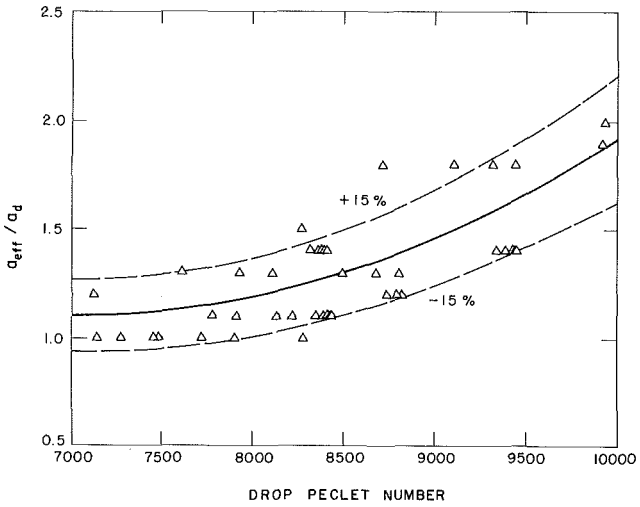

Fig. 8 a_{eff}/a_d versus drop Peclet number

where Eö_n is the nozzle Eötvos number, defined as

$$\text{Eö}_n = \frac{\Delta\rho g d_n^2}{\sigma} \tag{8}$$

For conditions between the jetting velocity and the critical jetting velocity, the following correlation is recommended to determine the drop size (Steiner and Hartland, 1983):

$$d_D = d_{jc}\left[2.06\,\frac{V_{jc}}{V_n} - 1.47\,\ln\frac{V_{jc}}{V_n}\right] \tag{9}$$

Steiner and Hartland (1983) recommend maintaining a minimum Weber number (defined with nozzle velocity and the density of the dispersed phase) greater than two to prevent seeping along the surface and secure drop formation on all openings. Experience in my laboratory indicates that nozzle or perforation spacing should not be closer than 1.5 d_D to insure that jet or drop coalescence does not occur. For the case of bubbles that may be expanding, the spacing should be 1.5 times their expected largest cross-sectional diameter.

Drops or bubbles formed from jets or nozzles may behave differently according to their density, interfacial tension, volume, proximity to other drops and bubbles, and whether heat and/or mass transfer takes place between them and the surrounding continuous phase. For drops or bubbles rising through a continuous phase due to gravity, there are five dimensionless groups that govern their motion:

Reynolds Number

$$\text{Re}_c = \frac{\rho_c d_D V_D}{\mu_c} \tag{10}$$

Eötvos Number

$$\text{Eö} = \frac{\Delta\rho g d_D}{\sigma} \tag{11}$$

M-Group

$$M = \frac{g\mu_c^4\Delta\rho}{\rho_c^2\sigma^3} \tag{12}$$

Viscosity Group

$$K_1 = \mu_d/\mu_c \tag{13}$$

Density Ratio

$$\gamma = \rho_d/\rho_c \tag{14}$$

For an isothermal system and any particular combination of fluids, M, K, and γ are constant. Thus, Grace (1983) correlated drop or bubble behavior by plotting Re versus Eö for constant values of M for a large number of fluid pairs. He found that K and γ play a small role in the results. Figure 7 categorizes drops and bubbles into three regimes: the Spherical regime, the Ellipsoidal regime, and the Spherical Cap regime. An approximate curve is shown that separates the first two regimes. This author's personal experience indicates that the presence of even small amounts of impurities will shift the curve to the right at high Re.

The spherical regime contains the regime where the drops are nearly spherical. For spherical drops, little or no internal circulation takes place, and according to Sideman (1966), the onset of internal circulation as designated by a critical Re is hard to predict. This is especially true in the presence of surface contaminants, which tend to immobilize the interface. The presence of internal circulation, however, can significantly increase the heat transfer to a drop or bubble. Recently, Jacobs and Eden (1986), using experimental data from a sieve tray column with isobutane as the dispersed phase in a continuous phase of geothermal brine, produced the curve shown in Fig. 8 for the increase in effective thermal diffusivity of an assumed rigid drop due to probable internal circulation.

The Ellipsoidal regime and the Spherical Cap regime delineate regions where the bubbles or drops are strongly distorted and where no time-consistent geometry occurs. The continuous distortion of the dispersed phase leads to strong internal circulation and can greatly reduce any internal resistance to heat transfer. Unfortunately, this also leads to more unpredictable motion, higher drag, and greater probability of coalescence of bubbles or drops within a swarm. Thus, in designing a direct-contact heat exchanger, these regimes should be avoided if possible. When it is impossible to avoid these regimes, it is necessary to depend upon experience with similar equipment operating in the same regimes.

(A) Heat Transfer in Devices Without Phase Change. Direct-contact heat transfer in devices without a change in phase of either fluid are common in many process applications. They are perhaps most common when dealing with two immiscible liquids. Depending on the properties of

Downloaded 16 Dec 2010 to 193.140.21.150. Redistribution subject to ASME license or copyright; see http://www.asme.org/terms/Terms_Use.cfm

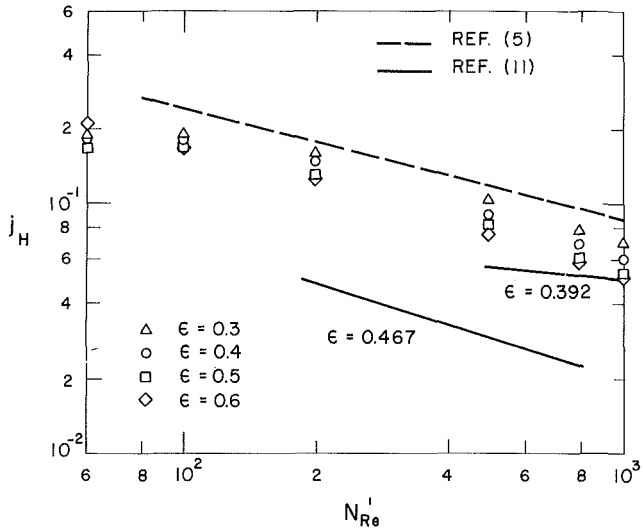

Fig. 9 Comparison of numerical calculations of Chilton-Colburn factor with correlations of McConnachie and Thodos (1963) and Bhatlacharyya and Pei (1975) (from Thompson and Jacobs, 1984)

the two fluids, the heat transfer can be dominated by either the external or internal to the drop resistance. Whereas the internal heat transfer is rather readily dealt with by a model for transient conduction in a sphere exposed to a fluid of time-varying temperature and a uniform external heat transfer coefficient (Jacobs and Golafshani, 1985) using an appropriate expression to account for the effective thermal diffusivity due to possible internal circulation, the heat transfer coefficient external to the drop is less well understood. The external-to-the-drop heat transfer coefficient depends upon the local volume fraction of the column occupied by the dispersed phase. For example, consider a relatively large-diameter column through which a single drop is rising or falling. The external flow is not significantly different than that for flow over a rigid sphere, if no internal circulation takes place. For this situation, a wide range of correlations are available covering the range of Peclet number Pe from 10^{-2} to 10^{7} (Sideman, 1966).

With internal circulation, drops and bubbles deform as already noted. A drop or bubble may take on a variety of shapes: however, still the only basis for a theoretical model to deal with internal circulation is the classical model of Hadamard first published in 1911. According to Sideman (1966), there are at least six published equations using the Hadamard model and an additional twelve based primarily on experimental data (most are derived from mass transfer analogies). He recommends the following correlation for rapidly circulating drops:

$$\mathrm{Nu}_{ci} = 2 + 1.13(\mathrm{Pe}K_v)^{0.5} \tag{15}$$

where

$$K_v = 1 - 1.45\,\frac{2+3\mu_d/\mu_c}{1+\left(\frac{\rho_d\mu_d}{\rho_c\mu_c}\right)^{1/2}}\,\mathrm{Re}_c^{-1/2} \tag{16}$$

Sideman gives for the critical diameter for transition to a circulating drop the expression

$$D_{CR} = \left[\frac{12(\sigma-\sigma_s)^{1/2}}{g(\rho_d-\rho_c)}\right] \tag{17}$$

where σ is the surface tension for a pure system and σ_s is that observed for the actual working fluids. Experimental data are generally needed for σ_s.

For circulating and oscillating drops, the following empirical equation for the external heat transfer coefficient is suggested:

$$\mathrm{Nu}_{co} = 50 + 0.0085\mathrm{Re}_c\mathrm{Pr}^{0.7} \tag{18}$$

For heat transfer inside the drops or bubbles, for rigid drops or where small circulation occurs, it is recommended that a transient conduction model be used together with the correction to the effective thermal diffusivity shown in Fig. 8, as mentioned previously.

Actual direct-contact heat exchangers seldom are designed with widely dispersed drops or bubbles. Rather, to optimize the heat transfer, they should be operated near the flooding point. Typically, this point might be reached at a dispersed phase volume fraction of between 15 and 40 percent, depending on their relative buoyancy, size, and the fluid properties of the two phases (Letan, 1988a, 1988b) and Jacobs (1988b). If one were to consider the region occupied by the continuous phase to be a spherical annulus, the distance between adjacent drop centers would be only 1.88 drop diameters for a 15 percent holdup and 1.35 for a 40 percent holdup situation. The fluid dynamics associated with single drops would not apply, nor would the heat transfer. Instead of an adverse pressure gradient occurring on the back of the drop with the associated wake formation and shedding, the adjacent drops may provide a favorable pressure gradient, and attached flow around nearly all if not all of the drop. The external heat transfer would thus more closely approximate that seen in packed beds of randomly oriented spherical particles. For such a situation, Thompson and Jacobs (1984) present a series of curves for Nu_{cdD} as a function of Re_{cdD} for various packing densities and continuous phase Pr. Their numerical solutions show good agreement with existing experimental data; although their results are typically higher by about 20 percent as shown in Fig. 9. No such analysis exists for the case of drops or bubbles with mobile interfaces.

(A.1) Spray Columns as Heat Exchangers. Steiner and Hartland's chapter in the *Handbook of Fluids in Motion* deals with the hydrodynamics of liquid–liquid spray columns. It provides expressions for estimating the rise of single drops and a review of the current status of means to estimate the behavior of drops in swarms. As pointed out by them, most of the empirical relations published are quite restrictive in their application and no single relation seems to hold. Therefore, this is an area ripe for further investigation. Nevertheless, simple models have been proposed by Letan (1976, 1988b) and Jacobs and Golafshani (1985) that appear to offer reasonable means to predict column performance if care is taken to eliminate recirculation by proper design of the inlet nozzles for both the continuous and disperse fluids (Jacobs, 1988b).

Although it is best to utilize heat transfer models based on the heat transfer to individual drops, a wide number of authors have proposed the use of volumetric heat transfer coefficients for preliminary design. A large number of correlations exist that utilize a small amount of data. Plass et al. (1979) utilized all existing data available through 1978 to develop the following correlation:

$$U_v = 1.2\times10^4\epsilon\ \frac{\mathrm{Btu}}{\mathrm{hrft^3\,°F}}\ \text{for}\ \epsilon<0.05 \tag{19}$$

$$U_v = \left[4.5\times10^4(\epsilon-0.05)e^{-0.57G_d/G_c}+600\right]\frac{\mathrm{Btu}}{\mathrm{hrft^3\,°F}}$$

$$\text{for}\ \epsilon\geq0.06 \tag{20}$$

where ϵ is the void fraction or holdup.

Equations (19) and (20) utilized data from a wide range of fluids but excluded all data utilizing liquid metals. Most of the data dealt with organic-aqueous systems and with drops from 2 mm to 6 mm in diameter. It is doubtful that the correlation

Downloaded 16 Dec 2010 to 193.140.21.150. Redistribution subject to ASME license or copyright; see http://www.asme.org/terms/Terms_Use.cfm

would be very acceptable as a predictive tool for significantly different conditions. Such correlations are also suspect when little is known about the total column arrangement in the experiments from which the data is taken. If back mixing (axial mixing) occurred to any significant extent, the data could be strongly influenced (See Steiner and Hartland, 1985).

Recirculation in a spray column can be due to the design of the continuous phase injector as demonstrated by Kim and Jacobs (1987). It can also be due to wake shedding from the drops. In fact, Letan and Kehat (1968) attribute much of the back mixing in spray columns to this phenomenon. They propose a model for heat transfer that treats the wakes as a third phase and neglect the surface heat transfer coefficients entirely, as the drops are assumed to be perfectly mixed. (This would require very large drops and clean systems.) Although this idea has drawn a lot of attention, and may play a significant role in low holdup situations, it is probably not applicable at high holdup as has already been mentioned. In fact, Jacobs and Golafshani (1985) have shown that for the isobutane-water system that Letan and Kehat used in their early study, the internal resistance in the drops governed the heat transfer.

(*A.2*) *Sieve Tray Columns.* Sieve tray columns are widely used as mass transfer devices because they produce very high mass transfer coefficients through the repeated reformation of the drops or bubbles comprising the dispersed phase. It is this same feature that makes them attractive as heat exchangers. As can be seen in Fig. 3, the sieve tray column is composed of essentially the same components as a spray column plus the trays. The trays are designed in much the same way as a dispersed phase injector, in that the perforations in the trays should operate between the jetting velocity and the critical jetting velocity. The head providing for the pressure drop across the nozzles is obtained from a sufficiently thick layer of the coalesced, dispersed phase above or below the tray. This depth is achieved by the use of what is called a downcomer, which directs the downward or upward flow of the continuous phase as well as acting as a dam for the dispersed phase. In a recent paper, Jacobs and Eden (1986) presented an analysis of a sieve tray column and proposed a model that described the heat transfer as an idealized crossflow heat exchanger when modeling the heat transfer process between individual trays. When comparing the model to experimental data, they found excellent agreement utilizing overall heat transfer coefficients, which accounted for the transient conduction in the drops and a surface heat transfer coefficient recommended by Whitaker (1972) for packed beds. For larger drops, where internal circulation was probable, the effective thermal diffusivity shown in Fig. 8 and described by equation (21) was used.

$$\alpha_{\text{eff}}/\alpha_d = [\text{Pe}_d/(7004(1+\mu_c/\mu_d))]^{1.65} \tag{21}$$

The results of the study indicated that the use of larger drops (which could reduce the internal thermal resistance) did not overcome the advantage due to the larger surface area of a system of smaller drops for the same volumetric flow rate of the dispersed phase. Of course, they warn that heat transfer alone cannot dictate column design, and volumetric throughput also depends on drop or bubble size. When comparing the heat transfer achievable with a spray column and a sieve tray column for the same fluid throughputs, drop diameters, and column diameter, Jacobs and Eden (1986) claim that the equivalent volumetric heat transfer coefficients for the sieve tray column can be three to four times as large as for the spray column when internal-to-the-drop heat transfer governs the design. This, of course, is attributable to the drop reforming and the reduction of the diffusional resistance. While this might lead to one deciding to use very close tray spacing, the associated pressure drop and increasing use of the column for coalesced, dispersed phase soon renders such a decision faulty. As with conventional heat exchangers, proper design of direct contactors requires choosing the optimum compromise.

(B) Heat Transfer With Change of Phase

(*B.1*) *Condensation.* Perhaps the most common direct contactor currently in use that is based on heat transfer to drops or bubbles is the barometric condenser. As noted in the Introduction, the industrial use of such condensers dates back more than eighty years (Hausbrand, 1933). In a literature review published in 1977 by Jacobs and Fannir, direct-contact condensers were first classified as being "drop type," "jet and sheet type," and "film type." Drop-type condensation refers to condensation on sprays or drops of liquid coolant that are injected into a chamber filled with vapor or a gas-vapor mixture. Early work dealt primarily with the condensation of saturated pure vapors where the liquid and vapor are the same substance. Kutateladze (1966) was the first to recommend that drops be assumed spherical and that heat transfer be governed by the transient conduction within the drops. This assumption is reasonable in most situations as drops in such condensers are designed to lie in the range of 0.25–2.5 mm in diameter.

Ford and Lekic (1973) published the results of a study of condensation of steam on single drops of water. Utilizing the equations for transient conduction in a sphere suddenly having its surface temperature changed to the saturation temperature, they found that the drop growth rate was overpredicted. Jacobs and Cook (1978) developed a theoretical model accounting for the added resistance of the condensate that exactly predicted Ford and Lekic's experiments. Jacobs and Cook's model recognized that the ratio of the final drop radius to initial radius was given by

$$R_f/R_i = \left(1+\frac{1}{\text{Ja}}\right)^{1/3} \tag{22}$$

where

$$\text{Ja} = \frac{\rho_l h_{fq}}{\rho_d C_{pd}(T_{\text{SAT}} - T_{(t=0)})} \tag{23}$$

The model assumes that the condensate film is thin, as would be the case for large values of the Ja defined in equation (23). Thus, they were able to solve the problem of conduction in a sphere subject to the boundary condition

$$q'' = k_l \frac{T_{\text{SAT}} - T_{(R_i)}}{R(t) - R_i} \tag{24}$$

The nondimensional radius at time t was given as

$$\frac{R(t)}{R_i} = \left[1+\frac{3}{\text{Ja}}\int_0^1 \left(\frac{r}{R_i}\right)^2 \frac{(T_{r,t}-T_i)}{(T_{\text{SAT}}-T_i)}\frac{dr}{R_i}\right] \tag{25}$$

Due to their success in treating the problem of a vapor condensing on its own liquid, Jacobs and Cook (1978) extended their theory to deal with a secondary vapor condensing on an immiscible drop, where the coolant would have been treated such that the vapor condensate would wet the drop. Typical results are shown in Figs. 10 and 11.

Kulik and Rhodes (1978) have studied the effects of noncondensables in steam on condensation on water drops. Their study showed that the internal resistance was important for drops greater than 0.1 mm in diameter, even when noncondensable gases are present. However, a reliable method of predicting the external resistance with noncondensables present was not developed. This latter topic has been part of the aim of P.S. Ayyaswamy and co-workers (Chung and Ayyaswamy, 1981a, 1981b, 1984a, 1984b; Sundarajan and Ayyaswamy, 1984, 1985a, 1985b; Huang and Ayyaswamy, 1987a, 1987b). These studies have been aimed at theoretically modeling both the internal and the external flow around a drop. Except for very large drops or very high relative velocities, the internal

Downloaded 16 Dec 2010 to 193.140.21.150. Redistribution subject to ASME license or copyright; see http://www.asme.org/terms/Terms_Use.cfm

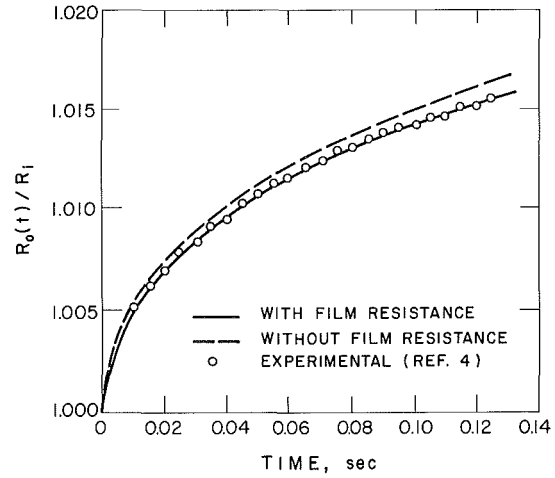

Fig. 10 Drop growth rate for steam condensing on a water drop; $T_{SAT} - T_j$ = 50°C (Jacobs and Cook, 1978)

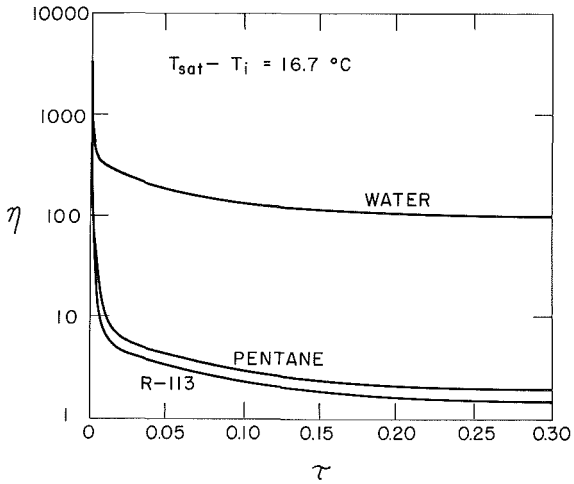

Fig. 11 Comparison of effective external nondimensional heat transfer coefficients for condensing steam, pentane, and R-113 on water drops (Jacobs and Cook, 1978)

circulation is small. Thus, the latter analyses are a bit of overkill when applied to barometric condensers where a small diameter and low vapor velocities are most practical. More concentration, however, is needed on the influence of noncondensables and drop spray statistics.

The prediction of drop size distribution statistics for a given nozzle is needed to predict heat transfer accurately. More information is needed on the formation of drops in spray nozzles and their size distribution even though such statistics have long been studied (Brown, 1951; Isachenko and Kushnyrev, 1974). In order to design a barometric condenser, for example, the vapor velocity must not exceed the terminal velocity of the smallest drop, yet to utilize the cooling capacity of the spray fully, the size of the largest drops must be known. From a practical viewpoint, this means that the diameter of the condenser vessel is dictated by consideration of the smallest drops and the height is dictated by the largest (Jacobs, 1985).

The fact that the interface between the vapor and the drop is not impermeable to noncondensable gases, especially highly soluble ones, offers other problems. For example, both CO_2 and H_2S are soluble in water. At the Geysers geothermal facility in California, the first 15 power plants installed used direct-contact condensers. The condensers were connected to open cooling towers and the H_2S absorbed in the condensers was subsequently released into the atmosphere. Air pollution standards led to curtailment of the use of the direct contactors on later plant expansion because no information was available to circumvent the problem. A better understanding of this mass transfer problem could have averted a costly refitting, and perhaps an adequate direct contact design could have been achieved.

In addition to the absorption problem, it is also possible that the coolant drops could contain dissolved gas. Heating the drops during the condensation process can lead to migration of the gas to the condensate interface, thereby greatly reducing the heat transfer by effectively lowering the liquid thermal conductivity and by introducing the gases into the surrounding vapor boundary layer. On the other hand, the gases going into solution in the drops could lower the effect of noncondensables on a gas–vapor mixture condensation problem. This problem has been addressed by Chung and Ayyaswamy (1981a); however, these effects need further examination.

Direct-contact condensers can also be designed wherein streams of bubbles can be injected into a continuous liquid. Such is the case in an open feedwater heater, although, it is more likely a series of jets that breakdown rather than a series of bubble trains. A wide range of experiments on this problem and models to describe the phenomena have been reported by Sideman (1982). Most have as their basis the early work by Floreschuetz and Chao (1965). In 1978, Jacobs and Major were the first to consider the resistance of the condensate film inside the bubble and to model successfully the effects of noncondensables. For bubbles smaller than 4.5 mm in diameter, they found that the collapse was dominated by diffusion of the noncondensables; for larger bubbles, the early bubble distortion effectively kept the vapor gas mixture uniformly mixed as proposed earlier by Isenberg and Sideman (1970). A problem of considerable debate in developing models for bubble condensation is the correct boundary condition in the external liquid boundary layer, particularly if the condensate is immiscible in the coolant. Lerner et al. (1984), argued for a slip boundary condition while Jacobs and Major (1982) assumed that the condensate moved at the potential flow as did the coolant. Grace (1983) indicates that the appropriate boundary condition is a function of the Eötvos number and is dependent on whether or not impurities are present. In examining all of the models described by Sideman (1982), it is clear that a variety of effects can be used to explain the experimental data and that each modeler has equally rational arguments. Thus, more thorough models and better experiments are necessary.

In applying single bubble data to heat exchanger systems, Moalem-Maron et al. (1972) developed a model for condensation of a bubble train. Golafshani (1983) improved on the model by using the more sophisticated model of Jacobs and Major (1982) to account for the resistance of the condensate and to account for the effects of the noncondensable gases that might be present. The results of Golafshani (1983) indicated that for no noncondensables present, the different models for single bubble collapse had small effects on the behavior of the bubble train. Thus, it appears that small differences in single bubble theory have little effect on heat exchanger design.

Despite the relative acceptability of the theories, Johnson et al. (1983) and Sudhoff (1982) have found the experiments are plagued by a so-called persistent bubble. Johnson carried out experiments in a very deep heat exchanger. He reports that visual observation indicates that the persistent bubble finally disappears. He concludes that this is due to absorption of the noncondensable gases present into the liqud. So far, none of the other investigators have offered any hypothesis for this phenomenon although all of the experimental investigations have reported it.

If Johnson's arguments concerning the persistent bubble are valid, it may be that a heat exchanger could be designed with such a depth that condensation can be accomplished and gases

Downloaded 16 Dec 2010 to 193.140.21.150. Redistribution subject to ASME license or copyright; see http://www.asme.org/terms/Terms_Use.cfm

easily separated. This requires investigation of condensation with gases that are noncondensable but slightly soluble.

More recent studies of bubble collapse deal with an interesting phenomenon that may have some interesting applications to the cooling of electronics. This phenomenon deals with the collapse of vapor bubbles in an immiscible coolant that is lighter than the condensate. This causes the bubbles to decelerate after the condensation is near completion and fall backward somewhat like a "spouted-bed-device" (a device where a fluid is injected into a gas and falls back into a pool from which it is pumped to another heat exchanger and cooled or heated before being reinjected into the gas) (Kalman et al., 1987; Lerner et al., 1987).

(B.2) Boiling. The evaporation of drops of immiscible fluids in a warm continuous phase has numerous industrial applications including desalination processes, and extraction of heat from geothermal brines (Jacobs, 1988b) or from solar ponds (Wright, 1988). Sideman (1966) deals with a wide range of studies on this problem, including work with both single and multidrop systems. Unfortunately, none of the early work sheds light on either the problem of nucleation or how complete evaporation occurred, despite the wide range of experimental studies conducted. In the 1970s, continued work on desalination in Great Britain (Simpson et al., 1974) led to further understanding of the evaporation process, but not to understanding of the nucleation phenomenon, nor the behavior of evaporation droplet swarms. For example, for single drops it is clear that significant superheating of the liquid can occur before evaporation commences. If the degree of superheating brings the drop temperature close to the Spinodal limit, then the drop may explode. This limit is seldom reached in process heat transfer, yet the degree of superheat before nucleation occurs is not known. For drops where evaporation is occurring, the interfacial tension between the two fluids may keep the liquid in the drop at the drop surface. For the vapor–liquid interface to be at least at the saturation temperature means that during the evaporation process, the liquid must remain superheated. This is the basis for the Simpson et al. model. The results indicate that the instantaneous value of the heat transfer coefficient increases with increasing ratio of the instantaneous to initial drop diameter raised to the 1/6 power up to 90 percent evaporation. This is consistent with their experiments and with those of Sideman (1966).

More recent studies of the evaporation of drops in an immiscible liquid have based their work on that of Sideman (1964, 1967) and Simpson (1974). Among these works are included those of Raina et al. (1982, 1984a, 1984b, 1985) and Battya (1983). All of these single bubble studies assume that the heat transfer depends primarily on the external heat transfer and the portion of the two-phase bubble's wall wetted by the evaporating liquid. Jacobs and Boehm (1980) found that multidrop systems were impossible to correlate based on single-phase systems due to foaming and, therefore, presented only a simple correlation of volumetric heat transfer based on holdup prior to the initiation of vaporization. More recently, Boehm and co-workers (Coban, 1986; Goodwin, 1985) have found reasonable success using the single bubble model of Raina (1985) for low to moderate holdup systems. The latter model accounts for sloshing and is essentially the same as that of Sideman (1966). If such models were to be extended to high holdups, they will have to account for the change in external-to-the-drop heat transfer coefficients.

Evaporation of drops moving through a gas–vapor mixture occurs in gas quenching systems and in combustion systems, to name a few applications. Extensive studies have been reported in the literature. Prakash (1980), Sirignano (1983), and Law (1984) have made careful reviews of the literature, which include their own efforts. While much of what they report has been directed at the combustion problem, it is generally applicable to the broader applications of process heat transfer. In fact, the studies directed at internal circulation in drops are probably more applicable to large drops than to the fine ones used in fuel sprays for combustors. Because of the existence of these extensive reviews, the reader is referred to them for further information.

Direct-Contact Heat Transfer to Jets and Sheets

The use of jets and sheets in process heat transfer normally is applied to the heating or cooling of a gas stream, although it could be applied to heating of a liquid using a submerged vaporous jet. For the former application, sieve tray columns can provide small laminar or turbulent jets of liquid that fall from tray to tray, and baffle tray columns can provide nearly impervious sheets. The gas stream would normally flow across the jets or sheets. The heat transfer coefficient external to the jet or sheet would, therefore, not be unlike that for a tube bundle in crossflow (Crabb, 1981). Care would have to be taken to keep the gas phase velocity sufficiently low so as not to break up the liquid or to cause jet coalescence. In addition, the boundary conditions at the liquid surface would be different and unless the gas was saturated, evaporation would likely occur. For a saturated gas stream, the injection of a cool liquid can be used as a means of stripping the gas of unwanted vapors. Thus, such equipment as mentioned normally involves heat transfer with change of phase.

Although the liquid jets emanating from the perforations in a tray in a sieve tray column may be designed to be laminar and continuous, they are susceptible to breakdown as discussed by Bogy (1979). Such jets are susceptible to surface instabilities that may make them wavy, and eventually turbulent, if they do not first fragment (List, 1982). If the jets or sheets are continuous and remain laminar, the calculation of the internal resistance to heat transfer follows essentially the type of analysis for a Graetz problem. In fact, this type of analysis was directly applied by Kutateladze (1952) in evaluating the problem of steam condensation on a cylindrical jet and on a sheet of water. He assumed that the outside surface of the jet or sheet was suddenly changed to that of the saturated vapor. He also assumed that the velocity in the fluid was uniform both radially and axially.

The use of jets and sheets in barometric condensers was first discussed by Hausbrand (1933) and later by How (1956) and then Fair (1972). None of these authors dealt with the heat transfer coefficients necessary for design. In 1952, Kutateladze suggested the use of the Graetz solution, and this lead was followed by Hasson et al. (1964a, 1964b) who expanded the work to deal with fan jets. Tatel and Tamir (1969) extended the work to deal with noncondensables being present in the vapor, but ignored the condensate's added resistance. Jacobs and Nadig (1987) recently solved the problem of an axisymmetric laminar jet or a sheet including both the resistance of the condensate and the effects of noncondensables for the vapor and fluid being the same or immiscible fluids. They propose presenting curves of coolant capacity utilization rather than heat transfer coefficients for design purposes. Such a curve is shown in Fig. 12 for a steam–air, water system. Knowing the noncondensable concentration and the desired degree of utilization, the Graetz number, and thus, the length of the sheet can be determined. Extension of this work is needed to apply to wavy and turbulent jets and to fragmenting ones. In dealing with the later phenomenon, Lui et al. (1988) have indicated that the fragmentation may not significantly alter the heat transfer from that of a continuous jet. Their experiments have shown good agreement between a fragmenting jet and the theory of Jacobs and Nadig (1987) for a continuous one. Work is also needed dealing with vapor velocity and high pressure effects.

Downloaded 16 Dec 2010 to 193.140.21.150. Redistribution subject to ASME license or copyright; see http://www.asme.org/terms/Terms_Use.cfm

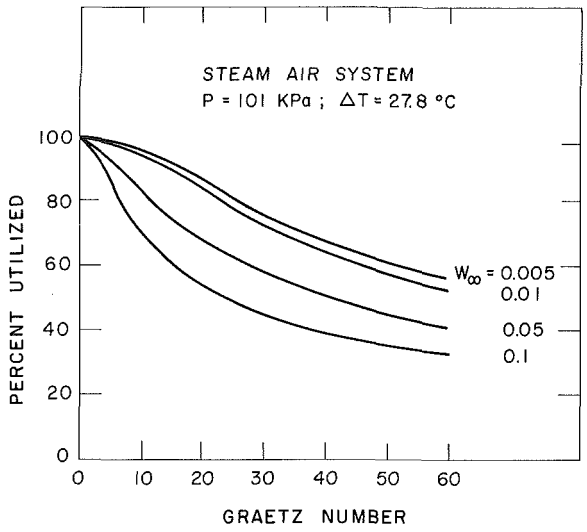

Fig. 12 Degree of coolant capacity utilized as a function of noncondensible gas concentration and Graetz number (Jacobs and Nadig, 1987)

Condensation on high-velocity liquid jets have been studied by Del-Tin (1982, Lineham (1970), and turbulent jets by Kim and Mills (1988) and Wassel (1985). Earlier, Mills et al. (1982) studied both sensible heat transfer and heat transfer with evaporation from turbulent jets. His results indicate that for a turbulent jet that the heat transfer is primarily dependent only on the external-to-the-jet thermal resistance. Similar results were found by Iciek (1983).

The injection of a vapor jet into a continuous pool has many applications, including applications in the chemical process industry and even in waste treatment. Although the basic problem of a jet discharging into a pool has been studied for a long time, two of the first definitive treatments were due to Weimer et al. (1973), and Joung et al. (1974). These studies of condensing jets led to numerous other studies by Faeth and coworkers at The Pennsylvania State University (Chen and Faeth, 1982, 1983). More recently, Sun (1985) has carried out studies on turbulent bubbly jets that arise from the injection of a two-phase jet into a continuous pool. Although sophisticated numerical models were used, it was pointed out that to analyze practical flows, e.g., condensing and evaporating jets, present methods must be extended as they do not yet consider adequately heat and mass transfer between phases and the effect of polydispersions.

Direct-Contact Heat Transfer to Thin Films

The use of thin films to achieve high mass transfer rates is common throughout the process industries. The standard forced draft, wet cooling tower is an excellent example where in both mass transfer and sensible heat transfer occur. Other examples include the packed bed shown in Fig. 4. Packed beds can be used with a liquid and a gas-vapor phase, or for heat transfer between two immiscible liquids when only one of the liquids wets the packing material. They are also used in heating the bed material itself (Murthy and Naranya, 1978). For two-fluid systems, the heavier fluid is normally chosen to be the one wetting the surfaces. A variety of packing materials have been developed and are described in Trebal (1963) and similar texts. They are generally classified as being random packing materials and structured packings. Random packings are normally difficult to model, with the exception of beds of spheres. Most heat transfer data and information on wetting of packings is proprietary, although experimental studies exist in the literature for the more common packings (Jacobs et al., 1978; Schroder and Pohl, 1982; Schulman and Margolis, 1957). However, numerous studies have been carried out for simple geometries such as vertical flat plates, and for spheres (Robertson, 1985; Gunn, 1978; Seban, 1978; Gunn and Vortmeyer, 1982; Kozlov et al., 1978; Niyogi and Pavlenco, 1978; Dukler, 1960; etc.). These studies have a degree of application to structured packings.

Most studies of falling films have assumed negligible or constant shear at the free surface, and have assumed heat transfer from the wall (Seban, 1978). However, the free surface is seldom free of shear and this very phenomenon can lead to the interface instability, waves, and eventually turbulence or stripping of liquid from the surface. Boyadiev et al. (1976a, 1976b) were the first to study nonconstant interfacial shear. They dealt with two infinitely thick fluids that remain stratified and show a similarity solution for cocurrent flow but not for countercurrent flow. Recently, Jacobs and Fletcher (1988) have analyzed the case of a falling film on a vertical flat plate with countercurrent gas stream. They show a transition as the free-stream velocity is increased from a gas side boundary layer growing from the top to one growing from the bottom of the film as the free-stream velocity is increased. Their analysis is restricted to laminar flows. Turbulent gas flows, both cocurrent and countercurrent, have been studied in wetted wall columns (Hikita et al., 1976a, 1976b; Dukler et al., 1984; Hughmark, 1980). An important problem to be studied by these efforts is the onset of flooding (Moalem-Maron and Dukler, 1984; Taitel et al., 1982; etc.). Jacobs and Fletcher (1988) argue that this point may be reached when the liquid interfacial velocity reverses.

Heat transfer studies to thin films flowing over adiabatic surfaces without mass transfer are relatively few in number. Jacobs et al. (1976) studied parallel flows of immiscible liquids and concluded that such a situation was not practical for efficient heat exchange. For the case of a turbulent liquid film exposed to a gas stream, the heat transfer is governed by the gas side coefficient (Gimbutis, 1974). For a laminar film with a countercurrent gas stream, Jacobs and Fletcher (1988) show that the overall heat transfer decreases with increasing gas stream velocity until the gas boundary layer reversal mentioned previously, and then increases indicating a worst-case operating condition exists.

For the case of packed beds, a recent survey by Bohn (1988) indicates that most heat transfer studies must currently rely on mass transfer researches. However, there are a number of applicable studies (Shulman, 1957; Rowe, 1965; Gunn, 1978; Robertson, 1985; Gunn and Vortmeyer, 1982; etc.) There are, of course, also studies of flooding that are applicable, such as Schroder (1982) and Lee (1982). Nevertheless, future work is needed to evaluate the applicability of the mass transfer data to heat transfer design.

Condensation on falling films has been studied by many investigators for the case of laminar films (Murthy and Sastri, 1974, 1976; Rao and Sarma, 1984; Finklestein and Tamir, 1976; Tamir and Rachmilev, 1974; Jacobs and Bogart, 1980; Jacobs et al., 1982; Jacobs and Nadig, 1983). For turbulent gas-vapor streams, Renz and Odenthal (1979) and Wassel and Mills (1982) provide some insight. If the gas-vapor stream is turbulent and the film remains laminar, the heat transfer is still governed by the transport within the film, but the effects of noncondensables is reduced. If the film is turbulent, Wassel and Mills claim the heat transport is only a function of the gas side Peclet number.

Application of the above studies to packed beds requires knowledge of the characteristics of the packing and the degree to which it is wetted by the coolant. Studies in packed beds have been reported by numerous investigators. The early work is summarized by Jacobs et al. (1979) who also carried out their own experiments. More recently, Bharathan and Althof (1984) have carried out an experimental study for the condensation of steam in the presence of large amounts of air. Their study was aimed at the OTEC problem as was that of Wassel

Downloaded 16 Dec 2010 to 193.140.21.150. Redistribution subject to ASME license or copyright; see http://www.asme.org/terms/Terms_Use.cfm

and Mills (1982). Bharathan and Althof (1984) report a good correlation of their data following the scheme recommended by Jacobs et al. (1979) despite the fact that their data undoubtedly involved a turbulent gas stream, while the latter dealt with flow rates and packings that would indicate laminar flows for both coolant and vapor streams. Further, the latter work dealt with streams essentially free of noncondensables. The application of the simple geometry studies to packed beds is not very obvious unless simple and structured packings are used. However, Jacobs (1988a) indicates that the work of Jacobs et al. (1982) can be applied to the data of Jacobs et al. (1979) marching layer-by-layer through the column when uniform spheres were used as the packing, with good results.

Evaporation from thin films has normally been researched for the case of the heat transfer from the supporting structure (Seban, 1978). Analyses based on these models have been directed toward annular two-phase boiling studies (Michyoshi, 1978; Kozlov, 1978; Kelly, 1982). However, they are equally applicable to problems where the gas-vapor mixture is the heat source (Bharathan, 1988; Wassel and Mills, 1982; Wassel and Ghiaasiaan, 1985). They also apply to the design of wet cooling towers where the low concentration of vapor in the air induces the evaporation (Campbell, 1988). The reader is referred to Campbell's paper for current design practices and future research needs.

Summary

This paper has reviewed much of the current and past research on direct-contact heat transfer between two fluid streams. It is clear that, although much is still to be learned about this topic, considerable information exists in the literature. There are definite advantages to the use of direct contactors, and the general heat transfer community, and particularly those involved in process design, need to pay more attention to them as economical alternatives.

For the heat transfer researcher, the subject of direct-contact heat transfer opens many fundamental paths of inquiry. Some of these have been mentioned herein; however, many more can be discerned by reading the literature. While many possible studies can be conducted utilizing pure systems, most industrial problems involve impure ones and these systems must be studied. Finally, as noted by Crowe (1988), it is necessary to develop adequate computational models for these two or more phase systems if optimum designs are to be made. Thus, the general topic of direct-contact heat transfer for process technology offers fertile fields of endeavor. Welcome to them!

References

Battya, P., Raghaven, V. R., and Seetharamu, K. N., 1983, "A Theoretical Analysis of Direct Contact Evaporation of a Moving Drop in an Immiscible Liquid," *Proceedings of the Third International Conference on Numerical Methods in Thermal Problems*, Seattle, Washington.

Bharathan, D., 1988, "Direct Contact Evaporation," *Direct Contact Heat Transfer*, F. Kreith and R. F. Boehm, eds., Hemisphere Publishing Corp., Chap. 11, pp. 203–221.

Bharathan, D., and Althof, J., 1984, "An Experimental Study of Steam Condensation on Water in Countercurrent Flow in Presence of Inert Cases," ASME Paper No. 84-WA-SOL-25.

Bohn, M. S., 1988, "Air-Molten Salt Direct Contact Heat Transfer Analysis," *Direct Contact Heat Transfer*, F. Kreith and R. F. Boehm, eds., Hemisphere Publishing Corp., App. 2, pp. 257–298.

Bogy, D. B., 1979, "Drop Formation in a Circular Liquid Jet," *Annual Reviews of Fluid Mechanics*, Vol. 11, pp. 207–228.

Boyadjiev, C., Mitev, P, and Sapundzhier, T., 1976a, "Laminar Boundary Layers of Cocurrent Gas–Liquid Stratified Flows – I: Theory," *International Journal of Multiphase Flow*, Vol. 3, pp. 57–60.

Boyadjiev, C., Mitev, P., and Beshkov, V., 1976b, "Laminar Boundary Layers at a Moving Interface Generated by Countercurrent Gas–Liquid Stratified Flow," *International Journal of Multiphase Flow*, Vol. 3, pp. 61–66.

Brown, G., 1951, "Heat Transmission During Condensation of Steam on a Spray of Water Drops," *Institution of Mechanical Engineers, General Discussion on Heat Transfer*, pp. 49–51.

Campbell, J. C., 1988, "Thermal Design of Water Cooling Towers," *Direct Contact Heat Transfer*, F. Kreith and R. F. Boehm, Hemisphere Publishing Corp., App. 6, pp. 371–390.

Chen, L.-D., and Faeth, G. M., 1982, "Condensation of Submerged Vapor Jets in Subcooled Liquids," ASME JOURNAL OF HEAT TRANSFER, Vol. 104, pp. 774–780.

Chen, L.-D., and Faeth, G. M., 1983, "Structure of Turbulent Reacting Gas Jets Submerged in Liquid Metals," *Combustion Science and Technology*, Vol. 31, pp. 277–296.

Chung, J. N., and Ayyaswamy, P. S., 1981a, "Material Removal Associated With Condensation on a Droplet in Motion," *International Journal of Multiphase Flow*, Vol. 7, pp. 329–342.

Chung, J. N., and Ayyaswamy, P. S., 1981b, "Laminar Condensation Heat and Mass Transfer of a Moving Drop," *AIChE Journal*, Vol. 27, pp. 327–377.

Chung, J. N., Ayyaswamy, P. S., and Sadhal, S. S., 1984a, "Laminar Condensation on a Moving Drop, Part 1, Singular Perturbation Technique," *Journal of Fluid Mechanics*, Vol. 139, pp. 105–130.

Chung, J. N., Ayyaswamy, P. S., and Sadhal, S. S., 1984b, "Laminar Condensation on a Moving Drop, Part 2, Numerical Solutions," *Journal of Fluid Mechanics*, Vol. 139, pp. 131–144.

Coban, T., and Boehm, R., 1986, "Numerical and Experimental Modeling of Three Phase Direct Contact Heat Exchangers," *Proceedings of the Eighth International Heat Transfer Conference*, Paper No. SA-08.

Crabb, D., et al., 1981, "A Round Jet Normal to a Cross-Flow," *Journal Fluids Engineering*, Vol. 103, pp. 142–153.

Crowe, C. T., 1988, "Computational Techniques for Two Phase Flow and Heat Transfer," *Direct Contact Heat Transfer*, F. Kreith and R. F. Boehm, eds., Hemisphere Publishing Corp., Chap. 3, pp. 41–58.

Del-Tin, G., Lavagno, E., and Malandrone, M., 1982, "Pressure and Temperature Measurements in a Vapor Condensing Jet," *Proceedings of the 7th International Heat Transfer Conference*, Vol. 6, pp. 159–164.

Dukler, A. E., 1960, "Fluid Mechanics and Heat Transfer in Vertical Falling Film Systems," *AIChE Chemical Engineering Progress Series, Heat Transfer – STORRS*, Vol. 56, No. 30, pp. 1–10.

Dukler, A. E., Smith, L., and Chopra, H., 1984, "Flooding and Upward Film Flows in Tubes – I: Experimental Studies," *International Journal of Multiphase Flow*, Vol. 10, No. 5, pp. 585–597.

Fair, J. R., 1972, "Designing Direct Contact Coolers/Condenser," *Chemical Engineering*, pp. 91–100.

Fair, J. R., 1988, "Industrial Practices and Needs," *Direct Contact Heat Transfer*, F. Kreith and R. F. Boehm, eds., Hemisphere Publishing Corp., Chap. 2, pp. 25–39.

Finklestrein, Y., and Tamir, A., 1976, "Interfacial Heat Transfer Coefficients of Various Vapors in Direct Contact Condensation," *The Chemical Engineering Journal*, Vol. 12, pp. 199–209.

Ford, J. D., and Lekic, A., 1973, "Rate of Growth of Drops During Condensation," *International Journal of Heat and Mass Transfer*, Vol. 16, pp. 61–66.

Gimbutis, G., 1974, "Heat Transfer of a Turbulent Vertical Falling Film," *Proceedings of the 5th International Heat Transfer Conference*, Vol. II, pp. 85–89.

Golafshani, M., 1983, "Bubble Type Direct Contact Condensers," MS Thesis, Department of Mechanical and Industrial Engineering, University of Utah.

Goldstick, R. J., KVB, Inc., 1981, "Survey of Flue Gas Condensation Heat Recovery Systems," GRI 80/0152, The Gas Research Institute.

Goodwin, P., Coban, M., and Boehm, R., 1985, "Evaluation of the Flooding Limits and Heat Transfer of a Direct Contact Three Phase Spray Column," ASME Paper No. 85-HT-19.

Grace, J. R., "Hydrodynamics of Liquid Drops in Immiscible Liquids," *Handbook of Fluids in Motion*, The Butterfield Group, Ann Arbor, MI, Chap. 38, pp. 1003–1025.

Gunn, D. J., 1978, "Transfer of Heat and Mass to Particles in Fixed and Fluidized Beds," *International Journal of Heat and Mass Transfer*, Vol. 21, pp. 467–476.

Gunn, D. J., and Vortmeyer, D., 1982, "Heat Transfer in Fixed Bed Chemical Reactors," *Proceedings of the 7th International Heat Transfer Conference*, Vol. 6, pp. 13–18.

Hasson, D., Luss, D., and Peck, R., 1964a, "Theoretical Analysis of Vapor Condensation on Laminar Jets," *International Journal of Heat and Mass Transfer*, Vol. 7, pp. 969–981.

Hasson, D., Luss, D., and Navon, V., 1964b, "An Experimental Study of Steam Condensing on a Laminar Water Sheet," *International Journal of Heat and Mass Transfer*, Vol. 7, pp. 983–1001.

Hausbrand, E., 1933, *Condensing and Cooling Apparatus*, 5th ed., Van Nostrand, New York.

Hikita, H., and Ishimi, K., 1976a, "Frictional Pressure Drop for Laminar Gas Streams in Wetted Wall Columns With Cocurrent and Countercurrent Gas–Liquid Flow," *Journal of Chemical Engineering of Japan*, Vol. 9, No. 5, pp. 357–361.

Hikita, H., and Ishimi, K., 1976b, "Mass Transfer into Turbulent Gas Streams in Wetted Wall Columns With Cocurrent and Countercurrent Gas–Liquid Flow," *Journal of Chemical Engineering of Japan*, Vol. 9, No. 5, pp. 362–367.

Hikita, H., Ishimi, K., Omotehana, Y., and Fukase, T., 1978, "Mass Transfer Into Turbulent Gas Streams in Wetted Wall Columns With Cocurrent

Downloaded 16 Dec 2010 to 193.140.21.150. Redistribution subject to ASME license or copyright; see http://www.asme.org/terms/Terms_Use.cfm

and Countercurrent Gas–Liquid Flow," *Journal of Chemical Engineering of Japan*, Vol. 11, No. 2, pp. 96–101.

How, H., 1956, "How to Design Barometric Condensers," *Chemical Engineering*, pp. 174–182.

Huang, L. J., and Ayyaswamy, P. S., 1987a, "Drag Coefficients Associated With a Moving Drop Experiencing Condensation," ASME JOURNAL OF HEAT TRANSFER, Vol. 109, pp. 1003–1006.

Huang, L. J., and Ayyaswamy, P. S., 1987b, "Heat and Mass Transfer Associated With a Spray Drop Experiencing Condensation: A Fully Transient Analysis," *International Journal of Heat and Mass Transfer*, in press.

Hughmark, G. A., 1980, "Mass Transfer and Flooding in Wetted Wall and Packed Columns," *Ind. Engineering Chemical Fundamentals*, Vol. 19, No. 4, pp. 385–389.

Iciek, J., 1983, "The Hydrodynamics of a Free Liquid Jet and Their Influence on Direct Contact Heat Transfer – III. Direct Contact Heating of a Cylindrical Free Falling Liquid Jet," *International Journal of Multiphase Flow*, Vol. 9, pp. 167–179.

Isachenko, V. P., and Kushnyrev, V. I., 19XX, "Condensation in Dispersed Liquid Sprays," *Proceedings of the Fifteenth International Heat Transfer Conference*, Vol. III, pp. 217–220.

Isenberg, J., Moalem-Maron, D., and Sideman, S., 1970, "Direct Contact Heat Transfer with Change of Phase: Bubble Collapse With Translatory Motion in Single and Two Component Systems," *Proceedings of the Fourth International Heat Transfer Conference*, Vol. 5, Paper No. B2.5.

Jacobs, H. R., 1985, "Direct Contact Condensers," *Heat Exchange Design Handbook*, Hemisphere Press, New York, Section 2.6.8, Supplement No. 2.

Jacobs, H. R., 1988, "Direct Contact Condensation," *Direct Contact Heat Transfer*, F. Kreith, and R. F. Boehm, eds., Hemisphere Publishing Corp., Chap. 12, pp. 223–234.

Jacobs, H. R., 1988, "Thermal and Hydraulic Design of Direct Contact Spray Columns for Use in Extracting Heat from Geothermal Brines," *Direct Contact Heat Transfer*, F. Kreith and R. F. Boehm, eds., Hemisphere Publishing Corp., App. 5, pp. 343–370.

Jacobs, H. R., and Boehm, R. F., 1980, "Direct Contact Binary Cycles," *Sourcebook on the Production of Electricity from Geothermal Brine*, J. Kestin, U.S.D.O.E., Washington, D.C., DOE/RA/4051-1, Section 4.2.6.

Jacobs, H. R., and Bogart, J. A., 1980, "Condensation on an Immiscible Thin Film," ASME Paper No. 80-HT-110.

Jacobs, H. R., Bogart, J. A., and Pensel, R. W., 1982, "Condensation on a Thin Film Flowing Over an Adiabatic Sphere," *Proceedings of the 7th International Heat Transfer Conference*, Vol. 5, pp. 89–94.

Jacobs, H. R., and Cook, D. S., 1978, "Direct Contact Condensation on a Non-circulating Drop," *Proceedings of the 6th International Heat Transfer Conference*, Vol. 3, pp. 389–393.

Jacobs, H. R., and Eden, T. J., 1986, "Direct Contact Heat Transfer in a Sieve Tray Column," *Heat Transfer 1986, Proceedings of the 8th International Heat Transfer Conference*, San Francisco, CA, 6 pp.

Jacobs, H. R., and Fannir, H., 1977, "Direct Contact Condensers: A Literature Survey," U.S.D.O.E. Report DGE/1523-3.

Jacobs, H. R., and Fletcher, M. J., "Heat Transfer From a Falling Film to a Countercurrent Gas Stream," to be presented at the 1988 AIChE/ASME National Heat Transfer Conference.

Jacobs, H. R., and Golafshani, M., 1985, "A Heuristic Evaluation of the Governing Mode of Heat Transfer in a Liquid–Liquid Spray Column," ASME Paper No. 85-HT-50 (to be published in ASME JOURNAL OF HEAT TRANSFER, 1988).

Jacobs, H. R., Johnson, R., and Boehm, R. F., 1976, "Heat Transfer and Temperature Distribution in Liquid–Liquid Direct Contact Parallel Flow of Immiscible Fluids," ASME Paper No. 76-HT-25.

Jacobs, H. R., and Major, B. H., 1982, "The Effect of Noncondensible Gases on Bubble Condensation in an Immiscible Liquid," ASME JOURNAL OF HEAT TRANSFER, Vol. 104, pp. 487–492.

Jacobs, H. R., and Nadig, R., 1983, "Condensation on an Immiscible Falling Film in the Presence of a Noncondensible Gas," *Heat Exchanges for Two Phase Applications*, ASME HTD – Vol. 27, pp. 99–106.

Jacobs, H. R., and Nadig, R., 1987, "Condensation on Coolant Jets and Sheets Including the Effects of Noncondensible Gases," ASME JOURNAL OF HEAT TRANSFER, Vol. 109, pp. 1013–1020.

Jacobs, H. R., Thomas, K. D., and Boehm, R. F., 1979, "Direct Contact Condensation of Immiscible Fluids in Packed Beds," *Condensation Heat Transfer*, ASME, New York, pp. 103–110.

Johnson, K. M., Jacobs, H. R., and Boehm, R. F., 1983, "Collapse Height for Condensing Vapor Bubbles in an Immiscible Liquid," *Proceedings of the Joint ASME/JSME Heat Transfer Conference*, Vol. 2, pp. 155–163.

Johnson, R. E., and Sadhal, S. S., 1985, "Fluid Mechanics of Compound Multiphase Drops and Bubbles," *Ann. Rev. of Fluid Mechanics*, Vol. 17, pp. 289–320.

Joung, R. J., Yang, K. T., and Novotny, J. L., 1974, "Vapor–Liquid Interaction in High Velocity Vapor Jet Condensing in a Coaxial Water Flow," *Proceedings of the 5th International Heat Transfer Conference*, Vol. 3, pp. 226–230.

Kalman, H., Ullman, A., and Letan, R., 1987, "Visualization Studies of a Freon 113 Bubble Condensing in Water," ASME JOURNAL OF HEAT TRANSFER, Vol. 109, pp. 543–545.

Kelly, R. E., and Goussis, D., 1982, "Instability of a Liquid Film Flowing Down a Heated Inclined Plane," *Proceedings of the 7th International Heat Transfer Conference*, Vol. 5, pp. 319–324.

Kim, C. B., and Jacobs, H. R., 1987, "Numerical Study on the Operational Performance of Spray Column Direct Contact Heat Exchangers," *KSME Journal*, Vol. 1, No. 1, pp. 9–12.

Kim, S., and Mills, A. F., 1988, "An Experimental Study of Condensation on Turbulent Liquid Jets," submitted for publication in ASME JOURNAL OF HEAT TRANSFER.

Kozlov, V. M., Musvik, A. B., Ivanov, V. G., and Miranov, Y. L., 1978, "Investigation Into Hydrodynamics and Heat Exchange in Film Flows," *Proceedings of the 6th International Heat Transfer Conference*, Vol. 1, pp. 487–492.

Kulik, E., and Rhodes, E., 1978, "Heat Transfer Rates to Moving Droplets in Air/Steam Mixtures," *Proceedings of the 6th International Heat Transfer Conference*, Vol. 1, pp. 469–474.

Kutaleladze, S. S., and Borishanskii, V. H., 1973, *A Concise Encyclopedia of Heat Transfer*, Academic Press, New York.

Law, C. K., 1984, "Heat and Mass Transfer in Combustion: Fundamental Concepts and Analytical Techniques," *Progress in Energy and Combustion Science*, Vol. 10, pp. 295–318.

Lee, H. M., and McCarthy, G. E., 1982, "Liquid Carry-over in Air–Water Countercurrent Flooding," *Proceedings of the 7th International Heat Transfer Conference*, Vol. 5, pp. 237–242.

Lee, S. C., and Bankoff, S. G., 1983, "Stability of Steam–Water Countercurrent Flow in an Inclined Channel: Flooding," ASME JOURNAL OF HEAT TRANSFER, Vol. 105, pp. 713–718.

Lerner, Y., Kalman, H., and Letan, R., 1987, "Condensation of an Accelerating-Decelerating Bubble: Experimental and Phenomenological Analysis," ASME JOURNAL OF HEAT TRANSFER, Vol. 109, pp. 509–517.

Lerner, Y., and Letan, R., 1985, "Dynamics of Condensing Bubbles: Effects of Injection Frequency," ASME Paper No. 85-HT-47.

Letan, R., 1976, "Design of a Particle Direct Contact Heat Exchangers: Uniform Countercurrent Flow," ASME Paper No. 76-HT-27.

Letan, R., 1988, "Design of a Direct Contact Liquid-Liquid Heat Exchanger," *Direct Contact Heat Transfer*, F. Kreith and R. F. Boehm, eds., Hemisphere Publishing Corp., App. 4, pp. 335–342.

Letan, R., 1988, "Liquid-Liquid Processes," *Direct Contact Heat Transfer*, F. Kreith and R. F. Boehm, eds., Hemisphere Publishing Corp., Chap. 6, pp. 83–116.

Letan, R., and Kehat, E., 1968, "The Mechanism of Heat Transfer in a Spray Column Heat Exchanger," *AIChE Journal*, Vol. 14, No. 3, pp. 398–405.

Lineham, J. H., and Groimes, M. A., 1970, "Condensation of a High Velocity Vapor on a Subcooled Liquid Jet in Stratified Flow," *Proceedings of the 4th International Heat Transfer Conference*, Vol. VI, Cs. 2.6.

List, E. J., 1982, "Turbulent Jets and Plumes," *Annual Reviews of Fluid Mechanics*, Vol. 14, pp. 189–212.

Michiyoshi, I., 1978, "Two Phase Two Component Heat Transfer," *Proceedings of the 6th International Heat Transfer Conference*, Vol. 6, pp. 219–233.

Mills, A. F., Kim, S., et al., 1982, "Heat and Mass Transport in Turbulent Liquid Jets," *International Journal of Heat and Mass Transfer*, Vol. 25, pp. 889–897.

Mitev, P., and Boyadjiev, V., 1978, "Mass Transfer by Cocurrent Gas–Liquid Stratified Flow," *Letters in Heat and Mass Transfer*, Vol. 5, pp. 349–354.

Moalem-Maron, D., and Dukler, A. E., 1984, "Flooding and Upward Film Flow in Vertical Tubes – II: Speculation on Film Flow Mechanisms," *International Journal of Multiphase Flow*, Vol. 10, No. 5, pp. 599–621.

Moalem-Maron, D., and Sideman, S., "Condensation of Bubble Trains: An Approximate Solution," *Progress in Heat and Mass Transfer*, Vol. 6, pp. 155–177.

Mori, Y. H., 1987, "Artificial Transformation of the Direct Contact Condensation Pattern of Steam Bubbles in a Hydrophobic Liquid Medium," ASME JOURNAL OF HEAT TRANSFER, Vol. 109, pp. 1007–1012.

Murthy, M. V. K., and Narayana, K. B., 1978, "Heat and Mass Transfer in Food Products," *Proceedings of the 6th International Heat Transfer Conference*, Vol. 6, pp. 339–354.

Murthy, N. S., and Sastri, V. M. K., 1974, "Condensation on a Falling Laminar Liquid Film," *Proceedings of the 5th International Heat Transfer Conference*, Vol. III, pp. 231–235.

Murthy, N. S., and Sastri, V. M. K., 1976, "Condensation on a Falling Laminar Sheet," *Canadian Journal of Chemical Engineering*, Vol. 54, pp. 633–635.

Niyogi, K. K., and Pavlenco, G. F., 1978, "Heat and Mass Transfer in Wetted Surface Cooling Towers," *Proceedings of the 6th International Heat Transfer Conference*, Vol. 2, pp. 97–103.

Nusselt, W., 1916, "Die Oberflachenkondensation des Wasserdamfes," *Z. Ver. Dt. Ing.*, Vol. 60, pp. 541, 569.

Ohlander, R. S., Oshmyanshu, S., Nichols, K., and Werner, D., 1983, "Final Phase Testing and Evaluation of the 500 kWe Direct Contact Pilot Plant at East Mesa," U.S.D.O.E. Report No. DOE/SF/11700 TI.

Plass, S. B., Jacobs, H. R., and Boehm, R. F., 1979, "Operational Characteristics of a Spray Column Type Direct Contact Preheater," *AIChE Symposium Series*, No. 189, pp. 227–234.

Prakash, S., and Sirignano, W. A., 1980, "Theory of Convection Droplet Vaporization With Unsteady Heat Transfer in the Circulating Phase," *International Journal of Heat and Mass Transfer*, Vol. 23, pp. 253–268.

Raina, G., and Grover, P., 1982, "Direct Contact Heat Transfer With Change of Phase: Theoretical Model," *AIChE Journal*, Vol. 28, pp. 515–517.

Downloaded 16 Dec 2010 to 193.140.21.150. Redistribution subject to ASME license or copyright; see http://www.asme.org/terms/Terms_Use.cfm

Raina, G., and Grover, P., 1985, "Direct Contact Heat Transfer With Change of Phase: Theoretical Model Incorporating Sloshing Effects," *AIChE Journal*, Vol. 31, pp. 507–510.

Raina, G., and Wanchoo, R., 1984a, "Direct Contact Heat Transfer With Phase Change: Theoretical Expression for Instantaneous Velocity of a Two-Phase Bubble," *International Communications in Heat and Mass Transfer*, Vol. 11, pp. 227–237.

Raina, G., Wanchoo, R., and Grover, P., 1984b, "Direct Contact Heat Transfer With Phase Change: Motion of Evaporating Droplets," *AIChE Journal*, Vol. 30, pp. 835–837.

Rao, V. D., and Sarma, P. K., 1984, "Condensation Heat Transfer on Laminar Liquid Film" ASME JOURNAL OF HEAT TRANSFER, Vol. 106, pp. 518–523.

Renz, V., and Odenthal, H. P., 1979, "Numerical Prediction of Heat and Mass Transfer During Condensation From a Turbulent Gas Vapor Stream Onto a Vertical Film," *Condensation Heat Transfer*, ASME, New York, pp. 27–34.

Robertson, M. E., 1985, "Mass Transfer in Packed Beds of Spherical Particles," MS Thesis, Department of Mechanical and Industrial Engineering, University of Utah, Salt Lake City, UT, 1985.

Rogers, J. T., 1981, "Laminar Falling Film Flow and Heat Transfer Characteristics on Horizontal Tubes," *The Canadian Journal of Chemical Engineering*, Vol. 59, pp. 213–222.

Rowe, P. N., and Claxton, K. T., 1965, "Heat and Mass Transfer From a Single Sphere to Fluid Flowing Through an Array," *Transactions of Chemical Engineers*, Vol. 43, pp. 321–331.

Schroder, J. J., and Pohl, U., 1982, "Minimum Flowrates and Rewetting Rates of Falling Films," *Proceedings of the 7th International Heat Transfer Conference*, Vol. 5, pp. 83–88.

Seban, R. A., 1978, "Transport to Falling Films," *Proceedings of the 6th International Heat Transfer Conference*, Vol. 6, pp. 417–428.

Shulman, H. L., and Margolis, J. E., 1957, "Performance of Packed Columns," *AIChE Journal*, Vol. 3, pp. 157–161.

Sideman, S., 1966, "Direct Contact Heat Transfer Between Immiscible Liquids," *Advances in Chemical Engineering*, Vol. 6, Academic Press, New York, pp. 207–286.

Sideman, S., and Isenberg, J., 1967, "Direct Contact Heat Transfer With Change of Phase: Bubble Growth in Three-Phase Systems," *Desalination*, Vol. 2, pp. 207–214.

Sideman, S., and Moalem-Maron, D., 1982, "Direct Contact Condensation," *Advances in Heat Transfer*, Academic Press, New York, pp. 228–276.

Sideman, S., and Taitel, Y., 1964, "Direct Contact Heat Transfer With Change of Phase: Evaporation of Drops in an Immiscible Liquid Medium," *International Journal of Heat and Mass Transfer*, Vol. 7, pp. 1273–1289.

Simpson, H. C., Beggs, G. C., and Nazir, 1974, "Evaporation of Butane Drops in Brine," *Desalination*, Vol. 15, pp. 11–23.

Sirignano, W. A., 1983, "Fuel Droplet Vaporization and Spray Combustion Theory," *Progress in Energy and Combustion Science*, Vol. 9, pp. 291–322.

Skelland, A. H. P., and Johnson, K. R., 1974, "Jet Break-up in Liquid–Liquid Systems," *Canadian Journal of Chemical Engineering*, Vol. 52, pp. 732–738.

Steiner, L., and Hartland, S., 1983, "Hydrodynamics of Liquid–Liquid Spray Columns," *Handbook of Fluids in Motion*, The Butterfield Group, Ann Arbor, MI, Chap. 40, pp. 1049–1091.

Sudhoff, B., 1982, "Directer Warmeubergang bei der Kondensation in Blap finsaulen," Ph.D. Dissertation, Universitat Dortmund, Federal Republic of Germany.

Sun, T. Y., 1985, "A Theoretical and Experimental Study of Noncondensible Turbulent Bubbly Jets," Ph.D. Dissertation, Department of Mechanical Engineering, The Pennsylvania State University.

Sundararajan, T., and Ayyaswamy, P. S., 1984, "Hydrodynamics and Heat Transfer Associated With Condensation on a Moving Drop: Solutions for Intermediate Reynolds Numbers," *Journal of Fluid Mechanics*, Vol. 149, pp. 33–58.

Sundararajan, T., and Ayyaswamy, P. S., 1985a, "Heat and Mass Transfer Associated With Condensation on a Moving Drop: Solution for Intermediate Reynolds Numbers by a Boundary Layer Formulation," ASME JOURNAL OF HEAT TRANSFER, Vol. 107, pp. 409–416.

Sundararajan, T., and Ayyaswamy, P. S., 1985b, "Numerical Evaluation of Heat and Mass Transfer to a Moving Drop Experiencing Condensation," *Numerical Heat Transfer*, Vol. 8, pp. 689–706.

Taitel, Y., Barneas, D., and Dukler, A. E., 1982, "A Film Model for the Prediction of Flooding and Flow Reversal for Gas-Liquid Flow in Vertical Tubes," *International Journal of Multiphase Flow*, Vol. 8, No. 1, pp. 1–10.

Taitel, Y., and Tamir, A., 1969, "Condensation in the Presence of a Non-condensible Gas in Direct Contact," *International Journal of Heat and Mass Transfer*, Vol. 12, pp. 1157–1169.

Tamir, A., and Rachmilev, I., 1974, "Direct Contact Condensation of an Immiscible Vapor on a Thin Film of Water," *International Journal of Heat and Mass Transfer*, Vol. 17, pp. 1241–1251.

Thompson, R. J., and Jacobs, H. R., 1984, "Mass and Simultaneous Convective Heat Transfer for Flow in a Packed Bed of Spherical Particles," *AIChE Symposium Series*, Vol. 80, No. 236, pp. 240–248.

Treybal, R. E., 1963, *Liquid Extraction*, 2nd ed., McGraw-Hill, New York.

Van De Sande, E., and Smith, J. M., 1976, "Jet Break-up and Air-Entrainment by Low Velocity Turbulent Jets," *Chemical Engineering Science*, Vol. 31, pp. 219–224.

Weimer, J. C., Faeth, G. M., and Olson, D. R., 1973, "Penetration of Vapor Jets in Subcooled Liquids," *AIChE Journal*, Vol. 19, pp. 552–558.

Whitaker, S., 1972, "Forced Convection Heat Transfer Correlations for Flow in Pipes, Past Flat Plates, Single Cylinders, Single Spheres and for Flow in Packed Beds and Tube Bundles," *AIChE Journal*, Vol. 18, pp. 361–371.

Wright, J. D., 1988, "Design of Direct Contact Preheater/Boilers for Solar Pond Power Plants," *Direct Contact Heat Transfer*, F. Kreith and R. F. Boehm, eds., Hemisphere Publishing Corp., App. 3, pp. 299–334.

Downloaded 16 Dec 2010 to 193.140.21.150. Redistribution subject to ASME license or copyright; see http://www.asme.org/terms/Terms_Use.cfm

J. H. Lienhard
Professor,
Heat Transfer/Phase Change Laboratory,
Mechanical Engineering Department,
University of Houston,
Houston, TX 77204-4792
Fellow ASME

Burnout on Cylinders

The cylinder is the most thoroughly studied boiling burnout configuration, starting with Nukiyama's pioneering study and continuing through the present. This review paper summarizes much of what is known about the peak boiling heat flux in this arrangement taking into account such variables as size, properties of the boiled liquid, gravity, liquid subcooling, velocity of an imposed crossflow, and certain "nuisance" variables, as well.

Preface

It might seem terribly restrictive to devote a long review article to such a seemingly limited subject as the burnout heat flux in a single geometry. The reason for doing so is that it allows us "to see the world in a grain of sand." If we can understand the burnout problem in one particular geometry, we will be in a far better position to understand it generally.

The horizontal cylinder geometry is the simplest and most commonly studied heater configuration. If we fail to look deeply enough we might be reminded of the policeman who found a little boy searching about in the light of the only street lamp on a dark street. "What's the trouble?" he asked the boy. "I lost a quarter," the boy replied. "Where did you hear it fall?" asked the policeman. "Across the street, about a half a block down," the boy told him. "When then, why on earth are you looking here!" the policeman exploded. The boy backed up a step and said, "B-b-but sir, the light's brightest over here."

However, the extensive study of burnout on cylinders has had far greater value than one might first think. While the cylinder geometry *has* been overworked by virtue of its experimental simplicity—while it is a geometry for which we have been given a great deal of imperfect data and flawed analysis—the other side of the coin is that it is the geometry for which we have available the largest fund of convincing information.

The best way to sort out what is, and what is not, known about the peak boiling heat flux q_{max} (or burnout limit) is to concentrate on the best-understood configuration. The reason is that correct analytical descriptions must represent sets of situations that are *similar* to one another. First in the hierarchy of similar variables are those whose variations cause basic changes in physical mechanisms. That normally places geometry at the head of the list of variables that must be held constant in describing a phenomenon.

Within the scope of a specified cylindrical heater geometry, we look at the following variables:

- geometric scale;
- physical properties of the boiled liquid;
- gravity;
- liquid subcooling;
- liquid crossflow velocity; and
- certain nuisance variables, including:
  - heater surface condition;
  - geometry of the liquid container;
  - blockage effects;
  - etc.

Although the study of the cylinder avoids mechanism changes that occur as a consequence of changing the geometry, other mechanism changes can occur as we vary any of the quantities listed above.

Contributed by the Heat Transfer Division for publication in the JOURNAL OF HEAT TRANSFER. Manuscript received by the Heat Transfer Division April 15, 1988. Keywords: Boiling, Reviews.

Early Studies of Burnout on Cylinders—1920 to 1958

We begin by looking briefly at the study of burnout from 1920 until 1958 when a burnout theory was finally developed—one that could be systematically exploited in different situations.

The first complete boiling curves were obtained by metallurgists (Pilling and Lynch, 1920). (See Lienhard and Witte, 1985.) They reported how the cooling rate of metal samples varied with the cylinder temperature when they were quenched. Figure 1 shows their boiling curves for eight different initial liquid bath temperatures. The cooling rate is proportional to the heat flux, and the cylinder temperature is linear in ΔT. Hence these curves are, in reality, boiling curves. At the higher bath temperatures, the full range of boiling curve behavior is evident.

When Nukiyama (1934) made his celebrated observations of the peak and minimum heat fluxes, he was unaware of the Pilling and Lynch study. Nukiyama used very small diameter horizontal cylinders in his study. We subsequently find that his cylinders were so small that most of his observations lay in a region where the boiling mechanism was suffering a transition, and that his data therefore have only qualitative importance. He also had to vary the heat flux as the independent variable, and was therefore unable to obtain a complete boiling curve. We include a typical Nukiyama boiling curve in Fig. 2.

With the exception of the important observations of Cichelli and Bonilla (1945), and Bonilla and Perry (1941), on horizontal flat plates, the most influential studies of burnout in the two decades following Nukiyama's study, were also generally made on cylindrical heaters.

Drew and Mueller (1937) made the earliest experiments in which the heater temperature was varied independently (or nearly so), and they also used horizontal cylinders. Theirs were the first (very limited) steady-state transition boiling data. Farbar and Scorah (1948) produced what they represented as complete boiling curves for horizontal cylindrical heaters; but they used an experimental technique that yielded, not transition boiling, but simultaneous nucleate and film boiling on the same heater.

The first reliable burnout measurements in this geometry actually did not appear until a decade and a half after Nukiyama (1934) had captured our imagination with his experiments. Typical were the data of Rohsenow and his students at MIT (see, e.g., Addoms, 1948); of Kutateladze, Borishanskii, and others in Leningrad (see, e.g., Kutateladze, 1948, 1952); and, a bit later, of Westwater and his students (see, e.g., Westwater and Santangelo, 1955, and Pramuk and Westwater, 1956). Westwater also improved Drew and Mueller's (1939) technique of heating a tube with pressurized condensing water to create a nearly specifiable wall temperature, and thus provided the first useful transition boiling data for any configuration.

Of course, many other people produced burnout data for cylinders before 1958; but the papers above, for many reasons, were major landmarks that—rightly or wrong-

Copyright © 1988 by ASME
Downloaded 16 Dec 2010 to 193.140.21.150. Redistribution subject to ASME license or copyright; see http://www.asme.org/terms/Terms_Use.cfm

ly—were shaping people's opinions about pool boiling burnout on cylinders.

The Adoption of the Hydrodynamic Theory—1958 to 1974

Early Combat Over a New Idea. A common supposition marked most studies of burnout all the way into the middle 1960s. That is the notion that burnout is dictated by processes that go on right at the heater surface. A major consequence of this notion is that the gross geometry of the heater is unimportant. This view was overturned during the years from 1958 to 1974 in a surprisingly vitriolic struggle.

The struggle over mechanisms of burnout can better be understood in terms of Kuhn's (1962) analysis of scientific revolution. Thomas Kuhn, a noted historian of science, pointed out that science evolves not so much by accretion as by revolution—that when the normal rules of science fail to resolve a problem, then a crisis follows. Several things happen during a crisis: Scientists go back to question the foundations of their science; they improve the precision of their measurements in an attempt to isolate and explain the failure; and they square off in combat among competing schools. Finally, a new mode of *normal science* emerges with a new group of practitioners—usually the young and the outsiders. The previous scientists only rarely will be converted to the new way of thinking.[1]

Several competing schools had taken form by 1958 (see discussion by Lienhard and Witte, 1985). Not the least of these was based on the concept that burnout was a consequence of hydrodynamic flooding such as occurs in a distillation tower. That idea had first been advanced by Bonilla and Perry (1941), and they provided a somewhat crude correlation of burnout based upon it. Kutateladze (1952) next picked up the idea and used it to motivate a dimensional analysis that gave his well-known burnout expression:

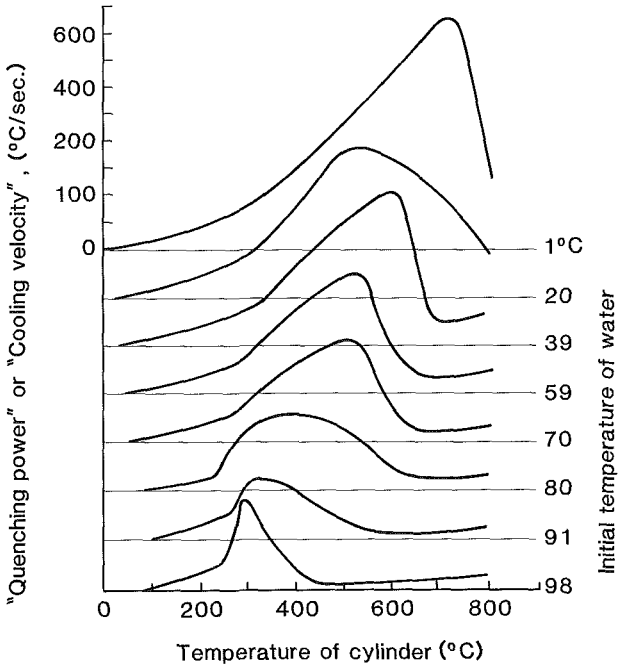

Fig. 1 One of Pilling and Lynch's (1920) sets of quenching curves: the first boiling curves.

[1]The reader who is familiar with Kuhn (1962) will wonder why I have so scrupulously avoided using the word *paradigm*. The reason is one that Kuhn himself later acknowledged. The word was entirely too catchy. Everyone used it, and few understood what lay behind it in Kuhn's detailed analysis. The term *normal science* is safer.

Nomenclature

A, $A_{cond.}$ = area; area of vapor jets on which condensation occurs

A_{jet}, A_{heater} = cross-sectional area of the vapor jets; area of the heater per escaping vapor jet

c_p = specific heat at constant pressure

Fr = Froude number = $u_\infty/(2gR)^{1/2}$

f = used to denote a functional relationship

G = gravity influence parameter, defined in equation (9)

g = gravitational acceleration

h_{fg}, $h_{fg,1}$ = latent heat of vaporization at constant temperature; "integral" or constant-composition latent heat of vaporization

Ja, Ja_e = volumetric Jakob number = $\rho_f c_p \Delta T_{sub}/\rho_g h_{fg}$; modified volumetric Jakob number based on an effective subcooling (see equation (45*a* and *b*))

Ku = Kutateladze number, defined in equation (1)

k = thermal conductivity

L, L' = characteristic length; $L/[g(\rho_f - \rho_g)/\sigma]^{1/2}$

MESC = Mechanical Energy Stability Criterion

Nu = Nusselt number defined in equation (36)

Pe = effective Peclet number, defined in equation (30)

Pr = Prandtl number = ν/α

q, q_{max} = heat flux; peak or "burnout" q in saturated liquids

$q_{cond.}$ = heat flux conducted from the vapor jet interface to the surrounding subcooled liquid, expressed on a per-unit-heater-area basis

q_{maxmax} = molecular effusion limited q (see equation (20))

$q_{max,sub}$ = q_{max} in subcooled boiling

$q_{max,SL}$ = In the context of binary boiling, we use this symbol to represent the value that q_{max} would have had if it were not influenced by induced subcooling. The letters SL reflect the fact that it might be predicted by the Sun–Lienhard expression, equation (4).

R, R_{eff} = radius of a horizontal cylindrical heater; effective radius of the vapor region around the heater during moderately and highly subcooled boiling

Downloaded 16 Dec 2010 to 193.140.21.150. Redistribution subject to ASME license or copyright; see http://www.asme.org/terms/Terms_Use.cfm

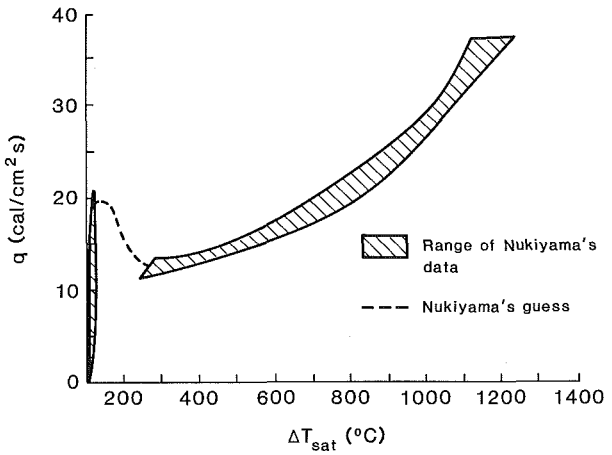

Fig. 2 One of Nukiyama's (1934) sets of boiling curves. The data for several wires are represented in the cross-hatched areas. The dashed line is Nukiyama's conjectured transition boiling region.

$$\mathrm{Ku} \equiv \frac{q_{\max}}{\rho_g^{1/2} h_{fg} [\sigma g (\rho_f - \rho_g)]^{1/4}} = \text{const} \tag{1}$$

where Ku is called the Kutateladze number.

Two problems were inherent in Kutateladze's correlation. The first is that equation (1) does not include a characteristic length. Hence it did not imply any particular geometry. Actually the inclusion of a characteristic length in the dimensional analysis yields a second dimensionless group

$$L' = \frac{L}{\sqrt{\sigma / g (\rho_f - \rho_g)}} \tag{2}$$

where L is any characteristic length. For the cylinder geometry, L is the cylinder radius R. In what follows we generally use an R' (an L' based on $L = R$) as a dimensionless length. Accordingly, equation (1) should be modified to the form

$$\mathrm{Ku} = f(L') \neq \text{const} \tag{3}$$

for burnout from finite bodies.

Correlations in the form of equation (3) were not exploited until the middle 1960s when Bobrovich et al. (1964) and Lienhard and Watanabe (1966) independently used them to isolate the role of geometric scale within different geometries. By 1966 it was becoming clear on both sides of the ocean that equation (1) did not represent burnout for anything other than an infinite flat plate. (Yet we still see it being widely misused today.)

But in 1952 Kutateladze fixed the constant in equation (1) at 0.131 by comparing it with the available burnout data, almost all of which had been obtained on horizontal cylinders. The experimental scatter of those data (which in fact represented quite a range of R') was fairly wide, of course; and no particular point was made about the geometry since no one at the time felt it made any difference. The result was that those who were aware of the equation during the 1950s took it to represent burnout for any geometry and any size of heater.

Zuber's (1959) doctoral dissertation (completed in 1958) presented the well-known analytical development of equation (1) based on the Taylor and Helmholtz instabilities of the vapor escape process (for details see, e.g., Lienhard and Witte, 1985, or Lienhard 1987). Zuber put analytical flesh and blood on Bonilla's column-flooding idea. In doing so he explicitly took burnout to be geometry-independent, although his analysis actually represented the flat-plate geometry. He showed that he could get several values of the constant in equation (1) depending on whether he used critical or "most-dangerous" wavelengths in the hydrodynamic theory. The oft-quoted value of the constant equal to $\pi/24$ (= 0.131) was a compromise among these values that perfectly replicated Kutateladze's correlation. (Figure 3 is Kutateladze's comparison of equation (1) with data, as it was used by Zuber.)

Zuber had introduced equation (1) to the Western world and aggressively given it a rationale that flew in the teeth of

Nomenclature (cont.)

R' = $R/[\sigma/g(\rho_f - \rho_g)]^{1/2}$
R_{gas} = ideal gas constant on a per-unit-mass basis
Ra = Rayleigh number defined in equation (37)
r = ρ_f/ρ_g
St = Strouhal number = $2R/u_\infty \tau$
$T, T_{sat}, T_w, T_{bath}, T_f$ = temperature, saturated liquid temperature, temperature of the wall of a heater, bath temperature in pool boiling, liquid temperature in binary boiling
t = time
u_∞, u_g = velocity of the incoming liquid flow, relative velocity of vapor in a jet
We_g = Weber number = $\rho_g u_\infty^2 2R/\sigma$
x = mole fraction of one component in the liquid phase of a binary mixture
y = mole fraction in the vapor phase when the x is the equilibrium mole fraction in the liquid phase
α = vapor sheet thickness divided by $2R$; thermal diffusivity of the boiled liquid
β = volumetric coefficient of thermal expansion
$\Delta T, \Delta T_{sub}$ = $T_w - T_{sat}$; $T_{sat} - T_{bath}$
Δq_{sub} = difference between q in film-transition, and film, boiling, $q_{max} - q_{max,SL}$
θ = retreating contact angle
ν = kinematic viscosity
ρ_f, ρ_g = saturated liquid and vapor densities, respectively
σ = surface tension
τ = period of jet breakdown in subcooled pool boiling or bubble breakoff during flow boiling
ϕ = dimensionless q_{max}, either the value given in equation (8) for flow boiling, or $q_{max,sub}/q_{maxmax}$ for subcooled pool boiling (distinguished in context)
ϕ_{pred} = a value of ϕ predicted for flow boiling in the absence of gravity
χ = an effective Peclet number appropriate to highly subcooled pool boiling

Subscripts

1, 2 = denoting the two components of a binary mixture
f, g = denoting the saturated liquid and vapor states

Downloaded 16 Dec 2010 to 193.140.21.150. Redistribution subject to ASME license or copyright; see http://www.asme.org/terms/Terms_Use.cfm

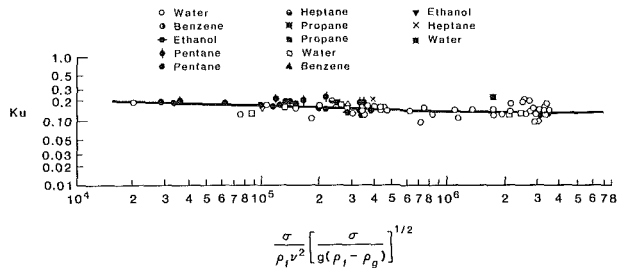

Fig. 3 Kutateladze's (1952) burnout data correlation as quoted by Zuber (1958), and as used to suggest that Ku = 0.131

models that placed the q_{max} instability right at the surface of the heater. At the same time, he had overlooked the fact that, since his hydrodynamic mechanism was based on a geometry-dependent wake structure, q_{max} had to depend on R'. His statement of equation (1) was thus extremely vulnerable to experimental contradiction, and for many years he was severely challenged in the literature (see discussion by Lienhard and Witte, 1985).

The theory, which had been particularly ill-received by chemical engineers, received its first strong support when the noted chemical engineer Westwater joined forces with Zuber and his dissertation advisor, Tribus (Zuber et al., 1963). They extended the theory to create a modestly successful subcooled q_{max} correlation.

The Predictions and Experiments of Wong, Sun, and Dhir and Others. Lienhard and Wong (1964) provided the second major support for the hydrodynamic theory by both predicting and measuring the Taylor waves during saturated film boiling on horizontal cylinders. This calculation, by the way, showed a clear dependence of wavelength on R'.

A byproduct of this prediction was a rational correlation of the minimum film boiling heat flux, which also showed a strong R' dependence. This correlation, which has been widely quoted, suffers from a problem endemic to minimum heat flux work—that the minimum heat flux is seriously affected by contact angle unless nonwetting is perfect (see the discussion by Ramilison and Lienhard 1987). Nevertheless, it provided another element in the demonstration of an R' dependence.

But it was several years before Sun and Lienhard (1970) could complete a hydrodynamic prediction of q_{max} specific to any particular geometry. For horizontal cylinders they obtained

$$Ku = 0.1164 + 0.297\exp(-3.44\sqrt{R'}) \tag{4}$$

which has the form of equation (3). Equation (4) predicted what were, by then, hundreds of available q_{max} data for cylinders within about ±15 percent. The data scatter included some minor, but inescapable, systematic variations among the boiled liquids.

The next step in the elaboration of the hydrodynamic theory was a set of experiments by Bakhru and Lienhard (1972) in which they measured q_{max} on very small horizontal cylinders for which R' lay in the range $0.0076 \le R' \le 0.0806$. These experiments showed what Lienhard and Wong's measurements had only hinted—that the hydrodynamic processes vanished as R' was reduced below 0.1. This failure is illustrated for horizontal cylinders in Fig. 4. We thus emphasize that

$$\text{Hydrodynamic}\begin{Bmatrix}\text{predictions}\\ \text{correlations}\end{Bmatrix}\text{ of } q_{max} \text{ fail for } R' \text{ or } L' < 0.1 \tag{5}$$

During the late 1960s, Dhir and others made the last important steps in presenting a mature hydrodynamic theory. These

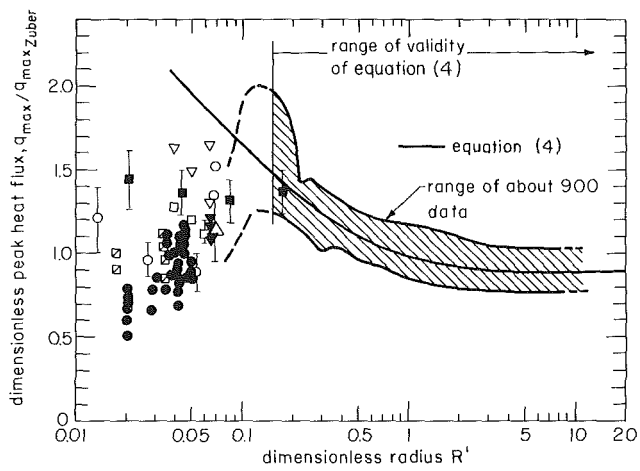

Fig. 4 Illustration of the failure of the hydrodynamic theory, as characterized by equation (3), at low values of R' or L'

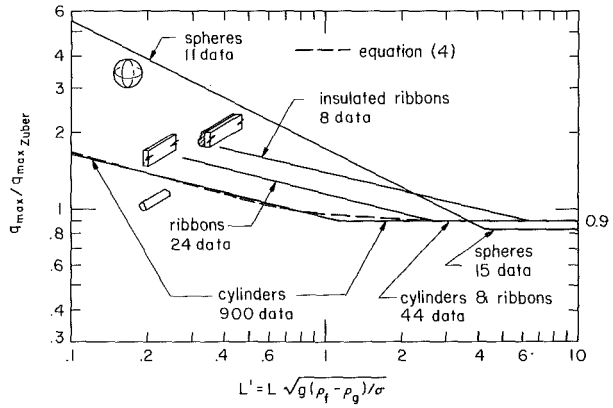

Fig. 5 Lienhard and Dhir's (1973a) collected burnout curves for various geometry

contributions (summarized by Lienhard and Dhir, 1973a) included:

- The articulation of equation (3) for many geometries. These included ribbons (one or both sides active) and finite flat plates (see Lienhard and Dhir, 1973b); spheres (Ded and Lienhard, 1972); as well as cylinders (see a collected set of predictions in Fig. 5).
- A procedure for creating additional hydrodynamic predictions in new geometries (Lienhard and Dhir, 1973b).
- The inclusion of viscosity in the hydrodynamic theory (see Dhir and Lienhard, 1973, 1974).

The Role of Size, Gravity, Surface Condition, and Nuisance Variables. The interest of NASA in the influence of gravity on boiling provided the motive and much of the funding for the articulation of the hydrodynamic theory. This work finally clarified the influence of gravity on q_{max} for pool boiling. Equation (3) tells us that

$$q_{max} = g^{1/4} f[(g)^{1/2}] \tag{6}$$

It was now clear that the function becomes a constant when R' (or L') is large (see Fig. 5) so q_{max} depends on the quarter power of g. For smaller cylinders (or for lower gravity) the g dependence is more complicated.

The influence of surface condition and other nuisance variables, on the other hand, was not sorted out in this work because care had been taken to eliminate them. Scrupulous care had been taken in our experiments, and in those of most other investigators, to keep the heaters clean and uniformly smooth, and the liquids pure. The selection of boiled fluids and heater materials had generally resulted in well-wetted

Downloaded 16 Dec 2010 to 193.140.21.150. Redistribution subject to ASME license or copyright; see http://www.asme.org/terms/Terms_Use.cfm

heaters with low contact angles. Electrical fields—long known to exert an influence on boiling—had been eliminated.

There was precedent for not pursuing the effects of surface variables. While the flat-plate experiments of Berenson (1960) had shown enormous influences of surface condition on nucleate boiling, they had shown minimal influences in burnout. Other less well-controlled experiments had produced conflicting claims about the influence of surface condition on q_{max}. But the controlled experiments, around which the theory had been developed, consistently showed no serious influence of these variables on burnout.

The question of blockage effects on pool boiling burnout was addressed by Elkassabgi and Lienhard (1987). They varied both the spacing of side walls from a cylinder, and the depth of the cylinder below the surface. They discovered that the depth of immersion exerted no influence unless it was coupled with sidewall blockage, and that sidewalls had to be less than 15 diameters apart to exert any influence on q_{max}.

Burnout During Crossflow on Cylinders

The Mechanical Energy Stability Criterion. In one sense boiling on a cylinder is never without a component of superposed flow. In *pool* boiling, the rising vapor entrains liquid and pulls a certain amount of it up past the cylinder. This entrainment is a viscous phenomenon. Dhir and Lienhard (1974) showed a definite influence of very high viscosities on q_{max} through the role of viscosity in the Helmholtz instability. However, correlation of the influence of viscosity has not succeeded in isolating any influence on burnout at lower viscosities, even though viscosity causes entrainment. We are therefore disinclined to think that such convection is important in this geometry.

Measurements of burnout on horizontal cylinders in liquid cross*flows* have been made by many people since the 1950s. The first, like other early boiling observations, were made with limited control of the various system variables. The first carefully controlled data that drew wide attention to the problem were those of Vliet and Leppert (1964) (also described by Leppert and Pitts, 1964). These observations, made in nearly saturated liquids, on cylinders long enough to minimize end effects, were accompanied with photographs that provided the first clear sense of what was going on in this interesting geometry. These data were followed by the observations of McKee and Bell (1969) who studied burnout on short cylinders in water, and the measurements of Cochran and Andracchio (1974) in water and Freon-113.

Vliet's photographs also revealed a startlingly simple vapor removal geometry (sketched in Fig. 6) near burnout on cylinders in a crossflow. In 1973, Lienhard and Eichhorn looked at those pictures and concluded that burnout ought to be the straightforward result of a Helmholtz instability in the two-dimensional vapor sheet. Haggerty and Shea (1955) had already analyzed the instability of such flows, and the prediction of q_{max} based on this analysis only required two pieces of information: the susceptible Helmholz wavelength λ_H, and the dimensionless thickness of the sheet α.

It took three years for Lienhard and Eichhorn (1976) to arrive at a strategy providing even one of the two missing pieces of information. They suggested that the wake should become unstable when the vapor carries more mechanical energy into it than can be absorbed in the new surface energy of the escaping bubbles. This so-called *mechanical energy stability criterion* or *MESC* could be used to eliminate one of the two unknowns, but not both. They chose to eliminate the wavelength λ_H. This left the dimensionless sheet thickness α, which they were unable to measure or predict. To eliminate it, they substituted measured q_{max} data into their expression and calculated α. They then used these results to make a separate

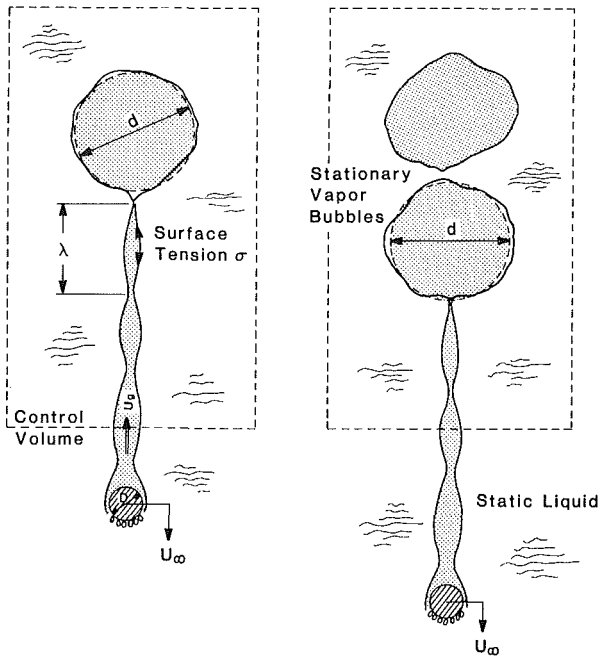

Fig. 6 Burnout vapor removal configuration near burnout from a cylinder in a liquid crossflow

experimental correlation for α. Their q_{max} correlation took the form

$$\phi = f(\mathrm{We}_g, r) \tag{7}$$

where

$$\phi \equiv \frac{\pi q_{max}}{u_\infty \rho_g h_{fg}}; \quad \mathrm{We}_g = \frac{(2R)\rho_g u_\infty^2}{\sigma}; \quad r \equiv \frac{\rho_f}{\rho_g} \tag{8}$$

In making this correlation, they added the data of Min (1975) to those of the previous investigators. These data, by the way, made it clear that the vapor sheet shown in Fig. 6 was established after a transition that occurred at very low velocities. For slow enough flows, the original jets and columns behavior was retained. The data also required that equation (7) be written in different ways for slow and rapid flows.

Learning by Iteration. Lienhard and Eichhorn's (1976) prediction was plagued with two problems: Their mechanical energy balance was incomplete; it turned out that such a balance was far more subtle than they realized. The second problem was their failure to recognize some extremely important system variables. We next look at these complications. However, it is worth pointing out that their MESC itself has generally proved to be a valid enough tool for analyzing boiling burnout. It was also formulated by Lienhard and Eichhorn (1979) (and subsequently extended by Sharan and Lienhard, 1985) for the burnout of liquid jets impinging on disk heaters. It was successfully applied to pool boiling burnout by Lienhard and Hasan (1979).

Subsequent studies have made one emendment after another for the MESC analysis of burnout in cylinder crossflows[2]:

Hasan et al. (1981) noted that gravity influences many of the existing data. They developed an apparatus that would permit the liquid to flow upward over the heater or downward past it. These data were plotted against velocity, which was now either positive or negative in the gravity field. (A typical plot for one heater is shown in Fig. 7.) On the basis of such

[2]While this correction process is uncomfortable, it has been required in every prediction of boiling yet developed by anybody. Where the field of boiling has developed a poor reputation, it has been because of our resistance to iterating and correcting what we know to be imperfect predictions.

Downloaded 16 Dec 2010 to 193.140.21.150. Redistribution subject to ASME license or copyright; see http://www.asme.org/terms/Terms_Use.cfm

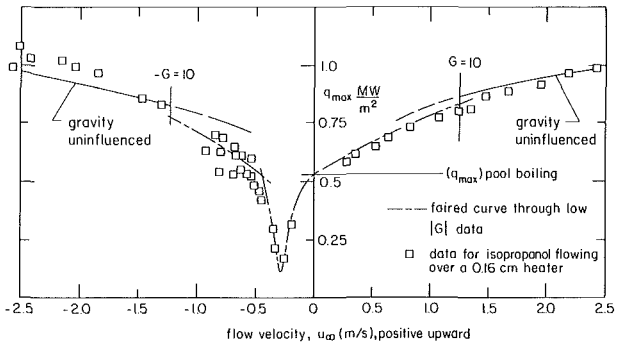

Fig. 7 Hasan et al.'s (1981) identification of a velocity above which burnout is uninfluenced by gravity

data, they identified the absolute value of a velocity beyond which the right and left sides of the figure were mirror images of one another—in which the orientation in the gravity field was irrelevant. Using these values, they suggested that the criterion[3]:

$$G \equiv u_\infty (\rho_f / g\sigma)^{1/4} \geq 10 \tag{9}$$

would assure that gravity did not influence burnout in this configuration. They also provided a new correlation for the gravity-free regime.

Next (with Ungar's (1978) help) Kheyrandish and Lienhard (1985) found that, when a-c current is used to supply the heaters, its frequency will sometimes set the Helmholtz wavelength. This was never the case for pool boiling. But when the much greater flow-boiling heat-removal all occurs near the front of the cylinder, a-c creates much larger 120 Hz temperature fluctuations that set the wavelength in the sheet. This required Kheyrandish and Lienhard (1965) to provide two correlations: one for a-c heated cylinders and one for non-a-c heated cylinders.

When the frequency of breakoff is an independently specified exterior variable, then equation (7) must be amended to include another dimensionless variable

$$\phi = f(\mathrm{We}_g, r, \mathrm{St}) \tag{10}$$

The new independent variable is the Strouhal number St, or dimensionless frequency

$$\mathrm{St} \equiv 2R/u_\infty \tau \tag{11}$$

which equals $2R/$(breakoff wavelength) at burnout. When the waves grow naturally, the period τ, appropriate to the most rapidly growing Helmholtz-unstable wave, is a dependent variable so it does not appear in the dimensionless functional equation.

They also discovered (see Kheyrandish and Lienhard, 1985) another omission in the previous use of the MESC. Lienhard and Eichhorn (1976) had neglected the surface energy absorbed in the bubble that breaks away from the vapor sheet. Taking account of the a-c/non-a-c problem and the missing surface-energy term in the balance, Kheyrandish and Lienhard (1985) obtained still better correlations of the data.

The next iteration was made by Sadasivan and Lienhard (1986) who observed alternating-current-influenced burnout in yet another gravity orientation, namely liquid flowing across a cylinder *normal* to the gravity field. An important outcome of this study was the discovery that q_{max} differed negligibly between the vertical and horizontal flows shown in Fig. 8. That is because gravity affects burnout by thinning the sheet, and burnout occurs at the same sheet thickness in either

[3] Criterion (9) was intentionally constructed to reflect that fact that the data of Hasan et al. did not reveal any influence of heater size. We shall see that subsequent studies suggest that such a criterion probably *should* reflect some influence of size.

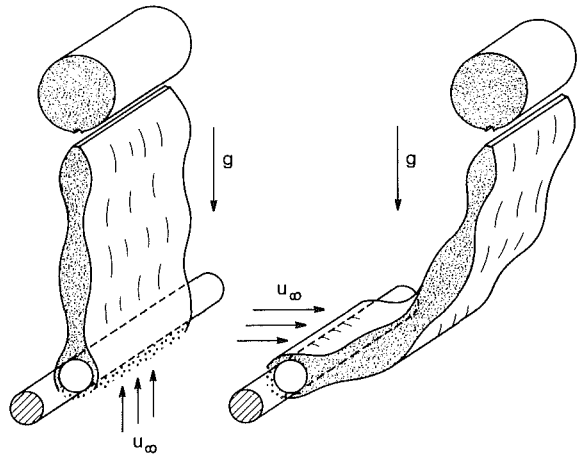

Fig. 8 The patterns of vapor removal during liquid upflows and *sideflows across a cylinder*

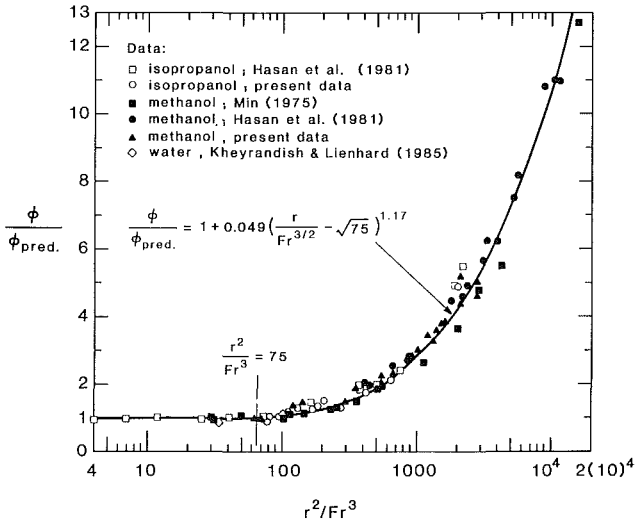

Fig. 9 Sadasivan and Lienhard's (1987) correlation of a-c-influenced data showing the regions of gravity influence and noninfluence

case. They correlated these data using yet another version of the MESC. They also refined the gravity correction. It is probably not worth repeating this derivation of the MESC because it was still not yet correct or complete. However, the correlation based upon it takes the form of equation (7), and it is as accurate and all-encompassing as any yet in print.

Sadasivan and Lienhard's (1986) correlations are shown in Figs. 9 and 10 for a-c-driven burnout and non-a-c-driven burnout. These correlations are based on the data of Sadasivan and Lienhard (1986), Vliet and Leppert (1964), Cochran and Andracchio (1964), Min (1975), Hasan et al. (1981), Yilmaz and Westwater (1980), Broussard and Westwater (1984), and Ungar (1987). To create these correlations, they added another parameter to equation (7) (or (10)) to accommodate the influence of gravity

$$\phi = f(\mathrm{We}_g, r, \mathrm{St}, \text{and a gravity parameter}) \tag{12}$$

where, of course, the last two parameters only appear if a-c and gravity exert an influence. They did not adopt G as the gravity parameter since other experiments had suggested that the characteristic dimension *did* influence the gravity transition.

They sought (by strictly empirical means) to find how the onset of gravity influence depended on We_g, r, and a Froude number defined as $\mathrm{Fr} \equiv u_\infty/(2Rg)^{1/2}$. Least-squares calculations showed that the transition was uninfluenced by We_g, so

Downloaded 16 Dec 2010 to 193.140.21.150. Redistribution subject to ASME license or copyright; see http://www.asme.org/terms/Terms_Use.cfm

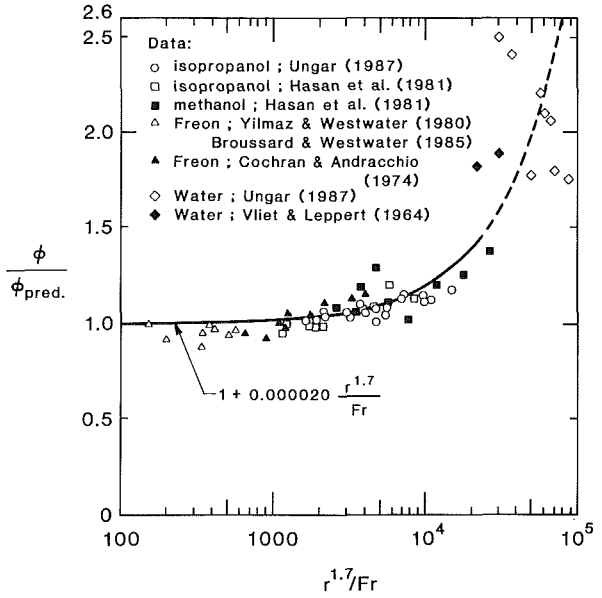

Fig. 10 Sadasivan and Lienhard's (1987) correlation of a-c-uninfluenced data showing the regions of gravity influence and noninfluence

they looked for a gravity parameter in form of a power law dependence on r and Fr.

The process of correlation yielded different gravity influence parameters for a-c and non-a-c-influenced burnout. In both cases Sadasivan and Lienhard (1986) used a form of equation (10) to correlate ϕ. (This gravity-uninfluenced value is called ϕ_{pred}.)

The criteria for burnout to be *un*influenced by gravity are:

$$\text{for a-c-influenced data:} \quad r^2/\text{Fr}^3 \leq 75$$

and (13)

$$\text{for a-c-uninfluenced data:} \quad r^{1.7}/\text{Fr} \gtrsim 3000$$

These criteria are approximate as is obvious from Figs. 9 and 10) and the one for a-c-influenced data is the more reliable.

Using the data deemed to be gravity-uninfluenced, under these criteria, they obtained for 120 Hz a-c-influenced burnout:

$$\phi_{\text{pred}} = 0.0017 r^{0.91} \text{We}_g^{-0.2} \left[1 + 13.3 r^{0.3} \text{We}_g^{-0.27} \left(1 - \sqrt{\pi \left(\frac{240R}{u_\infty} \right) \phi_{\text{pred}}} \right)^{1/3} \right] \tag{14}$$

which represents the data within an rms error of ±12.3 percent. For burnout that is not influenced by either a-c or gravity they obtained

$$\phi_{\text{pred}} = \alpha + \left[\frac{4\alpha^2}{\text{We}_g} \left(1 - \sqrt{\phi_{\text{pred}}(\phi_{\text{pred}} - \alpha)} \left(\frac{\text{We}_g}{6\alpha^3} \right)^{1/4} \right) \right]^{1/3} \tag{15}$$

where α was given as $0.077 r^{0.314} \text{We}_g^{-0.12}$. This represents the data within an rms error of ±11.4 percent.

Finally, for both upflows or crossflows they represent the region of gravity influence in a-c-influenced burnout with

$$\frac{\phi}{\phi_{\text{pred}}} = 1 + 0.049 \left(\frac{r}{\text{Fr}^{3/2}} - \sqrt{75} \right)^{1.17} \tag{16}$$

which is accurate within an rms error of ±10.0 percent. In the a-c-uninfluenced regime, however, they only obtained the very approximate relation (see Fig. 10)

$$\phi/\phi_{\text{pred}} = 1 + 0.000020 r^{1.7}/\text{Fr} \tag{17}$$

which represents all the data, except the widely scattered ones for water, within an rms error of ±11.0 percent.

However, the failure of the gravity- and a-c-uninfluenced water data of both Ungar (1987) and Vliet and Leppert (1964) to correlate well in these coordinates is clearly more than a nuisance variable problem. It remained for Ungar (1987) to clarify this failure.

The other issue that is made clear by Figs. 9 and 10 is that gravity can exert a greater influence on $q_{\max}$, when $q_{\max}$ is influenced by a-c. That seems reasonable since a naturally growing, unforced wave is the most rapidly growing wave. The sheet is therefore shorter when it breaks off and one would expect gravity to have less time to act upon the sheet. Still, if we look carefully at the data, we discover that, while $q_{\max}$ is less influenced by gravity in the a-c-uninfluenced case, we nevertheless find that it starts to deviate at a lower value of the Froude number.

The latest step in the problem of determining $q_{\max}$ during saturated flow boiling over a cylinder was Ungar's (1987) study. (See also details given by Ungar and Eichhorn 1988.) Ungar (1987) made the most extensive observations of the vapor removal process in this geometry, and the most complete formulation of the mechanical energy balance as well. His experiments were made in liquid upflows, and in most cases were gravity influenced. He also developed a technique for *measuring* the outer amplitude of the wavy sheet to obtain an approximation to α.

Ungar's (1987) observations showed that α is more complicated than many of us had hoped it was. For example, he found that α varies in the flow-wise direction. He found that periodic breakoff seems to occur only in gravity-influenced upflows—otherwise breakoff becomes very ragged. He found other ways in which the simple sausagelike bubble-breakoff model deteriorates.

He accompanied these observations with a formulation of the mechanical energy balance that appears to be complete. But, being complete, it is no longer a stability criterion (an MESC) but rather an equation that can be solved for α. This equation gave α values that were either imaginary or only a small fraction of the observed values. The reason is that the actual sheets proved to be too messy to conform to the mathematical description.

Ungar (1987) based a hydrodynamic prediction of $q_{\max}$ on Haggerty and Shea's stability criterion. He eliminated u_g/u_∞ from Lienhard and Eichhorn's (1976) energy balance statement, $\phi = \alpha[1 + u_g/u_\infty]/\pi$, and obtained

$$\phi = \alpha[1 + 2\pi \text{St} \sqrt{3\alpha/2\text{We}_g}] \tag{18}$$

where gravity appears in a Froude number in independent empirical correlations for St and α

$$\text{St} = 0.947(\text{Fr} + 0.614)^{3/2} \text{ and } \alpha = 0.28\, \text{Fr}^{0.141(r)^{0.258}} \tag{19}$$

The effective values of α (above) were obtained by substituting data in equation (18) and correlating the results. Equation (19) gives effective α's a half to a third of the α's measured at the outer edge of the sheet.

Ungar's (1987) burnout prediction takes the form of equation (12) and is restricted to a-c-uninfluenced burnout at values of $G \leq 8$, in liquid upflows. Its accuracy is comparable to Sadasivan's (1986) correlation in the same range.

After Ungar's work, our hopes for making a pure prediction of $q_{\max}$ have been considerably diminished, although it is clear that data can be well correlated with equation (12).

The Idea of an Effusion Limit to Burnout

Ungar's (1987) $q_{\max}$ observations in *saturated* water reached heat fluxes of almost 2 MW/m^2. Recent unpublished results

Downloaded 16 Dec 2010 to 193.140.21.150. Redistribution subject to ASME license or copyright; see http://www.asme.org/terms/Terms_Use.cfm

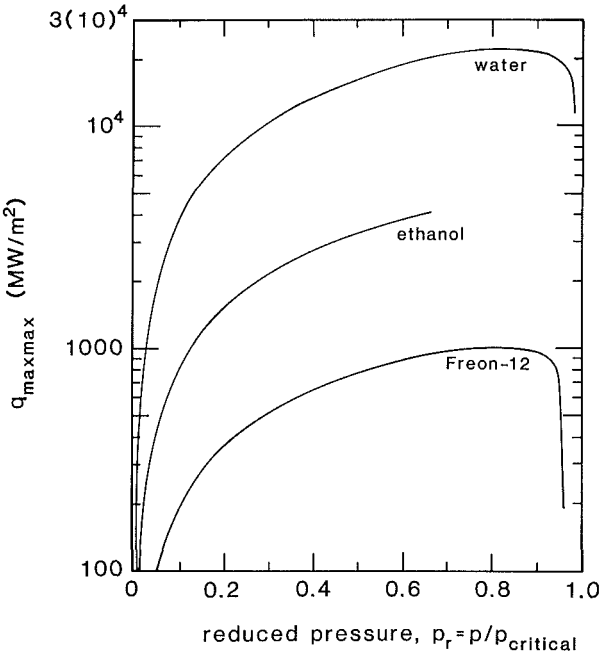

Fig. 11 The pressure dependence of q_{maxmax} as reported by Gambill and Lienhard (1986)

by Kheyrandish and Ungar in the Heat Transfer/Phase Change Laboratory using subcooled water have yielded heat fluxes as high as 14 MW/m^2. Enormously high heat fluxes are attainable in flow boiling.

Gambill and Lienhard (1986) recently asked what the limit of boiling heat fluxes in this (or any other) configuration might be. Obviously, we would achieve the upper limit on a boiling process if the molecules that naturally leave by effusion were allowed to get away, but none were allowed to return to the surface. This upper bound was computed exactly by Schrage (1953), and it can be closely approximated as

$$q_{\text{maxmax}} = \rho_g h_{fg} \sqrt{R_{\text{gas}} T_{\text{sat}} / 2\pi} \tag{20}$$

where R_{gas} is the ideal gas constant.

Figure 11 shows typical values of this characteristic limit extreme boiling (or, for that matter, condensing) heat fluxes for some common liquids. It is apparent that astounding heat fluxes are attainable. The limit q_{maxmax} reaches the astonishing value of more than 20 GW/m^2 at high pressure.

How much of this limit can actually be reached? Gambill and Lienhard (1986) sought out the highest measured burnout heat fluxes and used them to plot Fig. 12. These data show that one may reach about 10 percent of the conceptual limit. The data in Fig. 12 represent all kinds of boiling configurations; however all of them combine subcooling with forced convection. The configurations include jets impinging on disks, twisted-tape generated swirl in tubes, and many others. The data point labeled #22 is Weatherhead's (1955) observation of q_{max} for a horizontal cylinder in a high-speed liquid crossflow. The highest actual heat flux represented in this set is point #8—Ornatskii and Vinyarskii's (1965) result for high-pressure subcooled water, flowing 90 to 100 m/s, in a 1/2 cm i.d. tube. Their value is $q_{\text{max}} = 224.5$ MW/m^2. (I like to picture this as the energy output of 150,000 toasters passing through the area of my desk top, and driven by a very modest temperature difference.)

The failure of the 10 percent limit rule at high pressure is a consequence of two problems. One is that, as ρ_f/ρ_g shrinks at high pressures, it becomes hard to create configurations that do not provide regions of (inefficient) single-phase heat convection. The limit, in other words, becomes harder to reach in practice. The other reason is that it becomes nearly impossible to create heat sources to supply liquids with the terribly high heat fluxes that would otherwise be attainable at high pressures.

The heat flux may thus become limited because it is too close to q_{maxmax}—not because the vapor escape path becomes unstable. It may be limited because the process of molecular effusion is insufficient to carry away as much energy as a vapor escape path would otherwise permit it. We call this behavior *effusion-limited* burnout, and it will figure prominently in a theory of subcooled boiling on cylinders.

Toward a Theory of Subcooled Boiling Burnout

Subcooled Pool Boiling: The First 30 Years. The problem of predicting pool boiling burnout in subcooled liquids has received intermittent attention for the past 30 years. Perhaps work was less intense than in other areas of boiling because, strictly speaking, true steady pool boiling cannot be subcooled. The boiled liquid in a stagnant pool will eventually warm to the saturation temperature.

However, a submerged body in a large bath can operate in quasi-static subcooled boiling for a long time. Thus the subcooled burnout limit is important in the short term. Furthermore, if the cool liquid is replenished, either by slow fluid motion or a cooling process in the liquid bath, something very close to pool conditions can be maintained indefinitely. Finally, since subcooled behavior is of paramount importance in flow boiling, it is important that we understand the zero velocity limit if we are to reach a general understanding of burnout in flow boiling.

Kutateladze (1951) first looked at subcooled boiling burnout heat flux $q_{\text{max,sub}}$, and argued that since some fraction of the heat had to go to warming the liquid to its boiling point before boiling could occur, one could represent $q_{\text{max,sub}}$ as

$$\frac{q_{\text{max,sub}}}{q_{\text{max}}} = \text{const}(\text{Ja}) \tag{21}$$

where the Jakob number Ja $\equiv \rho_f c_p \Delta T_{\text{sub}} / \rho_g h_{fg}$; $\Delta T_{\text{sub}} \equiv$ the liquid subcooling, $(T_{\text{sat}} - T_{\text{bath}})$; and $q_{\text{max}} \equiv$ the saturated peak heat flux.

Kutateladze and Schneiderman (before 1953) measured $q_{\text{max,sub}}$ on horizontal cylinders. Their limited data in water, ethanol, and iso-octane suggested that $q_{\text{max,sub}}$ varied in direct proportion to Ja and thus to ΔT_{sub}; but they also suggested that the constant in equation (21) should contain the factor $(\rho_f/\rho_g)^{0.077}$ to account for the "recirculation of unheated subcooled liquid." The maximum subcoolings they imposed were 64°C in water, 20°C in ethanol, and 76°C in iso-octane. They made their measurements on graphite rods, whose diameters they failed to report.

Zuber et al. (1963) suggested in 1961 that subcooling would augment burnout by condensing a fraction of the departing vapor on the walls of the jets through which it flowed. This meant that additional vapor would have to be generated at a heater surface before Helmholtz instability caused burnout. The amount of vapor condensed must then be established by transient heat conduction in the moving liquid–vapor interface. Thus they obtained a correlation that explicitly displays the familiar formula for transient conduction into a semi-infinite medium

$$\frac{q_{\text{max,sub}}}{q_{\text{max}}} = 1 + \text{const} \frac{2k\Delta T_{\text{sub}}}{q_{\text{max}} \sqrt{\pi \tau \alpha}} \tag{22}$$

where τ was an approximation to the lifetime of the vapor jets. The Zuber–Tribus–Westwater mechanism was the most plausible of the early explanations of subcooled burnout; but, for reasons that become clear below, it did not provide very good correlation of the existing subcooled data.

Ivey and Morris (1962) (see also Ivey and Morris, 1966) pro-

Downloaded 16 Dec 2010 to 193.140.21.150. Redistribution subject to ASME license or copyright; see http://www.asme.org/terms/Terms_Use.cfm

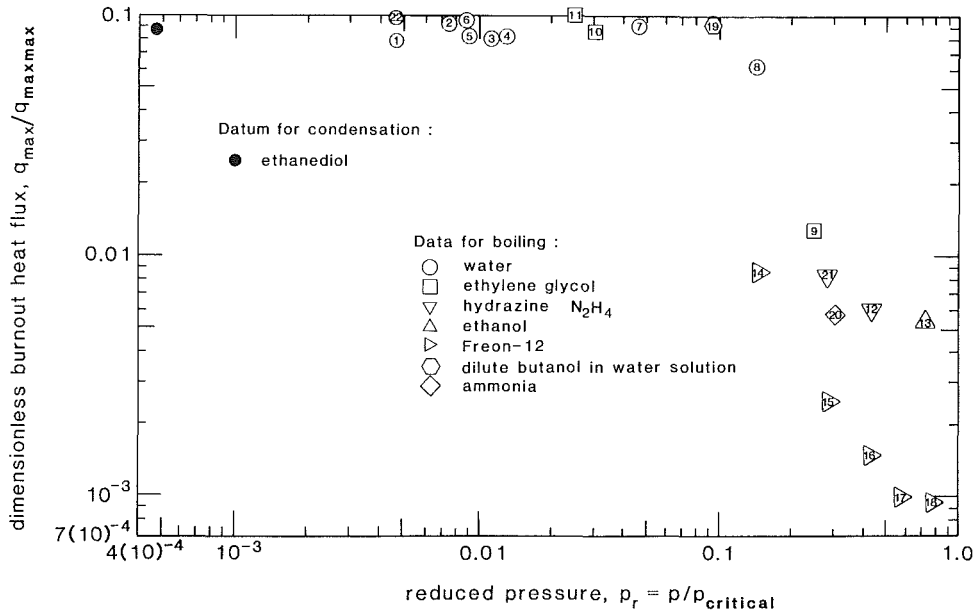

Fig. 12 Pressure dependence of the highest measured burnout heat fluxes, after Gambill and Lienhard (1988)

vided the following modification of Kutateladze and Schneiderman's correlation:

$$\frac{q_{max,sub}}{q_{max}} = 1 + 0.1\left(\frac{\rho_g}{\rho_f}\right)^{1/4} \text{Ja} \qquad (23)$$

Equation (23) correlated theirs and Kutateladze's data for horizontal wires 1.22 to 2.67 mm in diameter in water, in the range $0 < \Delta T_{sub} \leq 72°C$. The correlation was only accurate within ±25 percent, and it failed to represent data for other geometries.

Thus, by 1966, it had been established that $q_{max,sub}$ varied more or less as ΔT_{sub}, at least when ΔT_{sub} was not too great. However, the influence of both geometry and geometric scale had not been clarified at all. Furthermore, the fact that the thermal conductivity had to enter the process (as indicated by Zuber et al. 1963 was still largely neglected.

Elkassabgi and Lienhard (1988) provided the most extensive subcooled pool boiling burnout data set. They made 631 observations of q_{max} on cylindrical electric resistance heaters ranging from 0.80 to 1.54 mm in diameter. They boiled four liquids—isopropanol, acetone, methanol, and Freon-113—at atmospheric pressure, and they reached subcoolings as high as 140°C.

Typical results of their experiments are shown in Fig. 13. These $q_{max,sub}$ data (for isopropanol in this case) have been normalized by Sun and Lienhard's (1970) saturated q_{max} prediction, equation (4). The purpose of using the hydrodynamic prediction of q_{max} to reduce the data on an otherwise dimensional plot was to make it feasible to put data for different wire sizes on the same graph. While equation (4) may not correctly account for geometric scale at high subcooling, this normalization nevertheless made it possible to see that $q_{max,sub}$ passed through three identifiable regimes of boiling behavior as ΔT_{sub} was increased.

These three regimes of subcooled burnout behavior were more sharply evident in photographs. In the "region of low subcooling" the familiar jets-and-columns behavior of saturated boiling was preserved, although the jets diminished slightly in size. In the "region of intermediate subcooling" the jets gave way to fairly large bubbles that continued to condense after they left the wire.

The most dramatic behavior lay in the "region of high subcooling." Here two unexpected things happened: The burnout

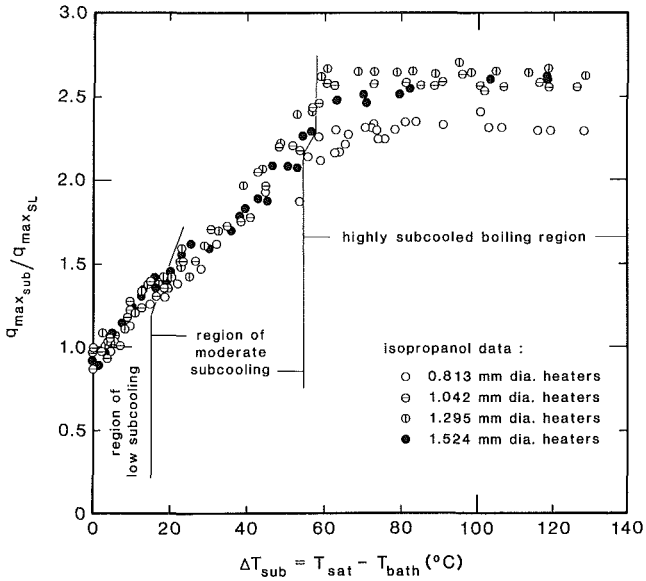

Fig. 13 The effect of liquid subcooling on the peak heat flux, for heaters of various sizes in isopropanol after Elkassabgi and Lienhard (1988)

heat flux reached a ceiling that was independent of ΔT_{sub}, and the bubble departure pattern took on the appearance of saturated film boiling. At high superheats, very small bubbles left the wire and rose, without condensing, in a thin sheet of liquid that had been heated all the way to T_{sat} by the wire. Elkassabgi and Lienhard (1988) identified this hitherto unnoticed high-subcooling region by developing extensive sets of data for extreme subcoolings where other investigators had only provided a few points.

The Region of Low Subcooling. The mechanism for burnout in the region of low subcooling is the same Helmholtz instability process that occurs in saturated boiling. In this case, however, more vapor must be supplied to the escaping jets, to make up that portion that condenses on the jet walls before burnout occurs.

This is the essence of the Zuber et al. (1963) mechanism. Like Zuber et al., Elkassabgi and Lienhard (1988) noted q_{max}

Downloaded 16 Dec 2010 to 193.140.21.150. Redistribution subject to ASME license or copyright; see http://www.asme.org/terms/Terms_Use.cfm

should be added to the transient heat flux from the saturated interface of the vapor jets to the surrounding subcooled liquid. The *average* transient conduction is well known. It may be renormalized as follows to give a flux per unit area of the *heater*:

$$q_{\text{cond.}} \equiv \frac{2k\Delta T_{\text{sub}}}{\sqrt{\pi\alpha\tau}} \frac{A_{\text{cond.}}}{A_{\text{heater}}} \tag{24}$$

where $A_{\text{cond.}}$ is the jet surface on which the condensation process takes place. Elkassabgi and Lienhard (1988) used MESC arguments to show that τ must take the following form:

$$\tau = \text{const} \frac{\rho_g^{1/2}\sigma^{1/4}}{[g(\rho_f - \rho_g)]^{3/4}} \tag{25}$$

They then wrote the subcooled peak heat flux in the following variation of equation (22):

$$\frac{q_{\text{max,sub}}}{q_{\text{max}}} = 1 + \frac{q_{\text{cond.}}}{q_{\text{max}}} \tag{26}$$

where q_{max} is the saturated burnout heat flux, and

$$A_{\text{cond.}} = \tau \frac{dA_{\text{cond.}}}{dt} \tag{27}$$

Additional MESC arguments were used to estimate the rate of generating interfacial surface. The result was

$$\frac{dA_{\text{cond.}}}{dt} \sim \frac{\rho_g u_g^3}{\sigma} A_{\text{jet}} \sim \frac{\sigma^{3/4}}{\rho_g^{1/2}[g(\rho_f - \rho_g)]^{1/4}} A_{\text{jet}} \tag{28}$$

Finally they combined equations (24), (25), (26), (27), (28), and (4), and noted that $A_{\text{jet}}/A_{\text{heater}}$ should depend weakly on R'. The result was

$$\frac{q_{\text{max,sub}}}{q_{\text{max}}} = 1 + f(R')\text{Ja}/\text{Pe}^{1/4} \tag{29}$$

where q_{max} could represent either Sun and Lienhard's (1970) prediction or the actual measured value of q_{max} in a saturated liquid, and where Pe is an effective Peclet number

$$\text{Pe} \equiv \frac{\sigma^{3/4}}{\alpha[g(\rho_f - \rho_g)]^{1/4}\rho_g^{1/2}} \tag{30}$$

Figure 14 shows their low-subcooling data plotted in accordance with equation (29). Three difficulties arose in making this plot. The first was that of normalizing the ordinate. We have noted that equation (4) shows some systematic error among the various fluids. Therefore average measured q_{max} values are used in place of equation (4) to normalize the ordinate.

The second difficulty was that of locating a given data point in the correct region of subcooling. Elkassabgi and Lienhard (1988) eventually had to do this after the fact by empirical correlation.

The third difficulty—specifying the function $f(R')$—conveniently vanished. Least-squares correlation revealed that $f(R')$ was approximately the constant 4.28. Consequently equation (29) was reduced to

$$\frac{q_{\text{max,sub}}}{q_{\text{max}}} = 1 + 4.28\ \text{Ja}/\text{Pe}^{1/4} \tag{31}$$

based on experimentally determined values of q_{max}. Equation (31) represented the data within an rms error of ± 5.95 percent.

The Region of Intermediate Subcooling. Elkassabgi and Lienhard's (1988) photographs made it clear that the low subcooling mechanism was not appropriate to the vapor escape process at higher subcoolings. The jets and columns vanish as bubbles grow and condense in a region that is increasingly restricted to the neighborhood close to the cylinder.

Their photographs for high subcooling revealed intense bubble growth and condensation action near the surface. This action is undoubtedly coupled with mass transfer *through* the bubbles, as postulated by Edwards and Snyder (1954). (See, e.g., Snyder and Robin, 1968.) Consequently, fairly limited liquid–solid contact occurs around the heater, and the liquid outside this highly active vapor bubble layer is saturated.

So the cylinder has an effective radius R_{eff} larger than R by the thickness of the bubble layer, with heat transfer occurring by *natural convection* from the saturated liquid to the surrounding subcooled liquid. Normally, natural convection would not be terribly effective; however in this case the no-slip condition (between the saturated interface and the bubble layer) is largely removed *by* the bubble layer. Therefore burnout occurs in this region when the efficient phase-change process in the bubble layer reaches the limit of heat that can be removed by the not-quite-as-efficient natural convection process outside the vapor layer.

If heat transfer is determined in this way, the dimensional functional equation for $q_{\text{max,sub}}$ is

$$q_{\text{max,sub}} = f(\Delta T_{\text{sub}},\ R_{\text{eff}},\ g,\ \beta,\ k,\ \alpha,\ \nu) \tag{32}$$

where β is the coefficient of thermal expansion of the liquid, ν is the kinematic viscosity, and R_{eff} is the sum of the cylinder radius and one departing bubble diameter. The use of Fritz's (1937) departing bubble diameter (for saturated pool boiling) gives

$$R_{\text{eff}} = R(1 + 0.02\ \theta/R') \tag{33}$$

where the second term is the Fritz radius. (The constant 0.02

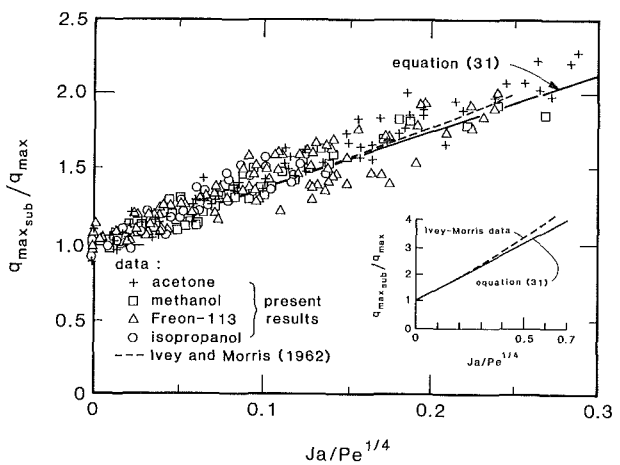

Fig. 14 Elkassabgi and Lienhard's (1988) correlation of $q_{\text{max,sub}}$ data in the region of low subcooling in accordance with equation (31)

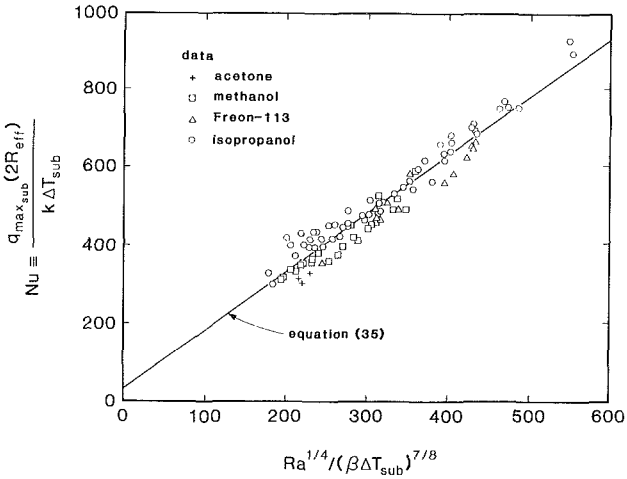

Fig. 15 Elkassabgi and Lienhard's (1988) correlation of $q_{\text{max,sub}}$ data in the region of moderate subcooling, in accordance with equation (35)

Downloaded 16 Dec 2010 to 193.140.21.150. Redistribution subject to ASME license or copyright; see http://www.asme.org/terms/Terms_Use.cfm

was verified for the subcooled burnout configuration by least-squares correlation.) Equation (32) has eight variables in four dimensions and thus reduces to four dimensionless groups

$$\frac{q_{\max,\text{sub}} R_{\text{eff}}}{k\Delta T_{\text{sub}}} = f\left(\frac{gR_{\text{eff}}^3}{\alpha\nu},\ \beta\Delta T_{\text{sub}},\ \text{Pr}\right) \tag{34}$$

Correlating data with this equation, Elkassabgi and Lienhard (1988) obtained for the region of moderate subcooling

$$\text{Nu} = 28 + 1.50\ \text{Ra}^{1/4}/(\beta\Delta T_{\text{sub}})^{7/8} \tag{35}$$

where the Nusselt number for this case is defined as

$$\text{Nu} \equiv \frac{q_{\max,\text{sub}}(2R_{\text{eff}})}{k\Delta T_{\text{sub}}} \tag{36}$$

and the Rayleigh number is

$$\text{Ra} \equiv \frac{g\beta\Delta T_{\text{sub}}(2R_{\text{eff}})^3}{\alpha\nu} \tag{37}$$

The familiar 1/4 power exponent of Ra in equation (35) is the result of the correlation and it was *not assumed.* (So too was the 7/8 exponent of $(k\Delta T_{\text{sub}})$.) The use of equation (35) requires measured values of the retreating contact angle θ, which enters both Nu and Ra through R_{eff} in equation (33).

Equation (35) is plotted with all of the available data for the moderately subcooled region in Fig. 15. It represents the data accurately within an rms error of ±7.06 percent.

The Region of High Subcooling. In the third region of boiling, the boiling configuration is similar to that in the range of moderate subcooling. Rapidly changing, growing, and collapsing, bubbles form and reform a thin structure of liquid-vapor interfaces in which there occurs rapid transient conduction related to repeated contacts with the heater surface. The maximum heat fluxes in this region are very high—typically three times the saturated values—yet they no longer depend on ΔT_{sub}.

The fact that these heat fluxes have reached a ΔT_{sub}-independent limit calls for a new mechanism of boiling—one that occurs when the phase-change heat transfer process can no longer keep up with natural convection. Elkassabgi and Lienhard (1988) noted that this must be some fraction of the molecular effusion limit given by equation (20). Indeed their data rather consistently gave $\phi \equiv q_{\max,\text{sub}}/q_{\max\max}$ on the order of 0.01 with slightly larger values for smaller wires.

This raised a dimensional difficulty since the Taylor wavelength no longer provides a second length parameter. They concluded that the relevant system parameters must be related to the transient heating of liquid in the structure of the changing liquid-vapor interface, and they wrote

$$\phi = \phi\left(\alpha,\ R,\ \frac{R}{\sqrt{R_{\text{gas}}T_{\text{sat}}}}\right) \tag{38}$$

where the last term is the characteristic time required for molecules to traverse the characteristic dimension of the system.

$$\text{time to transit } R = \frac{R}{\sqrt{R_{\text{gas}}T_{\text{sat}}}} \tag{39}$$

These four variables are expressed in just two dimensions so equation (38) can be rearranged into

$$\phi = \phi(\chi) \tag{40}$$

where the new group χ is another form of Peclet number

$$\chi \equiv R(R_{\text{gas}}T_{\text{sat}})^{1/2}/\alpha \tag{41}$$

The highly subcooled data are shown in Fig. 16 on ϕ versus χ coordinates. The choice of α for the liquid in equation (38) was validated by four additional $q_{\max,\text{sub}}$ data obtained on steel heaters with a thermal diffusivity three times that of nichrome, which are included here. (The steel heater data correlate perfectly with the nichrome data when they are plotted on the coordinates required by equation (40).) The final correlation was

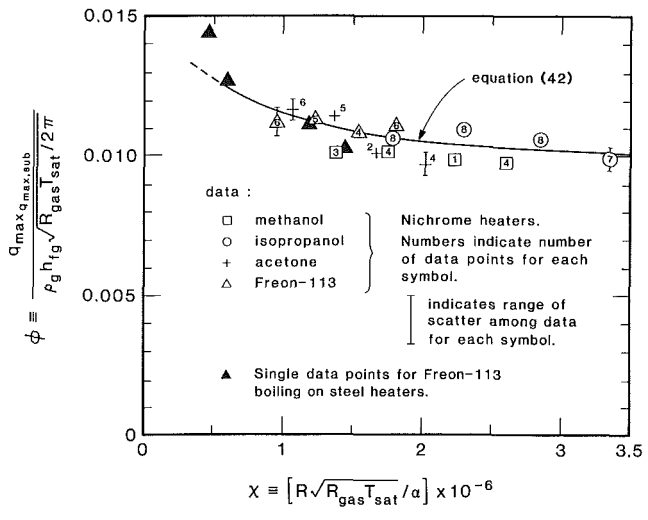

Fig. 16 Elkassabgi and Lienhard's (1988) correlation of $q_{max,sub}$ data in the region of high subcooling, in accordance with equation (42)

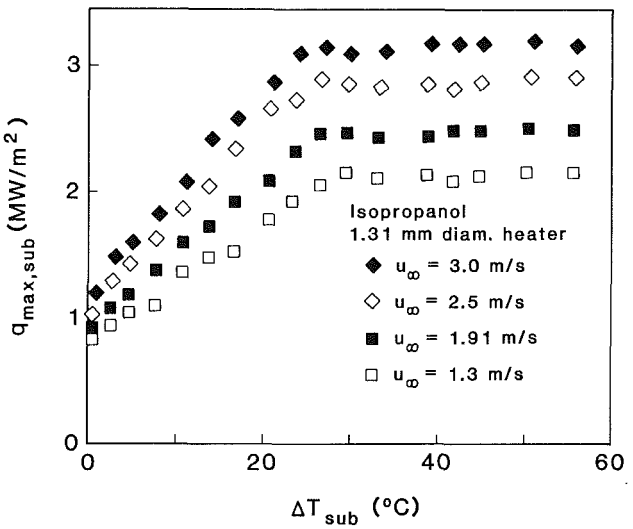

Fig. 17 Flow boiling burnout data of Kheyrandish (1988) for methanol passing over a horizontal cylinder

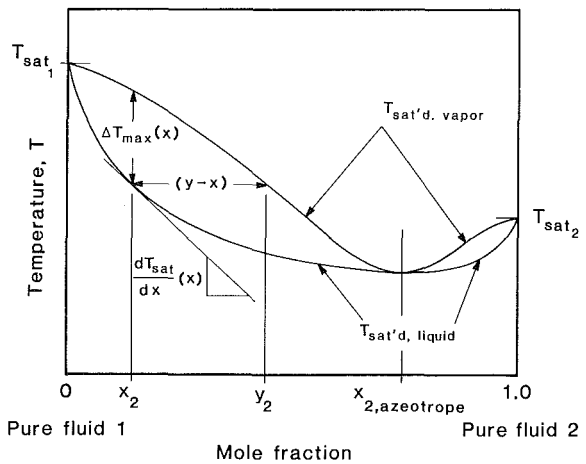

Fig. 18 Schematic equilibrium phase diagram for a typical binary azeotropic mixture, showing nomenclature

Downloaded 16 Dec 2010 to 193.140.21.150. Redistribution subject to ASME license or copyright; see http://www.asme.org/terms/Terms_Use.cfm

$$\phi = 0.01 + 0.0047\exp(-1.11\times10^{-6}\chi) \quad (42)$$

which represents the data with an rms deviation of 6.82 percent.

Summary of the Subcooled Boiling Correlations. Elkassabgi and Lienhard (1988) discovered that *most* of the existing subcooled boiling data for horizontal cylinders are data for which R' was too small, for which a significant liquid crossflow had been imposed, or for which the system parameters had been incompletely reported. The only previous data that they could legitimately compare with their correlations were the low-subcooling data of Ivey and Morris (1962). These data are for water, which was not used in building the correlation; yet they are perfectly represented by it.

The common wisdom before 1987 was that q_{max} increased linearly with ΔT_{sub}. Elkassabgi and Lienhard's (1988) study bore this out at low ΔT_{sub}, but showed that it is inaccurate in the moderate subcooling region and completely incorrect when ΔT_{sub} is large.

A serious, and yet unresolved, problem with the three new $q_{max,sub}$ predictions is determining which of them is appropriate for a heater of a given size in a given liquid at a given ΔT_{sub}. To date, this determination must often be made after the fact.

Subcooled Flow Boiling. No theory of subcooled burnout has yet been created for *flow* boiling. However, Kheyrandish (1988) has measured q_{max} during flow boiling over horizontal cylinders using the apparatus described by Lienhard and Kheyrandish (1985) and Ungar (1987). A typical set of these data is shown in Fig. 17. The data mirror those of Elkassabgi and Lienhard (1988) in that q_{max} rises in a seemingly linear fashion with ΔT_{sub} up to a limiting value. At higher values of ΔT_{sub}, q_{max} becomes independent of ΔT_{sub}.

In the limited data he has thus far obtained, Kheyrandish (1988) has only seen two subcooled boiling regimes: One is an approximately linear region that is undoubtedly kin to the region of low subcooling in pool boiling. The other is a high subcooling region that is almost certainly effusion limited. Elkassabgi and Lienhard's (1988) middle range of natural convection limited burnout is absent. But that absence lends support to their arguments since there could be no such region in a forced convection process.

In the effusion-limited region, q_{max} increases with velocity. However, the velocities are modest in this experiment (see Fig. 17)—nothing like those needed to reach Gambill and Lienhard's (1988) apparent limit of q_{max}/q_{maxmax}.

The range of these measurements is limited, thus far. They involve only one fluid and they cover restrictive ranges of velocity and heater size. The data do, however, strongly support Elkassabgi and Lienhard's (1988) observation of an effusion-limited burnout in highly subcooled boiling by displaying it in clear and dramatic terms.

Toward a Theory of Burnout in Binary Liquids

The process industries have wanted to understand burnout in mixtures for fifty years. Reddy (1987) and Reddy and Lienhard (1988) have given comprehensive critical reviews of the literature on burnout in binary mixtures. Most of this literature has been devoted to cylindrical heaters.

Van Stralen and several co-workers, in particular, made many observations of burnout on small horizontal cylinders in binary mixtures, starting in the 1950s. Van Stralen and Sluyter (1969) took a particular interest in the fact that small concentrations of one liquid in a binary mixture could greatly increase q_{max}.

Unfortunately, most of the early interpretations of this phenomenon suffered because the influences of geometry and geometric scale on burnout had not yet been identified or properly diagnosed. Yet, not only were those influences present, but many of the data also fell in regions of low R'. Therefore, most interpretations of the role of composition were muddied by these unrecognized influences.

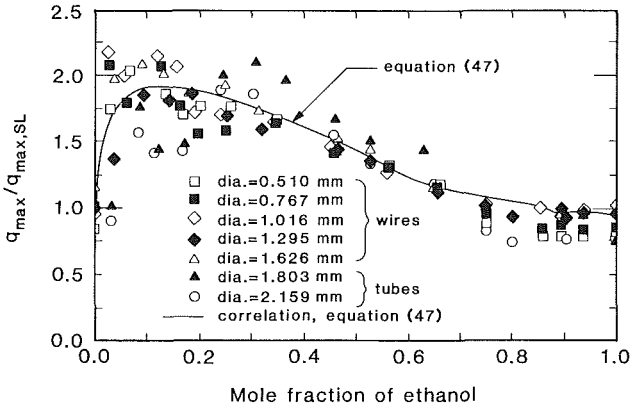

Fig. 19 Reddy and Lienhard's (1988) q_{max} data normalized to eliminate the role of geometric scale and displaying their final correlation

Two particularly important insights emerged during the 1960s. Carne (1964a, 1964b) questioned the use of the equilibrium latent heat of vaporization. Figure 18 shows a typical phase-equilibrium diagram for a binary azeotropic mixture. The equilibrium h_{fg} is the enthalpy difference between the liquid and vapor at the same temperature. But Carne suggested that a flash evaporation process occurred at constant *composition* during boiling. Actually, it is doubtful that pure flash evaporation occurs; Thome (1983) subsequently argued that the actual process lies somewhere *between* equilibrium and flash evaporation.

McEligot (1964) took the second important step toward understanding binary boiling when he noted that vapor leaves the liquid at a higher temperature than that at which it would condense. The surrounding liquid, at the original concentration, is thus effectively subcooled. This subcooling is greatest at low alcohol concentrations in water (owing to the shape of its phase-equilibrium diagram), and so too is the heat flux augmentation.

This induced subcooling idea can only be made useful when both its *magnitude* and its *effect* on the burnout heat flux are known. McEligot (1964) had access to neither. Elkassabgi and Lienhard's (1988) descriptions of the various regions of subcooling on burnout in pure fluids were not made until 1987, and the extent of induced subcooling in interfaces of boiling binary liquids remains unpredictable. Of course, one must also know the path of the evaporation process in the phase-equilibrium diagram. Thome and Shock's (1984) study, 20 years later, provided a cogent discussion of these problems.

Finally, as Kutateladze et al. (1966) first pointed out, the shape of the phase-equilibrium diagram must also be made a part of any q_{max} prediction for binary liquids. Several different pairs of information may be used to characterize the diagram completely. If the liquid and vapor mole fractions of component 1 are called x and y, then $T(x)$ and $T(y)$ would clearly be one such pair. Another would be

$$(x-y)\frac{dT_{sat}}{dx} \quad (43)$$

After the mid-1960s, work on burnout in binary mixtures slacked off. The issue did not go away, but the flow of new ideas abated. However, two papers served to revitalize interest in the subject: Thome and Shock's (1983) broad review of the theoretical bases of the problem and Yang's (1987) recent attempt to organize a new correlation of prior data. (Unfortunately Yang's paper still failed to deal systematically with geometric considerations.)

Downloaded 16 Dec 2010 to 193.140.21.150. Redistribution subject to ASME license or copyright; see http://www.asme.org/terms/Terms_Use.cfm

Reddy and Lienhard (1988) set about to incorporate all the ideas described above in describing a new, well-controlled, and complete set of data. They measured q_{max} in ethanol/water mixtures (which clearly exhibits a maximum q_{max} at low ethanol compositions) and they used the horizontal cylinder geometry because the most was already known about it. Finally, they stayed within a size range ($0.1 \leq R' \leq 0.7$) for which the hydrodynamic mechanisms are clearly defined.

Their complete q_{max} data are shown in Fig. 19, where they have been normalized in accordance with theoretical considerations explained below. Despite the normalization, it is clear that the smaller heaters display a maximum at low alcohol concentrations, while data for the larger heaters become increasingly scattered at low concentrations.

Means for Identifying the Effective Subcooling. Since, as McEligot (1964) noted, the maximum in q_{max} must be caused by induced subcooling, Reddy and Lienhard (1988) sought to evaluate that subcooling quantitatively. They did this by comparing the increase of q_{max} over the conventional hydrodynamic value, with the increase of q_{max} predicted to occur as a consequence of subcooling.

To estimate this difference Δq_{sub}, they calculated a pure hydrodynamic value of q_{max} to subtract from the experimental q_{max}. They obtained the hydrodynamic value using equation (4) slightly adjusted to account for its small systematic error in the pure-fluid limits. The use of equation (4) was crucial here because it properly took into account the influence of geometry. They then equated this Δq_{sub} to the extreme right-hand term in equation (31) and solved the result to get the effective ΔT_{sub}.

The resulting values of ΔT_{sub}, plotted in Fig. 19, show a clear trend in x, with ΔT_{sub} vanishing at the azeotrope. ΔT_{sub} must stay close to zero for $x \geq x_{azeotrope}$, since the saturated liquid and vapor curves for alcohol/water remain very close together in this region. The numerical values of ΔT_{sub} are all fairly small—all below 2°C—thus vindicating the use of the low-subcooling equation (31).

Burnout Correlation. Reddy and Lienhard (1988) began with a dimensional analysis of burnout. Their dimensional functional equation for q_{max} was

$$q_{max} = f(h_{fg},\ g(\rho_f - \rho_g),\ \rho_g,\ R,\ c_p,$$
$$T_g(k) - T_f(x),\ \alpha,\ \text{mass diffusivity})$$

The ten variables are expressible in N, m, s, °C. Hence the dimensional equation reduced to six dimensionless groups

$$\text{Ku} = f(R',\ \text{Ja}_e,\ \rho_f/\rho_g,\ \text{Pe},\ \text{Lewis No.}) \tag{44}$$

Two of these groups are probably unimportant: Mass diffusivity is normally so slow with respect to boiling processes that the Lewis number should not play an important role. Elkassabgi and Lienhard (1988) found by least-squares fitting that ρ_f/ρ_g played no role in the kindred problem of burnout in single-component subcooled liquids, so it should also be unimportant here.

The x-dependent shape of the phase equilibrium diagram is represented in a new effective Jakob number Ja_e, based on the effective subcooling of the liquid, which varies with x. Two candidate Jakob numbers based on two representations of the subcooling are

$$\text{Ja}_e \equiv \frac{\rho_f c_p (x-y)}{\rho_g h_{fg}} \frac{dT_f}{dx} \tag{45a}$$

and

$$\text{Ja}_e \equiv \frac{\rho_f c_p [T_g(x) - T_f(x)]}{\rho_g h_{fg}} \tag{45b}$$

Other Ja_e could have been created using other characterizations of the subcooling. However, equation (45*b*) proved to work better than any others that Reddy tried.

We have already seen that we can combine Ku and R' by carrying the R' dependence in q_{max}. Thus Reddy and Lienhard (1988) sought a correlation of the form

$$\frac{q_{max}}{q_{max,SL}} = \frac{1}{1 - f(\text{Ja}_e,\ \text{Pe})} \tag{46}$$

where the single-phase q_{max} is identified as $q_{max,SL}$ since it can be represented by the Sun–Lienhard (1970) prediction, equation (4). They were unable to isolate any influence of Pe on q_{max}. However, the range of variation of Pe was not large enough to justify any general conclusion about its role in binary liquid burnout. It was only clear that Pe did not influence burnout in the range represented by the ethanol/water system at 1 atm.

A simple least-squares fit of their data then gave:

$$\frac{q_{max}(1 + 0.10x)}{q_{max,SL}} = (1 - 0.170\text{Ja}_e^{0.308})^{-1} \tag{47}$$

which represented the data for wires within an rms deviation of ±8 percent. (Equation (47) is included in Fig. 19.) Data for stainless steel tubes exhibit pretty broad scatter in Fig. 19 at low values of x. Changing from wires to tubes changes the heat transfer boundary condition from a nearly uniform wall temperature to a nearly uniform heat flux, and it is clear that burnout is sensitive to this change. (If the tube data were included, the rms error of equation (47) would increase to ±15 percent.)

Challenges to the Hydrodynamic Theory

On the Nature of Challenges to a Theory. The hydrodynamic theory of burnout, especially as applied to cylindrical heaters, has clearly served our understanding very well. I have painted a generally rosy picture of its successes. But we began this essay by referring to Thomas Kuhn's (1962) theory of scientific revolution. Kuhn drove home the message that workers in a field are the most resistant to admitting change in that field. We do not easily admit any inadequacies in what we have done, and we are *extremely* ill-disposed to give competing theories a fair hearing. That problem dogged the people who gave us the hydrodynamic theory, and *we* must try to avoid fighting the new ideas that will clearly be needed to complete *our* understanding of burnout.

Kuhn (1962) shows that seemingly minor imperfections in a given body of theory—the problems that look like mere incompleted details at first—are often storm signals that a theory is in need of major revision. The failure of Rayleigh's theory of radiation at small wavelengths was, for example, a warning that classical statistical mechanics must fail dramatically at low temperatures.

We accordingly have to be alert to the content of competing burnout theories; and we should carefully ask what our more resistant unsolved problems in the field are.

Storm Signals. Practitioners in the field have historically proved to be least qualified to identify correctly the problems that threaten a body of theory. Indeed, for me to do so, I must reveal those nagging doubts that I do not like to speak aloud; and that is not easy to do.

I have mentioned many unresolved problems in passing. But we need means to separate the true storm signals from mere unanswered questions. Elkassabgi and Lienhard (1988) failed to figure out how to predict the regions of subcooled boiling *a priori*; and Reddy and Lienhard (1988) were unable to determine the path of evaporation on the phase-equilibrium diagram. Dozens of such questions either have not been around long enough to attract the interest of one clever person, or are so difficult that we might never expect to answer them.

Downloaded 16 Dec 2010 to 193.140.21.150. Redistribution subject to ASME license or copyright; see http://www.asme.org/terms/Terms_Use.cfm

Kuhn (1962) points out that certain storm signals (he uses the word *anomalies*) are exceptions to theory that, at first, seem small enough to shrug off, but which show their faces consistently and which become increasingly clear as measurement is refined. Such anomalies often signal the need for radical extension or even replacement of a theory. Three potential storm signals that bother me include:

1 The seemingly minor systematic inaccuracies of the Sun-Lienhard (1970) equation from fluid to fluid. (Such variations are inconsistent with dimensional analysis based on purely hydrodynamic burnout and should not occur.)

2 The fact that q_{max} has consistently shown some dependence on surface condition. (*In most cases this dependence is minor, but circumstances exist in which it can* be greatly magnified.)

3 The failure of the theory to account explicitly for the recurring collapse of vapor jets in the mechanism of pool boiling. (These jets are taken to be static vapor escape conduits until they suffer collapse, yet observations show that, at heat fluxes below q_{max}, they periodically break down and reestablish themselves. What is the mechamism of their collapse and reformation, and how does it relate to Helmholtz instability?)

The first assaults launched against the hydrodynamic theory were rooted in the idea that burnout must be surface-influenced. Those of us who have developed the theory have generally made light of such influences because they have usually been minor, at least in the geometries we have studied. But if surface effects *do* give rise to items (1) and (2) above, whether they are minor or not, the theory is still incomplete if it cannot take them into account. If they occur, they well might be very important in another geometry. That is exactly what recent work is suggesting.

Liaw and Dhir's Accounting of Surface Influences. Liaw and Dhir (1987a) recently provided a detailed study of water boiling on a large vertical plate. In particular, they discovered that, as surface wetting just begins to deteriorate, q_{max} falls off dramatically. Increasing the sessile-drop contact angle from 27 to 90 deg caused q_{max} to fall off 35 percent in this geometry. They also measured local void densities and suggested a hydrodynamic model, consistent with these observations, to explain the influence of contact angle on q_{max} (see Liaw and Dhir, 1987b).

This is not entirely surprising. It is known (see e.g., Winterton, 1983) that nucleate boiling and the entire multivalued boiling curve vanish so that there is no q_{max} when mercury boils on surfaces that will not be wetted at all. Heating instead undergoes a transition directly from natural convection into film boiling.

But, Liaw and Dhir's work differs from previous surface-influence attacks in two interesting ways. It is convincingly systematic, and it displays large influences of contact angle, even while a good measure of wetting is still present.

The problem is that the vertical plate is *not* a well-understood geometry. We are left to ask if one could repeat the work in other configurations. Figure 4 reflects a huge number of data for cylinders—with all kinds of surface conditions. Sun and Lienhard's (1970) prediction represents these data within ±15 percent scatter. Systematic influences of the surface–liquid interaction are certainly present here, but these influences are far less than Liaw and Dhir (1987) have obtained in the vertical plate geometry. The work of Elkassabgi and Lienhard (1988) makes it clear that about ±10 percent of this scatter probably reflects the different liquid–surface combinations. Similar systematic minor, but inescapable, variations of q_{max} with surface conditions were found both by Berenson (1960) and by Ramilison and Lienhard (1987) in the *horizontal* flat plate geometry.

If the contact angle influences burnout on cylinders, then that influence is certainly muted in comparison with its influence in the vertical plate configuration. But, whether or not it is large, if such an influence is present then the hydrodynamic theory cannot be considered complete until it accommodates it.

The Haramuro-Katto Challenge. Haramura and Katto (1983) recently offered a competing hydrodynamic model for burnout. Figure 21 contrasts their model with the conventional hydrodynamic one. They suggested that the nucleate boiling heat flux is limited by a thin liquid sublayer along the surface, which is perforated by many small vapor jets. They suppose that the sublayer becomes unstable if its thickness ever exceeds one fourth of the Helmholtz unstable wavelength in the small jets.

Haramuro and Katto (1983) assumed that, during pool boiling, large vapor bubbles grow directly above the heater surface and leave with a known frequency. The bubbles are fed by an evaporating liquid sublayer, which is replenished only after

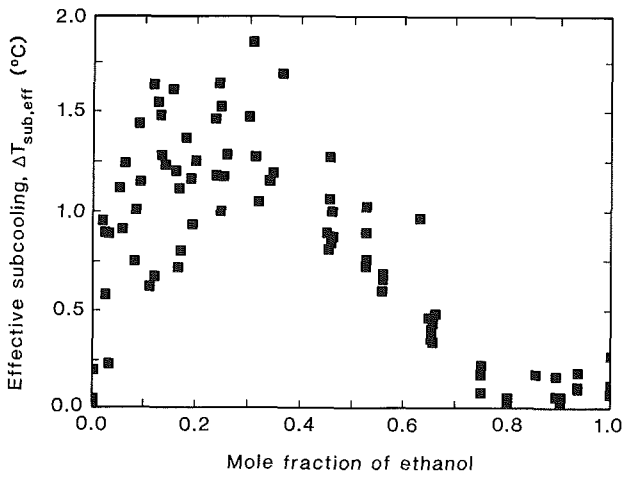

Fig. 20 Reddy and Lienhard's (1988) effective subcooling inferred from the present data using the low-subcooling correlation of Elkassabgi and Lienhard

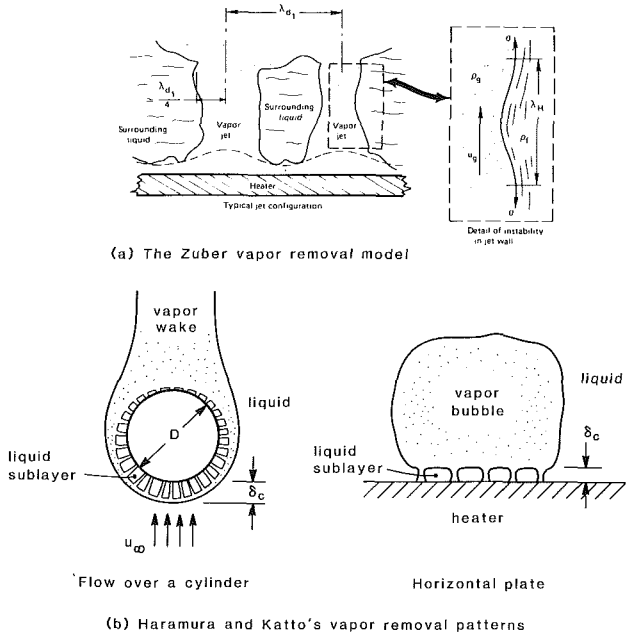

Fig. 21 Comparison of the vapor removal configurations near burnout according to (*a*) the conventional pool boiling model envisioned by Zuber (1961), Sun and Lienhard (1970), and others; and (*b*) the Haramura and Katto (1983) models for both pool and flow boiling

Downloaded 16 Dec 2010 to 193.140.21.150. Redistribution subject to ASME license or copyright; see http://www.asme.org/terms/Terms_Use.cfm

each large bubble departs. Burnout is presumed to occur when the entire sublayer evaporates away before the bubble buoys away. The problem is that, although a liquid sublayer is present in pool boiling, the large vapor bubbles are separated from the sublayer by long, large vapor jets. The sublayer clearly can be replenished continuously.

For flow boiling, Haramura and Katto (1983) imagine that a liquid sublayer moves at the free-stream velocity along the heater (under the vapor). They presume its thickness at the upstream stagnation point is the same as in pool boiling, and that burnout occurs when the sublayer just evaporates away as it reaches the downstream stagnation point. The problem here is that no such sublayer has ever been observed and we can be fairly certain that none ever will be.

Unfortunately, most of the assumptions underlying Haramura and Katto's (1983) theory have not been borne out in experiments and some are implausible. Their q_{max} formulas, of course, still take the form of equations (3) and (7), and are in reasonable agreement with the data to which they have been shaped. Indeed, the data with which they compare their flow boiling theory are largely ones that have been strongly influenced by gravity, while their theory takes no account of gravity.

Still, their ideas have a potential value that should not be shrugged off. The notion that the Helmholtz instability might actually occur in the feeder structure instead of in the jets themselves could well be the key to bringing a muted surface influence into equation (3). Indeed, elements of this notion are at the root of the hydrodynamic theory of Liaw–Dhir (1987b) for vertical plates.

Conclusion

The horizontal cylinder geometry has provided the most complete set of burnout data and burnout-related data of any configuration. Leaving questions of practical application aside for a moment, if we seek only to understand and elaborate the hydrodynamic theory, it is the test configuration to which we should look. For example, when Bhattacharya and Lienhard (1972) sought to check the validity of hydrodynamic mechanisms by observing them in high current density electrolysis on cylinders, they succeeded because burnout was well understood in this geometry. Still it is obvious that we must also look to other configurations since they might well expose effects that cylinders do not make evident.

We have demonstrated the power of the hydrodynamic theory when it is applied to boiling with all kinds of systemic variation in this geometry. But we have also made a plea that investigators retain both their critical logic and their flexibility of mind when they use it. Like most theories it is still incomplete.

The field of boiling has suffered because we have been lax in carrying out the great debates that have characterized other sciences. Ideas have been accepted too lightly or rejected out of prejudice. We have been too quick to judge a theory by whether or not it yields a formula that works—not by whether it represents reality accurately. As a consequence, too many of our formulas themselves ultimately prove to be unreliable. This situation is presently being severely aggravated by funding agency pressures to look at problems only if their applicability is immediate.

But whether the hydrodynamic theory survives intact or undergoes radical modification, it—in combination with one well-defined geometry—has taken our fundamental understanding of burnout very far indeed.

Acknowledgments

I am very grateful to R. Eichhorn, R. P. Reddy, P. Sadasivan, E. K. Ungar, and the conscientious anonymous reviewer, for critical readings of this manuscript and for their advice.

References

Addoms, J. N., 1948, "Heat Transfer at High Rates to Water Boiling Outside Cylinders," D.Sc. Thesis, Mech. Engr. Dept., MIT, Cambridge, MA.

Bakhru, N., and Lienhard, J. H., 1972, "Boiling From Small Cylinders," *Int. J. Heat Mass Transfer*, Vol. 15, pp. 2011–2025.

Berenson, P. J., 1960, "Transition Boiling From a Horizontal Surface," MIT Heat Transfer Lab. Tech. Report. No. 17, Mar.

Bhattacharya, A., and Lienhard, J. H., 1972, "Hydrodynamic Transition in Electrolysis," ASME *Journal of Basic Engineering*, Vol. 94, No. 4, pp. 804–810.

Bobrovich, G. I., Gogonin, I. I., and Kutataladze, S. S., 1964, "Influence of Size of Heater Surface on the Peak Pooling Boiling Heat Flux," *Jour. Appl. Mech. and Tech., Phys.*, No. 4, pp. 137–138.

Bonilla, C. F., and Perry, C. W., 1941, "Heat Transmission to Binary Liquid Mixtures," *Trans. AIChE*, Vol. 37, p. 685.

Broussard, R. A., and Westwater, J. W., 1984, "Boiling Heat Transfer of Freon 113 Flowing Normal to a Tube: Effect of Tube Diameter," 19th AIAA Thermophys. Conf., June 25–28, Snowmass, CO.

Carne, M., 1964a, "Studies of the Critical Heat Flux for Some Binary Mixtures and Their Components," *Can. J. Chem. Engr.*, Vol. 41, pp. 235–241.

Carne, M., 1964b, "Some Effects of Test Section Geometry, in Saturated Pool Boiling, on the Critical Heat Flux for Some Organic Liquids and Their Mixtures," AIChE Preprint No. 6, ASME/AIChE Heat Transfer Conf., Cleveland, OH, Aug.

Cichelli, M. T., and Bonilla, C. F., 1945, "Heat Transfer to Liquids Boiling Under Pressure," *Trans. AIChE*, Vol. 41, p. 755.

Cochran, T. H., and Andracchio, C. R., 1964, "Forced Convection Peak Heat Flux on Cylindrical Heaters in Water and Refrigerant 113," NASA D-7553, Feb.

Ded, J., and Lienhard, J. H., 1972, "The Peak Pool Boiling Heat Flux From a Sphere," *AIChE J.*, Vol. 18, No. 2, pp. 337–342.

Dhir, V. K., and Lienhard, J. H., 1973, "Taylor Stabilitiy of Viscous Fluids and Applications to Film Boiling," *Int. J. Heat Mass Transfer*, Vol. 16, pp. 2097–2109.

Dhir, V. K., and Lienhard, J. H., 1974, "Peak Pool Boiling Heat Flux in Viscous Liquids," ASME JOURNAL OF HEAT TRANSFER, Vol. 96, No. 1, pp. 71–78.

Drew, T. B., and Mueller, C., 1937, "Boiling," *Trans. AIChE*, Vol. 33, p. 449.

Edwards, D. K., 1954, "The Role of Interphase Mass Transfer in the Mechanism of Nucleate Boiling," Master's Thesis, Mech. Engr. Dept., University of California, Berkeley, CA.

Elkassabgi, Y., and Lienhard, J. H., 1987, "Sidewall and Immersion-Depth Effects on Pool Boiling Burnout for Horizontal Cylindrical Heaters," ASME JOURNAL OF HEAT TRANSFER, Vol. 109, No. 4, pp. 1055–1057.

Elkassabgi, Y., and Lienhard, J. H., 1988, "The Peak Pool Boiling Heat Flux From Horizontal Cylinders in Subcooled Liquids," ASME JOURNAL OF HEAT TRANSFER, Vol. 110, No. 2, pp. 479–486.

Farber, E. A., and Scorah, R. L., 1948, "Heat Transfer to Water Boiling Under Pressure," *Trans. ASME*, Vol. 70, pp. 369–384.

Fritz, W., 1937, "Maximum Volume of Vapor Bubbles," *Z. für Physik*, Vol. 36, pp. 379–384.

Gambill, W. R., and Lienhard, J. H., 1986, "An Upper Bound for the Boiling Heat Flux," ASME-JSME Thermal Engineering Joint Conference, Honolulu, HI, Mar. 22–27.

Haggerty, W. W., and Shea, I. F., 1955, "A Study of the Stability of Plane Fluid Sheets," ASME *Journal of Applied Mechanics*, Vol. 22, pp. 509–514.

Haramura, Y., and Katto, Y., 1983, "A New Hydrodynamic Model of Critical Heat Flux, Applicable Widely to Both Pool and Forced Convection Boiling on Submerged Bodies in Saturated Liquids," *Int. J. Heat Mass Transfer*, Vol. 26, No. 3, pp. 389–399.

Hasan, M. Z., Hasan, M. M., Eichhorn, R., and Lienhard, J. H., 1981, "Boiling Burnout During Crossflow Over Cylinders, Beyond the Influence of Gravity," ASME JOURNAL OF HEAT TRANSFER, Vol. 103, No. 3, pp. 478–484.

Ivey, H. J., and Morris, D. J., 1962, "On the Relevance of the Vapour-Liquid Exchange Mechanism for Sub-cooled Boiling Heat Transfer at High Pressure," UKAEA Report No. AEEW-R 137.

Ivey, H. J., and Morris, D. J., 1966, "Critical Heat Flux of Saturation and Subcooled Pool Boiling in Water at Atmospheric Pressure," *Proc. 3rd Int. Heat Transfer Conf.*, Vol. III, Chicago, IL, Aug. 10, pp. 129–142.

Kheyrandish, K., and Lienhard, J. H., 1985, "Mechanisms of Burnout in Saturated and Subcooled Flow Boiling Over a Horizontal Cylinder," AIChE/ASME Nat'l. Heat Transfer Conf., Denver, CO, Aug. 4–7.

Kheyrandish, K., 1988, Doctoral work in progress, University of Houston, Houston, TX.

Kuhn, T. S., 1962, *The Structure of Scientific Revolution*, The University of Chicago, Chicago, IL (see 2nd ed., 1970).

Kutateladze, S. S., 1948, "On the Transition to Film Boiling Under Natural Convection," *Kotloturbostroenie*, No. 3, p. 10.

Kutateladze, S. S., 1951, "Hydrodynamic Theory of Changes in the Boiling Process Under Free Convection Conditions," *Isv. Akad. Nauk. SSSR, Otd. Tekh. Nauk.*, No. 4, p. 529.

Kutateladze, S. S., 1952, *Teploperedacha pri Kondensatsii i Kipenii*, State Sci.

Downloaded 16 Dec 2010 to 193.140.21.150. Redistribution subject to ASME license or copyright; see http://www.asme.org/terms/Terms_Use.cfm

and Tech. Pubs. of Lit. on Mach., Moscow (also published in English as *Heat Transfer in Condensation and Boiling*, 2nd ed., AEC-tr-3770, Phys. and Math., 1959.)

Kutateladze, S. S., and Schneiderman, L. L., 1953, "Experimental Study of Influence of Temperature of Liquid on Change in the Rate of Boiling," USAEC Rept, AEC tr. 3405, pp. 95–100.

Kutateladze, S. S., Bobrovich, G. I., Gogonin, I. I., Mamontova, N. N., and Moskvichova, V. N., 1966, "The Critical Heat Flux at the Pool Boiling of Some Binary Liquid Mixtures," *Proc. 3rd Int. Heat Transfer Conf.*, Chicago, IL, Vol. 3, pp. 149–159.

Leppert, G., and Pitts, C. C., 1964, "Boiling," *Advances in Heat Transfer*, T. F. Irvine, Jr. and J. P. Hartnett, eds., Vol. 1, Academic Press, New York.

Liaw, S. P., and Dhir, V. K., 1987a, "Void Fraction Measurements During Saturated Pool Boiling of Water on Partially Wetted Vertical Surfaces," *Radiation Phase-Change Heat Transfer and Thermal Systems*, ASME HTD-Vol. 81, pp. 103–110.

Liaw, S. P., and Dhir, V. K., 1987b, "Framework for a Unified Model for Nucleate and Transition Pool Boiling," *Radiation Phase-Change Heat Transfer and Thermal Systems*, ASME HTD-Vol. 81, pp. 51–58.

Lienhard, J. H., and Wong, P. T. Y., 1964, "The Dominant Unstable Wavelength and Minimum Heat Flux During Film Boiling on a Horizontal Cylinder," ASME JOURNAL OF HEAT TRANSFER, Vol. 86, No. 1, pp. 220–226.

Lienhard, J. H., and Watanabe, K., 1966, "On Correlating the Peak and Minimum Boiling Heat Fluxes with Pressure and Heater Configuration," ASME JOURNAL OF HEAT TRANSFER, Vol. 88, No. 1, pp. 94–100.

Lienhard, J. H., and Dhir, V. K., 1973a, "Extended Hydrodynamic Theory of the Peak and Minimum Pool Boiling Heat Fluxes," NASA CR-2270, July.

Lienhard, J. H., and Dhir, V. K., 1973b, "Hydrodynamic Prediction of Peak Pool-Boiling Heat Fluxes From Finite Bodies," ASME JOURNAL OF HEAT TRANSFER, Vol. 95, No. 2, pp. 152–158.

Lienhard, J. H., and Eichhorn, R., 1976, "Peak Boiling Heat Flux on Cylinders in a Crossflow," *Int. J. Heat Mass Transfer*, Vol. 19, pp. 1135–1142.

Lienhard, J. H., and Eichhorn, R., 1979, "On Predicting Boiling Burnout for Heaters Cooled by Liquid Jets," *Int. J. Heat Mass Transfer*, Vol. 22, pp. 774–776.

Lienhard, J. H., and Hasan, M. M., 1979, "On Predicting Boiling Burnout With the Mechanical Energy Stability Criterion," ASME JOURNAL OF HEAT TRANSFER, Vol. 101, No. 2, pp. 276–279.

Lienhard, J. H., and Witte, L. C., 1985, "An Historical Review of the Hydrodynamic Theory of Boiling," *Chem. Engr. Revs.*, Vol. 3, Nos. 3 and 4, pp. 187–280.

Lienhard, J. H., 1987, *A Heat Transfer Textbook*, 2nd ed., Prentice-Hall Inc., Englewood Cliffs, NJ.

McEligot, D. M., 1964, "Generalized Peak Heat Flux for Dilute Binary Mixtures," *AIChE J.*, Vol. 10, No. 1, pp. 130–131.

McKee, H. R., and Bell, K. J., 1969, "Forced Convection Boiling From a Cylinder Normal to the Flow," *Chem. Engr. Symposium Series*, Vol. 92, No. 65, pp. 222–230.

Min, T. K., 1975, Master's Thesis, Mech. Engr. Dept., Univ. of Kentucky, Lexington, KY.

Nukiyama, S., 1934, "The Maximum and Minimum Values of the Heat Q Transmitted From Metal to Boiling Water under Atmospheric Pressure" (tr. by C. J. Lee from *J. Jap. Soc. Mech. Engr.*, Vol. 37, 1934, pp. 367–374), *Int. J. Heat Mass Transfer*, Vol. 9, 1966, pp. 1419–1433.

Ornatskii, A. P., and Vinyarskii, L. S., 1965, "Heat Transfer Crisis in a Forced Flow of Underheated [Subcooled] Water in Small-Bore Tubes," *High Temp.*, Vol. 3, No. 3, pp. 400–406.

Pilling, N. B., and Lynch, T. D., 1920, "Cooling Properties of Technical Liquids," *Trans. Am. Inst. of Mining and Met. Engrs.*, Vol. 62, pp. 665–688.

Pramuk, F. S., and Westwater, J. W., 1956, "Effect of Agitation on the Critical Temperature Difference for a Boiling Liquid," *Chem. Engr. Symp. Series*, Vol. 52, No. 18, pp. 79–83.

Reddy, R., 1987, "The Critical Heat Flux in Binary Mixtures of Water and Ethanol," M.S. Thesis, Mech. Engr. Dept., Univ. of Houston, Houston, TX.

Reddy, R., and Lienhard, J. H., 1988, "The Peak Boiling Heat Flux in Saturated Ethanol–Water Mixtures," ASME/AIChE Heat Transfer Conference, Houston, TX, July.

Snyder, N. W., and Robin, T. T., 1968, "Mass-Transfer Model in Subcooled Nucleate Boiling," ASME Paper No. 68-HT-51.

Ramilison, J. M., and Lienhard, J. H., 1987, "Transition Boiling and the Correlation of Ransition-Film Boiling," ASME JOURNAL OF HEAT TRANSFER, Vol. 109, No. 3, pp. 746–752.

Sadasivan, P., 1986, "Gravity Influences on Boiling Burnout During Flow Across Cylinders," M.S. Thesis, Mech. Engr. Dept., University of Houston, Houston, TX.

Sadasivan, P., and Lienhard, J. H., 1987, "Burnout of Cylinders in Flow Boiling: the Role of Gravity Influences on the Vapor Plume," ASME/AIChE Heat Transfer Conference, Pittsburgh, PA.

Schrage, R. W., 1953, *Interphase Mass Transfer*, Columbia University Press, New York, Chapt. II.

Sharan, A., and Lienhard, J. H., 1985, "On Predicting Burnout in the Jet-Disc Configuration," ASME JOURNAL OF HEAT TRANSFER, Vol. 107, No. 2, pp. 398–401.

Shock, R. A. W., 1977, "Nucleate Boiling in Binary Mixtures," *Int. J. Heat Mass Transfer*, Vol. 20, pp. 701–709.

Sun, K. H., and Lienhard, J. H., 1970, "The Peak Pool Boiling Heat Flux on Horizontal Cylinders," *Int. J. Heat Mass Transfer*, Vol. 13, pp. 1425–1439.

Thome, J. R., 1983, "Prediction of Binary Mixture Boiling Heat Transfer Coefficients Using only Phase Equilibrium Data," *Int. J. Heat Mass Transfer*, Vol. 26, No. 7, pp. 965–974.

Thome, J. R., and Shock, R. A. W., 1984, "Boiling of Multicomponent Liquid Mixtures," *Advances in Heat Transfer*, Vol. 106, pp. 59–156.

Ungar, E. K., 1987, "Saturated Pool and Flow Boiling From Horizontal Cylinders," Doctoral Dissertation, Mech. Engr. Dept., University of Houston, Houston, TX.

Ungar, E. K., and Eichhorn, R., 1988, "A New Hydrodynamic Prediction of the Peak Heat Flux From Horizontal Cylinders in Low Speed Upflow," ASME/AIChE Heat Transfer Conference, Houston, TX, July.

Van Stralen, S. J. D., 1959, "Heat Transfer to Boiling Binary Liquid Mixtures," *Br. Chem. J.*; Part I, Vol. 4, pp. 8–17; Part II, Vol. 4, pp. 78–82; Part III, Vol. 6, pp. 834–840; Part IV, Vol. 7, pp. 90–97.

Vliet, G. C., and Leppert, G., 1964, "Critical Heat Flux for Nearly Saturated Water Flowing Normal to a Cylinder," ASME JOURNAL OF HEAT TRANSFER, Vol. 86, No. 1, pp. 59–67.

Weatherhead, R. T., 1955, "Boiling Burnout Heat Flux for Wires in Water Crossflow at Atmospheric Pressure," Report NDA-9 (Boiling Burnout Progress Report No. 5).

Westwater, J. W., and Santangelo, J. G., 1955, "Photographic Study of Boiling," *Ind. Engr. Chem.*, Vol. 47, pp. 1605–1610.

Yang, Y. M., 1987, "An Estimation of Pool Boiling Critical Hear Flux for Binary Mixtures," *Proc 2nd ASME/JSME Joint Thermal Engr. Conf.*, Honolulu, Vol. 5, pp. 439–446.

Yilmaz, S., and Westwater, J. W., 1980, "Effect of Velocity on Heat Transfer to Boiling Freon-113," ASME JOURNAL OF HEAT TRANSFER, Vol. 102, No. 1, pp. 26–31.

Zuber, N., 1959, "Hydrodynamic Aspects of Boiling Heat Transfer," Ph.D. thesis, UCLA, Los Angeles, CA (also available as AECU-4439 Physics and Mathematics).

Zuber, N., Tribus, M., and Westwater, J. W., 1963, "The Hydrodynanic Crisis in Pool Boiling of Saturated and Subcooled Liquids," *International Developments in Heat Transfer*, ASME, New York, No. 27, pp. 230–236.

Downloaded 16 Dec 2010 to 193.140.21.150. Redistribution subject to ASME license or copyright; see http://www.asme.org/terms/Terms_Use.cfm

An Evaluation of Film Condensation on Horizontal Integral-Fin Tubes

P. J. Marto
Department of Mechanical Engineering,
Naval Postgraduate School,
Monterey, CA 93943
Fellow ASME

This paper reviews nearly fifty years of progress that has been made in our understanding of film condensation on horizontal, integral-fin tubes. Both experimental and theoretical developments pertaining to single tubes and tube bundles are discussed. Special attention is given to the importance of surface tension, and appropriate research directions are provided.

Introduction

Low-profile integral-fin tubes have been used in heat exchangers since the early 1940s when it was discovered that such tubes could be manufactured at reasonable cost while providing a significant increase in the rate of heat transfer per unit length of tube in liquid-to-liquid heat exchangers. It was not long thereafter that integral fins were shown to be effective in condensing applications (Armstrong, 1945; Katz et al., 1945, 1947). Since then, they have been used commonly in surface condensers in the refrigeration and process industries with low surface tension liquids.

At first, fin shapes, dimensions, and spacings were limited by manufacturing techniques, and the primary concern was to increase the surface area. The effect of surface tension forces on the condensate film near the tips of the fins was completely neglected until addressed by Gregorig (1954) for vertical fluted tubes. His work stimulated research in the effective utilization of surface tension forces to thin the condensate film at the tips of the flutes or fins and enhance the condensation heat transfer process. However, with horizontal tubes, Katz et al. (1946) found that surface tension forces can also cause condensate "holdup," "retention," or "flooding" between fins, thereby reducing the effective surface area for condensation, and decreasing the heat transfer. For this reason, tubes with low fin densities were generally used.

In the decade following the world-wide energy crisis of 1973–74, an emphasis to design and manufacture more effective, more compact, and perhaps cheaper heat exchangers occurred. As a result, the need and benefits of enhancing shell-side condensation received considerable attention (Webb, 1981; Marto and Nunn, 1983; Marto, 1984; Webb et al., 1984). Numerous condensation enhancement schemes have since been explored (Cooper and Rose, 1981; Marto, 1986; Renz, 1986) but the use of integral-fin tubes remains the most common. Today, integral-fin tubes are available from many manufacturers in a variety of materials including aluminum, copper and its alloys, stainless steel, and titanium. Fin densities vary from about 350 to 1600 fins per meter (fpm). In addition, more advanced surface structures (e.g., Hitachi Thermoexcel-C, Wolverine Turbo-C) have been introduced to take advantage of the ability of three-dimensional fin geometries to provide even thinner condensate films (Arai et al., 1977).

With these significant developments, it is somewhat surprising to discover that there remains, at present, no generalized, yet simple, design method to predict accurately the thermal performance of surface condensers operating with a bundle of horizontal finned tubes in a given vapor/liquid environment. Important questions remain to be answered. For example, what fin shape, size, and spacing will yield maximum heat transfer for a given vapor, tube wall, and coolant combination? Or, what is the best tube when consideration is given to condensate inundation, vapor velocity, and the tube bundle layout? The results of very recent experimental and theoretical research programs around the world have provided significant new insight toward understanding all the complex phenomena that occur in this two-phase heat transfer situation, but more research must still be done.

The purpose of this paper is to provide a critical review of the published literature on film condensation of pure vapors on horizontal, integral-fin tubes. It follows the development of this subject from the inception of the integral-fin tube nearly fifty years ago to our current understanding. It focuses on horizontal tubes, but the phenomena reviewed, in which the use of surface tension forces is stressed, may be useful for other surface orientations (e.g., downward-facing surfaces as investigated by Honda et al. (1986) and Hijikata et al. (1987)). The author hopes that the paper will provide a source of useful information to engineers and researchers alike so that, in the future, improved surface condenser designs for various applications may be a reality.

Single Tubes in Quiescent Vapor

Condensate Flooding

Experimental Results. It is well known that when a horizontal finned tube comes in contact with a highly wetting liquid (i.e., a liquid having a contact angle equal to, or very near, zero), surface tension forces will cause the liquid to be retained between fins on the bottom portion of the tube. This phenomenon is known as liquid "holdup," "retention," or "flooding," and was first investigated by Katz et al. (1946), who measured static (i.e., no condensation occurring) liquid retention of several test fluids on various integral-fin tubes having different fin densities. They found that as much as 100 percent of the tube circumference could be flooded by the retained liquid. Rudy and Webb (1981) made condensate retention measurements on finned tubes having three different fin densities (748, 1024, and 1378 fins per meter) and a "spine-fin" tube using R-11, *n*-pentane, and water under static and dynamic (i.e., during condensation) conditions. They found, for example, that for the 1024 fins-per-meter tube, R-11, *n*-pentane, and water flooded 26, 42, and 100 percent of the tube circumference, respectively. Further, they observed that condensate flooding under dynamic conditions was not significantly different than under static conditions. Honda et al. (1983) reported measurements with methanol and R-113 using three integral-fin tubes (1020, 1562, and 2000 fins per meter) and a "saw-tooth" fin (Thermoexcel-C) tube under dynamic conditions. For the 2000-fin-per-meter tube, measurements were made under both static and dynamic con-

Contributed by the Heat Transfer Division for publication in the JOURNAL OF HEAT TRANSFER. Manuscript received by the Heat Transfer Division March 10, 1988. Keywords: Condensation, Finned Surfaces, Reviews.

Copyright © 1988 by ASME

Downloaded 16 Dec 2010 to 193.140.21.150. Redistribution subject to ASME license or copyright; see http://www.asme.org/terms/Terms_Use.cfm

ditions. The flooding level was almost the same for both conditions, and they observed that the condensate film between fins increased rather abruptly at a circumferential position around the tube below which the interfin spaces were completely flooded with condensate. Yau et al. (1984) made measurements under simulated condensation conditions. (Liquid from a cloth suspended above the test tube was drained uniformly onto the test tube so that the entire tube was wetted). They tested a family of 13 specially machined, rectangular-fin tubes with water, ethylene glycol, and R-113. Their data were in good agreement with the previously mentioned measurements.

Very recently, this flooding phenomenon has been carefully studied by Masuda and Rose (1987). By observing static liquid retention on finned tubes, they discovered that the liquid is not only retained on the bottom portion of the tube, but also on the upper portion in the form of a small liquid "wedge" between the flanks of the fins and the tube surface in the interfin space. This is depicted schematically in Fig. 1(*a*), which shows the retained liquid (shaded area) between trapezoidal-shape fins. The radius of curvature of the liquid "wedge" varies with position around the tube and has been written by Masuda and Rose (1987) as

$$r = \sigma/\rho g z \tag{1}$$

where z is the vertical distance from the bottom of the tube to a point on the tube surface in the interfin space. As a result, the intersection of the liquid and the tube surface forms a curve resembling a parabola. Similar retained-liquid profiles have been observed by Marto et al. (1987) during condensation of steam on wire-wrapped smooth tubes. Figures 1(*b*) and 1(*c*) show radial sections of the liquid profiles between fins at various circumferential positions, comparing the behavior with closely spaced fins ($b<2h$, Fig. 1(*b*)) to widely spaced fins ($b>2h$, Fig. 1(*c*)). In the former case, the liquid "wedges" from each of the fin flanks meet at the center of the interfin space prior to reaching the top of the fin (Fig. 1(*b*)(2)), whereas in the latter case, the "wedges" reach the top of the fin before they meet (Fig. 1(*c*)(2)). Masuda and Rose (1987) therefore proposed four flooding conditions (Fig. 1(*b*)(2), Fig. 1(*b*)(3), Fig. 1(*c*)(2), and Fig. 1(*c*)(3)) and defined a flooding angle ϕ_f for each of these situations as the angle measured from the top of the tube to the position where each of the above-mentioned conditions occurs. The most common definition of flooding is represented in Fig. 1(*b*)(3). At this point, the entire fin flank is wetted with liquid and the contact angle at the fin tip is zero. Farther around the tube,

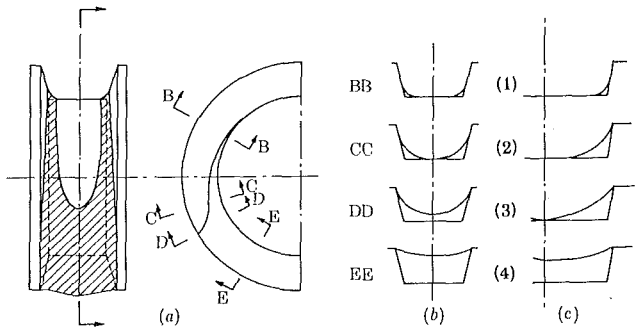

Fig. 1 Liquid retention on a finned tube (Masuda and Rose, 1987)

Nomenclature

a = coefficient defined in equation (6)
a_1 = coefficient defined in equation (8)
A_{ef} = effective finned-tube surface area $= \eta_f A_f + A_u$
A_f = surface area of fins
A_u = surface area of interfin tube space
A_s = surface area defined in equation (23)
b = fin spacing
b_b = fin spacing at base of fins
b_c = critical fin spacing such that the tube is just fully flooded by retained condensate
C_{BK} = coefficient defined in equation (10)
C_N = correction factor due to condensate inundation on finned tubes
D_{eq} = equivalent diameter defined in equation (11)
D_o = diameter to the outside of the fin tips
D_r = diameter to the fin roots
f = proportion of surface area covered with falling condensate
f_f = proportion of rectangular fin flanks blanked by retained liquid, defined in equation (4)
f_t = proportion of interfin tube surface of rectangular fin tube blanked by retained liquid, defined in equation (5)
f_x = x component of normalized gravity
F = factor defined in equation (36)
Fr = Froude number $= U^2/gD_0$
g = gravitational acceleration
G = mass flow rate in half of a fin channel
h = fin height
h_{fg} = specific enthalpy of vaporization
H = factor defined in equation (21)
k = thermal conductivity
K = permeability of porous strip
L = length of condensing tube
$\bar{L}$ = effective condensing length on the side of a fin, defined in equation (12)
m = factor defined in equation (20)
n, N = number of tubes in a vertical column
Nu = Nusselt number
p = pressure
q = heat flux
r = radius of curvature of condensate
r_b = radius of curvature of condensate at the bottom of a fin
r_t = radius of curvature of condensate at the top of a fin
R_o = radius to the outside of the fin tips
R_r = radius to the fin roots
s = distance along the condensate surface
s = inundation exponent defined in equation (37)
S_m = maximum length of the convex condensate surface along a fin
S_T = total length of the condensate surface from the fin tip to the center of the drainage channel
t = fin thickness
t_b = thickness of fin base
t_p = thickness of porous drainage strip
T_c = temperature of the coolant
T_s = vapor saturation temperature
T_w = wall temperature
T_{wo} = wall temperature at the base of the fins
$\bar{T}_{wo}$ = average wall temperature at the base of the fins
ΔT = temperature difference $= (T_s - T_w)$
U = vapor velocity
v = average velocity of condensate in a porous drainage strip
x = distance from the fin tip
x = vertical distance along a porous drainage strip
x_1 = overflow point on a porous drainage strip

Downloaded 16 Dec 2010 to 193.140.21.150. Redistribution subject to ASME license or copyright; see http://www.asme.org/terms/Terms_Use.cfm

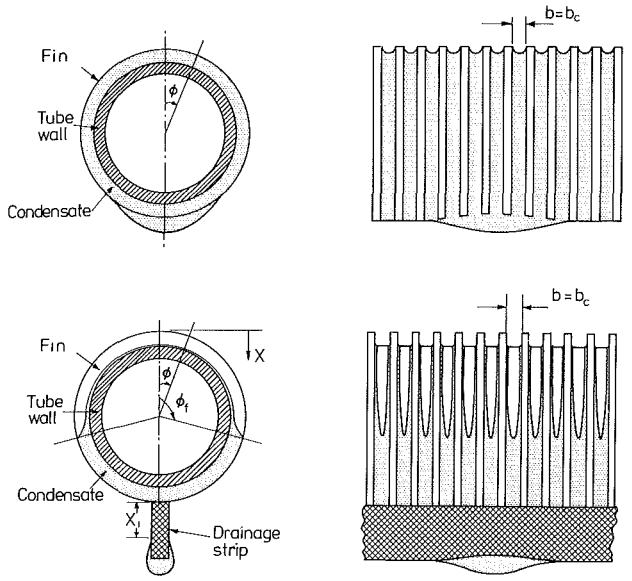

Fig. 2 Liquid retention on finned tubes: (*a*) a "just fully flooded" tube; (*b*) case (*a*) with a porous drainage strip

the liquid fills up the interfin space more and more and the contact angle at the fin tip increases. Figure 2(a) depicts the special case of a finned tube with rectangular-shape fins where the spacing between fins b is equal to a critical value b_c such that the tube is just fully flooded (i.e., $\phi_f = 0$). In this unique situation, the entire fin flank around the tube is covered with liquid and the radius of curvature of the liquid–vapor interface at the very top of the tube is equal to half the fin spacing $b_c/2$. This radius of curvature continues to increase around the tube until it approaches infinity at the very bottom of the tube (except in the region near a departing droplet).

As investigated by Honda et al. (1983), Honda and Nozu (1985), Yau et al. (1984), and Marto et al. (1988b), it is possible to reduce the amount of flooding significantly by using longitudinal condensate drainage strips placed at the very bottom of the tube. Figure 2(b) depicts the case of the fully flooded tube shown in Fig. 2(a) but with a porous drainage strip in place. The porous drainage strip creates a low-pressure region at the bottom of the tube, pulling the condensate into its pores. This principle is commonly used in heat pipe wicks (Chi, 1976; Dunn and Reay, 1982). The liquid is pulled down off the tube, exposing portions of the fin flanks and the interfin spaces. Notice, however, that a liquid "wedge" persists at the base of the fins to the top of the tube. If enough suction can be created at the base of the tube, it is possible to pull the condensate completely off (except for the "wedges" at the root of the fins) the tube. This would create a dramatic improvement in heat transfer. Yau et al. (1984), using solid drainage strips with two different finned tubes (fin spacings of 1.5 and 2.0 mm), found that the flooding angle ϕ_f was increased for R-113, ethylene gylcol, and water by about 10, 20, and 40 percent, respectively. Honda et al. (1983), using porous drainage strips of large porosity (0.8 mm effective pore diameter) with three finned tubes (fin spacings of 0.4, 0.5, and 0.7 mm), found that the flooding angle was increased for R-113 from 8 to 22 percent and for methanol from 13 to 61

Nomenclature (cont.)

x_b = distance from the fin tip to the end of the condensate thin film region
z = vertical distance from the bottom of the tube to a point on the tube surface in the interfin space
Z = dimensionless thickness of condensate in the channel = Δ/h
Z_b = dimensionless thickness of condensate defined in equation (19)
α_b = heat transfer coefficient in flooded region of a finned tube
α_f = heat transfer coefficient along the fin surface
α_u = heat transfer coefficient on the unfinned surface
α_{BK} = average heat transfer coefficient of the Beatty and Katz (1948) model, equation (9)
α_{HN} = average heat transfer coefficient of the Honda and Nozu (1987) model, equation (33)
α_{KB} = average heat transfer coefficient of the Karkhu and Borovkov (1971) model, equation (22)
α_O = average heat transfer coefficient of the Owen et al. (1983) model, equation (27)
α_{RW} = average heat transfer coefficient of the Rudy and Webb (1981) model, equation (24)
α_W = average heat transfer coefficient of the Webb et al. (1985) model, equation (28)
$\bar{\alpha}$ = measured average heat transfer coefficient
$\bar{\alpha}_1$ = measured average heat transfer coefficient for the first tube in a vertical column
$\bar{\alpha}_N$ = measured average heat transfer coefficient for N tubes in a vertical column
$\bar{\alpha}_o$ = measured average heat transfer coefficient of a smooth tube, or of a finned tube at zero velocity
$\bar{\alpha}_o$ = average heat transfer coefficient for a smooth tube as predicted by Nusselt theory
δ = condensate film thickness along a fin
Δ = condensate film thickness in the interfin space
ϵ = angle shown in Fig. 15
ϵ_A = finned tube to smooth tube area ratio
ϵ_q = heat transfer enhancement ratio, defined as the ratio of the finned tube vapor-side coefficient to smooth tube value at the same heat flux and based upon the smooth tube surface area of diameter D_r
$\epsilon_{\Delta T}$ = heat transfer enhancement ratio, defined as the ratio of finned tube vapor-side coefficient to smooth tube value at the same vapor-to-wall temperature difference and based upon the smooth tube surface area of diameter D_r
Γ = flow rate of falling condensate per unit length for one side of a tube
λ = Taylor instability wavelength defined in equation (38)
κ = curvature of the condensate film
κ_o = curvature of the condensate film at the tip of the fin
ρ = density
σ = surface tension
ϕ = angle measured from the top of the tube
ϕ_f = flooding angle defined in equation (2)
θ = fin-tip half angle
θ_m = maximum rotation angle of the normal to the convex condensate surface
θ_T = total rotation angle of the normal to the convex condensate surface from the fin tip to the center of the condensate channel
η_f = fin efficiency
μ = dynamic viscosity
ν = kinematic viscosity
ξ = active area enhancement defined in equation (3)
ζ = condensate shape parameter defined in equation (8)

Downloaded 16 Dec 2010 to 193.140.21.150. Redistribution subject to ASME license or copyright; see http://www.asme.org/terms/Terms_Use.cfm

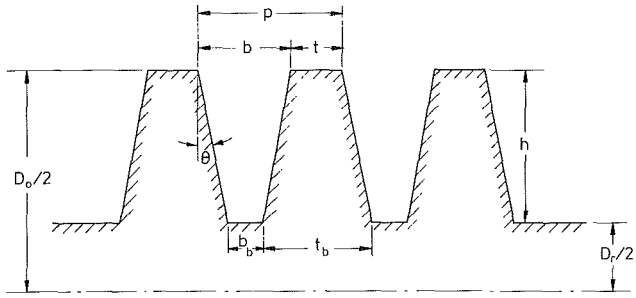

Fig. 3 Geometric variables of a finned tube

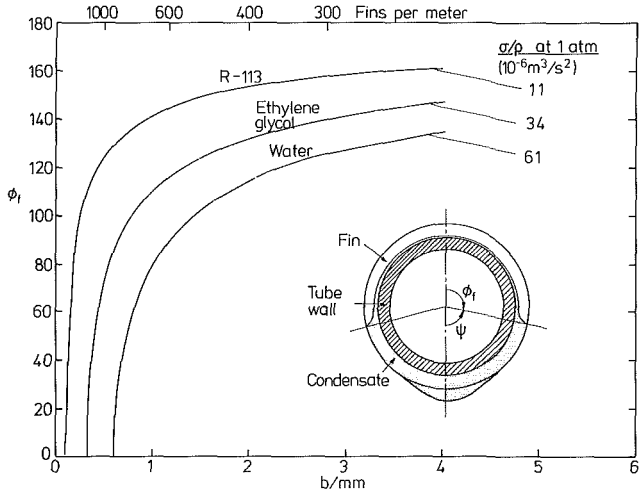

Fig. 4 Flooding angle versus fin spacing and σ/ρ

percent. The largest increases occurred for the tube with the smallest fin spacing. Marto et al. (1988b), using porous drainage strips of small porosity (about 0.05 mm effective pore diameter) with one finned tube (fin spacing of 0.5 mm), found that, with a strip height of 8 mm or more, water was pulled completely off the tube under static conditions.

Theoretical Results. Honda et al. (1983) made a theoretical analysis of the static meniscus between low, trapezoidal-shape fins (sketched in Fig. 3) using several assumptions about meniscus shape:

1 The meniscus is in contact with the fin tip and has a zero contact angle.

2 The radius of curvature of the liquid–vapor interface in the interfin space is much smaller in the longitudinal direction than in the circumferential direction.

3 The fin height h and the fin-tip spacing b are much smaller than the tube radius.

4 At the tube bottom, the radius of curvature of the liquid–vapor interface is infinite.

They arrived at the following approximate expression for the flooding angle ϕ_f for $h > b/2$

$$\phi_f = \cos^{-1}\left\{\left[\frac{2\sigma\cos\theta}{\rho g b R_o}\right] - 1\right\} \tag{2}$$

which compared very favorably with their own experimental data and the data of Katz et al. (1946) and Rudy and Webb (1981). A similar result was derived independently by Owen et al. (1983). Rudy and Webb (1983, 1985) developed a generalized model to predict condensate flooding on horizontal, integral-fin tubes based upon their observation that the vertical rise height of liquid between rectangular-shape fins is the same for a horizontal tube as it is for a vertical plate. Neglecting vapor shear effects, they made a static force balance on the liquid retained between adjacent fins of arbitrary shape, which included surface tension forces and gravity forces. For rectangular-shape fins (i.e., $\theta = 0$), their expression agrees identically with the result of Honda et al. (1983).

Equation (2) predicts that the flooding angle should decrease (i.e., more flooding should occur) with an increase in fin density and/or an increase in surface tension-to-density ratio. Equation (2) is plotted in Fig. 4 for a tube with an outside diameter of 21.05 mm and rectangular-shape fins of thickness 0.5 mm. Results are shown for R-113, ethylene glycol, and water. Notice that the tube is fully flooded (i.e., $\phi_f = 0$) at a critical fin spacing b_c equal to 0.6, 0.33, and 0.1 mm for water, ethylene glycol, and R-113, respectively. If a flooding angle of 90 deg is chosen arbitarily to be a desirable flooding condition, then equation (2) clearly shows that the chosen fin spacing for water, ethylene glycol, and R-113 should be about 1.2, 0.6, and 0.2 mm respectively.

Condensate flooding is obviously a very important phenomenon that must be treated properly when using horizontal finned tubes to enhance heat transfer. Masuda and Rose (1987) reasoned that the retained liquid on a finned tube is much thicker than condensate films that are controlled solely by gravity and viscosity, and therefore, the thermal resistance of the retained liquid during condensation is relatively large. In other words, those parts of the tube surface beneath retained liquid are essentially blanked off from heat transfer. This reasoning led them to the definition of active surface area, which is the bare tube surface area under static conditions. As seen from Fig. 1 (a), this active surface area includes all of the fin tips and that portion of the fin flanks and tube wall not covered by retained liquid. In selecting a finned tube for a given liquid, a design tradeoff exists. As the fin density is increased to create more total surface area, more liquid is retained on the tube, blanking off a larger portion of the surface for effective condensation. Thus, an optimum fin spacing must exist.

Masuda and Rose (1987) have defined an active surface area enhancement ξ as the *unblanked* area of a finned tube (i.e., the area of the fin tips together with the *unblanked* portions of the fin flanks and the interfin tube surface) divided by the area of a smooth tube of root diameter D_r. They showed that this ratio can be expressed as

$$\xi = \frac{\pi(D_r + 2h)t + \phi_f D_r b(1 - f_t) + 2h(D_r + h)\phi_f(1 - f_f)}{\pi D_r(b + t)} \tag{3}$$

where

$$f_f = \int_0^{\phi_f} rD_r d\phi/(\phi_f D_r h) \simeq (\sigma/\rho g R_r h)(\tan(\phi_f/2)/\phi_f) \tag{4}$$

$$f_t = 2\int_0^{\phi_f} rD_r d\phi/(\phi_f D_r b) \simeq (2\sigma/\rho g R_r b)(\tan(\phi_f/2)/\phi_f) \tag{5}$$

Figure 5 shows the calculated dependence of ξ on fin spacing for three fluids having different values of σ/ρ. (Note that the curves are cut off at the left when $\phi_f = 0$ and at the right when $b = 2h$.) These calculations were made for a finned tube (root diameter D_r equal to 12.7 mm) having rectangular-shape fins (height h equal to 1.59 mm and thickness t equal to 0.5 mm). The results show clearly that an optimum active surface area enhancement exists. In particular, the maximum surface area enhancements for water, ethylene glycol, and R-113 occur for spacings close to 1.5, and 1.0, and 0.5 mm, respectively.

Heat Transfer

Experimental Results. Table 1 is a chronological listing of pertinent references that provide experimental heat transfer data for horizontal finned tubes. In studying the table, several

Downloaded 16 Dec 2010 to 193.140.21.150. Redistribution subject to ASME license or copyright; see http://www.asme.org/terms/Terms_Use.cfm

Downloaded 16 Dec 2010 to 193.140.21.150. Redistribution subject to ASME license or copyright; see http://www.asme.org/terms/Terms_Use.cfm

Table 1 Chronological summary of experimental data

Year	Reference	Fluid	Absolute pressure	Test tubes		Technique used to determine $\bar{\alpha}$	Remarks
			kPa	Material	Geometry		
1945	Katz et al.	Steam	273	Copper	2 smooth and 18 commercial finned tubes (157 to 945 FPM)	Wilson (1915) plot	Possibility that dropwise conditions may have occurred in some runs.
1947	Katz et al.	R-12	788	Copper	1 smooth and 6 commercial finned tubes (151 to 630 FPM)	Wilson (1915) plot	Obtained heat transfer coefficients for both saturated and superheated vapor.
1948	Beatty and Katz	Methyl chloride Sulfur dioxide R-22 Propane n-Butane n-Pentane	720, 994 582 1200, 1819 1049 307, 582 135	Copper	1 smooth and 6 finned tubes (272 and 610 FPM)	Wilson (1915) plot	Correlated data using equivalent tube diameter made up of vertical fin surfaces and horizontal tube surfaces.
				Nickel	1 finned tube (257 FPM)		
1971	Karkhu and Borovkov	Steam R-113	111	Brass	3 special trapezoidal-fin tubes (782 and 1238 FPM)	Not available	Vapor-side heat transfer coefficients were 50–100 percent higher than for smooth tube.
				Copper	1 commercial finned tube (1190 FPM)		Heat transfer was about the same as for smooth tube.
1975	Mills et al.	Steam	6.4[a]	Copper Brass 70-30 Cu/Ni	1 special trapezoidal-fin tube (1420 FPM)	Wall temperature measurement using thick-wall tube	Downward vapor velocity 0.6 to 2.6 m/s. Heat transfer enhancements (over Nusselt) for Cu, Br and Cu/Ni (at $\Delta T = 9°C$) were 4.0, 3.6, 2.6.
1977	Arai et al.	R-12	Not available	Copper	1 commercial finned tube (748 FPM) and various, specially machined saw-tooth fin tubes (650 to 3000 FPM)	Not available	Found that most important geometric parameter was interval of grooves. The optimum groove pitch was determined to be 0.7 mm.
1978	Kisaragi et al.	R-113	Not available	Copper	1 smooth, 6 commercial finned, 6 special finned, and 3 porous coated tubes	Not available	Average coefficient measured for 8 tubes in vertical row. Porous-coated fin tube gave fourfold improvement over 748 FPM tube.
1980	Carnavos	R-11	148[a]	Copper	1 smooth and 11 enhanced geometry tubes	Overall resistance with calculated tube-side and wall resistances removed	Approach vapor velocity of 0.02 m/s. Heat transfer enhancements (over smooth tube at $\Delta T = 10°C$) were 2.9 to 4.0.
1980	Shekriladze and Rusishvili	Steam Ethyl alcohol	101	Stainless steel Steel 20 Copper	2000 and 3000 FPM 2000 and 3000 FPM 2000 and 3000 FPM	Not available	Compared data to previously determined analytical results and found qualitative agreement.
1981	Shklover et al.	Steam	22-16	Stainless steel	1 smooth, 3 threaded (1600, 2000 FPM), and 1 rolled tube (625 FPM)	Wall resistance included in $\bar{\alpha}$; overall resistance with tube-side resistance removed.	Finely finned stainless steel tubes did not exhibit a much better performance than smooth tubes.
1982	Sauer and Williams	R-11	Not available	Copper	1 smooth and 1 commercial finned tube (748 FPM)	Wall temperature measurement	Measured condensing heat transfer coefficients on finned tube were much less than predicted by Beatty and Katz correlation.
1982	Rudy	R-11	160	Copper	4 finned tubes (748, 1024, and 1378 FPM)	Wall temperature measurement	Data used to verify theoretical model.
1983 1985	Honda et al.	R-113 Methanol	101–151[a] 102–154[a]	Copper	1 smooth, 3 finned (1020, 1563, and 2000 FPM), and 1 saw-tooth fin tube (1389 FPM)	Wall temperature measurement	Heat transfer enhancement of finned tubes (over smooth tube at $\Delta T = 5°C$) were: 6–9 for R-113 and 5–6 for methanol.
					Used solid and porous drainage strips		Heat transfer augmentation increased with porous drainage strips.

Downloaded 16 Dec 2010 to 193.140.21.150. Redistribution subject to ASME license or copyright; see http://www.asme.org/terms/Terms_Use.cfm

Table 1 (continued)

1984	Kabov	R-12 R-21	572–1900[a] 521	Brass	1 finned tube (1333 FPM)	Not available	Systematically varied distance between fins. Fin spacing found to be very important parameter.
				Copper	8 finned tubes (385 to 1075 FPM)		
1984 1985 1986	Yau et al.	Steam	101	Copper	1 smooth tube and 13 specially machined, rectangular-fin tubes (50–100 FPM)	Overall resistance with calculated wall resistance and previously measured tube-side resistance removed	Heat transfer enhancement (over smooth tube at constant ΔT was found to be 3.6 at optimum fin spacing of 1.5 mm.
					Used solid drainage strips		Solid drainage strips increased heat transfer another 30 percent.
1984 1986	Wanniarachchi et al.	Steam	11.3 and 101	Copper	1 smooth tube and 6 specially machined, rectangular-fin tubes (95–667 FPM)	Overall resistance with calculated wall resistance and independently measured tube-side resistance removed. Results also obtained using modified Wilson plot technique (Nobbs, 1975)	Optimum fin spacing was 1.5 mm. At this spacing, heat transfer enhancements (over smooth tube at constant flux) were 5.2 and 3.6 for atmospheric and vacuum conditions.
1985	Masuda and Rose	R-113	101	Copper	1 smooth tube and 13 specially machined, rectangular-fin tubes (50–1000 FPM)	Modified Wilson plot technique (Nobbs, 1975)	Optimum fin spacing was 0.5 mm. For this tube, enhancement ratio (over smooth tube at constant ΔT) was 7.3.
1985	Wanniarachchi et al.	Steam	11.3 and 101	Copper	24 specially machined, rectangular-fin tubes (with various fin spacings, thicknesses, and heights)	Overall resistance with calculated wall resistance and independently measured tube-side resistance removed	Best fin spacing between 1.5 to 2.0 mm. Minor effect of thickness. Best performance with tall fins
1986	Mitrou	Steam	11.3 and 101	Copper Aluminum Cu/Ni Stainless steel	Various threaded tubes	Modified Wilson plot technique (Nobbs, 1975)	Tube wall thermal conductivity is very important.
1986	Marto, et al.	Steam	11.3 and 101	Copper	1 smooth tube and 4 specially machined, finned tubes having different fin shapes (500 FPM)	Modified Wilson plot technique (Nobbs, 1975)	Fin shape caused 10–15 percent change in heat transfer coefficient.
1988	Masuda and Rose	Ethylene glycol	101	Copper	1 smooth tube and 13 specially machined, rectangular-fin tubes (50–1000 FPM)	Modified Wilson plot technique (Nobbs, 1975)	Best fin spacing was 1.0 mm. For this tube, enhancement ratio (over smooth tube at constant ΔT) was 4.7.
1988	Marto et al.	R-113	101	Copper	1 smooth tube and 24 specially machined, rectangular-fin tubes (with various fin spacings, thicknesses, and heights)	Modified Wilson plot technique (Nobbs, 1975)	Best fin spacing between 0.2 to 0.5 mm. Heat transfer performance increased with thinner and taller fins.
1988	Sukhatme et al.	Steam	11.3 and 101	Copper	1 finned tube with rectangular-fins to which were attached various solid and porous drainage strips	Modified Wilson plot technique (Nobbs, 1975)	Heat transfer performance increased by as much as 65 percent using drainage strips.
1988	Sukhatme, et al.	R-11	150–250	Copper	1 smooth tube, 9 specially machined, trapezoidal-fin tubes (945–2205 FPM) and 3 specially enhanced tubes	Wall temperature measurement	Best integral-fin tube had 1417 FPM, a fin-tip half angle of 10 deg and a height of 1.22 mm. For this tube, enhancement ratio (over smooth tube at $\Delta T = 10°C$) about 9.0

[a]Pressure values estimated from measured saturation temperature.

interesting observations can be made. First, after the initial investigations in the mid-1940s, there was a 23 year gap in reported experimental findings. Apparently, the need for further work did not become evident until the energy crisis of 1973-74, and the recent surge in experimental results in the 1980s is remarkable. Second, finned tube technology has advanced considerably, exhibiting a trend toward higher fin densities and different shapes. In recent years, systematic investigations of various families of tubes have become common. Most of the data have been accumulated for copper tubes and various refrigerants, although recent data for other flluids, including steam, have become available.

Another important observation pertains to the difficulty in interpreting and using the results. In obtaining film condensation heat transfer data of pure vapors, there are numerous operational difficulties that can alter the accuracy of the experimental results. For example, the presence of noncondensing gases in the vicinity of the test tube, or partial dropwise condensing conditions on the surface of the tube, or a substantial local vapor velocity near the tube can influence the heat transfer significantly. Many of the investigations fail to provide information on the operational problems in obtaining the data and fail to quote resultant uncertainties in the measured results. Another very important issue pertains to the method of determining the average vapor-side heat transfer coefficient $\bar{\alpha}$. The original investigations used the Wilson (1915) plot technique. Others have used a direct measurement technique using wall temperature measurements. Still others have used modified versions of these two techniques. A comparison of these techniques was recently made by Wanniarachchi et al. (1986). In general, depending upon which technique is used, they found that there may be variations of 10 to 15 percent in the quoted vapor-side heat transfer coefficient. More confusion exists with the various results due to the choice of surface area used in calculating the results. For example, some investigators have chosen the fin "envelope" surface area (i.e., the surface area of a smooth tube of diameter equal to the outer diameter of the fins D_o). Others use the area of a smooth tube of fin root diameter D_r. Still others use the total surface area (equal to the fin area plus the tube surface area) or a total effective surface area, which corrects the fin surface area with a fin efficiency. Finally, heat transfer enhancements with relation to a smooth tube have been reported based either on constant heat flux or on constant vapor-to-wall surface temperature difference and, as shown by Masuda and Rose (1985) and Yau et al. (1986), these two definitions yield very different numerical results ($\epsilon_q = \epsilon_{\Delta T}^{4/3}$). As a result of these various inconsistencies, great care must be exercised in using published experimental data. A brief review of the important experimental findings is provided below.

Beatty and Katz (1948) measured condensing heat transfer coefficients for several low surface tension fluids on a commercially available, horizontal integral-fin copper tube having 610 fins per meter (about 16 fins per inch). The tube had a fin root diameter of 15.88 mm and a fin height of 1.46 mm. For R-22, data were also obtained for several special tubes of different fin heights and thermal conductivities. They used these data to arrive at a theoretically based correlation for the average heat transfer coefficient $\bar{\alpha}$, which is described later in the paper. Karkhu and Borovkov (1971) obtained data for R-113 and steam condensing on three different trapezoidal-shape finned tubes of brass and one trapezoidal-shape finned tube of copper in order to study the influence of surface tension forces on film flow and heat transfer. The tubes had a root diameter of 18 mm, and had either 782 or 1238 fins per meter. The brass tubes had a fin-tip thickness of 0.14 mm, a fin-base spacing of 0.14 mm, and a fin-tip half angle of between 10 and 30 deg. The copper tube had a fin-tip thickness of 0.64 mm, a fin-base spacing of 0.20 mm, and a fin-tip half angle of 17 deg. Measured heat transfer coefficients were between 50 and 100 percent higher than for a smooth tube. Kisaragi et al. (1977) condensed R-113 on copper low-fin and high-fin tubes containing 748, 1024, and 1378 fins per meter, as well as on several specially prepared, spiral-groove tubes and porous-coated, finned tubes. Defining the thermal conductance per unit length of tube as the heat transfer rate per unit temperature difference and per unit length, they reported a remarkable improvement of this conductance over the standard 748 fins-per-meter (i.e., 19 fins-per-inch) tube. In particular, they found that a twofold enhancement in the conductance is possible with the grooved tubes and a fourfold enhancement is possible with the porous-coated finned tubes, presumably due to the additional thinning of the condensate film that occurs near the fin tips of these special tubes. Carnavos (1980) measured condensing heat transfer coefficients for R-11 on eleven different augmented tubes and on a smooth tube. The augmented tubes included flat-sided finned surfaces, fluted surfaces, and knurled surfaces. Heat transfer enhancements (based upon the "envelope" outside surface area) over the smooth tube at the same condensing film temperature difference of 10 K were about 3–4. Rudy (1982) obtained data for R-11 condensing on four copper, integral-fin tubes. Three of the tubes were commercially available with 748, 1024, and 1378 fins per meter. The fourth tube was a 748 fin-per-meter tube machined down in diameter to reduce the fin height from 1.53 to 0.85 mm. Based upon the "envelope" outside surface area, the 1378 fin-per-meter showed a heat transfer coefficient 71 percent higher than the 748 fin-per-meter tube and 49 percent higher than the 1024 fin-per-meter tube.

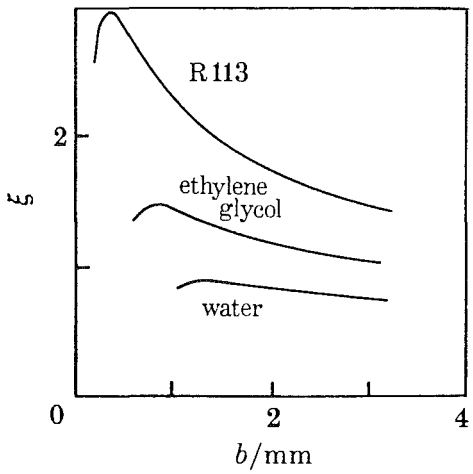

Fig. 5 Active area enhancement (Masuda and Rose, 1987)

Honda et al. (1983) and Honda and Nozu (1985) obtained condensing data for R-113 and methanol on several copper, integral-fin tubes. Two of the tubes had trapezoidal-shape fins (fin-tip half angle less than 5 deg) while the third had rectangular-shape fins. This third tube exhibited the best performance, showing an enhancement factor over a smooth tube (based upon the "envelope" outside surface area) at the same overall vapor-to-wall temperature difference (5 K) of 8.8 and 4.9 for R-113 and methanol, respectively. Kabov (1984) measured condensing heat transfer coefficients for R-12 and R-21 on several families of tubes having different fin spacings and heights. One family had a fin root diameter of 17.7 mm, a fin height of 1.0 mm, a fin thickness of 0.5 mm, and spacings of 0.25, 0.4, 1.0, and 2.1 mm. He determined that fin spacing is one of the principal parameters controlling heat transfer. Very recently, Sukhatme et al. (1988) measured the heat transfer performance of R-11 condensing on horizontal, integral-fin tubes having trapezoidal-shape fins of outside diameter near 24 mm. They systematically varied the fin densi-

Downloaded 16 Dec 2010 to 193.140.21.150. Redistribution subject to ASME license or copyright; see http://www.asme.org/terms/Terms_Use.cfm

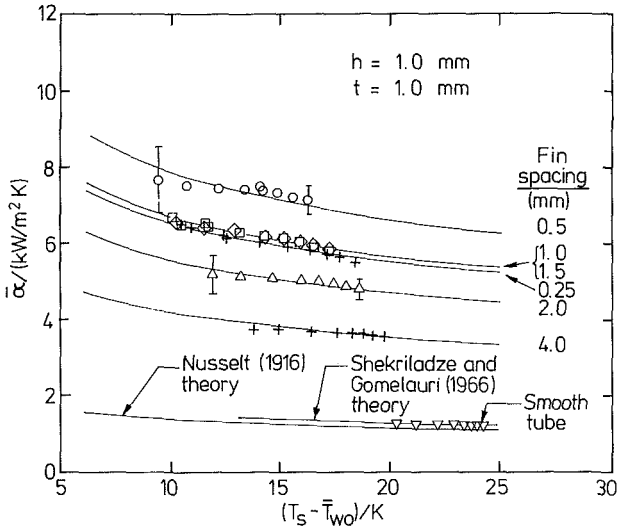

Fig. 6 Variation of R-113 heat transfer coefficient with wall subcooling (Marto et al., 1988a)

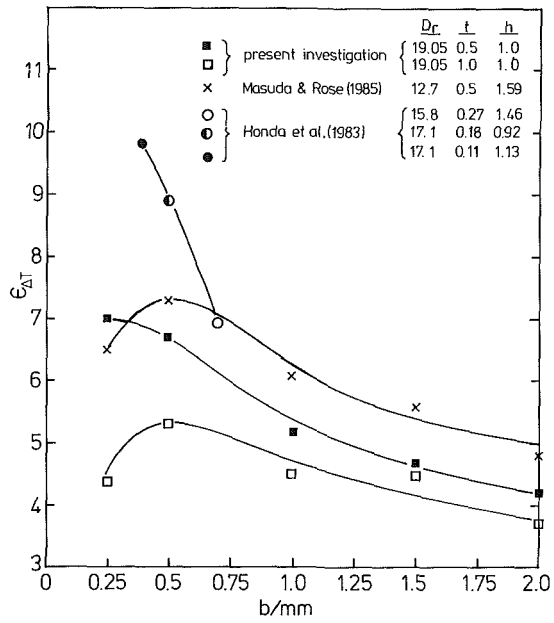

Fig. 7 Dependence of R-113 heat transfer enhancement upon fin geometry (Marto et al., 1988a)

ty, fin height, and fin-tip half angle. The best performing tube had a fin density of 1417 fins per meter (fin spacing about 0.35 mm), a fin-tip half angle of 10 deg, and a fin height of 1.22 mm. This tube had an enhancement ratio (compared to a smooth tube of the same outside diameter) at the same condensing film temperature difference (about 3 K) of about 10.

In recent years, a wide variety of data has been generated by two collaborative, experimental programs: one in the U.S. (Wanniarachchi et al., 1984, 1985, 1986; Marto et al., 1986, 1988a, 1988b) and the other in England (Yau et al., 1984, 1985, 1986; Masuda and Rose, 1985, 1988). Both programs have been conducted in a systematic fashion (e.g., varying one fin geometric variable such as fin spacing while holding all the other geometric variables constant) in order to generate a broad data base for analysis and design. Over 60 different finned tubes have been specially manufactured and tested so far in an effort to observe the effects of fin spacing, thickness, height, shape, and material. Three test fluids have been chosen (steam, ethylene glycol, and R-113) in order to give a large variation in the surface tension to density ratio σ/ρ. All the data have been gathered with great care to insure accuracy in the measurements and minimal disturbances caused by dropwise conditions and/or noncondensing gases. Figure 6 shows some representative heat transfer coefficient data for R-113 at atmospheric pressure condensing on one family of tubes (Marto et al., 1988a). The average heat transfer coefficient $\bar{\alpha}$ is based upon the nominal surface area of a smooth tube having a diameter equal to the root diameter of the finned tube D_r. It is also based upon the average outside wall temperature at the root of the fins $\bar{T}_{wo}$, which is inferred from a modified Wilson plot technique (Wanniarachchi et al., 1986). The data were obtained for copper tubes with a root diameter of 19.05 mm, containing rectangular-shape fins whose thickness t and height h were kept constant at 1.0 mm. The spacing between fins was 0.25, 0.5, 1.0, 1.5, 2.0, and 4.0 mm. Vapor flowed downward over the test tube at a velocity of about 0.4 m/s. Data for a 19.05 mm diameter (equal to root diameter of finned tube) smooth tube are also shown for comparison, as well as typical uncertainty bands. The smooth tube data are slightly above the Nusselt (1916) theory due to the small downward vapor velocity and if vapor velocity effects are included, using the theory of Shekriladze and Gomelauri (1966), excellent agreement with the data occurs. The finned tube data show that an optimum spacing exists, near 0.5 mm. The solid curves through the data represent least-squares fits using the relation

$$q = a(T_s - \bar{T}_{wo})^{3/4} \tag{6}$$

Using equation (6), the heat transfer enhancement ratio $\epsilon_{\Delta T}$ defined as the ratio of the finned-tube vapor-side coefficient to the smooth-tube value at the same vapor-to-wall temperature difference and based upon the smooth tube surface area, simply reduces to

$$\epsilon_{\Delta T} = \frac{a_f}{a_s} \tag{7}$$

where a_f and a_s are the coefficients in equation (6) for the finned and smooth tubes respectively. Figure 7 compares the heat transfer enhancement ratio data of Marto et al. (1988a) for R-113 with those of Honda et al. (1983) and Masuda and Rose (1985). All the tubes were copper and had rectangular-shape fins[1]; in addition, all the data were taken near atmospheric pressure. Unfortunately, the dimensions of the tubes and the fins were different, making it very difficult to assess completely the significance of the results. Nevertheless, a few important trends are evident. It appears that the enhancement ratio increases as fin thickness decreases and an optimum fin spacing appears to lie between 0.25 and 0.5 mm. Enhancements between 7 and 10 are readily evident. Also, the fin height to tube root diameter h/D_r may be an important variable. These trends are discussed in more detail in Marto et al. (1988a).

Figure 8 shows a similar comparison for steam, comparing the data of Wanniarachchi et al. (1986) to those of Yau et al. (1986). Once again, the different tube geometries used create a problem in assessing results, but all the data exhibit a clear optimum fin spacing near 1.5 mm. At this optimum spacing, the enhancements range between 2.4 and 3.2, depending upon operating pressure and tube dimensions. Smaller enhancements occur at lower operating pressures, presumably due to higher surface tension (i.e., more flooding) and condensate viscosity at lower temperatures. In comparing the results shown in Fig. 8 to those in Fig. 7, an unexplainable inconsistency appears. For R-113, the data of Masuda and Rose (1985) are higher than the data of Marto et al. (1988a). However, for steam (at atmospheric pressure, 101 kPa) just the opposite is true. The reason for this inconsistency is not known at present, and further testing at each laboratory with

[1] Actually, the first two tubes listed for Honda et al. (1983) had trapezoidal-shape fins with fin tip half angles θ near 5 deg.

Downloaded 16 Dec 2010 to 193.140.21.150. Redistribution subject to ASME license or copyright; see http://www.asme.org/terms/Terms_Use.cfm

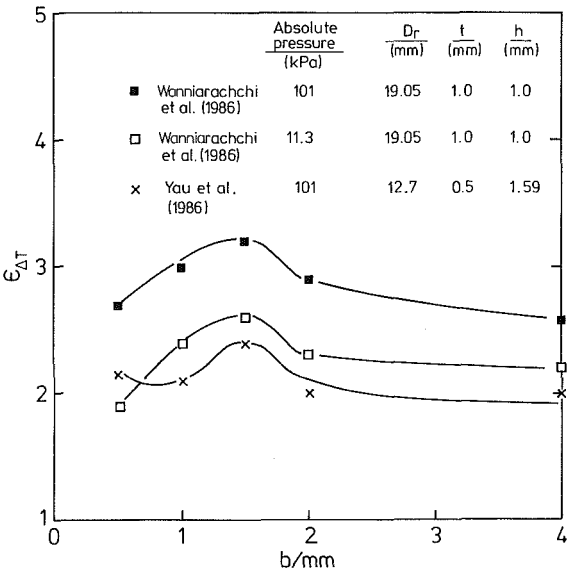

Fig. 8 Dependence of steam heat transfer enhancement upon fin geometry

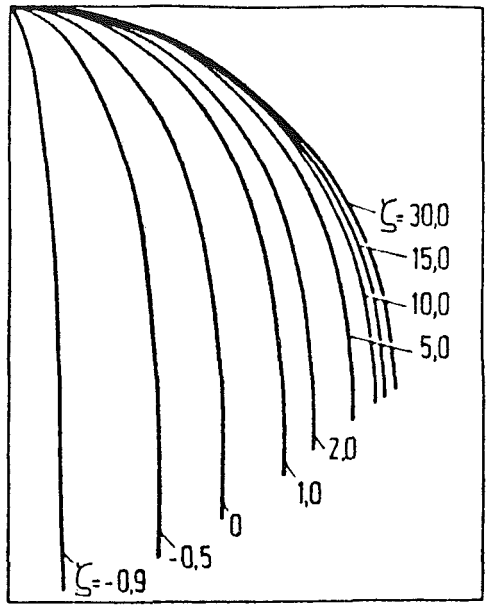

Fig. 10 Variation of condensate film profiles (Adamek, 1981)

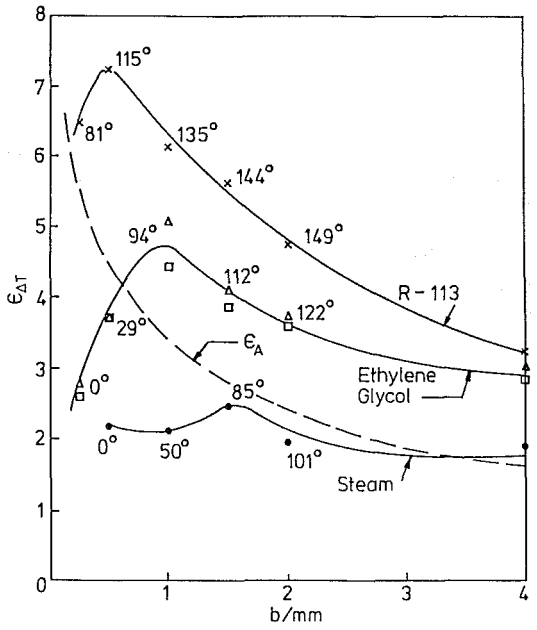

Fig. 9 Dependence of heat transfer enhancement upon fin spacing for three test fluids (Masuda and Rose, 1988)

identical tube geometries will be required before it can be properly resolved.

Figure 9 shows the composite results of Yau et al. (1985, 1986) and Masuda and Rose (1985, 1988) for a single family of copper tubes with R-113, ethylene glycol, and steam. Except for steam, the data show that the heat transfer enhancement $\epsilon_{\Delta T}$ is greater than the surface area enhancement ϵ_A (area ratio of the finned tube to a smooth tube of diameter equal to the finned tube root diameter). The data show that apparently the maximum heat transfer enhancement ratio increases and the optimum fin spacing decreases as the surface tension to density ratio of the condensate σ/ρ decreases (Fig. 4). Maximum enhancements of 7.3, 4.7, and 2.4 occur at spacings near 0.5, 1.0, and 1.5 mm for R-113, ethylene glycol, and steam, respectively. The numbers adjacent to each data point represent the calculated flooding angles using equation (2). Masuda and Rose (1988) observe that the maximum enhancement occurs when the tubes are approximately half flooded (i.e., $\phi_f \sim 90$ deg). They also note that for ethylene glycol and steam, even when the tube is fully flooded (i.e., $\phi_f = 0$), significant enhancements are evident. This indicates that significant heat transfer occurs at or near the fin tip, or that secondary condensate flow effects within the channels enhance the heat transfer. Masuda and Rose (1987) recognized a close resemblance between the experimental heat transfer enhancement ratio curves shown in Fig. 9 and the active surface area enhancement ratios shown in Fig. 5. The results show that heat transfer enhancement seems to be related to the *unblanked* area of a finned tube. Masuda and Rose (1987) therefore postulated that improved heat transfer results would occur by radiusing the fin roots between fins. Although this would decrease the *total* surface area of the finned tube (compared to sharp-cornered fin roots), it would increase the *unblanked* surface area by preventing condensate "wedges" to form on the upper part of the tube.

Marto et al. (1986) have reported on the effect of fin shape during condensation of steam on horizontal finned tubes. They tested four copper tubes containing specially machined fins whose shapes resembled (but were not precisely equal to) a rectangle, a triangle, a trapezoid, and a parabola. All the tubes were manufactured with a fin height of 1.0 mm, a fin-root spacing of 1.5 mm, and a fin-root thickness of 0.5 mm. The different fin shapes created slightly varying surface areas. The experimental results showed that the heat transfer enhancement ratio of the parabolic-shape fin was about 10 to 15 percent higher than the other fin shapes after correcting for the slightly different surface areas. They therefore concluded that a near-parabolic fin tip is superior to the other shapes, confirming the earlier results of Adamek (1981) and Mori et al. (1979) for vertical surfaces. Each of these investigations showed that the optimum fin shape for maximum surface-tension-induced drainage is one which exhibits a large curvature (i.e., a small radius of curvature) at the fin tip with a continuously decreasing curvature toward the fin root. For example, Adamek (1981) has described the curvature of the condensate profile by

$$\kappa(s) = \frac{1}{r(s)} = \begin{cases} \kappa_o - a_1 s^{\zeta}, & 0 < \zeta < \infty \quad (8a) \\ a_1 s^{\zeta} - \kappa_o, & -1 < \zeta < 0 \quad (8b) \end{cases}$$

Downloaded 16 Dec 2010 to 193.140.21.150. Redistribution subject to ASME license or copyright; see http://www.asme.org/terms/Terms_Use.cfm

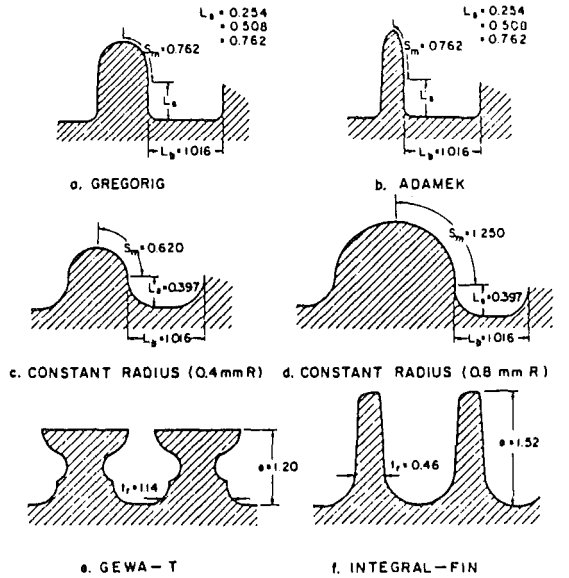

Fig. 11(a) Cross sections of fin surfaces

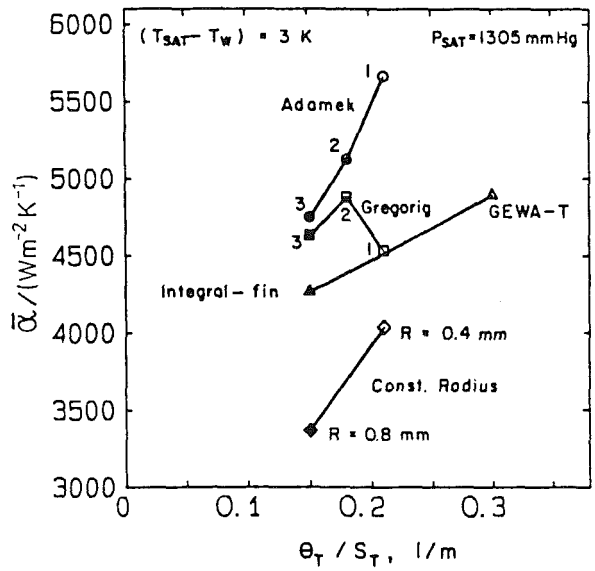

Fig. 11(b) Heat transfer results

Fig. 11 Effect of fin shape on film condensation of R-11 on vertical fluted plates (Kedzierski and Webb, 1987)

where a_1, κ_o, and ζ are geometric parameters, and s is the path length along the curved condensate film. This description of various curvatures is shown in Fig. 10 for R-11 (Adamek, 1981). Adamek (1981) has shown theoretically that for a vertical surface, the best heat transfer around the fin crest region is given by a curve with a shape parameter $\zeta = -0.5$. The Gregorig (1954) shape ($\zeta = 2.0$) does not perform as well. Recently, Kedzierski and Webb (1987) have reported experimental data for accurately machined fins on vertical, water-cooled plates. Very precise fin shapes were manufactured by using an electric discharge machining (EDM) process. Figure 11(a) shows cross sections of their machined surfaces. There were three Gregorig ($\zeta = 2.0$) surfaces and three Adamek ($\zeta = -0.5$) surfaces each having three different channel depths for the same fin-tip shape and dimensions. In addition, there were two constant-radius surfaces and finally, two surfaces fabricated to simulate commercially available shapes. Data were taken for R-11 condensing at an absolute pressure of 173 kPa. Figure 11(b) shows their results for the average vapor-side heat transfer coefficient (based on the total plate surface

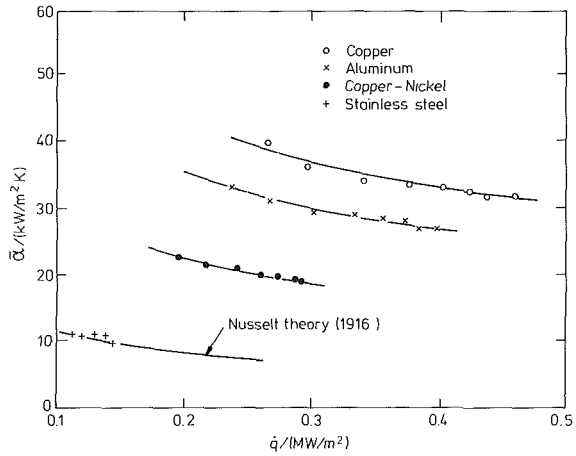

Fig. 12 Effect of wall thermal conductivity on the heat transfer coefficient of steam on spirally threaded tubes (Mitrou, 1986)

area) versus the ratio θ_T/S_T. Kedzierski and Webb (1987) define θ_T as the angle that the arc length along the fin turns starting from the fin tip and ending at the center of the channel. The total arc length S_T is the distance measured along the surface from the fin tip to the center of the channel. They mention that the ratio θ_T/S_T is equal to the average curvature of the fin $\bar{\kappa}$. Their results show that, except for the Gregorig – 1 surface, higher heat transfer coefficients occurred for surfaces with larger average curvature (i.e., larger values of θ_T/S_T). In fact, the Adamek surfaces outperformed all the other surfaces, verifying the earlier theoretical predictions of Adamek (1981). Kedzierski and Webb (1987) used a variation of the Wilson (1915) plot method to separate the overall surface heat transfer rate into its components due to the convex fin tip, the channel sides, and the channel bottom. Their results showed that, along the convex surface, the Adamek fin shape performed about 50 percent better than the Gregorig fin shape.

All of the above-mentioned results are for copper tubes. Mitrou (1986) has shown that tube material can alter the heat transfer results substantially. Figure 12 is a plot of his data for condensation of steam on spirally threaded tubes of copper, aluminum, copper-nickel, and stainless steel. There is a clear trend with thermal conductivity. As the thermal conductivity of the fin decreases, the added thermal resistance in the fin (i.e., a lower fin efficiency) reduces the film condensation heat transfer. In fact, the data for stainless steel are about the same as predicted by the Nusselt (1916) theory for a smooth tube. Similar results have been obtained by Mills et al. (1975) and Shklover et al. (1981).

As mentioned earlier, condensate flooding on finned tubes may be substantially reduced by using longitudinal drainage strips at the bottom of the tube to pull the condensate off. Marto et al. (1988b) have reported on a systematic experimental investigation of the effect of both solid and porous drainage strips on condensation of steam on an integral-fin tube. The finned tube had a root diameter of 19.05 mm and had rectangular fins 1.0 mm high, 1.0 mm thick, and spaced only 0.5 mm apart. This tube was selected since, without a drainage strip, it was fully flooded by water (i.e., $\phi_f = 0$). Tests were conducted with this finned tube containing various drainage strips to study the effects of strip height, thickness, and porosity. Figure 13 is an illustration of their average steam-side heat transfer coefficient versus heat flux at a pressure near atmospheric. The data were taken with different porous strip heights of 8, 11, and 15 mm, at a constant strip thickness of 3 mm, and indicate that the heat transfer coefficient increases by up to 40 percent with increases in porous strip height. The results with the 11 mm and 15 mm high

Downloaded 16 Dec 2010 to 193.140.21.150. Redistribution subject to ASME license or copyright; see http://www.asme.org/terms/Terms_Use.cfm

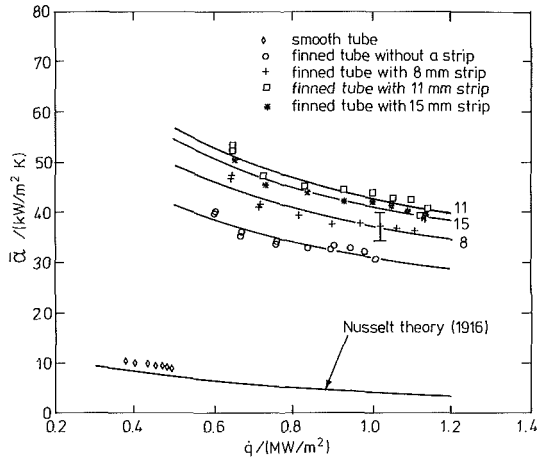

Fig. 13 Effect of porous drainage strip height on the average steam condensing heat transfer coefficient on a finned tube (Marto et al., 1988b)

strips, however, were about the same, implying that an upper limit may exist on the strip height, beyond which no further improvement occurs. This trend is in agreement with the experimental results of Honda and Nozu (1985) for methanol. Honda et al. (1983) found that porous drainage strips could increase the heat transfer enhancement from 1.13 to 1.36 for R-113 and from 1.39 to 2.08 for methanol. Yau et al. (1986) obtained data for steam condensing on two fin tubes to which was attached a solid drainage strip of copper, which was 0.5 mm thick and 8 mm high. They found that the strip improved the steam-side heat transfer coefficient by about 25 to 30 percent.

Theoretical Results. The first theoretical model of film condensation on a horizontal, finned tube was proposed by Beatty and Katz (1948). They neglected surface tension forces completely and considered only gravity-driven, Nusselt-type condensation on the vertical fin flanks and on the tube surface between fins. By adding up the contributions of the fin flanks (using Nusselt theory for a vertical plate) and the tube surface (using Nusselt theory for a horizontal tube), they arrived at an average heat transfer coefficient[2]

$$\alpha_{BK} = \eta_f \alpha_f \frac{A_f}{A_{ef}} + \alpha_u \frac{A_u}{A_{ef}} \tag{9}$$

where η_f represents the fin efficiency and A_{ef} is an effective total surface area (equal to $\eta_f A_f + A_u$). Upon substituting in the well-known Nusselt expressions for α_f and α_u, they arrived at the following simple result:

$$\alpha_{BK} = C_{BK} \left\{ \frac{k^3 \rho^2 g\, h_{fg}}{\mu\, \Delta T\, D_{eq}} \right\}^{1/4} \tag{10}$$

where

$$\left\{ \frac{1}{D_{eq}} \right\}^{1/4} = 1.30 \eta_f \frac{A_f}{A_{ef}} \frac{1}{\bar{L}^{1/4}} + \frac{A_u}{A_{ef}} \frac{1}{D_r^{1/4}} \tag{11}$$

and

$$\bar{L} = \pi (D_o^2 - D_r^2)/4D_o \tag{12}$$

When equation (10) was compared to their experimental data, they found that agreement to within about 10 percent was possible by using a leading coefficient C_{BK} equal to 0.689 (which is within 5 percent of the Nusselt value of 0.728 for a horizontal smooth tube). Equation (10) has been used successfully in the refrigeration industry for many years. However, since it was based upon experimental data for low surface tension fluids with a low fin density tube, and since surface tension effects were completely neglected in its derivation, it should not be valid for high surface tension fluids and/or for tubes with high fin densities. As pointed out above, surface tension forces influence condensation heat transfer on finned tubes in two opposing ways. First, surface tension creates condensate flooding which decreases the heat transfer. Secondly, it helps to thin the condensate film on regions of the fin flanks and the tube surface, which increases the heat transfer. It is interesting to note, therefore, that by neglecting surface tension forces in the Beatty–Katz (1948) expression, the two opposing trends tend to cancel one another out, thereby extending, unintentionally, the range of validity of the expression.

[2]Beatty and Katz (1948) did not consider the fin tips in their analysis. This, presumably, was due to the fact that the commercially manufactured fins that they used had no appreciable fin-tip thickness. A corrected expression for the equivalent tube diameter D_{eq}, which includes the contribution from the fin tips, was proposed by Smirnov and Lukanov (1972).

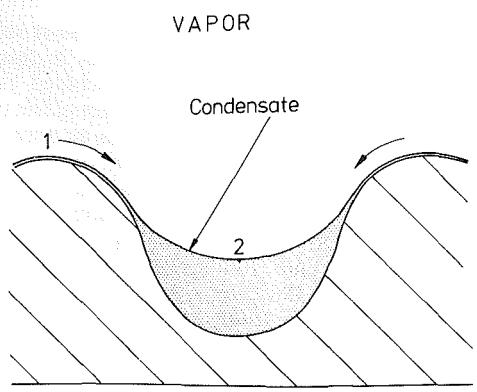

Fig. 14 Sketch of a fluted surface (Gregorig, 1954)

Gregorig (1954), in studying film condensation on finely rippled or fluted vertical surfaces, realized that surface tension on a curved surface can induce a pressure gradient many times larger than that induced by gravity. Figure 14 shows a schematic of a vertical fluted surface. At point 1, the pressure in the liquid is larger than the local vapor pressure because of the convex shape of the condensate surface. At point 2, just the opposite is true because of the concave shape. Therefore, a pressure gradient exists from point 1 to point 2 that drives the condensate toward the trough region of the surface. More precisely, the local pressure gradient along the liquid-vapor interface due to the surface tension is

$$\frac{dp}{ds} = \frac{d}{ds}\left(\frac{\sigma}{r}\right) \tag{13}$$

where r is the local radius of curvature and s is the path length along the curved condensate surface. Gregorig (1954) assumed that on the convex portion of a fluted surface only surface tension forces (and not gravity) are important. He then carried out a Nusselt-type analysis to arrive at an expression for the local condensate film thickness $\delta(s)$

$$\frac{1}{r(s)} = \frac{1}{r_o} - \frac{3\mu k \Delta T}{\sigma \rho h_{fg}} \int_0^s \left[\int_0^s \frac{ds}{\delta(s)} \right] \frac{ds}{\delta(s)^3} \tag{14}$$

Using equation (14), he then questioned what the shape of the profile must be in order for a constant film thickness to result. In this (but by no means optimum) situation, with δ equal to a constant, equation (14) simply reduces to a parabolic expression

$$\frac{1}{r(s)} = \frac{1}{r_o} - \frac{3\mu k \Delta T}{\sigma \rho h_{fg} \delta^4} \frac{s^2}{2} \tag{15}$$

Since $1/r(s)$ is the curvature of the surface $\kappa(s)$, then when equation (15) is compared to equation (8*a*) due to Adamek (1981), it is clear that the two equations are equal when the

Downloaded 16 Dec 2010 to 193.140.21.150. Redistribution subject to ASME license or copyright; see http://www.asme.org/terms/Terms_Use.cfm

Adamek shape parameter $\zeta = 2.0$. Gregorig (1954) solved for the resulting average heat transfer coefficient in this special case, using numerical integration, and concluded that very thin condensate films on the crests of the flutes offset the thick films in the troughs or channels, resulting in an average heat-transfer coefficient many times that on a smooth surface. This work stimulated a variety of improved analyses to predict the thermal performance of vertical fluted surfaces and to understand further the importance of surface tension forces (Zener and Lavi, 1974; Fujii and Honda, 1978; Panchal and Bell, 1980; Honda and Fujii, 1984; Joos, 1985; Panday and Bilek, 1985). These investigations studied the importance of gravity versus surface tension forces on the fin tips and in the troughs or channels, and offered a variety of mathematical solutions to solve this complex problem.

The first analysis that recognized the importance of surface tension on horizontal finned tubes was made by Karkhu and Borovkov (1971), who studied film condensation on trapezoidal-shape fins. They divided the finned surface into two regions: the fin flanks on which the vapor condensed and on which the condensate flowed radially toward the fin root under the influence of surface tension forces (i.e., gravity was neglected), and the channel between fins on which the collected condensate from the fin flanks flowed around the tube under the influence of gravity (i.e., surface tension was neglected). Since the film thickness in the channel was assumed to be large, heat transfer was neglected in this second region. They treated condensate flooding on the bottom part of the tube by assuming that the effective circumference for heat transfer was limited to $\phi < 150$ deg. They assumed a uniform radial pressure gradient along the fin flank given by

$$\frac{\partial p}{\partial x} \simeq \frac{\Delta p}{\Delta x} \simeq \frac{\sigma \cos\theta}{r_t (h-\Delta)} \tag{16}$$

where Δ is the local thickness of the condensate in the channel and where r_t, the radius of curvature of the condensate at the fin tip, was approximated (see Fig. 3) as

$$r_t \simeq \frac{t}{2}(1+\tan\theta) \tag{17}$$

Substituting this expression for the pressure gradient into the momentum equation for the condensate along the fin yielded the following result for the local condensate film thickness as a function of distance from the fin tips x:

$$\delta(x) = \left\{ \frac{2\mu k (T_s - T_w)(1+\tan\theta)(h-\Delta)tx}{\sigma \rho h_{fg} \cos\theta} \right\}^{1/4} \tag{18}$$

They then coupled the flow of condensate from the fin flanks to the mass flow in the channel and numerically solved for the dimensionless thickness of the condensate in the channel Z (equal to Δ/h) and the condensate mass flow rate in half of the channel $G(Z)$ as a function of angular position around the tube ϕ. Upon comparing these results to their experimental data, an empirical expression for the dimensionless channel film thickness at $\phi = 150$ deg resulted as follows:

$$Z_b = 1.6\, H^{0.2}(1 - 0.35\, H^{-0.3} m) \tag{19}$$

where

$$m = \frac{t_b}{2h \tan\theta} \tag{20}$$

and

$$H = \frac{2.8\sigma^{1/4}\mu^{3/4}k^{3/4}R_o(T_s - T_w)^{3/4}}{\rho^{7/4}h^{7/2}(t/2)^{1/4}h_{fg}^{3/4}\sin^3\theta(1+\tan\theta)^{1/4}(\cos\theta)^{1/4}} \tag{21}$$

In equation (21), an average temperature difference along the fin was used, which was calculated from the solution of the heat conduction equation within the fin. Karkhu and Borovkov (1971) then used equations (19)–(21) to find the mass flow rate in half of a fin channel $G(Z_b)$, which was then used to find an average heat transfer coefficient

$$\alpha_{KB} = \frac{G(Z_b)h_{fg}}{A_s(T_s - T_o)} \tag{22}$$

Equation (22) is based upon the finned surface area associated with half a fin channel[3]

$$A_s = \left(\frac{t}{2} + \frac{t_b}{2} + \frac{2h}{\cos\theta}\right)\pi R_o \tag{23}$$

and the fin root temperature difference $(T_s - T_o)$. When equation (22) was compared to their experimental data, agreement to within ± 5 percent was found. Improvements to the above solution were later made by Zozulya et al. (1977) and Rifert (1980).

Edwards et al. (1973) analyzed both evaporation and condensation on horizontal tubes with triangular-shape, spiral grooves. They analyzed fluid flow in the grooves under the influence of surface tension and gravity, and heat transfer at the fin tips by solving the fin equation. They found that wall conductivity has a significant effect and that an optimum groove angle and pitch exists. During condensation, they postulated that the predominant heat transfer may not occur at the fin tip but at a position along the fin where the meniscus changes shape from being convex to concave and the film becomes very thin. This thinning effect along the fin flanks was studied in detail both analytically and experimentally by Hirasawa et al. (1980). They concluded that the condensate film near the bottom of a narrow channel becomes thinned locally due to a suction effect that is caused by the liquid flowing in the channel. This local thinning creates a significant local heat transfer enhancement. A similar local thinning effect between widely spaced fins was noted by Rifert et al. (1985).

Several important contributions have been made by Webb and co-workers to understand the role of surface tension. Based upon their study of condensate flooding, Rudy and Webb (1981) proposed that the Beatty and Katz (1948) heat transfer coefficient be simply modified to allow for condensate flooding

$$\alpha_{RW} = \alpha_{BK}\frac{\phi_f}{\pi} \tag{24}$$

Equation (24) neglects heat transfer through the flooded portion of the tube. Rudy and Webb (1981) found that this equation underpredicted their R-11 data on a 1378 fin-per-meter tube by 35 percent, and postulated that some other mechanism was causing condensate drainage on the fins. Webb et al. (1982), using a vertical plate with rectangular-shape, "spine fins," showed that the Beatty and Katz (1948) model, equations (9)–(12), did a poor job of predicting their test results. They therefore proposed a new surface-tension-drained model, which was based on an assumption similar to that used earlier by Karkhu and Borovkov (1971): Namely, that on the condensate surface around a fin, the pressure gradient is constant

$$\frac{dp}{dx} = \frac{\Delta p}{\Delta x} = \frac{2\sigma}{h}\left(\frac{1}{t} + \frac{1}{b}\right) \tag{25}$$

Webb et al. (1982) used this result to replace the gravity force per unit volume term used in the Nusselt, gravity-drainage model, arriving at the following expression for the surface-tension-driven heat transfer coefficient on the fin surface:

$$\alpha_f = 0.943\left\{\frac{k^3\rho h_{fg}}{\mu\Delta T}\right\}^{1/4}\left\{\frac{2\sigma}{h^2}\left(\frac{1}{t} + \frac{1}{b}\right)\right\}^{1/4} \tag{26}$$

When this expression was substituted into the Beatty and Katz (1948) expression, equation (9), they found that the prediction

[3] The factor of 2 appearing in the last term of equation (23) was mistakenly omitted in the Karkhu and Borovkov (1971) paper.

Downloaded 16 Dec 2010 to 193.140.21.150. Redistribution subject to ASME license or copyright; see http://www.asme.org/terms/Terms_Use.cfm

agreed with their experimental data to within 10 percent. Rudy and Webb (1983) applied this result to a horizontal integral-fin tube by using equation (24) together with the Beatty and Katz (1948) model as modified above. They concluded that the simplified linear pressure gradient model was not adequate in predicting the trends of their experimental data, and that a more detailed pressure gradient form was required. Owen et al. (1983) corrected equation (24) to allow for heat transfer in the flooded part of the tube, and proposed the following expression for the average heat transfer coefficient

$$\alpha_O = \alpha_{BK}\frac{\phi_f}{\pi} + \alpha_b\left(1 - \frac{\phi_f}{\pi}\right) \tag{27}$$

where α_b is the heat transfer coefficient in the flooded part of the tube. They estimated this coefficient by using a one-dimensional radial conduction model through the fins and the condensate, and found agreement with earlier data to ± 30 percent. Rudy et al. (1984) and Webb et al. (1985) proposed a refined model, which includes surface tension drainage on the fin flanks, gravity drainage on the interfin tube surface, and heat transfer in the flooded zone. Their expression for the average heat transfer coefficient can be written as[4]

$$\alpha_W = \frac{\phi_f}{\pi}\left(\eta_f\alpha_f\frac{A_f}{A_{ef}} + \alpha_u\frac{A_u}{A_{ef}}\right) + \left(1 - \frac{\phi_f}{\pi}\right)\alpha_b \tag{28}$$

They calculated a flooding angle ϕ_f using a relationship similar to equation (2), and on the fin flanks, they used the heat transfer coefficient proposed by Adamek (1981). His result for various convex surfaces is

$$\alpha_f = 2.149\frac{k}{S_m}\left\{\frac{\rho\sigma h_{fg}\theta_m S_m}{\mu k\Delta T}\frac{(\zeta+1)}{(\zeta+2)^3}\right\}^{1/4} \tag{29}$$

where S_m is the maximum length of the convex surface, θ_m is the maximum rotation angle of the normal to the convex surface, and ζ is the convex shape parameter defined in equation (8). On the tube surface in the interfin space, they used a modified Nusselt expression for α_u, which takes into account the additional condensate from the fin flanks. Finally, in the flooded region, they used a two-dimensional conduction approach for the fin–liquid combination. Using this model, with values of ζ chosen between -0.77 and -0.85 to approximate the shape of their fins, their predicted heat transfer coefficients were within ± 20 percent of their R-11 experimental values. Wanniarachchi et al. (1986) compared their data for steam to the model of Webb et al. (1985),[5] and found that, except for the fully flooded tube, the model predicted their experimental data to about ± 20 percent. For the fully flooded tube, the model underpredicted the data by as much as 100 percent under vacuum conditions and 200 percent at atmospheric pressure.

The most complete approach to solving the problem has been made by Honda and Nozu (1984, 1987) and Honda et al. (1987c), who treated the problem as a composite one involving vapor-to-coolant heat transfer through a finned tube wall. Figure 15 shows the physical model and coordinates used by Honda and Nozu (1987). Their fins were trapezoidal in shape except for rounded corners near the fin tips. They divided the tube into unflooded (u) and flooded (f) regions, using equation (2) to determine the flooding angle. On the fin surface, they assumed that the condensate flow was driven by surface tension and gravity whereas in the interfin space between fins only gravity was present. The fin surface was divided into a thin film region toward the top of the fin and a thick film region near the bottom. In the thick film region, they assumed

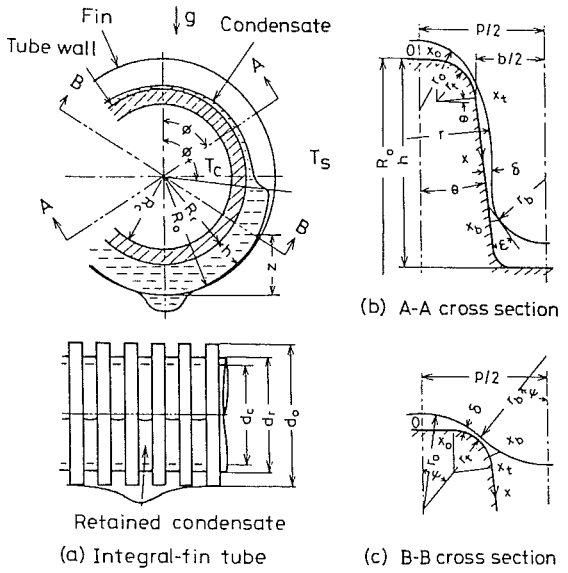

Fig. 15 Physical model of condensation on a finned tube (Honda and Nozu, 1987)

that the radius of curvature of the liquid–vapor interface r_b varied with position around the tube according to equation (1). Heat transfer in the thick film region was neglected. In the thin film region, they numerically solved the following differential equation for the film thickness $\delta(x)$

$$\frac{1}{3\nu}\frac{d}{dx}\left\{\left(\rho g f_x - \sigma\frac{d}{dx}\left(\frac{1}{r}\right)\right)\delta^3\right\} = \frac{k(T_s - T_w)}{\delta h_{fg}} \tag{30}$$

where f_x is the x component of normalized gravity and r is the radius of curvature of the condensate film, which depends in a complex way on the film thickness and its derivatives. To solve this fourth-order differential equation, they assumed the following four boundary conditions:

$$\frac{d\delta}{dx} = \frac{d^3\delta}{dx^3} = 0, \qquad x = 0 \tag{31}$$

$$\frac{d\delta}{dx} = \tan\epsilon \text{ and } r = -r_b, \qquad x = x_b \tag{32}$$

where ϵ is the angle shown in Fig. 15(b). Based on their numerical results, approximate expressions for the Nusselt numbers in both the unflooded (Nu_{du}) and flooded (Nu_{df}) regions were then obtained, and the overall average Nusselt number was written as

$$\mathrm{Nu}_{HN} = \frac{\alpha_{HN}D_o}{k} = \frac{\mathrm{Nu}_{du}\eta_u(1-\tilde{T}_{wu}) + \mathrm{Nu}_{df}\eta_f(1-\tilde{T}_{wf})}{(1-\tilde{T}_{wu})\tilde{\phi}_f + (1-\tilde{T}_{wf})(1-\tilde{\phi}_f)} \tag{33}$$

where the subscripts u and f pertain to the unflooded and flooded regions, η represents the fin efficiency, $\tilde{\phi}_f = \phi_f/\pi$, and $\tilde{T}_w = (T_w - T_c)/(T_s - T_c)$. The values of $\tilde{T}_{wu}$ and $\tilde{T}_{wf}$ were determined by solving the circumferential wall heat conduction equation. The authors pointed out that this wall temperature variation must be considered since the heat transfer rates between the unflooded and flooded regions were so different. Honda and Nozu (1987) compared their predicted results to the experimental data of various investigators (including 11 fluids and 22 tubes) and found agreement to within ± 20 percent. Honda et al. (1987c) extended the previous analysis to include condensate flow and heat transfer in the space between fins. In so doing, they included axial wall temperature variations between the fin root and the tube sur-

[4] Rudy et al. (1984) mistakenly have an additional area ratio in the third term of equation (28), which should not be present.

[5] Wanniarachchi et al. (1986) used a value of $\zeta = -0.95$ and used one-dimensional conduction in the flooded region rather than two-dimensional conduction as proposed by Webb et al. (1985).

Downloaded 16 Dec 2010 to 193.140.21.150. Redistribution subject to ASME license or copyright; see http://www.asme.org/terms/Terms_Use.cfm

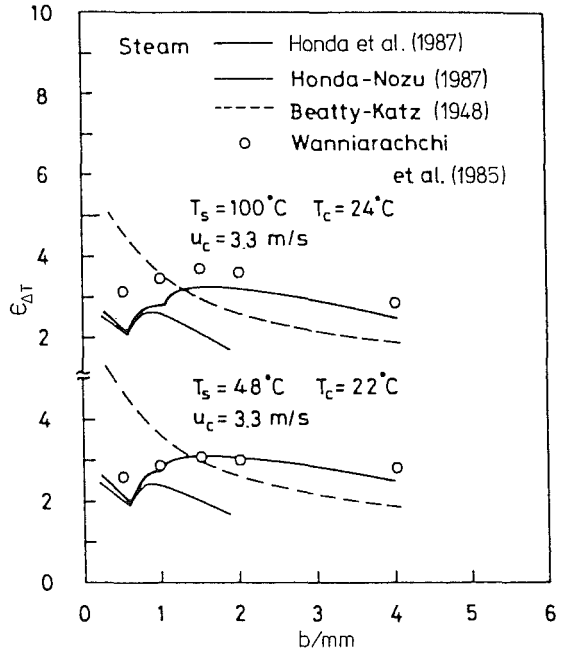

Fig. 16 Comparison of measured and predicted heat transfer enhancements of steam on finned tubes (Honda et al., 1987c)

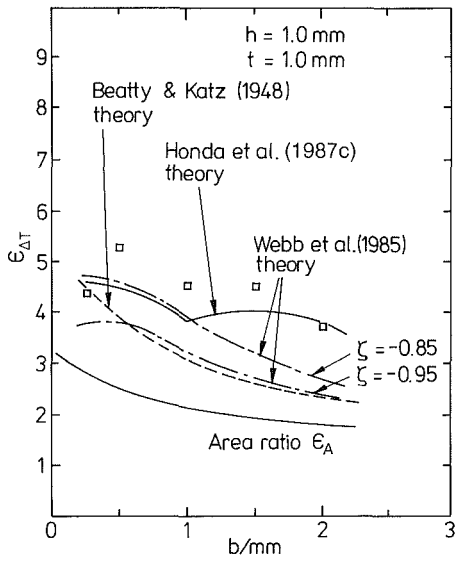

Fig. 17 Comparison of measured and predicted heat transfer enhancements of R-113 on finned tubes (Marto et al., 1988a)

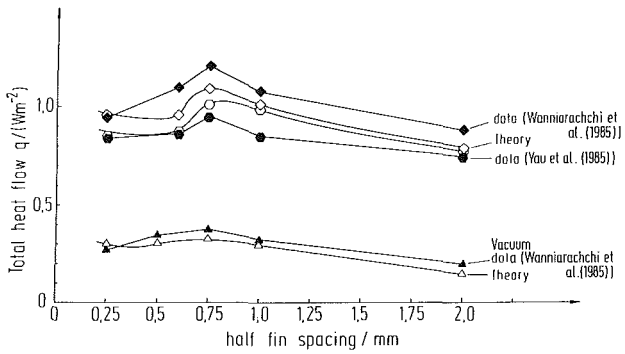

Fig. 18 Comparison of steam test data with theoretical prediction of Adamek and Webb (1988)

face near the fin root. The expression for the flooding angle was also extended to allow for large fin spacings (as compared to fin height). These authors found that for large fin spacings and low condensation rates, surface tension forces create thin film regions not only on the fin surface but also on the interfin tube surface. This effect had been postulated earlier by Thomas (1968) and has been recently experimentally confirmed by Shekarriz and Plumb (1988). The extended analysis of Honda et al. (1987c) therefore predicts larger heat transfer coefficients at large fin spacings than their earlier model.

Figure 16 is a plot of the experimental heat transfer enhancement ratio of Wanniarachchi et al. (1985) for steam and the predictions of Beatty and Katz (1948), Honda and Nozu (1987), and Honda et al. (1987c). The comparison is made for one family of copper tubes with a fin root diameter of 19.05 mm, containing rectangular-shape fins whose thickness and height were constant at 1.0 mm. The spacing between fins was varied from 0.5 mm to 4.0 mm. The Beatty and Katz (1948) model underpredicts the data at large fin spacings and overpredicts it at small fin spacings. The Honda and Nozu (1987) model underpredicts the data especially at large fin spacings, whereas the Honda et al. (1987c) extended model shows reasonable agreement, except for the smallest fin spacing where complete flooding occurs. The dip in both Honda models at a fin spacing of 0.5 mm is caused by the unique circumstances of complete flooding. As the spacing between fins is decreased toward the critical spacing for complete flooding, more of the tube circumstances becomes flooded and heat transfer should decrease. However, once the tube is completely flooded, then a further decrease in fin spacing results in replacing low thermal conductivity liquid within the channels with high conductivity metal, and heat transfer should increase. The second dip in the Honda et al. (1987c) model at a fin spacing slightly more than 1 mm is due to a change in mechanism that occurs in their model between "closely spaced" and "widely spaced" fins. A similar comparison is shown in Fig. 17, which shows the data of Marto et al. (1988a) for R-113 and the predictions of Beatty and Katz (1948), Webb et al. (1985), and Honda et al. (1987c). The data were obtained using the same family of tubes used for steam. (One additional tube with a spacing of only 0.25 was tested because of the low surface tension of R-113.) Surprisingly, the Beatty and Katz (1948) model underpredicts the data by as much as 75 percent. The Webb et al. (1985) model depends upon the selection of the Adamek (1981) condensate shape parameter ζ. Unfortunately, it is very difficult to know what value of ζ to use, especially for the case of rectangular-shape fins. The best agreement is evident with the Honda et al. (1987c) model.

Adamek and Webb (1988) have recently extended an earlier analysis of Adamek (1985) to predict film condensation on horizontal integral-fin tubes having rectangular or trapezoidal shape fins. Three additional effects were included: condensation at the bottom of the channel along the interfin tube surface in the unflooded part of the tube, condensation along a very small length of the fin flank in the flooded part of the tube, and condensation on the fin tip. The first effect was accounted for by a Nusselt-type, gravity-drainage model with mass addition from the fin flanks. They assumed that on the lateral side of a rectangular or trapezoidal fin, the flow of condensate due to surface tension could be approximated by a constant-pressure-gradient model (see for example equation (26)) corrected for the fin efficiency.[6] The second effect was accounted for by determining the existence of a short thin-film length near the fin tip (this length was estimated to be less than 0.2 mm), along which surface-tension-drainage due to a con-

[6]The fin efficiency was calculated following a numerical procedure recently prescribed by Adamek and Kedzierski (1988).

Downloaded 16 Dec 2010 to 193.140.21.150. Redistribution subject to ASME license or copyright; see http://www.asme.org/terms/Terms_Use.cfm

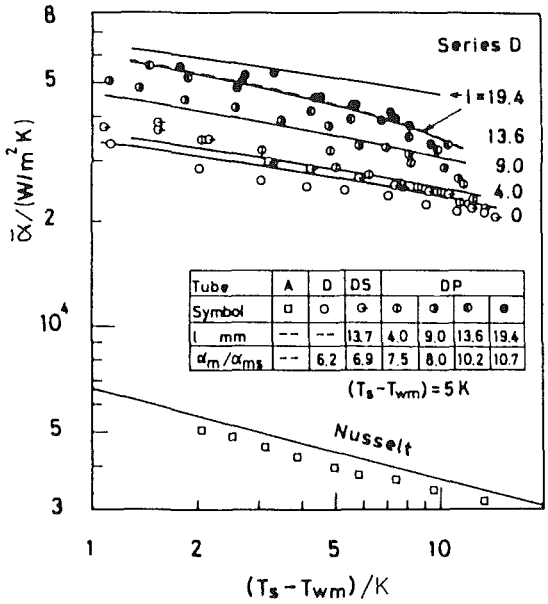

Fig. 19 Comparison of measured and predicted heat transfer coefficients of methanol on finned tubes with porous drainage strips (Honda and Nozu, 1985)

stant pressure gradient occurs. The third effect was included by using Nusselt (1916) theory for a horizontal tube of diameter D_o. Thus the condensate that formed on the fin tips was assumed to drain around the circumference of the fin and not radially inward toward the channel bottom. Using this extended model, Adamek and Webb (1988) compared their heat transfer predictions to the experimental data of Yau et al. (1985) and Wanniarachchi et al. (1985) for steam. The results are shown in Fig. 18, demonstrating excellent agreement (within about ±10 to 15 percent) over the complete range of fin spacings.

Honda and Nozu (1985) modified the analytical model of Honda and Nozu (1984) (later published as Honda and Nozu, 1987) to include the effect of a porous, longitudinal drainage strip mounted at the base of the fins as shown schematically in Fig. 2(*b*). At the tube bottom, they assumed that the retained condensate was pulled by gravity and surface tension forces into the porous drainage strip. The condensate flow through the porous strip was governed by Darcy's law with a pressure gradient given by

$$\frac{dp}{dx} = \rho g - \frac{\mu v}{K} \tag{34}$$

where x is the vertical distance along the strip, v is the average condensate velocity in the strip, and K is the permeability of the porous material. They then made a pressure balance between the flooding point on the tube (i.e., $\phi = \phi_f$) and the condensate overflow point ($x = x_1$) at the bottom of the strip, and arrived at an expression for the flooding angle ϕ_f under these conditions

$$\phi_f = \cos^{-1}\left\{\left[\frac{2\sigma \cos\theta/b - \rho g(1-F/K)x_1}{\rho g R_o}\right] - 1\right\} \tag{35}$$

where F is a factor that is related to the average heat flux along the tube q (based on the nominal surface area $\pi D_o L$)

$$F = \frac{\pi D_o q v}{\rho g\, h_{fg} t_p} \tag{36}$$

Equation (35) was then substituted into equation (33) to arrive at an average Nusselt number. Figure 19 shows a comparison of the results of this modified model to their experimental data for methanol. Tube A was a 19.05 mm diameter smooth tube and Tube D contained rectangular-shape fins ($t = 0.11$ mm, $b = 0.4$ mm, and $h = 1.13$ mm) on a root diameter of 17.1 mm. In addition to the data for the plain finned tube (D), data were also obtained for tube D with a solid drainage strip (DS) and with a porous drainage strip (DP). As expected, the porous drainage strip enhances the heat transfer significantly. The solid curves in Fig. 19 are the predicted results from the modified model for different porous strip heights of 4.0, 9.0, 13.6, and 19.4 mm. The predictions appear to agree well with the data except for the tube DP19. Honda and Nozu (1985) discussed this discrepancy and suggested a revised result (lower curve), which agrees well with the data. The results, in general, show that there appears to be an upper limit in effective strip height, which is apparently determined by the capillary limit of the porous strip.

Effect of Condensate Inundation

It is well known that shell-side condensation in an actual surface condenser is widely different from that which occurs on a single tube. One of the reasons for this difference is the effect of condensate inundation. Nusselt (1916) considered the idealized case where the condensate from a smooth tube is assumed to drain by gravity (i.e., no vapor shear) as a continuous laminar sheet directly onto the top of the tube below it. He arrived at the well-known expression for the ratio of the average heat transfer coefficient for a vertical column of N tubes compared to the coefficient for the top tube

$$\frac{\bar{\alpha}_N}{\bar{\alpha}_1} = N^{-s} \tag{37}$$

where $s = 1/4$. Kern (1958) assumed that the condensate drains as discrete droplets or columns, which cause disturbances in the condensate film, and predicted a less conservative relationship with $s = 1/6$. Fujii (1983) reviewed the physics of the inundation process, and recommended an improved model, which considers how much the condensate spreads axially when it strikes a lower tube as a droplet or column. Numerous experimental studies have been made using smooth tubes (e.g., Nobbs, 1975), but the data in general are widely scattered, making it very difficult to verify the analytical models. Very little information has been published for finned tubes, and most of this information pertains to refrigerants and small tube bundles.

Katz et al. (1947b) measured condensation heat transfer coefficients for R-12 in a 40-tube commercial condenser. The finned tubes had 590 fins per meter and were placed in a triangular array with a pitch-to-diameter ratio of 1.3. They presented several empirically derived design charts for multitube condensers, which included a correction to be applied to the Nusselt (1916) expression, equation (37). Katz and Geist (1948) obtained data for six finned tubes (590 fins per meter) in an in-line vertical column using R-12, acetone, *n*-butane, and steam. The pitch-to-diameter ratio was 1.75. They found that with finned tubes, the effect of condensate inundation was much less than predicted by Nusselt (1916). In fact, their data can be correlated by equation (37) with an inundation exponent s of about 0.06. Pearson and Withers (1969) measured coefficients using two identical, 60-tube condensers with R-22. One condenser contained finned tubes with 748 fins per meter while the other had tubes with 1024 fins per meter. The tubes in each condenser were arranged in a triangular array with a pitch-to-diameter ratio of 1.25. They suggested that the average heat transfer coefficient data for a bundle could be predicted by correcting the single, finned-tube expression of Beatty and Katz (1948), equations (9)–(12), with a factor $C_N/N^{1/4}$, where $C_N = 1.34$ and 1.31 for the 1024 and 748 fin-per-meter tubes, respectively. Smirnov and Lukanov (1972) made tests with an 80-tube bundle using R-11. The tubes contained 490 rather thick, trapezoidal-shape fins per meter and were placed in a triangular array with a pitch-to-diameter ratio

Downloaded 16 Dec 2010 to 193.140.21.150. Redistribution subject to ASME license or copyright; see http://www.asme.org/terms/Terms_Use.cfm

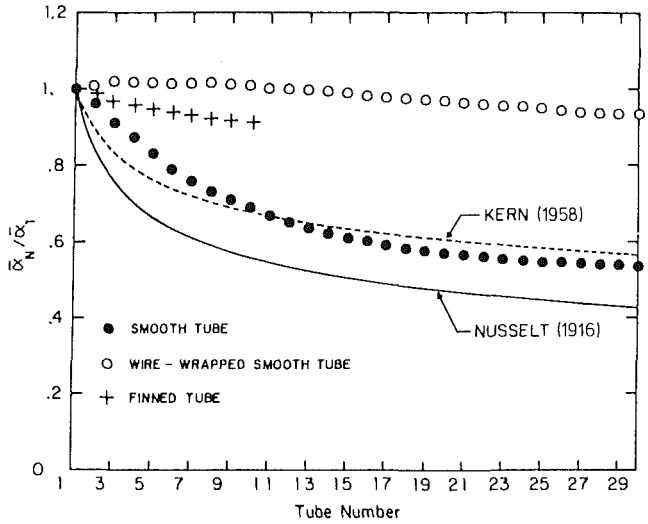

Fig. 20 Preliminary data showing influence of condensate inundation on the steam condensing heat transfer coefficient on smooth and enhanced tubes

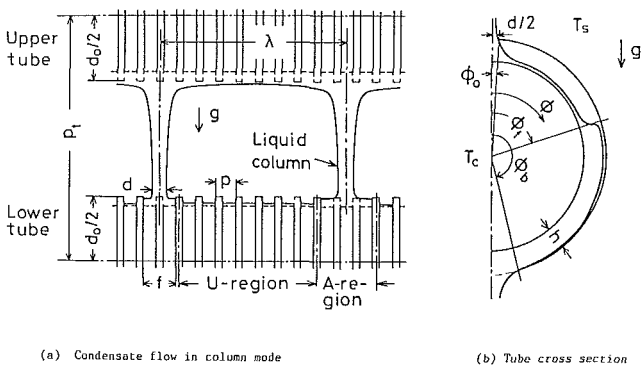

Fig. 21 Condensate inundation model of Honda et al. (1987b)

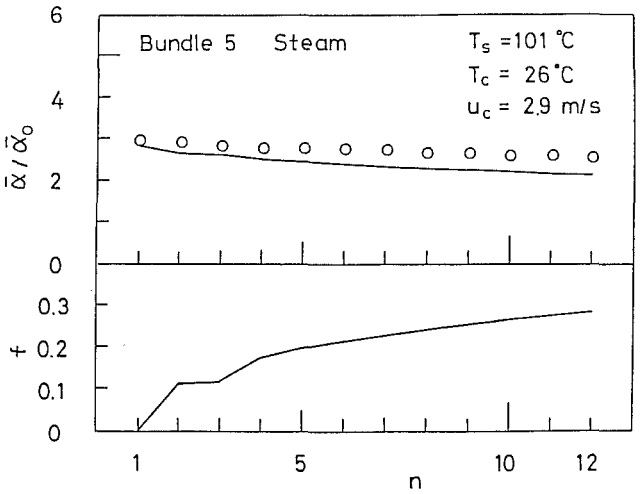

Fig. 22 Comparison of measured and predicted results for condensation of steam in a finned-tube bundle (Honda et al., 1987b)

of 1.3. Quite surprisingly, they found that the local heat transfer coefficient within the bundle fell more sharply from the first to the fifth tube row than predicted by the Nusselt (1916) theory. Farther down in the bundle, however, a slight increase occurred with tube row. These results are clearly contrary to those of the other previous investigations and the reasons for this difference are unknown.

Edwards et al. (1973), in their analysis of spirally threaded tubes as mentioned above, found that the effect of condensate inundation for a threaded tube was much less than for a smooth tube. They also showed that the effect of inundation was more pronounced for finer-pitched threads. Mills et al. (1975) experimentally studied the effect of an overhead liquid drip rate during steam condensation on a threaded tube (1420 threads per meter) in order to simulate a bundle effect. They found no significant decrease in heat transfer at a drip rate of up to ten equivalent tubes. Some preliminary data for steam, obtained at the Naval Postgraduate School, are shown in Fig. 20. The data were taken for five active tubes[7] in a vertical column with a pitch-to-diameter ratio of 1.5. Additional tubes were simulated using a perforated tube. The apparatus is described in detail by Brower (1985). Results were obtained for a smooth tube, a wire-wrapped smooth tube (wire diameter of 1.6 mm and wire pitch of 8 mm) and an integral-fin tube (fin height and thickness of 1.0 mm and fin spacing of 1.5 mm). The data show that the effect of condensate inundation appears to be less significant with a wire-wrapped or a finned tube than with a smooth one. Presumably, the presence of wires or fins on the tube surface prevents the condensate that drips onto the tube from spreading significantly. In addition, surface tension forces tend to thin the film between wires or fins because of the low-pressure regions created in the condensate under the concave "wedges" of liquid formed at the base of the wires or fins.

Several analyses of condensate inundation in finned-tube bundles have been made recently. Ishihara and Palen (1983) presented an overall approach, which includes gravity-controlled laminar, laminar-rippled, transition, and turbulent flow regimes. The local liquid film Reynolds number is used to determine the transition point from one regime to another. In the laminar regime, they proposed the use of the Beatty and Katz (1948) relationship for a single tube together with a correction factor similar to that used by Pearson and Withers (1969) (i.e., $C_N/N^{1/4}$). In the other regimes, they suggested adapting existing smooth tube predictions for the case of finned tubes. They proposed that the fins cause an earlier transition to occur from laminar to laminar-rippled flow. Also, an empirical Prandtl number effect was recommended in the laminar-rippled regime. They compared this proposed model to a range of data obtained prior to 1979 (351 data points using several fluids and several bundles), and found general agreement to within about ±30 percent. El-Meghazy (1986) analyzed condensate flow on an integral-fin surface containing circular-shape fin tips and fin channels. He found that the ratio of tip radius to channel radius is a very important design parameter whose selection depends on the number of tube rows in the bundle. He also made some condensation measurements with simulated horizontal finned-tube bundles using steam and R-11, and found that the finned tubes displayed an inundation exponent s equal to 0.15.

Honda et al. (1987b) have proposed an adaption of the Honda and Nozu (1987) model for a single integral-fin tube to account for condensate inundation effects. Based upon earlier experimental observations by Honda et al. (1987a) of condensate drainage from a column of finned tubes, they proposed a physical model that allows for drainage to occur either in a column mode or a sheet mode. The transition from one mode to the other was dependent upon a dimensionless parameter $K=\Gamma(g/\rho)^{1/4}/\sigma^{3/4}$, where Γ is the condensate flow rate per unit length for one side of a tube. They assumed that the column mode would occur for $K \leq 0.42$. Figure 21 shows a schematic of their column-mode model. The condensate was assumed to fall in columns, which were spaced at a Taylor wavelength (Yung et al., 1980)

[7] The data for the finned tube were for only one active tube with condensate simulation from a perforated tube.

Downloaded 16 Dec 2010 to 193.140.21.150. Redistribution subject to ASME license or copyright; see http://www.asme.org/terms/Terms_Use.cfm

$$\lambda = 2\pi\sqrt{2\sigma/\rho g} \tag{38}$$

This condensate was assumed to spread axially over a few channels, giving a condensate affected region (A). Between affected regions, the tube was assumed to have an unaffected region (U). The proportion of the surface area covered by impinging condensate was defined as f. They adapted their earlier heat transfer model to include this condensate flow, and arrived at an average heat transfer rate per tube on a row-by-row basis. Figure 22 is a plot of their prediction relative to experimental data for steam on a column of finned tubes (data from Fig. 20). The ratio $\bar{\alpha}/\bar{\alpha}_o$ is the average heat transfer coefficient (based on an equivalent smooth tube area) for a finned tube within the bundle divided by the average value for a single tube as predicted by Nusselt (1916) theory. The agreement between the data and the theory is very good, both showing a slight deterioration farther down in the bundle. The comparison is carried out to 12 tubes where the surface area fraction covered by condensate f is about 0.3. At this point, the column drainage mode shifts to the sheet mode. Their numerical results for a set of realistic finned tube geometries and operating conditions revealed that for R-12, the optimum fin spacing for a bundle is near 0.3 mm whereas for steam, the optimum is near 1.3 mm. These values of fin spacing are very close to the experimentally determined values for a single tube, thus indicating that the effect of inundation for a finned tube is not as important as for a smooth tube.

Effect of Vapor Velocity

All of the above-reported results have been obtained with low-velocity vapor. However, in actual surface condensers, depending upon the application, vapor velocities may be quite appreciable. In this situation, large interfacial shear forces on the condensate film could subsequently alter the condensate flow around the tube, resulting in an appreciable change in the heat transfer. The problem of film condensation with appreciable vapor shear is a complex one, and many theoretical and experimental investigations have been conducted with single, smooth tubes. For example, Rose (1988) has recently provided a comprehensive review of the fundamentals involved, and important experimental results have been recently reported by Memory and Rose (1986) and Honda et al. (1986). In addition, Cavallini et al. (1986) provided recent data for a bundle of tubes.

With integral-fin tubes, however, information on the effect of vapor velocity is almost nonexistent. The only work that reports directly on the effect of vapor velocity is that of Gogonin and Dorokhov (1981). They reported data for R-21 condensing on two different 800 fin-per-meter tubes over a range of vapor velocities (up to 8 m/s), operating pressure, and heat fluxes. Figure 23 compares their data for the finned tubes with those for a smooth tube. It shows the relative heat transfer coefficient ratio $\overline{Nu}/\overline{Nu}_o$[8] versus the square root of the Froude number ($Fr = U^2/gD_o$) and indicates clearly that the effect of vapor velocity for the finned tubes is very small in comparison to the effect for smooth tubes. Ishihara and Palen (1983) discuss heat transfer in finned-tube bundles at high vapor velocities, and suggest a forced-convection type of correlation with a correction factor to include two-phase flow effects. Unfortunately, they provide no further quantitative information on the differences between smooth and finned tubes. Webb (1984) surveyed the effect of vapor velocity in shell-side refrigeration condensers, and found no published information other than the data of Gogonin and Dorokhov (1981). However, he calculated the range of vapor velocities in these condensers and discovered that the largest vapor velocity was 0.6 m/s. He therefore concluded that in refrigeration condensers, the shell-side vapor velocity should not significantly affect the heat transfer coefficient with finned tubes. Yau et al. (1986), in their measurements of steam condensation on a family of finned tubes, obtained data with downward vapor velocities of 0.5, 0.7, and 1.1 m/s. Even though this range of velocity is very small, it perhaps is important to point out that they detected almost the same influence of vapor velocity on their finned tube data as their smooth tube data (i.e., the finned-to-plain tube enhancement was essentially the same at all three vapor velocities). This result is contrary to the observation of Gogonin and Dorokhov (1981), and implies that the influence of vapor velocity on finned tube condensation is far from being resolved.

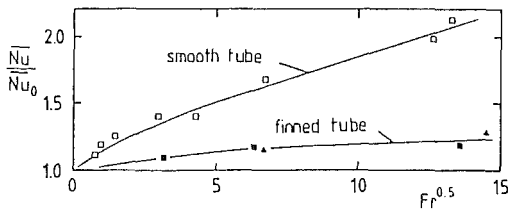

Fig. 23 Influence of vapor velocity on smooth tube and finned tube heat transfer (Gogonin and Dorokhov, 1981)

Conclusions

Significant progress has been made in understanding the role of surface tension during film condensation from a quiescent vapor to a single, horizontal, integral-fin tube. Condensate flooding significantly affects finned tube performance, and heat transfer enhancements, in general, are larger than surface area enhancements created by adding fins. A significant data base for various tube sizes, fin geometries, and operating fluids is now being gathered, but care must be exercised in using the data due to variations in the definitions of several important quantities such as surface area, enhancement ratio, etc. An effort should therefore be made to standardize data reduction procedures.

Fin spacing, the most studied fin variable to date, has been shown to be very important. As the ratio of the surface tension to density of the operating fluid goes up, the optimum fin spacing increases and the magnitude of the heat transfer enhancement decreases. Fin shape may be an important variable for situations where there is a small degree of condensate flooding, and when using high conductivity metals, tall thin fins are desirable. Condensate drainage devices may also prove to be very useful in providing additional heat transfer enhancement, especially for high surface tension fluids. Although several very promising theoretical models exist, no simple accurate design equation is as yet available.

There is a clear need for additional research into the effects of condensate inundation and vapor shear on finned tube performance. Existing evidence suggests that the effect of condensate inundation for an integral-fin tube is less than for a smooth one, though this result may be very sensitive to fin spacing. Additional data (including visual data) are therefore needed for various tube bundle configurations, showing condensate drainage patterns and tube flooding angles as a function of surface tension-to-density ratio and tube/fin geometry. Almost no information is available with regard to the effect of vapor velocity on finned tube performance. Although vapor shear may not be important in refrigeration condensers, it could possibly be a controlling factor in other applications.

Acknowledgment

Portions of this work were supported by the National

[8] In the Nusselt number $\overline{Nu}_o$, Gogonin and Dorokhov (1981) do not define the heat transfer coefficient $\bar{\alpha}_o$ clearly. As a result, some ambiguity exists. In this paper, $\bar{\alpha}_o$ is interpreted as the average heat transfer coefficient in a quiescent vapor.

Downloaded 16 Dec 2010 to 193.140.21.150. Redistribution subject to ASME license or copyright; see http://www.asme.org/terms/Terms_Use.cfm

Science Foundation through Grant No. CBT-8603582. The author is also deeply appreciative of the partial financial assistance received from the UK Science and Engineering Research Council while on sabbatical leave at Queen Mary College, University of London.

References

Adamek, T., 1981, "Bestimmung der Kondensation-grossen auf Feingewellten Oberflachen zur Auslegun Aptimaler Wandprofile," *Warme- und Stoffübertragung*, Vol. 15, pp. 255–270.

Adamek, T., 1985, "Rechenmodell der Filmkondensation on Engberippten Kondensatorrohren," *Warme- und Stoffübertragung*, Vol. 19, pp. 145–157.

Adamek, T., and Kedzierski, M. A., 1988, Private Communication.

Adamek, T., and Webb, R. L., 1988, "Extended Prediction Theory for Film Condensation on Finned Surfaces Including Heat Transfer Within the Channel," *Int. J. Heat Mass Transfer*, Vol. 31 (submitted).

Arai, N., Fukushima, T., Arai, A., Nakayama, T., Fujie, K., and Nakayama, Y., 1977, "Heat Transfer Tubes Enhancing Boiling and Condensation in Heat Exchangers of a Refrigerating Machine," *Trans. ASHRAE*, Vol. 83, pp. 58–70.

Armstrong, R. M., 1945, "Heat Transfer and Pressure Loss in Small Commercial Shell-and-Finned-Tube Heat Exchangers," *Trans. ASME*, Vol. 67, pp. 675–681.

Beatty, K. O., and Katz, D. L., 1948, "Condensation of Vapors on Outside of Finned Tubes," *Chem. Eng. Prog.*, Vol. 44, No. 1, pp. 55–70.

Brower, S. K., 1985, "The Effects of Condensate Inundation on Steam Condensation Heat Transfer in a Tube Bundle," M.S. Thesis, Naval Postgraduate School, Monterey, CA.

Carnavos, T. C., 1980, "An Experimental Study: Condensing R-11 on Augmented Tubes," ASME Paper No. 80-HT-54.

Cavallini, A., Frizzerin, S., and Rossetto, L., 1986, "Condensation of R-11 Vapor Flowing Downward Outside a Horizontal Tube Bundle," *Proc. 8th Int. Heat Transfer Conference*, C. L. Tien et al., eds., Hemisphere Publishing Corp., Washington, DC, Vol. 4, pp. 1707–1712.

Chi, S. W., 1976, *Heat Pipe Theory and Practice*, McGraw-Hill, New York.

Cooper, J. R., and Rose, J. W., 1981, "Condensation Heat-Transfer Enhancement by Vapour-Side Surface Geometry Modification," *Proc. HTFS Research Symp.*, Oxford, Paper No. RS402, pp. 647–672.

Dunn, P. D., and Reay, D. A., 1982, *Heat Pipes*, 3rd ed., Pergamon Press, New York.

Edwards, D. K., Gier, K. D., Ayyaswamy, P. S., and Catton, I., 1973, "Evaporation and Condensation in Circumferential Grooves on Horizontal Tubes," ASME Paper No. 73-HT-25.

El-Meghazy, I. M., 1986, "Enhancing Condensation Heat Transfer on Finned Tubes in Condensers," Ph.D. Thesis, Technical University of Warsaw, Poland.

Fujii, T., 1983, "Condensation in Tube Banks," *Proc. Symp. on Condensers: Theory and Practice*, I. Chem. E. Symp. Ser. No. 75, pp. 3–22.

Fujii, T., and Honda, H., 1978, "Laminar Filmwise Condensation on a Vertical Single Fluted Plate, " *Proc. 6th International Heat Transfer Conference*, Hemisphere Publishing Corp., Washington, DC, Vol. 2, pp. 419–424.

Gogonin, I. I., and Dorokhov, A. R., 1981, "Enhancement of Heat Transfer in Horizontal Shell-and-Tube Condensers," *Heat Transfer—Soviet Research*, Vol. 3, No. 3, pp. 119–126.

Gregorig, R., 1954, "Film Condensation on Finely Rippled Surfaces With Consideration of Surface Tension," *Z. Angew. Math. Phys.*, Vol. 5, pp. 36–49.

Hijikata, K., Simoda, K., and Mori, Y., 1987, "Condensation Heat Transfer Enhancement on a Downward Facing Surface by the Gravity," *Proc. 2nd ASME-JSME Thermal Engineering Joint Conference*, P. J. Marto and I. Tanasawa, eds., Vol. 5, pp. 393–400.

Hirasawa, S., Hijikata, K., Mori, Y., and Nakayama, W., 1980, "Effect of Surface Tension on Condensate Motion in Laminar Film Condensation (Study of Liquid Film in a Small Trough)," *Int. J. Heat Mass Transfer*, Vol. 23, pp. 1471–1478.

Honda, H., Nozu, S., and Mitsumori, K., 1983, "Augmentation of Condensation on Horizontal Finned Tubes by Attaching a Porous Drainage Plate," *Proc. ASME-JSME Thermal Engineering Joint Conference*, Y. Mori and W.-J. Yang, eds., Vol. 3, pp. 289–296.

Honda, H., and Fujii, T., 1984, "Semi-empirical Equation for Condensation Heat Transfer on Vertical Fluted Tubes," ASME HTD-Vol. 38, pp. 99–106.

Honda, H., and Nozu, S., 1984, "A Prediction Method for Heat Transfer During Film Condensation on Horizontal Low Integral-Fin Tubes," *Fundamentals of Phase Change: Boiling and Condensation*, ASME HTD-Vol. 38, pp. 107–114.

Honda, H., and Nozu, S., 1985, "Effect of Drainage Strips on the Condensation Heat Transfer Performance of Horizontal Finned Tubes," *Proc. Int. Symp. on Heat Transfer*, Vol. 2, Paper No. 85-ISHT-II-32 (also 1987, in *Heat Transfer Science and Technology*, Hemisphere Publishing Corp., Washington DC, pp. 455–462).

Honda, H., Nozu, S., and Furukawa, Y., 1986, "Effect of Porous Drainage Strips on Film Condensation on Downard-Facing Horizontal Surfaces," *Proc. 8th Int. Heat Transfer Conference*, C. L. Tien et al. eds., Hemisphere Publishing Corp., Washington DC, Vol. 4, pp. 1713–1718.

Honda, H., Nozu, S., Uchima, B., and Fujii, T., 1986, "Effect of Vapour Velocity on Film Condensation of R-113 on Horizontal Tubes in a Crossflow," *Int. J. Heat Mass Transfer*, Vol. 29, pp. 429–438.

Honda, H., and Nozu, S., 1987, "A Prediction Method for Heat Transfer During Film Condensation on Horizontal Low Integral-Fin Tubes," ASME Journal of Heat Transfer, Vol. 109, pp. 218–225.

Honda, H., Nozu, S., and Takeda, Y., 1987, "Flow Characteristics of Condensate on a Vertical Column of Horizontal Low Finned Tubes," *Proc. 2nd ASME-JSME Thermal Engineering Joint Conference*, P. J. Marto and I. Tanasawa, eds., Vol. 1, pp. 517–524.

Honda, H., Nozu, S., and Takeda, Y., 1987, "A Theoretical Model of Film Condensation in a Bundle of Horizontal Low Finned Tubes," *Boiling and Condensation in Heat Transfer Equipment*, ASME HTD-Vol. 85, pp. 79–85.

Honda, H., Nozu, S., and Uchima, B., 1987, "A Generalized Prediction Method for Heat Transfer During Film Condensation on a Horizontal Low Finned Tube," *Proc. 2nd ASME-JSME Thermal Engineering Joint Conference*, P. J. Marto and I. Tanasawa, eds., JSME, Vol. 4, pp. 385–392.

Ishihara, K. I., and Palen, J. W., 1983, "Condensation of Pure Fluids on Horizontal Finned Tube Bundles," *Proc. Symp. on Condensers: Theory and Practice*, I. Chem. E. Symp. Ser. No. 75, pp. 429–446.

Joos, F. M., 1984, "Thin Liquid Films on Arbitrary Surfaces With Condensation or Evaporation," *Fundamentals of Phase Change: Boiling and Condensation*, ASME HTD-Vol. 38, pp. 123–132.

Kabov, O. A., 1984, "Film Condensation of Immobile Vapor on a Horizontal Finned Cylinder," *Heat Transfer—Soviet Research*, Vol. 16, No. 6, pp. 76–83.

Karkhu, V. A., and Borovkov, V. P., 1971, "Film Condensation of Vapor at Finely-Finned Horizontal Tubes," *Heat Transfer—Soviet Research*, Vol. 3, No. 2, pp. 183–191.

Katz, D. L., Beatty, K. O., and Foust, A. S., 1945, "Heat Transfer Through Tubes With Integral Spiral Fins," *Trans. ASME*, Vol. 67, pp. 665–674.

Katz, D. L., and Geist, J. M., 1948, "Condensation on Six Finned Tubes in a Vertical Row," *Trans. ASME*, Vol. 70, pp. 907–914.

Katz, D. L., Hope, R. C., and Datsko, S. C., 1946, "Liquid Retention on Integral-Finned Tubes," Department of Engineering Research, University of Michigan, Ann Arbor, MI, Project No. M592.

Katz, D. L., Hope, R. E., Datsko, S. C., and Robinson, D. B., 1947, "Condensation of Freon-12 With Finned Tubes, Part I. Single Horizontal Tubes," *J. Am. Soc. Refrigerating Engineers*, Vol. 53, pp. 211–217.

Katz, D. L., Hope, R. E., Datsko, S. C., and Robinson, D. B., 1947, "Condensation of Freon-12 With Finned Tubes, Part II. Multitube Condensers," *J. Am. Soc. Refrigerating Engineers*, Vol. 53, pp. 315–319, 352–354.

Kedzierski, M. A., and Webb, R. L., 1987, "Experimental Measurements of Condensation on Vertical Plates With Enhanced Fins," *Boiling and Condensation in Heat Transfer Equipment*, ASME HTD-Vol. 85, pp. 87–95.

Kern, D. Q., 1958, "Mathematical Development of Loading in Horizontal Condensers," *AIChE J.*, Vol. 4, pp. 157–160.

Kisaragi, T., Enya, S., Ochiai, J., Kuwahara, K., and Tanasawa, I., 1978, "On the Improvement of Condensation Heat Transfer on Horizontal Tubes," JSME Paper No. 780-1, pp. 1–5.

Marto, P. J., 1984, "Heat Transfer and Two-Phase Flow During Shell-Side Condensation," *Heat Trans. Engrg.*, Vol. 5, Nos. 1–2, pp. 31–61.

Marto, P. J., 1986, "Recent Progress in Enhancing Film Condensation Heat Transfer on Horizontal Tubes," *Heat Trans. Engrg.*, Vol. 7, Nos. 3–4, pp. 61–71.

Marto, P. J., Mitrou, E., Wanniarachchi, A. S., and Rose, J. W., 1986, "Film Condensation of Steam on Horizontal Finned Tubes: Effect of Fin Shape," *Proc. 8th Int. Heat Transfer Conference*, C. L. Tien et al., eds., Hemisphere Publishing Corp., Washington, DC, Vol. 4, pp. 1695–1700.

Marto, P. J., Mitrou, E., Wanniarachchi, A. S., and Katsuta, M., 1987, "Film Condensation of Steam on a Horizontal Wire-Wrapped Tube," *Proc. 2nd ASME-JSME Thermal Engineering Joint Conference*, P. J. Marto and I. Tanasawa, eds., Vol. 1, pp. 509–516.

Marto, P. J., and Nunn, R. H., 1983, "The Potential of Heat Transfer Enhancement in Surface Condensers," *Proc. Symp. on Condensers: Theory and Practice*, I.Chem.E. Symp. Ser. No. 75, pp. 23–39.

Marto, P. J., Zebrowski, D., Wanniarachchi, A. S., and Rose, J. W., 1988, "Film Condensation of R-113 on Horizontal Finned Tubes," *Fundamentals of Phase Change: Boiling and Condensation*, Proc. 1988 National Heat Transfer Conf., H. R. Jacobs, ed., ASME, Vol. 2, pp. 583–592.

Marto, P. J., Wanniarachchi, A. S., Cakan, O., and Rose, J. W., 1988, "Enhancement of Steam Condensation on a Horizontal Finned Tube by Using Drainage Strips," *Proc. 2nd U.K. National Heat Transfer Conference*, Glasgow, Scotland (submitted).

Masuda, H., 1985, "Film Condensation Heat Transfer on Low Integral-Fin Tubes," Ph.D. Thesis, Queen Mary College, University of London.

Masuda, H., and Rose, J. W., 1985, "An Experimental Study of Condensation of Refrigerant 113 on Low Integral-Fin Tubes," *Proc. Int. Symp. on Heat Transfer*, Beijing, China, Vol. 2, Paper No. 32 (also 1987, in *Heat Transfer Science and Technology*, Hemisphere Publishing Corp., Washington, DC, pp. 480–487).

Masuda, H., and Rose J. W., 1987, "Static Configuration of Liquid Films on Horizontal Tubes With Low Radial Fins: Implications for Condensation Heat Transfer," *Proc. Roy. Soc. London*, A410, pp. 125–139.

Masuda, H., and Rose, J. W., 1988, "Condensation of Ethylene Glycol on Horizontal Integral-Fin Tubes," ASME Journal of Heat Transfer, Vol. 110 (to be published).

Memory, S. B., and Rose, J. W., 1986, "Film Condensation of Ethylene Glycol on a Horizontal Tube at High Vapor Velocity," *Proc. 8th Int. Heat*

Downloaded 16 Dec 2010 to 193.140.21.150. Redistribution subject to ASME license or copyright; see http://www.asme.org/terms/Terms_Use.cfm

Transfer Conference, C. L. Tien et al., eds., Hemisphere Publishing Corp., Washington, DC, Vol. 4, pp. 1607-1612.

Mills, A. F., Hubbard, G. L., James, R. K., and Tan, C., 1975, "Experimental Study of Film Condensation on Horizontal Grooved Tubes," *Desalination*, Vol. 16, pp. 121-133.

Mitrou, E., 1986, "Film Condensation Heat Transfer on Horizontal Finned Tubes," M.S. Thesis, Naval Postgraduate School, Monterey, CA.

Mori, Y., Hijikata, K., Hirasawa, S., and Nakayama, W., 1979, "Optimized Performance of Condensers With Outside Condensing Surface," *Condensation Heat Transfer*, P. J. Marto and P. G. Kroeger, eds., ASME, New York, pp. 55-62.

Nobbs, D. W., 1975, "The Effect of Downward Vapor Velocity and Inundation on the Condensation Rates on Horizontal Tubes and Tube Banks," Ph.D. Thesis, University of Bristol, England.

Nusselt, W., 1916, "Die Oberflachen-Kondensation des Wasserdampfes," *VDI Zeitung*, Vol. 60, pp. 541-546, 569-575.

Owen, R. G., Sardesai, R. G., Smith, R. A., and Lee, W. C., 1983, "Gravity Controlled Condensation on Low Integral-Fin Tubes," *Proc. Symp. on Condensers: Theory and Practice*, I.Chem.E. Symp. Ser. No. 75, pp. 415-428.

Panchal, C. B., and Bell, K. J., 1980, "Analysis of Nusselt-Type Condensation on a Vertical Fluted Surface," *Num. Heat Trans.*, Vol. 3, pp. 357-371.

Panday, P. K., and Bilek, A., 1985, "Condensation of Pure Vapor on Longitudinally Grooved Vertical Cylinders," *Proc. 4th Int. Conf. on Numerical Methods in Thermal Problems*, pp. 218-228.

Pearson, J. F., and Withers, J. G., 1969, "New Finned Tube Configuration Improves Refrigerant Condensing," *Trans. ASHRAE*, Vol. 75, pp. 77-82.

Renz, U., 1986, "Measures to Improve Heat Transfer in Condensation," *German Chemical Engineering*, Vol. 9, No. 1, pp. 30-41.

Rifert, V. G., 1980, "A New Method for Calculating Rates of Condensation on Finned Tubes," *Heat Transfer—Soviet Research*, Vol. 12, No. 3, pp. 142-147.

Rifert, V. G., Barabash, P. A., Vizel, Y. F., and Trokoz, Y. Y., 1985, "Effect of Surface Tension on the Hydrodynamics and Heat Transfer in Condensation of Vapor on Finned or Corrugated Surfaces," *Heat Transfer—Soviet Research*, Vol. 17, No. 1, pp. 18-27.

Rose, J. W., 1988, "Fundamentals of Condensation Heat Transfer: Laminar Film Condensation," *JSME International J.*, Vol. 31 (to be published).

Rudy, T. M., 1982, "A Theoretical and Experimental Study of Condensation on Single, Integral-Fin Tubes," Ph.D. Thesis, The Pennsylvania State University, University Park, PA.

Rudy, T. M., and Webb, R. L., 1981, "Condensate Retention on Horizontal Integral-Fin Tubing," *Advances in Heat Transfer*, ASME HTD-Vol. 18, pp. 35-41.

Rudy, T. M., and Webb, R. L., 1983, "An Analytical Model to Predict Condensate Retention on Horizontal, Integral-Fin Tubes," *Proc. of ASME-JSME Thermal Engineering Conference*, Y. Mori and W.-J. Yang, eds., Vol. 1, pp. 373-378.

Rudy, T. M., and Webb, R. L., 1983, "Theoretical Model for Condensation on Horizontal, Integral-Fin Tubes," *Heat Transfer Seattle*, AIChE Symp. Ser. No. 225, Vol. 79, pp. 11-18.

Rudy, T. M., Kedzierski, M. A., and Webb, R. L., 1984, "Investigation of Integral-Fin-Type Condenser Tubes for Process Industry Applications," I.Chem.E. Symp. Ser. No. 86, pp. 633-647.

Rudy, T. M., and Webb, R. L., 1985, "An Analytical Model to Predict Condensate Retention on Horizontal Integral-Fin Tubes," ASME JOURNAL OF HEAT TRANSFER, Vol. 107, pp. 361-366.

Sauer, H. J., and Williams, P. E., 1982, "Condensation of Refrigerant-Oil Mixtures on Low-Profile Finned Tubing," *Proc. 7th Int. Heat Transfer Conference*, U. Grigull et al., eds., Hemisphere Publishing Corp., Washington, DC, Vol. 4, pp. 147-152.

Shekarriz, A., and Plumb, O. A., 1988, "Experimental Investigation of Enhancement of Film Condensation on a Horizontal Tube Using Capillary Porous Fins," *J. Thermophysics and Heat Transfer* (submitted).

Shekriladze, I. G., and Gomelauri, V. I., 1966, "Theoretical Study of Laminar Film Condensation of Flowing Vapor," *Int. J. Heat Mass Trans.*, Vol. 9, pp. 581-591.

Shekriladze, I. G., and Rusishvili, D. G., 1980, "Heat Transfer in Condensation on Capillary Surfaces," *Heat Transfer—Soviet Research*, Vol. 12, No. 4, pp. 48-49.

Shklover, G. G., Mil'man, O. O., Baskov, V. S., and Ankudinov, G. A., 1981, "Heat Transfer in Condensation of Steam on Finely-Finned Horizontal Tubes," *Heat Transfer—Soviet Research*, Vol. 13, No. 2, pp. 108-114.

Smirnov, G. F., and Lukanov, I. I., 1972, "Study of Heat Transfer from Freon-11 Condensing on a Bundle of Finned Tubes," *Heat Transfer—Soviet Research*, Vol. 4, No. 3, pp. 51-56.

Sukhatme, S. P., Jagadish, B. S., and Prabhakaran, P., 1988, "Film Condensation of R-11 Vapour on Single Horizontal Enhanced Condenser Tubes," ASME JOURNAL OF HEAT TRANSFER, Vol. 110 (submitted).

Thomas, D. G., 1968, "Enhancement of Film Condensation Rate on Vertical Tubes by Longitudinal Fins," *AIChE J.*, Vol. 14, No. 4, pp. 644-649.

Wanniarachchi, A. S., Marto, P. J., and Rose, J. W., 1984, "Filmwise Condensation of Steam on Externally-Finned Horizontal Tubes," *Fundamentals of Phase Change: Boiling and Condensation*, ASME HTD-Vol. 38, pp. 133-141.

Wanniarachchi, A. S., Marto, P. J., and Rose, J. W., 1985, "Film Condensation of Steam on Horizontal Finned Tubes: Effect of Fin Spacing, Thickness and Height," *Multiphase Flow and Heat Transfer*, ASME HTD-Vol. 47, pp. 93-99.

Wanniarachchi, A. S., Marto, P. J., and Rose, J. W., 1986, "Film Condensation of Steam on Horizontal Finned Tubes: Effect of Fin Spacing," ASME JOURNAL OF HEAT TRANSFER, Vol. 108, pp. 960-966.

Webb, R. L., 1981, "The Use of Enhanced Surface Geometries in Condensers: An Overview," *Power Condenser Heat Transfer Technology*, P. J. Marto and R. H. Nunn, eds., Hemisphere Publishing Corp., Washington, DC, pp. 287-324.

Webb, R. L., 1984, "Shell-side Condensation in Refrigerant Condensers," *Trans. ASHRAE*, Vol. 90, pt. 1.

Webb, R. L., Keswani, S. T., and Rudy, T. M., 1982, "Investigation of Surface Tension and Gravity Effects in Film Condensation," *Proc. 7th Int. Heat Transfer Conference*, U. Grigull et al., eds., Hemisphere Publishing Corp., Washington, DC, Vol. 5, pp. 175-180.

Webb, R. L., Harman, L. L., and Hui, T. S., 1984, "Enhanced Tubes in Electric Utility Steam Condensers," *Heat Transfer in Heat Rejection Systems*, S. Sengupta and Y. S. Mussalli, eds., ASME HTD-Vol. 37, pp. 17-25.

Webb, R. L., Rudy, T. M., and Kedzierski, M. A., 1985, "Prediction of the Condensation Coefficient on Horizontal Integral-Fin Tubes," ASME JOURNAL OF HEAT TRANSFER, Vol. 107, pp. 369-376.

Wilson, E. E., 1915, "Basis for Rational Design of Heat-Transfer Apparatus," *Trans. ASME*, Vol. 37, pp. 47-82.

Yau, K. K., Cooper, J. R., and Rose, J. W., 1984, "Effects of Drainage Strips and Fin Spacing on Heat Transfer and Condensate Retention for Horizontal Finned and Plain Condenser Tubes," *Fundamentals of Phase Change: Boiling and Condensation*, ASME HTD-Vol. 38, pp. 151-156,

Yau, K. K., Cooper, J. R., and Rose, J. W., 1985, "Effects of Fin Spacing on the Performance of Horizontal Integral-Fin Condenser Tubes," ASME JOURNAL OF HEAT TRANSFER, Vol. 107, pp. 377-383.

Yau, K. K., Cooper, J. R., and Rose, J. W., 1986, "Horizontal Plain and Low-Finned Condenser Tubes—Effect of Fin Spacing and Drainage Strips on Heat Transfer and Condensate Retention," ASME JOURNAL OF HEAT TRANSFER, Vol. 108, pp. 946-950.

Yung, D., Lorenz, J. J., and Ganic, E. N., 1980, "Vapor/Liquid Interaction and Entrainment in Falling Film Evaporators," ASME JOURNAL OF HEAT TRANSFER, Vol. 102, pp. 20-25.

Zener, C., and Lavi, A., 1974, "Drainage Systems for Condensation," ASME *Journal of Engineering for Power*, Vol. 96, pp. 209-215.

Zozulya, N. V., Karkhu, V. A., and Borovkov, V. P., 1977, "An Analytic and Experimental Study of Heat Transfer in Condensation of Vapor on Finned Surfaces," *Heat Transfer—Soviet Research*, Vol. 9, No. 2, pp. 18-22.

Downloaded 16 Dec 2010 to 193.140.21.150. Redistribution subject to ASME license or copyright; see http://www.asme.org/terms/Terms_Use.cfm